Evidence-Based Complementary and Alternative Medicine

Traditional Chinese Medicine for Digestive System Tumors

Lead Guest Editor: Xueliang Wu
Guest Editors: Shangxiang Chen and Tianyi Liu

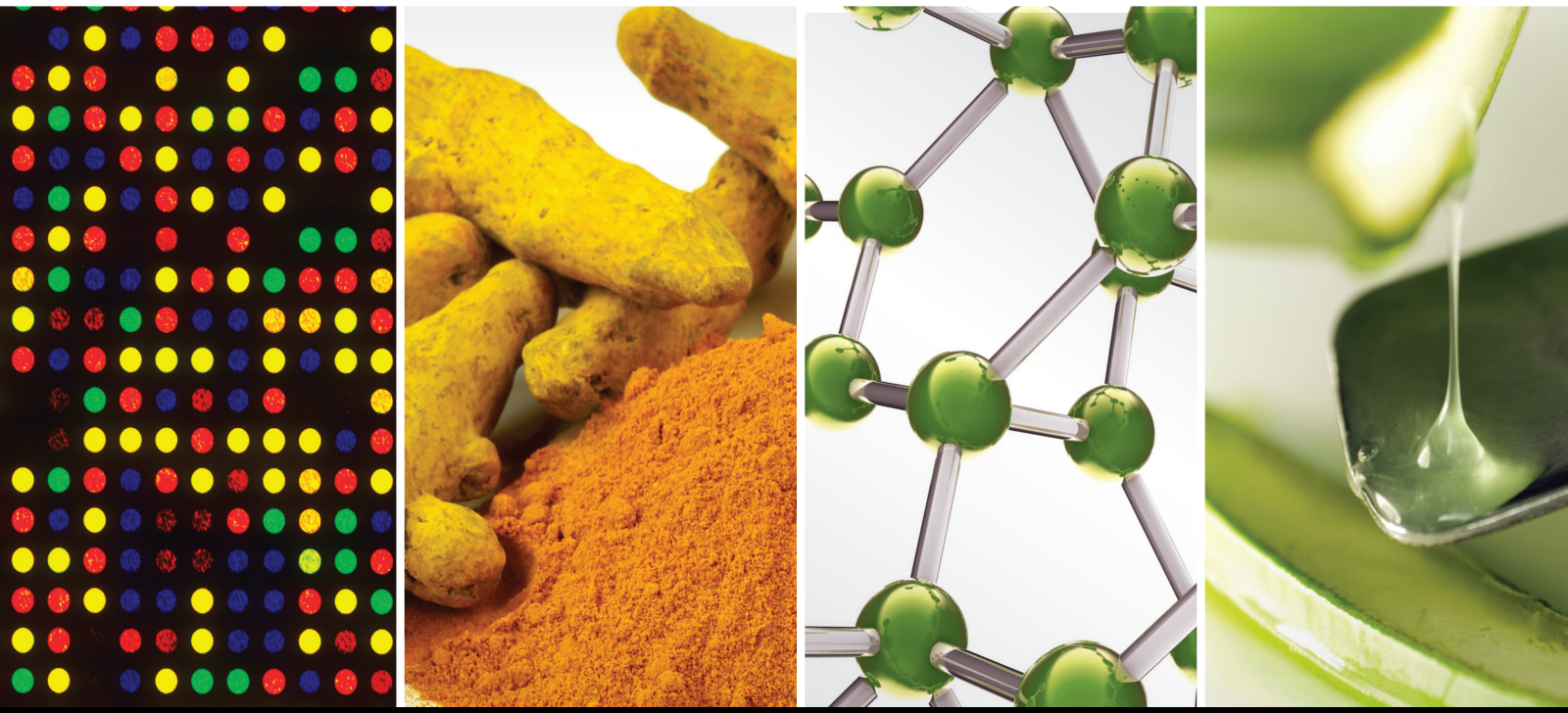

Traditional Chinese Medicine for Digestive System Tumors

Evidence-Based Complementary and Alternative Medicine

Traditional Chinese Medicine for Digestive System Tumors

Lead Guest Editor: Xueliang Wu
Guest Editors: Shangxiang Chen and Tianyi Liu

Chief Editor

Associate Editors

Academic Editors

Contents

Retracted: High-Throughput Sequencing Investigation of Bacterial Diversity in Chronic Suppurative Otitis Media and Middle Ear Cholesteatoma
Evidence-Based Complementary and Alternative Medicine
Retraction (1 page), Article ID 9753435, Volume 2023 (2023)

Retracted: Efficacy Evaluation of the VFQ-25 Scale in Patients with Different Degrees of Vitreous Opacity After Nd : YAG Laser Ablation
Evidence-Based Complementary and Alternative Medicine
Retraction (1 page), Article ID 9870497, Volume 2023 (2023)

Retracted: Delayed Surgery to Preserve Kidney with Grade IV Injury
Evidence-Based Complementary and Alternative Medicine
Retraction (1 page), Article ID 9835328, Volume 2023 (2023)

Retracted: Clinical Efficacy of Topical Tacrolimus on Conjunctival Hyperemia Caused by Prostaglandin Analogues
Evidence-Based Complementary and Alternative Medicine
Retraction (1 page), Article ID 9795630, Volume 2023 (2023)

Retracted: The Analysis of the Effect of Blood Transfusion on Changes of Blood Platelet Parameters in Patients with Leukemia Treated with Chemotherapy
Evidence-Based Complementary and Alternative Medicine
Retraction (1 page), Article ID 9787616, Volume 2023 (2023)

Retracted: LncRNA Gm43843 Promotes Cardiac Hypertrophy via miR-153-3p/Cacna1c Axis
Evidence-Based Complementary and Alternative Medicine
Retraction (1 page), Article ID 9841426, Volume 2023 (2023)

Retracted: A Three-Year Prospective Study Assessing the Application of Chromosomal Microarray Analysis in 576 High-Risk Pregnant Women
Evidence-Based Complementary and Alternative Medicine
Retraction (1 page), Article ID 9806751, Volume 2023 (2023)

Retracted: The Change of Aqueous Humor Cytokine Levels after Anti-VEGF in Diabetic Macular Edema: A Systematic Review and Meta-Analysis
Evidence-Based Complementary and Alternative Medicine
Retraction (1 page), Article ID 9797136, Volume 2023 (2023)

Retracted: *Vitis vinifera* L. Flavones Regulate Hippocampal Neurons via Autophagy in APP/PS1 Alzheimer Model Mice
Evidence-Based Complementary and Alternative Medicine
Retraction (1 page), Article ID 9795602, Volume 2023 (2023)

Retracted: Noncoding RNAs and Virus and Treatment in Allergic Rhinitis
Evidence-Based Complementary and Alternative Medicine
Retraction (1 page), Article ID 9898150, Volume 2023 (2023)

Contents

Contents

Contents

Contents

Hindawi
Evidence-Based Complementary and Alternative Medicine
Volume 2023, Article ID 9793852, 1 page
https://doi.org/10.1155/2023/9793852

Retraction

Retracted: Surfactant without Endotracheal Tube Intubation (SurE) versus Intubation-Surfactant-Extubation (InSurE) in Neonatal Respiratory Distress Syndrome: A Systematic Review and Meta-Analysis

Evidence-Based Complementary and Alternative Medicine

Received 10 October 2023; Accepted 10 October 2023; Published 11 October 2023

This article has been retracted by Hindawi following an investigation undertaken by the publisher [1]. This investigation has uncovered evidence of one or more of the following indicators of systematic manipulation of the publication process:

(1) Discrepancies in scope

(2) Discrepancies in the description of the research reported

(3) Discrepancies between the availability of data and the research described

(4) Inappropriate citations

(5) Incoherent, meaningless and/or irrelevant content included in the article

(6) Peer-review manipulation

The presence of these indicators undermines our confidence in the integrity of the article's content and we cannot, therefore, vouch for its reliability. Please note that this notice is intended solely to alert readers that the content of this article is unreliable. We have not investigated whether authors were aware of or involved in the systematic manipulation of the publication process.

Wiley and Hindawi regrets that the usual quality checks did not identify these issues before publication and have since put additional measures in place to safeguard research integrity.

We wish to credit our own Research Integrity and Research Publishing teams and anonymous and named external researchers and research integrity experts for contributing to this investigation.

The corresponding author, as the representative of all authors, has been given the opportunity to register their agreement or disagreement to this retraction. We have kept a record of any response received.

References

[1] L. Wang, M. Zhang, and Q. Yi, "Surfactant without Endotracheal Tube Intubation (SurE) versus Intubation-Surfactant-Extubation (InSurE) in Neonatal Respiratory Distress Syndrome: A Systematic Review and Meta-Analysis," *Evidence-Based Complementary and Alternative Medicine*, vol. 2022, Article ID 6225282, 16 pages, 2022.

Hindawi
Evidence-Based Complementary and Alternative Medicine
Volume 2023, Article ID 9870761, 1 page
https://doi.org/10.1155/2023/9870761

Retraction

Retracted: Cardiac External Counterpulsation Attenuates Myocardial Injury by Regulating NRF2-mediated Ferroptosisin and Oxidative stress Injury

Evidence-Based Complementary and Alternative Medicine

Received 3 October 2023; Accepted 3 October 2023; Published 4 October 2023

This article has been retracted by Hindawi following an investigation undertaken by the publisher [1]. This investigation has uncovered evidence of one or more of the following indicators of systematic manipulation of the publication process:

(1) Discrepancies in scope
(2) Discrepancies in the description of the research reported
(3) Discrepancies between the availability of data and the research described
(4) Inappropriate citations
(5) Incoherent, meaningless and/or irrelevant content included in the article
(6) Peer-review manipulation

The presence of these indicators undermines our confidence in the integrity of the article's content and we cannot, therefore, vouch for its reliability. Please note that this notice is intended solely to alert readers that the content of this article is unreliable. We have not investigated whether authors were aware of or involved in the systematic manipulation of the publication process.

Wiley and Hindawi regrets that the usual quality checks did not identify these issues before publication and have since put additional measures in place to safeguard research integrity.

We wish to credit our own Research Integrity and Research Publishing teams and anonymous and named external researchers and research integrity experts for contributing to this investigation.

The corresponding author, as the representative of all authors, has been given the opportunity to register their agreement or disagreement to this retraction. We have kept a record of any response received.

References

[1] S. Wang, B. Wang, G. Guo, and Y. Chen, "Cardiac External Counterpulsation Attenuates Myocardial Injury by Regulating NRF2-mediated Ferroptosisin and Oxidative stress Injury," *Evidence-Based Complementary and Alternative Medicine*, vol. 2022, Article ID 6477778, 7 pages, 2022.

Hindawi
Evidence-Based Complementary and Alternative Medicine
Volume 2023, Article ID 9853204, 1 page
https://doi.org/10.1155/2023/9853204

Retraction

Retracted: Synchronous Colorectal Liver Metastases considering Infectious Complications: Simultaneous or Delayed Surgery?

Evidence-Based Complementary and Alternative Medicine

Received 3 October 2023; Accepted 3 October 2023; Published 4 October 2023

This article has been retracted by Hindawi following an investigation undertaken by the publisher [1]. This investigation has uncovered evidence of one or more of the following indicators of systematic manipulation of the publication process:

(1) Discrepancies in scope
(2) Discrepancies in the description of the research reported
(3) Discrepancies between the availability of data and the research described
(4) Inappropriate citations
(5) Incoherent, meaningless and/or irrelevant content included in the article
(6) Peer-review manipulation

The presence of these indicators undermines our confidence in the integrity of the article's content and we cannot, therefore, vouch for its reliability. Please note that this notice is intended solely to alert readers that the content of this article is unreliable. We have not investigated whether authors were aware of or involved in the systematic manipulation of the publication process.

In addition, our investigation has also shown that one or more of the following human-subject reporting requirements has not been met in this article: ethical approval by an Institutional Review Board (IRB) committee or equivalent, patient/participant consent to participate, and/or agreement to publish patient/participant details (where relevant).

Wiley and Hindawi regrets that the usual quality checks did not identify these issues before publication and have since put additional measures in place to safeguard research integrity.

We wish to credit our own Research Integrity and Research Publishing teams and anonymous and named external researchers and research integrity experts for contributing to this investigation.

The corresponding author, as the representative of all authors, has been given the opportunity to register their agreement or disagreement to this retraction. We have kept a record of any response received.

References

[1] L. Huang, X. Tang, J. Fang, Z. Zheng, and H. Wei, "Synchronous Colorectal Liver Metastases considering Infectious Complications: Simultaneous or Delayed Surgery?" *Evidence-Based Complementary and Alternative Medicine*, vol. 2022, Article ID 5268554, 7 pages, 2022.

Hindawi
Evidence-Based Complementary and Alternative Medicine
Volume 2023, Article ID 9846920, 1 page
https://doi.org/10.1155/2023/9846920

Retraction

Retracted: Prognostic Value of Lactate Dehydrogenase, Melanoma Inhibitory Protein, and S-100B Protein in Patients with Malignant Melanoma

Evidence-Based Complementary and Alternative Medicine

Received 3 October 2023; Accepted 3 October 2023; Published 4 October 2023

This article has been retracted by Hindawi following an investigation undertaken by the publisher [1]. This investigation has uncovered evidence of one or more of the following indicators of systematic manipulation of the publication process:

(1) Discrepancies in scope
(2) Discrepancies in the description of the research reported
(3) Discrepancies between the availability of data and the research described
(4) Inappropriate citations
(5) Incoherent, meaningless and/or irrelevant content included in the article
(6) Peer-review manipulation

The presence of these indicators undermines our confidence in the integrity of the article's content and we cannot, therefore, vouch for its reliability. Please note that this notice is intended solely to alert readers that the content of this article is unreliable. We have not investigated whether authors were aware of or involved in the systematic manipulation of the publication process.

Wiley and Hindawi regrets that the usual quality checks did not identify these issues before publication and have since put additional measures in place to safeguard research integrity.

We wish to credit our own Research Integrity and Research Publishing teams and anonymous and named external researchers and research integrity experts for contributing to this investigation.

The corresponding author, as the representative of all authors, has been given the opportunity to register their agreement or disagreement to this retraction. We have kept a record of any response received.

References

[1] S. Fan, X. Liu, Y. Wu et al., "Prognostic Value of Lactate Dehydrogenase, Melanoma Inhibitory Protein, and S-100B Protein in Patients with Malignant Melanoma," *Evidence-Based Complementary and Alternative Medicine*, vol. 2022, Article ID 9086540, 7 pages, 2022.

Hindawi
Evidence-Based Complementary and Alternative Medicine
Volume 2023, Article ID 9840736, 1 page
https://doi.org/10.1155/2023/9840736

Retraction

Retracted: Analysis of the Clinical Efficacy of Azacytidine + Venetoclax in the Treatment of Elderly Patients with Relapsed Refractory Acute Myeloid Leukemia

Evidence-Based Complementary and Alternative Medicine

Received 3 October 2023; Accepted 3 October 2023; Published 4 October 2023

This article has been retracted by Hindawi following an investigation undertaken by the publisher [1]. This investigation has uncovered evidence of one or more of the following indicators of systematic manipulation of the publication process:

(1) Discrepancies in scope
(2) Discrepancies in the description of the research reported
(3) Discrepancies between the availability of data and the research described
(4) Inappropriate citations
(5) Incoherent, meaningless and/or irrelevant content included in the article
(6) Peer-review manipulation

The presence of these indicators undermines our confidence in the integrity of the article's content and we cannot, therefore, vouch for its reliability. Please note that this notice is intended solely to alert readers that the content of this article is unreliable. We have not investigated whether authors were aware of or involved in the systematic manipulation of the publication process.

Wiley and Hindawi regrets that the usual quality checks did not identify these issues before publication and have since put additional measures in place to safeguard research integrity.

We wish to credit our own Research Integrity and Research Publishing teams and anonymous and named external researchers and research integrity experts for contributing to this investigation.

The corresponding author, as the representative of all authors, has been given the opportunity to register their agreement or disagreement to this retraction. We have kept a record of any response received.

References

[1] W. Wang, Q. Luo, Q. Chen, A. Pang, and K. Fang, "Analysis of the Clinical Efficacy of Azacytidine + Venetoclax in the Treatment of Elderly Patients with Relapsed Refractory Acute Myeloid Leukemia," *Evidence-Based Complementary and Alternative Medicine*, vol. 2022, Article ID 8691835, 4 pages, 2022.

Hindawi
Evidence-Based Complementary and Alternative Medicine
Volume 2023, Article ID 9795740, 1 page
https://doi.org/10.1155/2023/9795740

Retraction

Retracted: Traditional Chinese Medicine Based Acupoint Application for Asthma Treatment in Children: A Meta-Analysis and Systematic Review

Evidence-Based Complementary and Alternative Medicine

Received 3 October 2023; Accepted 3 October 2023; Published 4 October 2023

This article has been retracted by Hindawi following an investigation undertaken by the publisher [1]. This investigation has uncovered evidence of one or more of the following indicators of systematic manipulation of the publication process:

(1) Discrepancies in scope

(2) Discrepancies in the description of the research reported

(3) Discrepancies between the availability of data and the research described

(4) Inappropriate citations

(5) Incoherent, meaningless and/or irrelevant content included in the article

(6) Peer-review manipulation

The presence of these indicators undermines our confidence in the integrity of the article's content and we cannot, therefore, vouch for its reliability. Please note that this notice is intended solely to alert readers that the content of this article is unreliable. We have not investigated whether authors were aware of or involved in the systematic manipulation of the publication process.

Wiley and Hindawi regrets that the usual quality checks did not identify these issues before publication and have since put additional measures in place to safeguard research integrity.

We wish to credit our own Research Integrity and Research Publishing teams and anonymous and named external researchers and research integrity experts for contributing to this investigation.

The corresponding author, as the representative of all authors, has been given the opportunity to register their agreement or disagreement to this retraction. We have kept a record of any response received.

References

[1] Y. Wang, T. Guo, F. Yang et al., "Traditional Chinese Medicine Based Acupoint Application for Asthma Treatment in Children: A Meta-Analysis and Systematic Review," *Evidence-Based Complementary and Alternative Medicine*, vol. 2022, Article ID 7500056, 15 pages, 2022.

Hindawi
Evidence-Based Complementary and Alternative Medicine
Volume 2023, Article ID 9786270, 1 page
https://doi.org/10.1155/2023/9786270

Retraction

Retracted: Analysis of Influencing Factors for Exercise Ventilation Efficiency of COPD Patients

Evidence-Based Complementary and Alternative Medicine

Received 3 October 2023; Accepted 3 October 2023; Published 4 October 2023

This article has been retracted by Hindawi following an investigation undertaken by the publisher [1]. This investigation has uncovered evidence of one or more of the following indicators of systematic manipulation of the publication process:

(1) Discrepancies in scope

(2) Discrepancies in the description of the research reported

(3) Discrepancies between the availability of data and the research described

(4) Inappropriate citations

(5) Incoherent, meaningless and/or irrelevant content included in the article

(6) Peer-review manipulation

The presence of these indicators undermines our confidence in the integrity of the article's content and we cannot, therefore, vouch for its reliability. Please note that this notice is intended solely to alert readers that the content of this article is unreliable. We have not investigated whether authors were aware of or involved in the systematic manipulation of the publication process.

Wiley and Hindawi regrets that the usual quality checks did not identify these issues before publication and have since put additional measures in place to safeguard research integrity.

We wish to credit our own Research Integrity and Research Publishing teams and anonymous and named external researchers and research integrity experts for contributing to this investigation.

The corresponding author, as the representative of all authors, has been given the opportunity to register their agreement or disagreement to this retraction. We have kept a record of any response received.

References

[1] Y.-m. Ge, S. Nie, N. Jia, Q.-F. Xu, B. Xu, and H.-Y. Wang, "Analysis of Influencing Factors for Exercise Ventilation Efficiency of COPD Patients," *Evidence-Based Complementary and Alternative Medicine*, vol. 2022, Article ID 8376085, 7 pages, 2022.

Hindawi
Evidence-Based Complementary and Alternative Medicine
Volume 2023, Article ID 9782478, 1 page
https://doi.org/10.1155/2023/9782478

Retraction

Retracted: Evaluation of lncRNA FOXD3-AS1 as a Biomarker for Early-Stage Lung Cancer Diagnosis and Subtype Identification

Evidence-Based Complementary and Alternative Medicine

Received 3 October 2023; Accepted 3 October 2023; Published 4 October 2023

This article has been retracted by Hindawi following an investigation undertaken by the publisher [1]. This investigation has uncovered evidence of one or more of the following indicators of systematic manipulation of the publication process:

(1) Discrepancies in scope
(2) Discrepancies in the description of the research reported
(3) Discrepancies between the availability of data and the research described
(4) Inappropriate citations
(5) Incoherent, meaningless and/or irrelevant content included in the article
(6) Peer-review manipulation

The presence of these indicators undermines our confidence in the integrity of the article's content and we cannot, therefore, vouch for its reliability. Please note that this notice is intended solely to alert readers that the content of this article is unreliable. We have not investigated whether authors were aware of or involved in the systematic manipulation of the publication process.

Wiley and Hindawi regrets that the usual quality checks did not identify these issues before publication and have since put additional measures in place to safeguard research integrity.

We wish to credit our own Research Integrity and Research Publishing teams and anonymous and named external researchers and research integrity experts for contributing to this investigation.

The corresponding author, as the representative of all authors, has been given the opportunity to register their agreement or disagreement to this retraction. We have kept a record of any response received.

References

[1] X. Liu, W. Chen, Y. Qi, and Y. Zhu, "Evaluation of lncRNA FOXD3-AS1 as a Biomarker for Early-Stage Lung Cancer Diagnosis and Subtype Identification," *Evidence-Based Complementary and Alternative Medicine*, vol. 2022, Article ID 5702014, 11 pages, 2022.

Hindawi
Evidence-Based Complementary and Alternative Medicine
Volume 2023, Article ID 9765415, 1 page
https://doi.org/10.1155/2023/9765415

Retraction

Retracted: Efficacy of Periodontal Endodontics Combined with Diode Laser (DL) Therapy on Severe Periodontitis

Evidence-Based Complementary and Alternative Medicine

Received 3 October 2023; Accepted 3 October 2023; Published 4 October 2023

This article has been retracted by Hindawi following an investigation undertaken by the publisher [1]. This investigation has uncovered evidence of one or more of the following indicators of systematic manipulation of the publication process:

(1) Discrepancies in scope
(2) Discrepancies in the description of the research reported
(3) Discrepancies between the availability of data and the research described
(4) Inappropriate citations
(5) Incoherent, meaningless and/or irrelevant content included in the article
(6) Peer-review manipulation

The presence of these indicators undermines our confidence in the integrity of the article's content and we cannot, therefore, vouch for its reliability. Please note that this notice is intended solely to alert readers that the content of this article is unreliable. We have not investigated whether authors were aware of or involved in the systematic manipulation of the publication process.

In addition, our investigation has also shown that one or more of the following human-subject reporting requirements has not been met in this article: ethical approval by an Institutional Review Board (IRB) committee or equivalent, patient/participant consent to participate, and/or agreement to publish patient/participant details (where relevant).

Wiley and Hindawi regrets that the usual quality checks did not identify these issues before publication and have since put additional measures in place to safeguard research integrity.

We wish to credit our own Research Integrity and Research Publishing teams and anonymous and named external researchers and research integrity experts for contributing to this investigation.

The corresponding author, as the representative of all authors, has been given the opportunity to register their agreement or disagreement to this retraction. We have kept a record of any response received.

References

[1] S. Liu, X. Zhang, and Q. Zhou, "Efficacy of Periodontal Endodontics Combined with Diode Laser (DL) Therapy on Severe Periodontitis," *Evidence-Based Complementary and Alternative Medicine*, vol. 2022, Article ID 5689900, 7 pages, 2022.

Hindawi
Evidence-Based Complementary and Alternative Medicine
Volume 2023, Article ID 9753435, 1 page
https://doi.org/10.1155/2023/9753435

Retraction

Retracted: High-Throughput Sequencing Investigation of Bacterial Diversity in Chronic Suppurative Otitis Media and Middle Ear Cholesteatoma

Evidence-Based Complementary and Alternative Medicine

Received 3 October 2023; Accepted 3 October 2023; Published 4 October 2023

This article has been retracted by Hindawi following an investigation undertaken by the publisher [1]. This investigation has uncovered evidence of one or more of the following indicators of systematic manipulation of the publication process:

(1) Discrepancies in scope

(2) Discrepancies in the description of the research reported

(3) Discrepancies between the availability of data and the research described

(4) Inappropriate citations

(5) Incoherent, meaningless and/or irrelevant content included in the article

(6) Peer-review manipulation

The presence of these indicators undermines our confidence in the integrity of the article's content and we cannot, therefore, vouch for its reliability. Please note that this notice is intended solely to alert readers that the content of this article is unreliable. We have not investigated whether authors were aware of or involved in the systematic manipulation of the publication process.

Wiley and Hindawi regrets that the usual quality checks did not identify these issues before publication and have since put additional measures in place to safeguard research integrity.

We wish to credit our own Research Integrity and Research Publishing teams and anonymous and named external researchers and research integrity experts for contributing to this investigation.

The corresponding author, as the representative of all authors, has been given the opportunity to register their agreement or disagreement to this retraction. We have kept a record of any response received.

References

[1] X. Cheng, A. Tuoheti, X. Huang, and X. Gu, "High-Throughput Sequencing Investigation of Bacterial Diversity in Chronic Suppurative Otitis Media and Middle Ear Cholesteatoma," *Evidence-Based Complementary and Alternative Medicine*, vol. 2022, Article ID 9616582, 9 pages, 2022.

Hindawi
Evidence-Based Complementary and Alternative Medicine
Volume 2023, Article ID 9870497, 1 page
https://doi.org/10.1155/2023/9870497

Retraction

Retracted: Efficacy Evaluation of the VFQ-25 Scale in Patients with Different Degrees of Vitreous Opacity After Nd : YAG Laser Ablation

Evidence-Based Complementary and Alternative Medicine

Received 15 August 2023; Accepted 15 August 2023; Published 16 August 2023

This article has been retracted by Hindawi following an investigation undertaken by the publisher [1]. This investigation has uncovered evidence of one or more of the following indicators of systematic manipulation of the publication process:

(1) Discrepancies in scope
(2) Discrepancies in the description of the research reported
(3) Discrepancies between the availability of data and the research described
(4) Inappropriate citations
(5) Incoherent, meaningless and/or irrelevant content included in the article
(6) Peer-review manipulation

The presence of these indicators undermines our confidence in the integrity of the article's content and we cannot, therefore, vouch for its reliability. Please note that this notice is intended solely to alert readers that the content of this article is unreliable. We have not investigated whether authors were aware of or involved in the systematic manipulation of the publication process.

Wiley and Hindawi regrets that the usual quality checks did not identify these issues before publication and have since put additional measures in place to safeguard research integrity.

We wish to credit our own Research Integrity and Research Publishing teams and anonymous and named external researchers and research integrity experts for contributing to this investigation.

The corresponding author, as the representative of all authors, has been given the opportunity to register their agreement or disagreement to this retraction. We have kept a record of any response received.

References

[1] S. Zhang, K. Yang, and B. Wang, "Efficacy Evaluation of the VFQ-25 Scale in Patients with Different Degrees of Vitreous Opacity After Nd : YAG Laser Ablation," *Evidence-Based Complementary and Alternative Medicine*, vol. 2022, Article ID 5075447, 5 pages, 2022.

Hindawi
Evidence-Based Complementary and Alternative Medicine
Volume 2023, Article ID 9835328, 1 page
https://doi.org/10.1155/2023/9835328

Retraction

Retracted: Delayed Surgery to Preserve Kidney with Grade IV Injury

Evidence-Based Complementary and Alternative Medicine

Received 15 August 2023; Accepted 15 August 2023; Published 16 August 2023

This article has been retracted by Hindawi following an investigation undertaken by the publisher [1]. This investigation has uncovered evidence of one or more of the following indicators of systematic manipulation of the publication process:

(1) Discrepancies in scope
(2) Discrepancies in the description of the research reported
(3) Discrepancies between the availability of data and the research described
(4) Inappropriate citations
(5) Incoherent, meaningless and/or irrelevant content included in the article
(6) Peer-review manipulation

The presence of these indicators undermines our confidence in the integrity of the article's content and we cannot, therefore, vouch for its reliability. Please note that this notice is intended solely to alert readers that the content of this article is unreliable. We have not investigated whether authors were aware of or involved in the systematic manipulation of the publication process.

In addition, our investigation has also shown that one or more of the following human-subject reporting requirements has not been met in this article: ethical approval by an Institutional Review Board (IRB) committee or equivalent, patient/participant consent to participate, and/or agreement to publish patient/participant details (where relevant).

Wiley and Hindawi regrets that the usual quality checks did not identify these issues before publication and have since put additional measures in place to safeguard research integrity.

We wish to credit our own Research Integrity and Research Publishing teams and anonymous and named external researchers and research integrity experts for contributing to this investigation.

The corresponding author, as the representative of all authors, has been given the opportunity to register their agreement or disagreement to this retraction. We have kept a record of any response received.

References

[1] Y. Li, L. Xiao, W. Xu, L. Zhao, and M. Xiao, "Delayed Surgery to Preserve Kidney with Grade IV Injury," *Evidence-Based Complementary and Alternative Medicine*, vol. 2022, Article ID 5066278, 5 pages, 2022.

Hindawi
Evidence-Based Complementary and Alternative Medicine
Volume 2023, Article ID 9795630, 1 page
https://doi.org/10.1155/2023/9795630

Retraction

Retracted: Clinical Efficacy of Topical Tacrolimus on Conjunctival Hyperemia Caused by Prostaglandin Analogues

Evidence-Based Complementary and Alternative Medicine

Received 15 August 2023; Accepted 15 August 2023; Published 16 August 2023

This article has been retracted by Hindawi following an investigation undertaken by the publisher [1]. This investigation has uncovered evidence of one or more of the following indicators of systematic manipulation of the publication process:

(1) Discrepancies in scope

(2) Discrepancies in the description of the research reported

(3) Discrepancies between the availability of data and the research described

(4) Inappropriate citations

(5) Incoherent, meaningless and/or irrelevant content included in the article

(6) Peer-review manipulation

The presence of these indicators undermines our confidence in the integrity of the article's content and we cannot, therefore, vouch for its reliability. Please note that this notice is intended solely to alert readers that the content of this article is unreliable. We have not investigated whether authors were aware of or involved in the systematic manipulation of the publication process.

Wiley and Hindawi regrets that the usual quality checks did not identify these issues before publication and have since put additional measures in place to safeguard research integrity.

We wish to credit our own Research Integrity and Research Publishing teams and anonymous and named external researchers and research integrity experts for contributing to this investigation.

The corresponding author, as the representative of all authors, has been given the opportunity to register their agreement or disagreement to this retraction. We have kept a record of any response received.

References

[1] J. Yang, Y. Shi, and H. Chen, "Clinical Efficacy of Topical Tacrolimus on Conjunctival Hyperemia Caused by Prostaglandin Analogues," *Evidence-Based Complementary and Alternative Medicine*, vol. 2022, Article ID 3700720, 6 pages, 2022.

Hindawi
Evidence-Based Complementary and Alternative Medicine
Volume 2023, Article ID 9787616, 1 page
https://doi.org/10.1155/2023/9787616

Retraction

Retracted: The Analysis of the Effect of Blood Transfusion on Changes of Blood Platelet Parameters in Patients with Leukemia Treated with Chemotherapy

Evidence-Based Complementary and Alternative Medicine

Received 15 August 2023; Accepted 15 August 2023; Published 16 August 2023

This article has been retracted by Hindawi following an investigation undertaken by the publisher [1]. This investigation has uncovered evidence of one or more of the following indicators of systematic manipulation of the publication process:

(1) Discrepancies in scope
(2) Discrepancies in the description of the research reported
(3) Discrepancies between the availability of data and the research described
(4) Inappropriate citations
(5) Incoherent, meaningless and/or irrelevant content included in the article
(6) Peer-review manipulation

The presence of these indicators undermines our confidence in the integrity of the article's content and we cannot, therefore, vouch for its reliability. Please note that this notice is intended solely to alert readers that the content of this article is unreliable. We have not investigated whether authors were aware of or involved in the systematic manipulation of the publication process.

Wiley and Hindawi regrets that the usual quality checks did not identify these issues before publication and have since put additional measures in place to safeguard research integrity.

We wish to credit our own Research Integrity and Research Publishing teams and anonymous and named external researchers and research integrity experts for contributing to this investigation.

The corresponding author, as the representative of all authors, has been given the opportunity to register their agreement or disagreement to this retraction. We have kept a record of any response received.

References

[1] Y. He, S. Liang, Y. Xu, C. Wan, F. Ma, and B. Wang, "The Analysis of the Effect of Blood Transfusion on Changes of Blood Platelet Parameters in Patients with Leukemia Treated with Chemotherapy," *Evidence-Based Complementary and Alternative Medicine*, vol. 2022, Article ID 2901993, 4 pages, 2022.

Hindawi
Evidence-Based Complementary and Alternative Medicine
Volume 2023, Article ID 9841426, 1 page
https://doi.org/10.1155/2023/9841426

Retraction

Retracted: LncRNA Gm43843 Promotes Cardiac Hypertrophy via miR-153-3p/Cacna1c Axis

Evidence-Based Complementary and Alternative Medicine

Received 8 August 2023; Accepted 8 August 2023; Published 9 August 2023

This article has been retracted by Hindawi following an investigation undertaken by the publisher [1]. This investigation has uncovered evidence of one or more of the following indicators of systematic manipulation of the publication process:

(1) Discrepancies in scope
(2) Discrepancies in the description of the research reported
(3) Discrepancies between the availability of data and the research described
(4) Inappropriate citations
(5) Incoherent, meaningless and/or irrelevant content included in the article
(6) Peer-review manipulation

The presence of these indicators undermines our confidence in the integrity of the article's content and we cannot, therefore, vouch for its reliability. Please note that this notice is intended solely to alert readers that the content of this article is unreliable. We have not investigated whether authors were aware of or involved in the systematic manipulation of the publication process.

Wiley and Hindawi regrets that the usual quality checks did not identify these issues before publication and have since put additional measures in place to safeguard research integrity.

We wish to credit our own Research Integrity and Research Publishing teams and anonymous and named external researchers and research integrity experts for contributing to this investigation.

The corresponding author, as the representative of all authors, has been given the opportunity to register their agreement or disagreement to this retraction. We have kept a record of any response received.

References

[1] Y. Cai and Y. Li, "LncRNA Gm43843 Promotes Cardiac Hypertrophy via miR-153-3p/Cacna1c Axis," *Evidence- Based Complementary and Alternative Medicine*, vol. 2022, Article ID 2160804, 13 pages, 2022.

Hindawi
Evidence-Based Complementary and Alternative Medicine
Volume 2023, Article ID 9806751, 1 page
https://doi.org/10.1155/2023/9806751

Retraction

Retracted: A Three-Year Prospective Study Assessing the Application of Chromosomal Microarray Analysis in 576 High-Risk Pregnant Women

Evidence-Based Complementary and Alternative Medicine

Received 8 August 2023; Accepted 8 August 2023; Published 9 August 2023

This article has been retracted by Hindawi following an investigation undertaken by the publisher [1]. This investigation has uncovered evidence of one or more of the following indicators of systematic manipulation of the publication process:

(1) Discrepancies in scope
(2) Discrepancies in the description of the research reported
(3) Discrepancies between the availability of data and the research described
(4) Inappropriate citations
(5) Incoherent, meaningless and/or irrelevant content included in the article
(6) Peer-review manipulation

The presence of these indicators undermines our confidence in the integrity of the article's content and we cannot, therefore, vouch for its reliability. Please note that this notice is intended solely to alert readers that the content of this article is unreliable. We have not investigated whether authors were aware of or involved in the systematic manipulation of the publication process.

Wiley and Hindawi regrets that the usual quality checks did not identify these issues before publication and have since put additional measures in place to safeguard research integrity.

We wish to credit our own Research Integrity and Research Publishing teams and anonymous and named external researchers and research integrity experts for contributing to this investigation.

The corresponding author, as the representative of all authors, has been given the opportunity to register their agreement or disagreement to this retraction. We have kept a record of any response received.

References

[1] M. Jiang, S. Huang, X. Ma et al., "A Three-Year Prospective Study Assessing the Application of Chromosomal Microarray Analysis in 576 High-Risk Pregnant Women," *Evidence-Based Complementary and Alternative Medicine*, vol. 2022, Article ID 1533346, 5 pages, 2022.

Hindawi
Evidence-Based Complementary and Alternative Medicine
Volume 2023, Article ID 9797136, 1 page
https://doi.org/10.1155/2023/9797136

Retraction

Retracted: The Change of Aqueous Humor Cytokine Levels after Anti-VEGF in Diabetic Macular Edema: A Systematic Review and Meta-Analysis

Evidence-Based Complementary and Alternative Medicine

Received 8 August 2023; Accepted 8 August 2023; Published 9 August 2023

This article has been retracted by Hindawi following an investigation undertaken by the publisher [1]. This investigation has uncovered evidence of one or more of the following indicators of systematic manipulation of the publication process:

(1) Discrepancies in scope

(2) Discrepancies in the description of the research reported

(3) Discrepancies between the availability of data and the research described

(4) Inappropriate citations

(5) Incoherent, meaningless and/or irrelevant content included in the article

(6) Peer-review manipulation

The presence of these indicators undermines our confidence in the integrity of the article's content and we cannot, therefore, vouch for its reliability. Please note that this notice is intended solely to alert readers that the content of this article is unreliable. We have not investigated whether authors were aware of or involved in the systematic manipulation of the publication process.

Wiley and Hindawi regrets that the usual quality checks did not identify these issues before publication and have since put additional measures in place to safeguard research integrity.

We wish to credit our own Research Integrity and Research Publishing teams and anonymous and named external researchers and research integrity experts for contributing to this investigation.

The corresponding author, as the representative of all authors, has been given the opportunity to register their agreement or disagreement to this retraction. We have kept a record of any response received.

References

[1] A. Wang and H. Wang, "The Change of Aqueous Humor Cytokine Levels after Anti-VEGF in Diabetic Macular Edema: A Systematic Review and Meta-Analysis," *Evidence-Based Complementary and Alternative Medicine*, vol. 2022, Article ID 9779951, 10 pages, 2022.

Hindawi
Evidence-Based Complementary and Alternative Medicine
Volume 2023, Article ID 9795602, 1 page
https://doi.org/10.1155/2023/9795602

Retraction

Retracted: *Vitis vinifera* L. Flavones Regulate Hippocampal Neurons via Autophagy in APP/PS1 Alzheimer Model Mice

Evidence-Based Complementary and Alternative Medicine

Received 8 August 2023; Accepted 8 August 2023; Published 9 August 2023

This article has been retracted by Hindawi following an investigation undertaken by the publisher [1]. This investigation has uncovered evidence of one or more of the following indicators of systematic manipulation of the publication process:

(1) Discrepancies in scope
(2) Discrepancies in the description of the research reported
(3) Discrepancies between the availability of data and the research described
(4) Inappropriate citations
(5) Incoherent, meaningless and/or irrelevant content included in the article
(6) Peer-review manipulation

The presence of these indicators undermines our confidence in the integrity of the article's content and we cannot, therefore, vouch for its reliability. Please note that this notice is intended solely to alert readers that the content of this article is unreliable. We have not investigated whether authors were aware of or involved in the systematic manipulation of the publication process.

Wiley and Hindawi regrets that the usual quality checks did not identify these issues before publication and have since put additional measures in place to safeguard research integrity.

We wish to credit our own Research Integrity and Research Publishing teams and anonymous and named external researchers and research integrity experts for contributing to this investigation.

The corresponding author, as the representative of all authors, has been given the opportunity to register their agreement or disagreement to this retraction. We have kept a record of any response received.

References

[1] P. Zhang, Z. Maimaiti, G. Aili, F. Yuan, and H. Xiao, "*Vitis vinifera* L. Flavones Regulate Hippocampal Neurons via Autophagy in APP/PS1 Alzheimer Model Mice," *Evidence-Based Complementary and Alternative Medicine*, vol. 2022, Article ID 8554184, 7 pages, 2022.

Hindawi
Evidence-Based Complementary and Alternative Medicine
Volume 2023, Article ID 9898150, 1 page
https://doi.org/10.1155/2023/9898150

Retraction

Retracted: Noncoding RNAs and Virus and Treatment in Allergic Rhinitis

Evidence-Based Complementary and Alternative Medicine

Received 8 August 2023; Accepted 8 August 2023; Published 9 August 2023

This article has been retracted by Hindawi following an investigation undertaken by the publisher [1]. This investigation has uncovered evidence of one or more of the following indicators of systematic manipulation of the publication process:

(1) Discrepancies in scope

(2) Discrepancies in the description of the research reported

(3) Discrepancies between the availability of data and the research described

(4) Inappropriate citations

(5) Incoherent, meaningless and/or irrelevant content included in the article

(6) Peer-review manipulation

The presence of these indicators undermines our confidence in the integrity of the article's content and we cannot, therefore, vouch for its reliability. Please note that this notice is intended solely to alert readers that the content of this article is unreliable. We have not investigated whether authors were aware of or involved in the systematic manipulation of the publication process.

Wiley and Hindawi regrets that the usual quality checks did not identify these issues before publication and have since put additional measures in place to safeguard research integrity.

We wish to credit our own Research Integrity and Research Publishing teams and anonymous and named external researchers and research integrity experts for contributing to this investigation.

The corresponding author, as the representative of all authors, has been given the opportunity to register their agreement or disagreement to this retraction. We have kept a record of any response received.

References

[1] Z. Lei, G. Feng, Z. Wang, and Z. Ning, "Noncoding RNAs and Virus and Treatment in Allergic Rhinitis," *Evidence-Based Complementary and Alternative Medicine*, vol. 2022, Article ID 1979447, 8 pages, 2022.

Hindawi
Evidence-Based Complementary and Alternative Medicine
Volume 2023, Article ID 9865432, 1 page
https://doi.org/10.1155/2023/9865432

Retraction

Retracted: Valproic Acid Inhibits Peripheral T Cell Lymphoma Cells Behaviors via Restraining PI3K/AKT Pathway

Evidence-Based Complementary and Alternative Medicine

Received 8 August 2023; Accepted 8 August 2023; Published 9 August 2023

This article has been retracted by Hindawi following an investigation undertaken by the publisher [1]. This investigation has uncovered evidence of one or more of the following indicators of systematic manipulation of the publication process:

(1) Discrepancies in scope

(2) Discrepancies in the description of the research reported

(3) Discrepancies between the availability of data and the research described

(4) Inappropriate citations

(5) Incoherent, meaningless and/or irrelevant content included in the article

(6) Peer-review manipulation

The presence of these indicators undermines our confidence in the integrity of the article's content and we cannot, therefore, vouch for its reliability. Please note that this notice is intended solely to alert readers that the content of this article is unreliable. We have not investigated whether authors were aware of or involved in the systematic manipulation of the publication process.

Wiley and Hindawi regrets that the usual quality checks did not identify these issues before publication and have since put additional measures in place to safeguard research integrity.

We wish to credit our own Research Integrity and Research Publishing teams and anonymous and named external researchers and research integrity experts for contributing to this investigation.

The corresponding author, as the representative of all authors, has been given the opportunity to register their agreement or disagreement to this retraction. We have kept a record of any response received.

References

[1] Z. Peng, J. Xiong, and H. Dong, "Valproic Acid Inhibits Peripheral T Cell Lymphoma Cells Behaviors via Restraining PI3K/AKT Pathway," *Evidence-Based Complementary and Alternative Medicine*, vol. 2022, Article ID 7350489, 9 pages, 2022.

Hindawi
Evidence-Based Complementary and Alternative Medicine
Volume 2023, Article ID 9864167, 1 page
https://doi.org/10.1155/2023/9864167

Retraction

Retracted: HDAC2 Induces DNA Methyltransferase DNMT3B Expression to Regulate the Wnt Signaling Pathway and Thus Promotes Glioma Development and Progression

Evidence-Based Complementary and Alternative Medicine

Received 8 August 2023; Accepted 8 August 2023; Published 9 August 2023

This article has been retracted by Hindawi following an investigation undertaken by the publisher [1]. This investigation has uncovered evidence of one or more of the following indicators of systematic manipulation of the publication process:

(1) Discrepancies in scope
(2) Discrepancies in the description of the research reported
(3) Discrepancies between the availability of data and the research described
(4) Inappropriate citations
(5) Incoherent, meaningless and/or irrelevant content included in the article
(6) Peer-review manipulation

The presence of these indicators undermines our confidence in the integrity of the article's content and we cannot, therefore, vouch for its reliability. Please note that this notice is intended solely to alert readers that the content of this article is unreliable. We have not investigated whether authors were aware of or involved in the systematic manipulation of the publication process.

Wiley and Hindawi regrets that the usual quality checks did not identify these issues before publication and have since put additional measures in place to safeguard research integrity.

We wish to credit our own Research Integrity and Research Publishing teams and anonymous and named external researchers and research integrity experts for contributing to this investigation.

The corresponding author, as the representative of all authors, has been given the opportunity to register their agreement or disagreement to this retraction. We have kept a record of any response received.

References

[1] X. Ren, Z. Jiang, and K. Xu, "HDAC2 Induces DNA Methyltransferase DNMT3B Expression to Regulate the Wnt Signaling Pathway and Thus Promotes Glioma Development and Progression," *Evidence-Based Complementary and Alternative Medicine*, vol. 2022, Article ID 1948766, 8 pages, 2022.

Hindawi
Evidence-Based Complementary and Alternative Medicine
Volume 2023, Article ID 9762457, 1 page
https://doi.org/10.1155/2023/9762457

Retraction

Retracted: Heparin-Binding Protein Aggravates Acute Lung Injury in Septic Rats by Promoting Macrophage M1 Polarization and NF-κB Signaling Pathway Activation

Evidence-Based Complementary and Alternative Medicine

Received 1 August 2023; Accepted 1 August 2023; Published 2 August 2023

This article has been retracted by Hindawi following an investigation undertaken by the publisher [1]. This investigation has uncovered evidence of one or more of the following indicators of systematic manipulation of the publication process:

(1) Discrepancies in scope
(2) Discrepancies in the description of the research reported
(3) Discrepancies between the availability of data and the research described
(4) Inappropriate citations
(5) Incoherent, meaningless and/or irrelevant content included in the article
(6) Peer-review manipulation

The presence of these indicators undermines our confidence in the integrity of the article's content and we cannot, therefore, vouch for its reliability. Please note that this notice is intended solely to alert readers that the content of this article is unreliable. We have not investigated whether authors were aware of or involved in the systematic manipulation of the publication process.

Wiley and Hindawi regrets that the usual quality checks did not identify these issues before publication and have since put additional measures in place to safeguard research integrity.

We wish to credit our own Research Integrity and Research Publishing teams and anonymous and named external researchers and research integrity experts for contributing to this investigation.

The corresponding author, as the representative of all authors, has been given the opportunity to register their agreement or disagreement to this retraction. We have kept a record of any response received.

References

[1] Y. Zhang, W. Sun, and L. Zhang, "Heparin-Binding Protein Aggravates Acute Lung Injury in Septic Rats by Promoting Macrophage M1 Polarization and NF-κB Signaling Pathway Activation," *Evidence-Based Complementary and Alternative Medicine*, vol. 2022, Article ID 3315601, 7 pages, 2022.

Hindawi
Evidence-Based Complementary and Alternative Medicine
Volume 2023, Article ID 4946642, 7 pages
https://doi.org/10.1155/2023/4946642

Review Article

Meta-Analysis of Capecitabine versus 5-Fluorouracil in Advanced Gastric Cancer

Zhongliang Wu, Xingfa Zhang, Chongxiang Zhang, and Yi Lin

Department of Gastrointestinal Surgery, The Third Affiliated Hospital of Guizhou Medical University, Duyun, Guizhou Province, China

Correspondence should be addressed to Yi Lin; liyi712114@163.com

Received 12 August 2022; Revised 17 September 2022; Accepted 10 October 2022; Published 27 June 2023

Academic Editor: Xueliang Wu

Objective. To investigate the effect of capecitabine versus 5-fluorouracil in advanced gastric cancer patients. *Methods*. We searched PubMed, Cochrane Library, Embase, and other databases from database establishment to June 2022, containing randomized controlled trials (RCT) on capecitabine and 5-fluorouracil in advanced gastric cancer patients. A meta-analysis was conducted to evaluate the effect of capecitabine versus 5-fluorouracil on overall response rate, neutropenia, thrombocytopenia, stomatitis, hand-foot syndrome, nausea and vomiting, alopecia, and diarrhea. *Results*. Eight RCTs with a total of 1998 patients with advanced gastric cancer were finally included, including 982 with capecitabine and 1016 with 5-fluorouracil. Compared with 5-fluorouracil, capecitabine use was significantly associated with an improved overall response rate in patients (RR 1.13, 95% CI 1.02–1.25, $P = 0.02$). Compared with 5-fluorouracil, treatment with capecitabine was significantly associated with decreased neutropenia events (RR 0.78, 95% CI 0.62–0.99, $I^2 = 86\%$, $P = 0.04$), and a decreased risk of stomatitis (RR 0.73, 95% CI 0.64–0.84, $I^2 = 40\%$, $P < 0.0001$) in patients with advanced gastric cancer. In terms of hand-foot syndrome, capecitabine was associated with increased hand-foot syndrome events than 5-fluorouracil (RR 2.00, 95% CI 1.21–3.31, $P = 0.007$). In terms of thrombocytopenia, nausea and vomiting, alopecia, and diarrhea, the effect of capecitabine and 5-fluorouracil were similar ($P > 0.05$). *Conclusions*. Compared with 5-fluorouracil, capecitabine treatment improves the overall response rate and reduces the risk of neutropenia and stomatitis in advanced gastric cancer patients. It should be noted that capecitabine treatment may also increase the occurrence of hand-foot syndrome. Capecitabine is similar to 5-fluorouracil in causing thrombocytopenia, nausea and vomiting, alopecia, and diarrhea.

1. Introduction

Gastric cancer is derived from the mucosal epithelium, the vast majority of which are gastric adenocarcinomas, and more than half appear in the antrum [1]. Gastric cancer in the early stage has no obvious symptoms, or some nonspecific symptoms, such as epigastric discomfort and belching, therefore most individuals are found with advanced gastric cancer. Reference [2]. Epidemiological studies show that 0.99 million people worldwide have gastric cancer and 0.74 million people die of this disease annually [3]. There is a clear difference in incidence between males and females, with males being two to three times more prevalent than females [4]. Gastric cancer is a disease caused by both environmental and genetic factors, which is associated with genes, ethnicity, family history, geographical environment, smoking, dietary and life factors, and *Helicobacter pylori* infection [5]. At present, the treatment methods for gastric cancer include surgical treatment, chemotherapy, radiotherapy, molecular targeted therapy, and immunotherapy. The preferred way for gastric cancer is surgical treatment. However, advanced gastric cancer patients often do not have the chance of surgery [6]. Therefore, it is particularly important to select the treatment regimen for them. In recent years, molecular targeted therapy and immunotherapy have emerged endlessly, but traditional chemotherapy still plays a major role [7]. 5-Fluorouracil is the most commonly used uracil antimetabolite and is widely used to treat malignant tumors by converting to a 5-fluorodeoxyuracil nucleotide in vivo to achieve inhibition of DNA synthesis.

Capecitabine, a thymidine phosphorylase active fluoropyrimidine carbamate, is a prodrug of 5-fluorouracil. Compared with 5-fluorouracil, capecitabine has no cytotoxicity. At the location of the tumor, capecitabine can be converted into 5-fluorouracil through the tumor-related vascular factor (thymidine phosphorylase), thereby minimizing the damage to normal cells. It has been shown that the capecitabine combination regimen can reduce mortality compared with 5-fluorouracil (hazard ratio (HR) 0.86, 95% confidence interval (95% CI) 0.80–0.99) [8]. However, it has also been suggested that treatment with capecitabine did not significantly prolong survival compared with 5-fluorouracil (10.5 versus 9.3 months) [9]. Therefore, the effect of capecitabine versus 5-fluorouracil remains controversial. This study aimed to investigate the effect of capecitabine versus 5-fluorouracil on overall response rate, neutropenia, thrombocytopenia, nausea and vomiting, alopecia, and diarrhea through a meta-analysis.

2. Materials and Methods

2.1. Literature Search. A literature search of PubMed, Embase, and Cochrane Library was performed to include published randomized controlled trials (RCTs) on capecitabine and 5-fluorouracil published from database establishment to June 2022. Search terms were as followed: advanced gastric cancer; advanced gastric malignancy; gastric carcinoma; gastric neoplasm; capecitabine/siroda; 5-fluorouracil; chemotherapy. The retrieved articles and references of the studies were read to try to find out the target articles as much as possible. Published clinical trials and relevant review articles in oncology journals were hand-searched.

2.2. Inclusion and Exclusion Criteria. Inclusion criteria were as follows: (1) RCT; (2) individuals aged ≥ 18 years with a definite diagnosis of advanced gastric cancer, despite of sex, and race; (3) capecitabine-based chemotherapy was used in the experimental group and 5-fluorouracil-based chemotherapy was used in the control group; (4) data on overall response rate and adverse events were provided in the study.

Exclusion criteria were as follows: (1) animal studies; (2) sample size < 20; (3) diagnostic criteria for advanced gastric cancer were not given; (4) the needed data was not shown, or contact authors were still not available. All searches were limited to randomized clinical trials (RCTs) reported in journals or conferences, with no publication date or language restrictions.

2.3. Data Extraction and Quality Assessment. Two independent researchers extracted the needed data from the included studies: first author, publication year, the sample size of both groups, patient age, patient sex, chemotherapy regimen, overall response rate, neutropenia, thrombocytopenia, stomatitis, hand-foot syndrome, nausea and vomiting, alopecia, and diarrhea. The quality was assessed by the Cochrane collaboration's risk of bias evaluation tool, including seven aspects. We also attempted to reach out to the authors for supplemental data. A third researcher will help to deal with the differences.

2.4. Outcome Measures. Primary outcome measures: overall response rate. Overall response rate = (complete response + partial response)/total number × 100%. Safety measures: neutropenia, thrombocytopenia, stomatitis, hand-foot syndrome, nausea and vomiting, alopecia, and diarrhea.

2.5. Statistical Analysis. Analysis was carried out on an intent-to-treat basis, and all randomized patients were included according to their allocated treatment. $P < 0.05$ was defined as statistically significant. RR and its 95% CI were used to analyze the effect of treatment on overall response rate, neutropenia, thrombocytopenia, stomatitis, hand-foot syndrome, nausea and vomiting, alopecia, and diarrhea in advanced gastric cancer. The $\chi 2$ test was used to identify the heterogeneity among RCTs. We use the fixed-effect model when $P \geq 0.1$ and I2 ≤ 50% were considered to be small among studies; we use the random-effect model when $P < 0.1$ and $I^2 > 50\%$. Meta-analysis was performed by RevMan 5.3 software.

3. Results

3.1. Selection Process of Included Literature. As shown in Figure 1, 205 pieces of screened literature were determined. We excluded twenty-seven duplicate studies and 135 studies after reading the titles and abstracts, and the remaining 43 articles were read in full. We excluded thirty-five articles with conference abstracts or without outcome measures. 8 RCTs were included in the meta-analysis [8–15].

3.2. Clinical Characteristics of Included Articles. 1998 individuals with advanced gastric cancer were included, with 982 patients in the capecitabine arm and 1016 patients in the 5-fluorouracil arm (Table 1). The age ranged from 52 to 63 years in patients with capecitabine and from 52 to 63 years in patients with 5-fluorouracil. Both groups were predominantly male, ranging from 16 to 392 males in the capecitabine group and 13 to 393 males in the 5-fluorouracil group. Chemotherapy regimens in the capecitabine arm included cisplatin/capecitabine, docetaxel/capecitabine, and docetaxel/oxaliplatin/capecitabine. Chemotherapy regimens in the 5-fluorouracil group included irinotecan/5-fluorouracil, docetaxel/cisplatin/5-fluorouracil, and docetaxel/oxaliplatin/5-fluorouracil.

3.3. Risk of Bias. The overall study design of the included articles was good and the study quality was high (Figure 2). In terms of random sequence generation and allocation concealment, all eight studies were low risk. In terms of investigator and subject double-blinding, 5 studies were low risk and 3 were an uncertain risk. Six studies have a low risk of blinding of outcome assessment and two were an uncertain risk.

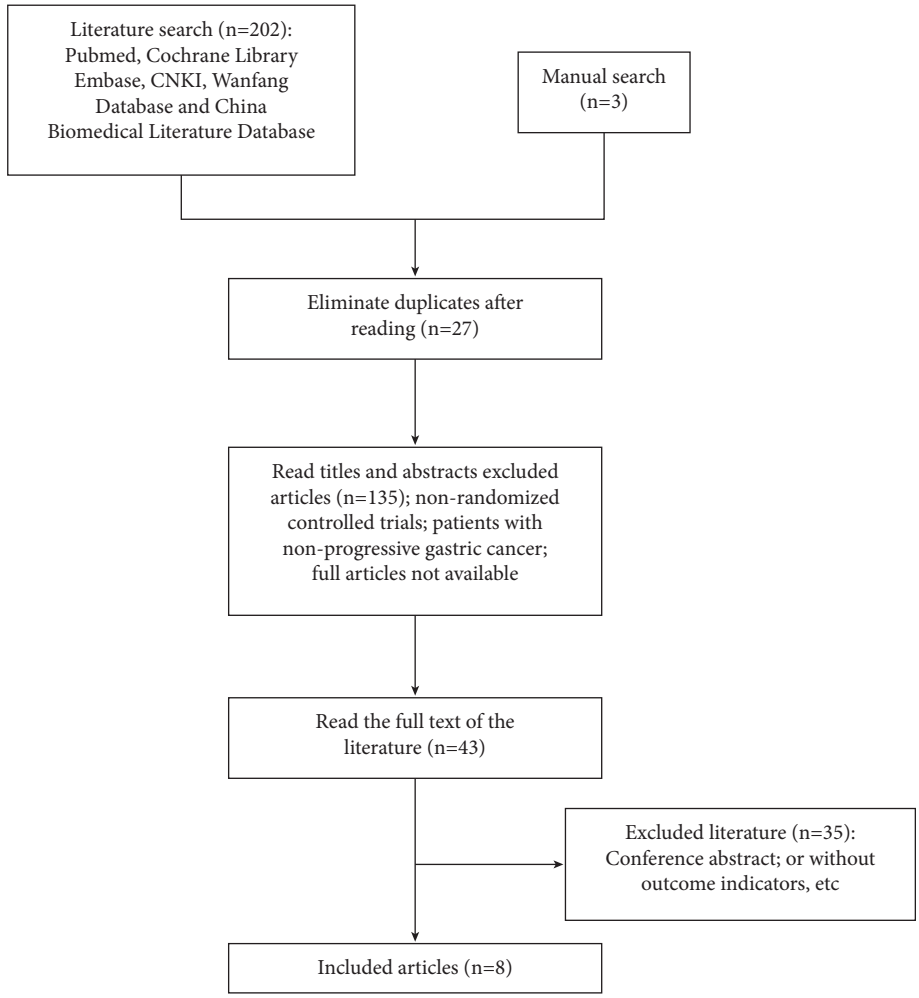

Figure 1: The screening process of included literature.

3.4. Effect of Capecitabine and 5-Fluorouracil on Overall Response Rate. A total of 8 articles were included in Figure 3 to show the effect of capecitabine and 5-fluorouracil on the overall response rate. Capecitabine use was significantly associated with an increased overall response rate compared with 5-fluorouracil (RR 1.13, 95% CI 1.02–1.25, $I^2 = 65\%$, $P = 0.02$).

3.5. Effect of Capecitabine and 5-Fluorouracil on Neutropenia and Thrombocytopenia. Figure 4 shows the effect of capecitabine versus 5-fluorouracil on neutropenia. Compared with 5-fluorouracil, treatment with capecitabine was significantly associated with decreased neutropenia events in advanced gastric cancer patients (RR 0.78, 95% CI 0.62–0.99, $I^2 = 86\%$, $P = 0.04$). Capecitabine tended to reduce the occurrence of thrombocytopenia compared with the 5-fluorouracil group (RR 0.79, 95% CI 0.38 to 1 .62, $I^2 = 82\%$, $P = 0.52$) (Table 2).

4. Nonhematologic Adverse Events

Compared with 5-fluorouracil, the intervention with capecitabine was significantly associated with decreased stomatitis events (RR 0.73, 95% CI 0.64–0.84, $I^2 = 40\%$, $P < 0.0001$). In terms of hand-foot syndrome, capecitabine was associated with increased hand-foot syndrome events than 5-fluorouracil (RR 2.00, 95% CI 1.21–3.31, $I^2 = 69\%$, $P = 0.007$). Capecitabine was not significantly different from 5-fluorouracil in nausea and vomiting (RR 0.97, 95% CI 0.91–1.03, $I^2 = 0\%$, $P = 0.27$). Capecitabine did not differ significantly from 5-fluorouracil in alopecia (RR 0.95, 95% CI 0.89–1.02, $I^2 = 26\%$, $P = 0.17$). Compared with 5-fluorouracil treatment, capecitabine did not significantly affect diarrhea (RR 1.02, 95% CI 0.78–1.33, $I^2 = 67\%$, $P = 0.90$).

5. Discussion

This study found that capecitabine was significantly associated with an improved overall response rate compared with 5-fluorouracil in advanced gastric cancer individuals. In addition, capecitabine reduces the risk of neutropenia and stomatitis compared with 5-fluorouracil. However, it is noteworthy that capecitabine may increase the occurrence of hand-foot syndrome. Capecitabine is similar to 5-fluorouracil in causing thrombocytopenia, nausea and vomiting, alopecia, and diarrhea.

Table 1: Clinical characteristics of included literature.

First author	Year	Sample size (capecitabine/ 5-fluorouracil)	Age, years (capecitabine/ 5-fluorouracil)	Number of males (capecitabine/ 5-fluorouracil)	Capecitabine arm chemotherapy regimen	5-Fluorouracil arm chemotherapy regimen
Cunningham [8]	2008	494/508	63/63	392/393	Epirubicin/cisplatin/capecitabine, or epirubicin/oxaliplatin/capecitabine	Epirubicin/cisplatin/5-fluorouracil, or epirubicin/oxaliplatin/5-fluorouracil
Kang [9]	2009	139/137	56/56	103/108	Cisplatin/capecitabine	Cisplatin/5-fluorouracil
Li [10]	2016	55/50	52/52	35/34	Epirubicin/oxaliplatin/capecitabine	Irinotecan/5-fluorouracil/leucovorin calcium
Ochenduszko [11]	2015	29/27	58/60	16/13	Epirubicin/oxaliplatin/capecitabine	Docetaxel/cisplatin/5-fluorouracil
Ocvirk [12]	2012	40/45	56/55	32/34	Epirubicin/cisplatin/capecitabine	Epirubicin/cisplatin/5-fluorouracil
Sumpter [13]	2005	96/108	63/62	82/79	Epirubicin/cisplatin/capecitabine, or epirubicin/oxaliplatin/capecitabine	Epirubicin/cisplatin/5-fluorouracil, or epirubicin/oxaliplatin/5-fluorouracil
Tebbutt [14]	2010	47/53	59/61	42/42	Docetaxel/capecitabine	Docetaxel/cisplatin/5-fluorouracil
Van Cutsem [15]	2014	82/88	59/58	74/69	Docetaxel/oxaliplatin/capecitabine	Docetaxel/oxaliplatin/5-fluorouracil

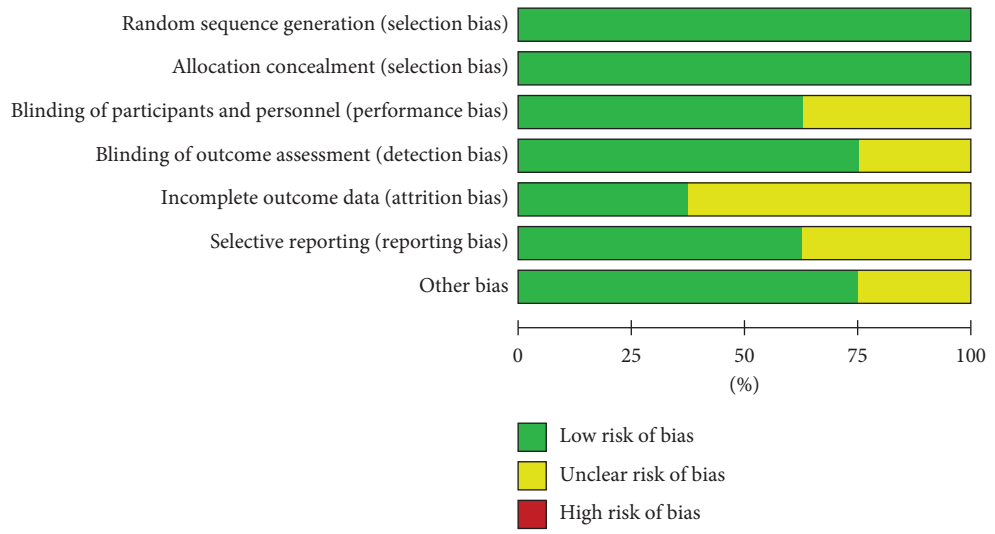

Figure 2: Risk of bias of included literature.

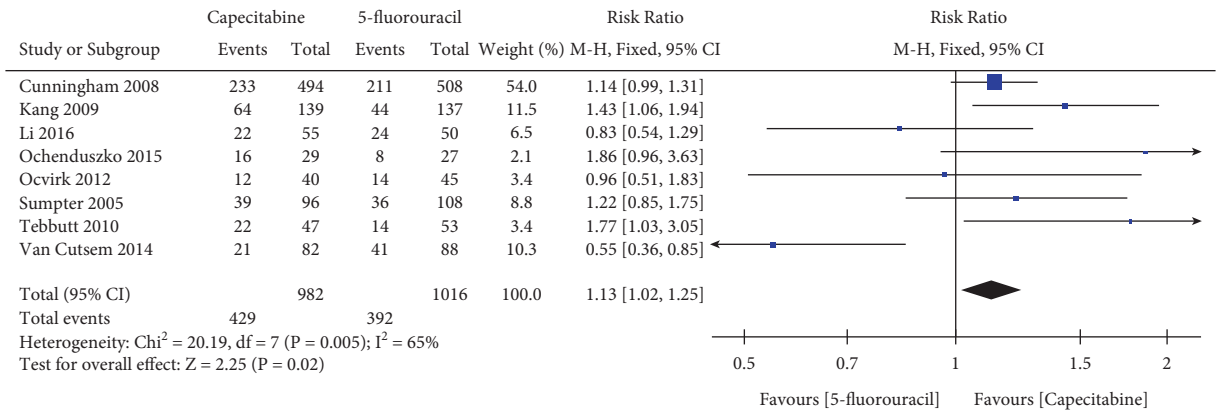

Figure 3: Effect of capecitabine and 5-fluorouracil on overall response rate.

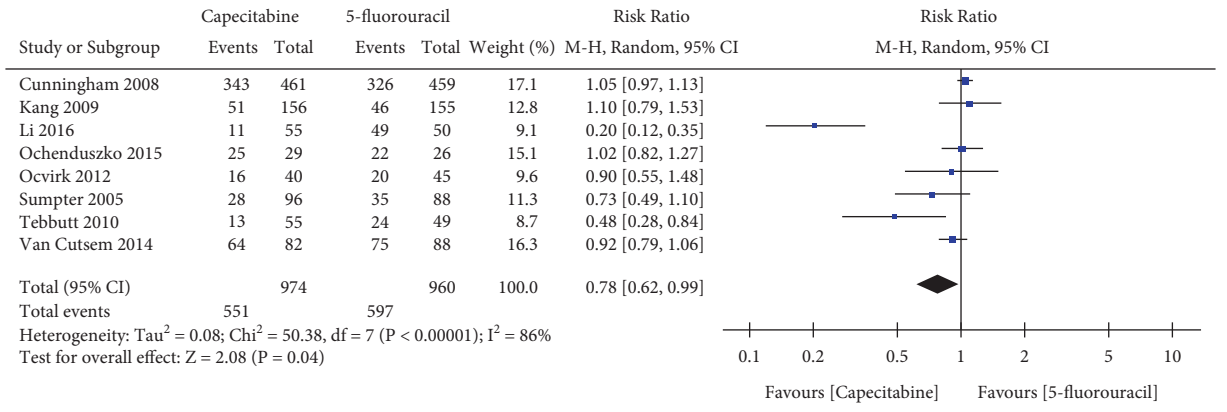

Figure 4: Effect of capecitabine and 5-fluorouracil on neutropenia.

Over the past years, the incidence of gastric cancer has slightly decreased, which may be attributed to the improvement of people's health awareness, the progress of screening methods, and the development of molecular targeted therapy and immunotherapy [16]. However, it should be reminded that the survival rate is still low, and the five-year survival rate is still about 20% in most regions and countries of the world [17]. For advanced gastric cancer, traditional chemotherapy remains the main treatment modality. Therefore, improving disease response rate and survival rate are the main objectives when selecting chemotherapeutic agents.

Table 2: Safety analysis of capecitabine and 5-fluorouracil.

Adverse reactions	Capecitabine arm (number of events/sample size)	5-Fluorouracil group (# events/sample size)	RR	95% CI	P Value	I^2 (%)
Thrombocytopenia	130/811	146/813	0.79	0.38–1.62	0.52	82
Nausea and vomiting	580/969	598/969	0.97	0.91–1.03	0.27	0
Hand-foot syndrome	300/878	173/872	2.00	1.21–3.31	0.007	69
Alopecia	454/689	477/693	0.95	0.89–1.02	0.17	26
Stomatitis	238/878	322/872	0.73	0.64–0.84	<0.0001	40
Diarrhea	372/878	364/872	1.02	0.78–1.33	0.90	67

A meta-analysis published in 2014, which included 26 studies with a total of 1585 patients, suggested that chemotherapy regimens containing capecitabine had similar efficacy compared with chemotherapy regimens containing 5-fluorouracil [18]. However, by further updating the literature and expanding the sample size, this study found that capecitabine may be superior in improving the overall response rate (RR 1.13, $P = 0.02$). Similar to this study, capecitabine-based chemotherapy regimens have also been suggested to show longer overall survival compared with conventional 5-FU-based chemotherapy regimens [19].

In terms of safety, treatment with capecitabine was significantly associated with decreased neutropenia events (RR 0.78, $P = 0.04$) and stomatitis (RR 0.73, $P < 0.0001$) compared with 5-fluorouracil. Similar to this study, an additional meta-analysis also found a significant reduction in serious leukopenia in capecitabine patients [19]. However, it is noteworthy that capecitabine may significantly increase the occurrence of hand-foot syndrome compared with 5-fluorouracil (RR 2.00, 95% CI 1.21–3.31 $P = 0.007$). Grade 1 or 2 hand-foot syndrome can be managed by ointment or appropriate reduction [20]. Some studies suggest that the hands and feet have many exocrine glands, and the excretion of capecitabine from the suboriferous is the cause of the hand-foot syndrome. In addition, the hand-foot syndrome caused by capecitabine may be related to the destruction of the deep capillary network and the overexpression of cyclooxygenase (COX-2).

The limitations of the study were as follows: (1) the primary endpoint evaluated in this study was the overall response rate without assessing survival. Although the overall response rate is clearly associated with survival, survival is the more important indicator. Future studies are needed to further evaluate survival. (2) Adverse reactions such as neutropenia, thrombocytopenia, nausea and vomiting, alopecia, stomatitis, and diarrhea were assessed in this study, but safety events such as anemia and peripheral neuropathy were not assessed. (3) Although the chemotherapy treatments included in the study are based on capecitabine or 5-fluorouracil, there are some differences between the chemotherapy plans in different studies, which may affect the results of the study. (4) Meta-analysis is mainly used to identify the relevant relationship, and a large sample of head-to-head R CT is needed in the future to further compare the effect of capecitabine and 5-fluorouracil.

In summary, capecitabine treatment improves overall response rates and reduces the risk of neutropenia and stomatitis compared with 5-fluorouracil. It should be noted that treatment with capecitabine may also increase the occurrence of hand-foot syndrome. Capecitabine is similar to 5-fluorouracil in causing thrombocytopenia, nausea and vomiting, alopecia, and diarrhea.

Data Availability

The analyzed data sets generated during the study are available from the corresponding author upon reasonable request.

Conflicts of Interest

The authors declare that they have no conflicts of interest.

References

[1] P. Correa, "Gastric cancer: overview," *Gastroenterology Clinics of North America*, vol. 42, no. 2, pp. 211–217, 2013.

[2] E. C. Smyth, M. Nilsson, H. I. Grabsch, N. C. van Grieken, and F. Lordick, "Gastric cancer," *The Lancet*, vol. 396, no. 10251, pp. 635–648, 2020.

[3] P. Karimi, F. Islami, S. Anandasabapathy, N. D. Freedman, and F. Kamangar, "Gastric cancer: descriptive epidemiology, risk factors, screening, and prevention," *Cancer Epidemiology, Biomarkers & Prevention*, vol. 23, no. 5, pp. 700–713, 2014.

[4] J. Ferlay, H. R. Shin, F. Bray, D. Forman, C. Mathers, and D. M. Parkin, "Estimates of worldwide burden of cancer in 2008: globocan 2008," *International Journal of Cancer*, vol. 127, no. 12, pp. 2893–2917, 2010.

[5] D. E. Guggenheim and M. A. Shah, "Gastric cancer epidemiology and risk factors," *Journal of Surgical Oncology*, vol. 107, no. 3, pp. 230–236, 2013.

[6] R. E. Sexton, M. N. Al Hallak, M. Diab, and A. S. Azmi, "Gastric cancer: a comprehensive review of current and future treatment strategies," *Cancer and Metastasis Reviews*, vol. 39, no. 4, pp. 1179–1203, 2020.

[7] Z. Song, Y. Wu, J. Yang, D. Yang, and X. Fang, "Progress in the treatment of advanced gastric cancer," *Tumour Biol*, vol. 39, no. 7, Article ID 101042831771462, 2017.

[8] D. Cunningham, N. Starling, S. Rao et al., "Capecitabine and oxaliplatin for advanced esophagogastric cancer," *New England Journal of Medicine*, vol. 358, no. 1, pp. 36–46, 2008.

[9] Y. K. Kang, W. K. Kang, D. B. Shin et al., "Capecitabine/cisplatin versus 5-fluorouracil/cisplatin as first-line therapy in patients with advanced gastric cancer: a randomised phase III noninferiority trial," *Annals of Oncology*, vol. 20, no. 4, pp. 666–673, 2009.

[10] J. W. Li, "Comparison of efficacy of modified EOX and FOLFIRI regimens in treatment of metastatic gastric cancer,"

World Chinese Journal of Digestology, vol. 24, no. 12, p. 1866, 2016.

[11] S. Ochenduszko, M. Puskulluoglu, K. Konopka et al., "Comparison of efficacy and safety of first-line palliative chemotherapy with EOX and mDCF regimens in patients with locally advanced inoperable or metastatic HER2-negative gastric or gastroesophageal junction adenocarcinoma: a randomized phase 3 trial," *Medical Oncology*, vol. 32, no. 10, p. 242, 2015.

[12] J. Ocvirk, M. Rebersek, E. Skof, Z. Hlebanja, and M. Boc, "Randomized prospective phase II study to compare the combination chemotherapy regimen epirubicin, cisplatin, and 5-fluorouracil with epirubicin, cisplatin, and capecitabine in patients with advanced or metastatic gastric cancer," *American Journal of Clinical Oncology*, vol. 35, no. 3, pp. 237–241, 2012.

[13] K. Sumpter, C. Harper-Wynne, D. Cunningham et al., "Report of two protocol planned interim analyses in a randomised multicentre phase III study comparing capecitabine with fluorouracil and oxaliplatin with cisplatin in patients with advanced oesophagogastric cancer receiving ECF," *British Journal of Cancer*, vol. 92, no. 11, pp. 1976–1983, 2005.

[14] N. C. Tebbutt, M. M. Cummins, T. Sourjina et al., "Randomised, non-comparative phase II study of weekly docetaxel with cisplatin and 5-fluorouracil or with capecitabine in oesophagogastric cancer: the AGITG ATTAX trial," *British Journal of Cancer*, vol. 102, no. 3, pp. 475–481, 2010.

[15] E. Van Cutsem, C. Boni, J. Tabernero et al., "Docetaxel plus oxaliplatin with or without fluorouracil or capecitabine in metastatic or locally recurrent gastric cancer: a randomized phase II study," *Annals of Oncology*, vol. 26, no. 1, pp. 149–156, 2015.

[16] A. P. Thrift and H. B. El-Serag, "Burden of gastric cancer," *Clinical Gastroenterology and Hepatology*, vol. 18, no. 3, pp. 534–542, 2020.

[17] R. Siegel, J. Ma, Z. Zou, and A. Jemal, "Cancer statistics," *CA: A Cancer Journal for Clinicians*, vol. 64, no. 1, pp. 9–29, 2014.

[18] H. B. Xu, F. Huang, R. Su, F. M. Shen, and Q. Z. Lv, "Capecitabine plus oxaliplatin (XELOX) compared with 5-fluorouracil/leucovorin plus oxaliplatin (FOLFOXs) in advanced gastric cancer: meta-analysis of randomized controlled trials," *European Journal of Clinical Pharmacology*, vol. 71, no. 5, pp. 589–601, 2015.

[19] Y. Ma, L. Tang, H. X. Wang, Y. C. Xu, Y. Ma, and F. C. Zhang, "Capecitabine for the treatment for advanced gastric cancer: efficacy, safety and ethnicity," *Journal of Clinical Pharmacy and Therapeutics*, vol. 37, no. 3, pp. 266–275, 2012.

[20] N. Boku, M. H. Ryu, K. Kato et al., "Safety and efficacy of nivolumab in combination with S-1/capecitabine plus oxaliplatin in patients with previously untreated, unresectable, advanced, or recurrent gastric/gastroesophageal junction cancer: interim results of a randomized, phase II trial (ATTRACTION-4)," *Annals of Oncology*, vol. 30, no. 2, pp. 250–258, 2019.

Hindawi
Evidence-Based Complementary and Alternative Medicine
Volume 2023, Article ID 9402155, 12 pages
https://doi.org/10.1155/2023/9402155

Research Article

Nourishing Kidney Promoting Ovulation Decoction (NKPOD) Attenuates Polycystic Ovary Syndrome by Downregulating miRNA-224

Yinhua Guo, Xingli Tong, Peipei Tang, Wenting Zuo, and Yong Tan

Department of Reproductive Medicine, Jiangsu Hospital of Traditional Chinese Medicine, Affiliated Hospital of Nanjing University of Traditional Chinese Medicine, Nanjing 210000, Jiangsu, China

Correspondence should be addressed to Yong Tan; tcmtanyong@163.com

Received 4 August 2022; Revised 27 September 2022; Accepted 6 October 2022; Published 20 April 2023

Academic Editor: Xueliang Wu

Background. Currently, exploring effective agents is urgently required for polycystic ovary syndrome (PCOS) treatment. Although nourishing kidney promoting ovulation decoction (NKPOD) as a traditional Chinese medicine decoction is widely employed to increase pregnancy rates, whether NKPOD attenuates ovulation disorders in PCOS patients remains unknown. Here, we aim to explore the clinical significance and the underlying mechanisms of NKPOD in ovulation disorders. *Methods*. PCOS patients were recruited to confirm the clinical significance of NKPOD in attenuating ovulation disorder. Subsequently, regulation targets of NKPOD were identified through network pharmacology analysis. Additionally, a series of experiments were performed to observe the impacts of NKPOD on miRNA-224 transcription through transcription factor AR. *Results*. In this study, NKPOD administration improved hormone dysregulation and reproductive outcomes in PCOS patients. Interestingly, 100 potential targets related to NKPOD and PCOS were screened, and transcription regulation was observed to be the most enriched function. Mechanistically, NKPOD inhibited miRNA-224 transcription through reducing AR expression, in which AR as a transcription factor directly regulated miRNA-224 transcription. *Conclusions*. Collectively, these findings highlight the therapeutic effect of NKPOD on PCOS, which could provide promising therapeutic agents for PCOS.

1. Introduction

Polycystic ovary syndrome (PCOS) is an endocrine disease which is characterized by anovulatory cycles/oligo, polycystic ovaries, hirsutism, and insulin resistance [1]. Accumulating evidence indicates that arrested follicular growth and abnormality of early follicle development are critical factors in the pathogenesis of PCOS [2–4]. At present, approximately 5% to 20% of females will develop PCOS during their reproductive age [2, 5]. Mounting evidence indicates that PCOS increases the risk of type 2 diabetes, cardiovascular disease, obesity, metabolic syndrome, and endometrial cancer [6–8]. Additionally, pregnant women with PCOS are more vulnerable to miscarriages and ovarian hyperstimulation syndrome [9]. Therefore, exploring effective agents is urgently required for the treatment of PCOS.

Traditional Chinese medicine (TCM) has been widely applicable to treatment for PCOS [10], and nourishing kidney promoting ovulation decoction (NKPOD), which is composed of twelve kinds of Chinese herbal medicines, is one of them, including Angelicae sinensis Radix, Paeoniae Radix alba, Rhizoma Dioscoreae, Rehmanniae Radix Preparata, Cortex Moutan, Poria, Semen Cuscutae, Dipsaci Radix, Cuscutae Semen, Cornu Cervi, Faeces Trogopterori, and Carthami flos. Modern pharmacological studies have shown that some active ingredients in NKPOD play a role in regulating oocyte competency and embryo development [10–12]. For example, animal experiments showed that Bushen-zhu-yun decoction including Angelicae sinensis Radix significantly alleviated pathological changes in the ovary, altered hormone levels of serum, and reduced the apoptotic rate of granulosa cells [13], while an experimental study

demonstrated that Cuscuta-Salvia ameliorated the pathological changes in the liver, ovaries, and adipose tissue [14]. Multicomponents and multiple targeting characteristics of NKPOD play a common role in the protective effect of PCOS; thus, expanding the knowledge of NKPOD in PCOS treatment will be interesting.

During the development of the oocyte and embryo, numerous miRNAs are produced, and they function through posttranscriptional gene regulation [15, 16]. Several previous studies have demonstrated that miRNA-224 is a marker of PCOS and regulates oocyte competency and embryo development [17, 18]. As an example, miRNA-224 is involved in the growth of follicular granulosa cell by transforming growth factor-β1 and estradiol (E2) [19]. Another research of miRNA-224 revealed bisphenol-A exposure changes in serum E2 levels and follicle-stimulating hormone levels through transcriptional regulation on miRNA-224 in preantral ovarian granulosa cells [18]. These pieces of evidence suggest that miRNA-224 could be involved in later development of follicles.

In this study, we explore and present the NKPOD-treatment-mechanism relationships with clinical research, network pharmacology methods, and *in vitro* experiments. We use these methods to give a dependable result of the NKPOD on attenuating polycystic ovary syndrome. Furthermore, we investigate whether NKPOD could regulate the expression of miRNA-224 and the underlying mechanism.

2. Methods

2.1. Clinical Samples. From January 2018 to June 2020, the PCOS patients (age <38 years) who underwent *in vitro* fertilization and embryo transfer and intracytoplasmic sperm injection (IVF-ET/ICSI)-assisted pregnancy in the Reproductive Medicine Department of Jiangsu Traditional Chinese Medicine Hospital were collected. The basic clinical characteristics, embryo laboratory indexes, and the OHSS incidence of the two groups were analyzed and compared (Table 1). The diagnostic criteria for PCOS referred to as PCOS formulated by experts of the European Society of Human Reproduction and Embryology and the American Society of Reproductive Medicine (ESHRE/ASRM) in Rotterdam in 2003 were as follows: (a) clinical manifestations of hyperandrogenemia and/or hyperandrogen, (b) anovulation or rare ovulation, and (c) ultrasound showing ovarian polycystic changes (ovarian volume greater than 10 ml in one or both ovaries and/or > 12 follicles with a diameter of 2–9 mm). After excluding Cushing's syndrome, congenital adrenocortical hyperplasia, androgen-secreting tumors, and other diseases, if 2 of the above three are consistent, it can be diagnosed as polycystic ovary syndrome. Among them, hyperandrogenemia is based on the fact that the fasting testosterone value in the morning of menstruation D3 is higher than the upper limit of normal. The standard of rare ovulation was a menstrual cycle >35 days. The ultrasound image of the polycystic ovary is based on the standard that the number of bilateral ovarian sinus follicles (AFC) shown by transvaginal ultrasound is greater than 12. The selected patients with normal ovarian function were younger than 38 years and had regular menstrual cycles (28–30 d), normal basic reproductive hormones, and a number of follicles in both ovarian sinuses (unilateral AFC = 6–10). The two groups had no ovarian cysts, hyperprolactinemia, ovarian tumors, endometriosis, ovarian surgery, chemotherapy and radiotherapy, hypothyroidism/hyperthyroidism, and other endocrine diseases, and the chromosomes of the couple were normal. The Ethics Committee of the Jiangsu Hospital of Traditional Chinese Medicine (2019NL-KS74) approved this study. Written informed consent was obtained from all participants included in the study.

Table 1: Comparison of general information in the two groups.

Item	NC group ($n = 9$)	PCOS group ($n = 9$)	P value
Age (year)	30.11 ± 3.59	29.78 ± 5.38	0.88
Primary infertility	7	7	0.71
Secondary infertility	2	2	
Course of disease (year)	2.56 ± 1.33	2.78 ± 1.64	0.76

2.2. NKPOD Administration. NKPOD that met the standards set by the Chinese Pharmacopoeia (2015 Edition) [20] contained Angelicae sinensis Radix (10 g), Paeoniae Radix alba (10 g), Rhizoma Dioscoreae (10 g), Rehmanniae Radix Preparata (10 g), Cortex Moutan (10 g), Poria (10 g), Semen Cuscutae (9 g), Dipsaci Radix (10 g), Cuscutae Semen (10 g), Cornu Cervi (10 g), Faeces Trogopterori (10 g), and Carthami flos (5 g). All components were provided by Jiangsu Traditional Chinese Medicine Hospital. All the components were soaked in cold water for 30 minutes; then, NKPOD was soaked in water to a final volume of 1 L. All the components were extracted by boiling in 400 mL water for 1 h.

2.3. Sample Collection and Detection. For collection of serum, blood was collected on the 2nd–5th day of the menstrual cycle and the elbow vein blood of the patient was extracted. After centrifugation ($2{,}000 \times g$ for 5 min; $10{,}000 \times g$ for 5 min) at 4°C, the serum was taken and stored in the −80°C refrigerator for testing. For collection of follicular fluid, the diameter of the selected experimental follicles was more than 18 mm. The follicular fluid was obtained when the follicles were punctured, and the eggs were taken under the guidance of vaginal B-ultrasound. About 4 ml of clear follicular fluid without blood pollution was left. After centrifugation, the supernatant was left and stored in the refrigerator at −80°C for testing. For collection of granulosa cells, the eggs were punctured according to the egg taken as the standard, the follicular fluid was retained, human lymphocyte separation solution was added, the granulosa cell layer between the two liquid levels was absorbed after centrifugation, PBS was added, the supernatant was discarded after centrifugation, and the lower layer had granulosa cells. Granulosa cells for experimental research and oocytes for IVF-ET/ICSI were collected. The granulosa cells

were grown in DMEM/F12 (1 : 1; Thermo Fisher Scientific, Inc., Waltham, MA, USA) supplemented with 10% fetal bovine serum (FBS) (Thermo Fisher Scientific) and 1% antibiotics (Thermo Fisher Scientific), including penicillin (100 U/ml) and streptomycin (100 g/ml), at 37°C with 5% CO_2. The serum levels of luteinizing hormone (LH), E2, testosterone (T), follicle-stimulating hormone (FSH), and anti-Mullerian hormone (AMH) were measured by electrochemiluminescence; additionally, clinical information about participants was collected, including stimulation duration of gonadotropin (Gn), total Gn doses, the number of oocytes punctured and oocytes retrieved, the number of 2PN and 2PN cleavage numbers, and the number of embryos transferred and high-quality embryos. The number of dominant follicles, ovulation, pregnancies, and abortions was also recorded. D3 embryo grades were as follows [21]: (a) grade I: an embryo with blastomeres of equal size; in addition, no cytoplasmic fragmentation was found; (b) grade II: an embryo with blastomeres of equal size and minor; in addition, cytoplasmic fragmentation covers ≤10% of the embryo surface; (c) grade III: an embryo with blastomeres of equal or unequal size; in addition, cytoplasmic fragmentation covers >10% of the embryo surface; (d) grade IV: an embryo with few blastomeres of any size; in addition, severe fragmentation covers ≥50% of the embryo surface; (e) grade V: an embryo with few blastomeres of any size; in addition, severe fragmentation covers ≥50% of the embryo surface; grades I and II are called high-quality embryos, and grades I ~ III are available embryos.

2.4. Plasmid Construction and Transfection. The full-length cDNA of AR was cloned into pcDNA3.1 (Thermo Fisher Scientific, Inc., Waltham, MA, USA). The corresponding empty vector (pcDNA3.1-NC) and AR plasmid (pcDNA3.1-AR) were transfected into granulosa cells using Lipofectamine 3000 reagent (Thermo Fisher Scientific). G418 treatment (2 mg/ml) was performed to structure stably transfected cells. Subsequently, granulosa cells were subjected to qRT-PCR analysis to evaluate AR expression.

2.5. Pharmacological Network Analysis. The components potential targets of Angelicae sinensis Radix, Paeoniae Radix alba, Rhizoma Dioscoreae, Rehmanniae Radix Preparata, Cortex Moutan, Poria, Semen Cuscutae, Dipsaci Radix, Cuscutae Semen, Cornu Cervi, Faeces Trogopterori, and Carthami flos were identified by the Traditional Chinese Medicine Systems Pharmacology Database and Analysis Platform (TCMSP, https://tcmsp-e.com/) with drug likeness (DL ≥ 0.1) and oral bioavailability (OB ≥ 30%). The potential targets of Angelicae sinensis Radix, Paeoniae Radix Alba, Rhizoma Dioscoreae, Rehmanniae Radix Preparata, Cortex Moutan, Poria, Semen Cuscutae, Dipsaci Radix, Cuscutae Semen, Cornu Cervi, Faeces Trogopterori, and Carthami flos were also obtained from the TCMSP (https://tcmsp-e.com/). Subsequently, PCOS-related genes were obtained from the GeneCards database (https://www.genecards.org/) and the Comparative Toxicogenomics Database (CTD, https://ctdbase.org/). Using Cytoscape software (version 3.8.2, Bethesda, MD, USA), we visualized the composition-target network. In addition, protein-protein interactions (confidence score >0.9) were selected using STRING (https://www.string-db.org/) and Cytoscape software. The core targets were analyzed using plug-in components (CytoNCA) through analysing betweenness, bloseness, degrees, eigenvectors, LAC, and networks. The visualization of gene ontology (GO) terms was performed by using the clusterProfiler package in R.

2.6. Bioinformatic Analysis. The transcription factors for miRNA-224 and predicted sites of AR-binding in miRNA-224 promoters were acquired through TransmiRNA v2.0 (https://www.cuilab.cn/transmiRNA) and hTFtarget (https://bioinfo.life.hust.edu.cn/hTFtarget#!/). The DNA motif of AR was predicted from JASPAR (https://jaspar.genereg.net/).

2.7. Western Blot Assay. Total proteins from granulosa cells were extracted and separated by SDSPAGE gels (10%) and then transferred to PVDF membranes (0.22 μm, Merck Millipore, Billerica, Massachusetts, USA). After blocking with skim milk powder (5%), the membranes incubated with the androgen receptor (AR) antibody (NO. ab108341, Abcam, Cambridge, UK), p-AR antibody (NO. ab45089, Abcam), or glyceraldehyde-3-phosphate dehydrogenase (GAPDH) antibody (NO. ab181602, Abcam) at 4°C overnight. Next, secondary antibodies (NO. ab205718, ab205719, Abcam) were incubated. An ECL detection system (Bio-Rad, Hercules, USA) was used to measure the protein bands. GAPDH was used as a control.

2.8. Real-Time Quantitative PCR (RT-qPCR). Total RNA was extracted from granulosa cells using Magnetic Tissue/Cell/Blood Total RNA Kit (Tiangen Biochemical Technology Co., Ltd, Beijing, China). Then, RNA was reverse-transcribed using QuantScript RT Kit (Tiangen) by following the standard protocols. Real-time PCR was carried out using ReliaTM SYBR QPCR Mix (Nanjing Detai Bioengineering Co., Ltd, Nanjing, China). The level of miRNA-224 was normalized to U6, and the relative level was calculated. U6 primers were as follows: forward: 5′-GCT TCG GCA GCA CAT ATA CTA A-3′ and reverse: 5′-AAC GCT TCA CGA ATT TGC GT-3′. miRNA-224 primers were as follows: forward: 5′-TCA AGT CAC TAG TGG TTC CGT -3′ and reverse: 5′-GGC TTT GTA GTC ACT AGG GCA-3′. miRNA-224-3p primers were as follows: forward: 5′- TGA TGT GGG TGC TGG TGT C -3′ and reverse: 5′- TTG TGT TGG GGC AGT ACT G -3′. miRNA-224-5p primers were as follows: forward: 5′- CTG GTA GGT AAG TCA CTA -3′ and reverse: 5′- TCA ACT GGT GTC GTG GAG -3′.

2.9. Dual-Luciferase Assay. The wild-type reporter of miRNA-224 promoters (pmiRNAGLO-WT) or the mutant reporter (pmiRNAGLO- MUT) was cotransfected with pcDNA3.1-NC or pcDNA3.1-AR into HEK293T cells. After transfection for 24 h, HEK293T cells were washed with PBS

and subjected to the dual-luciferase reporter assay system (Promega) for luciferase level measurement. Luciferase activities were normalized to that of Renilla.

2.10. Chromatin Immunoprecipitation (ChIP). By following the manufacturer's instructions, ChIP assays were conducted using ChIP Assay Kit (Beyotime, Haimen, China). Granulosa cells were crosslinked with formaldehyde and sonicated to an average length of 200–1000 bp. Subsequently, IP was performed with an AR antibody (Abcam) or IgG. Finally, precipitated DNA was detected by qRT-PCR.

2.11. Statistical Analysis. Quantitative data are presented as the mean ± SD and analyzed by using SPSS software (version 22.0, IBM, Chicago, USA). Normality of distribution was assessed using the Kolmogorov–Smirnov test. The Mann–Whitney U tests or Student's t-test was performed for two-group comparisons. Differences between the two groups after treatment were measured using covariance analysis. The threshold for statistical significance was set at $P < 0.05$.

3. Results

3.1. NKPOD Attenuates Ovulation Disorders in PCOS Patients. In this study, we investigated the function of NKPOD in regulating ovulation disorders in PCOS patients. Interestingly, NKPOD administration resulted in a significant decrease of BIM in PCOS patients ($P < 0.001$; Figure 1(a)). PCOS patients displayed higher levels of AMH, while the increase was partly reversed by NKPOD administration ($P < 0.001$; Figure 1(b)). The influence of NKPOD on T levels in PCOS patients was verified; the results demonstrated that NKPOD administration significantly impaired PCOS-mediated promotion of serum T levels ($P < 0.01$; Figure 1(c)). Similar results were observed in LH levels ($P < 0.05$; Figure 1(d)). To further explore the effects of NKPOD on attenuating ovulation disorders, we confirmed the serum of E2. Interestingly, higher E2 levels were observed in PCOS patients receiving NKPOD administration ($P < 0.05$; Figure 1(e)). Moreover, we found that the increased FSH levels in PCOS patients were partially reversed by NKPOD ($P < 0.01$; Figure 1(f)). Collectively, these data demonstrate that NKPOD exerts a therapeutic effect on PCOS.

3.2. NKPOD Improves Reproductive Outcomes in PCOS Patients. Subsequently, we further elucidated whether NKPOD influences reproductive outcomes in PCOS patients. Stimulation duration and total Gn doses were not changed in PCOS patients with NKPOD treatment ($P > 0.05$; Figures 2(a) and 2(b)). Notably, after exposure to NKPOD, we noted that the changes in the number of oocytes punctured and oocytes retrieved were not significant compared with those in the NC group ($P > 0.05$; Figure 2(c)). However, a higher number of oocytes were found in PCOS patients with NKPOD exposure ($P < 0.05$; Figure 2(d)). Furthermore, we noted that NKPOD administration significantly increased the number of 2PN and 2PN cleavage numbers ($P < 0.05$; Figures 2(e) and 2(f)). Consistent with 2PN, comparisons analysis demonstrated that NKPOD administration had significant effects on increasing the number of embryos transferred and high-quality embryos ($P < 0.05$; Figures 2(g) and 2(h)). We further evaluated the influences of NKPOD on reproductive outcomes and found that NKPOD treatment led to a significant increase in pregnancy rates in PCOS patients ($P < 0.05$; Table 2). Furthermore, we assessed the safety of NKPOD administration. Importantly, all PCOS patients were examined for blood, urine, stool routine, ECG, and liver and kidney function after each course of treatment. The results showed that there were no obvious abnormalities and that there were no serious adverse reactions in all patients. Taken together, our findings highlight the important role of NKPOD in improving reproductive outcomes in PCOS patients.

3.3. NKPOD Component-Target Network Construction. To elucidate the underlying molecular mechanism, in which NKPOD attenuating ovulation disorders, we investigated the targets of NKPOD through network pharmacology. The components and potential targets of Angelicae sinensis Radix, Paeoniae Radix alba, Rhizoma Dioscoreae, Rehmanniae Radix Preparata, Cortex Moutan, Poria, Semen Cuscutae, Dipsaci Radix, Cuscutae Semen, Cornu Cervi, Faeces Trogopterori, and Carthami flos, which constitute NKPOD, were identified, as displayed in Table S1. After screening with OB and DL, a total of 63 components were obtained from the TCMSP. 1857 possible targets of these components were also obtained from the TCMSP (Table S1). Subsequently, a total of 954 genes related to PCOS were obtained from the GeneCards database (1260 genes) and CTD (12894 genes), as shown in Figure 3(a) and Table S2. Interestingly, a total of 954 genes, which were both related to NKPOD and PCOS, were confirmed (Figure 3(b) and Table S3). As demonstrated in Figure 3(c), we structured the compound-target network, including 161 nodes, 61 bioactive compounds and 100 targets. Subsequently, the proposed protein-protein interactions of 100 targets are constructed and displayed in Figure 3(d). After hiding disconnected nodes, 91 nodes and 686 edges were found in the network. To investigate the crucial nodes, betweenness, closeness, degrees, eigenvectors, LAC, and networks were used to identify 24 nodes and 240 edges. To investigate the potential functions of these targets, we performed functional enrichment analysis and found 1867 GO biological terms (FDR cutoff = 0.01, Table S4 and Figure 3(e)). The results of Figure 3(e) revealed the top 10 enriched GO-BP terms, including nuclear receptor activity, ligand-activated transcription factor activity, DNA-binding transcription factor binding, steroid hormone receptor activity, ubiquitin-like protein ligase binding, RNA polymerase II-specificDNA-binding transcription factor binding, transcription coactivator-binding serine

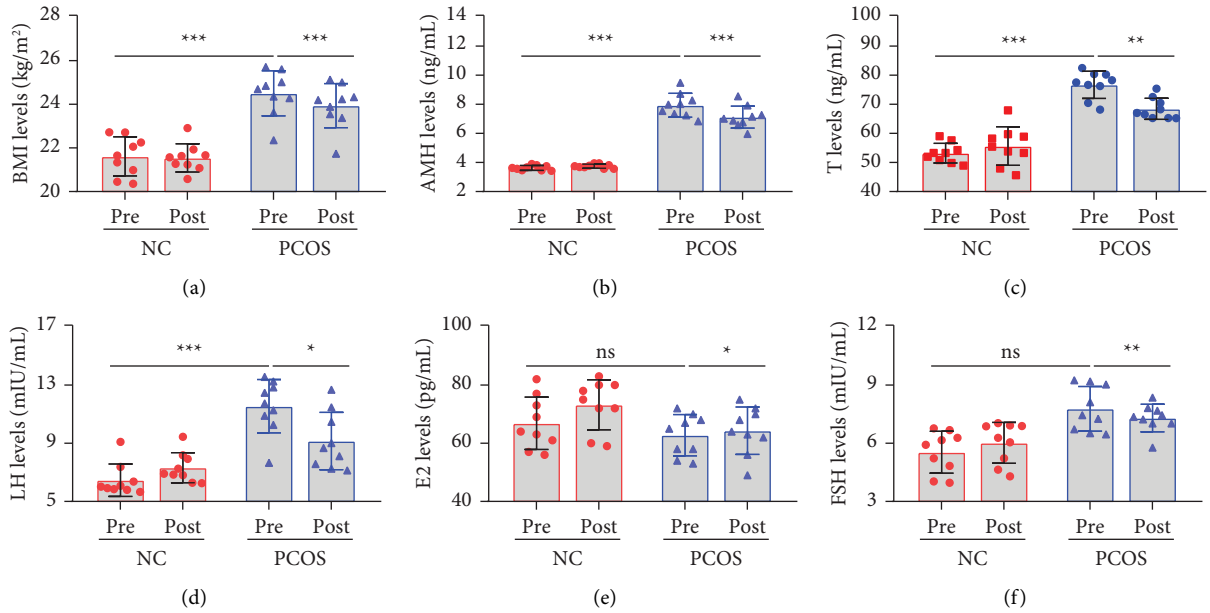

Figure 1: NKPOD administration alleviates hormone dysregulation in PCOS patients. (a) The changes in the BMI of PCOS patients receiving NKPOD administration. (b) The changes in anti-Müllerian hormone (AMH) of PCOS patients with NKPOD treatment. (c) After NKPOD treatment, the levels of testosterone (T) in PCOS patients. (d) The changes in luteinizing hormone (LH) of PCOS patients receiving NKPOD administration. (e) The changes in estradiol (E2) of PCOS patients receiving NKPOD administration. (f) The changes in follicle-stimulating hormone (FSH) in PCOS patients receiving NKPOD administration. ns represents ($P > 0.05$), * ($P < 0.05$), ** ($P < 0.01$), and *** ($P < 0.001$).

Table 2: Comparison of ovulation and pregnancy between the two groups.

Item	NC group ($n = 9$)	PCOS group ($n = 9$)	P value
Ovulation	1	6	0.016
Gestation	1	5	0.046
Abortion	0	0	1

hydrolase activity, serine-type endopeptidase activity, and ubiquitin protein ligase binding.

3.4. NKPOD Inhibits AR Expression. To investigate the possible mechanism of NKPOD on attenuating ovulation disorders, we measured miRNA-224 abundance in PCOS patients. As expected, significant increased miRNA-224 abundance was discovered in follicular fluid, granulosa cells, and serum of PCOS patients (Figures 4(a)–4(c)). Particularly, NKPOD showed a stronger ability to lower miRNA-224 abundance in follicular fluid, granulosa cells, and serum of PCOS patients (Figures 4(a)–4(c)). Similar results were obtained for miRNA-224-3p (Figures 4(d)–4(f)) and miRNA-224-5p (Figures 4(g)–4(i)). Taken together, these results imply that NKPOD inhibits miRNA-224 transcription. To understand the mechanism by which NKPOD regulated miRNA-224 transcription, we investigated the transcription factor for miRNA-224. Interestingly, AR was identified as the only target of miRNA-224 transcription factors and NKPOD regulatory targets (Figure 4(j)). The predicted sites of AR-binding in miRNA-224 promoters by TransmiRNA v2.0 (https://www.cuilab.cn/transmiRNA) are shown in Figure 4(k). Additionally, the motif of AR predicated by the JASPAR database (https://jaspar.genereg.net/) is displayed in Figure 4(l). Next, we explored the effects of NKPOD on the expression of AR in granulosa cells; western blotting was performed and displayed that AR expression was significantly upregulated in PCOS patients, whereas the increased AR expression was inhibited by NKPOD treatment (Figures 4(m) and 4(n)). Interestingly, the inhibition effect of NKPOD on phosphorylation of AR was determined, in which the elevated p-AR/AR levels in granulosa cells of PCOS patients were significantly attenuated by NKPOD treatment (Figures 4(m) and 4(o)).

3.5. miRNA-224 Is Confirmed as the Target of AR. To further understand the mechanism by which AR regulated miRNA-224 transcription, the ChIP assay was used, and we pointed out that the miRNA-224 promoter was strongly enriched in the AR pellet in granulosa cells (Figures 5(a) and 5(b)). Subsequently, we performed the luciferase reporter assay through constructing the wild-type and mutant-binding sequences (Figure 5(c)). The results showed that relative luciferase activity was dramatically enhanced in the miRNA-224promoter-WT + AR overexpression group, but there was no apparent change in the miRNA-224promoter-MUT + AR overexpression group (Figures 5(d) and 5(e)). Next, we further investigated the regulation of AR on miRNA-224 transcription. The effects of AR overexpression on miRNA-224 transcription were further unveiled. qRT-PCR results showed that miRNA-224 expression was significantly upregulated in granulosa cells transfected

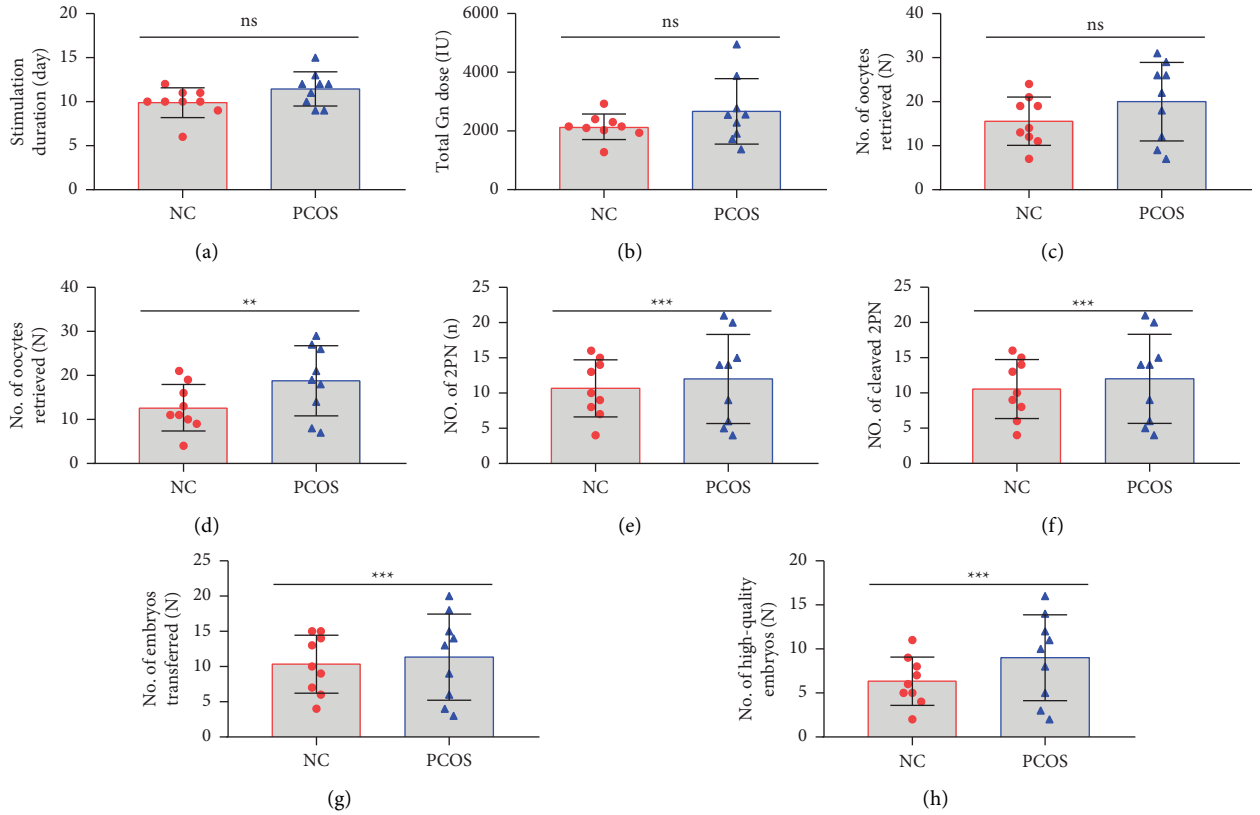

Figure 2: NKPOD changes the pregnancy outcome in PCOS patients. The changes in stimulation duration of Gn (a) and total Gn doses (b) in PCOS patients with NKPOD treatment. (c, d) The effect of NKPOD treatment on the number of oocytes punctured and oocytes retrieved in PCOS patients. The influence of NKPOD treatment on the number of 2PN (e) and 2PN cleavage numbers (f) in PCOS patients with NKPOD treatment. The influence of NKPOD treatment on the number of embryos transferred (g) and number of high-quality embryos (h) in PCOS patients receiving NKPOD administration. ns represents ($P > 0.05$), $^{**}(P < 0.01)$, and $^{***}(P < 0.001)$.

with pcDNA3.1-AR compared with the cells transfected with pcDNA3.1-NC (Figure 5(f)). To sum up, AR is involved in miRNA-224 transcription.

4. Disscussion

Meta-analyses and systematic reviews of observational studies and trials with a small sample size have demonstrated the effectiveness of TCM in improving PCOS's clinical outcomes [12, 22, 23]. Although some components of NKPOD, as a traditional Chinese medicine decoction, have been widely used in the treatment of infertility and have shown some efficacy [23–25], pronounced knowledge gaps remain existed regarding the therapeutic effect of NKPOD on PCOS through systematic research and regulatory mechanisms. In the present study, we discovered that NKPOD administration can alleviate hormone and ovulatory aberrations caused by PCOS, including significantly reducing the levels of BMI, AMH, T, LH, and FSH and increasing the abundance of E2. Furthermore, we discovered that NKPOD treatment contributed to gestation in PCOS patients, increasing the number of oocytes, number of 2PN and 2PN cleavage numbers, and number of embryos transferred and high-quality embryos as well as pregnancy rates. Subsequently, we explored the regulatory mechanism and found that NKPOD inhibited AR expression, which indicates that AR expression is positively correlated with miRNA-224 transcription. In particular, AR directly regulated miRNA-224 transcription through binding with the promoter of miRNA-224. This study provides novel insights into understanding the efficacy and mechanism of NKPOD in improving ovulation disorders and provides an experimental basis for the clinical application of NKPOD in PCOS (Figure 5(g)).

Accumulating evidence indicates that an intrinsic abnormality of early follicle development and arrested follicular growth are critical factors in the pathogenesis of PCOS [8, 26]. Furthermore, hormonal perturbation will have a profound impact on adult endocrine and reproductive status [27, 28]. However, currently, there are still no effective drugs for PCOS, so it is of great significance to find new drugs for the treatment of PCOS. In this study, we sought to investigate the effect of NKPOD on hormonal levels of PCOS patients. Interestingly, our study provided clear evidence that NKPOD administration can alleviate the hormone dysregulation caused by PCOS, including significantly reducing the levels of BMI, AMH, T, LH, and FSH and increasing the abundance of E2. These beneficial effects provide a theoretical basis for the application of NKPOD in PCOS treatment. Subsequently, we first explored the

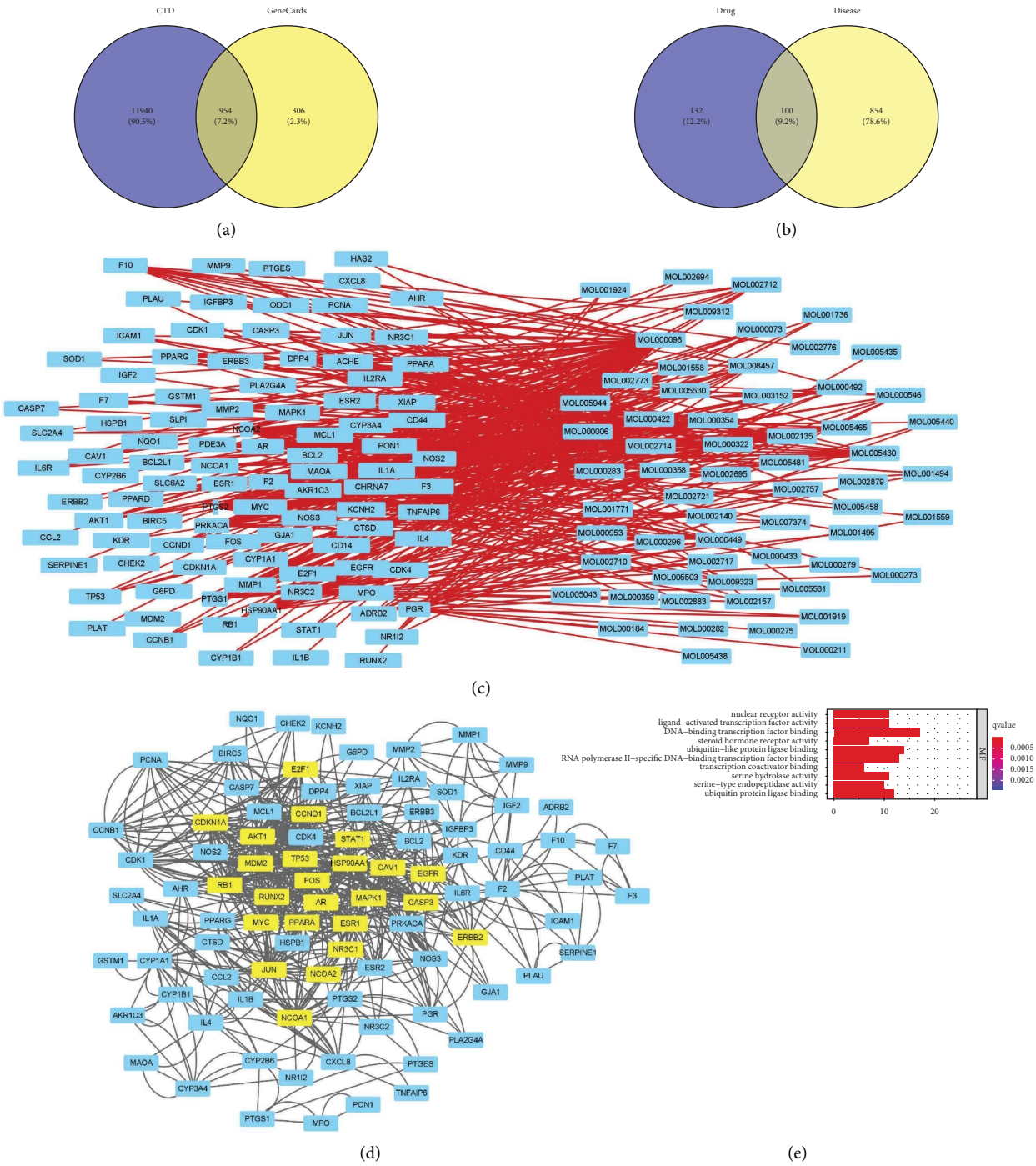

Figure 3: Network pharmacology was constructed to elucidate the candidate targets. (a) The Venn diagram of candidate genes related to PCOS. (b) The Venn diagram of candidate targets related to PCOS and NKPOD. (c) The component-target network. The left nodes represent bioactive compounds. The right nodes represent the intersection targets of PCOS and NKPOD. The edges represent the interactions among them. (d) The protein-protein interaction network. The yellow nodes represent core nodes. (e) The GO enrichment analysis of the 100 putative targets.

benefit of NKPOD on the outcome of IVF-ET/ICSI. Interestingly, although there is no difference in some indicators, including stimulation duration of Gn, total Gn doses, and the number of oocytes punctured and oocytes retrieved, we found that PCOS patients with NKPOD treatment can obtain a higher number of oocytes, 2PN, 2PN cleavage numbers, embryos transferred, and high-quality embryos as well as higher pregnancy rates. At present, despite increased efforts to treat PCOS, the prognosis for improved fertility is usually poor in a considerable number of patients; the beneficial effect indicates that NKPOD is a promising

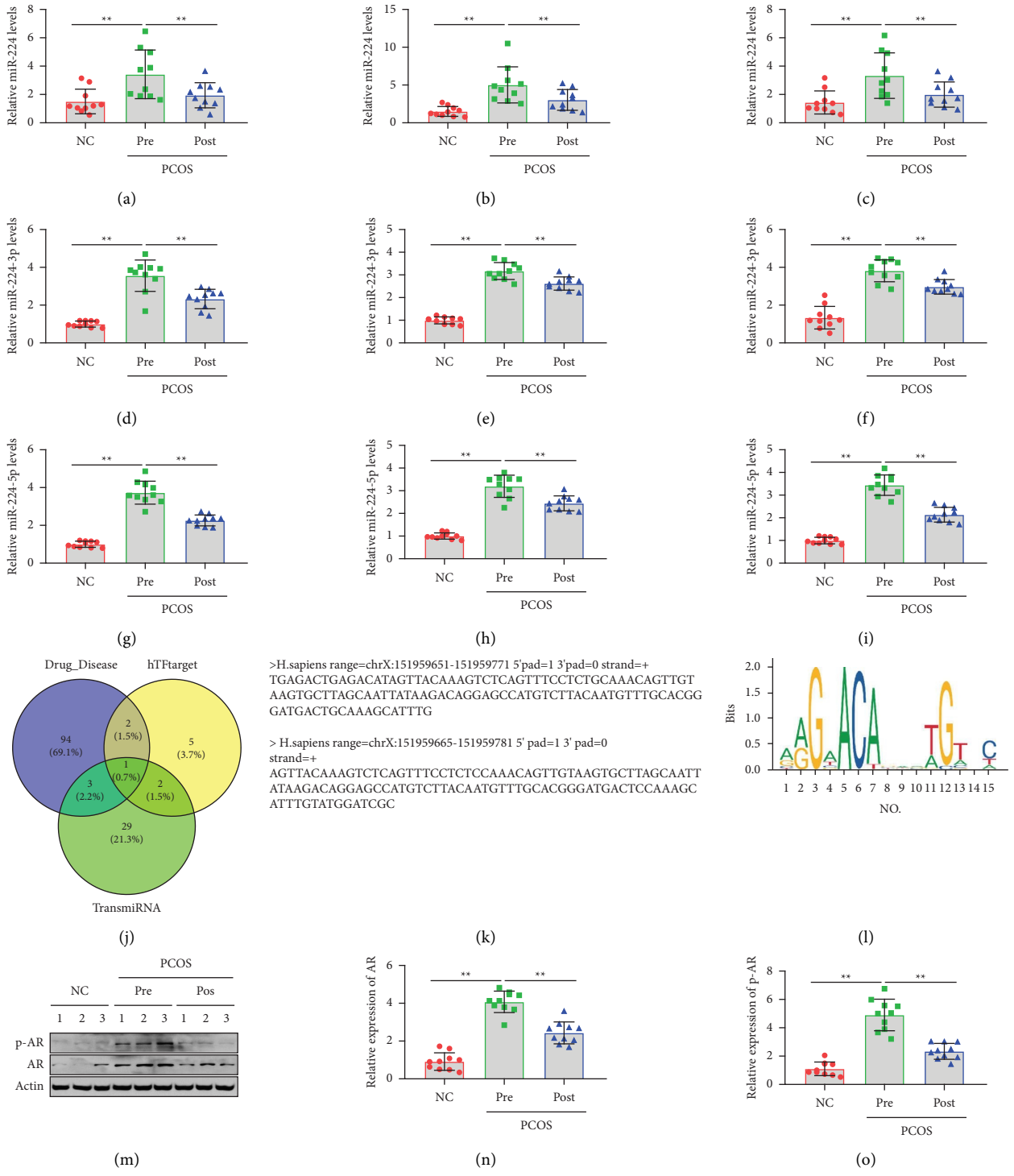

Figure 4: NKPOD regulates miRNA-224 transcription through AR. qRT-PCR detected relative miRNA-224 levels in granulosa cells (a), follicular fluid (b), and blood (c). qRT-PCR detected relative miRNA-224-3p levels in granulosa cells (d), follicular fluid (e), and blood (f). qRT-PCR detected relative miRNA-224-5p levels in granulosa cells (g), follicular fluid (h), and blood (i). (j) The Venn diagram of candidate genes related to NKPOD targets and transcription factors for miRNA-224. (k, l) The DNA motif of AR predicted from JASPAR (https://jaspar.genereg.net/) and 2 predicted binding sites of AR in miRNA-224 promoters. The regulation of NKPOD on AR expression (m, n) and AR phosphorylation (m, o). $^{**}(P < 0.01)$.

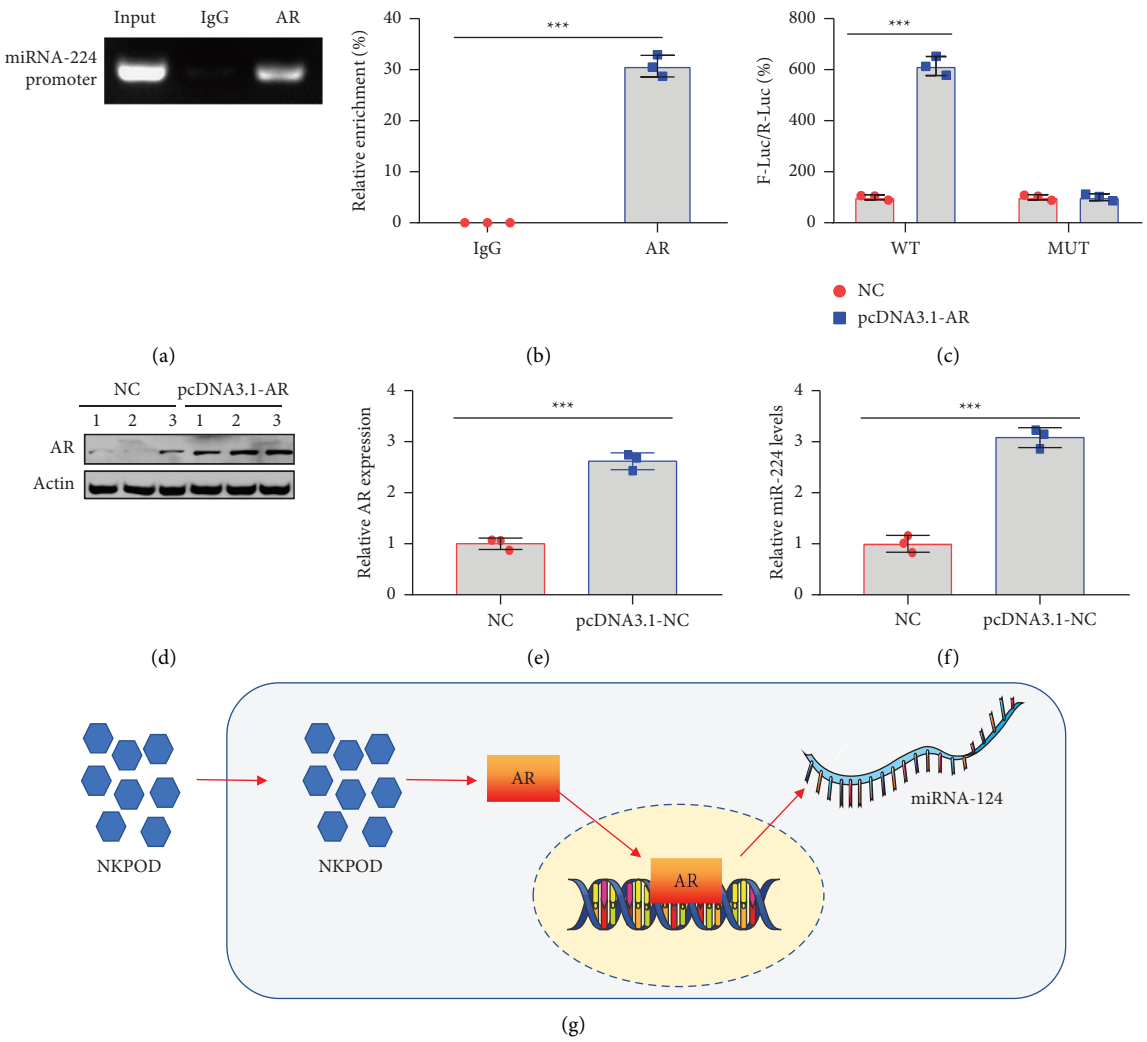

Figure 5: AR is the transcription factor for miRNA-224. (a, b) The affinity of AR in the promoter region of miRNA-224 assessed by the ChIP assay. (c) Luciferase activity detection verified the binding of AR to the miRNA-224 promoter. (d, e) The expression of AR in granulosa cells after transcription of pcDNA3.1-AR. (f) The levels of miRNA-224 in granulosa cells with AR overexpression. (g) A working model of NKPOD on attenuating polycystic ovary syndrome in PCOS patients via activating miRNA-224 transcription through AR. *** ($P < 0.001$).

treatment option for PCOS. Additionally, no obvious adverse reaction and higher pregnancy rates show the superiority of NKPOD treatment of PCOS, for PCOS ovulation disorder infertility TCM provides objective basis.

NKPOD consists of 12 ingredients: Angelicae sinensis Radix, Paeoniae Radix alba, Rhizoma Dioscoreae, Rehmanniae Radix Preparata, Cortex Moutan, Poria, Semen Cuscutae, Dipsaci Radix, Cuscutae Semen, Cornu Cervi, Faeces Trogopterori, and Carthami flos. Although the regulatory targets of some ingredients have been clarified, the regulatory relationship of NKPOD-target-PCOS has not been clarified. In recent years, network pharmacology has attracted global attention. Interestingly, network pharmacology provides an effective method for component screening and prediction of drug targets. In our study, we present the NKPOD-target relationships, which give a dependable result of the NKPOD effects on PCOS. A total of 100 potential targets including 24 core targets were identified to be associated with PCOS. Among the 24 core targets, some of them such as AR [29], epidermal growth factor receptor (EGFR) [30], and RAC-alpha serine/threonine-protein kinase (AKT1) [31] have previously been confirmed through experiments. For example, Jiang et al. [32] reported that miRNA-93 promotes ovarian granulosa cell proliferation through targeting cyclin-dependent kinase inhibitor 1A in PCOS. However, some targets such as peroxisome proliferator-activated receptor alpha and heat shock protein HSP 90-alpha have not yet been confirmed with regard to PCOS through experiments. Therefore, these putative targets that have been

discovered provide a foundation for future research. Interestingly, through GO enrichment analysis, we noted that the 100 putative targets were mainly involved in the regulation of gene transcription. These potential targets and molecular function provide a basis for further research and the feasibility of TCM theory in guiding clinical NKPOD application.

At present, the pathogenesis of PCOS has not been fully elucidated. Changes in miRNAs are obvious pathology in PCOS progression, and miRNAs markers have been used to detect and study this disease [33, 34]. miRNA-224 is one of the u-regulated miRNAs located in an intron of a transforming growth factor-β (TGF-β) responsive gene and gamma-aminobutyric acid receptor subunit epsilon [35, 36]. There are numerous *in vitro* studies that have shown the potential role of miRNA-224 in the ovaries. miRNA-224 has a regulatory effect on cumulus expansion [17, 37]. It has been previously reported that miRNA-224 negatively affected ovulation in the mouse model by decreasing the expression of Ptx3 and Smad4 [32]. Notably, in this study, negative regulation of NKPOD on miRNA-224, miRNA-224-3p, and miRNA-224-5p was noticed. Considering the regulation of NKPOD on putative targets including transcription factors as well as the function of transcription factor activity, we speculated that NKPOD may regulate miRNA-224 abundance by regulating the activity of transcription factors. Using bioinformatic methods, we discovered only one common target (AR), which is related to the transcription factor of miRNA-224, NKPOD targets, and PCOS-related genes. Due to the relationship between AR and PCOS [38], we believe that the regulation of miRNA-224 abundance by NKPOD requires the involvement of AR. As expected, AR was verified as the transcription factor activating miRNA-224 transcription. Mechanism investigation further validated that NKPOD administration eliminated the stability of AR. The combined data elucidate a crucial mechanism of NKPOD in improving ovulation disorder in PCOS patients.

However, we are aware of some limitations in this study. First, the sample size of PCOS patients was relatively limited, and larger population is necessary to validate the role of NKPOD. Furthermore, the regulation of NKPOD on other targets lacks experimental data support, so it will be interesting to study them in the future. In summary, to our knowledge, this is the first report that generally investigates the clinical implication and mechanism of NKPOD in PCOS. The results present that NKPOD improves ovulation disorder in PCOS patients through AR-mediated transcriptional inhibition of miRNA. These findings provide novel insights into understanding the efficacy and mechanism of NKPOD in improving ovulation disorder and provide an experimental basis for the clinical application of NKPOD in PCOS.

Data Availability

The data used to support the findings of this study are available from the corresponding author upon request.

Ethical Approval

This work was approved by the Ethics Committee of the Jiangsu Hospital of Traditional Chinese Medicine (2019NL-KS74).

Consent

Written informed consent was obtained from all participants included in the study.

Conflicts of Interest

The authors declare no conflicts of interest.

Authors' Contributions

YT contributed to the study conception and design. Material preparation, data collection, and analysis were performed by YHG, XLT, PPT, and WTZ. The initial draft of the manuscript was written by YHG and XLT. PPT and WTZ were responsible for data visualisation and literature review. YT contributed to the critical revision of the manuscript. All the authors have read and approved the final manuscript.

Acknowledgments

This work was supported by the grants from the 2018 Jiangsu Province Traditional Chinese Medicine Science and Technology Project (Grant no. YB201818).

Supplementary Materials

Table S1: the components and possible targets of NKPOD. Table S2: the common targets of the GeneCards Database and CTD. Table S3: the common targets related to NKPOD and PCOS. Table S4: GO biological terms. (*Supplementary Materials*)

References

[1] N. X. Jiang and X. L. Li, "The disorders of endometrial receptivity in PCOS and its mechanisms," *Reproductive Sciences*, vol. 29, 2021.

[2] B. Liao, J. Qiao, and Y. Pang, "Central regulation of PCOS: abnormal neuronal-reproductive-metabolic circuits in PCOS pathophysiology," *Frontiers in Endocrinology*, vol. 12, Article ID 667422, 2021.

[3] J. V. Kolhe, A. S. Chhipa, and S. Butani, "PCOS and depression: common links and potential targets," *Reproductive Sciences*, vol. 29, 2021.

[4] C. Tatone, G. Di Emidio, M. Placidi et al., "AGEs-related dysfunctions in PCOS: evidence from animal and clinical research," *Journal of Endocrinology*, vol. 251, no. 2, pp. R1–r9, 2021.

[5] E. Rudnicka, M. Kunicki, A. Calik-Ksepka et al., "Anti-müllerian hormone in pathogenesis, diagnostic and treatment of PCOS," *International Journal of Molecular Sciences*, vol. 22, no. 22, Article ID 12507, 2021.

[6] M. Phylactou, S. A. Clarke, B. Patel et al., "Clinical and biochemical discriminants between functional hypothalamic amenorrhoea (FHA) and polycystic ovary syndrome

(PCOS)," *Clinical Endocrinology*, vol. 95, no. 2, pp. 239–252, 2021.

[7] H. Zhao, C. Xing, J. Zhang, and B. He, "Comparative efficacy of oral insulin sensitizers metformin, thiazolidinediones, inositol, and berberine in improving endocrine and metabolic profiles in women with PCOS: a network meta-analysis," *Reproductive Health*, vol. 18, no. 1, p. 171, 2021.

[8] P. G. Artini, E. Malacarne, V. Tomatis, and A. D. Genazzani, "The relevance of inositols treatment for PCOS before and during ART," *European Review for Medical and Pharmacological Sciences*, vol. 25, no. 14, pp. 4799–4809, 2021.

[9] V. Kandasamy and U. Balasundaram, "Caesalpinia bonduc (L.) Roxb. as a promising source of pharmacological compounds to treat Poly Cystic Ovary Syndrome (PCOS): a review," *Journal of Ethnopharmacology*, vol. 279, Article ID 114375, 2021.

[10] P. Zhu, J. Z. Guan, Q. C. Hai, J. Jin, L. Shi, and L. Hua, "The clinical effectiveness and safety of traditional Chinese medicine Jinfeng pill in adjuvant treatment of infertility with polycystic ovary syndrome: a protocol for systematic review and meta-analysis," *Medicine (Baltimore)*, vol. 101, no. 4, Article ID e28676, 2022.

[11] Y. Chen, X. Chai, Y. Zhao, X. Yang, C. Zhong, and Y. Feng, "Investigation of the mechanism of zishen yutai pills on polycystic ovary syndrome: a network pharmacology and molecular docking approach," *Evidence-based Complementary and Alternative Medicine*, vol. 2021, Article ID 6843828, 14 pages, 2021.

[12] H. Qian, W. Xu, L. Cui et al., "Efficacy of Bushen Huatan Decoction combined with Baduanjin in the treatment of polycystic ovary syndrome with insulin resistance (IR-PCOS), kidney deficiency and phlegm dampness: study protocol for a randomized controlled trial," *Trials*, vol. 22, no. 1, p. 781, 2021.

[13] X. Jiang, Y. Yuan, M. Shi, S. Zhang, M. Sui, and H. Zhou, "Bushen-zhu-yun decoction inhibits granulosa cell apoptosis in rat polycystic ovary syndrome through estrogen receptor α-mediated PI3K/AKT/mTOR pathway," *Journal of Ethnopharmacology*, vol. 288, Article ID 114862, 2022.

[14] Y. Y. Zhang, J. X. Ma, Y. T. Zhu et al., "Investigation of the mechanisms and experimental verification of Cuscuta-Salvia in the treatment of polycystic ovary syndrome (PCOS) via network pharmacology," *Journal of Ovarian Research*, vol. 15, no. 1, p. 40, 2022.

[15] J. Wu and X. Chen, "Acupuncture therapy protects PCOS patients with diabetes by regulating miR-32-3p/PLA2G4A pathway," *Am J Transl Res*, vol. 13, no. 8, pp. 8819–8832, 2021.

[16] D. Yuan, J. Luo, Y. Sun, L. Hao, J. Zheng, and Z. Yang, "PCOS follicular fluid derived exosomal miR-424-5p induces granulosa cells senescence by targeting CDCA4 expression," *Cellular Signalling*, vol. 85, Article ID 110030, 2021.

[17] M. Vahdat-Lasemi, S. Hosseini, V. Jajarmi, B. Kazemi, and M. Salehi, "Intraovarian injection of miR-224 as a marker of polycystic ovarian syndrome declines oocyte competency and embryo development," *Journal of Cellular Physiology*, vol. 234, no. 8, pp. 13858–13866, 2019.

[18] C. Lite, S. S. S. J. Ahmed, W. Santosh, and B. Seetharaman, "Prenatal exposure to bisphenol-A altered miRNA-224 and protein expression of aromatase in ovarian granulosa cells concomitant with elevated serum estradiol levels in F(1) adult offspring," *Journal of Biochemical and Molecular Toxicology*, vol. 33, no. 6, Article ID e22317, 2019.

[19] F. An, X. Wu, Y. Zhang et al., "miR-224 regulates the aggressiveness of hepatoma cells through the IL-6/STAT3/SMAD4 pathway," *Turkish Journal of Gastroenterology*, vol. 32, no. 6, pp. 532–542, 2021.

[20] H. Y. J. C. P. J. Li, "The introduction on Chinese Pharmacopoeia 2015 edition volume II," *Chinese Pharmaceutical Journal*, pp. 1757–1760, 2015.

[21] C. Hnida, E. Engenheiro, and S. Ziebe, "Computer-controlled, multilevel, morphometric analysis of blastomere size as biomarker of fragmentation and multinuclearity in human embryos," *Human Reproduction*, vol. 19, no. 2, pp. 288–293, 2004.

[22] J. X. Ma, M. Ye, K. Ma et al., "Network pharmacology-based strategy for predicting active ingredients and potential targets of coptis chinensis franchin polycystic ovary syndrome," *Evidence-based Complementary and Alternative Medicine*, vol. 2021, Article ID 6651307, 15 pages, 2021.

[23] Z. Wang, K. Nie, H. Su et al., "Berberine improves ovulation and endometrial receptivity in polycystic ovary syndrome," *Phytomedicine*, vol. 91, Article ID 153654, 2021.

[24] Y. Lin, L. Xiang, and X. Li, "Exploring the mechanism of yijing decoction in treating polycystic ovary syndrome by using network pharmacology," *Current Medicinal Chemistry*, vol. 30, no. 21, 2022.

[25] Y. Xu, Y. M. Han, W. Xu, C. Shi, Y. E. Chen, and N. Li, "Clinical efficacy and safety of the Jinfeng pill in the adjuvant treatment of infertility in patients with polycystic ovary syndrome: a systematic review and meta-analysis of randomized controlled trial," *Annals of Palliative Medicine*, vol. 11, no. 1, pp. 352–362, 2022.

[26] B. Crespi, "Variation among human populations in endometriosis and PCOS A test of the inverse comorbidity model," *Evolution, Medicine, and Public Health*, vol. 9, no. 1, pp. 295–310, 2021.

[27] P. Dubey, S. Reddy, S. Boyd et al., "Effect of nutritional supplementation on oxidative stress and hormonal and lipid profiles in PCOS-affected females," *Nutrients*, vol. 13, no. 9, p. 2938, 2021.

[28] K. Ożegowska, S. Plewa, U. Mantaj, L. Pawelczyk, and J. Matysiak, "Serum metabolomics in PCOS women with different body mass index," *Journal of Clinical Medicine*, vol. 10, no. 13, p. 2811, 2021.

[29] T. Vezza, M. Rocha, and V. M. Víctor, "PGK1-AR axis: benefits of a novel actor in PCOS pathology," *EBioMedicine*, vol. 62, Article ID 103110, 2020.

[30] Q. Zheng, Y. Li, D. Zhang et al., "ANP promotes proliferation and inhibits apoptosis of ovarian granulosa cells by NPRA/PGRMC1/EGFR complex and improves ovary functions of PCOS rats," *Cell Death & Disease*, vol. 8, no. 10, p. e3145, 2017.

[31] S. Nekoonam, M. Naji, M. S. Nashtaei et al., "Expression of AKT1 along with AKT2 in granulosa-lutein cells of hyperandrogenic PCOS patients," *Archives of Gynecology and Obstetrics*, vol. 295, no. 4, pp. 1041–1050, 2017.

[32] L. Jiang, J. Huang, L. Li et al., "MicroRNA-93 promotes ovarian granulosa cells proliferation through targeting CDKN1A in polycystic ovarian syndrome," *Journal of Clinical Endocrinology and Metabolism*, vol. 100, no. 5, pp. E729–E738, 2015.

[33] J. Zhang, W. Xu, S. Li, J. Zhang, Y. Shang, and J. Gui, "The role of miRNA-339-5p in the function of vascular endothelial progenitor cells in patients with PCOS," *Reproductive BioMedicine Online*, vol. 44, no. 3, pp. 423–433, 2022.

[34] Y. Qin, Y. Wang, H. Zhao, Z. Yang, and Y. Kang, "Aberrant miRNA-mRNA regulatory network in polycystic ovary syndrome is associated with markers of insulin sensitivity and

inflammation," *Annals of Translational Medicine*, vol. 9, no. 18, p. 1405, 2021.

[35] H. Ren, Y. Shao, X. Ma, L. An, Y. Liu, and Q. Wang, "Interaction of circulating TGFβ regulatory miRNAs in different severity of diabetic kidney disease," *Archives of Physiology and Biochemistry*, vol. 2, no. 11, pp. 1–15, 2022.

[36] Y. Gong, X. Wei, W. Sun et al., "Exosomal miR-224 contributes to hemolymph microbiota homeostasis during bacterial infection in crustacean," *PLoS Pathogens*, vol. 17, no. 8, Article ID e1009837, 2021.

[37] M. Abdalla, H. Deshmukh, S. L. Atkin, and T. Sathyapalan, "MiRNAs as a novel clinical biomarker and therapeutic targets in polycystic ovary syndrome (PCOS): a review," *Life Sciences*, vol. 259, Article ID 118174, 2020.

[38] X. Liu, C. Sun, K. Zou et al., "Novel PGK1 determines SKP2-dependent AR stability and reprograms granular cell glucose metabolism facilitating ovulation dysfunction," *EBioMedicine*, vol. 61, Article ID 103058, 2020.

Hindawi
Evidence-Based Complementary and Alternative Medicine
Volume 2023, Article ID 2919811, 9 pages
https://doi.org/10.1155/2023/2919811

Research Article

Naringin Prevents Cognitive Dysfunction in Aging Rats by Inhibiting Toll-Like Receptor 4 (TLR4)/NF-κB Pathway and Endoplasmic Reticulum Stress

Xiao-jie Dai,[1] Yi Jia,[1] Rui Cao,[2] and Mei-ning Zhou [3]

[1]*Internal Medicine-Neurology, Xi'an Gaoxin Hospital, Shaanxi 710075, China*
[2]*Internal Medicine-Neurology, Qingyang People's Hospital, Qingyang, Gansu 745000, China*
[3]*The Third Affiliated Hospital of Xi'an Medical University, Xi'an, Shaanxi 710068, China*

Correspondence should be addressed to Mei-ning Zhou; zhoumeining0815@sina.com

Received 29 July 2022; Revised 23 August 2022; Accepted 23 September 2022; Published 21 February 2023

Academic Editor: Xueliang Wu

Objective. Naringin is a flavonoid derived from Chinese herbs. According to earlier studies, naringin may have the potential to alleviate aging-induced cognitive dysfunction. Therefore, this study attempted to explore the protective effect and underlying mechanism of naringin on aging rats with cognitive dysfunction. *Methods*. After the construction of a model of aging rats with cognitive dysfunction through subcutaneous injection of D-galactose (D-gal; 150 mg/kg), intragastric administration of naringin (100 mg/kg) was performed for treatment. Behavioral tests, including Morris water maze test (MWM), novel object recognition test (NORT), and fear conditioning test, were used to measure the cognitive function; ELISA and biochemical tests were used to determine the levels of interleukin (IL)-1β, IL-6, monocyte chemoattractant protein-1 (MCP-1), brain-derived neurotrophic factor (BDNF), nerve growth factor (NGF), malondialdehyde (MDA), and glutathione peroxidase (GSH-Px) in the hippocampus of rats in each group, respectively; H&E staining was used to observe the pathological changes in the hippocampus; Western blot was used to examine the expression of toll-like receptor 4 (TLR4)/NF-κB pathway-related proteins and endoplasmic reticulum (ER) stress-related proteins in the hippocampus. *Results*. The model was successfully constructed by subcutaneous injection of D-gal (150 mg/kg). The behavioral test results showed that naringin could ameliorate the cognitive dysfunction and alleviate the histopathological damage of hippocampus. Moreover, naringin significantly improve the inflammatory response (the levels of IL-1β, IL-6, and MCP-1 were decreased), oxidative stress response (MDA level was increased while GSH-Px activity was decreased), and ER stress (the expression of glucose-regulated protein 78 (GRP78), C/-EBP homologous protein (CHOP), and transcription factor 6 (ATF6) expression was downregulated), and increased the levels of neurotrophic factors BDNF and NGF in D-gal rats. Besides, further mechanistic studies revealed the downregulation of naringin on TLR4/NF-κB pathway activity. *Conclusion*. Naringin may inhibit inflammatory response, oxidative stress, and ER stress by downregulating TLR4/NF-κB pathway activity, thereby improving cognitive dysfunction and alleviating histopathological damage of hippocampus in aging rats. Briefly, naringin is an effective drug for the treatment of cognitive dysfunction.

1. Introduction

Despite a normal physiological process, aging raises the risk of diabetes, vasculopathy, hypertension, dyslipidemia, and dementia [1]. Individuals pay more and more attention to the aging issue with the increase in the aging population proportion and the number of aging countries. Studies have suggested that the old behave poorer than the young in memory, attention, visuospatial ability, or executive function [2]. The poor performance of the old is closely related to neurobiological changes in the hippocampus, such as a decrease in new neurons in the subgranular zone of the hippocampus [3]. And neurobiological changes in the hippocampus may be attributed to factors such as chronic inflammation, oxidative stress, and mitochondrial dysfunction. According to several types of research, the brain

falls short of defense mechanisms such as inflammation, oxidative damage, and antioxidant in different regions during aging [4]. Also, studies have demonstrated that inflammatory markers, such as tumor necrosis factor-α (TNF-α) and interleukin (IL)-1β, are elevated in the old and associated with age-related cognitive dysfunction and decline [5]. In addition, aging-induced protein damage and changes in redox status result in the accumulation of proteins with decreased folding abilities and misfolded proteins in the endoplasmic reticulum (ER) cavity, thereby activating a series of signaling pathways. The above process is called ER stress, and generally, the accumulation of ER stress can result in apoptosis [6]. Decreased learning and memory abilities caused by the deterioration of brain function during the physiological process of aging are tightly related to the accumulation of inflammation, oxidative damage, and ER stress.

Traditional Chinese medicine (TCM), a system of traditional medicine in the Chinese healthcare system over thousands of years, plays a crucial role in the treatment of chronic diseases such as lung cancer, coronary heart disease, allergies, diabetes, and infections [7]. Naringin, a natural flavanone glycoside, is mainly present in Chinese herbs, tomatoes, and citrus fruits. Prior studies have stated that the malignant behavior of various cancers, including esophageal cancer [8], gastric cancer [9], colorectal cancer [10], and ovarian cancer [11], was inhibited by naringin. In addition, various biological and pharmacological properties of naringin, such as anti-inflammation, antioxidation, and anti-apoptosis, have also been demonstrated by some studies [12–14]. Moreover, other research has revealed that naringin can effectively reduce the expression of inflammation-related factors. For example, Habauzit et al. claimed that naringin significantly inhibited the expression of proinflammatory cytokine IL-6 in the serum of aging Wistar rats [15]. Also, naringin has antioxidant abilities. Golechha et al. discovered that naringin inhibited oxidative stress in rats with pentylenetetrazole-induced epilepsy by binding to free radicals and regulating GSH levels [16]. Notably, Wang et al. discovered that oral naringin greatly improved learning and memory abilities and alleviated mitochondrial dysfunction in rats given a high-fat diet (HFD) for 20 weeks [17]. The above findings suggest that naringin has the potential to treat aging-induced cognitive dysfunction in old people, but there are few related studies at present. Therefore, based on the model of aging rats with cognitive dysfunction induced by subcutaneous injection of D-galactose (D-gal), the effect and possible mechanism of naringin on these rats were investigated through a series of behavioral tests, biochemical experiments, and other basic studies. And the objective of this paper was to propose novel perspectives for the prevention and improvement of aging-induced cognitive dysfunction.

2. Materials and Methods

2.1. Construction and Processing of the Rat Model. This study was approved by the Ethics Committee of The Third Affiliated Hospital of Xi'an Medical University (XAMU2022-05) and conducted under the approved guidelines. To explore the effect of naringin on cognitive dysfunction in aging rats, we constructed an aging rat model of cognitive dysfunction by subcutaneous injection of D-gal (150 mg/kg) following the method in the study by Garcez et al. [18]. Twenty Wistar rats (weight: 220 ± 20 g) were randomly divided into 4 groups ($n = 5$). In the control group, rats were injected subcutaneously and gavaged with an equal amount of saline. In the naringin gavage (NG) group, rats were injected subcutaneously with an equal amount of saline and gavaged with naringin (100 mg/kg/d, CAS NO. 10236-47-2, MedChemExpress, USA) for 8 weeks. In the D-gal group, after the construction of a model of aging rats with cognitive dysfunction through subcutaneous injection of D-gal (150 mg/kg), rats were treated with intragastric administration of an equal amount of saline. As for the D-gal + NG group, a model of rats with cognitive impairment was established by subcutaneous injection of D-gal (150 mg/kg), and then, rats were gavaged with naringin (100 mg/kg/d) for 8 weeks. At the end of the experimental cycle, the rats were subjected to the Morris water maze test (MWM) and novel object recognition test (NORT), followed by euthanasia. Finally, their hippocampal tissues were collected for subsequent tests.

2.2. Morris Water Maze Test. The MWM test was employed to assess the spatial learning and memory ability of rats in each group. MWM was a circular pool filled with water ($21 \pm 1^{\circ}$C), with a white inner wall, 150 cm diameter, and 50 cm height. The pool was divided into four quadrants labeled with different markers. After the last intervention, the rats were subjected to a training experiment for 4 consecutive days. First, the rats were placed in a water maze without any platforms for adaptive training. Specifically, the rats were allowed to swim freely in the water maze for 120 s, and then, they were taken out and cleaned to minimize the effects of factors such as grasping and water environment. After that, the navigation test was performed as follows. A transparent cylindrical escape platform with a diameter of 10 cm was placed in one of the quadrants randomly, and the surface of the platform was 2 cm from the water surface. Then, the rats facing the pool wall were randomly placed into one of the quadrants, the time of rats finding the platform (escape latency) was recorded, and the recording was stopped after 10 s of rats reaching the platform. If the platform was not found within 120 s, the rats were guided to the platform, and after 10 s, they were taken out. The test was conducted once in the morning and once in the afternoon for a total of 4 days. The escape latency, the number of crossing the intersections of platform quadrants, and the time spent in target quadrants were recorded by a computerized tracking/image analyzer system [19].

2.3. Novel Object Recognition Test. NORT was applied to assess cognitive dysfunction in rats based on the spontaneous tendency of rats to show more interactions with novel objects rather than familiar objects. On the first day of the adjustment phase, each rat was free to explore the open field

(a 55 cm × 55 cm × 38 cm white box) without objects. During the familiarization phase on the second day, each rat was placed in the white box containing two identical objects for 5 min. On the third day, one of the familiar objects was replaced with a novel one, i.e., rats were exposed to a familiar object and a novel object to test their recognition memory. The exploration time of rats to familiar objects (TF) and novel objects (TN) was recorded during each phase, and the recognition index (RI) of finding the novel object was calculated according to the formula of RI = TN/(TF + TN) [20].

2.4. Fear Conditioning Test. Contextual and tone fear conditioning (CFC and TFC) tasks were set to evaluate associative emotional memory, and rats were placed in a conditioning box to receive CFC and TFC training [21]. In the CFC test, rats were placed in a conditioning box with striped walls, grid floors, and bright lights for 5 min, followed by a 20 s of sound (80 dB) stimulation. Subsequently, a 0.8 mA foot shock was given for 3 s, a total of three times; 1 min later, the rats were returned to the cage. After 24 hours, the CFC test was performed. Briefly, the rats were placed again in the conditioning box for 5 min, and in this process, they didn't suffer sound and foot shock stimulation. After 24 hours of CFC testing, TFC testing was conducted. The rats were put in a box with a semicircular white wall and flat floor for 5 min, followed by sound stimulation twice (80 dB, 20 s, interval of 1 min). By the way, during TFC testing, the box was cleaned with 30% acetic acid, and the lamp was turned off. The whole process of the above testing was videotaped for subsequent analysis, the freezing behavior of rats associated with contextual fear memory caused by spontaneous activities and adverse experiences was recorded, and the percentage of freezing behavior time was calculated using Image FZ software.

2.5. ELISA Assay. Hippocampal tissues were isolated from the brain tissues (50 mg) of rats in each group. After the addition of PBS buffer, the tissues were fully homogenized and then centrifuged at 12,000 r/min for 30 min at 4°C to obtain the supernatant. Subsequently, the levels of IL-1β, IL-6, monocyte chemoattractant protein-1 (MCP-1), brain-derived neurotrophic factor (BDNF), and nerve growth factor (NGF) in the hippocampal tissues of rats in each group were measured in accordance with the corresponding ELISA assay kit (Solarbio, China) instructions strictly.

2.6. Malondialdehyde Level and Glutathione Peroxidase Activity Assay. Likewise, hippocampal tissues were isolated from the brain tissues (50 mg) of rats in each group. Then, PBS buffer was added, and the tissues were homogenized thoroughly. After centrifugation at 12,000 r/min for 30 min at 4°C, the supernatant was collected. Next, the levels of malondialdehyde (MDA) and glutathione peroxidase (GSH-Px) in rat hippocampal tissues were measured under the instructions of the biochemical assay kit (Nanjing Jiancheng Bioengineering Institute, China).

2.7. HE Staining. Hippocampal tissues (approximately 0.5 cm around the injury site) from rats in each group were collected. Then, the tissues were fixed in 4% paraformaldehyde for 24 h and embedded in paraffin, and 6 μm thick sections were made. The sections were subjected to dewaxing with xylene, dehydration with graded ethanol, hydration, and staining with HE staining kit (Solarbio, China). After dehydration with alcohol and xylene, the sections were sealed with neutral resin, and finally, histopathological changes of hippocampal tissues in rats were observed under a light microscope (Olympus, Japan), and rated images were collected.

2.8. Western Blot. The total protein was extracted from hippocampal tissues using RIPA lysate (Solarbio, China), followed by the detection of the concentration with a BCA kit (Solarbio, China). Next, 5 × loading buffer was added, and 20 μg of the total protein was boiled. After denaturation, the protein was separated by sodium dodecyl sulfate-polyacrylamide gel electrophoresis (SDS-PAGE). Later, the protein was transferred to a PVDF membrane (Millipore, USA), and the membrane was blocked with 5% skimmed milk powder for 2 to 3 h and then incubated overnight with the primary antibodies (antiglucose-regulated protein 78 (GRP78), anti-C/-EBP homologous protein (CHOP), anti-transcription factor 6 (ATF6), antitoll like receptor 4 (TLR4), anti-NF-κB 65 ($p65$), anti-p-$p65$, antitumor-necrosis-factor-α (TNF-α), anti-β-actin; Cell Signaling Technology, USA). Therefore, the membrane was washed with TBST 3 times and incubated with the secondary antibody (ZSGB-BIO, China) for 1 h at ambient temperature. Again with TBST washing 3 times, ECL chemiluminescent reagent (Biyotime, China) was added to the membrane. Then, the protein was developed by a gel imaging system, and the images were collected. Ultimately, the gray level of the protein bands was analyzed by Image J software, and the relative protein expression was calculated by taking β-actin as an internal reference.

2.9. Data Analysis. All data were expressed as mean ± standard deviation (SD) and visualized and statistically analyzed by GraphPad Prism 9.0 software. A one-way analysis of variance was used for comparison among multiple groups. $P < 0.05$ was deemed as the criterion for the significance of difference.

3. Results

3.1. Naringin Attenuates D-Galactose-Induced Spacial Learning and Memory Dysfunction in Rats. To reveal the effect of naringin on cognitive dysfunction in aging rats, we established an aging rat model with D-gal (150 mg/kg)-induced spacial learning and memory dysfunction. The results showed that, compared with the control group, rats in the D-gal group exhibited prolonged escape latency, reduced number of target quadrant crossing, and shortened time spent in the target quadrant. Besides, the recognition index

(RI), the percentage of time spent exploring familiar and novel objects, and the percentage of freezing time of rats in the D-gal group were significantly lower than the control group, suggesting that the model was successful. Moreover, compared with the D-gal group, rats in the D-gal + NG group showed shortened escape latency, increased number of target quadrant crossing, and prolonged time spent in the target quadrant, as well as a significant increase in the RI, the percentage of time spent exploring familiar and novel objects, and the percentage of freezing time (Figures 1(a)–1(f)). The above outcomes presented that naringin treatment could significantly attenuate D-gal-induced spatial learning and memory dysfunction in rats.

3.2. Naringin Alleviates D-Galactose-Induced Pathological Damage in Rat Hippocampus. The hippocampal tissues from each group were sectioned and stained with HE to directly observe the effect of naringin on D-gal-induced hippocampal histopathology in rats. Specifically, the hippocampal tissues in the D-gal group presented severe neuron and vertebral cell damage, while in the NG group, the cellular structure of the hippocampal tissues of D-gal rats was normal, and only a few cells suffered from karyopyknosis and cytoplasmic vacuolization (Figure 2). The above findings suggested that naringin significantly alleviated D-gal-induced pathological damage in the hippocampal tissues of rats.

3.3. Naringin Attenuates D-Galactose-Induced Inflammatory Response and Oxidative Stress in Rat Hippocampus. The imbalance of inflammatory response and oxidative stress further damaged hippocampal tissues. ELISA and biochemical assays were used to measure the levels of inflammatory factors and oxidative stress substances in the hippocampal tissues of each group. As shown in Figures 3(a)–3(e), the levels of proinflammatory cytokines IL-1β, IL-6, and MCP-1 in the D-gal group were significantly increased compared with those in the control group, while gavage with naringin could markedly inhibit the levels of IL-1β, IL-6, and MCP-1 in the D-gal group (Figures 3(a)–3(c)). As for oxidative stress, the level of MDA in the D-gal group was greatly increased, and the activity of GSH-Px was declined compared with the control group. After NG treatment, the level of MDA was considerably downregulated, and the activity of GSH-Px was restored (Figures 3(d) and 3(e)). In short, naringin could alleviate D-gal-induced inflammatory response and oxidative stress in rat hippocampus.

3.4. Naringin Inhibits D-Galactose-Induced Endoplasmic Reticulum Stress in Rat Hippocampus. ER stress is a marker of impaired hippocampal tissue function. In order to clarify the effect of naringin on D-gal-induced ER stress in rat hippocampal tissues, the expression levels of ER stress-related proteins (GRP78, CHOP, and ATF6) in the hippocampal tissues of rats in each group were examined. According to the experimental data, the expression levels of GRP78, CHOP, and ATF6 in the D-gal group were significantly increased while decreased in the D-gal + NG group (Figures 4(a)–4(d)). Briefly speaking, naringin was able to inhibit D-gal-induced ER stress in rat hippocampal tissues.

3.5. Naringin Increases the Levels of D-Galactose-Induced Neurotrophic Factors in Rat Hippocampus. Neurotrophic factors are essential factors to maintain the normal function of hippocampal tissues. We observed that the levels of BDNF and NGF in the D-gal group were much lower than those in the control group, while after NG treatment, BDNF and NGF levels in the hippocampal tissue of D-gal rats were significantly increased (Figures 5(a) and 5(b)). Briefly, naringin could increase the levels of neurotrophic factors in D-gal-induced rat hippocampal tissues.

3.6. Naringin Inhibits the TLR4/NF-κB Pathway in D-Galactose-Induced Rat Hippocampus. Studies reported that TLR4/NF-κB signaling pathway is associated with cognitive dysfunction caused by various factors [22, 23]. Nevertheless, it is unclear whether it plays a role in alleviating D-gal-induced cognitive dysfunction by naringenin. In order to further reveal the mechanism of naringin protecting rats from D-gal-induced cognitive dysfunction, the expression of TLR4/NF-κB pathway-related proteins was detected by western blot. The results disclosed that, compared with the control group, the protein expression levels of TLR4, p-NF-κB p65, and TNF-α and the ratio of p-NF-κB p65/NF-κB were significantly increased in the D-gal group, while compared with the D-gal group, the D-gal + NG group exhibited decreased TLR4, p-NF-κB p65, TNF-α protein expression levels, and p-NF-κB *p*65/NF-κB ratios (Figures 6(a)–6(d)). The above results indicated that D-gal could significantly activate the TLR4/NF-κB pathway in rat hippocampus, while naringin treatment could inhibit the activation of the TLR4/NF-κB pathway.

4. Discussion

The physiological process of aging involves progressive cognitive loss caused by brain function deterioration, including the decline in learning and memory skills [24]. The D-gal-induced aging model is widely used in antiaging studies due to its aging characteristics such as short life span, cognitive dysfunction, learning and memory dysfunction, and decreased immune function [25]. Moreover, conventional and quantitative D-gal injections in rats may trigger symptoms similar to natural aging [25]. It has been shown that in the D-gal-induced aging model in rats, excessive and long-term D-gal injection leads to excessive production of advanced glycosylation end-products (AGEs) and reactive oxygen species (ROS), which in turn produce intense oxidative stress and chronic inflammatory responses, thereby accelerating aging in rats [26]. Oxidative stress accumulation and chronic low-grade inflammation are considered as hallmarks of aging, which cause damage to neurons and synapses in the brain and eventually lead to impaired cognitive function [27]. Several studies have confirmed that

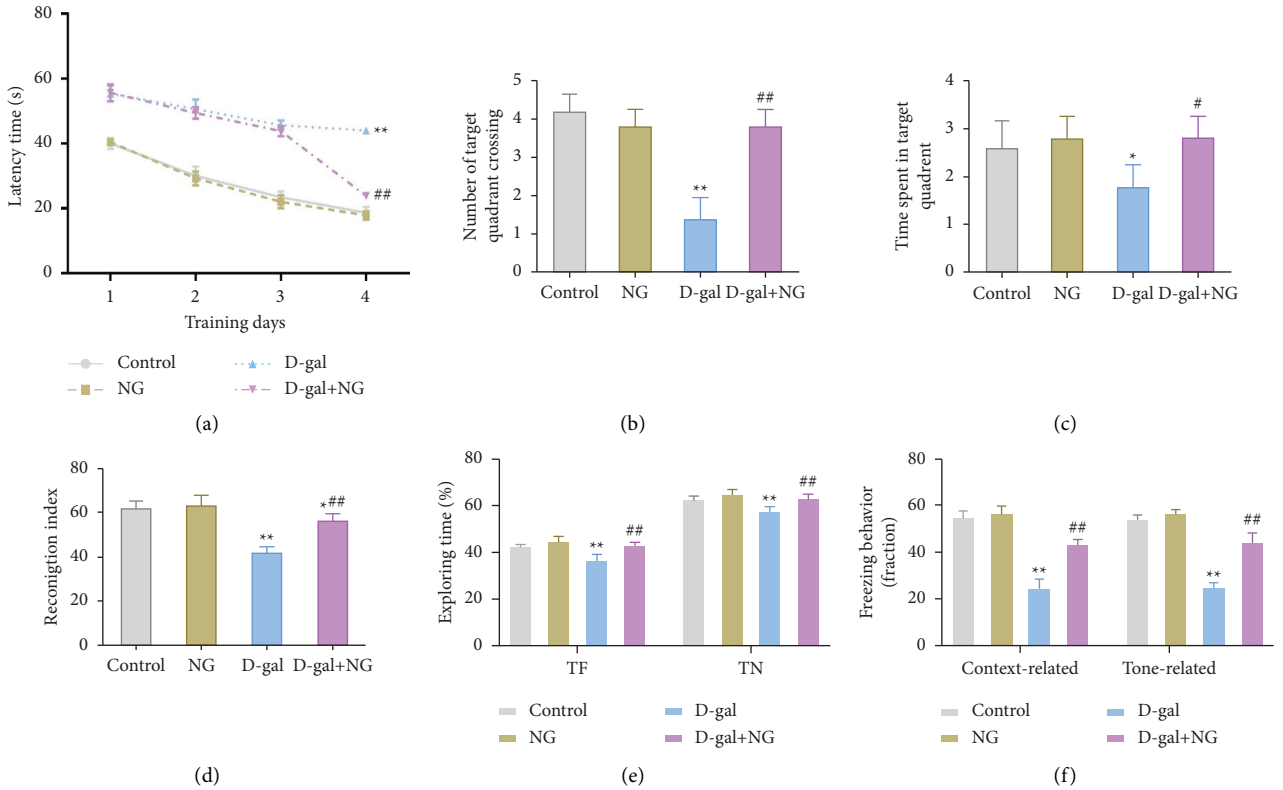

Figure 1: Naringin attenuates D-galactose-induced spatial learning and memory dysfunction in rats. (a)–(c): the effects of naringin on escape latency (a), the number of target quadrant crossing (b), and the time spent in the target quadrant (c) in aging rats observed through the Morris water maze test; (d)–(f): the novel object recognition test was applied to assess the effects of naringin on novel object exploration recognition index (d), percentage of time spent exploring familiar objects and novel objects (e), and percentage of time spent in contextual and context fear conditioning tests (f) in aging rats. $^{*}P < 0.05$, $^{**}P < 0.01$, vs. control; $^{\#}P < 0.05$ and $^{\#\#}P < 0.01$, vs. D-gal.

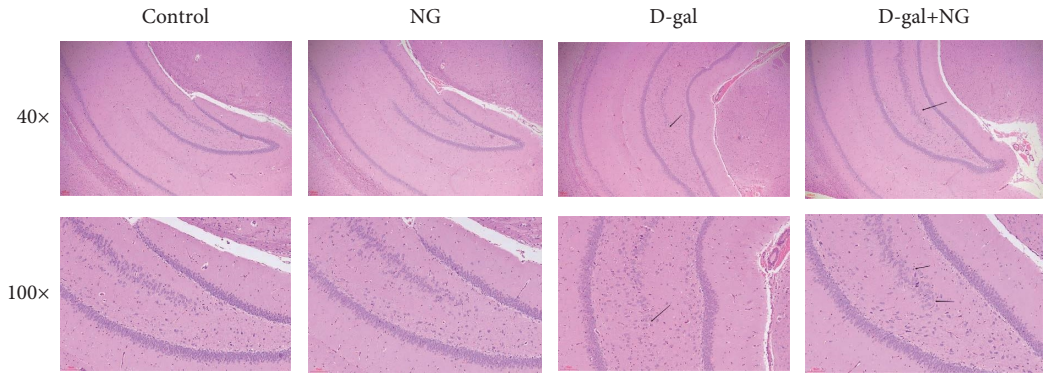

Figure 2: Naringin alleviates D-galactose-induced pathological damage in the rat hippocampus.

oxidative stress factors and proinflammatory factors are accumulated gradually while antioxidant factors and anti-inflammatory factors are markedly downregulated in both hippocampal tissues and serum of aging rats with cognitive dysfunction [28]. In our study, rats were subcutaneously injected with D-gal (150 mg/kg) for the construction of the aging rat model. The behavioral test results revealed that D-gal severely impaired the learning and memory ability and hippocampal tissues of rats, promoted inflammatory response, ER stress, and oxidative stress, and reduced the levels of neurotrophic factors. The above outcomes in this study indicated that an aging rat model of cognitive dysfunction was constructed successfully.

Generally, due to good anti-inflammatory and antioxidant effect, naringin can significantly inhibit the levels of inflammatory factors and oxidative stress in hippocampal tissues [29]. Moreover, as a novel drug for the treatment of Parkinson's disease, naringin activates antiapoptotic programs by inducing the production of neurotrophic substances such as BDNF and vascular endothelial growth factor

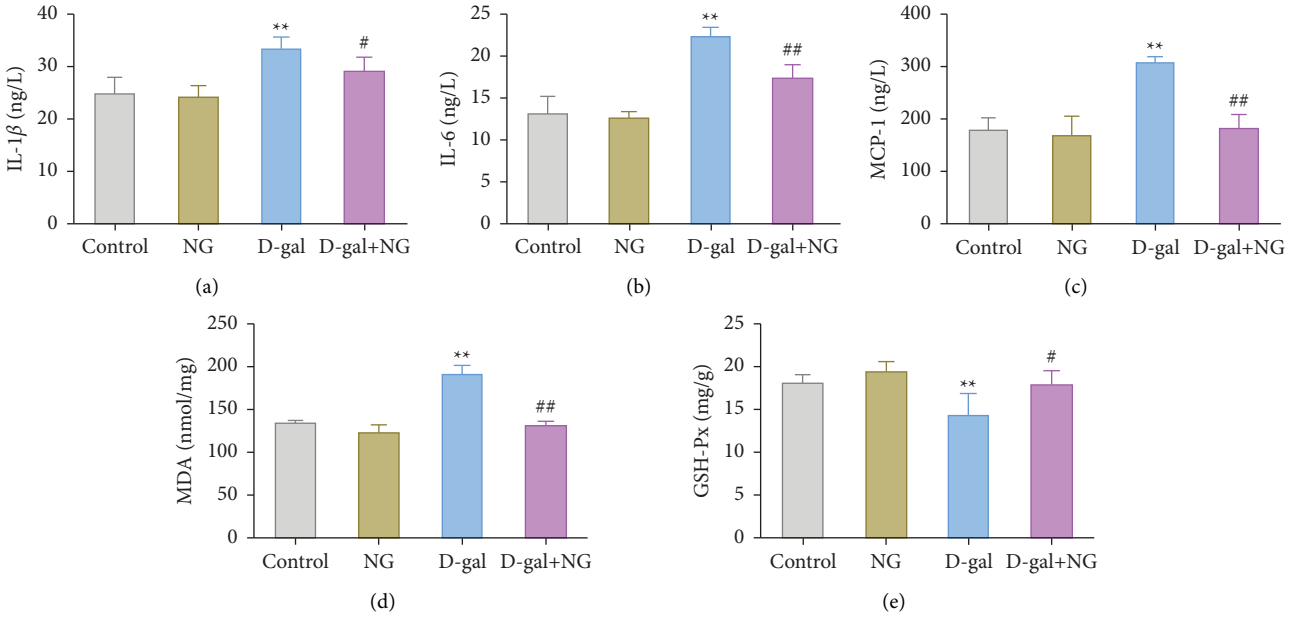

FIGURE 3: Naringin attenuates D-galactose-induced inflammatory response and oxidative stress in the rat hippocampus. (a)–(c): the levels of proinflammatory cytokines IL-1β (a), IL-6 (b), and MCP-1 (c) in the hippocampus of rats in each group detected by ELISA assay; (d)/(e): the levels of oxidative stress substance MDA (d) and the activity of GSH-Px (e) in the hippocampus of rats in each group detected by the biochemical kit; $^{**}P < 0.01$, vs. control; $^{\#}P < 0.05$ and $^{\#\#}P < 0.01$, vs. D-gal.

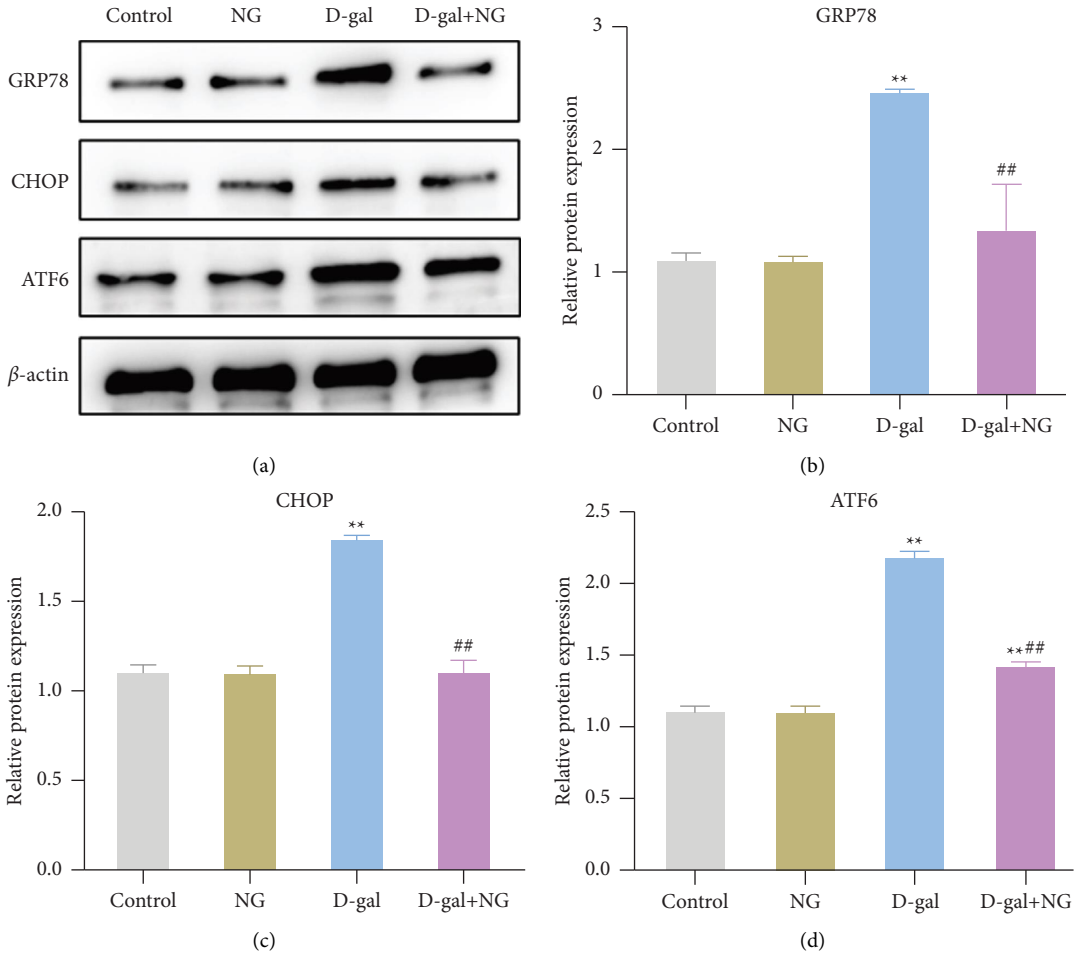

FIGURE 4: Naringin inhibits D-galactose-induced endoplasmic reticulum stress in the rat hippocampus. (a)–(d): the relative protein expression levels of ER stress-related proteins GRP78, CHOP, and ATF6 in the hippocampus of rats in each group detected by western blot; $^{**}P < 0.01$, vs. control; $^{\#\#}P < 0.01$, vs. D-gal.

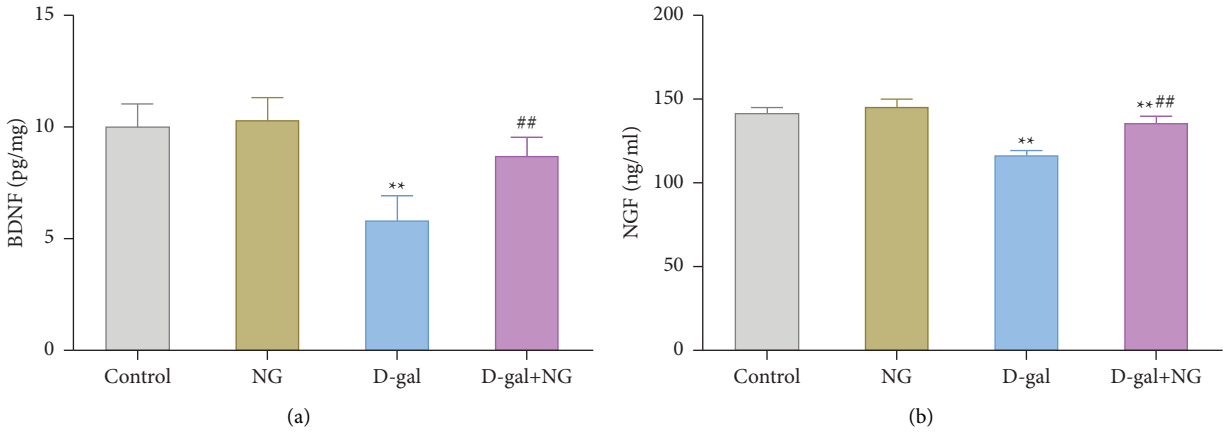

FIGURE 5: Naringin increases the levels of neurotrophic factors in the D-galactose-induced rat hippocampus. The levels of brain-derived neurotrophic factor (BDNF) (a) and nerve growth factor (NGF) (b) in the hippocampus of rats in each group were assessed by ELISA assay; $^{**}P < 0.01$, vs. control; $^{\#\#}P < 0.01$, vs. D-gal.

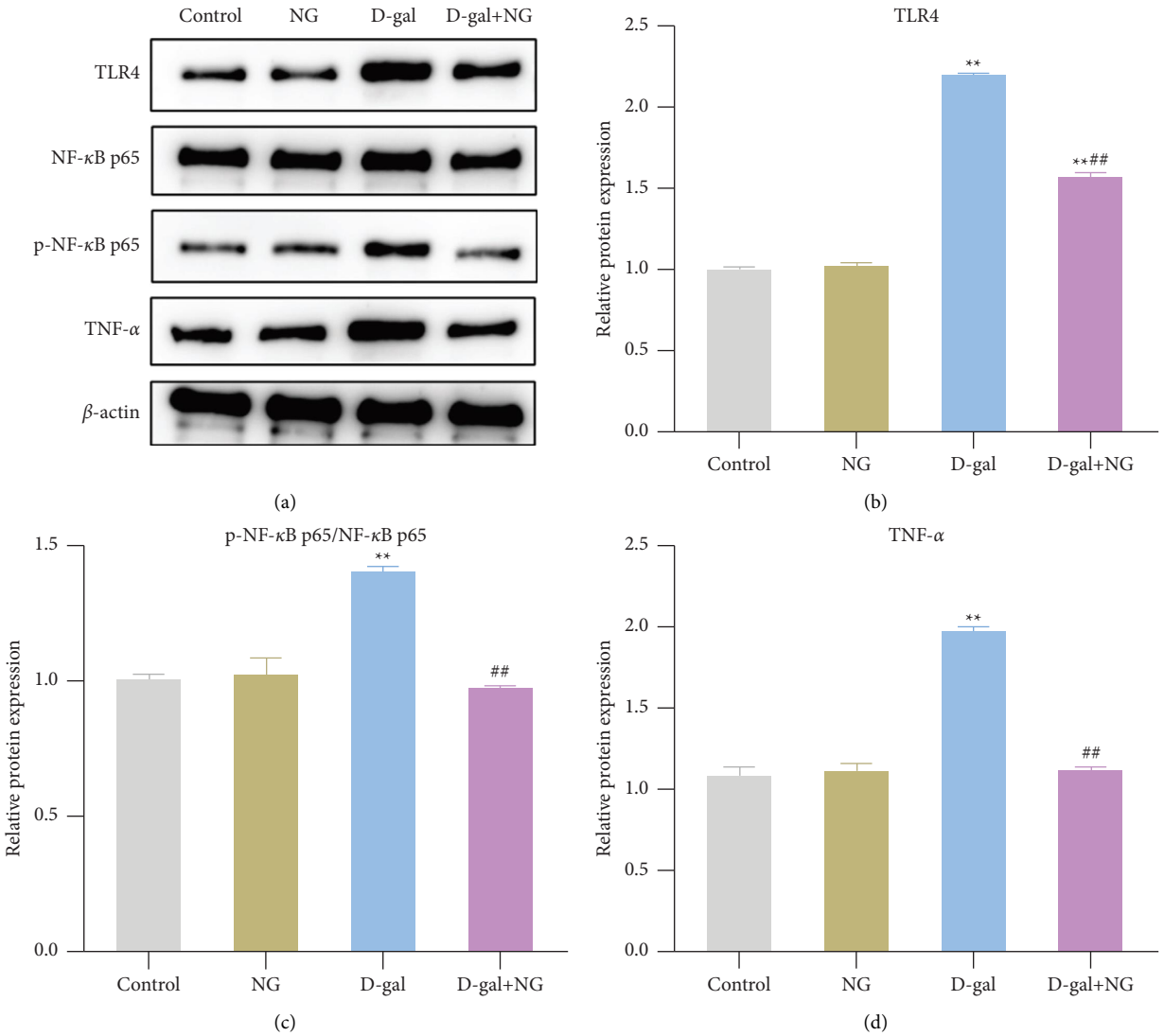

FIGURE 6: Naringin inhibits the TLR4/NF-κB pathway in D-galactose-induced rat hippocampus. (a)–(d): the relative protein expression levels of TLR4/NF-κB pathway-related proteins TLR4, p65 (NF-κB), p-p65 (p-NF-κB), and TNF-α in the hippocampus of rats in each group detected by western blot; $^{**}P < 0.01$, vs. control; $^{\#\#}P < 0.01$, vs. D-gal.

[30]. Intriguingly, in our research, naringin obviously improved the learning and memory abilities of the aging rats. Besides, naringin exerted anti-inflammatory and antioxidant effects by inhibiting the levels of inflammatory cytokines IL-1β, IL-6, and MCP-1 and regulating the levels or activity of oxidative stress-related substances in the hippocampus of aging rats. Furthermore, naringin could notably increase the levels of BDNF and NGF in the hippocampus of D-gal group rats. Ramalingayya et al. discovered that naringin greatly alleviated short-term episodic memory deficits in rats [31]. Jiang et al. pointed out that naringin provided neuroprotection for CCL2-induced cognitive dysfunction in aging rats by attenuating neuronal apoptosis in the hippocampus [32]. In a word, naringin has a good neuroprotective effect.

ER is a vital organelle and a crucial component of the proteostasis network. Aging-caused ER function declines result in the accumulation of the misfolded proteins in the ER cavity, thereby leading to ER stress [33]. GRP78, one of the members of the heat shock protein family in ER cavity, is a hallmark of ER stress [34]. During ER stress, GRP78 binds to unfolded proteins and activates multipartner complexes, then results in the increase of ER protein folding capacity and accumulation of unfolded or misfolded proteins, and finally induces apoptosis [34]. In prior reports, naringin exhibited its inhibition effect on ER stress. For instance, Wang et al. stated that naringin alleviated cerebral ischemia-reperfusion injury in rats by inhibiting ER stress [35]. And Albayrak et al. discovered that naringin could affect ER stress in colon cancer cells through ATF4/CHOP pathway [13]. In our paper, naringin was able to significantly reduce protein levels of GRP78, CHOP, and ATF6 in hippocampal tissues of D-gal rats. All of the above findings suggest that naringin can effectively reduce ER stress in the hippocampus of D-gal aging rats.

TLR4, as a critical receptor for both innate and adaptive immunity, can activate NF-κB signaling and further induce downstream inflammatory response [36]. After activation and translocation to the nucleus, NF-κB induces a series of gene expressions mediating immunity, cell adhesion, inflammation, and apoptosis [37, 38]. Previous research has proved that naringin affects neuronal apoptosis via the TLR4/NF-κB pathway [39]. In our investigation, naringin could significantly downregulate the activity of the TLR4/NF-κB pathway activated by D-gal. Chtourou et al. also claimed that naringin might inhibit TLR4/NF-κB pathway through antioxidation and anti-inflammation [40]. However, our study involved neither the exploration of the specific mechanism of naringin regulating TLR4/NF-κB nor the detection of the activity of additional signaling pathways that may be related to TLR4/NF-B. As a result, it is unclear whether naringin exerts a protective effect by virtue of other signaling pathways, and the mechanism of action of naringin also needs further exploration and validation.

5. Conclusion

In summary, naringin inhibits D-gal-induced inflammatory response, oxidative stress, and ER stress in rats, alleviates pathological damage, and increases the levels of neurotrophic factors in rat hippocampus, thereby alleviating cognitive dysfunction in aging rats. According to further mechanistic studies, naringin may exert its protective effect by inhibiting the activity of the TLR4/NF-κB signaling pathway. In short, naringin is a beneficial option for the treatment of elderly patients with cognitive dysfunction.

Data Availability

The data used to support the findings of this study are available from the corresponding author upon request.

Conflicts of Interest

The authors declare that they have no conflicts of interest.

References

[1] C. Y. Santos, P. J. Snyder, W. C. Wu, M. Zhang, A. Echeverria, and J. Alber, "Pathophysiologic relationship between Alzheimer's disease, cerebrovascular disease, and cardiovascular risk: a review and synthesis," *Alzheimer's and Dementia: Diagnosis, Assessment & Disease Monitoring*, vol. 7, no. 1, pp. 69–87, 2017.

[2] D. Tromp, A. Dufour, S. Lithfous, T. Pebayle, and O. Despres, "Episodic memory in normal aging and Alzheimer disease: insights from imaging and behavioral studies," *Ageing Research Reviews*, vol. 24, pp. 232–262, 2015.

[3] A. Olariu, K. M. Cleaver, and H. A. Cameron, "Decreased neurogenesis in aged rats results from loss of granule cell precursors without lengthening of the cell cycle," *Journal of Comparative Neurology*, vol. 501, no. 4, pp. 659–667, 2007.

[4] C. Gemma, J. Vila, A. Bachstetter, and P. C. Bickford, "Frontiers in neuroscience oxidative stress and the aging brain: from theory to prevention," in *Brain Aging: Models, Methods, and Mechanisms*, D. R. Riddle, Ed., CRC Press/Taylor & Francis Copyright © 2007, Taylor & Francis Group, LLC, Boca Raton, FL, USA, 2007.

[5] J. N. Trollor, E. Smith, E. Agars et al., "The association between systemic inflammation and cognitive performance in the elderly: the Sydney Memory and Ageing Study," *The age*, vol. 34, no. 5, pp. 1295–1308, 2012.

[6] H. M. Zeeshan, G. H. Lee, H. R. Kim, and H. J. Chae, "Endoplasmic reticulum stress and associated ROS," *International Journal of Molecular Sciences*, vol. 17, no. 3, p. 327, 2016.

[7] J. Huang and F. Lei, "Research progress of traditional Chinese medicine to treat Alzheimer′s disease," *China Journal of Chinese Medicine*, vol. 45, no. 5, pp. 989–1006, 2013.

[8] F. Yang, T. Jiang, L. Zhang, Y. Qi, and Z. Yang, "Naringin inhibits the proliferation and invasion of Eca109 esophageal cancer cells and promotes its apoptosis by blocking JAK/STAT signal pathway," *Xi Bao Yu Fen Zi Mian Yi Xue Za Zhi*, vol. 37, no. 12, pp. 1085–1091, 2021.

[9] S. Raha, S. M. Kim, H. J. Lee et al., "Naringin induces lysosomal permeabilization and autophagy cell death in AGS gastric cancer cells," *American Journal of Chinese Medicine*, vol. 48, no. 3, pp. 679–702, 2020.

[10] D. Albayrak, O. Doğanlar, S. Erdoğan et al., "Naringin combined with NF-κB inhibition and endoplasmic reticulum stress induces apoptotic cell death via oxidative stress and the PERK/eIF2α/ATF4/CHOP Axis in HT29 colon cancer cells," *Biochemical Genetics*, vol. 59, no. 1, pp. 159–184, 2021.

[11] H. Zhu, X. Zou, S. Lin, X. Hu, and J. Gao, "Effects of naringin on reversing cisplatin resistance and the Wnt/β-catenin pathway in human ovarian cancer SKOV3/CDDP cells," *Journal of International Medical Research*, vol. 48, no. 10, Article ID 30006051988786, 2020.

[12] H. Zhao, M. Liu, H. Liu, R. Suo, and C. Lu, "Naringin protects endothelial cells from apoptosis and inflammation by regulating the Hippo-YAP Pathway," *Bioscience Reports*, vol. 40, no. 3, Article ID 20193431, 2020.

[13] B. Salehi, P. V. T. Fokou, M. Sharifi-Rad et al., "The therapeutic potential of naringenin: a review of clinical trials," *Pharmaceuticals*, vol. 12, no. 1, Article ID 12010011, 2019.

[14] E. Hernández-Aquino and P. Muriel, "Beneficial effects of naringenin in liver diseases: molecular mechanisms," *World Journal of Gastroenterology*, vol. 24, no. 16, pp. 1679–1707, 2018.

[15] V. Habauzit, S. M. Sacco, A. Gil-Izquierdo et al., "Differential effects of two citrus flavanones on bone quality in senescent male rats in relation to their bioavailability and metabolism," *Bone*, vol. 49, no. 5, pp. 1108–1116, 2011.

[16] M. Golechha, V. Sarangal, J. Bhatia, U. Chaudhry, D. Saluja, and D. S. Arya, "Naringin ameliorates pentylenetetrazol-induced seizures and associated oxidative stress, inflammation, and cognitive impairment in rats: possible mechanisms of neuroprotection," *Epilepsy and Behavior*, vol. 41, pp. 98–102, 2014.

[17] D. Wang, J. Yan, J. Chen, W. Wu, X. Zhu, and Y. Wang, "Naringin improves neuronal insulin signaling, brain mitochondrial function, and cognitive function in high-fat diet-induced obese mice," *Cellular and Molecular Neurobiology*, vol. 35, no. 7, pp. 1061–1071, 2015.

[18] M. L. Garcez, R. C. S. Cassoma, F. Mina et al., "Folic acid prevents habituation memory impairment and oxidative stress in an aging model induced by D-galactose," *Metabolic Brain Disease*, vol. 36, no. 2, pp. 213–224, 2021.

[19] X. Ma, M. Song, Y. Yan et al., "Albiflorin alleviates cognitive dysfunction in STZ-induced rats," *Aging (Albany NY)*, vol. 13, no. 14, pp. 18287–18297, 2021.

[20] H. Scholtzova, E. Do, S. Dhakal et al., "Innate immunity stimulation via toll-like receptor 9 ameliorates vascular amyloid pathology in tg-SwDI mice with associated cognitive benefits," *Journal of Neuroscience*, vol. 37, no. 4, pp. 936–959, 2017.

[21] D. Moreira-Silva, D. C. Carrettiero, A. S. A. Oliveira et al., "Anandamide effects in a streptozotocin-induced alzheimer's disease-like sporadic dementia in rats," *Frontiers in Neuroscience*, vol. 12, p. 653, 2018.

[22] J. Shi, X. Zou, K. Jiang, and F. Wang, "SIRT1 mediates improvement of cardiac surgery-induced postoperative cognitive dysfunction via the TLR4/NF-κB pathway," *World Journal of Biological Psychiatry*, vol. 21, no. 10, pp. 757–765, 2020.

[23] X. Jin, M. Y. Liu, D. F. Zhang et al., "Baicalin mitigates cognitive impairment and protects neurons from microglia-mediated neuroinflammation via suppressing NLRP3 inflammasomes and TLR4/NF-κB signaling pathway," *CNS Neuroscience and Therapeutics*, vol. 25, no. 5, pp. 575–590, 2019.

[24] Z. Ungvari, S. Tarantini, A. J. Donato, V. Galvan, and A. Csiszar, "Mechanisms of vascular aging," *Circulation Research*, vol. 123, no. 7, pp. 849–867, 2018.

[25] K. F. Azman and R. Zakaria, "D-Galactose-induced accelerated aging model: an overview," *Biogerontology*, vol. 20, no. 6, pp. 763–782, 2019.

[26] F. Ullah, T. Ali, N. Ullah, and M. O. Kim, "Caffeine prevents d-galactose-induced cognitive deficits, oxidative stress, neuroinflammation and neurodegeneration in the adult rat brain," *Neurochemistry International*, vol. 90, pp. 114–124, 2015.

[27] L. E. B. Bettio, L. Rajendran, and J. Gil-Mohapel, "The effects of aging in the hippocampus and cognitive decline," *Neuroscience & Biobehavioral Reviews*, vol. 79, pp. 66–86, 2017.

[28] C. J. Chen, F. C. Cheng, S. L. Liao, W. Y. Chen, N. N. Lin, and J. S. Kuo, "Effects of naloxone on lactate, pyruvate metabolism and antioxidant enzyme activity in rat cerebral ischemia/reperfusion," *Neuroscience Letters*, vol. 287, no. 2, pp. 113–116, 2000.

[29] K. H. Jeong, U. J. Jung, and S. R. Kim, "Naringin attenuates autophagic stress and neuroinflammation in kainic acid-treated Hippocampus in vivo," *Evid Based Complement Alternat Med*, vol. 2015, Article ID 354326, 15 pages, 2015.

[30] W. Rong, J. Wang, X. Liu et al., "Naringin treatment improves functional recovery by increasing BDNF and VEGF expression, inhibiting neuronal apoptosis after spinal cord injury," *Neurochemical Research*, vol. 37, no. 8, pp. 1615–1623, 2012.

[31] G.V. Ramalingayya, M. Nampoothiri, and P.G. Nayak, "Naringin and rutin alleviates episodic memory deficits in two differentially challenged object recognition tasks," *Pharmacognosy Magazine*, vol. 12, no. 45, pp. 63–70, 2016.

[32] J. Y. Long, J. M. Chen, Y. J. Liao, Y. J. Zhou, B. Y. Liang, and Y. Zhou, "Naringin provides neuroprotection in CCL2-induced cognition impairment by attenuating neuronal apoptosis in the hippocampus," *Behavioral and Brain Functions*, vol. 16, no. 1, p. 4, 2020.

[33] A. Baiceanu, P. Mesdom, M. Lagouge, and F. Foufelle, "Endoplasmic reticulum proteostasis in hepatic steatosis," *Nature Reviews Endocrinology*, vol. 12, no. 12, pp. 710–722, 2016.

[34] B. M. Gardner, D. Pincus, K. Gotthardt, C. M. Gallagher, and P. Walter, "Endoplasmic reticulum stress sensing in the unfolded protein response," *Cold Spring Harbor Perspectives in Biology*, vol. 5, no. 3, Article ID 13169, 2013.

[35] L. Wang, Z. Zhang, and H. Wang, "Naringin attenuates cerebral ischemia-reperfusion injury in rats by inhibiting endoplasmic reticulum stress," *Translational Neuroscience*, vol. 12, no. 1, pp. 190–197, 2021.

[36] M. Yamamoto, S. Sato, H. Hemmi et al., "TRAM is specifically involved in the Toll-like receptor 4-mediated MyD88-independent signaling pathway," *Nature Immunology*, vol. 4-, no. 11, pp. 1144–1150, 2003.

[37] S. Vallabhapurapu and M. Karin, "Regulation and function of NF-κB transcription factors in the immune system," *Annual Review of Immunology*, vol. 27, no. 1, pp. 693–733, 2009.

[38] W. Sun, Y. Gao, X. Yu et al., "Psoriasis 1' reduces psoriasis-like skin inflammation by inhibiting the VDR-mediated nuclear NF-κB and STAT signaling pathways," *Molecular Medicine Reports*, vol. 18, no. 3, pp. 2733–2743, 2018.

[39] H. Wang, Y. S. Xu, M. L. Wang et al., "Protective effect of naringin against the LPS-induced apoptosis of PC12 cells: implications for the treatment of neurodegenerative disorders," *International Journal of Molecular Medicine*, vol. 39, no. 4, pp. 819–830, 2017.

[40] Y. Chtourou, B. Aouey, M. Kebieche, and H. Fetoui, "Protective role of naringin against cisplatin induced oxidative stress, inflammatory response and apoptosis in rat striatum via suppressing ROS-mediated NF-κB and P53 signaling pathways," *Chemico-Biological Interactions*, vol. 239, pp. 76–86, 2015.

Hindawi
Evidence-Based Complementary and Alternative Medicine
Volume 2023, Article ID 5628551, 6 pages
https://doi.org/10.1155/2023/5628551

Research Article

Role of Laryngopharyngeal Reflux Changes in Children with Adenoid Hypertrophy: A Randomized Controlled Prospective Study

Yu Zhou,[1] Ruixia Ma,[2] Jiangbo Luo,[3] Zhikai Wang,[1] and Pei Yang[1]

[1]*Department of Otorhinolaryngology Head and Neck Surgery, General Hospital of Ningxia Medical University, Yinchuan, Ningxia 750001, China*
[2]*Department of Otorhinolaryngology Head and Neck Surgery, The First People's Hospital of Yinchuan, Yinchuan, Ningxia 750001, China*
[3]*Department of Otorhinolaryngology Head and Neck Surgery, Ningxia Wuzhong Hongsipu District People's Hospital, Wuzhong, Ningxia 750001, China*

Correspondence should be addressed to Pei Yang; yangpei2698@163.com

Received 1 August 2022; Revised 7 September 2022; Accepted 12 October 2022; Published 6 February 2023

Academic Editor: Xueliang Wu

Objectives. This prospective randomized controlled analysis aimed to assess the changes in laryngopharyngeal reflux (LPR) in children with adenoid hypertrophy (AH). Study design: a prospective, randomized, and controlled analysis. *Methods*. The reflux symptom index (RSI) and the reflux finding score (RFS) scores were used to evaluate the laryngopharyngeal reflux changes in children diagnosed with adenoid hypertrophy. The pepsin concentration in salivary samples was examined, and the positive pepsin was used to assess the sensitivity and specificity of RSI, RFS, and RSI combined with RFS in forecasting LPR. *Results*. In 43 children with AH, the sensitivity of the RSI and RFS scale (used alone or in combination) in diagnosing pharyngeal reflux in children with adenoid hypertrophy was lower. Pepsin expression was identified in 43 items of salivary samples, with a total positive rate of 69.77%, most of which were optimistic. The expression level of pepsin was positively correlated with the grade of adenoid hypertrophy ($r = 0.576$, $P < 0.01$). Based on the positive rate of pepsin, we found that the sensitivity and specificity of RSI and RFS were 5.77%, 35.03%, and 91.74%, 55.89%. Moreover, there was a noticeable distinction in the number of acid reflux episodes between the LPR-positive and LPR-negative groups. *Conclusion*. There is a special connection between LPR change and children's AH. LPR exerts a crucial role in the progression of children's AH. Because of the low sensitivity of RSI and RFS, it is not suitable for LPR children to choose AH.

1. Introduction

Adenoid hypertrophy (AH) is one of the most common respiratory diseases in children. The incidence rates of AH in children and adolescents range from 40 to 71% [1]. The main clinical symptoms of AH are snoring, mouth-open breathing, nasal congestion, and so on. Remarkably, it has been shown that long mouth-open breathing may lead to an "adenoid face" [2]. Adenoids are the immune organs of the body, containing lymphocytes at different stages of development [3]. Adenoid hypertrophy may block the eustachian tube's posterior nostril and pharyngeal orifice, leading to diseases of the adjacent organs [4]. One of the most critical complications of AH is obstructive sleep apnea (OSA), which has a significant impact on children's growth and learning [5]. Therefore, AH has been paid more and more attention by clinicians and parents, striving for early diagnosis and treatment.

Laryngopharyngeal reflux (LPR) is an upper respiratory tract (UAT) disease, which is related to the reflux of gastric or duodenal contents, resulting in morphological changes of UAT [6]. LPR causes damage and structural changes to laryngeal epithelial mucosa through repeated stimulation of the throat mucosa by gastric acid, pepsin, and bile acid in the

gastric contents [7]. Emerging pieces of evidence suggests that 5%–10% of patients in the otolaryngology department have symptoms of LPR [8]. Recent studies have shown that LPR might be one of the pathogenic factors for adenoid hypertrophy in children [9]. A recent study studied 30 children with adenoidal hypertrophy and found that gastroesophageal reflux in infants under 1-year-old was 88% and 32% for infants under one-year-old [10]. Another group reported that the prevalence of LPR was 46.7% in 30 children with adenoidal hypertrophy, which is much higher in the control group [11]. Similarly, it has been found that the reflux substances such as gastric acid and pepsin might act as antigens to stimulate the immune response of adenoid lymphoid tissue, resulting in AH [12]. However, the study on the laryngopharyngeal reflux changes in children's adenoid hypertrophy is mainly unknown.

In this study, the expression of pepsin in adenoid tissue was detected to investigate the correlation between adenoid hypertrophy and pharyngeal reflux change. The possibility and accuracy of the RSI and RFS in predicting the correlation between children's adenoid hypertrophy and LPR change were assessed.

2. Materials and Methods

2.1. Clinical Data. Children with adenoidal hypertrophy (nasal obstruction >50%) in the department of otorhinolaryngology in the General Hospital of Ningxia Medical University were selected for the study. Inclusion criteria were as follows: Nasal endoscopy showed adenoid grade III~IV, mouth-open breathing, snoring, recurrent or chronic otitis media, or sinusitis caused by adenoid hypertrophy. Exclusion criteria were follows: (1) Antacid drugs that have been used in the recent three months; (2) suffering from immune system diseases or other severe system diseases; (3) upper respiratory tract infection occurred within two weeks; and (4) long-term use of antibiotics, hormones, and other drugs in the recent three months. This study was approved by the Ethics Committee of the General Hospital of Ningxia Medical University. All experimental samples were obtained and used with the written consent of the patient's family.

2.2. Electronic Nasopharyngoscopy. All children underwent electronic nasopharyngoscopy before the operation, and adenoid hypertrophy was divided into four grades according to the grading method proposed by Cassano and Gelardi [13]. Level I: nasal cavity ≤25% after hypertrophic adenoid obstruction; Level II: 26%–50% of nostrils after hypertrophic adenoids block; Level III: 51%–75% of nostrils after hypertrophic adenoids block; and Level IV: 76%–100% of nostrils after hypertrophic adenoids block. Hypertrophy of grade III ~ IV with clinical symptoms is adenoidal hypertrophy.

2.3. RFS and RSI Scores. The RSI score developed by Belafsky was filled in by the family members (young children) or children (older children). Each item was divided into 0–5 points according to the throat symptoms, and the total score >13 points were positive; otherwise, it was negative. Two doctors independently scored the physical signs under the electronic laryngoscope. According to the RFS scale developed by Belafsky, the total score >7 was positive; otherwise, it was negative.

2.4. Detection of Pepsin Concentration in Saliva. Saliva was collected from the patients who participated in the study. Patients were offered 30 mL of germ-free pliable pipes to collect saliva. Pliable pipes were centrifuged for 10 min at 5000 rpm, collected the supernatant, and added to the human pepsin kit (Yonghui Biotechnology Co., Ltd.). Salivary samples were examined using an automatic enzyme labeling instrument (Thermo). Sixteen ng/ml was used as the critical value to consider the positive pepsin of salivary samples.

2.5. Statistical Analysis. SPSS 22.0 software was used for data processing. Continuous data were expressed as mean ± standard deviation if normally distributed and as median or else. A T-test is used for normal distribution and homogeneity of variance, and the Wilcoxon test is used for otherwise. Spearman correlation analysis is selected for nonbivariate normal distribution data. The statistically significant value is $P < 0.05$.

3. Results

3.1. RSI Scores in Children with Adenoidal Hypertrophy. Among 43 children with AH, 21 cases (48.8%) had grade III hypertrophy, and 22 cases (51.2%) had grade IV hypertrophy. Among them, 2 cases (4.7%) had RSI >13 points, 14 cases (32.6%) had RFS >7 points, and 1 case was positive in both scores. According to the RSI scores, the symptoms of 43 children with AH included: hoarseness or dysphonia in 5 cases (11.6%), excessive sputum or nasal regurgitation in 24 cases (55.8%), cough after eating or lying down in 17 cases (35.9%), throat clearing in 25 cases (58.1%), dyspnea in 4 cases (9.3%), annoying cough in 23 cases (53.5%), heartburn, chest pain, and stomach pain in 2 cases (4.7%, Table 1).

3.2. RFS Scores in Children with Adenoidal Hypertrophy. According to the RFS scores, 43 children with adenoidal hypertrophy showed symptoms under the electronic laryngoscope: 5 cases (11.6%) of pseudovocal fold groove, 10 cases (23.3%) of partial or complete disappearance of the laryngeal chamber, 6 cases (13.9%) of diffuse erythema of laryngeal cavity, 12 cases (27.9%) of vocal cord edema, 23 cases (53.5%) of mucus attachment in the larynx, 6 cases (13.9%) of in diffuse laryngeal edema, 7 cases (16.3%) of in thickening of posterior commissural mucosa, and 0 cases (0%) of granuloma (Table 2).

3.3. Correlation Analysis of Adenoidal Hypertrophy and Pepsin Expression. Pepsin, a reliable marker for diagnosing laryngeal reflux, has been abundantly recognized in various diseases, such as vocal cord polyps in adults and laryngeal malacia in children [12]. In this study, the expression of

Table 1: RSI scale.

Symptom	Cases	Proportion (%)
Hoarseness or dysphonia	5	11.6
Excessive sputum or nasal mucus reflux	24	55.8
Cough after eating or lying down	17	35.9
Dyspnea or recurrent asphyxia	4	9.3
Foreign body sensation in the throat	25	58.1
Heartburn, chest pain, stomach pain	2	4.7
Bad for swallowing food, water, or tablets	10	23.3
Annoying cough	23	53.5
Throat clearing	25	58.1

Table 2: RFS scales (electronic laryngoscopy of children).

Laryngoscopic appearance	Cases	Proportion (%)
Pseudovocal groove exists	5	11.6
Partial or complete disappearance of laryngeal chamber	10	23.3
Diffuse erythema of laryngeal cavity	6	13.9
Edema of the vocal cord	12	27.9
Mucus attachment in the larynx	23	53.5
Diffuse laryngeal edema	6	13.9
Thickening of posterior commissural mucosa	7	16.3
Granuloma	0	0

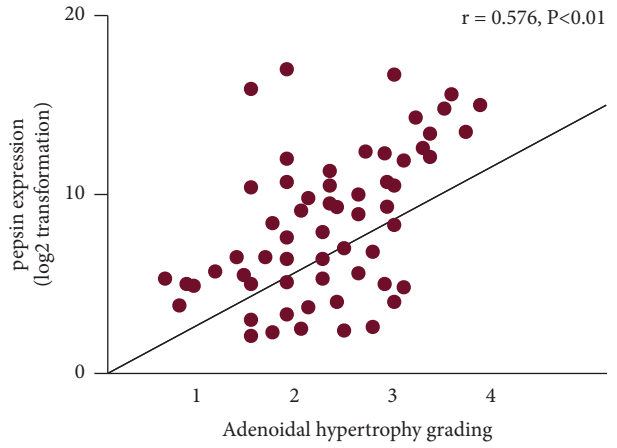

Figure 1: The relationship between AH grading and pepsin expression.

pepsin in salivary samples was detected. Based on the thresholds of 16 ng/mL, the prevalence of positive pepsin was markedly increased in LPR (+) group compared with that in the LPR (−) group ($P < 0.05$). Furthermore, the pepsin concentration was markedly enhanced in the LPR (+) group compared with that in the LPR (−) group ($P < 0.05$). In 43 cases of salivary samples, the total positive rate of pepsin is 69.77%, of which 7 cases (16.28%) were strongly positive, 13 cases (30.23%) were positive, 9 cases (20.93%) were weakly positive, and 13 cases (30.23%) were negative. Spearman's correlation analysis showed that the higher the grade of AH, the higher the pepsin expression intensity (Figure 1, Table 3; $r = 0.576$, $P < 0.01$).

Table 3: Comparison between adenoid hypertrophy grading and pepsin expression.

Pepsin expression	*Adenoidal hypertrophy grading*			
	Level 1	Level 2	Level 3	Level 4
−	—	—	9	4
+	—	—	6	3
++	—	—	5	8
+++	—	—	2	5
χ^2	7.68			
r	0.576			
P	0.003			

Table 4: Sensitivity and specificity of RSI, RFS, and RSI combined with RFS in diagnosing pharyngeal reflux.

	Pepsin (+)	Pepsin (−)
RSI (+)	3	1
RSI (−)	25	9
RFS (+)	18	8
RFS (−)	16	5
RSI + RFS (+)	20	9
RSI + RFS (−)	15	7

RSI: reflux symptom index; RFS: reflux finding score.

3.4. Consistency Analysis between Pepsin Expression in Adenoids and Reflux Tables. The positive pepsin in adenoid tissues was used as the diagnostic standard of pharyngeal reflux. Based on the pepsin expression, the sensitivity of RSI, RFS, and RSI combined with RFS was 5.77%, 35.03%, and 38.46%, respectively, and the specificity was 91.74%, 55.89%, and 53.67%, respectively (Table 4).

Table 5: Patients characteristics.

	Total ($n = 43$)	LPR (+) ($n = 8$)	LPR (−) ($n = 35$)	P
Age	6.73 ± 3.08	6.91 ± 3.04	6.52 ± 2.82	0.51
Sex (no, %)				
Female	20 (46.4%)	5 (62.5%)	20 (57.1%)	0.39
Male	23 (53.5%)	3 (37.5%)	15 (42.9%)	
LPR (median)	20	49	27	0.70
Acid regurgitation (median)	12	46	20	0.06
Mouth breathing (no, %)	34 (79.1%)	5 (62.5%)	29 (82.9%)	0.70
Snoring (no, %)	28 (65.1%)	4 (50%)	24 (68.6%)	0.34
Stoppage of breathing (no, %)	3 (6.9)	1 (1.3%)	2 (5.7%)	0.40
URTI (no, %)	4 (9.3%)	2 (25%)	2 (5.7%)	0.28
Heartburn (no, %)	2 (4.7%)	1 (1.3%)	1 (2.9%)	0.08

URTI: upper respiratory tract infection; LPR: laryngopharyngeal reflux.

3.5. Patients' Characteristics. The characteristics of patients with LPR diagnosis are exhibited in Table 5. A total of 43 children with adenoidal hypertrophy were enrolled in the study. The age range of the children was 2–10 years old, with an average of 5.4 years old. The course of the disease was 3–52 months, with an average of 16.3 months. LPR was detected in 8 (18.6%) subjects. No differences in age, sex, LPR, acid regurgitation, mouth breathing, snoring, stoppage of breathing, URTI, and heartburn were observed between patients in the LPR (+) and LPR (−) groups.

3.6. The Reflux Episodes Number in LPR Positive and Negative Patients. Figures 2 and 3 show a marked difference in the number of acids and total quantity of reflux episodes between the LPR-positive and LPR-negative groups (all $p < 0.05$).

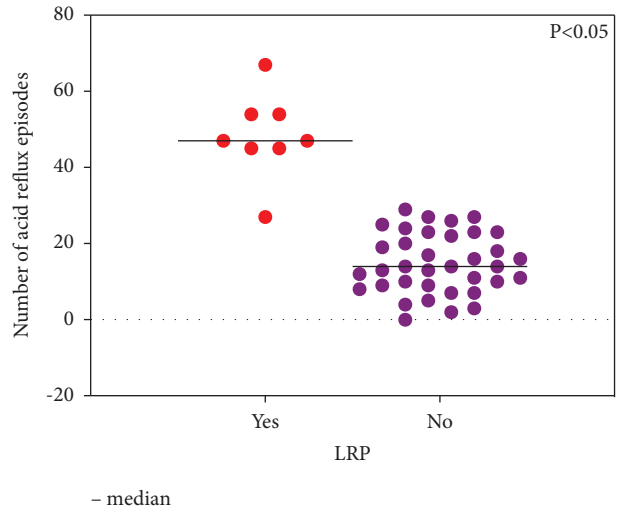

Figure 2: Number of acid reflux episodes in LPR (+) and LPR (−) groups.

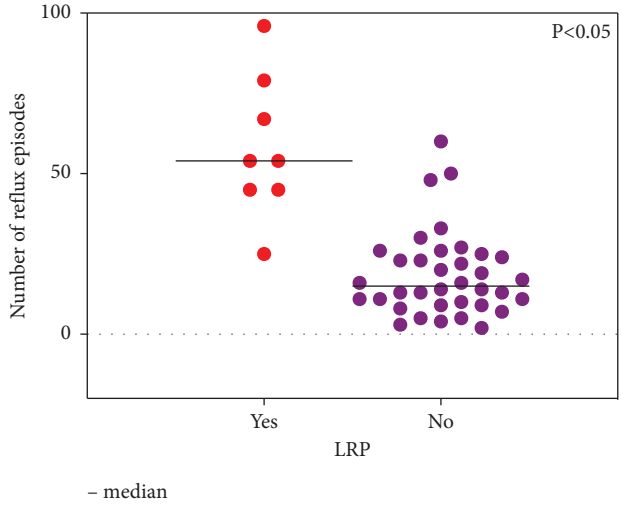

Figure 3: Total quantity of reflux episodes in LPR (+) and LPR (−) groups.

4. Discussion

Adenoidal hypertrophy often causes nasal congestion and mouth-opening breathing in children and affects physical development [14]. Increasing evidence indicates that AH might be caused by viruses, bacterial infections, allergic inflammation, the influence of second-hand smoke, and other factors [15]. In recent years, studies have found that throat reflux plays a critical role in the occurrence and development of adenoid hypertrophy, chronic sinusitis, chronic rhinitis, secretory otitis media, asthma, and laryngeal dysfunction. Keles et al. performed 24-hour esophageal pH monitoring in 30 children with adenoidal hypertrophy and observed that the incidence of pharyngeal reflux was significantly enhanced compared with that in the control group [16]. They indicated that pharyngeal reflux plays an essential role in the process of adenoidal hypertrophy. A recent study investigated 207 children diagnosed with chronic adenoiditis and observed that 87 cases were suspected of upper respiratory reflux, of which 29% had reflux symptoms [17]. Han et al. evaluated 997 children who underwent adenoidectomy and found that 81 children had gastroesophageal reflux and 8 had postoperative complications. They believed that reflux was a risk factor for complications after adenoidectomy [18]. Moreover, another study has highlighted that the increased respiratory movement of OSA in children (mainly due to adenoid hypertrophy) produces tremendous negative pressure, which

induces reflux, then produces inflammation and sensory abnormalities in the throat, leading to the aggravation of OSA [19].

RSI and RFS are the simplest clinical screening methods for diagnosing pharyngeal reflux [20]. The diagnostic value of this scale for adult pharyngeal reflux has been recognized [21]. However, their diagnostic value in children with pharyngeal reflux remains largely unknown. In this study, the positive adenoid pepsin in children was used as the gold standard to evaluate the correlation and accuracy of RSI and RFS in predicting adenoid hypertrophy and pharyngeal reflux. We found that RSI and RFS scales, whether applied alone or in combination, have low sensitivity in diagnosing pharyngeal reflux in children with adenoidal hypertrophy, suggesting that these two scales are unsuitable for the preliminary screening of children with adenoidal hypertrophy in the diagnosis of pharyngeal reflux. In RSI, we found that most children with adenoidal hypertrophy had excessive sputum or nasal regurgitation (55.8%), annoying cough (53.5%), and cough after eating or lying down (35.9%). In RFS, we found that most children with adenoidal hypertrophy had mucus attachment in the larynx (53.5%), partial or complete disappearance of the laryngeal chamber (23.3%), and vocal cord edema (27.9%).

Gastric reflux contains gastric acid, pepsin, bile, trypsin, and other components [22]. Among them, pepsin is an essential proteolytic enzyme in the digestive system, and it is also the main invasive component in pharyngeal reflux [23]. In this study, pepsin was detected in hypertrophic adenoids, and the positive rate was as high as 69.77%, suggesting that pharyngeal reflux widely existed in children with hypertrophic adenoids. At the same time, the higher the grade of adenoid hypertrophy, the higher the expression intensity of pepsin ($r = 0.576$, $P < 0.01$), indicating that pepsin plays an essential role in developing adenoid hypertrophy.

In conclusion, we found that RSI and RFS scales have low sensitivity and poor diagnostic value for AH children and are unsuitable for diagnosing pharyngeal reflux in children with AH. In addition, AH in children is correlated with pathological reflux of gastric contents such as pepsin. Pathological reflux of gastric contents to the nasopharynx might be one of the causes of adenoid hypertrophy.

Data Availability

The labeled dataset used to support the findings of this study are available from the corresponding author upon request.

Conflicts of Interest

The authors declare that they have no conflicts of interest.

Authors' Contributions

Yu Zhou and Ruixia Ma have contributed equally to this work.

Acknowledgments

This research was supported by the Science and Technology Department of Ningxia (No. 2021CMG03036).

References

[1] M. C. Leal, D. Seabra Ramos, T. Pinto Bezerra et al., "The prevalence of adenoid hypertrophy among children with zika related microcephaly," *Multidisciplinary Digital Publishing Institute*, vol. 13, 2021.

[2] L. Marusiakova, P. Durdik, M. Jesenak et al., "Ciliary beat frequency in children with adenoid hypertrophy," *Pediatric Pulmonology*, vol. 55, no. 3, pp. 666–673, 2020.

[3] K. Masna, A. Zwierz, K. Domagalski, and P. Burduk, "The impact of the thermal seasons on adenoid size, its mucus coverage and otitis media with effusion: a cohort study," *Journal of Clinical Medicine*, vol. 10, no. 23, p. 5603, 2021.

[4] T. Zhao, J. Zhou, J. Yan et al., "Automated adenoid hypertrophy assessment with lateral cephalometry in children based on artificial intelligence," *Diagnostics*, vol. 11, no. 8, p. 1386, 2021.

[5] K. T. Kang, C. H. Chou, W. C. Weng, P. L. Lee, and W. C. Hsu, "Associations between adenotonsillar hypertrophy, age, and obesity in children with obstructive sleep apnea," *PLoS One*, vol. 8, no. 10, Article ID e78666, 2013.

[6] A. Madani, E. Wong, L. Sowerby, K. Fung, and J. C. Gregor, "Detecting the other reflux disease," *Journal of Family Practice*, vol. 59, no. 2, pp. 102–107, 2010.

[7] S. H. Lee and S. H. Huh, "Recent trends of laryngopharyngeal reflux disease," *Korean Journal of Otorhinolaryngology-Head and Neck Surgery*, vol. 54, no. 8, p. 519, 2011.

[8] H. Kavookjian, T. Irwin, J. D. Garnett, and S. Kraft, "The reflux symptom index and symptom overlap in dysphonic patients," *The Laryngoscope*, vol. 130, no. 11, pp. 2631–2636, 2020.

[9] F. Kong, Y. L. Sun, and B. Yuan, "Prevalence of pulmonary hypertension in children with adenoid or adenotonsillar hypertrophy: a meta-analysis," *International Journal of Pediatric Otorhinolaryngology*, vol. 153, 2021.

[10] M. Sagar, P. Sagar, S. Kabra, R. Kumar, and S. Mallick, "The concatenation of association between gastroesophageal reflux and obstructive adenotonsillar hypertrophy," *International Journal of Pediatric Otorhinolaryngology*, vol. 139, Article ID 110439, 2020.

[11] Y. D. Huang, J. J. Tan, X. Y. Han, F. F. Zeng, and X. P. Li, "Study on the correlation between adenoid hypertrophy and laryngopharyngeal reflux in children," *Lin chuang er bi yan hou tou jing wai ke za zhi = Journal of clinical otorhinolaryngology, head, and neck surgery*, vol. 32, p. 899, 2018.

[12] J. Ren, Y. Zhao, and X. Ren, "[An association between adenoid hypertrophy and exstra-gastroesophageal reflux disease]," *Journal of Clinical Otorhinolaryngology Head and Neck Surgery*, vol. 29, no. 15, pp. 1406–1408, 2015.

[13] P. Cassano and M. Gelardi, *Fibere Endoscopic Assessment of Rhinopharyngeal Obstruction Due to Adenoidal Hypertrophy*, 2000.

[14] H. Huang, L. Zhang, Q. Zhang, J. Zhong, L. Fua, and Y. Mou, "Comparison of the efficacy of two surgical procedures on adenoidal hypertrophy in children - ScienceDirect," *Archives de Pediatrie*, vol. 27, pp. 72–78, 2020.

[15] J. Xu, W. Dai, Q. Liang, and D. Ren, "The microbiomes of adenoid and middle ear in children with otitis media with effusion and hypertrophy from a tertiary hospital in China," *International Journal of Pediatric Otorhinolaryngology*, vol. 134, Article ID 110058, 2020.

[16] B. Keles, K. Ozturk, H. Arbag, E. Gunel, and B. Ozer, "Frequency of pharyngeal reflux in children with adenoid hyperplasia,"

International Journal of Pediatric Otorhinolaryngology, vol. 69, no. 8, pp. 1103–1107, 2005.

[17] P. R. Purnell, J. H. Ramadan, and H. H. Ramadan, "Can symptoms differentiate between chronic adenoiditis and chronic rhinosinusitis in pediatric patients," *Ear, Nose, & Throat Journal*, vol. 98, no. 5, pp. 279–282, 2019.

[18] Y. M. Han, S. J. Chung, S. Yoo et al., "Inverse correlation between gastroesophageal reflux disease and atrophic gastritis assessed by endoscopy and serology," *World Journal of Gastroenterology*, vol. 28, no. 8, pp. 853–867, 2022.

[19] C. A. Mccall and J. W. Winkelman, "Respiratory-related leg movements of sleep are associated with serotonergic antidepressants but not bupropion," *Journal of Clinical Sleep Medicine*, vol. 14, no. 9, pp. 1569–1576, 2018.

[20] S. A. Anzi, M. Turkalj, A. Oupan, M. Labor, D. Plavec, and T. Baudoin, "Eight weeks of omeprazole 20 mg significantly reduces both laryngopharyngeal reflux and comorbid chronic rhinosinusitis signs and symptoms: randomised, double-blind, placebo-controlled trial," *Clinical Otolaryngology*, vol. 43, 2017.

[21] L. Boom, M. Edens, and B. Rinia, "Reflux finding score and reflux symptom index as potential predictors for proton pump inhibitor response in globus pharyngeus patients: a prospective study," *Auris Nasus Larynx*, vol. 47, no. 4, pp. 609–615, 2020.

[22] L. Y. Zhang, J. Zhang, D. Li et al., "Bile reflux is an independent risk factor for precancerous gastric lesions and gastric cancer: an observational cross sectional study: ectional study," *Journal of Digestive Diseases*, vol. 22, no. 5, pp. 282–290, 2021.

[23] X. Xiong, S. He, F. Xu et al., "Gastroesophageal reflux disease and salivary pepsin in patients with heterotopic gastric mucosa in the upper esophagus," *Diseases of the Esophagus: Official Journal of the International Society for Diseases of the Esophagus*, vol. 35, no. 4, Article ID doab074, 2022.

Hindawi
Evidence-Based Complementary and Alternative Medicine
Volume 2023, Article ID 9731315, 27 pages
https://doi.org/10.1155/2023/9731315

Review Article

Clinical Evidence and Potential Mechanisms in Treating Radiation Enteritis with Modified Baitouweng Decoction

Zihong Wu,[1] **Bei Yin**,[2] **Ziming Wang**,[3] **Enfeng Song**,[3] **and Fengming You**[1]

[1]*Hospital of Chengdu University of Traditional Chinese Medicine, Chengdu, China*
[2]*School of Second Clinical Medicine, Guangzhou University of Chinese Medicine, Guangzhou, China*
[3]*Department of Traditional Chinese Medicine, Renmin Hospital of Wuhan University, Wuhan, China*

Correspondence should be addressed to Fengming You; yfmdoc@163.com

Received 14 July 2022; Revised 12 November 2022; Accepted 24 November 2022; Published 30 January 2023

Academic Editor: Xueliang Wu

Objectives. To perform a meta-analysis and network analysis identification to evaluate the efficacy, safety, and potential mechanisms of modified Baitouweng decoction (mBTWD) in the treatment of radiation enteritis. *Methods*. We searched PubMed, Embase, Cochrane Library, Web of Science, CNKI, Wanfang Databases, SionMed, and Chinese Scientific Journals Database to collect the randomized controlled trials (RCTs) of mBTWD treating radiation enteritis. Rev.Man 5.3 and Stata 14.0 software are employed for meta-analysis. The GRADE online tool is used to evaluate the quality of evidence. Network analysis and molecular docking approach are applied to predict the potential targets and ingredients of representative drugs in mBTWD for the treatment of radiation enteritis. *Results*. Seventeen studies are eventually included, covering a total of 1611 patients: (1) The clinical efficacy is significantly higher in mBTWD groups than in control groups (RR = 1.24, 95% CI (1.17, 1.32), $P < 0.00001$). (2) mBTWD has certain advantages in improving TCM syndromes (MD = −3.41, $P < 0.00001$). (3) mBTWD has a certain positive effect on the improvement of intestinal signs and symptoms (RR = 1.23, $P = 0.0001$; OR = 3.51, $P < 0.00001$). (4) Indexes including CRP, KPS, and OB, are better in mBTWD groups than in control groups ($P < 0.00001$, $P = 0.002$, $P = 0.03$), but the credibility is downgraded for a small sample size. Adverse events and recurrence rates require further confirmation with larger sample sizes. (5) Univariate meta-regression for clinical efficacy shows none of the coefficients are significantly associated with the estimated risk ratio. The clinical efficacy overestimates about 4.9% from publication bias. The quality of the included studies is low according to GRADE evidence. (6) Quercetin, isorhamnetin, and beta-sitosterol are the main ingredients from representative drugs in mBTWD and its key targets are MYC, TP53, and MAPK14/MAPK1. *Conclusions*. mBTWD may be effective in the treatment of radiation enteritis, but its long-term benefits, safety, and molecular mechanisms remain unclear due to the poor quality of the evidence. Larger sample sizes, high-quality studies, and basic research are essential in the future.

1. Introduction

Radiation therapy is an important treatment therapy for pelvic/abdominal malignancies such as cervical cancer and rectal cancer. While effectively killing cancer cells and controlling local diffusion and distant metastasis of lesions, radiation enteritis often occurs. Oxidative stress caused by the local high doses of radiation can produce a large number of reactive oxide species (ROS), which can cause DNA damage of normal intestinal epithelial cells, atrophy and ulceration of intestinal mucosa, and finally form radioactive enteritis [1]. Approximately 90% of patients with pelvic and abdominal tumors have been reported to have irreversible changes in their defecation habits after radiation therapy, leading to a decrease in the quality of life of approximately 50% of patients [2]. Patients with radiation enteritis mainly present with diarrhea, bellyache, mucous stool, tenesmus, and anal distention, even serious conditions such as intestinal obstruction, intestinal perforation, and fistula formation. These intestinal symptoms lead to a significant reduction in the patient's willingness to continue with radiation therapy [3, 4]. With the improvement of treatment methods, more and more tumor patients benefit from longer survival due to active management of side effects. The

treatment of radiation enteritis is mainly symptomatic treatment such as antidiarrheal, anti-inflammatory, analgesic, and fluid rehydration. Commonly used drugs include dexamethasone, gentamicin, lidocaine, and montmorillonite powder. Moreover, the administration is mostly by reserved enema (Re) or per os (Po). These treatments can alleviate symptoms to some extent, but there is often a risk of incomplete treatment, aggravating infection, and high recurrence rate.

Chinese herbal formula is a long-established, complementary, and alternative medical treatment with curative efficacy, and it is now widely accepted and studied in countries around the world [5]. In recent years, traditional Chinese medicine (TCM) made some achievements in the treatment of radiation enteritis, especially the herbal retention enema reflects the unique advantages of TCM. Baitouweng decoction (BTWD) is from the Treatise on Typhoid Fever, written by Zhang Zhong Jing in the Han Dynasty, and it is a representative formula for the treatment of febrile dysentery. The base ingredients of the modified Baitouweng decoction (mBTWD) are mainly Baitouweng decoction, which consists of four herbs: *Pulsatilla* (Baitouweng), *Coptis chinensis* (Huanglian), tractat (Huangbo), and ash bark (Qinpi). Modern pharmacological studies show that the representative drugs in mBTWD have a good effect on intestinal inflammation. These ingredients regulate intestinal microbiota through FXR/TGR5 and IL-6/STAT3 signaling pathways, restore Th17/Treg cell balance, and improve intestinal immune function and epithelial barrier in mice with enteritis [6–8] (Figure 1). However, the effects and benefits of mBTWD on radiation enteritis are still uncertain, and the mechanism of mBTWD in the treatment of radiation enteritis remains to be further discovered.

In this study, we conducted a meta-analysis to summarize the clinical evidence for mBTWD in the treatment of radiation enteritis. Based on the results of the meta-analysis, we employ network analysis and molecular docking techniques to preliminarily predict the active components and key targets of mBTWD at the molecular level for the treatment of radiation enteritis. This study aims to provide a scientific reference for the clinical application of mBTWD in the treatment of radiation enteritis.

2. Materials and Methods

This study is registered with the International Platform of Registered Systematic Review and Meta-analysis Protocols (INPLASY) (https://inplasy.com) as INPLASY 202190053.

2.1. Search Strategies. We searched PubMed, Embase, Cochrane Library, Web of Science, China National Knowledge Infrastructure (CNKI), Wanfang Databases, SionMed, and the Chinese Scientific Journal Database from inception until March 1, 2022. The search strategy in PubMed is as follows: ((((“Baitouweng Decoction”(Title/Abstract)) OR (“BTWD”(Title/Abstract))) OR (“Baitouweng Tang”(Title/Abstract))) OR (Baitouweng* (Title/Abstract))) AND (((“Radiation enteritis”(Title/Abstract)) OR (“Radiation proctitis”(Title/Abstract))) OR (“Radiation colitis”(Title/Abstract))).

2.2. Inclusion/Exclusion Criteria. The inclusion criteria are constructed following the principle of PICOS. (1) Participants: all subjects are patients with abdominal/pelvic tumors complicated with radiation enteritis, regardless of age, sex or nationality. The diagnostic criteria refer to the consensus of Chinese experts on the diagnosis and treatment of radiation enteritis in 2021 [9]. (2) Interventions: the experimental groups are treated with mBTWD alone or combined with conventional western medicine (CWM), and the CWM is the same as the control groups. There are no special restrictions on the dose of herbs, and the methods of administration include retention enema and per os. The treatment course is longer than 14 days. (3) Controls: control groups receive the CWM recommended by expert consensus or just a placebo, and the methods of administration also include retention enema and per os. For example, montmorillonite powder retention enema or oral, or montmorillonite combined with gentamicin, dexamethasone, and procaine for retention enema. (4) Outcomes: the outcome indices mainly include clinical efficacy, TCM symptom score, colonoscopy score/grade, and radiation enteritis grading, KPS score, serum inflammatory factor level, fecal occult blood, adverse events, and recurrence rate. (5) Types of studies: all studies are RCTs and the studies included are not restricted by journals.

Exclusion criteria: (1) Studies on animal testing and basic research. (2) Nonrandomized controlled trial. (3) Studies with data loss, duplicate publications, or unclear outcome indicators. (4) The experimental groups combine acupuncture, massage, and other TCM therapy. (5) The control groups are treated with TCM.

2.3. Data Extraction. Two researchers independently conducted the literature retrieval according to the inclusion/exclusion criteria, then performed a preliminary screening by reading titles and abstracts. Next, they read the full text for rescreening and discuss the inconsistencies in screening results. If no agreement is reached, the third researcher will coordinate to solve it. The extracted contents mainly include the following: (1) basic characteristics, including the first author, publication year, sample size, and mean age. (2) Diagnostic criteria. (3) Intervention measures, including drug composition and dose, route of administration, and treatment cycle. (4) Outcome indicators, including efficacy standards and symptom rating scales. (5) Study design and methods. If some details are not fully reported in the study, the researcher will contact the original author.

2.4. Quality Evaluation. The Cochrane Handbook [10] is utilized to assess the risk of bias of all included RCTs. And the main types of bias are divided into six categories. (1) Selection bias: random sequence generation and allocation concealment. (2) Performance bias: blindness of participants and personnel. (3) Detection bias: blinding of outcome

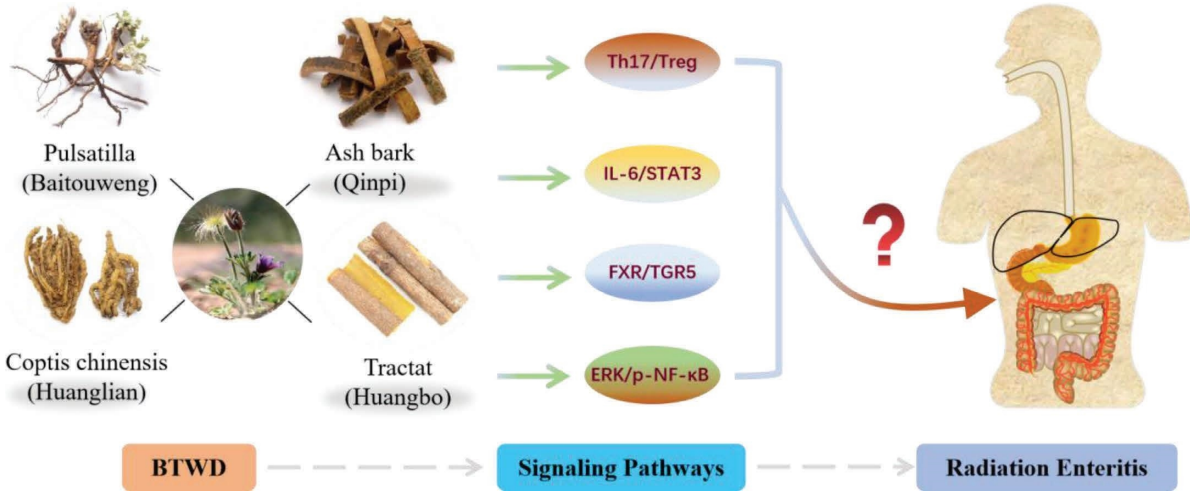

Figure 1: Molecular mechanisms of representative drugs in mBTWD for the treatment of radiation enteritis.

assessment. (4) Attrition bias: incomplete outcome data. (5) Reporting bias: selective reporting. (6) Other bias: each bias risk is divided into three grades: high bias risk, low bias risk, and unknown bias risk.

2.5. Statistical Analysis and GRADE Evidence. RevMan5.3 and Stata 14.0 software is used for data processing. The risk ratio (RR) or odds ratio (OR) are used for dichotomous variables and the weighted mean differences are used for continuous variables. And 95% confidence intervals (CI) are calculated for all effect sizes. Cochran's Q and χ^2 test statistics are utilized to test the heterogeneity across studies. The fixed-effects model is adopted with low heterogeneity ($P > 0.1$, $I^2 < 50\%$). If there is heterogeneity in the studies ($P \leq 0.1$, $I^2 \geq 50\%$), the random-effects model is chosen. Sensitivity analysis, subgroup analysis, and univariate meta-regression analysis are employed to deal with high heterogeneity.

A meta-regression analysis is essentially an observational study that uses regression analysis to explore the effect of certain trial or case characteristics (covariates) on the combined effect in a meta-analysis in an attempt to clarify the sources of heterogeneity across studies and to explore the effect of covariates on the combined effect. Univariate meta-regression analyses are conducted to explore the cause of heterogeneity and association between factors including intervention, drug deliver, sample size, mean age, duration and publication year, and the clinical efficacy of mBTWD on radiation enteritis when there are over 10 studies included. Egger's test is a simple quantitative method for testing the symmetry of funnel plots by linear regression, developed by Matthias Egger et al. in 1997 to overcome the shortcomings of the funnel plot method. The theoretical basis of Begg's test is based on Kendall's tau rank correlation method, which determines the existence of "publication bias" by the presence of Kendall's correlation between the standardized effect estimates and the variance of the effect estimates. The trim and fill method aims to identify and correct funnel plot asymmetries caused by publication bias. This method allows both the number of missing studies to be estimated and the inclusion of missing studies to be rerun in a meta-analysis, correcting for the combined effect size of the intervention. Egger's test, Begg's test, and the funnel-plot-based trim and fill method are used to deal with the potential publication bias.

The online Grading of Recommendations Assessment, Development, and Evaluation (GRADE) tool [11] is used to evaluate the quality of evidence (https://gdt.gradepro.org/app/). The GRADE standard is a grading of the body of evidence that takes into account the type of study design, methodological quality, consistency of results, and directness of evidence. It has been adopted by over 100 international organisations and associations worldwide as one of the international standards for evaluating interventional evidence. We mainly use the risk of bias, inconsistency, indirectness, imprecision, and other considerations to evaluate quality. There are four levels of evidence: quality of evidence-high, moderate, low, or very low.

2.6. Network Analysis and Molecular Docking. Firstly, the chemical constituents of representative drugs, Baitouweng, Huanglian, Huangbo, and Qinpi, are collected by searching the Traditional Chinese Medicine Systems Pharmacology (TCMSP) database (https://tcmspw.com/tcmsp.php). The main active compounds are obtained with oral bioavailability (OBA) greater than or equal to 30% and drug-like (DL) greater than or equal to 0.18 as screening conditions [12]. Then we screen the target protein corresponding to the active ingredients and convert the target protein name into the corresponding Gene Symbol. The UniProtKB database (https://www.uniporot.org/) is used to check the target information.

Secondly, we set the keywords to "radiation enteritis" to search for the genes related to radiation enteritis from the five sources: GeneCards (https://www.pharmgkb.org/), OMIM (https://omim.org/) and TTD (https://db.idrblab.net/ttd/). All targets associated with radiation enteritis are obtained after repeated genes. The R language program and

Venny 2.1 software are used to predict the drug-disease common targets. Then we use the Perl program and Cytoscape 3.8.2 software to build a compound-target-disease network.

Thirdly, common drug-disease targets are imported into the STRING database (https://string-db.org/cgi/input.pl), setting the species as "Homo Sapiens" and the Protein-protein interaction (PPI) network is formed. We then import the PPI network into Cytoscape 3.8.2 software and simplify it according to four topology attributes (DC, Degree Centrality; BC, Between Ness Centrality; CC, Closeness Centrality; EC, Eigenvec Tor Centrality). Thus, we obtain the final core target PPI network.

Next, ClueGO plug-ins are used to conduct Gene Ontology (GO) functional enrichment analysis and Kyoto Encyclopedia of Genes and Genomes (KEGG) pathway analysis for the core targets to screen out the main gene items and signal pathways related to radiation enteritis. GO is divided into three parts: BP (biological process), CC (cellular component), and MF (Molecular Function) [13].

Finally, ligand files and receptor files for molecular docking need to be prepared. (1) Ligand files: 2D structures of small molecule ligands of each core target are downloaded from the PubChem database (https://pubchem.ncbi.nlm.nih.gov/) and are converted from 2D to 3D structures with ChemOffice software. We then optimize them with the AutoDockTools (Version 1.5.6) and save them in PDBQT format as ligand files. (2) Receptor files: the PDB files of the 3D structures of the core target are downloaded from Protein Data Bank (PDB) database (https://www.rcsb.org/). Then we process them with Pymol software (Version 3.2.2) and AutoDockTools software (Version 1.5.6) and save them in PDBQT format as receptor files. (3) Molecular docking: AutoGrid software is used to determine the active pocket of the docking receptor, AutoDock Vina software (Version 1.1.2) is selected for molecular docking, and Pymol software (Version 3.2.2) software is used for analysis and mapping. At the same time, dexamethasone, the commonly used drug in radiation enteritis treatment, is selected as a positive control for analysis and verification.

3. Results

3.1. Retrieval Results and Study Characteristics. A total of 306 related studies were preliminarily retrieved, 37 duplicate articles were removed, and 212 articles were excluded after reading titles and abstracts. The remaining 57 papers were read in full and 17 studies selected that met the inclusion criteria (Figure 2).

The baseline of the 17 included studies is consistent. The intervention groups receive mBTWD alone or in combination with conventional western medicine. The control groups are given a placebo, gentamicin, dexamethasone, montmorillonite powder, procaine/lidocaine, or combination therapy. The main route of administration is retention enema [9, 14–22]; three studies report the route of administration of retention enema combined with per os [23–25], and four studies report oral administration [26–29]. A total of 1611 patients are enrolled. The baseline characteristics of included trials are shown in Table 1. The compositions of mBTWD from the included studies are shown in Table 2.

3.2. Risk of Bias and Quality Assessment. All of the included studies are randomized controlled trials (RCTs). The risk of bias is assessed according to Cochrane Manual standards. (1) Randomization is mentioned in all included studies, and seven studies [9, 15–17, 25, 27, 29] mention the "random number table." However, none of the studies mention distribution hiding methods. (2) None of the studies is designed to mention "blindness." Although blindness is inadequate in the three studies [9, 14, 15], the outcomes are judged by the system evaluators to be mainly objectively detectable indicators and unlikely to be affected by the lack of blindness. (3) Only two studies [9, 16] describe the missing data, and two studies [14, 29] identify no cases of deletions. No absence or exclusion is reported in the remaining studies. (4) Only one study [16] publishes all prestated results, with no selective reporting. The remaining studies could not be evaluated for too few indicators or the absence of project proposals, raising suspicions about selective reporting. (5) Two studies [21, 22] are considered high-risk because of potential sources of bias associated with a particular trial design. As a result, the quality of the included studies is low (Figure 3).

3.3. Primary Outcome Measure

3.3.1. Clinical Efficacy. Fifteen studies [9, 14, 16–24, 26–29] compare the clinical efficacy of mBTWD with CWM in 1413 patients with radiation enteritis. Due to the moderate heterogeneity of this meta-analysis ($\text{Chi}^2 = 25.48$, $P = 0.03$, $I^2 = 45\%$), a random-effects model is carried out for the meta-analysis to estimate the RR (Figure 4(a)). From the forest plots, we find that the study [18] deviates significantly from the invalid vertical line; after eliminating this study, the heterogeneity decreases ($\text{Chi}^2 = 16.66$, $P = 0.22$, $I^2 = 22\%$) (Figure 4(b)). In addition, we also analyze that differences in drug deliver may be a source of heterogeneity, so we perform a subgroup analysis comprising three subgroups: reserved enema (Re), per os (Po), and Re + Po. The heterogeneity of each subgroup is further reduced ($\text{Chi}^2 = 7.5$, $P = 0.38$, $I^2 = 7\%$; $\text{Chi}^2 = 6.09$, $P = 0.11$, $I^2 = 51\%$; $\text{Chi}^2 = 0.16$, $P = 0.69$, $I^2 = 0\%$) and the differences in each subgroup are statistically significant ($P < 0.00001$; $P = 0.002$; $P < 0.00001$). The clinical efficacy of the mBTWD intervention groups is significantly higher than that of the control groups (RR = 1.24, 95% CI (1.17, 1.32), $P < 0.00001$) (Figure 5). The results show that different drug deliver produce heterogeneity to some extent.

Next, we read the full text of the excluded study [18] in detail and found that it lacks clear diagnostic criteria, suggesting that this is a low-quality study and should be excluded.

3.3.2. Total Score of TCM Syndrome. The main symptom (bellyache, diarrhea, tenesmus, mucosanguineous feces, burning pain in the anus, and so on) of patients is scored

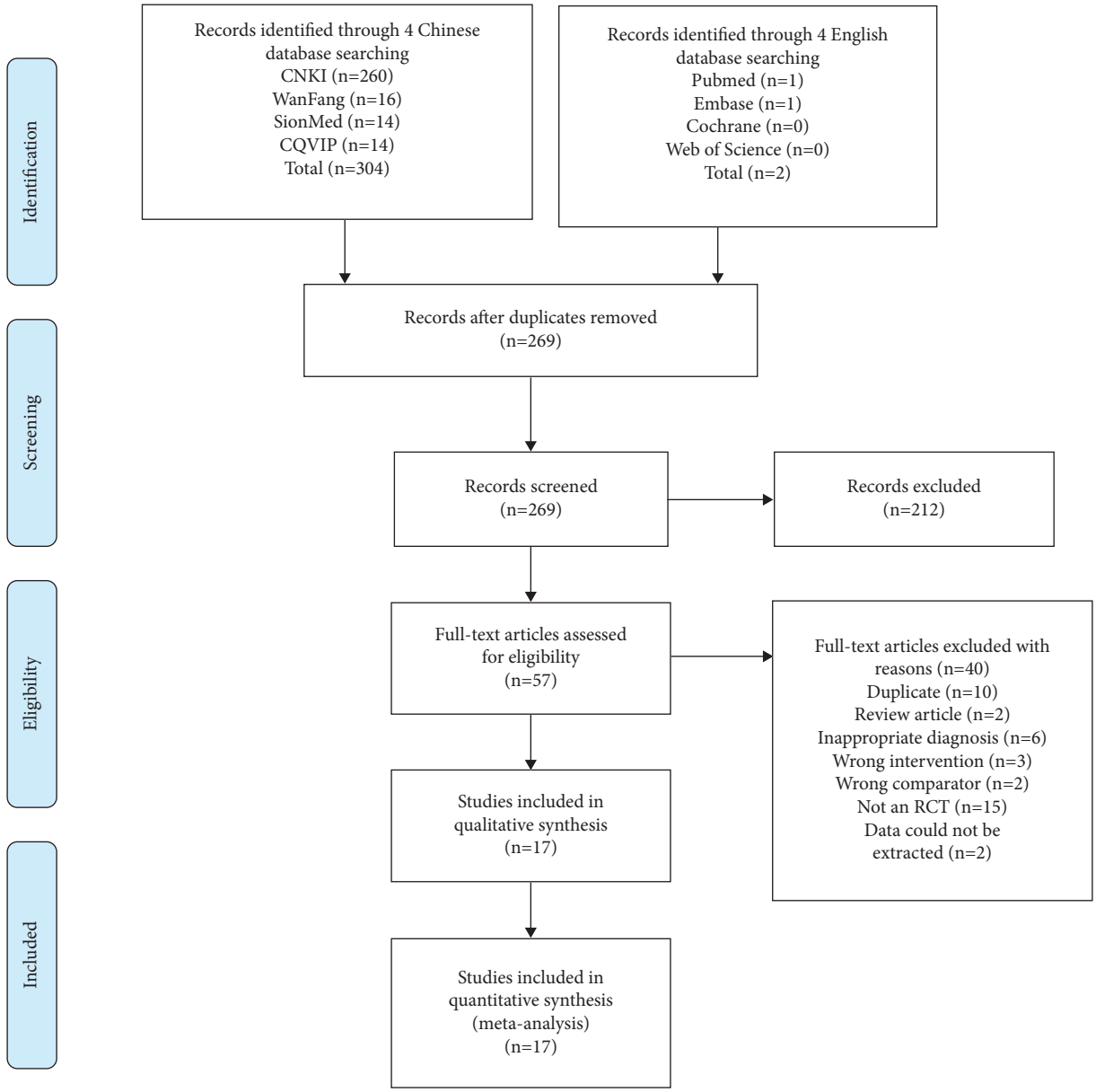

Figure 2: Flow diagram of eligible study selection.

according to the quantitative criteria of TCM syndrome (SFDA, 2002): 0 = none, 1 = mild, 2 = moderate, 3 = severity. Moreover, Stata 14.0 software is used to combine effect sizes. A total of 7 studies describe TCM syndrome's total score regarding this standard, one study [16] is excluded from describing the discrete variables. The remaining 6 studies [9, 14, 15, 21, 22, 29] include a total of 476 patients. The results of the meta-analysis show a moderate heterogeneous in the total score of the TCM syndrome ($\text{Chi}^2 = 10.02$, $P = 0.07$, $I^2 = 50\%$) (Figure 6(a)). It can be seen from the forest plots that the study [14] has the least overlap with other studies; then a sensitivity analysis is conducted and heterogeneity is significantly reduced after this study is removed ($\text{Chi}^2 = 5.11$, $P = 0.28$, $I^2 = 22\%$) (Figure 6(b)). After careful reading of this study, we find that the score of systemic symptoms is included, while other studies are mainly based on the local symptom of the intestinal tract. Therefore, we believe that this is due to heterogeneity caused by differences in trial design, so it is excluded.

According to the results of the meta-analysis, the difference in the TCM syndrome total score between the two groups after treatment is statistically significant (MD = −3.41, 95% CI (−3.75, −3.06), $P < 0.00001$) (Figure 6(b)). Therefore, we discover that mBTWD has certain advantages in improving bellyache, diarrhea, tenesmus, mucosanguineous feces, and burning pain in anus syndromes.

3.3.3. Colonoscopy Score/Grade and Radiation Enteritis Grading. Two studies [9, 14] report the comparison of the colonoscopy score of radiation enteritis patients between the mBTWD and CWM groups. The results show a high

Table 1: Basic characteristics of included studies.

First-author (year)	Sample size	Age (year)	Tumor types	Randomised methods	Diagnosis standard	Drug deliver	Intervention	Control	Duration (day)	Outcomes
Chen 2020 [14]	41/42	49.21 ± 8.25/ 49.74 ± 9.71	Cervical cancer	NR	CCDTRP (2018)	reserved enema	mBTWD (50 ml, qd) + A + rhGM-CSF	A + rhGM-CSF (50 ml, qd)	14	(1), (2), (3), (4), (5)
Zhao 2011 [26]	35/36	49.5 ± 7.6/ 50.8 ± 7.9	Pelvic tumor	NR	NOHS (2002)	Po	mBTWD (150 ml, bid)	Blank control	35	(1), (3)
Jiang 2008 [23]	60/30	24–78/25–76	Gynecological cancer	NR	SDTMTC	Re + Po	mBTWD (50 ml, qd, Re) + (100 ml, bid, Po)	B (50 ml, qd)	20	(1)
Lai 2021 [15]	60/60	48.6 ± 7.3/ 50.3 ± 8.6	Cervical cancer	NRT	CCDTRP (2018)	Re	mBTWD (100 ml, bid)	B (100 ml, bid)	20	(2), (3), (4), (7)
Lei 2019 [16]	35/36	49.80 ± 11.66/ 49.69 ± 11.22	Pelvic tumor	NRT	NOHS (2002)	Re	mBTWD (100 ml, qd)	C (100 ml, qd)	14	(1), (2), (3), (4), (5), (6), (7)
Lei 2010 [17]	40/33	40–60	Cervical cancer	NRT	MOR (2001)	Re	mBTWD (150 ml, qd)	A (150 ml, qd)	60	(1)
Xia 2016 [18]	24/24	37–68/36–65	Cervical cancer	NR	NR	Re	mBTWD (100 ml, qd)	B (100 ml, qd)	60	(1)
Yang 2012 [19]	29/29	34–73/36–75	Pelvic tumor	NR	NR	Re	mBTWD (100 ml, qd)	B (100 ml, qd)	20	(1)
Jiang 2011 [27]	52/46	48.9 ± 7.8/ 47.8 ± 8.5	Cervical cancer	NRT	MOR (2001)	Po	mBTWD (150 ml, bid) + E	D	14	(1)
Yao 2014 [24]	203/189	25–78/26–79	Pelvic tumor	NR	NOHS (2002)	Re + Po	mBTWD (50 ml, qd, Re) + (100 ml, bid, Po)	Antibiotic (iv) + A + B (50 ml, qd)	20	(1), (3), (7)
Li 2008 [20]	32/27	32–65	Abdominal tumor	NR	GGCCDT (2003)	Re	mBTWD (100 ml, qd) + Symptomatic treatment	Symptomatic treatment	15	(1)
Tong 2012 [25]	47/42	56/53	Pelvic tumor	NRT	MOR (2001)	Re + Po	mBTWD (50 ml, qd)	C (50 ml, qd)	NR	(3), (4), (7)
Ma 2021 [9]	30/30	57.87 ± 6.62/ 58.83 ± 5.97	Abdominal tumor	NRT	CCDTRP (2018)	Re	BTWD (100 ml, qd)	C (100 ml, qd)	20	(1), (2), (3), (5), (6)
Wang 2017 [21]	42/42	60.5 ± 2.1/ 63.0 ± 3.2	NR	NR	NR	Re	mBTWD (200 ml, qd) + Xilei San (3 g)	B + adrenalin (200 ml, qd)	NR	(1), (2)
Zhang 2013 [22]	34/34	56.62 ± 9.82/ 52.29 ± 9.77	NR	NR	CCDTRP (2018)	Re	mBTWD (200 ml, qd) + Xilei San (3 g)	B + adrenalin (200 ml, qd)	14	(1), (2)
Ye 2007 [28]	43/43	NR	Pelvic tumor	NR	NR	Po	mBTWD	Blank control	NR	(1)
Wang 2021 [29]	27/34	52.7 ± 5.6/ 51.3 ± 4.4	Pelvic tumor	NRT	CCDTRP (2018)	Po	mBTWD (200 ml, bid) + Montmorillonite (3 g, tid)	Montmorillonite (3 g, tid)	NR	(1), (2), (3), (4)

Note. NR, not report. RNT, random number table. CCDTRP (2018), the consensus of Chinese experts on diagnosis and treatment of radiation proctitis (2018). NOHS (2002), national occupational health standards (2002). MOR (2001), modern oncology radiation therapy (2001). SDTMTC, standard for the diagnosis and treatment of common malignant tumors in China. GGCCDT (2003), graphic gastroenterology -clinical classical diagnosis and treatment methods (2003). Re, retention enema. Po, per os. BTWD, Baitouweng decoction. mBTWD, modified BTWD. A, 0.9% NaCl solution 50 ml + gentamicin 160,000 U + dexamethasone 10 mg + montmorillonite powder 3 g. B, 0.9% NaCl solution 100 ml + gentamicin 160,000 U + dexamethasone 5 mg + procaine/lidocaine 10 ml. C, 0.9% NaCl solution 100 ml + dexamethasone 10 mg + montmorillonite powder 6 g. D, norfloxacin (0.2 g, tid) + berberine (0.3 g, tid) + yunnan baiyao (0.5 g, tid). rhGM-CSF, recombinant human granulocyte-macrophagecolony-stimulating factor for injection. (1) clinical efficacy, (2) TCM symptom score, (3) colonoscopy score (grade) and radiation enteritis grading, (4) KPS score, (5) serum inflammatory factor level, (6) fecal occult blood, and (7) adverse events and recurrence rate.

Table 2: mBTWD composition of included studies.

First-author (year)	Formula	Components
Chen 2020 [14]	mBTWD	Pulsatillia Radix (Baitouweng, Chinese bulbul) 12 g; Coptidis Rhizoma (Huanglian, Goldthread) 12 g; Phellodendri Chinrnsis Cortex (Huangbo, Tractat) 12 g; Fraxini Cortex (Qinpi, Ash bark) 15 g; Burnet (Diyu, Sanguisorba officinalis) 15 g; Saposhnicovia divaricate (Fangfeng, Radix sileris) 9 g
Zhao 2011 [26]	mBTWD	Pulsatilliae Radix (Baitouweng, Chinese bulbul) 15 g; Coptidis Rhizoma (Huanglian, Goldthread) 5 g; Phellodendri Chinrnsis Cortex (Huangbo, Tractat) 10 g; Fraxini Cortex (Qinpi, Ash bark) 10 g; Sophora japonica (Huaihua, Flos sophorae) 10 g; Aucklandia (Muxiang, Costustoot) 10 g; Pueraria (Gegen, The root of kudzu vine) 15 g; Corydalis tuber (Yanhusuo, Rhizoma corydalis) 10 g; Licorice (Gancao, Glycyrrhiza) 6 g; Atractylodes (Baizhu, Rhizoma atractylodis) 10 g; Nepeta (Jingjie, Schizonepeta) 10 g; Red peony root (Chishao, Radix paeoniae rubra) 10 g; Rheum officinale (Dahuang, Chinese rhubarb) 6 g; Coloured malt (Maiya, Malt culms) 10 g; Amomum (Sharen, Fructus amomi) 3 g
Jiang 2008 [23]	mBTWD	Pulsatilliae Radix (Baitouweng, Chinese bulbul) 15 g; Coptidis Rhizoma (Huanglian, Goldthread) 6 g; Phellodendri Chinrnsis Cortex (Huangbo, Tractat) 10 g; Burnet (Diyu, Sanguisorba officinalis) 15 g; Red peony root (Chishao, Radix paeoniae rubra) 30 g; White peony root (Baishao, Radix paeoniae alba) 15 g; Angelica sinensis (Danggui, Chinese angelica) 20 g; Paeonia suffruticosa (Mudanpi, Moutan bark) 15 g; Radix scrophulariae (Xuanshen, Figwort root) 15 g; Field thistle (Xiaoji, cephalanoplos segetum) 10 g; Notoginseng powder (Sanqifen, Notoginseng root) 3 g; Cacumen biotae (Cebaiye, Chinese arborvitae twig) 15 g; Sophora japonica (Huaihua, Flos sophorae) 15 g; Licorice (Gancao, Glycyrrhiza) 10 g
Lai 2021 [15]	mBTWD	Pulsatilliae Radix (Baitouweng, Chinese bulbul) 30 g; Coptidis Rhizoma (Huanglian, Goldthread) 30 g; Radix Scutellariae (Huangqin, Scutellaria baicalensis) 30 g; Burnet (Diyu, Sanguisorba officinalis) 15 g; Sophora japonica (Huaihua, Flos sophorae) 15 g; Pueraria (Gegen, The root of kudzu vine) 30 g; Cultured calculus bovis (Tiwaipeiyuniuhuang, Cultured bezoar in vitro) 0.3 g; Philippine violet herb (Zihuadiding, Chinese violet) 15 g
Lei 2019 [16]	mBTWD	Pulsatilliae Radix (Baitouweng, Chinese bulbul) 15 g; Coptidis Rhizoma (Huanglian, Goldthread) 10 g; Phellodendri Chinrnsis Cortex (Huangbo, Tractat) 10 g; Fraxini Cortex (Qinpi, Ash bark) 15 g; Burnet (Diyu, Sanguisorba officinalis) 15 g; White peony root (Baishao, Radix paeoniae alba) 15 g; Angelica sinensis (Danggui, Chinese angelica) 15 g; Poria cocos (Fuling, Tuckahoe) 15 g; Rheum officinale (Dahuang, Chinese rhubarb) 5 g; Aucklandia (Muxiang, Costustoot) 15 g; Areca-nut (Binglang, Areca catechu) 15 g; Rhizoma atractylodis (Cangzhu, Atractylodes) 15 g; Licorice (Gancao, Glycyrrhiza) 6 g
Lei 2010 [17]	mBTWD	Pulsatilliae Radix (Baitouweng, Chinese bulbul) 10 g; Coptidis Rhizoma (Huanglian, Goldthread) 5 g; Phellodendri Chinrnsis Cortex (Huangbo, Tractat) 5 g; Fraxini Cortex (Qinpi, Ash bark) 10 g; Burnet (Diyu, Sanguisorba officinalis) 15 g; Sophora flavescens (Kushen, Radix sophorae flavescentis) 10 g; Common bletilla pseudobulb (Baiji, Rhizoma bletillae) 10 g; Aucklandia (Muxiang, Costustoot) 10 g; Hedyotis diffusa (Baihuasheshecao, Oldenlandia) 10 g; Corydalis tuber (Yanhusuo, Rhizoma corydalis) 10 g; Red peony root (Chishao, Radix paeoniae rubra) 10 g
Xia 2016 [18]	mBTWD	Pulsatilliae Radix (Baitouweng, Chinese bulbul) 30 g; Coptidis Rhizoma (Huanglian, Goldthread) 30 g; Phellodendri Chinrnsis Cortex (Huangbo, Tractat) 30 g; Sophora flavescens (Kushen, Radix sophorae flavescentis) 30 g; Common bletilla pseudobulb (Baiji, Rhizoma bletillae) 30 g; Hedyotis diffusa (Baihuasheshecao, Oldenlandia) 30 g; White peony root (Baishao, Radix paeoniae alba) 30 g
Yang 2012 [19]	mBTWD	Pulsatilliae Radix (Baitouweng, Chinese bulbul) 30 g; Coptidis Rhizoma (Huanglian, Goldthread) 30 g; Phellodendri Chinrnsis Cortex (Huangbo, Tractat) 30 g; Burnet (Diyu, Sanguisorba officinalis) 30 g; Sophora japonica (Huaihua, Flos sophorae) 30 g; Porslane (Machixian, Portulacae herba) 30 g; Honeysuckle (Jinyinhua, Lonicera japonica) 30 g

Table 2: Continued.

First-author (year)	Formula	Components
Jiang 2011 [27]	mBTWD	Pulsatilliae Radix (Baitouweng, Chinese bulbul) 15 g; Coptidis Rhizoma (Huanglian, Goldthread) 3 g; Phellodendri Chinrnsis Cortex (Huangbo, Tractat) 6 g; Fraxini Cortex (Qinpi, Ash bark) 9 g; Burnet (Diyu, Sanguisorba officinalis) 12 g; Dried rehmannia root (Shengdihuang, Radix rehmanniae recen) 12 g; Paeonia suffruticosa (Mudanpi, Moutan bark) 6 g; Red peony root (Chishao, Radix paeoniae rubra) 9 g; Sophora japonica (Huaihua, Flos sophorae) 12 g; Licorice (Gancao, Glycyrrhiza) 6 g
Yao 2014 [24]	mBTWD	Pulsatilliae Radix (Baitouweng, Chinese bulbul) 15 g; Coptidis Rhizoma (Huanglian, Goldthread) 6 g; Fraxini Cortex (Qinpi, Ash bark) 10 g; Burnet (Diyu, Sanguisorba officinalis) 20 g; Astragalus membranaceus (Huangqi, Radix Astragali) 30 g; Atractylodes (Baizhu, Rhizoma atractylodis) 10 g; Angelica sinensis (Danggui, Chinese angelica) 10 g; Dried rehmannia root (Shengdihuang, Radix rehmanniae recen) 15 g; White peony root (Baishao, Radix paeoniae alba) 15 g; Taraxacum (Pugongying, Dandelion) 10 g; Aucklandia (Muxiang, Costustoot) 6 g; Areca-nut (Binglang, Areca catechu) 6 g; Licorice (Gancao, Glycyrrhiza) 5 g
Li 2008 [20]	mBTWD	Pulsatilliae Radix (Baitouweng, Chinese bulbul) 15 g; Coptidis Rhizoma (Huanglian, Goldthread) 6 g; Phellodendri Chinrnsis Cortex (Huangbo, Tractat) 12 g; Fraxini Cortex (Qinpi, Ash bark) 12 g; Burnet (Diyu, Sanguisorba officinalis) 15 g; Saposhnicovia divaricata (Fangfeng, Radix sileris) 12 g
Tong 2012 [25]	mBTWD	Pulsatilliae Radix (Baitouweng, Chinese bulbul) 15 g; Coptidis Rhizoma (Huanglian, Goldthread) 12 g; Radix Scutellariae (Huangqin, Scutellaria baicalensis) 6 g; Fraxini Cortex (Qinpi, Ash bark) 12 g; Pueraria (Gegen, The root of the kudzu vine) 9 g; Fructus schizandrae (Wuweizi, Chinese magnoliavine fruit) 6 g; Cuttle bone (Wuzeigu, The inkfish bone) 10 g
Ma 2021 [9]	BTWD	Pulsatilliae Radix (Baitouweng, Chinese bulbul) 30 g; Coptidis Rhizoma (Huanglian, Goldthread) 12 g; Phellodendri Chinrnsis Cortex (Huangbo, Tractat) 24 g; Fraxini Cortex (Qinpi, Ash bark) 24 g
Wang 2017 [21]	mBTWD	Pulsatilliae Radix (Baitouweng, Chinese bulbul) 30 g; Coptidis Rhizoma (Huanglian, Goldthread) 10 g; Phellodendri Chinrnsis Cortex (Huangbo, Tractat) 10 g; Fraxini Cortex (Qinpi, Ash bark) 20 g; Burnet (Diyu, Sanguisorba officinalis) 10 g; White peony root (Baishao, Radix paeoniae alba) 10 g; Red peony root (Chishao, Radix paeoniae rubra) 10 g; Sophora japonica (Huaihua, Flos sophorae) 10 g; Patrinia (Baijiangcao, White flower Patrinia Herb) 30 g; Aucklandia (Muxiang, Costustoot) 6 g
Zhang 2013 [22]	mBTWD	Pulsatilliae Radix (Baitouweng, Chinese bulbul) 30 g; Coptidis Rhizoma (Huanglian, Goldthread) 10 g; Phellodendri Chinrnsis Cortex (Huangbo, Tractat) 10 g; Fraxini Cortex (Qinpi, Ash bark) 20 g; Burnet (Diyu, Sanguisorba officinalis) 10 g; White peony root (Baishao, Radix paeoniae alba) 10 g; Red peony root (Chishao, Radix paeoniae rubra) 10 g; Sophora japonica (Huaihua, Flos sophorae) 10 g; Common bletilla pseudobulb (Baiji, Rhizoma bletillae) 10 g; Patrinia (Baijiangcao, White flower Patrinia Herb) 30 g; Aucklandia (Muxiang, Costustoot) 6 g
Ye 2007 [28]	mBTWD	Pulsatilliae Radix (Baitouweng, Chinese bulbul) 10 g; Coptidis Rhizoma (Huanglian, Goldthread) 12 g; Phellodendri Chinrnsis Cortex (Huangbo, Tractat) 12 g; Fraxini Cortex (Qinpi, Ash bark) 12 g; Burnet (Diyu, Sanguisorba officinalis) 15 g; Porslane (Machixian, Portulacae herba) 30 g; Sophora flavescens (Kushen, Radix sophorae flavescentis) 10 g; Sophora japonica (Huaihua, Flos sophorae) 15 g; Coix Seed (Yiyiren, Semen coicis) 20 g; Aucklandia (Muxiang, Costustoot) 10 g
Wang 2021 [29]	mBTWD	Pulsatilliae Radix (Baitouweng, Chinese bulbul) 15 g; Phellodendri Chinrnsis Cortex (Huangbo, Tractat) 10 g; Radix Scutellariae (Huangqin, Scutellaria baicalensis) 10 g; Red peony root (Chishao, Radix paeoniae rubra) 20 g; Angelica sinensis (Danggui, Chinese angelica) 15 g; Aucklandia (Muxiang, Costustoot) 10 g; Patrinia (Baijiangcao, White flower Patrinia Herb) 10 g; Coix Seed (Yiyiren, Semen coicis) 10 g; White peony root (Baishao, Radix paeoniae alba) 10 g; Citrus (Chenpi, Tangerine Peel) 10 g; Hairyvein agrimony (Xianhecao, Agrimonia pilosa ledeb) 10 g; Licorice (Gancao, Glycyrrhiza) 5 g 1.Hemafecia: Sophora japonica (Huaihua, Flos sophorae) 10 g, Burnet (Diyu, Sanguisorba officinalis) 15 g, Palm shell charcoal (Zongyutan, Palm kernel shell activated carbon) 15 g

Note. mBTWD, modified Baitouweng decoction.

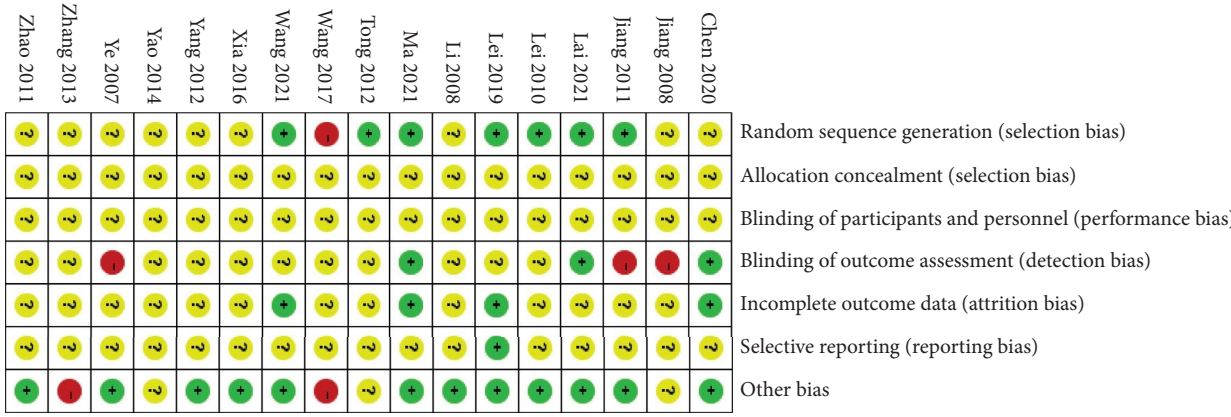

Figure 3: Risk of bias summary.

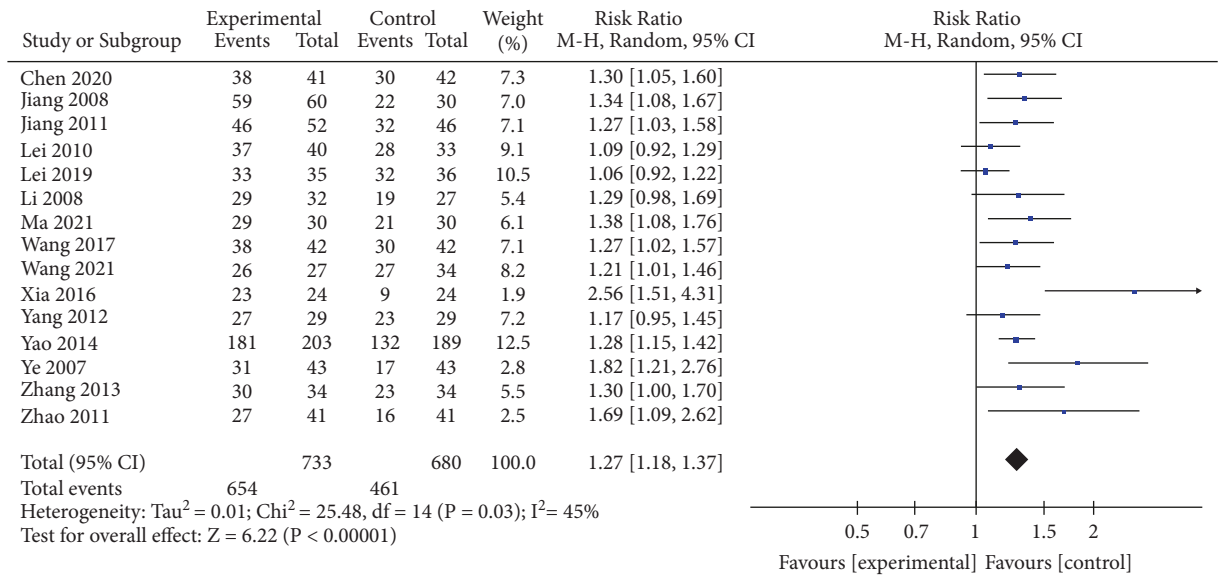

(a)

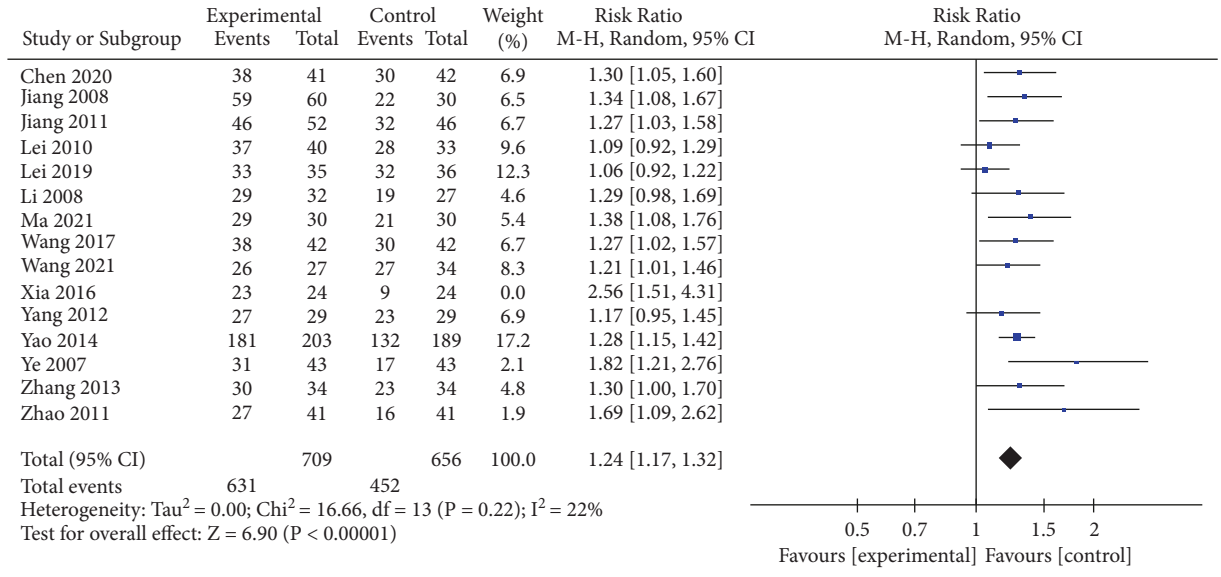

(b)

Figure 4: (a and b) Forest plots of the clinical efficacy.

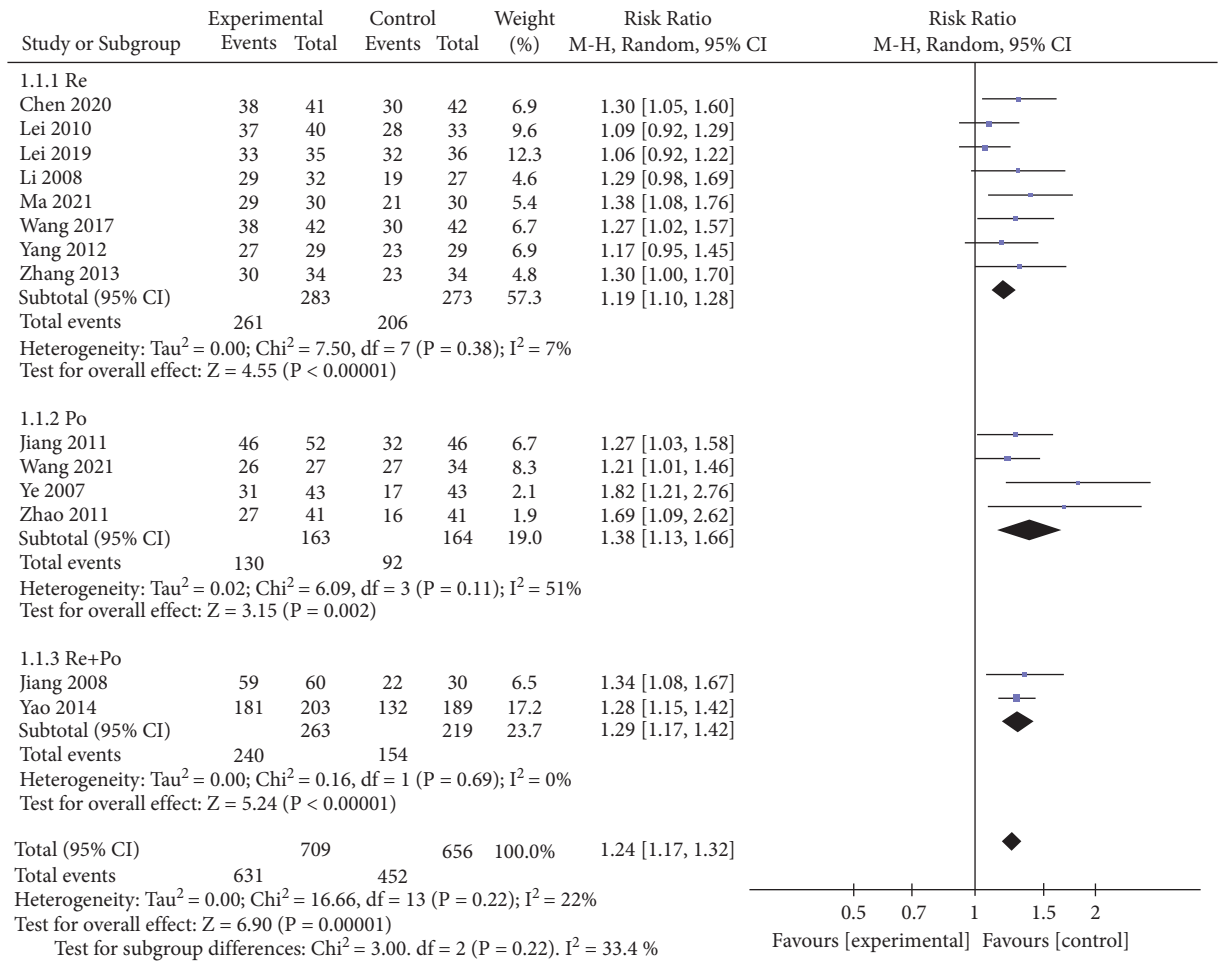

Figure 5: Subgroup analysis of clinical efficacy. Re, retention enema; Po, per os.

heterogeneity ($\text{Chi}^2 = 5.35$, $P = 0.02$, $I^2 = 81\%$) (Figure 7). After careful reading of that two studies, we find the heterogeneity may come from different scoring criteria. Instead of a random-effects model, there is a statistically significant difference between the two groups (MD = −0.71, 95% CI (−1.22, −0.20), $P = 0.006$) (Figure 7).

Two studies [16, 24], with a total of 463 patients, compare the efficacy of mBTWD alone with combined CWM by estimating the grade of colonoscopy. According to the Gareau classification criteria of Gareau et al. [30], intestinal mucosal injury under colonoscopy is divided into degrees 0 to IV: 0-II, intestinal mucosal injury is significantly improved or normalized; III to normal; III-IV, the injury of the intestinal mucosa is serious or irreversible. Meta-analysis is conducted according to 0-II and III-IV, respectively, and the results show good homogeneity between studies of different grades ($\text{Chi}^2 = 0.33$, $P = 0.57$, $I^2 = 0\%$; $\text{Chi}^2 = 0.22$, $P = 0.64$, $I^2 = 0\%$) (Figure 8). Moreover, there is a significant difference in colonoscopy grade between the two groups after treatment (RR = 1.23, 95% CI (1.11, 1.36), $P = 0.0001$; RR = 0.51, 95% CI (0.36, 0.72), $P = 0.0001$) (Figure 8).

Six studies [9, 15, 16, 25, 26, 29], with a total of 483 patients, report the comparison of radiation enteritis grading between the mBTWD and CWM groups. According to the RTOG/EORCT radiation injury classification scheme [31], the intestinal reaction after radiotherapy is classified into degrees 0–IV: 0–II, the intestinal reaction is significantly improved or restored to normal; III-IV, the intestinal reaction is serious or irreversible. The meta-analysis is conducted according to 0-II and III-IV, respectively; there is little heterogeneity among these studies at different grades ($\text{Chi}^2 = 4.54$, $P = 0.47$, $I^2 = 0\%$; $\text{Chi}^2 = 4.54$, $P = 0.47$, $I^2 = 0\%$) (Figure 9). Moreover, there is a significant difference in radiation enteritis grading between the two groups after treatment (OR = 3.51, 95% CI (2.22, 5.54), $P < 0.00001$; OR = 0.29, 95% CI (0.18, 0.45), $P < 0.00001$) (Figure 9).

Overall results show that mBTWD can significantly improve intestinal mucosal injury and reduce the degree of intestinal reaction after radiotherapy.

3.3.4. C-Reactive Protein Level. Two studies [9, 16] report a comparison of C-reactive protein (CRP) levels between groups, with both control groups treated with 0.9% NaCl solution 100 ml + dexamethasone 10 mg + montmorillonite powder 6 g. No heterogeneity is found in the results ($\text{Chi}^2 = 0.19$, $P = 0.66$, $I^2 = 0\%$) (Figure 10). Therefore, with a fixed effect model, there is a significant difference in mBTWD versus CWM (MD = −5.28, 95% CI (−7.41, −3.14), $P < 0.00001$) (Figure 10).

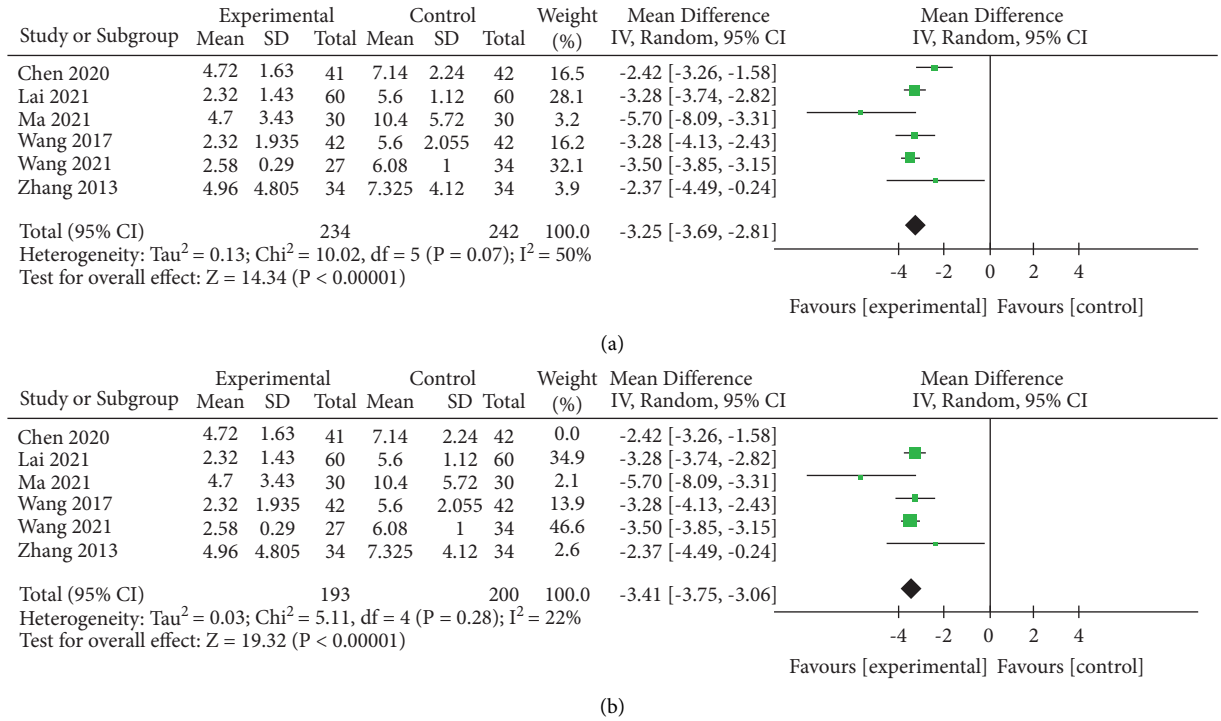

Figure 6: Forest plots of the total score of TCM syndrome. (a) Original data. (b) After eliminating the study with a large heterogeneity.

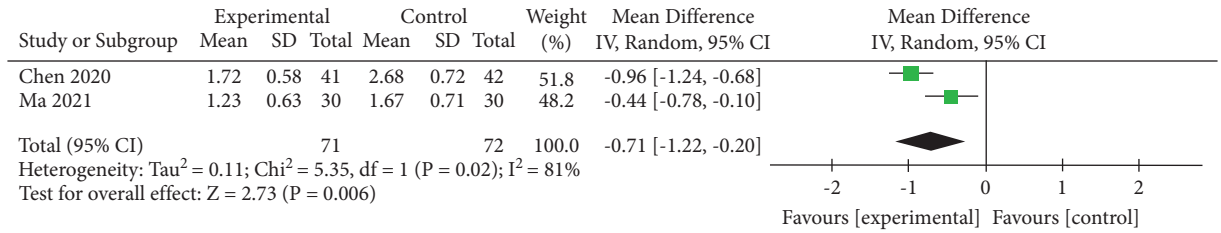

Figure 7: Forest plots of colonoscopy score.

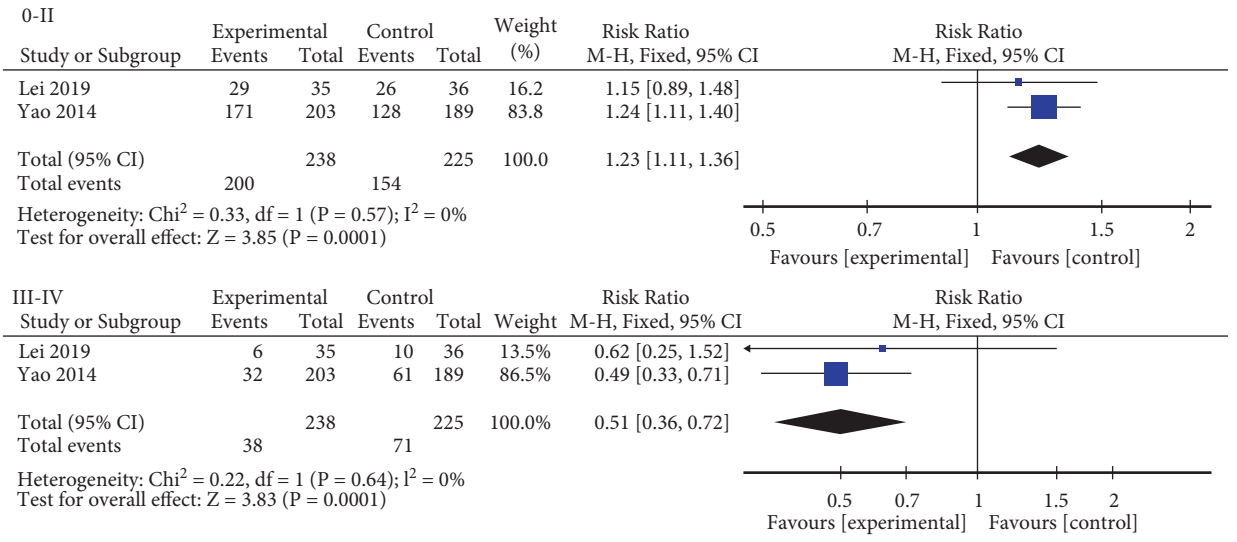

Figure 8: Forest plots of colonoscopy grade (0–IV degree). 0–II, the injury of the intestinal mucosa is significantly improved or restored to normal; III-IV, the injury of the intestinal mucosa is serious or irreversible.

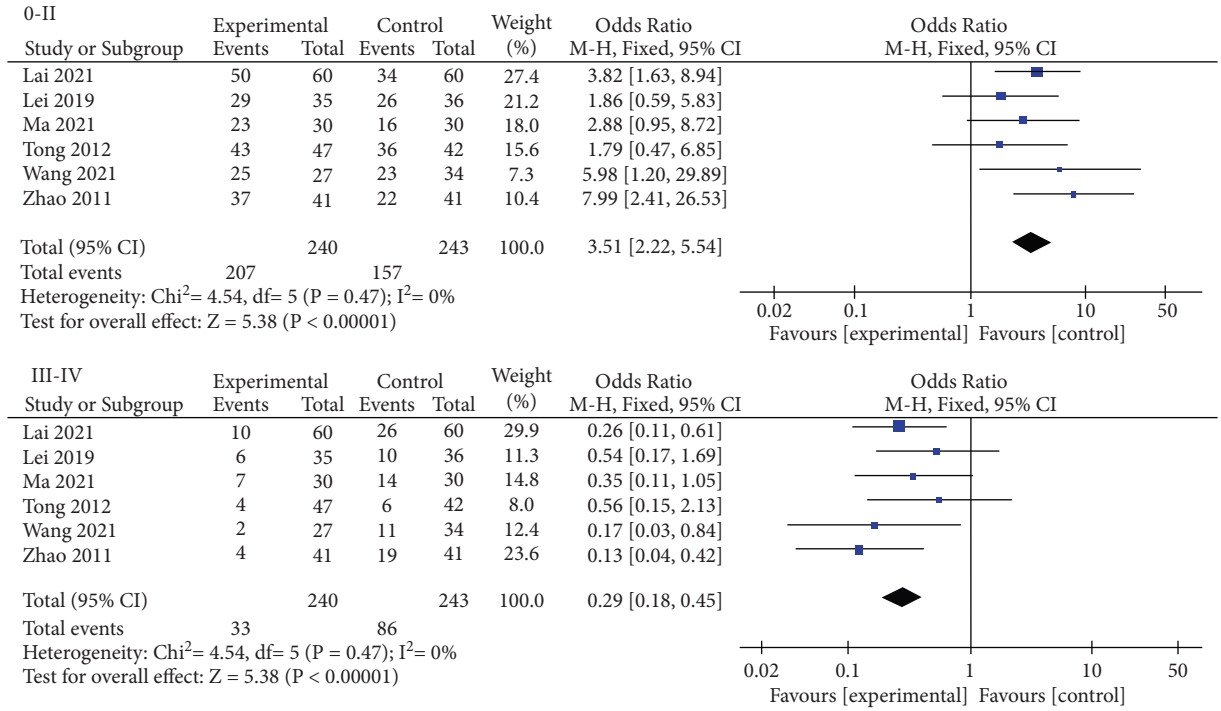

Figure 9: Forest plots of radiation enteritis classification (0, IV degree). 0-II, the intestinal reaction is significantly improved or restored to normal; III-IV, the intestinal reaction is serious or irreversible.

3.3.5. Karnofsky Performance Scale. Five studies report the comparison of the Karnofsky performance scale (KPS) score [32] among mBTWD and CWM groups. Three of these studies [14, 15, 29] with a total of 264 radiation enteritis patients, describing continuous variables. As shown in Figure 11(a), there is a high heterogeneity in the results ($\text{Chi}^2 = 59.03$, $P < 0.00001$, $I^2 = 97\%$). Then, a subgroup analysis is performed due to differences in KPS score before treatment: KPS = 40–60 and KPS > 60 before treatment. The results show that heterogeneity decreased significantly after the subgroup analysis ($\text{Chi}^2 = 1.13$, $P = 0.29$, $I^2 = 12\%$). Moreover, the KPS score is significantly different between the two groups (MD = 15.32, 95% CI (5.62, 25.01), $P = 0.002$) (Figure 11(a)).

Two studies [16, 25] with a total of 160 patients report the number of patients with a KPS greater than 80 after treatment, which is a dichotomous variable. There is little heterogeneity in the results ($\text{Chi}^2 = 0.07$, $P = 0.79$, $I^2 = 0\%$) (Figure 11(b)). And the difference between the two groups is statistically significant (RR = 1.23, 95% CI (1.02, 1.48), $P = 0.03$) (Figure 11(b)).

3.3.6. Fecal Occult Blood. Two studies [9, 16] with a total of 131 patients report the comparison of occult fecal blood (OB) between mBTWD and the CWM groups. We mainly analyze the number of patients with negative or weakly positive fecal occult blood tests (OB: 0~+) after treatment. There is slight heterogeneity in the results ($\text{Chi}^2 = 0.01$, $P = 0.91$, $I^2 = 0\%$) (Figure 12). Hence, the improvement of fecal occult blood is significantly different between the two groups (RR = 1.47, 95% CI (1.03, 2.08), $P = 0.03$) (Figure 12).

3.3.7. Safety. No serious adverse events occur in nearly all of the studies, and there is no significant difference in the incidence of adverse events between the intervention groups and the control group.

Two studies with 481 radiation enteritis patients that compared mBTWD with CWM are identified in this analysis [24, 25]. The heterogeneity between the two studies is large ($\text{Chi}^2 = 3.72$, $P = 0.05$, $I^2 = 73\%$) (Figure 13). Hence, the difference in the rate of recurrence between the two groups is not statistically significant (RR = 0.07, 95% CI (0.00, 2.21), $P = 0.13$) (Figure 13).

3.4. Univariate Meta Regression. Since more than 10 studies are included in the analysis of clinical efficacy, we conduct a univariate meta regression here to explore the association between the clinical efficacy indicator and the difference in intervention, drug delivery, sample size, publication year, or other characteristics of the studies including the mean age and duration of treatment. Both dichotomous and continuous covariates are employed in the regression models; the results of the univariate meta-regression analyses are presented in Table 3 and Figure 14. It is found that the association with the effect size of the intervention (mBTWD with CWM) on the clinical efficacy of mBTWD in the treatment of radiation enteritis is not statistically significant (meta-regression coefficient 1.014, CI 0.859, 1.198, $P = 0.852$, $I^2 = 39.730\%$, $\text{Tau}^2 = 0.328\%$), suggesting that the difference in the intervention is unlikely to increase clinical efficacy with the baseline levels. Then none of the coefficients of other covariates are significantly associated with the estimated risk ratio, and for this specific reason, multivariate analyses are not performed.

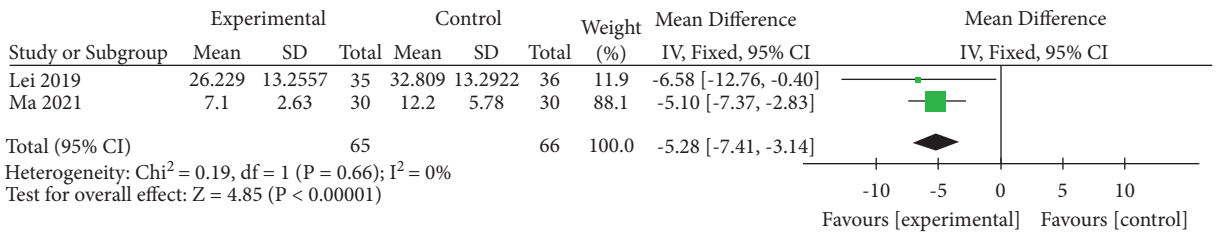

Figure 10: Forest plots of CRP level. CRP, C-reactive protein.

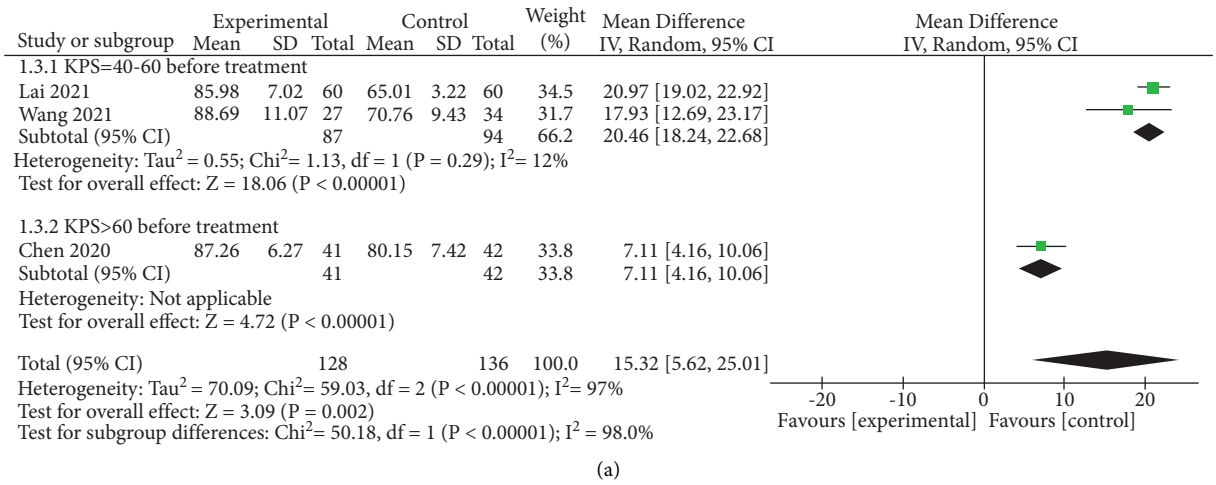

(a)

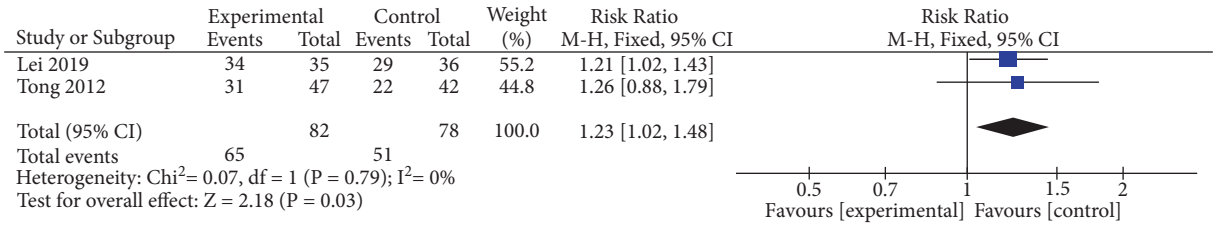

(b)

Figure 11: Forest plots of KPS score. KPS, Karnofsky. (a) Continuous variable. (b) Dichotomous variable.

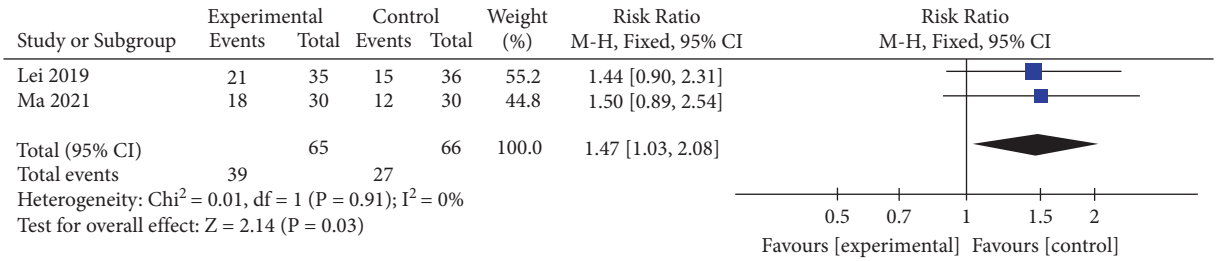

Figure 12: Forest plots of fecal occult blood.

3.5. Publication Bias. Since most clinical outcome variables contain less than 10 studies, performing the funnel plot could be of little significance, so it is difficult to fully identify the risk of publication bias. Specifically, the meta-analysis of the clinical efficacy indicator contained up to 15 eligible studies for us to conduct a Funnel plot, as shown in Figure 15(a), visual inspection of the funnel plot suggests a little asymmetry, indicating the existence of publication bias.

Furthermore, we accurately perform publication bias using Egger's test (Figure 15(b)) and Begg's test (Figure 15(c)). All analyses are performed with Stata 14.0 software and results are shown with 95% confidence intervals. Both Egger's test and Begg's test detect the existence of publication bias (coefficient = 2.175, $P = 0.006$), indicating that the validity and generalization of our conclusions would be limited and affected due to possible publication bias.

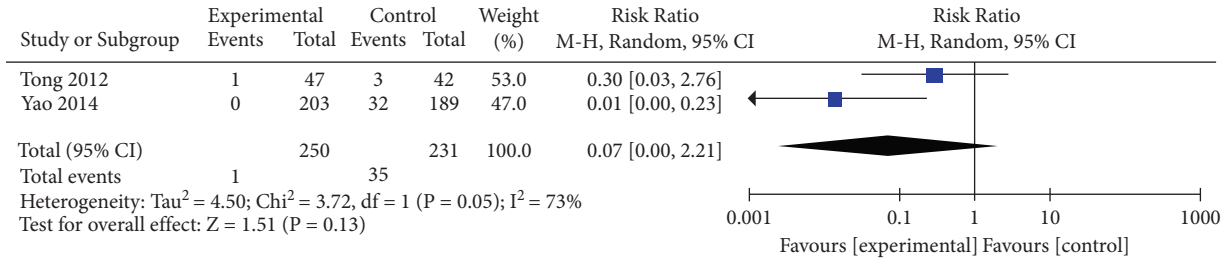

Figure 13: Forest plots of recurrence rate.

Table 3: Univariate meta-regression analyses of clinical efficacy.

Univariate meta-regression models	No. of studies	I^2 (%)	Tau^2 (%)	P value	Estimated risk ratio* (95% CI)
Intervention					
mBTWD with CWM	6	39.730	0.328	0.852	1.014 (0.859, 1.198)
mBTWD without CWM	9				
Drug deliver					
Re	9			0.800	1.030 (0.801, 1.326)
Po	4	38.560	0.321	0.520	0.941 (0.770, 1.149)
Re + Po	2				
Sample size	15	39.440	0.004	0.878	1.000 (0.993, 1.001)
Mean age	14▲	34.660	0.003	0.747	1.002 (0.984, 1.022)
Duration	12■	45.510	0.006	0.849	1.000 (0.994, 1.007)
Publication year	15	38.400	0.003	0.567	0.995 (0.978, 1.013)

Note. *Statistics including Tau^2, I^2, and P values are derived from meta-regression models conducted with Stata 14.0, estimated risk ratio is obtained using the conventional fixed-effects model with 95% confidence interval (CI). Both dichotomous and continuous covariates are employed in the regression models. ▲Ye and Wang [28] report related data without mean age. ■Ye and Wang [28], Wang [21], and Wang et al. [29] report related data without duration time.

Thus, we try to employ another Funnel-plot-based trim and fill method to deal with the potential impact of publication bias, as shown in Figure 15(d). In the trim and fill method, we can re-estimate the actual effect size by filling in the "missing" studies and forming a new pooled estimate until the funnel plot reaches a new symmetry. After 4 iterations, the procedure identifies and trims 4 studies (4 inserted studies as their theoretical counterparts) until the distribution is symmetrical, with the overall effect size estimated as RR = 1.21 (95% CI from 1.12 to 1.31, $P < 0.001$). Compared with our initial pooled effect size of RR = 1.27, which is substantially larger than the bias-corrected effect size and indicates that the potential publication bias made the initial results overestimated (approximately 4.9%), the real effect when controlling for selective publication bias could be slightly lower. This indicates that our results are still robust even with the occurrence of publication bias.

3.6. Assessment Quality of Evidence. Several types of evidence for mBTWD in the treatment of radiation enteritis are included in our meta-analysis; the GRADE evidence rating levels performed with the online tool are shown in Table 4. The evidence quality for clinical efficacy and recurrence rate is rated as very low due to serious clinical or statistical heterogeneity problems in risk of bias, inconsistency, imprecision, or publication bias. The quality of the evidence for KPS is rated low with other conditions rated moderate. The criteria and reasons for upgrading or lowering the quality of evidence for each outcome are as follows. (1) Study design: all studies included in this paper are randomized controlled trials that satisfied our inclusion criteria. (2) Risk of bias: although sensitivity analysis that excludes trials with a high risk of bias does not change the main results, all of these studies are downgraded due to a lack of blinding. (3) Inconsistency: high statistical heterogeneity ($I^2 > 50\%$) occurrence will downgrade the evidence quality to a lower level; three outcomes are marked as serious inconsistency. (4) Indirectness: mBTWD is implemented in the treatment of radiation enteritis and is directly related to those clinical outcomes in our study, so there is no downgrade of evidence. (5) Imprecision: the evidence will be downgraded if the 95% CI crosses no treatment effect or if the estimated effect size is significantly different ($P > 0.05$). (6) Other Considerations: downgrades if serious publication bias is detected to be significant ($P < 0.05\%$), which occurs in the clinical efficacy analysis.

3.7. Sensitivity Analysis. With evidence of the publication bias, we also propose sensitivity analyses to investigate the potential causes of heterogeneity and identify unbalanced or disproportionate contributions to the observed bias from these trials. Sensitivity analyzes are performed using *metainf* command with Stata 14.0, by repeating the baseline meta-analysis by excluding assumed "biased" trials one-by-one to

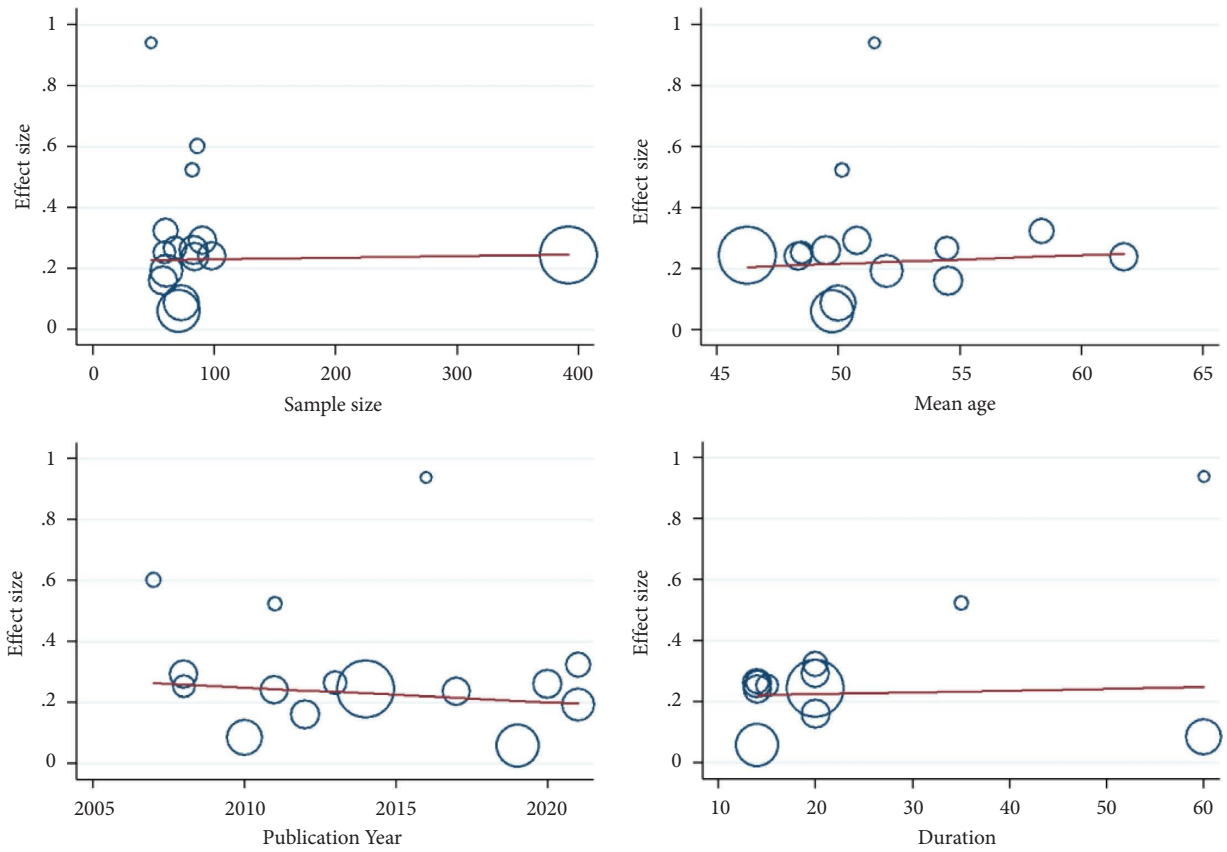

Figure 14: Meta-regression of clinical efficacy with continuous covariates.

assess their impact on the overall estimate; relevant results are shown in Figure 16(a). It is shown that dropping out trials one by one may have little impact on the overall estimated effect size while expanding the confidential levels from (1.18, 1.36) to (1.17, 1.38). Among those excluded studies, dropping Xia [18] and Ye and Wang [28] may lead to a lower effect size while excluding Lei [17] and Lei [16] could cause a higher effect size. For better visual inspection, we also introduce the Galbraith plot to identify possible outlier studies that have an excessive influence on the overall estimate (Figure 16(b)). From the Galbraith plot, we could draw a similar conclusion that these four studies [16–18, 28] are the main possible outliers with a higher risk of heterogeneity and can be correlated with publication bias.

3.8. Network Analysis and Molecular Docking Results

3.8.1. Active Ingredients and Targets Screening Results. According to the OB and DL characteristics of the compounds, a total of 65 active ingredients are obtained from the TCMSP database; there are 11 in Baitouweng (BTW), 37 in Huangbo (HB), 14 in Huanglian (HL), and 3 in Qinpi (QP). After removing the duplicate ingredients, a total of 51 are left (Table 5). Then, we screen the corresponding targets of the active ingredients, and 987 human-derived target proteins are obtained after the duplicate targets are removed. The Cytoscape 3.8.2 software is used to connect the active ingredients-targets network. The network consists of 175 nodes and 381 edges, these nodes represent compounds and the corresponding targets, and edges represent interactions between compounds and target proteins (Figure 17).

3.8.2. Prediction and Construction of Drug-Disease Networks. Five databases (OMIM, GeneCards, PharmGkb, DrugBank, and TTD) are searched to obtain 2642 disease targets related to radiation enteritis. Using the R language program and Venny2.1 software, the intersection of mBTWD and radiation enteritis targets is selected, and finally 139 common drug-disease targets are screened out. Finally, Cytoscape 3.8.2 software is used to build the mBTWD active ingredients-targets-radiation enteritis network (Figure 18). Of these, quercetin (MOL000098) interacted with 114 targets, isorhamnetin (MOL000354) interacted with 21 targets, and beta-sitosterol (MOL000358) interacted with 18 targets. Other compounds, such as stigmasterol (MOL000449) and aureusidin (MOL001978), are associated with multiple targets, suggesting that the compounds in BTWD may exert pharmacological effects against radiation enteritis by acting together on these targets.

3.8.3. PPI Network of Key Targets. These 139 drug-disease common targets are imported into the STRING database, and the PPI network of targets for mBTWD against radiation enteritis could be obtained by removing the noncorrelated targets. Then the PPI network is imported into Cytoscape

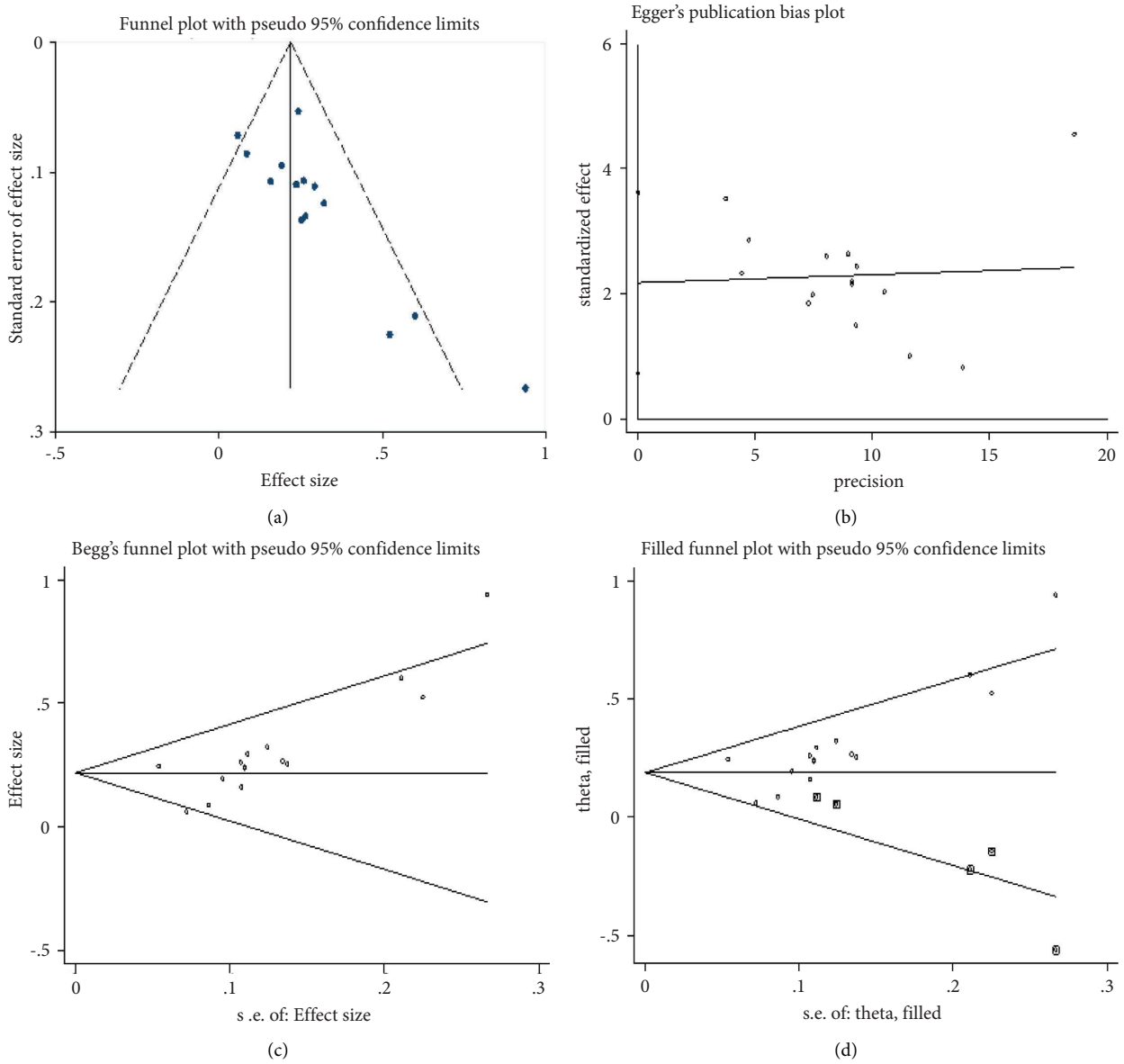

Figure 15: Funnel plots of clinical efficacy of mBTWD in treating radiation enteritis. (a) Basic funnel plot. (b) Egger's funnel plot. (c) Begg's funnel plot. (d) Filled funnel plot of metatrim analysis.

3.8.2 software, and the CytoNCA plug-in is used to calculate the median value of network nodes. Finally, eleven key targets are obtained, and the PPI network of core targets is constructed. The larger the node, the darker the color, and the higher the DC value (Figure 19). From the network, we can see that the top four are MYC, TP53, MAPK14, and MAPK1, and their DC values are 9, 8, 8, and 8, respectively. These results indicate that these targets are the key targets of BTWD in the treatment of radiation enteritis.

3.8.4. GO and KEGG Enrichment Analysis of Key Targets. The ClueGO plug-in is used to perform GO functional annotation and KEGG signal pathways enrichment analysis for the key targets of BTWD in the treatment of radiation enteritis (filter criteria $P < 0.05$). The GO enrichment analysis mainly refers to biological process (BP), and a total of 2183 GO items are obtained, mainly involving response to lipopolysaccharide, response to xenobiotic stimulus, and response to molecule of bacterial origin and wound healing (Figure 20(a)). A total of 172 signal pathways are identified in the KEGG enrichment analysis, which are found in the lipid and atherosclerosis, PI3K-Akt signaling pathway, and chemical carcinogenesis-receptor activation (Figure 20(b)).

According to the results of the KEGG enrichment analysis, we select the "hsa0415" (PI3K-Akt signaling pathway) to draw a pathway map using the Pathview plug-in. And the red nodes indicate that the key target genes exist in the regulatory network (Figure 21).

Table 4: GRADE evidence for mBTWD in treating radiation enteritis.

No. of studies	Study design	Risk of bias	Inconsistency	Indirectness	Imprecision	Other considerations	Quality of evidence
Clinical efficacy							
15	RCTs	Serious	Serious	Not serious	Not serious	Publication bias	⊕○○○ very low
Tcm syndrome total score							
6	RCTs	Serious	Not serious	Not serious	Not serious	None	⊕⊕⊕○ moderate
Colonoscopy score							
2	RCTs	Serious	Not serious	Not serious	Not serious	None	⊕⊕⊕○ moderate
Colonoscopy grade (0–II)							
2	RCTs	Serious	Not serious	Not serious	Not serious	None	⊕⊕⊕○ moderate
Colonoscopy grade (III-IV)							
2	RCTs	Serious	Not serious	Not serious	Not serious	None	⊕⊕⊕○ moderate
Radiation enteritis grading (0–II)							
6	RCTs	Serious	Not serious	Not serious	Not serious	None	⊕⊕⊕○ moderate
Radiation enteritis grading (III-IV)							
6	RCTs	Serious	Not serious	Not serious	Not serious	None	⊕⊕⊕○ moderate
CRP							
2	RCTs	Serious	Not serious	Not serious	Not serious	None	⊕⊕⊕○ moderate
KPS							
3	RCTs	Serious	Serious	Not serious	Not serious	None	⊕⊕○○ low
OB							
2	RCTs	Serious	Not serious	Not serious	Not serious	None	⊕⊕⊕○ moderate
Recurrence rate							
2	RCTs	Serious	Serious	Not serious	Serious	None	⊕○○○ very low

Moderate quality means the estimated effect sizes and their confidence levels may be affected by further studies; low quality represents that the estimated effect sizes and their confidence levels are likely to be affected or changed by further research; very low-quality shows that the estimated effect sizes and their confidence levels are confronted of huge uncertainty.

3.8.5. Molecular Docking of Active Ingredients and Key Targets. According to the PPI network, the key targets of mBTWD in the treatment of radiation enteritis are MYC, TP53, MAPK14, and MAPK1. Molecular coupling is performed for the 4 core targets with the active ingredients of mBTWD and the positive control drug dexamethasone. Affinity $< -5.0\ \text{kJ}\cdot\text{mol}^{-1}$ indicated good binding activity between ligands and receptors [33]. The results show that MAPK1 has the highest binding activity with quercetin (affinity $= -8.5\ \text{kJ}\cdot\text{mol}^{-1}$), followed by TP53 with quercetin (affinity $= -8.3\ \text{kJ}\cdot\text{mol}^{-1}$). MAPK14 with aureusidin (affinity $= -7.7\ \text{kJ}\cdot\text{mol}^{-1}$), MAPK14 with isorhamnetin (affinity $= -7.2\ \text{kJ}\cdot\text{mol}^{-1}$). Additionally, the binding activity of these active ingredients with the key targets is stronger than the positive control drug dexamethasone (Table 6). The optimal molecular docking diagram is shown in Figure 22.

4. Discussion

4.1. Summary of the Evidence and Results. Radiation enteritis is a common side effect of radiotherapy in patients with pelvic/abdominal malignancy. The small intestine is quite sensitive to radiation, and radiotherapy could easily cause intestinal wall damage, leading to inflammatory infiltration of intestinal epithelial cells. Patients present with an intolerable change in stool habits that last for a long time, causing the discontinuation of radiotherapy, which severely impair their quality of life and reduce survival [34]. Acute radiotoxicity mainly damages the intestinal mucosa, leading to a decrease in the normal intestinal villous epithelial barrier and presenting as abdominal pain. Chronic radiation toxicity primarily affects the muscular and serosal layers, causing vascular degeneration and fibrosis, and manifests itself as chronic diarrhea and malabsorption, the formation of ischemic intestinal disease, intestinal flora disorder, and chronic enteritis, followed by an intestinal mucosal ulcer, perforation or abscess, and finally, the formation of intestinal obstruction and microbial over-propagation [35, 36]. Evidence also suggests that gut microbiota dysbiosis plays an important role in the development of radiation enteritis, and it is a reminder that radiation injury can be relieved by modifying the local microecosystem [1, 2]. Therefore, some formulae of Chinese medicine with an anti-inflammatory effect, such as Baitouweng decoction, may be a complementary means for recurrent radiation enteritis that is difficult to control by conventional western medicine.

The results of this meta-analysis show that mBTWD alone or in combination with CWM can benefit patients with radiation enteritis with better clinical efficacy than CWM alone. Due to the moderate heterogeneity ($P = 0.03$, $I^2 = 45\%$), we eliminate the study [18] for its unclear diagnostic criteria by sensitivity analysis. In addition, subgroup analysis is performed according to different drug deliver (Re, Po, and Re + Po) to identify possible sources of heterogeneity; we find that the heterogeneity of these subgroups are decreased ($P = 0.38$, $I^2 = 7\%$; $P = 0.11$, $I^2 = 51\%$; $P = 0.69$, $I^2 = 0\%$), this indicates that there is indeed some heterogeneity in different drug deliver. In light of the P value results of Re and Po ($P < 0.00001$; $P = 0.002$), we believe that the difference in efficacy of retention enema seems to be

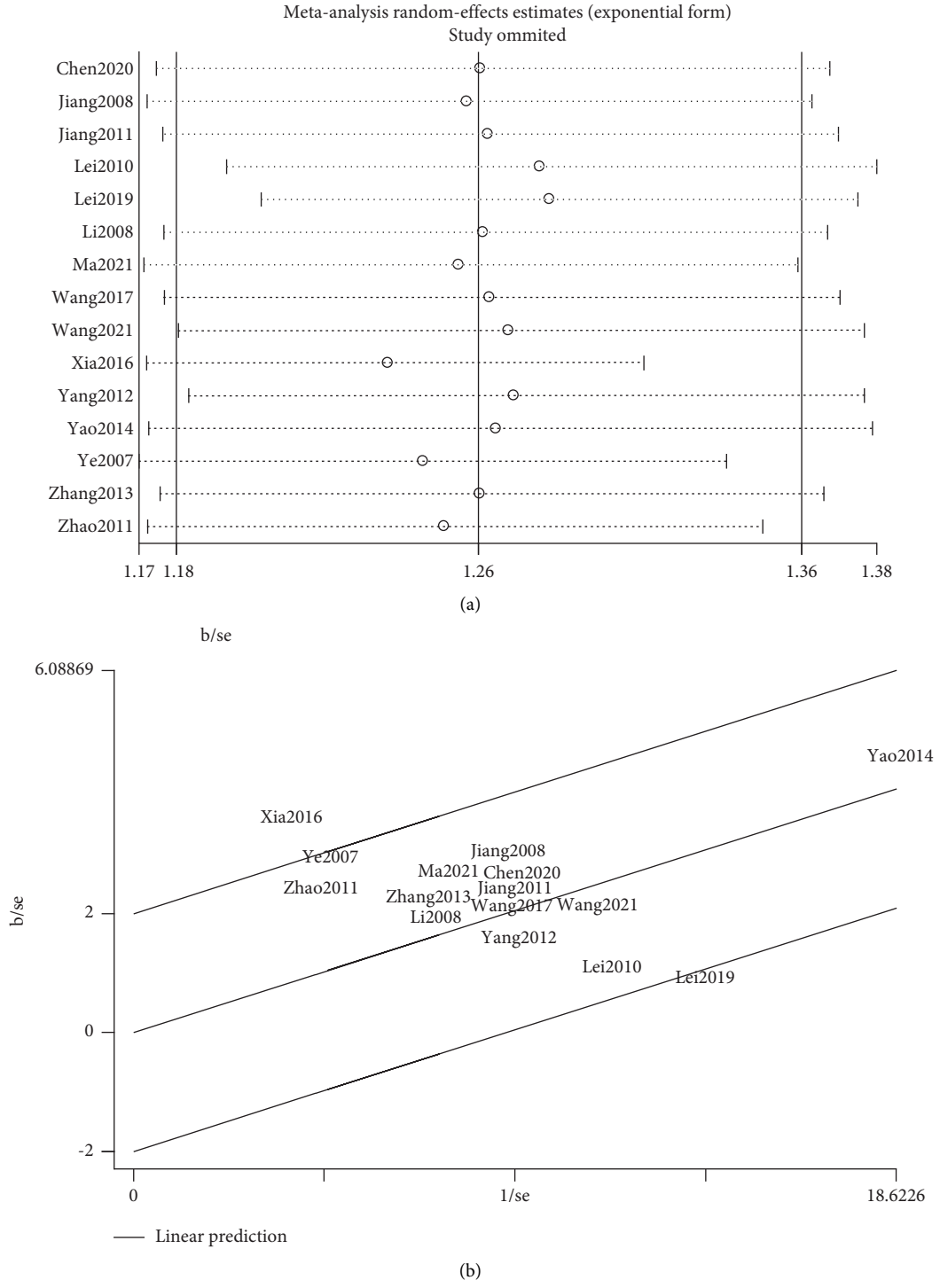

Figure 16: Sensitivity analyses of the clinical efficacy of mBTWD in treating radiation enteritis. (a) The one-by-one dropped out estimation results. (b) The Galbraith plot.

more significant. This might be due to the reason the TCM decoction can be quickly absorbed into the blood through the intestinal mucosa after the enema, acting directly on the lesions and avoiding the elimination of drugs by the hepatoenteric circulation [37]. To sum up, based on the remaining 14 studies, we have reason to think that mBTWD has a good clinical effect on radiation enteritis, and the effect can be increased by about 24% compared with the control groups (RR = 1.24, $P < 0.00001$). A study comparing montmorillonite powder alone or combined with dexamethasone in the treatment of acute radiation enteritis reports that the clinical efficacy of the two groups is 72.09% and 97.67%, respectively [38]. While the results of the meta-analysis in this article show that the mean clinical efficacy of

Table 5: The main active ingredients of representative drugs in mBTWD.

Mol ID	MolName	OBA (%)	DL	Herb
MOL001971	Pulchinenoside c_qt	37.79	0.76	BTW
MOL001973	Sitosteryl acetate	40.39	0.85	BTW
MOL001978	Aureusidin	53.42	0.24	BTW
MOL001979	Lan	42.12	0.75	BTW
MOL001984	3beta, 23-Dihydroxy-lup-20 (29)-ene-28-o-alpha-l-rhamnopyranosyl-(1-4)-beta-d-glucopyranosyl (1-6)-beta-d-glucopyranoside_qt	37.59	0.79	BTW
MOL001985	Zinc01615307	56.38	0.87	BTW
MOL001987	B-sitosterol	33.94	0.7	BTW
MOL000211	Mairin	55.38	0.78	BTW
MOL000354	Isorhamnetin	49.6	0.31	BTW
MOL000449	Stigmasterol	43.83	0.76	BTW, HB
MOL000358	Beta-sitosterol	36.91	0.75	BTW, HB, QP
MOL001454	Berberine	36.86	0.78	HB, HL
MOL001458	Coptisine	30.67	0.86	HB, HL
MOL002636	Kihadalactone a	34.21	0.82	HB
MOL013352	Obacunone	43.29	0.77	HB, HL
MOL002641	Phellavin_qt	35.86	0.44	HB
MOL002643	Delta 7-stigmastenol	37.42	0.75	HB
MOL002644	Phellopterin	40.19	0.28	HB
MOL002651	Dehydrotanshinone ii a	43.76	0.4	HB
MOL002652	Delta7-dehydrosophoramine	54.45	0.25	HB
MOL002656	Dihydroniloticin	36.43	0.81	HB
MOL002659	Kihadanin a	31.6	0.7	HB
MOL002660	Niloticin	41.41	0.82	HB
MOL002662	Rutaecarpine	40.3	0.6	HB, HL
MOL002663	Skimmianin	40.14	0.2	HB
MOL002666	Chelerythrine	34.18	0.78	HB
MOL002668	Worenine	45.83	0.87	HB, HL
MOL002670	Cavidine	35.64	0.81	HB
MOL002671	Candletoxin a	31.81	0.69	HB
MOL002672	Hericenone h	39	0.63	HB
MOL002673	Hispidone	36.18	0.83	HB
MOL000622	Magnograndiolide	63.71	0.19	HB, HL
MOL000762	Palmidin a	35.36	0.65	HB, HL
MOL000785	Palmatine	64.6	0.65	HB, HL
MOL000787	Fumarine	59.26	0.83	HB
MOL000790	Isocorypalmine	35.77	0.59	HB
MOL000098	Quercetin	46.43	0.28	HB, HL
MOL001131	Phellamurin_qt	56.6	0.39	HB
MOL001455	(s)-canadine	53.83	0.77	HB
MOL001771	Poriferast-5-en-3beta-ol	36.91	0.75	HB
MOL002894	Berberrubine	35.74	0.73	HB, HL
MOL005438	Campesterol	37.58	0.71	HB
MOL006401	Melianone	40.53	0.78	HB
MOL006413	Phellochin	35.41	0.82	HB
MOL006422	Thalifendine	44.41	0.73	HB
MOL002897	Epiberberine	43.09	0.78	HL
MOL002903	(r)-canadine	55.37	0.77	HL
MOL002904	Berlambine	36.68	0.82	HL
MOL002907	Corchoroside a_qt	104.95	0.78	HL
MOL006709	Aids214634	92.43	0.55	QP
MOL006710	8-(beta-d-glucopyranosyloxy)-7-hydroxy-6-methoxy-2h-1-benzopyran-2-one	36.76	0.42	QP

mBTWD combination therapy is approximately 89.2%. This suggests that for the treatment of acute radiation enteritis, mBTWD combined with dexamethasone can be effective in relieving symptoms.

mBTWD combination therapy can significantly improve the symptoms of TCM. Compared to western medicine treatment alone, mBTWD combination therapy alleviates symptoms of bellyache, diarrhea, tenesmus, and muco-sanguineous feces in patients with radiation enteritis, and the total score of the TCM syndrome decreases by an average of 3.41 points ($MD = -3.41$, $P < 0.00001$). Furthermore, mBTWD could improve the local bowel symptoms in

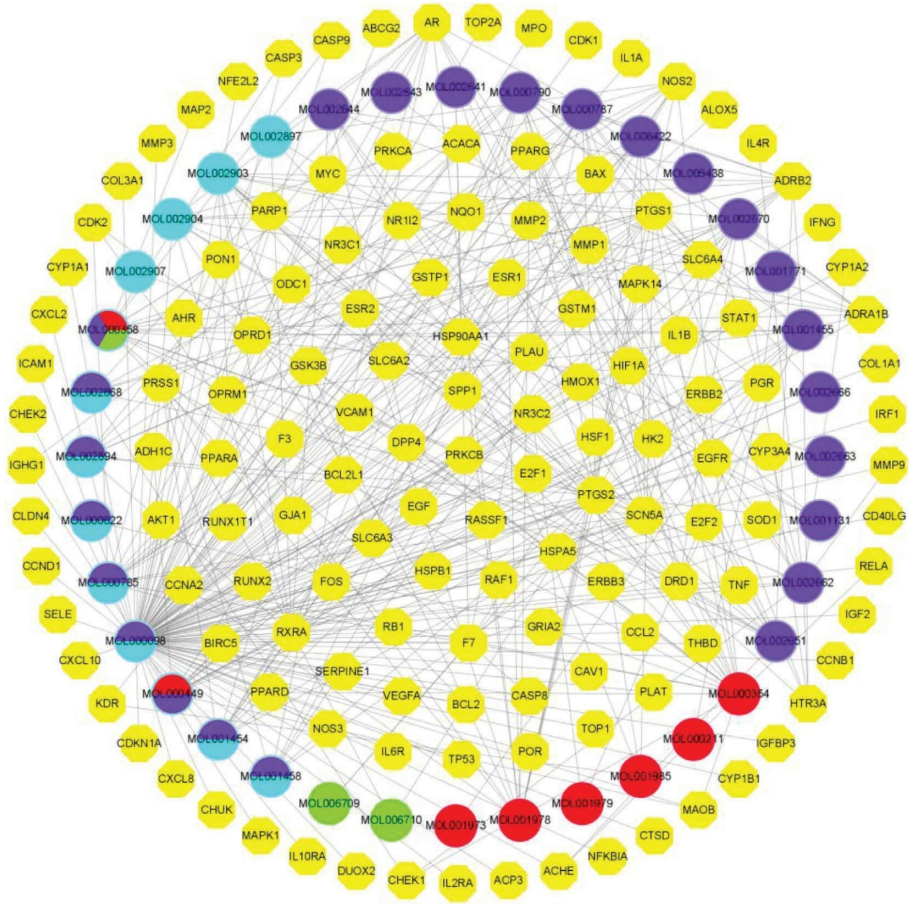

Figure 17: Network of active ingredients-targets. Yellow: human-derived target proteins. Red: Baitouweng. Purple: huangbo. Light blue: huanglian. Green: Qinpi. Mixed color: multidrug.

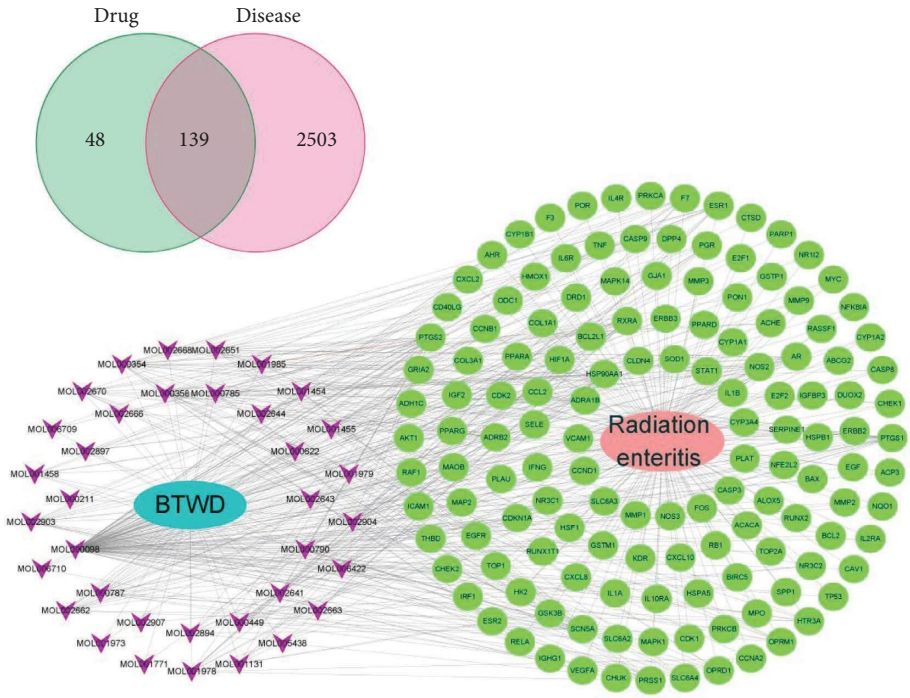

Figure 18: Network of BTWD active ingredients-targets-radiation enteritis.

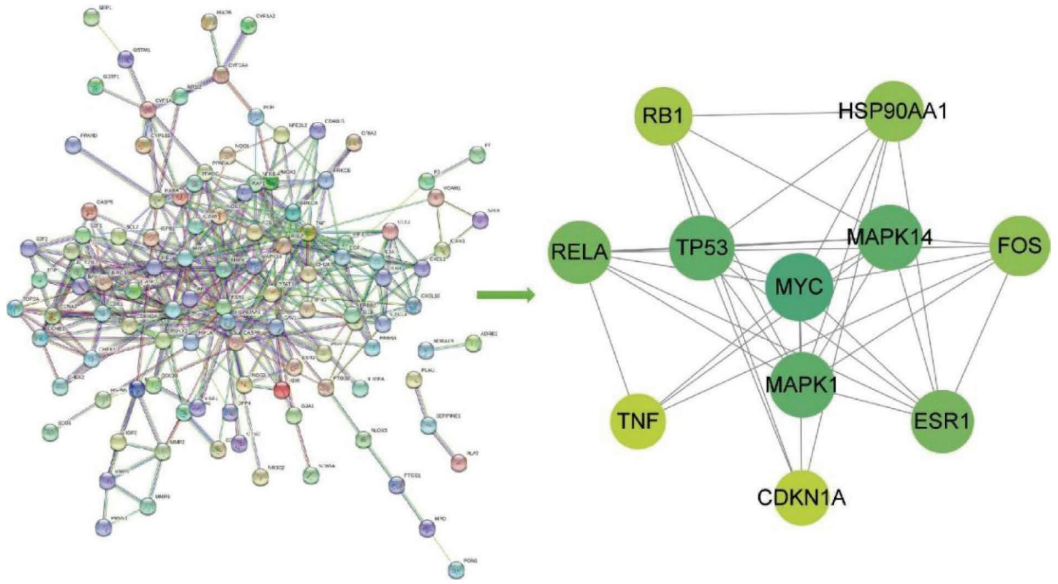

Figure 19: PPI network of the key targets for representative drugs in mBTWD against radiation enteritis.

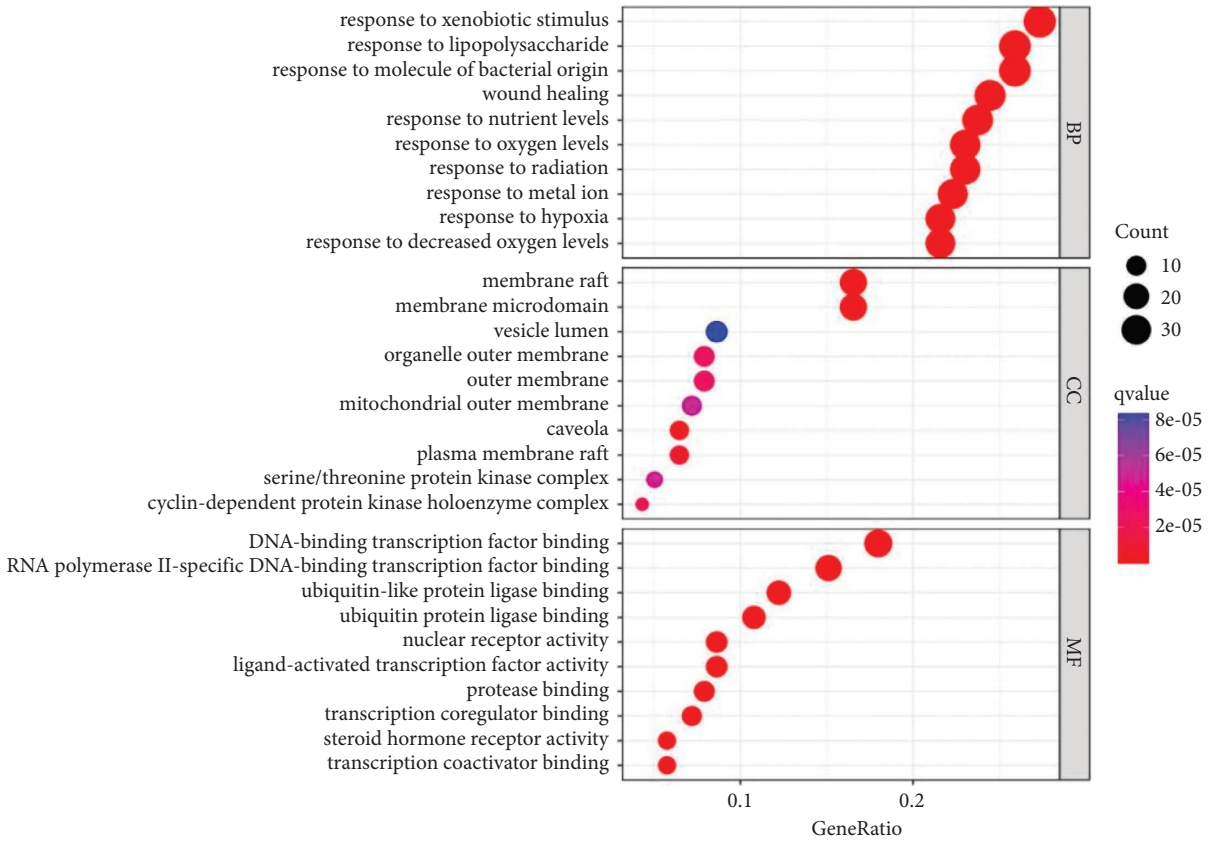

(a)

Figure 20: Continued.

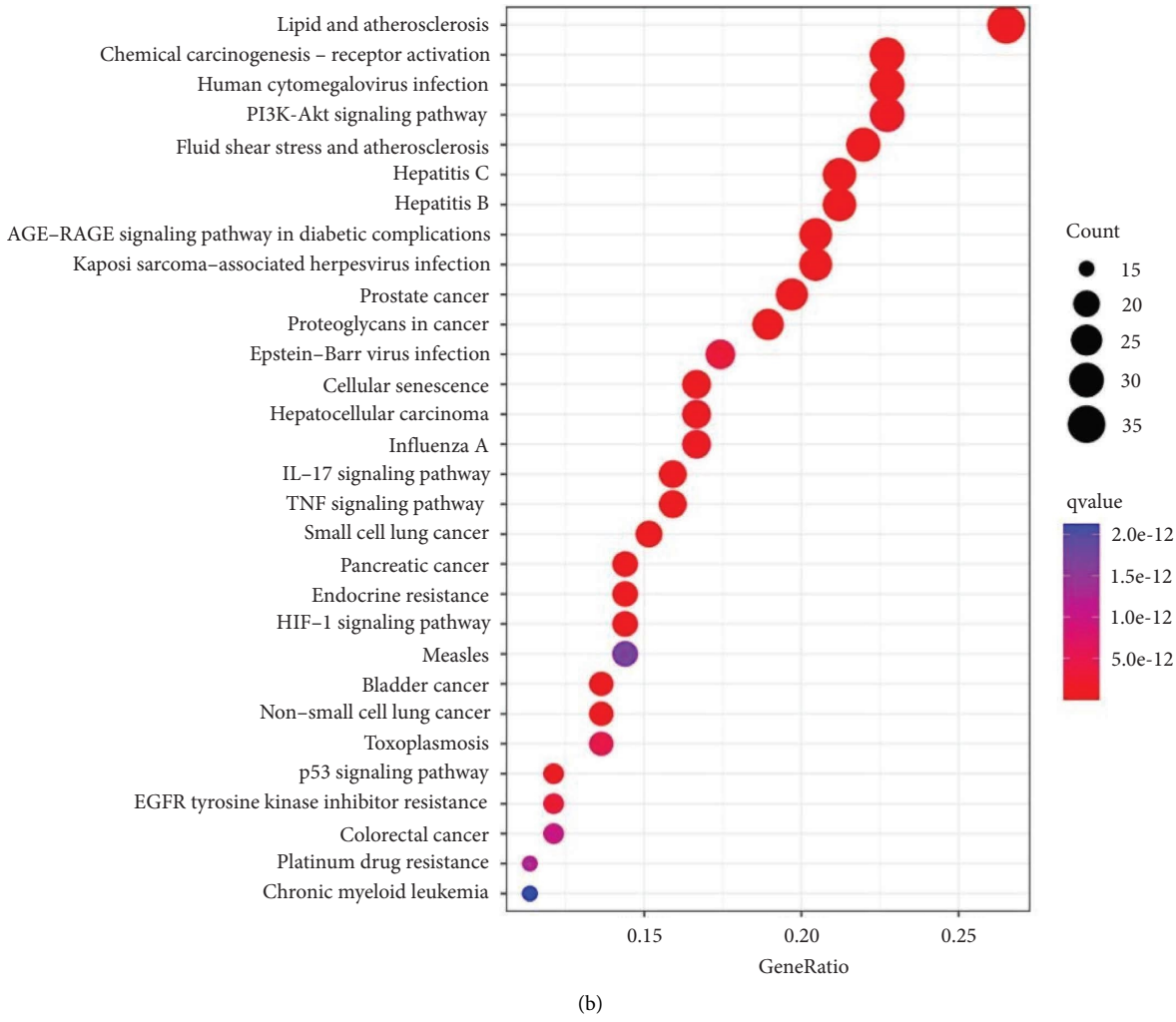

(b)

Figure 20: GO and KEGG enrichment analysis of the key targets for mBTWD against radiation enteritis. (a) GO functional annotation. (b) KEGG signaling pathways.

patients. The intestinal mucosal improvement rate in the mBTWD groups is about 23% higher than that in the CWM groups (RR = 1.23, $P = 0.0001$), correspondingly, the deterioration rate decreases by nearly half compared to the control groups (RR = 0.51, $P = 0.0001$). Colonoscopy objective signs are reported in four studies, two of which report colonoscopic intestinal mucosa scoring and another two are grading. However, these two studies of continuous variables show great heterogeneity due to different scoring criteria ($P = 0.02$, $I^2 = 81\%$), and sensitivity analysis are unable to be conducted due to the small sample size. Another two studies estimate the grade of colonoscopy (0–IV degree) according to the same criteria, both 0-II and III-IV have strong homogeneity ($P = 0.57$, $I^2 = 0\%$; $P = 0.64$, $I^2 = 0\%$). Another 6 studies also report the subjective symptoms of radiation enteritis grading (0–IV degree), in order to reduce the heterogeneity, we select the OR for statistical analysis, both 0–II and III-IV have strong homogeneity ($P = 0.47$, $I^2 = 0\%$; $P = 0.47$, $I^2 = 0\%$). The improvement rate of the radiation enteritis classification in the mBTWD groups is 3.51 times higher than that in the CWM groups (OR = 3.51, $P < 0.00001$); correspondingly, the deterioration rate is only 0.29 times that of the CWM groups (OR = 0.29, $P < 0.00001$). Similarly, we compare the findings obtained with previous studies and the data show a higher efficacy of colonoscopy after mBTWD treatment compared to montmorillonite alone (82.03 vs. 65.12%) [38]. These results indicate that, in general, mBTWD has a certain positive effect on the improvement of intestinal mucosal signs and symptoms and is significantly correlated with the reduction of the rate of deterioration.

Only two studies with a total of 161 samples report the CRP level, there is no heterogeneity in the results ($P = 0.66$, $I^2 = 0\%$), and the CRP level decreases by an average of 5.28 mg/L compared with the control groups after treatment (MD = −5.28, $P < 0.00001$). Five studies report the KPS score, including three continuous variables and two dichotomies: for the continuous variables, a subgroup analysis is performed according to the KPS score before treatment (KPS = 40–60 and KPS > 60) and the results are fine ($P = 0.29$, $I^2 = 12\%$), after treatment, the KPS score improved by an average of 15.32 points compared to the control groups (MD = 15.32, $P = 0.002$); for dichotomies

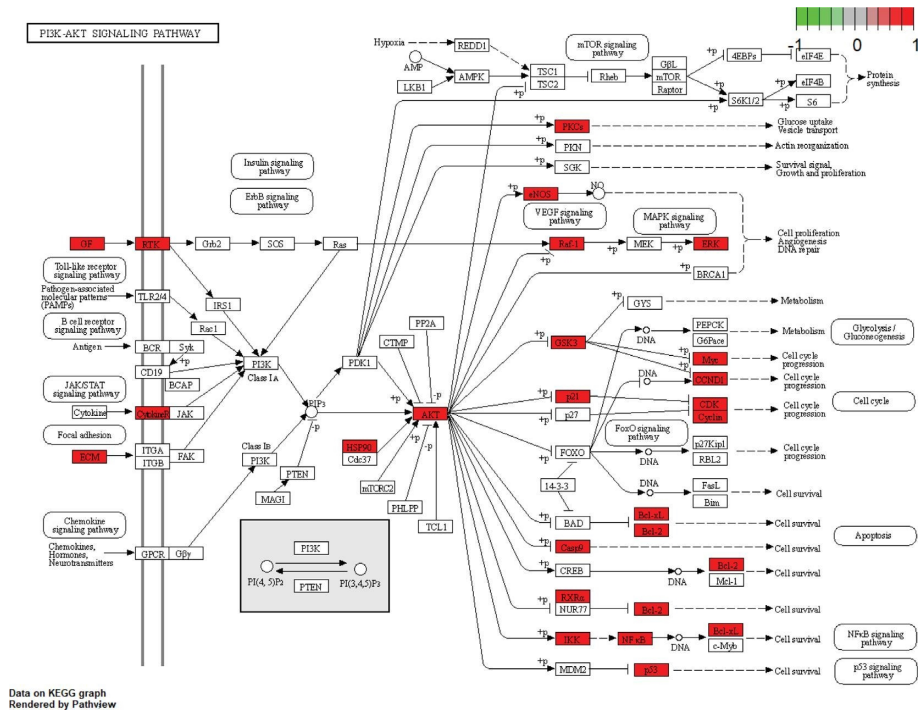

Figure 21: PI3K-Akt signaling pathway.

Table 6: Molecular docking of active ingredients with key targets from representative drugs in mBTWD.

Target protein	PDB ID	PubChem CID	MolName	Affinity/kJ·mol^{-1}
MYC	1A93	5743	Dexamethasone	−0.0
		5280343	Quercetin	−2.8
TP53	6WQX	5743	Dexamethasone	−7.9
		5280343	Quercetin	−8.3
MAPK14	1A9U	5743	Dexamethasone	−5.4
		5281220	Aureusidin	−7.7
		5281654	Isorhamnetin	−7.2
MAPK1	1PME	5743	Dexamethasone	−5.5
		5280343	Quercetin	−8.5

variables, there is also little heterogeneity ($P = 0.79$, $I^2 = 0\%$) and the rate of improvement of life quality in the mBTWD groups is about 23% higher than that of the CWM groups (RR = 1.23, $P = 0.03$); these results indicate that mBTWD is effective in improving the quality of life of patients with radiation enteritis. Although only 2 studies report the fecal occult blood, the improvement rate is about 47% higher than the control groups (RR = 1.47, $P = 0.03$), suggesting that mBTWD have better hemostasis. Due to fewer included studies and small sample size, we think that the credibility of these meta-analysis results of CRP levels, KPS score, and fecal occult blood is not high.

We are also interested in safety except for efficacy. Fortunately, no serious adverse events occur in both the intervention and control groups, indicating that both mBTWD and conventional western medicine treatments are safe and reliable. However, some studies have reported a certain recurrence rate after treatment, but the difference is not statistically significant between the two groups (RR = 0.07, $P = 0.13$). As noted previously, due to the small sample size and the low quality of the evidence, adverse events and recurrence rates also need to be further confirmed. In the future, larger sample sizes and more studies are needed to reach true scientific conclusions.

Based on Egger's test, Begg's test, and Funnel-plot-based trim and fill method, we find that there is indeed publication bias in the reports of clinical efficacy in existing studies; the potential publication bias makes the initial results overestimated by about 4.9%. This indicates that our results are still robust even with the occurrence of publication bias. According to the results of the GRADE evidence, the included overall quality of the studies is low, mainly for the reason that almost all the studies do not follow the double-blind rule and there is publication bias. With the evidence of publication bias, we also propose sensitivity analyses to investigate the potential causes of heterogeneity. The results show that the heterogeneity decreased significantly after eliminating some individual studies one by one, the evidence

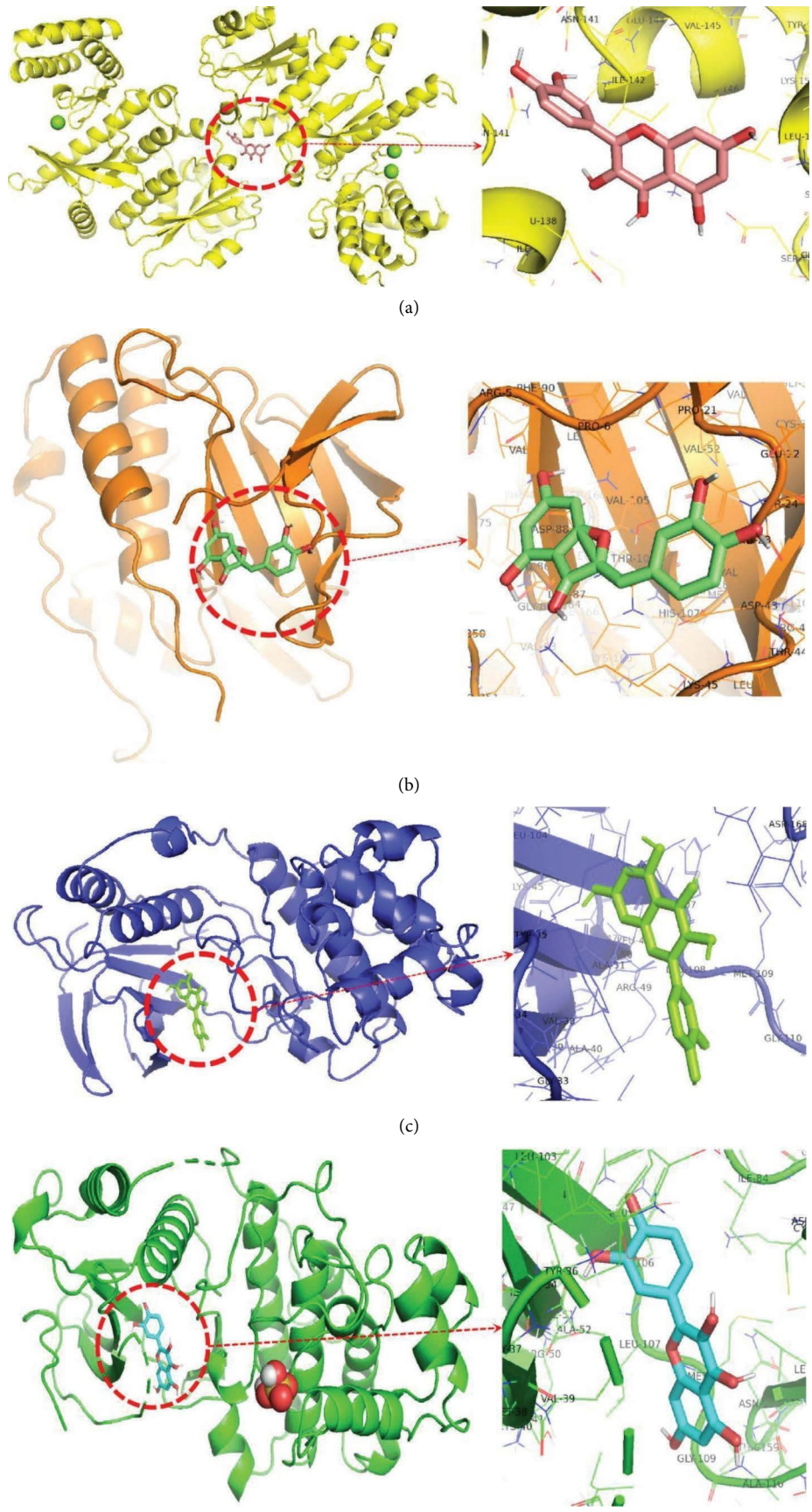

Figure 22: Three-dimensional structure diagram of molecular docking. (a) TP53-quercetin. (b) MAPK14- aureusidin. (c) MAPK14-isorhamnetin. (d) MAPK1-quercetin.

quality of these studies is relatively low and most of them lacked rigorous and clear inclusion or exclusion criteria.

4.2. Potential Molecular Mechanism. The results of network analysis show that BTWD could act on radiation enteritis with multiple targets, components, and pathways. A total of 51 ingredients are discovered and 139 common targets are screened out, such as quercetin, isorhamnetin, and beta-sitosterol, which could reduce the level of inflammatory factors, a powerful antioxidant, endothelial cell protection, and antitumor effects [39–42]. These components may be the key factors in the treatment of radiation enteritis. From the PPI network, the top four are MYC, TP53, MAPK14, and MAPK1; both TP53 and MAPK regulated many biological processes, including apoptosis, protein biosynthesis, oncogenesis, and the cell cycle [43, 44], indicating that these targets are the key targets of BTWD in the treatment of radiation enteritis. GO and KEGG enrichment analysis results also mainly involve some microbial infection and antitumor biological process which are related to the incidence of radiation enteritis. Molecular docking technology further verified the better binding activity of main active ingredients and key targets in BTWD from a quantitative perspective, even better than that of positive control drugs. However, these conclusions are only the results of network pharmacological prediction and lack of further molecular validation.

4.3. Limitations and Prospects for Future Research. This study also has several limitations. (1) The research has design flaws, the quality of evidence in existing studies is generally low without involving a specific randomized control grouping method, allocation concealment, blinding, and there is certain publication bias. (2) The included RCT studies are conducted only in China with small sample sizes and lacking larger sample studies in other languages, resulting in low-quality evidence. (3) The inclusion criteria and outcomes evaluation of some studies are not unified, and the course of radiation enteritis is not clearly defined, leading to an increased risk of heterogeneity. (4) There are too few reports on adverse events and recurrence rate, which could not objectively present the safety problems of mBTWD, and there may be false negative results. (5) The composition of mBTWD varies greatly and is not rigorous enough, the addition or subtraction of mBTWD contains many other herbs, and the dosage of mBTWD has not been unified or standardized, which made it difficult to determine the relationship between its efficacy and other ingredients or doses. (6) Network analysis and molecular docking techniques can only predict the possible targets and signaling pathways of representative drugs in mBTWD treatment of radiation enteritis, lacking further molecular verification, and the molecular mechanism needs further demonstration.

With the limitations of current studies, future studies are expected to strictly follow the randomly assigned, blinded, allocation concealment principles or to improve the quality of studies by increasing sample sizes, uniforming inclusion criteria, or outcomes measuring standards. In future studies, it is necessary to define the main components of mBTWD clearly and restrict the dose range to reduce heterogeneity. Based on the results of this meta-analysis, we recommend herbs like Baitouweng, Huanglian, Huangbo, Qinpi, and Diyu be chosen for the clinical application of mBTWD in the treatment of radiation enteritis, and the dosage of each drug could also be adjusted accordingly. Moreover, more detailed information, including withdrawal, adverse events, recurrence rate, and follow-up times, should be recorded and discussed adequately. In particular, the results based on the network analysis and molecular docking indicate that the most probable active ingredients or targets should be experimentally validated to clarify the potential pharmacological mechanisms.

5. Conclusion

Although this meta-analysis provides relatively poor quality evidence to validate the efficacy and safety of mBTWD in the treatment of radiation enteritis, the clinical significance of this study lies in two aspects. It provides both an option and an idea for radiation enteritis treatment. In addition, it further supports the unique advantages and usage of traditional Chinese medicine to relieve symptoms and improve the quality of life in cancer patients. However, there are still some limitations. The risk of adverse events and recurrence rate is under-reported, and further experiments should be performed to validate the predicted ingredients and targets. Therefore, it is necessary to design scientifically rigorous large-sample RCTs and supplement basic studies to evaluate the clinical evidence and molecular mechanism of mBTWD in the future treatment of radiation enteritis.

Abbreviations

CNKI:	China national knowledge infrastructure
CWM:	Conventional western medicine
DL:	Drug like
GO:	Gene ontology
GRADE:	Grading of recommendations assessment, development and evaluation
INPLASY:	International platform of registered systematic review and meta-analysis protocols
KEGG:	Kyoto encyclopedia of genes and genomes
mBTWD:	Modified baitouweng decoction
NR:	Not reported
OB:	Occult blood
OBA:	Oral bioavailability
OR:	Odds ratio
Po:	Per os
RCTs:	Randomised controlled trials
Re:	Reserved enema
rhGM-CSF:	Recombinant human granulocyte-macrophage colony stimulating factor for injection
RNT:	Random number table
ROS:	Reactive oxide species
RR:	Risk ratio
TCM:	Traditional chinese medicine

TCMSP: Traditional chinese medicine systems pharmacology.

Conflicts of Interest

The authors declare that they have no conflicts of interest.

Authors' Contributions

Conceptualization was performed by Z.H.W.; methodology was developed by F.M.Y.; data curation was performed by Z.H.W., Y. B., and Z. M. W.; original draft was written by Z.H.W.; review and editing were performed by Z.H.W., E.F. S., and F.M.Y.; project administration was performed by F.M.Y.; funding acquisition was done by F.M.Y. All the authors have read and agreed to the published version of the manuscript.

Acknowledgments

This research was supported by the National Nature Science Foundation of China (no. 82074315), with the project title of "Tongxieyaofang" Effect in Delaying Colon Cancer Progression through Inhitibion of Stress-induced TSC22D3 Over-expression and Recovering of Th1/Tc1 Immune Responses from the Perspective of "Simultaneous Regulation of Form, Qi, and Spirit."

References

[1] Y. Jian, D. Zhang, M. Liu, Y. Wang, and Z. X. Xu, "The impact of gut microbiota on radiation-induced enteritis," *Frontiers in Cellular and Infection Microbiology*, vol. 11, Article ID 586392, 2021.

[2] Y. Li, H. Yan, Y. Zhang et al., "Alterations of the gut microbiome composition and lipid metabolic profile in radiation enteritis," *Frontiers in Cellular and Infection Microbiology*, vol. 10, Article ID 541178, 2020.

[3] M. F. Hale, "Radiation enteritis: from diagnosis to management," *Current Opinion in Gastroenterology*, vol. 36, no. 3, pp. 208–214, 2020.

[4] Q. Lian, J. Xu, S. Yan et al., "Chemotherapy-induced intestinal inflammatory responses are mediated by exosome secretion of double-strand DNA via AIM2 inflammasome activation," *Cell Research*, vol. 27, no. 6, pp. 784–800, 2017.

[5] S. Li, M. Huang, G. Wu et al., "Efficacy of Chinese herbal formula sini zuojin decoction in treating gastroesophageal reflux disease: clinical evidence and potential mechanisms," *Frontiers in Pharmacology*, vol. 11, p. 76, 2020.

[6] Z. Miao, L. Chen, H. Feng et al., "Baitouweng decoction ameliorates ulcerative colitis in mice partially attributed to regulating Th17/treg balance and restoring intestinal epithelial barrier," *Frontiers in Pharmacology*, vol. 11, Article ID 531117, 2020.

[7] C. Xuan-qing, L. Xiang-yu, and L. Shi-jia, "Baitouweng decoction alleviates dextran sulfate sodium-induced ulcerative colitis by regulating intestinal microbiota and the IL-6/STAT3 signaling pathway," *Journal of Ethnopharmacology*, vol. 265, Article ID 113357, 2021.

[8] Y. L. Hua, Y. Q. Jia, X. S. Zhang et al., "Baitouweng Tang ameliorates DSS-induced ulcerative colitis through the regulation of the gut microbiota and bile acids via pathways involving FXR and TGR5," *Biomedicine & Pharmacotherapy*, vol. 137, Article ID 111320, 2021.

[9] H. Q. Ma, *Clinical Observation of Baitouweng Decoction Retention Enema in the Treatment of Damp-Heat Radiation Proctitis*, Anhui University of Traditional Chinese Medicine, Hefei, China, 2021.

[10] J. P. T. Higgins, D. G. Altman, P. C. Gotzsche et al., "The Cochrane Collaboration's tool for assessing risk of bias in randomised trials," *BMJ*, vol. 343, p. d5928, 2011.

[11] J. L. Brozek, E. A. Akl, P. Alonso-Coello et al., "Grading quality of evidence and strength of recommendations in clinical practice guidelines," *Allergy*, vol. 64, no. 5, pp. 669–677, 2009.

[12] A. Daina, O. Michielin, and V. Zoete, "SwissADME: a free web tool to evaluate pharmacokinetics, drug-likeness and medicinal chemistry friendliness of small molecules," *Scientific Reports*, vol. 7, no. 1, Article ID 42717, 2017.

[13] The Gene Ontology Consortium, "The gene Ontology resource: 20 years and still GOing strong," *Nucleic Acids Research*, vol. 47, no. D1, pp. D330–D338, 2019.

[14] S. X. Chen, Y. Zhao, N. N. Han et al., "Effect of Baitouweng decoction retention enema combined with rhGM-CSF on acute radiation proctitis caused by pelvic radiotherapy of stage II~III cervical cancer and its inflammatory reaction," *Shannxi Journal of Traditional Chinese medicine*, vol. 41, no. 01, pp. 46–49, 2020.

[15] X. Y. Lai, X. N. Lan, M. S. He, and J. Y. M, "Clinical observation of self-made traditional Chinese medicine decoction in the treatment of radiation proctitis induced by radiotherapy of cervical cancer," *Evaluation and Analysis of Drug-use in Hospitals of China*, vol. 21, no. 03, pp. 278–280+284, 2021.

[16] D. M. Lei, *Clinical Effectiveness of Baitouweng Tang in the Treatment of Acute Radiation Proctitis (Fire Damp Heat Syndrome)*, Chengdu University of Traditional Chinese Medicine, Chengdu, China, 2019.

[17] R. F. Lei, "A summary of 40 cases of radiation proctitis treated by traditional Chinese medicine retention enema," *Guiding Journal of Traditional Chinese Medicine and Pharmacy*, vol. 16, no. 08, pp. 42-43, 2010.

[18] G. P. Xia, "Clinical observation on treating radiation proctitis by TCM enema," *Clinical Journal of Chinese Medicine*, vol. 8, no. 08, pp. 114-115, 2016.

[19] Y. T. Yang, "Observation of therapeutic effect of Traditional Chinese medicine retention enema on radiation proctitis," *Journal of Guangdong Medical College*, vol. 30, no. 06, pp. 630-631, 2012.

[20] H. Q. Li, "Retention enema with baitouweng Decoction for treating 32 cases of chronic radiation enteritis," *Henan Traditional Chinese Medicine*, no. 09, pp. 28-29, 2008.

[21] G. Q. Wang, "Clinical observation on treating acute radiation proctitis with the Baitouweng decoction plus Xilei San," *Clinical Journal of Traditional Chinese Medicine*, vol. 9, no. 11, pp. 75-76, 2017.

[22] J. Zhang, J. H. Zhou, C. H. Li, and Q. Y. Fan, "Therapeutic effect of jiawei baitouweng decoction combined with xilei san on acute radiation proctitis," *Chinese Journal of Clinical Medicine*, vol. 25, no. 10, pp. 852-853, 2013.

[23] Z. J. Jiang, F. Ge, and H. J. Fan, "Therapeutic effect of oral Chinese medicine combined with enema on radiation proctitis," *Medical Journal of Chinese People's Health*, vol. 22, p. 2669+2691, 2008.

[24] J. Yao, Y. H. Jiang, and S. P. Wang, "Clinical observation of 392 cases of radiation proctitis treated by oral Chinese medicine and enema," *Chinese Journal of Clinical Research*, vol. 27, no. 04, pp. 481–483, 2014.

[25] L. Tong, C. Li, and C. S. Xu, "Clinical observation on radiotherapy combined with Chinese Medicine enema for 47 cases of radiation enteritis," *Journal of Traditional Chinese Medicine*, vol. 53, no. 21, pp. 1838–1840, 2012.

[26] J. X. Zhao, L. Shi, C. Liang, J. H. Chen, and J. G. Chen, "Study on preventive and therapeutic effect of baitouwengtangjiawei to acute radioactive enteritis in pelvic tumor radiotherapy," *Journal of Zhejiang University of Traditional Chinese Medicine*, vol. 35, no. 02, pp. 177–179, 2011.

[27] R. Jiang, J. Xiao, L. M. Li, and N. H. Xiong, "The clinical observation of pulsatillae decoction healing radioactive proctitis after cervical cancer," *Journal of Jiangxi University of TCM*, vol. 23, no. 02, pp. 38-39, 2011.

[28] H. B. Ye and D. W. Wang, *Prevention and treatment of 43 cases of radiation proctitis with Baitouweng decoction*, p. 55, Henan Traditional Chinese Medicine, Zhengzhou, China, 2007.

[29] X. H. Wang, L. J. Chen, H. X. Zhang, and Q. N. Liu, "Clinical evaluation of shaoyao Decoction combined with Baitouweng Decoction in the treatment of damp-heat radiation proctitis," *Journal of Medical Theory & Practice*, vol. 34, no. 18, pp. 3179–3181, 2021.

[30] M. G. Gareau, E. Wine, D. M. Rodrigues et al., "Bacterial infection causes stress-induced memory dysfunction in mice," *Gut*, vol. 60, no. 3, pp. 307–317, 2011.

[31] T. Herrmann, A. Knorr, and K. Dorner, "The RTOG/EORTC classification criteria for early and late radiation reactions," *Radiobiologia, Radiotherapia*, vol. 28, no. 4, pp. 519–528, 1987.

[32] P. J. Thuluvath, A. J. Thuluvath, Y. Savva, and T. Zhang, "Karnofsky performance status following liver transplantation in patients with multiple organ failures and probable acute-on-chronic liver failure," *Clinical Gastroenterology and Hepatology*, vol. 18, no. 1, pp. 234–241, 2020.

[33] J. Eberhardt, D. Santos-Martins, A. F. Tillack, and S. Forli, "AutoDock Vina 1.2.0: New Docking Methods, Expanded Force Field, and Python Bindings," *Journal of Chemical Information and Modeling*, vol. 61, no. 8, pp. 3891–3898, 2021.

[34] L. Loge, C. Florescu, A. Alves, and B. Menahem, "Radiation enteritis: diagnostic and therapeutic issues," *Journal of Visceral Surgery*, vol. 157, no. 6, pp. 475–485, 2020.

[35] M. Hauer-Jensen, J. W. Denham, and H. J. N. Andreyev, "Radiation enteropathy--pathogenesis, treatment and prevention," *Nature Reviews Gastroenterology & Hepatology*, vol. 11, no. 8, pp. 470–479, 2014.

[36] L. N. Lu, W. J. Li, L. H. Chen et al., "Radiation-induced intestinal damage: latest molecular and clinical developments," *Future Oncology*, vol. 15, no. 35, pp. 4105–4118, 2019.

[37] Z. X. Yan, Y. M. Liu, T. Ma et al., "Efficacy and safety of retention enema with traditional Chinese medicine for ulcerative colitis: a meta-analysis of randomized controlled trials," *Complementary Therapies in Clinical Practice*, vol. 42, Article ID 101278, 2021.

[38] W. Chen, Q. Ma, L. Yang, L. Zhang, J. Zhu, and W. Lin, "Curative effects of montmorillonite powder combined with dexamethasone on acute radiation enteritis," *Am J Transl Res*, vol. 13, no. 6, pp. 7270–7275, 2021.

[39] P. Singh, Y. Arif, A. Bajguz, and S. Hayat, "The role of quercetin in plants," *Plant Physiology and Biochemistry*, vol. 166, pp. 10–19, 2021.

[40] M. Reyes-Farias and C. Carrasco-Pozo, "The anti-cancer effect of quercetin: molecular implications in cancer metabolism," *International Journal of Molecular Sciences*, vol. 20, no. 13, p. 3177, 2019.

[41] X. Tian, X. Peng, J. Lin et al., "Isorhamnetin ameliorates Aspergillus fumigatus keratitis by reducing fungal load, inhibiting pattern-recognition receptors and inflammatory cytokines," *Investigative Ophthalmology & Visual Science*, vol. 62, no. 3, p. 38, 2021.

[42] Y. H. Jiang, X. Li, W. Niu, D. Wang, B. Wu, and C. H. Yang, "β-Sitosterol regulated microRNAs in endothelial cells against an oxidized low-density lipoprotein," *Food & Function*, vol. 11, no. 2, pp. 1881–1890, 2020.

[43] E. Thoenen, A. Curl, and T. Iwakuma, "TP53 in bone and soft tissue sarcomas," *Pharmacology & Therapeutics*, vol. 202, pp. 149–164, 2019.

[44] E. M. W. Hepworth and S. D. Hinton, "Pseudophosphatases as regulators of MAPK signaling," *International Journal of Molecular Sciences*, vol. 22, no. 22, p. 12595, 2021.

Hindawi
Evidence-Based Complementary and Alternative Medicine
Volume 2023, Article ID 9765415, 1 page
https://doi.org/10.1155/2023/9765415

Retraction

Retracted: Efficacy of Periodontal Endodontics Combined with Diode Laser (DL) Therapy on Severe Periodontitis

Evidence-Based Complementary and Alternative Medicine

Received 3 October 2023; Accepted 3 October 2023; Published 4 October 2023

This article has been retracted by Hindawi following an investigation undertaken by the publisher [1]. This investigation has uncovered evidence of one or more of the following indicators of systematic manipulation of the publication process:

(1) Discrepancies in scope
(2) Discrepancies in the description of the research reported
(3) Discrepancies between the availability of data and the research described
(4) Inappropriate citations
(5) Incoherent, meaningless and/or irrelevant content included in the article
(6) Peer-review manipulation

The presence of these indicators undermines our confidence in the integrity of the article's content and we cannot, therefore, vouch for its reliability. Please note that this notice is intended solely to alert readers that the content of this article is unreliable. We have not investigated whether authors were aware of or involved in the systematic manipulation of the publication process.

In addition, our investigation has also shown that one or more of the following human-subject reporting requirements has not been met in this article: ethical approval by an Institutional Review Board (IRB) committee or equivalent, patient/participant consent to participate, and/or agreement to publish patient/participant details (where relevant).

Wiley and Hindawi regrets that the usual quality checks did not identify these issues before publication and have since put additional measures in place to safeguard research integrity.

We wish to credit our own Research Integrity and Research Publishing teams and anonymous and named external researchers and research integrity experts for contributing to this investigation.

The corresponding author, as the representative of all authors, has been given the opportunity to register their agreement or disagreement to this retraction. We have kept a record of any response received.

References

[1] S. Liu, X. Zhang, and Q. Zhou, "Efficacy of Periodontal Endodontics Combined with Diode Laser (DL) Therapy on Severe Periodontitis," *Evidence-Based Complementary and Alternative Medicine*, vol. 2022, Article ID 5689900, 7 pages, 2022.

Hindawi
Evidence-Based Complementary and Alternative Medicine
Volume 2022, Article ID 5689900, 7 pages
https://doi.org/10.1155/2022/5689900

Research Article

Efficacy of Periodontal Endodontics Combined with Diode Laser (DL) Therapy on Severe Periodontitis

Sijia Liu,[1] Xu Zhang,[2] and Quanying Zhou [3]

[1]*Wuhan Hospital of Traditional Chinese Medicine, Department of Stomatology, No. 303 Sixin Avenue, Hanyang, Wuhan 430000, Hubei, China*
[2]*Wuchang Hospital Affiliated to Wuhan University of Science and Technology (Stomatology), No. 116 Yangyuan Street, Wuchang District, Wuhan 430063, Hubei, China*
[3]*Wuhan 9th Hospital, Department Stomatology, No. 20, Jilin Street, Qingshan District, Wuhan 430080, Hubei, China*

Correspondence should be addressed to Quanying Zhou; 2016122389@jou.edu.cn

Received 31 July 2022; Revised 17 August 2022; Accepted 20 September 2022; Published 15 October 2022

Academic Editor: Xueliang Wu

Background. For a long time, the impact of severe periodontitis on the pulp has been the focus of periodontal clinical research. Whether the teeth with severe periodontitis should be treated with pulp has also become the focus of clinical research. *Aims*. To explore the effect of periodontal endodontic therapy combined with DL therapy on severe periodontitis. *Materials and Methods*. The clinical data of 100 patients with severe periodontitis from January 2020 to July 2022 were selected and included in the retrospective study. According to the different retrieval treatment methods, they were divided into the control group and the treatment group with 50 cases in each group. The control group received periodontal endodontic treatment, and the treatment group received DL treatment on the basis of the control group. The differences in periodontal probing depth (PD), toothache degree, bleeding index (BI), inflammatory factors, plaque index (PLI), and attachment loss (AL) between the two groups were compared and analyzed. *Results*. After 3 months of treatment, the bleeding index (BI), plaque index (PLI), and periodontal probing depth (PD) of the treatment group were significantly lower than those of the control group, and the difference was statistically significant ($P < 0.05$). The attachment loss (AL) of the group was not significantly different from that of the control group ($P > 0.05$). Before treatment, there was no significant difference in the levels of inflammatory factors between the two groups ($P > 0.05$). After 3 months of treatment, the levels of IL-6 and CRP in the treatment group were significantly lower than those in the control group, and the difference was statistically significant ($P < 0.05$). Before treatment, there was no significant difference in the levels of inflammatory factors between the two groups ($P > 0.05$). After 3 days of treatment, the VAS score of the treatment group was significantly lower than that of the control group, and the difference was statistically significant ($P < 0.05$).After treatment, there were no complications during follow-up in the two groups. *Conclusion*. The application of DL treatment has a significant effect, which can promote the healing of periodontal tissue, reduce the depth of periodontal pockets, and reduce the degree of toothache, thereby providing a reference for clinical treatment.

1. Introduction

Severe periodontitis is one of the difficult aspects of periodontal treatment due to the fact that severe periodontitis not only destroys the periodontal tissue [1], but it also leaves the pulp in a subclinical state through periodontal pulp traffic branches, and the presence of diseased pulp will prevent the healing of periodontal tissue after periodontal treatment [2]. Severe periodontitis is a common disease in dentistry, the onset of which is associated with multiple factors, and early patients have no obvious symptoms, mostly just secondary gingival bleeding or halitosis, with symptoms similar to gingival inflammation [3]. With the development of the disease, patients can develop corresponding symptoms, which affect the chewing function of teeth and reduce the quality of life of patients [4]. Severe periodontitis tends to involve several tissues, while the anatomical structure between periodontal and pulpal tissues

is relatively special, involving dentin tubules and apical foramina [5]. The relationship between the two tissues is interoperable, and unilateral lesions and infections may affect the other side, resulting in combined periodontal and pulpal lesions that make treatment more difficult [6].

A large number of studies in recent years have shown the efficacy of periodontal-endodontic treatment of severe periodontitis, which can reduce the depth of periodontal pockets and positively control the disease [7]. However, in view of the limitations of the results achieved by single treatment, it has been suggested that DL can be combined to enhance the therapeutic effect from different mechanisms of action [8]. The principle of action of DL is a treatment that uses mechanical, photochemical, thermal, and biological promotion effects to accelerate the inflammation relief at the lesion site [9]. The laser has a bactericidal effect, especially in periodontal soft tissues, as DL has an affinity for hemoglobin and gingival pigments, allowing precise soft tissue separation, sealing of blood vessels, and removal of the working area, while reducing postoperative swelling [10]. In addition, DL has the advantages of portability, affordability, and ease of operation [11]. DL is more effective and less invasive than traditional methods. DL allows precise cutting of soft tissues and complete debridement of diseased tissues while looking directly at the affected tooth and has the efficacy of removing subgingival plaque and tartar and inhibiting periodontitis pathogens, and it has been widely used in periodontal treatment in recent years [12]. Therefore, in this study, periodontal endodontic treatment combined with DL treatment was performed in patients with severe periodontitis.

2. Material and Methods

2.1. Research Object. The clinical data of 100 patients with severe periodontitis from January 2020 to July 2022 were selected for inclusion in the retrospective study. Fifty cases each were divided into a comparison group and a treatment group according to the retrieval treatment method. Diagnostic criteria for periodontitis are as follows [13]: adjacent CAL detected in more than 2 nonadjacent teeth; or the presence of buccal or lingual CAL ≥3 mm in >2 teeth, along with PD ≥ 3 mm.

2.2. Criteria for Nadir Discharge. Inclusion criteria are as follows:(i) age 18 to 70 years old, clinical attachment loss ≥5 mm, apical radiograph showing alveolar bone destruction exceeding 1/2 of root length, degree of loosening less than 3 degrees, sluggish pulp viability test, and no clinical pulp tooth with inflammation symptoms; (ii) there is no obvious loosening of the tooth, no full crown restoration, periodontal and endodontic joint disease, or grade III furcation disease; (iii) in order to avoid false negative or false positive results of the electrical measuring instrument at the same time, perform a pulp temperature test on the affected tooth, choose the thermal diagnosis method of gutta-percha, first measure the control tooth, and then measure the test tooth. Sexual pain. Exclusion criteria are as follows: (i) women who are pregnant, breastfeeding, or planning to become pregnant within the past 3 months, patients with acute periodontal abscess or acute necrotizing gingivitis; (ii) history of periodontal treatment within the past 3 months, within the past 3 months history of taking antibiotics, nonhormonal anti-inflammatory drugs and immune preparations, and other systemic diseases; (iii) patients with systemic diseases, smokers, dentin sensitivity, poor restorations, or night grinding.

2.3. Methods. The control group was given periodontal endodontic treatment, that is, a comprehensive specialist examination was performed on the patients, detailed medical history and periodontal records were taken, and oral hygiene education was given to the patients, and the test teeth were selected. Full-mouth ultrasonic supragingival scaling was performed first, the clinical indicators of the test teeth were recorded, and a standard series of periapical films were taken. Root canal treatment was performed on the teeth of test group 1 (the criteria for the success of root canal treatment were X-ray that showed the root canal filling was tight, and the root filling was 0.5-2 m away from the apex. Satisfied), one week after treatment, ultrasonic scaler and Gracey subgingival scaling device were used to complete subgingival scaling and root planing in two times.

The treatment group was combined with DL treatment on the basis of the control group, that is, adjusting the DL display screen to the periodontal scaling, according to the depth of periodontal probing, gently probe the 400 m optical fiber into the bottom of the periodontal pocket, and lift it 2 mm and move it to feel it. Its form. Start the laser (wavelength 980 nm, power 2 W), keep the tip of the fiber in contact with the epithelial tissue, and make a "zigzag" movement in the periodontal pocket smoothly and slowly. When the periodontal pocket is less than 6 mm, the laser irradiation time is about 30 s, and when the periodontal pocket is larger than 6 mm, the irradiation time is 45 s. Routine ultrasonic subgingival scaling and manual root planing were then performed. After the conventional treatment, the laser treatment is used again for about 20~30 s for the purpose of hemostasis and periodontal debridement.

2.3.1. Observation Indexes. (i) PD: 6 sites (labial-buccal/lingual mesial, central, and distal) were recorded for each tooth, in millimeters (mm), rounded up, and the probing force was controlled at 20-25 g. BI: record both buccal and lingual surfaces for each tooth. The scoring criteria are as follows: 0 is healthy gums without inflammation and bleeding; 1 is inflammatory changes in the color of the gums without bleeding on probing; 2 is punctate bleeding after probing; 3 is bleeding after probing that spreads along the gingival margin; 4 is bleeding that overflows and overflows the gingival sulcus; 5 is spontaneous bleeding. PLI: plaque index scoring method was employed, the buccal and lingual surfaces of each tooth are recorded, and the scoring standard is as follows: 0 is sterile plaque in the gingival margin area and 1 is thin plaque on the tooth surface in the gingival margin area; however, it is not easy to see by visual

inspection. The side of the probe tip is used to scrape out plaque. AL: when the gingiva is coronal to the cementoenamel junction, AL is the periodontal probing depth distance from the cementoenamel junction to the gingival margin. (ii) 4 mL of fasting venous blood was extracted from patients for inflammatory factor levels, and after centrifugation at 3000 r/min for 10 min, the supernatant was taken, and the American Beckman Coulter AU-5800 automatic biochemical analyzer was used which was provided by Beijing Hotgen Biotechnology Co Ltd. The enzyme-linked immunosorbent assay kit was used to detect the levels of interleukin-6 (IL-6) and C-reactive protein (CRP). Evaluation, instruct the patient to score the toothache in the past 24 hours according to their own subjective feelings and combined with the scale, with a total score of 0 to 10 points. The higher the score, the higher the pain, and the average score is calculated.

2.4. Statistical Analysis. All statistical data in this study were entered into Excel software by the first author and the corresponding author, and the statistical processing software was SPSS25.0 for calculation. Repeated measure analysis of variance between groups was used to measure the measurement which was expressed as mean ± standard deviation ($X \pm SD$). Material. One-way analysis of variance was used for comparison between groups, and the count data were tested by x^2. Count data expressed as a percentage (%) were tested by χ^2. The risk factors with significant differences were screened. Included data that did not conform to a normal distribution were described by M (QR), using the Mann–Whitney test. The statistical significance was $P < 0.05$.

3. Results

3.1. Comparison of General Clinical Data. The comparison of general data such as gender, age, number of carious tooth surfaces, number of bits, and body mass index of the two groups of patients did not have significant statistical differences by independent sample *t*-test and chi-square test ($P > 0.05$) (see Table 1).

3.2. Comparison of Clinical Efficacy. Before treatment, there was no significant difference in clinical efficacy between the two groups. After 3 months of treatment, the bleeding index (BI), plaque index (PLI), and periodontal probing depth (PD) of the treatment group were significantly lower than those of the control group, and the difference was statistically significant ($P < 0.05$). The attachment loss (AL) of the group was not significantly different from that of the control group ($P > 0.05$) (see Figure 1).

3.3. Comparison of Inflammatory Factor Levels. Before treatment, there was no significant difference in the levels of inflammatory factors between the two groups ($P > 0.05$). After 3 months of treatment, the levels of IL-6 and CRP in the treatment group were significantly lower than those in the control group, and the difference was statistically significant ($P < 0.05$) (see Figure 2).

3.4. Toothache Comparison. Before treatment, there was no significant difference in the levels of inflammatory factors between the two groups ($P > 0.05$). After 3 days of treatment, the VAS score of the treatment group was significantly lower than that of the control group, and the difference was statistically significant ($P < 0.05$) (see Figure 3).

4. Discussion

DL is one of the most popular new periodontal techniques, which is easy to operate and the laser fiber can reach areas that cannot be reached by traditional mechanical methods, and can work on affected teeth with anatomical abnormalities such as deep periodontal pockets, root bifurcations, and root surface depressions [14]. When the DL beam is irradiated to biological tissues, it can produce thermal, photochemical, and biostimulatory effects to accelerate the inflammatory absorption and improve local microcirculation at the lesion site, which has good periodontal treatment functions with the ability to sterilize, promote healing, reduce bleeding, and remove epithelium from periodontal pockets [15]. Therefore, laser therapy that is applied to the adjuvant treatment of periodontal diseases has attracted wide attention from scholars at home and abroad [16]. DL is a tissue-penetrating laser, mainly applied to soft tissues, and the heat generated has minimal effect on the roots of teeth, and the energy generated can be absorbed by endogenous chromophores, of which hemoglobin has the highest absorption rate and can play the best role within the blood environment [17]. DL has the advantages of small size, light weight, low cost, adjustable wavelength, and stable output power, and it has a very broad development prospect [18].

Our study found that after 3 months of treatment, the bleeding index (BI), plaque index (PLI), and periodontal probing depth (PD) of the treatment group were significantly lower than those of the control group, indicating that the application of DL treatment had a significant effect. The reasons are as follows: periodontitis is a chronic inflammatory disease caused by bacterial infection, and the removal of pathogenic bacteria in the periodontal pocket is an important part of the treatment of periodontitis [19]. When measured four weeks after the completion of basic periodontal treatment, the subgingival microbial flora will change, in which the number of periodontal pathogens is significantly reduced [20]. The microbiota recolonized long after basic treatment. The microbial structure was very different from that of mature dental plaque in a shorter period of time after treatment, but the microbial structure and mature dental plaque structure after a long time of treatment were largely the same except for a few bacteria [21–25]. But this microbial change must be controlled by regular subgingival scaling and root planing performed during supportive periodontal therapy [26]. The addition of laser irradiation at this critical stage of treatment can

Table 1: Comparison of clinical data between two groups of patients (n, $\overline{x} \pm s$).

Clinical parameter	Comparison group (50)	Treatment group (50)	χ^2/t	P
Sex (male/female)	23/27	24/26	0.040	0.841
Age (years)	56.13 ± 6.32	55.91 ± 6.67	0.169	0.866
Number of decayed tooth surfaces	44.78 ± 3.32	44.34 ± 3.25	0.670	0.505
Number of digits	123.62 ± 10.66	123.26 ± 10.64	0.169	0.866
Body mass index (kg/m^2)	26.78 ± 2.32	26.94 ± 2.25	0.350	0.727

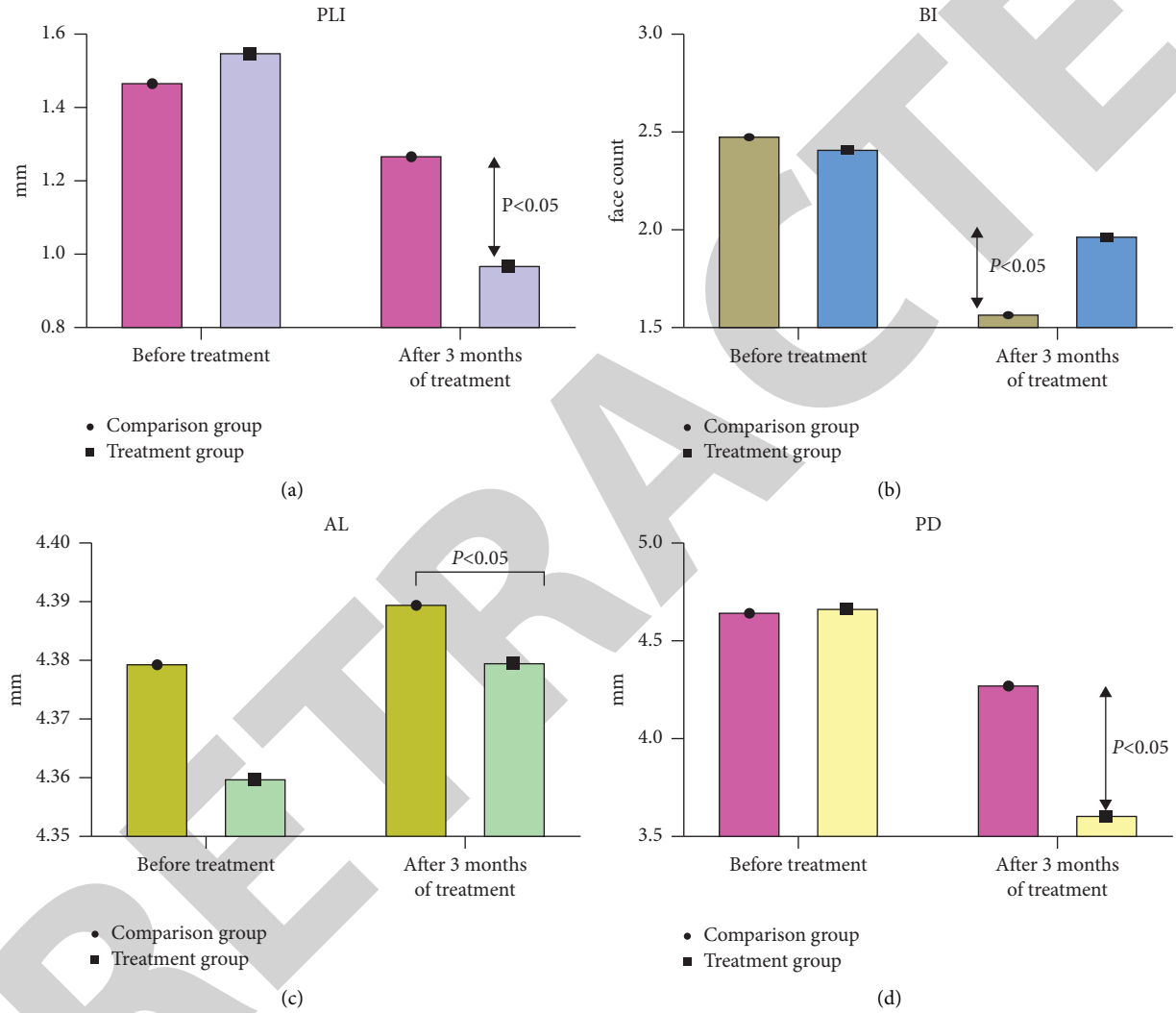

Figure 1: Clinical efficacy comparison (all statistical clinical efficacy comparison data in this study were entered into Excel software by the first author and corresponding author, and the statistical processing software was SPSS25.0 for calculation. An independent sample t-test analysis was performed between the two groups to measure the values which were expressed as mean ± standard deviation. It was found that before treatment, there was no significant difference in clinical efficacy between the two groups. After 3 months of treatment, the bleeding index (BI), plaque index (PLI), and periodontal probing depth (PD) were significantly lower than those in the control group, and the difference was statistically significant ($P < 0.05$), while the attachment loss (AL) in the treatment group was not significantly different from that in the control group ($P < 0.05$).

effectively improve periodontal healing, achieve deeper bacterial suppression, and hopefully prolong the interval between repairs [27]. In the treatment of soft tissue, the use of DL treatment has a bactericidal effect. Since DL cannot remove dental calculus, it is only used here as an auxiliary means to treat its bactericidal and detoxifying effects [28]. DL treatment applied to the blood-rich periodontal pocket can better absorb the laser beam, and the resulting thermal effect can cause immediate damage to the cell wall structure of Gram-negative bacteria, but basically does not damage the root surface [29]. Biostimulatory effects can reduce vascular permeability, reduce inflammation, reduce congestion and

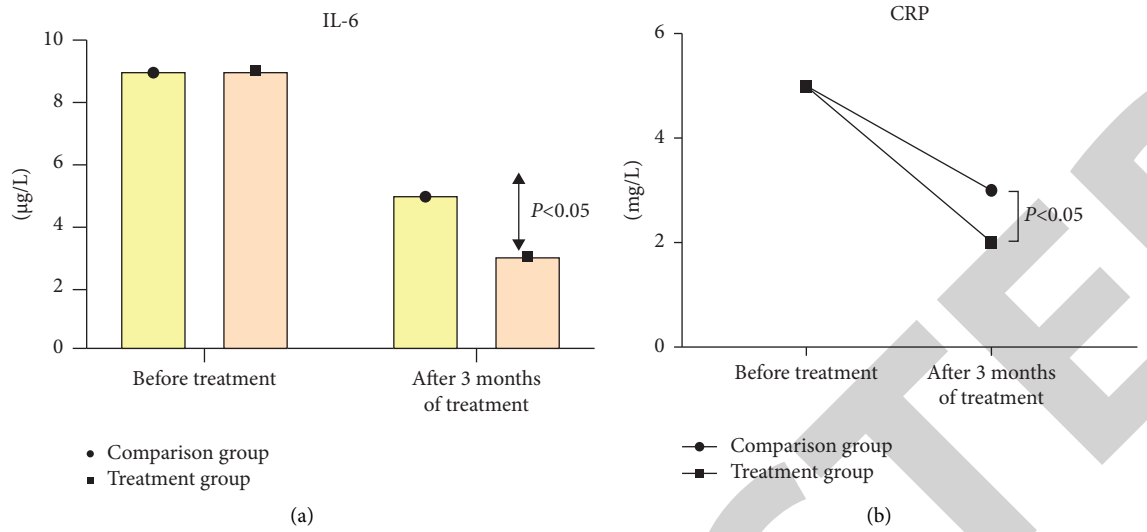

Figure 2: Comparison of inflammatory factor levels (all statistical inflammatory factor level comparison data in this study were entered into Excel software by the first author and corresponding author, and the statistical processing software was SPSS25.0 for calculation. An independent sample t-test analysis was performed between the two groups to measure the measured values which were expressed as mean ± standard deviation. It was found that there was no significant difference in the levels of inflammatory factors between the two groups before treatment ($P > 0.05$). After 3 months of treatment, the levels of IL-6 and CRP in the treatment group were significantly lower than those in the control group, and the difference was statistically significant ($P < 0.05$).

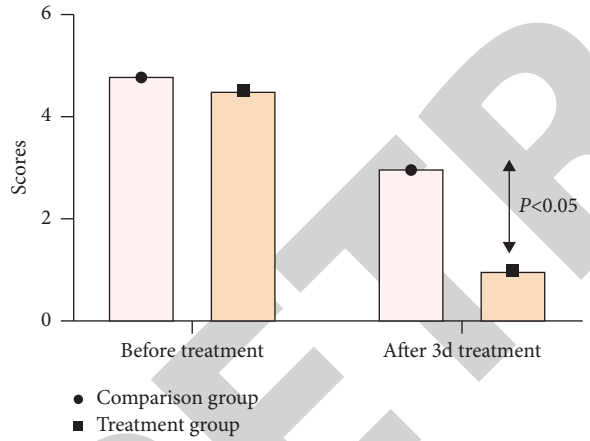

Figure 3: Toothache degree comparison (all statistical toothache degree comparison data in this study were entered into Excel software by the first author and corresponding author, and the statistical processing software was SPSS25.0 for calculation. An independent sample *t*-test analysis was performed between the two groups to measure the measured values which were expressed as mean ± standard deviation. It was found that before treatment, there was no significant difference in the levels of inflammatory factors between the two groups ($P > 0.05$). The VAS score was significantly lower than that of the control group, and the difference was statistically significant ($P < 0.05$).

edema, improve tissue blood circulation, promote angiogenesis and stimulate tissue regeneration, and are inexpensive, small, and simple to operate [30].

In our study, we found that IL-6 and CRP in the treatment group were significantly lower than those in the control group after 3 months of treatment, suggesting that DL treatment can effectively control the inflammatory response of the organism and improve the condition. The reasons are as follows: DL is currently a more common type of laser in oral diseases, which can be highly absorbed by water and water-rich tissues, producing a photothermal effect with less thermal damage compared to other lasers [31]. It is able to achieve a low thermal effect treatment and exerts a more refined effect of plaque and tartar removal [32]. It also stimulates fibroblasts, promotes the synthesis of collagen and extracellular matrix on the root surface, improves their biocompatibility, and provides good conditions for fibroblast attachment [33]. Also, the ability to remove the staining layer of the tooth surface in the bifurcation zone and promote the regeneration of periodontal tissues can further confirm that the combined treatment can enhance clinical efficacy and promote gingival health [34]. The pathological process of periodontitis is accompanied by the release of several inflammatory factors, which can be used for the evaluation of the disease [35]. IL-6 induces a variety of inflammatory responses and is able to inhibit the production of several periodontal membrane cells [36]. When subjected to microbial invasion, the nonspecific immune mechanisms of the body are activated and hepatocytes increase the synthesis of CRP [37]. CRP can bind to ligands to activate the complement and mononuclear phagocyte systems, enhancing the ability to undergo external microorganisms [38].

In our study, we found that the VAS scores of the treatment group were significantly lower than those of the control group after 3 d of treatment, indicating that the combined treatment was effective in improving the toothache and achieving significant therapeutic effects. Laser removal of diseased tissues by periodontal reversal, combined with laser to promote periodontal tissue repair, can

achieve a strong therapeutic effect through continuous treatment, effectively relieving toothache and enhancing the therapeutic effect [39]. Inflammation of periodontal tissue in teeth with severe periodontitis can affect the pulp tissue and can lead to loss of attachment and irreducible inflammatory changes in the pulp or even necrosis [40]. Timely and complete DL treatment of teeth with severe periodontitis with sluggish pulp vitality can control the progression of inflammation and facilitate periodontal tissue healing [41]. Few studies have tracked the long-term prognosis of teeth with severe periodontitis after DL treatment, and further follow-up studies are needed in the future to determine the long-term efficacy of treatment [42]. However, the present study has some clinical implications, as most of the teeth with severe periodontitis with sluggish pulp vitality already have some degree of pulp degeneration or necrosis [43]. Patient's pain, and is also in line with the principle of minimally invasive treatment in the broad sense [44]. It is also in line with the principle of minimally invasive treatment in the broad sense [45].

Our study has certain limitations which are as follows: lack of long-termfollow-up, no observation of patients' recurrence, and our study does not meet the needs of multifaceted and multilevel observation of clinical trials. In conclusion, the application of DL treatment is effective in promoting periodontal tissue healing and reducing the depth of periodontal pockets, reducing the degree of tooth pain, and thus providing a reference for clinical treatment.

Data Availability

No data were used to support this study.

Conflicts of Interest

The authors declare that they have no conflicts of interest.

Authors' Contributions

Sijia Liu and Xu Zhang are co-first authors, and both authors contributed equally to the article.

References

[1] L. H. Theodoro, R. A. C. Marcantonio, M. Wainwright, and V. G. Garcia, "LASER in periodontal treatment: is it an effective treatment or science fiction?" *Brazilian Oral Research*, vol. 35, no. Supp 2, 2021.

[2] L. Zheng and J. Kang, "Evaluation of 6-year maintenance effect of periodontal non-surgical treatment of a case of chronic periodontitis with deformed radicular groove," *Journal of West China Journal of Stomatology*, vol. 29, no. 3, pp. 327–329, 2011.

[3] B. Tan, J. Xiao, and W. Wu, "Application of root canal therapy in the treatment of recurrent periodontal abscess,".

[4] X. Zhang, C. Sun, and C. Xue, "Semiconductor diode laser and its application in periodontal surgery," *Chinese Journal of Practical Stomatology*, vol. 6, no. 4, pp. 250–253, 2013.

[5] Y. Li, X. Wang, J. Xu, X. Zhou, and K. Xie, "The clinical study on the use of diode laser irradiation in the treatment of periodontal-endodontic combined lesions," *West China Journal of Stomatology*, vol. 30, no. 2, pp. 161–164, 2012.

[6] M. Giannelli, F. Materassi, T. Fossi, L. Lorenzini, and D. Bani, "Treatment of severe periodontitis with a laser and light-emitting diode (LED) procedure adjunctive to scaling and root planing: a double-blind, randomized, single-center, split-mouth clinical trial investigating its efficacy and patient-reported outcomes at 1 year," *Lasers in Medical Science*, vol. 33, no. 5, pp. 991–1002, 2018.

[7] F. Katsikanis, D. Strakas, and I. Vouros, "The application of antimicrobial photodynamic therapy (aPDT, 670 nm) and diode laser (940 nm) as adjunctive approach in the conventional cause-related treatment of chronic periodontal disease: a randomized controlled split-mouth clinical trial," *Clinical Oral Investigations*, vol. 24, no. 5, pp. 1821–1827, 2020.

[8] S. Chandra and P. Shashikumar, "Diode laser—a novel therapeutic approach in the treatment of chronic periodontitis in type 2 diabetes mellitus patients: a prospective randomized controlled clinical trial," *Journal of Lasers in Medical Sciences*, vol. 10, no. 1, pp. 56–63, 2018.

[9] T. Kaplan, G. P. Sezgin, and S. Sönmez Kaplan, "Effect of a 980-nm diode laser on post-operative pain after endodontic treatment in teeth with apical periodontitis: a randomized clinical trial," *BMC Oral Health*, vol. 21, no. 1, p. 41, 2021.

[10] S. Pourshahidi, H. Ebrahimi, A. Mansourian, Y. Mousavi, and M. Kharazifard, "Comparison of Er, Cr: YSGG and diode laser effects on dentin hypersensitivity: a split-mouth randomized clinical trial," *Clinical Oral Investigations*, vol. 23, no. 11, pp. 4051–4058, 2019.

[11] A. Crispino, M. M. Figliuzzi, C. Iovane et al., "Effectiveness of a diode laser in addition to non-surgical periodontal therapy: study of intervention," *Annali di Stomatologia*, vol. 6, no. 1, pp. 15–20, 2015.

[12] T. M. Lobo and D. G. Pol, "Evaluation of the use of a 940 nm diode laser as an adjunct in flap surgery for treatment of chronic periodontitis," *Journal of Indian Society of Periodontology*, vol. 19, no. 1, pp. 43–48, 2015.

[13] H. Meng, "An introduction to the new international classification of periodontal disease and peri-implant disease in 2018," *Journal of Chinese Journal of Stomatology*.vol. 54, no. 2, pp. 73–78, 2019.

[14] L. Chambrone, U. D. Ramos, and M. A. Reynolds, "Infrared lasers for the treatment of moderate to severe periodontitis: an American Academy of periodontology best evidence review," *Journal of Periodontology*, vol. 89, no. 7, pp. 743–765, 2018.

[15] Y. Cherepynska, O. Volkova, E. Riabokon, and T. Baglyk, "Analysis of the long-term clinical results of using 940 μm diode laser in patients with generalized moderate chronic periodontitis," *Georgian Med News*, no. 270, pp. 24–30, 2017.

[16] L. Jokar, M. Bayani, H. Hamidi, M. Keivan, and S. Azari-Marhabi, "A comparison of 940 nm diode laser and cryosurgery with liquid nitrogen in the treatment of gingival physiologic hyperpigmentation using split mouth technique: 12 months follow up," *Journal of Lasers in Medical Sciences*, vol. 10, no. 2, pp. 131–138, 2019.

[17] C. Yang, X. Wang, and Y. Wang, "Effect of diode laser combined with minocycline hydrochloride in nonsurgical periodontal therapy: a randomized clinical trial," *BMC Oral Health*, vol. 22, no. 1, p. 71, 2022.

[18] A. Shahnaz, R. Jamali, F. Mohammadi, A. Khorsand, N. Moslemi, and R. Fekrazad, "A preliminary randomized clinical trial comparing diode laser and scalpel periosteal incision during implant surgery: impact on postoperative

Hindawi
Evidence-Based Complementary and Alternative Medicine
Volume 2023, Article ID 9898150, 1 page
https://doi.org/10.1155/2023/9898150

Retraction

Retracted: Noncoding RNAs and Virus and Treatment in Allergic Rhinitis

Evidence-Based Complementary and Alternative Medicine

Received 8 August 2023; Accepted 8 August 2023; Published 9 August 2023

This article has been retracted by Hindawi following an investigation undertaken by the publisher [1]. This investigation has uncovered evidence of one or more of the following indicators of systematic manipulation of the publication process:

(1) Discrepancies in scope

(2) Discrepancies in the description of the research reported

(3) Discrepancies between the availability of data and the research described

(4) Inappropriate citations

(5) Incoherent, meaningless and/or irrelevant content included in the article

(6) Peer-review manipulation

The presence of these indicators undermines our confidence in the integrity of the article's content and we cannot, therefore, vouch for its reliability. Please note that this notice is intended solely to alert readers that the content of this article is unreliable. We have not investigated whether authors were aware of or involved in the systematic manipulation of the publication process.

Wiley and Hindawi regrets that the usual quality checks did not identify these issues before publication and have since put additional measures in place to safeguard research integrity.

We wish to credit our own Research Integrity and Research Publishing teams and anonymous and named external researchers and research integrity experts for contributing to this investigation.

The corresponding author, as the representative of all authors, has been given the opportunity to register their agreement or disagreement to this retraction. We have kept a record of any response received.

References

[1] Z. Lei, G. Feng, Z. Wang, and Z. Ning, "Noncoding RNAs and Virus and Treatment in Allergic Rhinitis," *Evidence-Based Complementary and Alternative Medicine*, vol. 2022, Article ID 1979447, 8 pages, 2022.

Hindawi
Evidence-Based Complementary and Alternative Medicine
Volume 2022, Article ID 1979447, 8 pages
https://doi.org/10.1155/2022/1979447

Research Article

Noncoding RNAs and Virus and Treatment in Allergic Rhinitis

Zhu Lei,[1] Guangrui Feng,[2] Zhiguo Wang,[3] and Zhifeng Ning[4]

[1]*Otolaryngology Department, Xianning First People's Hospital, Xianning 437100, Hubei, China*
[2]*Cardiovascular Medicine Department, The First Affiliated Hospital of Hubei University of Science and Technology, Xianning 437100, Hubei, China*
[3]*Dermatology Department, The First Affiliated Hospital of Hubei University of Science and Technology, Xianning 437100, Hubei, China*
[4]*Human Anatomy Department, Basic Medicine College, Hubei University of Science and Technology, Xianning 437100, Hubei, China*

Correspondence should be addressed to Zhifeng Ning; zhifengn123@163.com

Received 1 July 2022; Revised 31 July 2022; Accepted 17 August 2022; Published 15 October 2022

Academic Editor: Xueliang Wu

Allergic rhinitis (AR) is a type I hypersensitivity reaction disease caused by inhaled allergens and immunoglobulin *E* (IgE)-mediated. Noncoding RNA (ncRNA) is an important regulator involved in gene expression and can be detected in the cytoplasm or extracellular fluid, which mainly includes microRNAs (miRNA, length 22–24 nucleotides), long noncoding RNAs (lncRNA, length >200 nucleotides), and circRNAs. LncRNA and miRNA both participate in the regulation of immune function. Some respiratory viral infections can aggravate allergic rhinitis, such as a respiratory syncytial virus (RSV) and human metapneumovirus (hMPV). However, the interaction between viral infection and allergy is complex and the mechanism is still unclear. In this review, we summarized the interactions of noncoding RNAs and viruses in the occurrence and development of AR, along with the treatments focusing on the noncoding RNAs in the past five years.

1. Introduction

Allergic rhinitis (AR) is a type I hypersensitivity reaction disease caused by inhaled allergens and immunoglobulin *E* (IgE)-mediated. At present, the morbidity of AR is estimated between 10% and 40% worldwide, with even up to 50% in some countries [1–3]. When allergic rhinitis patients first contact with an allergen, they never develop any clinical symptoms but have them during the sensitization stage. At this phase, dendritic cells (DCs) of the nasal mucosa take up the allergen, process it, and nest it to the draining lymph node, presenting it to the naive $CD4^+$T cells [4, 5]. Subsequently, naive $CD4^+$T cells are activated and differentiated into allergen-specific helper T cells type 2 (Th2 cells), which activate B cells to differentiate into plasma cells, resulting in the production of allergen-specific IgE [6–8] and release into the circulatory system. When the body is exposed to the same allergen again that can be specifically combined with IgE. This promotes effector cells' release of multiple inflammatory mediators, including histamine, leukotriene, prostaglandin D2, and other products [9].

Noncoding RNA (ncRNA) is an important regulator involved in gene expression and can be detected in the cytoplasm or extracellular fluid, which mainly includes microRNAs (miRNA, length 22–24 nucleotides), long noncoding RNAs (lncRNA, length >200 nucleotides), and circRNAs [10, 11]. All ncRNA were evolutionarily conserved and coded independently [12]. LncRNA and miRNA both participate in immune regulatory responses by regulating the differentiation of bone marrow hematopoietic stem cells and activating mononuclear macrophages and DCs [13]. More interestingly, a large number of noncoding fragments were found in peripheral blood cells of patients with asthma, including natural antisense chains, pseudogenes, and differential expression of ncRNA between genes [14]. In addition, some scholars found a large number of lncRNA in $CD4^+$ and $CD8^+$T cells, with phased expression [15, 16]. At the same time, the role of miRNA in regulating innate

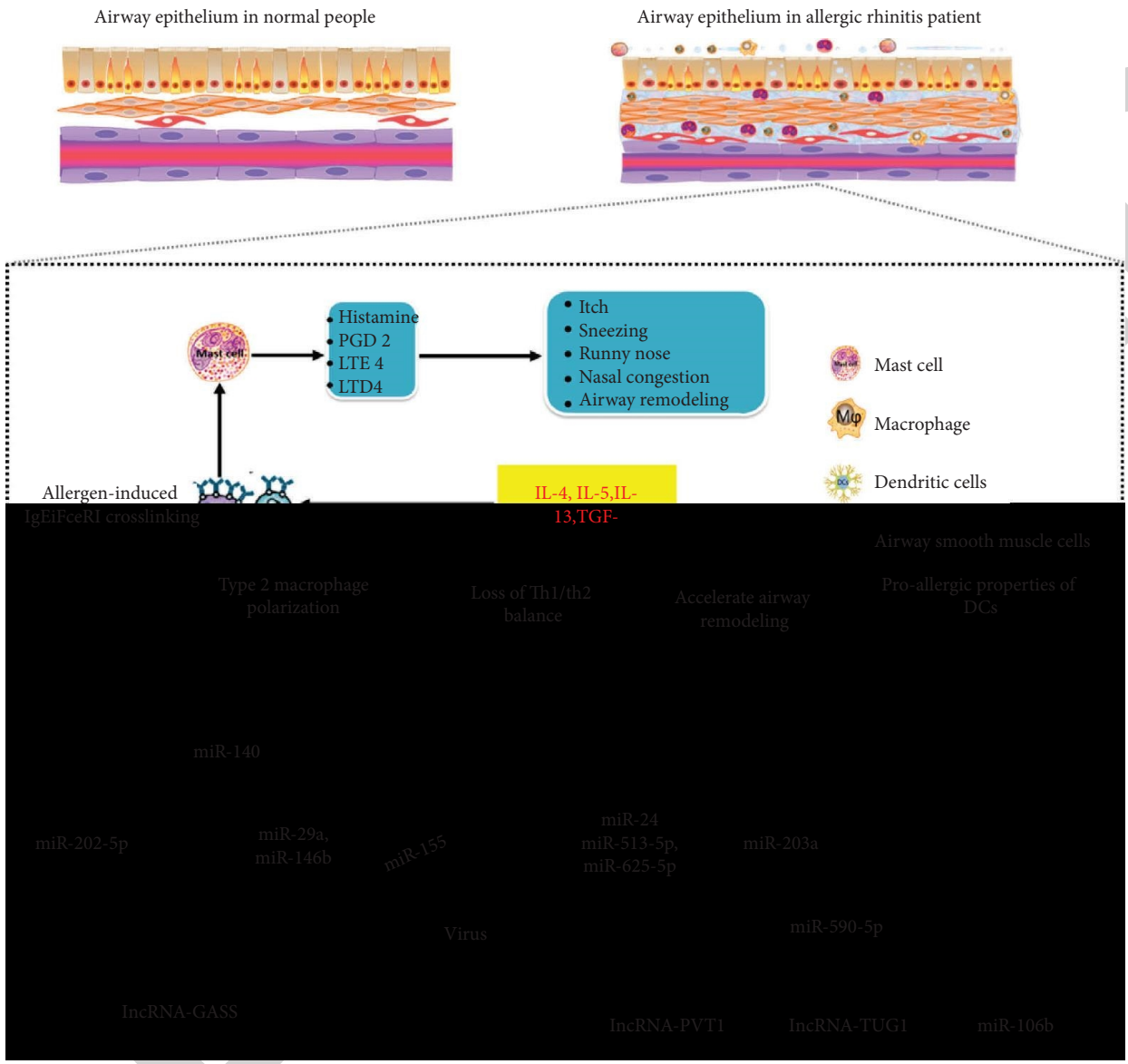

Figure 1: Mechanism of allergic rhinitis. The interaction networks between ncRNA and virus copromote the occurrence of allergic rhinitis. Black arrows mark the positive effects between elements, whereas red stop bars denote inhibitory effects.

immune responses, especially macrophages and granulocytes, has been shown to alter cell development, differentiation, and the release of inflammatory factors. In addition, Th2 cells are important mediators of type I allergy, and it has been reported that ncRNA promotes Th2 cell migration to target organs by regulating chemokine gene expression [17]. These results suggest that the noncoding RNA regulatory network may play a potential role in the development of allergic rhinitis (Figure 1).

Viral tinfections are known to aggravate AR. Although, the interaction between viral infection and allergy is complex and the mechanisms remain unclear. Some studies suggest that coregulatory molecules and cytokines may play a role [18]. Viral regulation of B7 family inhibitory molecules in epithelial cells leads to suppression or termination of immune responses [19]. Programmed cell death ligands 1 (PD-L1, B7–H1, CD274) and (PD-L2, B7-DC, CD273) belong to the B7 family and are widely expressed in activated T cells, B cells, monocytes, dendritic cells, macrophages, and other cells to regulate activation or inhibition [20]. NcRNA can act as a regulator of translation by participating in transcriptional and post-transcriptional gene regulation, heterochromatin formation, histone modification, DNA methylation, RNA splicing, and gene expression [21]. Many respiratory virus infections can significantly alter the expression profile of host ncRNA, and some affected ncRNA have been shown to play an important role in viral replication and/or host response [22], such as a respiratory syncytial virus (RSV) and human metapneumovirus (hMPV).

In this review, we will focus on how noncoding RNA and viruses interact to jointly regulate the occurrence and development of allergic rhinitis, as well as the latest research progress on virus-like particles and targeted noncoding RNA therapy in the treatment of allergic rhinitis patients.

1.1. The Interaction between miRNA and Virus Copromotes the Occurrence of AR. Infectious eukaryotic viruses play an important role in acute upper respiratory tract infections. RSV and hMPV are the main viruses that cause allergic rhinitis and are also risk factors for AR [23]. These viruses cause lung injury through various immune pathways, such as activation of preinflammatory mediators (including TNF-α, interleukin, and chemotherapeutic factors), as well as activation of white blood cells at the infection site, resulting in impaired lung function, persistent bronchial hyperreactivity, and airway inflammation, promoting Th2 cell sensitization and inducing allergic rhinitis [24]. Microarray and high-throughput sequencing techniques have been used to identify changes in miRNA expression after RSV/hMPV infection. Changes in miRNA expression after RSV infection have been demonstrated in a variety of cells and tissues such as bronchial epithelial cells (NHBEs), nasal mucosa, and dendritic cells [25]. Members of the LEt-7 family have been shown to decrease in both animal models and human studies of asthma and allergic rhinitis. Conversely, the activation of the JAK1/STAT3 signaling pathway inhibits IL-13 production and SOCS4 gene transcription, thus inhibiting the expression of various inflammatory factors in AR. A group of core miRNAs involved in atopic diseases includes up-regulation of miR-21, MiR-223, MiR-146a, MiR-142-5p, MiR-142-3p, MiR-146b, and MiR-155 and down-regulation of let-7 family , MiR-193b and MiR-375. Most of the miRNAs involved increased Th2 cytokine secretion (MiR-124b and MiR-146b), decreased Th1 cytokine secretion (MiR-513-5p and MiR-625-5p) or promoted T cell differentiation into Th2 (MiR-21 and MiR-19a) [26, 27]. In a study of 30 patients with allergic rhinitis, we collected nasal irrigation fluid and isolated type 2 macrophages (M2) by flow cytometer. MiR-202-5p was highly expressed in macrophages of patients with allergic rhinitis compared with healthy controls, promoting M2 polarization by targeting MATN2 [28]. MiR-155 plays an important role in the development of the immune system, the differentiation of immune cells, and the maintenance of immune function. The nasal mucosa of patients with allergic rhinitis shows enrichment of ILC2 and miR-155. Highly expressed miR-155 may enhance IL-4 levels by promoting ILC2 expression, thereby promoting Th2 inflammation [29]. After RSV infection, SOCS1 and SOCS3 expressions can be induced to further reduce the phosphorylation level of STAT, which is conducive to virus survival [30]. MiR-155 and its target gene SOCS1 are key regulators of effector $CD8^+$ T cells and affect cytokine signal transduction through STAT5. SOCS1 is a direct target of miR-155, and the inhibition of miR-155 can restore SOCS1 expression. Overexpression of miR-155 can reduce SOCS1 expression level [31]. Therefore, SOCS1 expression was induced after RSV infection, and the expression level of miR-155 was up-regulated. Overexpression of miR-155 can increase the surface level of IL-4 and promote the inflammatory response of allergic rhinitis patients. On the other hand, up-regulated miR-155 can inhibit RSV replication by upregulating STAT phosphorylation levels. Therefore, miR-155 can be used as a therapeutic target for patients with RSV-induced allergic rhinitis. We summarized the miRNA that plays a regulatory role in allergic rhinitis over the years (Table 1).

1.2. LncRNA and Viruses Play Important Roles in the Occurrence of AR. Studies have found that lncRNA is associated with AR. One study showed that analysis of lncRNA cores showed that there were 2259 lncRNA in the nasal mucous membrane of AR patients, of which 1033 were up-regulated and 1226 down-regulated [38]. Genetic ontology table of enrichment results of gene ontology (GO) and pathway LncRNA-mRNA is involved in several biological processes related to the pathogenesis of AR enrichment in cell signaling pathways, such as positive regulation of IL-13 secretion and FcεRI signaling pathway and NF-κB signaling pathway [38]. Recently, it has been found that long non-coding RNA FOXD3-AS1 has a negative regulatory role in allergic rhinitis. LncFOXD3-AS1 expression in nasal mucosa was compared between patients with allergic rhinitis and healthy controls. Nasal epithelial cells (NECs) were then coincubated with lipopolysaccharide or recombinant IL-25, and NECs supernatant was then incubated with CD4+ T cells. The proportion of Th2 cells was detected by a flow cytometer. The results showed that lncFOXD3-AS1 expression was down-regulated in the nasal mucosa, and the proportion of Th2 cells in peripheral blood and the levels of IL-25, IL-4, and IL-13 were increased in AR patients, while overexpression of lncFOXD3-AS1 inhibited the expression and secretion of IL-25 in NECs, thus alleviating the inflammatory response in AR patients [39]. TNF-α and IL-6 are highly expressed in AR subjects and are important proinflammatory factors regulating the inflammatory response of AR. Studies have shown that their single nucleotide polymorphisms (SNPs) may be risk factors for AR susceptibility [40]. In addition, IL-6 is an inhibitor of T helper 1 (Th1) differentiation and plays an important role in regulating CD4+ T cell differentiation and IL-4 production during Th2 differentiation. Therefore, IL-6 is a key factor in regulating the pathogenesis of AR induced by the imbalance of Th1 and Th2 differentiation [41]. The research shows that down-regulated lncRNA-AK149641 can decrease the expression level of TNF-α and IL-6 by the activity of the NF-κB signaling pathway in OVA mice [42]. We have mentioned that respiratory syncytial virus (RSV) infection is a risk factor for allergic rhinitis. Recently, some scholars found that the expression level of LncRNA-PVT1 was down-regulated in the RSV-infected AR rat model. Subsequently, we up-regulated lncRNA-PVT1 with α-asarone and found that the viability, proliferation, and migration of RSV-ASMCs were significantly reduced, which is mediated by the PVT1/ miR-203a/E2F3 signaling pathway [43]. These results suggest that lncrNA-PVT1 can be an important target for the prevention and treatment of RSV-induced allergic rhinitis. Finally, we concluded that LncRNA participates in the regulation and development of allergic rhinitis in recent years (Table 2).

1.3. Recent Advances in the Treatment of Allergic Rhinitis, Focusing on ncRNA and Virus. According to the definition

Table 1: Summary of regulation and function with miRNA in allergic rhinitis.

miRNA	Expression	Targets	Pathways	Function
miR-133b	Down-regulated	TNF-α, il-4, and INF-α	Nlrp3	Up-regulation of miR-133b significantly reduced OVA-specific IgE concentrations, nasal friction, sneezing frequency, cytokines (TNF-α, IL-4, IL-5, and IFN-γ), and Nlrp3 expression levels [32].
miR-181a	Up-regulated	IL-10 and TGF-β	PI3K/Akt	Up-regulation of miR-181a promotes expression of TGF-β and IL-10 and is involved in the regulation of regulatory T cell differentiation and function in children with allergic rhinitis [33].
miR-375	Up-regulated	Thymic stromal lymphopoietin (TSLP) and type II innate lymphoid cells (ILC2)	JAK2/STAT3	Mediated regulation of ILC2 cells through TSLP in allergic rhinitis [34].
miR-233	Up-regulated	IL-35		Mir-223 and IL-35 levels were associated with Th1/Th2 cytokines, eosinophil counts, and clinical severity [35].
miR-30a-5p	Up-regulated	SOCS3	SOCS1/ SOCS3	Involved in T helper cell differentiation [36].
miR-202-5p	Up-regulated	CD4+T	MANT2	Promoted tregs differentiation [28].
miR-29	Down-regulated	CD276		Decreasing inflammatory response [37].

Table 2: Summary of regulation and function with lncRNA in allergic rhinitis.

lncRNA	Expression	Targets	Effectors	Function
Linc00632	Down-regulated	MiR-498	IL-13 and gm-csf	Linc00632 inhibited IL-13-induced GM-CSF, eotaxin, and MUAC5AC production in IL-13-treated NECs by targeting miR-498 [44].
SNHG16	Up-regulated	miR-106-5p	Leukemia inhibitory factor (LIF) and JAK1/STAT3	SNHG16 up-regulates LIF expression by binding with miR-106b-5p, thus promoting the activity of the JAK1/STAT3 pathway and promoting cell apoptosis, inflammation, and development of AR [45].
GAS5	Up-regulated	miR-140 and niR-21	IFN-γ and IL-2	GAS5 down-regulates the expression of target proteins, including miR-140 and miR-21, accelerates the imbalance of Th1/Th2, and promotes the inflammatory response of AR patients [46].
MIAT	Up-regulated	miR-10b-5p	Th17, IL4, IL6, and IL17	MIAT can promote allergic inflammation and symptoms by activating the th17/IL4/IL6 immune response via target-inhibited miR-10b-5p in AR patients [47].
NEAT1	Up-regulated	miR-511	NR4A2 and IL13	NEAT1 induced inflammatory cytokine production and apoptosis contributing to the pathogenesis of AR via the miR-511/NR4A2 axis [48].

proposed by the ARIA (allergic rhinitis and its effects on asthma) initiative allergic rhinitis is an IgE-mediated inflammatory response of the nasal epithelium with corresponding symptoms caused by exposure to allergens [49]. Although there are many drugs to treat allergic rhinitis, many of them are symptomatic treatments, such as inhibiting histamine release or reducing inflammation, which are not the most effective ways. In addition to active allergen avoidance, immunotherapy is considered the most effective treatment for type I allergies, which includes the use of allergen agents in various forms and through various channels. Allergen immunotherapy (AIT) is the only proven effective treatment in these areas[50]. Among them, virus-like particles (VLPs) provide a very effective platform for allergen immunity, with characteristics of high immunogenicity, low allergen, and high clinical efficacy [51]. CpG motifs (CpGs) short nucleotide sequences within the CpG motif have also been extensively studied as effective stimulators of dendritic cells and B cells. The way VLPs modulate the immune response highlights its particular promise as a platform for immunotherapy of allergic diseases. Due to the immunomodulatory properties associated with viral structure, they are also used as a treatment for allergic diseases, particularly allergic rhinitis and asthma. In fact, VLPs loaded with CpGs appear to promote the re-establishment of physiological immune response in patients with allergies, although the underlying immune mechanisms are not fully understood.

So how does AIT work? A dendritic cell, one of the antigen-presenting cells, is believed to play a central role in the absorption and processing of allergens to induce allergen-specific immune responses. In the presence of high doses of allergens, the physical immune system will tolerate the phenomenon, which leads to an imbalance between Th1 and Th2. Regulatory T cells (iTreg) and thymus-derived $FOXP3^{+}CD4^{+}CD25^{+}$ natural regulatory T cells (nTreg) both play an important role in controlling pathogenic effector T cells and maintaining the balance between immune tolerance and immunity, which can down-regulate dendritic cells, mast cells, eosinophil and basophils, and helper T cells [52]. What's more, IL-10 and TGF-β are inhibitory cytokines that play an important role in this regard. When we restored the balance between Th2/Th1/Treg with VLPs, the ratio between allergen-specific IgE and IgG4 antibodies was reduced, resulting in higher IgG4 production and reduced migration of inflammatory cells to tissues, resulting in reduced clinical symptoms in AR patients.

In addition, several ncRNA-virus products are being actively developed. RNA interference (RNAi) is a gene-specific RNA degradation process mediated by short interfering RNA (siRNA), which is a novel therapeutic vector for allergic rhinitis [53]. Calcium-activated potassium ion channel-3.1 (KCa3.1) plays an important role in the release of inflammatory factors by mast cells. Some scholars investigated the effect of lentivirus-mediated shRNA silencing KCa3.1 on hypersensitivity to allergic rhinitis in mice. The results showed that LV-KCA3.1-shrNA intervention could effectively attenuate hypersensitivity to AR and inhibit mast cell activity by inhibiting PI3K/AKT signaling pathway [54]. In addition, miRNA and lncRNA both play an important role in regulating the pathogenesis of allergic inflammation, such as regulating Th1 and Th2 polarization and participating in the release of eosinophils, T cells, mast cells, and basophil cytokines. Therefore, the construction of a complete RNA regulatory network can help us better find targets for AR therapy.

2. Discussion

In conclusion, miRNA can target AR-related gene expression, while lncRNA can combine with miRNA through competition, and total also involved in AR epigenetic modification. On the other hand, lncRNA also may be involved in the pathogenesis of AR through multiple functional pathways. In addition, extracellular exosomes lncRNA is gaining increasing attention in AR. Further exploration of RNA in many ways will greatly expand the genes and molecules involved in the research on the mechanism of action in AR and other allergic diseases will provide the accuracy of AR in future therapy and offer new directions. Viral infections, like respiratory syncytial virus (RSV) and human metapneumovirus (hMPV), could interact with the noncoding RNA. However, the interaction between viral infection, noncoding RNA, and allergy is complex. At present, the research on allergic rhinitis is more and more in-depth, and the regulatory network of lncRNA is gradually improved, which is conducive to the development of new treatment methods and the discovery of new molecular markers for rapid diagnosis and classification.

Data Availability

All data in this paper are available on the PUBMED website.

Conflicts of Interest

The authors declare that they have no conflicts of interest.

Authors' Contributions

Zhu Lei and Guangrui Feng contributed equally.

Acknowledgments

This study was supported by Hubei University of Science and Technology Ophthalmology and Otorhinolaryngology S(2020-2) for NZF. None.

References

[1] S. Dinmezel, C. Ogus, and H. Erengin, "The prevalence of asthma, allergic rhinitis, and atopy in Antalya, Turkey," *Allergy and Asthma Proceedings*, vol. 26, no. 5, pp. 403–409, 2005.

[2] C. Bachert, P. van Cauwenberge, and J. Olbrecht, "Prevalence, classification and perception of allergic and nonallergic rhinitis in Belgium," *Allergy*, vol. 61, no. 6, pp. 693–698, 2006.

[3] P. J. Bousquet, B. Leynaert, F. Neukirch et al., "Geographical distribution of atopic rhinitis in the European community

respiratory health survey I," *Allergy*, vol. 63, no. 10, pp. 1301–1309, 2008.

[4] M. Humbert, J. Bousquet, C. Bachert et al., "IgE-mediated multimorbidities in allergic asthma and the potential for omalizumab therapy," *Journal of Allergy and Clinical Immunology: In Practice*, vol. 7, no. 5, pp. 1418–1429, 2019.

[5] O. Palomares, M. Akdis, M. Martín-Fontecha, and C. A. Akdis, "Mechanisms of immune regulation in allergic diseases: the role of regulatory T and B cells," *Immunological Reviews*, vol. 278, no. 1, pp. 219–236, 2017.

[6] D. I. Bernstein, G. Schwartz, and J. A. Bernstein, "Allergic rhinitis: mechanisms and treatment," *Immunology and Allergy Clinics of North America*, vol. 36, no. 2, pp. 261–278, 2016.

[7] C. A. Janeway, P. Travers, and M. Walport, *Immunobiology: The Immune System in Health and Disease*, Garland Science, New York, NY, USA, 2001.

[8] F. Ihara, D. Sakurai, S. Yonekura et al., "Identification of specifically reduced Th2 cell subsets in allergic rhinitis patients after sublingual immunotherapy," *Allergy*, vol. 73, no. 9, pp. 1823–1832, 2018.

[9] J. Numminen, "Allergic rhinitis," *Duodecim*, vol. 133, no. 5, pp. 473–478, 2017.

[10] S. Bonnet, O. Boucherat, R. Paulin et al., "Clinical value of non-coding RNAs in cardiovascular, pulmonary, and muscle diseases," *American Journal of Physiology—Cell Physiology*, vol. 318, no. 1, pp. C1–C28, 2020.

[11] M. Losko, J. Kotlinowski, and J. Jura, "Long noncoding RNAs in metabolic syndrome related disorders," *Mediators of Inflammation*, vol. 2016, pp. 1–12, 2016.

[12] J. A. Vidigal and A. Ventura, "The biological functions of miRNAs: lessons from in vivo studies," *Trends in Cell Biology*, vol. 25, no. 3, pp. 137–147, 2015.

[13] M. R. Hadjicharalambous and M. A. Lindsay, "Long noncoding RNAs and the innate immune response," *Noncoding RNA*, vol. 5, no. 2, p. 34, 2019.

[14] E. Tsitsiou, A. E. Williams, S. A. Moschos et al., "Transcriptome analysis shows activation of circulating CD8+ T cells in patients with severe asthma," *The Journal of Allergy and Clinical Immunology*, vol. 129, no. 1, pp. 95–103, 2012.

[15] M. Li, K. Ma, Z. Feng, J. Wang, X. Zhou, and L. Zhou, "Differential long non-coding RNA expression profiles in the peripheral blood and CD4+ T cells of patients with active rheumatoid arthritis," *Experimental and Therapeutic Medicine*, vol. 20, no. 1, pp. 461–471, 2020.

[16] A. C. Wells, E. L. Pobezinskaya, and L. A. Pobezinsky, "Non-coding RNAs in CD8 T cell biology," *Molecular Immunology*, vol. 120, pp. 67–73, 2020.

[17] X. Y. Zhu, X. P. Wang, Y. Wang, and Y. Zhao, "Exosomal long non-coding RNA GAS5 suppresses Th1 differentiation and promotes Th2 differentiation via downregulating EZH2 and T-bet in allergic rhinitis," *Molecular Immunology*, vol. 118, pp. 30–39, 2020.

[18] A. K. Singh, P. Stock, and O. Akbari, "Role of PD-L1 and PD-L2 in allergic diseases and asthma," *Allergy*, vol. 66, no. 2, pp. 155–162, 2011.

[19] K. Ishiwata, N. Watanabe, M. Guo et al., "Costimulator B7-DC attenuates strong Th2 responses induced by *Nippostrongylus brasiliensis*," *The Journal of Immunology*, vol. 184, no. 4, pp. 2086–2094, 2010.

[20] M. T. Zdrenghea and S. L. Johnston, "Role of PD-L1/PD-1 in the immune response to respiratory viral infections," *Microbes and Infection*, vol. 14, no. 6, pp. 495–499, 2012.

[21] J. J. Quinn and H. Y. Chang, "Unique features of long non-coding RNA biogenesis and function," *Nature Reviews Genetics*, vol. 17, no. 1, pp. 47–62, 2016.

[22] W. Z. Wu, E. J. Choi, I. Lee, Y. S. Lee, and X. Bao, "Non-coding RNAs and their role in respiratory syncytial virus (RSV) and human metapneumovirus (hMPV) infections," *Viruses*, vol. 12, no. 3, p. 345, 2020.

[23] H. Bisgaard, M. N. Hermansen, K. Bonnelykke et al., "Association of bacteria and viruses with wheezy episodes in young children: prospective birth cohort study," *BMJ*, vol. 341, 2010.

[24] G. A. Rossi and A. A. Colin, "Infantile respiratory syncytial virus and human rhinovirus infections: respective role in inception and persistence of wheezing," *European Respiratory Journal*, vol. 45, no. 3, pp. 774–789, 2015.

[25] S. Wang, P. Liu, P. Yang, J. Zheng, and D. Zhao, "Peripheral blood microRNAs expression is associated with infant respiratory syncytial virus infection," *Oncotarget*, vol. 8, no. 57, pp. 96627–96635, 2017.

[26] S. Q. Yu, R. X. Zhang, and G. J. Liu, "Microarray analysis of differentially expressed microRNAs in allergic rhinitis," *Am Journal Rhinol Allergy*, vol. 25, no. 6, pp. e242–e246, 2011.

[27] F. Gómez, C. Rondón, M. Salas, and P. Campo, "Local allergic rhinitis: mechanisms, diagnosis and relevance for occupational rhinitis," *Current Opinion in Allergy and Clinical Immunology*, vol. 15, no. 2, pp. 111–116, 2015.

[28] L. Wang, X. Y. Liu, X. C. Song, L. Dong, and D. Liu, "MiR-202-5p promotes M2 polarization in allergic rhinitis by targeting MATN2," *International Archives of Allergy and Immunology*, vol. 178, no. 2, pp. 119–127, 2019.

[29] Y. Q. Zhu and Y. H. Liu, "A review on group 2 innate lymphoid cells and miR-155 in allergic rhinitis," *Lin Chung Er Bi Yan Hou Tou Jing Wai Ke Za Zhi*, vol. 31, no. 24, pp. 1940–1943, 2017.

[30] J. C. Dudda, B. Salaun, Y. Ji et al., "MicroRNA-155 is required for effector CD8+ T cell responses to virus infection and cancer," *Immunity*, vol. 38, no. 4, pp. 742–753, 2013.

[31] S. Wang, Y. Ling, Y. Y. Yao, G. Zheng, and W Chen, "Luteolin inhibits respiratory syncytial virus replication by regulating the MiR-155/SOCS1/STAT1 signaling pathway," *Virology Journal*, vol. 17, no. 1, p. 187, 2020.

[32] X. F. Li, J. Li, Q. Hu, and Y. Li, "MicroRNA-133b ameliorates allergic inflammation and symptom in murine model of allergic rhinitis by targeting nlrp3," *Cellular Physiology and Biochemistry*, vol. 42, no. 3, pp. 901–912, 2017.

[33] Q. X. Zeng, W. L. Liu, R. Z. Luo, and G. Lu, "MicroRNA-181a and microRNA-155 are involved in the regulation of the differentiation and function of regulatory T cells in allergic rhinitis children," *Pediatric Allergy and Immunology*, vol. 30, no. 4, pp. 434–442, 2019.

[34] X. Luo, Q. X. zeng, S. B. Yan, W. Liu, and R. Luo, "MicroRNA-375-mediated regulation of ILC2 cells through TSLP in allergic rhinitis," *World Allergy Organization Journal*, vol. 13, no. 8, 2020.

[35] G. X. Ruan, X. L. Wen, and Z. W. Yuan, "Correlation between miR-223 and IL-35 and their regulatory effect in children with allergic rhinitis," *Clinical Immunology*, vol. 214, 2020.

[36] C. Y. Zhao, W. Wang, H. C. Yao, and X. Wang, "SOCS3 is upregulated and targeted by miR30a-5p in allergic rhinitis," *International Archives of Allergy and Immunology*, vol. 175, no. 4, pp. 209–219, 2018.

[37] J. Wang, J. S. Yin, H. Peng, and A. Z. Liu, "MicroRNA-29 mediates anti-inflammatory effects and alleviation of allergic responses and symptoms in mice with allergic rhinitis,"

Hindawi
Evidence-Based Complementary and Alternative Medicine
Volume 2023, Article ID 9806751, 1 page
https://doi.org/10.1155/2023/9806751

Retraction

Retracted: A Three-Year Prospective Study Assessing the Application of Chromosomal Microarray Analysis in 576 High-Risk Pregnant Women

Evidence-Based Complementary and Alternative Medicine

Received 8 August 2023; Accepted 8 August 2023; Published 9 August 2023

This article has been retracted by Hindawi following an investigation undertaken by the publisher [1]. This investigation has uncovered evidence of one or more of the following indicators of systematic manipulation of the publication process:

(1) Discrepancies in scope
(2) Discrepancies in the description of the research reported
(3) Discrepancies between the availability of data and the research described
(4) Inappropriate citations
(5) Incoherent, meaningless and/or irrelevant content included in the article
(6) Peer-review manipulation

The presence of these indicators undermines our confidence in the integrity of the article's content and we cannot, therefore, vouch for its reliability. Please note that this notice is intended solely to alert readers that the content of this article is unreliable. We have not investigated whether authors were aware of or involved in the systematic manipulation of the publication process.

Wiley and Hindawi regrets that the usual quality checks did not identify these issues before publication and have since put additional measures in place to safeguard research integrity.

We wish to credit our own Research Integrity and Research Publishing teams and anonymous and named external researchers and research integrity experts for contributing to this investigation.

The corresponding author, as the representative of all authors, has been given the opportunity to register their agreement or disagreement to this retraction. We have kept a record of any response received.

References

[1] M. Jiang, S. Huang, X. Ma et al., "A Three-Year Prospective Study Assessing the Application of Chromosomal Microarray Analysis in 576 High-Risk Pregnant Women," *Evidence-Based Complementary and Alternative Medicine*, vol. 2022, Article ID 1533346, 5 pages, 2022.

Hindawi
Evidence-Based Complementary and Alternative Medicine
Volume 2022, Article ID 1533346, 5 pages
https://doi.org/10.1155/2022/1533346

Research Article

A Three-Year Prospective Study Assessing the Application of Chromosomal Microarray Analysis in 576 High-Risk Pregnant Women

Minmin Jiang,[1] **Shengwen Huang**,[1] **Xingwei Ma**,[1] **Ping Xie**,[2] **Lingyan Ren**,[1] **Qian Jin**,[1] **and Keyan Linghu**[1]

[1]*Prenatal Diagnosis Center, Guizhou Provincial People's Hospital, Guiyang 550004, China*
[2]*Department of Ultrasonography, Guizhou Provincial People's Hospital, Guiyang 550004, China*

Correspondence should be addressed to Minmin Jiang; drjiangminmin@outlook.com

Received 22 July 2022; Revised 21 September 2022; Accepted 22 September 2022; Published 15 October 2022

Academic Editor: Xueliang Wu

Background. The use of chromosomal microarray analysis (CMA) in prenatal diagnosis of chromosomal and genetic diseases has resulted in a significant improvement in the diagnosis of genetically caused congenital malformations, neurodevelopmental disorders, and congenital anomalies, with a high diagnostic yield in selected prenatal cases. *Objective*. The objective of this study was to evaluate the application of CMA in the prenatal diagnosis of high-risk pregnant women. *Method*. A total of 576 pregnancies were selected from May 2018 to October 2020 in our hospital, including amniotic fluid chromosome, karyotype analysis, and CMA detection. The study group was divided into two groups based on the indications for testing: group A has 88 patients at the age of 35 years or older, and group B patients were in high-risk pregnancies, which consisted of 33 cases of bad pregnancy history, 252 high-risk serological screenings, 70 high-risk non-invasive prenatal testing (NIPT), 65 cases of B-ultrasound indicated fetal development abnormalities or ultrasonic soft marker abnormalities, and 68 other cases of pregnant women or both who have genetic or chromosomal abnormalities. At last, we have an analysis of the detection rate from different testing methods. *Results*. Based on the follow-up test, 576 high-risk pregnant women showed an amniotic fluid chromosome karyotype rate of 18.1% (104/576), and the remaining 472 of these cases suffered a CNV ratio of 14.2% (67/472). 472 women of low clinical relevance are at 4.87% (23/472), 16 people showed a clear cause ratio = 3.39% (16/472), and 28 of the 472 (5.93%) cases showed polymorphism. *Conclusions*. In our study, CMA significantly improved the fetal detection rate and diagnosis rate in high-risk pregnant women, which proved to be a very useful method in the diagnosis of genetically caused neurodevelopmental disorders and congenital anomalies. The use of CMA in high-risk pregnant women is justified, and these women can detect an additional (3.40%, 16/472) of pathogenic microdeletions and microduplications in the cases.

1. Introduction

Chromosomal microarray analysis (CMA) is also called "molecular karyotype" technology, including array-based comparative genomic hybridization (aCGH) and single nucleotide polymorphism microarrays (SNP arrays). With the advantages of high resolution (0.1–0.3 mb), high efficiency, and high sensitivity, CMA can accurately locate abnormal fragments, display affected genes, and help identify disease-related genes. The chromosome karyotype analysis uses "fetal cells" as the test specimen and is recognized as the gold standard for genetic prenatal diagnosis of abnormal chromosome number, large fragment deletion/duplication (>10 mb), rearrangement, and inversion. Some studies have reported that about 12.4% to 35% of fetal ultrasound abnormalities are caused by chromosomal aberrations, of which about 25% are abnormal in karyotype structure or number, and about 10% are abnormal in chromosomal microstructure [1]. In addition, chromosomal microarray analysis (CMA) is a useful technique used to detect clinically significant microdefects or duplications with high sensitivity to submicroscopic aberrations [2]. In

2009, the American Society of Obstetricians and Gynecologists (ACOG) recommended the use of CMA for antenatal ultrasound abnormality detection. In 2013, ACOG and the American Society of Maternal and Fetal Medicine (SMFM) recommended that CMA be used as an alternative to traditional chromosome karyotyping techniques [3, 4]. In 2021, researchers investigated the clinical significance of chromosomal mosaicism (CM) in prenatal diagnosis through G-banding karyotyping and chromosomal microarray analysis (CMA) [5–7]. Some scholars believe that CMA cannot detect balanced ectopic, inverted, <30% mosaicism, and single-gene diseases, and the analysis of the results is complicated [8]. Therefore, it is not practical to completely replace traditional karyotyping in a short period of time [9].

In 2014, China released the expert consensus on the application of CMA prenatal diagnosis [10]. The late start and the lack of a comprehensive database of the Chinese populations have delayed its development to a certain extent. This study retrospectively analyzed the chromosome detection results of 576 high-risk pregnant women who underwent amniotic fluid chromosome karyotype analysis and CMA testing in our hospital from May 2018 to October 2020 to explore the application of chromosomal microarray analysis (CMA) in prenatal diagnosis.

2. Methods

2.1. Patients and Design. From May 2018 to October 2020, 576 high-risk pregnant women were selected, including 88 pregnant women located at the age of 35 years or older, 33 cases of bad pregnancy history, 252 high-risk serological screenings, 70 high-risk NIPTs, 65 cases of B-ultrasound indicated fetal development abnormalities or ultrasonic soft marker abnormalities, and 68 other cases of pregnant women or both who have suffered genetic or chromosomal abnormalities. They all underwent amniocentesis, chromosome karyotype analysis, and CMA technology detection at the Prenatal Diagnosis Center, Guizhou Provincial People's Hospital. All of the women were 35–53 years of age (mean, 38.7 years) and were at gestational 18–32 weeks (mean, 19.7 weeks). This study has obtained informed consent from the women before screening and diagnosis and was approved by the hospital medical ethics committee.

2.2. Interventional Prenatal Diagnosis. Before carrying out invasive prenatal diagnosis, we carried out necessary genetic counseling services for high-risk pregnant women, fully informed them of the technical advantages and possible risks, and had them sign an informed consent form. Amniocentesis under ultrasound guidance was used to quantify 30 ml of amniotic fluid, which was then sent to the genetic laboratory for chromosome karyotype analysis and CMA analysis.

2.3. Ultrasonography. Prenatal ultrasound grade III screening for selected high-risk pregnant women is referred to as "Prenatal Ultrasound Diagnosis of Fetal Malformations" [11]. Screen out fetuses with ultrasound soft indicators such as lateral ventricle normal high value, intestinal echo enhancement, renal pelvis separation, ventricular bright spot, choroid plexus cyst, single umbilical artery, and other ultrasound soft indicators, as well as cases of fetal structural malformations. Partial results were presented in supporting information (Figure S1).

2.4. Amniotic Fluid Cell Karyotype Analysis. First, 10 mL of amniotic fluid that centrifuge at 1500 r/min for 10 min, then discarded the supernatant. After adding amniotic fluid cell culture medium (PAN, Germany), we placed it in a 37°C, 5% volume fraction carbon dioxide cell incubator for about 5 to 7 days. Finally, we had to mix 10 μL of colchicine with the product for 2 hours, and routine G-banding chromosome analysis was performed. We were required to detect 20 karyotypes under the microscope (CytoVision®) and analyze 5 of them. Additionally, in cases of abnormal karyotype or chimera, no less than 60–100 cell division phases were analyzed [12]. Partial results were presented in supporting information (Figure S2).

2.5. Prenatal CMA Testing. The experimental reaction process refers to the experimental operation process provided by Illumina. Research and application of the whole genome HumanCyto SNP-12 BeadChip Kits chip provided by Illumina in the United States, which contains about 300,000 detection sites. It can detect abnormal chromosomal copy number changes and loss of heterozygosity, such as chromosome microdeletion/microduplication and chromosome subtelomere deletion syndrome, with clinical significance in the whole genome. After whole genome amplification, denaturation, and renaturation of fetal DNA, data collection is performed using the Iscan scanning system, and data analysis is performed using KaryoStudio software. The test results are compared and analyzed with the following public databases: http://omim.org/(OMIM database); http://genome.ucsc.edu/(UCSC database); http://ncbi.nlm.nih.gov/pubmed (NCBI database); and https://decipher.sanger.ac.uk/(DECIPHER database).

The nature of CNVs is determined through database comparison; pathological CNVs and benign CNVs are identified. For CNVs of unknown clinical significance, further family analysis is carried out to determine the source of abnormality and assist in evaluating the prognosis.

2.6. Statistical Methods. Data are collected using EXCEL forms, and counting data are expressed as the number of cases and percentages.

3. Results

3.1. Amniotic Fluid Chromosome Abnormalities. According to clear research objects and methods, 2719 samples were screened, which is the total number of pregnant women tested by related items in our hospital from May 2018 to October 2020, and 576 samples of high-risk pregnant women meeting the research conditions were

Table 1: 104 cases of abnormal karyotypes.

Case	Abnormal karyotype	N	Pregnancy outcome
1	47, XN, +21	29	Termination of pregnancy
2	47, XN, +18	9	Termination of pregnancy
3	47, XN, +13	2	Termination of pregnancy
4	47, XYY	5	3 terminations of pregnancy, 2 continue pregnancy
5	47, XXX	3	1 termination of pregnancy, 2 continue pregnancy
6	46, XN, 16qh+	4	Continue pregnancy
7	46, XN, 1qh+	6	Continue pregnancy
8	46, XN, 9qh+	2	Continue pregnancy
9	46, XN, 14ps+	2	Continue pregnancy
10	46, XN, 21ps+	6	Continue pregnancy
11	46, XN, 13ps+	2	Continue pregnancy
12	46, XN, 15ps+	1	Continue pregnancy
13	46, XN, 22ps+	1	Termination of pregnancy
14	46, X, Yqh+	5	Continue pregnancy
15	46, X, Yqh-	4	Continue pregnancy
16	MOS 45, X[13]/46, XN[68]	1	Continue pregnancy
17	MOS45, X[15]/46, XX[19]	1	Continue pregnancy
18	MOS45, x[4]/46,x, Yqh-[96]	1	Continue pregnancy
19	MOS46, XN, t(6; 10) (p22.2,q26) [2]14, ps+46,XN[48]	1	Continue pregnancy
20	MOS 45, X[13]/46, XN[68]	1	Continue pregnancy
21	46, XN, der(22)add(22)(p11.2)	1	Continue pregnancy
22	46, XN, t(1; 14) (q21; q24)	1	Continue pregnancy
23	46, XN, inv(9)(p12q13)	11	Continue pregnancy
24	46, XN, Inv(10) (p13q11.2)	1	Continue pregnancy
25	46, XN, der(9)del(9) (p24)dup(11) (q22)	1	Continue pregnancy
26	46, XN, der(14; 15) (q10:q10)	1	Continue pregnancy
27	47, XN, +13(57)/46, XN(3)	1	Continue pregnancy
28	46X, inv(Y) (P11.2G11.22)	1	Continue pregnancy

CNV abnormalities.

selected for analysis. There were 472 cases with normal karyotypes and 104 cases with abnormal karyotypes, including 29 cases of the 21-trisomy syndrome (27.9%, 29/104), 9 cases of the 18-trisomy syndrome (8.65%, 9/104), 2 cases of the 13-trisomy syndrome (1.92%, 2/104), superfemale 3 cases of the syndrome (2.88%, 3/104), 5 cases of the Klinefelter syndrome (4.80%, 5/104), 33 cases of polymorphism (31.7%, 33/104), and 23cases of abnormal chromosome structure (22.1%, 23/104) (Table 1).

Among the 472 cases with normal karyotype analysis, 67 cases were abnormal CNV, 16 cases (23.9%, 16/67) had clear pathogenicity, 18 cases (26.9%, 18/67) had polymorphism, and 33 cases had no clinically meaningful significance (49.3%, 33/67). Through analysis, it is found that 16 additional cases (3.40%, 16/472) of pathogenic CNV abnormalities can be detected by CMA technology in high-risk pregnant women (Table 2).

4. Discussion

Academically, structural variations above 1 kb in the DNA genome, including microdeletions and microduplications, are collectively called genome copy number variation (CNV). Such submicroscopic structural changes are also abnormalities in CNV, which cannot be passed through conventional karyotype analysis technology to distinguish [13]. As a high-resolution, high-efficiency molecular biology detection method, CMA can detect small fragments <50 bp that cannot be detected by traditional chromosome karyotypes, and the mutation detection rate is significantly improved.

The results of this study showed that the incidence of chromosome abnormalities accounted for 18.1% (104/576), the incidence of normal chromosome karyotypes and genome copy number variation was 11.6% and 14.2% (67/472), among which the pathogenic chromosomal microdeletions and microduplications accounted for 3.39% (16/472), and the report rate of unclear clinical significance was 4.87% (23/472). Based on chromosome karyotype analysis combined with CMA, 16 cases of karyotype-negative fetuses were detected with a chromosomal microstructural variation. The detection rate of pathogenic CNV abnormalities increased by 3.40%. This result was consistent with previous reports that CMA testing can significantly increase the mutation rate of chromosomal diseases. HILLMAN et al. [14] reported that the CMA confirmed that fetal cases with a normal chromosomal karyotype but abnormal ultrasound structure had a pathogenic rate higher than 3% to 5%.

For reports with unclear clinical significance, prenatal genetic counseling for high-risk pregnant women will generally confuse clinicians and pregnant women. Therefore, this study hopes to reduce the rate of reports with unclear clinical significance. In 2012, Wapner et al. [15] published a research article showing that the incidence of CNV with unclear clinical significance was about 2.5%. In

Table 2: 16 cases of abnormal detection of CNV with normal karyotype.

Case	Chromosome location	Microdeletions, microduplications	Karyotype
1	Chromosom2	2q31.2518 kb duplicate (verified from father)	46, XN
2	Chromosome2	2P 509 kb missing	46, XN
3	Chromosome22	22q11.21 1.3 mb repeat	46, XN
4	Chromosome20	20q13.13 209 kb duplicate	46, XN
5	Chromosome11	11q14.3 371 kb missing	46, XN
6	Chromosome15	15q11.2 1.04 mb repeat	46, XN
7	Chromosome4	4p15.1p14 913 kb microduplicate	46, XN
8	Chromosome5	5p 854 kb repeat; 16 to 718 kb deletion	46, XN
9	Chromosome8	8p2.25M repeat	46, XN
10	Chromosome12	12P11.22 224 kb duplicate	46, XN
11	Chromosome18	18p11.3 repeat 497 kb	46, XN
12	Chromosome5	arr5q21.1 (315 kb repeat), arr5q33.3 (228 kb repeat), arr5q32.1 (519 kb repeat)	46, XN
13	Chromosome21	Trisomy 21 repeats	46, XN
14	Chromosome11	11P11.12 repeat 878 kb	46, XN
15	Chromosome13	13q33.1 missing 323 kb	46, XN
16	Chromosome18	18P11.21 repeat 509 kb	46, XN

2018, the research article changed the reporting rate of CNV with unclear prenatal clinical significance from a 2.5% decline to 0.9% [16]. In the results of this study, the report rate of unclear clinical significance is 4.87%, which is much higher than the report of Wapner et al. [16]. This will be our next task. We will continue to accumulate a large number of clinical case studies in order to provide more reliable data for prenatal genetics, counseling, and clinical screening.

Application of CMA in prenatal consultation CMA technology can be described as a "double-edged sword" for prenatal diagnosis. The sensitivity to small fragments increases the positive rate of test results, reduces the birth of children with chromosomal defects, and can be used as a means of genetic evaluation and used for assisted reproduction. However, the clinical significance is unknown, and the results of complex mutations can cause anxiety in pregnant and lying-in women, and even terminate the pregnancy by mistake. In this study, a total of 16 copy variant sites were detected. After database comparison and analysis and parental chromosome comparison, the CMA test results were classified into pathogenic, possibly pathogenic, unknown significance, and possibly benign according to the American ACMG guidelines and benign classification methods for microstructure variation classification [3]. Perfect fetal prenatal consultation and effective case follow-up are of great significance for special microstructural variation sites. Furthermore, with more and more clinical experience of whole genome arrays, the availability, complexity, and scale of CNV databases continue to increase. At the same time, more special prenatal cases should be submitted to the ISCA/DEFAPHER database to build a good communication platform.

In conclusion, in prenatal diagnosis, it is recommended that high-risk pregnant women perform CMA detection on the fetus. Compared with traditional karyotyping, the detection rate of pathogenic chromosomal abnormalities has been significantly increased, and birth defects can be better avoided. At the same time, it is necessary to accumulate a large amount of clinical data for further research to provide references for clinical work.

Abbreviations

NIPT: Non-invasive prenatal testing
CNVs: Copy number variations
CMA: Chromosomal microarray analysis
aCGH: Array-based comparative genomic hybridization
SNP arrays: Single nucleotide polymorphism microarray
ACOG: American Society of Obstetricians and Gynecologists.
SMFM: Society of Maternal and Fetal Medicine.

Data Availability

Raw data are archived at the Prenatal Diagnosis Center, Guizhou Provincial People's Hospital, Guiyang, China. Data supporting the findings of this study are available from the corresponding author upon reasonable request.

Ethical Approval

Ethical approval for this study was obtained from the Guizhou Provincial People's Hospital Ethical Review Authority. Participants gave their informed consent for study participation by submitting the survey. The study was performed in accordance with the Declaration of Helsinki, and all methods were performed in accordance with the relevant guidelines and regulations.

Conflicts of Interest

The authors declare that they have no conflicts of interest.

Authors' Contributions

Minmin Jiang, Shengwen Huang, and Xingwei Ma conceptualized the study design. Ping Xie, Lingyan Ren, Qian Jin, and Keyan Linghu collected the data. Minmin Jiang performed the analysis and wrote the manuscript. Drafts were critically discussed and revised by all authors. All

Hindawi
Evidence-Based Complementary and Alternative Medicine
Volume 2023, Article ID 9795630, 1 page
https://doi.org/10.1155/2023/9795630

Retraction

Retracted: Clinical Efficacy of Topical Tacrolimus on Conjunctival Hyperemia Caused by Prostaglandin Analogues

Evidence-Based Complementary and Alternative Medicine

Received 15 August 2023; Accepted 15 August 2023; Published 16 August 2023

This article has been retracted by Hindawi following an investigation undertaken by the publisher [1]. This investigation has uncovered evidence of one or more of the following indicators of systematic manipulation of the publication process:

(1) Discrepancies in scope

(2) Discrepancies in the description of the research reported

(3) Discrepancies between the availability of data and the research described

(4) Inappropriate citations

(5) Incoherent, meaningless and/or irrelevant content included in the article

(6) Peer-review manipulation

The presence of these indicators undermines our confidence in the integrity of the article's content and we cannot, therefore, vouch for its reliability. Please note that this notice is intended solely to alert readers that the content of this article is unreliable. We have not investigated whether authors were aware of or involved in the systematic manipulation of the publication process.

Wiley and Hindawi regrets that the usual quality checks did not identify these issues before publication and have since put additional measures in place to safeguard research integrity.

We wish to credit our own Research Integrity and Research Publishing teams and anonymous and named external researchers and research integrity experts for contributing to this investigation.

The corresponding author, as the representative of all authors, has been given the opportunity to register their agreement or disagreement to this retraction. We have kept a record of any response received.

References

[1] J. Yang, Y. Shi, and H. Chen, "Clinical Efficacy of Topical Tacrolimus on Conjunctival Hyperemia Caused by Prostaglandin Analogues," *Evidence-Based Complementary and Alternative Medicine*, vol. 2022, Article ID 3700720, 6 pages, 2022.

Hindawi
Evidence-Based Complementary and Alternative Medicine
Volume 2022, Article ID 3700720, 6 pages
https://doi.org/10.1155/2022/3700720

Research Article

Clinical Efficacy of Topical Tacrolimus on Conjunctival Hyperemia Caused by Prostaglandin Analogues

Jing Yang,[1] Yiyu Shi,[1] and Haibo Chen[2]

[1]*Hainan Eye Hospital and Key Laboratory of Ophthalmology, Zhongshan Ophthalmic Center, Sun Yat-sen University, Haikou, Hainan 570311, China*
[2]*Department of Ophthalmology, Hainan Aier Ehope Eye Hospital, Haikou 570226, China*

Correspondence should be addressed to Haibo Chen; chenwave2022@163.com

Received 11 July 2022; Revised 13 September 2022; Accepted 16 September 2022; Published 14 October 2022

Academic Editor: Xueliang Wu

Objective. To evaluate the clinical efficacy of tacrolimus ophthalmic solution on conjunctival hyperemia caused by prostaglandin analogues. *Methods*. A retrospective analysis was performed on 120 patients diagnosed with bilateral primary open-angle glaucoma (POAG). The enrolled patients developed symptoms of conjunctival hyperemia during the administration of travoprost ophthalmic solution. The patients were divided into two groups: 0.004% travoprost solution was administered in the control group. A combination of 0.004% travoprost solution with tacrolimus was administered in the experimental group. Clinopathological parameters including intraocular pressure (IOP), subjective dry eye symptom score (SDES), hyperemia score, and noninvasive tear break-up time (NIBUT) were recorded at week 0, 1, 2, and 4. Two-way ANOVA for repeated measurement was employed for statistical analysis using SPSS 22.0 software. *Results*. At week 1, 2, and 4, the IOP and SDES of both the control and experimental groups were significantly lower when compared the values at week 0 (before treatment). No significant differences in the IOP values between the two groups were observed at all time points. At week 2, the SDES and hyperemia score were lower in the experimental group than those in the control group, and the NIBUT was significantly longer in the experimental group. The above parameters showed no significant difference at week 4 between the two groups, although the average SDES and hyperemia score were slightly lower in the experimental group. *Conclusion*. Tacrolimus ophthalmic solution can relieve conjunctival hyperemia, improve ocular surface conditions, and reduce discomfort caused by prostaglandin analogues.

1. Introduction

Glaucoma is the second most common eye disease which can eventually lead to blindness [1]. The increased intraocular pressure (IOP) is a major risk factor associated with the progression of glaucoma. Since the effectiveness of the optic neuroprotective therapy is uncertain [2], the main therapeutic goal in glaucoma treatment is to lower IOP, reduce retinal ganglion cell loss, and maintain the visual function. There are different strategies to lower IOP [3]. Prostaglandin analogues (PGAs) are the main therapeutic to reduce IOP in glaucoma patients, which shows a good IOP-lowering effect at daily dosing frequency [4, 5]. However, these drugs cause side effects such as conjunctival hyperemia, eyelash elongation, eyelid, and iris pigmentation [6, 7]. Conjunctival hyperemia appears to be a major symptom at the early stage of PGA administration, which impinges on the eye vision and patients' compliance with medication [8, 9]. At present, there are no effective strategies to ameliorate conjunctival hyperemia caused by PGAs.

Tacrolimus (also known as FK506) is a fermentation product isolated from *Streptomyces tsukubaensis* and belongs to macrolide antibiotics [10]. It is a powerful immunosuppressant commonly used in transplantation, which acts by inhibiting the release of interleukin-2 (L-2) and the activation of T lymphocytes [11, 12]. Topical tacrolimus have been reported to show beneficial effects in inflammatory and allergic eye diseases [13, 14]. Since conjunctival hyperemia is usually triggered by microvasculature vasodilation upon inflammatory responses [15, 16], it is plausible that

tacrolimus may alleviate the inflammatory conditions in conjunctival hyperemia caused by PGAs.

In this study, a total number of 120 patients diagnosed with POAG and developed the symptoms of conjunctival hyperemia after PGA administration were randomly divided into the control group (0.004% travoprost solution) and the experimental group (a combination of 0.004% travoprost solution with tacrolimus). The ocular parameters including intraocular pressure (IOP), subjective dry eye symptom score (SDES), hyperemia score, and noninvasive tear break-up time (NIBUT) were followed for 4 weeks after treatment. We found that the administration of tacrolimus ophthalmic solution can relieve conjunctival hyperemia and reduce eye discomfort. Our data suggest that topical tacrolimus administration can serve as a potential strategy for alleviating conjunctival hyperemia induced by PGAs.

2. Subjects and Methods

2.1. Subjects. A total number of 120 patients (65 men and 55 women) who had been diagnosed with bilateral primary open angle glaucoma (POAG) and developed conjunctival hyperemia after 3–5 days' treatment of travoprost ophthalmic solution were enrolled in the study. This was a single-blinded study in which the medical staffs were aware of the treatment while the patients were not informed of the details of the medication. The patients' ages ranged between 28 and 67 years, with an average age at 50.3 ± 8.9 years (mean $\pm$ SD). The diagnostic criteria for POAG were based on the Chinese Glaucoma Guidelines (2020) [17]. All those patients had not been treated by any other medications and did not have any medical records of PGA-treated hyperemia before the enrollment in the study. Patients with other immunological disorders, ocular surface diseases, or who had undergone ocular surgery were excluded from the analysis. This study was approved by ethical committee of our hospital and all the enrolled patients signed an informed consent.

2.2. Methods. The patients were randomly assigned into the control and experimental groups ($n = 60$ in each group). Fisher's randomization technique was employed for random assignment [18]. All the enrolled patients suffered from conjunctival hyperemia within 5 days after topical application of 0.004% travoprost ophthalmic solution (TRAVATAN *Z* ophthalmic solution 0.004%, Alcon Laboratories Inc., 200 μL/per eye, once a day at 9 : 00 pm). Patients in the control group continued to be treated with travoprost ophthalmic solution only; while patients in the experimental group received a mixture of travoprost solution and tacrolimus, with travoprost ophthalmic solution at final concentration of 0.004%, and Talymus ophthalmic solution at final concentration of 0.1% (Senju Pharmaceutical Co., Ltd). All the solutions were administrated 200 μL/per eye, 4 times a day.

2.3. Observation Indexes. Intraocular pressure (IOP) : IOP was measured by a Goldmann tonometer for 3 times at each time point, and the average value was recorded as the IOP.

Subjective dry eye symptoms score (SDES) : SDES was assessed by questionnaire on week 0, 1, 2, and 4. The scoring criteria: Score 0: no dryness, foreign body sensation and burning sensation; Score 1: occasional occurrence of the above symptoms; Score 2: intermittent occurrence of the above symptoms; Score 3: persistent occurrence of the above symptoms. The scores of the patients in each group were summed at each time point and divided by the total number of patients as SDES.

Ocular redness index and noninvasive tear film break-up time (NIBUT) : the ocular redness index and NIBUT were measured by Oculus Keratograph.

2.4. Statistical Analysis. SPSS 22.0 was used for statistical analysis, and data were summarized as mean $\pm$ standard deviation. Two-way ANOVA for repeated measurement was used for the statistical comparison between the two groups, with Tukey's test as the post hoc test. $P < 0.05$ was considered to be statistically significant.

3. Results

After treatment with travoprost ophthalmic solution for 1 week, patients in both the groups showed typical symptoms of conjunctival hyperemia (see Figure 1) and high conjunctival index (see Figure 2). In the experimental groups administrated with tacrolimus ophthalmic solution, the symptoms of conjunctival hyperemia and high conjunctival index were significantly ameliorated after 3 weeks (see Figure 3 and Figure 4).

IOP: compared with week 0 (before travoprost ophthalmic solution and tacrolimus ophthalmic solution treatment), the IOP values at week 1, 2, and 4 were significantly reduced in both the groups ($P < 0.05$). However, there was no significant difference between IPO values of the two groups at all time points ($P < 0.05$) (Table 1).

SDES : compared with week 0, the SDES values at week 1, 2, and 4 were significantly higher in both the groups ($P < 0.05$). At week 0 and week 1, there were no statistical differences in the SDES between the two groups. However, at week 2 the SDES in the experimental group was significantly lower than that of the control group ($P < 0.05$) (Table 1). At week 4, the SDES was also slightly lower in the experimental group, although the difference between the two groups was not significant ($P > 0.05$).

Hyperemia score: compared with week 0, hyperemia scores at week 1 and 2 were significantly higher in both the groups ($P < 0.05$). At week 0, 1, and 4, hyperemia scores remained at a similar level between the two groups. At week 2, the hyperemia score in the experimental group was significantly lower than that of the control group ($P < 0.05$) (Table 1).

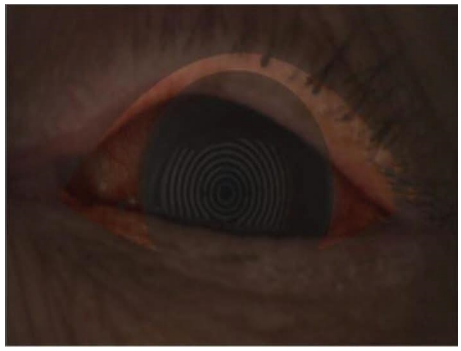

Figure 1: Conjunctival congestion after travoprost treatment for 1 week.

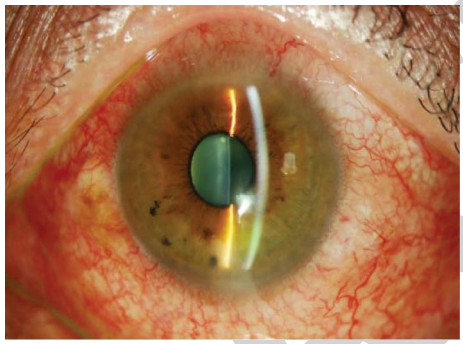

Figure 2: High hyperemia index after 1 week of travoprost treatment.

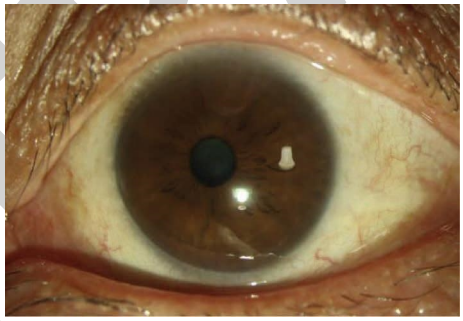

Figure 3: Conjunctival congestion was relieved after tacrolimus treatment for 3 weeks.

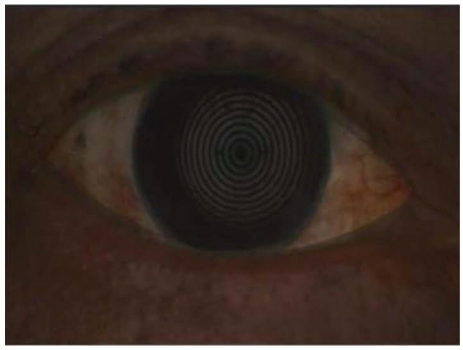

Figure 4: Hyperemia index decreased after tacrolimus treatment for 3 weeks.

Table 1: Comparison of the IOP, SDES, hyperemia score, and NIBUT in the two groups at different time points ($\overline{X} \pm s$).

Indexes	Week_0	Week_1	Week_2	Week_4
Experimental group				
IOP(mmHg)	26.4 ± 4.1	18.7 ± 3.5[1)]	16.2 ± 2.9[1)]	16.4±3.7[1)]
SDES	0.60 ± 0.51	1.88 ± 0.58[1)]	1.41 ± 0.39[1), 2)]	1.26±0.29[1)]
Hyperemia score	1.02 ± 0.51	2.85 ± 0.56[1)]	1.43 ± 0.44[1), 2)]	1.25 ± 0.21
NIBUT (s)	13.76 ± 2.51	5.34 ± 2.21[1)]	9.43 ± 2.44[1), 2)]	11.26 ± 3.29
Control group				
IOP(mmHg)	25.2 ± 5.3	19.5 ± 2.9[1)]	17.7 ± 3.3[1)]	16.9 ± 4.2[1)]
SDES	0.70 ± 0.48	1.90 ± 0.74[1)]	1.85 ± 0.50[1)]	1.33 ± 0.31[1)]
Hyperemia score	1.09 ± 0.48	2.96 ± 0.74[1)]	2.09 ± 0.56[1)]	1.33 ± 0.42
NIBUT (s)	12.89 ± 1.96	5.96 ± 1.99[1)]	6.41 ± 1.56[1)]	10.69 ± 3.42

NIBUT : compared with week 0, NIBUT values at week 1 and 2 were significantly lower in both the groups ($P < 0.05$). No statistical differences in NIBUT were observed between the two groups at week 0, 1, and 4. At week 2, NIBUT was significantly longer in the experimental group ($P < 0.05$) (Table 1).

(1) Indicates $p < 0.05$ when compared to the value at week 0.

(2) Indicates $p < 0.05$ when compared to the control group.

4. Discussion

Lowering the IOP by medication is an effective treatment for patients with hypertension or primary open-angle glaucoma [3]. Nonadherence to glaucoma eye treatment is a significant barrier limiting the treatment outcome in glaucoma patients. Medication compliance depends on many factors, such as the cost, convenience, and side effects [19,20]. Prostaglandin analogues (PGAs) are a class of unsaturated fatty acids derived from arachidonic acid in the cyclooxygenase pathway. PGAs are able to reduce the IOP by increasing the blood flow in retinal vasculatures and nursing the optic nerve in the retina [21]. In clinical practice, prostaglandins and its analogues are widely used to lower the IOP in glaucoma patients.

The administration of PGAs is accompanied by local side effects, such as conjunctival hyperemia, eyelash elongation and eyelid pigmentation [22]. It has been suggested that conjunctival hyperemia after PGA administration can be triggered by the preservative in the solution [22], since better ocular tolerance was observed when the patients were treated with preservative-free latanoprost. Experimental evidence indicates that latanoprost, which contains the highest concentration of benzalkonium chloride, seems to result in a lower incidence of conjunctival hyperemia [23].

The onset of conjunctival hyperemia involves conjunctival vasodilation, which is mediated by intracellular calcium and endothelium-derived nitric oxide [24]. However, recent evidence also suggests that conjunctival hyperemia can be induced by ocular vasodilation due to infectionor non-infectious agents [15,16]. Tacrolimus functions as a calcineurin inhibitor and is widely as an immunosuppressant in transplantation [14,25]. Since calcineurin is calcium-dependent phosphatase involved in the activation of immune responses [26], we attempted to investigate its potential effect on the conjunctival hyperemia caused by PGAs. Although tacrolimus ophthalmic solution showed no significant effect on the IOP, the administration of tacrolimus improved the ocular surface condition, alleviated subjective dry eye symptom and hyperemia, and prolonged noninvasive tear break-up time after 2 weeks. However, there was no significant difference observed at week 4 between the two groups, although the average SDES and hyperemia score in the experimental group were slightly lower. We reasoned that the patients became adapted to the PGA treatment gradually, and the conjunctival hyperemia improved itself without tacrolimus treatment at week 4. This can also be evidenced by the observation that, at week 4 the hyperemia score and NIBUT became comparable to those of week 0 (before treatment) in both the groups. Overall, these data suggest that the administration of tacrolimus produces a temporary or short-term relieving effect on conjunctival hyperemia caused by PGAs. We also found that some patients developed intolerable hyperemia after the long-term use of PGAs. After tacrolimus medication, the symptoms of hyperemia were significantly improved and PGA therapy could be continued. It is also worth mentioning that we did not find any side effects or additional symptoms associated with tacrolimus administration.

The preservatives in the ophthalmic solution may have a toxic effect on the ocular surface and induce inflammation [27]. Topical administration of tacrolimus has been reported to show beneficial effects in inflammatory and allergic eye diseases [13,14]. Since conjunctival hyperemia can be induced by pathological retinal vasodilation in response to inflammation [15,16], it is speculated that tacrolimus ophthalmic solution may suppress the inflammatory responses triggered by PGA administration or the preservatives in the solution. However, to what extent the immunosuppressant activity of tacrolimus contributes to its beneficial effects on conjunctival hyperemia needs to be clarified in the future studies.

One of the major limitations of our study is the single-blindness, in which the medical staff were aware of the medication in each group. A double-blinded study design would provide more convincing data by excluding subjective judgment. Moreover, a larger cohort of patients from multiple medical centers would provide more valid conclusion of the effect of tacrolimus on conjunctival

hyperemia. In addition, the optimal orders of the administration of tacrolimus and PGAs should be clinically practiced to maximize the treatment outcome.

In conclusion, topical administration of tacrolimus ophthalmic solution can significantly relieve conjunctival hyperemia caused by PGAs in POAG patients. It ameliorates the ocular surface conditions, reduces the discomfort and improves the medication compliance in the patients. Our study provides evidence for the beneficial effect of tacrolimus on conjunctival hyperemia. However, in order to maximize the effect of tacrolimus, the optimal clinical practice of tacrolimus administration together with prostaglandin usage remains to be explored in glaucoma treatment.

Data Availability

All data used in this study are presented in the manuscript.

Additional Points

Topical tacrolimus administration improves the SDES and hyperemia score in POAG patients. Topical tacrolimus administration does not affect the IOP values in POAG patients. Topical tacrolimus administration reduces discomfort in POAG patients.

Conflicts of Interest

The authors declare that they have no conflicts of interest.

Acknowledgments

This work is supported by the Youth Fund Project of Hainan Natural Science Foundation (project no.: 820qn414) and Hainan health industry scientific research project (project no: 20a200322).

References

[1] A. K. Schuster, C. Erb, E. M. Hoffmann, T. Dietlein, and N. Pfeiffer, "The diagnosis and treatment of glaucoma," *Deutsches Arzteblatt International*, vol. 117, no. 13, pp. 225–234, 2020.

[2] S. He, D. L. Stankowska, D. Z. Ellis, R. R. Krishnamoorthy, and T Yorio, "Targets of neuroprotection in glaucoma," *Journal of Ocular Pharmacology and Therapeutics*, vol. 34, pp. 85–106, 2018.

[3] R. Conlon, H. Saheb, and I. I. K. Ahmed, "Glaucoma treatment trends: a review," *Canadian Journal of Ophthalmology*, vol. 52, no. 1, pp. 114–124, 2017.

[4] T. Wenquan, Z. Feng, and L. Ke, "Efficacy and safety of prostaglandin analogues in primary open-angle glaucoma or ocular hypertension patients: a meta-analysis," *Medicine (Baltimore)*, vol. 98, no. 30, Article ID e16597, 2019.

[5] F. G. A. Carlos, A. G. Jairo, I. R. P. Ariel, and Amaya-Restrepo, "Systematic review of prostaglandin analogues for retained placenta," *International Journal of Gynecology & Obstetrics*, vol. 143, no. 1, pp. 19–23, 2018.

[6] K. Inoue, M. Shiokawa, R. Higa et al., "Adverse periocular reactions to five types of prostaglandin analogs," *Eye*, vol. 26, no. 11, pp. 1465–1472, 2012.

[7] S. DI Staso, L. Agnifili, S. Cecannecchia, A. DI Gregorio, and M Ciancaglini, "*In vivo* analysis of prostaglandins-induced ocular surface and periocular adnexa modifications in patients with glaucoma," *In Vivo*, vol. 32, no. 2, pp. 211–220, 2018.

[8] R. M. Feldman, "Conjunctival hyperemia and the use of topical prostaglandins in glaucoma and ocular hypertension," *Journal of Ocular Pharmacology and Therapeutics*, vol. 19, no. 1, pp. 23–35, 2003 Feb.

[9] S. Rei, S. Toshihiro, and M. Hiroshi, "Time course of prostaglandin analog-related conjunctival hyperemia and the effect of a nonsteroidal anti-inflammatory ophthalmic solution," *Journal of Glaucoma*, vol. 25, no. 3, pp. 204–208, 2016.

[10] M. Uchino, H. Ikeuchi, H. Matsuoka et al., "Topical tacrolimus therapy for antibiotic-refractory pouchitis," *Diseases of the Colon & Rectum*, vol. 56, no. 10, pp. 1166–1173, 2013.

[11] S. Ivulich, M. Dooley, C. Kirkpatrick, and G. Snell, "Clinical challenges of tacrolimus for maintenance immunosuppression post–lung transplantation," *Transplantation Proceedings*, vol. 49, no. 9, pp. 2153–2160, 2017.

[12] Q. Wu, D. Liu, X. Zhang et al., "Development and effects of tacrolimus-loaded nanoparticles on the inhibition of corneal allograft rejection," *Drug Delivery*, vol. 26, no. 1, pp. 290–299, 2019.

[13] L. Rebibo, C. Tam, Y. Sun et al., "Topical tacrolimus nanocapsules eye drops for therapeutic effect enhancement in both anterior and posterior ocular inflammation models," *Journal of Controlled Release*, vol. 333, pp. 283–297, 2021.

[14] N. Erdinest, H. Ben-Eli, and A. Solomon, "Topical tacrolimus for allergic eye diseases," *Current Opinion in Allergy and Clinical Immunology*, vol. 19, no. 5, pp. 535–543, 2019.

[15] C. W. McMonnies, "Conjunctival tear layer temperature, evaporation, hyperosmolarity, inflammation, hyperemia, tissue damage, and symptoms: a review of an amplifying cascade," *Current Eye Research*, vol. 42, no. 12, pp. 1574–1584, 2017.

[16] R. B. Singh, L. Liu, S. Anchouche et al., "Ocular redness – I: etiology, pathogenesis, and assessment of conjunctival hyperemia," *Ocular Surface*, vol. 21, pp. 134–144, 2021.

[17] Group Ophthalmology Society of Chinese Medical Association, "Chinese guidelines for Glaucoma(2020)," *Chinese Journal of Ophthalmology*, vol. 56, no. 08, pp. 573–586, 2020.

[18] K. Suresh, "An overview of randomization techniques: an unbiased assessment of outcome in clinical research," *Journal of Human Reproductive Sciences*, vol. 4, no. 1, pp. 8–11, 2011.

[19] M. C. Velez-Gomez and E. M. Vasquez-Trespalacios, "Adherence to topical treatment of glaucoma, risk and protective factors: a review," *Archivos de la Sociedad Espanola de Oftalmologia*, vol. 93, no. 2, pp. 87–92, 2018.

[20] S. Jack, A. Noy, and G. Anat, "Barriers to glaucoma medication compliance among veterans: dry eye symptoms and anxiety disorders," *Eye and Contact Lens: Science and Clinical Practice*, vol. 44, no. 1, pp. 50–54, 2018.

[21] I. Francesco, B. Elena, A. Nicoletta, S. Brambilla, B. Duquesroix, and A. C. Kothe, "Prostaglandin analogues and nitric oxide contribution in the treatment of ocular hypertension and glaucoma," *British Journal of Pharmacology*, vol. 176, no. 8, pp. 1079–1089, 2019.

[22] E. A. Ammar, V. Guillaume, and K. K. Raoul, "Objective ocular surface tolerance in patients with glaucoma treated with topical preserved or unpreserved prostaglandin analogues," *European Journal of Ophthalmology*, vol. 29, no. 6, pp. 645–653, 2019.

Hindawi
Evidence-Based Complementary and Alternative Medicine
Volume 2023, Article ID 9840736, 1 page
https://doi.org/10.1155/2023/9840736

Retraction

Retracted: Analysis of the Clinical Efficacy of Azacytidine + Venetoclax in the Treatment of Elderly Patients with Relapsed Refractory Acute Myeloid Leukemia

Evidence-Based Complementary and Alternative Medicine

Received 3 October 2023; Accepted 3 October 2023; Published 4 October 2023

This article has been retracted by Hindawi following an investigation undertaken by the publisher [1]. This investigation has uncovered evidence of one or more of the following indicators of systematic manipulation of the publication process:

(1) Discrepancies in scope
(2) Discrepancies in the description of the research reported
(3) Discrepancies between the availability of data and the research described
(4) Inappropriate citations
(5) Incoherent, meaningless and/or irrelevant content included in the article
(6) Peer-review manipulation

The presence of these indicators undermines our confidence in the integrity of the article's content and we cannot, therefore, vouch for its reliability. Please note that this notice is intended solely to alert readers that the content of this article is unreliable. We have not investigated whether authors were aware of or involved in the systematic manipulation of the publication process.

Wiley and Hindawi regrets that the usual quality checks did not identify these issues before publication and have since put additional measures in place to safeguard research integrity.

We wish to credit our own Research Integrity and Research Publishing teams and anonymous and named external researchers and research integrity experts for contributing to this investigation.

The corresponding author, as the representative of all authors, has been given the opportunity to register their agreement or disagreement to this retraction. We have kept a record of any response received.

References

[1] W. Wang, Q. Luo, Q. Chen, A. Pang, and K. Fang, "Analysis of the Clinical Efficacy of Azacytidine + Venetoclax in the Treatment of Elderly Patients with Relapsed Refractory Acute Myeloid Leukemia," *Evidence-Based Complementary and Alternative Medicine*, vol. 2022, Article ID 8691835, 4 pages, 2022.

Hindawi
Evidence-Based Complementary and Alternative Medicine
Volume 2022, Article ID 8691835, 4 pages
https://doi.org/10.1155/2022/8691835

Research Article

Analysis of the Clinical Efficacy of Azacytidine + Venetoclax in the Treatment of Elderly Patients with Relapsed Refractory Acute Myeloid Leukemia

Wei Wang, Quanfang Luo, Qinpin Chen, Aiping Pang, and Kuiyan Fang

Department of Hematology, Nanxishan Hospital of Guangxi Zhuang Autonomous Region, Guilin, Guangxi Province, China

Correspondence should be addressed to Wei Wang; weiwang9258@163.com

Received 5 August 2022; Revised 17 September 2022; Accepted 27 September 2022; Published 14 October 2022

Academic Editor: Xueliang Wu

Objective. To explore the clinical efficacy of azacytidine + venetoclax in the treatment of elderly patients with relapsed refractory acute myeloid leukemia (AML). *Method*. The present study included 20 elderly patients with relapsed refractory AML from January 2019 to January 2021. These patients were randomized into treatment groups ($n = 10$, azacytidine alone) and control groups ($n = 10$, azacytidine + venetoclax) by a random number table. The differences in efficacy, adverse reactions, hematology parameters, and immune functions in elderly patients with relapsed refractory AML in two groups were analyzed. *Results*. The total efficiency for elderly patients with relapsed refractory AML was 90.00% and significantly higher than that in the control group (40.00%), $P < 0.05$; PLT and WBC after treatment in the treatment group were significantly higher than those in the control group, and Hb was significantly lower than in the control group, $P < 0.05$; CD4+, CD3+, and CD4+/CD8+ after treatment in both groups were significantly lower than those before treatment, $P < 0.05$; CD4+, CD3+, and CD4+/CD8+ after treatment were not significantly different between the two groups, $P > 0.05$; the incidences of adverse reactions were not significantly different between the two groups, $P > 0.05$. *Conclusion*. Azacytidine + venetoclax in the treatment of elderly patients with relapsed refractory AML could improve efficacy and hematology parameters with high safety, which is of great significance.

1. Introduction

AML is a hematological malignancy. The main feature of AML patients is the clonal proliferation of undifferentiated or abnormally differentiated myeloid cells in the peripheral blood and bone marrow [1, 2]. AML can cause fever, infection, hemorrhage, and anemia, damage the patient's health and even threaten the patient's life. Thus, effective measures are necessary to improve the prognosis [3–5]. Venetoclax is a selective small molecule inhibitor of B-cell lymphoma factor-2 (Bcl-2) and is used in combination with demethylated drugs in the treatment of AML [6, 7]. Azacytidine is a DNA-demethylation drug for AML and is effective in the treatment of relapsed refractory AML [8, 9]. In order to explore the clinical efficacy of azacytidine + venetoclax in the treatment of elderly patients with relapsed refractory AML, the present study included 20 elderly patients with relapsed refractory AML from January 2019 to January 2021 to analyze and clinical value of azacytidine + venetoclax was summarized.

2. Information and Methods

2.1. Information. The present study included 20 elderly patients with relapsed refractory AML from January 2019 to January 2021.

These patients were randomized into treatment groups ($n = 10$) and control groups ($n = 10$) by a random number table.

Inclusion criteria: a: diagnosed as relapsed refractory AML per criteria for diagnosis and efficacy of hematological diseases; b: and aged ≥60 years old; c: normal liver, kidney, and heart functions; d: good compliance.

Exclusion criteria: a: comorbid with other tumors; b: central nervous system is invaded; c: history of drug allergy.

All patients signed informed consent and this study was approved by the Ethics Committee.

2.2. Methods. Patients in the treatment group received azacytidine + venetoclax. Cycle 1, azacytidine, 75 mg/m^2, sc, days 1–7; venetoclax, day 1, 100 mg, day 2, 200 mg, days 3–28, 400 mg, po. A cycle consists of 28 days. The dosage and administration of azacytidine in subsequent cycles were the same as in cycle 1. The dosage of venetoclax was 400 mg from day 1 to the end of the cycle, po. Patients in the control group received azacytidine alone. The regimen of azacytidine is referred to the treatment group.

Patients in both groups received alkalization and hydration during the treatment to prevent tumor lysis syndrome. Patients with high WBC were orally administered hydroxyurea. Subsequent treatment could be continued only when WBC dropped to $<20 \times 10^9$/L.

2.3. Measurements. The efficacy and adverse reactions in both groups were observed. The differences in hematological parameters and immunological parameters before and after the treatment were analyzed.

Efficacy: complete response (CR): PLT in peripheral blood $>100 \times 10^9$/L, neutrophils $>1.5 \times 10^9$/L, proportion of bone marrow blast cells <0.05, no leukemia cells in differential blood count; partial response (PR): neither PLT nor neutrophils in peripheral blood meets the criteria of CR, proportion of bone marrow blast cells is 0.05–0.25 and drops by >50% than that before the treatment; no response (NR): these criteria are not met; the sum of the CR rate and the PR rate is the total efficiency.

Adverse reactions: mainly nausea, vomiting, pulmonary infection, fever, and lower PLT.

Hematology parameters: Venous blood samples of 5 ml were collected from fasting patients. Serum was collected after centrifugation. A hematology analyzer was used to measure PLT count, Hb, and WBC count.

Immunological parameters: CD4+, CD3+, and CD4+/CD8+ measured by flow cytometry.

Data were collected before and after the treatment.

2.4. Statistical Analysis. Statistical analysis was performed with SPSS 21.0. Enumeration data were represented by n (%) and analyzed by chi-square test. Measurement data were represented by mean ± SD and analyzed by Student's t-test. $P < 0.05$ indicated statistical significance.

3. Results

3.1. General Information. In the treatment group, the mean age was 70.21 ± 8.39 years (60–83 years), including two M0 patients, three M2 patients, three M4 patients, two M5 patients, and five males and five females. In the control group, the mean age was 70.44 ± 7.61 years (61–82 years), including two M0 patients, three M2 patients, two M4 patients, three M5 patients, and 6 males and 4 females. Basic information of elderly patients with relapsed refractory AML in two groups were not significantly different ($P > 0.05$), indicating comparability between the two groups. Table 1

3.2. Efficacy. As shown in Table 2, total efficiency for elderly patients with relapsed refractory AML in the treatment group was 90.00% and significantly higher than that in the control group (40.00%), $P < 0.05$.

3.3. Hematology Parameters. As shown in Table 3, PLT and WBC after treatment in both groups were significantly higher than those before treatment, and Hb after treatment was significantly lower than that before the treatment, $P < 0.05$; PLT and WBC after treatment in the treatment group were significantly higher than those in the control group, and Hb was significantly lower than that in the control group. All the differences were significant, $P < 0.05$.

3.4. Immunological Parameters. As shown in Table 4, CD4+, CD3+, and CD4+/CD8+ after the treatment in both groups were significantly lower than those before the treatment, $P < 0.05$; CD4+, CD3+ and CD4+/CD8+ after treatment were not significantly different between two groups, $P > 0.05$.

3.5. Adverse Reactions. As shown in Table 5, the incidences of adverse reactions between two groups were not significantly different ($P > 0.05$).

4. Discussion

The incidence of relapsed refractory AML in the elderly is relatively high. This disease will damage the patient's physical and mental health with a high mortality and poor prognosis [10]. Thus, effective treatment is necessary to improve the prognosis for patients with relapsed refractory AML.

In the present study, total efficiency for elderly patients with relapsed refractory AML was 90.00% and significantly higher than that in the control group (40.00%), $P < 0.05$; PLT and WBC after treatment in the treatment group were significantly higher than those in the control group, and Hb was significantly lower than in the control group, $P < 0.05$; CD4+, CD3+, and CD4+/CD8+ after the treatment in both groups were significantly lower than those before the treatment, $P < 0.05$; CD4+, CD3+, and CD4+/CD8+ after treatment were not significantly different between the two groups, $P > 0.05$; the incidences of adverse reactions were not significantly different between two groups, $P > 0.05$. This indicated that azacytidine + venetoclax for elderly patients with relapsed refractory AML could improve efficacy and hematology parameters, have little effect on immunological parameters, and would not increase the incidence of adverse reactions. Venetoclax is a selective Bcl-2 inhibitor that can bind to Bcl-2 protein, promote the release of proapoptosis Bax and Bim, change the

Table 1: General information.

Item	Treatment group ($n = 10$)	Control group ($n = 10$)	χ^2/t	P
Gender			0.202	0.653
Male	5 (50%)	6 (60%)		
Female	5 (40%)	4 (40%)		
Age (years old)	70.21 ± 8.39	70.44 ± 7.61	0.064	0.949
Classification			0.400	0.940
M0	2 (20%)	2 (20%)		
M2	3 30%)	3 (30%)		
M4	3 (30%)	2 (20%)		
M5	2 (20%)	3 (30%)		

Table 2: Efficacy [n (%)].

Group	n	CR	PR	NR	Total efficiency
Treatment group	10	3 (30.00)	6 (60.00)	1 (10.00)	9 (90.00)
Control group	10	1 (10.00)	3 (30.00)	6 (60.00)	4 (40.00)
X^2	—	—	—	—	5.495
P	—	—	—	—	0.019

Table 3: Hematology parameters ($\overline{x} \pm s$).

Group	n	PLT ($\times 10^9$/L)		Hb (g/L)		WBC ($\times 10^9$/L)	
		Before	After	Before	After	Before	After
Treatment group	10	71.23 ± 5.69	239.45 ± 32.05	90.45 ± 6.98	74.29 ± 5.14	2.36 ± 0.29	5.71 ± 0.89
Control group	10	70.89 ± 7.02	202.18 ± 20.36	90.22 ± 7.03	79.63 ± 3.20	2.41 ± 0.33	4.40 ± 0.78
T	—	0.119	3.104	0.073	2.789	0.360	3.500
P	—	0.907	0.006	0.942	0.012	0.723	0.003

Table 4: Immunological parameters ($\overline{x} \pm s$).

Group	n	CD4+ (%)		CD3+ (%)		CD4+/CD8+	
		Before	After	Before	After	Before	After
Treatment group	10	36.89 ± 2.34	31.56 ± 5.78	50.26 ± 5.45	38.45 ± 5.16	1.50 ± 0.26	1.32 ± 0.25
Control group	10	37.01 ± 1.69	32.02 ± 6.41	49.78 ± 4.32	39.02 ± 4.47	1.52 ± 0.31	1.34 ± 0.29
T	—	0.131	0.169	0.218	0.264	0.156	0.165
P	—	0.897	0.868	0.830	0.795	0.878	0.871

Table 5: Adverse reactions [n (%)].

Group	n	Nausea and vomiting	Pulmonary infection	Fever	Lower PLT	Total
Treatment group	10	2 (20.00)	1 (10.00)	1 (10.00)	1 (10.00)	5 (50.00)
Control group	10	2 (20.00)	1 (10.00)	2 (20.00)	1 (10.00)	6 (60.00)
X^2	—	—	—	—	—	0.202
P	—	—	—	—	—	0.653

permeability of the mitochondrial outer membrane, activate caspase, and recover the patient's apoptosis [11, 12]. Venetoclax has certain efficacy in the treatment of elderly patients with relapsed refractory AML, yet the efficacy of venetoclax alone is not ideal. Azacytidine is a cytidine analogue. When it binds to RNA and DNA, it has cytotoxicity and specific inhibition on cell cycle; when it binds to DNA methyltransferase, it inhibits methylation of newly synthesized DNA and further promotes recovery of hematopoietic stem cell function [11]. Azacytidine can regulate the differentiation of leukemia cells and induce apoptosis of leukemia cells [12]. Azacytidine is an inhibitor of DNA methyltransferase and can increase the sensitivity of AML to drugs and efficacy [13]. In terms of deficiencies, the current evidence is inadequate to definitively conclude because this study was a single-center study with a relatively small sample size and a relatively short duration of follow-up.

Hindawi
Evidence-Based Complementary and Alternative Medicine
Volume 2022, Article ID 1705193, 7 pages
https://doi.org/10.1155/2022/1705193

Research Article

Detection and Analysis of the Oral Flora in Patients with Recurrent Aphthous Stomatitis

Ruolin Cai,[1] **Wei Bi**,[2] **and Youcheng Yu**[2]

[1]*Department of Stomatology, Zhongshan Hospital (Xiamen), Fudan University, Xiamen 361015, China*
[2]*Department of Stomatology, Zhongshan Hospital, Fudan University, Shanghai 200032, China*

Correspondence should be addressed to Youcheng Yu; yu.youcheng@zs-hospital.sh.cn

Received 22 July 2022; Accepted 28 September 2022; Published 13 October 2022

Academic Editor: Xueliang Wu

The present study detected differences in the oral mucosal flora in healthy people and patients diagnosed with recurrent aphthous stomatitis (RAS) using the 16S ribosomal RNA high-throughput sequencing (rRNA-seq). All samples were collected from the lower lip mucosa of 100 healthy individuals and 100 patients with RAS. After the extraction, DNA was subjected to PCR amplification for the bacterial 16S rRNA gene, before subjecting to high-throughput sequencing, and matched to a database. Most bacterial species and most unique bacteria were from the healthy control group, and the amount of operational taxonomic units (OTUs) calculated was similar in the ulcer and nonulcer sites. *Firmicutes*, *Proteobacteria,* and *Bacteroidetes* were most abundant in the healthy group and in ulcer, nonulcer, and healed ulcer sites at the phylum level. Meanwhile, the number of *Prevotella* was significantly elevated in ulcer sites ($P < 0.05$). Healthy people had more species of bacteria inhabiting their oral mucosa than did RAS patients, and patients with ulcers had the lowest abundance of bacterial species. We suggest that the number of *Prevotella* is associated with RAS.

1. Introduction

Recurrent aphthous stomatitis (RAS) is a chronic inflammatory common ulcerative disease in the oral mucosa with an incidence ratios of ten to twenty percent [1]. RAS was classified into three categories according to different clinical presentations: herpetiform (multiple small pinpoint ulcers), major (ulcers >10 mm in diameter), and minor (ulcers ≦10 mm in diameter) [2]. The general clinical characteristics include an oval/round shallow ulcer, with a gray-white pseudomembrane on the surface and a thin erythematous halo envelope, with obvious pain. The pathogenesis is primarily divided into the attack period (prodromal period/ulcer period), healing period, and intermittent period, with different durations. RAS is generally self-limiting. The predilection sites of RAS are the lips, tongue, and gingiva. Noticeably, RAS is extremely painful, and the healing time is longer than traumatic ulcers of the same size [3]. RAS affects the normal functions of the oral cavity, such as eating and speaking, as well as teeth brushing.

The causes of RAS are not clear, and there are obvious individual differences. Recent studies suggested that the occurrence of RAS was due to local inflammation caused by an imbalance in the oral mucosal flora [2]. Aas et al. found that the predominant bacterial flora in the healthy oral cavity was highly variable between people and was site-specific [1]. Seoudi et al. found that colonization of *Rothia dentocariosa* was increased at nonulcer sites in RAS patients, and the oral mucosa of healthy controls (HCs) had higher abundances of *Neisseria* and *Veillonella* than the patient groups [4].

However, study results are regionally variable. For example, Hijazi showed that oral Streptococcaceae species were predominant in HCs compared to the ulcerated sites of RAS patients but not in HCs compared with uninfected sites in RAS patients in the UK [5]. In contrast, Bankvall showed that the noninflamed buccal mucosa' microbiota varied between HCs and patients in Gothenburg, Sweden [6]. Yun-Ji found that increased *Acinetobacter johnsonii* and decreased *Streptococcus salivarius* in the mucosa were related with RAS risk in Koreans [7]. Some scholars believe that

Helicobacter pylori infection is linked with an increased risk of RAS [8, 9], but others believe that *Helicobacter pylori* is not directly related to RAS [10].

Relevant literature suggests that oral mucosal flora differs between healthy people and patients with RAS, but the detection results in patients with RAS vary between studies, which may be due to the use of different populations and detection methods.

Many methods for bacterial species analysis are emerging. High-throughput sequencing is a relatively advanced and accurate method that is becoming increasingly mature, and it is able to simultaneously sequence massive DNA molecules up to millions of molecules. High-throughput sequencing method enabled us to perform a detailed and comprehensive analysis of not only the transcriptome but also the genome of a species. Therefore, this study utilized high-throughput sequencing method to compare variations in oral mucosal flora between patients with RAS and healthy group.

2. Materials and Methods

The ethics committee of Zhongshan Hospital, Fudan University, Shanghai, China approved this study. All parents in this research were noted of the purpose and signed informed consent in written. The oral medicine specialist diagnosis is minor aphthous ulcer.

2.1. Subject Selection. This experiment recruited patients at Zhongshan Hospital, Fudan University, Shanghai, China from September 2018 to August 2019. All volunteers underwent strict physical, laboratory, and oral examinations.

The inclusion criteria as follows:

(1) Healthy volunteers with confirmed results from physical, laboratory, and oral examinations.

(2) Confirmed results from systemic and laboratory examinations (oral disease was diagnosed as RAS from the patient's history of treatment and clinical examination).

(3) Lived in Shanghai for more than five years.

The exclusion criteria were as follows:

(1) Smoking or drinking history.

(2) Pregnancy or lactation.

(3) The presence of chronic systemic diseases.

(4) Abnormal red blood cell, vitamin B12, vitamin D, folate, ferritin, iron ion, or zinc ion indexes.

(5) Any antibiotics taken in the preceding 3 months.

(6) Any kind of treatment for RAS in the preceding six months.

(7) The use of any medication.

(8) The presence of other mucosal diseases.

(9) Dental caries.

2.2. If There Is a Periodontal Disease

(1) A high-sugar diet.

(2) Go to bed after 23 : 00.

All participants were banned from using antibacterial mouthwashes, and they were asked to brush their teeth twice daily for two weeks before sampling. At the time of sampling, the participant's ulcer is minor ulcer (diameter: 5~10 mm).

2.3. Sample Collection. Time point of all the sample collection is in the morning. The same operator used a sterile throat swab to repeatedly scrape the lower lip mucosa 5 times, while ensuring that the throat swab did not touch the teeth and other parts during the sampling process. Direct swabs of healthy sites on the lower lip mucosa in RAS patients and HCs were collected. Swab samples were also collected from ulcers on the lower lip mucosa in RAS patients, and these sites were sampled again when the ulcer healed. The samples were stored in a −20°C freezer. The swabs did not touch the teeth at the time of sampling.

2.4. Extraction and Amplification of DNA. Total DNA was extracted under the instructions of the EZNA® Soil Kit (Omega Bio-Tek, Norcross, GA, US). DNA purity and concentration were assessed by a NanoDrop2000, and the quality of the extracted DNA was examined using DNA electrophoresis. Using the primers 806R (5′-GGACTACHVGGGTWTCTAAT-3′) and 338F (5′-ACTCCTACGGGAGGCAGCAG-3′), the polymerase chain reaction amplification of the V3-V4 variable region was performed using an ABI GeneAmp® 9700 and the program 95°C predenaturation for 180s was carried out, and then 27 cycles of 95°C denaturation for 30 s, annealing for 30s at 55°C, and extension for 30s at 72°C, with an extension for 600s at 72°C were carried out. Followed by the 20-μl volume amplification system includes 10 ng DNA template, 2 μl 2.5 mM dNTPs, 4 μl of 5x FastPfu buffer, 0.4 μl FastPfu polymerase, and 0.8 μl primer (5 μM).

2.5. Illumina MiSeq Sequencing. The PCR products were enriched by electrophoresis of 2% agarose gel, and an AxyPrep DNA Gel Extraction Kit (Axygen Biosciences, Union City, CA, USA) was applied to purify the PCR product, followed by the elution with Tris-HCl. After detection of DNA using 2% agarose electrophoresis, QuantiFluor™-ST (Promega, USA) was utilized for quantification of PCR product. The amplified fragments were applied to build a library of PE 2∗300 according to the standard procedures provided by the Illumina MiSeq platform.

The following steps were used to construct the library: (1) connect the "Y"-shaped adapter; (2) screen and remove the self-linking fragments of the adapter using magnetic beads; (3) enrich the library template using PCR amplification; and

Table 1: Distribution of research subjects according to age and gender.

		HC group	RAS group
Age (years)		43 ± 7.9	37 ± 9.6
Gender	Male	50	50
	Female	50	50

(4) produce single-stranded DNA fragments through denature using sodium hydroxide.

Sequencing was completed through Illumina's MiSeq PE300 platform (Shanghai Meiji Biomedical Technology Co, Ltd), with the original data transmitted to the database of NCBI.

2.6. Processing of Sequencing Data. This research applied Trimmomatic software to control the original sequencing, and the software FLASH was utilized for splicing, as follows:

(1) Set a window of 50 bp. If the average value of quality was below 20 in the window, all the later sequences in the window were removed from the front, and the sequences were removed after quality control if its length did not reach 50 bp.

(2) The sequences were joined at both ends according to the overlapping bases. During splicing, the max mismatching ratio was 0.2 between overlaps, with its length ≥10 bp. Sequences were either joined or removed.

(3) The sequence was split into each sample according to the primer and the barcode at both or either end of the sequence. The barcodes were exactly matched. The primer allowed mismatches of 2-base, while sequences were removed if ambiguous bases exist.

The software UPARSE was utilized for performing operational taxonomic unit (out) clustering of sequences at a sequence similarity of 97%, and a single chimera or a sequence was eliminated during the process of clustering. The RDP classifier was used to annotate and classify sequence and perform comparisons with the comparison threshold set to 70% in the Silva database (SSU123).

3. Results

The two hundreds enrolled subjects included 100 RAS patients and 100 HCs. Half of the RAS group was male, and the range of their age is 37 ± 9.6 years. Half of the HC group was male with the age range of 43 ± 7.9 years (Table 1).

A Venn diagram in Figure 1 illustrated that 223 OTUs appeared in all the four groups. There were 357 OTUs in the healthy group (a) highly similar to the ulcer site (b) in the RAS group during the ulceration stage; 294 OTUs in the healthy group (a) and the nonulcer site (c) were highly similar; 411 OTUs were highly similar in the healthy group (a) and the healed ulcer site (d); 279 OTUs were highly similar between the ulcer site (b) and the nonulcer site (c) in the RAS group during ulceration; 336 OTUs were highly similar between the ulcer site (b) and the healed ulcer site

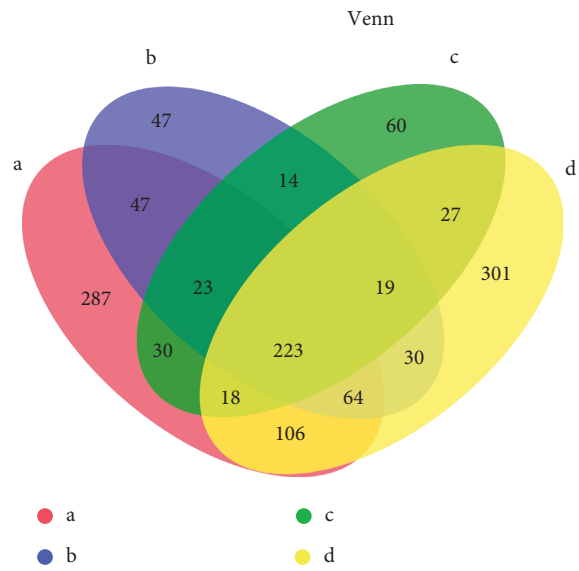

Figure 1: Comparison of oral microbial communities between groups using Venn diagrams. (a) Healthy group; (b) ulcer site; (c) nonulcer site; (d) healed ulcer site.

(d); 287 OTUs were highly similar between the nonulcer site (c) and the healed site (d).

The healthy group (a) had the highest number of OTUs, with 798; the ulcer site had the least number of OTUs, with 467. Meanwhile, the healthy group had the highest unique OTUs, with 287. The account of OTUs was similar between the healthy group (a) and the healed ulcer sites (d), and the numbers of OTUs in these two groups were highest.

Phylum-level comparisons between flora composition and relative richness showed that *Firmicutes*, *Proteobacteria*, *Actinobacteria*, *Bacteroidetes*, *Fusobacteria*, and *Patescibacteria* were the first six dominant bacterial phyla (Figure 2). The most abundant species was *Firmicutes* in all four groups. *Patescibacteria*, *Actinobacteria,* and *Fusobacteria* were more abundant in the healthy group. Much more *Actinobacteria* and *Fusobacteria* were present in the healthy group. *Firmicutes* was much more abundant than the other phyla at nonulcer sites, and *Proteobacteria* was much more abundant than the other phyla at ulcerated sites.

Significant differences for some bacteria were revealed by genus-level diversity comparisons of high-throughput sequencing findings. The abundance of *Prevotella* ($P < 0.05$) at the ulcer sites in RAS patients was increased (Figure 3; Figure 4). Samples from the ulcer sites were relatively independent from the other samples.

4. Discussion

The pathogenesis of RAS is not clear. Factors affecting RAS include genetic factors, immunological factors, bacterial factors, dietary habits, hormonal disorders, a lack of micronutrients, mechanical trauma, mental factors, systemic diseases, and oxidative stress. Some studies noted that a lack of micronutrients (e.g., vitamins, serum iron, ferritin, and folic acid) may affect the occurrence and development of RAS, but this result is controversial [11–14]. Some studies

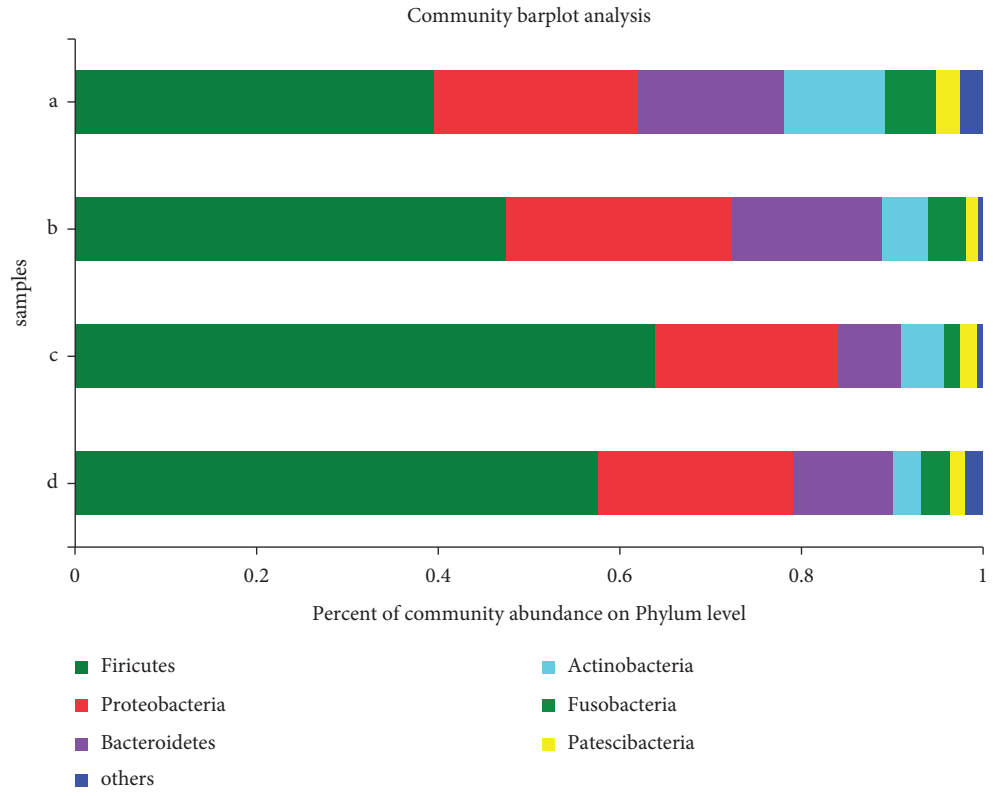

Figure 2: Relative abundance of species in the oral microbial community at the phylum level of each group. (a) Healthy group; (b) ulcer site; (c) nonulcer site; (d) healed ulcer site.

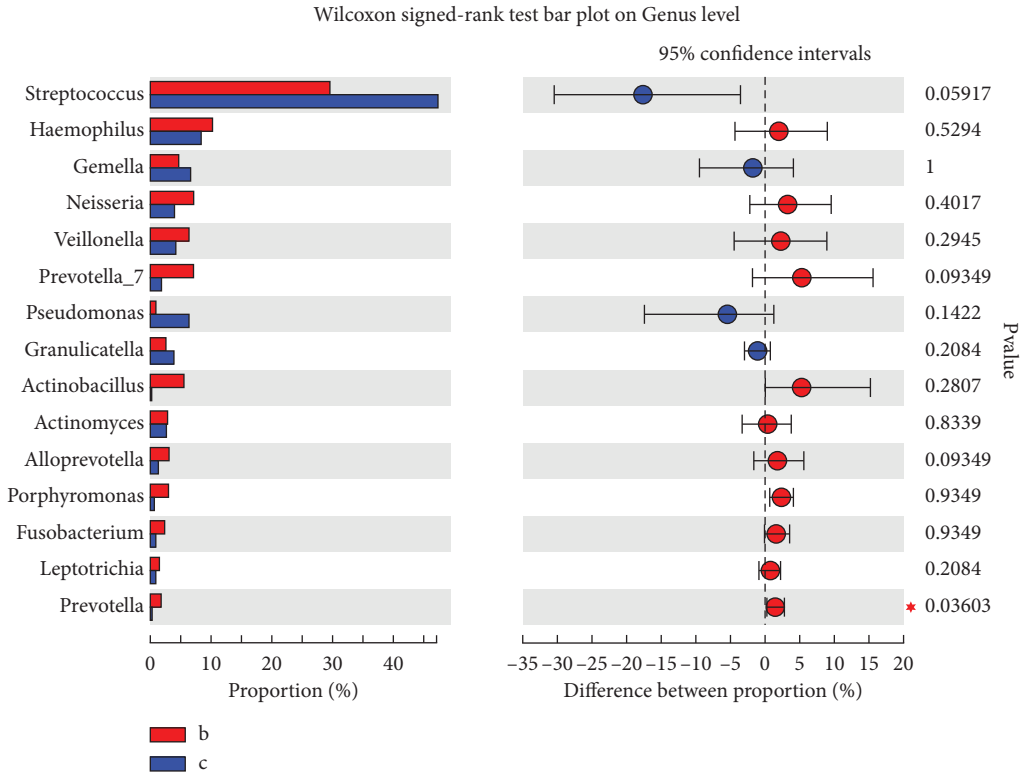

Figure 3: Comparison of the oral microbiota between ulcer and nonulcer sites at the genus level. (b) Ulcer site; (c) nonulcer site. $^{*}p < 0.05$.

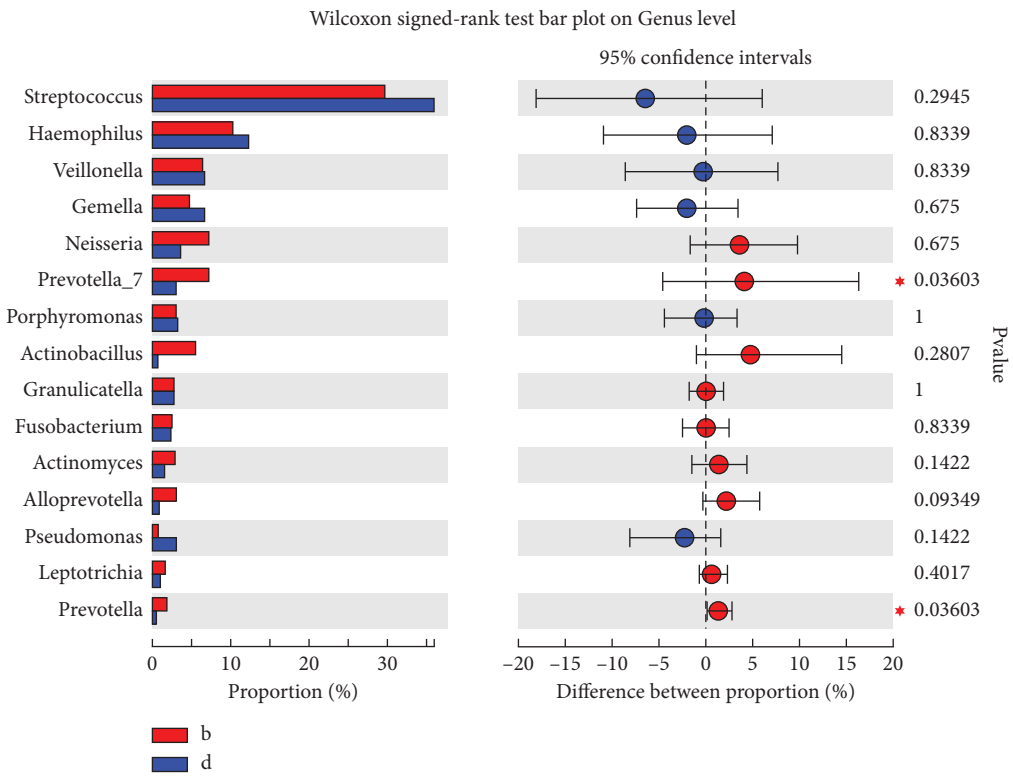

Figure 4: Comparison at the genus level of the oral microbiota between ulcer and healed ulcer sites. (b) Ulcer site; (d) healed ulcer site. * $p < 0.05$.

showed that vitamin B12 treatment was effective in patients suffering from RAS [13, 15]. A Turkish study on serum zinc and vitamin D reported an association between zinc deficiency and RAS [16]. Another study reported insufficient levels of vitamin D in patients with RAS comparing to HCs [17–20]. Du et al. found that frequent consumption of carbonated beverages and frequent thirst increased the possibility of RAS, and the consumption of nuts provided protection [21].

As for mental factors, studies have shown that the frequency of staying up late and the cumulative duration of staying up late will affect the severity of RAS attacks. At the same time, the length of sleep time may affect mental state and easily lead to depression and anxiety. These negative emotions will aggravate RAS and the frequency of attacks and the severity of ulcers [13, 23–26].

At the same time, taking drugs such as glucocorticoids, thalidomide, and other drugs [27] and suffering from certain autoimmune diseases such as Crohn's disease and PFAPA (periodic fever, aphthous stomatitis, pharyngitis, and adenitis) syndrome also affect RAS [28].

The present study detected folate, ferritin, vitamin B12, vitamin D, iron ions, and zinc ions in all participants. The daily drinking frequency and amount were normal in the RAS group, and they reported no frequent consumption of carbonated drinks, no consumption of nuts, and a light diet on weekdays.

According to the existing articles on RAS flora research, it can be found that the methods of flora detection can be roughly divided into several categories: microscopy, T-RFLP, HOMIM analysis, MALDI-TOF-MS, and high-throughput sequencing. The T-RFLP method is to design universal primers based on the conserved regions of bacteria, in which the 5′ end of one primer is labeled with a fluorescent substance. Extract the DNA of the sample to be analyzed and perform PCR amplification to obtain a PCR product with a fluorescent label, which is then digested with the corresponding restriction enzymes. The nucleotide sequences are also different, resulting in different positions of restriction sites, so the lengths of the restriction fragments produced are also different. Then, the sequencer is used for determination, and the fluorescent label at the end of the fragment will be detected, resulting in different peaks, each of which represent at least one bacterium or several closely related bacteria. The HOMIM analysis method is to directly extract the total DNA from the sample and directly perform detection and analysis through the chip. MALDI-TOF-MS isolates and cultivates the bacterial flora of the sample then extracts the polypeptides of the bacteria for detection, and compares them according to the information in the database to obtain the type of bacteria. The principle of the high-throughput sequencing method has been described in "Materials and methods". High-throughput sequencing is a relatively advanced and accurate method, and the sequencing technology is becoming more and more mature. It can sequence hundreds of thousands or even millions of DNA strands at the same time. Therefore, the detection method of this experiment adopts high-throughput

sequencing technology to ensure the accuracy of the experimental data.

In the present study, HCs possess the largest amount of oral mucosa flora species. In contrast, the number of oral flora species in RAS patients decreased by different degrees at different stages during the disease course. During the ulcer stage, both ulcerated (467 OTUs) and healthy sites (414 OTUs) had the fewest bacterial flora species. The number of oral flora increased during the intermittent stage (788 OTUs). At the phylum level, six dominant species of oral mucosa were highly similar between the group of RAS patients and the group of healthy control. However, the dominant species levels differed between the four sites. The flora at the ulcer site in RAS patients was different from the other sites. Previous studies inquired into the composition of the oral bacterial community within healthy controls, while the RAS patients may have suffered from background noise due to the individual differences [22]. Therefore, the present study compared the oral microbiota within the same individual. We found that the increase in *Prevotella* abundance within communities of bacteria was strongly associated with RAS ($P < 0.05$). *Prevotella* belongs to *Bacteroidetes*, which is a Gram-negative anaerobe. The increase in the number of *Prevotella* during the onset of RAS may disrupt the local microecological balance.

5. Conclusion

The results of this experiment showed differences in the oral mucosal flora between the healthy control and RAS groups and suggested that the increased presence in *Prevotella* was correlated with RAS.

Data Availability

The data used for the study are included within the article.

Ethical Approval

The ethical approval number is FDU-20180813-523.

Conflicts of Interest

The authors declare that there are no conflicts of interest.

References

[1] J. A. Aas, B. J. Paster, L. N. Stokes, I. Olsen, and F. E. Dewhirst, "Defining the normal bacterial flora of the oral cavity," *Journal of Clinical Microbiology*, vol. 43, no. 11, pp. 5721–5732, 2005.

[2] L. Marchini, M. S. Campos, A. M. Silva, L. C. Paulino, and F. G. Nobrega, "Bacterial diversity in aphthous ulcers," *Oral Microbiology and Immunology*, vol. 22, no. 4, pp. 225–231, 2007.

[3] C. Scully and D. H. Felix, "Oral medicine--update for the dental practitioner. Aphthous and other common ulcers," *British Dental Journal*, vol. 199, no. 5, pp. 259–264, 2005.

[4] N. Seoudi, L. A. Bergmeier, F. Drobniewski, B. Paster, and F. Fortune, "The oral mucosal and salivary microbial community of Behcet's syndrome and recurrent aphthous stomatitis," *Journal of Oral Microbiology*, vol. 7, no. 1, Article ID 27150, 2015.

[5] K. Hijazi, T. Lowe, C. Meharg, S. H. Berry, J. Foley, and G. L. Hold, "Mucosal microbiome in patients with recurrent aphthous stomatitis," *Journal of Dental Research*, vol. 94, pp. 87S–94S, 2015.

[6] M. Bankvall, F. Sjoberg, G. Gale, A. Wold, M. Jontell, and S. Ostman, "The oral microbiota of patients with recurrent aphthous stomatitis," *Journal of Oral Microbiology*, vol. 6, no. 1, Article ID 25739, 2014.

[7] Y. J. Kim, Y. S. Choi, K. J. Baek, S. H. Yoon, H. K. Park, and Y. Choi, "Mucosal and salivary microbiota associated with recurrent aphthous stomatitis," *BMC Microbiology*, vol. 16, no. 1, p. 57, 2016.

[8] I. Adler, A. Muino, S. Aguas et al., "*Helicobacter pylori* and oral pathology: relationship with the gastric infection," *World Journal of Gastroenterology*, vol. 20, no. 29, pp. 9922–9935, 2014.

[9] N. R. Edgar, D. Saleh, and R. A. Miller, "Recurrent aphthous stomatitis: a review," *J Clin Aesthet Dermatol*, vol. 10, no. 3, pp. 26–36, 2017.

[10] C. C. Gomes, R. S. Gomez, L. G. Zina, and F. R. Amaral, "Recurrent aphthous stomatitis and *Helicobacter pylori*," *Medicina Oral, Patología Oral y Cirugía Bucal*, vol. 21, no. 2, pp. e187–e191, 2016.

[11] C. Scully and S. Porter, "Oral mucosal disease: recurrent aphthous stomatitis," *British Journal of Oral and Maxillofacial Surgery*, vol. 46, no. 3, pp. 198–206, 2008.

[12] P. Lopez-Jornet, F. Camacho-Alonso, and N. Martos, "Hematological study of patients with aphthous stomatitis," *International Journal of Dermatology*, vol. 53, no. 2, pp. 159–163, 2014.

[13] I. Volkov, I. Rudoy, T. Freud et al., "Response: Re: effectiveness of vitamin B12 in treating recurrent aphthous stomatitis: a randomized, double-blind, placebo-controlled trial," *The Journal of the American Board of Family Medicine*, vol. 22, no. 5, 616 pages, 2009.

[14] R. V. Lalla, L. E. Choquette, R. S. Feinn et al., "Multivitamin therapy for recurrent aphthous stomatitis: a randomized, double-masked, placebo-controlled trial," *Journal of The American Dental Association*, vol. 143, no. 4, pp. 370–376, 2012.

[15] R. Taleb, B. Hafez, N. El Kassir, H. El Achkar, and M. Mourad, "Role of vitamin B12 in treating recurrent aphthous stomatitis: a review," *International journal for vitamin and nutrition research. Internationale Zeitschrift fur Vitamin- und Ernahrungsforschung. Journal international de vitaminologie et de nutrition*, pp. 1–8, 2020.

[16] G. S. Ozler, "Zinc deficiency in patients with recurrent aphthous stomatitis: a pilot study," *Journal of Laryngology & Otology*, vol. 128, no. 6, pp. 531–533, 2014.

[17] A. Oztekin and C. Oztekin, "Vitamin D levels in patients with recurrent aphthous stomatitis," *BMC Oral Health*, vol. 18, no. 1, p. 186, 2018.

[18] S. A. Al-Maweri, E. Halboub, G. Al-Sufyani, A. Y. Alqutaibi, A. Shamala, and A. Alsalhani, "Is vitamin D deficiency a risk factor for recurrent aphthous stomatitis? A systematic review and meta-analysis," *Oral Diseases*, vol. 26, no. 6, pp. 1116–1123, 2020.

[19] B. Nalbantoglu and A. Nalbantoglu, "Vitamin D levels in children with recurrent aphthous stomatitis," *Ear, Nose, & Throat Journal*, vol. 99, no. 7, pp. 460–463, 2020.

[20] S. H. Al-Amad and H. Hasan, "Vitamin D and hematinic deficiencies in patients with recurrent aphthous stomatitis,"

Clinical Oral Investigations, vol. 24, no. 7, pp. 2427–2432, 2020.

[21] Q. Du, S. L. Ni, Y. L. Fu, and S. H. Liu, "Analysis of Dietary Related Factors of Recurrent Aphthous Stomatitis Among College Students," vol. 2018, 2018 Evidence-Based Complementary and Alternative Medicine.

[22] Z. Yang, Q. Cui, R. An et al., "Comparison of microbiomes in ulcerative and normal mucosa of recurrent aphthous stomatitis (RAS)-affected patients," *BMC Oral Health*, vol. 20, no. 1, p. 128, 2020.

[23] R. Ma, H. Chen, T. Zhou et al., "Effect of bedtime on recurrent aphthous stomatitis in college students," *Oral Surgery, Oral Medicine, Oral Pathology and Oral Radiology*, vol. 119, no. 2, pp. 196–201.e2, 2015.

[24] L. B. Huling, L. Baccaglini, L. Choquette, R. S. Feinn, and R. V Lalla, "Effect of stressful life events on the onset and duration of recurrent aphthous stomatitis," *Journal of Oral Pathology & Medicine*, vol. 41, no. 2, pp. 149–152, 2012.

[25] A. V. Keenan and S. Spivakovksy, "Stress associated with onset of recurrent aphthous stomatitis," *Evidence-Based Dentistry*, vol. 14, no. 1, p. 25, 2013.

[26] G. C. Kiran and B. A. Reginald, "Aphthous ulcers, salivary peroxidase and stress: are they related?" *Journal of Oral & Maxillofacial Pathology Jomfp*, vol. 19, no. 1, p. 37, 2015.

[27] "SLEBIODA Z, SZPONAR E, 27 KOWALSKA A. Etiopathogenesis of recurrent aphthous stomatitis and the role of immunologic aspects: literature review," *Archivum Immunologiae et Therapiae Experimentalis*, vol. 62, no. 3, pp. 205–215, 2013.

[28] Q. Yao and D. E. Furst, "Autoinflammatory diseases: an update of clinical and genetic aspects," *Rheumatology*, vol. 47, no. 7, pp. 946–951, 2008.

Hindawi
Evidence-Based Complementary and Alternative Medicine
Volume 2022, Article ID 3360966, 9 pages
https://doi.org/10.1155/2022/3360966

Research Article

LEARNS Model as Perioperative Education Strategy for Patients with Laryngeal Tumors

Biaoxin Zhang,[1] Qinzhi Sun,[1] Shaohua Hu,[2] Yinxiang Yu,[1] Cuixia Hu,[1] Dejuan Zhao,[1] Jing Xu,[1] Jun Fang,[1] and Lulu Wang[1]

[1]*Department of Otolaryngology Head and Neck Surgery, The First Affiliated Hospital of Anhui Medical University, Hefei, Anhui 230022, China*
[2]*Nursing Department, The First Affiliated Hospital of Anhui Medical University, Hefei, Anhui 230022, China*

Correspondence should be addressed to Lulu Wang; luluwang0816@163.com

Received 6 August 2022; Accepted 17 September 2022; Published 12 October 2022

Academic Editor: Xueliang Wu

Objective. To evaluate LEARNS model as a perioperative strategy for health education and nursing supervision of patients with laryngeal tumors. *Methods*. LEARNS scheme based on the best practice guidelines was applied to patients in the observation group: (1) analyze the needs of patients (Listen_L); (2) establish therapeutic partnership (Establish_E); (3) adopt intentional intervention (Adopt_A); (4) reinforce health awareness (Reinforce_R); (5) implement feedback assessment of knowledge (Name_N); (6) strengthen self-management based on community resources (Strengthen_S). In the control group, traditional medical care instructions were provided to the patients by medical staff. Parameters such as anxiety status, treatment compliance, nursing satisfaction, self-care ability, and life quality were compared between the observation and control groups. *Results*. Upon admission, there was no significant difference in self-care ability and anxiety level between two groups. However, the anxiety level of observation group was significantly lower than that of the control group 1 day before operation and 7 days after operation. Postoperative treatment compliance and nursing satisfaction were also improved in the observation group. In addition, self-care ability and life quality in the observation group were significantly enhanced as compared to the control group. *Conclusion*. As a mutual learning process between nurses and patients, LEARNS model motivates nurses to assess the needs of patients voluntarily. Furthermore, evidence-based education reinforces the self-care ability and health awareness of the patients. Our data suggests that LEARNS model is of great value in improving the life quality of the patients with laryngeal tumors and nursing satisfaction.

1. Introduction

Larynx is an important organ for breathing, swallowing, and pronunciation. Laryngectomy is the main treatment for laryngeal tumors. Due to the complete or partial loss of laryngeal function after laryngectomy, patients need to wear a tracheal tube or fistula for a long time as a medical assistance [1]. After the operation, patients will suffer from a series of changes in physical, psychological and social life, including impaired breathing and swallowing capability [2], functional aphonia [3], depression and anxiety [4], uncertainty feeling of illness [5], malnutrition [6], interpersonal disorders and impaired life quality [7]. In the meanwhile, patients need to master a series of self-care skills related to wound care, airway management, diet and nutrition, and other self-care management knowledge after radiotherapy and chemotherapy [8]. Therefore, postoperative orientation for patients with laryngeal tumors is of great value to enhance self-management ability and prepare for postoperative challenges.

The LEARNS model based on best practice guidelines is a mature educational module for patient-centered and patient-oriented health awareness promotion [9]. LEARNS model encourage nurses to actively converse with patients instead of waiting for their complaints. The LEARNS processes requires nurses to actively assess the needs of patients

(Listen), establish a beneficial therapeutic partnership (Establish), adopt intentional intervention methods (Adopt), reinforce health awareness of the patients (Reinforce), implement feedback assessment of health literacy (Name), and strengthen self-management strategies (Strengthen) [10]. The core guideline is to create a client-centered care environment without embarrassment and blame. Nurses serve as catalysts to start conversations with patients to promote their health awareness, build knowledge and skills essential for postoperative care and formulate self-management strategies. The final goal is to enhance health literacy and self-efficacy of the patients, which has been proved to optimize patient outcomes and self-management in different scenarios [10–12]. However, this type of patient-centered orientation program is seldom adopted in the health care system of Chinese hospitals.

In this study, we aimed to investigate the effect of LEARNS model on health education and nursing supervision of patients with laryngeal tumors. Among 60 patients who were diagnosed with laryngeal cancer, 30 patients in the control group were provided with the regular health education and 30 patients in the experimental group (observation group) were trained with the LEARNS health education model. Perioperative anxiety level, patients' compliance during the treatment, satisfaction degree of nursing staff, perioperative self-care ability and the quality of life between the two groups of patients were assessed. Based on our study, a standardized procedure of perioperative health education for patients with laryngeal tumors could improve the health literacy, self-management ability and life quality of patients with laryngeal tumors.

2. Methods

2.1. Subjects Enrollment. A total number of 60 patients who were diagnosed with laryngeal cancer and underwent laryngeal tumor resection in the Otorhinolaryngology Head and Neck Surgery Department of our hospital in Anhui Province from January 2019 to April 2021 were enrolled in this study. This study was approved by the Ethics Committee of The First Affiliated Hospital of Anhui Medical University. All the 60 patients signed the written informed consent.

2.1.1. Inclusion Criteria. (1) Patients diagnosed pathologically with laryngeal tumors and underwent laryngectomy; (2) patients were in a stable condition and able to cooperate with the guidelines and instruction given by the nurses; (3) patients were capable of listening, speaking, reading and writing, with the age ≥18 years old; (4) patients were recruited on the voluntary basis and signed the informed consent.

2.1.2. Exclusion Criteria. (1) Patients diagnosed with the recurrence or metastasis of laryngeal tumors in the past six months; (2) patients diagnosed with other type of tumors or mental illnesses in the treatment stage; (3) patients suffered from severe heart, lung, liver and kidney dysfunction; (4) patients suffered from severe communication disorders or unable to correctly understand the questionnaire and instructions provided.

2.1.3. Falling-Off Criteria. Patients with incomplete data and those who did not complete the survey and questionnaires for various reasons.

2.2. Grouping Method. According to the order of admission time, enrolled subjects were randomly divided into two groups. 30 patients in the control group were provided with the regular health education model, and 30 patients in the experimental group (observation group) were trained with the LEARNS health education model. Fisher randomization technique was employed for random assignment. The statistical power of sample size was evaluated using online tool: https://www.stat.ubc.ca/~rollin/stats/ssize/n2.html.

2.3. Intervention Measures for the Control Group (Conventional Health Education Model). Perioperative health education was provided in accordance with the general nursing routines and health education pathways of surgical patients, including preoperative examination, preoperative preparation, psychological care, postoperative body movement, diet guidance, postoperative tracheal tube care (such as airway humidification, Sputum suction, cannula disinfection, pronunciation and communication method guidance), medication guidance, discharge guidance and return visit education.

2.4. Experimental Group (LEARNS Model) Intervention Measures

2.4.1. Establishment of an Evidence-Based Nursing Research Team. An evidence-based nursing research team comprising head nurses, nursing backbones, and guideline inspectors in the department was formed to implement the LEARNS model. The research team was divided into three subgroups: nursing management team, clinical practice team, and quality control team. Members of each group summarized and discussed the research process and problems on a monthly basis.

2.4.2. Conduct Evidence-Based Nursing Training on the Research Team. Domestic experts on evidence-based nursing was invited to conduct homogenization training for research team members on evidence-based medicine, evidence-based nursing and application of best practice guidelines to ensure the standardized conduct of interventions.

2.4.3. Gap Analysis. To analyze the gap between the best practice guidelines based on LEARNS model and the current status of perioperative health education for patients with laryngeal tumors (see Table 1 for details).

2.4.4. Assessment of the Learning Needs. The learning needs assessment questionnaires were distributed to patients in the observation group on a regular basis. The content included:

Table 1: Analysis of the gap between LEARNS guidelines and current health education.

Guide mode	Guide meaning	Current clinical status	Ways to improve
L (listen)	Understand patient needs	Based on symptoms and positive indicators	Conduct a needs assessment
E (establish)	Establish a therapeutic partnership	Preaching teacher-student relationship	Master guidelines and standardized training, change nursing concept
A (adopt)	Adopt intentional intervention	Indoctrination	Evaluate the individuality and differential needs, plan multi-mode education
R (reinforce)	Improve health awareness	Based mainly on biochemical indicators	Focus on the psychology and improve self-management efficiency
N (name)	Learning feedback	No systematic evaluation of the educational process	Develop a health education process and dynamically evaluate the outcome
S (strengthen)	Self-management using community resources	Short-term education during hospitalization	Continue nursing health education with the assistance of information platform

Table 2: Assessment of learning and needs of patients with laryngeal tumors.

Survey item	Demand content (in order of priority)
Learning duration ways of learning	Study 1 hour a day or study every other day oral explanations and demonstrations given by nurses, video materials playing, official guidelines from the hospital, information searching on internet
Learning tools	Video, audio, pictures, leaflets, brochures, science and education books, web materials
Learning contents	Cannula disinfection, wound dressing, airway humidification, postoperative nutritional management, handling of common accidents in the cannula, learning platform use, psychological adjustment, guidance on pronunciation and communication methods, review content and procedures
Resources	Internet search, science books, hospital information platform, professional books, community presentations

study time, ways of learning, study tools, study content, and available resources. A descriptive analysis of the evaluation results was shown in Table 2.

2.4.5. Clinical Application of LEARNS Model. According to the LEARNS model, we identified the existing problems in the current perioperative health education for patients with laryngeal tumors and assessed the learning needs of the patients. We reformulated the process of perioperative health education for patients with laryngeal tumors, as shown in Figure 1.

2.5. Observation Index

2.5.1. General Information Questionnaire. Designed by the research team and contained surveys about general sociodemographic data, clinical nursing data and health education status. General sociodemographic information includes: gender, age, occupation, habitual residence address, marital status, religious belief, contact information, education level, economic level, and method of payment of medical expenses. Clinical nursing information includes: operation time, operation method, tracheal cannula type, airway humidification method, presence or absence of difficulty in expectoration, cannula blockage, bleeding, decoupling, subcutaneous emphysema and other complications. The status of health education includes: concerns, degree of coping with distress, health education obtained, knowledge requirements and specific content, family and social support.

2.5.2. Anxiety Self-Rating Scale (Self-Rating Anxiety Scale, SAS). Containing 20 items (Supplementary file), each item was based on a 4-point scoring method (from 1 to 4 points). The total score was calculated by summing up the scores of all items. The total rough score was multiplied by 1.25 and the integer part was considered as the standard score. The full score was set as 100 points. The critical cutoff value for SAS was 50 points. Higher total score indicated a higher level of anxiety. Evaluations were performed on admission, 1 day before surgery and 7 days after surgery.

2.5.3. Evaluation of Treatment Compliance. Score A: actively accepted the treatment plan and nursing guidance, and successfully completed the treatment. Score B: partially accepted treatment plan and nursing guidance, and completed most of the treatment and nursing care procedures. Score C: those who did not understand the treatment plan and occasionally did not cooperate with the treatment and nursing care. Evaluation was performed on the 7th day after surgery.

2.5.4. Patient and Family Satisfaction. Self-designed nursing satisfaction questionnaire; the total score was 100 points; patients with ≥96 points were considered as very satisfied, patients with 90–95 points were relatively satisfactory, and those with <90 points were unsatisfactory. The assessment was conducted on the day of discharge.

2.5.5. Self-Care Ability Scale (Exercise Self-Care Agency, ESCA). Composed of 4 dimensions of self-care skills (12 items), self-responsibility (8 items), self-management literacy (9 items) and health knowledge level (14 items), with a total of 43 items (Supplementary file). A score of 0 to 4 (Five-level scoring method) was assigned to each item, with a total score of 172 points. 0 = very different from me, 1 = something not like me, 2 = no comment, 3 = something like me, 4 = very like me.

According to the total score of the scale and the score of each dimension, the self-care abilities were divided into 3 levels: 0–57 as low level; 58–115 as medium level; 116–172 as high level. A higher score of each dimension indicated a stronger self-care ability. The CVI (Core Values Index) value for the validity of the scale was 0.98, and the Cronbach's coefficient was 0.93. The evaluation was performed 4 weeks after the operation.

2.5.6. Washington Medical University Quality of Life Scale (The University of Washington Quality of Life Scale, UW-QOL). UW-QoL is one of the most frequently reported health-related quality of life (HR-QoL) questionnaires specifically in head and neck cancer, and since its first publication in 1993, it has been used in many different cohorts [13, 14]. This self-assessment questionnaire was

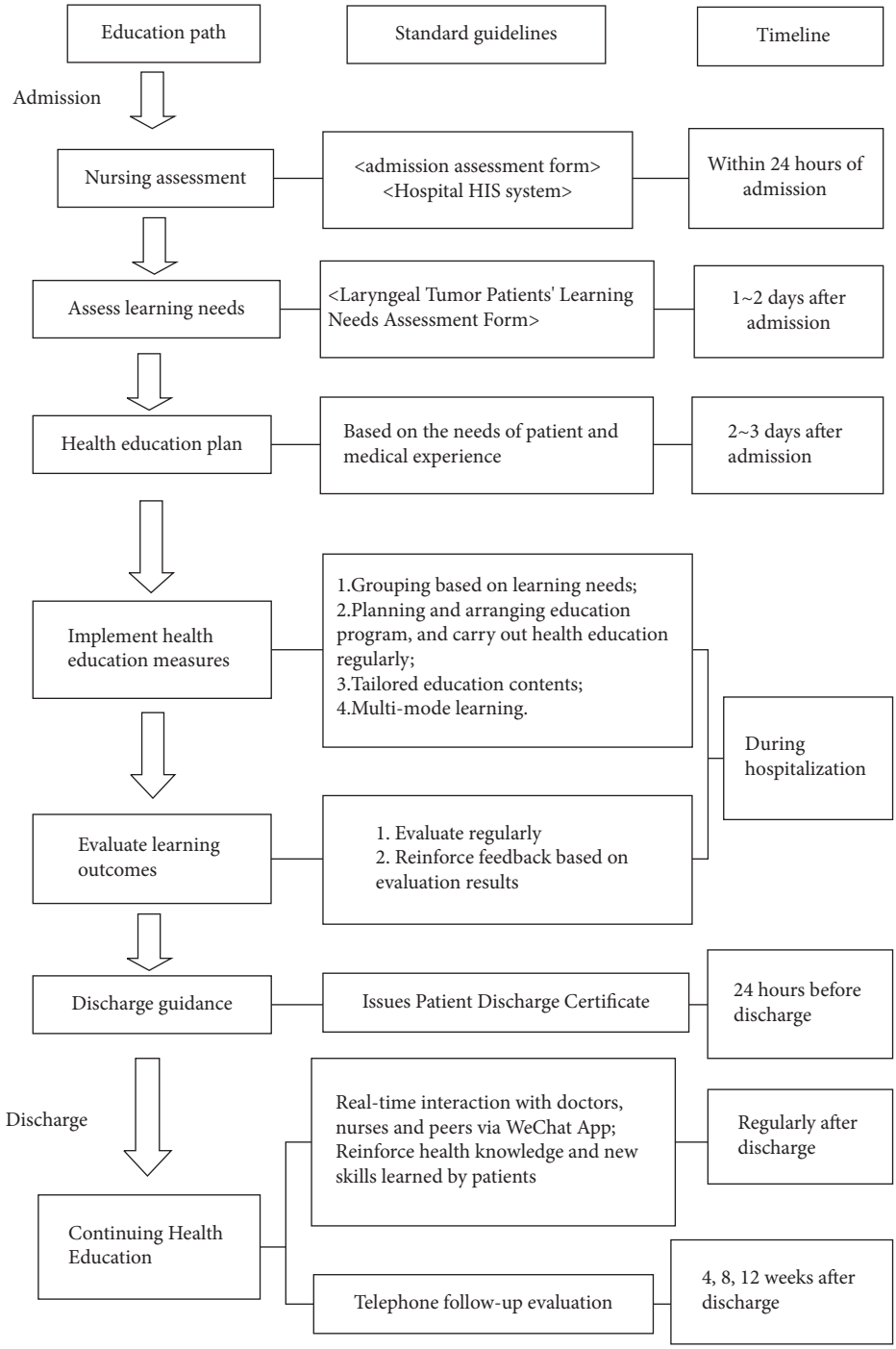

Figure 1: Health education flow chart of learns mode for patients with laryngeal tumors during perioperative period.

dedicated to patients with head and neck tumors including 12 specific questions concerning the quality of life, 3 comprehensive questions[?]Patients can add questions that are not included in the scale[?]. The 12 specific items were: pain, appearance, entertainment, vitality, swallowing, chewing, language, shoulder function, taste, saliva, mood and anxiety. Each item was divided into 3 to 5 levels, and the score ranged from 0 to 100 points. The higher the score, the better the quality of life is. The assessment was carried out 12 weeks after the operation.

2.6. Data Processing and Statistical Analysis. Epidata3.1 software was used for data entry and SPSS18.0 software was employed for statistical analysis. Measurement data were described by (mean ± SD : $X \pm S$); t-test was used for comparison between two groups in anxiety score before and after surgery; count data were described by case; Chi-square (χ^2) statistic test and rank sum test were used for comparison of parameters including, treatment compliance, nursing satisfaction, self-management ability and quality of life between two groups. The test level $a = 0.05$,

Table 3: Comparison of anxiety levels between the two groups of patients (n, $X \pm S$).

	Number (n)	Anxiety score on admission	Anxiety score 1 day before surgery	Anxiety score 7 days after surgery
Observation group	30	57.33 ± 12.63	61.50 ± 10.33	55.23 ± 9.96
Control group	30	57.23 ± 13.39	66.83 ± 9.99	60.57 ± 9.87
t value		0.030	−2.033	−2.084
P value		0.976	0.047	0.042

Statistics: unpaired student's t test.

and the difference was considered as statistically significant when $P < 0.05$.

3. Results

3.1. Anxiety Level Comparison. We first assessed the anxiety level of the patients enrolled in the control group and experimental group. There was no significant difference in anxiety between the two groups of patients when they were admitted to the hospital; the anxiety level of the observation group was significantly lower than that of the control group 1 day before surgery and 7 days after surgery (Table 3).

3.2. Treatment Compliance and Nursing Satisfaction Comparison. The treatment compliance of the two groups of patients was evaluated on the 7th day after operation, and the nursing satisfaction was evaluated on the day of discharge. Our data demonstrated that the observation group with LEARNS model showed a better treatment compliance and a relatively higher level of nursing satisfaction (Table 4).

3.3. Comparison of Self-Care Ability and Quality of Life. The self-care ability of patients was evaluated at 4 weeks after operation, and the quality of life was measured at 12 weeks after operation. The observation group with the implementation of LEARNS model showed a significantly higher level of self-care capacity and life quality than the control group (Table 5).

4. Discussions

4.1. LEARNS Mode Could Effectively Reduce the Perioperative Anxiety Level of Patients with Laryngeal Tumors. The results of this study showed that the anxiety level of the two groups of patients with laryngeal tumors was reduced after operation. In the observation group with the LEARNS model implementation, the anxiety score decreased from 61.50 ± 10.33 (1 day before surgery) to 55.23 ± 9.96 (7 days after surgery), and the perioperative anxiety level was significantly lower as compared with the control group with conventional health education model. This indicates that conventional health education is an effective health education model that is widely used and verified by clinical practice to relieve the stress and anxiety of perioperative patients [15–17]. However, the conventional health education model in health care focuses on the evaluation, diagnosis, treatment and nursing of the clinical symptoms or positive indicators of disease progression [18]. According to a previous study, most of nurses in clinical cares have insufficient empathy and motivation to assess the health needs and feelings of the patients [19]. Additionally, routine patient education by nurses usually happens in one-way guidance and passive reception manner, which does not foster self-evaluation and autonomous learning by the patients [20].

In contrast, LEARNS model is an evidence-based practical education process of two-way learning between nurses and patients. It follows the patient-centered principle, which prompts nurses to engage both their mind and body in understanding the needs and feeling of the patients [21]. On the other hand, the involvement of patients in the design of learning program and needs assessment can also motivate the independent learning and promote the health literacy of the patients. The LEARNS model therefore not only promotes the interactive therapeutic partnership, but also fosters evidence-based patient education and learning processes. As sufficient interactions with patients and evidence-based education have been demonstrated to improve the treatment outcome [22], LEARNS model which requires nurses to actively converse with patients instead of waiting for their complaints are expected to ameliorate the anxiety of the patients. This is particularly important for patients with laryngectomy, who are prone to a series of mental problems such as communication disorders, decline in social function, and self-esteem decline after surgery [23, 24].

4.2. LEARNS Model Improves the Perioperative Treatment Compliance and Nursing Satisfaction of Patients with Laryngeal Tumors. In this study, the treatment compliance of the two groups of patients was evaluated on the 7th day after the operation, and the nursing satisfaction was evaluated on the day of discharge. The results showed that the perioperative treatment compliance and nursing satisfaction of LEARNS model group was significantly higher than the group receiving conventional health education. The majority of patients with laryngeal tumors were diagnosed and treated in the middle and late stages of the tumor. Although they are treated with total or partial laryngectomy, the generally poor prognosis and the long course of the disease progression makes the expectation of recovery very low [25]. Conventional health education mainly focuses on treatment and education for specific clinical symptoms. The lack of patient needs and feeling assessment makes it difficult to meet the overall

Table 4: Comparison of treatment compliance and nursing satisfaction.

	Number (n)	Treatment compliance (n)			Nursing satisfaction (n)		
		A	B	C	Very satisfied	Relatively satisfied	Not satisfied
Observation group	30	21	8	1	20	9	1
Control group	30	13	13	4	12	15	3
Z value			−2.175			−2.104	
P value			<0.05			<0.05	

Statistics: rank sum test.

Table 5: Comparison of postoperative self-care ability and quality of life between the two groups (n, %, $X \pm S$).

	Number (n)	Self-care ability score				Life quality score
		Low	Medium	High	Total score ($X \pm S$)	
Observation group	30	0	1 (3.33%)	29 (96.67%)	131.23 ± 11.21	85.23 + 8.74
Control group	30	0	7 (23.33%)	23 (76.67%)	125.10 ± 10.67	80.03 + 9.68
X^2 /t value			5.192		2.170	2.182
P value			0.023		0.034	0.033

Statistics: chi-square (χ^2) statistic test.

psychological, spiritual, social, and cultural needs of patients, which may lower the treatment compliance [26].

The LEARNS model based on the best practice guidelines not only embodies humanistic care, but also implicates an active and interactive patient education program for patients with laryngeal tumors. A previous study indicates that, the awareness of the disease and acceptance of the prognosis are key factors affecting the therapeutic compliance [27]. The response of a patient to treatment is also closely related to their cognitive evaluation and emotional experience of the disease [28]. Therefore, positive cognitive evaluation and emotion regulation can improve health promotion behavior and the acceptance of the treatment. In this study, the LEARNS model was used to fully assess the knowledge of patients with laryngeal tumors on the outcome and development of their own diseases, evaluated the health needs of patients, and establish cooperative partnerships between nurses and patients. The patients were also involved in the formulation and implementation of health education programs to reinforce their health literacy, which could contribute to the improved compliance with perioperative treatment.

4.3. LEARNS Model Improves the Perioperative Self-Care Ability and Quality of Life of Patients with Laryngeal Tumors. In this study, the self-care ability of patients was evaluated at 4 weeks after operation, and the quality of life was evaluated at 12 weeks after operation. The results showed that the self-care ability and life quality in the observation group were higher than those of the control group ($P < 0.05$). The score of self-care skills, self-responsibility, self-concept and health knowledge level were also higher than those of the control group, and the health knowledge level showing the most obvious advantage. This indicates that the LEARNS health education model is more organized, structured and purposeful. It is based on evidence-based practice and combined with the preliminary evaluation results to clarify the gap of self-care skills and knowledge (including tracheal tube replacement, cleaning, disinfection, gas Tract humidification, tracheotomy wound care, treatment of tracheal tube blockage, tube slippage, wound bleeding and functional exercises, etc.). Through the cooperation with patients and multi-professional teams, targeted health education programs could improve self-care ability and skills more efficiently.

In addition, after the application of LEARNS model, the sense of self-responsibility and self-awareness have been significantly improved. This may be attributable to the teaching feedback evaluation [29]. Nurses actively conducted dialogues with patients through written materials, telephone calls, computer technology and multimedia. This could strengthen the self-management skills and foster continuous learning.

Our study suffers from the following limitations: (1) The sample size is small and increased cohort number from multiple clinical centers would provide more solid conclusions; (2) During the analysis and patient recruitment, other confounding factors such as family history of exercise and education, and the accessibility to the community health care resources need to be reconciled; (3) A prolonged duration of follow-up would provide more insights into whether LEARNS module procures beneficial effect on the prognosis of the patients.

5. Conclusion

The LEARNS model based on the best practice guidelines is a new form of perioperative health education for patients with laryngeal tumors. The core guideline is to create a client-centered care environment without embarrassment and blame, which relieves patient anxiety and effectively implement high-quality nursing. The therapeutic partnership with patients not only helps build knowledge and skills essential for postoperative self-management, but also improves the satisfaction of both

nurses and patients. Evidence-based practical education also contributes to enhanced self-care ability, improved therapeutic compliance and an overall higher quality of life.

Data Availability

All data used in this study are presented in the manuscript.

Ethical Approval

All procedures performed in studies involving human participants were in accordance with the ethical standards of the institutional and/or national research committee and with the 1964 Helsinki declaration and its later amendments or comparable ethical standards. This study was approved by the Ethics Committee of The First Affiliated Hospital of Anhui Medical University.

Consent

Informed consent was obtained from all individual participants included in the study.

Conflicts of Interest

All authors declare that they have no conflicts of interest.

Authors' Contributions

Biaoxin Zhang and QinzhiSun contributed to this work equally.

Acknowledgments

This study was supported by Acute and Critical Care Fund Project of the First Affiliated Hospital of Anhui Medical University (2020JWZZHL-01); National Natural Science Foundation Youth Cultivation Program of the First Affiliated Hospital of Anhui Medical University in 2019 (2019kj23).

Supplementary Materials

Categories of questions in Self-Rating Anxiety Scale (SAS) and Exercise Self-care Agency (ESCA) assessment. (*Supplementary Materials*)

References

[1] S. Stawicki, A. Cipriano, M. Mao et al., "An overview of complications associated with open and percutaneous tracheostomy procedures," *International Journal of Critical Illness and Injury Science*, vol. 5, no. 3, pp. 179–188, 2015.

[2] I. Carmignani, L. G. Locatello, I. Desideri et al., "Analysis of dysphagia in advanced-stage head-and-neck cancer patients: impact on quality of life and development of a preventive swallowing treatment," *European Archives of Oto-Rhino-Laryngology*, vol. 275, no. 8, pp. 2159–2167, 2018.

[3] M. Taito, S. Taito, M. Banno et al., "Voice rehabilitation for laryngeal cancer after radiotherapy: a systematic review and meta-analysis," *European Archives of Oto-Rhino-Laryngology*, vol. 276, no. 6, pp. 1573–1583, 2019.

[4] Y. Wang, W. Lu, and X. Shen, "Assessment of preoperative psychologic distress in laryngeal cancer patients," *Acta Oto-Laryngologica*, vol. 139, no. 2, pp. 184–186, 2019.

[5] A. Taylor, M. Wells, G. Hubbard, and A. Worth, "From an illusion of certainty into a reality of uncertainty: a longitudinal qualitative study of how people affected by laryngeal cancer use information over time," *European Journal of Oncology Nursing*, vol. 23, pp. 15–23, 2016.

[6] J. Cui, S. Chen, Q. Bo et al., "Preoperative prognostic nutritional index and nomogram predicting recurrence-free survival in patients with primary non-muscle-invasive bladder cancer without carcinoma in situ," *OncoTargets and Therapy*, vol. 10, pp. 5541–5550, 2017.

[7] L. T. Terlingen, W. Pilz, M. Kuijer, B. Kremer, and L. W. Baijens, "Diagnosis and treatment of oropharyngeal dysphagia after total laryngectomy with or without pharyngoesophageal reconstruction: systematic review," *Head & Neck*, vol. 40, no. 12, pp. 2733–2748, 2018.

[8] I. C. Cnossen, C. F. Van Uden-Kraan, S. E. J. Eerenstein et al., "An online self-care education program to support patients after total laryngectomy: feasibility and satisfaction," *Supportive Care in Cancer*, vol. 24, no. 3, pp. 1261–1268, 2016.

[9] K. R. Haase, "The role of the internet in the cancer experience: synthesizing patient and provider views to forge new directions for care," *Canadian Oncology Nursing Journal*, vol. 29, no. 3, pp. 204–209, 2019.

[10] A. J. Hoffman, "Enhancing self-efficacy for optimized patient outcomes through the theory of symptom self-management," *Cancer Nursing*, vol. 36, no. 1, pp. E16–E26, 2013.

[11] S. Rees and A. Williams, "Promoting and supporting self-management for adults living in the community with physical chronic illness: a systematic review of the effectiveness and meaningfulness of the patient-practitioner encounter," *JBI Library of Systematic Reviews*, vol. 7, no. 13, pp. 492–582, 2009.

[12] V. Duprez, D. Beeckman, S. Verhaeghe, and A. Van Hecke, "Self-management support by final year nursing students: a correlational study of performance and person-related associated factors," *International Journal of Nursing Studies*, vol. 74, pp. 120–127, 2017.

[13] M. Kolator, B. Mikuła, A. Maciejczyk, and T. Zatoński, "Polish validation of the University of Washington "quality of life" questionnaire in patients with cancer of the larynx," *British Journal of Oral and Maxillofacial Surgery*, vol. 57, no. 3, pp. 226–231, 2019.

[14] D. C. Laraway and S. N. Rogers, "A structured review of journal articles reporting outcomes using the University of Washington quality of life scale," *British Journal of Oral and Maxillofacial Surgery*, vol. 50, no. 2, pp. 122–131, 2012.

[15] F. Poland, N. Spalding, S. Gregory, J. McCulloch, K. Sargen, and P. Vicary, "Developing patient education to enhance recovery after colorectal surgery through action research: a qualitative study," *BMJ Open*, vol. 7, no. 6, Article ID e013498, 2017.

[16] M. F. Lemos, S. V. Lemos-Neto, L. Barrucand, N. Vercosa, and E. Tibirica, "Preoperative education reduces preoperative anxiety in cancer patients undergoing surgery: usefulness of the self-reported Beck anxiety inventory," *Brazilian Journal of Anesthesiology*, vol. 69, no. 1, pp. 1–6, 2019.

[17] L. Bailey, "Strategies for decreasing patient anxiety in the perioperative setting," *AORN Journal*, vol. 92, no. 4, pp. 445–460, 2010.

[18] M. Jasemi, L. Valizadeh, V. Zamanzadeh, and B. Keogh, "A concept analysis of holistic care by hybrid model," *Indian Journal of Palliative Care*, vol. 23, no. 1, pp. 71–80, 2017.

[19] S. Babaei and F. Taleghani, "Compassionate care challenges and barriers in clinical nurses: a qualitative study," *Iranian Journal of Nursing and Midwifery Research*, vol. 24, no. 3, pp. 213–219, 2019.

[20] C. Budgen and L. Gamroth, "An overview of practice education models," *Nurse Education Today*, vol. 28, no. 3, pp. 273–283, 2008.

[21] D. R. Brown, R. Ludwig, G. A. Buck, D. Durham, T. Shumard, and S. S. Graham, "Health literacy: universal precautions needed," *Journal Of Allied Health*, vol. 33, no. 2, pp. 150–155, 2004.

[22] C. C. Cutilli, "Excellence in patient education," *Nursing Clinics of North America*, vol. 55, no. 2, pp. 267–282, 2020.

[23] S. Zhang, H. Chen, M. Zhang, X. Sun, and X. Liu, "Reduction of depression symptoms in laryngeal cancer patients receiving psychology services," *American Journal of Translational Research*, vol. 12, no. 10, pp. 6637–6645, 2020.

[24] X. Li, J. Li, Y. Shi et al., "Psychological intervention improves life quality of patients with laryngeal cancer," *Patient Preference and Adherence*, vol. 11, pp. 1723–1727, 2017.

[25] K. He, Q. Li, Y. Hou, Y. He, and X. Yue, "Effect of a refined nursing model based on nursing quality feedback on the postoperative mental state of patients with laryngeal cancer," *American Journal of Translational Research*, vol. 13, no. 6, pp. 6525–6533, 2021.

[26] W. T. Gude and N. Peek, "Control theory to design and evaluate audit and feedback interventions," *Studies in Health Technology and Informatics*, vol. 263, pp. 159–170, 2019.

[27] J. Jin, G. E. Sklar, V. Min Sen Oh, and S. Chuen Li, "Factors affecting therapeutic compliance: a review from the patient's perspective," *Therapeutics and Clinical Risk Management*, vol. 4, no. 1, pp. 269–286, 2008.

[28] D. Kozlowski, M. Hutchinson, J. Hurley, J. Rowley, and J. Sutherland, "The role of emotion in clinical decision making: an integrative literature review," *BMC Medical Education*, vol. 17, no. 1, p. 255, 2017.

[29] A. Burgess and C. Mellis, "Feedback and assessment for clinical placements: achieving the right balance," *Advances in Medical Education and Practice*, vol. 6, pp. 373–381, 2015.

Hindawi
Evidence-Based Complementary and Alternative Medicine
Volume 2022, Article ID 2557952, 4 pages
https://doi.org/10.1155/2022/2557952

Research Article

Study on the Effect of Different Endoscopic Auxiliary Treatment of Gastric Mucosal Microtumor

Xiongping Zhong, Fuqun Wang, Dehui Zeng, Yijin Chen, and Shengbing Wang

Department of Gastroenterology, Meizhou People's Hospital, Meizhou, Guangdong Province, China

Correspondence should be addressed to Shengbing Wang; chengb18774@163.com

Received 8 July 2022; Revised 4 August 2022; Accepted 10 August 2022; Published 11 October 2022

Academic Editor: Xueliang Wu

Objective. To explore the effect of endoscopy in the treatment of gastric mucosal microtumors. *Methods*. A total of 229 patients with gastric mucosal microtumors were treated in our hospital from January 2016 to December 2021. All patients were divided into three groups group A, group B, and group C. Group A was treated with a transparent cap combined with circle-assisted endoscopic resection, group B with ligator combined with circle-assisted endoscopic resection, and group C with endoscopic mucosal tumor resection. The effects of the three groups were observed. *Results*. There were 47 patients in group A, 17 males, and 30 females, aged 36–69 years, with an average age of 55.6 ± 9.2 years. There were 54 patients in group B, 18 males, and 36 females, aged 38–72 years, with an average age of 57.6 ± 7.7 years. There were 128 patients in group C, 29 males, and 99 females, aged 33–78 years, with an average age of 55.6 ± 8.4 years. There is no significant difference in age and sex between group A, group B, and group C ($P > 0.05$). The incidence of postoperative complications in group B (66.7%) was significantly higher than that in group A (57.4%) and group C (53.9%) (all $P < 0.05$). The incidence of postoperative complications in group A (57.4%) was higher than that in group C (53.9%), and the difference was statistically significant ($P < 0.05$). *Conclusion*. Endoscopic mucosal resection and ligation combined with circle-assisted endoscopic resection are effective and safe in the treatment of gastric mucosal microtumors, but it needs to be combined with targeted nursing measures. The transparent cap combined with ring-assisted endoscopic resection has a significant effect on the treatment of gastric mucosal micromasses, reducing operative complications.

1. Introduction

A gastric submucosal tumor is a neoplastic or nonneoplastic space-occupying lesion originating from the tissue below the gastric mucosa [1]. It is a common lesion of the upper digestive tract. On average, 1 case can be found every 200 times of upper gastrointestinal endoscopy [2]. Among them, some small tumors in the gastric mucosa lack clinical symptoms, most of which are found during gastroscopy or other imaging examinations [3]. Patients have only some nonspecific symptoms such as stomach discomfort, nausea, abdominal distension, anorexia, indigestion, and so on [4]. Because of the deep location of the microtumor, it is a difficult problem for clinicians to make an effective treatment plan [5].

In recent years, with the improvement of people's health awareness and living standards, endoscopic technology has been rapidly developed and widely used, and the level of diagnosis and treatment has been gradually improved [6]. A variety of endoscopic resection techniques have been used in the diagnosis and treatment of gastric submucosal tumors [7]. Compared with surgery, endoscopic resection has the advantages of a definite curative effect, high safety, less trauma, and quick recovery [8]. At present, the existing endoscopic treatment techniques include transparent cap combined with circle-assisted endoscopic resection, ligator combined with circle-assisted endoscopic resection, endoscopic mucosal tumor resection, and so on [9]. Endoscopic mucosal tumor resection has a better surgical effect and less risk, so it has been used as a standard measure for endoscopic treatment of gastric mucosal microtumors [10]. At the same time, other endoscopic resection based on this technique has also been gradually developed and applied in the

clinic, such as transparent cap combined with circle-assisted endoscopic resection and ligator combined with circle-assisted endoscopic resection, which is used in the clinic [11]. Gastric submucosal tumors are a safe and effective treatment, with the advantages of simple operation and less trauma, reduce patient mortality, and improve patients' quality of life, which has been promoted and applied in the clinic [12].

At present, there are many studies on gastric submucosal masses, but there are still some deficiencies in the domestic and foreign studies on the efficacy of endoscopic-assisted treatment of gastric mucosal micromasses at home and abroad [13]. The application of endoscopic-assisted treatment of gastric mucosal micromasses is still controversial [14]. In summary, it is particularly important to pay attention to the endoscopic treatment of gastric mucosal microtumors [15]. This study retrospectively studied the clinical data of patients who had been treated under endoscopy and had identified the pathological type as gastric mucosal microtumors in our hospital, explored the application efficacy of different ways of endoscopic-assisted treatment of gastric mucosal microtumors, and analyzed the clinical effects of different endoscopic treatment, so as to provide more reference basis for clinical workers in the endoscopic diagnosis and treatment of gastric mucosal microtumors.

2. Methods

2.1. Study Design and Participants. A total of 229 patients with gastric mucosal microtumors from January 2016 to December 2021 were selected. All patients were randomly divided into three groups: group A, group B, and group C. There were 47 patients in group A, 17 males, and 30 females, aged 36–69 years. There were 54 patients in group B, 18 males, and 36 females, aged 38–72 years. There were 128 patients in group C, 29 males, and 99 females, aged 33–78 years. All subjects obtained informed consent. The ethics committee of Meizhou People's Hospital approved the research plan. All participants underwent a complete medical history and clinical examination.

2.2. Inclusion and Exclusion Criteria. Inclusion criteria were as follows: (1) Patients who met the diagnostic criteria of gastric submucosal tumors in the guidelines for Clinical diagnosis and treatment of tumors and were diagnosed by imaging examination. (2) Patients and their families knew about the study, the purpose of examination, and the possible risks of the operation, agreed to endoscopic treatment or surgical treatment, and signed the informed consent form. (3) Smooth gastric mucosa without ulcer, no lymph node, and distant metastasis. (4) Complete postoperative follow-up data. Exclusion criteria were as follows: (1) Patients with digestive tract stricture and perforation. (2) Patients with acute inflammation of the digestive tract. (3) Patients with heart, lung, brain, kidney, and other important organ failure or dysfunction, and who could not tolerate anesthesia. (4) Those who take anticoagulants, hematological diseases, and blood coagulation disorders.

2.3. Observation Index. The comparison of postoperative complications was as follows:

Postoperative patients fasted with water, were routinely treated with acid suppression, nutritional support, and mucosal repair and were observed for complications such as dyspnea, fever, hematemesis, gastrointestinal bleeding, or abdominal distension.

From the date of discharge, the patients were followed up by telephone, WeChat, and other means. The patients were asked to return to the clinic for gastroscopy or ultrasonic gastroscopy for 3~6 months and 1 year to observe and evaluate the wound healing status and whether there were complications such as residual lesions or recurrence.

2.4. Statistical Analysis. The SPSS23.0 statistical software was used to process the data, in which ($x \pm s$) represented the measurement data, while the counting data were expressed by the number of cases (n), (%) represented the intergroup rate, and the comparison between groups was made by the analysis of variance. The difference was statistically significant ($P < 0.05$).

3. Result

A total of 229 patients with gastric mucosal microtumors from January 2016 to June 2021 were selected. All patients were randomly divided into three groups group A, group B, and group C. There were 47 patients in group A, 17 males, and 30 females, aged 36–69 years, with an average age of 55.6 ± 9.2 years. There were 54 patients in group B, 18 males, and 36 females, aged 38–72 years, with an average age of 57.6 ± 7.7 years. There were 128 patients in group C, 29 males, and 99 females, aged 33–78 years, with an average age of 55.6 ± 8.4 years. There was no difference in the age, sex, intraoperative blood loss, intraoperative perforation rate, and endoscopic complete resection rate of the selected patients ($P > 0.05$), Table 1.

3.1. Comparison of Complication Rates among the Three Groups. The incidence of postoperative complications in group B was significantly higher than that in group A and group C (all $P < 0.05$). The incidence of postoperative complications in group A was higher than that in group C, and the difference was statistically significant ($P < 0.05$), Table 2.

4. Discussion

A gastric submucosal tumor is one of the most common clinical tumors [16]. In recent years, although the incidence of gastric submucosal tumors is increasing year by year, the overall prognosis of the disease is good. Surgery or endoscopic resection is the main treatment [17, 18]. The gastric submucosal tumor is a kind of lesion that originated from the submucous layer, its surface is covered by normal mucosal tissue, showing as a protuberant lesion, and routine biopsy usually cannot obtain an accurate pathological diagnosis, so it has a high risk of malignant transformation

Table 1: Baseline characteristics of participants.

	Group A ($N = 47$)	Group B ($N = 54$)	Group C ($N = 128$)
Gender (male/female, example)	17/30	18/36	29/99
Age ($x \pm S$, year)	55.6 ± 9.2	57.6 ± 7.7	55.6 ± 8.4
Intraoperative blood loss (ml)	0.2 ± 0.9	0.3 ± 1.2	3.1 ± 10.0
Intraoperative perforation rate (%)	82.1%	83.3%	40.8%
Endoscopic complete resection rate (%)	93.6%	92.8%	92.5%

Table 2: Comparison of the incidence of complications among the three groups (n (%)).

Group	n	Dyspnea	Fever	Abdominal distension	Gastrointestinal bleeding	Abdominal pain	Total incidence (%)
Group A	47	0 (0)	2 (4.3)	1 (2.1)	0 (0)	24 (51.1)	27 (57.4)
Group B	54	0 (0)	1 (1.9)	5 (9.3)	0 (0)	30 (55.6)	36 (66.7)
Group C	128	0 (0)	3 (2.3)	4 (3.1)	2 (1.6)	60 (46.9)	69 (53.9)

[19, 20]. The main clinical manifestations are gastrointestinal obstruction, gastrointestinal bleeding, abdominal pain, and fever, which seriously threaten the life safety and quality of life of patients [21].

Conventional laparotomy is the most important and effective treatment for large gastric submucosal tumors [22]. Endoscopic treatment is mainly used for patients with small submucosal tumors (< 20 mm), of which endoscopic submucosal tumor resection is more effective and less risky for submucosal tumors with diameters of 10–20 mm, endoscopic mucosal resection is a minimally invasive procedure for the treatment of submucosal tumors of the gastrointestinal tract, the utility model has the advantages of accurate positioning, high block resection rate, reducing the chance of residual and recurrence, realizing radical treatment, less trauma, few complications, no change of the structure of the digestive tract, safety and effectiveness in treating the pathological changes of the digestive tract and so on [23, 24]. At present, it has been accepted by international endoscopists and is widely used in the endoscopic resection of digestive tract lesions [25]. Now it has been used as a standard measure for endoscopic treatment of submucosal gastric masses. However, for gastric submucosal tumors with smaller diameters (< 10 mm), endoscopic mucosal resection is too complex and difficult to operate [26–28]. Therefore, transparent cap-assisted endoscopic full-thickness resection is also known as transparent cap suction tumor stripping, which is gradually applied in the clinic. Transparent cap-assisted endoscopic full-thickness resection has the advantages of simple and fast operation, short operation time, high resection integrity rate, and sufficient postoperative resection tissue for the identification of the nature of gastric submucosal tumors with a diameter of less than 10 mm [29].

The results of this study showed that the incidence of complications in group A was lower than those in group B. The results show that a transparent cap combined with ring-assisted endoscopic resection is very beneficial to the treatment of gastric mucosal microtumors, reducing the incidence of complications. The results show that a transparent cap combined with ring-assisted endoscopic resection can effectively promote early postoperative recovery and reduce the incidence of complications.

Based on the above findings, although endoscopic mucosal resection and ligator combined with circle-assisted endoscopic resection with ligator combined with ligation are effective and safe measures for the treatment of gastric mucosal microtumors, they should also be combined with targeted nursing measures. In order to reduce the amount of intraoperative bleeding and reduce the incidence of complications. The transparent cap combined with ring-assisted endoscopic resection has a significant effect on the treatment of small gastric mucosal tumors, reduces surgical complications, and improves the level of diagnosis and treatment. In conclusion, the transparent cap combined with ring-assisted endoscopic resection is more suitable for the endoscopic treatment of small gastric mucosal tumors.

Data Availability

The data used to support the findings of this study are available from the corresponding author upon request.

Conflicts of Interest

The authors declare that they have no conflicts of interest..

References

[1] A. Dhali, A. Sarkar, S. Ray, D. N. Biswas, G. K. Dhali, and A. Mahajan, "Hepatic artery pseudo-aneurysm rupturing into hepato-gastric fistula, a rare cause of massive upper gastrointestinal hemorrhage: case report," *Radiology Case Reports*, vol. 17, no. 1, pp. 133–136, 2022.

[2] J. D. Prologo, "Percutaneous CT-guided cryovagotomy," *Techniques in Vascular and Interventional Radiology*, vol. 23, no. 1, Article ID 100660, 2020.

[3] A. Gosselin-Tardif, M. Abou-Khalil, J. Mata et al., "Laparoscopic versus open subtotal gastrectomy for gastric adenocarcinoma: cost-effectiveness analysis," *BJS Open*, vol. 4, no. 5, pp. 830–839, 2020.

[4] M. D. Spann, C. V. Aher, W. J. English, and D. B. Williams, "Endoscopic management of erosion after banded bariatric procedures," *Surgery for Obesity and Related Diseases*, vol. 13, no. 11, pp. 1875–1879, 2017.

[5] D. Zhang, Q. Lin, R. Shi, L. Wang, J. Yao, and Y. Tian, "Ligation-assisted endoscopic submucosal resection with apical mucosal incision to treat gastric subepithelial tumors

originating from the muscularis propria," *Endoscopy*, vol. 50, no. 12, pp. 1180–1185, 2018.

[6] R. S. Azzam, "Are the persistent symptoms to proton pump inhibitor therapy due to refractory gastroesophageal reflux disease or to other disorders?" *Arquivos de Gastroenterologia*, vol. 55, no. 1, pp. 85–91, 2018.

[7] L. Monino, J. M. Gonzalez, V. Vitton, and M. Barthet, "Antireflux mucosectomy band in treatment of refractory gastroesophageal reflux disease: a pilot study for safety, feasibility and symptom control," *Endoscopy International Open*, vol. 8, no. 2, pp. E147–E154, 2020.

[8] E. N. F. T. Enigma, T. Tran-Nguyen, G. Fernandez-Esparrach et al., "Biopsy sampling in upper gastrointestinal endoscopy: a survey from 10 tertiary referral centres across europe," *Digestive Diseases*, vol. 39, no. 3, pp. 179–189, 2021.

[9] F. Rettura, F. Bronzini, M. Campigotto et al., "Refractory gastroesophageal reflux disease: a management update," *Frontiers of Medicine*, vol. 8, Article ID 765061, 2021.

[10] F. Bas-Cutrina, C. F. Consiglieri, J. Bosch-Schips, and J. B. Gornals, "Endoscopic band ligation plus single-incision needle knife biopsy for small subepithelial deep-layer tumor: easy and effective," *Endoscopy*, vol. 51, no. 07, pp. E191–E192, 2019.

[11] Y. W. Guo, H. B. Miao, Z. F. Wen, J. Y. Xuan, and H. X. Zhou, "Procedure-related complications in gastric variceal obturation with tissue glue," *World Journal of Gastroenterology*, vol. 23, no. 43, pp. 7746–7755, 2017.

[12] M. Sonmez, D. Ficai, A. Ficai et al., "Applications of mesoporous silica in biosensing and controlled release of insulin," *International Journal of Pharmaceutics*, vol. 549, no. 1-2, pp. 179–200, 2018.

[13] L. Chen, X. Ming, R. Gu et al., "Treatment experience of delayed massive gastrointestinal bleeding caused by intra-abdominal arteriointestinal fistula in gastric cancer patients after radical gastrectomy," *World Journal of Surgical Oncology*, vol. 17, no. 1, p. 201, 2019.

[14] K. Hashiba, C. A. Cappellanes, P. R. de Siqueira et al., "Applying basic principles of surgery may pave the way for more effective endoscopic bariatric techniques," *Endoscopy International Open*, vol. 9, no. 7, pp. E1049–E1054, 2021.

[15] M. Ogawa, S. Arihiro, N. Matsuhashi et al., "The early therapeutic response at 2 weeks is a crucial predictor of proton pump inhibitor-refractory gastroesophageal reflux disease," *Esophagus*, vol. 18, no. 2, pp. 398–406, 2021.

[16] R. D. Naik, M. H. Meyers, and M. F. Vaezi, "Treatment of refractory gastroesophageal reflux disease," *Gastroenterology and Hepatology*, vol. 16, no. 4, pp. 196–205, 2020.

[17] K. Tsuchida, H. Saeki, M. Yasukawa et al., "Short-Term outcomes of laparoscopic-assisted total gastrectomy using the endoscopic purse-string suture instrument ENDO-PSI," *Gan To Kagaku Ryoho*, vol. 46, no. 13, pp. 2503–2505, 2019.

[18] K. K. Limpias, N. Hosoe, K. Takabayashi et al., "Endoscopic removal of foreign bodies: a retrospective study in Japan," *World Journal of Gastrointestinal Endoscopy*, vol. 12, no. 1, pp. 33–41, 2020.

[19] M. Naga, M. Wahba, H. Okasha et al., "Comparative study of tissue adhesive therapy versus band ligation in control of actively bleeding esophageal varices," *Acta GastroenterolOGY Belg*, vol. 83, no. 1, pp. 5–10, 2020.

[20] S. Shibasaki, K. Suda, M. Nakauchi et al., "Robotic valvuloplastic esophagogastrostomy using double flap technique following proximal gastrectomy: technical aspects and short-term outcomes," *Surgical Endoscopy*, vol. 31, no. 10, pp. 4283–4297, 2017.

[21] A. Patel and R. Yadlapati, "Diagnosis and management of refractory gastroesophageal reflux disease," *Gastroenterology and Hepatology*, vol. 17, no. 7, pp. 305–315, 2021.

[22] Q. J. Zhuang, N. D. Tan, S. F. Chen, M. Y. Zhang, and Y. L. Xiao, "Magnetic sphincter augmentation in treating refractory gastroesophageal reflux disease: a systematic review and meta-analysis," *Journal of Digestive Diseases*, vol. 22, no. 12, pp. 695–705, 2021.

[23] S. J. Spechler, "Refractory gastroesophageal reflux disease and functional heartburn," *Gastrointestinal Endoscopy Clinics of North America*, vol. 30, no. 2, pp. 343–359, 2020.

[24] P. Rao, C. R. Schmidt, and B. A. Boone, "Robot assisted distal pancreatectomy with celiac Axis resection (DP-CAR) for pancreatic cancer: surgical planning and technique," *Journal of Visualized Experiments*, vol. 174, 2021.

[25] G. Du, E. Jiang, Y. Qiu et al., "Feasibility and preliminary technical experience of single incision plus one port laparoscopic total gastrectomy combined with π-shaped esophagojejunal anastomosis in surgical treatment of gastric cancer," *Zhonghua Wei Chang Wai Ke Za Zhi*, vol. 21, no. 5, pp. 556–563, 2018.

[26] T. Lin, J. Yu, Y. Hu et al., "Preliminary experience of dual-port laparoscopic distal gastrectomy for gastric cancer," *Zhonghua Wei Chang Wai Ke Za Zhi*, vol. 22, no. 1, pp. 35–42, 2019.

[27] P. M. Sy, N. Anton, Y. Idoux-Gillet et al., "Pickering nanoemulsion as a nanocarrier for pH-triggered drug release," *International Journal of Pharmacy*, vol. 549, no. 1-2, pp. 299–305, 2018.

[28] W. M. Seleem, A. S. Hanafy, and S. I. Mohamed, "Endoscopic management of refractory gastroesophageal reflux disease," *Scandinavian Journal of Gastroenterology*, vol. 53, no. 4, pp. 390–397, 2018.

[29] T. Wu, R. Sun, M. Zhang et al., "A new diagnostic method using air perfusion radiography under DSA for gastric stump-pleural fistula: report of five cases," *Thoracic Cancer*, vol. 10, no. 8, pp. 1736–1738, 2019.

Hindawi
Evidence-Based Complementary and Alternative Medicine
Volume 2023, Article ID 9853204, 1 page
https://doi.org/10.1155/2023/9853204

Retraction

Retracted: Synchronous Colorectal Liver Metastases considering Infectious Complications: Simultaneous or Delayed Surgery?

Evidence-Based Complementary and Alternative Medicine

Received 3 October 2023; Accepted 3 October 2023; Published 4 October 2023

This article has been retracted by Hindawi following an investigation undertaken by the publisher [1]. This investigation has uncovered evidence of one or more of the following indicators of systematic manipulation of the publication process:

(1) Discrepancies in scope
(2) Discrepancies in the description of the research reported
(3) Discrepancies between the availability of data and the research described
(4) Inappropriate citations
(5) Incoherent, meaningless and/or irrelevant content included in the article
(6) Peer-review manipulation

The presence of these indicators undermines our confidence in the integrity of the article's content and we cannot, therefore, vouch for its reliability. Please note that this notice is intended solely to alert readers that the content of this article is unreliable. We have not investigated whether authors were aware of or involved in the systematic manipulation of the publication process.

In addition, our investigation has also shown that one or more of the following human-subject reporting requirements has not been met in this article: ethical approval by an Institutional Review Board (IRB) committee or equivalent, patient/participant consent to participate, and/or agreement to publish patient/participant details (where relevant).

Wiley and Hindawi regrets that the usual quality checks did not identify these issues before publication and have since put additional measures in place to safeguard research integrity.

We wish to credit our own Research Integrity and Research Publishing teams and anonymous and named external researchers and research integrity experts for contributing to this investigation.

The corresponding author, as the representative of all authors, has been given the opportunity to register their agreement or disagreement to this retraction. We have kept a record of any response received.

References

[1] L. Huang, X. Tang, J. Fang, Z. Zheng, and H. Wei, "Synchronous Colorectal Liver Metastases considering Infectious Complications: Simultaneous or Delayed Surgery?" *Evidence-Based Complementary and Alternative Medicine*, vol. 2022, Article ID 5268554, 7 pages, 2022.

Hindawi
Evidence-Based Complementary and Alternative Medicine
Volume 2022, Article ID 5268554, 7 pages
https://doi.org/10.1155/2022/5268554

Research Article

Synchronous Colorectal Liver Metastases considering Infectious Complications: Simultaneous or Delayed Surgery?

Lijun Huang, Xiao Tang, Jiafeng Fang, Zongheng Zheng, and Hongbo Wei

Department of Gastrointestinal Surgery, The Third Affiliated Hospital of Sun Yat-sen University, Guangzhou 510630, Guangdong Province, China

Correspondence should be addressed to Zongheng Zheng; zhengzh@mail.sysu.edu.cn and Hongbo Wei; weihb@mail.sysu.edu.cn

Received 29 June 2022; Revised 24 July 2022; Accepted 28 July 2022; Published 11 October 2022

Academic Editor: Xueliang Wu

Background. Simultaneous or delayed surgery for synchronous colorectal liver metastases is performed in the clinic; which method is better is still up for debate. In particular, infectious complications are rarely compared. This study aims to investigate the differences between simultaneous and delayed surgery for synchronous colorectal liver metastases by comparing infectious complications and prognosis. *Methods*. Firstly, the patients' information from a single institution's database was retrospectively analyzed. Then the patients were divided into a simultaneous group and a delayed group according to synchronous colorectal liver metastases. Analyzing the postoperative complications within 30 days, the progression-free survival, and the overall survival in the two groups. *Results*. The simultaneous group had a higher neo-adjuvant chemotherapy rate (42.0% VS. 16.0% in the delayed group, $P < 0.05$) and laparoscopic surgery rate (89.8% VS. 72.0% in the delayed group, $P < 0.05$) than the delayed group. Moreover, the simultaneous group had a higher liver-related infection rate (17.0 VS. 0.0% in the delayed group, $P < 0.05$). *Conclusion*. Although there was no difference in survival rate between delayed and simultaneous surgeries, the delayed surgery have fewer liver-related infections compared with the simultaneous surgery in synchronous colorectal liver metastases patients. Delayed surgery could be a better treatment method for synchronous colorectal liver metastases patients.

1. Introduction

Colorectal cancer (CRC) is the third most frequent cancer disease, which claims more than 880,000 lives each year worldwide. It has been a major public health concern in the world [1–3]. Nearly 50% of CRC patients develop liver metastases, and at the time of initial diagnosis, 15% to 25% of CRC patients have synchronous liver metastases (SLM) [4]. Surgery containing resection or ablation of the liver metastasis is the curative way of dealing with the SLM [5]. A thorough resection of liver metastasis would improve survival and be associated with a 5-year survival rate of up to 40% [6–8]. However, the timing of the operation remains a matter of debate. Resection of synchronous colorectal liver metastasis can be performed via simultaneous surgery or delayed surgery. Simultaneous surgery means simultaneous resection on the same operative day. Delayed surgery indicates the two surgeries are carried out on separate operative days with a period of recovery. Compared with simultaneous surgery, delayed surgery is a traditional choice and focuses on the resection of the primary tumor first, followed by subsequent resection of the liver metastases in 3–6 months [9]. However, it is often thought that simultaneous surgery may avoid delayed removal of metastatic disease and reduce the risk of cancer spreading further [10]. However, it may lead to more surgical morbidity, especially in complex colorectal or liver resection, and should be considered [11].

Some retrospective and prospective studies reported that it was safe or not to treat liver metastasis along with primary cancer simultaneously. Compared with delayed liver surgery following resection of colorectal cancer, the simultaneous approach may have clear advantages in the hospital stay interval, the operation time, and most of all, avoiding another surgery [4, 12]. However, some studies report much higher mortality and severe complication rate in the

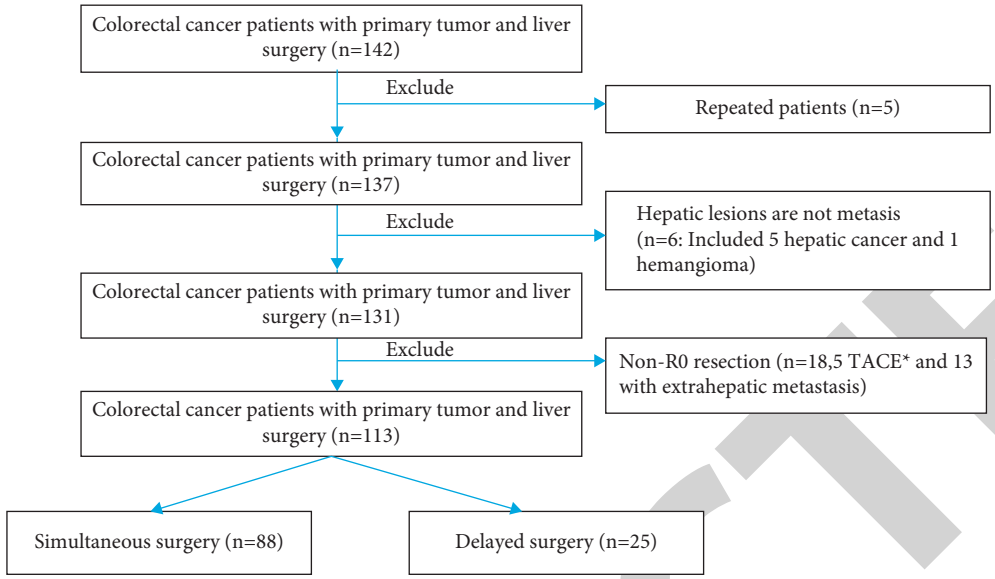

Figure 1: Sample screening scheme diagram.

simultaneous procedure [13, 14]. Therefore, the choice between simultaneous or delayed resection of the colorectal and liver remains controversial.

So far, most studies have compared the safety of the two methods in terms of postoperative complications. However, few studies pay close attention to infectious complications. As a common complication, perioperative infection not only influences the safety but also the long-term survival of the patients [5, 15]. Considering the complications of infection, more studies are needed on simultaneous and delayed surgery with simultaneous colorectal liver metastases. In our institution, the simultaneous way was well accepted, while the delayed way was chosen in a few cases, especially for some complex cases. It seems that the simultaneous surgery would lead to more infectious complications. Therefore, we conducted this retrospective study to compare the safety and prognosis of simultaneous surgery and delayed surgery. We aimed to investigate the differences between simultaneous and delayed surgery for synchronous colorectal liver metastases by comparing infectious complications and prognosis.

2. Materials and Methods

2.1. Samples Collection and Design. Colon cancer with liver metastasis patients who underwent liver resection from July 2011 to November 2020 in the Third Affiliated Hospital of Sun Yat-sen University was included.

2.1.1. Inclusion Criteria. Age ≥18; histologically confirmed adenocarcinoma of the primary tumor; liver metastases found at the same time; no extrahepatic metastases; tumor R0 removing after the surgical treatments.

2.1.2. Exclusion Criteria. Non-R0 resection of the hepatic lesions; hepatic lesions confirmed nonmetastases after surgery; extrahepatic metastases were found during the surgical interval of the delayed way.

The sample screening scheme was shown in Figure 1. Firstly, colorectal cancer patients with primary tumors and liver surgery (142 patients) were collected. After excluding repeated patients, patients with the nonmetastatic hepatic lesion, and patients with non-R0 resection, 113 patients were selected and divided into two groups: simultaneous group ($n = 88$) and delayed group ($n = 25$). The simultaneous group also called the synchronous group and defined as curative treatment of SLM, either with resection, radiofrequency ablation (RFA), or microwave ablation (MWA), was performed in one operation with resection of the primary tumor. While the delayed group was defined as curatively resecting the primary tumor first, followed by treatment of SLM a few months later. Examined variables including baseline clinic pathological data, operative factors, perioperative elements, infectious outcomes, and prognostic outcomes were collected by reviewing the hospital's archiving system or by contacting the patients and their treating doctors.

2.2. Data Definition and Management. For the delayed group, the bleeding volume and operation time in the separated surgery were added together to compare with the synchronous group. The overall survival (OS) time was defined as the time from the resection of the primary tumor to the death of the patient or the end point of follow up. The progression-free survival (PFS) time was defined as the time from the resection of the primary tumor to the progression of cancer or the end point of follow up. Complications were based on a standardized grading scale and the Clavien-Dindo classification of surgical complications [16]. This study was approved by the Ethics Committee of the Third Affiliated Hospital, Sun Yat-Sen University. The ethics number was [2022]02-031-01.

2.3. Statistical Analysis. Statistical analysis was performed using SPSS 21.0 (IBM SPSS Statistics 21.0). Continuous variables were expressed as mean ± standard deviation (SD),

Table 1: Group information and characteristics of two groups.

Characteristics	Simultaneous group $n = 88$	Delayed group $n = 25$	P Value
Gender (male/female)	59/29	20/5	0.213
Mean age	60.1 ± 12.7	59.7 ± 13.4	0.908
BMI (kg/m2)	22.40 ± 3.25	22.76 ± 3.55	0.637
Intestinal obstruction (Y/N*)	13/75	7/18	0.126
Abdominal infection (Y/N)	1/87	1/24	0.338
History of abdominal surgery (Y/N)	12/76	3/22	0.831
Diabetes (Y/N)	15/73	5/20	0.733
Cardiovascular disease (Y/N)	28/60	5/20	0.251
Pulmonary disease (Y/N)	2/86	0/25	0.447
Hepatic disease (Y/N)	12/76	2/23	0.450
Smoking (Y/N)	17/71	3/22	0.398
Alcohol abuse (Y/N)	10/78	3/22	0.930
Site of primary tumor (right colon/left colon/rectum)	23/33/32	4/10/11	0.558
Size of the primary tumor (≤3 cm/>3 cm)	38/50	12/13	0.669
Differentiation (well or medial/poor)	79/9	22/3	0.800
Number of liver metastases	2.4 ± 1.8	2.4 ± 2.6	0.996
The biggest size of liver metastases (cm)	2.7 ± 1.6	2.2 ± 1.4	0.196
Location of liver metastases (right lobe/left lobe/both)	44/13/31	5/2/18	0.149
Red blood cell transfusion (Y/N)	3/85	5/20	0.004
Parenteral nutrition (Y/N)	7/81	3/22	0.994
Neo-adjuvant chemotherapy (Y/N)	37/51	4/21	0.017
Oral antibiotics preparation (Y/N)	28/60	9/16	0.694
ASA score (I, II/III, IV, V)	83/5	25/0	0.223

*Y/N is Yes/No.

and any significant differences between the two groups were assessed by Student's t-test. Categorical variables were assessed by the chi-square test. Progression-free survival and overall survival were calculated using the Kaplan-Meier method, and differences in survival were estimated using the generalized log-rank test. In all analyses, $P < 0.05$ was considered to indicate statistical significance.

3. Results

3.1. Samples Screening and Analysis. As shown in Figure 1, data from these 113 patients were used to do the analyses. The endpoint of follow up was February 23, 2022. The median follow up time was 38 months (16–121 months). No one dropped off. To end, 40 patients died, and the overall survival rate was 64.6%.

The preoperative characteristics of the two groups were shown in Table 1. Totally, there were 79 males and 34 females; and the median age was 60.0 ± 12.8 years (age range 20–84 years). There was a similar distribution in gender, age, BMI, intestinal obstruction, abdominal infection, history of abdominal surgery, diabetes, cardiovascular disease, pulmonary disease, hepatic disease, smoking, alcohol abuse, site of the primary tumor, size of the primary tumor, differentiation, number of liver metastases, biggest size of liver metastases, location of liver metastases, parenteral nutrition, oral antibiotics preparation, and ASA score. While the synchronous group had fewer red blood cell transfusion rate compared with the delayed group (3.4% VS. 20.0%, $P = 0.004$) and a higher neo-adjuvant chemotherapy rate (42.0% VS. 16.0%, $P = 0.017$).

3.2. Comparison of Intraoperative Characteristics. As for the intro-operative characteristics (shown in Table 2), there are no differences in the right colectomy rate, stoma rate, and red blood cell transfusion rate. The difference between surgical way for liver lesions and combined organ resection among them was not significant ($P > 0.05$). They had similar bleeding volume and operation time, but the delayed group had a lower laparoscopic surgery rate for the primary tumor compared with the simultaneous group (72.0% VS. 89.8%, $P = 0.024$).

3.3. Comparison of Postoperative Characteristics. As for the post operative characteristics, the comparison of Management, Pathology, and Clinical Risk Score (CRS) was operated on (Table 3). Moreover, the CRS, as a clinical score, is usually used to assess the risk of recurrence of colorectal cancer liver metastases, and 3–5 is divided into high risk of recurrence.

There was no perioperative death or severe liver failure. For the cases with complications, the total number was 37, and the hospital stay after surgery ranged from 10 to 107 days while the median was 14 days. Meanwhile, Table 4 showed that the simultaneous group had a higher liver-related infection rate (17.0 VS. 0.0% in the delayed group, $P = 0.027$), but there was no difference in other complications between groups.

3.4. Comparison Analysis of PFS and OS between Groups. The PFS and OS rate trends were similar in both groups, which was shown in Figure 2. The 1-year, 3-year, and 5-year

Table 2: Comparison of intro-operative characteristics.

Characteristics	Simultaneous group $n = 88$	Delayed group $n = 25$	P value
Surgery for primary tumor (laparoscopic/open)	79/9	18/7	0.024
Right colectomy (Y/N)	23/65	4/21	0.294
Stoma (Y/N)	5/83	2/23	0.671
Surgery for liver lesions (ablation/resection/both)	61/22/5	22/3/0	0.147
Combined organ resection (Y/N)	1/87	0/25	0.592
Red blood cell transfusion (Y/N)	9/79	3/22	0.800
Bleeding volume (ml)	157.05 ± 353.51	78.40 ± 70.10	0.272
Operation time (min)	340.40 ± 97.66	324.08 ± 88.67	0.454

Table 3: Comparison of postoperative characteristics.

Characteristics		Simultaneous group $n = 88$	Delayed group $n = 25$	P value
Management	Time of preventive antibiotic use (POD*)	4.76 ± 3.56	4.96 ± 2.68	0.797
	Time of abdominal drainage (POD)	4.55 ± 3.67	5.56 ± 7.67	0.356
	Postoperative hospital stay (POD)	14.07 ± 18.00	9.32 ± 7.44	0.053
	Postoperative chemotherapy	88/0	25/0	NA
Pathology	Tumor invasion (1–3/4)	24/64	3/22	0.114
	Lymph node (P/N**)	59/29	20/5	0.213
	Vascular cancer thrombus (Y/N)	23/65	7/18	0.852
	Nerve invasion (Y/N)	18/70	9/16	0.108
CRS***	1/2 VS. 3/4/5	13/33 VS. 39/3/0	2/13 VS. 10/0/0	0.455

∗ POD, postoperation day; ** P/N, positive/negative; *** CRS, Clinical Risk Score.

Table 4: Occurred postoperative complications.

	Clavien-dindo grade*	Simultaneous group $n = 88$	Delayed group $n = 25$	P value
Bleeding		8	1	0.278
	II/IIIa/IIIb/IVa/IVb	7/0/0/1/0	1/0/0/0/0	
Bowl obstruction		4	0	0.407
	II/IIIa/IIIb/IVa/IVb	4/0/0/0/0	0/0/0/0/0	
Liver-related infection		15	0	0.027
Bile leakage	II/IIIa/IIIb/IVa/IVb	0/1/0/0/0	0/0/0/0/0	
Abscess around liver	II/IIIa/IIIb/IVa/IVb	2/9/1/1/1	0/0/0/0/0	
Bowl-related infection		4	2	0.497
Anastomotic leakage	II/IIIa/IIIb/IVa/IVb	0/0/3/0/0	0/0/1/1/0	
Abscess around intestine	II/IIIa/IIIb/IVa/IVb	0/1/0/0/0	0/0/0/0/0	
Wound infection		7	1	0.333
	II/IIIa/IIIb/IVa/IVb	6/1/0/0/0	0/1/0/0/0	
Others**		8	2	0.865
	II/IIIa/IIIb/IVa/IVb	6/1/0/1/0	1/0/0/0/1	
Total		32	5	0.124

*Postoperative usage of analgesics and antiemetic is a routine treatment in our department. We cannot distinguish Grade 1 complications, so complications are defined as more than Grade 2. ∗ ∗ Other complications contain urinary tract infection, pulmonary infection, and catheter-related infection.

PFS rate was 54.5%, 37.0%, and 32.8% in the simultaneous group, while 48.0%, 8.9%, and 8.9% in the delayed group. As for OS rate, 96.6%, 64.8% and 55.5% in the simultaneous group and 96.0%, 70.3% and 58.7% in the delayed group, respectively.

4. Discussion

Surgical site infections, especially intro-abdominal infections, like liver abscesses and anastomotic leakage, can influence the safety and long-term survival of colorectal cancer patients with synchronous liver metastases after surgery [5, 15, 17, 18]. We firstly focused on the infectious complications after surgical treatments of CRC with SLM and found that the simultaneous group had a higher infection rate. These results suggested that surgeons should pay more attention to the liver-related infection when doing the synchronous procedure, not just the total surgical site infection rate. Doughtie et al. reported similar results [19]. They compared the infectious complications in combined

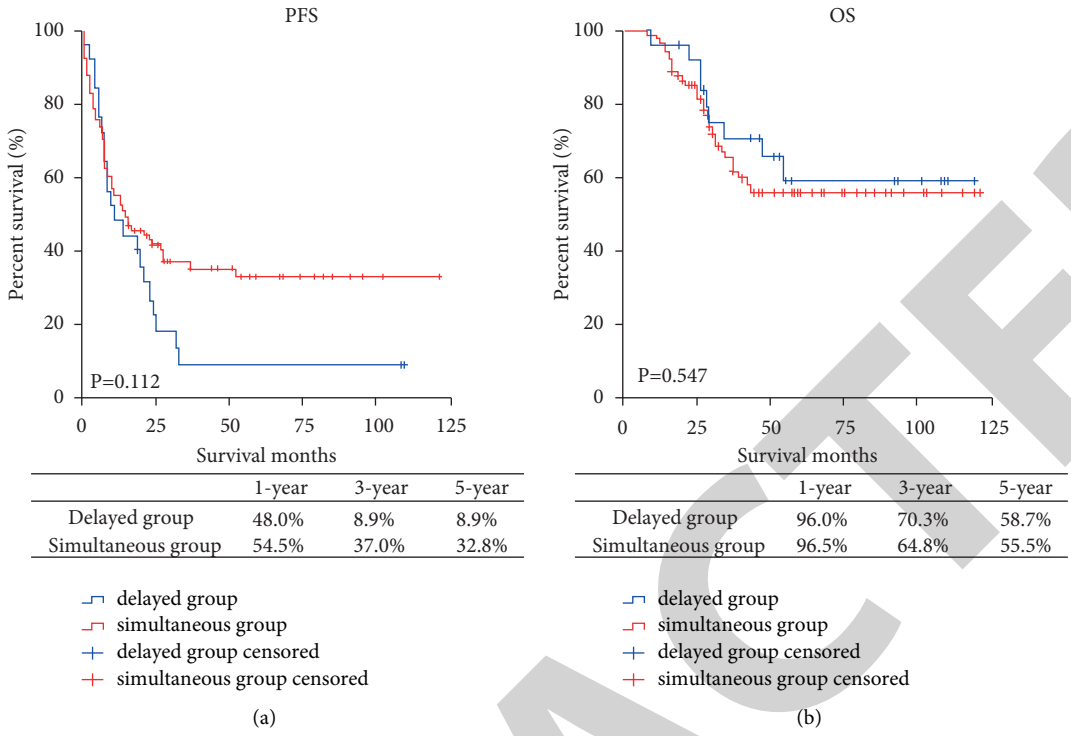

	1-year	3-year	5-year
Delayed group	48.0%	8.9%	8.9%
Simultaneous group	54.5%	37.0%	32.8%

	1-year	3-year	5-year
Delayed group	96.0%	70.3%	58.7%
Simultaneous group	96.5%	64.8%	55.5%

Figure 2: Comparison of the PFS (a) and OS, (b) between groups.

colon resection and ablation of colorectal liver metastases and found that high-grade (grade, III to V) complications and liver-specific complications were significantly increased in the combined ablation group. In 2020, a meta-analysis study reported the overall morbidity rate in the simultaneous resection group was 39.2%, compared to 32.8% in the staged resection group, with a pooled number of 7639 patients. No significant difference was found (OR 1.04; 95% CI 0.89–1.22; $P == 0.63$) [4]. The authors also gave data that compared anastomotic leaks, bile leaks, intra-abdominal abscesses, and subphrenic abscesses. The complication rates of the simultaneous resection group were all higher except for bile leak, but with no significant difference [4]. They did not compare the overall intro-abdominal infection rate. Another meta-analysis study containing 5300 patients in 2018 also confirmed that no statistically significant differences were found in safety and efficacy between the simultaneous and delayed hepatectomy cohorts, but the shorter length of hospital stay in the simultaneous group [20]. In 2021, a single prospective randomized controlled study was designed as a multi-center study with aimed at 222 enrolled patients. However, the enrollment was stopped at Number 85 due to no evidence of a difference in major complications between groups, and the potential of bad prognosis in the staged group [12]. When we went through the data again, the abdominal infection rate was 33.3% (13/39) in simultaneous resection and 13.0% (6/45) in delayed resection ($P < 0.05$). All these results suggested the safety of simultaneous colorectal and hepatic resection was unclear, and no study discussed the infectious complications alone. Our retrospective data showed that there might be more infections in simultaneous resection, suggesting that safety should be judged again.

It is still controversial whether synchronous colorectal cancer liver metastases (SLM) should be resected simultaneously with primary cancer or should be delayed. Firstly, both two procedures have their advantages and disadvantage. From the perspective of safety, the number of operations and anesthesia can be saved during the same period of surgery. Moreover, Gavriilidis et al. have reported that the hospital stay was significantly reduced during the same period of surgery [20]; However, a single operation may lead to a large wound area, much more operation time, and a high complication rate. Jessica Bogach et al. have even found in a retrospective cohort study that the 90-day postoperative mortality was higher[14], and the risk of each operation in a staged way might be low, but the interval between operations increased the number of chemotherapy, and might also increase the incidence of complications [21]. However, there was also some literature indicating that chemotherapy did not increase perioperative complications [22].

Furthermore, in terms of long-term prognosis, the preliminary results of a French multi-center randomized controlled study have shown that the staged group may have poor overall survival [5]. The main reason was that the disease progression of 8 cases in the staging group led to the termination of the experiment. This indicated that the study design was not perfect, and the oncology safety of the enrolled patients was not much enough considered. Thus, the results are not convincing. Bogach et al. have reported that simultaneous surgery may shorten the median overall survival (40 months, 95%CI 35–46 vs. 78 months, 95%CI

59–86) from a large retrospective cohort study [14]. Some recent reports have shown that PFS and OS are not significantly different, but the selection bias is obvious [4, 20]. Therefore, the pros and cons of these two surgical methods in terms of long-term survival are currently uncertain. Finally, it is still inconsistent about the definition of simultaneous liver metastasis of colorectal cancer in the published literature, including simultaneous discovery, and 3, 6, or 12 months separated, also cannot be homogenized [14]. Here are the results showing that based on the initial assessment of radically resectable concurrent liver metastases of colorectal cancer as the research object, the PFS and OS of concurrent surgery are equivalent to staged surgery. However, it may increase post-operative perihepatic infectious complications, which is similar to the conclusions of the published paper. The pros and cons of these two surgical methods still need to be clarified by high-quality research.

Nowadays, both surgical methods have been used in clinics. Our institution's experience was that, first, the surgical plan selection of the simultaneous or staged resection mainly depends on the evaluation of the liver surgeon. Second, because of the diverse surgical methods (TaTME and other surgical methods) for middle and lower rectal cancer [23], the operation is complicated and difficult, the complication rate of anastomotic leakage has significantly increased [24, 25], and the same period surgery should be avoided as much as possible. Therefore, when designing RCT studies, we should not include middle and low rectal cancer, and try to exclude the cases that cannot be controlled by systemic therapy, so as to avoid the case of prospective RCT in France, where the tumors of 8 staging cases have progressed to unresectable tumors. The study was terminated in advance with the conclusion that the prognosis of staged resection was poor [12]. From the meta-analysis and large population cohort studies [4, 14, 20], when the condition of the patients is good and liver and rectal lesion resection is relatively simple and safe, simultaneous surgery could avoid the problems caused by multiple operations. Further, the surgical safety and long-term prognosis are not weaker than staged surgery. Therefore, we speculated that both simultaneous and staged surgery have their advantages, but more research is needed to clarify the respective surgical indications. It may be a more meaningful direction to start from infection-related complications.

Due to the limitations of retrospective research, case selection may be biased; furthermore, the period is large, and the choice of treatment methods may be different. However, the results of our study still have certain guiding significance for the selection of surgical methods for this type of patient.

5. Conclusions

Delayed surgery for synchronous colorectal liver metastases may have fewer infectious complications, especially hepatic infections, than the simultaneous way with no different survival rate. High-quality prospective studies are still needed to detect which way is better or to set up the surgical indications for simultaneous colorectal and hepatic resection of colorectal cancer with synchronous liver metastases. And we should pay more attention to the hepatic infection rate in the following studies to confirm the benefit of the delayed way.

Data Availability

The data used to support the findings of this study are available from the corresponding author upon request.

Conflicts of Interest

The authors state no conflicts of interest.

Authors' Contributions

Lijun Huang and Xiao Tang are co-first authors. Zong Heng Zheng and Hongbo Wei conceived and designed the experiments. Lijun Huang and Xiao Tang performed the experiments. Lijun Huang and Jiafeng Fang operated literature search and analyzed the data. Lijun Huang wrote the paper. All authors read and approved the final manuscript. Lijun Huang and Xiao Tang contributed equally to this work.

Acknowledgments

This study was supported by the grant from National Natural Science Foundation of China Youth Program (Grant no. 81901471) and Wu Jieping Medical Foundation (Grant No. 320.2710.1822).

References

[1] F. Bray, J. Ferlay, I. Soerjomataram, R. L. Siegel, L. A. Torre, and A. Jemal, "Global cancer statistics 2018: GLOBOCAN estimates of incidence and mortality worldwide for 36 cancers in 185 countries," *CA: A Cancer Journal for Clinicians*, vol. 68, no. 6, pp. 394–424, 2018.

[2] WHO, *Globocan: World Health Organization*, WHO, Geneva, Switzerland, 2019.

[3] S. Ø Jensen, N. Øgaard, M. B. W. Ørntoft et al., "Novel DNA methylation biomarkers show high sensitivity and specificity for blood-based detection of colorectal cancer—a clinical biomarker discovery and validation study," *Clinical Epigenetics*, vol. 11, no. 1, p. 158, 2019.

[4] S. Hajibandeh, S. Hajibandeh, A. Sultana et al., "Simultaneous versus staged colorectal and hepatic resections for colorectal cancer with synchronous hepatic metastases: a meta-analysis of outcomes and clinical characteristics," *International Journal of Colorectal Disease*, vol. 35, no. 9, pp. 1629–1650, 2020.

[5] W. W. Kim, K. H. Kim, S. H. Kim et al., "Comparison of hepatic resection and radiofrequency ablation for the treatment of colorectal liver metastasis," *Indian Journal of Surgery*, vol. 77, no. S3, pp. 1126–1130, 2015.

[6] P. E. Serrano, C. S. Gu, M. Husien et al., "Risk factors for survival following recurrence after first liver resection for colorectal cancer liver metastases," *Journal of Surgical Oncology*, vol. 120, no. 8, pp. 1420–1426, 2019.

[7] E. K. Abdalla, R. Adam, A. J. Bilchik, D. Jaeck, J. N. Vauthey, and D. Mahvi, "Improving resectability of hepatic colorectal metastases: expert consensus statement," *Annals of Surgical Oncology*, vol. 13, no. 10, pp. 1271–1280, 2006.

Hindawi
Evidence-Based Complementary and Alternative Medicine
Volume 2023, Article ID 9864167, 1 page
https://doi.org/10.1155/2023/9864167

Retraction

Retracted: HDAC2 Induces DNA Methyltransferase DNMT3B Expression to Regulate the Wnt Signaling Pathway and Thus Promotes Glioma Development and Progression

Evidence-Based Complementary and Alternative Medicine

Received 8 August 2023; Accepted 8 August 2023; Published 9 August 2023

This article has been retracted by Hindawi following an investigation undertaken by the publisher [1]. This investigation has uncovered evidence of one or more of the following indicators of systematic manipulation of the publication process:

(1) Discrepancies in scope
(2) Discrepancies in the description of the research reported
(3) Discrepancies between the availability of data and the research described
(4) Inappropriate citations
(5) Incoherent, meaningless and/or irrelevant content included in the article
(6) Peer-review manipulation

The presence of these indicators undermines our confidence in the integrity of the article's content and we cannot, therefore, vouch for its reliability. Please note that this notice is intended solely to alert readers that the content of this article is unreliable. We have not investigated whether authors were aware of or involved in the systematic manipulation of the publication process.

Wiley and Hindawi regrets that the usual quality checks did not identify these issues before publication and have since put additional measures in place to safeguard research integrity.

We wish to credit our own Research Integrity and Research Publishing teams and anonymous and named external researchers and research integrity experts for contributing to this investigation.

The corresponding author, as the representative of all authors, has been given the opportunity to register their agreement or disagreement to this retraction. We have kept a record of any response received.

References

[1] X. Ren, Z. Jiang, and K. Xu, "HDAC2 Induces DNA Methyltransferase DNMT3B Expression to Regulate the Wnt Signaling Pathway and Thus Promotes Glioma Development and Progression," *Evidence-Based Complementary and Alternative Medicine*, vol. 2022, Article ID 1948766, 8 pages, 2022.

Hindawi
Evidence-Based Complementary and Alternative Medicine
Volume 2022, Article ID 1948766, 8 pages
https://doi.org/10.1155/2022/1948766

Research Article

HDAC2 Induces DNA Methyltransferase DNMT3B Expression to Regulate the Wnt Signaling Pathway and Thus Promotes Glioma Development and Progression

Xing Ren, Zhan Jiang, and Ke Xu

Department of Oncology, Radiotherapy Center, Chongqing General Hospital, Chongqing, China

Correspondence should be addressed to Ke Xu; plebron@une.edu

Received 13 July 2022; Revised 11 August 2022; Accepted 16 August 2022; Published 11 October 2022

Academic Editor: Xueliang Wu

Purpose. To investigate the role and molecular mechanism of HDAC2 in glioma. *Methods*. GSE16011, GSE31262, and GSE90598 datasets were used to identify co-expressed genes, GO analysis, and KEGG analysis to identify gene enrichment pathways, and PPI networks were constructed to identify gene interrelationships. HDAC2 enrichment on DNMT3B promoter and DNMT3B enrichment on Bcl2 CpG island was detected by a ChIP assay. The expression, prognosis, and hierarchical distribution of HDAC2, DNMT3B, and Bcl2 were examined in the CGGA database, and the correlation between HDAC2 and DNMT3B, Bcl2, and DNMT3B and Bcl2 was assessed. *Results*. The HDAC2-DNMT3B-Bcl2 axis is differentially expressed and interacts in gliomas. HDAC2 activates the transcriptional activity of DNMT3B, and DNMT3B inhibits the expression of Bcl2. HDAC2 and DNMT3B are highly expressed in gliomas and have a poor prognosis, while Bcl2 is lowly expressed in gliomas and has a good prognosis. *Conclusion*. HDAC2 promotes DNMT3B transcriptional repression of Bcl2 expression and Wnt pathway activity, thereby activating glioma cell activity in vitro and in vivo.

1. Introduction

Glioma is a common neurosurgical malignancy with an annual incidence of approximately 3–8 per 100,000 and 30,000 deaths per year. Like other tumors, glioma is caused by genetic and environmental carcinogenic factors. Gliomas are initially undetectable with no apparent symptoms, and as they increase in size or become cystic, symptoms of increased intracranial pressure or cerebrovascular compression such as localized epilepsy appear. When glioma is diagnosed, there are limitations to various treatments due to the specificity of its location, and it cannot be cured entirely, which is highly harmful to human beings. The specific treatment modalities for glioma are surgery, radiation, and chemotherapy. Although surgery has made some progress [1], it is challenging to eradicate glioma because of its aggressiveness and high recurrence rate; radiotherapy is not sensitive to most glioma tumors, and some sensitizers need to be added to assist in treatment. Although traditional chemotherapy is not as fast as surgery and radiotherapy, chemotherapy is still essential. It plays a vital role in glioma recurrence and the killing of residual tumor cells. Studies have shown that ACNU combined with TMZ is often used as adjuvant therapy after surgery and radiotherapy and is effective in preventing glioma recurrence after surgery. [2, 3]. However, the biggest problem facing chemotherapy for glioma is the increase in drug resistance, which is why glioma is challenging to cure, making it one of the worst prognoses among systemic tumor diseases [4]. Therefore, exploring the causes of chemotherapy resistance in glioma patients and trying to find drug resistance targets are of profound significance for glioma prognosis. Numerous studies have shown that histone deacetylase HDAC2 appears to be highly expressed in multiple types of cancer cells. For example, a study of tissue sections from clinical prostate cancer patients revealed that HDAC2 was differentially expressed in different grades of prostate cancer tissues, with higher expression with increasing progression [5]. A study of

sections from patients with squamous laryngeal carcinoma revealed that HDAC2 expression was significantly higher in the cancer site than that in the paracancerous tissue, and the survival rate of patients with low expression HDAC2 laryngeal squamous cell carcinoma was high under the same radiotherapy conditions [6]. This shows that the expression of HDAC2 is closely related to the grade of tumor progression, patient survival rate, and drug resistance. Numerous studies have demonstrated HDAC2 overexpression involving transcriptional processes of tumor-related genes such as oncogenes. Some researchers further investigated the relationship between HDAC2 and glioma [7] and found that HDAC2 expression was significantly higher in glioma multidrug-resistant cell lines than that in chemotherapy drug-sensitive lines. HDAC2 belongs to class I HDACs. Based on homology analysis, HDACs were classified into four categories: class I HDACs mainly include HDAC2, 2, 3, 8; class II consists of HDAC4, 5. HDACs are mainly composed of HDAC4, 5, 6, 7, 9, 10. Class III, the silent information regulator 2-related enzyme class, is an NAD + -dependent class of enzymes [8]; class IV HDACs occupy a separate class because they are different from classes I and II, mainly including HDAC21. HDACs are modified when the ATGC arrangement order of DNA HDAC2, as one of the more critical HDACs, has become a keen focus of researchers. HDAC2 mainly regulates histone and some nonhistone modifications. Rampalli et al. [9, 10] investigators found that SMAR1-related proteins in breast cancer are associated with HDAC2 by recruitment of HDAC2 Sin3 and retinoblastoma pocket proteins and inhibited the effects of cyclinD1 on cell cycle aspects by deacetylating the upstream region of cyclinD1 promoter on cyclin and found that the mechanism of action of oncogene SMAR1 is closely related to HDAC2.

The effect of HDAC2 expression on the morbidity trend and prognostic factors of prostate cancer patients was investigated. The deterioration grade of such cancer was proportional to HDAC2 expression. The high expression of HDAC2 in ERG (ETS-related gene) negative tumor cells is closely related to the gene fusion of TMPRSS2-ERG, expression of ERG, and deletion of PTEN, 5q, and 6q. The prognostic impact of HDAC2 is not dependent on established clinicopathological parameters and is expected to be a clinical, biochemical indicator for determining the risk grade of prostate cancer [11]. Aghdassi et al. [12] also found that invasive pancreatic cancer spread and metastasis were associated with the downregulation of E-calcine mucin, which is regulated by deacetylases 1 and 2. Overexpression of deacetylases 1 and 2 can reduce the amount of E-calcine mucin, allowing tumor cells to shuttle through the basement membrane to invade surrounding paracancerous tissues, resulting in enhanced tumor cell invasion and migration.

In contrast, HDACIs (histone deacetylase inhibitors) can inhibit the activity of some HDACs and therefore reduce the migratory force of tumor cells. Kumagai et al. [13, 14] found that in addition to E-calcine mucin, other anticancer factors such as retinoic acid receptor RARα, cycle regulator p21/WAF1, and transcription factor C/EBPα are also involved in HDACI-induced growth inhibition in pancreatic cancer. HDACIs, such as valproate (VPA) in combination with temozolomide (TMZ), a classical chemotherapeutic agent for glioma, can significantly increase E-calcine mucin expression in lung cancer in vitro experiments and enhance the efficacy of chemotherapeutic agents by enhancing antitumor treatment [15]. Amaravadi et al. [16] found that HDAC2 inhibitor TSA could enhance the expression of mRNA for the 5-hydroxytryptamine transporter (5-HTT) in HepG2 and THP-1 cell lines; the mechanism of action of HDAC2 was found to be enhanced by acetylation of histone H4 bound to the 5-HTT promoter region leading to the expression of 5-HTT by the chromatin immunoprecipitation technique. The expression of 5-HTT correlated with the phenomenon of autophagy in tumor cells, suggesting that HDAC2 plays a role in tumor cell autophagy and apoptosis through the downregulation of 5-HTT expression.

2. Materials and Methods

2.1. Gene Database. The GEO database (https://www.ncbi.nlm.nih.gov/geo/) provided GSE16011, GSE31262, and GSE90598. DEGs between GBM samples and healthy brain tissue were analyzed using *R* software. Affy *R* tool processed the downloaded raw data, while the limma *R* package identified DEGs. DEGs were discovered using volcano's differential expression volcano charting with |log2FC| 2 and p0.01.

2.2. Gene Function Analysis. GO and KEGG analyses were performed on genes to determine the enrichment function and the pathway of DEG. The enrichment results were constructed and visualized by the Barplot package. The STRING database (https://string-db.org/) is mainly used for protein interaction network analysis.

2.3. Glioma Database. This study employed the TCGA (Cancer Genome Atlas) database to compare HDAC2, DNMT3B, and Bcl2 expression between glioma and normal individuals. The China Glioma Genome Atlas Project (CGGA) database is a user-friendly web tool for studying brain tumor datasets from a Chinese cohort of more than 2,000 samples. The CGGA database analyzed the expression levels of HDAC2, DNMT3B, and Bcl2 in WHO-graded gliomas. The median expression values of each gene in the glioma samples were calculated, and they were classified into high (above median) and low (below median) expression groups. The prognostic results obtained from the CGGA database, including overall survival, were used to plot Kaplan–Meier survival curves, and the relationship between gene expression and HDAC2 and DNMT3B, DNMT3B and Bcl2, and HDAC2 and Bcl2 expression in gliomas established gene correlations.

2.4. Statistical Analysis. All experiments were performed in triplicate, and all data are expressed as mean ± standard error (SE). Differences between two groups were analyzed by Student's t-test, differences between at least three groups

were determined using one-way ANOVA, and results for glioma activity were analyzed using two-way ANOVA. Post hoc analyses were performed after one-way or two-way ANOVA. An SPSS 22.0 for Windows was used to perform these analyses (SPSS, IL, USA), and $P < 0.05$ was considered a significant difference between groups.

3. Results and Analysis

3.1. Identification of Differentially Expressed DEGs in GBM. Using the GSE16011 dataset, 346 DEGs were upregulated and 241 were downregulated in GBM samples compared to normal human brain tissue (Figure 1(a)). 286 upregulated and 222 downregulated DEGs were found in GSE31262 (Figure 1(b)). 277 upregulated and 162 downregulated DEGs were found in the GSE90598 dataset (Figure 1(c)). 28 genes were co-upregulated and 16 were co-downregulated in the three datasets (Figure 1(d)).

3.2. Enrichment Analysis of DEGs. Most of the differential genes in the biological process (BP) category mediated "nervous system development," "transcriptional regulation," "DNA replication," and "apoptosis" (Figure 2(a)). Most differential genes in this category are located in "cytoplasm," "centrosome," and "apoptosis" (Figure 2(a)) and "centrosome," "plasma membrane," and "cell surface" (Figure 2(b)). Different genes conduct "protein binding," "transcription factor activity," "methylation activity," "transcriptional activity," and "transcriptional regulatory activity" in the MF category, "Regulatory transcription" (Figure 2(c)). In the KEGG pathway enrichment analysis, we observed that the genes were predominantly enriched in the Wnt pathway (Figure 2(d)). We found that the differential genes in glioma mainly affect the apoptotic process and may influence transcriptional activity and DNA methyl transfer activity.

3.3. HDAC2-DNMT3B-Bcl2 Regulation May Occur in Gliomas. The interactions between differential genes were explored, and a PPI network was constructed. With confidence = 0.6, 52 linkages and 38 nodes were found in the network, and the gene axis was observed. We found that DNMT3B has some binding relationship to Bcl2; in the previous GO enrichment analysis, we found that the gene performs a DNA methylation transfer function. In the PPI network, HDAC2-DNMT3B-Bcl2 is the most likely glioma gene axis (Figure 3(a)). Raw signal analysis showed HDAC2 at 329–339 bp on the DNMT3B promoter (Figure 3(b)). In cultured glioma cells T98 G and A172, HDAC2 and DNMT3B binding was confirmed. The ChIP test identified enrichment on DNMT3B promoter, and HDAC2 downregulation dramatically reduced the enrichment of HDAC2 at 329–339 bp, demonstrating that HDAC2 and DNMT3B bind to each other in glioma cells T98 G and A172 (Figure 3(c)). The CpG island of Bcl2 was produced using MethPrimer, positioned at 454–613 bp of the promoter (Figure 3(d)).

HDAC2 was elevated in gliomas, and patients with high HDAC2 expression had a poorer prognosis. We examined the HDAC2 distribution data of WHO patients with different grades from the CGGA database to determine the link between HDAC2 expression and glioma grade (Figure 4(a)). DNMT3B was considerably enhanced in gliomas in the CGGA database, and high expression was related to shorter overall survival in all glioma grades. Bcl2 expression was much lower in gliomas, and low expression was linked to poor patient survival and WHO grade progression (Figure 4(b)). HDAC2-DNMT3B-Bcl2 was positively associated with the glioma database (Figure 4(d)).

4. Discussion

The concept of histone acetylation modification was introduced by Vincent et al. [53] back in the 1860s. Histone deacetylases are enzymes that act on histones and related nonhistone proteins and are mainly found on the nucleosomal units that constitute chromosomes; therefore, histone modifications are closely related to gene expression on chromosomes.

Histone acetylation modifications, i.e., entire ATGC order of DNA, alter gene function through structural acetylation modifications of histones. In addition to histone acetylation modification, there are other aspects, such as DNA methylation, chromosome remodeling, noncoding RNA regulation, and genomic imprinting. In this experiment, we focus on histone acetylation; i.e., the transfer and deacylation of acetyl groups. In normal cells, this process is at an emotional level. When stimulated by external factors, such as radiotherapy and chemotherapy in tumor patients, the balance is disturbed, leading to cellular derangement, in which histone deacetylases (HDACs) and histone acetylases (HATs) play an important role.

HDACs [16] de CH3CO- makes histones with corresponding + charge, which has a mutual attraction with DNA(-), making nucleosomes dense and tightly curved and chromosomes in a closed state, which is unfavorable for gene expression; HATs, on the contrary, add acetyl groups to histones with the corresponding (-) charge, which repels DNA(-), making nucleosomes sparse and chromosomes lose, which is favorable for the gene transcription process. Therefore, the imbalance of HDACs and HATs is associated with various gene-related diseases, especially in tumors, as it is closely related to the expression of various oncogenes and oncogenes. Different types of HDACs act at different sites in different cells. Their actions are not random but target specific transcription factors in the nucleus to inhibit the expression of relevant oncogenes, leading to dysregulation of a cycle, proliferation, and differentiation and contributing to tumorigenesis [17].

HDACs act in tumor cells mainly through the following actions: through chromatin remodeling as in acute promyelocytic HDACs act on cycle-related factors, such as the p21 cytokine-dependent kinase inhibitor CDKI class, an important one [18], and class I HDACs are dependent on Sp1/Sp3 to inhibit p21 expression in colon cancer [19, 20]. To ensure accurate entry of cells into the cycle, cells have cycle checkpoints [21], monitoring cells from G1 to S phase or from G2 to M phase. Activating the checkpoint pathway

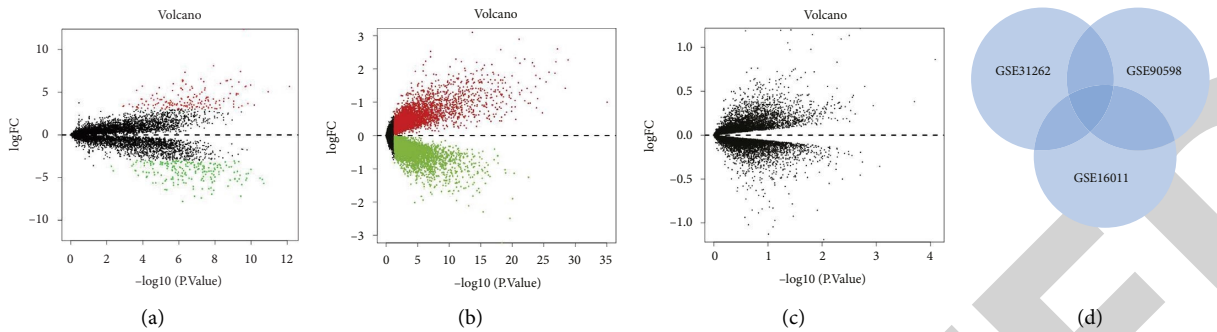

Figure 1: Search for differential genes in GBM. (a) Plotting volcanoes to identify differential genes in GSE16011. (b) Identification of differential genes in GSE31262 dataset. (c) Identification of differential genes in GSE90598. (d) Wayne plot overlap to calculate common upregulated and downregulated genes.

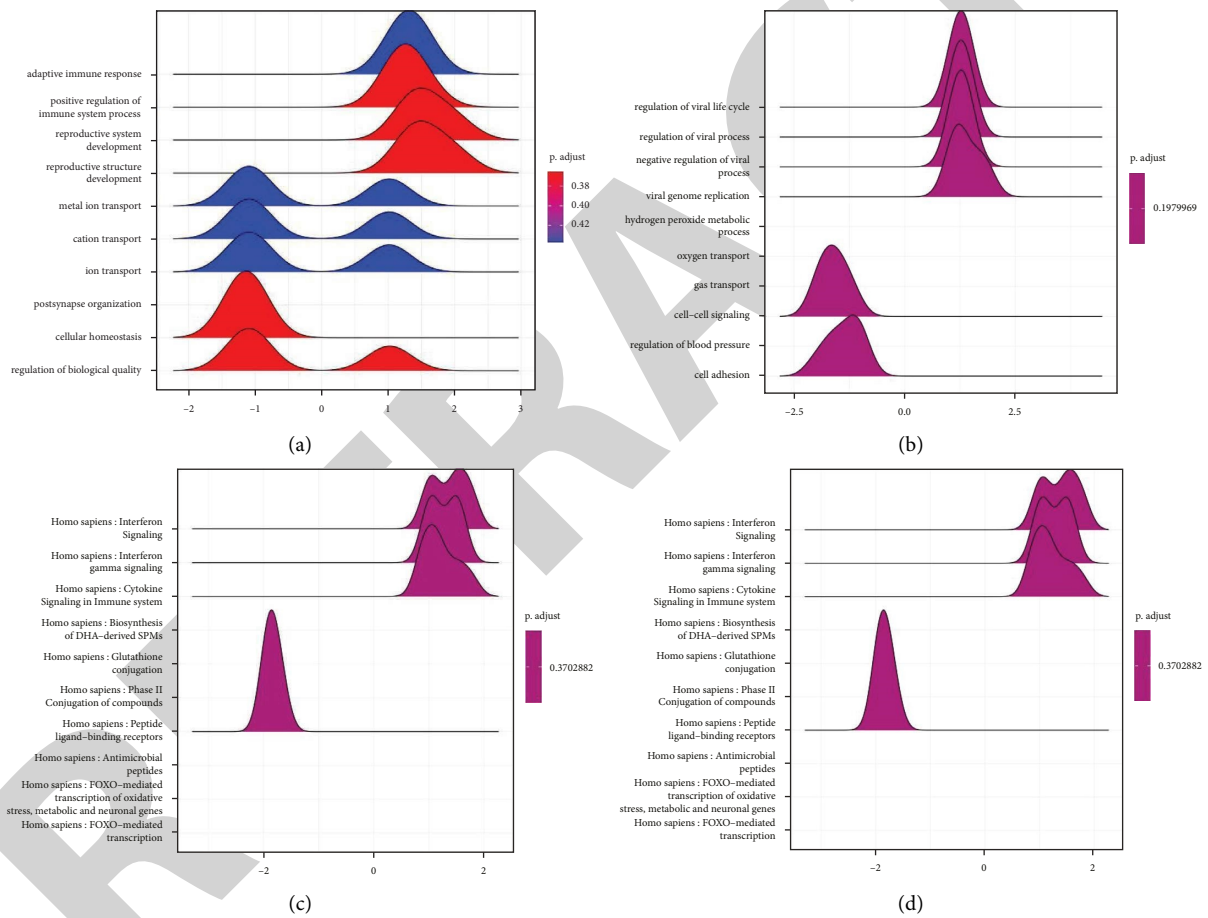

Figure 2: Functional enrichment analysis of genes. (a)–(c) GO analysis of genes with the terms biological process, cellular component, and molecular function, respectively. (d) KEGG pathway enrichment analysis of genes.

leads to phosphorylation and activation of checkpoint proteins, such as ATR, ATM, CHK1, CHK2, and p51. In addition to phosphorylation, acetylation and deacetylation of cell cycle proteins have a huge impact. HDACs de HDACs are not only associated with the cell cycle but also with apoptosis. HDAC3 in class I HDACs have a clear anti-apoptotic effect, and caspase-dependent inactivation of HDAC3 cleavage can activate apoptotic factors and thus trigger apoptosis [22]. In addition to this, HDAC5 in class II HDACs combined with vascular endothelial growth factor (VEGF) is involved in tumor angiogenesis, and the PKD-dependent phosphorylation-specific deletion of HDAC5 inhibits VEGF-mediated expression of an oligomeric nuclear receptor (RN4A1), endothelial cell migration, and angiogenesis in vitro [23]. It can be seen that HDACs are mainly involved in chromatin remodeling, act on cyclin and related apoptotic proteins, and are associated with tumor angiogenesis.

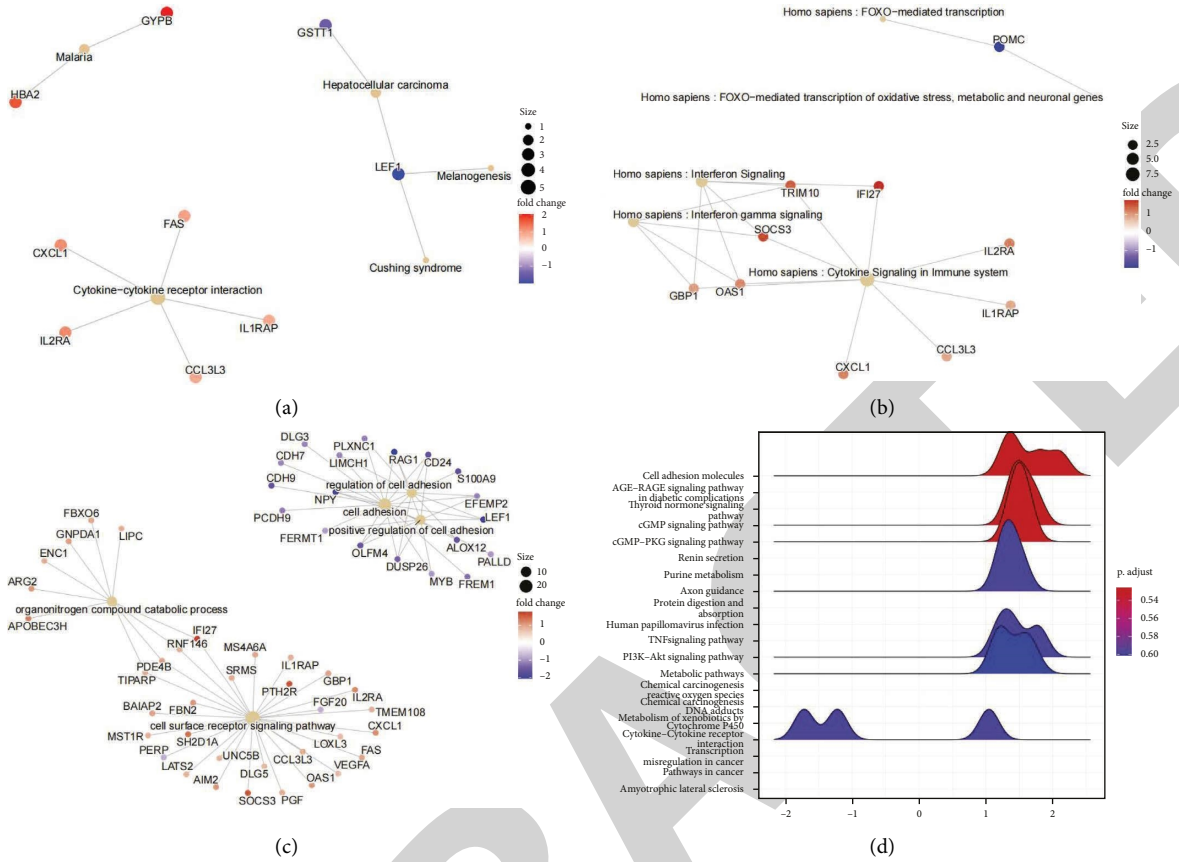

Figure 3: Probe the axis of gene action in GBM. (a) Protein interactions between genes found by STRING. (b) Predicted binding site to HDAC2 on DNMT3B promoter obtained. (c) ChIP experiment to verify the relationship between HDAC2 and DNMT3B. (d) Raw letter analysis to obtain the CpG island of the Bcl2 promoter. (e) ChIP experiment to verify the enrichment of DNMT3B HDAC2-DNMT3B-Bcl2 expression correlates in glioma.

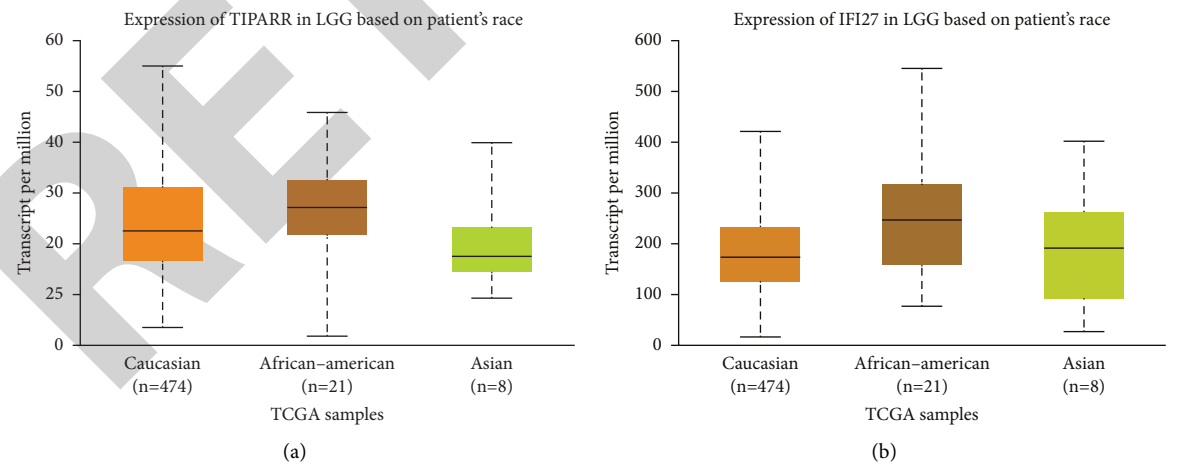

Figure 4: Continued.

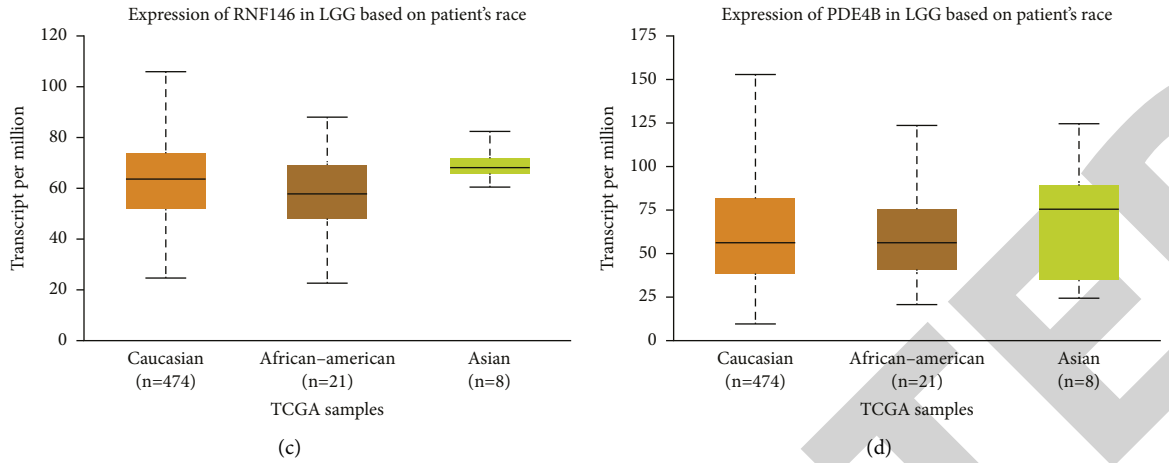

Figure 4: Detection of gene prognosis. (a) Detection of TIPARP expression, (b) IFI27 expression, (c) RNF146 expression, and (d) PDE48 expression in GBM.

HDACs are closely related to drug resistance in various types of tumor cells. Kikuchi et al. found that the sensitivity of multiple myeloma cells to bortezomib both in vivo and in vitro depended on the expression of HDAC2, implying that HDACs are closely related to proteasome inhibitors. Catley reported that NVP-LAQ824, an inhibitor of HDACs and hydroxamic acid salt derivative, affects proteasome activity in multiple myeloma. This compound uniquely affects multiple myeloma cell adhesion-mediated drug resistance (CAM-DR). It hasa unique effect. Shearer and Saunders [24] found a series of molecules and proteins (p21, CXCR4, syndecan-1, IGF-1, cyclinB2, cyclinF, and Bcl2) were affected by HDACs inhibitors SAHA and bortezomib by the microarray technique. Lung cancer cells also exhibit HDAC activity in resisting cell death through epithelial-mesenchymal transition [23], and many HDAC inhibitors have been widely used in clinical treatment [25]. HDAC2, as part of the transcriptional coblocker complex, is an important and ubiquitous regulator of gene expression. Sheng et al. [26] found that HDAC2 overexpression may induce the proliferation or differentiation of prostate cancer. However, a contrary study found that HDAC2 and suppression of HDAC2 triggered the development of hematological malignancies. This suggests that HDAC2 has a dual identity in tumor development [27]. However, in most classes of tumors, HDAC2 overexpression is a worsening effect on tumors, as in the melatonin treatment study of lung adenocarcinoma [28], where melatonin downregulated HDAC2 expression and led to acetylation of histone H3 in two cell lines, A549 and PC9, and enhanced melatonin-induced apoptosis after the addition of HDAC2 siRNA to bring it down.

We focused on HDAC2 in class I HDACs in the context of glioma drug resistance. Glioma is one of the most difficult tumors to treat, mainly due to its site-specificity and drug resistance [29]. Different individuals have different sensitivity to chemotherapeutic drugs, so finding glioma drug resistance targets is the basis for improving the clinical efficacy of glioma. In our previous study, we screened glioma drug resistance-related genes by gene microarray CHIP and identified 21 differentially expressed genes (including six upregulated genes and 15 downregulated genes); they were related to cell growth and differentiation, apoptosis, and signal transduction, respectively [30], among which HDAC2 was most obviously upregulated. In order to verify the accuracy of the microarray, the gene was confirmed to be highly expressed in drug-resistant gliomas by RT-PCR, so HDAC2 was studied as an important target. HDAC2 is highly expressed in several types of solid tumors, and abnormal expression of HDAC2 [31] can lead to chromosomal structural instability and DNA repair defects, which are associated with the repair of nonhomologous end-joins of broken double strands. HDAC2 expression was found to differ significantly between malignant prostate cancer focal tissue and adjacent benign paracancerous tissue by immunohistochemical staining, revealing that HDAC2 expression differs in similar tumor cells with different degrees of deterioration [32]. Thus, HDAC2 could be a reference indicator for predicting tumor deterioration grade. The HDAC2-DNMT3B-Bcl2 axis in gliomas is differentially expressed and interacting, HDAC2 activates the transcriptional activity of DNMT3B, and DNMT3B inhibits the expression of Bcl2. HDAC2 and DNMT3B are highly expressed in gliomas and have a poor prognosis, while Bcl2 is low expressed in gliomas and has a better prognosis. HDAC2-DNMT3B-Bcl2 promotes Wnt pathway activity in cells and tissues. Low expression of HDAC2 inhibited cell proliferation and migration activity and promoted apoptosis. In contrast, DNMT3B inhibited the downregulation of HDAC2 by increasing cell activity and decreasing apoptosis, and Bcl2 inhibited the effect of DNMT3B to decrease cell activity and increase apoptosis. In vivo, tumorigenic assays showed that HDAC2 downregulation and Bcl2 inhibited tumorigenic activity and enhanced apoptosis in glioma cells, while DNMT3B promoted tumorigenic activity and inhibited apoptosis in tissues.

Data Availability

The analyzed datasets generated during the study are available from the corresponding author upon request.

Conflicts of Interest

The authors declare that they have no conflicts of interest.

References

[1] D. I. Pitskhelauri, A. E. Bykanov, V. Y. Zhukov, I. A. Kachkov, S. B. Buklina, and A. S. Tonoyan, "Review of surgical treatment of insular gliomas: Challenges and opportunities," *Voprosy neirokhirurgii imeni N.N. Burdenko*, vol. 79, no. 2, pp. 111–116, 2015.

[2] D. G. Kim, H. J. Yang, I. A. Park et al., "Gliomatosis cerebri: clinical features, treatment, and prognosis," *Acta Neurochirurgica*, vol. 140, no. 8, pp. 755–762, 1998.

[3] M. Sanson, S. Cartalat-Carel, S. Taillibert et al., "Initial chemotherapy in gliomatosis cerebri," *Neurology*, vol. 63, no. 2, pp. 270–275, 2004.

[4] T. Inoue, T. Kumabe, M. Kanamori, Y. Sonoda, M. Watanabe, and T. Tominaga, "Prognostic factors for patients with gliomatosis cerebri: retrospective analysis of 17 consecutive cases," *Neurosurgical Review*, vol. 34, no. 2, pp. 197–208, 2011.

[5] K. Halkidou, L. Gaughan, S. Cook, H. Y. Leung, D. E. Neal, and C. N. Robson, "Upregulation and nuclear recruitment of HDAC1 in hormone refractory prostate cancer," *The Prostate*, vol. 59, no. 2, pp. 177–189, 2004.

[6] R. Zhao, K. Chen, J. Cao, H. Yu, L. Tian, and M. Liu, "A correlation analysis between HDAC1 over-expression and clinical features of laryngeal squamous cell carcinoma," *Acta Oto-Laryngologica*, vol. 136, no. 2, pp. 172–176, 2016.

[7] N. Keshelava, E. Davicioni, Z. Wan et al., "Histone deacetylase 1 gene expression and sensitization of multidrug-resistant neuroblastoma cell lines to cytotoxic agents by depsipeptide," *Journal of the National Cancer Institute*, vol. 99, no. 14, pp. 1107–1119, 2007.

[8] J. M. Denu, "The Sir 2 family of protein deacetylases," *Current Opinion in Chemical Biology*, vol. 9, no. 5, pp. 431–440, 2005.

[9] A. J. Wilson, D. S. Byun, N. Popova et al., "Histone deacetylase 3 (HDAC3) and other class I HDACs regulate colon cell maturation and p21 expression and are deregulated in human colon cancer," *Journal of Biological Chemistry*, vol. 281, no. 19, pp. 13548–13558, 2006.

[10] S. Rampalli, L. Pavithra, A. Bhatt, T. K. Kundu, and S. Chattopadhyay, "Tumor suppressor SMAR1 mediates cyclin D1 repression by recruitment of the SIN3/histone deacetylase 1 complex," *Molecular and Cellular Biology*, vol. 25, no. 19, pp. 8415–8429, 2005.

[11] C. Burdelski, O. M. Ruge, N. Melling et al., "HDAC1 overexpression independentlypredicts biochemical recurrence and is associated with rapid tumor cell proliferation and genomic instability in prostate cancer," *Experimental and Molecular Pathology*, vol. 98, no. 3, pp. 419–426, 2015.

[12] A. Aghdassi, M. Sendler, A. Guenther et al., "Recruitment of histone deacetylases HDAC1 and HDAC2 by the transcriptional repressor ZEB1 downregulates E-cadherin expression in pancreatic cancer," *Gut*, vol. 61, no. 3, pp. 439–448, 2012.

[13] T. Kumagai, N. Wakimoto, D. Yin et al., "Histone deacetylase inhibitor suberoylanilide hydroxamic acid (Vorinostat, SAHA) profoundly inhibits the growth of human pancreatic cancer cells," *International Journal of Cancer*, vol. 121, no. 3, pp. 656–665, 2007.

[14] F. U. Weiss, I. J. Marques, J. M. Woltering et al., "Retinoic acid receptor antagonists inhibit miR-10a expression and block metastatic behavior of pancreatic cancer," *Gastroenterology*, vol. 137, no. 6, pp. 2136–2145.e7, 2009.

[15] W. Liao, G. Jordaan, M. K. Srivastava, S. Dubinett, S. Sharma, and S. Sharma, "Effect of epigenetic histone modifications on E-cadherin splicing and expression in lung cancer," *American Journal of Cancer Research*, vol. 3, no. 4, pp. 374–389, 2013.

[16] R. K. Amaravadi, D. Yu, J. J. Lum et al., "Autophagy inhibition enhances therapy-induced apoptosis in a Myc-induced model of lymphoma," *Journal of Clinical Investigation*, vol. 117, no. 2, pp. 326–336, 2007.

[17] M. H. Malim and M. Emerman, "HIV-1 accessory proteins--ensuring viral survival in a hostile environment," *Cell Host and Microbe*, vol. 3, no. 6, pp. 388–398, 2008.

[18] D. Escors and K. Breckpot, "Lentiviral vectors in gene therapy their current status and future potential," *Archivum Immunologiae et Therapiae Experimentalis*, vol. 58, no. 2, pp. 107–119, 2010.

[19] S. Watanabe and H. M. Temin, "Encapsidation sequences for spleen necrosis virus, an avian retrovirus, are between the 5' long terminal repeat and the start of the gag gene," *National Academy of Sciences of the United States of America*, vol. 79, no. 19, pp. 5986–5990, 1982.

[20] T. Dull, R. Zufferey, M. Kelly et al., "A third-generation lentivirus vector with a conditional packaging system," *Journal of Virology*, vol. 72, no. 11, pp. 8463–8471, 1998.

[21] R. Zufferey, D. Nagy, R. J. Mandel, L. Naldini, and D. Trono, "Multiply attenuated lentiviral vector achieves efficient gene delivery in vivo," *Nature Biotechnology*, vol. 15, no. 9, pp. 871–875, 1997.

[22] T. Schnell, P. Foley, M. Wirth, J. Munch, and K. Uberla, "Development of a self-inactivating, minimal lentivirus vector based on simian immunodeficiency virus," *Human Gene Therapy*, vol. 11, no. 3, pp. 439–447, 2000.

[23] R. Zufferey, T. Dull, R. J. Mandel et al., "Self-inactivating lentivirus vector for safe and efficient in vivo gene delivery," *Journal of Virology*, vol. 72, no. 12, pp. 9873–9880, 1998.

[24] R. F. Shearer and D. N. Saunders, "Experimental design for stable genetic manipulation in mammalian cell lines lentivirus and alternatives," *Genes to Cells*, vol. 20, no. 1, pp. 1–10, 2015.

[25] M. Peviani, M. Kurosaki, M. Terao et al., "Lentiviral vectors carrying enhancer elements of Hb9 promoter drive selective transgene expression in mouse spinal cord motor neurons," *Journal of Neuroscience Methods*, vol. 205, no. 1, pp. 139–147, 2012.

[26] S. Sheng, Y. Kang, Y. Guo, Q. Pu, M. Cai, and Z. Tu, "Overexpression of Sirt3 inhibits lipid accumulation in macrophages through mitochondrial IDH2 deacetylation," *International Journal of Clinical and Experimental Pathology*, vol. 8, no. 8, pp. 9196–9201, 2015.

[27] W. Yang, B. Pan, T. Zhang, Z. Wang, L. Zhang, and Y. Guo, "The morphological changes of SW620 cells induced by overexpression of human sorting nexin 3," *Xi Bao Yu Fen Zi Mian Yi Xue Za Zhi*, vol. 31, no. 8, pp. 1057–1061, 2015.

[28] K. Blakely, T. Ketela, and J. Moffat, "Pooled lentiviral shRNA screening for functional genomics in mammalian cells," *Methods in Molecular Biology*, vol. 781, pp. 161–182, 2011.

[29] D. E. Root, N. Hacohen, W. C. Hahn, E. S. Lander, and D. M. Sabatini, "Genome-scale loss-of-function screening with a lentiviral RNAi library," *Nature Methods*, vol. 3, no. 9, pp. 715–719, 2006.

Hindawi
Evidence-Based Complementary and Alternative Medicine
Volume 2023, Article ID 9841426, 1 page
https://doi.org/10.1155/2023/9841426

Retraction

Retracted: LncRNA Gm43843 Promotes Cardiac Hypertrophy via miR-153-3p/Cacna1c Axis

Evidence-Based Complementary and Alternative Medicine

Received 8 August 2023; Accepted 8 August 2023; Published 9 August 2023

This article has been retracted by Hindawi following an investigation undertaken by the publisher [1]. This investigation has uncovered evidence of one or more of the following indicators of systematic manipulation of the publication process:

(1) Discrepancies in scope
(2) Discrepancies in the description of the research reported
(3) Discrepancies between the availability of data and the research described
(4) Inappropriate citations
(5) Incoherent, meaningless and/or irrelevant content included in the article
(6) Peer-review manipulation

The presence of these indicators undermines our confidence in the integrity of the article's content and we cannot, therefore, vouch for its reliability. Please note that this notice is intended solely to alert readers that the content of this article is unreliable. We have not investigated whether authors were aware of or involved in the systematic manipulation of the publication process.

Wiley and Hindawi regrets that the usual quality checks did not identify these issues before publication and have since put additional measures in place to safeguard research integrity.

We wish to credit our own Research Integrity and Research Publishing teams and anonymous and named external researchers and research integrity experts for contributing to this investigation.

The corresponding author, as the representative of all authors, has been given the opportunity to register their agreement or disagreement to this retraction. We have kept a record of any response received.

References

[1] Y. Cai and Y. Li, "LncRNA Gm43843 Promotes Cardiac Hypertrophy via miR-153-3p/Cacna1c Axis," *Evidence- Based Complementary and Alternative Medicine*, vol. 2022, Article ID 2160804, 13 pages, 2022.

Hindawi
Evidence-Based Complementary and Alternative Medicine
Volume 2022, Article ID 2160804, 13 pages
https://doi.org/10.1155/2022/2160804

Research Article

LncRNA Gm43843 Promotes Cardiac Hypertrophy via miR-153-3p/Cacna1c Axis

Yuhua Cai[1] and Yunpeng Li[2]

[1]*Department of Cardiology, Jingzhou First Municipal Hospital, Jingzhou 434000, Hubei Province, China*
[2]*Department of Cardiovasology, Dongfeng Hospital, Hubei University of Medicine, Shiyan 442000, Hubei Province, China*

Correspondence should be addressed to Yunpeng Li; nami147636756@163.com

Received 4 August 2022; Revised 30 August 2022; Accepted 9 September 2022; Published 10 October 2022

Academic Editor: Xueliang Wu

Long noncoding RNAs (lncRNAs) have been reported to engage in many human diseases, including cardiac hypertrophy. Cardiac hypertrophy was mainly caused by excessive pressure load, which can eventually lead to a decline in myocardial contractility. Gm43843, a novel lncRNA, has not been well explored in cardiac hypertrophy so far. Herein, we are going to search the function and the underlying molecular mechanism of Gm43843 in cardiac hypertrophy. Gm43843 levels were measured via qRT-PCR in mouse myocardial cells when they are treated with angiogenin II (Ang II) or transfected with different plasmids. Western blot assay was implemented to detect the cardiac hypertrophy-related protein markers, while the cell was analyzed via immunofluorescence (IF) assay to evaluate the hypertrophy. Meanwhile, the binding of Gm43843 and the putative targets was examined based on mechanistic assay results. We found that Gm43843 expression was increased with the elevated concentration of Ang II. Inhibited Gm43843 was detected to reduce the hypertrophy of mouse myocardial cells. Meanwhile, Gm43843/miR-153-3p/Cacna1c axis was found to modulate cardiac hypertrophy. In short, Gm43843 promotes cardiac hypertrophy via miR-153-3p/Cacna1c axis.

1. Introduction

Cardiac hypertrophy is a slow but effective compensatory function, which happened under long-term pressure overload [1]. Pathological cardiac hypertrophy poses a high risk of myocardial ischemia, which will lead to a deficiency in myocardial contractility, and eventually causes heart failure [2]. The major treatment for cardiac hypertrophy is surgical therapy [3]. Nevertheless, a lack of knowledge in the pathogenesis of cardiac hypertrophy makes the prevention of this disease difficult [4]. Thence, it has become vitally important for us to explore the underlying molecular mechanism in cardiac hypertrophy.

Noncoding RNAs (ncRNAs) are a group of genes, lacking protein-coding ability, but play important roles in modulating the biological behavior of cells [5–8]. Meanwhile, increasing long ncRNAs (lncRNAs) have been found to have a connection with the progression of cardiac hypertrophy by acting as competing endogenous RNAs (ceRNAs), that is, to sponge microRNAs (miRNAs) and modulate downstream messenger RNA (mRNA) expression [9]. For instance, lncRNA MIAT has been revealed to sequester miR-93 and regulate the expression of TLR4 in cardiac hypertrophy, functionally promoting the progression of cardiac hypertrophy [10]. Additionally, lncRNA MIAT contributes to cardiac hypertrophy by modulating the miR-93/Akt3 axis [11]. LncRNA-ROR can also modulate the progression of cardiac hypertrophy via miR-133 [12]. Gm43843 is a novel lncRNA that has not been well investigated so far. Limited evidence has suggested that lncRNA Gm15834 is allowed to facilitate myocardial hypertrophy by serving as a miR-30b-3p sponge and elevating ULK1 expression [13]. In our study, we are going to search for the function of Gm43843 in cardiac hypertrophy.

MiR-153-3p is a crucial regulator identified in various diseases. Specifically, in cardiac diseases, it has been found

that miR-153-3p contributes to mitochondrial fragmentation in cardiac hypertrophy [9]. The regulatory influence of miR-153-3p on cardiomyocyte apoptosis by directly targeting βII spectrin has also been uncovered [14]. Recent evidence has also pointed out that miR-153-3p is able to affect cardiomyocyte apoptosis induced by formaldehyde [14]. Herein, we aim to figure out whether miR-153-3p is a participant of the Gm15834-centered ceRNA regulatory axis.

mRNA calcium voltage-gated channel subunit alpha1C (Cacna1c) has been recognized as the effector of a wide range of neuropsychiatric syndromes [15]. Importantly, it has once been revealed that Cacna1c targeted by miR-221/222 is related to the change in cardiac ion channel expression and current density [16]. Cacna1c is also essential for cardiac electrophysiological development and maturation [17]. Therefore, it is one of the major targets of our study to uncover the function of Cacna1c in cardiac hypertrophy. Atrial natriuretic factor (ANF), brain natriuretic peptide (BNP), and β-myosin heavy chain (β-MHC) have been known as the biomarker of cardiac hypertrophy progression [11, 18]. In our study, these markers were detected to reflect hypertrophy. Meanwhile, the surface area of mouse myocardial cells was also assessed for investigating the hypertrophy variation.

In this study, the specific molecular mechanism of lncRNA Gm43843 in cardiac hypertrophy will be scrutinized, with the ceRNA network taken into consideration.

2. Materials and Methods

2.1. Cell Culture and Treatment. The mouse myocardial cells (H9C2 and MCM) were available from the ATCC (Manassas, VA). The cell culture environment was kept with 5% CO_2 at 37°C. Dulbecco's modified Eagle's medium (DMEM) supplemented with 1% antibiotics and 10% fetal bovine serum (FBS) was procured from Gibco (Grand Island, NY). To induce cardiac hypertrophy, H9C2 and MCM cells were severally processed with angiotensin II (Ang II; Sigma–Aldrich, St. Louis, MI) at 0.5 or 1 mmol/L concentration for 48 h.

2.2. RNA Extraction and Quantitative Real-Time PCR (qRT-PCR). Total RNA was isolated from cardiomyocytes utilizing TRIzol reagent (Thermo Fisher Scientific, Waltham, MA), followed by reverse transcription with the application of a reverse transcription system (Thermo Fisher Scientific). qRT-PCR was conducted on ABI 7900 Detection System (Applied Biosystems, Foster City, CA) by use of the SYBR-Green PCR Master Mix kit (Takara, Shiga, Japan). Relative expression of genes, normalized to GAPDH or U6, was calculated via the $2^{-\Delta\Delta Ct}$ approach.

2.3. Plasmid Transfection. The synthesized short hairpin RNAs (shRNAs) and control-shRNAs (GenePharma, Shanghai, China) were available to silence Gm43843 and Cacna1c using Lipofectamine3000 (Thermo Fisher Scientific). In addition, the miR-153-3p mimics and NC mimics, miR-153-3p inhibitor and NC inhibitor, as well as the pcDNA3.1-Cacna1c and pcDNA3.1-NC were all available from GenePharma for 48 h of plasmid transfection.

2.4. Western Blot. Total protein was extracted from cells by use of RIPA lysis buffer (Beyotime, Shanghai, China). Thereafter, the separation of proteins was achieved by using 10% SDS-PAGE (Bio-Rad, Hercules, CA), and the samples were then moved to PVDF membranes (Millipore, Bedford, MA). Following sealing with 5% fat-free milk, the membranes were cultivated at 4°C overnight with primary antibodies for ANP (1 : 2000; Abcam, Cambridge, MA), BNP (1 : 2000; Abcam), β-MHC (1 : 2000; Abcam) and control GAPDH (1 : 2000; Abcam). Later, secondary antibodies (1 : 5000; Abcam) were added to the culture for 1 h at 37°C. Finally, proteins were evaluated by the ECL detection system (Pierce, Rockford, IL, USA).

2.5. Immunofluorescence (IF). Processed H9C2 and MCM cells were fixed utilizing cold methanol (Sigma–Aldrich), followed by incubation with primary antibodies against α-actin (Abcam) and secondary antibodies conjugated to Alexa Fluor 488. Images were at last taken via fluorescence microscope (Olympus, Tokyo, Japan). After randomly examining 50 cells in 3 independent experiments, we obtained the average value for analyses. Image-Pro Plus 6.0 software was used to evaluate the surface area.

2.6. Fluorescence In Situ Hybridization (FISH). The subcellular localization of Gm43843 was examined through the FISH kit (Roche, Mannheim, Germany). Cells were cultured with a hybridization solution containing a specific Gm43843 probe (Sigma–Aldrich). The nuclei were dyed in DAPI (Sigma–Aldrich) for 10 min. At last, cells were captured via a fluorescence microscope to record images of fluorescence.

2.7. Subcellular Fraction. Nuclear/cytoplasmic fractionation PARIS Kit (Thermo Fisher Scientific) was used for collecting nuclear and cytoplasmic fractions of cells. The qRT-PCR was performed to determine the relative expression of Gm43843, GAPDH (cytoplasmic reference), and U6 (nuclear reference).

2.8. Luciferase Reporter Assay. The wild-type and mutated Gm43843 or Cacna1c fragments covering miR-153-3p binding sites were subcloned into pmirGLO dual-luciferase vector (Promega, Madison, WI). The acquired Gm43843-WT/Mut and Cacna1c-WT/Mut reporter vectors were cotransfected into cells with miR-153-3p mimics or NC mimics for 48 h. Luciferase activity was measured with a dual-luciferase reporter assay system (Promega).

2.9. RNA Pull Down. The wild-type and mutated miR-153-3p fragment covering Gm43843 or Cacna1c binding sites were labeled separately with biotin into Bio-miR-153-3p-WT/Mut probes. Biotinylated RNA was incubated with cell

lysates and magnetic beads, and the RNAs in the complexes pulled down were purified and detected by qRT-PCR.

2.10. Bioinformatics Prediction. StarBase website (https://starbase.sysu.edu.cn/) was employed for projecting candidate miRNAs targeted by Gm43843 with no specific condition. This database was also applied for screening potential mRNA likely binding with miR-153-3p in the subset of microT. The potential binding sequences of Gm43843 and Cacna1c covering miR-153-3p binding sites were obtained from starBase as well.

2.11. Statistical Analysis. All assays were run thrice. Values were shown as mean ± SD. GraphPad Prism 7 software (GraphPad Software, La Jolla, CA, USA) was utilized for statistical analysis with Student's *t*-test for two groups or one-way/two-way ANOVA for three or more groups with one or two variables. Tukey and Dunnett's approaches were applied as post hoc tests. The level of significance was specified as $p < 0.05$.

3. Results

3.1. Inhibited Gm43843 Relieved Cardiac Hypertrophy. Reportedly, lncRNAs play vital parts in the progression of cardiac hypertrophy [10, 19, 20]. Herein, we discussed the role of lncRNA Gm43843 in cardiac hypertrophy. Above all, it was noticed that Gm43843 expression increased upon the elevation of Ang II concentration in mouse myocardial cells (H9C2 and MCM) (Figure 1(a)). Thence, we predicted that Gm43843 played its regulatory function in H9C2 and MCM cells. Furthermore, inhibition efficiency of Gm43843 was detected via qRT-PCR assay (Figure 1(b)). As presented in Figures 1(c)-1(d), Ang II (1 mmol/L) significantly increased the mRNA and protein levels of the biomarkers of cardiac hypertrophy (ANF, BNP, and β-MHC) in H9C2 and MCM cells. When Gm43843 was inhibited, their expressions were decreased. These findings indicated that Ang II (1 mmol/L) induced H9C2 and MCM cell hypertrophy. However, Gm43843 inhibition decreased the hypertrophy symptom. Meanwhile, the IF assay assessed the cell surface area (Figure 1(e)). Results found that cell surface area expanded after Ang II (1 mmol/L) treatment, but reduced again by silenced Gm43843. In conclusion, inhibited Gm43843 relieved cardiac hypertrophy.

3.2. MiR-153-3p Could Bind to Gm43843 in H9C2 and MCM Cells. It has been scrutinized that cytoplasmic lncRNAs can function as ceRNAs to regulate downstream RNA expression [21]. In our study, we firstly investigated the location of Gm43843 in H9C2 and MCM cells (Figures 2(a)-2(b)). We could see from the result that Gm43843 was mainly located in the cytoplasm in H9C2 and MCM cells. Thence, we further searched the miRNAs that were predicted to bind to Gm43843 via the starBase website and their expressions were assessed in H9C2 and MCM cells treated with Ang II (1 mmol/L) (Figure 2(c)). We could see that mmu-miR-153-3p was down-regulated in H9C2 and MCM cells upon Ang II (1 mmol/L) treatment. Meanwhile, the binding site of Gm43843 and mmu-miR-153-3p was manifested based on starBase prediction (Figure 2(d)). After the high miR-153-3p overexpression efficiency was verified (Figure 2(e)), we confirmed the binding relationship between Gm43843 and miR-153-3p as the luciferase activity of Gm43843-WT was weakened due to miR-153-3p augmentation (Figure 2(f)). RNA pull-down assay further supported the above finding, since Bio-miR-153-3p-WT probes largely pulled down Gm43843 but Bio-miR-153-3p could not (Figure 2(g)). To sum up, miR-153-3p is directly targeted by Gm43843 in H9C2 and MCM cells.

3.3. Cacna1c Is Able to Combine with miR-153-3p in H9C2 and MCM Cells. In this part, we further explored the target gene of miR-153-3p to complete the ceRNA network. According to the starBase website, we found 700 mRNAs in the subset of microT. All of these mRNAs were implemented into qRT-PCR assay to detect the most suitable mRNA whose expression could be affected by inhibited Gm43843 and overexpressed miR-153-3p in H9C2 cells with or without Ang II treatment (Figure 3(a)). Xkr4 and Cacna1c were found. Meanwhile, the expression of Xkr4 and Cacna1c was investigated with different concentrations (0.5 and 1 mmol/L) of Ang II in H9C2 and MCM cells via qRT-PCR assay (Figure 3(b)). We detected that only Cacna1c expression increased with the elevation of Ang II concentration. Thence, Cacna1c was selected as the target. We presented the binding site of Cacna1c and mmu-miR-153-3p (Figure 3(c)). The binding affinity between Cacna1c and mmu-miR-153-3p was corroborated, as the wild type of Cacna1c luciferase activity was observed to be reduced on account of miR-153-3p up-regulation (Figure 3(d)). Cacna1c was also substantially pulled down by the wild type of Bio-miR-153-3p in H9C2 and MCM cells (Figure 3(e)). In a word, Cacna1c could bind to miR-153-3p in H9C2 and MCM cells.

3.4. Cacna1c Inhibition Could Relieve the Hypertrophy of H9C2 and MCM Cells. Previous studies have claimed the function of Cacna1c in the progression of cardiomyocyte hypertrophy [22–24]. In our study, we further investigated the function of Cacna1c in H9C2 and MCM cells. We first knocked down Cacna1c in H9C2 and MCM cells (Figure 4(a)). Then, we found that ANF, BNP, and β-MHC expressions were both inhibited by silenced Cacna1c (Figures 4(b)-4(c)). Meanwhile, the IF assay delineated that cell surface area was reduced when Cacna1c was inhibited in H9C2 and MCM cells (Figure 4(d)). To conclude, Cacna1c inhibition could relieve the hypertrophy of H9C2 and MCM cells.

3.5. Gm43843/miR-153-3p/Cacna1c Axis Could Modulate the Hypertrophy of H9C2 and MCM Cells. We further studied the function of the Gm43843/miR-153-3p/Cacna1c axis in

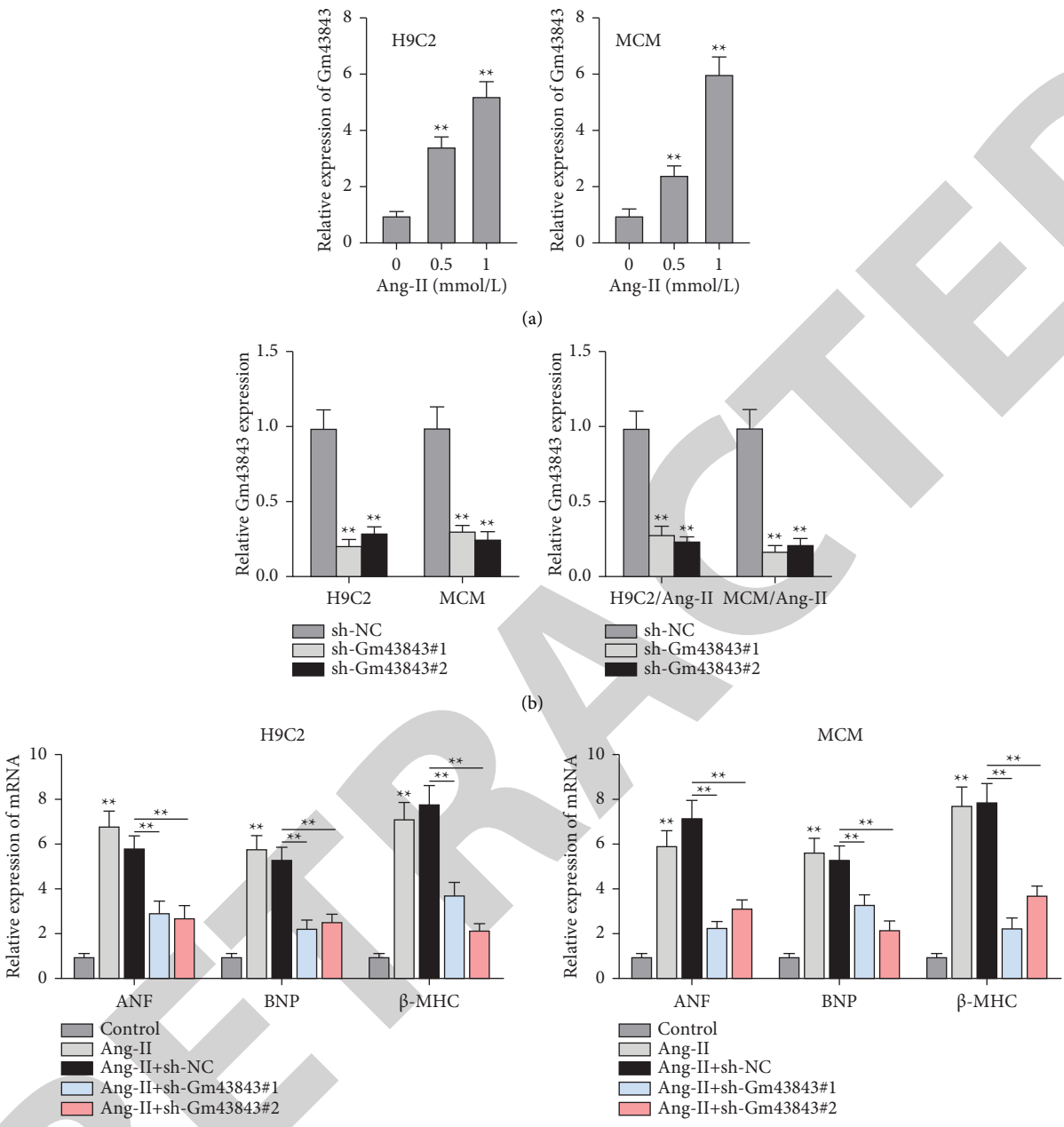

Figure 1: Continued.

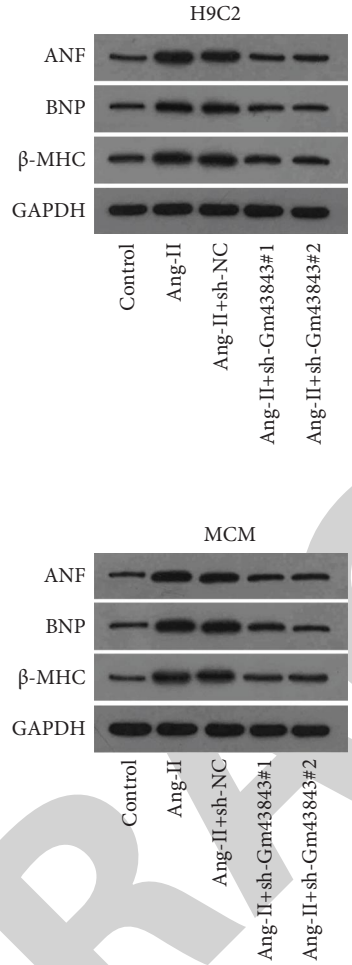

(d)

Figure 1: Continued.

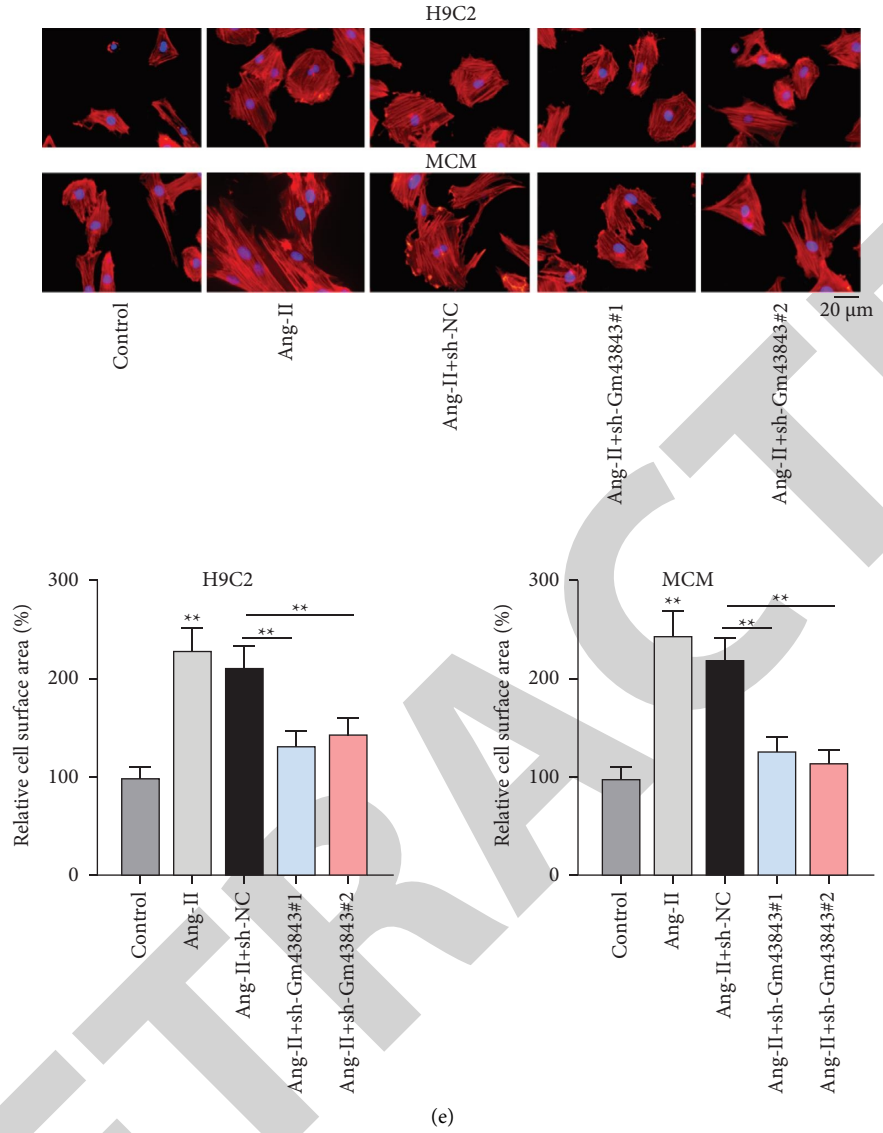

Figure 1: Inhibited Gm43843 relieved cardiac hypertrophy. (a) Gm43843 expression was detected via qRT-PCR assay when mouse myocardial cells (H9C2 and MCM) were treated with Ang II. (b) The inhibition efficiency of Gm43843 was monitored via qRT-PCR assay in H9C2 and MCM cells with or without the treatment of Ang II. (c-d) QRT-PCR assay and western blot assay were implemented to detect ANF, BNP, and β-MHC expression at mRNA and protein levels. (e) IF assay examined the variation of H9C2 and MCM cell surface. $^{**}P < 0.01$.

cardiac hypertrophy. We found that Cacna1c expression was significantly decreased with the silencing of Gm43843, but recovered with the inhibition of miR-153-3p (Figure 5(a)). After that, we overexpressed Cacna1c and the overexpression efficiency was proved to be high (Figure 5(b)). It was detected that RNA expressions and protein levels of ANF, BNP, and β-MHC were inhibited by Gm43843 depletion, but then, they were rescued by miR-153-3p inhibition or Cacna1c overexpression (Figures 5(c)-5(d)). Meanwhile, the IF assay found that lessened cell surface area due to knockdown of Gm43843 was increased again after miR-153-3p inhibition or Cacna1c augment (Figure 5(e)). In conclusion, Gm43843 could modulate the hypertrophy of H9C2 and MCM cells through miR-153-3p/Cacna1c.

4. Discussion

Accumulating evidence has proved that lncRNA can play regulating roles in cardiac hypertrophy. For example, Plscr4 increment can reduce Ang II-induced cardiomyocyte hypertrophy by regulating the expression of miR-214 and Mfn2 [25]. LncRNA CASC15 upregulated in cardiomyocytes treated with Ang II can increase the cell surface area of cardiomyocytes in cardiac hypertrophy by modulating the miR-432-5p/TLR4 pathway [26]. Meanwhile, H19 inhibition can activate cardiomyocyte hypertrophy, and H19 can regulate miR-675 targeting CaMKIIδ in cardiac hypertrophy [27]. In our study, we searched the role of Gm43843 in mouse myocardial cells treated with Ang II for inducing

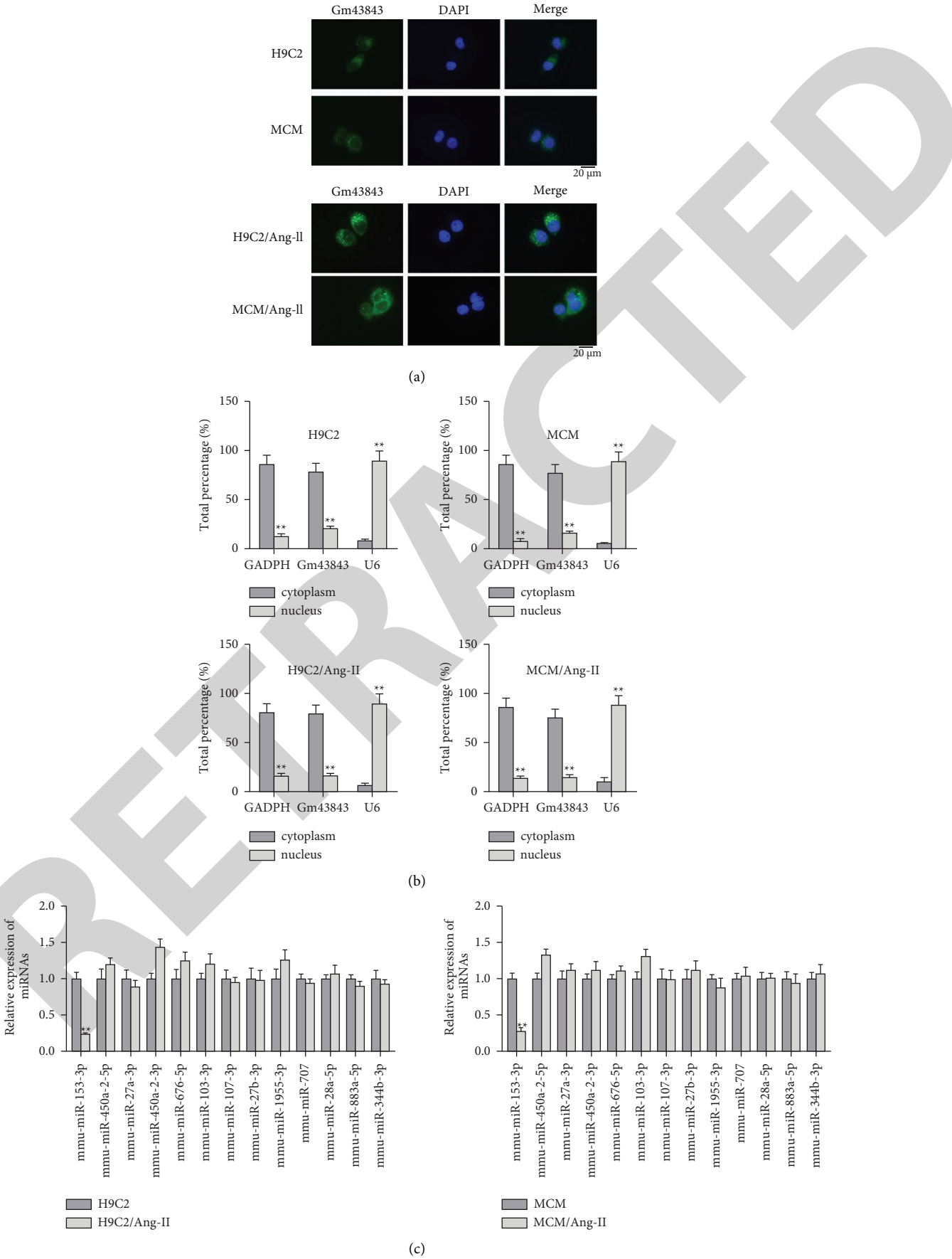

Figure 2: Continued.

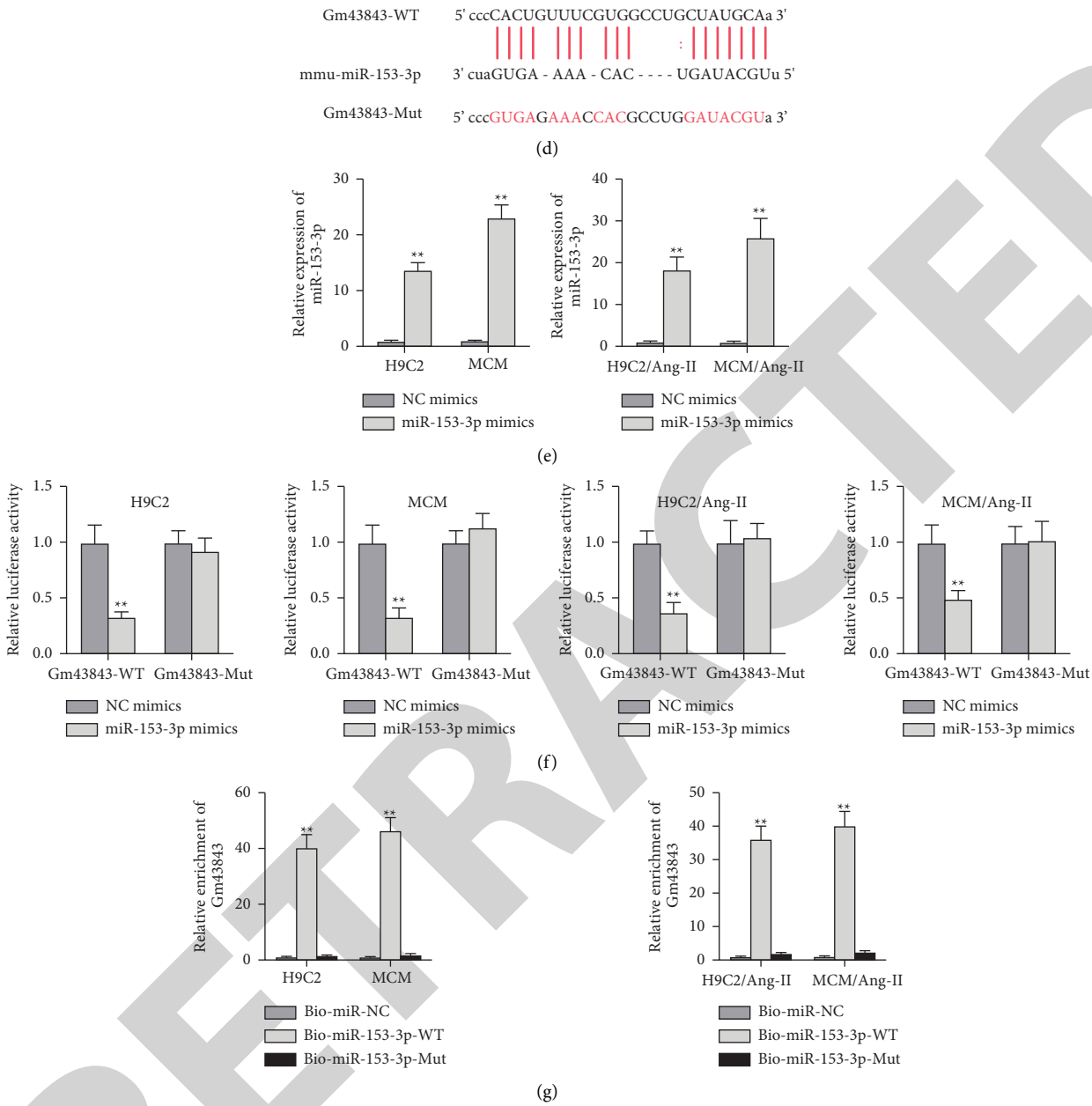

Figure 2: Gm43843 sequesters miR-153-3p in H9C2 and MCM cells. (a-b) The location of Gm43843 was investigated by FISH assay and subcellular fraction assay in H9C2 and MCM cells with or without Ang II treatment. (c) Thirteen miRNA candidates were searched from the starBase website, and their expression was detected in H9C2 and MCM cells treated with Ang II (1 mmol/L) via qRT-PCR assay. (d) The wide-type and mutated binding sites of Gm43843 and mmu-miR-153-3p were presented based on starBase prediction. (e) The overexpression efficiency of miR-153-3p was verified by qRT-PCR assay. (f-g) Luciferase reporter assay and RNA pull-down assay evaluated the binding relationship between Gm43843 and mmu-miR-153-3p. $^{**}P < 0.01$.

hypertrophy. Gm43843 expression was found up-regulated with the Ang II concentration increasing. Furthermore, Gm43843 inhibition was observed to relieve the cardiac hypertrophy of mouse myocardial cells. Meanwhile, the IF assay reassured that silenced Gm43843 played an inhibitory role in cardiac hypertrophy.

Previous studies have reported the ceRNA character of lncRNAs, which indicated that lncRNAs can function as miRNA sponges to form a miRNA/mRNA pathway to modulate the progression of human disease [28–30]. For example, lncRNA HOXD-AS1 can sponge to miR-130a-3p activating the expression of SOX4 to enhance the progression of liver cancer [31]. LncRNA TDRG1 can modulate cervical cancer cell growth, migration, and invasion via the miR-326/MAPK1 axis [32]. In our study, we firstly located Gm43843 in the cytoplasm in mouse myocardial cells.

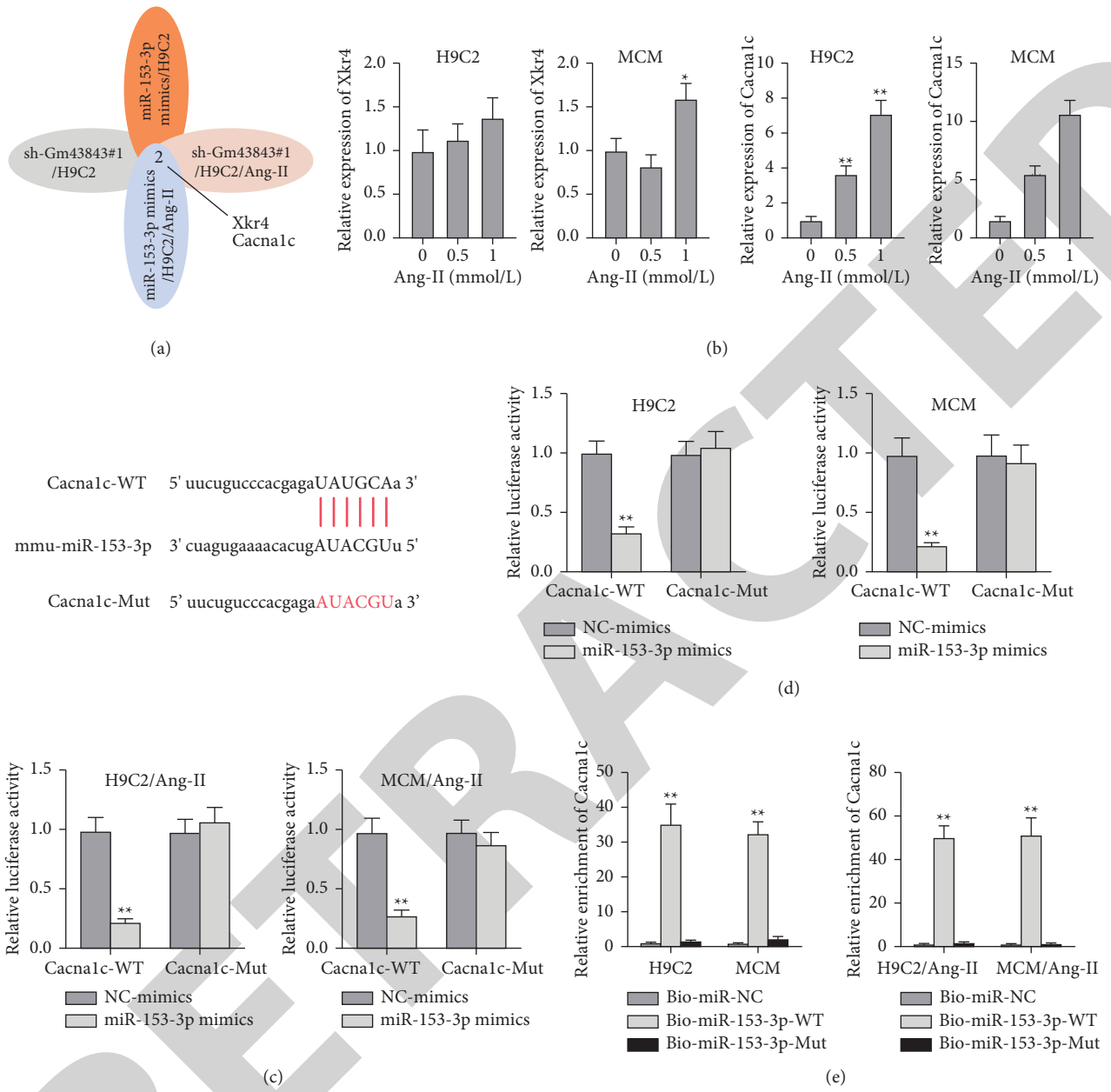

Figure 3: Cacna1c could bind to miR-153-3p in H9C2 and MCM cells. (a) QRT-PCR assay examined the most suitable mRNA whose expression could be affected by inhibited Gm43843 and overexpressed miR-153-3p in H9C2 cells. (b) Xkr4 and Cacna1c mRNA levels were investigated in H9C2 and MCM cells via qRT-PCR assay with the treatment of different concentrations (0.5 and 1 mmol/L) of Ang II. (c) The binding site of Cacna1c and mmu-miR-153-3p was displayed on the basis of starBase prediction. (d-e) Luciferase reporter and RNA pull-down assays reassured the binding in Cacna1c and mmu-miR-153-3p. $^{*}P < 0.05$, $^{**}P < 0.01$.

Mmu-miR-153-3p was corroborated to bind to Gm43843. Furthermore, Cacna1c was validated to bind to mmu-miR-153-3p.

Increasing molecular genetic testing has suggested that Cacna1c-linked disorders account for pathogenic variants and clinical findings. Cacna1c is related to calcium channel function and individuals with a pathogenic variant of this gene have a risk for cardiovascular disease [33]. Specifically, previous studies have unveiled that Cacna1c was involved in the progression of cardiomyocyte hypertrophy [22–24]. CACNA1C expression could be inhibited by miR-135b in cardiomyocytes to relieve the symptom of pathological cardiac hypertrophy [23]. In our study, we found the expression of Cacna1c was up-regulated with

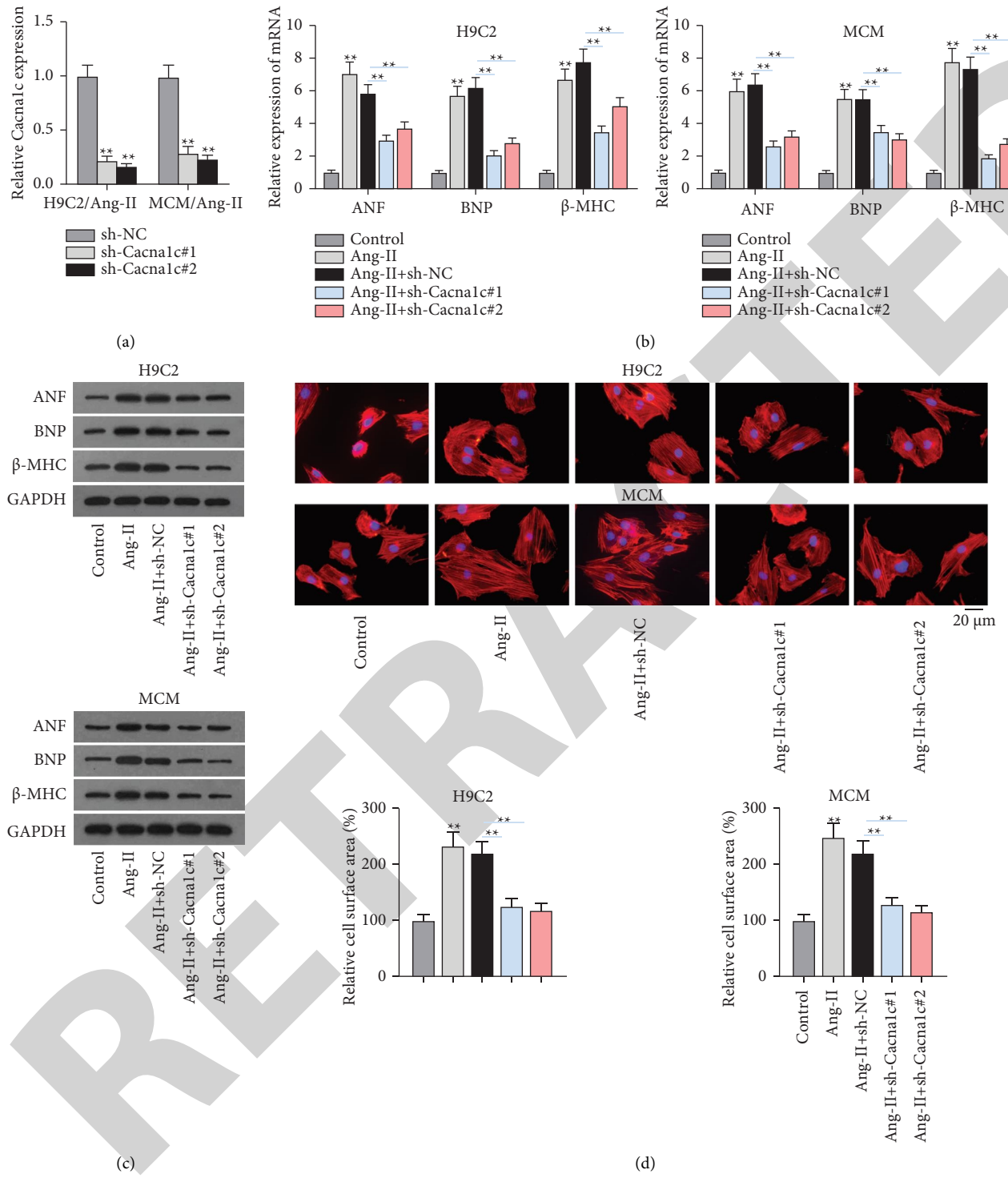

Figure 4: Cacna1c inhibition relieves the hypertrophy of H9C2 and MCM cells. (a) The inhibition efficiency of sh-Cacna1c was investigated by qRT-PCR assay in cells treated with Ang II. (b-c) QRT-PCR assay and western blot assay were implemented to detect the hypertrophy-related protein markers in Ang II-treated H9C2 and MCM cells upon Cacna1c depletion. (d) IF assay revealed the changes in H9C2 and MCM cell surface when Cacna1c was inhibited. $^{**}P < 0.01$.

Ang II inducement. It was worth noting that Cacna1c inhibition decreased the expression and protein level of ANF, BNP, and β-MHC, as well as reduced the cell surface area of mouse cardiomyocytes. Last but not least, it was verified that miR-153-3p inhibition or Cacna1c augmentation was able to abrogate the suppressive

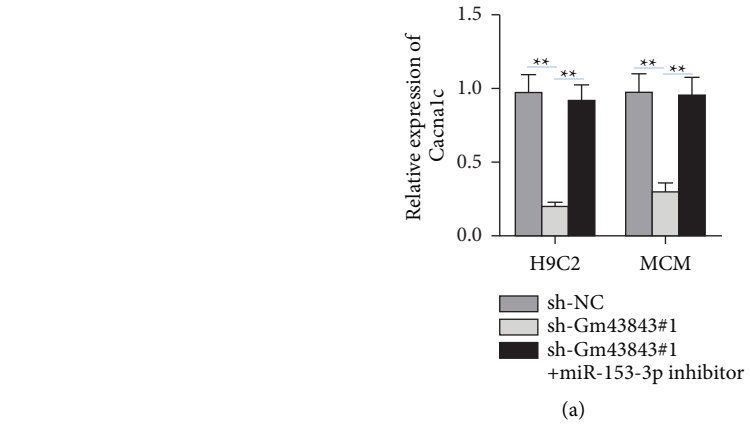

(a)

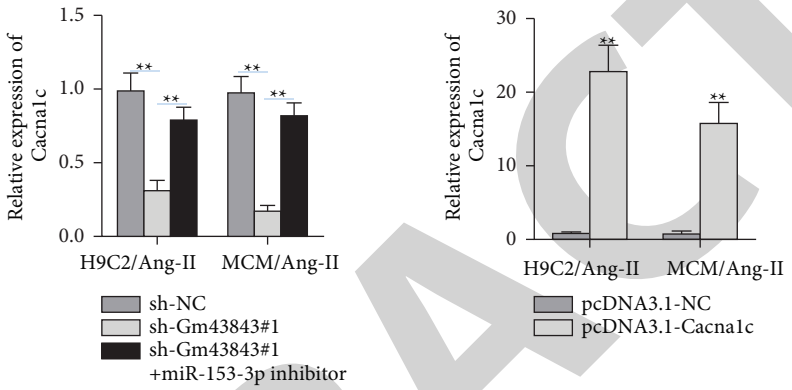

(b)

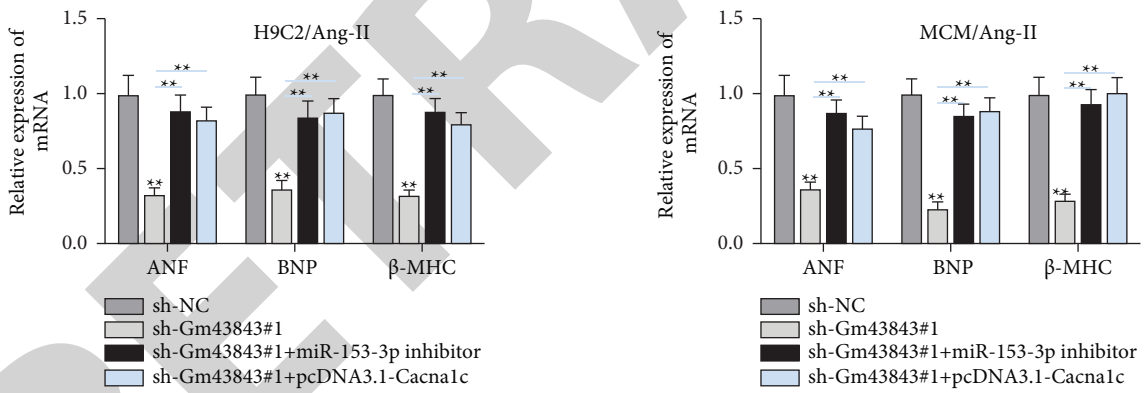

(c)

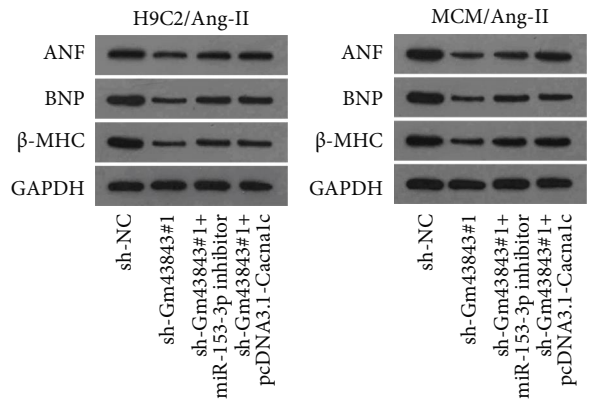

(d)

Figure 5: Continued.

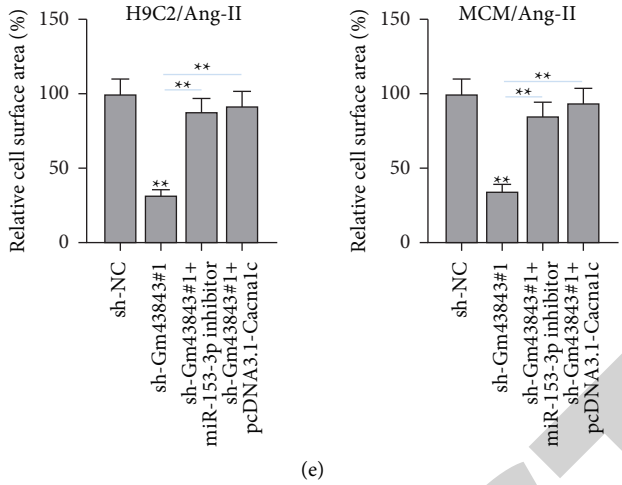

(e)

Figure 5: Gm43843/miR-153-3p/Cacna1c modulates the hypertrophy of H9C2 and MCM cells. (a) Cacna1c level variation upon Gm43843 depletion and miR-153-3p inhibition in Ang II-treated cells was evaluated via qRT-PCR. (b) Overexpression efficiency of Cacna1c was detected by qRT-PCR assay in cells after Ang II treatment. (c-d) The expression of ANF, BNP, and β-MHC at mRNA or protein levels was analyzed. (e) IF assay detected the surface of H9C2 and MCM cells. $^{**}P < 0.01$.

impact of Gm43843 deficiency on the hypertrophy of mouse cardiomyocytes.

To conclude, Gm43843 promotes cardiac hypertrophy via miR-153-3p/Cacna1c axis. Although human cells and clinical samples need to be involved in the future study for further confirmation of the validity of the axis, our study can still provide a novel perspective for a more in-depth understanding of the molecular mechanism in cardiac hypertrophy.

Data Availability

The data used in this study are presented in the manuscript.

Conflicts of Interest

The authors declare that they have no conflicts of interest.

References

[1] J. Veselka, N. S. Anavekar, and P. Charron, "Hypertrophic obstructive cardiomyopathy," *The Lancet*, vol. 389, no. 10075, pp. 1253–1267, 2017.

[2] T. Stanton and F. G. Dunn, "Hypertension, left ventricular hypertrophy, and myocardial ischemia," *Medical Clinics of North America*, vol. 101, no. 1, pp. 29–41, 2017.

[3] B. C. Bernardo, K. L. Weeks, L. Pretorius, and J. R. McMullen, "Molecular distinction between physiological and pathological cardiac hypertrophy: experimental findings and therapeutic strategies," *Pharmacology & Therapeutics*, vol. 128, no. 1, pp. 191–227, 2010.

[4] A. Diwan and G. W. Dorn, "Decompensation of cardiac hypertrophy: cellular mechanisms and novel therapeutic targets," *Physiology*, vol. 22, no. 1, pp. 56–64, 2007.

[5] The ENCODE Project Consortium, "An integrated encyclopedia of DNA elements in the human genome," *Nature*, vol. 489, no. 7414, pp. 57–74, 2012.

[6] A. Jandura and H. M. Krause, "The new RNA world: growing evidence for long noncoding RNA functionality," *Trends in Genetics*, vol. 33, no. 10, pp. 665–676, 2017.

[7] M. Klingenberg, A. Matsuda, S. Diederichs, and T. Patel, "Non-coding RNA in hepatocellular carcinoma: mechanisms, biomarkers and therapeutic targets," *Journal of Hepatology*, vol. 67, no. 3, pp. 603–618, 2017.

[8] M. Esteller, "Non-coding RNAs in human disease," *Nature Reviews Genetics*, vol. 12, no. 12, pp. 861–874, 2011 Nov 18.

[9] T. Wang, M. Zhai, S. Xu et al., "NFATc3-dependent expression of miR-153-3p promotes mitochondrial fragmentation in cardiac hypertrophy by impairing mitofusin-1 expression," *Theranostics*, vol. 10, no. 2, pp. 553–566, 2020.

[10] Y. Li, J. Wang, L. Sun, and S. Zhu, "LncRNA myocardial infarction-associated transcript (MIAT) contributed to cardiac hypertrophy by regulating TLR4 via miR-93," *European Journal of Pharmacology*, vol. 818, pp. 508–517, 2018.

[11] Y. Wo, J. Guo, P. Li, H. Yang, and J. Wo, "Long non-coding RNA CHRF facilitates cardiac hypertrophy through regulating Akt3 via miR-93," *Cardiovascular Pathology*, vol. 35, pp. 29–36, 2018.

[12] F. Jiang, X. Zhou, and J. Huang, "Long non-coding RNA-ROR mediates the reprogramming in cardiac hypertrophy," *PLoS One*, vol. 11, no. 4, Article ID e0152767, 2016.

[13] C. Song, H. Qi, Y. Liu et al., "Inhibition of lncRNA Gm15834 attenuates autophagy-mediated myocardial hypertrophy via the miR-30b-3p/ULK1 axis in mice," *Molecular Therapy*, vol. 29, no. 3, pp. 1120–1137, 2021.

[14] P. Yang, Y. Yang, X. He et al., "miR-153-3p targets βII spectrin to regulate formaldehyde-induced cardiomyocyte apoptosis," *Frontiers in Cardiovascular Medicine*, vol. 8, Article ID 764831, 2021.

[15] A. L. Moon, N. Haan, L. S. Wilkinson, K. L. Thomas, and J. Hall, "CACNA1C: association with psychiatric disorders, behavior, and neurogenesis," *Schizophrenia Bulletin*, vol. 44, no. 5, pp. 958–965, 2018.

[16] S. Binas, M. Knyrim, J. Hupfeld et al., "miR-221 and -222 target CACNA1C and KCNJ5 leading to altered cardiac ion channel expression and current density," *Cellular and Molecular Life Sciences*, vol. 77, no. 5, pp. 903–918, 2020.

[17] W. Li, N. Z. Zheng, Q. Yuan et al., "NFAT5-mediated CACNA1C expression is critical for cardiac

Hindawi
Evidence-Based Complementary and Alternative Medicine
Volume 2023, Article ID 9870761, 1 page
https://doi.org/10.1155/2023/9870761

Retraction

Retracted: Cardiac External Counterpulsation Attenuates Myocardial Injury by Regulating NRF2-mediated Ferroptosisin and Oxidative stress Injury

Evidence-Based Complementary and Alternative Medicine

Received 3 October 2023; Accepted 3 October 2023; Published 4 October 2023

This article has been retracted by Hindawi following an investigation undertaken by the publisher [1]. This investigation has uncovered evidence of one or more of the following indicators of systematic manipulation of the publication process:

(1) Discrepancies in scope
(2) Discrepancies in the description of the research reported
(3) Discrepancies between the availability of data and the research described
(4) Inappropriate citations
(5) Incoherent, meaningless and/or irrelevant content included in the article
(6) Peer-review manipulation

The presence of these indicators undermines our confidence in the integrity of the article's content and we cannot, therefore, vouch for its reliability. Please note that this notice is intended solely to alert readers that the content of this article is unreliable. We have not investigated whether authors were aware of or involved in the systematic manipulation of the publication process.

Wiley and Hindawi regrets that the usual quality checks did not identify these issues before publication and have since put additional measures in place to safeguard research integrity.

We wish to credit our own Research Integrity and Research Publishing teams and anonymous and named external researchers and research integrity experts for contributing to this investigation.

The corresponding author, as the representative of all authors, has been given the opportunity to register their agreement or disagreement to this retraction. We have kept a record of any response received.

References

[1] S. Wang, B. Wang, G. Guo, and Y. Chen, "Cardiac External Counterpulsation Attenuates Myocardial Injury by Regulating NRF2-mediated Ferroptosisin and Oxidative stress Injury," *Evidence-Based Complementary and Alternative Medicine*, vol. 2022, Article ID 6477778, 7 pages, 2022.

Hindawi
Evidence-Based Complementary and Alternative Medicine
Volume 2022, Article ID 6477778, 7 pages
https://doi.org/10.1155/2022/6477778

Research Article

Cardiac External Counterpulsation Attenuates Myocardial Injury by Regulating NRF2-mediated Ferroptosisin and Oxidative stress Injury

ShiXiang Wang,[1] Bin Wang,[2] Guofeng Guo,[1] and Youquan Chen [1]

[1]*Department of Cardiovascular Medicine, The Third Affiliated Hospital of Guangzhou Medical University, Guangzhou 510150, Guangdong, China*
[2]*Department of Radiology, Heze Hospital of Traditional Chinese Medicine, Heze 274400, Shandong, China*

Correspondence should be addressed to Youquan Chen; 2012690388@gzhmu.edu.cn

Received 21 July 2022; Revised 9 September 2022; Accepted 20 September 2022; Published 10 October 2022

Academic Editor: Xueliang Wu

Objectives. To explore the role of the external counterpulsation (ECP) myocardial injury by controlling NRF2-mediated ferroptosis and oxidative stress damage in acute myocardial infarction. *Methods*. Twenty acute myocardial infarction (AMI) participants hospitalized from January 2021 to January 2022 were enrolled. In addition, 20 healthy individuals who had a physical examination at our hospital served as normal controls. Before the AMI patients were given ECP therapy, the blood samples were collected and echocardiography was performed as the data of AMI cohort. Then, the blood samples were collected and echocardiography was performed following the ECP therapy as the data of AMI + ECP cohort. The heart function was assessed by echocardiography test. *Results*. Our findings demonstrated that ECP could reduce heart damage in patients with AMI. In the current study, we found that ECP could reduce heart damage in patients with AMI through increasing the LV-EF% and enhancing LVEDV and LVESV, and the difference was statistically significant ($P < 0.05$). ECP could reduce the levels of oxidative stress and ferroptosis markers in blood samples of AMI patients, which was through the upregulation of NRF2 and HO-1 expression, and the difference was statistically significant ($P < 0.05$). Taken together, all data implied that ECP was able to attenuate myocardial injury by regulating NRF2-mediated ferroptosis and oxidative stress in AMI patients, and the difference was statistically significant ($P < 0.05$). *Conclusion*. Our findings in this research are that cardiac ECP is able to attenuate myocardial injury by regulating NRF2-mediated ferroptosis and oxidative stress injury in AMI patients. This certainly gives the possibility of a clinically effective treatment for AMI patients, although further clinical trials need to be validated.

1. Introduce

Acute myocardial infarction (AMI) is a leading contributor to fatalities and morbidities throughout the world [1]. Each year approximately 10% of people admitted to the emergency department with chest pain are given a diagnosis of cardiac arrest [2–4]. Presently, no therapeutic options are available to prevention of ischemic reperfusion injuries (IRI) in the heart, which leads to the need for an in-depth investigation of the pathophysiology. Many works have demonstrated that oxidative stress is the predominant reason for IRI, which can upregulate the generation of reactive oxygen species (ROS), driving the pathogenesis of IRI [5, 6]. Moreover, an additional essential source is the imbalance of iron homeostasis, which will result in an elevated level of free iron in the cardiomyocytes. This metal ion will be elevated by the release of hydroxyl radicals (-OH) through the Fenton reaction. Eventually, these activators accelerate cellular damage by attacking biomolecules, such as lipids and proteins, and initiating various cell death pathways [7]. AMI is a disorder that can be co-occurring with ischemic cardiopathy and is manifested when atherosclerotic plaques rupture and a growing blood clot entirely or

partially occludes a crown artery, limiting circulation to the heart.

NRF2 is a stress-induced transcription factor in which protein levels are maintained at essentially a low level by three distinct E3-ubiquitin ligase enzymatic complexes [8]. External counterpulsation (ECP) therapy is a noninvasive assisted cardiovascular apparatus that is approved by the U.S. Food and Drug Administration for refractory angina pectoris. Remarkably, many proteins and enzymes responsible for the prevention of lipid peroxidation, and the resulting initiation of iron toxicity, are the target genes of NRF2. NRF2/HO-1 is a property found in almost 100% of human cells. It is triggered, relocated to the nucleus, and bound to DNA via antioxidant-response elements (AREs). As a modulator of the antioxidative response system, it upregulates the expression of HO-1 to minimize oxidative stress [9]. Previous investigations have proven the clinical applications of NRF2/HO-1 in pediatric cardiovascular disorders [9].

As a result of genetic mutations, endogenous stress-induced modifications, competitive conjugation of other interacting partners, or exogenous pharmacological inhibition, NRF2 can then translocate to the nucleus and initiate transcription of genes containing antioxidant-response elements (ARE) [10]. It is insufflated in the inferior extremities to raise the diastolic pressure in the aorta, thus augmenting the coronary perfusion. The cuff is deflated under systole to decrease vessel compression and heart backload. The increased hemodynamics and velocity of flow generate a shearing strain on the endothelium, resulting in improved functionality of the endothelium. In individuals with coronary artery disease (CAD), ECP is capability of triggering the release of nitric oxide, a vasodilator, and diminishing those vasoconstrictors [11, 12]. Thus, the modulation of these pathways by a shear force in the endothelium may attenuate the progression of cardiovascular disease. However, the influence of ECP in ferroptosis and oxidative stress has not remained unclear to the mitigation of myocardial injury via NRF2/HO-1. This study was to explore the role of ECP in myocardial injury by controlling NRF2-mediated ferroptosis and oxidative stress damage in acute myocardial infarction.

2. The Information of Patients and Methods

2.1. General Information of Participants. Twenty AMI participants hospitalized from January 2021 to January 2022 were enrolled in current research. In addition, 20 healthy individuals who had a physical examination at our hospital served as normal controls. There exhibited no remarkable difference in general data between AMI patients and normal cases. Before the AMI patients were given ECP therapy, the blood samples were collected and echocardiography was performed as the data of AMI cohort. Then, the blood samples were collected and echocardiography was performed following the ECP therapy as the data of AMI + ECP cohort. Our study has been approved by the hospital's ethics committee. All patients have signed an informed consent form.

2.2. Echocardiography. Left ventricular end-diastolic volume (LVEDV, ml), left ventricular end-systolic volume (LVESV, ml), and left ventricular ejection fraction (LV-EF, %) were measured by echocardiography. The date among normal controls, AMI cohort, and AMI + ECP cohort were taken as comparisons to assess the cardiac functions.

2.3. ELISA Assay. All plasma was obtained from the blood samples. The evaluation of oxidative stress was verified via measurement of superoxide dismutase (SOD), glutathione peroxidase (GPx), catalase and reduced glutathione (GSH), and malondialdehyde (MDA) by using an ELISA kit (Lifespan Biosciences, USA). All experimental practices were performed according to the manufacturer's protocol. The experiment was repeated three times.

2.4. RT-qPCR Assay. For this test, β-actin was utilized as an internal reference gene and the mRNA expressed each gene was determined using the $2^{-\Delta\Delta ct}$ relative quantification approach and standardized to the expressed relative to the control group. At least a minimum of triple testing was replicated. Complete RNA was derived from the blood of both healthy volunteers and patients pre- and post-ECP treatment using TRIzol reagent (Takara, Japan) and reversely transcribed into cDNA in a cDNA synthesis kit (Takara). Quantitative PCR was undertaken on the Ultra SYBR One-StepRT-qPCR Kit (CWBIO, China) and gene-specific primers. The quantity of RNA was counted using the comparative threshold cycling method. All primers were customized by GenScript, Inc. The primers of ACSL4, TFR1, GPX4, NRF2, and HO-1 are displayed in Table 1.

2.5. Iron Content Measured by ELISA. For quantitative determination of iron Fe^{3+} and/or Fe^{2+}, the evaluation of iron metabolism was conducted using QuantiChrom™ Iron Assay Kit (Bio Assay Systems, US) by following the manufacturer's instructions. The blood samples were collected, homogenized in 5x volume of iron assay buffer on ice, and centrifuged ($13,000 \times g$, 10 min) at 4°C. The supernatant was collected, and 5 μl of iron reducer was added to each sample and incubated for 30 min at 37°C. Next, 100 μl of iron probe was added to each sample and incubated for 60 min at 37°C away from light. The intensity of the color was measured at 590 nm. A minimum of triple testing was replicated at least.

2.6. Statistical Analysis. IBMSPSS24.0 software was applied for statistical analysis. The measurement data were expressed by mean ± standard deviation. The counting data were expressed by frequency or rate. *T*-test was used when measurement data obey normal distribution, and rank sum test was used when it did not obey normal distribution. $\chi 2$ test was used to compare the classified counting data. Repeated measurement data were analyzed by repeated measurement analysis of variance. Main effect test results were used when there was no interaction, and simple effect analysis was carried out when there was an interaction.

Table 1: Primer sequences used for qPCR.

Gene		Sequence (5′ to 3′)
β-actin	F	GCACCCAGCACGATGAAAAT
	R	GACAATGGAGGGTCCGGATT
ACSL4	F	ATATTCGTCACCACTCACA
	R	AACCTTGCTCATAACATTCTT
TFR1	F	AGAATGGCTGGAGGGGTACT
	R	TTCTCTCCAGCAGCGCATAC
GPX4	F	CAGGAGCCAGGAAGTAAT
	R	CAGCCGTTCTTATCAATGAG
NRF2	F	GCCCACATTCCCAAACAAGAT
	R	CCAGAGAGCTATTGAGGGACTG
HO-1	F	GCAGAGGGTGATAGAAGAGG
	R	AAGGAAGCCAGCCAAGAG

$P < 0.05$ indicated that the difference between groups is statistically significant.

3. Results

3.1. ECP Could Reduce Cardiac Damages in Patients with AMI Compared with Controls. Following the ECP treatment to the AMI patients, LV-EF% of AMI + ECP cohort was increased remarkably than pre-ECP therapy (Figure 1(a)), and the difference was statistically significant ($P < 0.05$). However, LV-EF% of AMI + ECP cohort still showed lower than the normal controls, and the difference was statistically significant ($P < 0.05$). LVEDV and LVESV were upregulated after ECP therapy, which were considerably relieved before ECP therapy, and the difference was statistically significant ($P < 0.05$). In addition, there was no obvious distinction between normal controls and patients of AMI + ECP cohort (See Figures 1(b) and 1(c)). These data released that ECP could reduce heart damage in patients with AMI.

3.2. ECP Could Reduce the Levels of Oxidative-Stress Markers in Blood Samples of AMI Patients. The oxidative-stress biomarkers were assessed among controls, AMI, and AMI + ECP cohorts. The current data suggested that MDA and SOD levels of AMI cases were considerably higher than healthy control participants, and the difference was statistically significant ($P < 0.05$). However, MDA and SOD values were downregulated remarkably after ECP treatment, and the difference was statistically significant ($P < 0.05$). On the other hand, GSH and GPx were obviously raised than healthy cases when the patients were suffering from AMI, and the difference was statistically significant ($P < 0.05$). Following the ECP therapy, GSH and GPx levels of AMI + ECP cohort were improved obviously than pre-ECP treatment, and the difference was statistically significant ($P < 0.05$). Taken together, these results imply that ECP could reduce the levels of oxidative-stress markers in blood samples of AMI patients (Figure 2).

3.3. ECP Could Downregulate Levels of Ferroptosis in Blood Samples of AMI Patients. The level of plasma iron content was upregulated considerably when the cases were suffering from AMI. After ECP treatment, the plasma iron content was reduced obviously than AMI patients, and the difference was statistically significant ($P < 0.05$). In addition, the levels of ACSL4 and TFR1 were strongly expressed, while the GPX4 expression decreased in AMI patients than the normal healthy group, and the difference was statistically significant ($P < 0.05$). In AMI + ECP cohort, the expressed ACSL4 and TFR1 mRNA was suppressed remarkably, at the meanwhile, the GPX4 mRNA level was weakened greatly, and the difference was statistically significant ($P < 0.05$). All the data suggested that ECP therapy could downregulate markers of ferroptosis in blood samples of AMI patients (Figure 3).

3.4. ECP Could Activate the NRF2/HO-1 Pathway in Blood Samples of AMI Patients. Before the therapy of ECP to AMI patients, the lower expressions of NRF2 and HO-1 levels were exhibited in AMI cases than that in normal controls, and the difference was statistically significant ($P < 0.05$). However, the levels of NRF2 and HO-1 were evaluated after the patients accepted the ECP therapy (See Figure 4).

4. Discussion

In the current study, we found that ECP could reduce heart damage in patients with AMI through increasing the LV-EF % and enhancing LVEDV and LVESV. ECP could reduce the levels of oxidative stress and ferroptosis markers in blood samples of AMI patients, which was through the upregulation of NRF2 and HO-1 expression. Taken together, all data implied that ECP was able to attenuate myocardial injury by regulating NRF2-mediated ferroptosis and oxidative stress in AMI patients. This study was to explore the role of the external counterpulsation (ECP) myocardial injury by controlling NRF2-mediated ferroptosis and oxidative stress damage in acute myocardial infarction.

The management of myocardial infarction has greatly advanced in the previous four decades [3, 13]. Consequently, it has grown more widespread for patients to have survived the acute event. Medically indicated remedies to limit infarct size are vital, as massive infarcts can contribute to cardiogenic shock, fatal arrhythmias, or acute heart failure [14–16]. During reperfusion, cardiomyocytes are submitted to further oxidative stress, a mandatory process for myocardial resuscitation [17, 18]. This impairment, thought to be ischemia-reperfusion, contributes to a submerged wave of cell death and an inflammatory reaction. ROS generated during and after ischemia and reperfusion are thought to be the main cause of cell death.

Medications that decrease cell mortality are predicted to lessen infarct size, preventing adverse events and having tremendous clinical implications. The initial ischemia at the cytosolic level can result in an elevation of reactive oxygen species (ROS). The free radicals are generated as by-products of regular cell metabolism, and the elevated levels of ROS may result from enhanced productivity or diminished damage to such formed free radicals by enzymatic and nonenzymatic antioxidants [19]. Alteration in the enzymatic levels of these antioxidants can seriously influence the sensitization of diverse organs to oxidative stress and is consequently involved in myocardial damage [20]. Current

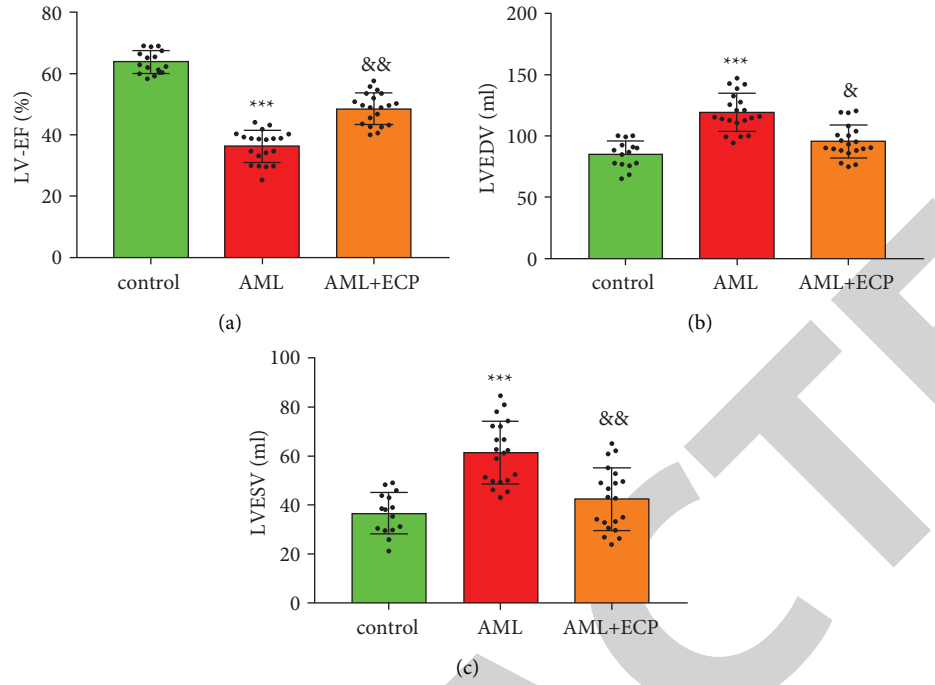

Figure 1: ECP could reduce heart damage in patients with AMI. LVEDV, LVESV, and LV-EF % were measured by echocardiography. $^{***}P < 0.001$ (control vs. AMI); $^{\&}P < 0.05$, $^{\&\&}P < 0.01$(AMI vs. AMI + ECP).

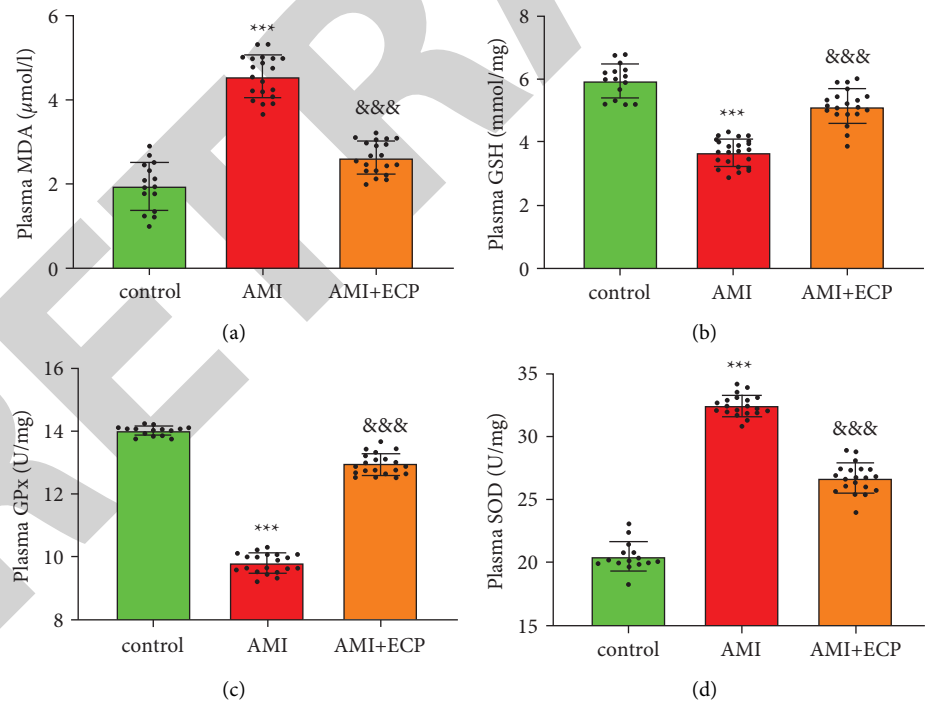

Figure 2: ECP could reduce oxidative-stress markers in blood samples of AMI patients. MDA (a), GSH (b), GPx (c), and SOD (d) were measured by ELISA. $^{***}P < 0.001$ (control vs. AMI); $^{\&\&\&}P < 0.001$ (AMI vs. AMI + ECP).

results demonstrated that MDA and SOD levels of AMI cases were considerably higher than healthy control participants. However, MDA and SOD values were down-regulated remarkably after ECP treatment. On the other hand, GSH and GPx were obviously raised than healthy cases when the patients were suffering from AMI. Following the ECP therapy, GSH and GPx levels of AMI + ECP cohort were improved obviously than pre-ECP treatment. MDA

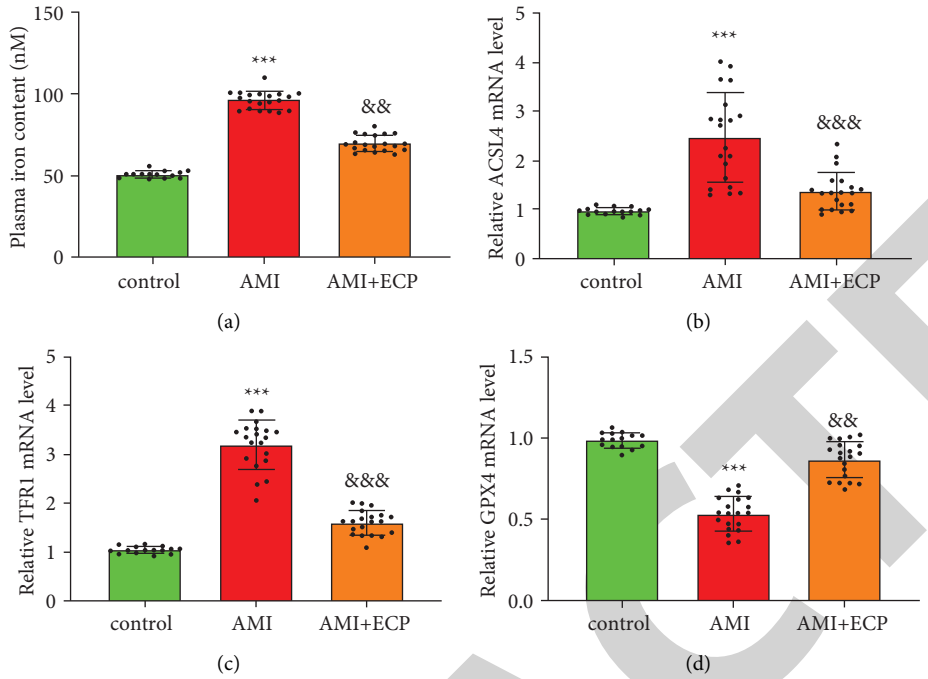

Figure 3: ECP could downregulate markers of ferroptosis in blood samples of AMI patients. Iron content (a) was measured by ELISA. The mRNA expressions of ACSL4 (b), TFR1 (c), and GPX4 (d) were measured by RT-qPCR. $^{***}P < 0.001$ (control vs. AMI); $^{\&\&}P < 0.01$ $^{\&\&\&}P < 0.001$(AMI vs. AMI + ECP).

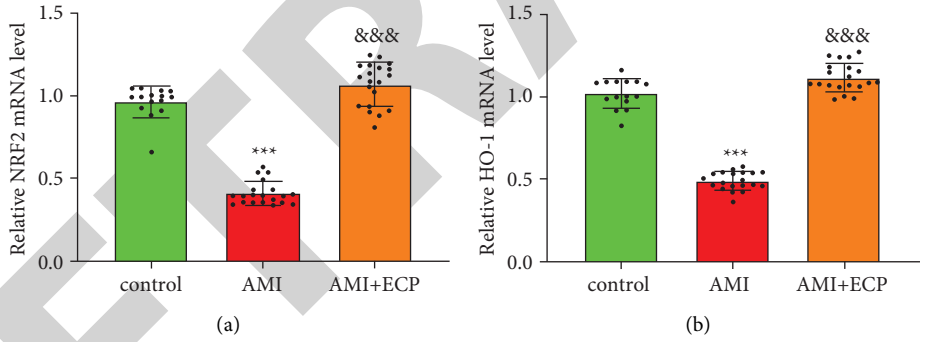

Figure 4: ECP could activate the NRF2 pathway in blood samples of AMI patients. The mRNA expressions of NRF2 (a) and HO-1(b) were measured by RT-qPCR. $^{*}P < 0.05$, and $^{***}P < 0.001$ (control vs. AMI); $^{\&\&}P < 0.01$ $^{\&\&\&}P < 0.001$(AMI vs. AMI + ECP).

and SOD were assessed as oxidative stress markers. The generation of oxidative free radicals and the magnitude of tissue impairment can be reflected indirectly by the measurement of lipid peroxidation and MDA [21]. SOD is an enzyme that cleaves the superoxide anion radical O_2- and has a major part in oxidation and antioxidation homeostasis in the body [22]. The alteration of serum MDA and SOD levels were in accordance with the apoptotic activity, while GSH and GPx activities exhibited the contrary pattern, indicating that the underlying therapeutic principle of AMI may be associated with antiapoptotic effect and oxidative stress [23]. Ferroptosis is primarily characterized by mitochondrial atrophy, in which the density of bilayer membranes improves and lipid peroxidation is accumulated. Myocardial ischemia-reperfusion injury (MIRI) is an unavoidable risk event for acute myocardial infarction. This part of the results implies that ECP can improve the function of injured myocardium, possibly through oxidative stress.

Ferroptosis is a newfound regulatory state form of cytosolic death depending on iron and ROS [24, 25]. It directly or indirectly influences GPX4 by induction of smaller molecules, which causes an overaccumulation of ROS in membrane-lipids due to redox inequality and damages the integrity of cytosolic membranes [26, 27]. Ferroptosis is closely associated with MIRI [28]. After ECP treatment, the plasma iron content was reduced obviously than AMI patients. In addition, the levels of ACSL4 and TFR1 were strongly expressed, while the GPX4 expression decreased in AMI patients than the normal healthy group. In AMI + ECP cohort, the expressed ACSL4 and TFR1 mRNA was suppressed remarkably, at the meanwhile, the GPX4 mRNA level was weakened greatly. All the data suggested that ECP

therapy could downregulate markers of ferroptosis in blood samples of AMI patients. ACSL4 and GPX4 are considered to be central factors participating in lipid peroxidation [29]. ACSL4 is a representative of the long-chain series of acyl-CoA synthetases that initiate long-chain fatty acids to produce cytosolic lipids, while GPX4 is thought to be the major enzyme that suppresses ferroptosis by transforming lipid hydroperoxide into nontoxic lipid alcohols [30]. Former investigations have indicated that ACSL4 is essential for the triggering of iron atrophy and that suppression of ACSL4 inhibits the occurrence of iron atrophy [30]. The translational element NRF2, which is encoded by the NFE2L2 gene, is most well-known for controlling the performance of antioxidant and detoxifying genes. Gene-knockout approaches have proven its general cytoprotective properties. It is featured by its reliance on iron and the accumulated lipid peroxides. TfR1 and iron phagosome have been determined to be essential modulators of iron accretion. TfR1 are membrane-based proteins that translocate iron from the extracellular surroundings into the cell and facilitate the building of the cellular iron pool required for ferroptosis [31].

NRF2 has been the subject of intensive research in cancer biology since its discovery in 1994, and the comprehension of the effect of NRF2 in cardiovascular disorders is just emerging [32]. Our current results displayed that before the therapy of ECP to AMI patients, the lower expressions of NRF2 and HO-1 levels were exhibited in AMI cases than that in normal controls. However, the levels of NRF2 and HO-1 were evaluated after the patients accepted the ECP therapy. It is proven that ECP could activate the NRF2 pathway in blood samples of AMI patients. There are some limitations in this study. First, the sample size of this study is not large and it is a single-center study, so bias is inevitable. In future research, we will carry out multicenter, large-sample prospective studies, or more valuable conclusions can be drawn.

5. Conclusion

In conclusion, our findings in this research are that cardiac ECP is able to attenuate myocardial injury by regulating NRF2-mediated ferroptosis and oxidative stress injury in AMI patients. This certainly gives the possibility of a clinically effective treatment for AMI patients, although further clinical trials need to be validated.

Data Availability

The datasets used and analyzed during the current study are available from the corresponding author upon reasonable request.

Conflicts of Interest

The authors declare that they have no conflicts of interest.

References

[1] M. Reindl, S. J. Reinstadler, H. J. Feistritzer et al., "Acute myocardial infarction as a manifestation of systemic vasculitis," *Wiener Klinische Wochenschrift*, vol. 128, no. 21-22, pp. 841–843, 2016.

[2] F. Vancheri, G. Longo, S. Vancheri, and M. Henein, "Coronary microvascular dysfunction," *Journal of Clinical Medicine*, vol. 9, no. 9, p. 2880, 2020.

[3] A. H. Shah, R. Puri, and A. Kalra, "Management of cardiogenic shock complicating acute myocardial infarction: a review," *Clinical Cardiology*, vol. 42, no. 4, pp. 484–493, 2019.

[4] A. A. Damluji, S. van Diepen, J. N. Katz et al., "Mechanical complications of acute myocardial infarction: a scientific statement from the American heart association," *Circulation*, vol. 144, no. 2, pp. e16–e35, 2021.

[5] S. Orellana-Urzúa, I. Rojas, L. Líbano, and R. Rodrigo, "Pathophysiology of ischemic stroke: role of oxidative stress," *Current Pharmaceutical Design*, vol. 26, no. 34, pp. 4246–4260, 2020.

[6] M. Xiang, Y. Lu, L. Xin et al., "Role of oxidative stress in reperfusion following myocardial ischemia and its treatments," *Oxidative Medicine and Cellular Longevity*, vol. 2021, Article ID 6614009, , 2021.

[7] T. Nakamura, I. Naguro, and H. Ichijo, "Iron homeostasis and iron-regulated ROS in cell death, senescence and human diseases," *Biochimica et Biophysica Acta (BBA)—General Subjects*, vol. 1863, no. 9, pp. 1398–1409, 2019.

[8] M. Dodson, R. Castro-Portuguez, and D. D. Zhang, "NRF2 plays a critical role in mitigating lipid peroxidation and ferroptosis," *Redox Biology*, vol. 23, Article ID 101107, 2019.

[9] X. Zhang, Y. Yu, H. Lei et al., "The nrf-2/HO-1 signaling Axis: a ray of hope in cardiovascular diseases," *Cardiology Research and Practice*, vol. 2020, Article ID 5695723, , 2020.

[10] C. W. S. Hoong, M. L. S. Tan, S. L. Kao, and E. Y. H. Khoo, "Effects of external counter-pulsation on endothelial function assessed by peripheral artery tonometry, levels of glycaemia and metabolic markers in individuals with type 2 diabetes mellitus," *Diabetes & Metabolic Syndrome: Clinical Research Reviews*, vol. 14, no. 6, pp. 2139–2145, 2020.

[11] A. Amritphale and N. Amritphale, "Refractory angina: the current state of mechanical therapies," *Current Cardiology Reports*, vol. 21, no. 6, p. 46, 2019.

[12] M. Akhtar, G. F. Wu, Z. M. Du, Z. S. Zheng, and A. D. Michaels, "Effect of external counterpulsation on plasma nitric oxide and endothelin-1 levels," *The American Journal of Cardiology*, vol. 98, no. 1, pp. 28–30, 2006.

[13] M. Tibaut, D. Mekis, and D. Petrovic, "Pathophysiology of myocardial infarction and acute management strategies," *Cardiovascular and Hematological Agents in Medicinal Chemistry*, vol. 14, no. 3, pp. 150–159, 2017.

[14] N. Uriel, G. Sayer, S. Annamalai, N. K. Kapur, and D. Burkhoff, "Mechanical unloading in heart failure," *Journal of the American College of Cardiology*, vol. 72, no. 5, pp. 569–580, 2018.

[15] B. Levy, N. Girerd, J. Amour et al., "HYPO-ECMO trial group and the international ecmo network (ECMONet). Effect of moderate hypothermia vs. normothermia on 30-day mortality in patients with cardiogenic shock receiving venoarterial extracorporeal membrane oxygenation: a randomized clinical trial," *JAMA*, vol. 327, no. 5, pp. 442–453, 2022.

[16] K. Brieger, S. Schiavone, F. J. Miller, and K. H. Krause, "Reactive oxygen species: from health to disease," *Swiss Medical Weekly*, vol. 142, 2012.

[17] K. Watanabe, M. Nagao, R. Toh et al., "Critical role of glutamine metabolism in cardiomyocytes under oxidative stress," *Biochemical and Biophysical Research Communications*, vol. 534, pp. 687–693, 2021.

Hindawi
Evidence-Based Complementary and Alternative Medicine
Volume 2023, Article ID 9846920, 1 page
https://doi.org/10.1155/2023/9846920

Retraction

Retracted: Prognostic Value of Lactate Dehydrogenase, Melanoma Inhibitory Protein, and S-100B Protein in Patients with Malignant Melanoma

Evidence-Based Complementary and Alternative Medicine

Received 3 October 2023; Accepted 3 October 2023; Published 4 October 2023

This article has been retracted by Hindawi following an investigation undertaken by the publisher [1]. This investigation has uncovered evidence of one or more of the following indicators of systematic manipulation of the publication process:

(1) Discrepancies in scope
(2) Discrepancies in the description of the research reported
(3) Discrepancies between the availability of data and the research described
(4) Inappropriate citations
(5) Incoherent, meaningless and/or irrelevant content included in the article
(6) Peer-review manipulation

The presence of these indicators undermines our confidence in the integrity of the article's content and we cannot, therefore, vouch for its reliability. Please note that this notice is intended solely to alert readers that the content of this article is unreliable. We have not investigated whether authors were aware of or involved in the systematic manipulation of the publication process.

Wiley and Hindawi regrets that the usual quality checks did not identify these issues before publication and have since put additional measures in place to safeguard research integrity.

We wish to credit our own Research Integrity and Research Publishing teams and anonymous and named external researchers and research integrity experts for contributing to this investigation.

The corresponding author, as the representative of all authors, has been given the opportunity to register their agreement or disagreement to this retraction. We have kept a record of any response received.

References

[1] S. Fan, X. Liu, Y. Wu et al., "Prognostic Value of Lactate Dehydrogenase, Melanoma Inhibitory Protein, and S-100B Protein in Patients with Malignant Melanoma," *Evidence-Based Complementary and Alternative Medicine*, vol. 2022, Article ID 9086540, 7 pages, 2022.

Hindawi
Evidence-Based Complementary and Alternative Medicine
Volume 2022, Article ID 9086540, 7 pages
https://doi.org/10.1155/2022/9086540

Research Article

Prognostic Value of Lactate Dehydrogenase, Melanoma Inhibitory Protein, and S-100B Protein in Patients with Malignant Melanoma

Shuwen Fan, Xiao Liu, Yizhu Wu, Ke Li, Xiaoyu Zhao, Wei Lin, and Jianjiang Liu

Department of Burn and Plastic Surgery, The First Affiliated Hospital of Soochow University, Suzhou, Jiangsu 215000, China

Correspondence should be addressed to Jianjiang Liu; sdfyyliu@163.com

Received 15 July 2022; Revised 11 August 2022; Accepted 30 August 2022; Published 4 October 2022

Academic Editor: Xueliang Wu

Objective. This investigation probed the prognostic potential for lactate dehydrogenase (LDH), melanoma inhibitory activity protein (MIA), and S-100B protein in cases of malignant melanoma. *Methods*. 84 cases were segregated into effective cohort ($n = 64$) and ineffective cohort ($n = 20$) depending on clinical efficacy. The cases were followed up for three years and segregated into mortality cohort ($n = 29$) and survival cohort ($n = 55$) depending upon 3-year survival. Serum LDH, MIA, and S-100B levels were compared across the effective and ineffective cohorts. Serum LDH, MIA, and S-100B levels in cases of different clinical stages were comparatively analyzed, with correlations of these indicators with the clinical stage being evaluated. ROC evaluated the prognostic potential of serum LDH, MIA, and S-100B. Cases were segregated into the high-level and low-level cohorts according to serum LDH, MIA, and S-100B levels, and the survival rates of cases were compared. *Results*. The levels of LDH, MIA, and S-100B in the effective cohort were significantly lower than those in the ineffective cohort. The AUC value of the composite indicator of serum LDH, MIA, and S-100B for effectiveness evaluation was (0.839). Serum LDH, MIA, and S-100B levels were positively linked to the clinical stage. AUC value of the composite indicator of serum LDH, MIA, and S-100B for prognosis evaluation prediction (0.942) was elevated compared to LDH (0.632), MIA (0.732), or S-100B (0.828) alone. Survival rate of cases of LDH ≥30.56 mg/L (57.14%, 32/56) was lower than that of cases of LDH <30.56 mg/L (82.14%, 23/28) (log-rank $\chi^2 = 4.672$, $P < 0.05$). The survival rate of MIA ≥5.34 ng/mL cases was lower than that of MIA <5.34 ng/mL cases. The survival rate of cases of S-100B ≥ 1.03ug/L was lower than that of S-100B < 1.03ug/L. *Conclusion*. Serum LDH, MIA, and S-100B protein levels are linked to the clinical stage. The lactate dehydrogenase, melanoma inhibitory protein, and S-100B protein are of good clinical effectiveness and have the prognostic potential for cases of malignant melanoma.

1. Introduction

Malignant melanoma (MM) is a malignant tumor of epithelial origin, and its incidence has shown an increasing trend in recent years. Ultraviolet radiation (UV) and malignant changes in moles are risk factors for MM. Surgical resection, radiotherapy, and chemotherapy are often employed in the clinical treatment of melanoma. It is reported that the 5-year survival rate of cases of MM in the United States is 98%, and the 5-year survival rate in cases of stage IV melanoma is 3%. Therefore, early prediction of melanoma cases is crucial, which is conducive to the personalized and accurate treatment of cases of MM [1–3].

Serum-based lactate dehydrogenase (LDH) is a critical member of the glycolytic enzymatic family, which might mediate the oxidation of lactic acid to pyruvate and increase serum LDH levels. Emerging evidence indicates that LDH is associated with heavy tumor load and poor prognosis [4, 5]. Melanoma inhibitory activity protein (MIA) is closely related to malignant tumor proliferation, metastasis, and invasion. Moreover, MIA could accelerate tumor cell apoptosis and block tumor angiogenesis [6, 7]. MIA can specifically inhibit the adhesion of melanoma cells to fibronectin and laminin, affecting tumor cell metastases; S-100b protein is highly expressed in MM and is also found to be elevated in the normal population [8–10]. S-100B proteomic expression

can reflect the tumor load of cases and is related to the recurrence and progression of the disease.

The current study explores the predictive value of LDH, MIA, and S-100B protein levels in the prognosis of patients with malignant melanoma.

2. Material and Methods

2.1. General Data. Eighty-four cases of advanced melanoma treated in our hospital from January 2013 to February 2019 were accepted, including 53 males and 31 females. Age ranged from 41 to 72 years, with a mean of 55.65 ± 5.72 years. The Hospital Ethics Committee accepted this investigation. Inclusion criteria: (1) All subjects were in line with the relevant standards of *Clinical Practice Guidelines for Pathological Diagnosis of Melanoma (2021 edition)* [11]; (2) All cases were the first onset; (3) All subjects had an expected survival time >3 months; (4) All subjects had complete clinicopathological data; (5) All subjects volunteered to participate in this study. Exclusion criteria: (1) Cases aged >75 years; (2) Cases of other malignant tumor diseases; (3) No drug, laser, or radiotherapy was given before enrollment; (4) Cases of autoimmune diseases; (5) Cases of severe cardiac/hepatic/renal dysfunction; (6) Cases of distant metastasis; (7) Cases of severe adverse reactions to chemotherapy.

2.2. Therapeutic Methods. After admission, all patients received relevant examination and chemotherapy risk assessment and were treated with high-dose recombinant human α-2b interferon combined with conventional chemotherapy. The recombinant human interferon α-2b of 3 million U + injection 2 mL was injected subcutaneously on d 3, 6 million U + 2 mL on d 6 and 9 million U + 2 mL on d 9. The treatment lasted 4 courses, 21 days as the course of treatment. The conventional chemotherapy regimen was dacarbazine + cisplatin + vincristine + doxorubicin, and the administration standard was as follows: intravenous drip of dacarbazine 100 mg/m^2 during d1 to d5; cisplatin 20 mg/m^2, vincristine 2 mg, and doxorubicin 50 mg were given intravenously during d1 to d8. On d1, 80 mg/m^2 of lomustine was taken orally. The treatment continued for four courses with 21 days as a course.

2.3. Clinical Effectiveness Evaluation. All cases were assessed depending on effectiveness parameters for solid tumors [12] and were segregated into complete response (CR), partial response (PR), stable disease (SD), and progressive disease (PD). CR: tumor diameter was reduced by ≥ 80%, no new lesions were developed, and the response was maintained for at least four weeks; PR: the tumor diameter was reduced by 50% to 79%, and the response remained for at least four weeks; SD: the tumor diameter was reduced by 30%~49%; PD: the tumor diameter was reduced by <29% or a had an increase, or new lesions emerged. Total response = CR + PR + SD.

2.4. Prognostic Evaluation. All cases were followed up remotely/outpatient-based follow-up for three years. Cases were segregated into mortality cohort and survival cohort according to 3-year survival.

2.5. Detection of Serum LDH, MIA, and S-100B Protein Levels. 10 mL of fasting venous blood was taken from individual cases in the morning and centrifuged at 2500 r/min for 15 min. The upper serum was collected and stored at −80°C. Serum LDH, MIA, and S-100B proteomic expression were identified through enzyme-linked immunosorbent assay (ELISA). The normal value of serum LDH is 100–300u/l. The average level of serum S-100B > 0.4 μg/kg indicates a poor prognosis.

2.6. Observation Indicators. (1) Serum LDH, MIA, and Smur100 B levels were compared between valid and ineffective cohorts. (2) The clinical value of serum lactate dehydrogenase, lactam, and Smur100B levels was evaluated by ROC curve. (3) Serum LDH, MIA, and S-100B levels in cases of different clinical stages were compared to evaluate the correlation of serum LDH, MIA, and S-100B levels with clinical stages. (4) The levels of serum lactate dehydrogenase, lactam, and Smur100B, including survival time and mortality cohort, were compared. (5) The prognostic potential of serum lactate dehydrogenase, lactam and Smur100 B levels were evaluated by ROC. (6) According to serum LDH, MIA, and S-100B levels, cases were segregated into the high-level and low-level cohorts. The survival curves of cases of differing serum LDH, MIA, and S-100B levels were evaluated, and the survival rates of cases of different levels were compared.

2.7. Statistical Analysis. Data were processed through SPSS® 24.0 and GraphPad Prism 5. Descriptive statistics were expressed as Mean ± SD ($\overline{x}$ ± S). Categorical variables were represented as n and %, chi-square test was employed to analyze the across cohorts, and rank sum test was employed for ranked data. The prognostic values of lactate dehydrogenase, melanoma inhibitory protein, and S-100B protein in patients with malignant melanoma in different groups were calculated by the Kaplan–Meier method, and the cumulative incidence was compared between groups by the log-rank method. ROC curve was employed to assess the evaluation value of serum LDH, MIA, and S-100B levels for the clinical effectiveness in patients with MM. Spearman correlation analysis was employed to evaluate the correlation across the AJCC stage and serum LDH, MIA, and S-100B

levels. Log-rank χ^2 test was employed to evaluate the survival rate among the two cohorts. All tests were two-sided, and $P < 0.05$ was considered a statistical significance.

3. Results

3.1. Clinical Effectiveness. A total of 11 cases of CR, 28 cases of PR, 25 cases of SD, and 20 cases of PD were identified. The total effective rate was 76.19% (64/84).

3.2. Comparison of Serum LDH, MIA, and S-100B Levels between the Influential and Ineffective Cohort. Serum LDH, MIA, and S-100B levels in the influential cohort were reduced compared with those in the ineffective cohort (all $P < 0.05$, Table 1).

3.3. Association between Serum LDH, MIA, and S-100B Levels and Clinical Effectiveness. The AUC value of the combined evaluation with serum LDH, MIA, and S-100B (0.839) was elevated compared to LDH alone (0.699) ($P < 0.05$, Table 2 and Figure 1).

3.4. Comparative Analysis of Serum LDH, MIA, and S-100B Levels in Differing Clinical Stages. Serum LDH, MIA, and S-100B levels in stages II, III, and IV were elevated compared with those in stage I, the levels of the above indicators in stage III and IV were elevated compared with those in stage II, and the levels in stage IV were elevated compared with those in stage III (all $P < 0.05$, Table 3).

3.5. Correlation Analysis of Serum LDH, MIA, And S-100B Levels with Clinical Stage. Serum LDH, MIA, and S-100B levels were positively linked to the clinical stage (all $P < 0.05$, Figure 2).

3.6. Comparative Analysis of Serum LDH, MIA, and S-100B Levels across Survival Cohort and Mortality Cohort. The serum LDH, MIA, and S-100B levels in the survival cohort were reduced compared with those in the mortality cohort (all $P < 0.05$, Table 4).

3.7. Prognostic Value of Serum LDH, MIA, and S-100B Levels. The AUC value of the combination of serum LDH, MIA, and S-100B indicators to predict prognosis (0.942) was better than LDH (0.632), MIA (0.732), or S-100B (0.828) alone (all $P < 0.05$, Table 5 and Figure 3).

3.8. Survival Curve Analysis of Cases of Differing Serum LDH, MIA, and S-100B Levels. The survival rate of cases of LDH ≥30.56 mg/L (57.14%, 32/56) was lower than that of cases of LDH<30.56 mg/L (82.14%, 23/28) (log-rank k $\chi^2 = 4.672$, $P < 0.05$). The survival rate of cases of MIA ≥5.34 ng/mL (55.38%, 36/65) was lower than that of cases of MIA <5.34 ng/mL (100%, 19/19) (log-rank $\chi^2 = 10.810$, $P < 0.05$). The survival rate of cases of S-100B ≥ 1.03 ug/L (26.77%, 17/40) was lower than that of cases of S-100B < 1.03 ug/L (86.36%, 38/44) (log-rank $\chi^2 = 17.060$, $P < 0.05$) (Figure 4).

4. Discussion

Cutaneous melanoma is a highly malignant tumor with a high recurrence rate and uncomplicated metastasis. Its prognosis is related to many factors, such as treatment timing, treatment method, and the presence of metastasis. Surgical resection is the first choice for clinical treatment of MM, but due to the number of lesions, anatomical location, and recurrence after surgical resection, surgery is not suitable for all cases of MM. Immunotherapy, targeted therapy, and other methods have been gradually applied to MM treatment. Recombinant human α-2b interferon is a secretory protein with antitumor, antivirus, and immunomodulatory functions. By imitating the function of interferon in the body, it plays a variety of biological activities, has the advantage of a fast metabolism, and can reduce the burden on the liver. In the present study, recombinant human interferon α-2b showed an excellent effect in MM treatment, with a total effective rate of 76.19% (64/84).

LDH exists widely in many human tissues and is involved in the glycolysis pathway. It is reported that glycolysis and LDH activity in malignant tumors is significantly higher than that in normal tissues. Therefore, the serum lactate dehydrogenase level in cancer patients increases, and lactate dehydrogenase is related to the prognosis of various malignant tumors [13, 14]. Previous studies have shown that LDH is an independent risk factor for prognosis MM cases, and the serum LDH level in MM cases is high [15, 16]. In addition, it has been reported that serum LDH levels have shown varying degrees of elevation, indicating anaerobic glycolysis in tissues before imaging manifestations in tumor cases. MIA is a secretory tumor growth suppressor that can regulate cell adhesion by specifically inhibiting melanoma cell adhesion to fibronectin laminin to regulate melanoma cell shedding from the extracellular matrix and ultimately affect tumor metastases. Evidence has indicated that MIA was highly expressed in the serum of MM patients, while overexpression of MIA may indicate a poor prognosis [17, 18]. S-100b protein is an acidic calcium-binding protein, widely existing in normal tissue cells of nerve ectodermal leaf, mesoderm, and ectoderm, or originating from cell tumors.

Most of them exist in cells and can be released into the blood when cells proliferate massively. It has been reported that S-100B protein is rarely expressed in nonmelanocyte tumors, and serum S-100B protein level is intimately linked with individual case tumor load. In addition, serum S-100B protein can reflect the therapeutic effect of patients and be employed as a prognostic indicator of MM. The elevation of the S-100B protein level in serum of MM cases occurred earlier than the onset of clinical symptoms [18, 19]. In the present study, the serum LDH, MIA, and S-100B levels in the influential cohort were reduced compared to the ineffective cohort, and the AUC value of the combined evaluation for clinical effectiveness with serum LDH, MIA, and S-100B (0.839) was higher than that with LDH (0.699) alone

Table 1: Comparison of serum LDH, MIA, and S-100B levels between the two cohorts ($\overline{x} \pm s$).

Cohort	LDH (mg/l)	MIA (ng/ml)	S-100B (ug/l)
Effective cohort ($n = 64$)	37.84 ± 16.35	7.68 ± 4.10	1.03 ± 0.45
Ineffective cohort ($n = 20$)	51.62 ± 20.44	13.11 ± 4.63	1.71 ± 0.68
t-value	3.095	5.019	4.177
P-value	0.003	<0.001	<0.001

Table 2: Evaluation value of serum LDH, MIA, and S-100B levels for clinical effectiveness.

Indicator	Cut-off value	AUC	SE	95% CI
LDH	31.56	0.699*	0.064	0.573~0.825
MIA	11.73	0.789	0.058	0.686~0.911
NWR	1.27	0.794	0.059	0.678~0.909
Combination		0.839	0.053	0.735~0.943

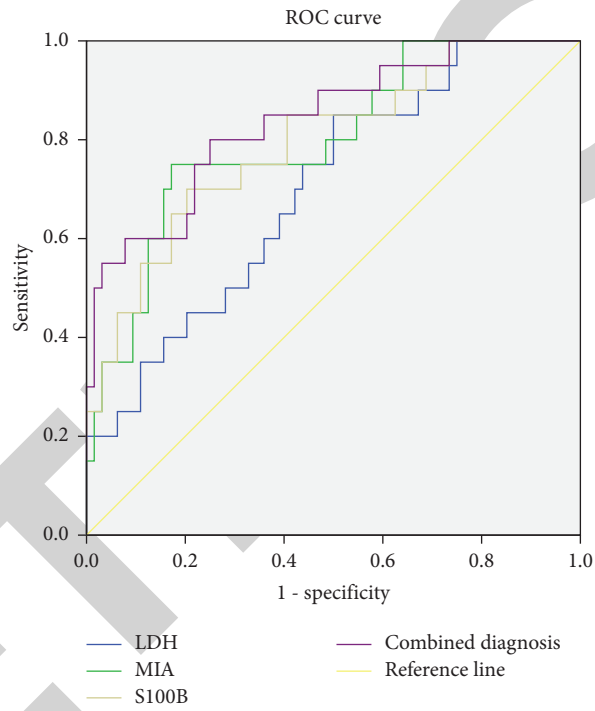

Figure 1: ROC curve analysis of evaluation value of LDH, MIA, and S-100B levels for clinical effectiveness. Note: Compared with combination, $^{*}P < 0.05$.

Table 3: Comparative analysis of serum LDH, MIA, and S-100B levels in differing clinical stages ($x \pm s$).

AJCC stage	LDH (mg/l)	MIA (ng/ml)	S-100B (ug/l)
Stage I ($n = 9$)	15.63 ± 1.89	2.99 ± 1.48	0.47 ± 0.17
Stage II ($n = 38$)	30.19 ± 4.31^{a}	6.39 ± 2.75^{a}	0.97 ± 0.37^{a}
Stage III ($n = 24$)	51.53 ± 5.43^{ab}	11.58 ± 2.70^{ab}	1.34 ± 0.42^{ab}
Stage IV ($n = 13$)	71.52 ± 10.28^{abc}	15.84 ± 2.83^{abc}	2.06 ± 0.47^{abc}
F-value	250.393	64.176	37.142
P-value	<0.001	<0.001	<0.001

Note: Compared with stage I, $^{a}P < 0.05$; compared with stage, $^{b}P < 0.05$; Compared with stage III, $^{c}P < 0.05$.

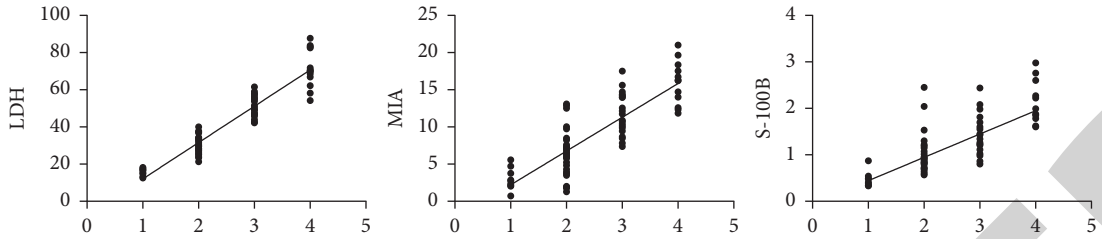

Figure 2: Correlation analysis of serum LDH, MIA, and S-100B levels with clinical stage.

Table 4: Comparative analysis of serum LDH, MIA, and S-100B levels across survival cohort and mortality cohort ($\overline{x} \pm s$).

Cohort	LDH (mg/l)	MIA (ng/ml)	S-100B (ug/l)
Survival cohort ($n = 55$)	37.97 ± 16.41	7.62 ± 4.38	0.96 ± 0.42
Mortality cohort ($n = 29$)	47.10 ± 20.31	11.54 ± 4.58	1.62 ± 0.62
t-value	2.230	3.840	5.087
P-value	0.029	<0.001	<0.001

Table 5: Prognostic values of serum LDH, MIA, and S-100B levels.

Indicator	Cut-off value	AUC	SE	95% CI
LDH	30.56	0.632*	0.063	0.509~0.755
MIA	5.34	0.732*	0.055	0.625~0.839
S-100B	1.03	0.828*	0.044	0.742~0.913
Combination		0.942	0.028	0.888~0.997

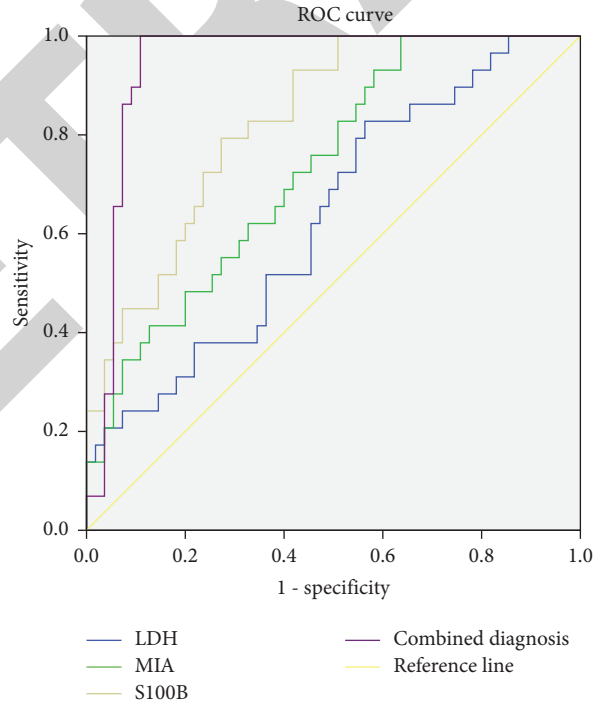

Figure 3: Prognostic value of serum LDH, MIA, and S-100B levels. Note: Compared with combination, $^*P < 0.05$.

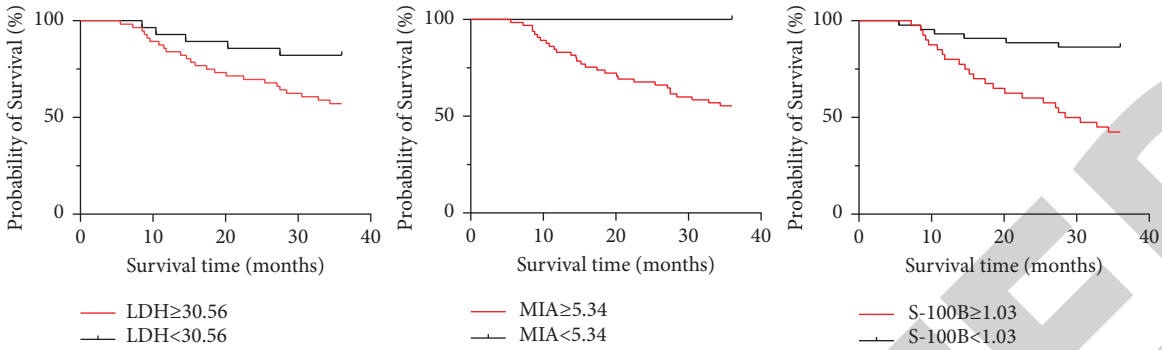

Figure 4: Survival curve analysis of cases of differing serum LDH, MIA, and S-100B levels.

($P < 0.05$). The result indicated that serum LDH, MIA, and S-100B levels are related to the therapeutic effect of recombinant human α-2b interferon on MM. These indicators can be employed to predict the clinical effectiveness of recombinant human α-2b interferon on MM.

AJCC stage is a commonly employed tool for clinically evaluating the severity and prognosis of malignant tumor diseases. However, the clinical application is subject to the subjective influence of the operator, which cannot be objective and cannot be applied to ultra-early diagnosis. In the present study, serum LDH, MIA, and S-100B levels of AJCC stage II, III, and IV were higher than those of stage I, serum LDH, those of stage III and IV were higher than those of stage II, those of stage IV were higher than those of stage III, suggesting the correlation of serum LDH, MIA, and S-100B levels with AJCC tumor stage. Spearman correlation analysis showed that serum LDH, MIA, and S-100B levels were positively linked to the clinical stage (all $P < 0.05$), suggesting that the elevation of serum LDH, MIA, and S-100B may be related to tumor progression. Detecting these tumor markers is convenient and plays a particular role in predicting recurrence and metastasis. Serum LDH, MIA, and S-100B levels are positively linked to the clinical stage, so the stability or progression of the disease can be judged based on the changes in serum LDH, MIA, and S-100B levels.

Tumor cell metabolism is unique and characterized by increased glucose uptake and glycolysis. Tumor cells metabolize energy through glycolysis regardless of oxygen availability. LDH is a crucial catalytic enzyme in the glycolysis pathway. LDH can promote pyruvate to generate lactate, and lactate accumulation can provide an acidic microenvironment conducive to tumor growth, invasion, and metastasis [20, 21]. Previous studies have shown that MIA and S-100B are closely related to the occurrence and development of MM [22, 23]. In the present study, the levels of serum LDH, MIA, and S-100B in the survival cohort were significantly reduced compared to those in the mortality cohort (all $P < 0.05$); the AUC value of serum LDH, MIA, and S-100B combined indicator (0.942) was higher than that with LDH (0.632), MIA (0.732), or S-100B (0.828) alone (all $P < 0.05$); the survival rates of cases of LDH ≥30.56 mg/L, MIA ≥5.34 ng/mL, or S-100B ≥ 1.03ug/L were lower than those of cases of LDH <30.56 mg/L, MIA ng/mL < 5.34, or S-100B < 1.03 ug/L. All these results suggested that serum LDH, MIA, or S-100B levels can be employed to evaluate the prognosis of MM. Elevated LDH levels are associated with the glycolysis pathway, which provides a favorable environment for tumor growth. MIA explicitly inhibits the adhesion of melanoma cells to fibronectin and laminin, affecting the metastasis of tumor cells, and its specific mechanism remains to be further explored. Previous studies have shown that S-100B is positively linked to the MM stage [24, 25], which is consistent with the results of the present study.

To sum up, serum LDH, MIA, and Smur100 B levels correlate with the clinical stage, and their combined detection is of value in evaluating the therapeutic effect and predicting the prognosis of MM cases. The limitation of this study is that a single-center retrospective study may lead to statistical bias. In a further study, a multicenter analysis could be performed to assess the correlation between serum lactate dehydrogenase, lactam, and Smur100B levels and MM.

Data Availability

The labeled dataset used to support the findings of this study are available from the corresponding author upon request.

Conflicts of Interest

The authors declare that they have no conflicts of interest.

References

[1] B. Ahmed, M. I. Qadir, and S. Ghafoor, "Malignant melanoma: skin cancer-diagnosis, prevention, and treatment[J]," *Critical Reviews in Eukaryotic Gene Expression*, vol. 30, no. 4, pp. 291–297, 2020.

[2] R. Cabrera and F. Recule, "Unusual clinical presentations of malignant melanoma: a review of clinical and histologic features with special emphasis on dermatoscopic findings," *American Journal of Clinical Dermatology*, vol. 19, pp. 15–23, 2018.

[3] T. Knackstedt, R. W. Knackstedt, R. Couto, and B. Gastman, "Malignant melanoma: diagnostic and management update," *Plastic and Reconstructive Surgery*, vol. 142, no. 2, pp. 202–216, 2018.

[4] D. Hermans, S. Gautam, J. C. García-Cañaveras et al., "Lactate dehydrogenase inhibition synergizes with IL-21 to promote

Hindawi
Evidence-Based Complementary and Alternative Medicine
Volume 2023, Article ID 9762457, 1 page
https://doi.org/10.1155/2023/9762457

Retraction

Retracted: Heparin-Binding Protein Aggravates Acute Lung Injury in Septic Rats by Promoting Macrophage M1 Polarization and NF-κB Signaling Pathway Activation

Evidence-Based Complementary and Alternative Medicine

Received 1 August 2023; Accepted 1 August 2023; Published 2 August 2023

This article has been retracted by Hindawi following an investigation undertaken by the publisher [1]. This investigation has uncovered evidence of one or more of the following indicators of systematic manipulation of the publication process:

(1) Discrepancies in scope
(2) Discrepancies in the description of the research reported
(3) Discrepancies between the availability of data and the research described
(4) Inappropriate citations
(5) Incoherent, meaningless and/or irrelevant content included in the article
(6) Peer-review manipulation

The presence of these indicators undermines our confidence in the integrity of the article's content and we cannot, therefore, vouch for its reliability. Please note that this notice is intended solely to alert readers that the content of this article is unreliable. We have not investigated whether authors were aware of or involved in the systematic manipulation of the publication process.

Wiley and Hindawi regrets that the usual quality checks did not identify these issues before publication and have since put additional measures in place to safeguard research integrity.

We wish to credit our own Research Integrity and Research Publishing teams and anonymous and named external researchers and research integrity experts for contributing to this investigation.

The corresponding author, as the representative of all authors, has been given the opportunity to register their agreement or disagreement to this retraction. We have kept a record of any response received.

References

[1] Y. Zhang, W. Sun, and L. Zhang, "Heparin-Binding Protein Aggravates Acute Lung Injury in Septic Rats by Promoting Macrophage M1 Polarization and NF-κB Signaling Pathway Activation," *Evidence-Based Complementary and Alternative Medicine*, vol. 2022, Article ID 3315601, 7 pages, 2022.

Hindawi
Evidence-Based Complementary and Alternative Medicine
Volume 2022, Article ID 3315601, 7 pages
https://doi.org/10.1155/2022/3315601

Research Article

Heparin-Binding Protein Aggravates Acute Lung Injury in Septic Rats by Promoting Macrophage M1 Polarization and NF-κB Signaling Pathway Activation

Ying Zhang,[1] **Wenqiao Sun**,[2] **and Licheng Zhang**[2]

[1]*Department of Diagnostic Ultrasound, Southern War Zone General Hospital, Guangzhou, Guangdong, China*
[2]*Minimally Invasive Interventional Oncology Department, Weihai Municipal Hospital, Cheeloo College of Medicine, Shandong University, Jinan, Shandong, China*

Correspondence should be addressed to Ying Zhang; qianqian20080807@126.com

Received 26 July 2022; Revised 16 September 2022; Accepted 20 September 2022; Published 3 October 2022

Academic Editor: Xueliang Wu

Objective. Heparin-binding protein (HBP) plays an important role in sepsis and is a prognostic biomarker in patients with sepsis, but the role of HBP in the pathogenesis of sepsis-associated acute lung injury (ALI) remains unclear. This study aimed to investigate the role of HBP in sepsis-induced ALI and its underlying molecular mechanisms. *Methods*. The cecal ligation and puncture (CLP) model was used to induce ALI in mice and randomly divided into 4 groups: control group, CLP (rats treated with cecal ligation and puncture), HBP (rats treated with CLP and HBP injection), and HBP + UFH (rats treated with CLP and injection of HBP and unfractionated heparin). Subsequently, HBP expression in rat serum and lung tissues was detected by qRT-PCR, edema and pathological changes in lung tissue by lung wet-to-dry weight ratio (W/*D*) and HE staining, myeloperoxidase (MPO) and superoxide dismutase (SOD) activities in lung tissues by detection kits. Additionally, ELISA and western blot were applied for the determination of IL-6, TNF-*α*, and IL-1*β* expression in rat bronchoalveolar lavage fluid, and iNOS, Arg-1, Mrc1, NF-*κ*Bp65, IKK*α*, I*κ*B*α*, and p-I*κ*B*α* expression in lung tissues. *Results*. The expression levels of HBP in serum and lung tissues of rats in the HBP group were significantly increased, the lung tissues were severely injured, accompanied by a significant increase in MPO activity but a significant decrease in SOD activity, and the levels of IL-6, TNF-*α*, and IL-1*β* in bronchoalveolar lavage fluid were significantly increased. In addition, the expression levels of iNOS, NF-*κ*B p65, IKK*α*, and p-I*κ*B*α* in the lung tissues of rats in the HBP group were significantly increased, while the addition of unfractionated heparin reversed the above results. *Conclusion*. HBP aggravates ALI in septic rats, and its mechanism may be related to the promotion of macrophage M1 polarization and activation of the NF-*κ*B signaling pathway.

1. Introduction

Sepsis is a systemic inflammatory response syndrome that damages the body, caused by a dysregulated host response to infection [1]. This disease occurs in patients with severe traumatic infections or with various chronic diseases, leading to life-threatening organ dysfunction [2,3]. The lung is one of the most vulnerable organs in sepsis, so sepsis patients are often complicated by acute lung injury (ALI), whose morbidity and mortality are increasing year by year [4,5]. However, the molecular mechanism of sepsis complicated by ALI remains unclear. Wang et al. showed that hederagenin inhibition by inhibiting the NF-*κ*B pathway and NLRP3 inflammasome activation reduces inflammatory response and macrophage M1 polarization, thereby playing a protective role against sepsis-induced ALI [6]. Jiao et al. found that exosomal miR-30d-5p from polymorphonuclear neutrophils contributed to sepsis-related ALI by inducing M1 macrophage polarization and priming macrophage pyroptosis through activating NF-*κ*B signaling [7]. Therefore, M1 macrophages and the NF-*κ*B signaling pathway play an important role in the pathogenesis of sepsis complicated with ALI.

Heparin-binding protein (HBP) belongs to the serine protease family, also known as cationic antibiotic protein 37 (CAP37), is a multifunctional inflammatory mediator present

in polymorphonuclear leukocyte (PMN) granules [8]. In the body attacked by sepsis, neutrophils activated by bacteria, toxins, and coagulation factor complexes [9,10] adhere to vascular endothelial cells to release HBP [11]. Subsequently, activation of Ca^{2+} and an increase in vascular permeability are induced, causing leakage of macromolecules and tissue injury. As a result, the body develops an inflammatory response, which destroys the stability of the internal environment and further leads to cell hypoxia, decreased effective circulating volume, organ failure, and consequently hypotension, or even shock [12,13]. Therefore, HBP can be used as a biomarker to predict the development and prognosis of sepsis [14]. Fisher et al. have found that HBP causes renal inflammation and capillary leakage [15]. There are studies indicating the involvement of HBP in the pathological process of ALI [16,17], but the mechanisms underlying this involvement are unclear. Therefore, in this study, cecal ligation and puncture (CLP) were performed to simulate the process of sepsis-induced ALI and, consequently, to obtain a rat model of sepsis. Then, the general conditions of rats in each group were observed, followed by the measurement of the changes of superoxide dismutase (SOD) and myeloperoxidase (MOP) activities in lung tissue, the levels of inflammatory cytokines in bronchoalveolar lavage fluid, and the expression of NF-κB signaling pathway-related proteins in lung tissue. This investigation seeks to explain the mechanism of HBP on sepsis-induced ALI and thus provide a theoretical basis for the clinical treatment of this disease.

2. Materials and Methods

2.1. Animals. A total of 24 male SD rats aged 6 weeks, weighing 180–220 g, were purchased from the Research Center of Shanghai Model Organisms and subsequently fed adaptively for one week. Feeding conditions were as follows: 24 ± 1°C, relative humidity: 65%, light cycle: 12 h light/12 h dark cycle, and free access to water. The animal experiments described in this study were authorized by the Experimental Animal Ethics Committee of the Guangdong Medical Experimental Center (2022-011).

2.2. Reagents. HBP and heparin sodium injections were purchased from Shanghai Sig Biotechnology Co., Ltd.; pentobarbital sodium and TRIzol ® kit from Beijing Solarbio Science&Technology Co., Ltd.; ELISA assay kits for tumor necrosis factor-α (TNF-α) and interleukin-1β (IL-1β), interleukin-6 (IL-6), as well as SOD and MOP kits from Nanjing Jiancheng Bioengineering Institute; qRT-PCR kit from VazymeBiotech; BCA protein assay kit from Beyotime Biotechnology Co., Ltd.; and antibodies from Abcam.

2.3. Methods

2.3.1. Model Preparation and Grouping. SD male rats were adaptively fed for a week. Before the operation, the rats were fasted but allowed to drink water. After monitoring general conditions and weighing, the rats were anesthetized with an intraperitoneal injection of 1% pentobarbital sodium at 50 mg/kg. A total of 24 SPF SD rats were randomly divided into the control group, CLP group, HBP group, and HBP + unfractionated heparin (UFH) group.

In the control group, the rats underwent laparotomy to expose the cecum without ligation and puncture and received a postoperative subcutaneous injection of normal saline at 30 mL/kg for fluid replacement. In the CLP group, after laparotomy for exposure of the cecum, the cecum was ligated at 1/2 and punctured once with a no.21 needle in the area with the least blood vessels. Subsequently, a small number of contents was extruded from the puncture site, the cecum was returned, and the incision was sutured. The rats also received a postoperative subcutaneous injection of normal saline at 30 mL/kg for fluid replacement. In the HBP group, the rats were injected intravenously with HBP 30 min before surgery, followed by the same modeling protocol as the CLP group. In the HBP + UFH group, the rats were injected intravenously with 0.4 U/g UFH and subsequently with an intravenous injection of HBP 30 min before surgery, followed by the same modeling protocol as in the CLP group. At 48 hours after surgery, rat serum, lung tissue, and bronchoalveolar lavage fluid were taken for index detection.

2.3.2. qRT-PCR. After collection of rat serum and lung tissues, total cellular RNA was extracted by utilizing the Trizol kit and stored at −80°C. After reverse transcription converting RNA to cDNA under the reverse transcription PCR kit instructions, the synthesized cDNA was tested for concentration and purity. Then, cDNA was taken for reaction according to the instructions of qRT-PCR with the reaction system: 95°C for 1 min; 35 cycles of 95°C for 40 s, 58°C for 40 s, and 72°C for 45 s; and 72°C for 10 min. Data analysis was performed with the $2^{-\Delta\Delta Ct}$ method [18]. The primer sequence used is shown in Table 1.

2.3.3. Detection of Lung Wet-to-Dry Weight Ratio (W/D). The W/*D* ratio was measured to judge the condition of pulmonary edema. Specifically, the wet weight was weighed immediately after the right lungs were separated from each group of rats. Their dry weight was weighed after the right lungs were dried on a hot blast stove at 80°C for 48 hours.

2.3.4. HE Staining. For histopathological analysis, lung tissue sections were dried and fixed for 30 s at ambient temperature. Then the sections were rinsed with 1 × PBS for 2 s and stained with hematoxylin (60°C) for 60 s. Next, on completion of another rinsing step with 1 × PBS for 10 s, differentiation was carried out utilizing 1% hydrochloric acid alcohol for 3 s, followed by a 2 s rinsing step with 1 × PBS. After that, eosin was employed for staining for a period of 3 min, and subsequently 1 × PBS for 2 s rinsing. Dehydration was completed with 70%, 80%, 95% ethanol, and absolute ethanol for 5 min, followed by clearing used xylene (3 times/5 min). Finally, the sections were observed under a microscope (BX63, Olympus, Japan) after coverslipping using gum. The experiment was repeated three times.

Table 1: Primer sequences for qRT-PCR.

Gene	Primer sequence
HBP	F 5′-ACAACCTCA ACGTCATCCTG G-3′ R 5′- GTCTTCATTGAGGGCGTTGC-3′
GAPDH	F 5′-ACTCCACTCACGGCAAATTC-3′ R 5′-TCTCCTATGGTGGTGACGACA-3′

2.3.5. Determination of Biochemical Indicators. Bronchoalveolar lavage fluid was taken to determine TNF-α, IL-1β, and IL-6 levels by ELISA, while lung tissues were processed for detection of MPO and SOD activities according to the kit instructions.

2.3.6. Western Blot. Proteins were extracted from lung tissue with RIPA lysis buffer (BioSharp, China), and their concentrations were determined with a Pierce-BCA protein analysis kit (Thermo Fisher Scientific, Rockford, IL, USA). Then, after separation using SDS-PAGE, the proteins were blotted onto a PVDF membrane, followed by a 1 h blocking step using 5% nonfat dry milk prepared in TBST. Subsequently, overnight co-incubation of the membrane and primary antibodies was carried out at 4°C, followed by shaking and rinsing with PBST solution for 10 min three times. Next, diluted secondary antibodies were added for another 2 h of incubation at an ambient temperature, followed by a rinsing step. After that, the ECL agent was evenly dripped, and the FliorchemHD2 imaging system was used for scanning and analysis.

2.4. Statistical Analysis. By using SPSS 10.0, a *t*-test for comparison between groups and a one-way analysis of variance for comparison among groups were performed. All outcomes were expressed as mean ± standard deviation (SD). A significant difference was suggested if $P < 0.05$.

3. Results

3.1. Upregulation of HBP Expression in Serum and Lung Tissue of Sepsis-Induced ALI Rats. For determining the successful construction of a rat model of sepsis-associated ALI, qRT-PCR was carried out to measure the expression of HBP in rat serum and lung tissues. Specifically, in comparison with the control group, CLP induced a marked increase in HBP expression. In sepsis-induced ALI rats, injection of HBP further increased HBP expression. However, in comparison with the HBP group, HBP + UFH injection led to a decrease in HBP expression in the serum and lung tissues (Figures 1(a) and 1(b)).

3.2. HBP Promotes Lung Tissue Damage in Sepsis-Induced ALI Rats. HE staining, lung W/*D* ratio, and lung injury score were applied to evaluate what effect HBP has on sepsis-induced ALI. In the control group, HE staining showed no obvious pathological injury but observed an intact and clear structure of lung tissue, less interstitial inflammatory cell infiltration in the alveoli, no obvious congestion and hemorrhage, an intact alveolar wall, and no edema in the alveoli. In the CLP group, the alveolar wall was destroyed, and the staining showed thickening and edema of the alveolar wall, collapse of the alveolar space, inflammatory cell infiltration, and red blood cell exudation in the alveolar wall and space. In the HBP group, lung injury was more severe than that in the CLP group, and specifically, the HE staining revealed a large number of inflammatory cell infiltration, red blood cell exudation accompanied by pulmonary vascular congestion, and exudative fluid in the alveolar space. Compared with the HBP group, the degree of lung injury was improved in the HBP + UFH group (Figure 2(a)).

In comparison with the control group, the lung injury score was significantly increased in the rats treated with CLP. And HBP injection further increased the lung injury score in sepsis-induced ALI rats. However, after injection of UFH, a reduction was identified in the lung injury score (Figure 2(b)). Consistent results were obtained by the W/*D* method as well as by the lung injury score (Figure 2(c)).

3.3. HBP Increases Oxidative Stress in Sepsis-Induced ALI Rats. Oxidative stress is the fundamental mechanism of multiple organ and multiple system injury in sepsis [19], so we further examined the effect of HBP on oxidative stress in the lungs of rats. Biochemical tests proved that CLP increased MPO activity but decreased SOD activity in the lung tissue of rats. Further, in comparison with the CLP group, the HBP group showed a marked increase in MPO activity and a decrease in SOD activity in the lung tissues. In comparison with the HBP group, decreased MPO activity and increased SOD activity were confirmed in the lung tissue of the HBP + UFH group (Figure 3(a) and 3(b)).

3.4. HBP Promotes Inflammatory Responses in Rats with Sepsis-Induced ALI. Sepsis is, essentially, the result of a continuously deteriorating inflammatory response in the body [20]. ELISA results confirmed that CLP contributed to the up-regulation of IL-6, TNF-α, and IL-1β expression in the bronchoalveolar lavage fluid of rats, and the upregulation was further promoted by HBP injection. However, after treatment with UFH, IL-6, TNF-α, and IL-1β expression in the bronchoalveolar lavage fluid was significantly decreased (Figure 4(a)-4(c)).

3.5. HBP Promotes M1 Polarization of Macrophages in Sepsis-Induced ALI Rats. As one of the crucial components of innate and adaptive immunity, macrophages can differentiate into phenotypes with different functions when the microenvironment changes, which is called macrophage polarization. Macrophage polarization significantly affected the immune regulation in septic cases [21]. As shown in Figure 5, CLP induced an increase in iNOS expression but no significant difference was identified in Arg-1 and Mrc1 expression. In comparison with the CLP group, a significant upregulation of iNOS expression and no marked changes in Arg-1 and Mrc1 expression were found in the HBP group ($P > 0.05$). Further, compared with the HBP group, the HBP + UFH group showed significantly decreased iNOS

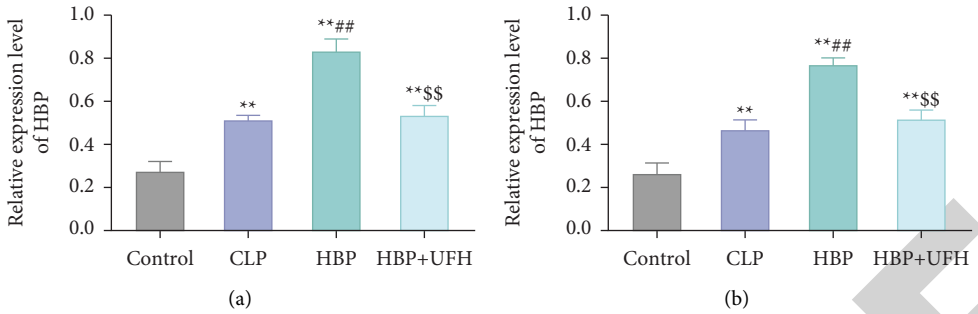

Figure 1: Upregulation of HBP expression in serum and lung tissue of sepsis-induced ALI rats. qRT-PCR-based detection of expression of heparin-binding protein in rat serum (a) and lung tissue (b). $^{**}P < 0.01$ vs. Control group, $^{\#\#}P < 0.01$ vs. CLP group, $P < 0.01$ *vs.* HBP group.

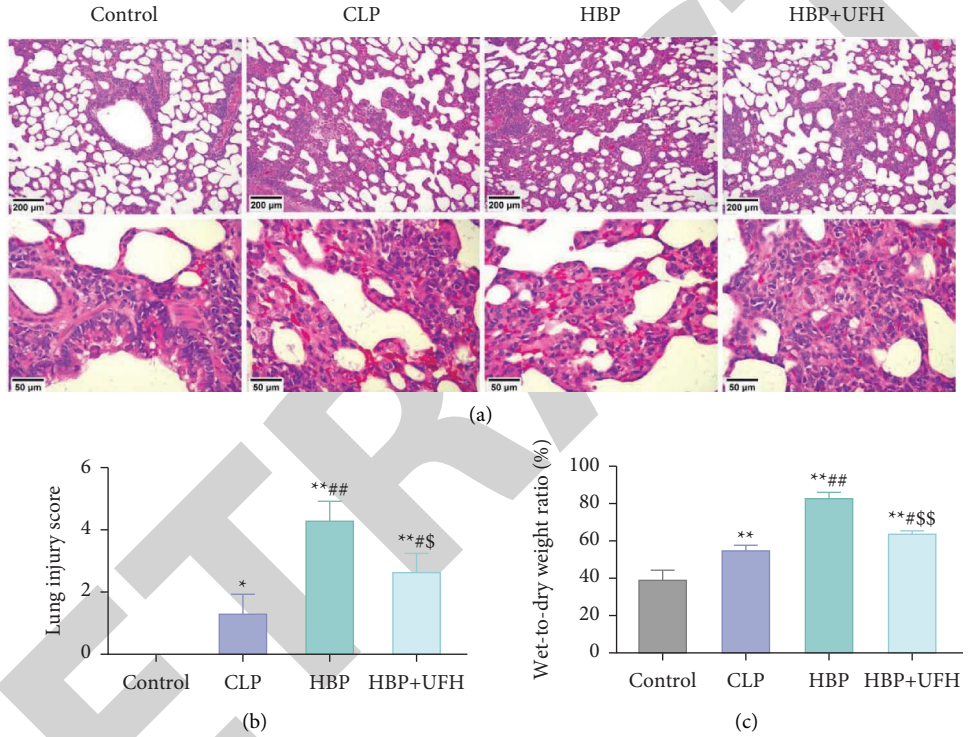

Figure 2: HBP promotes lung tissue damage in sepsis-induced ALI rats. a-b, HE staining and quantitative analysis for observing the histopathological changes of lung tissues; (c) Wet-to-dry method for quantifying water content of lung tissues. $^{**}P < 0.01$ vs. control group, $^{\#\#}P < 0.01$ vs. CLP group, and $P < 0.01$ *vs.* HBP group.

expression in the lung tissues, and Arg-1 and Mrc1 expressions were slightly increased, but the difference was not statistically significant.

3.6. HBP Activates the NF-κB Signaling Pathway in Sepsis-Induced ALI Rats. NF-κB is a key transcription factor of inflammation-related genes, playing a critical regulatory role in the 'waterfall cascade response' of inflammatory cytokines and in the development of sepsis [22]. Western blotting results proved that CLP increased NF-κB p65 expression in the nucleus, and treatment with HBP further promoted this increase. However, in comparison with the HBP group, HBP + UFH caused a significant decrease in NF-κB p65 nuclear expression (Figures 6(a) and 6(b)).

Additionally, CLP increased the ratios of IKKα and p-IκBα/IκBα in the lung tissues, and the increase in the ratios was further promoted by HBP injection. After treatment with HBP + UFH, the ratios of IKKα and p-IκBα/IκBα in the lung tissues were significantly decreased compared to the HBP group (Figures 6(c) –6(f)).

4. Discussion

Sepsis, a common acute critical disease, often leads to multiple organ and system injuries, especially in the lungs [23]. In this study, a rat model of sepsis was established by using CLP to explore the mechanism of HBP in sepsis-induced ALI. An increase of HBP in the CLP group and a further increase in the HBP group confirmed the successful construction of the

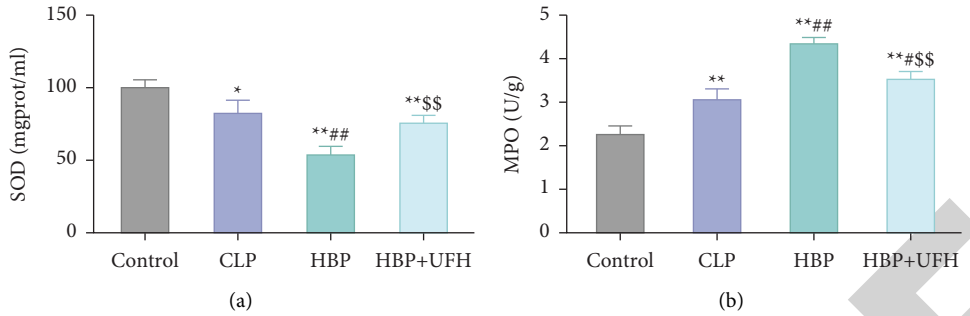

Figure 3: HBP increases oxidative stress in sepsis-induced ALI rats biochemical tests for detecting SOD activity (a) and MPO activity (b). $^{**}P < 0.01$ vs. control group, $^{\#\#}P < 0.01$ (v)s. CLP group, and $P < 0.01$*vs.* HBP group.

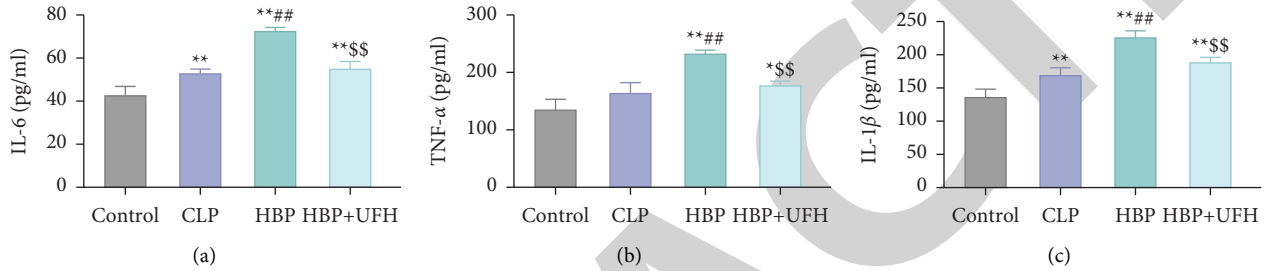

Figure 4: HBP promotes inflammatory responses in rats with sepsis-induced ALI. ELISA-based detection of IL-6 (a), TNF-α (b), and IL-1β (c) expression in the bronchoalveolar lavage fluid. $^{**}P < 0.01$ vs. control group, $^{\#\#}P < 0.01$ (v)s. CLP group, and $P < 0.01$*vs.* HBP roup.

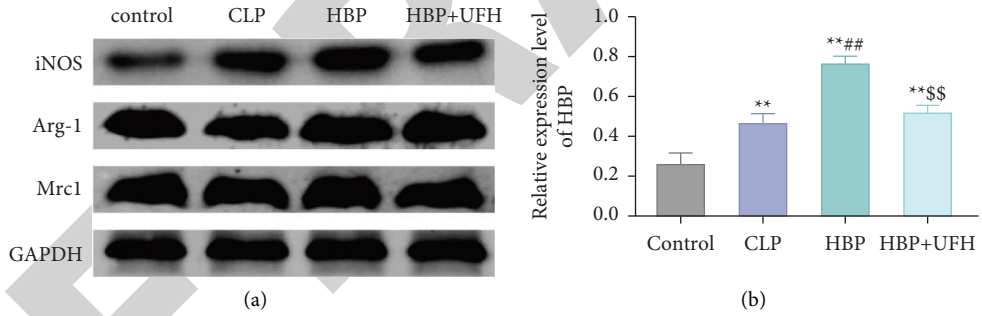

Figure 5: HBP promotes M1 polarization of macrophages in sepsis-induced ALI rats. Western blotting-based measurement (a) and gray-scale analysis (b) of iNOS, Arg-1, and Mrc1 in the lung tissues of rats. $^{**}P < 0.01$ vs. control group, $^{\#\#}P < 0.01$ (v)s. CLP group, and $P < 0.01$*vs.* HBP group.

model. When sepsis occurs, intravascular fluid and macromolecular proteins that normally cannot pass through the vascular wall extravasate into the alveolar space, resulting in increased protein content and aggravating pulmonary edema. The lung W/*D* ratio is an indicator reflecting the degree of pulmonary edema and pulmonary interstitial and alveolar vascular permeability [24], which was applied in our study. An increase in the water content of lung tissue was identified in the HBP group compared with the control and CLP groups, indicating that HBP aggravated pulmonary edema. However, the addition of UFH would decrease the water content. HE staining proved that the rats in the HBP group had more severe lung injury than the control and CLP groups, specifically showing a large number of inflammatory cell infiltration, red blood cell exudation accompanied by pulmonary vascular congestion and exudative fluid in the alveolar space. HBP significantly increased the lung injury score. Collectively, HBP aggravates lung injury.

MPO is a reductase present in neutrophils, and its activity in lung tissue quantitatively reflects the accumulation degree and activity of neutrophil polymorphonuclear granulocytes in the lungs. SOD, normally, is the most vital antioxidant enzyme in the body. SOD can rapidly scavenge superoxide anions and prevent the generation of oxygen free radicals, thus maintaining an oxidation-antioxidation balance and effectively avoiding peroxidation damage in tissues and cells. Therefore, SOD activity is commonly used to reflect the antioxidant enzyme activity and the ability to scavenge oxygen free radicals in the body [25]. In this study, HBP injection induced a significant increase in MPO activity and

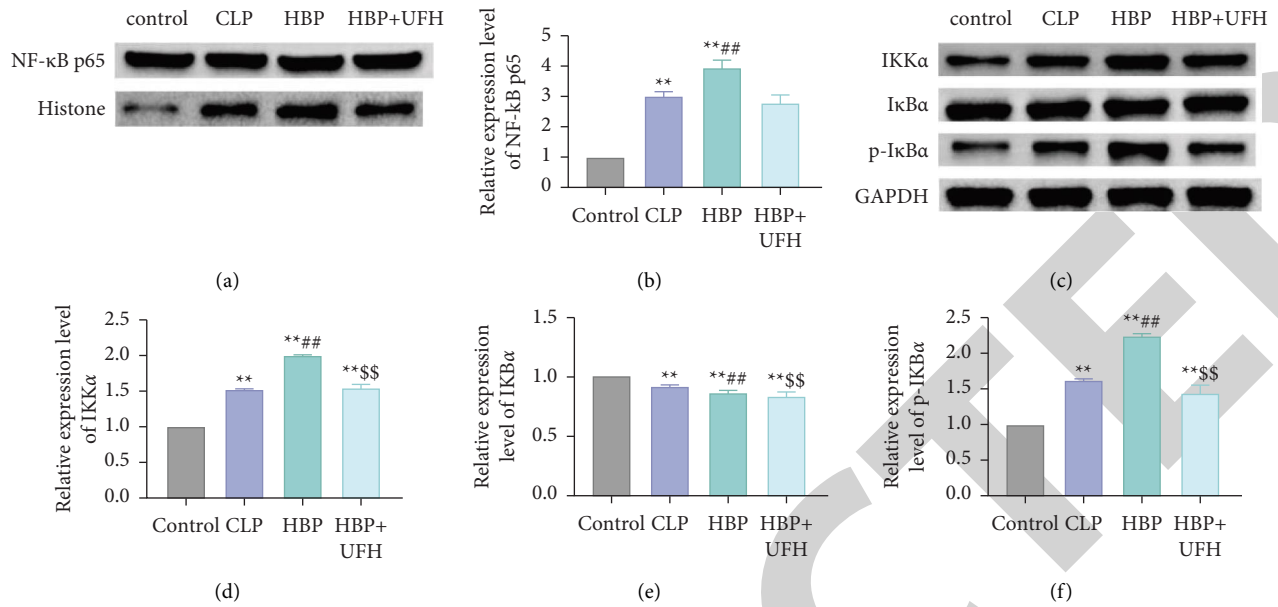

Figure 6: HBP activates the NF-κB signaling pathway in sepsis-induced ALI rats. a-b, Evaluation of NF-κB p65 nuclear expression in the lung tissues by western blotting; c-f, Measurement of the protein expression of IKKα (d), IκBα (e), and p-IκBα (f) in the lung tissues by western blotting. $^{**}P < 0.01$ vs. control group, $^{\#\#}P < 0.01$ (v)s. CLP group, and $P < 0.01$*vs*. HBP group.

a decrease in SOD activity in the lung tissue of rats treated with CLP. However, the addition of UFH led to a decrease in MPO activity and an increase in SOD activity. Collectively, HBP aggravates oxidative stress in the lungs of septic rats.

The lung, as an organ where macrophages accumulate, often has the most severe inflammatory response and injury, which leads to ALI, which is an important marker for severe sepsis [26]. Macrophages are one of the major sources of cytokine production. It has been shown that M1 macrophages are involved in the promotion of inflammation, while M2 macrophages in the resolution of inflammation [27–29]. Proinflammation by M1 macrophages is mainly achieved by secreting high levels of proinflammatory cytokines such as TNF-α, IL-6, and IL-1β, and generating active iNOS [30]. These cytokines play a key role in the pathophysiological process of ALI [30]. In this study, we found that in comparison with the control and CLP groups, the levels of IL-6, TNF-α, and IL-1β in the bronchoalveolar lavage fluid were significantly higher, and iNOS expression in the lung tissue was also increased in the HBP group. This finding indicates that HBP aggravates inflammatory responses and promotes macrophage M1 polarization in the lung tissue. However, it was able to reverse the above results in the presence of UFH, suggesting that the proinflammatory effect of HBP on ALI in septic rats may be related to the macrophage M1 polarization.

The NF-κB signaling pathway mainly exists in neurons, glial cells, and vascular endothelial cells, which is composed of the NF-κB family, IκB family, and IKK complex [31]. It has been reported that the NF-κB pathway is involved in the regulatory mechanism of sepsis through feedback regulation. When NF-κB is activated by various activating factors, the transcription of proinflammatory factors such as TNF-α, IL-6, and IL-1β is enhanced, and then the synthesis and release of these factors are increased, thus promoting NF-κB activation and NF-κB nuclear transfer [32]. Our results proved the increase of NF-κBp65 in the nucleus, IKKα and p-IκBα in the lung tissue, and the ratio of p-IκBα/IκBα in the HBP group compared with the control and CLP groups, suggesting that HBP can enhance the NF-κB pathway in the lung tissue of septic rats.

This study preliminarily demonstrates the important role of HBP in the pathophysiology of sepsis-induced ALI. However, this study has certain limitations. First, although this study shows that HBP inhibits M1 macrophage polarization and blocks activation of the NF-κB signaling pathway, the effect on M2 macrophages and whether other mechanisms are involved require further investigation. Second, this study has not been validated in cell experiments. In addition, in our experiments, we only used CLP to build a mouse model of sepsis-related ALI, which should be validated in other animal models of sepsis-related ALI. For example, whether there is a similar effect in the induction of sepsis-related ALI using LPS in mice. Therefore, it will be verified in future experiments.

5. Conclusion

The effect of HBP on sepsis-induced ALI is achieved by exacerbating oxidative stress, promoting macrophage M1 polarization to release proinflammatory factors, and activating the NF-κB signaling pathway. Therefore, inhibiting macrophage M1 polarization and blocking the NF-κB signaling pathway may be an effective new strategy for the treatment of ALI in septic rats.

Data Availability

The data used to support the findings of this study are available from the corresponding author upon request.

Hindawi
Evidence-Based Complementary and Alternative Medicine
Volume 2022, Article ID 9601020, 13 pages
https://doi.org/10.1155/2022/9601020

Research Article

The Effective Analysis for Blue Honeysuckle Extract in the Treatment of Hepatocellular Carcinoma

Chun-Peng Zhang,[1,2] Wei-Hua Li,[3] Jia-Ren Liu,[4] Guo-Dong Li,[2] Hao-Peng Zhang,[2] Jiu-Feng Wei,[2] Hong-Sheng Chen,[2] Jin-Lu Zhao,[2] Yun-Feng Wang,[5] Qiang Lv,[1] and Ming Liu[1]

[1]*Department of General Surgery, The Second Affiliated Hospital of Harbin Medical University, Harbin 150081, China*
[2]*Department of General Surgery & Bio-Bank of General Surgery, The Fourth Affiliated Hospital of Harbin Medical University, Harbin 150001, China*
[3]*Medical Imaging Department, Shenzhen Second People's Hospital-The First Affiliated Hospital of Shenzhen University Health Science Center, Shenzhen 518035, China*
[4]*Department of Laboratory Diagnosis, The Fourth Affiliated Hospital of Harbin Medical University, Harbin 150001, China*
[5]*Department of Hepatobiliary and Pancreatic Surgery, Heilongjiang Provincial Tumor Hospital, Harbin 150081, China*

Correspondence should be addressed to Ming Liu; mingliu35@hrbmu.edu.cn

Received 19 April 2022; Revised 6 May 2022; Accepted 7 July 2022; Published 29 September 2022

Academic Editor: Xueliang Wu

To further determine how BHE affected the growth of HCC cells, the proportion of each cell cycle phase was explored in HCC cells by flow cytometry. Blue honeysuckle (*Lonicera caerulea* L.) is a species of bush that grows in eastern Russia. Blue honeysuckle extract (BHE) is rich in bioactive phytochemicals which can inhibit the proliferation of tumor cells. The mechanism underlying the anticancer activity of BHE in primary liver cancer is poorly understood. The purpose of this study was to evaluate the growth inhibition mechanism of bioactive substances from blue honeysuckle on hepatocellular carcinoma (HCC) cells and to explore its protein and gene targets. The compounds in BHE were determined by high-performance liquid chromatography (HPLC) and liquid chromatography-mass spectrometry (LC-MS). Cell counting kit-8 (CCK8) assay was used to evaluate the effects of BHE on HCC cell proliferation, and flow cytometry assay (FCA) was used to determine how BHE arrested the proportion of each cell cycle phase in HCC cells. Western blot (WB) was performed to determine the expression of cell cycle-related proteins in HCC cells treated with different concentrations of BHE. The xenograft tumor animal models were established by HCC cell implantation. The results showed that cyanidin-3-o-glucoside and cyanidin-3-o-sophoroside which are the main biologically active components were detected in BHE. BHE is highly effective in inhibiting the proliferation of HCC cells by arresting the HCC cell cycle in the G2/M phase. BHE also downregulated the expression of conventional or classical dendritic cells-2 (cDC2) and cyclin B1 by promoting the expression of myelin transcription factor 1 (MyT1) in HCC cells. The weight and volume of xenografts were significantly decreased in the BHE treated groups when compared to the control group. BHE increased the expression of MyT1 in xenograft tissues. These findings showed that blue honeysuckle extract inhibits proliferation *in vivo* and *in vitro* by downregulating the expression of cDC2 and cyclin B1 and upregulating the expression of MyT1 in HCC cells.

1. Introduction

Hepatocellular carcinoma (HCC) is the most common primary malignant tumor of the liver. It is the sixth most common type of cancer and constitutes the fourth major cancer-related mortality worldwide in 2018. There are about 841,000 new HCC cases and 782,000 HCC-related deaths annually [1]. Worse yet is that both incidence and mortality of HCC show an upward trend worldwide in recent years, with a higher prevalence in Asia, accounting for nearly 70%

of new cases worldwide [2]. 55% of all HCC cases are diagnosed in China [3, 4]. The early stage of HCC tends to be asymptomatic, so the disease may have progressed to an advanced stage by the time of diagnosis. The therapeutic effects of current treatment approaches for HCC are also compromised by high relapse rates, leading to the poor long-term survival of HCC patients [5]. Surgery is a treatment mainstay, but its invasiveness may affect the postoperative quality of life and is associated with local recurrences. Thus, early chemoprevention, detection, diagnosis, and treatment are of great significance to enhance the prognosis of HCC patients [6, 7].

Plant antioxidants play an important role in mitigating the impact of oxidative stress on life genetic materials and cell structures, reducing the damage of chronic diseases, and facilitating the maintenance of the normal metabolism of tissue cells and various biological characteristics. These biological activities include oxidative damage attenuation, alleviation of radiation damage and inflammation, cardiomyocyte protection, bacteriostasis, gastroprotection [8, 9], hepatoprotection [10, 11], and other relevant properties [12, 13]. The chemoprophylaxis of blue honeysuckle stems from its high concentration of highly active phytochemicals and anthocyanins that have shown significant benefits against various human diseases [14]. In the past few decades, anthocyanins have captured great attention in the treatment of diseases including infections, neurological diseases, cancer [14–18], and diabetes [19, 20]. Blue honeysuckle (*Lonicera caerulea* L.), a fruit grown worldwide, is a nutrient-rich forest berry. The fruit of the blue honeysuckle is rich in a variety of vitamins, minerals, amino acids, flavonoids, carbohydrates, polyols, organic acids, and other bioactive substances [21, 22]. The health benefits of blue honeysuckle have been widely explored due to its rich bioactive components. These components mainly include phenolic acid, anthocyanin, and flavonoids, and vitamin B, magnesium, phosphorus, calcium, and potassium are secondary blue honeysuckle components [23, 24]. Blue honeysuckle contains great amounts of polyphenolic compounds [25, 26], such as anthocyanins, pelargonidin, peonidin, catechol, flavanols, and chlorogenic acid [27]. The total anthocyanin contents in blue honeysuckle are higher than that in other fruits [28]. Anthocyanins are the main polyphenolic compounds in blue honeysuckle [29], and the anthocyanin-3-glycoside is the main form of anthocyanin present in blue honeysuckle [24, 30, 31]. The blue honeysuckle contains higher contents of cyanidin-3-glucoside than other berries, including blueberries, blackberries, and raspberries [30]. Anthocyanins are mainly found in the peels of fruits, with a broad range of well-recognized biological activities including antimicrobial, anticancer, and anti-inflammatory activities [24]. Few studies have investigated the antitumor mechanism of fresh blue honeysuckle at the protein and molecular levels. In particular, efficient methods to extract bioactive substances from fresh blue honeysuckle and clarification of the molecular mechanisms underlying its antitumor activity have been sparingly explored. Thus, the aim of this study was to investigate the effects of blue honeysuckle extracts (BHE) on the proliferation of HCC cells by exploring its anti-neoplastic action and its molecular protein mechanism, which may provide a basis for the use of BHE as chemoprophylaxis and chemotherapeutic agents for primary liver cancer.

2. Materials and Methods

2.1. The Extraction of Fresh Blue Honeysuckle. Fully-ripe fresh blue honeysuckle was purchased from Greenfield Berries Ltd., Shangzhi City, Heilongjiang Province. Blue honeysuckles (200 g) were ground with 600 ml of 80% alcohol in a rough homogenate machine for 10 min, and the procedure was performed thrice. The crude blended samples were further mixed using a high rotary cutting homogenizer in an ice bath for 5 min. The homogenates were filtered through a Buchner funnel and vacuum filtered through three layers of Whatman#2 filter papers. The filtrate was rotary evaporated at 40°C for approximately 90 min in an evaporator to remove 95% of the solvent. Three replicates of blue honeysuckle extracts (BHE) were stored in aliquots at −80°C until required for further use.

2.2. The Content of Main Compounds in BHE by HPLC. Quantitative analysis of cyanidin-3-o-glucoside and cyanidin-3-o-sophoroside in BHE was performed on High-Performance Liquid Chromatography (HPLC) Surveyor (Thermo Fisher Scientific, Waltham, MA, USA) with a photo-diode array (PDA) detector scanning from 250 to 350 nm. The optimized mobile phases used were 0.1% phosphoric acid in ultrapure water (*A*) and acetonitrile (*B*), and the elution time was 30 min for equal concentration degree (*A*)/(*B*) (90 : 10). Chromatography was carried out at 30°C using Supersil ODS2 chromatographic column (4.6 mm × 250 mm, 5 μm). The chromatograms were recorded at 280 nm, and the 20 μL of injection was applied to the column.

2.3. Identification of Fresh BHE by LC-MS. The sample was analyzed by the AB Sciex 5600-Triple-Tof system, which consisted of surveyor autosampler, quaternary pump, online degassing machine, and electrospray ionization (ESI) with positive ionization mode. The flow-through analytical cell used Waters UPLC HSS T3 column (2.1 mm × 150 mm, 1.8 μm) and HSS T3 column (2.1 mm × 5 mm, 1.8 μm) with column temperature of 35°C, sample room temperature of 10°C, and the injection volume of 5 μL. The optimized mobile phases used were 0.1% formic acid in water (*A*) and 0.1% formic acid in acetonitrile (*B*) with gradient elution from 0 to 20 min at a flow rate of 0.3 ml/min. The ionization temperature was increased to 350°C, with a nebulizer and auxiliary gas at a pressure of 50 psi, and the capillary voltage was controlled at 4500 V.

2.4. Animal Treatment. Four-week-old athymic BALB/c female nude mice (weight 12~16 g) were purchased from Beijing Weitonglihua Laboratory Animal Technology Co. Ltd (Beijing, China) and acclimated for 7 days in the animal

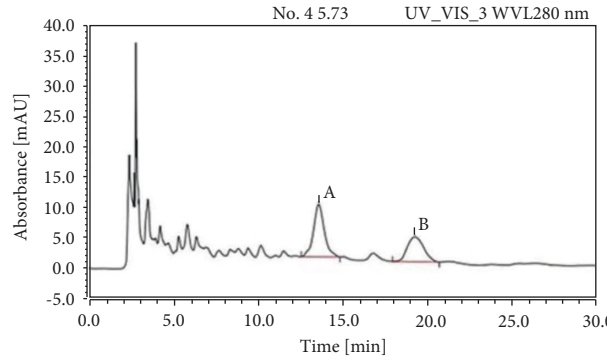

Figure 1: Contents of cyanidin-3-o-sophoroside and cyanidin-3-o-glucoside in blue honeysuckle extract. The contents of *A* and *B* were determined in blue honeysuckle extract (BHE) by HPLC. *A* for cyanidin-3-o-sophoroside and *B* for cyanidin-3-o-glucoside.

Table 1: The contents of cyanidin-3-o-sophoroside and cyanidin-3-o-glucoside in samples of blue honeysuckle (mg/g fresh weight).

Content	Cyanidin-3-O-sophoroside	Cyanidin-3-O-glucoside
1	0.568	0.543
2	0.577	0.556
3	0.589	0.533
Average	0.578 ± 0.011	0.544 ± 0.012

Table 2: The main components identified in BHE by LC-MS.

No.	tR (min)	[M-H]	Fragment ions	Tentatively identification
1	1.353	447.0	339.0 283.9 (M-Glc-Glc)	Cyanidin-3-O-glucoside isomer
2	2.873	375.1	213.0 (M-Glc), 168.0	—
3	3.359	447.0	284.9 (M-Rha-glc)	Cyanidin-3-O-glucoside
4	5.212	451.2	341.0, 162.8,61.9	—
5	5.509	609.0	564.3, 300.9, 61.9	Cyanidin-3-O-sophoroside
6	5.477	609.0	412.9, 315.0, 277.2	Cyanidin-3-O-sophoroside isomer
7	6.431	677.3	563.3, 451.2, 337.9, 225.1	—
8	6.797	791.1	563.3, 451.2, 337.9, 225.1, 146.9	—
9	7.080	903.3	695.3, 563.3, 451.2, 337.9, 225.1, 146.9	—
10	8.984	301	151.9, 61.9	Ellagic acid
11	9.350	421.0	197.7, 61.9	—

room. During the study, the mice were fed with sterilized food and water and were housed in a barrier environment under the standard light/dark cycle (12 h light, 12 h dark). The mice were maintained under standard conditions and cared for as per the institutional guidelines and ethical regulations of the National Cancer Institute of China. All protocols of animals were approved by the Committee of Ethics from Harbin Medical University (Harbin, China).

HepG2 cells or Huh7 cells (5×10^6) mixed with Matrigel (3 : 1) were placed subcutaneously on the right ventral dorsum of five-week-old athymic BALB/c female nude mice for a 7-days-of-growth to reach a tumor diameter of 5 mm. The mice with xenografts were randomly divided into 4 groups (5 mice/group): (I) mice received 0.9% normal saline daily by gavage as the control group; (II) mice received 7 g/kg/d of BHE (equivalent to 7 g fresh blue honeysuckle) by gavage; (III) mice received 40 mg/kg/d of anthocyanins by gavage; and (IV) mice received 30 mg/kg of intraperitoneal injection of 5-Fu alternately by gavage. The body weight and volume of the tumor were measured every 4 days. The activity of mice was also closely monitored. After 36 days of treatment, tumor xenografts were excised, collected, and weighed. Parts of xenografts were fixed for immunohistochemistry, and the others were frozen at 80°C for Western blot.

2.5. Cell Culture. HepG2 and Huh7 cells were donated by the Key Laboratory of Surgery Ministry, Harbin Medical University. Cells were grown in Dulbecco's modified Eagle's medium (DMEM) containing 10% FBS (fetal bovine serum, v/v), 100 units/ml penicillin, and 100 μg/ml at 37°C in a humidified incubator with 5% CO_2. Cells were sub-cultured every 2 days at 80–90% confluence for experiments.

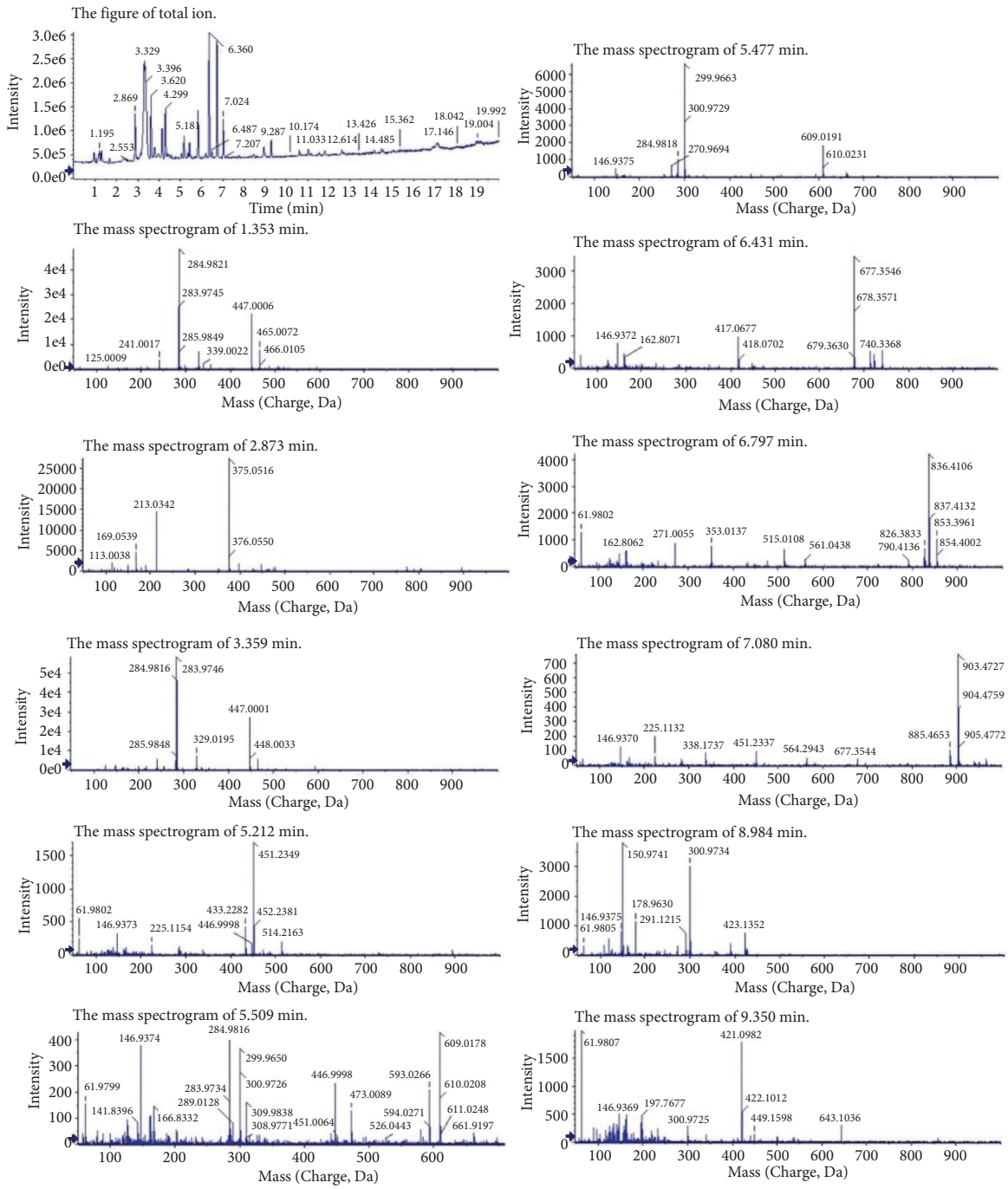

Figure 2: The total ion chromatogram and mass spectrograms of BHE. The compounds of BHE were identified by HPLC and LC-MS.

2.6. Cell Viability. The cell viability of BHE was assessed in HepG2 and Huh7 using the CCK8 (Dojindo Laboratories, Kumamoto, Japan) as in a previous study [32]. Cells were inoculated at a density of 3 × 103 cells/well in a 96-well plate and cultured in medium added with different BHE concentrations (0, 5, 10,15, 20, 30, or 40 mg/ml), anthocyanins (150 μg/ml) (Harbin, China), and 5-FU (10 μg/ml) (Sigma, USA) at 37°C for 24, 48, 72, or 96 h. Anthocyanins (150 μg/ml) and 5-FU (10 μg/ml) were used as the positive controls to evaluate the antitumor efficacy of blue honeysuckle extract from multiple perspectives. After treatment, 10 μL of CCK8 was added to each well and the cells were cultured for 2 h at 37°C. The optical density (OD) of each well was measured at 450 nm using a microplate reader (Bio-Rad Laboratories, Hercules, CA, USA). Cell viability was calculated using the following formula. Relative percentage of cell viability = (OD of the experimental group/OD of the control group) × 100%. The assay was performed in triplicate.

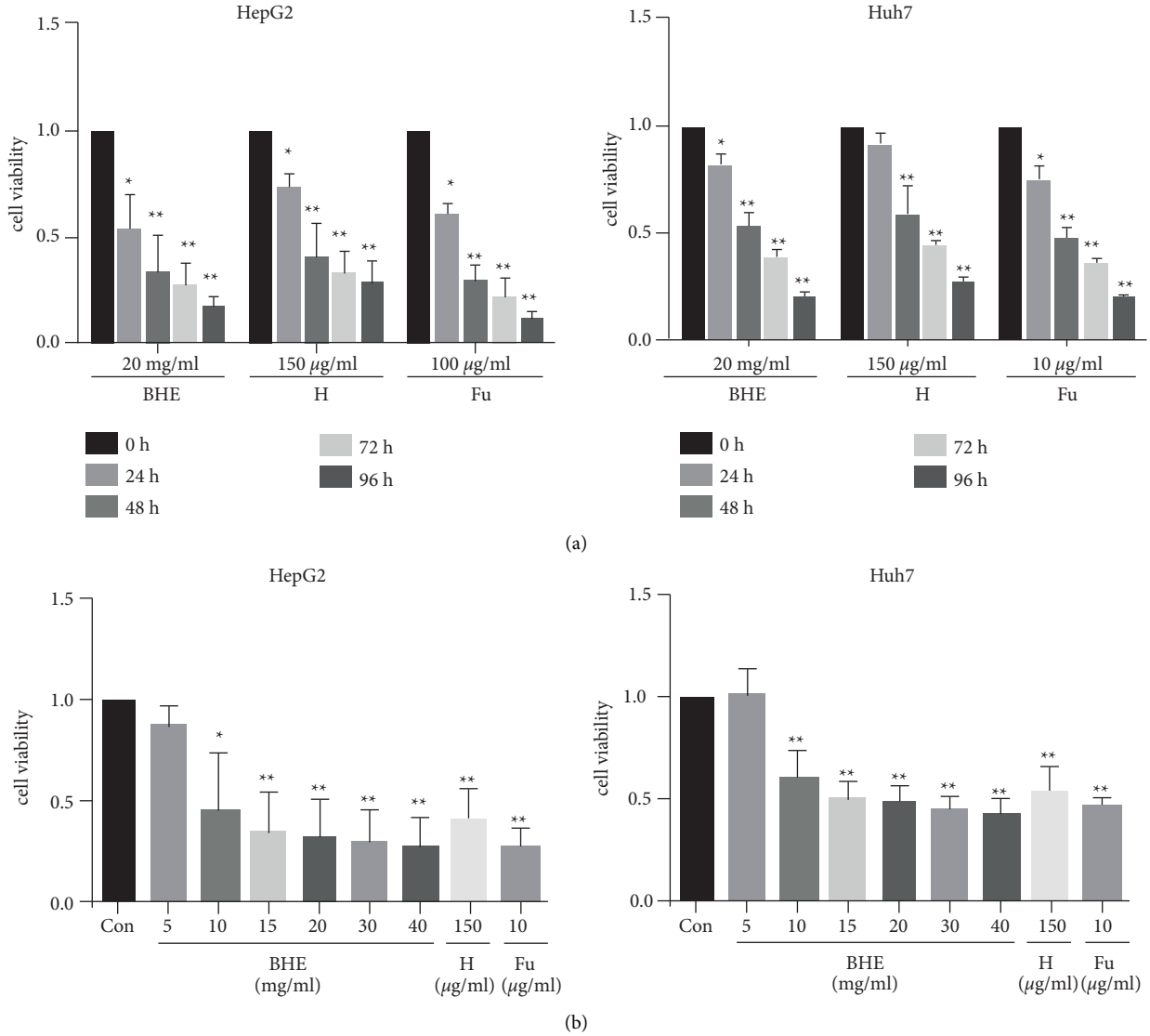

Figure 3: The cell viability of BHE in HepG2 and Huh7 cells. HepG2 cells or Huh7 cells were treated with 20 mg/ml of BHE, 150 μg/ml of anthocyanins, or 10 μg/ml of 5 FU for 24, 48, 72, or 96 h ($n = 6$). The cell viability was determined by the CCK8 assay. (a) The cell viability of BHE in HepG2 and Huh7 cells for 24, 48, 72, or 96 h. (b) The cell viability of BHE in HepG2 and Huh7 cells for 48 h. The data are expressed as mean ± standard deviation (S.D.). $^{*}P < 0.05$, $^{**}P < 0.01$, when compared to the negative control group.

2.7. Cell Cycle. The concentrations of BHE were selected for flow cytometry based on the results from CCK8 assay. The cells were inoculated in a culture flask, treated with different concentrations of BHE (0, 5, 10, or 20 mg/ml), anthocyanins (150 μg/ml), and 5 FU (10 μg/ml) at 5% CO_2 saturated humidity incubator at 37°C. After 48 h, cells were seeded at 1×10^6 cells/well and harvested by trypsinization for cell cycle analysis. After being rinsed with phosphate buffered saline (PBS), the cells were fixed with 1 ml of ice-cold 70% ethanol at −20°C overnight and were centrifuged (2,000g) at 4°C for 10 min. Cell pellets were collected, rinsed with PBS, and incubated in a 0.4 ml staining solution (PI: RNaseA, 5 : 1) for 30 min at 37°C, followed by fluorescence-activated cell sorting (FACS) using a FACSCalibur (FACSort, Becton-Dickinson, CA, USA) as in the previous study [33].

2.8. Western Blot. Western blot was performed to determine the levels of cyclin B1, cDC2, and MyT1 proteins as in the previous studies [34–36]. Cells were treated with different concentrations of BHE (0, 5, 10, or 20 mg/ml), anthocyanins (150 μg/ml), and 5 FU (10 μg/ml) for 48 h, rinsed twice with ice-cold PBS, and harvested by scraping. Total cellular protein was extracted using RIPA buffer (Cell Signaling Technology, MA, USA) with phenylmethane sulfonyl fluoride in the 1× proteinase inhibitor cocktail (Roche, Basel, Switzerland) per the manufacturer's instructions. Frozen xenograft tissues were soaked and lysed in cold RIPA buffer (Cell Signaling Technology) with phenyl methane sulfonyl fluoride in the 1× proteinase inhibitor cocktail (Roche, Basel) on ice. After stirring, the cells were homogenized with a high-rotation emulsifying

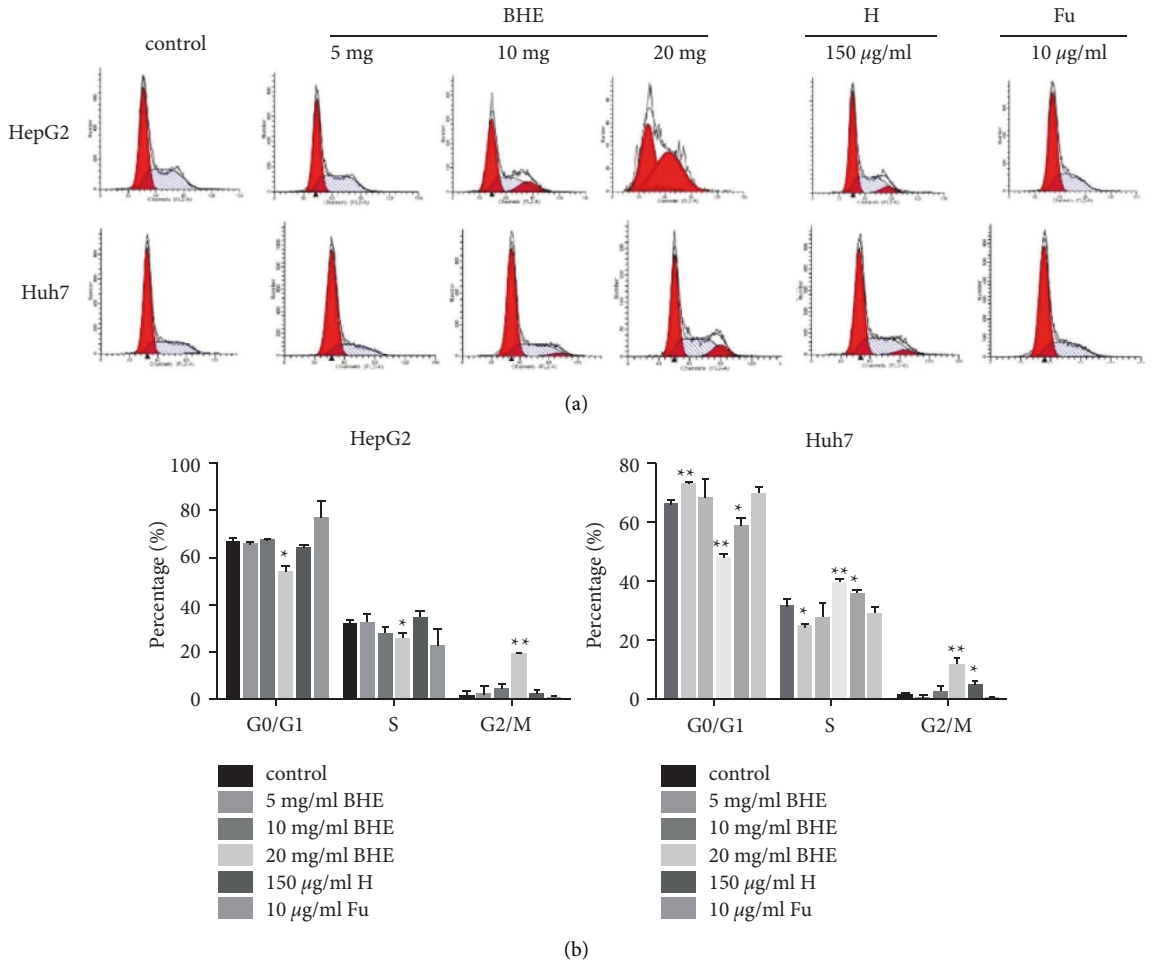

Figure 4: (a) The distribution of cell cycle in HepG2 and Huh7 cells. HepG2 and Huh7 cells were treated with different concentrations of BHE, 150 μg/ml of anthocyanins, or 10 μg/ml of 5 FU for 48 h. (b) The distribution of the cell cycle was determined in HepG2 and Huh7 cells by flow cytometry ($n = 3$). $^{*}P < 0.05$, $^{**}P < 0.01$, when compared to the negative control group.

homogenizer for 5 min to break the walls. The cells were then centrifuged (14000g, 4°C) for 10 min to obtain the supernatant. Total protein concentrations were determined using the BCA Protein Assay Kit (Beyotime, Shanghai, China). Proteins (30 μg) were separated using SDS-polyacrylamide gel electrophoresis (SDS-PAGE) and transferred onto polyvinylidene difluoride (PVDF) membranes. The membranes were blocked with 5% nonfat milk in PBS plus 0.05% Tween 20 (PBST) for 1 h at room temperature. Membranes were then incubated with primary antibodies against cyclin B1 (1 : 1000, San Ying Biotechnology, Wuhan, China), cDC2 (1 : 1000, San Ying Biotechnology, Wuhan, China), MyT1 (1 : 1000, San Ying Biotechnology, Wuhan, China), and β-actin (1 : 1000, San Ying Biotechnology, Wuhan, China) at 4°C overnight. Membranes were rinsed with PBST 3 times and then incubated with horseradish peroxidase-conjugated secondary antibodies for 2 h at room temperature. After being rinsed with PBST three times again, the enhanced chemiluminescence (ECL) reagents (Beyotime, Shanghai, China) were uniformly applied to the PVDF membrane according to the manufacturer's protocol for color development.

2.9. Immunohistochemistry. The expression of cyclin B1, cDC2, and MyT1 in xenografts was determined by immunohistochemistry as in the previous studies [37, 38]. Briefly, the sections of paraffin-embedded xenograft tumor tissue were dewaxed by xylene and hydrated with a graded ethanol solution. The sections were rinsed using PBS (pH 7.4) three times. The antigen retrieval was performed using the sodium citrate buffer (pH 6.0) at 95–100°C for 30 min, and the sections were cooled at room temperature. Then, the sections were pretreated in a 3% (v/v) hydrogen peroxide solution for 10 min to block endogenous peroxidase activity. After being rinsed with PBS three times, nonspecific binding serum was added to the sections for 10 min. Anti-cyclin B1, anti-cDC2, and anti-MyT1 antibodies at a dilution of 1 : 100 were added to the sections and incubated at 4°C overnight. After being rinsed with PBS three times, the sections were incubated with biotinylated secondary antibodies (Zhongshanjinqiao Biotechnology Inc, China) for 30 min at 37°C. 3,3-diaminobenzidine (DAB) solution was used for staining, and hematoxylin was used for counterstaining. The expression of cyclin B1, cDC2, and MyT1 was determined by light microscopy with a digital camera.

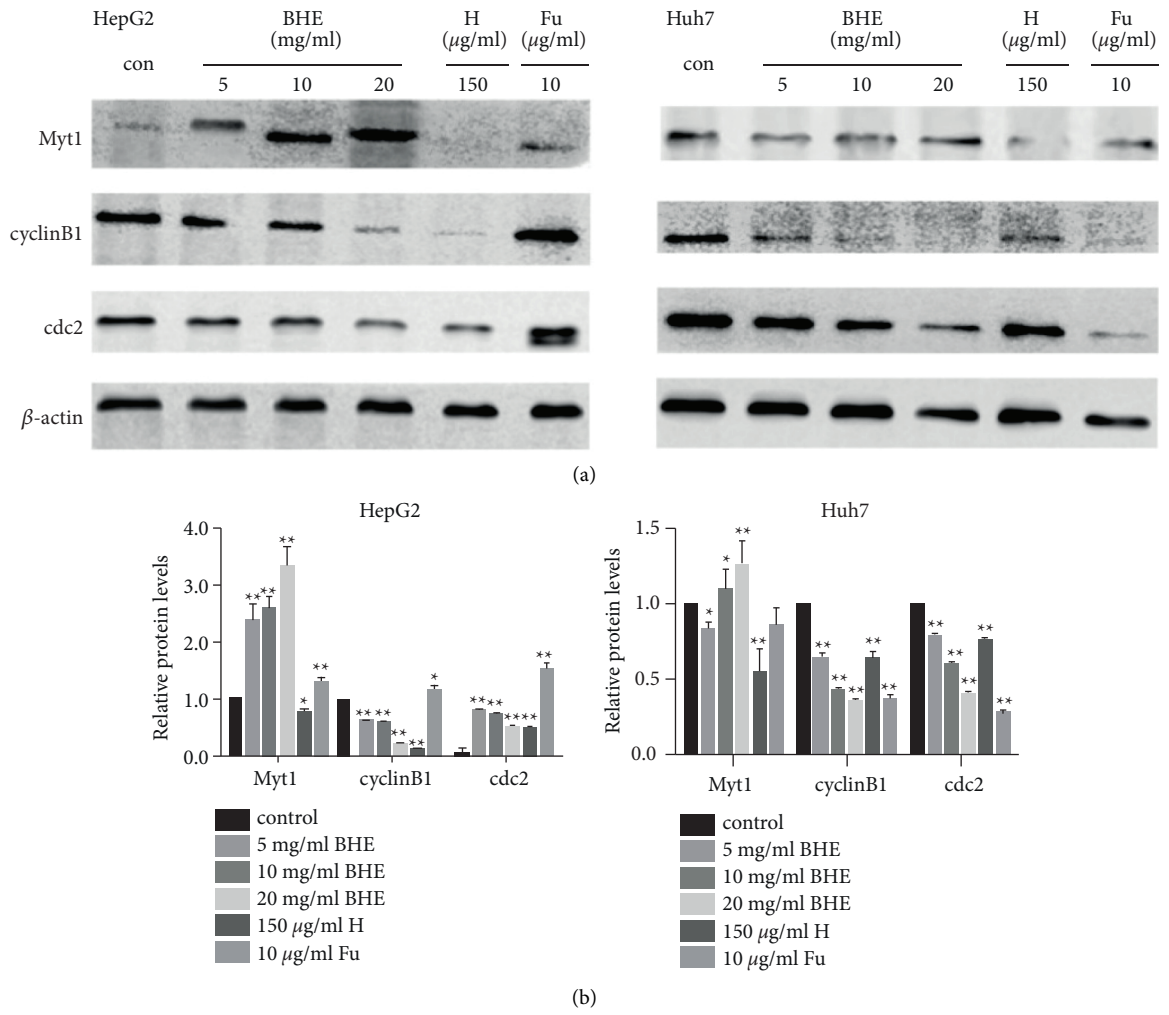

Figure 5: (a) The expression of cyclin B1, cDC2, and MyT1 proteins in HepG2 and Huh7 cells. HepG2 and Huh7 cells were treated with different concentrations of BHE, 150 μg/ml of anthocyanins, or 10 μg/ml of 5 FU for 48 h. (b) The expression of cyclin B1, cDC2, and MyT1 proteins was explored in HepG2 and Huh7 cells by Western blot. $^{*}P < 0.05$, $^{**}P < 0.01$, when compared to the negative control group.

2.10. Statistical Analyses. Data are expressed by means ± standard deviation (S.D.). Difference analysis was performed using GraphPad Prism 8.0 (GraphPad Software, USA). Student's *t*-test and variance analyses were performed to analyze the significance of differences with inter-group comparisons. Statistically significant results were defined as $P < 0.05$.

3. Results

3.1. The Components Identified in BHE. As shown in Figure 1, cyanidin-3-o-glucoside and cyanidin-3-o-sophoroside were identified in BHE by HPLC. The average contents of cyanidin-3-o-glucoside and cyanidin-3-o-sophoroside are shown in Table 1. There were 0.544 ± 0.012 mg and 0.578 ± 0.011 mg per 100 g of fresh blue honeysuckle for cyanidin-3-o-glucoside and cyanidin-3-o-sophoroside, respectively. Other components were also identified by LC-MS (Table 2), and several unknown components were found in BHE (Figure 2).

3.2. BHE Reduced the Proliferation of HCC Cells. To assess the effect of BHE on antitumor activity, a CCK8 assay was performed to determine the cell viability of HepG2 cells and Huh7 cells. BHE significantly inhibited the proliferation of HepG2 cells and Huh7 cells in a dose- and time-dependent manner ($P < 0.05$ and $P < 0.01$) (Figures 3(a) and 3(b)). The 50% inhibitory concentrations (IC_{50}) were 52.79 and 41.04 mg/ml in HepG2 and Huh7 cells, respectively. The positive controls, i.e., anthocyanins (150 μg/ml) and 5 FU (10 μg/ml), also showed potent inhibition of proliferation in both HepG2 and Huh7 cells (Figure 3).

3.3. BHE Arrested the Proportion of Each Cell Cycle Phase in HCC Cells. To further determine how BHE affected the growth of HCC cells, the proportion of each cell cycle phase was explored in HCC cells by flow cytometry as shown in Figure 4. BHE could affect the distribution of the cell cycle in HepG2 and Huh7 cells. After being cultivated with BHE at dose of 0, 5, 10, or 20 mg/ml or 150 μg/ml of anthocyanin for 48 h, the proportion of cell cycle at the G2/M phase increased

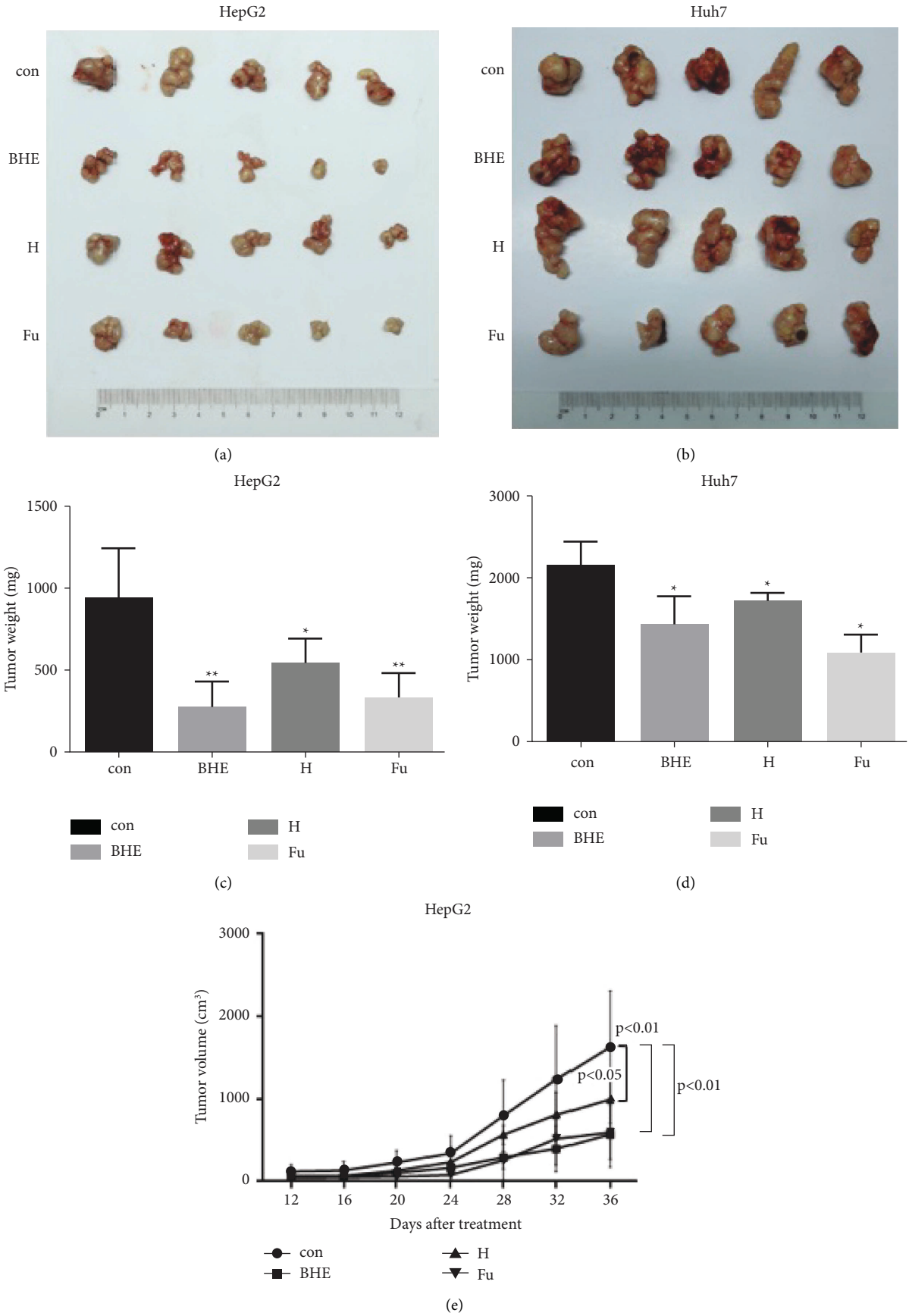

Figure 6: Continued.

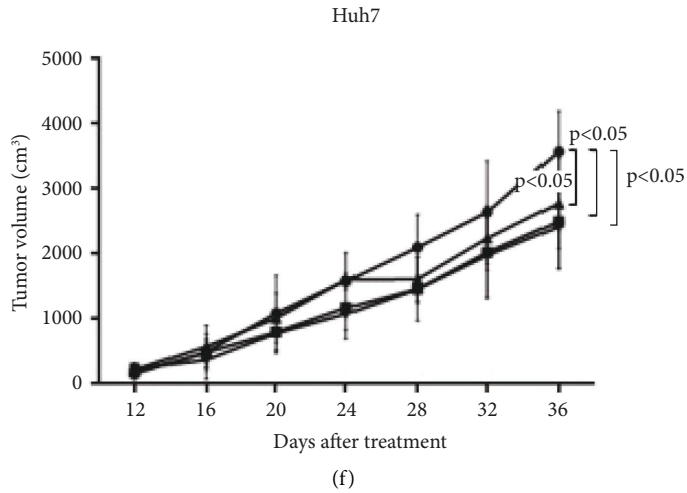

(f)

Figure 6: BHE inhibited the growth of xenografts in the model of nude mice. The BALB/c female nude mice were implanted with HepG2 cells or Huh cells for 7 days. The mice with xenografts were randomly divided into the positive control group, 7 g/kg/d of BHE (equivalent to 7 g fresh blue honeysuckle) group, 40 mg/kg/d of anthocyanins group, and 30 mg/kg of 5 Fu group (5 mice/group). The tumor sizes were measured every 4 days. After treatment for 36 days, xenografts were collected and weighted. (a) The size of HepG2 cell xenografts in nude mice. (b) The size of Huh cell xenografts in nude mice. (c) The weight of tumor in HepG2 cell xenografts of nude mice. (d) The weight of tumor in Huh cell xenografts of nude mice. (e) The changes of tumor volume in nude mice (HepG2 cells). (f) The changes of tumor volume in nude mice (Huh cells). $^{*}P < 0.05$, $^{**}P < 0.01$, when compared to the positive control group.

gradually from $1.33 \pm 2.16\%$ to $2.28 \pm 0.04\%$, $4.39 \pm 0.02\%$, $12.66 \pm 0.11\%$, and $2.11 \pm 0.02\%$ in HepG2 cells. However, the share of cell cycle at the G2/M phase changed from $1.57 \pm 0.01\%$ to $0.71 \pm 0.01\%$, $2.93 \pm 0.019\%$, $11.68 \pm 0.03\%$, and $4.89 \pm 0.02\%$ in Huh7 cells (Figure 4).

3.4. BHE Affected the Expression of Cell Cycle-Related Protein in HCC Cells. To explore the molecular mechanism of the BHE-arrested cell cycle at the G2/M phase, the expression of protein related to the cell cycle was examined in HepG2 and Huh7 cells by Western blot. After being cultivated with BHE (0, 5, 10, and 20 mg/ml), anthocyanin (150 μg/ml), or 5 FU (10 μg/ml) for 48 h, the expression of cyclin B1, cDC2, and MyT1 proteins was examined. The results are shown in Figure 5. BHE at the concentration of 20 mg/ml significantly upregulated the expression of MyT1 and downregulated the expression of cyclin B1 and cDC2 in both HepG2 and Huh7 cells ($P < 0.05$ and $P < 0.01$). However, the expression of cyclin B1 and cDC2 differed in HepG2 and Huh7 cells after treatment with anthocyanins or 5 FU. Anthocyanins significantly downregulated the expression of MyT1, cyclin B1, and cDC2 in both cell lines. 5 FU significantly downregulated the expression of MyT1, cyclin B1, and cDC2 in Huh7 cells and showed an opposite expression in HepG2 cells.

3.5. BHE Inhibited Growth of Xenografts in a Model of Mice. To further investigate the effects of BHE on anticancer activity, athymic BALB/c female nude mice were implanted with HepG2 and Huh7 cells. As shown in Figure 6, BHE significantly decreased the growth of xenografts in both HepG2 and Huh7 cells. BHE decreased both the weight of the tumor in the experimental termination and the volume of the tumor in a time-dependent manner ($P < 0.05$ and $P < 0.01$) (Figure 6). The weight of xenografts in the BHE group was 278 ± 105 g and 1432 ± 212 g in HepG2 and Huh7 cells, respectively, when compared to the control group (936 ± 178 g and 2140 ± 187 g) ($P < 0.05$ and $P < 0.01$). The final volumes of xenografts in the BHE group were $568 \pm 242\ mm^3$ and $2499 \pm 545\ mm^3$ in HepG2 and Huh7 cells, respectively, when compared to the control group ($1629 \pm 529\ mm^3$ and $3575 \pm 485\ mm^3$) ($P < 0.05$ and $P < 0.01$). The weight of the mice in the BHE group did not differ from the control group (data not shown). In addition, anthocyanins and 5 FU also showed an inhibitory effect on the growth of xenografts in this mouse model.

3.6. BHE Affected the Expression of MyT1, Cyclin B1, and cDC2 in Xenograft Tissues. To further investigate the possible mechanism of BHE inhibiting hepatocellular carcinoma growth *in vivo*, the expression of cyclin B1, cDC2, and MyT1 proteins was determined in xenograft tissues using Western blot and immunohistochemistry. The results are shown in Figures 7 and 8. BHE significantly decreased the expression of cyclin B1 and cDC2 and significantly increased the expression of MyT1 in xenograft tissues when compared to the group ($P < 0.05$ and $P < 0.01$).

4. Discussion

Cancer is one of the major causes of disease-related mortality worldwide. The pathogenesis of cancer is complex and involves alterations in cancer-related genes and tumor

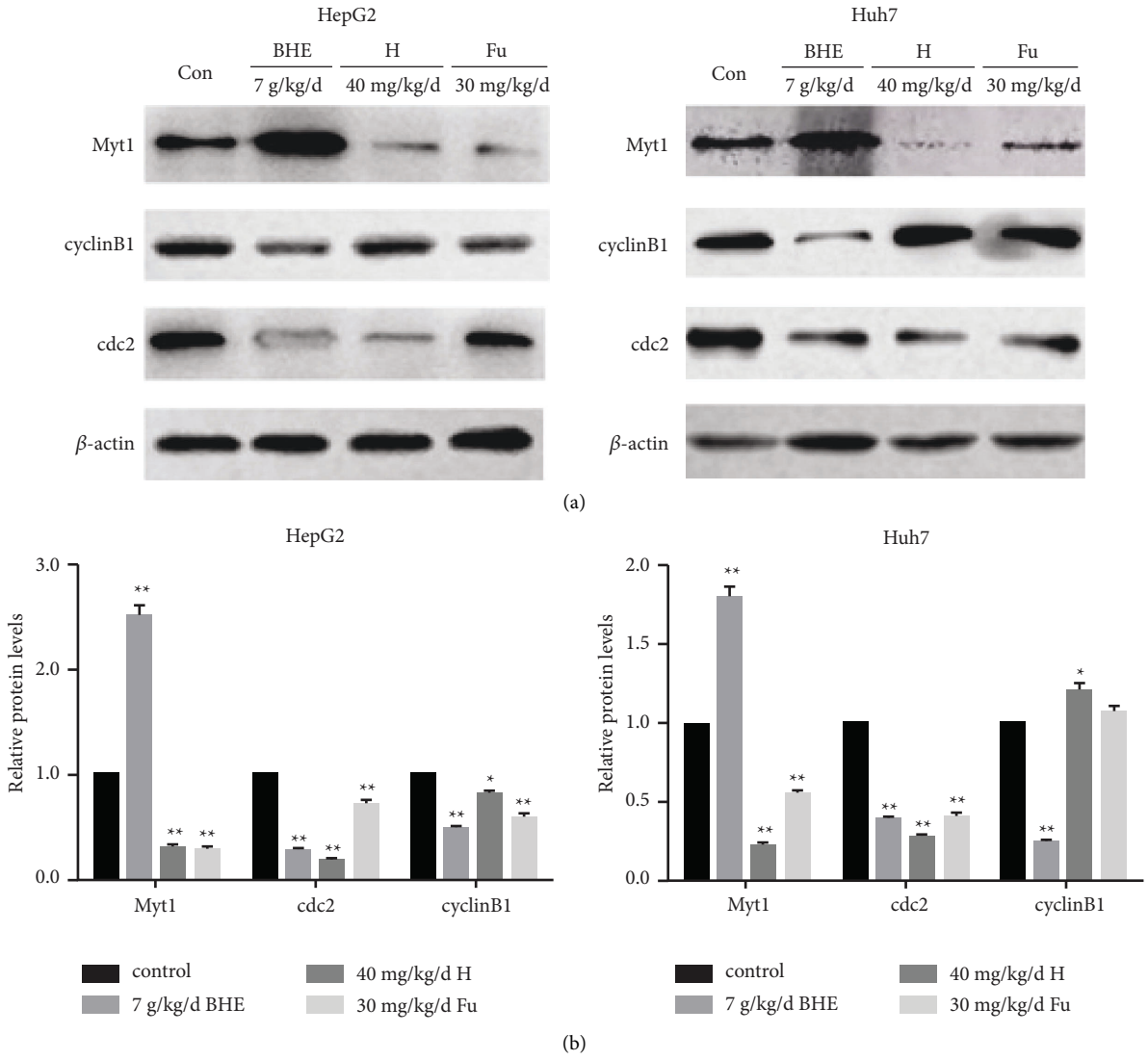

Figure 7: (a) The expression of cyclin B1, cDC2, and MyT1 proteins in xenograft tissues. (b) The expression of cyclin B1, cDC2, and MyT1 proteins in xenograft tissues analyzed by Western blot. $^{*}P < 0.05$, $^{**}P < 0.01$, when compared to the positive control group.

suppressor genes. Some cytokines also play roles in the occurrence and development of cancer. The actions of genes and cytokines lead to the malignant proliferation of cells, so inhibition of the proliferation of malignant cells is the cornerstone of tumor therapy. Our findings indicated that BHE could inhibit the proliferation of HCC cells in a dose-dependent manner.

Currently, the most common methods used to treat malignant tumors are surgery, chemotherapy, and radiotherapy. However, these approaches are associated with multiple toxic side effects, high recurrent rates, and drug resistance. Bioactive components from natural plants for antitumor purposes that cause fewer side effects might be another potentially effective approach for tumor therapy. The blue honeysuckle is rich in nutrients and bioactive substances, especially natural pigment anthocyanins, oxidized scavenger flavonoids, and plant fungicide organic phenolic acids. These bioactive components have strong antioxidant activities [22, 27]. Phytochemicals that are rich in BHE play an important role in inhibiting the development of different cancers, including colon [39–41], oral [42], lung [43], prostate [44], breast [45, 46], and skin cancer [47]. In the present study, the main biologically active components determined by HPLC in BHE were cyanidin-3-o-glucoside and cyanidin-3-o-sophoroside. The contents of cyanidin-3-o-glucoside and cyanidin-3-o-sophoroside of BHE were 0.544 ± 0.012 mg and 0.578 ± 0.011 mg per 100 g of fresh blue honeysuckle. Moreover, the compounds in BHE identified by LC-MS were cyanidin-3-o-glucoside, cyanidin-3-o-sophoroside, ellagic acid, and some unknown components.

In this study, BHE inhibited cell proliferation of HCC by arresting the cell cycle at the G2/M phase in HepG2 and Huh7 cells. The expression of the cDC2/cyclin B1 pathway in HepG2 and Huh7 cells was also determined. The cDC2 is the most important cell cycle gene in

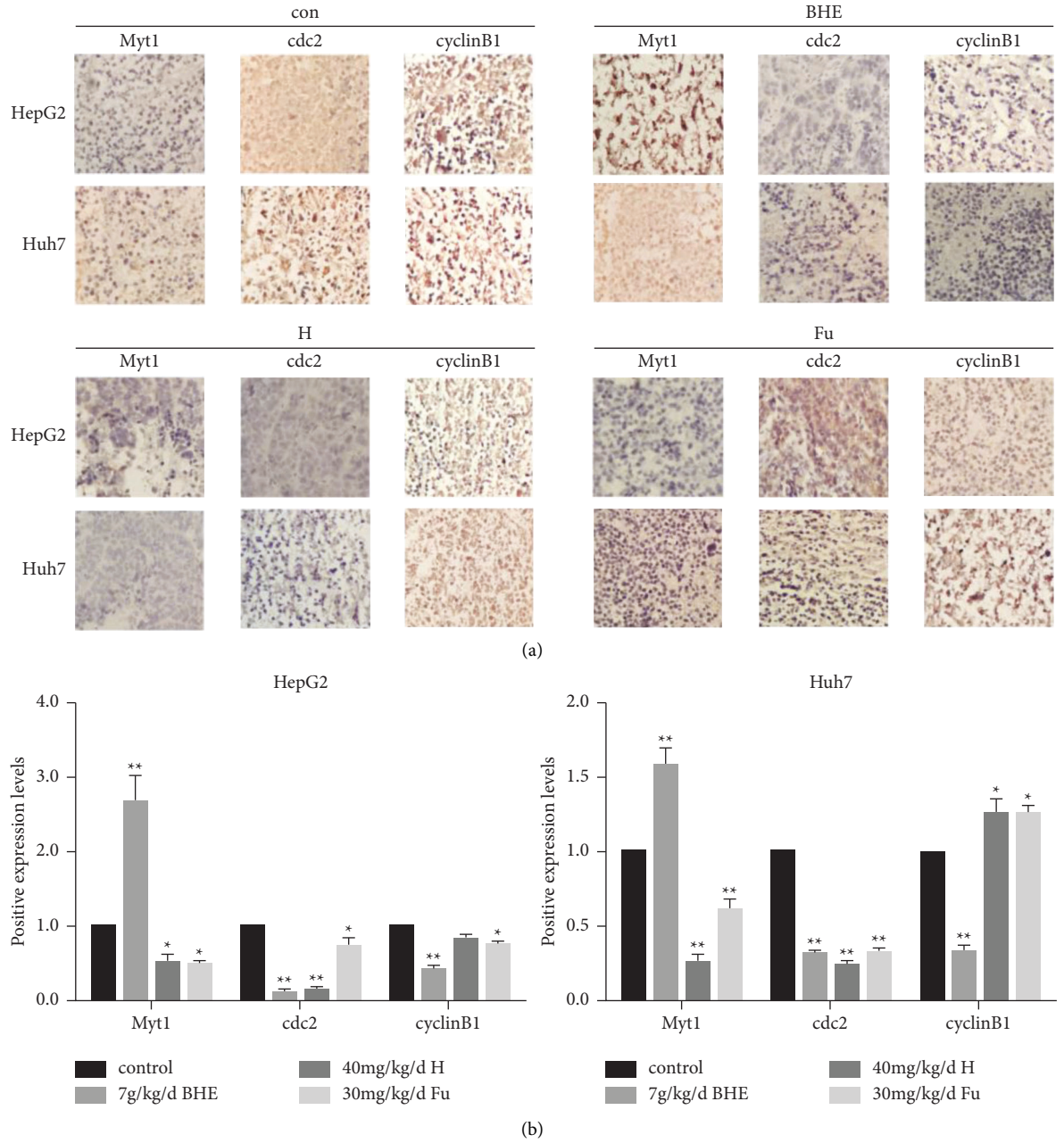

FIGURE 8: (a) The expression of cyclin B1, cDC2, and MyT1 proteins in xenograft tissues. (b) The expression of cyclin B1, cDC2, and MyT1 proteins in xenograft tissues analyzed by immunohistochemistry. $^{*}P < 0.05$, $^{**}P < 0.01$, when compared to the positive control group.

hematological malignant tumors [48, 49]. cDC2 inhibits the progression of the cell cycle and potentially induces apoptosis. The activation or over-expression of cDC2 promotes cell proliferation and imbalances the cell proliferation and apoptosis, which suggests the role of cDC2 in multiple tumorigenesis processes. Additionally, cyclin B-associated cDC2 regulates the G2/M phase [50]. The results of the present study suggested that BHE arrested the progression of the cell cycle at the G2/M phase by altering levels of MyT1, cyclin B1, and cDC2 in HepG2 and Huh7 cells.

A model of nude mice was established in this study, and the results showed that BHE inhibited the growth of xenografts and affected the expression of MyT1, cyclin B1, and cDC2. These findings confirmed that BHE inhibited the proliferation of HCC by arresting the cell cycle of HCC and affecting the expression of proteins related to the cell cycle. However, further clinical trials are required for the clinical application of blue honeysuckle extract.

5. Conclusion

BHE inhibits the cyclin B1/cDC2 signaling pathways to achieve antitumor effects, which demonstrates its great potential as a new anticancer drug for the treatment of patients with HCC and provides a theoretical basis for the

further development and utilization of blue honeysuckle in tumor therapy.

Data Availability

All data generated or analyzed during this study are included in this published article.

Conflicts of Interest

No conflicts of interest are declared by the authors.

Authors' Contributions

Chun-Peng Zhang and Wei-Hua Li have contributed equally to this work.

Acknowledgments

This work was supported by the Science and Technology Innovation Talent Foundation of Harbin (2017RAXXJ057).

References

[1] F. Bray, J. Ferlay, I. Soerjomataram, R. L. Siegel, L. A. Torre, and A. Jemal, "Global cancer statistics 2018: GLOBOCAN estimates of incidence and mortality worldwide for 36 cancers in 185 countries," *CA: A Cancer Journal for Clinicians*, vol. 68, no. 6, pp. 394–424, 2018.

[2] J. Ferlay, M. Colombet, I. Soerjomataram et al., "Estimating the global cancer incidence and mortality in 2018: GLOBOCAN sources and methods," *International Journal of Cancer*, vol. 144, no. 8, pp. 1941–1953, 2019.

[3] J. Rowe, Y. Ghouri, and I. Mian, "Review of hepatocellular carcinoma: epidemiology, etiology, and carcinogenesis," *Journal of Carcinogenesis*, vol. 16, p. 1, 2017.

[4] R. X. Zhu, W. K. Seto, C. L. Lai, and M. F. Yuen, "Epidemiology of hepatocellular carcinoma in the asia-pacific region," *Gut Liver*, vol. 10, no. 3, pp. 332–339, 2016.

[5] A. Villanueva and J. M. Llovet, "Targeted therapies for hepatocellular carcinoma," *Gastroenterology*, vol. 140, no. 5, pp. 1410–1426, 2011.

[6] G. A. Colditz and E. K. Wei, "Preventability of cancer: the relative contributions of biologic and social and physical environmental determinants of cancer mortality," *Annual Review of Public Health*, vol. 33, no. 1, pp. 137–156, 2012.

[7] W. P. Steward and K. Brown, "Cancer chemoprevention: a rapidly evolving field," *British Journal of Cancer*, vol. 109, pp. 1–7, 2013.

[8] J. R. Liu, H. W. Dong, X. R. Sun et al., "Effects of beta-ionone on mammary carcinogenesis and antioxidant status in rats treated with DMBA," *Nutrition and Cancer*, vol. 62, no. 1, pp. 58–65, 2009.

[9] J. R. Liu, X. R. Sun, H. W. Dong et al., "β-ionone suppresses mammary carcinogenesis, proliferative activity and induces apoptosis in the mammary gland of the sprague-dawley rat," *International Journal of Cancer*, vol. 122, no. 12, pp. 2689–2698, 2008.

[10] Y. Liu, M. Liu, B. Li et al., "Fresh raspberry phytochemical extract inhibits hepatic lesion in a Wistar rat model," *Nutrition and Metabolism*, vol. 7, no. 1, p. 84, 2010.

[11] H. S. Chen, M. Liu, L. J. Shi et al., "Effects of raspberry phytochemical extract on cell proliferation, apoptosis, and serum proteomics in a rat model," *Journal of Food Science*, vol. 76, no. 8, pp. T192–T198, 2011.

[12] J. Vostalova, A. Galandakova, I. Palikova et al., "*Lonicera caerulea* fruits reduce UVA-induced damage in hairless mice," *Journal of Photochemistry and Photobiology B: Biology*, vol. 128, pp. 1–11, 2013.

[13] C. Xie, J. Kang, M. E. Ferguson, S. Nagarajan, T. M. Badger, and X. Wu, "Blueberries reduce pro-inflammatory cytokine TNF-α and IL-6 production in mouse macrophages by inhibiting NF-κB activation and the MAPK pathway," *Molecular Nutrition & Food Research*, vol. 55, no. 10, pp. 1587–1591, 2011.

[14] S. Zafra-Stone, T. Yasmin, M. Bagchi, A. Chatterjee, J. A. Vinson, and D. Bagchi, "Berry anthocyanins as novel antioxidants in human health and disease prevention," *Molecular Nutrition & Food Research*, vol. 51, no. 6, pp. 675–683, 2007.

[15] A. J. Kim and S. Park, "Mulberry extract supplements ameliorate the inflammation-related hematological parameters in carrageenan-induced arthritic rats," *Journal of Medicinal Food*, vol. 9, no. 3, pp. 431–435, 2006.

[16] W. H. Shin, S. J. Park, and E. J. Kim, "Protective effect of anthocyanins in middle cerebral artery occlusion and reperfusion model of cerebral ischemia in rats," *Life Sciences*, vol. 79, no. 2, pp. 130–137, 2006.

[17] A. Tarozzi, F. Morroni, S. Hrelia et al., "Neuroprotective effects of anthocyanins and their in vivo metabolites in SH-SY5Y cells," *Neuroscience Letters*, vol. 424, no. 1, pp. 36–40, 2007.

[18] F. Cohen-Boulakia, P. E. Valensi, H. Boulahdour et al., "In vivo sequential study of skeletal muscle capillary permeability in diabetic rats: effect of anthocyanosides," *Metabolism*, vol. 49, no. 7, pp. 880–885, 2000.

[19] A. Jankowski, B. Jankowska, and J. Niedworok, "The effect of anthocyanin dye from grapes on experimental diabetes," *Folia Medica Cracoviensia*, vol. 41, no. 3-4, pp. 5–15, 2000.

[20] C. Pergola, A. Rossi, P. Dugo, S. Cuzzocrea, and L. Sautebin, "Inhibition of nitric oxide biosynthesis by anthocyanin fraction of blackberry extract," *Nitric Oxide*, vol. 15, no. 1, pp. 30–39, 2006.

[21] I. Palikova, K. Valentova, I. Oborna, and J. Ulrichova, "Protectivity of blue honeysuckle extract against oxidative human endothelial cells and rat hepatocyte damage," *Journal of Agricultural and Food Chemistry*, vol. 57, no. 15, pp. 6584–6589, 2009.

[22] I. Svarcova, J. Heinrich, and K. Valentova, "Berry fruits as a source of biologically active compounds: the case of *Lonicera caerulea*," *Biomedical Papers*, vol. 151, no. 2, pp. 163–174, 2007.

[23] G. Caprioli, R. Iannarelli, M. Innocenti et al., "Blue honeysuckle fruit (*Lonicera caerulea* L.) from eastern Russia: phenolic composition, nutritional value and biological activities of its polar extracts," *Food & Function*, vol. 7, no. 4, pp. 1892–1903, 2016.

[24] T. Jurikova, O. Rop, J. Mlcek et al., "Phenolic profile of edible honeysuckle berries (genus *lonicera*) and their biological effects," *Molecules*, vol. 17, no. 1, pp. 61–79, 2011.

[25] T. Jurikova, J. Sochor, O. Rop et al., "Evaluation of polyphenolic profile and nutritional value of non-traditional fruit species in the Czech Republic--a comparative study," *Molecules*, vol. 17, no. 8, pp. 8968–8981, 2012.

[26] H. P. Rupasinghe, M. M. Boehm, S. Sekhon-Loodu, I. Parmar, B. Bors, and A. R. Jamieson, "Anti-inflammatory activity of

haskap cultivars is polyphenols-dependent," *Biomolecules*, vol. 5, no. 2, pp. 1079–1098, 2015.

[27] A. Chaovanalikit, M. M. Thompson, and R. E. Wrolstad, "Characterization and quantification of anthocyanins and polyphenolics in blue honeysuckle (*Lonicera caerulea* L.)," *Journal of Agricultural and Food Chemistry*, vol. 52, no. 4, pp. 848–852, 2004.

[28] A. Wojdylo, P. N. N. Jáuregui, A. A. Carbonell-Barrachina, J. Oszmianski, and T. Golis, "Variability of phytochemical properties and content of bioactive compounds in *Lonicera caerulea* L. var. kamtschatica berries," *Journal of Agricultural and Food Chemistry*, vol. 61, no. 49, pp. 12072–12084, 2013.

[29] R. Myjavcova, P. Marhol, V. Kren et al., "Analysis of anthocyanin pigments in *Lonicera* (Caerulea) extracts using chromatographic fractionation followed by microcolumn liquid chromatography-mass spectrometry," *Journal of Chromatography A*, vol. 1217, no. 51, pp. 7932–7941, 2010.

[30] L. Chen, X. Xin, R. Lan, Q. Yuan, X. Wang, and Y. Li, "Isolation of cyanidin 3-glucoside from blue honeysuckle fruits by high-speed counter-current chromatography," *Food Chemistry*, vol. 152, pp. 386–390, 2014.

[31] Z. Gazdik, B. Krska, V. Adam et al., "Electrochemical determination of the antioxidant potential of some less common fruit species," *Sensors*, vol. 8, no. 12, pp. 7564–7570, 2008.

[32] H. Zhang, J. Liu, G. Li et al., "Fresh red raspberry phytochemicals suppress the growth of hepatocellular carcinoma cells by PTEN/AKT pathway," *The International Journal of Biochemistry & Cell Biology*, vol. 104, pp. 55–65, 2018.

[33] H. W. Dong, S. Zhang, W. G. Sun et al., "β-ionone arrests cell cycle of gastric carcinoma cancer cells by a MAPK pathway," *Archives of Toxicology*, vol. 87, no. 10, pp. 1797–1808, 2013.

[34] Q. Liu, H. W. Dong, W. G. Sun et al., "Apoptosis initiation of beta-ionone in SGC-7901 gastric carcinoma cancer cells via a PI3K-AKT pathway," *Archives of Toxicology*, vol. 87, no. 3, pp. 481–490, 2013.

[35] J. R. Liu, Q. Liu, J. Khoury et al., "Hypoxic preconditioning decreases nuclear factor κB activity via disrupted in schizophrenia-1," *The International Journal of Biochemistry & Cell Biology*, vol. 70, pp. 140–148, 2016.

[36] J. R. Liu, K. Yuki, C. Baek, X. H. Han, and S. G. Soriano, "Dexmedetomidine-induced neuroapoptosis is dependent on its cumulative dose," *Anesthesia & Analgesia*, vol. 123, no. 4, pp. 1008–1017, 2016.

[37] J. R. Liu, C. Baek, X. H. Han, P. Shoureshi, and S. G. Soriano, "Role of glycogen synthase kinase-3β in ketamine-induced developmental neuroapoptosis in rats," *British Journal of Anaesthesia*, vol. 110, 2013.

[38] L. H. Shan, W. G. Sun, W. Han et al., "Roles of fibroblasts from the interface zone in invasion, migration, proliferation and apoptosis of gastric adenocarcinoma," *Journal of Clinical Pathology*, vol. 65, no. 10, pp. 888–895, 2012.

[39] S. J. Duthie, P. T. Gardner, P. C. Morrice et al., "DNA stability and lipid peroxidation in vitamin E-deficient rats in vivo and colon cells in vitro," *European Journal of Nutrition*, vol. 44, no. 4, pp. 195–203, 2005.

[40] D. Serra, J. Paixao, C. Nunes, T. C. P. Dinis, and L. M. Almeida, "Cyanidin-3-glucoside suppresses cytokine-induced inflammatory response in human intestinal cells: comparison with 5-aminosalicylic acid," *PLoS One*, vol. 8, no. 9, Article ID e73001, 2013.

[41] S. C. Forester, Y. Y. Choy, A. L. Waterhouse, and P. I. Oteiza, "The anthocyanin metabolites gallic acid, 3-O-methylgallic acid, and 2, 4, 6-trihydroxybenzaldehyde decrease human colon cancer cell viability by regulating pro-oncogenic signals," *Molecular Carcinogenesis*, vol. 53, no. 6, pp. 432–439, 2014.

[42] H. Babich, A. Sedletcaia, and B. Kenigsberg, "In vitro cytotoxicity of protocatechuic acid to cultured human cells from oral tissue: involvement in oxidative stress," *Pharmacology & Toxicology*, vol. 91, no. 5, pp. 245–253, 2002.

[43] M. Amararathna, D. W. Hoskin, and H. V. Rupasinghe, "Anthocyanin-rich haskap (*Lonicera caerulea* L.) berry extracts reduce nitrosamine-induced DNA damage in human normal lung epithelial cells," *Food and Chemical Toxicology*, vol. 141, Article ID 111404, 2020.

[44] M. C. Yin, C. C. Lin, H. C. Wu, S. M. Tsao, and C. K. Hsu, "Apoptotic effects of protocatechuic acid in human breast, lung, liver, cervix, and prostate cancer cells: potential mechanisms of action," *Journal of Agricultural and Food Chemistry*, vol. 57, no. 14, pp. 6468–6473, 2009.

[45] C. Hui, Y. Bin, Y. Xiaoping et al., "Anticancer activities of an anthocyanin-rich extract from black rice against breast cancer cells in vitro and in vivo," *Nutrition and Cancer*, vol. 62, no. 8, pp. 1128–1136, 2010.

[46] W. Liu, J. Xu, S. Wu et al., "Selective anti-proliferation of HER2-positive breast cancer cells by anthocyanins identified by high-throughput screening," *PLoS One*, vol. 8, no. 12, Article ID e81586, 2013.

[47] Y. Nakamura, K. Torikai, Y. Ohto, A. Murakami, T. Tanaka, and H. Ohigashi, "A simple phenolic antioxidant protocatechuic acid enhances tumor promotion and oxidative stress in female ICR mouse skin: dose-and timing-dependent enhancement and involvement of bioactivation by tyrosinase," *Carcinogenesis*, vol. 21, no. 10, pp. 1899–1907, 2000.

[48] X. Chen, Y. Liao, D. Long, T. Yu, F. Shen, and X. Lin, "The Cdc2/Cdk1 inhibitor, purvalanol A, enhances the cytotoxic effects of taxol through Op18/stathmin in non-small cell lung cancer cells in vitro," *International Journal of Molecular Medicine*, vol. 40, no. 1, pp. 235–242, 2017.

[49] P. Liu, T. P. Kao, and H. Huang, "CDK1 promotes cell proliferation and survival via phosphorylation and inhibition of FOXO1 transcription factor," *Oncogene*, vol. 27, no. 34, pp. 4733–4744, 2008.

[50] L. Dai, Y. Liu, J. Liu et al., "A novel cyclinE/cyclinA-CDK inhibitor targets p27(Kip1) degradation, cell cycle progression and cell survival: implications in cancer therapy," *Cancer Letters*, vol. 333, no. 1, pp. 103–112, 2013.

Hindawi
Evidence-Based Complementary and Alternative Medicine
Volume 2022, Article ID 8746066, 7 pages
https://doi.org/10.1155/2022/8746066

Research Article

Effect of Transradial Artery Catheterization on Shock Patients

Hui Xu,[1] Wenyong Chen,[2] Mingming Huang,[3] and Zenggeng Wang[1]

[1]*Department of Emergency, Jiangxi Provincial People's Hospital, Nanchang, Jiangxi 330006, China*
[2]*Department of Emergency, Yongxiu County People's Hospital, Jiujiang, Jiangxi 330300, China*
[3]*Department of Emergency, Gongqingcheng People's Hospital, Jiujiang, Jiangxi 332020, China*

Correspondence should be addressed to Zenggeng Wang; wzglove123@163.com

Received 5 August 2022; Revised 13 September 2022; Accepted 17 September 2022; Published 28 September 2022

Academic Editor: Xueliang Wu

Objective. This study aimed to investigate the clinical effect of ultrasound-guided transradial catheterization (TRC) for ICU patients with shock. *Methods*. 120 shock patients registered in the ICU of our hospital from January 2019 to June 2022 were selected for prospective study. The control group (60 patients) were treated with palpation-guided TRC. The observation group was treated with ultrasound-guided TRC and was divided into the internal puncture group (internal TRC) and external puncture group (external TRC), with 30 cases in each. The first attempt success rate, total success rate, operation duration, complication, measurement of radial artery, and VAS scores were compared in these groups. *Results*. The success rate was higher in the observation group than in the control group ($P < 0.05$), and higher in the internal puncture group than in the external puncture group ($P < 0.05$). The first attempt success rate was significantly higher in the observation group than in the control group ($P < 0.05$), with no significant difference in between ($P > 0.05$). The number of attempts and operation duration were lower in the observation group than in the control group ($P < 0.05$), with significantly more operation duration in the internal puncture group than in the external puncture group ($P < 0.05$) and no significant difference in the number of attempts (both $P > 0.05$). The complication rate was significantly lower in the observation group than in the control group ($P < 0.05$) and there was no significant difference in between ($P > 0.05$). The radial artery diameter, cross-sectional area, and depth from the skin in the observation group were larger than those in the control group ($P < 0.05$) and there was no significant difference in between ($P > 0.05$). At 1, 6, 24, and 48 h after the surgery, the observation group showed lower VAS scores than the control group ($P < 0.05$). *Conclusion*. The ultrasound-guided TRC reduced the number of attempts, the complication rates, and the operation duration. For patients with shock, if Doppler ultrasound cannot detect blood flow, the success rate in the observation group was higher than that in the control group, and its advantage is worthy of promotion in severe patients.

1. Introduction

The term "shock" refers to a life-threatening circulatory failure caused by an imbalance between the supply and demand of cellular oxygen [1, 2]. The condition of shock patients changes rapidly, and the hemodynamic is extremely unstable. After hemodynamic disorder, intracoronary blood flow decreases, resulting in insufficient myocardial blood supply and oxygen supply [3]. Blood pressure and mean arterial pressure are two of the most important outcome measures in diagnosis and treatment for shock. It has become a routine treatment for shock patients to establish a vascular access with both real-time monitoring of blood pressure and convenient arterial blood collection as soon as possible. Meanwhile, with the surgical interventions for cardiovascular disease being taken widely, transradial catheterization (TRC) has gradually become one of the first options as the operative approach for interventional surgery due to the unaffected postoperative activities, quick postoperative hemostasis by compression, and easier observation of postoperative bleeding.

The radial artery is usually the first choice for arterial catheterization, because the radial and ulnar arteries have a rich lateral circulation that avoids ischemic necrosis of the anterior limb. However, obesity, ectopia, hypoperfusion (hypotension, low cardiac output), extreme-weak arterial

beats, and arterial spasm can all lead to failed arterial catheterization [4, 5]. In recent years, ultrasound guidance has been widely used in jugular catheterization, peripherally inserted central venous catheterization, and femoral venous catheterization, but there have been few applications reported in artery catheterization. For instance, ultrasound guidance for epidural surgery has gained popularity and interest, especially for lumbar epidural needle placement and catheterization, and its application in thoracic epidural surgeries has also been receiving attention [6]. Ultrasound-guided catheterization, as a "visual" new technology [7], makes the radial artery imaging clear and directly observes the radial artery orientation, anatomical variants, and the neighboring relationship with the surrounding tissues, which helps to find the best puncture point, improve the success rate, and reduce the injury with catheterization [8].

This study aimed to investigate the clinical value of ultrasound-guided TRC for ICU patients with shock, which may provide a novel insight for clinical application in severe patients.

2. Clinical Materials and Methods

2.1. General Clinical Data. 120 shock patients registered in the ICU of our hospital from January 2019 to June 2022 were selected for prospective study. Inclusion criteria: Patients met the diagnostic criteria for shock [9]. Exclusion criteria: Patients with a history of forearm surgery, local infection, local arterial embolization, or abnormal results of the quantitative SaO2-Allen test (negative). A total of 120 patients were included, aged from 15 to 95 years old, with a mean age of 62.13 ± and 19.81 years old. Patients enrolled in the study were randomized into the control and observation groups using a computer-generated list in the ratio of 1 : 1. The control group was treated with palpation-guided TRC (blind method). The observation group treated with ultrasound-guided TRC was divided into the internal puncture group (internal TRC) and the external puncture group (external TRC). There were 60 cases in the control group and 30 cases in either the internal puncture group or external puncture group. In the control group, there were 31 males and 29 females, aged 15.0–81.0 (64.3 ± 3.5), with a PACHEII score of 36.8 ± 5.3. In the external puncture group, there were 16 males and 14 females, aged 21.0–80.0 (65.1 ± 3.3), with a PACHEII score of 35.2 ± 4.6. In the internal puncture group, there were 17 males and 13 females, aged 20–95 (64.6 ± 3.1), with a PACHEII score of 36.5 ± 4.9. In addition, prior to TRC, the purpose and process of TRC were explained to all the patients themselves or their family members, and the informed consent form was signed by the authorized family members to obtain understanding and cooperation.

2.2. Methods. Patients were taken in the supine position or lifted 30 degrees by their heads, routinely assessed for radial artery beating, and evaluated with the Allen test. In both the groups, artery catheterization was processed using a 22G catheter from B. Braun.

The control group was treated with palpation-guided TRC. After disinfection of the left index and middle fingers, the operator palpated the artery beat using the left index and middle fingers to determine the puncture site. The catheter held by the operator's right hand was punctured into the radial artery along the arterial direction at 15°–30° oblique angle no matter using the direct method or the penetrating method and set lower when flashbacks of arterial blood were observed. The needle was withdrawn when the radial arterial blood flow was pressed and blocked by the end of the catheter near the heart. Then the cannula was connected to the disposable blood pressure transducer, disinfected, and fixed.

The authorized medical staff of our hospital (the first author of this paper) performed ultrasound-guided TRC in the observation group using a unified ultrasound system (M5s/M7 Series portable color Doppler ultrasound system, Shenzhen Mindray Biomedical Electronics Co., LTD.) with 7.5~10 MHz line array probe (7L4s). Patients were placed in the supine position or lifted 30 degrees by their heads and 15 degrees with their feet, with the left or right upper limb stretched out at 30°–60° and the wrist back stretched out at about 30° to fully expose the radial artery. A nursing cushion was placed underneath. Before the operation, the vessel condition and puncture site were determined according to the inclusion and exclusion criteria, and the relevant diameters were recorded. Internal puncture group: the disposable medical sterile protective cover was used for ultrasound probe protection. The probe was filled with couplant and fixed. The color Doppler system was set to upper limb artery mode. The vascular pulse and target puncture site were determined by color Doppler flow imaging (CDFI). The puncture was processed using the internal method. The pinpoint of the catheter was adjusted under color Doppler localization till it entered into the vessel. The catheter was withdrawn for fixation when the flashback of blood was observed. External puncture group: the disposable medical sterile protective cover was used for ultrasound probe protection. The probe was filled with couplant and fixed. The color Doppler system was set to upper limb artery mode. The vascular pulse and target puncture site were determined by CDFI. The puncture was processed using the external method. After the pinpoint was punctured into the center of the vascular lumen, the cannula was pushed forward by the left hand and the needle was drawn back by the right hand. If putting forward was not smooth, the direct method was switched to the penetrating method to withdraw the needle and put forward the cannula when the beating blood spouted. After successful puncture, a large disposable transparent film was used for fixation and the disposable pressure transducer was connected. All operations were performed by the same operator. On account of the severe shock of patients, another doctor was responsible for the emergency treatment and emergency operation during the operation.

2.3. Outcome Measures

(1) *First Attempt Success Rate*. The proportion of patients with successful first attempt of TRC to the total patients in group. First attempt success rate- = successful first attempt cases/total cases ∗ 100%.

(2) *Total Success Rate*. The proportion of patients with successful TRC to the total patients in group. Total success rate = total successful cases/total cases ∗ 100%.

(3) *Number of Attempts*. Number of attempts required for successful TRC.

(4) *Complication Rate*. During the catheterization, the proportion of patients with complications to the total patients (complications criteria: ① Local hematoma: swelling, ecchymosis, bulge, and waving feeling in the local skin near the catheter; ② puncture site bleeding: After successful TRC, blood flowing out from the puncture site; ③ local infection: Local redness and swelling near the catheter. Complication rate = complication cases/total cases ∗ 100%.

(5) *Operation Duration*. Time spent for successful TRC in both the groups. The control group recorded the time spent from palpation to successful TRC. The observation group recorded the time spent for ultrasound-guided TRC, including the image localization time (time from the probe being placed on the skin to the needle being punctured into the skin) and the catheterization duration.

(6) *Vascular Diameter, Cross-Sectional Area, and Depth from the Skin*. Measurement of the parameters were performed using the Sonosite built-in software.

(7) *Pain Status at 1, 6, 24, and 48 h after Surgery*. The visual analogue scale (VAS) score was used to assess pain degree, with a total score of 10, higher score indicating more severe pain.

2.4. Statistical Analysis. We planned to enroll 120 patients. We calculated that with this sample size the study would have 90% power to detect an increase in the first attempt success rate or total success rate from 70% in the control group to 90% in the puncture group at an α level of .05. The internal puncture and external puncture groups belonged to the observation group. They were estimated and both have an effect on shock patients. Thus, we used a separation ratio of 2 : 1 : 1.

Statistical analysis was conducted with SAS version 9.3 (SAS Institute Inc). All statistical tests were 2-sided. $P < 0.05$ was considered statistically significant.

3. Results

3.1. Comparison of General Data. The patients' age, sex, acute physiology, and acute Physiology and chronic health evaluation (PACHEII) were compared, and the results showed no significant difference (all $P < 0.05$), suggesting they were comparable.

3.2. Comparison of the Puncture Conditions. The results showed that the total success rate of TRC was significantly higher in the observation group than in the control group ($P < 0.05$) and higher in the internal puncture group than in the external puncture group, with significant differences ($P < 0.05$). The first attempt success rate was significantly higher in the observation group than in the control group ($P < 0.05$), with no significant difference in between ($P > 0.05$), as shown in Figure 1.

3.3. Comparison of Attempts and Operation Duration. The number of attempts and operation duration were less in the observation group than in the control group ($P < 0.05$), with significantly more operation duration in the internal puncture group than in the external puncture group ($P < 0.05$) and no significant difference in the number of attempts (both $P > 0.05$), as shown in Figure 2.

3.4. Comparison of Complications of Peripheral Arterial Catheters. The complication rate was significantly lower in the observation group than in the control group ($P < 0.05$) and there was no significant difference in between ($P > 0.05$), as shown in Table 1.

3.5. Comparison of Arterial Measurement and TRC-Related Information. The radial artery diameter, cross-sectional area, and depth from the skin in the observation group were larger than those in the control group ($P < 0.05$) and there was no difference in between ($P > 0.05$), as shown in Figure 3.

3.6. Comparison of Postoperative Pain Status. At 1, 6, 24, and 48 h after the surgery, the observation group showed lower VAS scores than the control group ($P < 0.05$) and there was no significant difference between the external puncture group and the internal puncture group ($P > 0.05$), as shown in Figure 4.

4. Discussion

The condition of shock patients changes rapidly with the possibility of massive bleeding, causing the patients to undergo frequent arterial blood collection and invasive arterial blood pressure monitoring. Radial artery blood collection has the advantages of small pain response, easy acceptance by patients, less pressure and preparation time, and less occurrence of hematoma, so the radial artery has become the preferred route of arterial catheterization for invasive blood pressure monitoring [10–12]. In clinical practice, however, there are often some shock patients in critical condition who have weak artery pulses due to limb swelling, insufficient capacity, and poor circulation. The traditional blind catheterization consists of anatomical localization and the palpation of the radial artery, which has a low first attempt success rate and causes multiple attempts at puncture, making it stressful and painful for patients awake. It is also easy to cause radial artery spasm, bleeding,

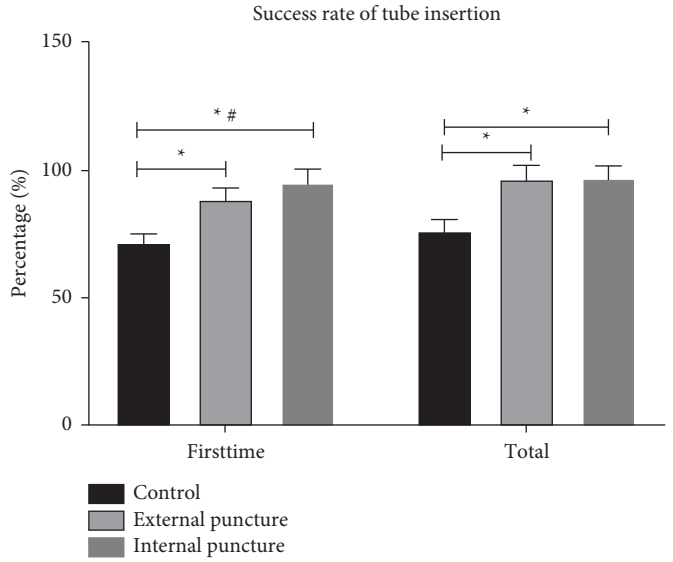

Figure 1: The puncture conditions in three groups. $^{*}P < 0.05$, compared with the control group; $^{\#}P < 0.05$, compared with the external puncture group.

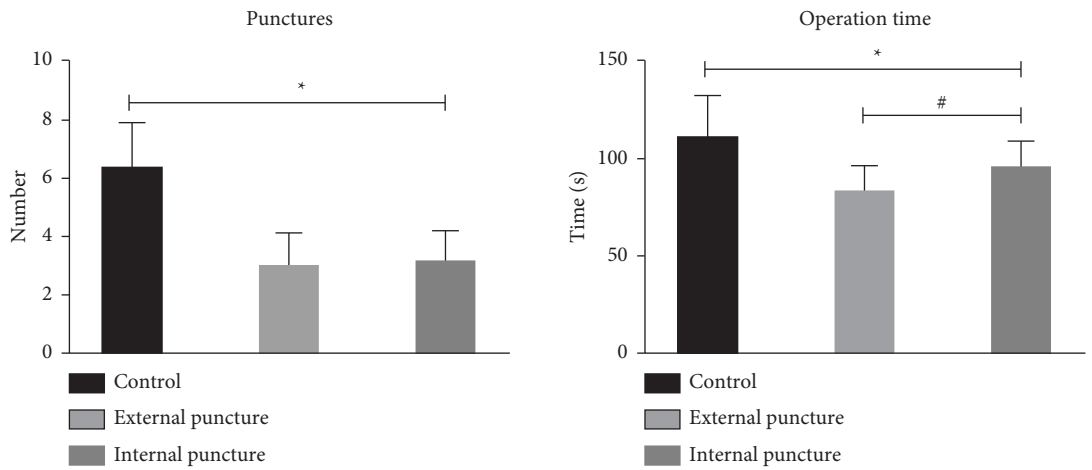

Figure 2: Attempts and operation duration in three groups. $^{*}P < 0.05$, compared with the control group; $^{\#}P < 0.05$, compared with the external puncture group.

Table 1: Complications of peripheral arterial catheters in three groups.

Group	Complication			Total	Incidence rate (%)
	Local hematoma	Puncture site bleeding	Local infection		
Control	8 (13.33)	5 (8.33)	2 (3.33)	15	25.00
External puncture	1 (3.33)	3 (10.00)	0 (0.00)	4	13.33
Internal puncture	2 (6.67)	1 (3.33)	0 (0.00)	3	10.00
t	4.537				
P	<0.001				

hematoma, and other complications, leading to puncture failure or catheterization and blood collection difficulty [13, 14]. The ultrasound-guided TRC clearly shows the arterial blood vessels and their surrounding tissues, and by using the high-quality imaging of the blood vessels by the ultrasound, the thickness, depth, and walking of the radial artery are clearly seen under the ultrasound. An external puncture is used during the puncture, and the radial artery image is placed in the middle of the probe and kept fixed. The needle is punctured through the midpoint of the probe,

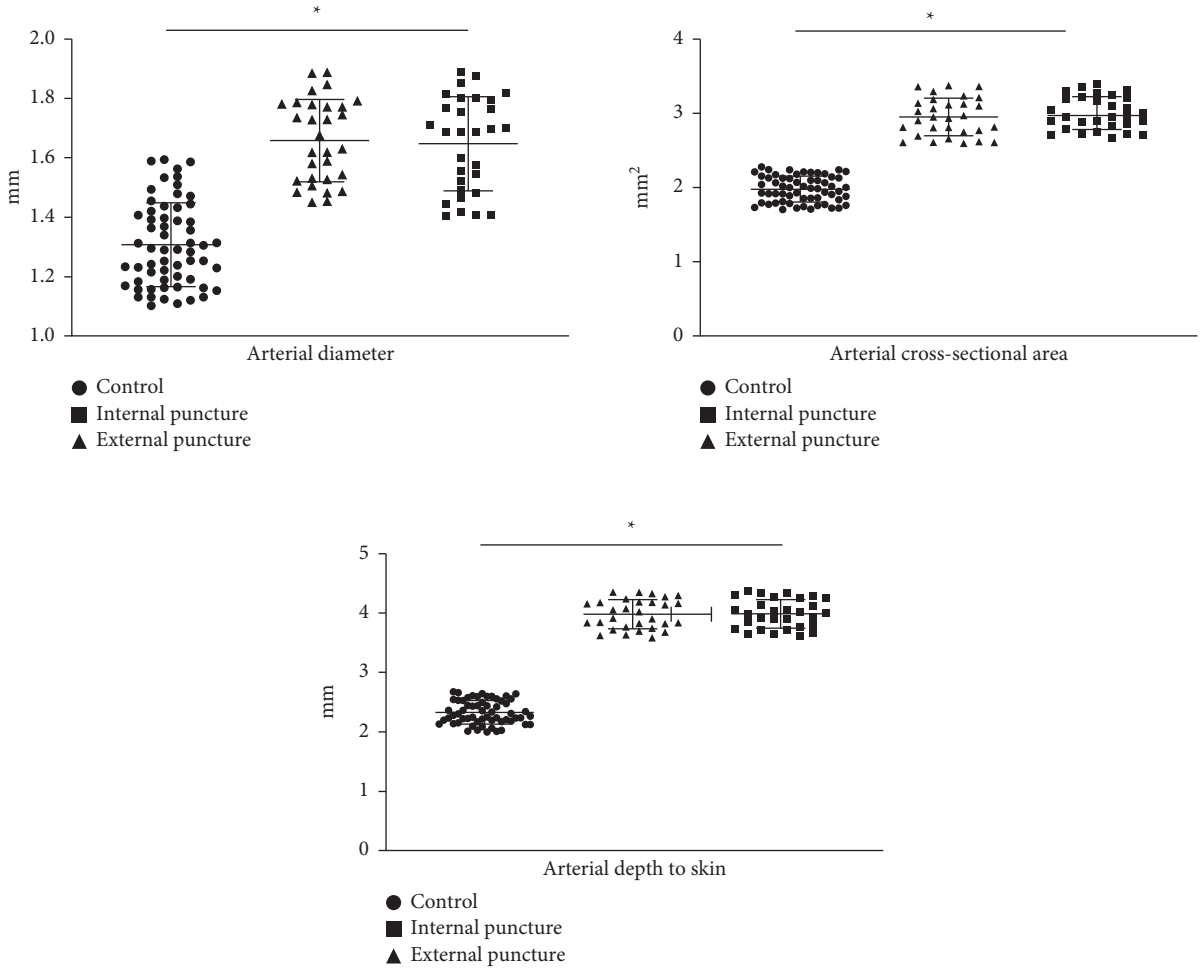

Figure 3: Arterial measurement and TRC-related information in three groups. $^{*}P < 0.05$, compared with the control group.

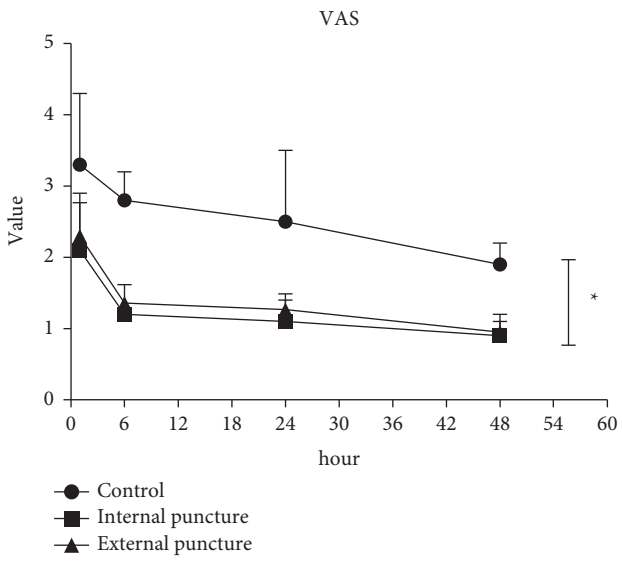

Figure 4: Postoperative pain status in three groups $^{*}P < 0.05$, compared with the control group.

which can greatly improve the success rate of arterial catheterization and reduce or even avoid the related complications [15–17].

Ultrasound technology has been widely used in clinical vascular puncture and has become the third "eye" of medical staff, reducing related complications and thus becoming more and more popularized in clinical practice. In recent years, with the emergence of high-frequency and high-definition ultrasound equipment and the continuous improvement of ultrasound probes, the application of ultrasound-guided TRC in the rescue and interventional treatment of acute and critical diseases is also on the rise, with more and more related studies. At present, ultrasound-guided catheterization includes internal puncture and external puncture with each having their own advantages and disadvantages and is been widely used for regional nerve block and central venipuncture. When the long-axis internal puncture is used, the ultrasound probe, the sheath, and the long-axis of vessel are in the same plane, and the long-axis section of the vessel and the trocar can be fully displayed during the puncture process, but the position relationship

between the pinpoint and the vessel in the short-axis section cannot be clearly displayed. On the other hand, the cross-sectional image of the vascular lumen captured during external puncture can clearly show the relationship between the positions of the trocar and the vessel in the short axis section, but sometimes it does not define the exact location of the pinpoint. Because the related complications of arterial puncture are more serious than those of venous puncture, how to reduce the complications is the focus of the current research. The results of this study showed that patients in need of TRC, palpation-guided group, may have multiple trials before success, which increased the number of attempts and operation duration. Compared to the palpation-guided control group, the ultrasound-guided group showed an increased first attempt success rate, significantly reduced number of attempts, less operation duration, and a lower VAS score in both the internal puncture group and the external puncture group, indicating that the ultrasound-guided TRC is a very effective and safe catheterization technique. It is worth noting that although the external puncture group was not significantly different from the internal puncture group in overall success rate, its first attempt success rate and operation duration were lower than those in the internal puncture group, and the reason for this difference may be related to the proficiency in the two methods. When using internal puncture, the left hand needs to fix the probe position continuously, and a little movement may lose the puncture plane. Therefore, internal puncture is more difficult than external one, and the beginners mostly prefer to use external puncture. Ball et al. [18] believe that although internal puncture has higher technical difficulty, it is clinically safer because the clear imaging of the needle tip in the lumen is better to avoid the vascular damage caused by catheter. When using external puncture, if the punctured blood vessel is relatively thin, due to the strong pressure of the anterior wall on the inner blood vessel caused by the large angle of insertion it can easily flatten the vessel and make the vessel lumen thinner, resulting in the vague position of the needle and a high risk of perforation through the posterior wall, thus causing hematoma. When internal puncture is used, its small angle of insertion causes limited pressure of the anterior wall to the blood vessel, with inconspicuous lumen changes. In addition, the position of the needle can be observed during the whole process, which can avoid the perforation through the posterior wall to a greater extent. Therefore, for shocked patients, the advantages of internal puncture are more prominent. Meanwhile, shock patients are often accompanied by coagulation dysfunction, so once the artery is perforated, it will easily cause hematoma and bleeding difficulties. Therefore, based on our research results, we suggested that internal puncture to be the main choice of TRC for shock patients.

Gu et al. [19] performed a meta-analysis of seven RCTs and showed that compared to palpation guidance, ultrasound guidance can improve the success rate of TRC and reduce the number of attempts, thus reducing the incidence of complications such as hematoma. In this study, the complication rate in the external puncture group and the internal puncture group was significantly lower than that in the control group. The patients involved were all critically ill, with insufficient volume, poor circulation, shock, systemic edema, and their arterial blood flow was unable to be seen using Doppler ultrasound. Therefore, the arterial catheterization became difficult, with inevitably repeated attempts, thus increasing the incidence of local hematoma, puncture bleeding, local infection, and so on. The external puncture group and the internal puncture group can quickly finish the localization of radial artery vessels and measure the size and depth of the arterial lumen. If the edema of the puncture site is too severe to form an image of blood flow, the arterial pulse of some patients can be observed alternately, thus solving the problem of arterial catheterization for severe patients and reducing the incidence of complications.

Although this study focused on patients with shock, the method we detected is suitable for every patient in need of TRC, and the success rate would be higher for patients with normal hemodynamics and good vascular filling. This method can also be used for patients undergoing radial puncture for interventional surgery. In addition, the operator's proficiency in ultrasound use is also key to the success of TRC. The operators of this study have all passed the standardized training on ultrasound for severe patients and have mastered the basic principles of ultrasound use, the selection and use of vascular probes, how to determine the artery/venous vessel and other ultrasound technologies. Due to the easy learning of ultrasound-guided puncture of blood vessels and its short training period, with the improvement of the hospital equipment, especially in the ICU wards, the equipment of ultrasound machines has been more and more popularized, creating better conditions for ultrasound-guided puncture. However, there were still some limitations. The sample size is quite small, thus we need more samples in our future research. Additionally, nonblinded design might have introduced bias, which should be avoided as much as possible in the future.

In conclusion, ultrasound-guided TRC made it possible to dynamically observe the radial artery vessels, thus benefiting by locating the puncture site and guiding the operation. It could effectively overcome the limitations of blind catheterization with simple, safe, and repeatable operations, greatly improving the first attempt success rate, reducing the number of attempts, reducing the incidence of complications, and reducing operation duration. Its superiority and practicability are worth promoting in severe patients.

Data Availability

The analysed datasets generated during the study are available from the corresponding author on reasonable request.

Conflicts of Interest

The authors declare that there are no conflicts of interest.

References

[1] H. Lier, M. Bernhard, and B. Hossfeld, "Hypovolemic and hemorrhagic shock," *Anaesthesist, Der*, vol. 67, no. 3, pp. 225–244, 2018.

[2] S. Patel, K. Holden, B. Calvin, B. DiSilvio, and T. Dumont, *Critical Care Nursing Quarterly*, vol. 45, no. 3, pp. 225–232, 2022.

[3] R. Ekart, S. Bevc, N. Hojs et al., "Relationship between subendocardial viability ratio and hemoglobin in patients with chronic kidney disease," *Clinical Nephrology*, vol. 88, no. S1, pp. 22–26, 2017.

[4] L. J. D. van Dijk, D. C. Bijdevaate, and A. Moelker, "Rupture of the radial artery after brachiocephalic stent placement per transradial access," *Journal of Vascular and Interventional Radiology*, vol. 29, no. 9, pp. 1281–1283, 2018.

[5] K. Schenke, A. Viertel, N. Joghetaei et al., "Distal transradial access for coronary angiography and interventions in everyday practice: data from the TRIANGLE registry (twitter initiated registry for coronary Angiography in Germany via distaL radial access)," *Cardiology Therapy*, vol. 10, no. 1, pp. 241–253, 2021.

[6] J. H. Lee, D. H. Kim, and W. U. Koh, "Real-time ultrasound guided thoracic epidural catheterization: a technical review," *Anesthesiology and Pain Medicine*, vol. 16, no. 4, pp. 322–328, 2021.

[7] D. Lee, J. Y. Kim, H. S. Kim, K. C. Lee, S. J. Lee, and H. J. Kwak, "Ultrasound evaluation of the radial artery for arterial catheterization in healthy anesthetized patients," *Journal of Clinical Monitoring and Computing*, vol. 30, no. 2, pp. 215–219, 2016.

[8] T. Ogura, A. K. Lefor, M. Nakamura, K. Fujizuka, K. Shiroto, and M. Nakano, "Ultrasound-guided resuscitative endovascular balloon occlusion of the aorta in the resuscitation area," *Journal of Emergency Medicine*, vol. 52, no. 5, pp. 715–722, 2017.

[9] A. Rhodes, "Surviving sepsis campaign: international guidelines for management of sepsis and septic shock," *Critical Care Medicine*, vol. 45, no. 3, pp. 486–552, 2016.

[10] T. Okabayashi, S. Yasuo, S. Tatsuaki et al., "Diagnosis and management of insulinoma," *World Journal of Gastroenterology*, vol. 19, no. 6, pp. 829–837, 2013.

[11] K. Ueda, S. Puangsuvan, M. Hove, and E. Bayman, "Ultrasound visual image-guided vs. Doppler auditory-assisted radial artery cannulation in infants and small children by non-expert anaesthesiologists: a randomized prospective study," *British Journal of Anaesthesia*, vol. 110, no. 2, pp. 281–286, 2013.

[12] K. Urasyanandana, D. Songsang, T. Aurboonyawat, E. Chankaew, P. Withayasuk, and A. Churojana, "Treatment outcomes in cerebral artery dissection and literature review," *Interventional Neuroradiology*, vol. 24, no. 3, pp. 254–262, 2018.

[13] D. Berk, Y. Gurkan, A. Kus, H. Ulugol, M. Solak, and K. Toker, "Ultrasound-guided radial arterial cannulation: long axis/in-plane versus short axis/out-of-plane approaches?" *Journal of Clinical Monitoring and Computing*, vol. 27, no. 3, pp. 319–324, 2013.

[14] M. Edanaga, M. Mimura, T. Azumaguchi, M. Kimura, and M. Yamakage, "Comparison of ultrasound-guided and blindly placed radial artery catheterization," *Masui*, vol. 61, no. 2, pp. 221–224, 2012.

[15] M. B. Stone, C. Moon, D. Sutijono, and M. Blaivas, "Needle tip visualization during ultrasound-guided vascular access: short-axis vs. long-axis approach," *The American Journal of Emergency Medicine*, vol. 28, no. 3, pp. 343–347, 2010.

[16] F. J. Carmona Monge, M. Martínez Lareo, and A. Núñez Reiz, "Ultrasound guided radial artery cannulation: procedure description and literature review," *Enfermería Intensiva*, vol. 22, no. 4, pp. 144–149, 2011.

[17] T. P. Nifong and T. J. McDevitt, "The effect of catheter to vein ratio on blood flow rates in a simulated model of peripherally inserted central venous catheters," *Chest*, vol. 140, no. 1, pp. 48–53, 2011.

[18] R. D. Ball, N. Scouras, S. Orebaugh, J. Wilde, and T. Sakai, "Randomized, prospective, observational simulation study comparing residents' needle-guided vs. free-hand ultrasound techniques for central venous catheter access," *British Journal of Anaesthesia*, vol. 108, no. 1, pp. 72–79, 2012.

[19] W. J. Gu, H. T. Tie, J. C. Liu, and X. T. Zeng, "Efficacy of ultrasound-guided radial artery catheterization: a systematic review and meta-analysis of randomized controlled trials," *Critical Care*, vol. 18, no. 3, p. R93, 2014.

Hindawi
Evidence-Based Complementary and Alternative Medicine
Volume 2023, Article ID 9870497, 1 page
https://doi.org/10.1155/2023/9870497

Retraction

Retracted: Efficacy Evaluation of the VFQ-25 Scale in Patients with Different Degrees of Vitreous Opacity After Nd : YAG Laser Ablation

Evidence-Based Complementary and Alternative Medicine

Received 15 August 2023; Accepted 15 August 2023; Published 16 August 2023

This article has been retracted by Hindawi following an investigation undertaken by the publisher [1]. This investigation has uncovered evidence of one or more of the following indicators of systematic manipulation of the publication process:

(1) Discrepancies in scope
(2) Discrepancies in the description of the research reported
(3) Discrepancies between the availability of data and the research described
(4) Inappropriate citations
(5) Incoherent, meaningless and/or irrelevant content included in the article
(6) Peer-review manipulation

The presence of these indicators undermines our confidence in the integrity of the article's content and we cannot, therefore, vouch for its reliability. Please note that this notice is intended solely to alert readers that the content of this article is unreliable. We have not investigated whether authors were aware of or involved in the systematic manipulation of the publication process.

Wiley and Hindawi regrets that the usual quality checks did not identify these issues before publication and have since put additional measures in place to safeguard research integrity.

We wish to credit our own Research Integrity and Research Publishing teams and anonymous and named external researchers and research integrity experts for contributing to this investigation.

The corresponding author, as the representative of all authors, has been given the opportunity to register their agreement or disagreement to this retraction. We have kept a record of any response received.

References

[1] S. Zhang, K. Yang, and B. Wang, "Efficacy Evaluation of the VFQ-25 Scale in Patients with Different Degrees of Vitreous Opacity After Nd : YAG Laser Ablation," *Evidence-Based Complementary and Alternative Medicine*, vol. 2022, Article ID 5075447, 5 pages, 2022.

Hindawi
Evidence-Based Complementary and Alternative Medicine
Volume 2022, Article ID 5075447, 5 pages
https://doi.org/10.1155/2022/5075447

Research Article

Efficacy Evaluation of the VFQ-25 Scale in Patients with Different Degrees of Vitreous Opacity After Nd : YAG Laser Ablation

Siwei Zhang,[1] **Kang Yang**,[2] **and Bin Wang**[1]

[1]*Department of Ophthalmology, Hefei Bright Eye Hospital, Hefei 230001, Anhui, China*
[2]*Department of Ophthalmology, Fuyang Women and Children's Hospital, Fuyang 236000, Anhui, China*

Correspondence should be addressed to Siwei Zhang; zhangsiwei1231@163.com

Received 1 August 2022; Revised 14 September 2022; Accepted 17 September 2022; Published 28 September 2022

Academic Editor: Xueliang Wu

Objective. To evaluate the effect of the VFQ-25 scale on the efficacy of Nd : YAG laser ablation in patients with different severity of vitreous opacities. *Methods*. From January 2020 to March 2021, data of patients who presented to our department and were diagnosed with vitreous opacity were collected, and the severity of vitreous opacity was divided into four grades: I, II, III, and IV. Preoperative visual acuity, intraocular pressure, dilated fundus, B ultrasound, and other examinations were performed, and the patients were scored using the VFQ-25 scale. All patients underwent Nd : YAG laser ablation and were followed for 6 months. The VFQ-25 scale was again used postoperatively to score the patient's efficacy. The general information and clinical characteristics of the patients we collected. The Spearman's test was used to evaluate the correlation between VFQ-25 score and Nd : YAG laser efficacy in patients. *Results*. A total of 80 patients (95 eyes) were included in this study. Vitreous opacities were grade I in 56 eyes (58.9%), grade II in 22 eyes (23.2%), grade III in 10 eyes (10.5%), and grade IV in 7 eyes (7.4%). Compared with preoperative scores, patients with vitreous opacity had significantly higher postoperative scores in terms of overall health (36.54 ± 17.06 vs 33.52 ± 16.74), overall visual acuity (60.39 ± 14.24 vs 57.56 ± 13.13), color vision (88.94 ± 12.56 vs 86.38 ± 12.37), and peripheral visual acuity (74.06 ± 18.38 vs 72.20 ± 18.79) items (all $P < 0.001$). The overall response rates of vitreous opacities I, II, III, and IV were 100%, 90.9%, 80.0%, and 71.4%, respectively. There was a significant correlation between the postoperative VFQ-25 total score, and the therapeutic effect of laser ablation for grade I vitreous opacities, with a correlation coefficient r of 0.417 ($P = 0.001$). The correlation coefficient r between the total score of postoperative VFQ-25 and the treatment effect of grade II vitreous opacity was 0.622 ($P = 0.002$). However, the correlation between the postoperative efficacy of grade III and IV patients and the VFQ-25 score was not significant. *Conclusion*. In patients with different degrees of vitreous opacity undergoing Nd : YAG laser vitreous ablation, the overall health, overall visual acuity, color vision, and peripheral visual acuity were improved after surgery, and the VFQ-25 score was significantly correlated with the postoperative efficacy, which is worthy of clinical use.

1. Introduction

The vitreous body is an extracellular matrix consisting of 98% water and macromolecules, the most important of which are hyaluronic acid and collagen in clear gel [1]. The vitreous structure changes caused by aging, inflammation, vitreoretinal dystrophy, diabetic vitreous disease, or myopia. The homogeneity of the vitreous decreases, and even formed elements will be precipitated, forming floating opacities such as dust and cloud floccules, that is, vitreous opacities [2]. Emerging evidence suggests that perception of vitreous opacities and associated visual disturbances are more prevalent than once thought [3]. Nd : YAG laser ablation is a new technology that has rapidly developed since the 1980s. It first achieved varying degrees of success in the treatment of posterior ocular diseases, while in recent years, the use of Nd : YAG laser ablation for vitreous opacities has attracted much attention [4]. In general, Nd : YAG laser ablation is safe, but it still does not seem to benefit all patients [5]. A scale, or marker, is needed to evaluate the efficacy of Nd : YAG laser ablation for vitreous opacities. The VFQ-25 scale is a practical tool for assessing visual function and vision-related quality of life and not only reflects disease status but also includes factors that affect quality of life, such as mental

status, and social functioning [6]. Currently, there are still a few studies using the VFQ-25 scale to evaluate the efficacy of Nd : YAG laser ablation in patients with different severity of vitreous opacities. The aim of this study was to assess the correlation between the VFQ-25 scale and treatment outcome by analyzing vitreous opacities treated with a 1064 nm neodymium : yttrium-aluminum-garnet laser (Nd: YAG laser).

2. Objects and Methods

2.1. Objective. From January 2020 to March 2021, the data of 95 eyes of 80 patients (28 males and 52 females, mean age 58 ± 12 years) who presented to our department and were diagnosed with vitreous opacity were collected.

Inclusion criteria is as follows: (1) vitreous opacity was confirmed by B ultrasound and slit lamp examination; (2) there were dust and cloud flocculent floaters in front of the eyes and affected life; and (3) the general health status was stable, and the symptoms were stable within half a year.

Exclusion criteria is as follows: (1) previous history of ocular surgery; (2) ocular diseases with uveitis, fundus lesions, and other ocular diseases affecting treatment or causing complications; (3) risk of retinal detachment; (4) unable to cooperate, or failed to adhere to treatment and follow-up; and (5) combined liver and kidney dysfunction, tumors or bleeding, and coagulation diseases. All patients were informed and signed a consent form. The study protocol was approved by the Ethics Committee of Hefei Bright Eye Hospital.

2.2. Severity Grading for Vitreous Opacities. Grade I refers to discomfort during vision, and monomeric opacities can be seen in the fundus; grade II refers to discomfort during vision, and several clear monomeric opacities can be seen in the fundus; grade III refers to obvious symptoms, an annular floating sensation during vision, and obvious annular opacities can be seen in the fundus; and grade IV refers to obvious symptoms, nebulous discomfort during vision, and a large number of opacities of different shapes can be seen in the fundus.

3. Method

3.1. Treatment Methods. All patients underwent visual acuity, intraocular pressure, dilated fundus, and B ultrasound. The Lumenis SmartV Selecta Duet Laser System was selected for laser treatment with parameters set to a starting energy of 2.0–8.0 mJ, single point emission, and energy parameters were progressively adjusted to vaporize the opacities. During the treatment, the number of pulses emitted per treatment is controlled within 500, and the time is controlled within 30 minutes according to the previous order after up and down. If there are still many opacities, elective retreatment is carried out.

3.2. Follow-up and Efficacy Determination. All patients were followed up until 6 months after laser treatment. Visual acuity, intraocular pressure, dilated fundus, and B ultrasound were re-examined to analyze the improvement of clinical symptoms. Criteria for curative effect determination is as follows: (1) markedly effective: the symptoms disappeared, and no complications were observed; (2) effective: the symptoms were improved, and no complications were observed; (3) ineffective: the symptoms were not improved, with or without complications. Overall response rate = (markedly effective + effective)/total number of eyes × 100%. The complications include lens injury, postoperative high intraocular pressure, glaucoma, retinal hemorrhage, and an increased number of floating objects.

3.3. Statistical Analysis. Continuous variables were presented as mean ± standard deviation, and a paired t-test was used to compare differences in the VFQ-25 scores before and after laser treatment in patients with vitreous opacities. Categorical variables were presented as frequencies (percentages) and differences in overall response rates among patients with different severity of vitreous opacities were assessed by the chi-square test. The Spearman's test was used to evaluate the correlation between VFQ-25 score and Nd : YAG laser efficacy in patients. Two-sided $P < 0.05$ was considered statistically significant. Data were analyzed using SPSS statistics 21.0 (IBM SPSS, Armonk, NY).

4. Results

4.1. Baseline Characteristics. As shown in Table 1, a total of 80 patients and 95 eyes were included in this study. The average age of patients was 58 ± 12 years, 65.0% (52/80) were female, and 18.8% (15/80) had a history of diabetes. Among the causes of vitreous opacity, posterior vitreous detachment accounted for 72.6% (69/95), vitreous liquefaction degeneration 16.8% (16/95), and high myopia 10.5% (10/95). In terms of severity grading, 56 eyes (58.9%) had grade I vitreous opacity, 22 eyes (23.2%) had grade II vitreous opacity, 10 eyes (10.5%) had grade III vitreous opacity, and 7 eyes (7.4%) had grade IV vitreous opacity.

4.2. VFQ-25 Score before and after Surgery. As shown in Table 2, compared with preoperative scores, patients with vitreous opacity had significantly higher postoperative scores for the items of general health (36.54 ± 17.06 vs 33.52 ± 16.74), overall visual acuity (60.39 ± 14.24 vs 57.56 ± 13.13), color vision (88.94 ± 12.56 vs 86.38 ± 12.37), and peripheral visual acuity (74.06 ± 18.38 vs 72.20 ± 18.79) ($P < 0.001$). However, the preoperative and postoperative scores of near vision activity, distance vision activity, social function, mental health, social activity role disorder, eye pain, social dependence, and driving were similar, and the differences were not statistically significant ($P > 0.05$).

4.3. Laser Treatment Effectiveness. As shown in Table 3, the significant rate of grade I vitreous opacity was 76.8%, the total effective rate was 100%, the significant rate of grade II vitreous opacity was 68.2%, the total effective rate was 90.9%, the significant rate of grade III vitreous opacity was 30.0%,

Table 1: Clinical characteristics of patients with vitreous opacity.

	Patients with vitreous opacity
Number, *n*	80
Number of eyes, *n*	95
Age, years	58 ± 12
Proportion of females, *n* (%)	52 (65.0)
History of diabetes, *n* (%)	15 (18.8)
Causes of vitreous opacity	
Posterior vitreous detachment	69 (72.6)
Vitreous liquefaction degeneration	16 (16.8)
High myopia	10 (10.5)
Severity grade	
Grade I	56 (58.9)
Grade II	22 (23.2)
Grade III	10 (10.5)
Grade IV	7 (7.4)

the total effective rate was 80.0%, the significant rate of grade IV vitreous opacity was 14.3%, and the total effective rate was 71.4%. For vitreous patients of different grades, the overall response rate after laser treatment was different, and the difference had statistical significance ($\chi^2 = 22.576$, $P = 0.001$).

Correlation of VFQ-25 with Treatment Effect.

As shown in Table 4, the postoperative total VFQ-25 score was significantly correlated with the therapeutic effect of laser ablation for grade I vitreous opacities, with a correlation coefficient r of 0.417 ($P = 0.001$). The correlation coefficient r between the total score of postoperative VFQ-25 and the treatment effect of grade II vitreous opacity was 0.622 ($P = 0.002$). The correlation coefficient r between the postoperative VFQ-25 score and the treatment effect of grade III vitreous opacity was 0.583 ($P = 0.077$). The correlation coefficient r between the postoperative VFQ-25 score and the treatment effect of grade IV vitreous opacity was 0.673 ($P = 0.097$).

5. Discussion

In patients with vitreous opacities, Nd: YAG laser ablation was found to significantly improve overall health, overall visual acuity, color vision, and peripheral visual acuity item scores. Different severity of vitreous opacity may lead to different therapeutic effects. Notably, the postoperative VFQ-25 score was significantly correlated with the treatment effect of laser ablation.

Vitreous opacity is most commonly caused by posterior vitreous detachment, and a small proportion can also be caused by vitreous liquefaction deformation and high myopia, and vitreous opacity can lead to blurred vision and decreased visual acuity [7]. Even if these symptoms are considered nonpathological, they may affect quality of life and mood for many patients and myopic patients with posterior vitreous detachment are more sensitive to these symptoms. Vitreous opacities that do not affect vision and daily life generally do not require treatment or administration of medication. For symptomatic patients with vitreous opacities, Nd : YAG laser vitreolysis may be a treatment option [8]. This treatment technique is noninvasive and allows precise localization of floaters within the vitreous cavity through a special optical lens followed by vaporization and ionization vaporization to form small molecular valorization gases such as CO, H2, CH4, and other gases to facilitate absorption, thereby treating vitreous opacities and improving patient symptoms [9].

Studies have shown that among patients with vitreous opacities undergoing Nd : YAG laser vitrectomy, 75% reported significant improvement and 25% reported moderate improvement [10]. This is in general agreement with our findings, where the overall response rate was 100% in patients with vitreous opacities of grade I and 71.4%–90.9% in patients with grades II–IV. Therefore, Nd : YAG laser vitrectomy is well-tolerated and effective treatment for vitreous opacities. In using this technique, the following points of attention are also required. First, the laser is confined to the middle and posterior vitreous. Anterior vitreous opacification has little impact on visual quality and visual acuity, but retinal and posterior lens capsule damage needs to be avoided, with a safe distance of 3–4 mm anterior to the retina and 2–3 mm posterior to the lens, and the operation is prohibited directly in front of the fovea, with a maximum energy of <8.0 Mj [11]. Second, the operating physician should pay attention to the movement of vitreous opacity to avoid laser action on the retina [5]. Third, specially designed convex contact lenses should also be used to lower the energy threshold for plasma formation and improve the safety of intravitreal YAG lasers [12].

The VFQ-25 score was developed with support from the National Eye Institute to create a survey measuring self-reported sight-targeted health status and further incorporate the impact of quality of life, such as emotional well-being and social functioning [13]. The VFQ25 score, which consists of 25 questions, has been widely used for glaucoma, cataracts, diabetic retinopathy, and low-vision diseases due to various causes [13]. In this study, the VFQ-25 score was used for the first time to evaluate the therapeutic effect of Nd : YAG laser vitrectomy in patients with vitreous opacity, and the results suggested that in patients with vitreous opacity, Nd: YAG laser ablation could significantly improve the scores of overall health, overall visual acuity, color vision, and peripheral visual acuity items.

Symptoms such as blurred vision and impaired vision are the main factors afflicting patients with vitreous opacity, but they also have further life and work impact. Previous studies have shown that the VFQ-25 score is a good scale for evaluating the severity of symptoms in patients with vitreous opacities and has reliable reliability and validity [14]. The VFQ-25 scale shows high internal consistency (Cronbach α range 0.739–0.932) and high test-retest reliability (intraclass correlation coefficient 0.876–0.975) [15]. This study also found that the VFQ-25 score was significantly associated with the treatment effect of laser ablation and could be used to evaluate the efficacy of laser ablation.

However, this study also has the following limitations: the study had a small sample size, no treatment control group was set and only the treatment effect at 6 months after surgery was observed in this study. In addition, we observed a significant correlation between the VFQ-25 score and

Table 2: VFQ-25 scores of patients with vitreous opacity before and after operation.

Item	Preoperative score	Post OPERATIVE SCORE	*P* Value
General health	33.52 ± 16.74	36.54 ± 17.06	<0.001
Overall visual acuity	57.56 ± 13.13	60.39 ± 14.24	<0.001
Near vision activity	72.07 ± 11.86	70.71 ± 12.18	0.147
Distance vision activity	55.45 ± 15.34	57.01 ± 15.56	0.219
Social functioning	72.87 ± 15.43	72.29 ± 13.73	0.742
Mental health	48.94 ± 15.59	47.61 ± 13.44	0.417
Role disorder in social activities	47.59 ± 14.93	45.68 ± 14.99	0.249
Color vision	86.38 ± 12.37	88.94 ± 12.56	<0.001
Peripheral vision	72.20 ± 18.79	74.06 ± 18.38	<0.001
Eye pain	78.61 ± 11.98	77.58 ± 9.85	0.418
Social dependence	71.25 ± 14.50	69.58 ± 14.87	0.082
Driving	70.05 ± 15.15	68.71 ± 14.83	0.077

Table 3: The laser treatment effect in patients with different severity of vitreous opacity.

	Number of eyes	Markedly effective	Effective	Invalid	Overall response rate,%
Grade I, *n* (%)	56	43 (76.8)	13 (23.2)	0 (0)	100
Grade II, *n* (%)	22	15 (68.2)	5 (22.7)	2 (9.1)	90.9
Grade III, *n* (%)	10	3 (30.0)	5 (50.0)	2 (20.0)	80.0
Grade IV, *n* (%)	7	1 (14.3)	4 (57.1)	2 (28.6)	71.4
X^2			22.576		
P Value			0.001		

Table 4: Correlation of the postoperative VFQ-25 total score with therapeutic effect of laser ablation.

	Correlation coefficient r	*P* Value
Grade I	0.417	0.001
Grade II	0.622	0.002
Grade III	0.583	0.077
Grade IV	0.673	0.097

postoperative efficacy in patients with grade I and II vitreous opacity. However, we did not observe a significant correlation in patients with grades III and IV, which may be related to our small sample size. Future large, prospective randomized controlled clinical trials are needed to evaluate the role of the VFQ-25 score in patients undergoing laser ablation for vitreous opacities.

In summary, in patients with different degrees of vitreous opacity undergoing Nd : YAG laser vitreous ablation, the VFQ-25 score was significantly correlated with the postoperative efficacy, which is worthy of clinical use.

Data Availability

The analyzed data sets generated during the study are available from the corresponding author on reasonable request.

Conflicts of Interest

The authors declare that they have no conflicts of interest.

Authors' Contributions

Siwei Zhang and Kang Yang contributed equally to this article.

References

[1] M. M. Le Goff and P. N. Bishop, "Adult vitreous structure and postnatal changes," *Eye*, vol. 22, no. 10, pp. 1214–1222, 2008.

[2] R. Milston, M. C. Madigan, and J. Sebag, "Vitreous floaters: etiology, diagnostics, and management," *Survey of Ophthalmology*, vol. 61, no. 2, pp. 211–227, 2016.

[3] B. F. Webb, J. R. Webb, M. C. Schroeder, and C. S. North, "Prevalence of vitreous floaters in a community sample of smartphone users," *International Journal of Ophthalmology*, vol. 6, no. 3, pp. 402–405, 2013.

[4] W. F. Tsai, Y. C. Chen, and C. Y. Su, "Treatment of vitreous floaters with neodymium YAG laser," *British Journal of Ophthalmology*, vol. 77, no. 8, pp. 485–488, 1993.

[5] Y. M. Delaney, A. Oyinloye, and L. Benjamin, "Nd:YAG vitreolysis and pars plana vitrectomy surgical treatment for vitreous floaters," *Eye*, vol. 16, no. 1, pp. 21–26, 2002.

[6] C. M. Mangione, P. P. Lee, P. R. Gutierrez, K. Spritzer, S. Berry, and R. D. Hays, "National eye Institute visual function questionnaire field test I development of the 25-item national eye Institute visual function questionnaire," *Archives of Ophthalmology*, vol. 119, no. 7, pp. 1050–1058, 2001.

[7] D. P. Sendrowski and M. A. Bronstein, "Current treatment for vitreous floaters," *Optometry - Journal of the American Optometric Association*, vol. 81, no. 3, pp. 157–161, 2010.

[8] C. P. Shah and J. S. Heier, "YAG laser vitreolysis vs sham YAG vitreolysis for symptomatic vitreous floaters a randomized clinical trial," *JAMA Ophthalmol*, vol. 135, no. 9, pp. 918–923, 2017.

Hindawi
Evidence-Based Complementary and Alternative Medicine
Volume 2022, Article ID 4891399, 10 pages
https://doi.org/10.1155/2022/4891399

Research Article

rhCNB Improves Cyclophosphamide-Induced Immunodeficiency in BALB/c Mice

Wenhua Zhong,[1] Hui Huang,[1] Zhaoxin Yang,[1] and Penghuan Chang[2]

[1]*College of Pharmacy, Hainan Medical University, Haikou 571199, China*
[2]*Department of Nursing, Haikou People's Hospital, Affiliated Haikou Hospital of Central South University Xiangya School of Medicine, Haikou 570100, China*

Correspondence should be addressed to Penghuan Chang; 1500468054@qq.com

Received 7 July 2022; Revised 25 August 2022; Accepted 1 September 2022; Published 26 September 2022

Academic Editor: Xueliang Wu

Background. This study aims to explore the immunomodulatory effect of rhCNB on mice with cyclophosphamide (CTX)-induced immunodeficiency through TLR_4/MAPK pathway. *Methods*. BALB/c mice were randomly divided into three groups: a negative control group, an immunosuppression model group, and a rhCNB treatment group. Tail vein injection of cyclophosphamide (40 mg/kg) was used to establish a mouse immunosuppression model. Intraperitoneal injection of rhCNB (20 mg/kg) was administered to the treatment group, whereas equal quantities of normal saline were given to the control group and model group. Perform peripheral blood routine of CD4, CD8, and CD19 lymphocyte subsets and peripheral blood Th1/Th2 cell subsets 24 hours after the last administration. RT-PCR was used to detect mRNA levels of TLR_4, P38, JNK, T-bet, and $GATA_3$, the spleen immune organ index was measured, and the histopathological status of the spleen and thymus was observed. *Results*. The results showed that compared with the control group, WBC, PLT, LYM, NEU, immune organ index, $CD4^+/CD8^+$ and $CD19^+$ subgroup ratio, and peripheral blood Th1/Th2 cell subgroups decreased in the model group. The mRNA levels of TLR_4, P38, JNK, T-bet, and $GATA_3$ decreased compared with the model group, while they increased in the treatment group. *Conclusions*. rhCNB has an immunomodulatory effect by regulating the expression of Th1/Th2 cytokine balance through the TLR_4/MAPK signaling pathway and promoting the differentiation and proliferation of lymphocytes, thereby improving the immune function.

1. Introduction

A malignant tumor is one of the major diseases threatening human life and health, and its mortality rate is second only to cardiovascular diseases [1–3]. Currently, the main treatments for malignant tumors are surgery, drug chemotherapy, radiotherapy, and chemotherapy. The body's bone marrow hematopoietic system and immune function are impaired when cancer cells are killed by radiation or drugs, which causes bone marrow suppression and a reduction in immune function. This would not only lower the quality of life for patients but also further reduce the effectiveness of the treatment, so one of cancer treatment goals is to lessen the influence on the body's immune system.

The recombinant human calcineurin B subunit (rhCNB) is a protein obtained by constructing the recombinant strain with high expression. TLR_4/NF-κB signaling pathway can activate the innate immune system, promote dendritic cell maturation, upregulate the expression of macrophages, and cause the production of TNF-α, IL-6, IL-12, IL-1β, and CCL_5, as well as mediate tumor cell apoptosis [4–7].

As a membrane recognition receptor protein, TLR is an important barrier against infectious diseases. The most common example is toll-like receptor 4 (TLR_4), which not only activates the genes related to innate immunity and adaptive immune response but also promotes the release of related cytokines to regulate immune function [8, 9]. Activated TLR_4 can activate the mitogen-activated protein kinase (MAPK) signaling pathway downstream [10]. The MAPK signaling pathway contributes to cell proliferation, differentiation, and adaptation to environmental stress [11]. Through the TLR_4 pathway, rhCNB can activate

macrophages, promote dendritic maturation, enhance the antigen-presenting effect of antigen-presenting cells, and promote activity of phagocytic and NK cells in macrophages. Besides, rhCNB induces the secretion of proinflammatory cytokines and chemokines, enhances cellular immunity, and causes apoptosis of tumor cells [7]. This study investigated how rhCNB affects the immune function of mice with cyclophosphamide (CTX)-induced immunodeficiency. The changes in TLR_4 and Th1/Th2 level and MAPK signal pathway were detected at the mRNA level to determine whether rhCNB regulates the immune function of immunosuppressed mice through TLR_4/MAPK pathway. The present research aims to provide reference for the further study of rhCNB in regulating immunologic function and related pharmacology after radiotherapy and chemotherapy.

2. Materials and Methods

2.1. Animals and Experimental Design. Female BALB/c mice (Changsha Tianqin Biotechnology Co., Changsha, China) aged six to eight weeks, weighing 18–22 g, were housed in polypropylene cages in specific pathogen-free rooms kept at 20–26°C with 40–70% relative humidity and a 12 h light cycle. All animals were given free access to standard rodent chow and filtered tap water *ad libitum*. All experiments were approved by and proceeded following the Hainan Medical College Animal Care and Use Committee (HYLL-2021-148).

The mice were randomly divided into the control group, the CTX group (40 mg/kg) [12], and the rhCNB group (20 mg/kg). The CTX group and rhCNB group were injected with 40 mg/kg CTX through tail veins for 3 days, while the control group received an equivalent volume of saline injection. On the 4^{th} day after the model was established, the rhCNB group received an intraperitoneal injection of rhCNB once a day for 5 days. Saline was administered intraperitoneally to both the CTX and control groups.

2.2. Reagents. Anti-mCD4-APC (553051), anti-mCD3e-PerCP (553067), anti-mCD8-PE (553032), anti-mCD4-PerCP (550954), anti-mIFN-γ-APC (554413), and anti-mIL-4-PE (554435) were purchased from BD Biosciences (Franklin Lakes, NJ, US). PrimeScriptTMRT reagent kit and MiniBEST Universal RNA Extraction kit were purchased from Takara Bio. Cyclophosphamide was obtained from Jiangsu Baxter Oncology Gmbh (Kantstr, Halle, Germany). rhCNB is a gift from Haikou Qili Pharmaceutical Co. Ltd. (Haikou, China).

2.3. Spleen Organ Index. The mice were weighed 24 hours following the last treatment, and then spleens of each mouse were collected and weighed immediately to determine the immune organ index.

2.4. HE Staining of Spleen and Thymus Tissue. Spleen and thymus tissue were isolated from mice, fixed in 4% paraformaldehyde, embedded in paraffin, and cut into sections of 3 μm. Following HE staining and sealing, these sections were examined under an optical microscope.

2.5. Hematological Examination. Blood was collected into EDTA-2K tubes by a retro-orbital bleeding method 24 hours after the last dose. Blood counts were performed using a hematology analyzer (ADVIA 2120i, Siemens, Germany), including white (WBC) and red blood cell (RBC) counts, platelet counts (PLT), lymphocyte percentage (LY%), and neutrophil ratio (NE%).

2.6. T-Lymphocyte and B-Lymphocyte Assay by Flow Cytometry. After being treated with RBC lysing buffer and PBS washing, the peripheral blood samples were incubated with anti-mouse CD3/CD4/CD8/CD19 antibodies (5 L) at 4°C for 1 hour. Utilizing BD FACS CaliburTM, flow cytometry analyses were carried out on the cells after they had been washed and resuspended in PBS (BD Biosciences, USA).

2.7. Detection of $CD4^+$ IFN-γ^+ and $CD4^+$ IL-4^+ Lymphocytes in Peripheral Blood by Flow Cytometry. Lymphocytes were separated from the peripheral blood of mice by a lymphocyte separation medium. Then, the cells in each tube were treated with Leuko Act Cktl with GolgiPlug (BD, 550583), and they were incubated for 4 hours at 37°C in an incubator with 5% CO_2. After stimulation, the cells were incubated with PerCP-anti-CD4 for 30 minutes at room temperature in the dark, washed, and then mixed with fixation/permeabilization solution (BD, 554714) to incubate for another 30 minutes at room temperature in the dark. After being washed, the samples were incubated for 30 minutes with anti-IL-4-PE and anti-IFN-γ-APC, then washed, and resuspended with 300 μL staining buffer. Samples were measured by flow cytometry.

2.8. Real-Time PCR. After tissues were subjected to Trizol reagent to isolate the quantitative real-time PCR total RNA, PrimeScriptTMRT reagent Kit (Takara Bio) was used to reverse-transcribe the RNA into cDNA. The cDNA was amplified by the MiniBEST Universal RNA Extraction Kit on a StepOnePlus Real-Time PCR System (Thermo Fisher Scientific). Primers are shown in Table 1. GAPDH was used as an internal control [13].

2.9. Statistical Analysis. Data are shown as mean ± SD. The statistical analysis program SPSS (v(0).24, SPSS Inc., Cary, NC) was used to determine the statistical significance of the differences between various groups using either Student's *t*-test or an ANOVA analysis for multiple comparisons. Values of $P < 0.05$ were considered statistically significant.

3. Results

3.1. Effect of rhCNB on Body Weight in Immunosuppressed Mice. Compared with the control group, mice in the model group gradually lost weight after being given

Table 1: Primers used for the RT-PCR study.

Gene name	Forward	Reverse
GAPDH	TGGGTGTGAACCATGAGAAG	GCTAAGCAGCAGTTGGTGGTGC
TLR_4	GCCATCATTATGAGTGCCAATT	AGGGATAAGAACGCTGAGAATT
P38	AGGAATTCAATGACGTGTACCT	AGGTCCCTGTGAATTATGTCAG
JNK	CCAGCCTTCAGATGCAGCAGTAAG	GGTGTGCTCAGTGGACATGGATG
ERK	ATCTCAACAAAGTTCGAGTTGC	GTCTGAAGCGCAGTAAGATTTT
T-bet	GATCACTCAGCTGAAAATCGAC	AGGCTGTGAGATCATATCCTTG
$GATA_3$	ATTACCACCTATCCGCCCTAT	CGGTTCTGCCCATTCATTTTAT

cyclophosphamide. After rhCNB intervention, the treatment group's body weight increased more slowly than that of the model group (Figure 1(a)). In addition, the mice in the model group showed upside-down coats, reduced mobility, and arched back after the administration of cyclophosphamide. After treatment with rhCNB, the mice in the treatment group had loose body hair, increased mobility, and reduced back phenomenon compared with the model group. It shows that rhCNB can reverse the weight loss induced by cyclophosphamide.

3.2. Effect of rhCNB on Immune Organ Index in Immunosuppressed Mice. The mice in the model group had significantly lower spleen index compared to the control group ($P < 0.05$). Compared with the model group, the spleen index of the mice in the treatment group increased, and the difference was statistically significant ($P < 0.05$). It indicates that rhCNB can significantly enhance the spleen index of immunosuppressed mice and increase the quality of the spleen (Figure 1(b)).

3.3. Effect of rhCNB on Histopathological Changes in Immunosuppressed Mice. The spleen body size of the model group was smaller than that of the control group, the lymphocytes in the cap area were loosely arranged, and a small number of lymphocytes underwent apoptosis. After rhCNB treatment, the number of splenic corpuscles and tightly arranged lymphocytes in the cap area increased, and no apoptotic cells were observed. Compared with the control group, the thymus medulla part of the model group was reduced, and the cortex part and the cortex-medullary ratio increased. Cell necrosis/apoptosis of the starry sky phenomenon can be seen in the cortex. After rhCNB treatment, the medulla part increased, the cortex decreased, and the cortex-medullary ratio decreased. It demonstrates that rhCNB can reduce the damage to the spleen and thymus induced by cyclophosphamide and can restore the function of immune organs with reduced immune function (Figure 2).

3.4. Effect of rhCNB on the Hematological Index in Immunosuppressed Mice. Cyclophosphamide, a commonly used modeling drug for inducing immunosuppressive animal models, reduces the body's immune function and decreases the number of WBCs, LYM, NEU, and PLT [14, 15]. The number of WBCs, LYM, NEU, PLT, and RBCs in the CTX model group was significantly reduced ($P < 0.05$) compared with the control group but significantly increased ($P < 0.05$) in the rhCNB treatment group compared with the CTX model group. It shows that rhCNB can lessen the cyclophosphamide-induced bone marrow suppression and restore the body's hematopoietic function (Figure 3).

3.5. Effect of rhCNB on T-Lymphocyte Subsets and B-Lymphocyte Subsets. The number of CD4 and CD8 lymphocytes as well as the ratio of $CD4^+/CD8^+$ T cells dropped in the model group as compared to the control group ($P < 0.05$) but increased in the rhCNB treatment group compared with the model group ($P < 0.05$) (Figures 4(a)–4(c)). Compared with the control group, the number of CD19 lymphoid subgroups in the model group decreased ($P < 0.05$) but increased compared with the model group ($P < 0.05$) (Figure 4(d)). It proves that rhCNB can promote the differentiation and proliferation of T cell subgroups and B cell subgroups in immunocompromised mice and regulate and improve the body's immune response (Figure 5).

3.6. Effect of rhCNB on Th1/Th2 Balance in Peripheral Blood of Immunosuppressed Mice. The content of IL-4 and IFN-γ in the model group was reduced compared with the control group ($P < 0.05$) but increased in the rhCNB treatment group compared with the model group ($P < 0.05$) (Figures 6(a) and 6(b)). The ratio of IFN-γ/IL-4 in the model group decreased compared with the control group but increased in the rhCNB treatment group compared with the model group ($P < 0.05$) (Figure 6(c)). The results reveal that rhCNB can regulate the function of cell subsets in immunosuppressed mice by encouraging the release of Th1/Th2 cytokines and enhance the function of cellular and humoral immunity, thus regulating the state of low immunity.

3.7. The mRNA Expression Levels of TLR_4, P38, JNK, ERK, T-Bet, and $GATA_3$ in the TLR_4/MAPK Signaling Pathway. The expression levels of TLR_4, P38, JNK, and ERK in the model group decreased as compared to the control group ($P < 0.05$) but increased in the rhCNB treatment group compared with the model group ($P < 0.05$) (Figures 7(c)–7(f)). Compared with the control group, the expression levels of T-bet and $GATA_3$ in the model group decreased ($P < 0.05$) but increased in the rhCNB treatment group compared with the model group ($P < 0.05$) (Figures 7(a) and 7(b)). It suggests that rhCNB can improve the immune

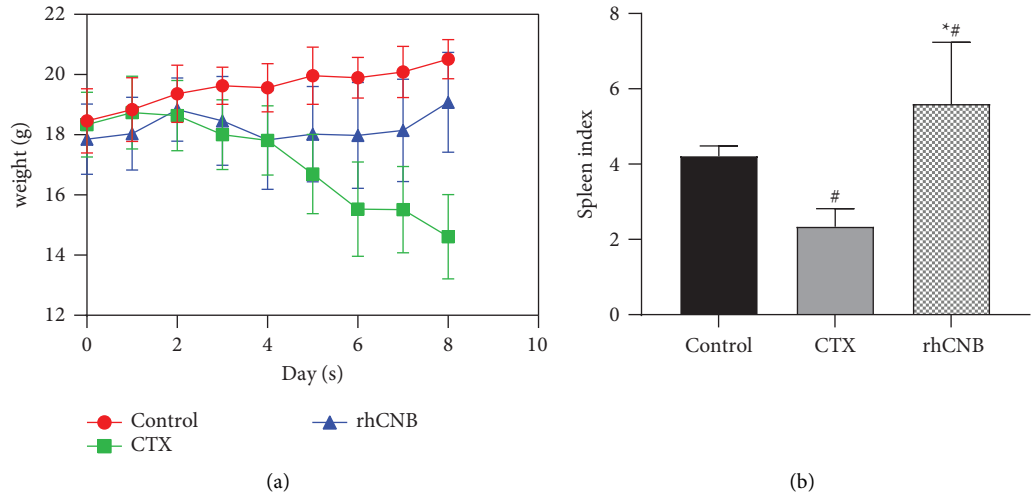

Figure 1: Body weight curve and spleen index. (a) The body weight curve. (b) The spleen index of mice (control is the negative control group, CTX is the model group, and rhCNB is the treatment group). Compared with control group, $^{\#}P < 0.05$; compared with model group, $^{*}P < 0.05$.

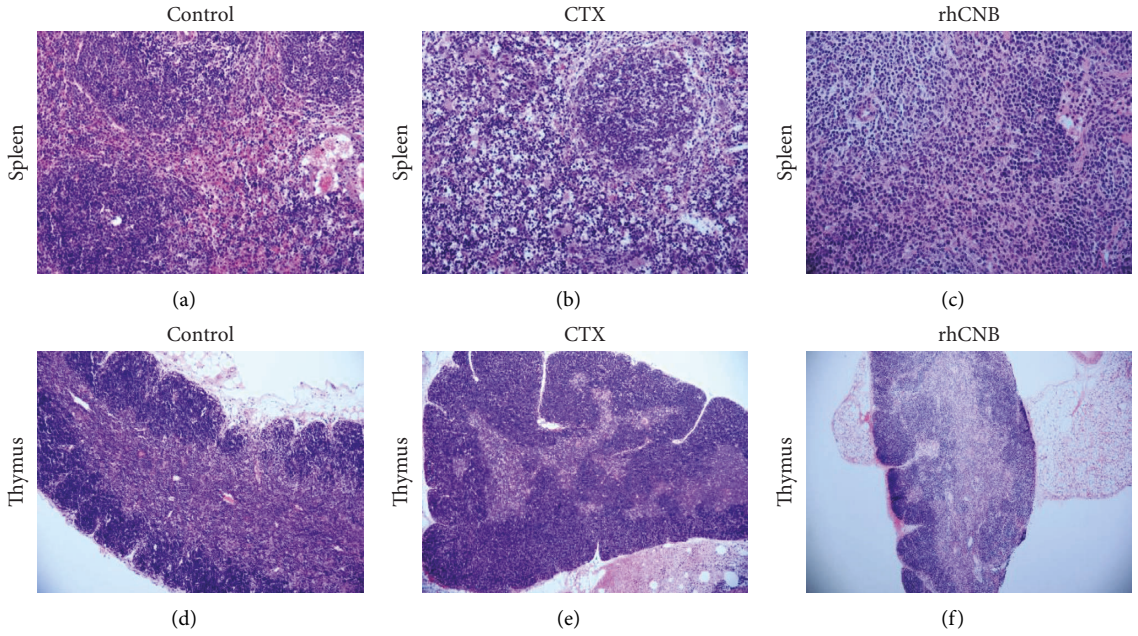

Figure 2: Effect of rhCNB on HE staining of the thymus (×200) and spleen (×400). (a, d) Normal tissue. (b) The spleen body shrinks, and the number of lymphocytes in the cap area decreases. (c) The volume of spleen corpuscle increased and the lymphocyte of cap area increased. (e) Glandular medulla area is partially reduced, the cortex increases, and the skin/medullary ratio increases. (f) The skin/medullary ratio decreases.

function of mice by regulating Th1/Th2 levels through TLR_4/MAPK signaling pathway.

4. Discussion

The current methods of treating malignant tumors are mainly surgery, drug chemotherapy, and radiotherapy. However, when tumor cells are killed by radiation and drugs, the body's bone marrow hematopoietic system and immune function will be damaged, which in turn leads to bone marrow suppression and reduces patients' immune function. As a result, patients' quality of life and treatment effect will be reduced. rhCNB is a protein drug with an anti-tumor effect, which can mediate tumor cell apoptosis by stimulating macrophages [16]. While rhCNB is an immunostimulatory protein, it has not yet been determined if it can ameliorate and regulate the immune suppression state of the body after radiotherapy and chemotherapy and restore immunological function in the body as a whole. Therefore, this study aims to investigate the effect of rhCNB on the

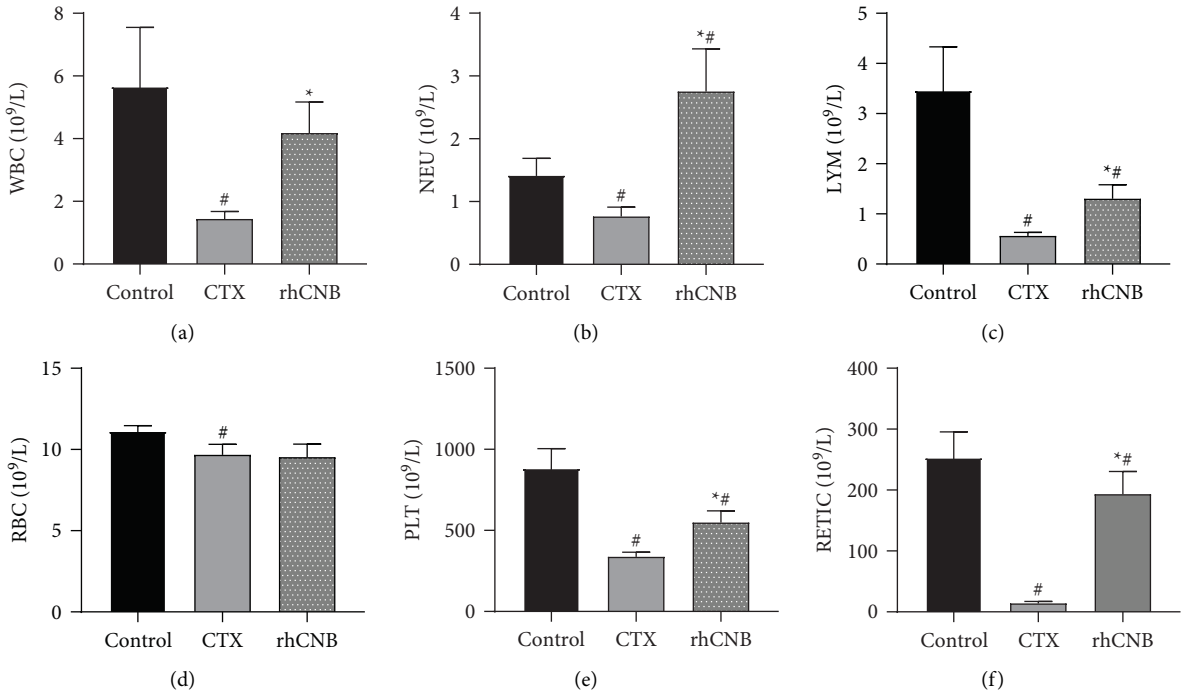

Figure 3: Analysis of rhCNB on hemogram of immunocompromised mice. The number of immune cells in the blood was analyzed to evaluate the immune function of mice.

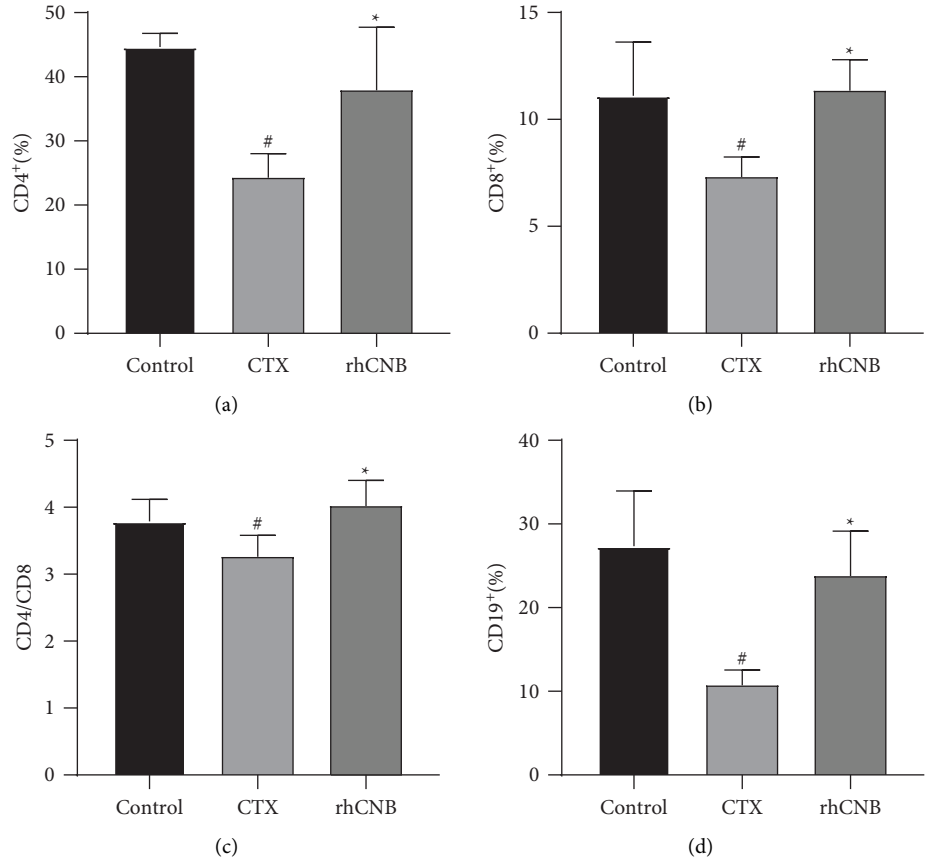

Figure 4: The results of peripheral blood lymphocyte subsets in each group. By analyzing the lymphatic subsets of T cells and B cells to evaluate the humoral and cellular immune functions of mice, it was found that rhCNB can improve the immune function of immunocompromised mice.

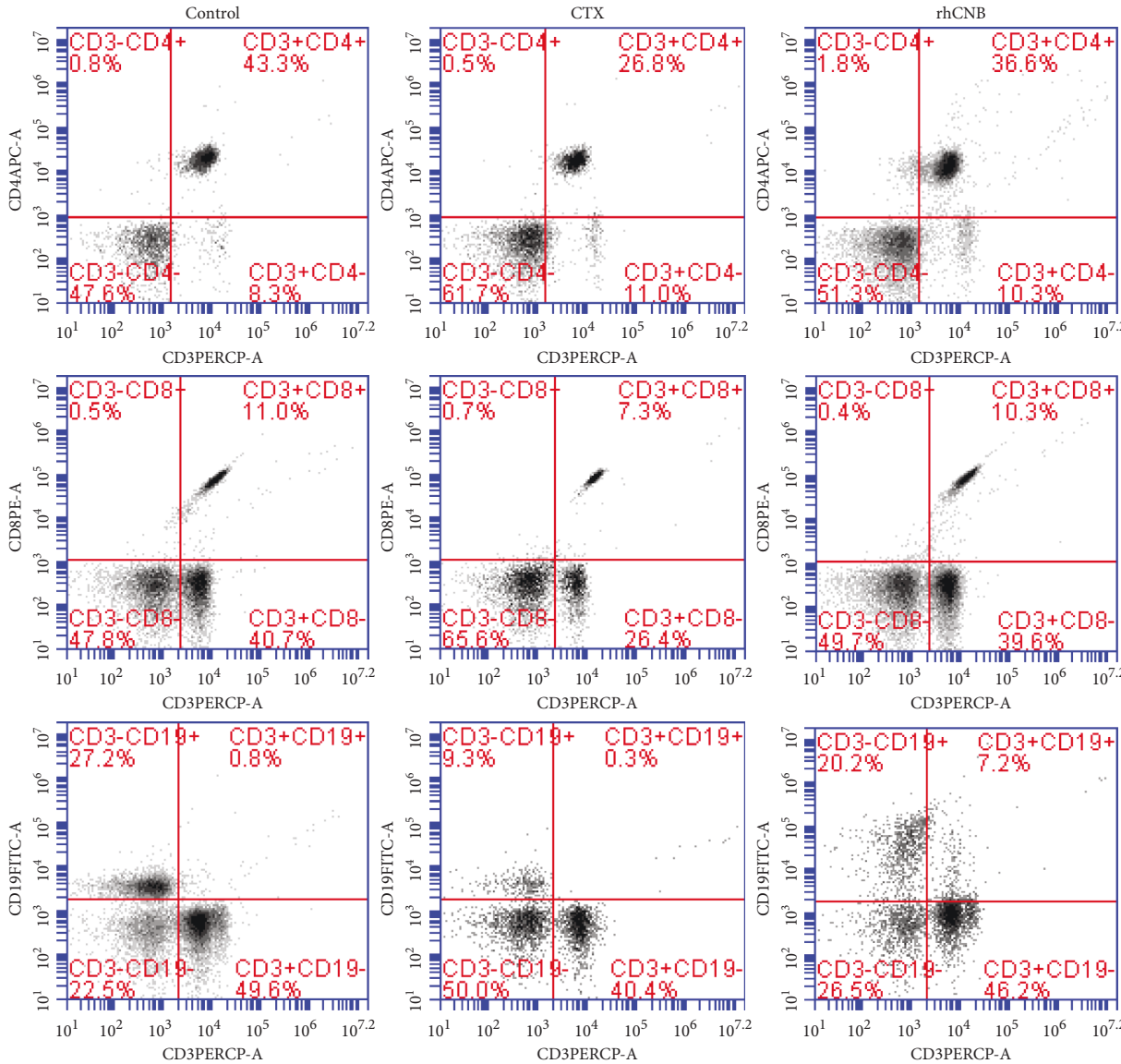

Figure 5: Examples of the detection results of peripheral blood lymphocyte subsets in each group. The flow cytometry was used to analyze the cell subsets, and the schematic diagram of the flow subsets in each group.

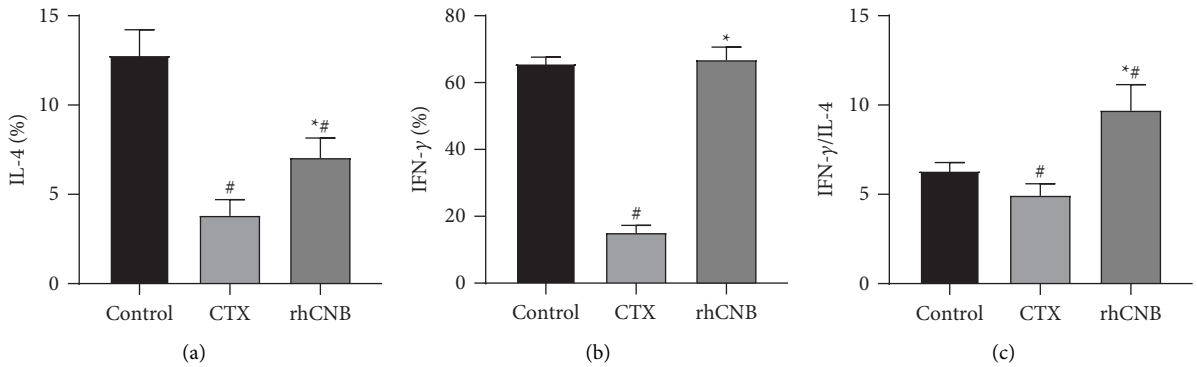

Figure 6: Results of flow cytometry IL-4 and IFN-γ. The effect of rhCNB on immune function was evaluated by analyzing the cytokines IFN-γ and IL-4 represented by Th1 and Th2. The results showed that rhCNB could restore the immune function of cyclophosphamide-induced immunocompromised mice.

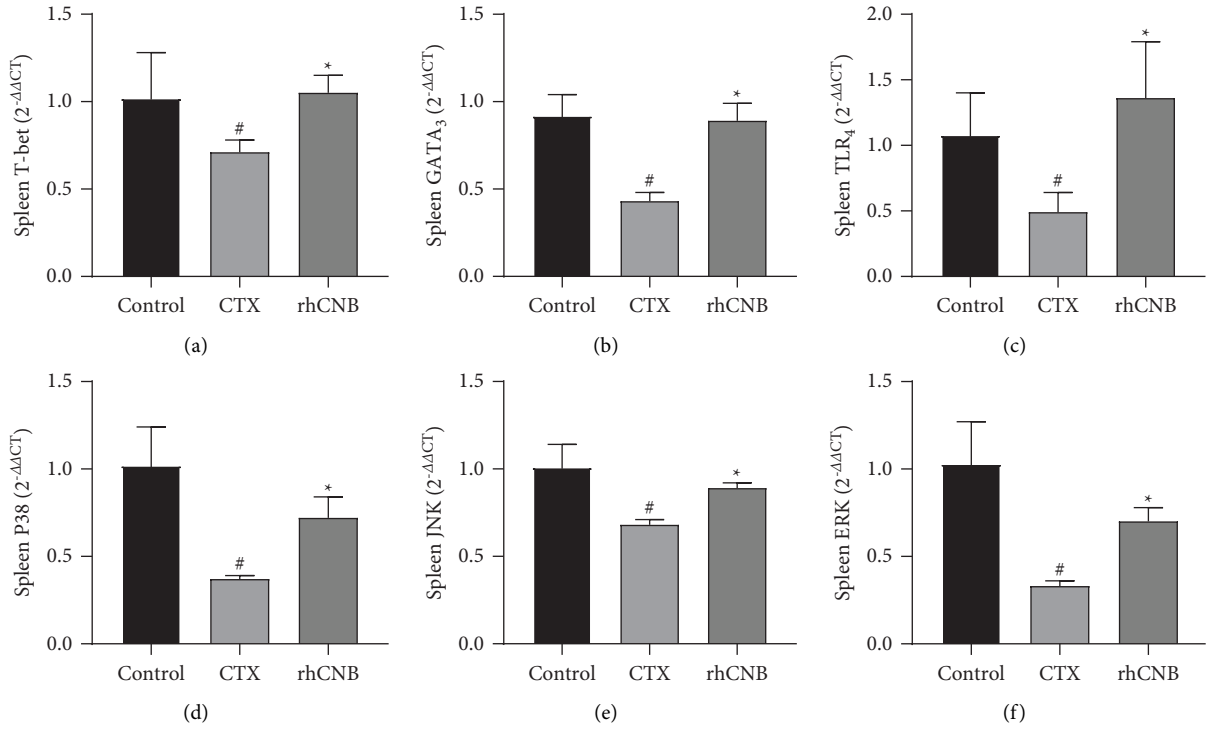

Figure 7: mRNA expression levels of related genes in spleen. The effect of rhCNB on the regulation of immune function was evaluated by PCR analysis of the spleen. The primer sequences are shown in Table 1. Data are shown as mean ± SD. The statistical analysis program SPSS was used to determine the statistical significance of the differences between various groups using either Student's *t*-test or an ANOVA analysis for multiple comparisons. Values of $P < 0.05$ were considered statistically significant.

immune system of mice with cyclophosphamide-induced immunodeficiency.

Although cyclophosphamide, a common cytotoxic agent, is frequently used to treat malignant tumors, it can cause atrophy of immune organs, weight loss, leukopenia, lymphopenia, bone marrow suppression, and thrombocytopenia and inhibit the humoral and cellular immunity of animals. Therefore, cyclophosphamide is often used as a model drug to replicate the animal model of immunosuppression and to study the immunomodulatory effect of drugs [17–21]. The spleen, the body's largest immune organ, is the body's cellular and humoral immune center. It can exert non-specific immune functions through phagocytosis and specific immune functions through T and B cell-mediated cellular and humoral immunity [22, 23]. This study observed the body weight of mice, the pathology of the spleen and thymus, the index of immune organs, and the blood cell counts. The results showed that rhCNB could significantly increase the immune organ index of immunosuppressed mice, increase the quality of spleen organs, and recover the weight loss induced by cyclophosphamide. The thymus and spleen are important immune organs to maintain immune homeostasis. The pathological results of the spleen and thymus indicated that rhCNB could recover the injury of the spleen and thymus induced by cyclophosphamide. The reduction of WBCs is the most common complication after chemotherapy. WBCs are considered to be mainly related to immune defense mechanisms, and the number of LYM and NEU can indicate how well the human body's immune system is functioning [24]. The results showed that compared with the model group, WBC, PLT, LYM, and NEU counts increased after rhCNB treatment, indicating that rhCNB can increase the WBC, PLT, LYM, and NEU counts in peripheral blood of immunocompromised mice induced by cyclophosphamide. In conclusion, the results suggest that rhCNB can enhance general health, promote the differentiation and proliferation of spleen and thymus lymphocytes, and influence immunological function. The peripheral blood picture results reveal that rhCNB can improve the cyclophosphamide-caused reduction in white blood cells, lymphocytes, neutrophils, and platelets. All these suggest that rhCNB can promote the production of immune cells in the body with low immune function, thus enhancing the immune function. By suppressing the activity of monocytes and macrophages, cyclophosphamide can prevent T lymphocytes and B lymphocytes from proliferating and differentiating [25–28]. Additionally, cyclophosphamide can affect cytokine production by activating the NF-κB pathway by affecting signaling pathways such as dendritic cells, TLR_2, and TLR_4 [29]. The results of flow cytometry showed that rhCNB could upregulate the expressions of $CD4^+$, $CD8^+$ T, and $CD19^+$ B subpopulations in immunocompromised mice, indicating that rhCNB can promote the differentiation and proliferation of T cells and B cells in immunocompromised mice and regulate and improve the immune response. These results were consistent with the fact that rhCNB could induce the proliferation of B lymphocytes and thymus lymphocytes around the splenic

cap in the model group. To maintain normal cellular and humoral immune functions, Th1 and Th2 cells are in a dynamic equilibrium state under normal conditions [30–32]. These immunomodulatory cytokines are involved in T cell proliferation, differentiation, activation, and immunomodulation. IFN-γ and IL-4, specific cytokines of Th1 and Th2 cells, respectively, can control the activity of downstream effector cells through Th1 and Th2 cells [33]. IFN-γ promotes the differentiation of Th1 cells by activating antigen-presenting cells and upregulating transcription factor T-bet. IL-4 is also a key regulator of the immune response, which can promote the transformation of immature T cells into Th2 cells [34]. Transcription factors T-bet and $GATA_3$ are the key factors for TH0 cells to differentiate into Th1 or Th2 cells and for maintaining Th1/Th2 homeostasis [35, 36]. The results showed that the levels of IL-4 and IFN-γ in the model group decreased and increased in the treatment group after rhCNB treatment. At the same time, the mRNA levels of T-bet and $GATA_3$ decreased in the model group and increased in the treatment group after rhCNB treatment. The results showed that rhCNB could regulate the above cytokine secretion pathways, hence regulating the body's immune response.

As a new anti-tumor protein drug, rhCNB can activate the innate immune system through the TLR4/NF-κB signaling pathway, promote the maturation of dendritic cells, upregulate the expression of macrophages, and induce tumor cell apoptosis [4]. MAPK, a downstream signaling pathway of TLRs, is an important molecular pathway that regulates immune response and is important for T cell proliferation, differentiation, and other related functions. The experimental results found that rhCNB could increase the mRNA levels of TLR_4, P38, JNK, and ERK in mice with cyclophosphamide-induced immunodeficiency. MAPKs can activate the immune response in T lymphocytes [37]. P38, ERK, and JNK are three pathways in the kinase family. Activated by mitogens and growth factors, ERK can regulate the proliferation and differentiation of Th2 cells [38]. JNK regulates the proliferation, differentiation, and associated cytokine production of CD4+ T cells [39, 40]. P38 mainly conducts inflammatory cytokines and various types of cell stress signals. Recent studies have found that the P38 MAPK signaling may promote the proliferation of T lymphocytes. Also, the activation of the p38MAPK/ERK1/2 signaling pathway can activate B cells, induce the synthesis and secretion of cytokines, and regulate inflammation and immune [41, 42]. In conclusion, rhCNB may stimulate T lymphocyte proliferation and cytokine production through the TLR_4/MAPK signal pathway, promote the differentiation and proliferation of relevant immune cells, and regulate the body's humoral and cellular immune functions. In addition, rhCNB could activate macrophages and promote dendritic maturation through the TLR_4 pathway, enhance antigen presentation of antigen-presenting cells, regulate cytokine secretion, and enhance immune response.

5. Conclusion

In summary, rhCNB can effectively improve the immunodeficiency induced by cyclophosphamide, enhance the immune response of the body by enhancing the function of immune organs and the phagocytosis of macrophages, and regulate Th1 and Th2 through the TLR_4/MAPK signal pathway. The secretion of cytokines promotes the differentiation and proliferation of T lymphocytes and B lymphocytes, regulates the balance of Th1/Th2, and finally boosts the immunity of immunocompromised mice.

Data Availability

The datasets used/analyzed in the current study are available from the corresponding author on reasonable request.

Conflicts of Interest

The authors declare that they have no conflicts of interest.

Authors' Contributions

Wenhua Zhong and Hui Huang contributed equally to this study.

Acknowledgments

This study was supported by the Hainan Provincial Key Research and Development Program of China (ZDYF2020158) and Hainan Provincial Natural Science Foundation of China (821RC1144).

References

[1] V. Ntziachristos, "Going deeper than microscopy: the optical imaging Frontier in biology," *Nature Methods*, vol. 7, no. 8, pp. 603–614, 2010.

[2] J. J. Wang, K. F. Lei, and F. Han, "Tumor microenvironment: recent advances in various cancer treatments," *European Review for Medical and Pharmacological Sciences*, vol. 22, no. 12, pp. 3855–3864, 2018.

[3] D. M. Hausman, "What is cancer?" *Perspectives in Biology and Medicine*, vol. 62, no. 4, pp. 778–784, 2019.

[4] N. Li, Z. Zhang, W. Zhang, and Q. Wei, "Calcineurin B subunit interacts with proteasome subunit alpha type 7 and represses hypoxia-induciblefactor-1α activity via the proteasome pathway," *Biochemical and Biophysical Research Communications*, vol. 405, no. 3, pp. 468–472, 2011.

[5] J. Li, J. Guo, Z. Su, M. Hu, W. Liu, and Q. Wei, "Calcineurin subunit B activates dendritic cells and acts as a cancer vaccine adjuvant," *International Immunology*, vol. 23, no. 5, pp. 327–334, 2011.

[6] J. Yang, N. Qin, H. Zhang, R. Yang, B. Xiang, and Q. Wei, "Cellular uptake of exogenous calcineurin B is dependent on TLR4/MD2/CD14 complexes, and CnB is an endogenous ligand of TLR_4," *Scientific Reports*, vol. 6, no. 1, Article ID 24346, 2016.

[7] J. Yang, H. Zhang, Z. Zhu, Y. Gao, B. Xiang, and Q. Wei, "The immunostimulatory effects and pro-apoptotic activity of rhCNB against Lewis lung cancer is mediated by Toll-like receptor 4," *Cancer Medicine*, vol. 8, no. 9, pp. 4441–4453, 2019.

[8] W. Fang, D. Bi, R. Zheng et al., "Identification and activation of TLR_4-mediated signalling pathways by alginate-derived guluronate oligosaccharide in RAW264.7 macrophages," *Scientific Reports*, vol. 7, no. 1, p. 1663, 2017.

[9] L. Zhou, Z. Liu, Z. Wang et al., "Astragalus polysaccharides exerts immunomodulatory effects via TLR4-mediatedMyD88-dependent signaling pathway in vitro and in vivo," *Scientific Reports*, vol. 7, no. 1, Article ID 44822, 2017.

[10] Y. Q. Wang, J. B. Mao, M. Q. Zhou et al., "Polysaccharide from Phellinus Igniarius activates TLR4-mediated signaling pathways in macrophages and shows immune adjuvant activity in mice," *International Journal of Biological Macromolecules*, vol. 123, pp. 157–166, 2019.

[11] Y. Li, T. Meng, N. Hao et al., "Immune regulation mechanism of Astragaloside IV on RAW264.7 cells through activating the NF-κB/MAPK signaling pathway," *International Immunopharmacology*, vol. 49, pp. 38–49, 2017.

[12] L. X. Chen, Y. L. Qi, Z. Qi et al., "A comparative study on the effects of different parts of panax ginseng on the immune activity of cyclophosphamide-induced immunosuppressed mice," *Molecules*, vol. 24, no. 6, p. 1096, 2019.

[13] L. Zhang, Z. Wang, B. Li et al., "The inhibition of miR-17-5p promotes cortical neuron neurite growth via STAT3/GAP-43 pathway," *Molecular Biology Reports*, vol. 47, no. 3, pp. 1795–1802, 2020.

[14] Y. Zhou, X. Chen, R. Yi et al., "Immunomodulatory effect of tremella polysaccharides against cyclophosphamide-induced immunosuppression in mice," *Molecules*, vol. 23, no. 2, p. 239, 2018.

[15] Y. Gong, J. Wu, and S. T. Li, "Immuno-enhancement effects of Lycium ruthenicum Murr. polysaccharide on cyclophosphamide-induced immunosuppression in mice," *International Journal of Clinical and Experimental Medicine*, vol. 8, no. 11, pp. 20631–20637, 2015.

[16] J. Li, M. Hu, J. Guo, Z. Su, and Q. Wei, "Calcineurin subunit B is an immunostimulatory protein and acts as a vaccine adjuvant inducing protective cellular and humoral responses against pneumococcal infection," *Immunology Letters*, vol. 140, no. 1-2, pp. 52–58, 2011.

[17] F. Khazaei, E. Ghanbari, and M. Khazaei, "Protective effect of royal jelly against cyclophosphamide-induced thrombocytopenia and spleen and bone marrow damages in rats," *Cell J*, vol. 22, no. 3, pp. 302–309, 2020.

[18] X. T. Chen, J. Li, H. L. Wang, W. M. Cheng, L. Zhang, and J. F. Ge, "Immunomodulating effects of fractioned polysaccharides isolated from Yu-Ping-Feng-Powder in cyclophosphamide-treated mice," *American Journal of Chinese Medicine*, vol. 34, no. 4, pp. 631–641, 2006.

[19] M. F. A. Elazab, A. M. Younes, A. Y. Gaafar, A. Z. Abu-Bryka, and M. M. Abdel-Daim, "Immunosuppressive effect of cyclophosphamide in Nile tilapia (*Oreochromis niloticus*)," *Environmental Science and Pollution Research*, vol. 28, no. 16, pp. 20784–20793, 2021.

[20] J. Deng, Y. F. Zhong, Y. P. Wu et al., "Carnosine attenuates cyclophosphamide-induced bone marrow suppression by reducing oxidative DNA damage," *Redox Biology*, vol. 14, pp. 1–6, 2018.

[21] C. Sun, J. Yang, L. Pan et al., "Improvement of icaritin on hematopoietic function in cyclophosphamide induced myelosuppression mice," *Immunopharmacology and Immunotoxicology*, vol. 40, no. 1, pp. 25–34, 2018.

[22] H. Y. Cui, C. L. Wang, Y. R. Wang et al., "Pleurotus nebrodensis polysaccharide (PN-S) enhances the immunity of immunosuppressed mice," *Chinese Journal of Natural Medicines*, vol. 13, no. 10, pp. 760–766, 2015.

[23] Q. Li, G. Chen, H. Chen et al., "Se-enriched G. frondosa polysaccharide protects against immunosuppression in cyclophosphamide-induced mice via MAPKs signal transduction pathway," *Carbohydrate Polymers*, vol. 196, pp. 445–456, 2018.

[24] M. D. Ficken and H. J. Barnes, "Effect of cyclophosphamide on selected hematologic parameters of the Turkey," *Avian Diseases*, vol. 32, no. 4, pp. 812–817, 1988.

[25] Z. Ren, C. He, Y. Fan et al., "Immuno-enhancement effects of ethanol extract from Cyrtomium macrophyllum (Makino) Tagawa on cyclophosphamide-induced immunosuppression in BALB/c mice," *Journal of Ethnopharmacology*, vol. 155, no. 1, pp. 769–775, 2014.

[26] P. Duggina, C. M. Kalla, S. R. Varikasuvu, S. Bukke, and V. Tartte, "Protective effect of centella triterpene saponins against cyclophosphamide-induced immune and hepatic system dysfunction in rats: its possible mechanisms of action," *Journal of Physiology & Biochemistry*, vol. 71, no. 3, pp. 435–454, 2015.

[27] T. Zhang, X. Y. Qin, X. Cao, W. H. Li, T. Gong, and Z. R. Zhang, "Thymopentin-loadedphospholipid-based phase separation gel with long-lasting immunomodulatory effects: in vitro and in vivo studies," *Acta Pharmacologica Sinica*, vol. 40, no. 4, pp. 514–521, 2019.

[28] L. Rivino and M. Q. Lim, "CD4(+) and CD8(+) T-cell immunity to Dengue - lessons for the study of Zika virus," *Immunology*, vol. 150, no. 2, pp. 146–154, 2017.

[29] M. K. Logani, S. Alekseev, M. K. Bhopale, W. S. Slovinsky, and M. C. Ziskin, "Effect of millimeter waves and cyclophosphamide on cytokine regulation," *Immunopharmacology and Immunotoxicology*, vol. 34, no. 1, pp. 107–112, 2012.

[30] S. Zhang, X. Liu, C. Sun et al., "Apigenin attenuates experimental autoimmune myocarditis by modulating Th1/Th2 cytokine balance in mice," *Inflammation*, vol. 39, no. 2, pp. 678–686, 2016.

[31] M. Diao, J. Min, F. Guo, and C. L. Zhang, "Effects of salbutamol aerosol combined with magnesium sulfate on T-lymphocyte subgroup and Th1/Th2 cytokines of pediatric asthma," *Experimental and Therapeutic Medicine*, vol. 13, no. 1, pp. 117–120, 2017.

[32] Y. Y. Shao, Y. M. Zhou, M. Hu et al., "The anti-allergic rhinitis effect of traditional Chinese medicine of shenqi by regulating mast cell degranulation and Th1/Th2 cytokine balance," *Molecules*, vol. 22, no. 3, p. 504, 2017.

[33] L. H. Glimcher and K. M. Murphy, "Lineage commitment in the immune system: the T helper lymphocyte grows up," *Genes & Development*, vol. 14, pp. 1693–1711, 2000.

[34] J. F. Lafreniere, P. Mills, M. Bouchentouf, and J. P. Tremblay, "Interleukin-4 improves the migration of human myogenic precursor cells in vitro and in vivo," *Experimental Cell Research*, vol. 312, no. 7, pp. 1127–1141, 2006.

[35] T. Nakayama, K. Hirahara, A. Onodera et al., "Th2 cells in health and disease," *Annual Review of Immunology*, vol. 35, no. 1, pp. 53–84, 2017.

[36] T. Nishimura, K. Iwakabe, M. Sekimoto et al., "Distinct role of antigen-specific T helper type 1 (Th1) and Th2 cells in tumor eradication in vivo," *Journal of Experimental Medicine*, vol. 190, no. 5, pp. 617–628, 1999.

[37] K. L. Jeffrey, M. Camps, C. Rommel, and C. R. Mackay, "Targeting dual-specificity phosphatases: manipulating MAP kinase signalling and immune responses," *Nature Reviews Drug Discovery*, vol. 6, no. 5, pp. 391–403, 2007.

[38] L. L. Sharp, D. A. Schwarz, C. M. Bott, C. J. Marshall, and S. M. Hedrick, "The influence of the MAPK pathway on T cell lineage commitment," *Immunity*, vol. 7, no. 5, pp. 609–618, 1997.

[39] T. Nakahara, Y. Moroi, H. Uchi, and M. Furue, "Differential role of MAPK signaling in human dendritic cell maturation and Th1/Th2 engagement," *Journal of Dermatological Science*, vol. 42, no. 1, pp. 1–11, 2006.

[40] Y. L. Zhang and C. Dong, "MAP kinases in immune responses," *Cellular and Molecular Immunology*, vol. 2, no. 1, pp. 20–27, 2005.

[41] W. Duan, J. H. P. Chan, K. McKay et al., "Inhaled p38αmitogen-activated protein kinase antisense oligonucleotide attenuates asthma in mice," *American Journal of Respiratory and Critical Care Medicine*, vol. 171, no. 6, pp. 571–578, 2005.

[42] S. Agrawal, S. Gollapudi, H. Su, and S. Gupta, "Leptin activates human B cells to secrete TNF-alpha, IL-6, and IL-10 via JAK2/STAT3 and p38MAPK/ERK1/2 signaling pathway," *Journal of Clinical Immunology*, vol. 31, no. 3, pp. 472–478, 2011.

Hindawi
Evidence-Based Complementary and Alternative Medicine
Volume 2022, Article ID 7856629, 11 pages
https://doi.org/10.1155/2022/7856629

Research Article

The Transcription Factor Otc4A Stimulates the Proliferation, Invasion, and Stemness of Colorectal Cancer Cells by Inhibiting the Regulation of miR-7-5p on TLR4

Jinsong He,[1] Liang Duan,[2] Yu Xie,[1] and Shoujiang Wei[1]

[1]*Department of Gastroenterology, Affiliated Hospital of North Sichuan Medical College, Nanchong, Sichuan 637000, China*
[2]*Department of Gastroenterology, Quxian People's Hospital, Dazhou, Sichuan 635299, China*

Correspondence should be addressed to Shoujiang Wei; nsmcwsj@163.com

Received 29 July 2022; Revised 31 August 2022; Accepted 8 September 2022; Published 26 September 2022

Academic Editor: Xueliang Wu

Background. To investigate the effects and mechanism of octamer-binding transcription factor 4 (Otc4A) on proliferation, invasion, and stemness of colorectal cancer (CRC) cells. *Methods*. Firstly, normal fetal human cells (FHC, colon epithelial cells) and HT29 cells (CRC cells) were cultured. The expression levels of Otc4A, miR-7-5p, and TLR4 in cells were then detected by qRT-PCR. CCK-8 was adopted to measure cell proliferation rate after Otc4A, miR-7-5p, and TLR4, respectively, were either knocked out or overexpressed in HT29 cells. Later, the cell viability was detected by cell cloning assay; cell invasion by transwell; cell sphere-forming ability by sphere-formation assay; protein expression level of Otc4A, p65, p-p65, and TLR4 by western blot; and the targeting relationships between miR-7-5p and Otc4A as well as miR-7-5p and TLR4 by dual-luciferase reporter assay. Finally, chromatin immunoprecipitation was applied to verify the interaction between Otc4A and miR-7-5p. *Results*. In HT29 cells, Otc4A expression was significantly increased. Additionally, the knockdown of Otc4A prevented HT29 cells from proliferating, migrating, forming spheres, and activating NF–B signaling. Otc4A could negatively regulate miR-7-5p, and miR-7-5p could target TLR4 expression. Besides, a negative correlation was found between Otc4A and miR-7-5p. Finally, the knockdown of miR-7-5p or overexpression of TLR4 could significantly reverse the effect of the knockdown of Otc4A on HT29 cells. *Conclusion*. The transcription factor Otc4A can regulate the level of TLR4 by inhibiting the expression of miR-7-5p and then promote the proliferation and invasion of CRC cell HT29 as well as enhance cell stemness.

1. Introduction

Colorectal cancer (CRC), a prevalent digestive tract malignancy, is the third most frequent malignancy after lung cancer and breast cancer in the world, especially in developed countries. It is reported that CRC ranks third among cancers worldwide in terms of morbidity and mortality [1], and the incidence of CRC is also mounting in developing countries. Among patients with CRC, 5% to 10% belong to familial hereditary diseases caused by familial adenomatous polyposis, and over 90% are manifested as sporadic tumors [2]. At present, scholars have improved their cognition of the CRC and its treatments due to the improvement of modern medical levels. However, the specific indicators for early diagnosis are still not sufficient, and most CRC patients have entered the middle and advanced stages when receiving clinical diagnosis. CRC is a major hazard to human health, and in fact, the survival of CRC patients with advanced invasion and metastasis is less than 10% at 5 years [3, 4]. Therefore, it is urgent to seek appropriate markers for improvement in screening and early diagnosis of CRC.

Octamer-binding transcription factor 4 (Otc4A), a totipotent or pluripotent stem cell marker, is crucial for embryonic stem cells to retain totipotency and self-renewal. Recent studies have established the critical function of Otc4A in the gene regulatory network of stem cell development [5], and over 1,000 genes are regulated by Otc4A. Related research studies have reported Otc4A expression in many tumor cells, such as MCF-7 cell lines in human breast cancer and breast cancer tissues, pancreatic cancer Capan-2,

Pan-1 cell lines, liver cancer Mahlava cell lines, gliomas, and bladder cancer tissues [6–8]. Some articles also pointed out that Otc4A overexpression can enhance stem-like properties of CRC cells, such as cell migration, invasion, and drug resistance [9]. Even yet, it is unclear exactly what part of Otc4A plays in the initiation of colorectal cancer. MicroRNAs (miRNAs) are endogenous noncoding RNAs around 18–25 nucleotides long, and specifically attach to the 3′-UTR of mRNAs to regulate an array of biological processes like gene expression, cell differentiation, proliferation, and apoptosis [10]. More than 700 miRNAs have already been identified, and it is reported that miRNAs not only are closely related to pathological processes such as tumors and inflammation [11, 12], but also have a pivotal role in predicting therapeutic strategies and targeted therapy [13]. As a tumor suppressor, MiR-7-5p prevents CRC cells from proliferating and migrating by suppressing Krüppel-like factor 4 expression [14]. However, the roles of Otc4A and miR-7-5p in CRC remain unclear. There are several subtypes of Otc4A. Otc4AA plays an important role in the early developmental stages of embryonic stem cells and in the maintenance of stem cells. The roles and functions of other variants and isoforms of Otc4A in biological systems are less well understood. In this study, we employed the Otc4AA variant as a research subject. Therefore, the effects of Otc4A and miR-7-5p on CRC were investigated in this study. This study aimed to provide reliable data support for searching for biomarkers and improving diagnosis of CRC.

2. Materials and Methods

2.1. Cell Culture. CRC cells HT29 and normal colon epithelial cells FHC were procured from the National Collection of Authenticated Cell Cultures. The purchased cells were grown in DMEM-F12 and RPMI-1640 medium supplemented with FBS (10%) and penicillin streptomycin (1%), and then CO_2 (5%) and humidity (95%) at 37°C were set to cultivate the cells.

2.2. Cell Culture and Transfection. HT29 cells were digested and passed after they entered the logarithmic growth phase. The logarithmic phase cells were then gathered and diluted to 2×106 cells/ml. Later, a six-well plate was chosen to seed the cells. Subsequently, the transfection was conducted once the cell confluence was between 80% and 90%. Otc4A knockout plasmid (si-Otc4A) and its negative control (si-NC), miR-7-5p mimics (miR-7-5p mimics) and negative mimics (NC mimics), negative inhibitor (NC-inhibitor) and miR-7-5p inhibitor (miR-7-5p inhibitor), and pcDNA3.1-TLR4 plasmids (TLR4) were constructed by Guangzhou RiboBio Co. Ltd. (China). As per the instructions of the lipo2000 transfection kit, the vectors in each group and the liposomes were diluted with a serum-free OptiMEM culture medium. Next, the liposomes with equal volumes were mixed with the vectors in each group. After incubating at ambient temperature for 20 minutes, they were introduced to the cultured cells for another 6 h culture. Then, a complete medium was used in place of the previous medium. In the end, the cells were harvested after 48 h transfection.

2.3. Real-Time Fluorescence Quantitative Polymerase Chain Reaction (RT-qPCR). Utilizing a total RNA extraction kit, the total RNA was isolated from the collected cells or tissues, and the extracted RNA was then kept at −80°C. Subsequent to the directions in the reverse transcription polymerase chain reaction (PCR) kit, cDNA was then created by reverse transcription. Following tests to ascertain the concentration and purity of the synthesized cDNA, PCR was performed under the guidelines of real-time PCR. The following was the reaction program: 95°C (1 min), 95°C (40 s), 58°C (40 s), and 72°C (45 s), with a 35-cycle, and 72°C (10 min). The data analysis technique adopted was the $2^{-\Delta\Delta Ct}$ method [15]. In Table 1, the primer sequences were displayed.

2.4. CCK-8 Method. After being digested, the logarithmic phase cells were diluted to 4×104 cells/mL. A further step involved seeding the cells in a 96-well plate (5000 cells per well). Additionally, each group received 6 replicate wells. The cells were cultured for 24 h, and after cell adhesion, the cells were starved by adding a serum-free medium for another 24 h. Then each well received a supplementation of fresh complete culture (90 μL) and CCK-8 solution (10 μL) for an additional 2 hours of culture. Ultimately, in order to detect the absorbance at 450 nm, a microplate reader was applied [16].

2.5. Cell Cloning Assay. The cells in the log phase were digested and passaged. The cells were counted, and the culture medium was taken to regulate cell concentration. The cells were then plated into dishes (200 cells per dish). Later, the dishes were gently shaken in a cross direction in order to disperse the cells evenly. Subsequently, static culture was conducted for 2–3 weeks in an environment of 37°C and 5% CO_2. The colonies that had over 50 cells were counted under a microscope, and the following formula was used to calculate the colony forming efficiency: the colony forming efficiency (%) = (number of clone cells/number of seeded cells) × 100.

2.6. Transwell Experiments. Matrigel was removed from a −20°C environment and left overnight at 4°C. After melting the Matrigel into liquid, a serum-free medium at 4°C was introduced to the Matrigel for a 1 : 6 dilution. The upper transwell chamber insert was then filled with 100 μl of Matrigel. Afterwards, the insert was placed at a temperature of 37°C for 3–5 h to solidify the Matrigel. The subsequent steps mirrored those of the migration test. Briefly speaking, the upper chamber received 100 μl cells, while the lower chamber received 500 μl 10% FBS medium. Subsequent to 48 hours of incubation, the cells were fixed first, then stained, and finally counted.

2.7. Cell Sphere-Formation Assay. Trypsin at a concentration of 0.25% was selected to lyse cells that were in a satisfactory growing state in each group. Later, the cells were collected, and they underwent two low-speed PBS washes. Further, the collected cells in each group were resuspended using the prepared stem cell culture medium, and the cell

Table 1: Primer sequences for qRT-PCR.

Genes	Primer sequences
Otc4A	F 5′-GAACATGTGTAAGCTGCGGCC-3′ R 5′-CCCTTCTGGCGCCGGTTAC-3′
miR-7-5p	F 5′-TGCGCTCAGCAAACATTTATTG-3′ R 5′-CCAGTGCAGGGTCCGAGGTATT-3′
TLR4	F 5′-CTGGGTGAGAAAGCTGGTAA-3′ R 5′-AGCCTTCCTGGATGATGTTGG-3′
U6	F 5′-CTCGCTTCGGCAGCACA-3′ R 5′-AACGCTTCACGAATTTGCGT-3′
GAPDH	F 5′-GTGAACCATGAGAAGTATG-3′ R 5′-CGGCCATCACGCCACAGTTTC-3′

concentration was increased to 10000 cells per milliliter. Next, the resulting cells were inoculated in a 24-well culture plate (1000 cells/well), with each group occupying 3 wells. By the way, the plate was dedicated to antiadhesion. Subsequently, the plate was shaken to make the cells distribute evenly, and then the incubation was conducted at 37°C with CO_2 (5%). After being in culture for 1–2 weeks, the cells were subjected to observation by means of a microscope. Finally, the number and the formation efficiency of cell spheres with a diameter longer than 75 μm were successively obtained.

2.8. Dual-Luciferase Reporter Assay. When the degree of cell fusion approached 80%–90%, transfection was carried out. The cotransfection of the established NC mimics and miR-7-5p mimics into TLR4 wild-type (TLR4-WT) and mutant (TLR4-MUT) or Otc4A wild-type (Otc4A-WT) and mutant (Otc4A-MUT) dual-luciferase reporter vectors was performed subsequently. Later, the cells were collected after the transfection and 48 hours of culture. Then, a condition of room temperature was set for cell lysis for 20 min. Subsequently, the luciferase substrate was added directly after the supernatant was collected by centrifugation. Next, luciferase activity was measured using a luminescence analyzer. Additionally, relative firefly luciferase activity was determined by taking Renilla luciferase activity as an internal control.

2.9. Chromatin Immunoprecipitation. The culture medium was removed when the cells reached 70%–80% confluence, and the supernatant was extracted for acquiring protein. The immune-precipitated beads were vortexed and shaken for 1 min to be fully resuspended. After that, 35 μl of magnetic beads were put into a 1.5 ml centrifuge tube that already contained 400 μl of binding buffer. Then the beads were fully resuspended and washed. Later, the magnetic separation was performed. After the solution became clear due to magnetic bead adsorption, the supernatant was aspirated and discarded. The EP tube was removed from the magnetic separator and washed once again. Then, 400 μl of binding buffer was added for the subsequent trials. The antibody binding reaction was performed as follows: on a rotary shaker at ambient temperature, the beads were first bound to the antibody for 15 minutes. Next, the beads were washed with binding buffer three times, slightly centrifuged, and rinsed three more times in the same buffer. Later, the beads and lysates were placed in a refrigerator overnight at 4°C for the last binding. After washing the beads again, magnetic separation was conducted. Subsequently, the supernatant was discarded, and 400 μl washing buffer was poured into the EP tube. Again, the washing buffer was taken once more to wash the beads four times repeatedly. During the last washing process, the beads were collected into a new centrifuge tube of 1.5 ml. Elution was performed, and 25 μl of 1 × SDS buffer was added. Then, the boiling water bath was conducted for 5 min. Finally, the beads were set up on a magnetic grate for magnetic separation, after which the supernatant was collected for WB detection.

2.10. Western Blot. Before being broken up by sonication in an ice bath, each group's cells underwent a 20-minute lysis with RIPA lysate. The protein concentration was then measured after collecting the supernatant proteins. Later, sodium dodecyl sulfate-polyacrylamide gel electrophoresis (SDS-PAGE) was performed, and the proteins were then transferred to PVDF membranes. Following that, blocking was done for 1 h at ambient temperature. After that, primary antibodies (Otc4A, p65, p-p65, TLR4, and β-actin) were added and the mixture was incubated at 4°C overnight. Subsequent to two rounds of washing the membranes, secondary antibodies that had been diluted and enzyme-labeled were added. After that, the membranes were incubated for another 1 h at ambient temperature. An internal control for the examination of the protein level was decided to β-actin.

2.11. Statistical Analysis. All obtained data were subjected to analysis using SPSS 26.0. Besides, *t*-test analysis was implemented between two groups, while one-way analysis of variance was conducted among multiple groups. In addition, Pearson phototropism was employed to examine how miR-7-5p, Otc4A, and TLR4 relate to one another. The test outcomes were described as mean ± standard deviation (SD), and $P < 0.05$ was regarded as the criterion for statistical significance.

3. Results

3.1. Knockdown of Otc4A Inhibits Malignant Phenotype, Stemness, and NF-κB Signaling Activation in Colorectal Cancer Cells. To begin with, the expression and function of Otc4A in CRC cells were examined. The examination results presented that HT29 cells had much higher levels of Otc4A expression than FHC cells (Figure 1(a)). The si-Otc4A group exhibited a markedly lower level of Otc4A expression as compared to the si-NC group, indicating a successful knockdown (Figure 1(b)). After the further knockdown of Otc4A, an obvious reduction was observed in the cell proliferation rate, viability, invasion ability, and sphere-forming ability of the cells (Figures 1(c)–1(f)), and so did the expression levels of Otc4A, p-P65, and the ratio of p-P65/P65 (Figure 1(g)). Microsphere culture is one of the methods to obtain stem cells and tumor stem cells. Tumor stem cells

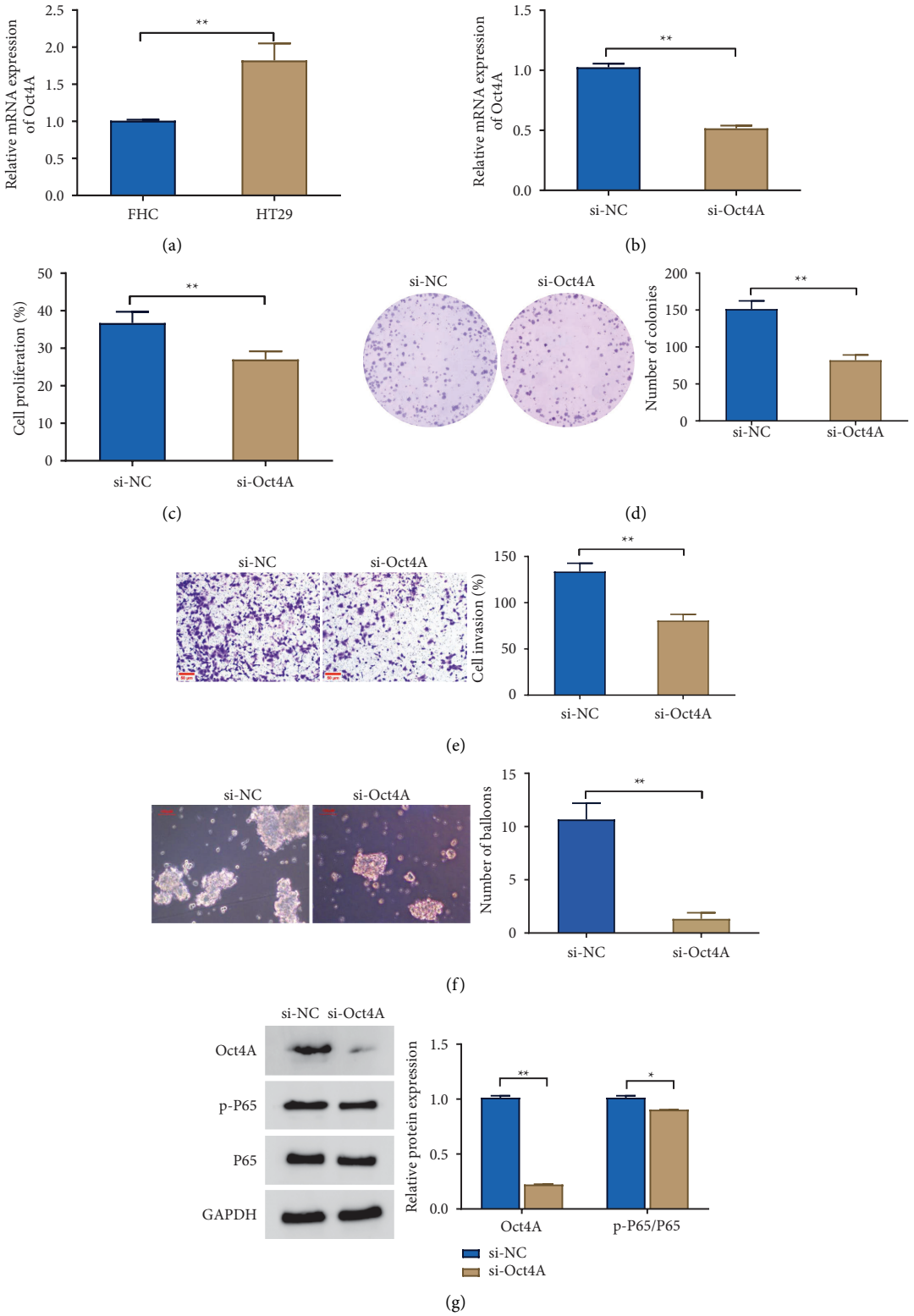

Figure 1: Effects of knockdown of Otc4A on the phenotype and stemness of colorectal cancer cells. qRT-PCR were used to detect Otc4A expression level in FHC and HT29 cells (a) and the si-NC and si-Otc4A groups (b); (c) CCK-8 for detecting the proliferation rate of cells; (d) cell cloning assay for the viability of cells; (e) Transwell for the invasion ability of cells; scale bar = 50 μm. (f) Sphere-forming assay for observing the sphere-forming ability of cells; scale bar = 100 μm. (g) Western blot for determining the expression level of Otc4A, p65, and p-p65. $^{*}P < 0.05$, $^{**}P < 0.01$. Each experiment was performed in triplicate.

can survive in a serum-free medium, while differentiated cells will die under such conditions. Thus, the sphere-forming ability of cells was observed by a sphere-forming assay, indicating the stemness of the tumor cells.

3.2. Negatively Regulatory Effect of Otc4A on miR-7-5p Expression in Colon Cancer Cells. The mechanism of Otc4A affecting CRC was further explored. In the miR-7-5p promoter region, Otc4A binding sites were determined by biological information tests (Figure 2(a)). Also, the co-transfection of miR-7-5p overexpression could apparently suppress the luciferase activity of the Otc4A-WT vector but not the Otc4A-MUT vector, according to the dual-luciferase reporter assay. The above outcomes indicated the interaction between Otc4A and miR-7-5p. Additionally, chromatin immunoprecipitation findings also showed that Otc4A and miR-7-5p bind to one another (Figure 2(b) and 2(c)). Besides, HT29 cells showed considerably lower miR-7-5p expression than FHC cells (Figure 2(d)). Furthermore, miR-7-5p expression was significantly elevated in the cells when Otc4A was knocked down, and an inverse correlation between Otc4A and miR-7-5p was discovered (Figures 2(e) and 2(f)).

3.3. TLR4 Serves as a Downstream mRNA of miR-7-5p. The downstream targets of miR-7-5p were further investigated. The Targetscan database (Fig. https://www.targetscan.org/vert_72) predicted as well as discovered the sites binding miR-7-5p and TLR4. Besides, the dual-luciferase reporter assay also indicated that overexpressing miR-7-5p considerably inhibited the luciferase activity of the TLR4-WT vector while having no obvious impact on the TLR4-MUT vector (Figure 3(a)). The above findings proved the targeting link between miR-7-5p and TLR4. Additionally, HT29 cells had significantly higher TLR4 expression than FHC cells did (Figure 3(b)). When miR-7-5p was overexpressed, its expression level went up, while the knockdown of miR-7-5p significantly declined the expression level in cells (Figure 3(c)). This result suggested a successful cell transfection. The levels of TLR4 mRNA and protein expression were correspondingly decreased or increased upon overexpression or knockdown of miR-7-5p in cells (Figures 3(d) and 3f). The correlation analysis also further showed that TLR4 was negatively correlated with miR-7-5p (Figure 3(f)). When compared to the si-NC group, the TLR4 expression level in the cells was noticeably lower in the si-Otc4A group, and Otc4A was positively correlated with TLR4 (Figures 3(g) and 3(h)).

3.4. Otc4A Regulates the Malignant Progression of HT29 Cells through miR-7-5p/TLR4 Axis. In this part, the roles of Otc4A, miR-7-5p, and TLR4 in CRC were further researched. We acquired the following results: firstly, different from the si-NC group, the si-Otc4A group exhibited a significant decrease in the proliferation rate, viability, invasion ability, sphere-forming ability, number of spheroids, and the expression level of TLR4 and p-p65, as well as the ratio of p-p65/p65 of the cells. However, the si-Otc4A + miR-7-5p inhibitor and si-Otc4A + TLR4 groups showed a remarkable increase in the proliferation rate, viability, invasion ability, sphere-forming ability, number of sphere-forming ability, TLR4 and p-p65 expression levels, and the ratio of p-p65/p65 of the cells, compared with the si-Otc4A group (Figure 4).

4. Discussion

CRC is the third most common malignancy after lung and breast carcinoma worldwide (especially in developed countries), and its incidence is increasing in developing countries [17]. As one of the heterogeneous cell populations with various characteristics, CRC arises with cancer cells of the colon, rectum, and appendix. Additionally, genes and the microenvironment are important factors in CRC pathogenesis [18]. In spite of the effectiveness of surgical and chemotherapy treatments, the prognosis allows for no optimism considering that many CRC patients suffer tumor recurrence or metastasis after surgery. One of the major clinical challenges of CRC is advanced diagnosis. Numerous gene mutations, dysregulated signaling networks, or an evident genetic variation among individuals all contribute to the complex pathogenesis of CRC. Therefore, molecular biological studies of biomarkers have important clinical implications.

Otc4A is included in the POU family of transcription factors. As a totipotent or pluripotent stem cell marker, Otc4A is critical for embryonic stem cells to retain totipotency and self-renewal. Otc4A is expressed in many different types of tumors, and its expression is associated with the tumorigenicity of pluripotent cells [19]. However, relevant studies on the expression of Otc4A in CRC tissues and its role in CRC are rare at home and abroad. Wang et al. [20] claimed that the positive expression of Otc4A could be a warning sign for distant recurrence and poor prognosis of rectal cancer in patients undergoing chemoradiotherapy before surgery. Studies have shown that Otc4A protein overexpression plays a role in the development of CRC in the development of colon cancer, and Otc4A is a key transcription factor for maintaining the survival of colon cancer tumor transcription factor critical for the survival of stem cell-like cells [21]. NF-κB falls into the category of a nuclear factor that binds to the gene regulatory region encoded by the immunoglobulin k light chain of activated B cells, and the abnormal activation of NF-κB could enhance cancer cell proliferation by binding to the cyclin D1 promoter [22]. Furthermore, the NF-κB signaling pathway promotes angiogenesis by regulating proangiogenic factors, vascular endothelial growth factor, and the proinflammatory cytokine IL-8 in cancer cells. A number of malignancies are impacted by abnormal NF-κB expressions [23]. NF-κB consists of five proteins, which are bound to IκBα in the cytoplasm at rest to form a complex. When IκBα is activated to form p-IκBα, IκBα is ubiquitinated and degraded to release bound NF-κB p65, which is further phosphorylated to form p-NF-κB p65, enhancing its localization signal into the nucleus to promote downstream gene expression. P65 is the

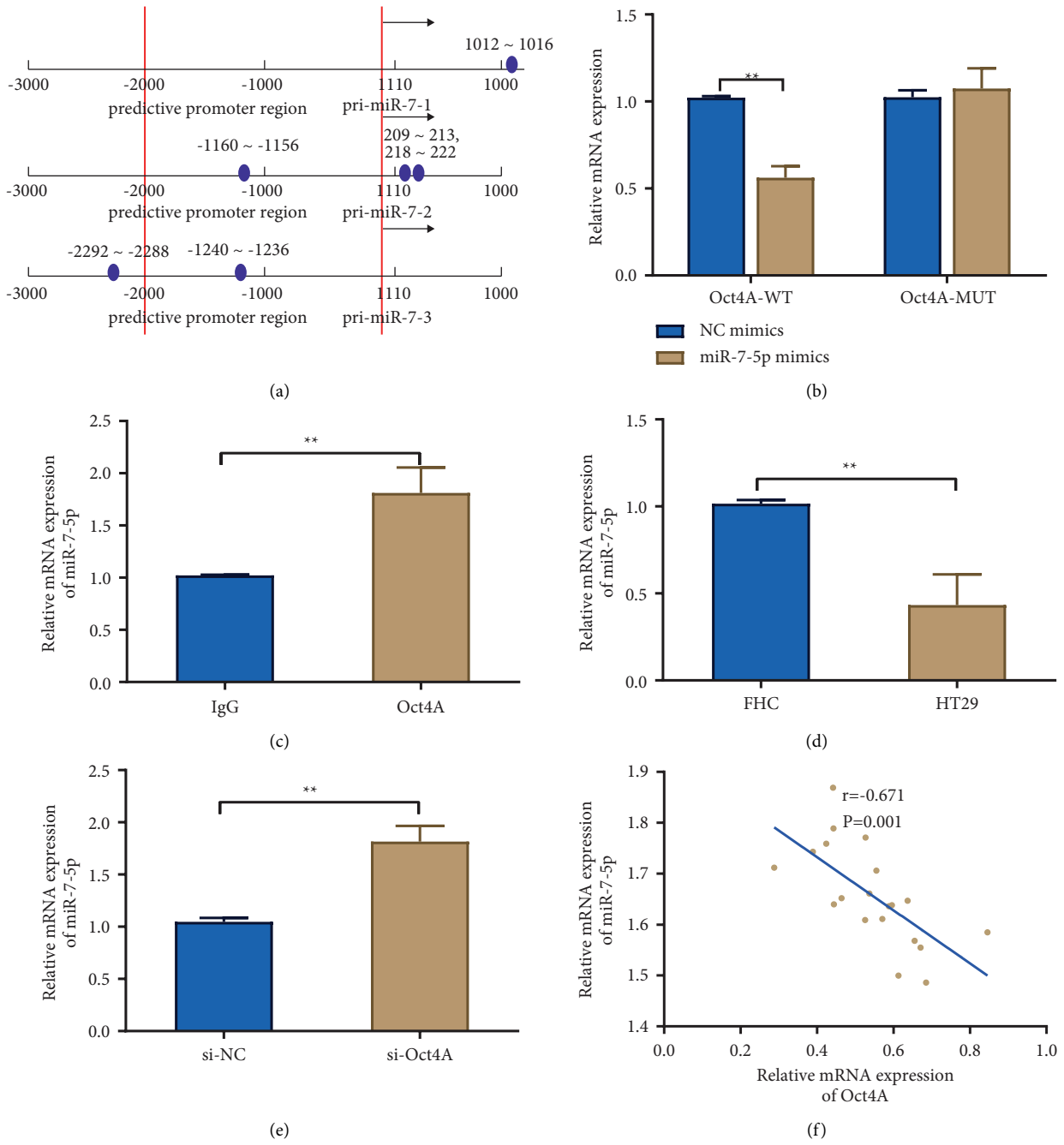

Figure 2: Effects of Otc4A on miR-7-5p in colorectal cancer cells. (a) The bioinformatics prediction was applied to obtain Otc4A binding sites in the miR-7-5p promoter region; (b) dual-luciferase reporter assay to verify the targeting relationship verified, $^{**}P < 0.01$; (c) chromatin immunoprecipitation to verify the interaction between Otc4A and miR-7-5p, $^{**}P < 0.01$; qRT-PCR to detect the expression level of miR-7-5p in FHC and HT29 cells (d) and in each group (e); $^{**}P < 0.01$; (f) the correlation analysis for the connection between Otc4A and miR-7-5. Each experiment was performed in triplicate.

most widely distributed heterodimer. Therefore, the NF-κB signaling pathway can be expressed by P65. In this study, knockdown of Otc4A inhibited the proliferation, migration, sphere formation, and NF-κB signaling activation of HT29 cells. The above findings in this study suggested that Otc4A was a cancer-promoting transcription factor, and with it, the NF-κB signaling pathway could be activated and CRC cell proliferation could be induced.

Numerous studies have revealed microRNAs (miRNAs) as novel and useful biomarkers that can be employed in the early diagnosis, treatment, and prognostic estimation of CRC [24]. Recent studies on the biological relationship between miR-7 and tumors have gradually increased. Some studies have discovered that a number of malignant tumors, such as CRC, lung carcinoma, and breast carcinoma, exhibit abnormal expression of miR-7 that implicates the proliferation,

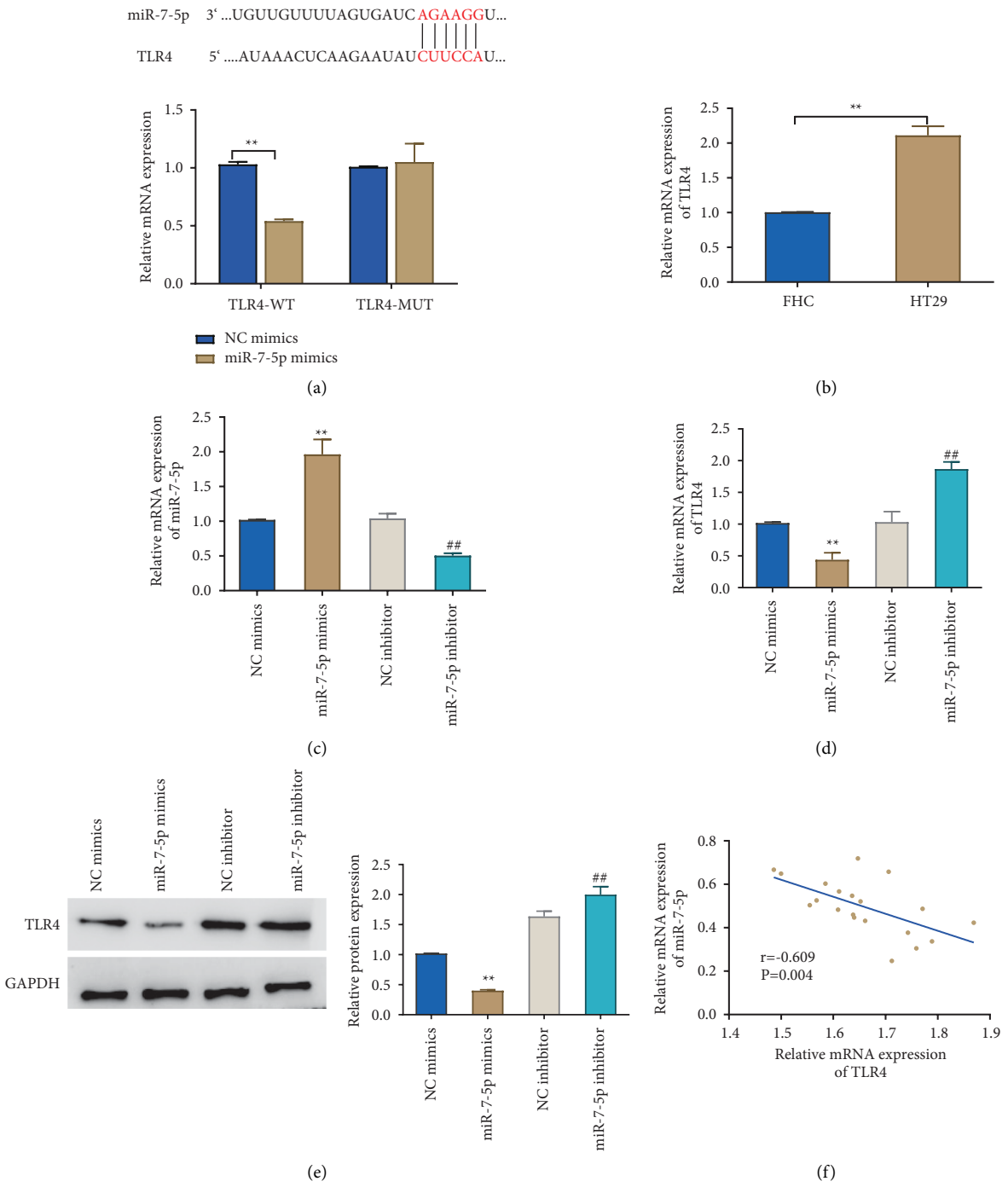

Figure 3: Continued.

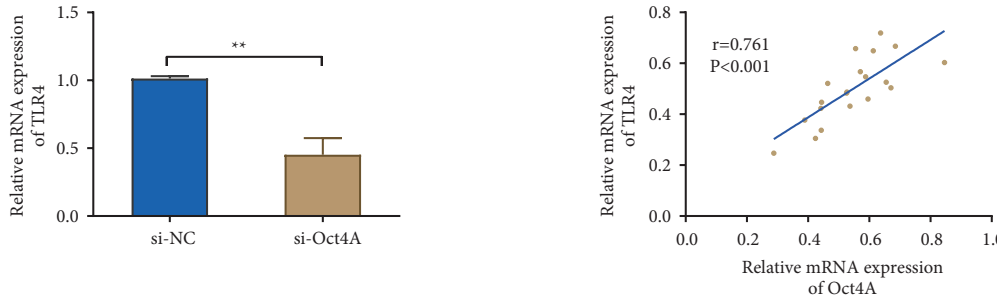

(g) (h)

Figure 3: Effects of miR-7-5p on TLR4 expression in colon cancer. (a) Database was utilized to predict the binding sites of miR-7-5p and TLR4; dual-luciferase reporter assay to verify the targeting relationship between miR-7-5p and TLR4; (b-d) qRT-PCR to check TLR4 expression level in FHC and HT29 cells (b) as well as miR-7-5p (c) and TLR4 (d) expression level in each group of cells; (e) Western blot to detect the protein level of TLR4 in cells; (f) correlation analysis for miR-7-5p and TLR4 expression; (g) qRT-PCR to observe the expression level of TLR4 in the si-NC and si-Otc4A groups; and (h) Correlation analysis for the association between Otc4A and TLR4 expression. $^{*}P < 0.05$, $^{**}P < 0.01$, $^{\#\#}P < 0.01$. Each experiment was performed in triplicate.

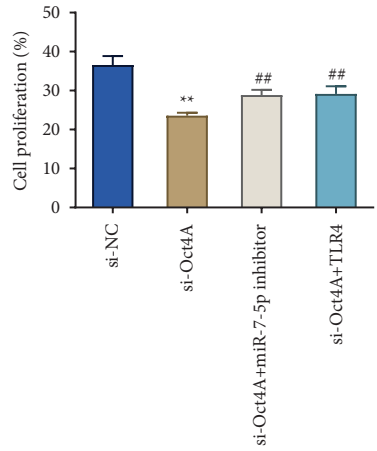

(a)

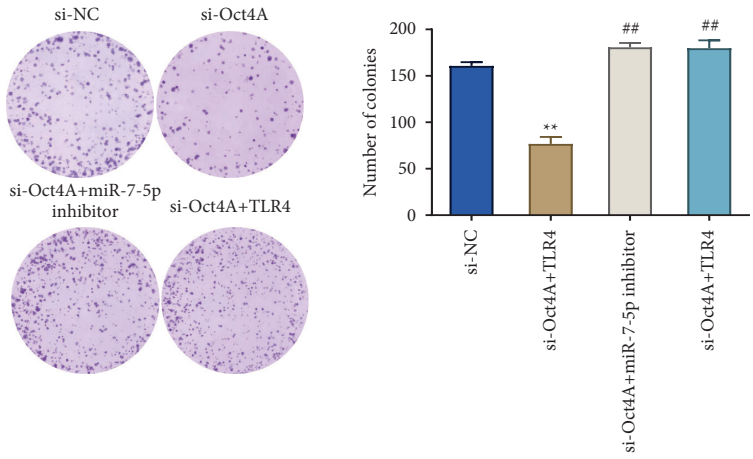

(b)

Figure 4: Continued.

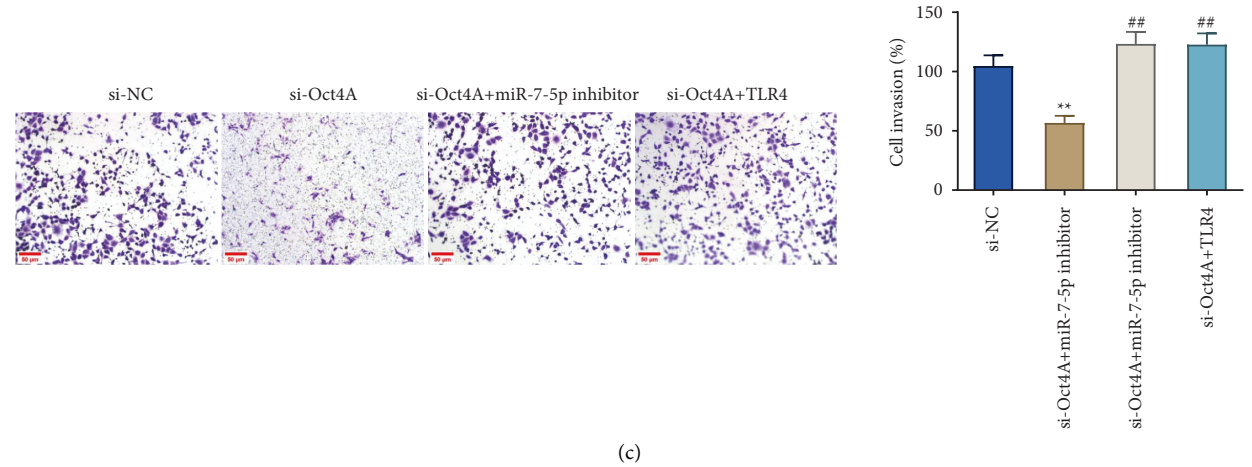

(c)

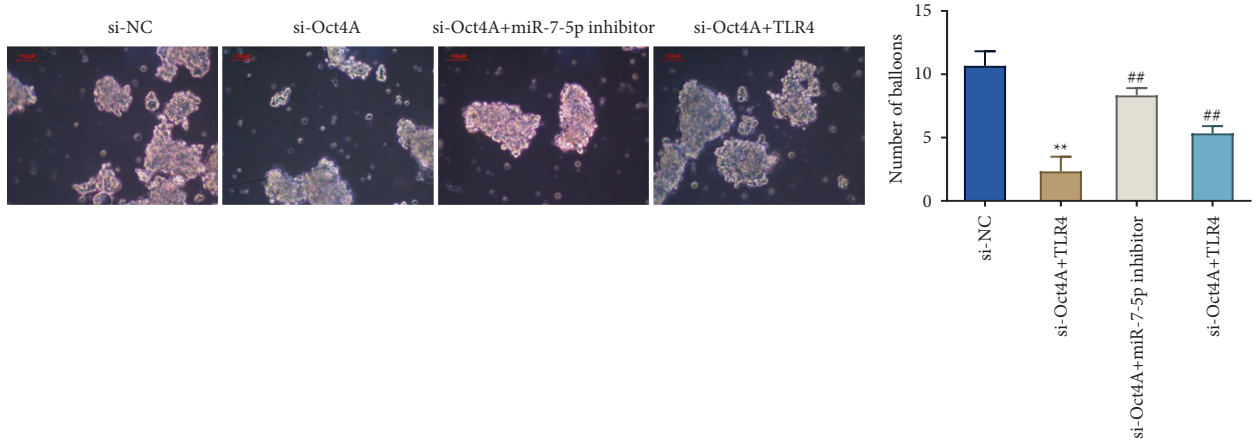

(d)

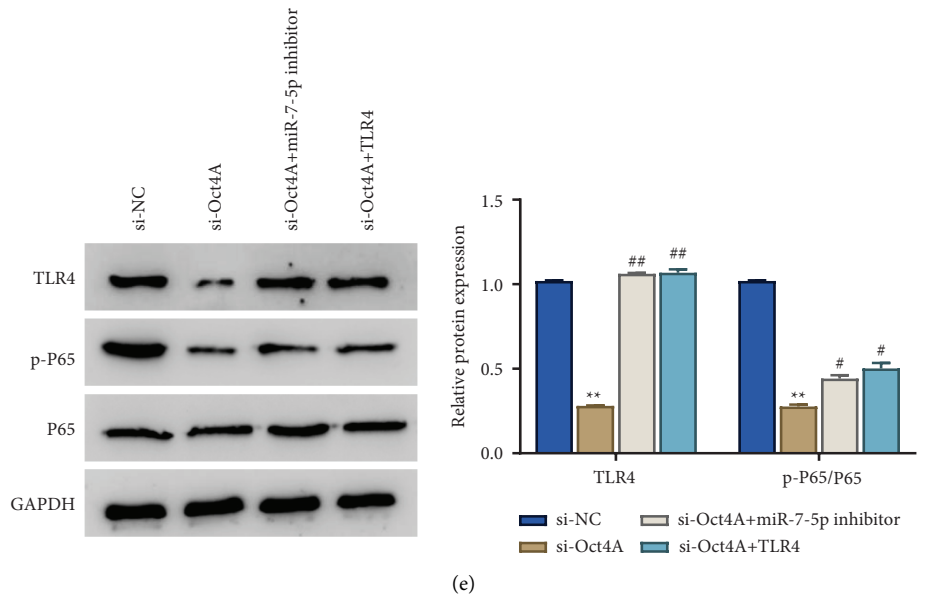

(e)

Figure 4: Roles of Otc4A, miR-7-5p, and TLR4 in colorectal cancer. (a) CCK-8 was adopted to detect the proliferation rate of cells; (b) cell cloning assay to confirm the viability of cells; (c) Transwell assay to detect the invasion ability of cells; scale bar = 50 μm. (d) Sphere-forming assay to observe the sphere-forming ability of cells; scale bar = 100 μm. (e) Western blot to detect the expression level of TLR4, p65, and p-p65 in cells. $^{**}P < 0.01$*vs.* the si-NC group; $^{\#}P < 0.05$, $^{\#\#}P < 0.01$*vs.* the si-Otc4A group. Each experiment was performed in triplicate.

differentiation, and apoptosis of tumor cells; and miR-7 also affects tumor growth, invasion, and metastasis [25]. Besides, MiR-7 can target p21-activated kinase 1, epidermal growth factor receptor, and insulin receptor substrate 1 to influence biological processes like proliferation, migration, apoptosis, and cell cycle of tumor cells in CRC by targeting [26]. Giles et al. [27] also came to the conclusion that miR-7-5p had the ability to inactivate the NF-κB pathway to suppress the growth and metastasis of melanoma, which suggests that miR-7-5p has the potential to be a treatment target for melanoma. Till now, however, there have been few studies on the connection between miR-7-5p and CRC. The membrane receptor TLR4 is closely related to intracellular inflammation and immune response. To be specific, when TLR4 is activated, MyD88 is urged to recruit the TIR domain of TLR4; then, the degradation of IκBα and the activation of NF-κB are induced; the transcription of proinflammatory factor genes such as TNF-α, IL-6, and IL-1β is enhanced; and the synthesis and release of TNF-α, L-6, and IL-1β are correspondingly increased; then the increase in the contents of TNF-α, IL-6, and IL-1β further strengthens the activation of NF-κB, promotes the nuclear transfer of NF-κB, and then aggravates immune inflammation [28]. In this paper, Otc4A was found to be a negative regulator of miR-7-5p, and TLR4 was found to be a downstream mRNA of miR-7-5p. Moreover, through the miR-7-5p/TLR4 axis, Otc4A regulated the proliferation, invasion, cell stemness, as well as NF-κB signaling of HT29 cells. The above results suggested that Otc4A is significant in promoting the malignant biological behavior of HT29 cells, and its mechanism may be achieved by preventing the miR-7-5p/TLR4 axis from activating the NF-κB signaling pathway.

In this study, it was found that the transcription factor Otc4A can regulate the level of TLR4 by inhibiting the expression of miR-7-5p and then promoting the proliferation and invasion of CRC cell HT29 and enhancing cell stemness. However, there are still some limitations to this study: First, we only conducted in vitro experiments, lacking evidence of in vivo experiments. We can collect patient samples and conduct further experiments in animals. Second, we did not further detect biomarkers of other stem cells. Finally, experiments were conducted on only one CRC cell line, and more cells could be used in the future.

5. Conclusion

Taken together, the cancer-promoting transcription factor Otc4A activates the NF-κB signaling pathway by reducing the regulatory effect of miR-7-5p on TLR4 level and then enhancing the proliferation, invasion, and cell stemness of CRC cells HT29. This study lays a solid experimental foundation for exploring biomarkers in the diagnosis and treatment of CRC.

Data Availability

The datasets used and/or analyzed during the current study are available from the corresponding author on reasonable request.

Conflicts of Interest

The authors declare that they have no conflicts of interest.

Authors' Contributions

Jinsong He and Shoujiang Wei were responsible for the conception or design of the work. Liang Duan and Yu Xie collected the data and wrote the manuscript. All the authors read and approved the final manuscript.

Acknowledgments

This work was supported by the Special fund for Science and Technology Strategic Cooperation of Nanchong Municipal Schools (20SXQT0151).

References

[1] L. A. Torre, F. Bray, R. L. Siegel, J. Ferlay, J. Lortet-Tieulent, and A. Jemal, "Global cancer statistics, 2012," *CA: A Cancer Journal for Clinicians*, vol. 65, no. 2, pp. 87–108, 2015.

[2] G. A. Calin, C. Sevignani, C. D. Dumitru et al., "Human microRNA genes are frequently located at fragile sites and genomic regions involved in cancers," *Proceedings of the National Academy of Sciences of the USA*, vol. 101, no. 9, pp. 2999–3004, 2004.

[3] R. Siegel, D. Naishadham, and A. Jemal, "Cancer statistics, 2012," *CA: A Cancer Journal for Clinicians*, vol. 62, no. 1, pp. 10–29, 2012.

[4] J. U. Marquardt, K. Fischer, K. Baus et al., "Sirtuin-6-dependent genetic and epigenetic alterations are associated with poor clinical outcome in hepatocellular carcinoma patients," *Hepatology*, vol. 58, no. 3, pp. 1054–1064, 2013.

[5] I. H. Park, R. Zhao, J. A. West et al., "Reprogramming of human somatic cells to pluripotency with defined factors," *Nature*, vol. 451, no. 7175, pp. 141–146, 2008.

[6] P. Wang, D. R. Branch, M. Bali, G. A. Schultz, P. E. Goss, and T. Jin, "The POU homeodomain protein OCT3 as a potential transcriptional activator for fibroblast growth factor-4 (FGF-4) in human breast cancer cells," *Biochemical Journal*, vol. 375, no. 1, pp. 199–205, 2003.

[7] Y. Atlasi, S. J. Mowla, S. A. Ziaee, and A. R. Bahrami, "OCT-4, an embryonic stem cell marker, is highly expressed in bladder cancer," *International Journal of Cancer*, vol. 120, no. 7, pp. 1598–1602, 2007.

[8] J. Shi, W. Shi, L. Ni et al., "OCT4 is epigenetically regulated by DNA hypomethylation of promoter and exon in primary gliomas," *Oncology Reports*, vol. 30, no. 1, pp. 201–206, 2013.

[9] C. J. Chang, Y. Chien, K. H. Lu et al., "Oct4-related cytokine effects regulate tumorigenic properties of colorectal cancer cells," *Biochemical and Biophysical Research Communications*, vol. 415, no. 2, pp. 245–251, 2011.

[10] T. A. Farazi, J. I. Spitzer, P. Morozov, and T. Tuschl, "miRNAs in human cancer," *The Journal of Pathology*, vol. 223, no. 2, pp. 102–115, 2011.

[11] D. P. Bartel, "MicroRNAs: genomics, biogenesis, mechanism, and function," *Cell*, vol. 116, no. 2, pp. 281–297, 2004.

[12] R. Rupaimoole and F. J. Slack, "MicroRNA therapeutics: towards a new era for the management of cancer and other diseases," *Nature Reviews Drug Discovery*, vol. 16, no. 3, pp. 203–222, 2017.

[13] M. Florczuk, A. Szpechcinski, and J. Chorostowska-Wynimko, "miRNAs as biomarkers and therapeutic targets in non-small cell lung cancer: current perspectives," *Targeted Oncology*, vol. 12, no. 2, pp. 179–200, 2017.

[14] M. Dong, Y. Xie, and Y. Xu, "miR-7-5p regulates the proliferation and migration of colorectal cancer cells by negatively regulating the expression of Kruppel-like factor 4," *Oncology Letters*, vol. 17, no. 3, pp. 3241–3246, 2019.

[15] A. L. Oberg, A. J. French, A. L. Sarver et al., "miRNA expression in colon polyps provides evidence for a multihit model of colon cancer," *PLoS One*, vol. 6, no. 6, Article ID e20465, 2011.

[16] F. Zhu, C. Cheng, H. Qin, H. Wang, and H. Yu, "A novel circular RNA circENTPD7 contributes to glioblastoma progression by targeting ROS1," *Cancer Cell International*, vol. 20, no. 1, p. 118, 2020.

[17] J. Ferlay, H. R. Shin, F. Bray, D. Forman, C. Mathers, and D. M. Parkin, "Estimates of worldwide burden of cancer in 2008: GLOBOCAN 2008," *International Journal of Cancer*, vol. 127, no. 12, pp. 2893–2917, 2010.

[18] S. Esmailzadeh, B. Mansoori, A. Mohammadi, D. Shanehbandi, and B. Baradaran, "siRNA-mediated silencing of HMGA2 induces apoptosis and cell cycle arrest in human colorectal carcinoma," *Journal of Gastrointestinal Cancer*, vol. 48, no. 2, pp. 156–163, 2017.

[19] X. Q. Wang, W. M. Ongkeko, L. Chen et al., "Octamer 4 (Oct4) mediates chemotherapeutic drug resistance in liver cancer cells through a potential Oct4-AKT-ATP-binding cassette G2 pathway," *Hepatology*, vol. 52, no. 2, pp. 528–539, 2010.

[20] S. Saigusa, K. Tanaka, Y. Toiyama et al., "Correlation of CD133, OCT4, and SOX2 in rectal cancer and their association with distant recurrence after chemoradiotherapy," *Annals of Surgical Oncology*, vol. 16, no. 12, pp. 3488–3498, 2009.

[21] W. Fang, M. Ni, M. Zhang, and H. Chen, "Prognostic value of OCT4 in colorectal cancer: analysis using immunohistochemistry and bioinformatics validation," *Biomarkers in Medicine*, vol. 14, no. 15, pp. 1473–1484, 2020.

[22] Z. Ren, L. Wang, J. Cui et al., "Resveratrol inhibits NF-kB signaling through suppression of p65 and IkappaB kinase activities," *Pharmazie*, vol. 68, no. 8, pp. 689–694, 2013.

[23] R. R. Rasmi, K. M. Sakthivel, and C. Guruvayoorappan, "NF-κB inhibitors in treatment and prevention of lung cancer," *Biomedicine & Pharmacotherapy*, vol. 130, Article ID 110569, 2020.

[24] Y. Zhang, M. Li, Y. Ding et al., "Serum MicroRNA profile in patients with colon adenomas or cancer," *BMC Medical Genomics*, vol. 10, no. 1, p. 23, 2017.

[25] L. Xu, M. Zhang, X. Zheng, P. Yi, C. Lan, and M. Xu, "The circular RNA ciRS-7 (Cdr1as) acts as a risk factor of hepatic microvascular invasion in hepatocellular carcinoma," *Journal of Cancer Research and Clinical Oncology*, vol. 143, no. 1, pp. 17–27, 2017.

[26] Y. Nagano, Y. Toiyama, Y. Okugawa et al., "MicroRNA-7 is associated with malignant potential and poor prognosis in human colorectal cancer," *Anticancer Research*, vol. 36, no. 12, pp. 6521–6526, 2016.

[27] A. Mohammadi, B. Mansoori, and B. Baradaran, "The role of microRNAs in colorectal cancer," *Biomedicine & Pharmacotherapy*, vol. 84, pp. 705–713, 2016.

[28] J. Wang, S. M. Fan, and J. Zhang, "Epigallocatechin-3-gallate ameliorates lipopolysaccharide-induced acute lung injury by suppression of TLR4/NF-κB signaling activation," *Brazilian Journal of Medical and Biological Research*, vol. 52, no. 7, Article ID e8092, 2019.

Hindawi
Evidence-Based Complementary and Alternative Medicine
Volume 2023, Article ID 9795740, 1 page
https://doi.org/10.1155/2023/9795740

Retraction

Retracted: Traditional Chinese Medicine Based Acupoint Application for Asthma Treatment in Children: A Meta-Analysis and Systematic Review

Evidence-Based Complementary and Alternative Medicine

Received 3 October 2023; Accepted 3 October 2023; Published 4 October 2023

This article has been retracted by Hindawi following an investigation undertaken by the publisher [1]. This investigation has uncovered evidence of one or more of the following indicators of systematic manipulation of the publication process:

(1) Discrepancies in scope

(2) Discrepancies in the description of the research reported

(3) Discrepancies between the availability of data and the research described

(4) Inappropriate citations

(5) Incoherent, meaningless and/or irrelevant content included in the article

(6) Peer-review manipulation

The presence of these indicators undermines our confidence in the integrity of the article's content and we cannot, therefore, vouch for its reliability. Please note that this notice is intended solely to alert readers that the content of this article is unreliable. We have not investigated whether authors were aware of or involved in the systematic manipulation of the publication process.

Wiley and Hindawi regrets that the usual quality checks did not identify these issues before publication and have since put additional measures in place to safeguard research integrity.

We wish to credit our own Research Integrity and Research Publishing teams and anonymous and named external researchers and research integrity experts for contributing to this investigation.

The corresponding author, as the representative of all authors, has been given the opportunity to register their agreement or disagreement to this retraction. We have kept a record of any response received.

References

[1] Y. Wang, T. Guo, F. Yang et al., "Traditional Chinese Medicine Based Acupoint Application for Asthma Treatment in Children: A Meta-Analysis and Systematic Review," *Evidence-Based Complementary and Alternative Medicine*, vol. 2022, Article ID 7500056, 15 pages, 2022.

Hindawi
Evidence-Based Complementary and Alternative Medicine
Volume 2022, Article ID 7500056, 15 pages
https://doi.org/10.1155/2022/7500056

Review Article

Traditional Chinese Medicine Based Acupoint Application for Asthma Treatment in Children: A Meta-Analysis and Systematic Review

Yijie Wang,[1] Tingting Guo,[2] Fushuang Yang,[2] Yongjun Li,[1] Lujia Liu,[1] Kexin Lin,[1] Zhijun Li,[3] and Youpeng Wang[3]

[1]*Heilongjiang University of Chinese Medicine, Harbin 150040, China*
[2]*Changchun University of Chinese Medicine, Changchun 130117, China*
[3]*The Second Affiliated Hospital of Heilongjiang University of Chinese Medicine, Harbin 150009, China*

Correspondence should be addressed to Youpeng Wang; wangyp8899@163.com

Received 22 July 2022; Revised 2 September 2022; Accepted 5 September 2022; Published 26 September 2022

Academic Editor: Xueliang Wu

Objective. By conducting a systematic review of the efficacy of acupoint application on children with asthma. *Methods*. We searched Chinese databases (CNKI, VIP, and Wanfang) and English databases (PubMed, Embase, and Cochrane Library) for studies from the establishment of the database to October 2021. The included literature studies were randomized control studies investigating the treatment of asthma in children by acupoint application. The primary outcomes included the cure rate, the resolution time of cough, and the resolution time of wheezing. The secondary outcomes included pulmonary function and interleukins. Stata 15 and RevMan 5.4 were used to analyze the extracted data. *Results*. A total of 24 related studies were included containing 2716 cases. The meta-analysis showed that TCM group was superior to control group in terms of cure rate, pulmonary function (FEV1), and resolution time of wheezing in children with asthma [RR = 1.26,95% (1.21,1.31), $P < 0.05$; SMD = 0.81, 95% CI (0.05,1.56), $P < 0.05$; WMD = −1.40, 95%CI (−1.75, −1.05), $P < 0.05$]. *Conclusions*. The present study shows that acupoint application is an effective treatment for children with asthma in China, especially in alleviating wheezing and improving quality of life.

1. Introduction

Asthma is a chronic and refractory disease that affects the quality of human life globally. This chronic inflammation is mainly related to airway hyper-responsiveness and reversible airflow limitation, which causes symptoms such as recurrent wheezing, shortness of breath, chest tightness, and cough [1]. In recent years, the incidence of asthma was increasing year by year. At present, there are about 334 million children with asthma in the world and 30 million children with asthma in China [2, 3]. Respiratory symptoms in children aged 5 to 16 years lack specificity, and they could develop asthma-like symptoms which may be caused by respiratory virus infection or prolonged disease course [4]. This results in overdiagnosis and abuse of adrenal cortical hormones (hormones), which make children and their families bear unnecessary costs and adverse reactions [5]; traditional Chinese medicine has a good clinical effect on children with asthma with low recurrence rate and side effects.

Asthma is a refractory disease with high rates of recurrence [6]. Therefore, the treatment principle of this disease in clinical practice basically aims to control the disease progression. Inhaled glucocorticoids, long-actingβ2-receptor agonists (LABA), and leukotriene receptor antagonists are the main controller medications. Short-actingβ2 receptor agonists (SABA) and inhaled anticholinergic drugs are the main relief drugs [7]. Acupoint application of traditional Chinese medicine has a long history. Acupoint application treatment is based on syndrome differentiation

and treatment; transdermal drug delivery can avoid the first pass effect of gastrointestinal digestive fluid and the liver and also avoid the "peak-valley phenomenon". In addition, the interlayer of skin tissue structure has storage capacity, which can make the blood concentration curve of drugs entering human tissues gentle and lasting. Previous studies reported that acupoint application could be used to treat childhood bronchial asthma, and the effective rate could reach 100% [8]. According to the theory of acupoint application, the mechanisms of asthma include acute airway obstruction and inversion of lung Qi which are mainly caused by long-term phlegm retention in the lungs and further aggravated by emotions, diet, fatigue, and physical weakness. Some studies believed that the pathogenesis of childhood bronchial asthma is retaining phlegm, which is directly related with the dysfunction of the liver, spleen, and kidneys. Exogenous lung wind, improper diet, and blockage of chest yang can contribute to asthma [9, 10]. However, the efficacy of acupoint application of traditional Chinese medicine in the treatment of childhood asthma is still unclear. Thus, a meta-analysis was conducted to compare the efficacy of acupoint application in the treatment of childhood asthma.

2. Materials and Methods

This meta-analysis was conducted in accordance with the Preferred Reporting Items for Systematic Reviews and meta-analysis (PRISMA) statement [11]. Scientific databases (PubMed, Embase, Web of Science, Cochrane Library, CBM, CNKI, and Wanfang) were comprehensively searched to identify relevant literature studies without language restriction. Relevant keywords, medical terms, and titles include acupoint application, children, asthma, and randomized controlled trials. The search results included original research papers published in online journals as of October 29, 2021, Specific search method, Supplementary material 1.

2.1. Inclusion and Exclusion Criteria. According to the aims of the study, the inclusion criteria were as follows: (1) the included population should meet the diagnostic criteria for asthma, (2) age <15 years old, (3) acupoint application intervention is the main therapeutic approach, (4) randomized controlled trials, and (5) complete original data.

Exclusion criteria were as follows: (1) conference abstracts and systematic reviews, (2) repeated publications, (3) animal experiments or nonclinical experiments, (4) articles with unreasonable experimental design, and (5) full text was not available.

2.2. Data Extraction. The following data were extracted from each eligible study: first author, country, subjects, number of participants, sex, age, intervention, comparator, treatment stage, treatment duration, follow-up time, lung function, cure rate, the resolution time of wheezing, serum IgE, and other related data. To ensure the quality of the meta-analysis, all eligible articles were independently reviewed and cross-checked by 2 researchers according to standardized methods. If there was any dissent, another reviewer was consulted. A consensus was reached on the selection of the final included studies.

2.3. Risk of Bias Assessment. Cochrane risk of bias tool was used to evaluate the risk of bias of each studies containing RCT and the following factors were taken into account: random sequence generation, allocation concealment, blinding of participants and researchers, blinding of outcome assessments, incomplete outcome data, selective reports of outcomes, and other sources of bias. The risk of bias in each aspect was scored as low, high, or unclear risk [12].

2.4. Statistical Analysis. Stata/SE12.0 software was used in this meta-analysis. The pooled enumeration data were expressed as relative risk (RR) and 95% confidence interval (CI). The pooled continuous variables were expressed as mean standard deviation (MD) and 95% CI operation. $P < 0.05$ was used as the standard to determine the difference to be statistically significant. Q-test (P-value) and chi-square test (I2) were used to determine the heterogeneity. The heterogeneity was considered not significant if $P \geq 0.1$ and $I2 \leq 50\%$, and the fixed-effects model was used to pool the data. Otherwise, the random-effects model was used to pool the data. The subgroup analysis was used to determine the source of the heterogeneity. Egger's test was performed to evaluate the publication bias, and $P > 0.05$ indicated that there was no publication bias; otherwise, publication bias existed.

3. Results

3.1. Literature Search and Screening. A total of 895 articles were initially retrieved. 563 articles were selected after removing duplicated publication. 464 articles were removed by reading the title and abstract. After reading the full text, 75 articles were removed due to incomplete results, unavailable data, and low quality of the literature, and 24 articles were finally involved in this analysis [13–34] with a total of 2716 patients. The flow chart of literature search is shown in Figure 1.

3.2. Basic Characteristics and Quality Evaluation of the Included Literature. The 24 literature studies included in this analysis were all randomized controlled studies published in Chinese. A total of 2716 subjects were included, among which 1384 subjects were in the experimental group and 1332 in the control group. The detailed characteristics of the literature are shown in Table 1. The plot for risk of bias is shown in Figure 2.

3.3. Meta-Analysis Results

3.3.1. Cure Rate. There were 18 studies [13–17, 19–23, 26, 27, 29–32, 35, 36] mentioning the cure rate of the two groups which was expressed as dichotomous variables. The treatment stage was used for subgroup

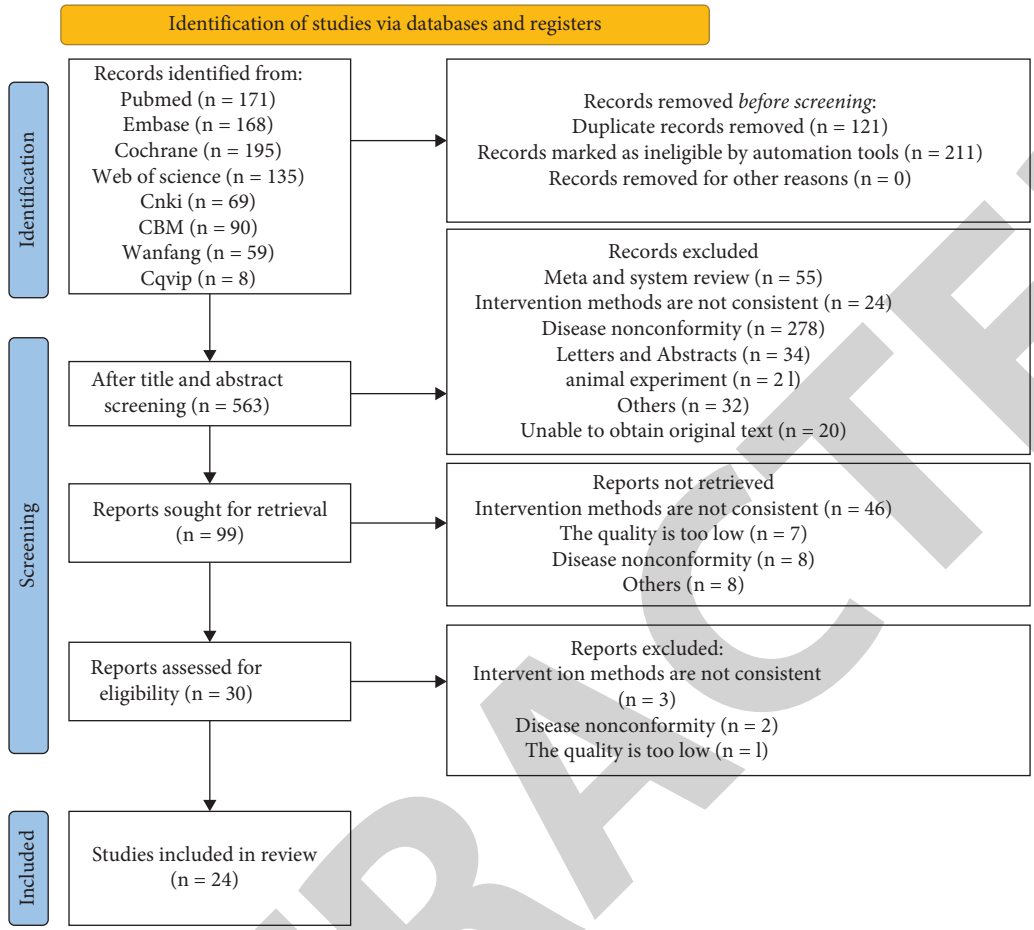

Figure 1: Results of literature screening and the process.

analysis. The fixed-effects model was employed (I2 = 48.1%, $P = 0.012$), and the pooled results showed that there was a statistically significant difference between the two groups [RR = 1.26, 95% (1.21, 1.31), $P < 0.05$]. The meta-analysis results presented that the effect of acupoint application was significantly superior to that of the control group in treating childhood asthma (Figure 3(a)).

A funnel plot was used to directly visualize publication bias, and Egger's and Begg's tests were used to analyze the funnel plot. The results of Egger's and Begg's test showed no significant difference ($P < 0.05$). Additionally, the results of sensitivity analysis showed that after excluding the study one by one, there was no significant change in effect size (Figures 3(b), 3)(c).

3.3.2. Pulmonary Function (FEV1). In the included articles, 8 studies [15–17, 22, 24, 28, 29, 33] mentioned FEV1-related indicators, which were presented as continuous variables. The random-effects model (I2 = 96.7%, $P = 0$) was used to pool the effect size, and the pooled results showed that the difference between the two groups was statistically significant [SMD = 0.81, 95%CI (0.05, 1.56), $P < 0.05$]. The meta-analysis results presented that the effect of acupoint application was significantly superior to that of the control group in improving pulmonary function (Figure 4(a)).

A funnel plot was used to directly visualize publication bias, and Egger 's and Begg 's tests were used to analyze the funnel plot. The results of Egger 's and Begg 's test showed no significant difference ($P < 0.05$). Additionally, the results of sensitivity analysis showed that after excluding the study one by one, there was no significant change in effect size (Figures 4(b), 4(c)).

3.4. Function (FEV1)

3.4.1. The Resolution Time of Wheezing. A total of 4 papers [13,22,28,33] reported the resolution time of wheezing, which was presented as a continuous variable. The random-effects model (I2 = 85.8%, $P = 0$) was used to pool the effect size. The pooled results showed that the difference between the two groups was statistically significant [WMD = −1.40, 95%CI (−1.75, −1.05), $P < 0.05$]. The meta-analysis results presented that the effect of acupoint application was significantly superior to that of the control group in improving asthma symptoms in children (Figure 5(a)). Sensitivity analysis showed that there was no significant change in effect size after removing the studies one by one (Figure 5(b)).

3.4.2. Serum IgE Level. A total of 4 studies [13, 17, 26, 35] reported serum IgE level which was expressed as continuous variables. The random-effects model (I 2 = 99.1%, $P = 0$) was

Table 1: Basic information of the included literature.

Number	Year	Author	Journal	Study type	Country	Intervention		Case		Age(mean ± sd)		Gender (male/female)		Stage	Period of treatment	Follow-up time
						Treatment group	Control group	Treatment group	Control group	Treatment group (year)	Control group (year)	Treatment group	Control group			
1	2009 [19]	Guo Juzhen	Journal of Sichuan of Acupoint Application	RCT	China	Inhalation of pumice aerosol, combined with acupoint application acupoint external application treatment	Just inhale pumice aerosol	40	32	—	—	23/17	18/14	—	30 days	3 to 6 months
2	2009 [20]	HE Wei	Chin Pediatr Integr Tradit West Med	RCT	China	Based on the treatment of relieving spasmolysis and relieving asthma, intermediate frequency drugs were added to the acupoint for treatment	Treatment of spasmolysis and asthma	60	60	—	—	40/20	46/14	Attack	3 days	—
3	2010 [21]	HU Aie	China Modern Doctor	RCT	China	The aerosol inhalation of Pulmicort in acute episode of asthma and the Chinese herbal acupoint application in its remission period were given to the treatment group	The aerosol inhalation of Pulmicort in acute episode of asthma was given to the control group	50	50	2.4	1.9	30/20	31/19	Duration and remission	3 years	—
4	2011 [26]	SHI Danmei	Clinical Journal of Chinese Medicine	RCT	China	Inhalation budesonide suspension + albuterol atomization solution + inhalation ipratropium bromide atomization, plus Chinese medicine acupoint application	Inhalation budesonide suspension + albuterol atomization solution + ipratropium bromide atomization solution for inhalation treatment	154	150	—	—	73/81	67/83	-	7 days	—
5	2010 [25]	Shi Pinying	Journal of Acupoint Application	RCT	China	On the basis of inhaling seretide for 6 months, Wu's blistering plaster for acupoint application was applied in dog-days	Treated with seretide inhalation 50 μg/100μ	40	40	7.9 ± 1.5	8.2 ± 1.9	23/17	24/16	In remission stage	6 months	—
6	2011 [32]	Zhang Xiuying	J. Pediatrics of TCM	RCT	China	Fu Jiu sticking therapy was administered in combination with beclomethasone dipropionate aerosol or budesonide inhalation powder	Treated with beclomethasone dipropionate aerosol or budesonide inhalation powder	60	60	—	—	38/22	39/21	In remission stage	3 years	—
7	2012 [15]	Deng Yuping	Hubei Journal of TCM Aug	RCT	China	On the basis of the treatment with inhalation of seretide powder, the treatment of winter disease in summer was added. On the first day of Tou Fu, Erfu, and Sanfu in summer every year, Sanfu acupoint application of cough and asthma was given	Treatment with inhalation seretide powder was given	80	80	7.59 ± 3.31	7.86 ± 2.95	48/32	45/35	In remission stage	1 year	—-
8	2012 [24]	Luo Jing-yan	Tianjin Med J	RCT	China	According to GINA regimen, inhaled glucocorticoid-based stepwise treatment was given, and inhaled budesonide aerosol was selected, on this basis, siji ointment was applied at point 2	Inhaled glucocorticoid-based step therapy was administered according to the GINA protocol, using budesonide aerosol inhalation	75	51	6.5 ± 1.3	6.4 ± 1.4	43/32	27/24	Duration	6 weeks	6 months
9	2012 [25]	Luo Jing-yan	Tianjin Journal of Acupoint Application	RCT	China	Inhaled glucocorticoid-based step therapy was administered according to the GINA protocol, using budesonide aerosol inhalation	Inhaled glucocorticoid-based step therapy was administered according to the GINA protocol, using budesonide aerosol inhalation	56	42	8.74 ± 1.64	8.61 ± 1.57	33/23	25/17	Duration	Once every 7=10 days, 6 times as a course of treatment	6 months
10	2012 [29]	Wu Fang	China Journal of Chinese Materia Medica	RCT	China	Xiaochuangao acupoint paste combined with fluticasone propionate aerosol	Inhale fluticasone propionate aerosol	30	30	7.6 ± 2.4	7.9 ± 2.5	15/15	16/14	In remission stage	1 year	1 year
11	2015 [34]	Zhao Juan	Clinical Journal of Acupoint Application	RCT	China	In addition to the routine use of glucocorticoid inhalation, observation group (20 cases) dog days into the volt is given selfmade acupoint application paste acupoint sticking	Used conventional glucocorticoid inhalation therapy	20	20	—	—	—	—	In remission stage	1 year	1 year

Table 1: Continued.

Number	Year	Author	Journal	Study type	Country	Intervention		Case		Age(mean ± sd)		Gender (male/female)		Stage	Period of treatment	Follow-up time
						Treatment group	Control group	Treatment group	Control group	Treatment group (year)	Control group (year)	Treatment group	Control group			
12	2016 [17]	Fang Junmei		RCT	China	On the basis of inhaling budesonide at less than 5 years old and inhaling sulide at more than 5 years old, combined with point mounting method during the dog and coldest days	Younger than 5 years, inhaled budesonide, older than 5 years, inhaled seretide	160	160	2.5-12	1.5-13	92/68	89/71	Duration	1 year	—
13	2017 [18]	Gu Hongdan	Chinese Archives of acupoint application	RCT	China	Treated with Xiao Chuan paste acupoint application combined with fluticasone propionate aerosol	Inhale fluticasone propionate aerosol	50	50	9.73 ± 2.42	9.65 ± 2.52	28/22	26/24	In remission stage	1 year	1 year
14	2017 [23]	Li Guiying	Journal of Clinic Nursing's practicality	RCT	China	Albuterol atomized inhalation combined with magnetic patch (acupoint application therapy) treatment	Treated with aerosol inhalation of salbutamol	40	40	—	—	—	—	—	30 days	—
15	2011 [25]	Shen Yi-yun	Guiding Journal of Acupoint Application and Pharmacology	RCT	China	On the basis of atomizing inhalation of Pulmicort, Bricanyl, and ipratropium bromide, acupoint sticking therapy with clearing heat stick combined with iontophoresis technology was given	Treated with Pulmicort, Bricanyl, and ipratropium bromide inhalation	60	60	6.53 ± 3.34	6.53 ± 2.09	31/29	28/32	Attack	5 days	—
16	2017 [28]	Shu Yifang	Journal of Clinical Medicine in Practice	RCT	China	Treated with the combination of budesonide and acupoint application with Chinese herbal medicine	Treated with budesonide atomization inhalation	40	40	9.1 ± 0.7	9.5 ± 0.5	19/21	24/16	—	36 days	—
17	2017 [35]	Zhou Fang	Chinese Journal of Traditional Medical Science and Technology	RCT	China	On the basis of inhaling pumice aerosol, wenyang Qucold paste was applied at summer acupoint	Give pumice aerosol inhalation	44	42	—	—	—	—	In remission stage	Three volts a course of treatment	—
18	2018 [36]	Zhao Meili	Guangxi Journal of Acupoint Application	RCT	China	Fluticasone propionate aerosol combined with acupoint application treatment, "relieving asthma cough external application powder"	Inhale fluticasone propionate aerosol	50	50	10.23 ± 2.85	9.66 ± 2.93	25/25	20/30	In remission stage	The experimental group was treated for 4 weeks as a course of treatment, the control group was treated for 10 days as a course of treatment, and the control group was treated with 4 times of application as a course of treatment	—
19	2020 [16]	Fan Xiaoni	Contemporary Medical Symposium	RCT	China	Salbutamol combined with acupoint stimulation was used for treatment	Treated with aerosol inhalation of salbutamol	40	40	4.57 ± 0.45	4.85 ± 0.46	23/17	22/18	Attack	2 weeks	—
20	2020 [33]	Zhao Baoling	Inner Mongolia Med J	RCT	China	Budesonide inhalation atomization treatment combined with "winter disease treatment in summer" three Fu stickers	Treated with budesonide atomization inhalation	49	49	9.33 ± 1.84	9.19 ± 1.73	24/25	26/23	—	36 days	—
21	2021 [22]	Le Lijun	Journal of Hubei Polytechnic University	RCT	China	Treated with acupoint application combined with budesonide atomization inhalation and symptomatic treatment	Treated with budesonide atomization inhalation	48	48	4.74 ± 2.87	4.34 ± 2.18	25/23	23/25	—	A course of treatment was given every week for 2 weeks	—
22	2021 [30]	Xie Jianling	Selfcare	RCT	China	On the basis of drug atomization inhalation treatment, acupoint application of "Shuji Point" was given	Treated with drug atomization inhalation	50	50	6.5 ± 3.1	6.1 ± 3.0	26/24	28/22	Duration	3 weeks	—
23	2021 [31]	Yang Dongyan	Practical Clinical Journal of Integrated Traditional Chinese and Western Medicine	RCT	China	Routine inhalation of budesonide aerosol treatment and Chinese medicine treatment of winter disease summer acupoint application	Treated with budesonide atomization inhalation	38	38	7.28 ± 0.49	7.30 ± 0.51	—	—	In remission stage	3 months	—

Table 1: Continued.

Number	Year	Author	Journal	Study type	Country	Intervention		Case		Age(mean ± sd)		Gender (male/female)		Stage	Period of treatment	Follow-up time
						Treatment group	Control group	Treatment group	Control group	Treatment group (year)	Control group (year)	Treatment group	Control group			
24	2015 [14]	Chen Yan	Today Nurse	RCT	China	Add acupoint application on the basis of Singulair or sulfone sprays	Treatment was given with Singulair or sulfone sprays	50	50	—	—	27/23	24/26	In remission stage	3 summer	—

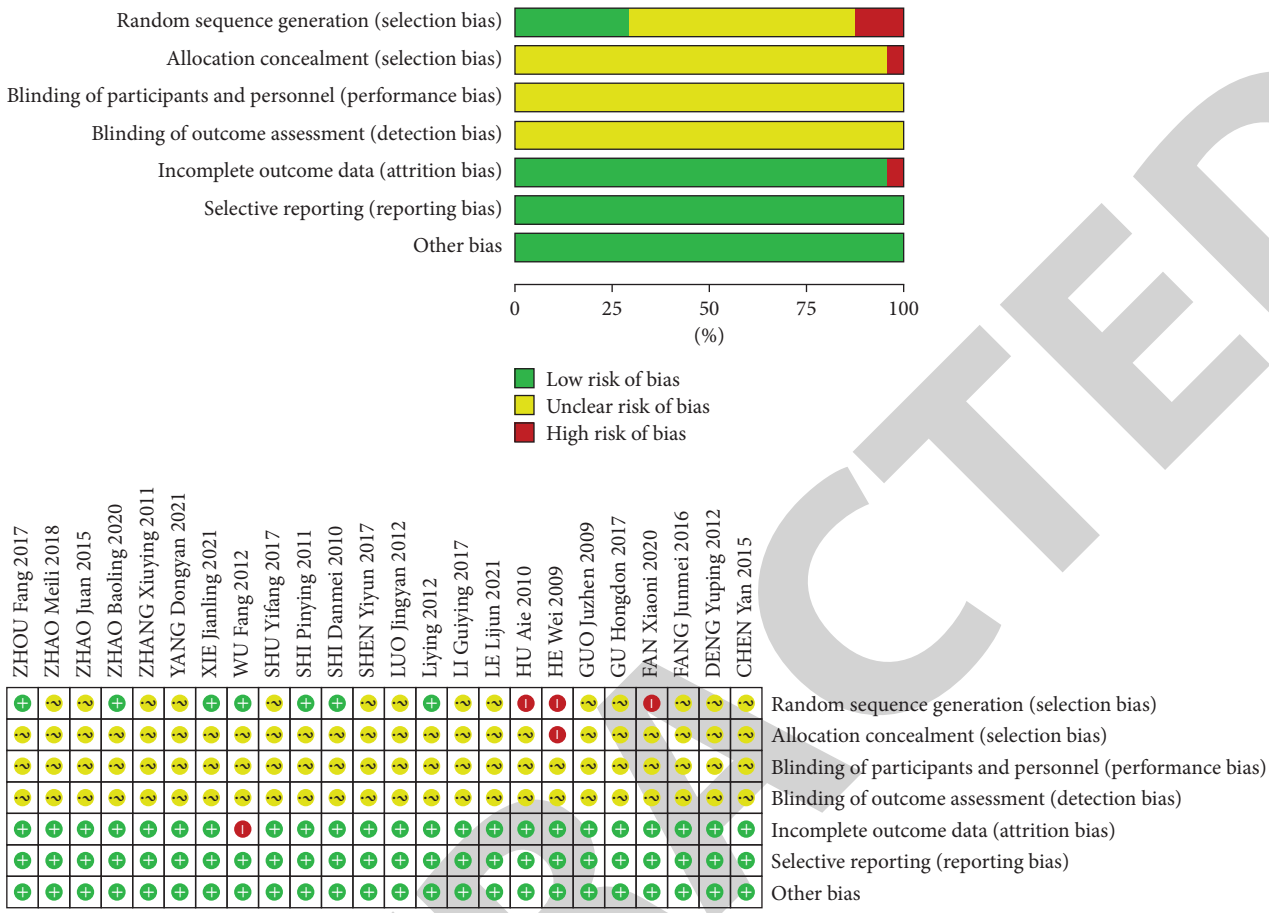

Figure 2: Risk of bias summary and graph.

used to pool the effect size. The pooled results showed that the difference between the two groups was not statistically significant [SMD = 1.39, 95%CI (−0.65, 3.44), $P < 0.05$]. The meta-analysis results demonstrated that there was no significant difference between the experimental group and the control group in the IgE level (Figure 6).

3.4.3. Occurrence of Asthma. A total of 4 [14, 31, 35, 37] studies reported the occurrence of asthma which were expressed as continuous variables. The random-effects model (I 2 = 98.2%, $P = 0$) was used to pool the effect size. The pooled results showed that the difference between the two groups was not statistically significant [SMD = −0.89, (−2.82, 1.04), $P > 0.05$]. The meta-analysis results demonstrated that there was no significant difference between the experimental group and the control group in the occurrence of asthma (Figure 7).

4. Discussion

With the improvement of medical conditions, increasing attention has been paid to the prevention and treatment of asthma. However, due to air pollution, changes in living and diet habits, and other factors [38], the incidence of childhood asthma has been increased. From the perspective of TCM, asthma belongs to the category of "wheezing disease" as termed by TCM. This concept was first mentioned in the "Huangdi Neijing". Wheezing disease is recurrent due to the failure in completely removing the etiological factor, subsequently aggravated by repeated exposure to exogenous pathogens [39]. Traditional Chinese medicine classifies asthma as "wind-cough" and "wheezing cough," and the treatment scheme adopts the principle of syndrome differentiation and treatment, treating both inside and outside. Li Yue Parallel Prose once said, "The reason of external governance is the reason of internal governance. Though it is treated externally, nothing can be treated internally." External treatment and internal treatment can complement and coordinate each other. Acupoint application has a long history in the external treatment of asthma. It can directly act on specific acupoints of the human body, and its multiple effects such as comprehensive drugs, acupoints, and meridians will direct the efficacy of the disease [39]. Based on the comprehensive analysis of the included literature studies, most of the basic drugs used for acupoint application were Chinese mustard seed, Asarum, Euphorbia kansui, and Rhizoma corydalis. White mustard has the function of warming lung and reducing phlegm. Relevant studies show that the efficacy of white mustard in adhesive can quickly penetrate into the skin and release stably [40]. Asarum pungent and warm, return to the heart, lung, and kidney

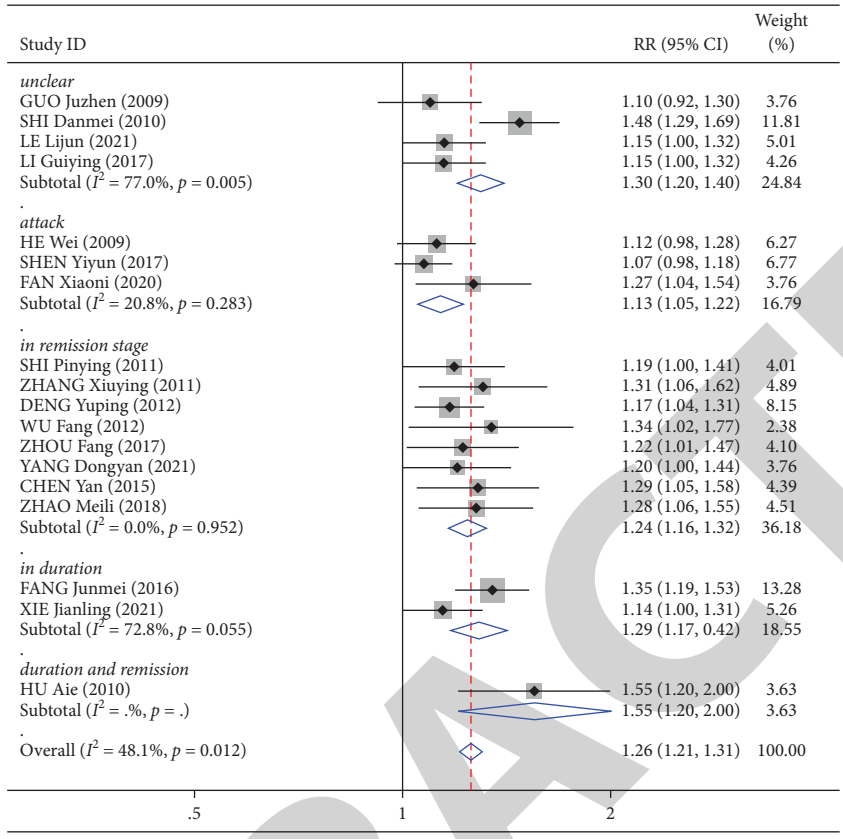

(a)

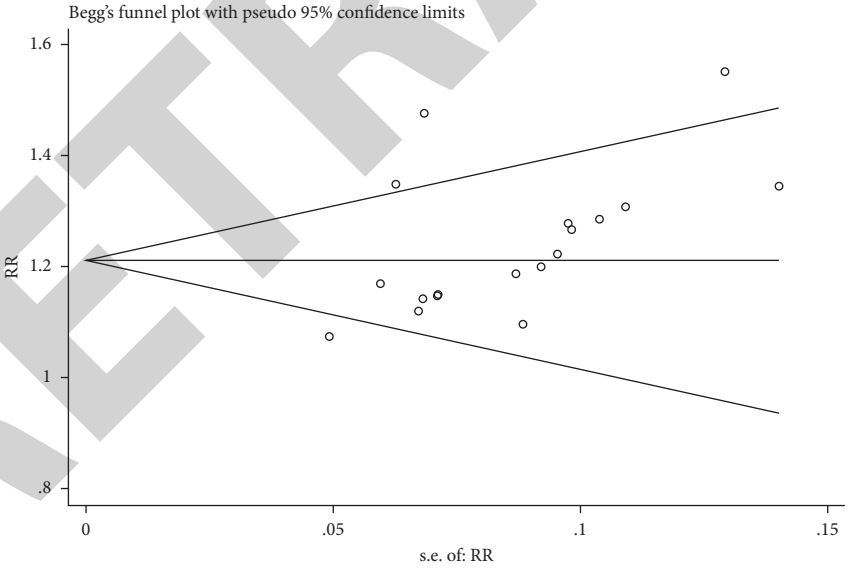

(b)

Figure 3: Continued.

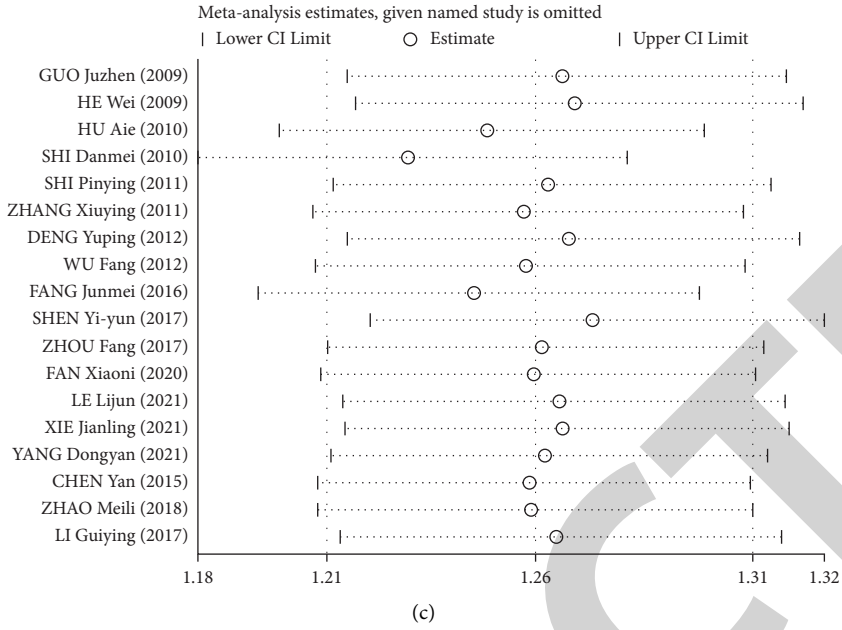

Figure 3: Forest plot, funnel plot, and sensitivity analysis of meta-analysis on cure rate.

meridian, has the effect of warming lung and hua Yin, etc. Asarum volatile oil can inhibit the release of inflammatory mediators, reduce histamine content, and fight against histamine or prostaglandin E caused by increased capillary permeability. Euphorbia kansui bitter cold, belongs to the lung, kidney, and spleen meridian, has the effect of purging water by drinking. Rhizoma corydalis tastes hard, warm, goes to the liver and stomach meridian, with qi, pain, blood circulation, and blood stasis [41]. The combination of the four herbs has the effect of relieving phlegm and benefiting qi, warming lung, and relieving cough. Acupoints are applied at the locations of lung acupoints, ding asthma acupoints, spleen deficiency, kidney deficiency, etc. The back acupoints are closely related to the sympathetic nerve. Stimulating acupoints can excite the sympathetic nerve, reduce the vagus nerve tension, and have the effect of relieving spasm and relieving cough [42].

The external therapy in acupoint application is an important approach to treat childhood asthma [43]. This therapy is easy to use, simple to operate, and good in compliance, showing a definite and rapid effect. Treatment is mainly based on acupoint application, pediatric massage, acupuncture, nasal drip of acupoint application, and fumigation and washing by using acupoint application. Among them, acupoint application is a common treatment method in pediatrics. Acupoint application can exert multiple effects in the treatment of asthma. The drug can not only be absorbed through the skin but can also promote the relaxation of bronchial smooth muscle, and thus dilate the bronchus and improve the symptoms of airway spasm. Meanwhile, through the special physiological amplification effect of the meridian points, it can exert anti-inflammatory effects, adjust the immune function of the body, improve blood circulation, and regulate the functions of the nerves, body fluids, and endocrine system, etc. Xunbin et al. [44] reported 111 cases and used acupoint application (Baijizi, Corydalis, Asarum, cinnamon, ginger juice, and starch) to conduct acupoint application on the specific points (Shuangfeishu, Shuangxinshu, Shuanggeshu, Shuangzusanli, Shuangfengmen, ShuangjueYinshu, Shuanggeshu, and Shuangpishu points). The results showed that the treatment was remarkably effective in 50 cases, effective in 7 cases, and ineffective in 2 cases, with a total effective rate of 96.1%. Yang Yafeng [45] treated childhood bronchial asthma by acupoint application, and the total effective rate was 92.5% after 1 year. It showed that the adjuvant therapy of acupoint application was also rather important in acute asthma attack. For children treated with Western medicine alone, the effective rate was 84.5%. The effective rate reached 97.9% after a combined use with acupoint application treatment. Acupoint application exerts a satisfactory auxiliary effect on the treatment of childhood bronchial asthma, which improves the clinical efficacy. This method is easy to operate in clinical practice, and it is safe and reliable for children to use without pain.

This study had several limitations. First, although we attempted to address heterogeneity through subgroup and sensitivity analyses, the heterogeneity in statistics and clinical data might raise doubts about the validity of this study. The heterogeneity of the study population made it challenging to prove that the results were meaningful. Second, the sample size was small, and the occurrence of asthma was low in many included studies with low quality. Third, the source of the research object is single. Thus, the uncertainty in the analysis was increased. The RCT methods in the included studies were generally poor since most risk items were unclear, especially the allocation concealment, blindness, and selective outcome reporting. This limitation might reduce the credibility of our conclusions.

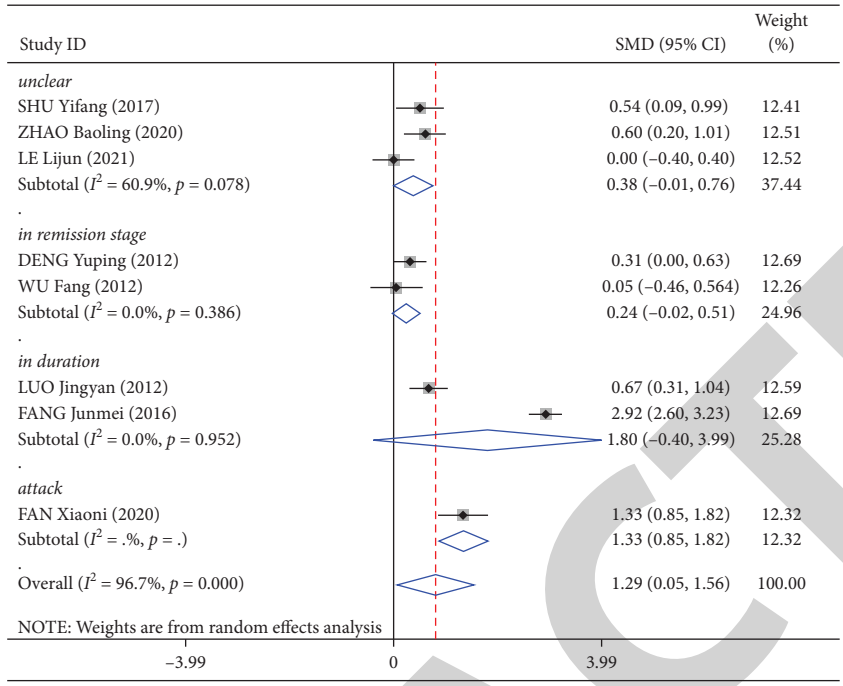

(a)

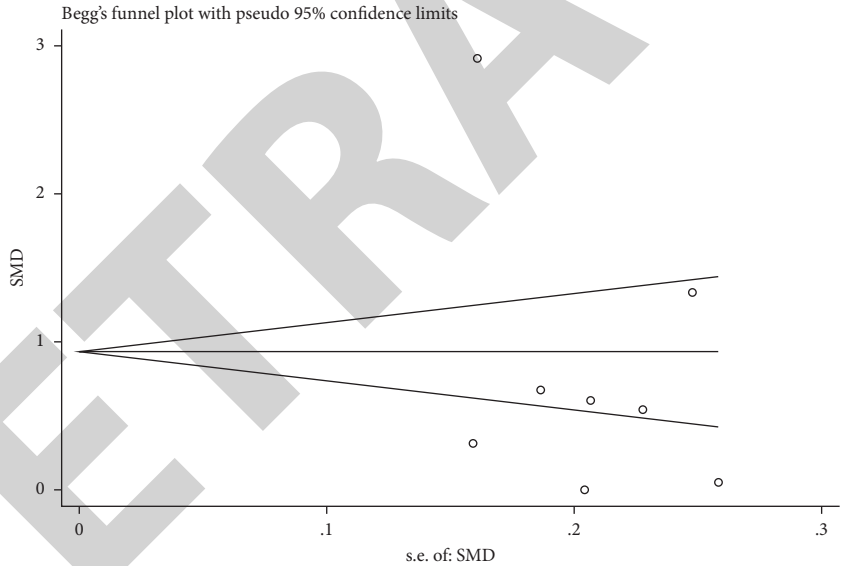

(b)

Figure 4: Continued.

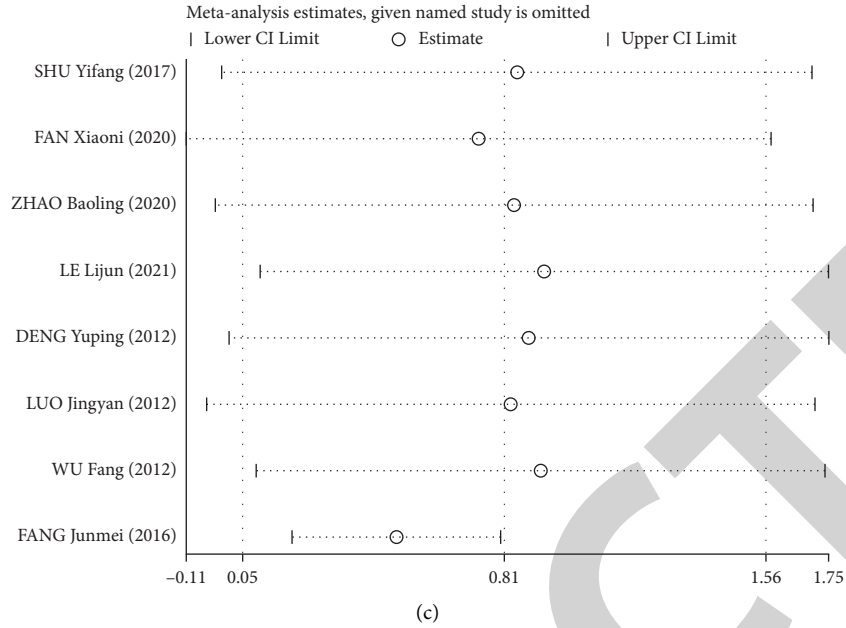

(c)

Figure 4: Forest plot, funnel plot, and sensitivity analysis of meta-analysis on pulmonary function (FEV1).

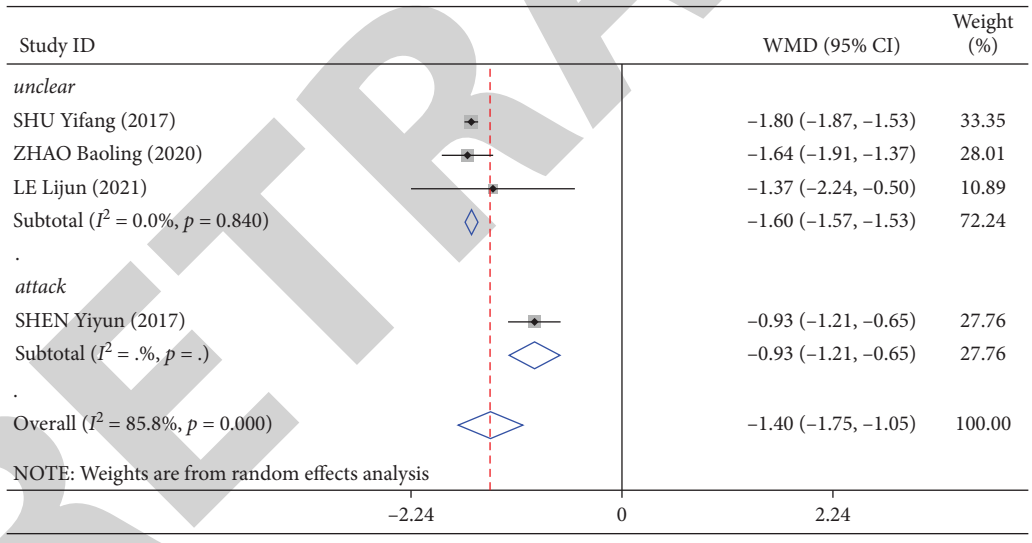

(a)

Figure 5: Continued.

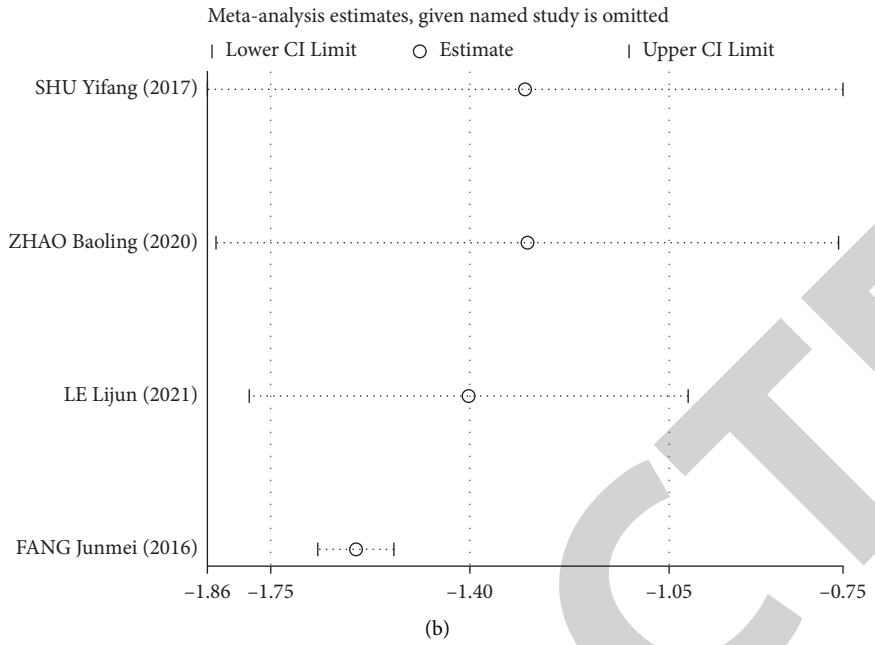

Figure 5: Forest plot and sensitivity analysis of meta-analysis on the resolution time of wheezing.

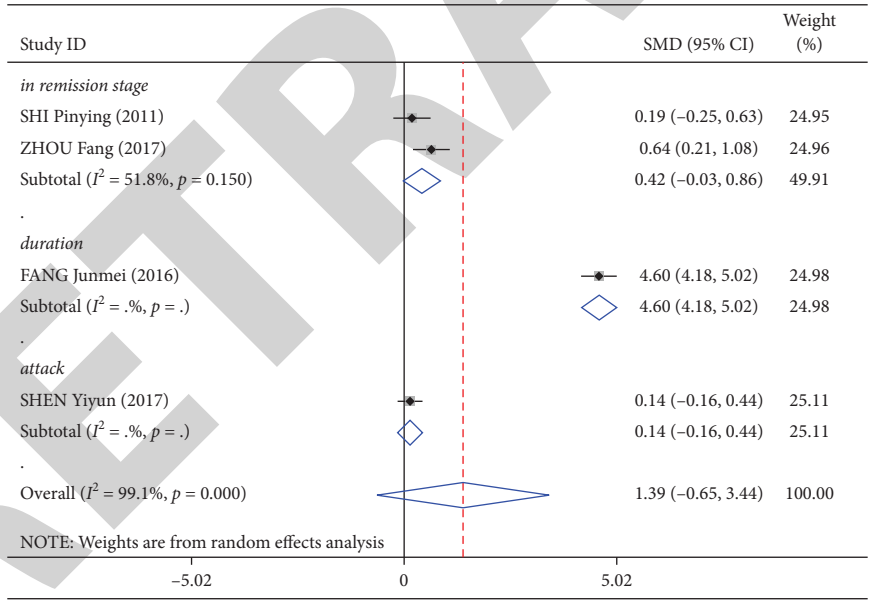

Figure 6: Forest plot of meta-analysis on serum IgE level.

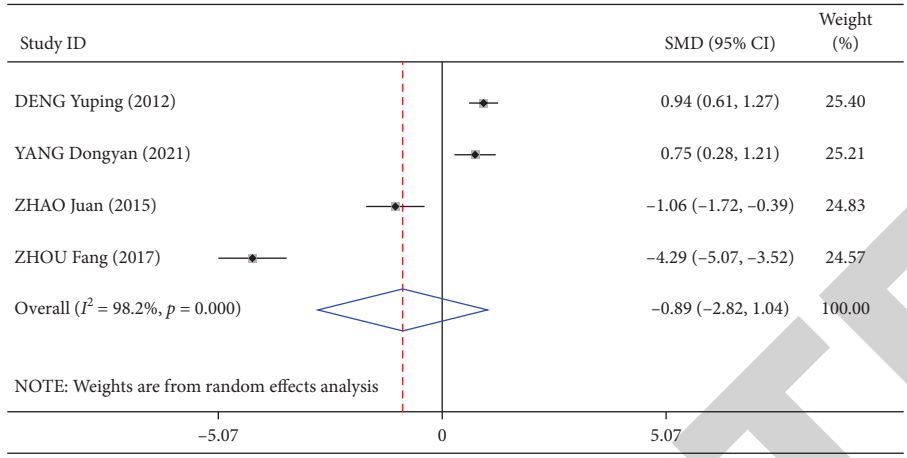

Figure 7: Forest plot of meta-analysis on the occurrence of asthma.

5. Conclusion

The present study shows that acupoint application is an effective treatment for children with asthma in China, especially in alleviating wheezing and improving quality of life. Due to the limitations of the study, further research should be conducted in the future with rigorous design, large sample size, sham/placebo control or blank/waiting control, and accurate report to support the evidence of acupoint application treatment in childhood asthma. Furthermore, since all studies were conducted in China, further studies in other countries are necessary to improve the applicability and generalizability of the results.

Data Availability

The data that support the findings of this study are available from the corresponding author upon reasonable request.

Conflicts of Interest

The authors declare no conflicts of interest and are responsible for the content and writing of the paper.

Authors' Contributions

Li ZJ and Wang YP designed the research. Wang YJ and Guo TT performed the research and contributed the analytic tools. Li YJ and Liu LJ searched the electronic databases and screened and extracted the studies. Yang FS and Lin KX analyzed the data. Wang YJ wrote the paper.

Acknowledgments

Not applicable. The study was supported by National Natural Science Foundation of China (No. 81874485).

Supplementary Materials

1. PRISMA_2020_checklist was uploaded as a supplementary file. 2. Search strategy was uploaded as a supplementary file. . (*Supplementary Materials*)

References

[1] G. Paçacı Çetin, B. Arslan, and İ. Yılmaz, "[Long-term macrolide therapy in asthma]," *Tuberk Toraks*, vol. 69, no. 4, pp. 520–534, 2021.

[2] A. L. Devonshire and R. Kumar, "Pediatric asthma: principles and treatment," *Allergy Asthma Process*, vol. 40, no. 6, pp. 389–392, 2019.

[3] S. D. Aaron, L. P. Boulet, H. K. Reddel, and A. S. Gershon, "Underdiagnosis and overdiagnosis of asthma," *American Journal of Respiratory and Critical Care Medicine*, vol. 198, no. 8, pp. 1012–1020, 2018.

[4] R. Azmeh, D. E. Greydanus, M. G. Agana et al., "Update in pediatric asthma: selected issues," *Disease-a-Month*, vol. 66, no. 4, Article ID 100886, 2020.

[5] X. Xu, D. Qiao, M. Mann, R. P. Garofalo, and A. R. Brasier, "Respiratory syncytial virus infection induces chromatin remodeling to activate growth factor and extracellular matrix secretion pathways," *Viruses*, vol. 12, pp. 804–8.

[6] D. Hakimeh and S. Tripodi, "Recent advances on diagnosis and management of childhood asthma and food allergies," *Ital Jounal Pediatrics*, vol. 39, no. 1, p. 80, 2013.

[7] R. B. O. C. M. A. Asthma Group, "Guidelines for the prevention and treatment of bronchial asthma (definition, diagnosis, treatment and management of bronchial asthma)," *Chinese Journal of Asthma(Electronic Version)*, vol. 2, no. 1, pp. 3–13.

[8] J. Zhou, "Observation on curative effect of 104 cases of infantile asthma treated in winter and summer treated," *Zhejiang Journal of Traditional Chinese Medicine*, vol. 46, no. 1, pp. 32-33.

[9] J. Zhang and C. Liu, "Application and progress of anti-IgE antibody in children with bronchial asthma," *Clinical Medication Journal*, vol. 16, no. 6, pp. 16–20.

[10] D. Zhu, C. Zhang, T. Lai, S. Ying, and H. Shen, "Research progress of on the intervention mechanism traditional Chinese medicine in airway remodeling in bronchial asthma," *Chinese Journal of Practical Internal Medicine*, vol. 36, no. 8, pp. 694–697.

[11] A. Liberati, D. G. Altman, J. Tetzlaff et al., "The PRISMA statement for reporting systematic reviews and meta-analyses of studies that evaluate health care interventions: explanation and elaboration," *PLoS Medicine*, vol. 6, no. 7, Article ID e1000100.

[12] J. P. T. Higgins, D. G. Altman, P. C. Gøtzsche et al., "The cochrane collaboration's tool for assessing risk of bias in randomised trials," *BMJ*, vol. 343, no. oct18 2, p. d5928, 2011.
[13] Y. Shen, C. Zhuang, and X. Liu, "Clinical observation on acupoint sticking therapy with clearing heat stick on hot asthma (mild)," *Guiding Journal of Traditional Chinese Medicine and Pharmacology*, vol. 23, no. 24, pp. 93–95.
[14] Y. Chen, "Application of acupoint application in the treatment of children with asthma in remission," *Today Nurse*, vol. 2, p. 96.
[15] Y. Deng, "Effect of kechuansanfutie on pulmonary function of remission stage of pediatric asthma," *Hubei Journal of Traditional Chinese Medicine*, vol. 34, no. 12, pp. 19-20.
[16] X. Fan, "Effect of aerosol inhalation combined with acupoint stimulation in the treatment of children with bronchial asthma and its effect on children's pulmonary function," *Contemporary Medicine Forum*, vol. 18, no. 18, pp. 128-129.
[17] J. Fang, W. Guo, and X. Jiang, "Observation of curative effect of Fujiutian acupoint sticking on prevention and treatment of bronchial asthma in children," *Zhejiang Clinical Medical Journal*, vol. 18, no. 9, pp. 1634–1636.
[18] H. Gu, "Influence of xiaochuan paste acupoint application on recrudesce and Th1/Th2 in Children with asthma," *Chinese Archives of Traditional Chinese Medicine*, vol. 35, no. 4, pp. 1014–1016.
[19] J. Guo and Y. Wan, "Observation on curative effect of 40 cases of children's asthma treated by integrated traditional Chinese and western medicine," *Journal of Sichuan Traditional Chinese Medicine*, vol. 27, no. 3, pp. 89-90.
[20] W. He, *Observation on the Clinical Effect of Medium Frequency Drug Acupoint Introduction in the Treatment of Children with Asthma*, Guangzhou University of Chinese Medicine, 2009.
[21] A. Hu, Z. Wen, and M. Lai, "Observation on the clinical efficacy of the combination of traditional Chinese and western medicine in the treatment of infantile asthma," *Chinese Modern Doctor*, vol. 48, no. 06, pp. 51-52.
[22] L. Le, "Clinical analysis of acupoint sticking combined with atomization inhalation in the treatment of children with asthma," *Journal of Hubei Institute of Technology*, vol. 37, no. 05, pp. 55–59.
[23] G. Li and Z. Mai, "Clinical observation of albuterol atomized inhalation combined with magnetic stickers in the treatment of variant asthma," *Journal of Clinic Nursing's Practicality*, vol. 2, no. 31, pp. 117-118.
[24] J. Luo and Y. Li, "Clinical observation of budesonide inhalation and acupoint sticking in the treatment of 75 children with asthma," *Tianjin Medical Journal*, vol. 40, no. 4, pp. 403-404.
[25] J. Luo, Y. Li, and J. Liu, "Analysis of life quality in children with asthma after treatment of GINA scheme and external application of Chinese medicine on acupoint," *Tianjin Journal of Traditional Chinese Medicine*, vol. 29, no. 3, pp. 243–245.
[26] P. Shi, J. Zhu, J. You, and M. Shen, "Effect of acupoint application with Wu's blistering plaster combined with seretide inhalation in preventing and treating children with asthma:40 Cases Report," *Journal of Traditional Chinese Medicine*, vol. 52, no. 4, pp. 314–316.
[27] D. Shi and X. Chen, "Observation on treating bronchial asthma in children by acupoint sticking," *Clinical Journal of Chinese Medicine*, vol. 2, no. 15, pp. 42-43.
[28] Y. Shu, X. Niu, and J. Wu, "Clinical efficacy of aerosol inhalation of budesonide combined with acupoints application with Chinese herbal medicine in the treatment of pediatric asthma," *Journal of Clinical Medicine in Practice*, vol. 21, no. 19, pp. 80–83.
[29] F. Wu, M. Yao, and Y. Zhu, "Clinical study on prevention of asthma recurrence in children with acupoint sticking therapy of winter disease and summer treatment of xiaochuan ointment," *Chinese Journal of Traditional Chinese Medicine*, vol. 37, no. 17, pp. 2646–2648.
[30] J. Xie, L. Guo, H. Zhang, and Z. Li, "Clinical effect analysis of "Mu-point acupuncture" acupoint application combined with drug atomization inhalation in the treatment of chronic persistent childhood asthma," *Self Care*, vol. 12, p. 261.
[31] D. Yang, "Observation of clinical effect of acupoint application therapy for winter disease and summer treatment in the treatment of children's asthma in remission stage," *Practical Clinical Journal of Integrated Traditional Chinese and Western Medicine*, vol. 21, no. 5, pp. 31-32.
[32] X. Zhang, L. Hu, Y. Gao, G. Zhao, and Y. Zheng, "Clinical observation of Fu Jiu sticking therapy in prevention and treatment of bronchial asthma," *Journal of Pediatrics of Traditional Chinese Medicine*, vol. 7, no. 6, pp. 41–43.
[33] B. Zhao, "Influence of "winter disease summer treatment" Chinese medicine acupoint sticking adjuvant therapy on children's asthma and pulmonary function, IL-6 and TNF-α Levels," *Inner Mongolia Medical Journal*, vol. 52, no. 2, pp. 160–162.
[34] Please provide references.
[35] F. Zhou, C. Hou, and Y. Fang, "Effect of warming yang and removing cold stick on acupoint sticking on children with asthma in remission," *Chinese Journal of Traditional Medical Science and Technology*, vol. 24, no. 6, pp. 791–793.
[36] M. Zhao, W. Li, S. Liang, F. Wang, M. Li, and Y. Zhang, "Observation on the effect of acupoint sticking combined with glucocorticoid inhalation in the prevention and treatment of children with bronchial asthma in remission stage," *Guangxi Journal of Traditional Chinese Medicine*, vol. 41, no. 5, pp. 32–34.
[37] J. Zhao and T. Zhou, "Clinical observation of self-made traditional Chinese medicine ointment in dog days acupoint in the treatment of remission period of the children with asthma," *Clinical Journal of Traditional Chinese Medicine*, vol. 27, no. 7, pp. 975-976.
[38] S. C. Dharmage, J. L. Perret, and A. Custovic, "Epidemiology of asthma in children and adults," *Front Pediatrics*, vol. 7, p. 246, 2019.
[39] R.g.o.t.P.P.C.o.t.C.A.o.I. Medicine, "Expert consensus on the prevention and treatment of asthma in children by integrated traditional Chinese and western medicine," *International Journal of Pediatrics*, vol. 47, no. 6, pp. 373–379.
[40] O. A. Dabbous, M. M. Soliman, N. H. Mohamed et al., "Evaluation of the improvement effect of laser acupuncture biostimulation in asthmatic children by exhaled inflammatory biomarker level of nitric oxide," *Lasers Medicine Science*, vol. 32, no. 1, pp. 53–59, 2017.
[41] R. K. Elnaggar, S. A. Moawd, S. E. Ali, A. M. Yousef, and A. R. Azab, "Potential impacts of Acu-TENS in the treatment of adolescents with moderate to severe bronchial asthma: a randomized clinical study," *Complementary Therapies in Medicine*, vol. 57, Article ID 102673, 2021.
[42] B. L. Wen, B. Y. Liu, J. Peng et al., "Clinical research of acupoint application for "treatment of winter disease in summer" used to prevent and treat bronchial asthma in children," *Journal of Traditional Chinese Medicine*, vol. 32, no. 1, pp. 31–39, 2012.

Hindawi
Evidence-Based Complementary and Alternative Medicine
Volume 2023, Article ID 9835328, 1 page
https://doi.org/10.1155/2023/9835328

Retraction

Retracted: Delayed Surgery to Preserve Kidney with Grade IV Injury

Evidence-Based Complementary and Alternative Medicine

Received 15 August 2023; Accepted 15 August 2023; Published 16 August 2023

This article has been retracted by Hindawi following an investigation undertaken by the publisher [1]. This investigation has uncovered evidence of one or more of the following indicators of systematic manipulation of the publication process:

(1) Discrepancies in scope
(2) Discrepancies in the description of the research reported
(3) Discrepancies between the availability of data and the research described
(4) Inappropriate citations
(5) Incoherent, meaningless and/or irrelevant content included in the article
(6) Peer-review manipulation

The presence of these indicators undermines our confidence in the integrity of the article's content and we cannot, therefore, vouch for its reliability. Please note that this notice is intended solely to alert readers that the content of this article is unreliable. We have not investigated whether authors were aware of or involved in the systematic manipulation of the publication process.

In addition, our investigation has also shown that one or more of the following human-subject reporting requirements has not been met in this article: ethical approval by an Institutional Review Board (IRB) committee or equivalent, patient/participant consent to participate, and/or agreement to publish patient/participant details (where relevant).

Wiley and Hindawi regrets that the usual quality checks did not identify these issues before publication and have since put additional measures in place to safeguard research integrity.

We wish to credit our own Research Integrity and Research Publishing teams and anonymous and named external researchers and research integrity experts for contributing to this investigation.

The corresponding author, as the representative of all authors, has been given the opportunity to register their agreement or disagreement to this retraction. We have kept a record of any response received.

References

[1] Y. Li, L. Xiao, W. Xu, L. Zhao, and M. Xiao, "Delayed Surgery to Preserve Kidney with Grade IV Injury," *Evidence-Based Complementary and Alternative Medicine*, vol. 2022, Article ID 5066278, 5 pages, 2022.

Hindawi
Evidence-Based Complementary and Alternative Medicine
Volume 2022, Article ID 5066278, 5 pages
https://doi.org/10.1155/2022/5066278

Research Article

Delayed Surgery to Preserve Kidney with Grade IV Injury

YunPeng Li,[1] Long Xiao,[2] WanChao Xu,[2] Liangyun Zhao,[2] and MinHui Xiao [2]

[1]*Department of Urology, The Fourth People's Hospital of Yunnan Province, Dali 671000, China*
[2]*Department of Urology, Yunnan First People's Hospital, Kunming 650000, China*

Correspondence should be addressed to MinHui Xiao; xiaominghui19689@163.com

Received 6 July 2022; Revised 21 August 2022; Accepted 29 August 2022; Published 22 September 2022

Academic Editor: Xueliang Wu

Background. Since the introduction of the ALARA ("as low as reasonably achievable") concept, the management of severe renal trauma has shifted. Our hospital promotes delayed surgical intervention for grade IV closed renal injury, to preserve renal function. In this study, we retrospectively reviewed the management and outcomes of patients with grade IV closed renal injury in our hospital. *Objective*. To evaluate the management and outcome of grade IV closed renal injury. *Methods*. We retrospectively reviewed the medical records of 45 patients with grade IV closed renal injury; namely, 36 men and 9 women with an average age of 35.6 years. All patients were diagnosed with grade IV closed renal injury in accordance with the guidelines of the American Association for the Surgery of Trauma. All hemodynamically-stable patients with renal trauma were treated conservatively for approximately 13 days and then underwent surgery only to clear the perirenal hematoma and not to repair or resect the affected kidney. Abstracted data included patient demographics, mechanism of injury, admission hemodynamics, CT findings, and mortality. The primary outcome was the success rate of nonsurgical treatment, and the secondary outcome was the complication of nonsurgical treatment. *Results*. All patients responded and were discharged, and no patients died. We followed 35 (77.8%) patients for at least 1 year. One patient with partially devitalized renal parenchyma underwent surgery to remove the affected kidney. Eleven patients (31.4%) suffered complications, namely, three (8.6%) cases of hypertension, four (11.4%) cases of hematuria, two cases (5.7%) of urinary tract infection, and two (5.7%) cases of urinoma. *Conclusions*. Delayed exploratory surgery only to remove the hematoma should be considered in hemodynamically-stable patients with grade IV closed renal injury. This approach can avoid high nephrectomy rates associated with emergency surgery and reduce the complications that result from conservative treatment without surgery.

1. Introduction

Traumatic kidney injury accounts for about 5% of all surgical injuries and is a common urological emergency. Kidney trauma is most common in traffic accidents, falling from a high altitude, and sports injuries [1–3]. Most of the local renal injury was low blunt renal injury (grades I–III), and others were severe renal injuries. Low-grade blunt kidney injury can be resolved by conservative treatment, which is widely accepted. However, severe renal injury, including grade IV and V blunt renal injury (renal fragmentation, hilar vascular tear, dissection with no blood supply to the kidney), requires surgical intervention, and nephrectomy is considered to be the appropriate treatment [4]. Due to limited prospective studies, the treatment of grade IV blunt renal trauma is controversial and there is no optimal treatment strategy. In the emergency treatment of this level of renal injury, the report indicates that surgery is unavoidable and that nephrectomy is necessary due to the location of the injury and associated vascular damage [4]. A review study showed that emergency nephrectomy was more common than nephron-sparing surgery in patients with grade IV blunt renal trauma [2, 3]. Intraoperatively, urologists are often unable to repair damaged kidneys in patients with grade IV blunt renal trauma due to acute renal hemorrhage, inflammation, severe trauma, perirenal hematoma, or anatomical confusion, leading to nephrectomy [5, 6]. In other studies, some patients with grade IV blunt renal trauma received only conservative treatment, and CT showed renal laceration involving the renal cortex, medulla, and collecting

system, injury involving the main arteries and veins of the kidney, and segmental renal infarction without renal laceration. In addition, for patients with stable hemodynamics, conservative treatment and observation are commonly used, and a series of imaging examinations are required due to the concomitant injury of other abdominal organs. Therefore, emergency surgical intervention is necessary, resulting in the removal of the affected kidney [7]. Based on these findings, management of grade IV blunt kidney injury remains an important clinical issue [8].

In our institution, from February 1994 to March 2016, hemodynamically-stable patients with grade IV closed renal trauma underwent conservative treatment for approximately followed by surgery only to remove the perinephric hematoma. This approach increased the likelihood of nephron-sparing compared with emergency surgery, and also significantly decreased the long-term complication rate. We describe our findings in these patients, in this report.

2. Methods

2.1. General Information. This is a retrospective case series including all adult patients with a grade IV blunt renal injury who were admitted between February 1994 to March 2016, to a third-class hospital in Yunnan Province, China. Renal injuries were graded based on computed tomographic (CT) findings and according to the American Association for the Surgery of Trauma Organ Injury Scale [1] which was defined as laceration through the parenchyma into the collecting system, vascular segmental venous or arterial injury, and any injury involving the collecting system (renal pelvis laceration and ureteric kidney pelvic disruption).

Based on these criteria, 45 patients with grade IV blunt renal injuries were included. We excluded patients with hemodynamic instability, other mental disorders, cognitive disabilities, or severe dysfunction of the heart, liver, and lung; included patients consisting of 36 men and nine women, with an age range of 4–72 years and an average age of 36.5 years (as shown in Table 1). Twelve patients sustained collision-related trauma, 27 sustained injuries following traffic accidents, and six patients experienced falls. Of the 45 patients, 24 patients sustained right kidney injury, and 21 patients sustained left kidney injury (as shown in Table 2). Based on patients' clinical manifestations, lower back pain was the most common complaint; gross hematuria occurred in 33 patients, and microscopic hematuria occurred in 12 patients. Physical examination revealed tenderness, a local mass, and percussion pain at the trauma site most often; two patients presented with ecchymosis, 24 patients presented with fever, and two patients presented with severe fever (> 39°C).

Table 1: Patients' clinical characteristics.

Clinical characteristics	*n*	%
Mean age (yr)	36.49 ± 15.207	
Male	36	80.0
Female	9	20.0
BMI (m/kg^2)	24.85 ± 3.44	
Creatinine/(μmol/L)		
Previous	67.32 ± 22.91	
Postoperation	62.84 ± 15.42	

BMI: body mass index.

Table 2: Injury position and type of Injury.

Type of injury	*n* (%)	Injury position	*n* (%)
Collision-related trauma	12 (26.7)	RK	7 (15.6)
		LK	5 (11.1)
Traffic accidents	27 (60.0)	RK	14 (31.1)
		LK	13 (28.9)
Falls	6 (13.3)	RK	3 (6.7)
		LK	3 (6.7)

RK: right kidney; LK: left kidney.

3. Treatment Methods

Methods After admission, all patients underwent routine urine examination, ultrasound examination, and CT examination and were confirmed to have grade IV closed renal injury (Figure 1). Conservative treatment lasted for about 13 days. Specific measures were as follows: first, ensure successful hemostasis, ensure the amount of blood transfusion when necessary, and monitor the patient's vital signs; nursing staff considers continuous testing of hematocrit measurement, let the patient rest in bed; consider clinical monitoring of the patient's physical condition and administer iv fluids if necessary. Treated with "Huayu Zhuxue Decoction" of traditional Chinese medicine: 10 g of raw dandelion, 12 g of dandelion, 6 g of wulingzhi, 15 g of white peony, 12 g of red peony, 6 g of peach kernel, 12 g of *Angelica sinensis*, 15 g of Achyranthes bidentata, 9 g of Dipsacus, 6 g of Jing mustard, 6 g of Panax notoginseng powder (for flushing), 6 g of roasted licorice, 24 g of chenneijin, 24 g of haijinsha and 3 g of amber powder (for flushing); 1 dose per day. Patients underwent surgery only to remove the perirenal hematoma and not to repair the lacerated kidney (Figure 2). Intraoperatively, we removed the perirenal organizing hematoma and addressed any urine extravasation. We did not dissect and control bleeding from the renal artery, which increased the ease and safety of the surgery. As seen in Figure 2, the lacerated edges of the kidney adhered closely to each other and were well-restored because of the organizing hematoma, which eliminated the need for further renal repair or nephrectomy. More recently, we used a laparoscope to remove the perinephric hematoma in some patients, and also achieved satisfactory results. We use and recommend an indwelling perinephric drainage tube (Figure 3).

4. Data and Outcomes

The following data were collected: demographics, mechanism of injury (collision-related trauma, traffic accidents, and fall), admission hemodynamics, CT findings, presence of free abdominal blood on CT scan (recorded as diffuse or confined around the kidney), and mortality. The primary outcome was the success rate of nonsurgical treatment, and the secondary outcome was the complication of nonsurgical treatment.

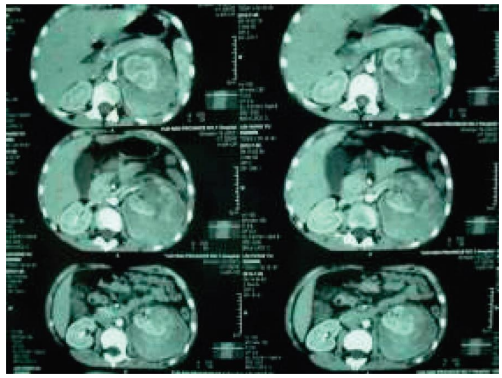

Figure 1: Computed tomographic image showing grade IV closed renal trauma. The perirenal hematoma is large and indicated by the arrow.

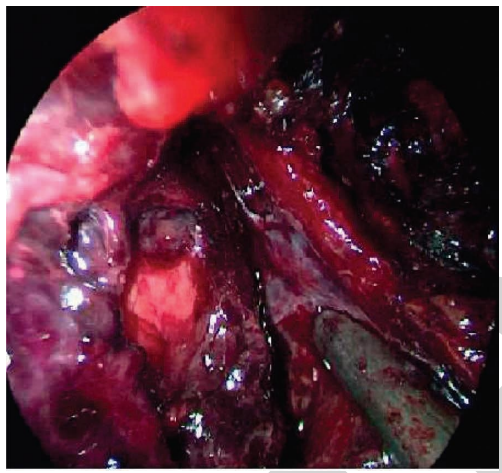

Figure 2: Intraoperative video image showing the perirenal organizational hematoma during the delayed surgery.

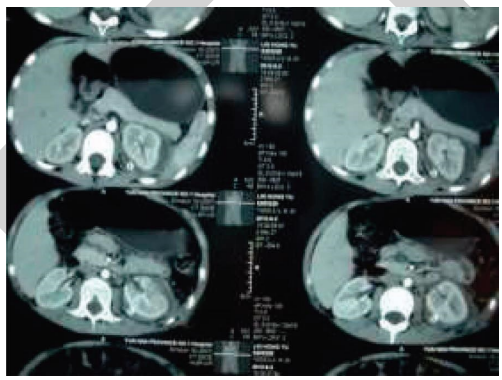

Figure 3: Computed tomographic image after the perirenal hematomas have been removed. The arrow indicates the perinephric drainage tube.

4.1. Statistical Analysis. SPSS 24.0 statistical software was used for analysis and statistical description according to data type. The measurement data conforming to normal distribution are expressed in mean ± standard deviation, the measurement data not conforming to normal distribution are expressed in median and quartile, and the counting data are expressed in frequency and percentage.

5. Results

All 45 included patients with grade IV closed renal injury underwent delayed surgical intervention, and one patient required nephrectomy secondary to poor adherence to the laceration margins. Kidneys in all remaining patients were successfully preserved, intraoperatively, and no patients died (as shown in Table 3).

Postoperative follow-up was performed for 35 patients for at least 1 year. Eleven of the 35 patients (31.4%, 11/35) developed complications related to kidney trauma(as shown in Table 2), namely, hypertension in three patients (8.6%, 3/35), for whom oral antihypertensive drugs controlled the symptom; four patients (11.4%, 4/35) developed microscopic hematuria; two patients (5.7%, 2/35) developed urinary tract infection, which responded to antibiotic therapy; and two patients (5.7%, 2/35) developed urinoma, which was treated with an indwelling drainage tube and which gradually dissolved (as shown in Table 4).

6. Discussion

Renal injury accounts for approximately 10% of all trauma cases, and the majority of patients sustain blunt renal trauma. The management of the renal injury is based on the mechanism of the injury, associated injuries, hemodynamic stability, and severity. Traditionally, grades I–III injuries have been managed conservatively, while patients with grade V injuries almost always undergo surgical exploration. For patients with severe renal injury (grades IV–V), except when life-saving measures are necessary; preserving renal function and minimizing the complications associated with kidney trauma should be the aim of therapies.

According to the criteria for nomenclature and classification of acute kidney injury agreed by the Taiwan AKI Working Group in 2021, grade IV laceration kidney injury runs through the renal cortex, medulla, and collecting system, and damage in the main branches of renal arteries and veins accompanied by bleeding can be treated conservatively or repaired in an emergency or delayed manner according to the actual situation of patients [9, 10]. Sun reported [11] that, in a cohort of 22 patients with a renal injury who underwent surgical intervention, nephrectomy was performed in 59% of patients. Su et al. [12] reported that 12 patients with severe kidney injury underwent surgery, and a nephrectomy was performed on 10 patients. In hemodynamically-stable patients with severe blunt renal trauma, choosing whether to perform surgery or nonoperative management can be difficult. The treatment of grade IV injuries is even more controversial because these patients can be managed conservatively or undergo urgent repair or delayed repair. Currently, most clinicians choose conservative treatment to avoid unnecessary nephrectomy and other unexpected risks [13]. Van et al. [14] reported, in a multicenter study of the nonsurgical treatment of severe blunt renal trauma in hemodynamically-stable patients, that

Table 3: Summary of operational characteristics.

Operational characteristics	*n* (%)
Delayed surgery	45 (100)
Preserved kidney success	44 (97.8)
Nephrectomy	1 (2.2)
Patients died	0

Table 4: Postoperative complications.

Adverse events	*n* (%)
Postoperative follow-up rate	35 (77.78, 35/45)
Hypertension	3 (8.6%, 3/35)
Microscopic hematuria	4 (11.4%, 4/35)
Urinary tract infection	2 (5.7%, 2/35)
Urinoma	2 (5.7%, 2/35)

the failure rate of nonsurgical treatment was only 6.5%. In the study, there were two important predictors: one was patient age > 55 years, and the other was vehicular trauma. If patients with grade IV or V renal trauma had both of these predictors and received conservative treatment, the failure rate was as high as 27.3%. Furthermore, the inconvenience and complications of conservative management increased patients' difficulties. Long periods of bed rest were extremely difficult for patients, especially for vital and active young children [15, 16]. Moreover, perirenal hematoma, if not cleared in time, may lead to infection and abscess formation, possibly even tissue fibrosis, which leads to hydronephrosis and more difficult future management.

Among our patients prior to the current study, 2 years after renal injury, two patients receiving conservative treatment required nephrectomy because of refractory hypertension. Therefore, we adopted the delayed exploratory surgery approach to treat patients with severe closed renal injury (grade IV). Specifically, hemodynamically-stable patients currently undergo conservative treatment for approximately 13 days and then undergo exploratory surgery, only to remove the perirenal hematoma. This approach is possible because of the "self-healing" ability of the kidney, which eliminates the need for kidney repair and reduces the surgical risk and difficulty. During conservative treatment, we used plain CT to dynamically observe the affected kidney, which can correctly have evaluated the extent of renal injury, determine the scope of the urinary extravasation and hematoma, and reveal devitalized renal tissues. CT examination is an important diagnostic and monitoring tool when evaluating renal injury [17–20]. In this study, raw dandelion, wulingzhi, peach kernel, and Schizonepeta were used to activate blood circulation and remove blood stasis, and Danpi was used to induce various drugs to the kidney to remove blood stasis and heat; *Angelica sinensis* and pseudo ginseng can not only promote blood circulation and remove blood stasis but also stop bleeding. We chose delayed exploratory surgery for several reasons. First, the kidney has a rich blood supply and strong compensatory and repair capability, often self-repairing once bleeding stops (Figure 4). Second, because patients undergo approximately

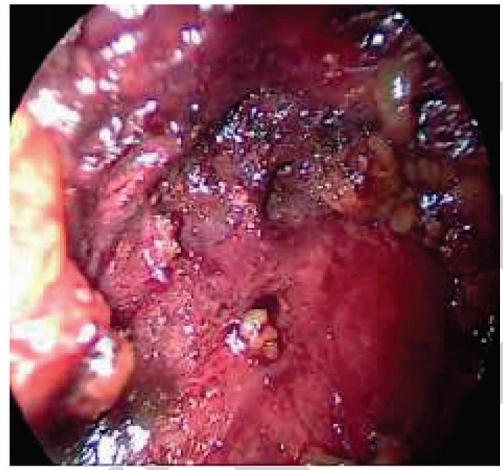

Figure 4: Intraoperative video image showing the self-healing ability of the kidney during the delayed surgery.

13 days of conservative treatment, delaying surgery avoids active hemorrhage resulting from the initial renal trauma. Because there is no active hemorrhage during the delayed surgery, and the surgical view is clear, urologists can operate precisely and better protect the kidney. Third, during delayed exploratory surgery, renal tissue edema has almost disappeared, and no conspicuous tissue adhesions between the kidney and surrounding tissues are present. Urologists can then more easily dissect the perirenal tissue and reveal the renal wound. Thirteen days after injury, renal tissue repair has passed the inflammatory stage and entered the tissue proliferation and granulation stage. It is well-known that granulation tissue fills and repairs the renal tissue wound, and has a strong resistance to infection. Therefore, because granulation tissue is not removed, it can provide a physiological basis for patients' rehabilitation. Although postoperatively, complications such as urine extravasation, hypertension, urinary infection, and urinoma are possible, the incidence of these complications is significantly lower compared with conservative treatment without delayed surgery [6, 7] If exploratory surgery is performed early after injury (< 10 days), although the surgical approach is easier, renal wound healing is poor and often requires repair, which increases the surgical difficulty. In contrast, if the exploratory surgery is delayed too long, because of renal fat adhesion and tissue organization, it is more difficult to identify the kidney and renal wound. Therefore, we recommend appropriately-delayed surgical treatment for hemodynamically-stable patients with grade IV closed renal injury to avoid the high nephrectomy rates associated with emergency surgery and to reduce the complications that result from conservative treatment without surgery. Delayed surgical intervention was appropriate for patients with grade IV closed renal injury, in our study.

7. Limitation

The study was subject to a number of limitations. First, because of the small number of patients, follow-up was difficult, and the lost-to-follow-up rate was high; no

Hindawi
Evidence-Based Complementary and Alternative Medicine
Volume 2022, Article ID 3261300, 15 pages
https://doi.org/10.1155/2022/3261300

Research Article

Pan-Cancer Analysis of BUB1B/hsa-miR-130a-3p Axis and Identification of Circulating hsa-miR-130a-3p as a Potential Biomarker for Cancer Risk Assessment

Xiaoxia Ding,[1] **Lele Chen**,[2] **Danfeng Xu**,[1] **Yong Yu**,[1] **Xiaohua Tao**,[1] **Yibin Fan**,[1] **and Youming Huang**[1]

[1]*Health Management Center, Department of Dermatology, Zhejiang Provincial People's Hospital, Affiliated People's Hospital, Hangzhou Medical College, Hangzhou, Zhejiang, China*
[2]*Department of Dermatology and Venereology, The First Affiliated Hospital of Wenzhou Medical University, Wenzhou, Zhejiang 325000, China*

Correspondence should be addressed to Youming Huang; huangyouming@hmc.edu.cn

Received 12 July 2022; Revised 19 August 2022; Accepted 24 August 2022; Published 22 September 2022

Academic Editor: Xueliang Wu

Based on the fact that very little was found in the literature on the question of potential molecules and mechanism for high risk of cancer in patients with psoriasis, this study was designed and performed based on bioinformatics analysis including WGCNA. The most striking result to emerge from the data is that BUB1B/hsa-miR-130a-3p axis, closely related to the development of psoriasis, also plays a remarkable role in multiple cancer development. The expression patterns of hsa-miR-130a-3p were found significantly changed in multiple tumors, which was also associated with prognosis. Additionally, hsa-miR-130a-3p was downregulated in lesion skin of psoriasis, but there was no difference in blood between psoriasis patients and normal controls. Circulating has-miR-130a-3p was found to have a higher level of blood in multiple tumor patients, suggesting that hsa-miR-130a-3p has the potential to be a blood biomarker for cancer risk assessment in patients with psoriasis.

1. Introduction

Psoriasis (Ps) is a hyperproliferative chronic inflammatory skin and joint disease with unknown etiology [1], which affects 2-3% of the population. According to previous studies, individuals with psoriasis are at an increased risk of cancer compared to the general population or a reference group without the disease [2, 3], but the underlying association is much less clear [4]. To improve the understanding of the underlying mechanisms of this increased risk, further research is needed.

MicroRNAs (miRNAs) interact with mRNAs and trigger translational suppression or mRNA degradation. MicroRNAs mutation and maladjustment are related to the occurrence and development of human diseases [5]. Accordingly, miRNAs, especially miR-21, miR-125b, miR-146a, and miR-203, may play a role in the pathogenesis of psoriasis. The underlying process affects keratinocytes proliferation and inflammation, as well as T-cell-mediated immunological failure [6]. Notably, plasma miRNAs are also involved in psoriasis pathogenesis targeting the VEGF, MAPK, and WNT signaling pathways [7]. Moreover, changes in miRNA expression or miRNA dysfunction have also been reported to be associated with cancer initiation, progression, and diagnosis in several studies [8, 9]. But still no studies focus on the role of psoriasis-related miRNAs in pan-cancer.

There is growing interest in microarray platforms as a way to detect genetic alterations and to determine biomarkers for many diseases [10]. Several biomarkers and pathways have been implicated in the development of psoriasis and multiple cancer types in previous studies on microarray data. For example, RNF114 was found to correlate with the development of psoriasis and gastric cancer

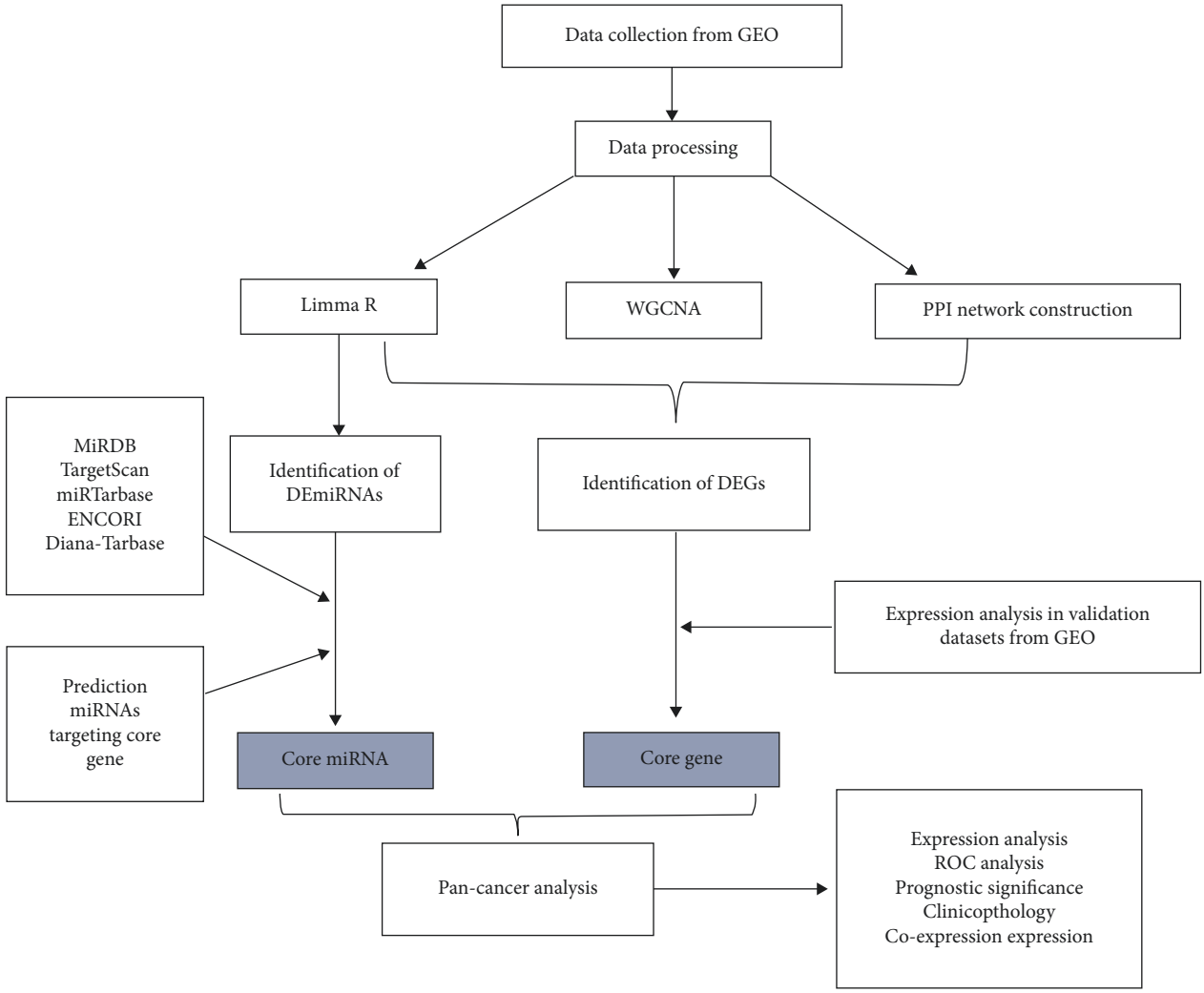

Figure 1: Flow chart.

[11]. The findings mentioned above point to a substantial correlation between psoriasis and cancer development. However, there has not been any pan-cancer analysis on the genes involved in the etiology of psoriasis, either mRNAs or miRNAs.

In this study, we analyzed and validated a total of 6 datasets, including blood samples and skin samples of healthy control and patients with psoriasis, by integrated bioinformatics methods. It was found that BUB1B/hsa-miR-130a-3p axis, closely related to the development of psoriasis, also plays a remarkable role in multiple cancer development. This study may provide a new insight into the mechanism of high cancer risk in patients with psoriasis.

2. Materials and Methods

The flow chart of this study is shown in Figure 1.

2.1. Dataset Collection. Gene expression datasets were collected from the Gene Expression Omnibus database (http://www.ncbi.nlm.nih.gov/geo) [12]. The uniformly normalized pan-cancer dataset was downloaded from the UCSC (https://xenabrowser.net/) database [13]: TCGA TARGET GTEx (PANCAN, $N = 19131$, $G = 60499$). miRNAseq data was obtained from Level 3 BCGSC miRNA Profiling in TCGA (https://portal.gdc.cancer.gov/) ALL (Pan-Cancer) project.

2.2. Data Processing and Differential Expression Analysis. The normalized expression matrix of microarray data was downloaded from the GSE dataset. Then, the probes were annotated with the annotation files from the dataset. For merging multiple datasets, we first merged the datasets using the R package inSilicoMerging [14], and then we removed the batch effects [15]. Then, the "limma R" package was used to obtain the differentially expressed genes (DEGs) between the different comparison groups and the control group in the dataset ($|\text{Log}\,2\text{FC}| > 1$, p adj value < 0.05) [16]. Venn plot was drawn between different comparison sets to get overlapped DEGs. Moreover, heatmap and box plot were conducted using "heatmap" and "ggplot2" packages of R software.

2.3. Weighted Correlation Network Analysis (WGCNA). First, we calculated the MAD (Median Absolute Deviation) of each gene separately using the gene expression profile, eliminated the top 50% of genes with the smallest MAD, removed the outlier genes and samples using the goodSamplesGenes method of the R package WGCNA [17], and further constructed a scale-free coexpression network. A power of $\beta = 5$ was chosen. To further analyze the module, we calculated the dissimilarity of the module eigen genes, chose a cutline for the module dendrogram, and merged modules with distance less than 0.25 along with a sensitivity set to 3. Finally, 14 non-grey modules were obtained. Additionally, we calculated the expression correlation with genes to obtain GS and also calculated the expression correlation of module eigenvectors with genes to obtain MM. Based on the cut-off criteria ($|\mathrm{MM}| > 0.8$ and $|\mathrm{GS}| > 0.1$), 698 genes with high connectivity in the clinical significant module were identified as hub genes.

2.4. Functional Correlation Analysis. For gene set functional enrichment analysis, we used GO annotations of genes from the R package org.Hs.eg.db (version 3.1.0) and KEGG annotation from rest API (https://www.kegg.jp/kegg/rest/keggapi.html) as background, mapped the genes to the background set, respectively, and used the R package clusterProfiler (version 3.14.3) for enrichment analysis to obtain gene set enrichment results [18]. Set the minimum gene set to 5 and the maximum gene set to 5000. A false discovery rate (FDR) < 0.05 and $p < 0.05$ were considered significant enrichment.

2.5. Construction of the PPI Network. To characterize the crucial DEGs, we used an online tool STRING (https://string-db.org/) to construct PPI networks with a minimum required interaction score of 0.4 [19]. For further analysis, Cytoscape software was used for the download of interaction information. Significant genes were determined by the CytoHubba plugin as hub genes [20]. The significant clusters within the PPI network were selected using the MCODE plugin.

2.6. Prediction and Validation of miRNAs Targeting Core Gene. The miRNA target predicting algorithms miRDB (http://mirdb.org/miRDB/) [21], TargetScan [22] (http://www.targetscan.org/), miRTarbase [23] (http://mirtarbase.cuhk.edu.cn/), ENCORI (https://stps://starbase.sysu.edu.cn/) [24], and Diana-Tarbase V8.0 [25] (https://dianalab.e-ce.uth.gr/) were used to predict miRNAs targeting core gene. The intersection of miRNAs obtained from multiple online tools and differently expressed mRNAs (DEmiRNAs) from the GSE142582 dataset was shown in an UpSetR-plot using the UpsetR R package [26].

2.7. Expression Analysis of BUB1B and hsa-miR-130a-3p in Pan-Cancer. We extracted the expression data of hsa-miR-130a-3p [MIMAT0000425] from various samples and then performed the log 2 transformation of each expression value. We calculated the difference in expression between paired tumor and adjacent normal tissues as well as normal and tumor samples in indicated tumor types using R software (version 3.6.4) and analyzed the difference in significance using unpaired Wilcoxon Rank Sum Tests. The final results were visualized by ggplot [27]. Moreover, the pan-cancer expression of BUB1B at the protein level was investigated using the Human Protein Atlas database (http://www.proteinatlas.org/) [28].

2.8. CancerMIRNome. CancerMIRNome is a comprehensive database with the human miRNome profiles of 33 cancer types from The Cancer Genome Atlas (TCGA) and 40 public cancer circulating miRNome profiling datasets from NCBI Gene Expression Omnibus (GEO) and ArrayExpress [29]. It was used to perform a different analysis of hsa-miR-130a-3p in pan-cancer.

3. Results

3.1. Data Preprocessing. After searching in the Gene Expression Omnibus database with inclusion criteria including (1) patients with psoriasis and (2) blood samples or skin samples, 6 datasets were chosen, and the detailed information and function are shown in Table 1. Briefly, GSE13355 and GSE14905 were merged to identify differentially expressed mRNAs; GSE142582 was used to explore differentially expressed miRNAs; GSE78097 and GSE55201 were validation datasets for DEmRNAs; and GSE55515 was another validation dataset for DEmiRNAs.

4. Differentially Expressed mRNAs in Patients with Psoriasis

Firstly, we removed the batch effects between GSE13355 and GSE14905. From the box plot (Figure 2(a)), we can observe that the sample distribution of each dataset before the batch effect is removed is quite different, suggesting that there is a batch effect, and the data distribution between the various data sets after the batch effect is removed tends to be consistent, and the median is on a line (Figure 2(b)). Then, we identified DEGs from 2 different comparison sets including PP versus NN and PP versus PN. DEGs were identified with the setting of cutoff at FDR < 0.05 and $|\log 2(\mathrm{FC})| \geq 1$. The DEGs from the 2 sets were presented as a volcano plot and heatmap plot (Figures 2(c)–2(f)). As shown in Figure 2(g), there are totally 498 upregulated DEGs and 308 downregulated DEGs from PP-NN set, while there are 448 upregulated and 219 downregulated DEGs from PP-PN set. Among them, 421 upregulated DEGs and 192 downregulated DEGs were overlapped between the 2 sets.

4.1. WGCNA Analysis and Attainment of Module DEGs. In this study, WGCNA analysis was conducted using the R package WGCNA. The expression patterns of the genes in the same module were similar and relevant to the average linkage clustering. We included 262 samples with clinical traits to filter outlier samples via sample clustering. A soft

Table 1: Detailed information of involved datasets.

Accession	Platform	Disease state	Tissue	Organism	Dataset contents	Purpose	Description
GSE13355	GPL570	Psoriasis and normal	Skin	Homo sapiens	58 PP 58 PN 64 NN	Exploration	PP = involved skin from cases PN = uninvolved skin from cases NN = normal skin from controls
GSE14905	GPL570	Psoriasis and normal	Skin	Homo sapiens	28 PP 28 PN 21 NN	Exploration	
GSE142582	GPL20301	Psoriasis and normal	Skin	Homo sapiens	5 PP 5 PN 5 NN	Exploration	
GSE78097	GPL570	Psoriasis and normal	Skin	Homo sapiens	14 MPs 13 SPs 6 CL	Validation	MPs = involved skin from mild cases SPs = involved skin from severe cases CL = normal skin
GSE55201	GPL570	Psoriasis and normal	Blood	Homo sapiens	27 PS 27 CL	Validation	PS = blood from cases CL = blood from controls
GSE55515	GPL11241	Psoriasis and normal	Blood	Homo sapiens	19 PS 15 CL	Validation	PS = blood from cases CL = blood from controls

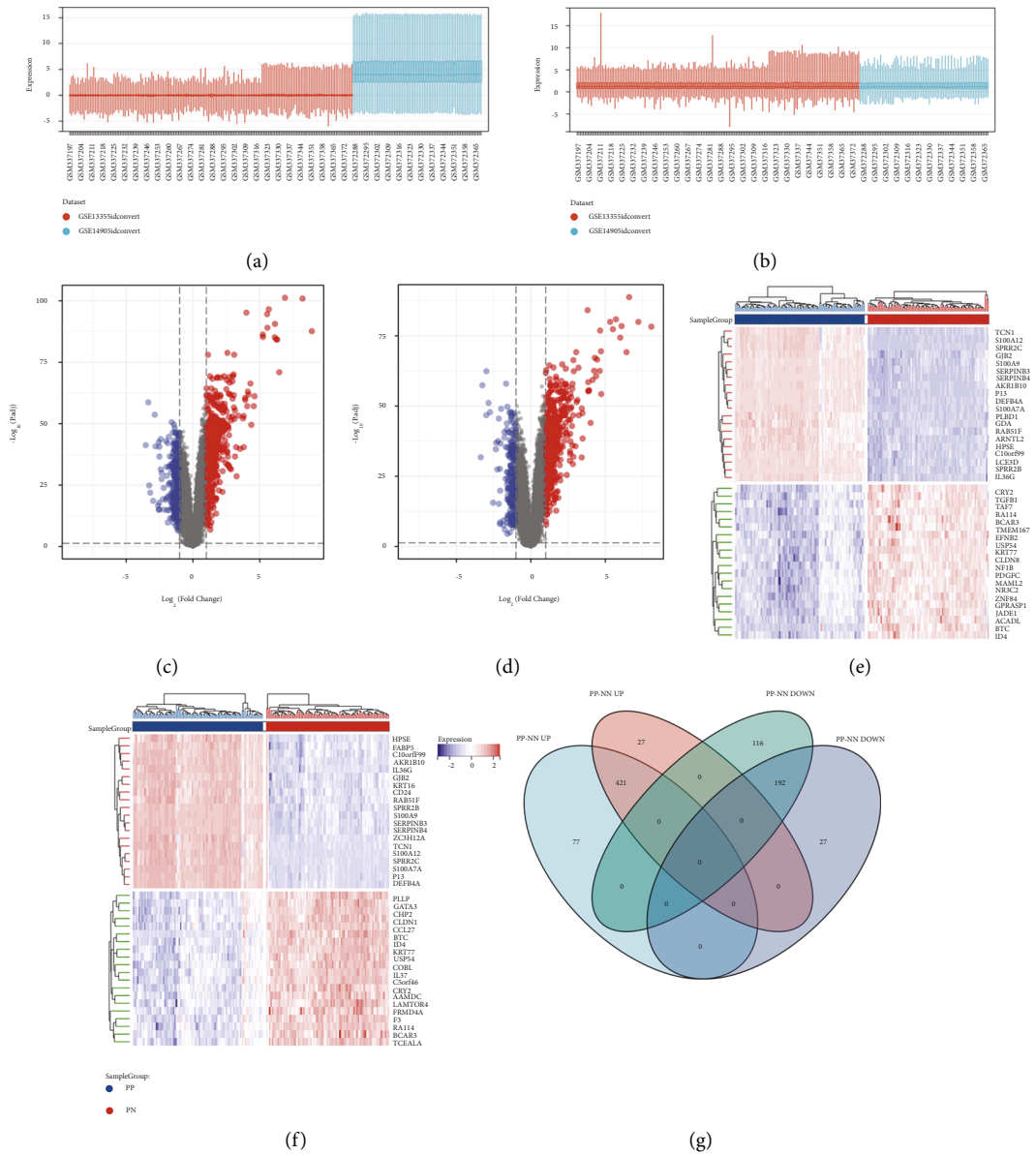

Figure 2: Differentially expressed genes (DEGs) exploring. (a) Box plot before batch effect is removed. (b) Box plot before batch effect is removed. (c) Volcano plot of DEGs from PP-NN set. (d) Volcano plot of DEGs from PP-PN set. (e) Heatmap plot of top 50 DEGs from PP-NN set. (f) Heatmap plot of top 50 DEGs from PP-NN set. (g) Venn plot of overlapped DEGs between 2 sets. (PP: lesion skin from psoriasis patients; PN: no-lesion skin from psoriasis patients; NN: normal skin from normal controls).

threshold (β) = 5 was set to ensure a scale-free network (Figure 3(a)). Similar modules with a height cut-off value of 0.25 were merged, and 14 non-grey modules were finally obtained (Figure 3(b)). Furthermore, the relationship between the modules and the clinical traits was evaluated to identify the hub module. The results showed that the turquoise module was significantly associated with the PP samples (Figure 3(c)). The module membership and gene significance of turquoise are shown in Figure 3(d). Additionally, we calculated the expression correlation with genes to obtain GS and also calculated the expression correlation of module eigenvectors with genes to obtain MM. Based on the cutoff criteria ($|MM| > 0.8$ and $|GS| > 0.1$), 697 genes with high connectivity in turquoise module were identified as hub genes. Subsequently, we plotted the Venn diagram between the modular hub genes and the abovementioned DEGs and finally obtained 297 upregulated genes and 43 downregulated genes (Figure 3(e)).

4.2. PPI Network Construction and Hub Genes Attainment. First, we used the STRING database and Cytoscape software to construct the network of the aforesaid DEGs from the turquoise module, containing 259 nodes and 1804 edges. The top three significant clusters (Figure 4(a)) within the PPI network were selected using MCODE plugin in Cytoscape software (Clusters 1, MCODE score = 42.978; Clusters 2, MCODE score = 19.818; Clusters 3, MCODE score = 5.053).

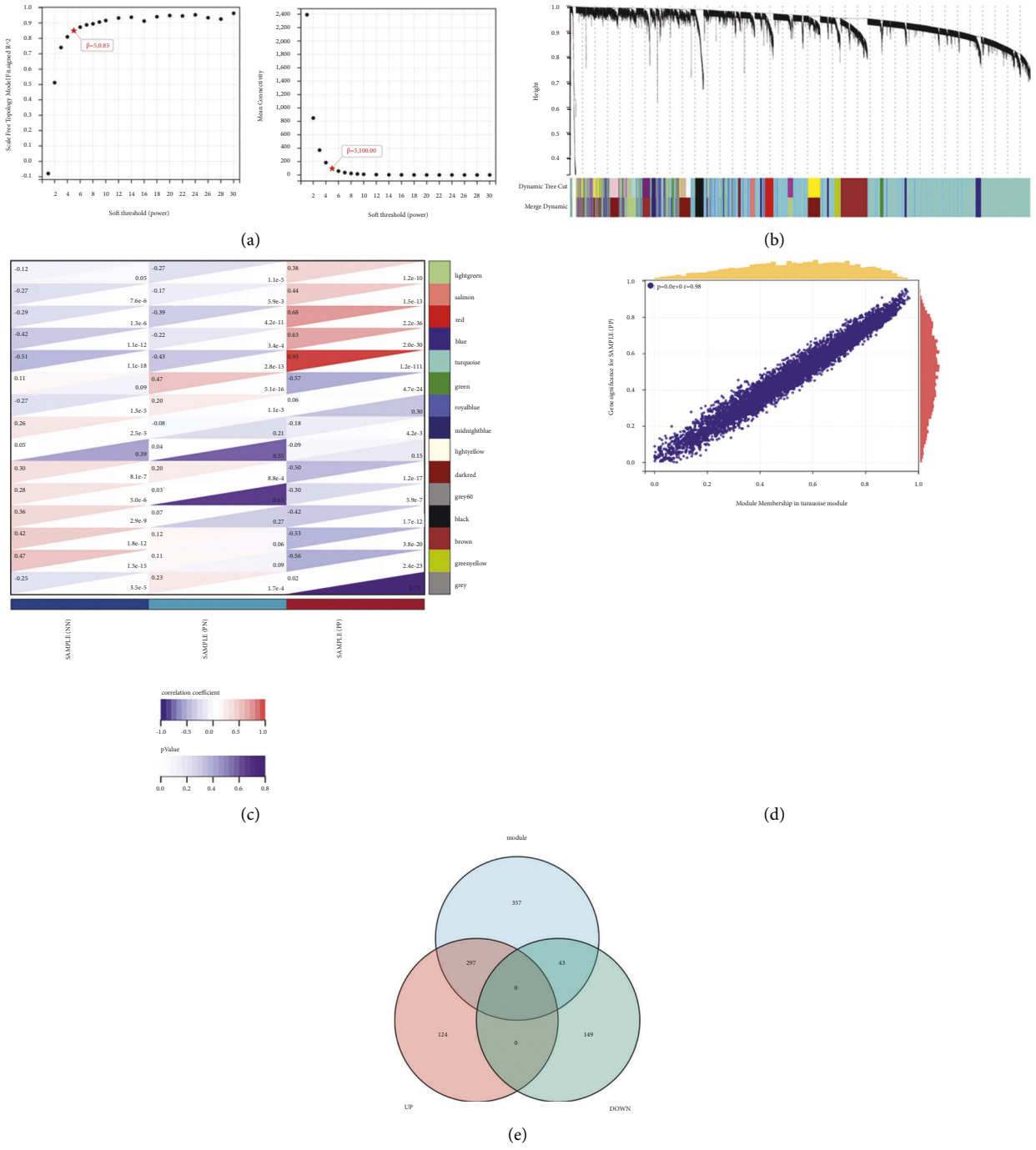

Figure 3: The result of WGCNA. (a) The lowest power for scale independence. (b) Repeated hierarchical clustering tree. (c) The associations between clinic traits and the modules. (d) Scatter plot of GS and MM correlation between turquoise module and PP samples. (e) Venn plot of 697 hub genes from turquoise module and overlapped DEGs from the above 2 different comparisons.

Then, the CytoHubba plugin was used to explore hub genes, and the top twenty were generated using DMNC, MCC, degree, EPC, and MNC methods. The intersection of the top 20 genes obtained from the five calculation methods was presented as an upset plot (Figure 4(b)). A total of 4 overlapped genes were obtained (TTK, KIF2C, BUB1B, and DLGAP5).

4.3. Expression Pattern Analysis of 4 Core Genes in the Validation Dataset. To further obtain more core genes, we analyzed the expression patterns of the four genes in the merge dataset as well as the validation dataset, GSE78097 and GSE55201. All 4 genes were highly expressed in psoriatic lesions compared to normal skin from psoriasis patients and normal controls (Figure 4(c)), but no difference was found

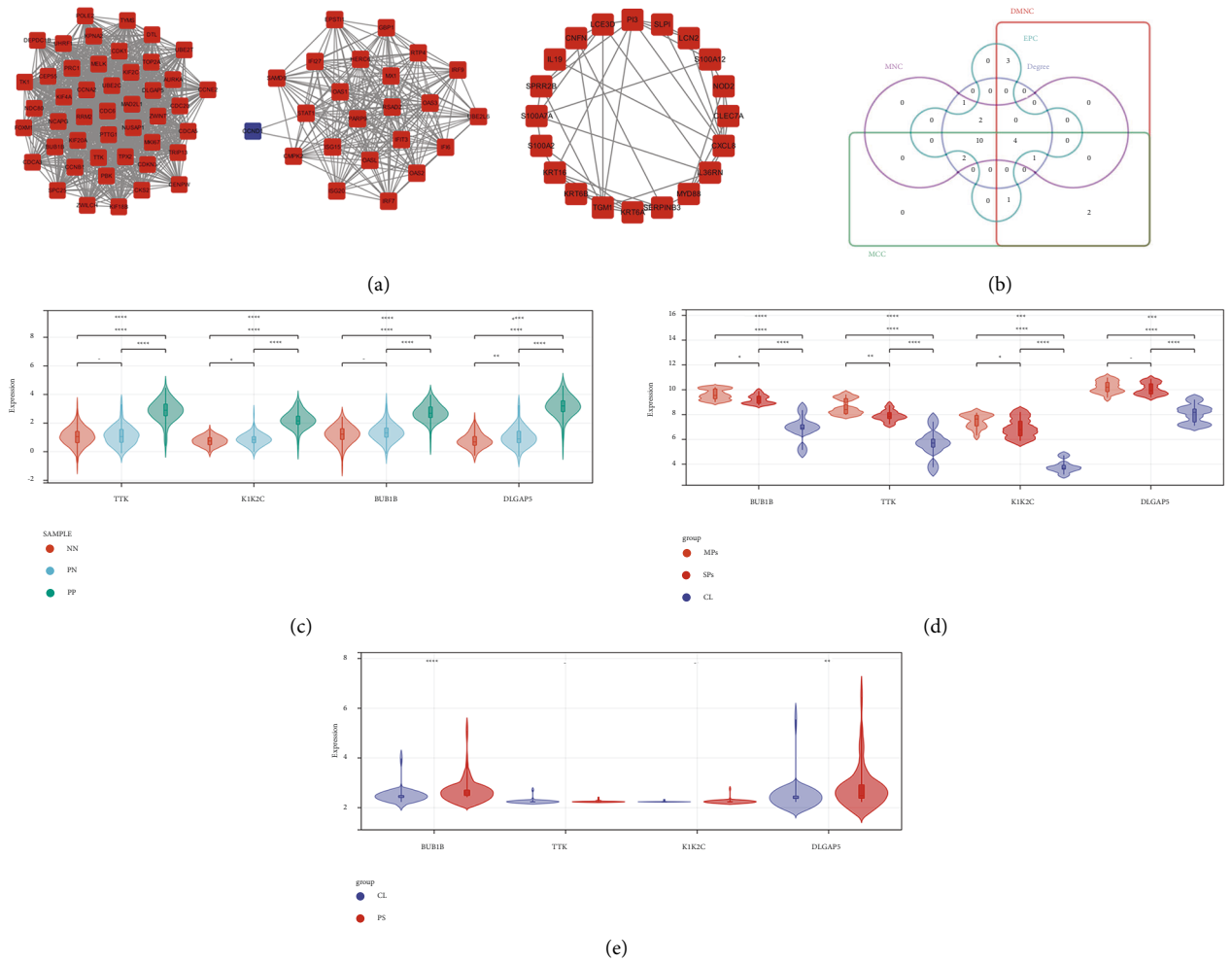

Figure 4: Further analysis of hub DEGs. (a) Clusters from MCODE in Cytoscape. (b) Overlapped genes of 5 different methods from CytoHubba plugin in Cytoscape. (c) Expression pattern of 4 overlapped genes in merged dataset (GSE13355 and GSE14905). (d) Expression pattern of 4 overlapped genes in GSE78097. (e) Expression pattern of 4 overlapped genes in GSE55201.

between normal skin from psoriasis patients and normal controls. As shown in Figure 4(d), BUB1B, TTK, and KIF2C were more highly expressed in psoriatic lesions compared to normal skin, which were more obvious in moderate psoriatic lesions than severe lesions. Differences in the DLGAP5 expression pattern exist only between lesions and normal skin, independent of lesion severity. Additionally, the expression of BUB1B and DLGAP5 in the blood samples of psoriasis patients was also higher than that of normal controls (Figure 4(e)). Combining the validation results of the above two datasets, BUB1B and DLGAP5 were considered to be core genes in the development of psoriasis. DLGAP5 has been reported to be correlated with clinical prognosis, immune cell infiltration, and tumor mutational burden across multiple tumors in previous studies [30]; thus, BUB1B was chosen for further analysis.

4.4. Identification and Function Enrichment Analysis of DEmiRNAs of Patients with Psoriasis. Differently expressed miRNAs (DEmiRNAs) of the GSE142582 dataset were obtained from 2 comparison sets including PP-PN and PP-NN. As shown in Figures 5(a)–5(c), a total of 140 DEmiRNAs for PP-NN set (57 upregulated and 83 downregulated) and 180 DEmiRNAs from PP-PN set (72 upregulated and 108 downregulated) were gained. Among them, 48 DEmiRNAs were overlapped between the above 2 sets (18 upregulated and 40 downregulated). Then, all the overlapped DEmiRNAs were used for DO enrichment analysis by miEAA. As shown in Figure 5(d), we ranked the results by the number of engaged DEmiRNAs, and the most involved diseases were multiple types of cancers. Additionally, mirPath (v 3.0) from DIANA-Tools is also used for KEGG enrichment analysis of those DEmiRNAs combined with DEGs from the hub module of the result of WGCNA. As shown in Figure 5(e), the top 1 involved pathway was cancer-related.

4.5. Prediction and Validation of miRNA Targeting BUB1B. Firstly, we predicted miRNAs targeting BUB1B using 5 different databases. The intersection of the predicted miRNAs with all overlapped DEmiRNAs is shown in Figure 5(f). With a threshold of simultaneous occurrence in at least three

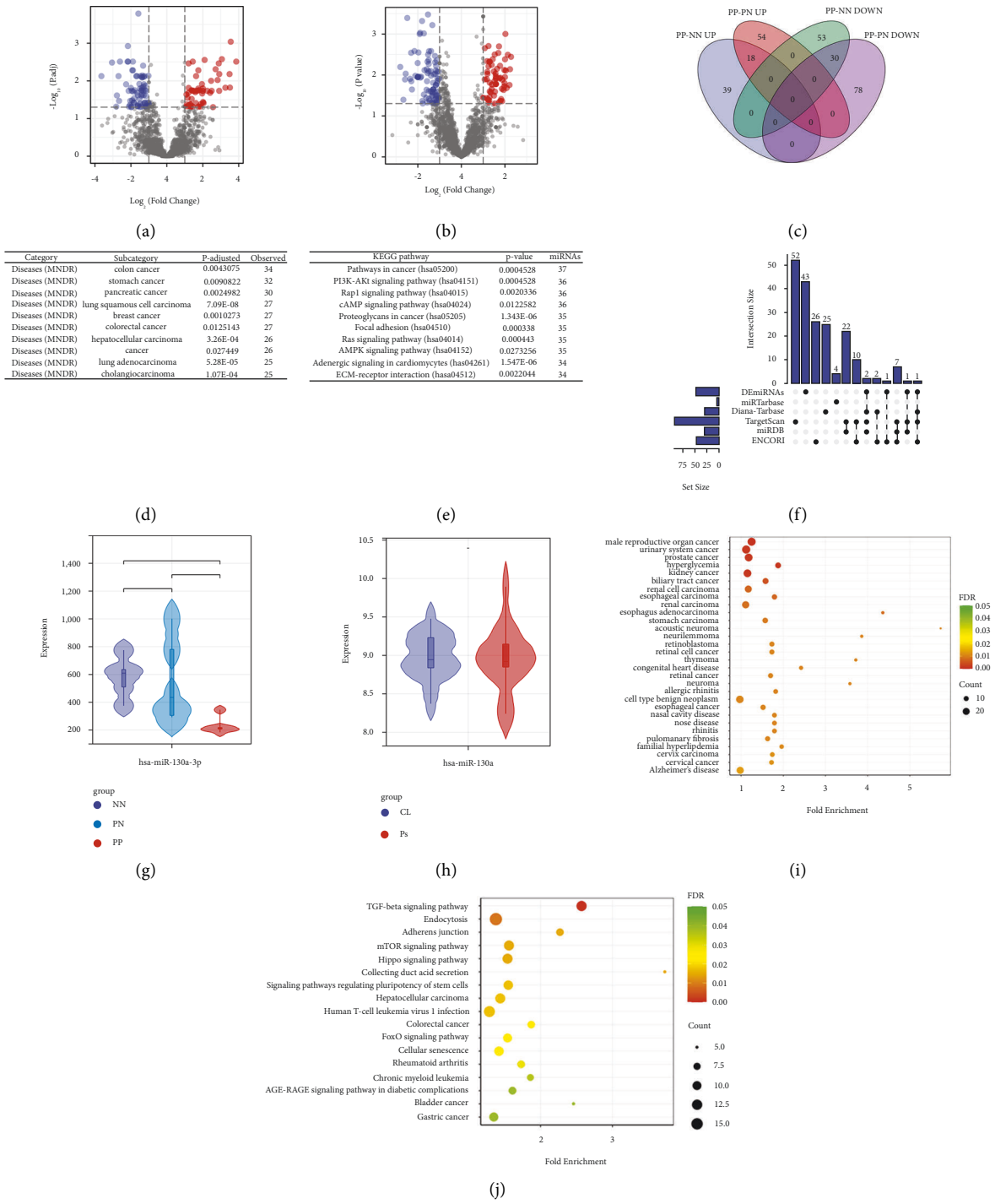

Category	Subcategory	P-adjusted	Observed
Diseases (MNDR)	colon cancer	0.0043075	34
Diseases (MNDR)	stomach cancer	0.0090822	32
Diseases (MNDR)	pancreatic cancer	0.0024982	30
Diseases (MNDR)	lung squamous cell carcinoma	7.09E-08	27
Diseases (MNDR)	breast cancer	0.0010273	27
Diseases (MNDR)	colorectal cancer	0.0125143	27
Diseases (MNDR)	hepatocellular carcinoma	3.26E-04	26
Diseases (MNDR)	cancer	0.027449	26
Diseases (MNDR)	lung adenocarcinoma	5.28E-05	25
Diseases (MNDR)	cholangiocarcinoma	1.07E-04	25

KEGG pathway	p-value	miRNAs
Pathways in cancer (hsa05200)	0.0004528	37
PI3K-AKt signaling pathway (hsa04151)	0.0004528	36
Rap1 signaling pathway (hsa04015)	0.0020336	36
cAMP signaling pathway (hsa04024)	0.0122582	36
Proteoglycans in cancer (hsa05205)	1.343E-06	35
Focal adhesion (hsa04510)	0.000338	35
Ras signaling pathway (hsa04014)	0.000443	35
AMPK signaling pathway (hsa04152)	0.0273256	35
Adenergic signaling in cardiomycytes (has04261)	1.547E-06	34
ECM-receptor interaction (hasa04512)	0.0022044	34

Figure 5: Differentially expressed miRNAs (DEmiRNAs) exploring and analysis. (a) Volcano plot of DEmiRNAs from PP-NN set. (b) Volcano plot of DEmiRNAs from PP-PN set. (c) Venn plot of DEmiRNAs from the above 2 comparisons. (d) Results of disease enrichment analysis of overlapped DEmiRNAs from 2 sets using miEAA. (e) Results of KEGG enrichment analysis of overlapped DEmiRNAs from 2 sets using mirPath. (f) Upset plot of overlapped DEmiRNAs and predicted miRNAs targeting BUB1B using different online tools. (g and h) Expression pattern of hsa-miR-130a-3p in GSE142582 (g) and GSE55515 (h). Results of diseases enrichment analysis (i) and KEGG enrichment analysis (j) of hsa-miR-130a-3p using CancerMIRNome.

databases, we obtained the only DEmiRNA targeting BUB1B, hsa-mir-130a-P3. Subsequently, we validated the expression pattern of hsa-miR-130a-3p in GSE142582 and GSE55515. As shown in Figure 5(g), hsa-miR-130a-3p was lowly expressed in the PP group compared with both the PN and NN group, while there was no statistical difference between the PN and NN groups. Conversely, the expression pattern of hsa-miR-130a-3p showed no difference in blood

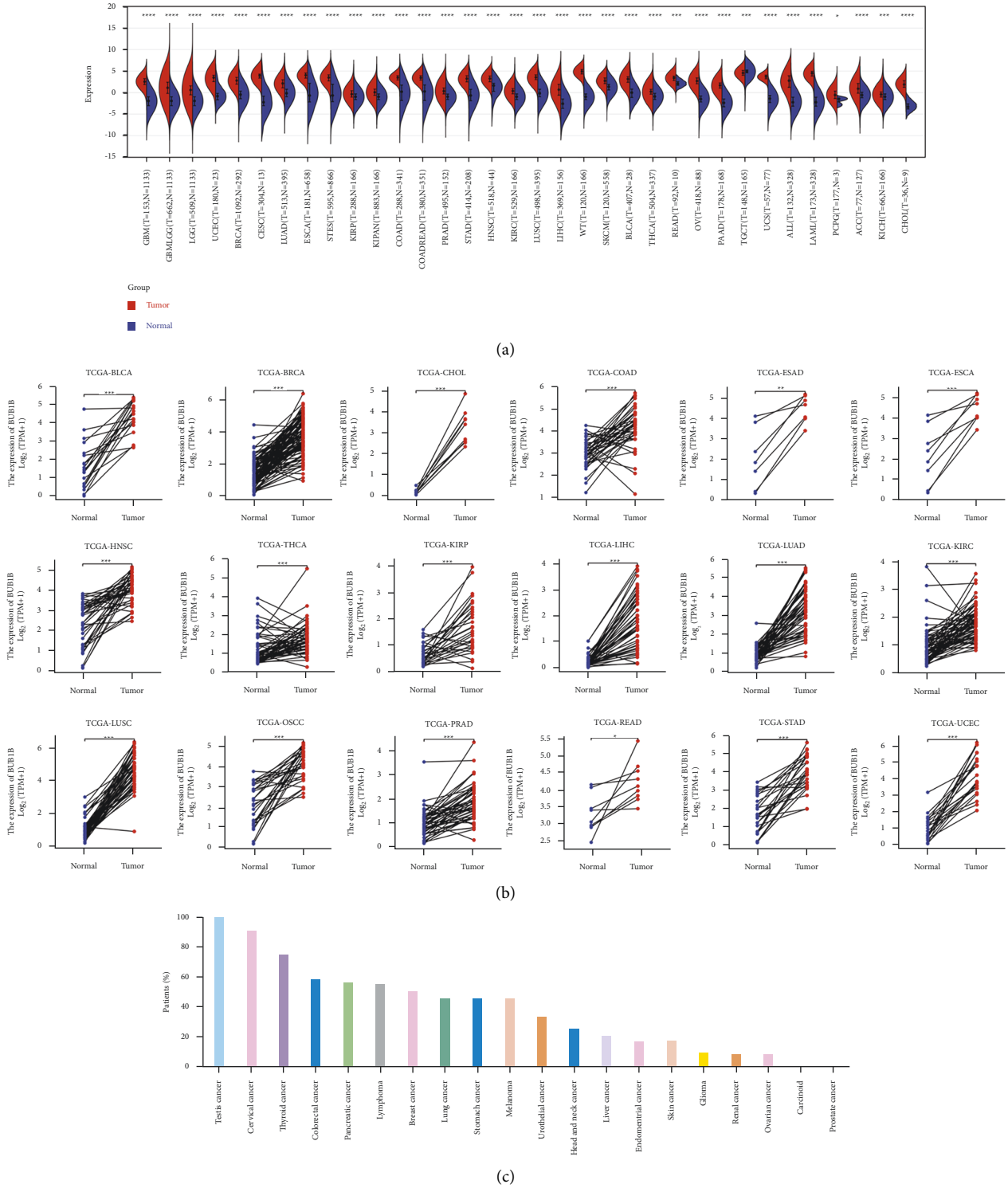

Figure 6: BUB1B expression pattern in pan-cancer; RNA expression pattern between normal and tumor samples (a) as well as paired tumor and normal tissues (b); protein expression pattern in pan-cancer using HPA database.

samples of psoriasis and normal controls (Figure 5(h)). The functional enrichment analysis was performed through CancerMIRNome. As shown in Figure 5(i), the diseases hsa-miR-130a-3p engaged in were the most cancer-related. The involved KEGG pathways are presented in Figure 5(j).

4.6. BUB1B Expression Analysis in Pan-Cancer. We calculated the difference in expression between normal and tumor samples in each tumor using R software (version 3.6.4) and difference significance analysis using unpaired Wilcoxon Rank Sum and Signed Rank Tests. As shown in Figure 6(a),

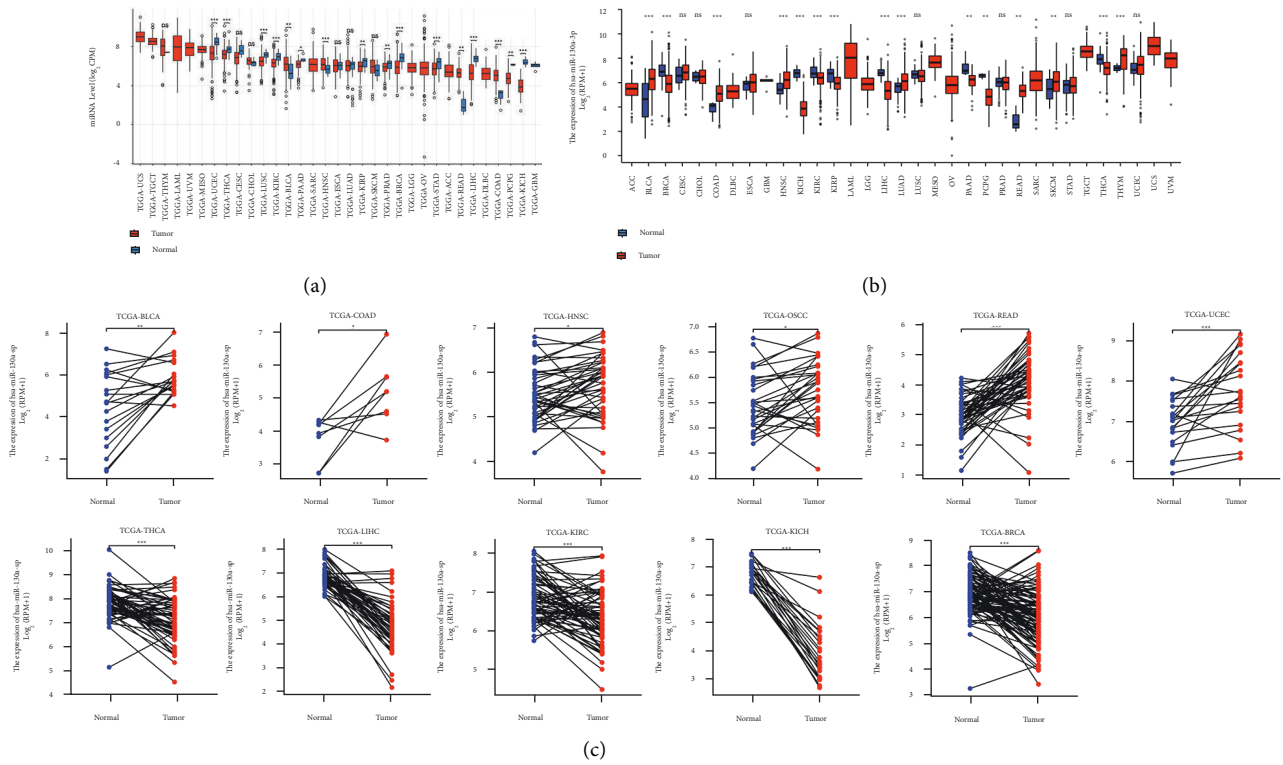

Figure 7: hsa-miR-130a-3p expression pattern in pan-cancer between normal and tumor samples ((a) figure from CancerMIRNome; (b) download dataset from TCGA) as well as paired tumor and normal tissues (c).

we observed significant upregulations in 33 tumors, including GBM, GBMLGG, LGG, UCEC, BRCA, CESC, LUAD, ESCA, STES, KIRP, KIPAN, COAD, COADREAD, PRAD, STAD, HNSC, KIRC, LUSC, LIHC, WT, SKCM, BLCA, THCA, READ, OV, PAAD, UCS, ALL, LAML, PCPG, ACC, KICH, and CHOL, and significant deregulation in THYM. For paired tumor and normal tissues in TCGA pan-cancer (Figure 6(b)), BUB1B was expressed at high levels in 18 tumors, including BLCA, BRCA, CHOL, COAD, ESAD, ESCA, HNSC, THCA, KIRP, LIHC, LUAD, KIRC, LUSC, OSCC, PRAD, READ, STAD, and UCEC. We continue to explore the protein level of BUB1B in pan-cancer using the HPA database. It was found that more than 50% of patients with 10 cancers exhibited high expression, including testis cancer, cervical cancer, thyroid cancer, colorectal cancer, pancreatic cancer, lymphoma, breast cancer, lung cancer, stomach cancer, and melanoma (Figure 6(c)).

4.7. Expression Analysis of hsa-miR-130a-3p in Pan-Cancer. After searching "hsa-miR-130a-3p" in "Query" section of CancerMIRNome (http://bioinfo.jialab-ucr.org/CancerMIRNome/), we obtained Figure 7(a). It was observed that hsa-miR-130a-3p had significant upregulations in 4 tumors (BLCA, HNSC, READ, and COAD) and downregulations in 12 tumors (UCEC, THCA, LUSC, KIRC, PAAD, KIRP, PRAD, BRCA, STAD, LIHC, PCPG, and KICH). As for the expression patterns analysis result from download dataset (Figure 7(b)), hsa-miR-130a-3p was found to have significant upregulations in 7 tumors (BLCA, COAD, HNSC, LUAD, READ, SKCM, and THYM) and downregulations in 8 tumors (BRCA, KICH, KIRC, KIRP, LIHC, PAAD, PCPG, and THCA). In paired comparison (Figure 7(c)), hsa-miR-130a-3p had significant upregulations in 6 tumors (BLCA, HNSC, OSCC, READ, COAD, and UCEC) and downregulations in 5 tumors (BRCA, KICH, KIRC, LIHC, and THCA).

4.8. Prognostic Significance of hsa-miR-130a-3p in Pan-Cancer. Using the CancerMIRNome database's "TCGA pan-cancer section," cox regression analysis of the results from 33 types of cancer suggested that the hsa-miR-130a-3p expression significantly correlated with OS in 6 types of cancer, including ACC, COAD, STAD, KIRC, LIHC, and UCS. Kaplan–Meier survival curves indicated that the unregulated hsa-miR-130a-3p expression was remarkably associated with poor OS in the ACC, COAD, STAD, and KIRC (Figure 8).

4.9. ROC Analysis of hsa-miR-130a-3p in Pan-Cancer. The results of ROC analysis of hsa-miR-130a-3p in various tumor types were obtained in the "TCGA pan-cancer part" of CancerMIRNome. As shown in Figure 9, a total of 5 cancers were found to have high AUC value (>0.85), including COAD, KICH, LIHC, PCPG, and READ. The results revealed that hsa-miR-130a-3p expression had excellent diagnostic value in multiple cancer types (Figure 10).

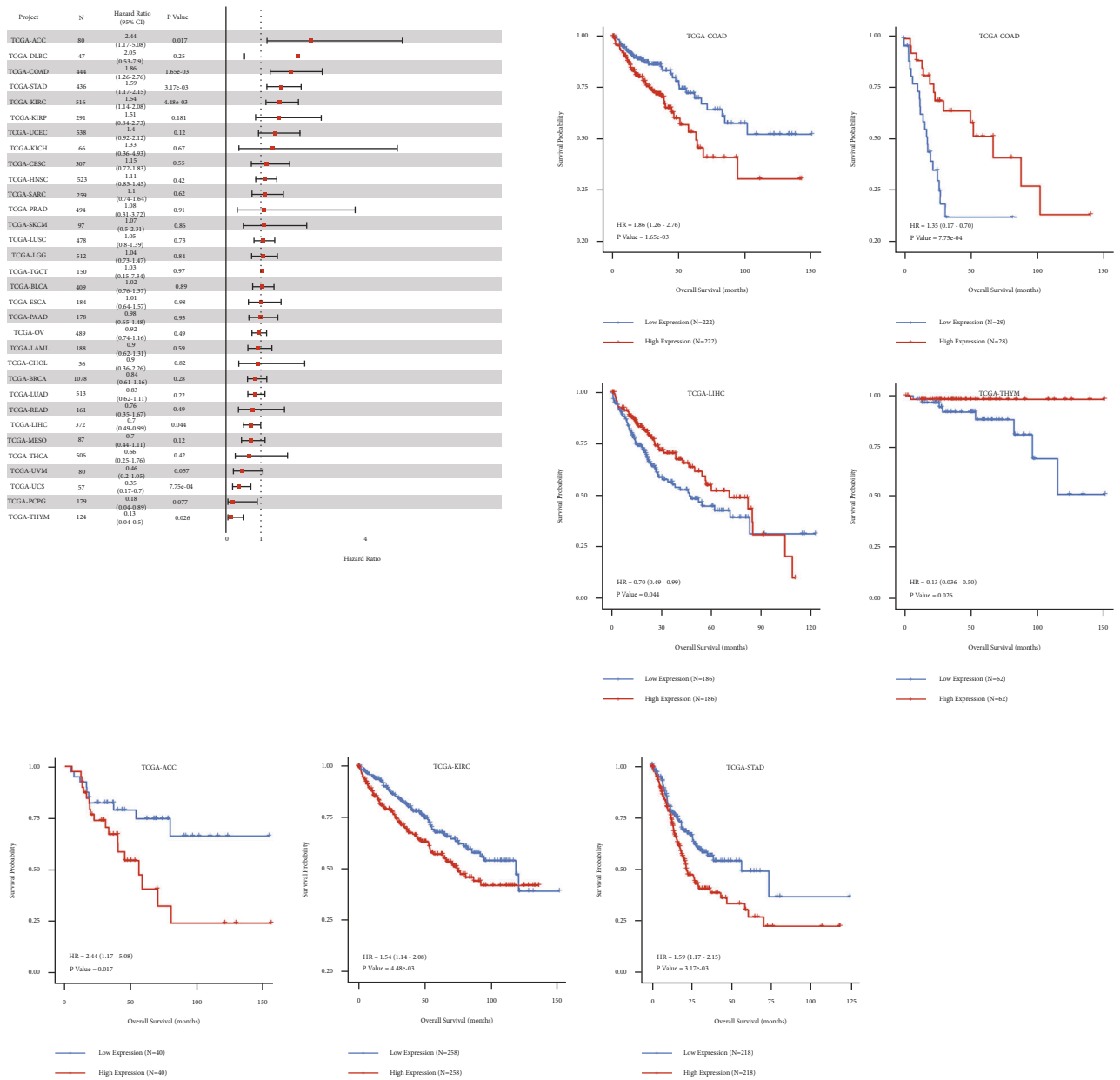

Figure 8: Association between the hsa-miR-130a-3p expression and OS in cancer patients. (a) A forest plot of hazard ratios of hsa-miR-130a-3p in 32 types of tumors. (b) Kaplan-Meier survival curves of OS for patients stratified by the different expressions of hsa-miR-130a-3p.

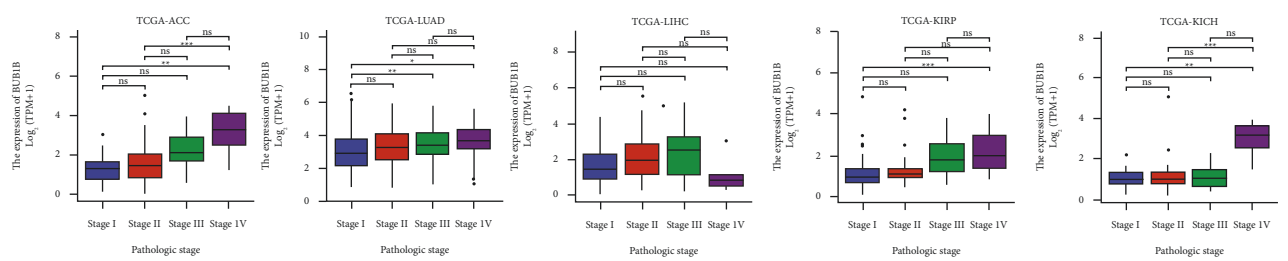

(a)

Figure 9: Continued.

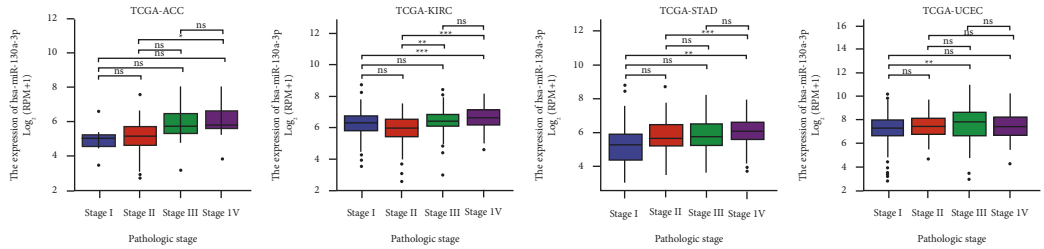

(b)

Figure 9: Correlations between the BUB1B and hsa-miR-130a-3p expression and the main pathological stages, including stage I, stage II, stage III, and stage IV.

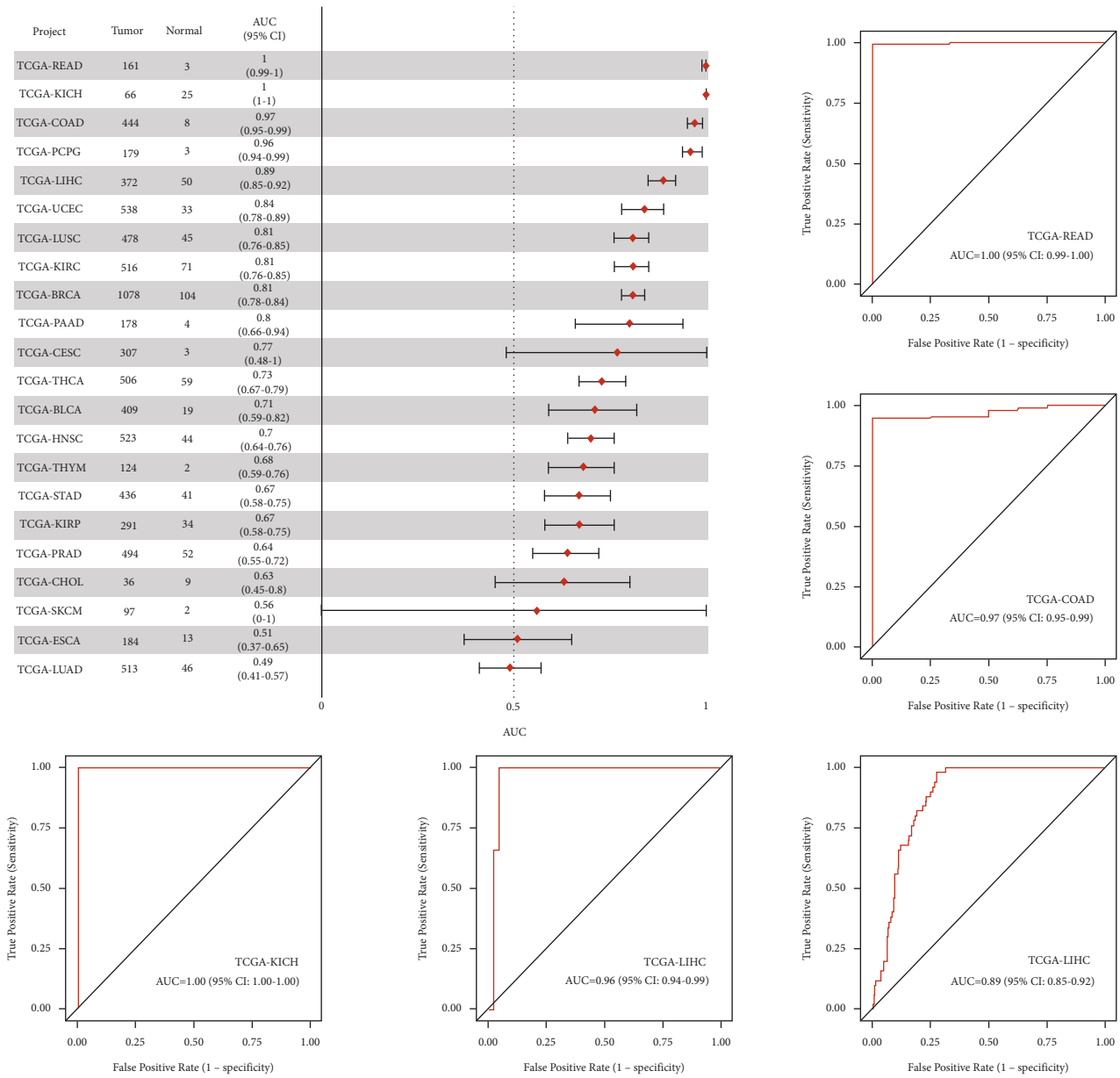

Figure 10: Forest plot and ROC curve of hsa-miR-130a-3p expression in pan-cancer.

Cancer	CancerFullName	SampleNum	Coefficient-R	p-value
ACC	Adrenocortical Carcinoma	79	0.476	9.34E-06
BLCA	Breast Urothelial Carcinoma	408	0.225	4.37E-06
BRCA	Breast Invasive Carcinoma	1085	0.109	3.35E-04
CESC	Cervical Squamous Cell Carcinoma and Endocervical Adenocarcinoma	306	-0.022	7.07E-01
CHOL	Cholangiocarcinoma	36	-0.18	2.94E-01
COAD	Colon Adenocarcinoma	450	-0.249	8.72E-08
DLBC	Lymphoid Neoplasm Diffuse Large B-cell Lymphoma	47	-0.077	6.07E-01
ESCA	Esophageal Carcinoma	162	0.129	1.01E-01
HNSC	Head and Neck Squamous Cell Carcinoma	497	0.08	7.64E-02
KICH	Kidney Chromophobe	65	0.359	3.29E-03
KIRC	Kidney Renal Clear Cell Carcinoma	517	0.198	5.86E-06
KIRP	Kidney Renal Papillary Cell Carcinoma	289	0.027	6.42E-01
LAML	Acute Myeloid Leukemia	83	0.065	5.58E-01
LGG	Brain Lower Grade Glioma	525	0.168	1.08E-04
LIHC	Liver Hepatocellular Carcinoma	370	0.009	8.56E-01
LUAD	Lung Adenocarcinoma	512	0.023	6.02E-01
LUSC	Lung Squamous Cell Carcinoma	475	0.061	1.83E-01
MESO	Mesothelioma	86	-0.072	5.13E-01
OV	Ovarian Serous Cystadenocarcinoma	376	0.196	1.33E-04
PAAD	Pancreatic Adenocarcinoma	178	0.176	1.89E-02
PCPG	Pheochromocytoma and Paraganglioma	183	0.093	2.13E-01
PRAD	Prostate Adenocarcinoma	495	-0.268	1.45E-09
READ	Rectum Adenocarcinoma	161	-0.201	1.05E-02
SARC	Sarcoma	261	0.1	1.07E-01
SKCM	Skin Cutaneous Melanoma	449	0.19	5.08E-05
STAD	Stomach Adenocarcinoma	372	0.004	9.42E-01
TGCT	Testicular Germ Cell Tumors	156	0.044	5.89E-01
THCA	Thyroid Carcinoma	509	0.054	2.21E-01
THYM	Thymoma	119	0.172	6.11E-02
UCEC	Uterine Corpus Endometrial Carcinoma	538	0.125	3.80E-03
UCS	Uterine Carcinosarcoma	56	-0.031	8.22E-01
UVM	Uveal Melanoma	80	-0.178	1.13E-01

Figure 11: Correlations of coexpression for BUB1B/hsa-miR-130a-3p in pan-cancer.

4.10. Pan-Cancer Analysis of the Correlation between hsa-miR-130a-3p, BUB1B Expression, and Clinicopathology. The expression of hsa-miR-130a-3p and BUB1B was assessed in cancer patients with different stages (I, II, III, and IV) to discover whether it is associated with clinicopathological features in multiple cancers. The results from the TCGA database revealed that the expression of hsa-miR-130a-3p was significantly upregulated in several advanced cancers, including ACC, KIRC, STAD, and UCEC (Figure 9(b)). As for BUB1B, upregulation in advanced ACC, KICH, KIRC, KIRP, and LUAD was revealed (Figure 9(a)).

4.11. Coexpression Analysis for BUB1B/hsa-miR-130a-3p in Pan-Cancer. After searching with hsa-miR-130a-3p and BUB1B in the "pan-cancer" section of ENCORI, we obtained the results shown in Figure 11. It was found that the correlation of BUB1B and hsa-miR-130a-3p coexpression was significant in multiple cancer types, especially in ACC, BLCA, COAD, KICH, PRAD, and READ.

5. Discussion

Based on the fact that very little was found in the literature on the question of potential molecules and mechanism for high risk of cancer in patients with psoriasis, this study was designed and performed. The most striking result to emerge from the data is that BUB1B/hsa-miR-130a-3p axis, closely related to the development of psoriasis, also plays a remarkable role in multiple cancer development.

After the identification and validation of DEGs, BUB1B and DLGAP5 were finally found as core genes in the development of psoriasis. In previous studies, several biomarkers as well as pathways have been reported to be correlated with the development of psoriasis, such as apoptosis, cell cycle, angiogenesis, inflammatory response, T cell immune response, VEGF, MAPK, WNT, JAK/STAT, NF-kappa B, and B cell response [7, 31]. It is the first time that BUB1B and DLGAP5 have been linked to the onset of psoriasis, though exact mechanisms are yet unknown. BUB1B, mitotic checkpoint serine/threonine-protein kinase BUB1 beta, is an essential component of the mitotic checkpoint, which is required for normal mitosis progression [32]. An impairment in BUB1B often leads to aneuploidy and chromosome instability, which can contribute to an increased cancer incidence [33, 34]. Furthermore, BUB1B mutations and abnormal expression can contribute to the development of cancer [35]. Consistent with the literature, this research revealed that BUB1B was significantly upregulated in multiple tumors across both paired and unpaired sample analyses, both RNA and protein levels. DLGAP5 (Discs Large Homolog Associated Protein 5), also known as HURP (Hepatoma Up-Regulated Protein) or KIAA0008, was identified as a cell-cycle-regulated protein [36], which is crucial for the movement of the spindle and helps establish the centromere during cell division [37]. According to previous studies, DLAG5 has been shown to be involved in many cancer types, including breast cancer, prostate cancer, and liver cancer [30, 37, 38]. All these results revealed that BUB1B as well as DLGAP5 may bridge the gap between psoriasis and cancers.

In this study, we likewise analyzed differentially expressed microRNAs in skin lesions of patients with psoriasis. KEGG enrichment analysis of these DEmiRNAs showed that they were highly associated with cancer development, which provides further evidence of a potential association between psoriasis and multiple cancers. Among them, hsa-miR-130a-5p was the only miRNA targeting BUB1B. In a series of subsequent analyses on hsa-miR-130a-3p in pan-cancer, we found that hsa-miR-130a-3p expression level was up- or downregulated in a variety of cancer types, some of which was also correlated with the clinical stage. This study supports evidence from previous observations that hsa-miR-130a-3p is a site-specific prognosis biomarker in colorectal cancer [39]. Based on the results of ROC analysis, we also found that hsa-miR-130a-3p was also a specific miRNA for LIHC, KICH, COAD, and PCPG.

Circulating miRNAs appear to be useful for preclinical diagnosis, since they are more sensitive and specific for early diagnosis, risk assessment, and monitoring disease progression

[40]. The assays of miRNA in blood samples have been developed as novel, minimally invasive biomarkers for the detection and the risk assessment of cancer [41]. Using the GEO dataset from the CancerMIRNome tool, circulating has-miR-130a-3p was found to have a higher level of blood in multiple tumor patients, which did not differ in blood between psoriasis patients and normal controls, suggesting that circulating has-miR-130a-3p has the potential to be a blood biomarker for cancer risk assessment in patients with psoriasis.

6. Conclusion

Through bioinformatics research, we discovered that the BUB1B/hsa-miR-130a-3p axis is closely related to the development of psoriasis as well as several cancer types. Circulating hsa-miR-130a-3p may be a potential biomarker for cancer risk assessment in psoriasis patients. These findings add to the growing body of research linking psoriasis to the development of cancer.

Data Availability

The article includes the study's original contributions; further questions should be addressed to the corresponding author.

Conflicts of Interest

The authors declare that there are no conflicts of interest.

Authors' Contributions

Xiaoxia Ding and Youming Huang drafted the manuscript and analyzed the data. Danfeng Xu and Yong Yu performed figure preparation and data analysis. Yibin Fan performed critical revision of the whole work. All authors contributed to the article and approved the submitted version.

Acknowledgments

This study was supported by the National Science Foundation of China (82073453).

References

[1] A. Karrys, I. Rady, and R.-C. N. Chamcheu, "Bioactive dietary VDR ligands regulate genes encoding biomarkers of skin repair that are associated with risk for psoriasis," *Nutrients*, vol. 10, no. 2, p. 174, 2018.

[2] J. H. Lee, H. J. Kim, and K. D. Han, "Cancer risk in 892 089 patients with psoriasis in Korea: a nationwide population-based cohort study," *Journal of Dermatology*, vol. 46, no. 2, pp. 95–102, 2019.

[3] A. M. Trafford, R. Parisi, E. Kontopantelis, C. E. M. Griffiths, and D. M. Ashcroft, "Association of psoriasis with the risk of developing or dying of cancer," *JAMA Dermatology*, vol. 155, no. 12, pp. 1390–1403, 2019.

[4] S. Vaengebjerg, L. Skov, A. Egeberg, and N. D. Loft, "Prevalence, incidence, and risk of cancer in patients with psoriasis and psoriatic arthritis," *JAMA Dermatology*, vol. 156, no. 4, pp. 421–429, 2020.

[5] M. Chen, B. Liao, and Z. Li, "Global similarity method based on a two-tier random walk for the prediction of microRNA–disease association," *Scientific Reports*, vol. 8, no. 1, p. 6481, 2018.

[6] Q. Liu, D.-H. Wu, L. Han et al., "Roles of microRNAs in psoriasis: immunological functions and potential biomarkers," *Experimental Dermatology*, vol. 26, no. 4, pp. 359–367, 2017.

[7] S. Xiao, X. Liu, X. Wang et al., "Plasma microRNA expression profiles in psoriasis," *Journal of Immunology Research*, vol. 2020, Article ID 1561278, 2020.

[8] V. Gonzalez-Villasana, M. H. Rashed, Y. Gonzalez-Cantú et al., "Presence of circulating miR-145, miR-155, and miR-382 in exosomes isolated from serum of breast cancer patients and healthy donors," *Disease Markers*, vol. 2019, Article ID 6852917, 2019.

[9] A. Honegger, D. Schilling, S. Bastian et al., "Dependence of intracellular and exosomal microRNAs on viral E6/E7 oncogene expression in HPV-positive tumor cells," *PLoS Pathogens*, vol. 11, no. 3, Article ID e1004712, 2015.

[10] Z. Su, H. Fang, H. Hong et al., "An investigation of biomarkers derived from legacy microarray data for their utility in the RNA-seq era," *Genome Biology*, vol. 15, no. 12, p. 523, 2014.

[11] Z. Feng, L. Li, Q. Zeng et al., "RNF114 silencing inhibits the proliferation and metastasis of gastric cancer," *Journal of Cancer*, vol. 13, no. 2, pp. 565–578, 2022.

[12] E. Clough and T. Barrett, "The gene expression omnibus database," *Methods in Molecular Biology*, vol. 1418, pp. 93–110, 2016.

[13] J. Navarro Gonzalez, A. S. Zweig, M. L. Speir et al., "The UCSC Genome Browser database: 2021 update," *Nucleic Acids Research*, vol. 49, no. D1, pp. D1046–D1057, 2021.

[14] J. Taminau, S. Meganck, C. Lazar et al., "Unlocking the potential of publicly available microarray data using inSilicoDb and inSilicoMerging R/bioconductor packages," *BMC Bioinformatics*, vol. 13, no. 1, p. 335, 2012.

[15] W. E. Johnson, C. Li, and A. Rabinovic, "Adjusting batch effects in microarray expression data using empirical bayes methods," *Biostatistics*, vol. 8, no. 1, pp. 118–127, 2007.

[16] M. E. Ritchie, B. Phipson, D. Wu et al., "Limma powers differential expression analyses for RNA-sequencing and microarray studies," *Nucleic Acids Research*, vol. 43, no. 7, p. e47, 2015.

[17] P. Langfelder and S. Horvath, "WGCNA: an R package for weighted correlation network analysis," *BMC Bioinformatics*, vol. 9, no. 1, p. 559, 2008.

[18] G. Yu, L.-G. Wang, Y. Han, and Q.-Y. He, "clusterProfiler: an R package for comparing biological themes among gene clusters," *OMICS: A Journal of Integrative Biology*, vol. 16, no. 5, pp. 284–287, 2012.

[19] D. Szklarczyk, A. L. Gable, D. Lyon et al., "STRING v11: protein-protein association networks with increased coverage, supporting functional discovery in genome-wide experimental datasets," *Nucleic Acids Research*, vol. 47, no. D1, pp. D607–D613, 2019.

[20] C.-H. Chin, S.-H. Chen, H.-H. Wu, C. W. Ho, M. T. Ko, and C. Y. Lin, "Cytohubba: identifying hub objects and sub-networks from complex interactome," *BMC Systems Biology*, vol. 8, no. S4, p. S11, 2014.

[21] Y. Chen and X. Wang, "miRDB: an online database for prediction of functional microRNA targets," *Nucleic Acids Research*, vol. 48, no. D1, pp. D127–D131, 2020.

[22] V. Agarwal, G. W. Bell, J.-W. Nam, and D. P. Bartel, "Predicting effective microRNA target sites in mammalian mRNAs," *eLife*, vol. 4, 2015.

[23] H.-Y. Huang, Y.-C.-D. Lin, and J. Li, "miRTarBase 2020: updates to the experimentally validated microRNA–target interaction database," *Nucleic Acids Research*, vol. 48, no. D1, pp. D148–D154, 2020.

[24] J.-H. Li, S. Liu, H. Zhou, L.-H. Qu, and J.-H. Yang, "starBase v2.0: decoding miRNA-ceRNA, miRNA-ncRNA and protein-RNA interaction networks from large-scaleCLIP-Seq data," *Nucleic Acids Research*, vol. 42, no. D1, pp. D92–D97, 2014.

[25] D. Karagkouni, M. D. Paraskevopoulou, S. Chatzopoulos et al., "DIANA-TarBase v8: a decade-long collection of experimentally supported miRNA–gene interactions," *Nucleic Acids Research*, vol. 46, no. D1, pp. D239–D245, 2018.

[26] A. Lex, N. Gehlenborg, H. Strobelt, R. Vuillemot, and H. Pfister, "UpSet: visualization of intersecting sets," *IEEE Transactions on Visualization and Computer Graphics*, vol. 20, no. 12, p. 1992, 2014.

[27] K. Ito and D. Murphy, "Application of ggplot2 to pharmacometric graphics," *CPT: Pharmacometrics & Systems Pharmacology*, vol. 2, no. 10, p. e79, 2013.

[28] "The human protein Atlas—spatial localization of the human proteome in health and disease–PMC," 2022, https://www.ncbi.nlm.nih.gov/pmc/articles/PMC7737765/.

[29] R. Li, H. Qu, S. Wang et al., "CancerMIRNome: an interactive analysis and visualization database for miRNome profiles of human cancer," *Nucleic Acids Research*, vol. 50, no. D1, pp. D1139–D1146, 2022.

[30] N. Tang, X. Dou, X. You, Q. Shi, M. Ke, and G. Liu, "Pan-cancer analysis of the oncogenic role of discs large homolog associated protein 5 (DLGAP5) in human tumors," *Cancer Cell International*, vol. 21, no. 1, p. 457, 2021.

[31] F. Benhadou, E. Glitzner, A. Brisebarre et al., "Epidermal autonomous VEGFA/Flt1/Nrp1 functions mediate psoriasis-like disease," *Science Advances*, vol. 6, no. 2, Article ID eaax5849, 2020.

[32] M. Kapanidou, S. Lee, and V. M. Bolanos-Garcia, "BubR1 kinase: protection against aneuploidy and premature aging," *Trends in Molecular Medicine*, vol. 21, no. 6, pp. 364–372, 2015.

[33] C. Y. Jiao, Q. C. Feng, C. X. Li et al., "BUB1B promotes extrahepatic cholangiocarcinoma progression via JNK/c-Jun pathways," *Cell Death & Disease*, vol. 12, no. 1, p. 63, 2021.

[34] C. Dominguez-Brauer, K. L. Thu, J. M. Mason, H. Blaser, M. Bray, and T. Mak, "Targeting mitosis in cancer: emerging strategies," *Molecular Cell*, vol. 60, no. 4, pp. 524–536, 2015.

[35] S. Hanks, K. Coleman, S. Reid et al., "Constitutional aneuploidy and cancer predisposition caused by biallelic mutations in BUB1B," *Nature Genetics*, vol. 36, no. 11, pp. 1159–1161, 2004.

[36] S. Bassal, N. Nomura, D. Venter, K. Brand, M. J. McKay, and P. J. van der Spek, "Characterization of a novel human cell-cycle-regulated homologue of drosophila dlg1," *Genomics*, vol. 77, no. 1-2, pp. 5–7, 2001.

[37] W. Liao, W. Liu, Q. Yuan et al., "Silencing of DLGAP5 by siRNA significantly inhibits the proliferation and invasion of hepatocellular carcinoma cells," *PLoS One*, vol. 8, no. 12, Article ID e80789, 2013.

[38] W.-X. Peng, C.-H. Gao, and G.-B. Huang, "High throughput analysis to identify key gene molecules that inhibit adipogenic differentiation and promote osteogenic differentiation of human mesenchymal stem cells," *Experimental and Therapeutic Medicine*, vol. 17, no. 4, pp. 3021–3028, 2019.

[39] L. M. Vieira, N. A. N. Jorge, J. B. de Sousa, J. C. Setubal, P. F. Stadler, and M. E. M. T. Walter, "Competing endogenous RNA in colorectal cancer: an analysis for colon, rectum, and rectosigmoid junction," *Frontiers in Oncology*, vol. 11, Article ID 681579, 2021.

[40] P. Goguet-Rubio, R. L. Klug, D. L. Sharma et al., "Existence of a strong correlation of biomarkers and miRNA in females with metabolic syndrome and obesity in a population of West Virginia," *International Journal of Medical Sciences*, vol. 14, no. 6, pp. 543–553, 2017.

[41] M. A. Moga, A. Bălan, O. G. Dimienescu, V. Burtea, R. M. Dragomir, and C. V. Anastasiu, "Circulating miRNAs as biomarkers for endometriosis and endometriosis-related ovarian cancer—an overview," *Journal of Clinical Medicine*, vol. 8, no. 5, p. 735, 2019.

Hindawi
Evidence-Based Complementary and Alternative Medicine
Volume 2022, Article ID 2483669, 8 pages
https://doi.org/10.1155/2022/2483669

Research Article

Protein Kinase N2 Reduces Hydrogen Peroxide-induced Damage and Apoptosis in PC12 Cells by AntiOxidative Stress and Activation of the mTOR Pathway

Lin Wang[1] **and Lin Zhang**[2]

[1]*Department of Orthopedics, Yijishan Hospital, Wannan Medical College, Wuhu 241000, Anhui, China*
[2]*Hangzhou TCM Hospital Affiliated to Zhejiang Chinese Medical University, Hangzhou 310053, Zhejiang, China*

Correspondence should be addressed to Lin Zhang; zhanglin_rei@163.com

Received 26 July 2022; Revised 2 September 2022; Accepted 9 September 2022; Published 21 September 2022

Academic Editor: Xueliang Wu

Objective. To investigate the role and mechanism of protein kinase N2 (PKN2) in hydrogen peroxide (H_2O_2)-induced injury of PC12 cells. *Methods*. PC12 cells were transfected with lentivirus to knock down or overexpress PKN2 and then were treated with 300 μM H_2O_2 to establish a cell model of oxidative stress injury. The cell viability of PC12 cells in each group was determined by the CCK-8 method. Biochemical assays were used to measure reactive oxygen species (ROS), malondialdehyde (MDA) levels, and superoxide dismutase (SOD) activity. Western blot was used to detect the protein expressions of PKN2, caspase-3, cleaved-caspase-3, PARP, cleaved-PARP, p-mTOR, and mTOR in PC12 cells in each group. *Results*. H_2O_2 treatment could significantly reduce PC12 cell viability and promote cell apoptosis and oxidative stress. PKN2 overexpression inhibited H_2O_2-induced apoptosis and oxidation damage by increasing PC12 cell viability, SOD activity, and p-mTOR protein expression, reducing intracellular ROS and MDA levels, and cleaved-caspase-3 and cleaved-PARP protein expression. *Conclusion*. PKN2 overexpression can alleviate H_2O_2-induced oxidative stress injury and apoptosis in PC12 cells by activating the mTOR pathway.

1. Introduction

Many central nervous system diseases, such as cerebral ischemia, spinal cord injury, Alzheimer's disease, Parkinson's disease, amyotrophic lateral sclerosis, Huntington's disease, and so on, often show neuron injury and death [1, 2]. These neurological disorders share common risk factors such as aging, oxidative stress, environmental stress, and protein dysfunction [3]. Oxidative stress damages the integrity of neurons causes cell necrosis or apoptosis and causes damage to the structure and function of the nervous system [4]. Since oxidative stress is a promising therapeutic target for nervous system disease treatments.

Protein kinase N (PKN) is a subfamily of AGC serine/threonine protein kinase. It consists of three subtypes, PKN1, PKN2, and PKN3. Because of its extensive biological functions, such as regulating the cell cycle, receptor transport, vesicle transport, cell apoptosis, and so on, it has attracted more and more attention [5]. PKN2, a member of the PKN2 family, has been found to promote axon growth and play an important role in the migration of neural crest in mouse mesodermal development [6, 7]. However, whether PKN2 has a protective effect on nerve cells and what mechanism is involved in this protective effect is not clear. Mammalian rapamycin (mTOR) is widely distributed in the central nervous system, which can promote the proliferation, differentiation, and survival of nerve cells and regulate synaptic plasticity [8]. PC12 cells are a recognized neuronal cell model for neuronal mechanistic studies and the detection of potentially neurotoxic substances [9]. In this study, the oxidative stress model of rat pheochromocytoma (PC12) cells induced by H_2O_2 was used to investigate

whether PKN2 has a protective effect on the H_2O_2-induced PC12 cell injury model and the possible mechanism of PKN2 and mTOR pathway.

2. Materials and Methods

2.1. Cell Culture. PC12 cells were purchased from the Shanghai Institute of life sciences, Chinese Academy of Sciences. PC12 cells were cultured in Dulbecco's Modified Eagle Medium (DMEM, Gibco, USA) containing 10% fetal bovine serum (FBS, Gibco, USA) and 1% penicillin-streptomycin (Gibco, USA) at 37°C, 5% of CO_2 incubator.

2.2. Cell Transfection and Grouping. Negative control lentivirus and PKN2 shRNA lentivirus, PKN2 overexpression lentivirus, and vector lentivirus were designed and synthesized by Wuhan University (sequence number: br005591). The RNAi target sequence was ACGCTCGGGTGATGTTKATTA, and the negative control target sequence was ttctccgaacgtcacgt. PC12 cells in the logarithmic growth phase were selected and transfected using Lipofectamine™ 3000 Transfection Reagent (Invitrogen) according to the manufacturer's instructions, and cells were grouped into control group, siNC group, PKN2i group, vector group, and PKN2-OE group. 72 h after transfection, the expression levels of PKN2 in each group of cells were detected by western blot.

2.3. Construction of Oxidative Stress Model. The transfected PC12 cells were treated with or without H_2O_2 (300 μM) for 8 h to induce an oxidative stress model [10, 11]. The transfected PC12 cells were divided into the control group, model group (H_2O_2), siNC + H_2O_2 group, PKN2i + H_2O_2 group, vector + H_2O_2 group, and PKN2-OE + H_2O_2 group. When the cells grow to a certain number, the cells are collected.

2.4. Cell Viability Assay. Cell viability was detected by the Cell Counting Kit-8 (CCK-8) assay. Transfected PC12 cells were seeded in a 96-well plate at 1×10^4 cells/well, 100 μL per well. Cell grouping and drug treatment were as described above. After 24 h, the medium was replaced with a DMEM medium containing 10 μL of CCK-8 solution (Beyotime), and the incubation was continued for 2 h. Then, the absorbance at 450 nm was measured using a microplate reader (BioTek Instruments).

2.5. Intracellular Oxygen Species (ROS), Malondialdehyde (MDA), and Superoxide Dismutase (SOD) Measurement. PC12 cells were seeded in 6-well plates at 1×106 cells/mL, and the cell supernatants were collected after cell grouping and administration as described above. Intracellular ROS, MDA, and SOD levels were determined using a ROS assay kit, lipid peroxidation assay kit, and SOD assay kit following the manufacturer's instructions (Nanjing Jiancheng).

2.6. Western Blot. PC12 cells were seeded in a 6-well plate at 1×10^6 cells/mL, and the cells were grouped and treated as described above. Cells were harvested, and total cell protein was extracted using RIPA lysis buffer (Solarbio) containing PMSF and phosphatase inhibitors, and the protein concentration was determined using a BCA protein detection kit (Beyotime). Protein samples were separated by SDS-PAGE electrophoresis, and proteins were transferred into a polyvinylidene fluoride (PVDF) membrane. Membranes were blocked with 5% skim milk or BSA for 1 h at room temperature. Then, the membranes were mixed with anti-PKN2-antibody, anticaspase-3-antibody, anticleaved-caspase-3-antibody, anti-PARP-antibody, anticleaved-PARP-antibody, anti-mTOR-antibody, anti-p-mTOR-antibody, and anti-GAPDH-antibody (all primary antibodies were purchased from Abcam, using ratio 1 : 1000) were incubated overnight. The next day, wash the membrane with TBST, then incubate the membrane with anti-IgG secondary goat anti-mouse antibody (1 : 5000, Abcam) or anti-IgG goat anti-rabbit antibody (1 : 5000, Abcam) at room temperature for 1h. The protein bands were displayed using the BeyoECL Star kit (Beyotime, China), and the gray values of the protein bands were determined by Image-Pro Plus software.

2.7. Statistical Analysis. SPSS 20.0 and GraphPad Prism 9.0 software were used for statistical analysis and visualization of experimental data. Comparisons between multiple groups were performed using one-way ANOVA, and differences between two groups were analyzed using Student's t-test. The experimental results are expressed as mean ± standard deviation (SD). $P < 0.05$ was considered a statistically significant difference.

3. Results

3.1. PKN2 Overexpression is Protective against H_2O_2-induced PC12 Cells. To investigate the effect of PKN2 on oxidative damage in PC12 cells. First, we knocked down or overexpressed PKN2 in PC12 cells by transfection and detected the transfection efficiency by western blot. Compared with the Si-NC group, PKN2 protein expression in the PKN2i group was significantly decreased, and compared with the vector group, the PKN2 protein expression in the PKN2-OE group was significantly increased (Figures 1(a), 1(b)).

Subsequently, the effect of PKN2 on H_2O_2-induced PC12 cell viability was detected by the CCK8 assay. The results showed that compared with the control group, the viability of PC12 cells was significantly reduced after H_2O_2 treatment, indicating that the oxidative damage model of PC12 cells was successfully established. Further analysis showed that compared with the siNC + H_2O_2 group, the cell viability of the PKN2i + $H2O_2$ group was significantly reduced. Compared with the vector + H_2O_2 group, the cell viability in the PKN2-OE + H_2O_2 group was significantly increased (Figure 1(c)). These results suggest that PKN2 overexpression can alleviate the toxic effects of H_2O_2 on PC12 cells.

3.2. PKN2 Overexpression Reduces H2O2-induced Oxidative Damage in PC-12 Cells. The production of ROS and MDA and the changes in SOD activity are important markers of oxidative stress in cells [12]. Previous studies have shown that

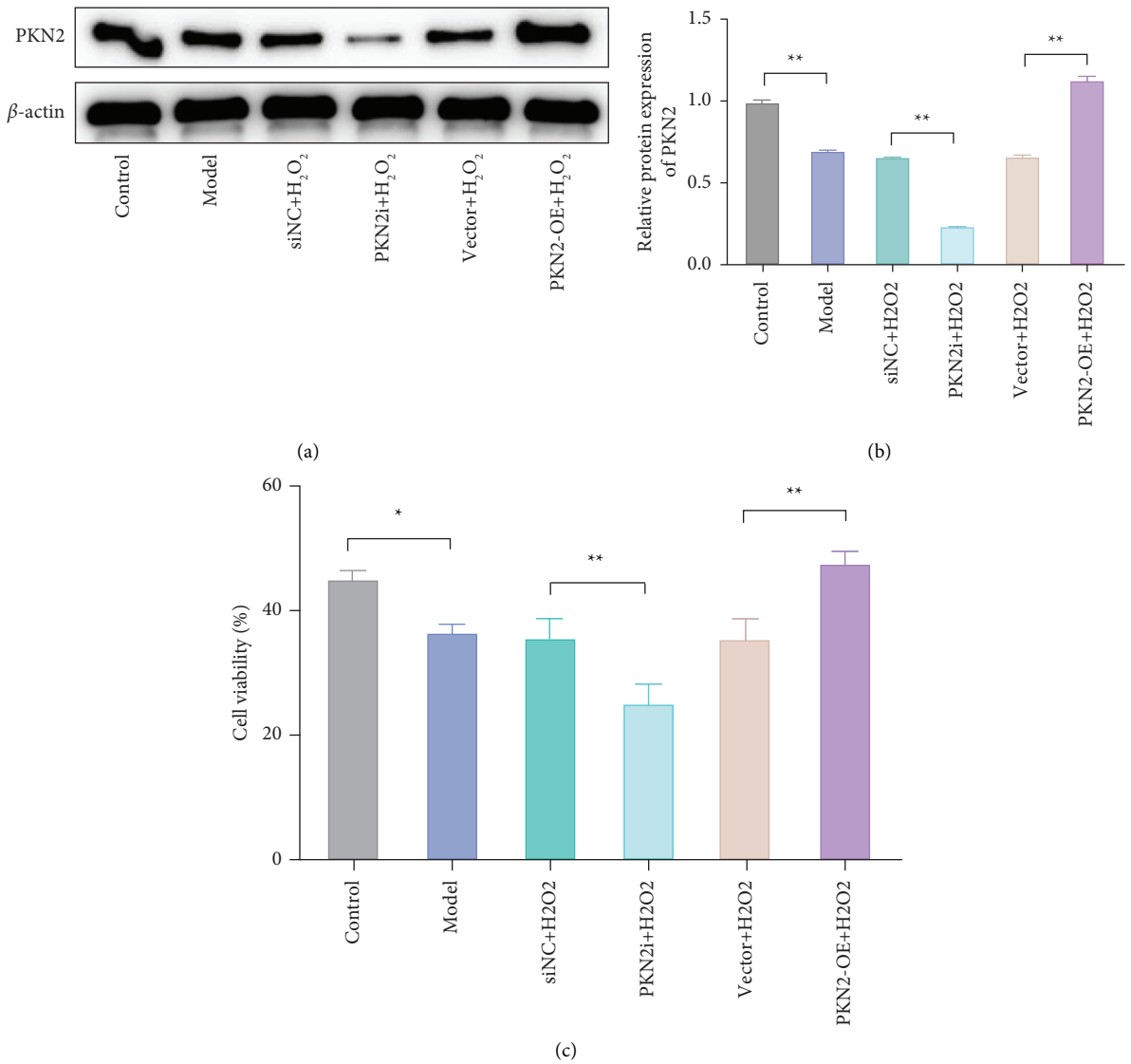

Figure 1: PKN2 overexpression has a protective effect on H_2O_2-induced PC12 cells. (a/b) PKN2 protein expression in PC12 cells after transfection were detected by western blot. (c) Effects of PKN2 knockdown or overexpression on H_2O_2-induced PC12 cell viability. $^{**}P < 0.01$ *vs.* control, siNC + H_2O_2, and vector + H_2O_2.

ROS is an important mediator of H_2O_2-induced cell death [13]. To explore the role of PKN2 in H_2O_2-induced oxidative stress in PC12 cells, we examined the production of ROS and MDA and the activity of SOD. The results showed that in PC12 cells, compared with the control group, the levels of ROS and MDA in the cells of the model group were significantly increased, and the activity of SOD was significantly decreased. Compared with the siNC + H_2O_2 group, knockdown of PKN2 could significantly increase the levels of ROS and MDA and decrease the activity of SOD. Compared with the vector + H_2O_2 group, PKN2 overexpression significantly decreased the levels of ROS and MDA in PC12 cells and increased the activity of SOD (Figures 2(a)–2(c)). The above results indicate that overexpression of PKN2 could significantly inhibit the oxidative damage of H_2O_2 on PC12 cells and exert an antioxidative stress effect.

3.3. PKN2 Overexpression Prevents H_2O_2-induced Apoptosis in PC12 Cells. The excessive accumulation of ROS caused by the dysfunction of mitochondria in cells is an important inducement for apoptosis [14]. Therefore, we further explore the effect of PKN2 on H_2O_2-induced apoptosis in PC12 cells. The results showed that compared with the control group, the expression of cleaved-PARP and cleaved-caspase-3 proteins in the cells of the model group was significantly increased. Compared with the siNC + H_2O_2 group, knockdown of PKN2 significantly increased the expression levels of cleaved-PARP and cleaved-caspase-3. Compared with the vector + H_2O_2 group, PKN2 overexpression could significantly reduce the expressions of cleaved-PARP and cleaved-caspase-3 proteins. In addition, PARP and caspase-3 expressions did not change significantly in each group of cells (Figures 3(a)(a)–

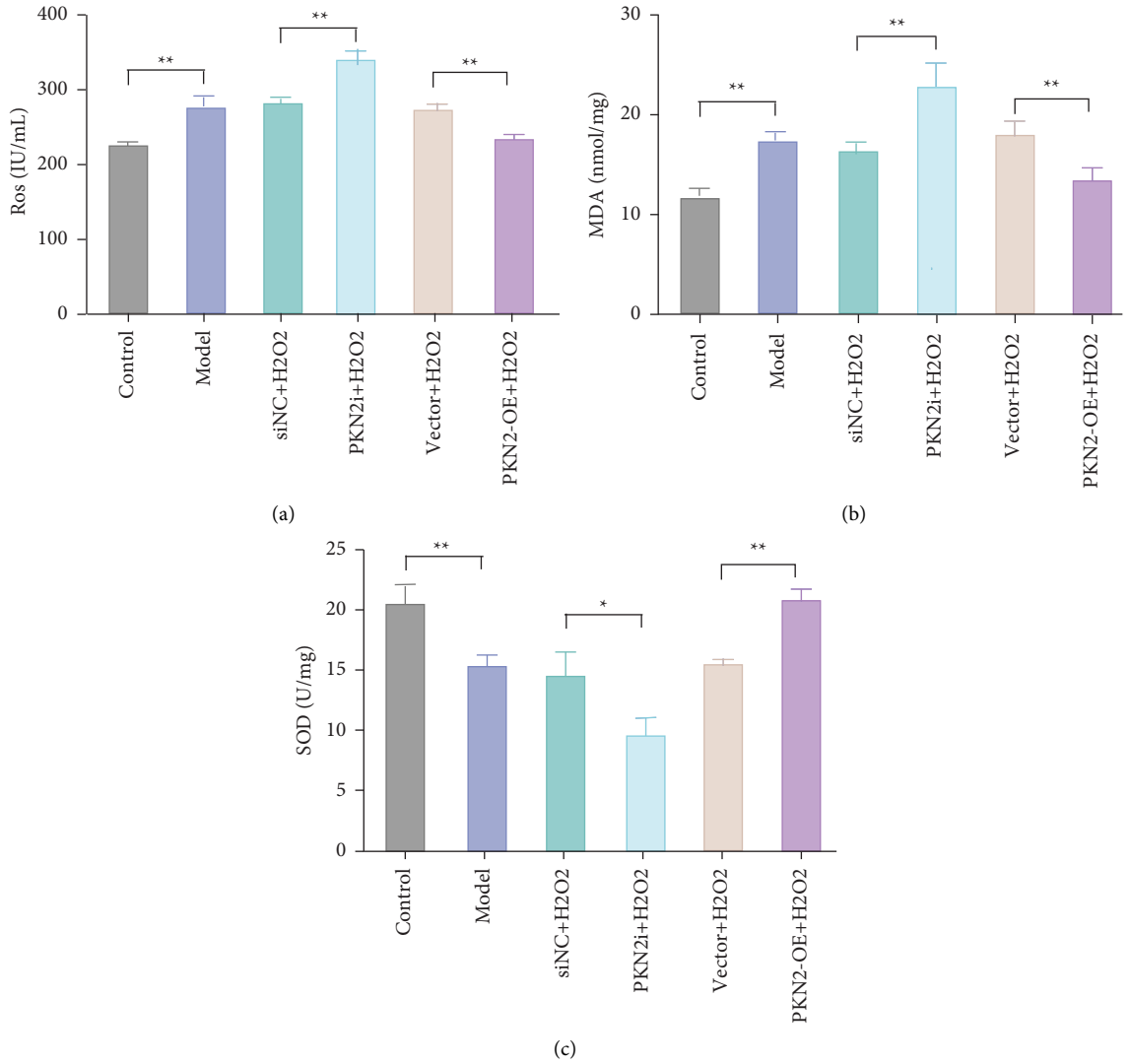

Figure 2: PKN2 overexpression reduces H_2O_2-induced oxidative damage in PC12 cells. (a–c) Quantitative analysis of intracellular levels of ROS, (a) MDA, and (b) relative activity of SOD in each group. $^{**}P < 0.01$ *vs.* control, siNC + H2O_2, and vector + H_2O_2.

3(e)). These results suggest that PKN2 overexpression may inhibit H_2O_2-induced apoptosis in PC12 cells by reducing the production of oxidative stress.

3.4. PKN2 Overexpression Inhibits H_2O_2-induced Apoptosis in PC12 Cells by Activating the mTOR Pathway. Studies have shown that the Mammalian target of rapamycin (mTOR) plays an important role in regulating autophagy and apoptosis, and activation of mTOR can alleviate ROS-mediated ER stress-induced apoptosis of CD_4 T cells [15]. In the present study, the mechanism of PKN2 on H_2O_2-induced apoptosis in PC12 cells were investigated by detecting mTOR pathway-related proteins. The results showed that the expression of p-mTOR protein and the ratio of p-mTOR/mTOR in the cells of the model group were significantly lower than those of the control group. Compared with the siNC + H_2O_2 group, knockdown of PKN2 could significantly reduce p-mTOR protein expression and p-mTOR/mTOR ratio. Compared with the vector + H_2O_2 group, PKN2 overexpression significantly increased p-mTOR protein expression and p-mTOR/mTOR ratio. At the same time, there was no significant change in the expression level of mTOR protein in the cells of each group (Figures 4(a)-4(b)). These results suggest that PKN2 overexpression may reduce H_2O_2-induced apoptosis in PC12 cells by activating the mTOR pathway.

4. Discussion

Diseases of the central nervous system often manifest as neuronal death. There is increasing evidence that oxidative stress is important pathogenesis of many central nervous system diseases [16–18]. Therefore, inhibiting oxidative stress can reduce neuronal damage, which is of positive significance for the prevention and treatment of neurological diseases. PC12 cells have been widely used in the study of neurological diseases [19]. In addition, H_2O_2, as a precursor of reactive oxygen species and reactive nitrogen species, can

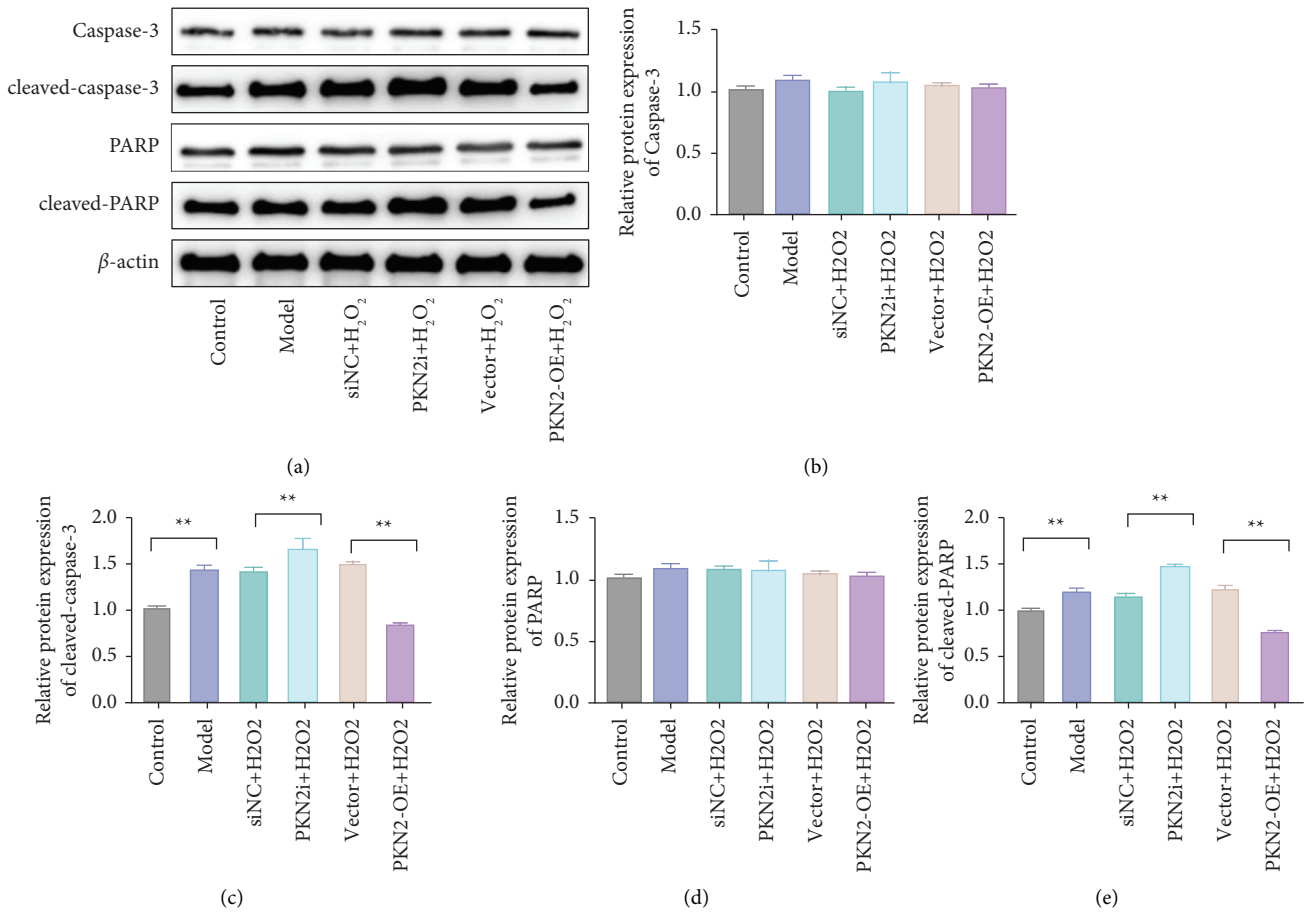

FIGURE 3: PKN2 overexpression prevents H_2O_2-induced apoptosis of PC12 cells. (a) The protein expression levels of PARP, cleaved PARP, caspase-3, and cleaved caspase-3 in cells of each group were detected by western blot. (b–e) Image-Pro Plus software to analyze the gray values of PARP, cleaved PARP, caspase-3, and cleaved-caspase-3 proteins in each group of cells $^{**}P < 0.01$ *vs.* control, siNC + H_2O_2, and vector + H_2O_2.

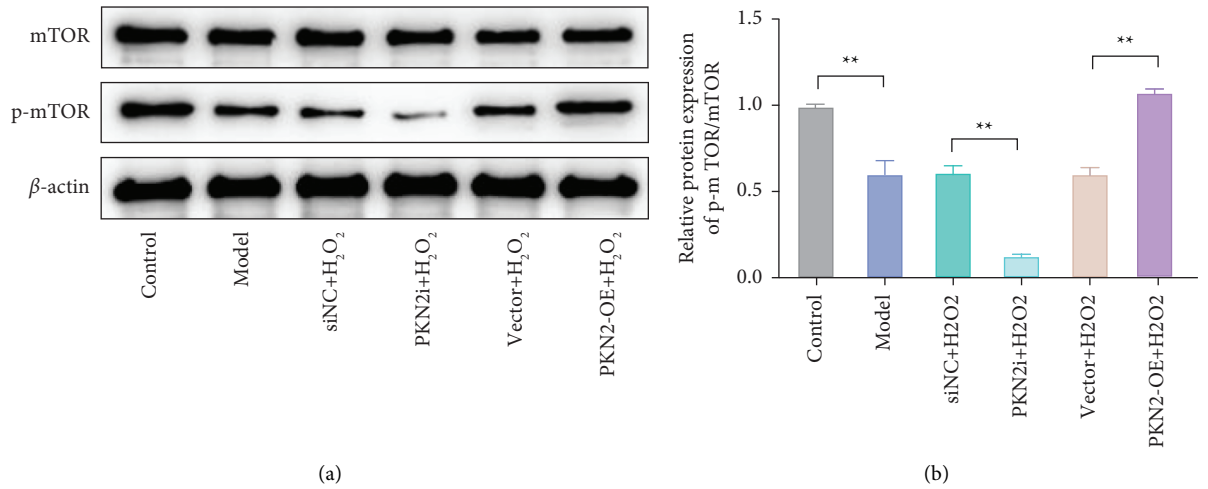

FIGURE 4: PKN2 overexpression inhibits H_2O_2-induced apoptosis in PC12 cells by activating the mTOR pathway. (a–b) Western blot detection of mTOR and p-mTOR protein expression and p-mTOR/mTOR ratio in cells of each group. $^{**}P < 0.01$ *vs.* control, siNC + H_2O_2, and vector + H_2O_2.

easily pass through biofilms and enter cells, thus, it has long been used as a stimulator to induce oxidative stress models [20, 21]. Therefore, in this study, PC12 cells were stimulated with H_2O_2 to induce an oxidative stress model to explore the effect of PKN2 on neuronal death and its mechanism.

ROS are a normal by-product of aerobic metabolism in eukaryotic cells. Low to moderate concentrations of ROS are involved in immune responses, signal transduction, and other processes under physiological conditions. However, excessive ROS production may cause oxidative damage to cellular biomolecules such as proteins, lipids, and nucleic acids [22]. Mammalian cells possess a variety of antioxidants and other cytoprotective factors that protect them from ROS damage [23]. SOD is the first-line antioxidant enzyme in organisms that catalyzes the conversion of superoxide to oxygen and hydrogen peroxide [24]. The generated hydrogen peroxide is converted into oxygen and water by catalase, thereby reducing the concentration of ROS [25]. When there is an imbalance between ROS production and degradation, excessive accumulation of ROS can lead to oxidative stress in cells, causing cell death. MDA is a relatively stable product of ROS attack on polyunsaturated fatty acids. Its content indirectly reflects the changes in intracellular oxygen-free radical content and the degree of lipid damage [26]. In this study, when PC12 cells were stimulated by H_2O_2, the levels of intracellular MDA and ROS were increased, and the cell viability and SOD activity were decreased. It can reduce H_2O_2-induced oxidative damage in PC12 cells and exert an antioxidative stress effect. Overexpression of PKN2 can significantly reduce the levels of MDA and ROS and increase the activity of intracellular SOD and cell viability, indicating that PKN2 overexpression can alleviate H_2O_2-induced oxidative damage in PC12 cells and play an antioxidative stress role. Mitochondria are the main site of reactive oxygen species production. H_2O_2 is a key reactive oxygen species produced by endogenous pathways in mitochondria [27]. When mitochondria are dysfunctional, excessive H_2O_2 can trigger the mitochondrial apoptosis pathway and eventually lead to apoptosis [28]. Due to its broad cytotoxicity to almost all cell types, H_2O_2 is currently the most widely used inducer to study apoptosis [29]. Consistent with previous findings [30–32], in the present study, caspase-3 was activated upon H_2O_2-induced apoptosis in PC12 cells, and the activated caspase-3 led to the cleavage of poly-ADP-ribose polymerase (PARP)-1, thereby triggering apoptosis. Therefore, cleaved caspase-3 and PARP-1 are often used as important markers for judging cell apoptosis [33, 34]. However, the overexpression of PKN2 not only inhibited the activation of caspase-3 but also inhibited the cleavage of PARP by caspase-3, and finally protected PC12 cells from H_2O_2-induced apoptosis.

mTOR is phosphorylated and activated by phosphatidylinositol 3-kinase (PI3K)/protein kinase B (Akt) in the canonical pathway and plays a role in inhibiting apoptosis and promoting cell survival [35]. Khallaghi et al. found that dimethylamine protects against oxidative stress in H_2O_2-induced PC12 cell injury by activating the mTOR signaling pathway [36]. In addition, animal experimental studies have shown that activation of the mTOR pathway is beneficial for reducing ischemia-reperfusion injury in rats by further inhibiting the process of inflammation, apoptosis, and oxidative stress [37]. In the present study, we found that PKN2 overexpression activates the mTOR pathway in PC12 cells to reduce H_2O_2-induced oxidative damage and apoptosis. It indicated that PKN2 may play an antioxidative damage and apoptosis effect by activating the mTOR pathway.

In conclusion, PKN2 participated in H_2O_2-induced oxidative stress injury by activating the mTOR signaling pathway, and its mechanism involves the regulation of mTOR protein phosphorylation. This study provides a reference for the study of the molecular mechanism of nerve injury and provides a potential new therapeutic target for the treatment of nervous system diseases. Because our experiment only explored mTOR signal pathway in PC12 cells, did not explore other signal pathways that PKN2 may play a role, and did not verify in primary nerve cells and animals, more research still needs to be further explored later.

5. Conclusion

In conclusion, PKN2 overexpression can alleviate the H_2O_2-induced PC12 cell damage via increasing cell viability and inhibiting cell apoptosis and oxidative stress. Further mechanism research showed that its protective effect in H_2O_2-induced PC12 cells may be related to the activated mTOR signaling pathway in PC12 cells.

Data Availability

The data used to support the findings of this study are available from the corresponding author upon request.

Ethical Approval

This article does not contain any studies with human participants performed by any of the authors.

Conflicts of Interest

The authors declare that they have no conflicts of interest.

Acknowledgments

This study was funded by Natural Science Foundation of Anhui Province (1708085QH209) and "Peak" cultivation program of scientific research capacity of Yijishan Hospital (GF2019G16).

References

[1] L. Wu, X. Xiong, X. Wu et al., "Targeting oxidative stress and inflammation to prevent ischemia-reperfusion injury," *Frontiers in Molecular Neuroscience*, vol. 13, p. 28, 2020.

[2] G. Cenini, A. Lloret, and R. Cascella, "Oxidative stress in neurodegenerative diseases: from a mitochondrial point of view," *Oxidative Medicine and Cellular Longevity*, vol. 2019, Article ID 2105607, 8 pages, 2019.

[3] A. Höhn, A. Tramutola, and R. Cascella, "Proteostasis failure in neurodegenerative diseases: focus on oxidative stress,"

Oxidative Medicine and Cellular Longevity, vol. 2020, Article ID 5497046, 21 pages, 2020.

[4] A. Singh, R. Kukreti, L. Saso, and S. Kukreti, "Oxidative stress: a key modulator in neurodegenerative diseases," *Molecules*, vol. 24, no. 8, p. 1583, 2019.

[5] B. Thauerer, S. Zur Nedden, and G. Baier-Bitterlich, "Protein kinase C-related kinase (PKN/PRK). potential key-role for PKN1 in protection of hypoxic neurons," *Current Neuropharmacology*, vol. 12, no. 3, pp. 213–218, 2014.

[6] W. J. Buchser, T. I. Slepak, O. Gutierrez-Arenas, J. L. Bixby, and V. P. Lemmon, "Kinase/phosphatase overexpression reveals pathways regulating hippocampal neuron morphology," *Molecular Systems Biology*, vol. 6, no. 1, p. 391, 2010.

[7] I. Quétier, J. Marshall, B. Spencer-Dene et al., "Knockout of the PKN family of rho effector kinases reveals a non-redundant role for PKN2 in developmental mesoderm expansion," *Cell Reports*, vol. 14, no. 3, pp. 440–448, 2016.

[8] Z. N. Zhang, L. Y. Liang, and J. H. Lian, "Research progress of PI3K/Akt/mTOR signaling pathway in central nervous system," *Journal of practical medicine*, vol. 36, no. 05, pp. 689–694, 2020.

[9] T. A. Slotkin, E. A. MacKillop, R. L. Melnick, K. A. Thayer, and F. J. Seidler, "Developmental neurotoxicity of perfluorinated chemicals modeled *in vitro*," *Environmental Health Perspectives*, vol. 116, no. 6, pp. 716–722, 2008.

[10] W. X. Lin, R. X. Ma, and F. Zy, "Effect of ligustrazine on oxidative stress induced by hydrogen peroxide in PC12 cells," *Jiangxi traditional Chinese medicine*, vol. 49, no. 02, pp. 29–31, 2018.

[11] Y. Guo, H. Qin, Z. Wei, L. Fang, and W. Min, "Protective effect and mechanism of pentapeptide from Changbai mountain walnut on oxidative damage of PC12 cells induced by hydrogen peroxide," *Food Science*, vol. 40, no. 13, pp. 143–149, 2019.

[12] Z. Ma, W. Zhang, Y. Wu et al., "Cyclophilin A inhibits A549 cell oxidative stress and apoptosis by modulating the PI3K/Akt/mTOR signaling pathway," *Bioscience Reports*, vol. 41, no. 1, Article ID BSR20203219, 2021.

[13] S. J. Dixon and B. R. Stockwell, "The role of iron and reactive oxygen species in cell death," *Nature Chemical Biology*, vol. 10, no. 1, pp. 9–17, 2014.

[14] A. Derakhshan, Z. Chen, and C. Van Waes, "Therapeutic small molecules target inhibitor of apoptosis proteins in cancers with deregulation of extrinsic and intrinsic cell death pathways," *Clinical Cancer Research*, vol. 23, no. 6, pp. 1379–1387, 2017.

[15] H. Wang, J. Chen, G. Bai, W. Han, R. Guo, and N. Cui, "mTOR modulates the endoplasmic reticulum stress-induced CD4+ T cell apoptosis mediated by ROS in septic immunosuppression," *Mediators of Inflammation*, vol. 2022, Article ID 6077570, 11 pages, 2022.

[16] X. Wang, X. Zhang, Q. Guan, and K. Wang, "Clinical effect of digital subtraction angiography combined with neurointerventional thrombolysis for acute ischemic cerebrovascular disease and its influence on vascular endothelial function and oxidative stress," *Oxidative Medicine and Cellular Longevity*, vol. 2022, Article ID 2777865, 8 pages, 2022.

[17] A. V. Venkataraman, A. Mansur, G. Rizzo et al., "Widespread cell stress and mitochondrial dysfunction occur in patients with early Alzheimer's disease," *Science Translational Medicine*, vol. 14, no. 658, Article ID eabk1051, 2022.

[18] A. T. Aborode, M. Pustake, W. A. Awuah et al., "Targeting oxidative stress mechanisms to treat Alzheimer's and Parkinson's disease: a critical review," *Oxidative Medicine and Cellular Longevity*, vol. 2022, Article ID 7934442, 9 pages, 2022.

[19] Gy Zhou, Z. Y. Chai, and H. Zp, "The role of mTOR/P70S6K pathway in anoxia/reoxygenation induced apoptosis of PC12 neurons," *Zhongnan pharmaceutical*, vol. 17, no. 07, pp. 1024–1029, 2019.

[20] K. Żamojć, M. Zdrowowicz, D. Jacewicz, D. Wyrzykowski, and L. Chmurzyński, "Fluorescent probes used for detection of hydrogen peroxide under biological conditions," *Critical Reviews in Analytical Chemistry*, vol. 46, no. 3, pp. 171–200, 2016.

[21] L. Wu, Y. Xi, and Q. Kong, "Dexmedetomidine protects PC12 cells from oxidative damage through regulation of miR-199a/HIF-1α," *Artificial Cells, Nanomedicine, and Biotechnology*, vol. 48, no. 1, pp. 506–514, 2020.

[22] G. Shadel and T. Horvath, "Mitochondrial ROS signaling in organismal homeostasis," *Cell*, vol. 163, no. 3, pp. 560–569, 2015.

[23] R. Li, Z. Jia, and M. A. Trush, "Defining ROS in biology and medicine," *Reactive oxygen species (Apex, NC)*, vol. 1, no. 1, pp. 9–21, 2016.

[24] S. S. Ali, H. Ahsan, M. K. Zia, T. Siddiqui, and F. H. Khan, "Understanding oxidants and antioxidants: classical team with new players," *Journal of Food Biochemistry*, vol. 44, no. 3, Article ID e13145, 2020.

[25] L. He, T. He, S. Farrar, L. Ji, T. Liu, and X. Ma, "Antioxidants maintain cellular redox homeostasis by elimination of reactive oxygen species," *Cellular Physiology and Biochemistry*, vol. 44, no. 2, pp. 532–553, 2017.

[26] C. Gallelli, S. Calcagnini, A. Romano et al., "Modulation of the oxidative stress and lipid peroxidation by endocannabinoids and their lipid analogues," *Antioxidants*, vol. 7, no. 7, p. 93, 2018.

[27] S. Basu, S. Rajakaruna, B. C. Dickinson, C. J. Chang, and A. S. Menko, "Endogenous hydrogen peroxide production in the epithelium of the developing embryonic lens," *Molecular Vision*, vol. 20, pp. 458–467, 2014.

[28] C. Dai, J. Li, S. Tang, J. Li, and X. Xiao, "Colistin-induced nephrotoxicity in mice involves the mitochondrial, death receptor, and endoplasmic reticulum pathways," *Antimicrobial Agents and Chemotherapy*, vol. 58, no. 7, pp. 4075–4085, 2014.

[29] J. Xiang, C. Wan, R. Guo, and D. Guo, "Is hydrogen peroxide a suitable Apoptosis inducer for all cell types?" *BioMed Research International*, vol. 2016, Article ID 7343965, 6 pages, 2016.

[30] B. Chen, R. Yue, Y. Yang et al., "Protective effects of (E)-2-(1-hydroxyl-4-oxocyclohexyl) ethyl caffeine against hydrogen peroxide-induced injury in PC12 cells," *Neurochemical Research*, vol. 40, no. 3, pp. 531–541, 2015.

[31] M. M. Jin, L. Zhang, H. X. Yu, J. Meng, Z. Sun, and R. R. Lu, "Protective effect of whey protein hydrolysates on H_2O_2-induced PC12 cells oxidative stress via a mitochondria-mediated pathway," *Food Chemistry*, vol. 141, no. 2, pp. 847–852, 2013.

[32] B. Jiang, J. Liu, Y. Bao, and L. An, "Catalpol inhibits apoptosis in hydrogen peroxide-induced PC12 cells by preventing cytochrome c release and inactivating of caspase cascade," *Toxicon*, vol. 43, no. 1, pp. 53–59, 2004.

[33] X. Zhang, Y. Wang, T. Velkov, S. Tang, and C. Dai, "T-2 toxin-induced toxicity in neuroblastoma-2a cells involves the generation of reactive oxygen, mitochondrial dysfunction and inhibition of Nrf2/HO-1 pathway," *Food and Chemical Toxicology*, vol. 114, pp. 88–97, 2018.

[34] T. Sairanen, R. Szepesi, M. L. Karjalainen-Lindsberg, J. Saksi, A. Paetau, and P. J. Lindsberg, "Neuronal caspase-3 and PARP-1 correlate differentially with apoptosis and necrosis in ischemic human stroke," *Acta Neuropathologica*, vol. 118, no. 4, pp. 541–552, 2009.

[35] R. R. Gao, H. Zhou, W. U. Ye-Ke, H. E. Yu, and W. U. Ke-Ming, "Effect of traditional Chinese medicine in regulating apoptosis and autophagy through mTOR pathway," *Chinese Journal of Experimental Traditional Medical Formulae*, vol. 25, no. 04, pp. 218–224, 2019.

[36] B. Khallaghi, F. Safarian, S. Nasoohi, A. Ahmadiani, and L. Dargahi, "Metformin-induced protection against oxidative stress is associated with AKT/mTOR restoration in PC12 cells," *Life Sciences*, vol. 148, pp. 286–292, 2016.

[37] L. Huang, C. Chen, X. Zhang et al., "Neuroprotective effect of curcumin against cerebral ischemia-reperfusion via mediating autophagy and inflammation," *Journal of Molecular Neuroscience*, vol. 64, no. 1, pp. 129–139, 2018.

Hindawi
Evidence-Based Complementary and Alternative Medicine
Volume 2022, Article ID 1092107, 10 pages
https://doi.org/10.1155/2022/1092107

Research Article

Knockdown of Long Noncoding RNA 01124 Inhibits the Malignant Behaviors of Colon Cancer Cells via miR-654-5p/HAX-1

Yu-jin Wu,[1] Zhi-quan Cai,[1] Run-ming He,[1] Xue-chuan Wang,[1] Long-ling Cong,[1] and Fang-hua Qiu[2]

[1]*Departments of Gastroenterology, The Affiliated TCM Hospital of Guangzhou Medical University, Guangzhou, Guangdong 510130, China*
[2]*Department of Hospital Office, The Affiliated TCM Hospital of Guangzhou Medical University, Guangzhou, Guangdong 510130, China*

Correspondence should be addressed to Fang-hua Qiu; fanghua_qiu@163.com

Received 19 July 2022; Revised 16 August 2022; Accepted 18 August 2022; Published 20 September 2022

Academic Editor: Xueliang Wu

Background. Previous studies have shown that long noncoding RNAs (lncRNAs) play a key role in cancer, including colon cancer (CC). However, the exact role of long noncoding RNA 01124 (LINC01124) in CC and its mechanisms of action remain unknown. In this study, we investigated the functional effects and the possible mechanism of LINC01124 in CC. *Methods.* We first determined the expression of LINC01124 in CC tissues (The Cancer Genome Atlas (TCGA) database) and cell lines (quantitative real-time polymerase chain reaction (qRT-PCR)). Functional analysis via Cell Counting Kit-8 (CCK-8), colony formation, cell cycle, wound healing and Transwell assays were performed, and a mechanistic experiment was performed with the western blotting. The function of LINC01124 was also determined in vivo using nude BALB/c mice. *Results.* The results showed that LINC01124 was upregulated in CC tissues and cell lines. Functional studies showed that knockdown of LINC01124 significantly suppressed the proliferation, migration, and invasion of colon cancer cells in vitro and in vivo. Subsequent mechanistic experiments indicated that LINC01124 acted as a sponge to suppress microRNA 654-5p, which targeted HAX-1. Downregulation of LINC01124 decreased the expression of HAX-1, and overexpression of the miR-654-5p inhibitor attenuated the sh-LINC01124-induced inhibition of CC cell proliferation, migration, and invasion. *Conclusion.* Collectively, this study revealed that the knockdown of LINC01124 inhibited the malignant behaviors of CC via the miR-654-5p/HAX-1 axis, suggesting that LINC01124 might be a therapeutic target for CC treatment.

1. Background

Colon cancer (CC) is the third most common malignancy worldwide [1], with more than 1.2 million newly diagnosed patients resulting in 551 thousand deaths each year worldwide [2]. High morbidity and mortality make colon tumors a serious threat to human health [3]. The lack of early diagnosis is one of the most important reasons for the high incidence of CC [4]. Another important reason is that malignant CC often possesses the characteristics of rapid progression and invasion, which can result in a poor prognosis [5, 6]. Therefore, identifying key molecules in the development of colorectal cancer (CRC) tumors may provide breakthroughs in the targeting and biomarker selection of antitumor drugs for this malignant disease.

Long noncoding RNA (lncRNA) is a nonprotein coding RNA transcript with a length greater than 200 nucleotides (nt) [7]. lncRNAs were found to be involved in regulating various processes, and their dysfunctions have been associated with the occurrence of many diseases, including tumors [8]. They can exert their effects on gene expression at transcriptional and post-transcriptional levels [9, 10]. For instance, lncRNAs can bind to DNA, RNA, and proteins to influence transcriptional initiation, RNA stability, or the activity of signaling pathways [10]. They can also serve as scaffolds for recruiting transcriptional factors to the

promoter region to affect gene expression. The involvement of lncRNAs and their critical roles have been reported in the development of cancers, such as malignant proliferation, metastasis, invasion, antiapoptosis effects, and therapeutic resistance [8, 11]. The dysregulation of many lncRNAs, such as lncRNA CCAT1, lncRNA POU6F2-AS2, and lncRNA ROR1-AS1, has been closely related to CRC progression [12, 13]. A previous study also confirmed that LINC01124 significantly inhibited the proliferation, migration, and invasive ability of non-small-cell lung carcinoma (NSCLC) cells [14]. However, the potential effect and mechanism of LINC01124 on CC remain unclear. Therefore, we decided to explore the potential functions of LINC01124 in CC.

HAX-1, located at chromosome 1 (1q21.3), is reported to play an important role in various tumors [15–18]. For example, HAX-1 was revealed to be overexpressed in hypopharyngeal squamous cell carcinoma and promoted cancer growth and migration [17]. HAX-1 was found to be targeted by miR-100 to regulate the sensitivity of breast cancer cells to cisplatin [16]. Moreover, in CRC, HAX-1 was reported to be targeted by miR-654-5p to regulate its malignancy behaviors [18].

LINC01124 is located at chromosome 2q31.1 and contains one exon. In the current study, we investigated the role of LINC01124 in the progression of CC and explored its underlying mechanisms. The results showed that LINC01124 was upregulated in CC tissues and cell lines. Knockdown of LINC01124 suppressed cell proliferation, migration, and invasion in vitro and in vivo. In addition, miR-654-5p was verified to be target miRNA of LINC01124, and we showed that sh-LINC01124 inhibited the progression of CC by modulating the miR-654-5p-HAX-1 signaling pathway. All these findings suggested that LINC01124 might be an underlying biomarker and a potential therapeutic target for CC.

2. Materials and Methods

2.1. Cell Culture. A human normal colonic epithelial cell line (NCM460) and 5 human CC cell lines (LoVo, SW620, HT29, HCT116, and SW480) were purchased from Nanjing Cobioer Biotechnology Co. Ltd. (Nanjing, Jiangsu, China). All CRC cell lines were cultured in RPMI 1640 (Roswell Park Memorial Institute 1640) medium supplemented with 10% fetal bovine serum (FBS, Gibco, Grand Island, NY, USA) and 1% penicillin-streptomycin. All cells were maintained in an incubator at 37°C with 5% CO_2 in a humidified atmosphere [19].

2.2. Transfection and Lentivirus Transduction. The miR-654-5p inhibitor and its negative control (Ctrl) were purchased from RiboBio, and oligonucleotide transfection was performed using Lipofectamine 2000 reagent (Invitrogen; Thermo Fisher Scientific, Inc.). Short hairpin RNA (shRNA) targeting LINC01124 was designed by GenePharma (Shanghai, China) and cloned into the pRNAT-u6.1/Neo plasmid (Biovector, Beijing, China). To establish a cell line with stable knockdown of LINC01124, the plasmid carrying sh-LINC01124 or sh-Ctrl was cotransfected with packaging vectors to produce pseudotyped lentiviruses, which were designated Lv-sh-LINC01124 and Lv-sh-Ctrl. The lentiviruses were concentrated by ultracentrifugation and then were used to infect CC cells [19].

2.3. Quantitative Real-Time Polymerase Chain Reaction (qRT-PCR). After transfection, total RNA was extracted from cells by TRIzol extraction (Invitrogen; Thermo Fisher Scientific, Inc.). Then, RNA samples were reverse transcribed into complementary DNA (cDNA) using a PrimeScript RT reagent kit (Takara). qRT-PCR analyses were performed with SYBR Green (Takara). The primers are shown in Table 1. The results were normalized to the expression of glyceraldehyde-3-phosphate dehydrogenase (GAPDH). Relative gene expression levels were calculated using the $2^{-\Delta\Delta ct}$ method [14].

2.4. Cell Proliferation Analysis. For the Cell Counting Kit-8 (CCK-8) assay, 2000 cells were seeded into 96-well plates in 100 μl of complete medium and cultured for 1, 2, 3, 4, and 5 days. At each time point, 10 μL of the CCK-8 solution (Dojindo, Kumamoto, Japan) was added to each well, and the absorbance was then measured at 450 nm using a microplate reader after 2 h at 37°C. The cells' cell viability was determined by measuring their absorbance. For colony formation assays, the cells were seeded into 12-well plates at a density of 500/well and incubated for 10–12 days. Then, colonies were stained with 0.1% crystal violet (Sigma) and counted [20].

2.5. Cell Cycle Analysis. HCT116 and SW480 cells were washed with cold PBS and then fixed with ice-cold 70% ethanol at 4°C overnight. On the second day, the cells were washed with PBS, and intracellular DNA was labeled with propidium iodide (PI, Sigma-Aldrich; Merck KGaA) at 4°C for 30 min and analyzed using BD FACSCalibur flow cytometry (BD Bioscience, San Jose, CA, USA). ModFit software (Verity Software House Inc., Topsham, ME, USA) was used to analyze the proportions of cells in the GO/G1, S, and G2/M phases [19].

2.6. Wound Healing Assay. Cells (1 × 10^5/well) were seeded into 6-well plates. The cells were starved in fetal bovine serum (FBS) free culture medium overnight. Then, a wound was made using a 200 μl pipette tip. Next, the cells were incubated with 2% FBS medium. The wound was imaged at 0 h and 36 h [20].

2.7. Transwell Invasion Assay. The transwell chamber (8-μm pore size, Corning, Cambridge, MA, USA) was used to perform the invasion assay. Cells (2 × 105/well) were cultured in the upper chamber with Matrigel (BD Biosciences), and a complete medium containing 20% FBS was added to the lower chamber. After incubation for 36 h at 37°C, cells adhering to the lower surface of the transwell membrane

Table 1: Sequences of primers for qRT-PCR.

Name	Sequence (5' to 3')
PCR primers for GAPDH	
Forward	GTGGCTGGCTCAGAAAAAGG
Reverse	GGGGAGATTCAGTGTGGTGG
PCR primers for LINC01124	
Forward	GGACTCCGAGCTTTCAACCA
Reverse	AGCGATCTGGTTCCTTAGCG

were fixed in 20% methanol and stained with 0.1% crystal violet. The number of invaded cells was analyzed [20].

2.8. Tumorigenesis Assay In Vivo. For the subcutaneous xenograft assay, 5×105 cells infected with sh-Ctrl or sh-LINC01124 were subcutaneously inoculated into the flanks of 5-week-old male athymic nude BALB/c mice. The tumor volumes were examined using calipers every three days. After 5 weeks, the mice were sacrificed by euthanasia. The tumors were then removed and weighed [19]. All animal studies were performed in strict accordance with the recommendations in the guidelines for the Animal Care and Use Committee of the Traditional Chinese Medicine University of Guangzhou (Permit number: 20190228035).

2.9. Luciferase Reporter Assay. The binding sequences of miR-654-5p and LINC01124 were predicted through online websites (https://www.mircode.org/and https://cm.jefferson.edu/ran22/Interacti-ve/). The potential binding sequences of miR-654-5p and LINC01124 (WT) and the mutant (Mut) miR-654-5p binding sequences in LINC01124 were inserted into a pmirGL3-basic vector (Promega Corporation, Madison, USA) to construct dual-luciferase reporter plasmids. Then, the cells were cotransfected with the WT (or Mut) plasmid and a Ctrl mimic or miR-654-5p mimic. After 48 h, luciferase activity was detected using a dual-luciferase reporter gene assay kit (Beyotime Institute of Biotechnology, Shanghai, China) according to the manufacturer's protocol. The relative luciferase activity was normalized to Renilla luciferase activity [20].

2.10. Western Blot. Protein samples were isolated with lysis buffer (RIPA) containing protease inhibitors. After quantification with a BCA kit (Beyotime, China), total protein (25 μg) was separated by 8–15% SDS-PAGE and transferred to polyvinylidene difluoride (PVDF) membranes. After blocking with 5% skimmed milk for 60 min, the membranes were incubated with primary antibodies anti-HAX-1 (ab137613, 1 : 500) and anti-GAPDH (#5174, CST, 1 : 1000) overnight, followed by incubation with fluorescence-conjugated secondary antibodies (1 : 1,000) for 30 min. Bands were detected by using a two-color infrared laser imaging system (Odyssey; Li-Cor, Lincoln, NE, USA) [20].

2.11. Statistical Analysis. All data in this study were obtained from experiments repeated at least three times and are presented as the mean ± standard deviation (SD). Two independent sample t-tests or one-way ANOVA for multiple comparisons were performed using SPSS v22.0 (IBM, Armonk, NY, USA). $^{**}p < 0.01$ or $^{*}p < 0.05$ was considered statistically significant [20].

3. Results

3.1. The Expression of LINC01124 Was Upregulated in CC Tissues and Cell Lines. To investigate the role of LINC01124 in CRC, we first analyzed the expression levels of LINC01124 in The Cancer Genome Atlas (TCGA) database (https://gepia.cancer-pku.cn/index.html). As shown in Figure 1(a), the expression of LINC01124 was significantly upregulated in CRC tissues. Next, we analyzed the expression of LINC01124 in CC cell lines. As illustrated in Figure 1(b), the expression of LINC01124 in all CC cell lines (LoVo, SW620, HT29, HCT116, and SW480) was significantly higher than that in the normal colonic epithelial cell line (NCM460). HCT116 and SW480 cells were chosen for downstream experiments based on their high expression. Our results show that LINC01124 was overexpressed in CC cell lines.

3.2. LINC01124 Knockdown Inhibited Cell Proliferation In Vitro. Loss-of-function experiments were performed by knocking down LINC01124 to explore the regulatory effect of LINC01124 on CC cell progression. We knocked down LINC01124 in HCT116 and SW480 cells. qRT-PCR results showed that the expression of LINC01124 was significantly downregulated in these cells by transfecting sh-LINC01124 (Figure 2(a)). We then performed CCK-8 and colony formation assays to evaluate cellular proliferation. The results demonstrated that knockdown of LINC01124 significantly inhibited cell proliferation (Figures 2(b)–2(d) and Supplementary Figure 1). More importantly, FACS analysis indicated that after transfection with sh-LINC01124, fewer cells entered the S phase and G2/M phase, while more cells were arrested in the G0/G1 phase (Figure 2(e)). Collectively, these findings suggest that knockdown of LINC01124 inhibited CC cell proliferation in vitro.

3.3. LINC01124 Knockdown Reduced Tumor Growth In Vivo. We further investigated the function of LINC01124 in vivo. sh-LINC01124 or control SW480 cells were subcutaneously injected into the flanks of nude mice. From the first week, we measured the tumor volumes at indicative time points. After 5 weeks, the mice were sacrificed, and the tumors were removed. As shown in Figures 3(a) and 3(b), knockdown of LINC01124 significantly inhibited tumor growth in vivo. Moreover, the tumors in the sh-LINC01124 group were smaller than those in the control group (Figure 3(c)). These findings indicate that knockdown of LINC01124 could reduce CC progression in vivo.

3.4. LINC01124 Knockdown Inhibited Cell Migration and Invasion. We assessed the effects of LINC01124 depletion on cell migration and invasion using wound healing and

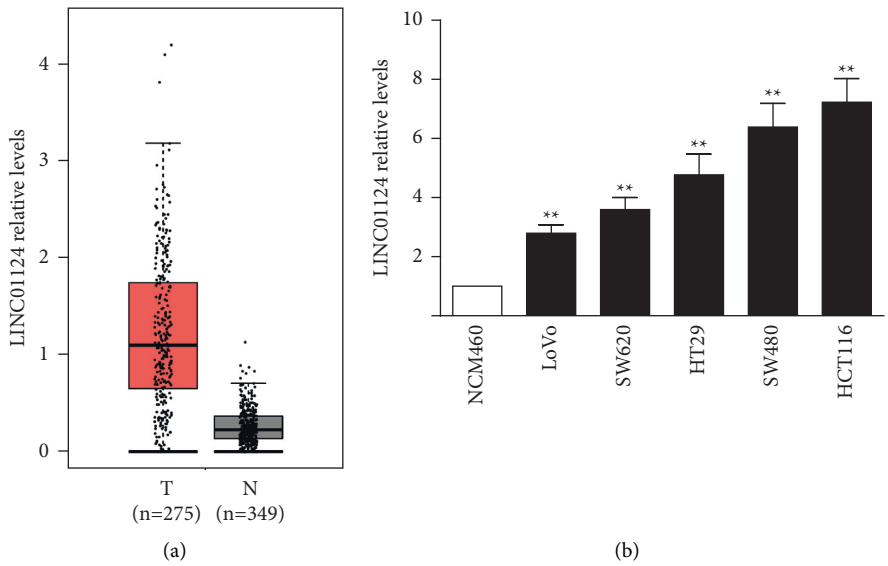

Figure 1: LINC01124 was upregulated in human colon cancer tissues and cell lines. (a) LINC01124 expression was analyzed in online public databases comparing 275 colon cancer tissues and 349 adjacent normal tissues. (b) Comparison of the relative LINC01124 expression levels between the normal colonic epithelial cell line (NCM460) and 5 CRC cell lines. Data are presented as the mean ± SD, $^{**}p < 0.01$.

transwell assays. As expected, knockdown of LINC01124 significantly suppressed the migration and invasion of HCT116 and SW480 cells (Figures 4(a) and 4(b)). Moreover, the expression of metastasis-related protein VIM was significantly downregulated, while another metastasis-related protein, CDH1, was upregulated in HCT116 cells transfected with sh-LINC01124 (Figure 4(c)). Collectively, these findings indicate that LINC01124 may act as an oncogene in CC.

3.5. LINC01124 Knockdown Inhibited the Progression of CC via the miR-654-5p/HAX-1 Axis. lncRNAs have been demonstrated to act as competing endogenous RNAs for miRNAs. Thus, two different mRNA target prediction algorithms, miRcode and RNA22, were used to predict the potential miRNAs that directly bind to LINC01124. Among all potential targets, we identified miR-654-5p, whose expression was downregulated in CC cells [18], as the most promising candidate. The potential binding sequences of miR-654-5p and LINC01124 are shown in Figure 5(a). Overexpression of miR-654-5p significantly suppressed the expression of LINC01124 (Figure 5(b)), and overexpression of LINC01124 significantly suppressed the expression of miR-654-5p (Supplementary Figure 2). To confirm the association of LINC01124 and miR-654-5p, the expression levels of these two RNAs were analyzed using TCGA data. As shown in Supplementary Tables 1, 2 and Supplementary Figure 3, there was an obvious negative correlation between LINC01124 and miR-654-5p, $r = 0.556966$. Moreover, the luciferase reporter assay indicated that overexpression of miR-654-5p suppressed the luciferase activity in HCT116 and SW480 cells transfected with the WT-LINC01124 vector (Figure 5(c)). It has been reported that miR-654-5p targets HAX-1 to regulate the malignant behaviors of CRC cells [18]; thus, we detected the expression of HAX-1 by the western blotting in HCT116 and SW480 cell lines transfected with sh-LINC01124 or cotransfected with sh-LINC01124 and miR-654-5p inhibitors. As shown in Figure 5(d), the expression of HAX-1 decreased when LINC01124 was knocked down; however, the opposite expression pattern of HAX-1 was observed when sh-LINC01124 and miR-654-5p inhibitors were cotransfected. Altogether, these findings demonstrated that LINC01124 is directly bounded to miR-654-5p in CC.

After confirming the direct interaction between miR-654-5p and LINC01124, rescue experiments were performed. sh-LINC01124 and miR-654-5p inhibitors were cotransfected into both HCT116 and SW480 cell lines. By assessing cell proliferation, migration, and invasion using colony formation, wound healing and transwell assays, we found that the miR-654-5p inhibitor partly reversed the suppressive effect of sh-LINC01124 on cell proliferation, migration, and invasion (Figures 5(e)–5(g)). Taken together, our findings suggested that LINC01124 acted as an oncogene via inhibition of miR-654-5p by targeting HAX-1.

4. Discussion

Due to limitations in the early diagnosis of CC, its 5-year survival rate is still less than 30% in many low-income countries [21, 22]. An increasing number of methods are being used to explore the pathogenesis of cancers, and accumulating evidence suggests that lncRNAs have important biological functions [23–25]. lncRNAs were once considered to be "transcriptional noise," but now lncRNAs have been proven to be involved in the regulation of tumorigenesis and progression as tumor suppressor genes or oncogenes [26–28].

For the past few years, an increasing number of researchers have focused on the effect of lncRNAs on CC. For

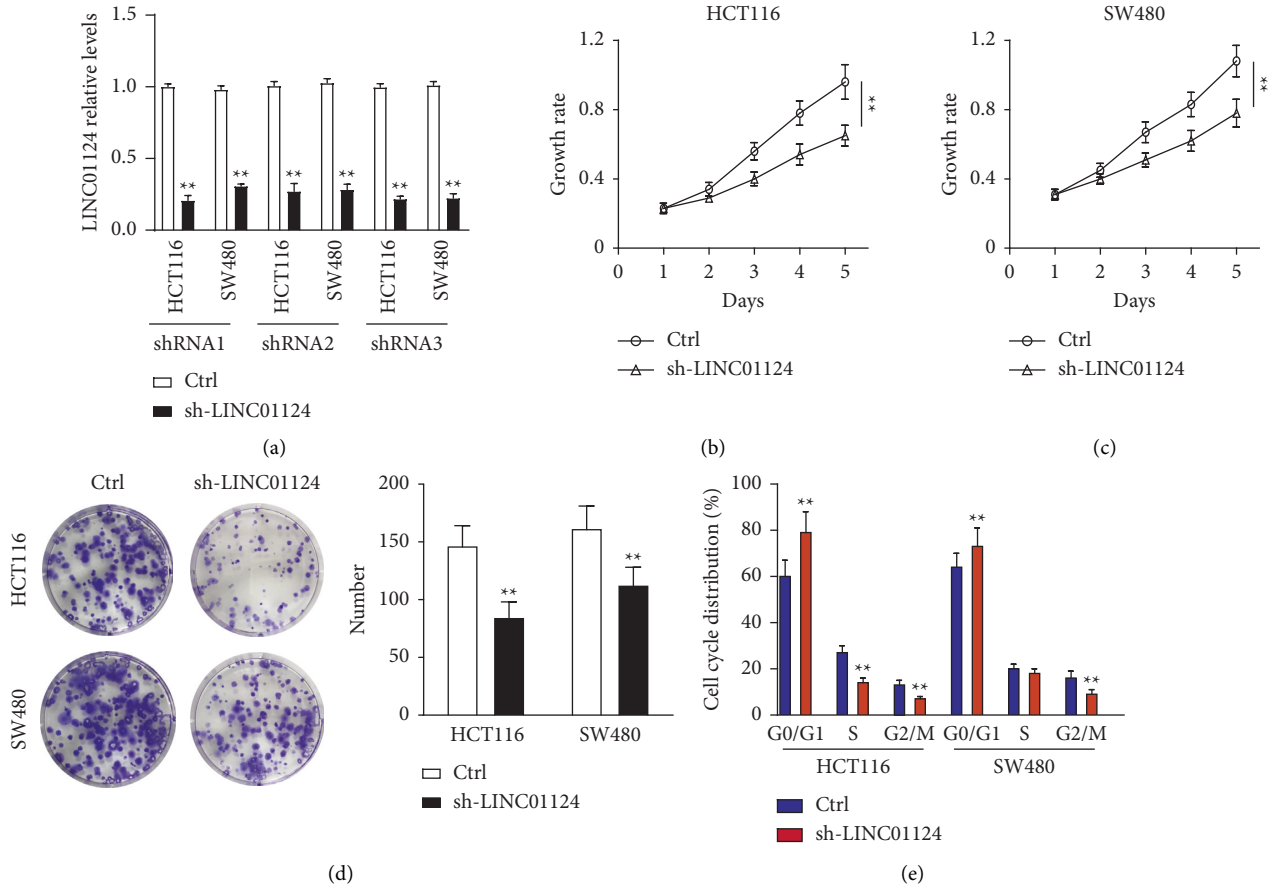

Figure 2: Knockdown of LINC01124 inhibited cell proliferation in vitro. (a) The inhibitory efficiency of sh-LINC01124 in LINC01124 expression by qRT-PCR. (b, c) CCK-8 assays and (d) colony formation assays were performed to assess the proliferation of HCT116 and SW480 cell lines. (e) Flow cytometry analysis was used for cell cycle evaluation. Data are presented as the mean ± SD, $^{**}p < 0.01$.

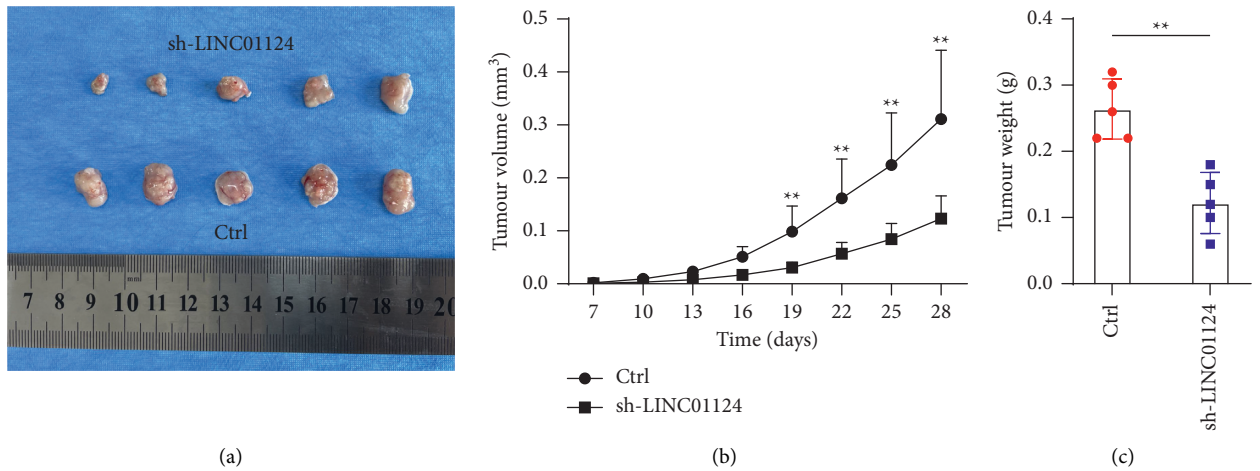

Figure 3: Knockdown of LINC01124 reduced tumor formation in nude mice xenografts. (a) Representative photos of xenografts. (b) The volumes in subcutaneous xenografts measured and calculated once a week for 5 weeks. (c) The tumor weight measured at the end of the experiments. Data are presented as the mean ± SD, $^{**}p < 0.01$.

example, some scholars have shown that lncRNA ROR1-AS1 promoted the proliferation of CC by suppressing the expression of DUSP5/CDKN1A [12], lncRNA NEAT1 regulated invasion and migration in CC via the miR-185-5p/IGF2 axis [29], lncRNA LINC00460 knockdown suppressed EMT in CC by downregulating ANXA2 [30], lncRNA POU6F2-AS2 promoted drug resistance in CC by regulating miR-377/BRD4 [13], and more. LINC01124, which is located

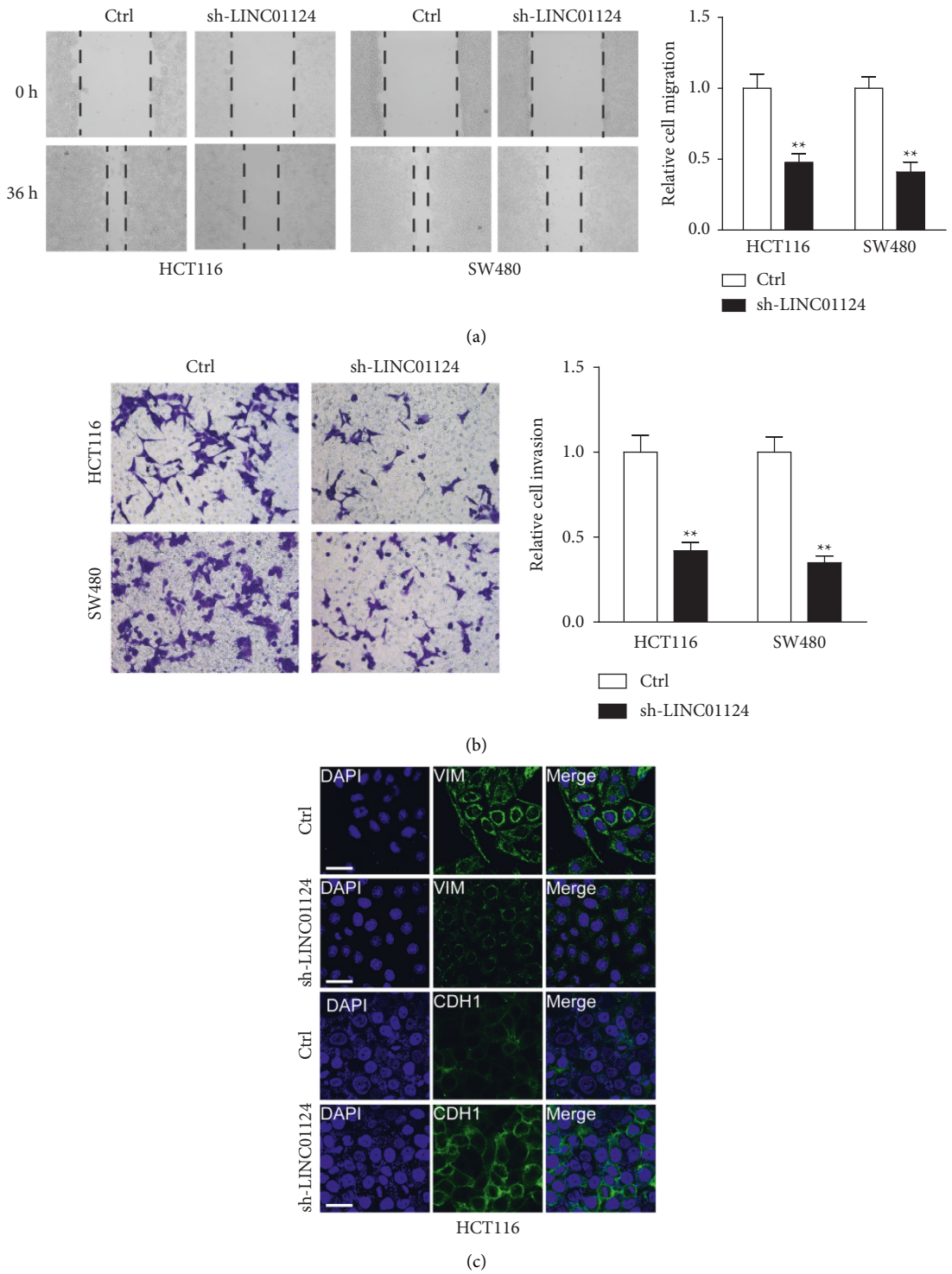

Figure 4: Knockdown of LINC01124 inhibited cell migration and invasion. (a) Wound healing assay to evaluate the effect of LINC01124 on the migration of HCT116 and SW480 cells (magnification, ×100). (b) Transwell assay to evaluate the effect of LINC01124 on the invasion of HCT116 and SW480 cells (magnification, ×200). (c) HCT116 cells were harvested for IF analysis by anti-VIM or anti-CHD1 (scale bar, 15 μm). Data are presented as the mean ± SD, $^{**}p < 0.01$.

at chromosome 2q31.1, was shown to act as a tumor suppressor in NSCLC. The expression level of LINC01124 was reported to be downregulated in tumor tissues compared with paired normal lung tissues, and LINC01124 significantly inhibited the proliferation, migration, and invasive ability of NSCLC cells [14]. However, the role of LINC01124

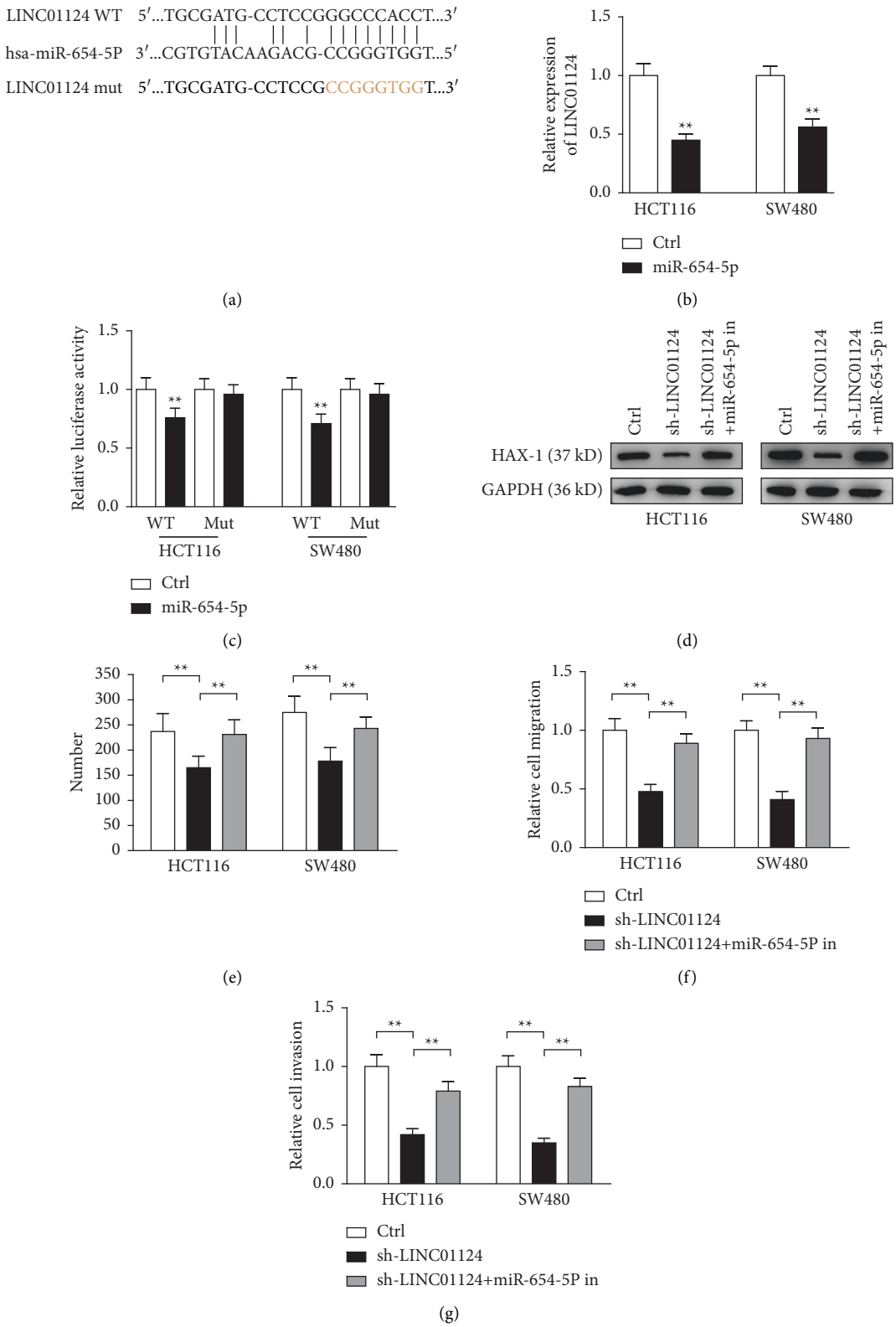

Figure 5: Knockdown of LINC01124 inhibited the progression of CC via the miR-654-5p/HAX-1 axis. (a) Predicted binding sites in LINC01124 of miR-654-5p. (b) Overexpression of miR-654-5p reduced the expression of LINC01124 in HCT116 and SW480 cell lines. (c) A dual-luciferase reporter assay was performed to assess the luciferase activity of HCT116 and SW480 cell lines transfected with WT-LINC01124 and mut-LINC01124. (d) Western blotting analysis of HAX-1 in HCT116 and SW480 cell lines. (e–g) Colony formation, wound healing, and transwell assays were performed with the indicated cell lines. Data are presented as the mean ± SD, $^{**}p < 0.01$.

in CC remained unclear. Here, we report for the first time that LINC01124 is upregulated in CC tissues and cell lines. The results showed that the downregulation of LINC01124 suppressed the proliferation, migration, and invasion of CC cell lines in vitro and in vivo. This function of LINC01124 in CC was the opposite of NSCLC cells.

Many studies have revealed some potential biological mechanisms of lncRNAs, and the theory of competing for endogenous RNAs (ceRNAs) is one of the commonly accepted theories [31]. ceRNAs can directly bind to miRNAs and affect the expression of target mRNAs, thus affecting the biological process of cells [32–34]. LINC01124 has not been reported to function as a ceRNA until recently, so we hypothesized that LINC01124 could regulate CC progression by binding to miRNAs. Using an online database, we found that miR-654-5p had a higher score for binding to LINC01124 and suppressed CC cell proliferation, migration, and invasion [18]. The luciferase reporter assay confirmed our prediction that LINC01124 could bind to miR-654-5p directly.

Hematopoietic cell-specific protein 1 (HS-1)-associated protein X-1 (HAX-1) is a 35 kDa protein that can interact with HS-1, an Src kinase substrate. HAX-1 was reported to be composed of a putative transmembrane domain, a putative PEST sequence, and an acid box [35]. It has emerged as an important factor in the mitochondrial-dependent cell death pathway, characterized by the activation and permeabilization of mitochondria, resulting in the release of cytochrome c and other proapoptotic molecules into cytosol [36]. Previous studies demonstrated that HAX-1 was involved in regulating mitochondrial membrane potential during apoptosis [37, 38]. In addition, HAX-1 protein was shown to interact with several cellular and viral proteins [39, 40]. Despite several studies demonstrating that HAX-1 might be important in apoptosis and proliferation [41, 42], its role in CRC remains under-investigated. In this present study, our experiments showed that the downregulation of LINC01124 significantly decreased the levels of HAX-1, which is the target gene of miR-654-5p. In addition, the miR-654-5p inhibitor rescued the effects of sh-LINC01124 on CC cell proliferation, migration, and invasion. All these findings suggested that the miR-654-5p/HAX-1 axis might be involved in the anti-CC effect of sh-LINC01124. Further bioinformatics analyses and in vitro and in vivo studies are needed to further validate the potential clinical significance of this axis in CC.

There were several limitations in this study. First, we did not use CC patients' tissues to determine the expression of LINC01124, which was only determined in the TCGA database. Second, immunohistochemistry was not performed to determine the association of LINC01124 with the survival of CC patients. Third, drug experiments were not performed to identify the optimal pharmacological therapies for patients overexpressing LINC01124. These issues could be clarified in future studies to confirm the clinical and real-world significance of LINC01124 as a therapeutic target for CC.

Taken together, our data for the first time showed that LINC01124 was upregulated in CC tissues and cell lines. Downregulation of LINC01124 was involved in malignant behaviors in CC. In addition, we identified miR-654-5p as a target of LINC01124. Thus, these findings indicate the potential role of the LINC01124/miR-654-5p/HAX-1 axis in CC, suggesting LINC01124 as a novel diagnostic and therapeutic target for CC.

Data Availability

The datasets used and/or analyzed during the current study are available from the corresponding author on reasonable request.

Ethical Approval

All animal studies were performed in strict accordance with the recommendations in the guidelines for the Animal Care and Use Committee of the Traditional Chinese Medicine University of Guangzhou. Permit number: 20190228035.

Disclosure

This manuscript has been preprinted (https://doi.org/10.21203/rs.3.rs-1445265/v2) [43].

Conflicts of Interest

The authors declare no conflicts of interest.

Authors' Contributions

Yujin Wu and Fanghua Qiu designed and wrote this article, Runming He and Zhiquan Cai completed Figures 1 and 2, Xuechuan Wang completed Figures 3 and 4, and Longling Cong and Yujin Wu completed Figure 5 and the supplementary materials.

Acknowledgments

This study was supported by the Guangdong Province Traditional Chinese Medicine Bureau (20173029), the Guangzhou Science and Technology Innovation Commission (201704020171), and the Guangzhou Municipal Health and Health Committee (2019A011014).

Supplementary Materials

Table S1: analysis of the expression levels of two RNAs LINC01124 and miR-654-5p using TCGA data. Table S2: analysis of the expression levels of two RNAs LINC01124 and miR-654-5p using TCGA data. Figure S1: knockdown of LINC01124 inhibited cell proliferation. Figure S2: the expression of miR-654-5p in ov-LINC01124 cells. Figure S3: the relationship of miR-654-5p and LINC01124. (*Supplementary Materials*)

References

[1] J. Weitz, M. Koch, J. Debus, T. Hohler, P. R. Galle, and M. W. Buchler, "Colorectal cancer," *The Lancet*, vol. 365, no. 9454, pp. 153–165, 2005.

[2] F. Bray, J. Ferlay, I. Soerjomataram, R. L. Siegel, L. A. Torre, and A. Jemal, "Global cancer statistics 2018: GLOBOCAN estimates of incidence and mortality worldwide for 36 cancers in 185 countries," *CA: A Cancer Journal for Clinicians*, vol. 68, no. 6, pp. 394–424, 2018.

[3] L. Lu, C. S. Mullins, C. Schafmayer, S. Zeißig, and M. Linnebacher, "A global assessment of recent trends in gastrointestinal cancer and lifestyle-associated risk factors," *Cancer Communications*, vol. 41, no. 11, pp. 1137–1151, 2021.

[4] S. Dueland, M. Hagness, P. D. Line, T. K. Guren, K. M. Tveit, and A. Foss, "Is liver transplantation an option in colorectal cancer patients with nonresectable liver metastases and progression on all lines of standard chemotherapy?" *Annals of Surgical Oncology*, vol. 22, no. 7, pp. 2195–2200, 2015.

[5] A. H. Cleven, S. Derks, M. X. Draht et al., "CHFR promoter methylation indicates poor prognosis in stage II microsatellite stable colorectal cancer," *Clinical Cancer Research*, vol. 20, no. 12, pp. 3261–3271, 2014.

[6] P. Chen, Q. Xi, Q. Wang, and P. Wei, "Downregulation of microRNA-100 correlates with tumor progression and poor prognosis in colorectal cancer," *Medical Oncology*, vol. 31, no. 10, p. 235, 2014.

[7] J. Jarroux, A. Morillon, and M. Pinskaya, "History, discovery, and classification of lncRNAs," *Advances in Experimental Medicine and Biology*, vol. 1008, pp. 1–46, 2017.

[8] J. Yuan, H. Yue, M. Zhang et al., "Transcriptional profiling analysis and functional prediction of long noncoding RNAs in cancer," *Oncotarget*, vol. 7, no. 7, pp. 8131–8142, 2016.

[9] Y. T. Tan, J. F. Lin, T. Li, J. J. Li, R. H. Xu, and H. Q. Ju, "LncRNA-mediated posttranslational modifications and reprogramming of energy metabolism in cancer," *Cancer Communications*, vol. 41, no. 2, pp. 109–120, 2021.

[10] X. Tang, X. Qiao, C. Chen, Y. Liu, J. Zhu, and J. Liu, "Regulation mechanism of long noncoding RNAs in colon cancer development and progression," *Yonsei Medical Journal*, vol. 60, no. 4, pp. 319–325, 2019.

[11] D. Liu, B. Xu, S. Chen et al., "Long non-coding RNAs and prostate cancer," *Journal of Nanoscience and Nanotechnology*, vol. 13, no. 5, pp. 3186–3194, 2013.

[12] X. Y. Wang, X. Jian, B. Q. Sun, X. S. Ge, F. J. Huang, and Y. Q. Chen, "LncRNA ROR1-AS1 promotes colon cancer cell proliferation by suppressing the expression of DUSP5/CDKN1A," *European Review for Medical and Pharmacological Sciences*, vol. 24, no. 3, pp. 1116–1125, 2020.

[13] G. Xu, H. Zhu, J. Xu et al., "Long non-coding RNA POU6F2-AS2 promotes cell proliferation and drug resistance in colon cancer by regulating miR-377/BRD4," *Journal of Cellular and Molecular Medicine*, vol. 24, no. 7, pp. 4136–4149, 2020.

[14] Z. B. Wang, H. Y. Zhang, and J. B. Lu, "Expression and effects of long non-coding RNA, LINC01124, in non-small cell lung cancer," *OncoTargets and Therapy*, vol. 12, pp. 11729–11736, 2019.

[15] H. Li, X. Yang, G. Wang et al., "KDM4B plays an important role in mitochondrial apoptosis by upregulating HAX1 expression in colorectal cancer," *Oncotarget*, vol. 7, no. 36, pp. 57866–57877, 2016.

[16] G. Wu, W. Zhou, X. Pan et al., "miR-100 reverses cisplatin resistance in breast cancer by suppressing HAX-1," *Cellular Physiology and Biochemistry*, vol. 47, no. 5, pp. 2077–2087, 2018.

[17] H. Wu, J. Chen, Q. Wang et al., "Abnormal expression of HAX-1 is associated with cellular proliferation and migration in human hypopharyngeal squamous cell carcinoma," *Molecular Medicine Reports*, vol. 16, no. 4, pp. 4664–4670, 2017.

[18] F. Huang, X. Wu, M. Wei et al., "miR-654-5p targets HAX-1 to regulate the malignancy behaviors of colorectal cancer cells," *BioMed Research International*, vol. 2020, Article ID 4914707, 6 pages, 2020.

[19] N. Jing, T. Huang, H. Guo et al., "LncRNA CASC15 promotes colon cancer cell proliferation and metastasis by regulating the miR-4310/LGR5/Wnt/β-catenin signaling pathway," *Molecular Medicine Reports*, vol. 18, no. 2, pp. 2269–2276, 2018.

[20] Y. Chen, F. Qiu, L. Huang et al., "Long noncoding RNA LINC00312 regulates breast cancer progression through the miR9/CDH1 axis," *Molecular Medicine Reports*, vol. 21, no. 3, pp. 1296–1303, 2020.

[21] M. Arnold, M. S. Sierra, M. Laversanne, I. Soerjomataram, A. Jemal, and F. Bray, "Global patterns and trends in colorectal cancer incidence and mortality," *Gut*, vol. 66, no. 4, pp. 683–691, 2017.

[22] J. Ferlay, M. Colombet, I. Soerjomataram et al., "Cancer incidence and mortality patterns in Europe: estimates for 40 countries and 25 major cancers in 2018," *European Journal of Cancer*, vol. 103, pp. 356–387, 2018.

[23] S. Loewer, M. N. Cabili, M. Guttman et al., "Large intergenic non-coding RNA-RoR modulates reprogramming of human induced pluripotent stem cells," *Nature Genetics*, vol. 42, no. 12, pp. 1113–1117, 2010.

[24] M. Huarte, M. Guttman, D. Feldser et al., "A large intergenic noncoding RNA induced by p53 mediates global gene repression in the p53 response," *Cell*, vol. 142, no. 3, pp. 409–419, 2010.

[25] T. R. Mercer, M. E. Dinger, and J. S. Mattick, "Long noncoding RNAs: insights into functions," *Nature Reviews Genetics*, vol. 10, no. 3, pp. 155–159, 2009.

[26] J. R. Evans, F. Y. Feng, and A. M. Chinnaiyan, "The bright side of dark matter: lncRNAs in cancer," *Journal of Clinical Investigation*, vol. 126, no. 8, pp. 2775–2782, 2016.

[27] C. Lin and L. Yang, "Long noncoding RNA in cancer: wiring signaling circuitry," *Trends in Cell Biology*, vol. 28, no. 4, pp. 287–301, 2018.

[28] B. A. Sullenger and S. Nair, "From the RNA world to the clinic," *Science*, vol. 352, no. 6292, pp. 1417–1420, 2016.

[29] S. T. Zhuang, Y. J. Cai, H. P. Liu, Y. Qin, and J. F. Wen, "LncRNA NEAT1/miR-185-5p/IGF2 axis regulates the invasion and migration of colon cancer," *Molecular Genetics and Genomic Medicine*, vol. 8, no. 4, Article ID e1125, 2020.

[30] W. Hong, H. Ying, F. Lin, R. Ding, W. Wang, and M. Zhang, "lncRNA LINC00460 silencing represses EMT in colon cancer through downregulation of ANXA2 via upregulating miR-433-3p," *Molecular Therapy. Nucleic Acids*, vol. 19, pp. 1209–1218, 2020.

[31] M. Cesana, D. Cacchiarelli, I. Legnini et al., "A long noncoding RNA controls muscle differentiation by functioning as a competing endogenous RNA," *Cell*, vol. 147, no. 4, pp. 947–369, 2011.

[32] R. O. Bak and J. G. Mikkelsen, "miRNA sponges: soaking up miRNAs for regulation of gene expression," *Wiley Interdisciplinary Reviews: RNA*, vol. 5, no. 3, pp. 317–333, 2014.

[33] B. K. Dey, A. C. Mueller, and A. Dutta, "Long non-coding RNAs as emerging regulators of differentiation, development, and disease," *Transcription*, vol. 5, no. 4, Article ID e944014, 2014.

[34] R. V. Kartha and S. Subramanian, "Competing endogenous RNAs (ceRNAs): new entrants to the intricacies of gene regulation," *Frontiers in Genetics*, vol. 5, p. 8, 2014.

[35] Y. Suzuki, C. Demoliere, D. Kitamura, H. Takeshita, U. Deuschle, and T. Watanabe, "HAX-1, a novel intracellular protein, localized on mitochondria, directly associates with HS1, a substrate of Src family tyrosine kinases," *The Journal of Immunology*, vol. 158, no. 6, pp. 2736–2744, 1997.

[36] J. R. Chao, E. Parganas, K. Boyd, C. Y. Hong, J. T. Opferman, and J. N. Ihle, "Hax1-mediated processing of HtrA2 by Parl allows survival of lymphocytes and neurons," *Nature*, vol. 452, no. 7183, pp. 98–102, 2008.

[37] A. H. Wyllie, J. F. R. Kerr, I. A. M. Macaskill, A. R. Currie, and A. R Currie, "Adrenocortical cell deletion: the role of ACTH," *The Journal of Pathology*, vol. 111, no. 2, pp. 85–94, 1973.

[38] V. Radhika, D. Onesime, J. H. Ha, and N. Dhanasekaran, "Galpha13 stimulates cell migration through cortactin-interacting protein Hax-1," *Journal of Biological Chemistry*, vol. 279, no. 47, pp. 49406–49413, 2004.

[39] E. Vafiadaki, D. A. Arvanitis, S. N. Pagakis et al., "The anti-apoptotic protein HAX-1 interacts with SERCA2 and regulates its protein levels to promote cell survival," *Molecular Biology of the Cell*, vol. 20, no. 1, pp. 306–318, 2009.

[40] V. S. R. K. Yedavalli, H. M. Shih, Y. P. Chiang et al., "Human immunodeficiency virus type 1 Vpr interacts with anti-apoptotic mitochondrial protein HAX-1," *Journal of Virology*, vol. 79, no. 21, pp. 13735–13746, 2005.

[41] A. Banerjee, K. Saito, K. Meyer et al., "Hepatitis C virus core protein and cellular protein HAX-1 promote 5-fluorouracil-mediated hepatocyte growth inhibition," *Journal of Virology*, vol. 83, no. 19, pp. 9663–9671, 2009.

[42] X. Li, J. Jiang, R. Yang et al., "Expression of HAX-1 in colorectal cancer and its role in cancer cell growth," *Molecular Medicine Reports*, vol. 12, no. 3, pp. 4071–4078, 2015.

[43] Y. Wu, R. He, Z. Cai, X. Wang, L. Cong, and F. Qiu, *Knockdown of long noncoding RNA 01124 inhibits the malignant behaviors of colon cancer cells by regulating miR-654-5p/HAX-1*, Research Square, https://www.researchsquare.com/article/rs-1445265/v2.

Hindawi
Evidence-Based Complementary and Alternative Medicine
Volume 2023, Article ID 9753435, 1 page
https://doi.org/10.1155/2023/9753435

Retraction

Retracted: High-Throughput Sequencing Investigation of Bacterial Diversity in Chronic Suppurative Otitis Media and Middle Ear Cholesteatoma

Evidence-Based Complementary and Alternative Medicine

Received 3 October 2023; Accepted 3 October 2023; Published 4 October 2023

This article has been retracted by Hindawi following an investigation undertaken by the publisher [1]. This investigation has uncovered evidence of one or more of the following indicators of systematic manipulation of the publication process:

(1) Discrepancies in scope

(2) Discrepancies in the description of the research reported

(3) Discrepancies between the availability of data and the research described

(4) Inappropriate citations

(5) Incoherent, meaningless and/or irrelevant content included in the article

(6) Peer-review manipulation

The presence of these indicators undermines our confidence in the integrity of the article's content and we cannot, therefore, vouch for its reliability. Please note that this notice is intended solely to alert readers that the content of this article is unreliable. We have not investigated whether authors were aware of or involved in the systematic manipulation of the publication process.

Wiley and Hindawi regrets that the usual quality checks did not identify these issues before publication and have since put additional measures in place to safeguard research integrity.

We wish to credit our own Research Integrity and Research Publishing teams and anonymous and named external researchers and research integrity experts for contributing to this investigation.

The corresponding author, as the representative of all authors, has been given the opportunity to register their agreement or disagreement to this retraction. We have kept a record of any response received.

References

[1] X. Cheng, A. Tuoheti, X. Huang, and X. Gu, "High-Throughput Sequencing Investigation of Bacterial Diversity in Chronic Suppurative Otitis Media and Middle Ear Cholesteatoma," *Evidence-Based Complementary and Alternative Medicine*, vol. 2022, Article ID 9616582, 9 pages, 2022.

Hindawi
Evidence-Based Complementary and Alternative Medicine
Volume 2022, Article ID 9616582, 9 pages
https://doi.org/10.1155/2022/9616582

Research Article

High-Throughput Sequencing Investigation of Bacterial Diversity in Chronic Suppurative Otitis Media and Middle Ear Cholesteatoma

Xiuqin Cheng,[1] Abulajiang Tuoheti,[1] Xiaobang Huang,[2] and Xingzhi Gu[3]

[1]*Diagnosis and Treatment Center of Otorhinolaryngology, People's Hospital of Xinjiang Uygur Autonomous Region, Urumqi, Xinjiang Uygur Autonomous Region, China*
[2]*Department of Otorhinolaryngology Head and Neck Surgery, Tianjin Beichen Hospital, Tianjin, China*
[3]*Otorhinolaryngology & Head and Neck Surgery, Sanya Central Hospital (Hainan Third People's Hospital), Sanya, Hainan, China*

Correspondence should be addressed to Xingzhi Gu; guxingzhixing@hainmc.edu.cn

Received 7 July 2022; Revised 31 July 2022; Accepted 11 August 2022; Published 19 September 2022

Academic Editor: Xueliang Wu

Background. Chronic otitis media is a common middle ear disease in otolaryngology. Bacterial infection is considered as the cause of the disease, but relying on conventional bacterial cultures can be problematic for identifying specific pathogens. Current research suggests that bacteria in microbial communities can only be identified by rDNA sequencing of bacteria. *Methods*. This cross-sectional study utilized broad-range PCR amplification of 16S rRNA genes with clone analysis to compare bacterial diversity in lesions from 6 patients with chronic suppurative otitis media (CSOM) and 10 patients with cholesteatoma of middle ear lesions. Bacteria were analyzed at the levels of phylum, order, family, genus, and species. *Results*. The age and sex difference between the patients with chronic suppurative otitis media and the patients with middle ear cholesteatoma were comparable ($P > 0.05$). Bacterial species abundance and species diversity were greater in cholesteatoma of the middle ear lesions than in CSOM lesions. The total number of detected operational taxonomic units (OTU) was 838, comprising 788 OTU detected in cholesteatoma pathological tissues, 230 in CSOM pathological tissues, and 180 OTU common to both groups. Proteus is a major part of CSOM (99.46%, $P = 0.000321$). The phyla detected in the Cholesteatoma samples were Proteus (Proteobacteria) (35.77%), thikum (Firmicutes) (44.21%, $P = 0.001071$), and Actinomycetes (Actinobacteria) (16.66%, $P = 0.032464$). At all bacterial taxonomic levels, the epithelial tissue of middle ear cholesteatoma was complex in terms of bacterial diversity, covering many Gram-positive and Gram-negative bacteria, likely related to bacterial microbiome formation. In contrast, the bacteriology of the CSOM lesions was relatively simple at all taxonomic levels, with all sequences characterized as belonging to Gram-negative bacteria. *Conclusion*. Our results suggest that persistent middle ear cholesteatoma infection may be a microbial flora disorder related to conditional pathogenic bacteria rather than a single bacterial infectious disease. The pathogen is relatively single in the diseased tissue of chronic suppurative otitis media, which is the main reason for its effective antiinfection treatment.

1. Introduction

Chronic otitis media, a common disease in otorhinolaryngology, is caused by inflammatory lesions in the middle ear and mastoid cavity and is characterized by ear discharge (otorrhea) and hearing loss. Some patients experience life-threatening complications [1, 2]. Clinically, chronic otitis media refers to chronic suppurative otitis media (CSOM) and middle ear cholesteatoma. Bacterial infection is the main pathogenic factor in chronic otitis media [3].

Bacterial culture of the external ear canal secretions is often used to confirm the presence of pathogenic bacteria, and various pathogenic bacteria, including methicillin-

resistant *Staphylococcus aureus*, have been obtained through this method [4].

Although sensitive antimicrobial agents based on culture results have been successfully used to treat patients, some cases of ineffective treatments have still been reported [5, 6]. Studies have confirmed that bacterial biofilm formation leading to resistance to antimicrobial agents may be among the reasons for the persistent symptoms in some patients [7–10]. Bacterial culture results are affected by many factors, including the inability of some bacteria to grow on standard medium and restrictions on specimen collection. Thus, in some cases, it is not easy to identify and treat the causative pathogen [11] successfully.

In recent years, there have been numerous reports on molecular techniques for the study of bacteria of otitis media. Previous work did not report any bacteria isolated from the middle ear secretions of children and adults by conventional bacterial culture methods. However, it confirmed that gene sequencing resulted in the isolation of various bacterial sequences, including the phylum and the genus Grapevine [12]. Neeff et al. demonstrated that analysis of CSOM and healthy human middle ear mucosa through molecular techniques could be accurately used to assess microbial communities in the middle ear or mastoid mucosa [13]. However, there are limited reports on the distribution of microbes in different types of chronic otitis media.

The current study used 16S rRNA gene amplicon sequencing to study microbial communities in CSOM and cholesteatoma of middle ear (CME) diseased tissues. Differences in microbial species abundance, diversity, and levels of phylum, class, order, family, genus, and species were compared. These analyses provide a basis for future studies on the characterization of bacteria at the molecular level in chronic otitis media.

2. Materials and Methods

2.1. Patient Information. All patients in this study had chronic otitis media and received surgical treatment in the otolaryngology department of Xinjiang Uygur Autonomous Region People's Hospital from January 2017 to June 2019. Among the 16 eligible patients, six cases were chronic suppurative otitis media, and 10 were middle ear cholesteatoma. None of the patients used antibiotic ear drops or systemic antibiotics before surgery, but according to the requirement for preventive use of antibiotics, all patients received intravenous cephalosporins 30 min~2 h before surgery. Patients were not associated with basic metabolic diseases such as diabetes or rheumatism and did not have external auditory canal fungal infections. The age and sex between the patients with chronic suppurative otitis media and the patients with middle ear cholesteatoma were comparable ($P > 0.05$).

The study was approved by the Ethics Committee of the People's Hospital of the Xinjiang Uygur Autonomous Region (Xinjiang District Hospital Ethics Committee 2015054). The patients or their authorized families had signed the informed consent.

The operation mode of canal wall up [CWU] tympanic forming or canal wall down [CWD] tympanic forming was selected according to the disease severity of the patient. After opening the tympanic sinus and mastoid cavity during the operation, the middle ear lesion tissue was retained (after cleaning the matrix, the epithelium and granulation tissue of cholesteatoma were retained). Following the collection of pathological tissues, the accompanying blood and floats were washed with normal saline, immediately placed into a specimen tube, frozen in liquid nitrogen, and then stored at −80°.

2.2. Absolute Quantification of 16S rRNA Amplicon Sequencing. Absolute quantification of 16S rRNA amplicon sequencing was performed by Genesky Biotechnologies Inc. (Shanghai, 201315, China). Briefly, total genomic DNA was extracted using a Fast DNA SPIN Kit for Soil (MP Biommedicals, Santa Ana, CA, USA) according to the manufacturer's instructions. The integrity of the genomic DNA was assessed through agarose gel electrophoresis, and the concentration and purity of genomic DNA were measured using a NanoDrop 2000 spectrophotometer and a Qubit 3.0 fluorometer.

The GC content was artificially synthesized. An appropriate proportion of spike-in mixture with known gradient copy numbers was then added to the sample DNA. The V3-V4 hypervariable regions of the 16s rRNA gene and spike-ins were amplified with the primers xxxF (5′-CCTACGGGNGGCWGCAG-3′) and xxxR (5′-GACTAACHVGGGTATCTAATCC-3′) and then sequenced using an Illumina NovaSeq 6000 sequencer.

2.3. Sequence Data Processing and Analysis. Raw read sequences were processed in QIME2 [14]. The adaptor and primer sequences were trimmed using the cutadapt plugin, and the DADA2 plugin was used for quality control and to identify amplicon sequence variants (ASVs) [15]. Taxonomic assignments of representative ASVs were performed with a confidence threshold of 0.8 by a pretrained Naive Bayes classifier trained on the Greengenes database (version 13.8). The spike-in sequences were then identified, and reads were counted. A standard curve for each sample was generated based on the read counts versus spike-in copy number, and the absolute copy number of ASVs in each sample was calculated using the read counts of the corresponding ASV. Since the spike-in sequence is not a component of the sample flora, the spike-in sequence was removed in the subsequent analysis [16].

3. Results

3.1. Analysis of Species Abundance and Diversity. High-throughput 16SrRNA gene sequencing technology was used to sequence samples from 16 patients with CSOM or cholesteatoma. A total of 4,672,171 raw sequences reads and 3,415,184 optimized sequence reads were obtained from the 16 patients with middle ear lesions (6 CSOM cases and 10

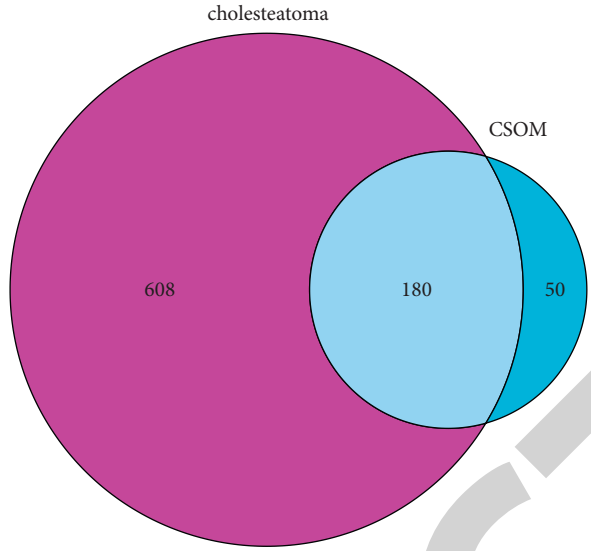

Figure 1: Venn diagram of OTUs of CSOM and cholesteatoma lesions.

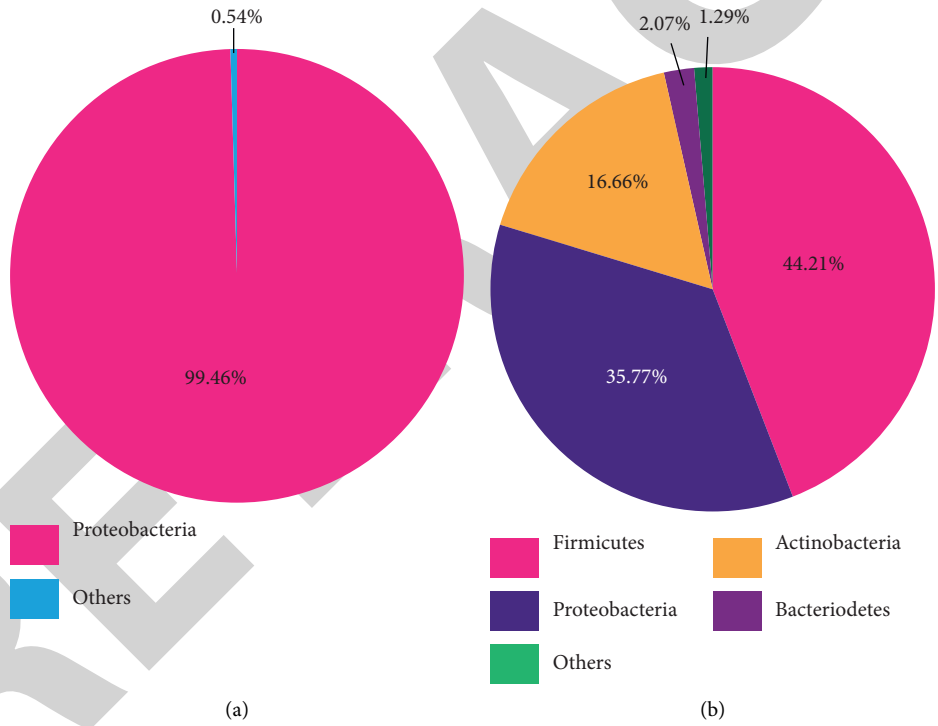

Figure 2: Pie charts showing phylum breakdown of bacterial communities obtained from CSOM (a) and cholesteatoma (b) pathological tissues.

cholesteatoma cases). The average sequence length from the total of 1,243,460,816 bases was 364.10 bp.

The sequences obtained from each patient group were 582,102 and 1,485,436 for CSOM and cholesteatoma, respectively.

3.2. Taxonomic Analysis of Pathological Tissue Flora from Patients with CSOM or Cholesteatoma. A total of 833 operational taxonomic units (OTU) were subjected to taxonomic classification, and 28 phyla, 50 classes, 63 orders, 128 families, 264 genera, and 232 species were identified and further analyzed.

Samples from different disease groups have certain common characteristics. Based on the OTU abundance table, each group's unique OTU and common OTU were screened and visualized. The total number of detected OTU was 838, comprising 788 OTU detected in cholesteatoma pathological tissues, 230 in CSOM pathological tissues, and 180 OTU common to both groups (Figure 1).

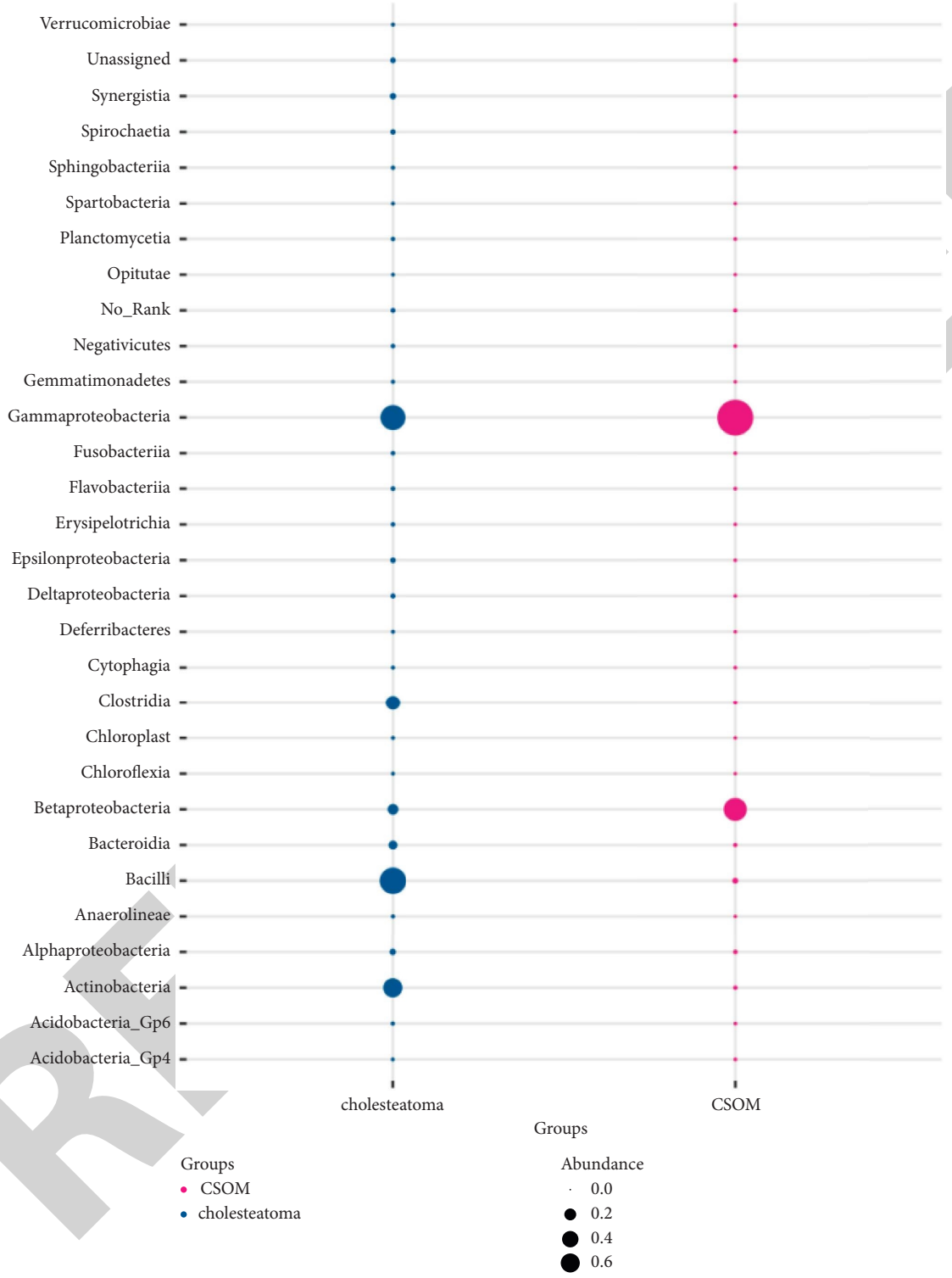

Figure 3: Bubble diagram of class level differences in bacterial communities of CSOM and cholesteatoma pathological tissues.

3.3. Phylum. Bacterial community analysis at the phylum level revealed that the community flora of CSOM tissues was simpler than that of Cholesteatoma samples. The phylum *Proteus (Proteobacteria)* was detected in both groups. The results confirmed that Proteus is a major part of CSOM (99.46%, $P = 0.000321$). In addition, the proteus phylum members such as *Pseudomonas aeruginosa* and *Escherichia coli* are the common Gram-negative pathogens. The microbial community of Cholesteatoma samples was more complex. The phyla detected in the Cholesteatoma samples were Proteus (*Proteobacteria*) (35.77%), thikum (*Firmicutes*) (44.21%, $P = 0.001071$), and *Actinomycetes*

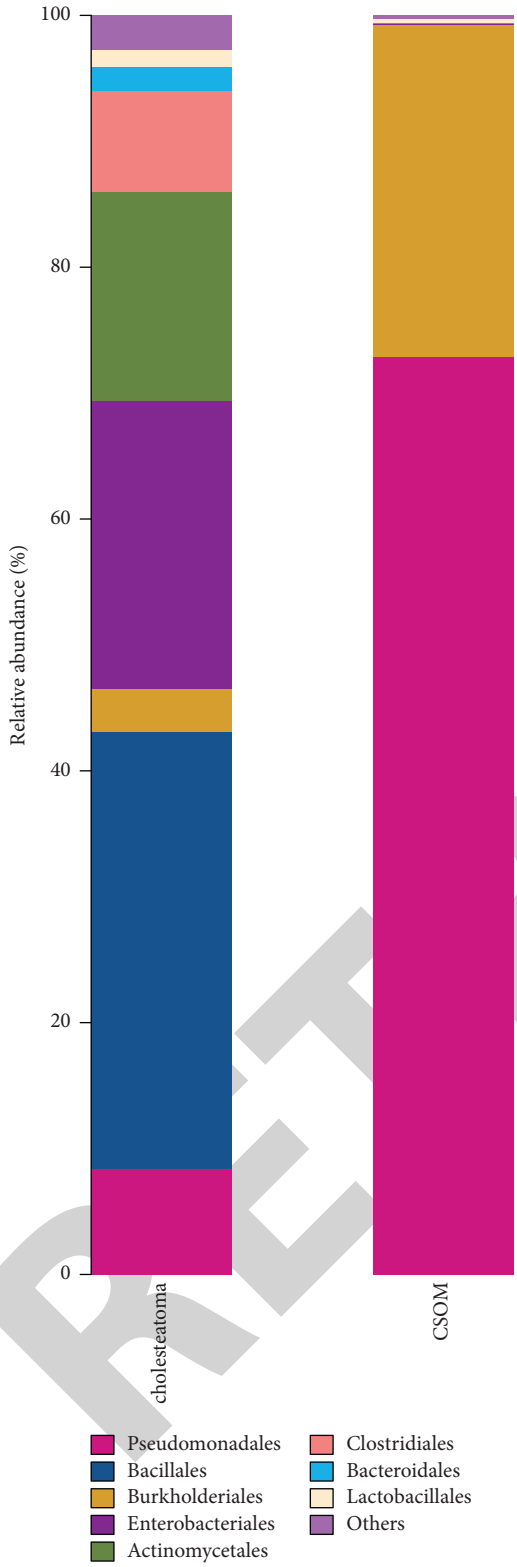

Figure 4: Bar plot diagram showing bacterial composition at the order level in CSOM and cholesteatomas pathological tissues.

(*Actinobacteria*) (16.66%, $P = 0.032464$). Thikum and Actinomycetes formed most Gram-positive bacteria (Figure 2).

3.4. Class. Bacterial sequence analysis at the class level showed statistically significant differences between the two groups (CSOM and cholesteatoma) in the classes *Gammaproteobacteria* γ-Proteus ($P = 0.03$), *Bacilli* ($P = 0.01034$), *Clostridia* ($P = 0.034$), and *Bacteroidia* ($P = 0.041$). In general, the measured species of the cholesteatoma lesions were higher than those of the CSOM group, indicating that the abundance of microbes was greater. In the CSOM group, *Gammaproteobacteria* γ- and β- Proteus (*Betaproteobacteria*) were predominantly detected, indicating that the number of microbial species present at the class level is relatively small in this group (Figure 3).

3.5. Order. At the order level, *Pseudomonadales* and *Burkholderiales* have an absolute advantage in CSOM, with *Pseudomonadales* being statistically significant ($P = 0.00129$). *Pseudomonas aeruginosa* strain PAO was identified in the bacterial species map at the sample sequencing level. In the cholesteatoma group, the statistically significant orders were *Bacillales* ($P = 0.011887$), *Clostridiales* ($P = 0.011887$), and *Bacteroidales* ($P = 0.002532$). The description of the bacterial communities at the order level also suggests that cholesteatoma is more complex in bacterial diversity (Figure 4).

3.6. Family. Analysis of sequencing results at the family level indicated that *Pseudomonadaceae* (37.74%), *Moraxellaceae* (35.13%), and *Alcaligenaceae* (26.13%) were predominant in the CSOM samples. In particular, the detection of *Pseudomonadaceae* ($P = 0.000976$) was statistically significant. Bacterial diversity at the family level in the cholesteatoma group was more complex than that of the CSOM group. Families with broad coverage in the cholesteatoma group were *Staphylococcaceae* (33.53%), *Enterobacteriaceae* (22.93%), *Brevibacteriaceae* (8.49%), *Pseudomonadaceae* (8.39%), and *Corynebacteriaceae* (6.31%). The statistically significant families *Porphyromonadaceae* and *Lachnospiraceae* are mostly conditional pathogenic bacteria (Figure 5).

3.7. Genus. Sequencing analysis of bacterial communities of CSOM and cholesteatoma lesions at the genus level revealed that 16 genera, including "Others" and "No_Rank," were detected across the two groups. However, only *Pseudomonas* was detected in both groups and showed a statistically significant difference in relative abundance between the two groups ($P = 0.000601$). *Pseudomonas* was significantly higher in the CSOM (37.74%) than in the middle ear cholesteatoma group (8.39%). Other genera detected in the CSOM group were *Acinetobacter* (35.13%) and *Alkaligenes* (26.02%) (Figure 6). Gram-negative genera were dominant. These genera include *Pseudomonas aeruginosa*, *Acinetobacter baumannii*, and fecal alkaloid bacteria, which are the most common resistant strains of nosocomial infections. In contrast, the composition of bacterial genera of the cholesteatoma group was more elaborate, comprising *Staphylococcus* (33.53%), *Providencia* (12.34%), Others (9.56%), *Proteus* (9.05%), *Brevibacterium* (8.49%), *Pseudomonas*

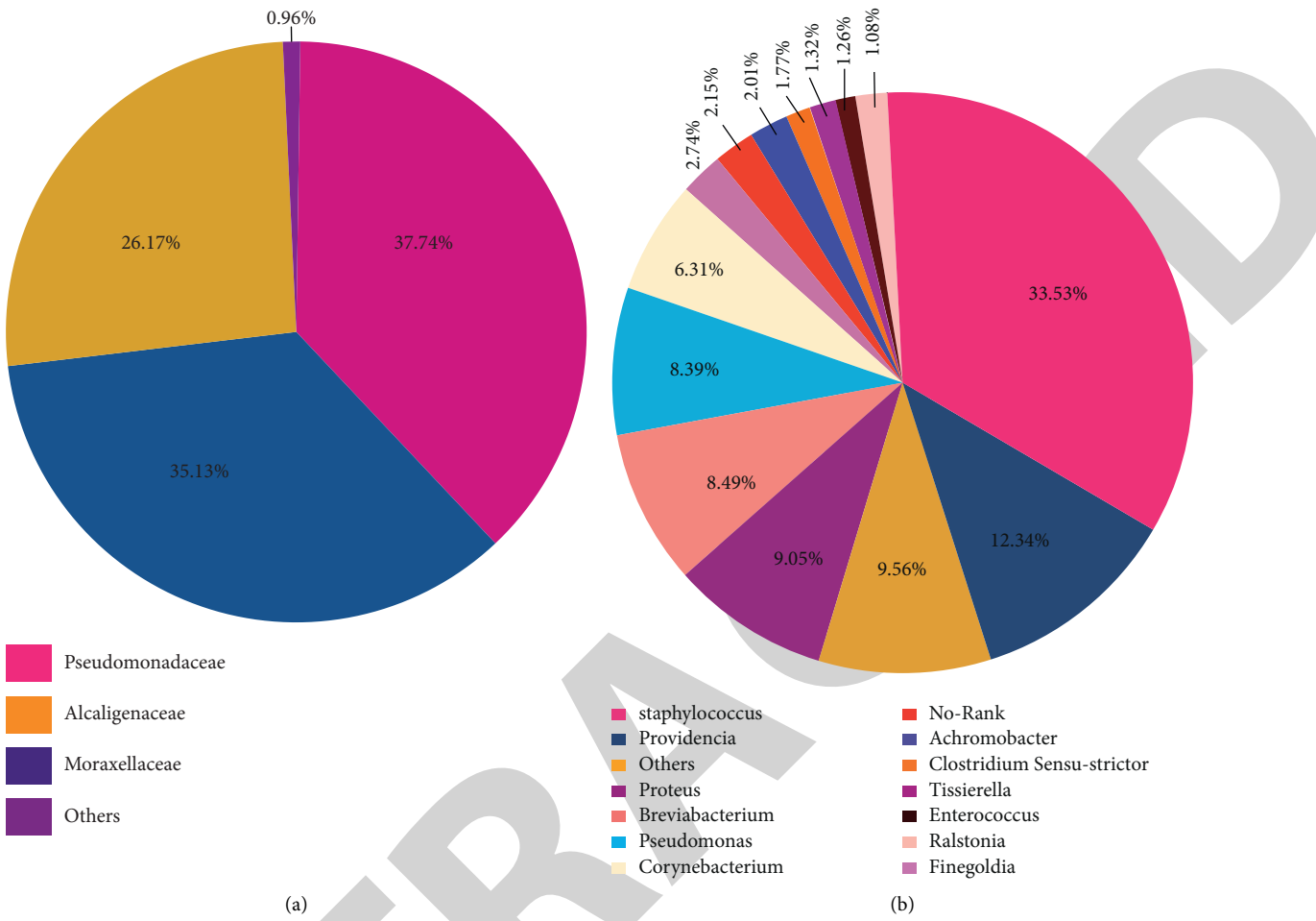

Figure 5: Pie charts showing composition of bacterial communities at the family level in CSOM (a) and cholesteatoma (b) lesions.

(8.39%), *Corynebacterium* (6.31%), *Finegoldia* (2.74%), No_Rank (2.15%), *Achromobacter* (2.09%), *Clostridium* (1.53%), *Tissierella* (1.32%), *Enterococcus* (1.26%), and *Ralstonia* (1.08%) (Figure 6). These genera are diverse and include Gram-positive and Gram-negative bacteria, cocci, bacilli, and aerobic and anaerobic bacteria.

3.8. Species. Sequencing analysis at the species level demonstrated that the pathogenic bacterial species composition in cholesteatoma lesions was more complex than in the CSOM lesions, while many more types of pathogenic bacteria were detected in the cholesteatoma group than in the CSOM group. The statistical results of the uncultured organism was $P = 0.001476$ while and the uncultured-bacterium was $P = 0.0043290$. The detection rate of *Pseudomonas aeruginosa* in the CSOM group was much higher than that in the middle ear cholesteatoma group ($P = 0.000576$, Figure 7).

4. Discussion

Although the clinical manifestations of each type of otitis media are different, surgery remains the treatment approach for both CSOM and middle ear cholesteatoma. There are slight differences in the use of antibiotics for treating the two types of otitis media, and the appropriate antimicrobial agent selection is solely based on ear secretion culture and drug sensitivity testing. In practical clinical work, the ear secretions' microbial culture results often do not meet the purpose of curing otitis media [17]. Clinicians rarely treat CSOM and middle ear cholesteatoma differently and do not select individualized treatments. Thus, there are limited studies on the detailed bacteriological differences between chronic otitis media and middle ear cholesteatoma.

In almost all molecular studies on the bacteriology of chronic otitis media, secretion swabs are collected from the middle ear cavity or the outer ear canal for gene sequencing. However, the collected secretions can be contaminated by bacteria in the external auditory canal or can be affected by the acquisition process. This may lead to false-positive results, and thus, these studies do not accurately reflect the true bacteriology of chronic otitis media [12, 18, 19]. Simultaneously, bacterial biofilm formation, like in many chronic inflammatory diseases, severely limits the ability to obtain positive results by conventional bacterial culture. Consequently, these analyses of chronic otitis media do not reflect the true clinical situation [20, 21].

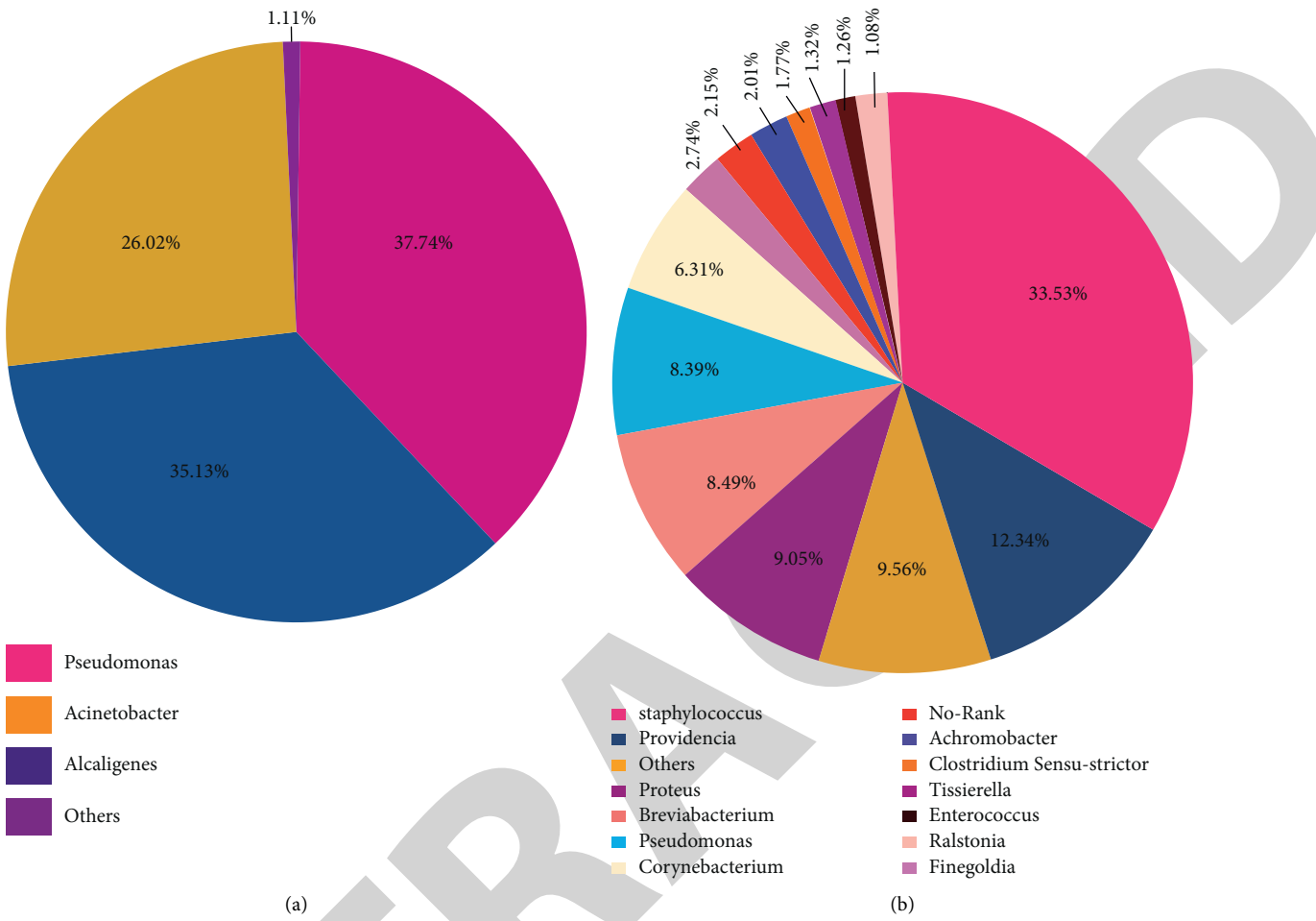

Figure 6: Pie charts showing genus-level composition of bacterial communities in CSOM (a) and cholesteatoma (b) lesions.

The use of gene sequencing might be an alternative approach for analyzing unusual or dominant flora in diseased tissue. Consequently, this approach may be beneficial for the study of the pathogenesis of otitis media. In this prospective study, high-throughput gene sequencing of CSOM and cholesteatoma tissues was performed. Bacterial species abundance and diversity differed between the two types of otitis media. The bacterial species abundance and diversity of the cholesteatoma group were greater than those of the CSOM group. This finding is congruent with previous studies [13]. Collectively, data from these studies suggests that the condition of bacterial infection in the middle ear in cholesteatoma may be different and more complex than that of CSOM.

The current study revealed that the bacterial community composition in the middle ear lesion tissue of cholesteatoma was significantly more complex than that of CSOM. The cholesteatoma group lesions contained numerous Gram-positive and Gram-negative bacteria, which might be associated with the patient's long-term illness, with the bacteria forming a unique microenvironment, a coexistence relationship, and biofilm. In contrast, the situation of CSOM lesions is relatively simple, with bacterial communities at all taxonomic levels (phyla, classes, orders, families, genera, and species) dominated by Gram-negative bacteria. These results indirectly explain why broad-spectrum antibiotics are sometimes effective in CSOM but not in middle ear cholesteatoma patients.

The current study's findings differ from previous bacteriological studies that reported that chronic otitis media usually produced only one or two kinds of bacteria. This phenomenon is due to the difficulties in cultivating various bacteria using conventional bacteriological techniques, meaning such studies cannot reflect the full picture of infections in patients. However, using high-throughput gene sequencing, the pathogenic bacteria detection rate in middle ear cholesteatoma lesions was significantly higher than in CSOM lesions. This phenomenon indicates that cholesteatoma has a higher bacterial species complexity, and it is not an infectious disease caused by a single pathogenic bacterial species. Cholesteatoma may therefore constitute a bacterial microenvironment, whereby the combination of multiple conditional pathogens leads to the continuous onset of clinical symptoms of middle ear cholesteatoma, and a series of complications eventually emerge. This finding warrants further attention in future research to identify the role of bacterial microenvironment formation in the pathogenic mechanism of middle ear cholesteatoma and

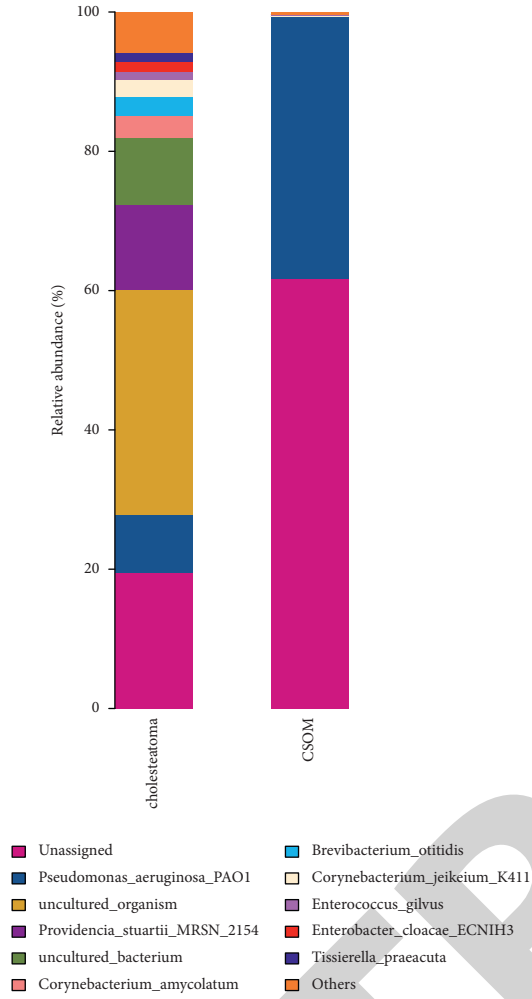

Figure 7: Bar plot showing species composition of bacterial communities of CSOM and cholesteatoma lesions.

eventually provide a basis for the prevention and early treatment of middle ear cholesteatoma.

Data Availability

The data used to support the findings of this study are available from the corresponding author upon request.

Disclosure

A preprint of this article has previously been published [22].

Conflicts of Interest

The authors declare that they have no conflicts of interest.

Acknowledgments

The authors thank all the participants of this study. Colleagues of the Otolaryngology Diagnosis and Treatment Center of Xinjiang Uygur Autonomous Region People's Hospital are acknowledged for their hard work in collecting cases and specimens. This study was financially supported by the National Science Foundation of China, Project No. 81560173.

References

[1] M. G. Li, P. J. Hotez, J. T. Vrabec, and D. T. Donovan, "Is chronic suppurative otitis media a neglected tropical disease?" *PLoS Neglected Tropical Diseases*, vol. 9, no. 3, Article ID e0003485, 2015.

[2] F. T. Orji, "A survey of the burden of management of chronic suppurative otitis media in a developing country," *Annals of Medical and Health Sciences Research*, vol. 3, no. 4, pp. 598–601, 2013.

[3] S. L. Vogt, J. Peña-Díaz, and B. B. Finlay, "Chemical communication in the gut: effects of microbiota-generated metabolites on gastrointestinal bacterial pathogens," *Anaerobe*, vol. 34, pp. 106–115, 2015.

[4] J. A. Yang, J. Y. Kim, Y. K. Yoon et al., "Epidemiological and genetic characterization of methicillin-resistant *Staphylococcus aureus* isolates from the ear discharge of outpatients with chronic otitis media," *Journal of Korean Medical Science*, vol. 23, no. 5, p. 762, 2008.

[5] R. Mittal, C. V. Lisi, R. Gerring et al., "Current concepts in the pathogenesis and treatment of chronic suppurative otitis media," *Journal of Medical Microbiology*, vol. 64, no. 10, pp. 1103–1116, 2015.

[6] B. Hiremath, R. S. Mudhol, and M. A. Vagrali, "Bacteriological profile and antimicrobial susceptibility pattern in chronic suppurative otitis media: a 1-year cross-sectional study," *Indian Journal of Otolaryngology and Head & Neck Surgery*, vol. 71, no. S2, pp. 1221–1226, 2019.

[7] R. B. Thornton, P. J. Rigby, S. P. Wiertsema et al., "Multi-species bacterial biofilm and intracellular infection in otitis media," *BMC Pediatrics*, vol. 11, no. 1, p. 94, 2011.

[8] R. B. Thornton, S. P. Wiertsema, L.-A. S. Kirkham et al., "Neutrophil extracellular traps and bacterial biofilms in middle ear effusion of children with recurrent acute otitis media—a potential treatment target," *PLoS One*, vol. 8, no. 2, Article ID 53837, 2013.

[9] X. Gu, Y. Keyoumu, L. Long, and H. Zhang, "Detection of bacterial biofilms in different types of chronic otitis media," *European Archives of Oto-Rhino-Laryngology*, vol. 271, no. 11, pp. 2877–2883, 2014.

[10] J. E. Dohar, P. A. Hebda, R. Veeh et al., "Mucosal biofilm formation on middle-ear mucosa in a nonhuman primate model of chronic suppurative otitis media," *Laryngoscope*, vol. 115, no. 8, pp. 1469–1472, 2005.

[11] B. L. Montgomery, "Lessons from microbes: what can we learn about equity from unculturable bacteria?" *mSphere*, vol. 5, no. 5, 2020.

[12] S. B. Minami, H. Mutai, T. Suzuki et al., "Microbiomes of the normal middle ear and ears with chronic otitis media," *Laryngoscope*, vol. 127, no. 10, pp. E371–E377, 2017.

[13] M. Neeff, K. Biswas, M. Hoggard, M. W. Taylor, and R. Douglas, "Molecular microbiological profile of chronic suppurative otitis media," *Journal of Clinical Microbiology*, vol. 54, no. 10, pp. 2538–2546, 2016.

[14] E. Bolyen, J. R. Rideout, M. R. Dillon et al., "Reproducible, interactive, scalable and extensible microbiome data science using QIIME 2," *Nature Biotechnology*, vol. 37, no. 8, pp. 852–857, 2019.

[15] B. J. Callahan, P. J. McMurdie, M. J. Rosen, A. W. Han, A. J. A. Johnson, and S. P. Holmes, "DADA2: high-resolution

Hindawi
Evidence-Based Complementary and Alternative Medicine
Volume 2022, Article ID 4731675, 8 pages
https://doi.org/10.1155/2022/4731675

Research Article

Skin Commensal Bacteria Modulates the Immune Balance of Mice to Alleviate Atopic Dermatitis-Induced Damage

Xianshui Yu,[1] Ting Chen,[2] Ning Huang,[1] Yanxia Jin,[1] and Ling Yang[1]

[1]*Department of Dermatology, 920th Hospital of Joint Logistics Support Force of Chinese People's Liberation Army, Kunming, Yunnan 650032, China*
[2]*Department of Pharmacy, 920th Hospital of Joint Logistics Support Force of Chinese People's Liberation Army, Kunming, Yunnan 650032, China*

Correspondence should be addressed to Ling Yang; kwqseb77@126.com

Received 26 July 2022; Revised 18 August 2022; Accepted 25 August 2022; Published 17 September 2022

Academic Editor: Xueliang Wu

Objective. Although studies indicate that *Staphylococcus epidermidis* (*S. epidermidis*) can regulate inflammation and anti-inflammatory cytokines, there is limited evidence supporting their effects on atopic dermatitis (AD). Here, we aimed to investigate the effects and potential mechanism of skin commensal bacteria on the immunity of mice with AD. *Methods*. Twenty-four female BALB/C mice were selected and divided randomly into 4 groups: normal group, atopic dermatitis model group (AD), atopic dermatitis/substrate group (AD/substrates), and atopic dermatitis/substrates/epidermidis group (AD/*S. epidermidis*). All the mice were given different ways. After 14 days, their skin conditions were scored, and the serum, ear tissue, and inguinal lymph node tissue were collected and analyzed. Furthermore, the flow cytometry was used to analyze the number of $CD4^{\circ}+^{\circ}CD25^{\circ}+^{\circ}Foxp3^{\circ}+^{\circ}$Treg in the mouse lymph node tissue. *Results*. Compared with the AD/substrate group, the mice ear thickness and dermatitis score were significantly reduced in the AD/*S. epidermidis* group; skin epidermis, acanthosis, the degree of keratinization, inflammatory cell infiltration in the dermis, and the number of mast cells were declined. The serum levels of IgE, IgG1, IgG2a, and TNF-α, IFN-γ, IL-4, and Eotaxin were significantly declined in the AD/*S. epidermidis* compared with the AD/substrate group. The proportion of $CD4^{\circ}+^{\circ}CD25^{\circ}+^{\circ}Foxp3^{\circ}+^{\circ}$Treg cells in the lymph node tissue was significantly increased in the AD/*S. epidermidis* group compared with the AD/substrate group. *Conclusion*. *Staphylococcus epidermidis* can regulate mice's immune balance to alleviate AD-induced skin damage.

1. Introduction

Atopic dermatitis (AD) is one of the most common chronic inflammatory skin diseases that mainly affects children [1], with a 20% prevalence in infants under two years old and 3% in adults worldwide [2]. Its prevalence has increased by 2 to 3-fold during the past decades in industrialized countries [3]. In America, it was found that the incidence of AD was approximately 10.7% (2011) in children and 7.2% (2015) in adults [4]. The main symptoms of AD are the destruction of the stratum corneum, eczema, and pruritus. Pruritus-caused skin scratches can severely damage the skin epidermal barrier, and subsequently, immunomodulatory proteins such as tumor necrosis factor (TNF)-α, interferon (IFN)-γ, and interleukin (IL-4) accumulate in the skin epithelial cells [5]. Immunomodulatory proteins are known to initiate and promote T helper (Th) 2 cell-mediated immune responses and stimulate B cells to undergo isotype switching from immunoglobulin (Ig) M to E [6]. However, increased IgE can result in the accumulation of eosinophil granulocytes in the dermis [7], thereby increasing immune imbalance-caused skin inflammation and aggravating AD symptoms. Besides, patients with AD are at increased risk of other atopic diseases, including asthma, allergic rhinitis, and food allergy [8]. Currently, AD treatment is focused on improving the severity of skin inflammation, including treatment with topical corticosteroids and calcineurin inhibitors, ultraviolet light, and systemic immunosuppression [9]. However, drugs

such as corticosteroids, calcineurin inhibitors (i.e., cyclosporine), and JAK inhibitors can cause side effects such as nausea, vomiting, diarrhea, skin thinning, and purpura [10]. In addition, the FDA has added a boxed warning to topical calcineurin inhibitors. Phototherapy is an alternative treatment option, but its use is limited due to high cost, inadequate local availability, and poor patient compliance [11]. Therefore, there is a need to develop alternative AD treatments.

The human skin is a complex barrier organ colonized by beneficial microorganisms interacting with their surroundings, including the host and other microbes. These interactions boost the barrier function of the skin. Therefore, a good symbiotic relationship between microbial communities is essential for the healthy skin [12]. Skin dysbiosis, defined as an imbalance of skin microbial organisms [13], is associated with an altered immune response and promotes the development of skin diseases. There is ample evidence showing that the skin of AD patients is more prone to *Staphylococcus aureus (S. aureus)* colonization and overgrowth [14]. Therefore, maintaining or restoring the skin microbial structure while specifically eliminating *S. aureus* is an ideal treatment strategy for AD.

Staphylococcus epidermidis belongs to a class of coagulase-negative staphylococci (CNS) and is a harmless commensal bacterium abundant on the human skin [15]. In natural ecology, *Staphylococcus epidermidis* plays a very important role in maintaining local homeostasis. In addition, it may compete with other potentially harmful microorganisms, such as *S. aureus*, to maintain a healthy skin flora. It is reported that polysaccharide adhesins on the surface of *Staphylococcus epidermidis* can activate human astrocytes through toll-like receptors (TLR) [16], and peptidoglycan (PG) derived from the astrocytes can activate human mononuclear THP-1 cells [17]. Some studies have reported that *Staphylococcus epidermidis* can also regulate the occurrence of IFN-γ, L-18, IL-12, and TNF [18]. According to the related reports, *Staphylococcus epidermidis* has a specific immunoregulatory function and can regulate the occurrence of inflammation and anti-inflammatory cytokines [19, 20]. The activation of immunoregulatory functions and regulation of cytokine occurrence are important defense mechanisms to prevent further damage by AD.

However, there are presently few studies on the effects of *Staphylococcus epidermidis* on AD. Therefore, in this study, an AD mouse model was established to explore the effects of *Staphylococcus epidermidis* on AD, with the objective of offering new methods and data for the clinical treatment of AD.

2. Materials and Methods

2.1. Experimental Animal. Twenty-four female SPF BALB/C mice (age: eight weeks) were housed in a temperature-controlled environment (202-21°C) with a relative humidity of 40–45% and 12 h light/dark cycles. After one week of standard diet feeding, the mice were taken through a follow-up test. This study was approved by the Ethics Committee of the 920th Hospital of Joint Logistics Support Force of Chinese People's Liberation Army (no. 2022-01-01), and the experiment was performed according to relevant guidelines and regulations.

2.2. Establishment of the Atopic Dermatitis Mouse Model. The female BALB/C mice were randomly divided into four groups (six mice per group). Mice without any treatment were set as the normal group. In the AD group, the mice's ears were painted with 2 nmol of MC903, a low-calcemic vitamin D3 analog, for 10 consecutive days [21, 22]. The topical application of MC903 induces the thymic stromal lymphopoietin (TSLP) expression in epidermal keratinocytes resulting in skin morphology changes and inflammation similar to immune perturbations observed in acute lesions of AD patients [22]. After one week of standard diet feeding, the hair on the back of the mice was removed. One fingertip unit of emulsion matrix was applied on the back of the mice twice a day (once in the morning and once in the afternoon). The mice were treated differently. For the AD/substrate group, the mice were painted with one fingertip unit of emulsion matrix on the back for seven successive days and with 2 nmol of MC903 on the ears. In the AD/*S. epidermidis* group, from the third day of painting with the emulsion matrix, the mice were painted with 150 μL of *Staphylococcus epidermidis* (10^7 CFU/mL; ATCC, USA) on the back once a day. After painting for five successive days, the ears were painted with 2 nmol of MC903. After 14 days, the serum, ear tissue, and inguinal lymph node tissue of the mice were collected.

2.3. Skin Severity Score. The mice ear thickness in each group was measured daily at the start of stimulation with MC903. Their skin conditions were scored (signs and symptoms: erythema/hemorrhage, edema, excoriation/erosion, scaling/dryness, and itch), and the scores were graded as 0 (none), 1 (mild), 2 (moderate), and 3 (severe) based on severity [23].

2.4. H and E Staining. Each mouse's right ear tissue was fixed with 4% paraformaldehyde for 48 h. Subsequently, the tissue was embedded and cut into 4-μm-thick sections. After deparaffinization with xylene, the sections were stained with hematoxylin for 5 min at an ambient temperature. Then, hydrochloric acid in ethanol was applied for tissue differentiation. After washing with water, the tissue was stained with eosin for 30 s. Then, alcohol was used to dehydrate. After treatment with dimethylbenzene, the tissue was mounted. The degree of keratinization and epidermal hyperplasia in the mouse tissue in each group were observed under a biomicroscope, and the thickness of the skin tissue *epidermis* was quantitatively analyzed.

2.5. Toluidine Blue Staining. After deparaffinization and hydration, sections of mice's right ear tissue were stained with 1% toluidine blue for approximately 20 minutes. Then, the sections were slowly rinsed with water for about 30 seconds, followed by using 95% alcohol for color separation.

The sections were cleared with xylene for 2 min and finally mounted with neutral gum. The mast cell infiltration was observed under a biomicroscope, and the thickness of the skin tissue *epidermis* was quantitatively analyzed.

2.6. ELISA Detection. The mice's whole blood was centrifuged at 3000 r/min at 4°C for 20 min, and the supernatant was collected. Their ear tissue was placed in a 2 mL tube for homogenizing. Homogenization beads and precooled PBS buffer (1 mL) were added to the tube. Then, the tissue was homogenized for 3 min at 50 Hz. After centrifugation at 12000 r/min at 4°C for 20 min, the supernatant was collected. The level of IgE, IgG1, and IgG2a in the serum and TNF-α, IFN-γ, IL-4, and Eotaxin in the mouse ear tissue in each group was evaluated following the ELISA kit instructions (MultiSciences (Lianke) Biotech Co., Ltd., China).

2.7. qRT-PCR. TRizol reagent (ThermoFisher, America) was used to extract the total RNA in the mouse ear tissue. Then, NanoDrop was used to check the concentration and purity of RNA. The cDNA was prepared following the random primer reverse transcription kit (Takala, Japan). The expression of TNF-α, IFN-i, IL-4s, and Eotaxin's mRNA was determined according to the instructions of the SYBR GREEN kit. GAPDH was used as an internal control for the analysis of the trial. The experiment was set up for 6 replicates. The $2^{-\Delta\Delta Ct}$ method was applied to calculate the relative expression of target genes according to the data obtained from qRT-PCR. Primer sequences are shown in Supplementary Table 1.

2.8. CD4°+°CD25°+°Foxp3°+°Treg Cell Assay. Surface fat and fibers of the lymph node tissue blocks of 5 mm^3 size were removed. After PBS was added to a 100-mesh stainless-steel mesh, the tissue was ground into cell suspension, which was then filtered using a 200-mesh nylon screening. After cell aggregates and uncrushed cell blocks were removed, the suspension was centrifuged. Then, PBS was used to resuspend for the preparation of single-cell suspension. Human lymphocytes separating medium was added to obtain mononuclear cells. After adding 2.5 μL of Percp-Cy5.5-CD4 monoclonal antibody and PE-CD25 monoclonal antibodies, the cells were incubated at 4°C in the dark for 30 min. Subsequently, permeabilization wash buffer was added. Then, 2.5 μL of APC-Foxp3 antibody was added, and the cells were incubated at 4°C for 30 min. Flow cytometry and the Cellquest software were used to evaluate and analyze the cells, respectively, and the ratio of Tregs cells in CD4 + cells was recorded.

2.9. Statistical Analysis. The results were expressed as mean ± standard deviation (SD). *T*-test analysis was utilized for the two-group comparisons and a one-way analysis for multigroup comparisons. All data were analyzed using the SPSS 25.0 software. Differences were considered to be statistically significant when $P < 0.05$.

3. Results

3.1. Skin Commensal Bacteria Can Alleviate MC903-Induced Atopic Dermatitis Symptoms in Mice. The effect of skin commensal bacteria on AD symptoms in mice was first evaluated. The results revealed that, compared with the normal group, the ear thickness and dermatitis severity score of the mice in the AD and AD/substrate groups were significantly increased. Notably, after painting with skin commensal bacteria, both the ear thickness and severity score were significantly reduced in the AD/*S. epidermidis* group compared with the AD/substrate group (Figures 1(a) and 1(b)).

The effects of skin commensal bacteria on the skin structure and the number of mast cells were evaluated. The results indicated that the skin tissue structure in the normal group was intact and normal, and there were no obvious abnormal changes in the dermis. In the AD and AD/substrate groups, the skin structure was severely damaged, with thickened *epidermis*, hyperkeratosis, acanthosis, edema of epidermal cells, dermal vasodilatation, and massive inflammatory cell infiltration. However, in the AD/*S. epidermidis* group, thickened *epidermis* and acanthosis were alleviated, the degree of keratinization was reduced, and dermal inflammatory cell infiltration was decreased compared with the AD/substrate group (Figure 1(c)). According to the toluidine blue staining results, compared with the normal group, the number of mast cells was significantly increased in the AD and AD/substrate groups. Notably, the number of mast cells in the AD/*S. epidermidis* group was reduced compared with the AD/substrate group (Figure 1(d)). Together, these results suggested that skin commensal bacteria could alleviate skin damage and reduce AD severity in mice.

3.2. Skin Commensal Bacteria Can Restore Immune Balance and Decrease the Inflammatory Factor Level in Mice with Atopic Dermatitis. The effects of skin commensal bacteria on immune and inflammatory factors were evaluated. Compared with the normal group, we found that the levels of immune factors (IgE, IgG1, and IgG2a), inflammatory factors (TNF-α, IFN-γ, and IL-4), and the expression and release levels of mRNA in Eotaxin were significantly upregulated in the serum of the AD and AD/substrate mice groups. However, there were no significant differences in these factors between the AD and AD/substrate groups. Notably, after skin commensal bacteria were added, both the immune and inflammatory factors in the serum were decreased in the AD/*S. epidermidis* compared with the AD/substrate group (Figures 2(a)–2(c)). Together, these results indicated that skin commensal bacteria might affect the immune balance and inflammatory reaction, relieving AD symptoms in mice.

3.3. Skin Commensal Bacteria Can Restore the Proliferation of CD4°+°CD25°+°Foxp3°+°Treg Cell in the Lymph Nodes. Flow cytometry was used to determine the effects of skin commensal bacteria on the recovery of immune function in

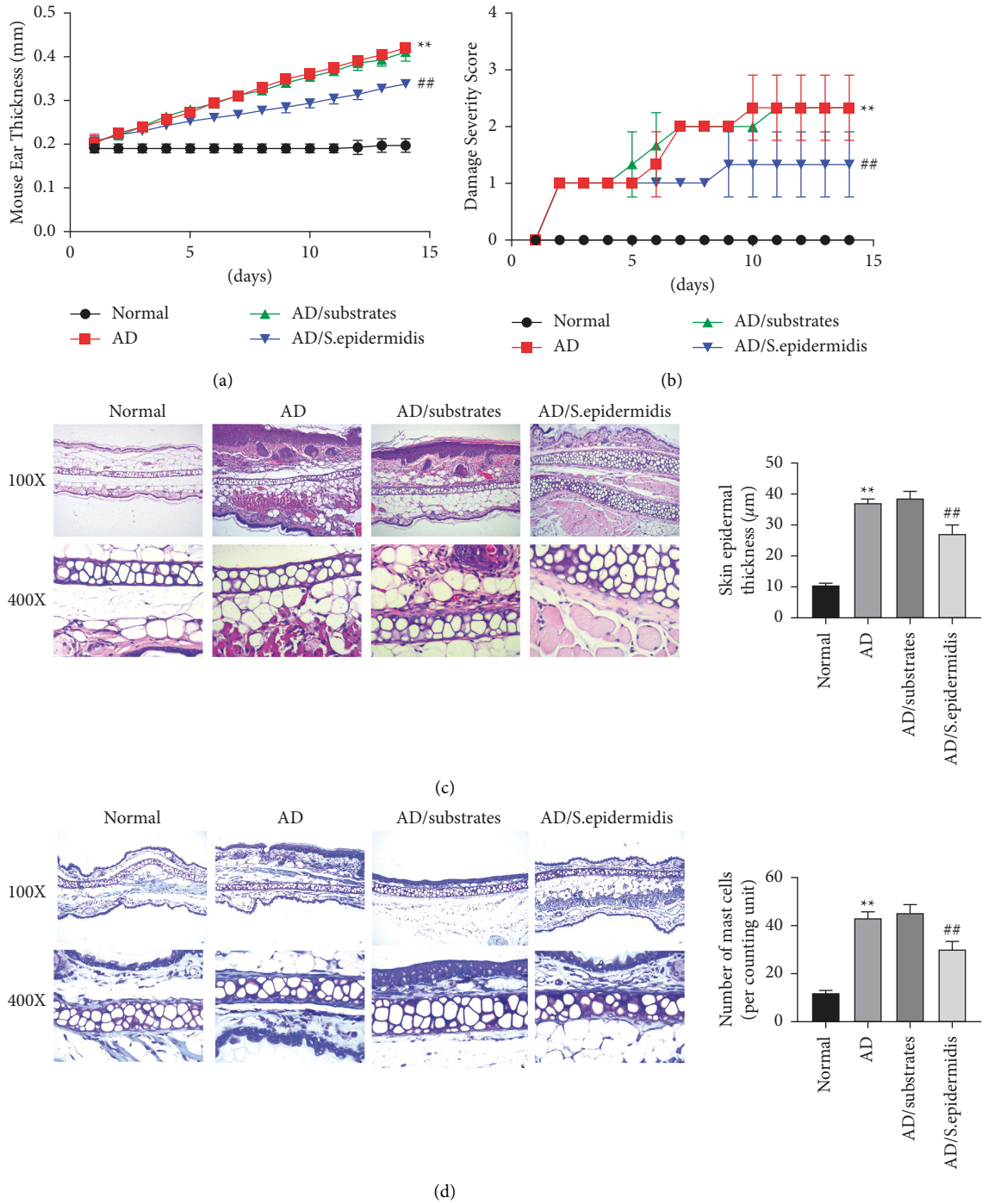

Figure 1: Effects of skin commensal bacteria on MC903-induced atopic dermatitis symptoms in mice. (a) The ear thickness of the mice in each group; (b) dermatitis severity score of mice in each group; (c) H and E staining was applied to observe the mouse ear tissue structure; (d) toluidine blue was used to observe infiltration of mast cells in the mouse ear tissue. $^{\#\#}P < 0.01$ *vs.* normal group and $^{\#\#}P < 0.01$ *vs.* AD/substrate group.

AD mice. The results revealed that the proportion of CD4˚+˚CD25˚+˚Foxp3˚+˚Treg cells in the mice lymph node tissue in the AD and AD/substrate groups was significantly lower than that in the normal group. The proportion of CD4˚+˚VCD25˚+˚Foxp3˚+˚Treg cells in the lymph node tissue was significantly increased in the AD/*S. epidermidis* group compared with the AD/substrate group (Figure 3). These results indicated that skin commensal bacteria could improve the immune function of AD mice.

4. Discussion

Atopic dermatitis is a refractory skin disease characterized by recurrent and difficult-to-recover eczema and pruritus

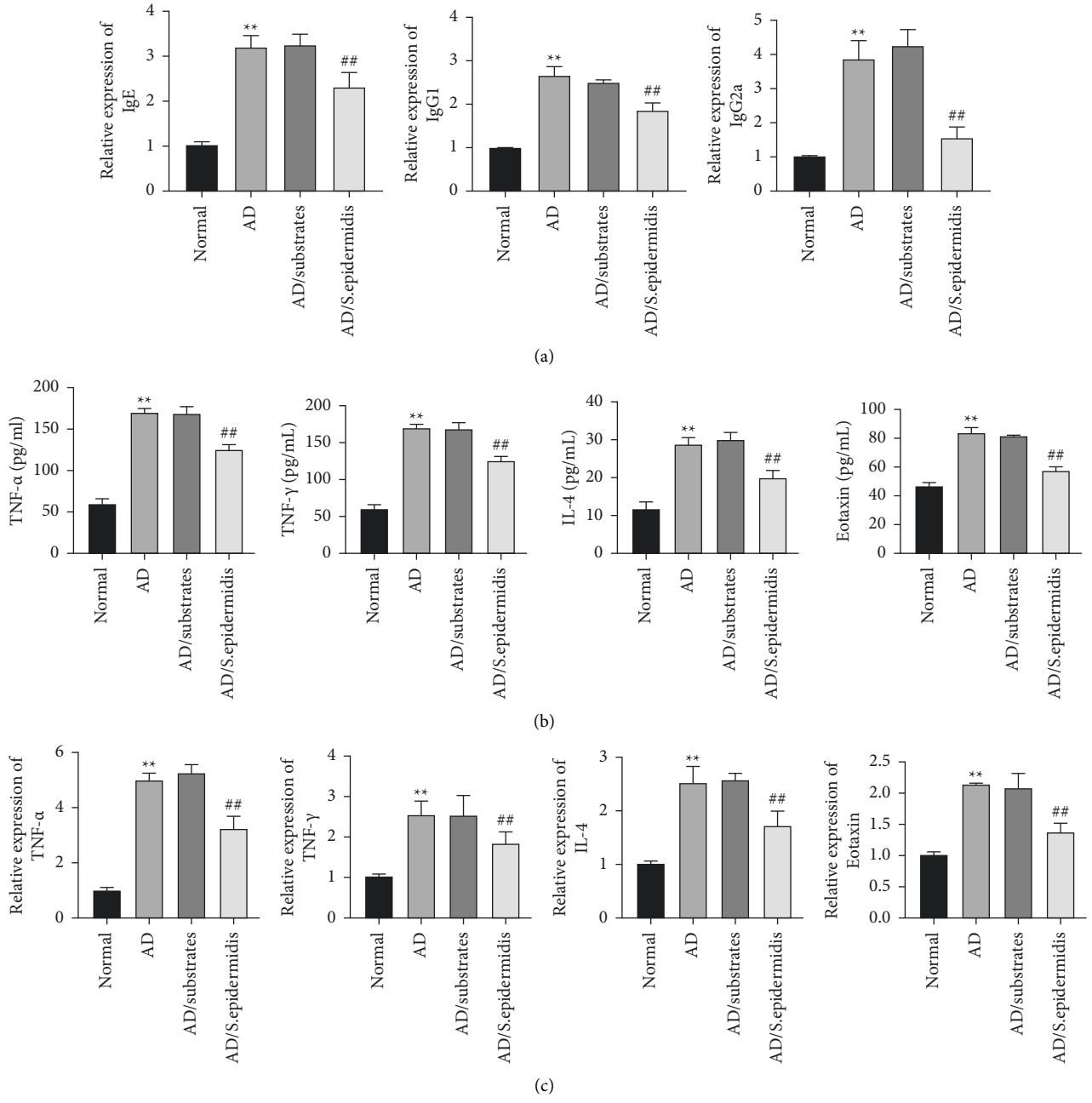

Figure 2: Effects of skin commensal bacteria on immune and inflammatory factors of mice with atopic dermatitis. a andb, ELISA was used to check the level of IgE, IgG1, and IgG2a in the mice serum (a); and TNF-α, IFN-γ, IL-4, and Eotaxin in the mouse ear tissue (b); and (c) QRT-PCR was used to measure the expression of TNF-α, IFN-γ, IL-4, and Eotaxin mRNA in the mouse ear tissue. $^{**}P < 0.01$ *vs.* normal group and $^{\#\#}P < 0.01$ *vs.* AD/substrate group.

[24]. While its prevalence has been increasing worldwide, the etiology of AD is not yet well understood, and there is currently no effective AD treatment. The current AD standard medical therapies, including topical corticosteroids and topical calcineurin inhibitors [24], can improve the condition of AD patients but have a lot of side effects. *S. aureus* skin colonization is considered an important factor in the pathogenesis of AD [25]. It was shown to exacerbate skin inflammation and allergic reactions by disrupting the adaptive and innate immune responses through several mechanisms [26]. On the other hand, *Staphylococcus epidermidis* is one of the most abundant species in the skin microbiota and has been shown to limit the growth of *Staphylococcus aureus* [27]. Based on these findings, we hypothesized that restoring immune balance through *Staphylococcus epidermidis* would be an effective AD treatment strategy. Expectedly, this study showed that *Staphylococcus epidermidis* significantly reduced dermatitis severity and skin damage in MC903-induced AD mice.

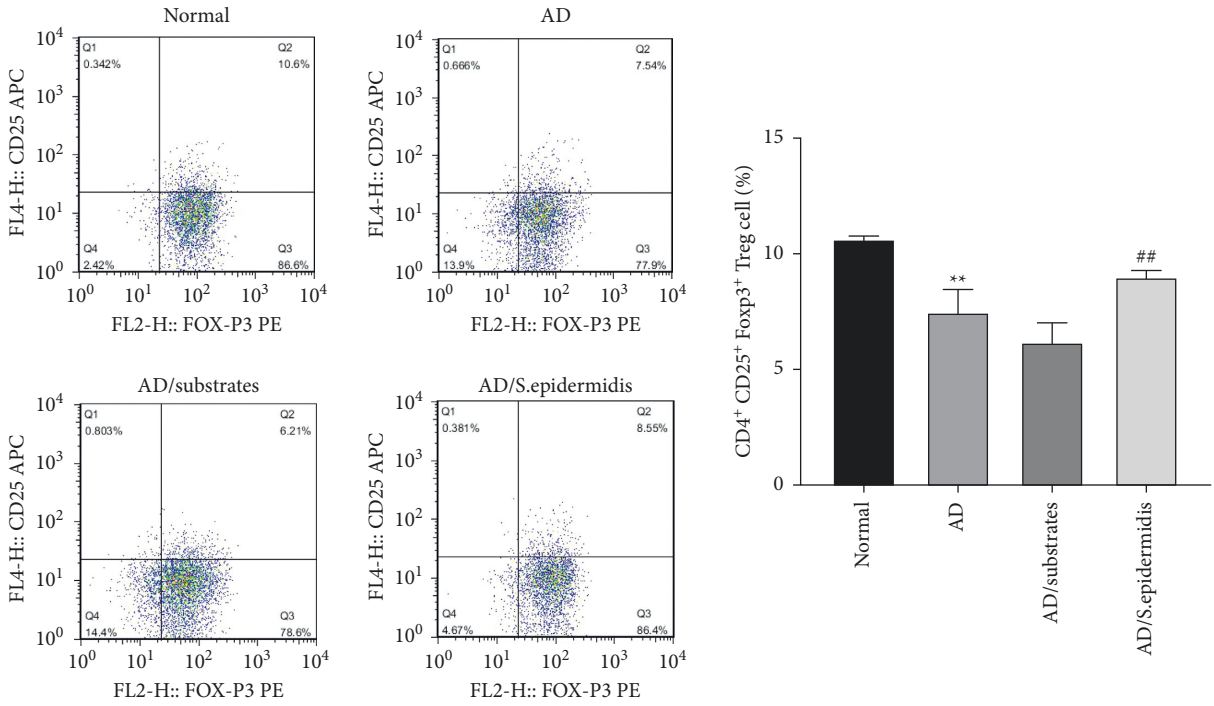

Figure 3: Effects of skin commensal bacteria on the proportion of CD4+ CD25+ Foxp3+Treg cells in the lymph node tissue of mice with atopic dermatitis. $^{**}P < 0.01$ vs. normal group and $^{\#\#}P < 0.01$ vs. AD/substrate group.

In a recent meta-analysis by Totte et al. [28], the authors reported that *Staphylococcus aureus* was significantly more prevalent on the lesional skin of AD patients than on the nonlesional skin of the same patients or the skin of healthy controls (70% vs. 39%), and its rate of colonization was shown to associate with disease severity. Although *S. epidermidis* is considered a beneficial skin microbe against *Staphylococcus aureus*, a recent study by Cau et al. [29] found that an overabundance of *Staphylococcus epidermidis* on some patients had similar harmful effects as *Staphylococcus aureus*. It was shown that some *Staphylococcus epidermidis* strains could impair the skin barrier and promote inflammation through the secretion of the cysteine protease EcpA, thereby increasing the disease severity [29]. Thus, *Staphylococcus epidermidis* may shift from a beneficial commensal to a deleterious pathogen similar to *Staphylococcus aureus* in the permissive growth conditions of the AD skin. Some unique coagulase-negative staphylococci (CoNS) strains, such as *Staphylococcus hominis A9* and *C5*, were shown effective in inhibiting and preventing *S. epidermidis*-induced skin damage [29]. *S. hominis A9* was shown to kill *S. aureus*, whereas *Staphylococcus hominis C5* synthetic autoinducing peptide was shown to inhibit the *Staphylococcus aureus* [29]. These indicate that such commensal CoNS strains are promising therapeutic tools in reducing *Staphylococcus aureus* colonization and the toxin production of both *Staphylococcus aureus* and *Staphylococcus epidermidis* in AD. The above findings indicate the complexity of the interactions between commensal CoNS and deleterious *S. aureus* and suggest that using *Staphylococcus epidermidis* as the treatment for dysbiosis in AD may further damage the skin and cause inflammation. Thus, a small molecule with a narrow-spectrum effect, especially on *Staphylococcus aureus*, might be an attractive alternative for the treatment of AD [30].

Mast cells are hematopoietic cells originating from bone marrow progenitor cells [31]. Mast cell-committed progenitors migrate through the circulation into the destination tissues and proliferate and differentiate into mature mast cells under the influence of the local microenvironment [32]. Mast cells are the key effector cells in allergic reactions. They are activated by IgE receptors, leading to degranulation and subsequent release of various inflammatory mediators such as histamine, serotonin, and tumor necrosis factor-α (TNF-α) [33, 34]. Most studies have shown an increase in the number of mast cells in skin lesions in AD models, so it is generally believed that mast cells contribute to skin inflammation [35]. The results of this study showed that *Staphylococcus epidermidis* decreased mast cell infiltration in mice ear tissues. These findings are consistent with those of Meng et al. who found that paeonol inhibited the development of 1-chloro-2,4-dinitrobenzene-induced AD in mice by differentiating mast cells and *T* cells [36].

AD is characterized by inflamed skin, impaired skin barrier function, and IgE-mediated sensitization to food and environmental allergens [37]. Currently, there are two main hypotheses explaining the pathogenesis of AD: (1) immune dysregulation causes Th2-predominant inflammation and IgE-mediated sensitization [38]; (2) intrinsic defects in skin barrier function. In addition, various inflammatory cytokines, mainly Th2 cell-derived cytokines, regulate and guide the nature of AD, including IL-4, TNF-α, IFN-γ, and Eotaxin [39]. IL-4 and IL-13 are the key drivers of the IgE isotype class switching, inflammation, and expression of receptors

on the surface of mast cells. IL-4 and IL-13 often activate the IL-4 receptor (IL-4R) to downregulate skin barrier proteins, thus affecting the skin barrier [40]. Therefore, reducing the expression of IL-4 and IL-13 is an effective AD treatment strategy. The results of this study showed that *Staphylococcus epidermidis* could reduce the level of TNF-α, IFN-γ, IL-4, and Eotaxin in the ear tissue and the level of IgE, IgG1, and IgG2a in mice's serum.

Numerous studies have shown that clinical symptoms of AD patients can be relieved by modulating the immune system. Simon et al. found that immunosuppressive drugs (i.e., cyclosporine and a mycophenolate mofetil) significantly improved the AD symptoms [41]. Beck et al. found that the symptoms of AD could be significantly alleviated by anti-IL-4 receptor antibody or anti-B cell antibody [42]. These findings suggested that immune dysfunction exerted a crucial role in the pathogenesis of AD. $CD4^{\circ}+^{\circ}$regulatory T cells (Treg) are indispensable in maintaining immune self-tolerance and homeostasis in the normal immune system, accounting for 10% of all the $CD4^{\circ}+^{\circ}$T cells in the peripheral circulation [43, 44]. Treg cells have been shown to prevent excessive inflammation and maintain immune tolerance. However, dysfunctional Treg can lead to autoimmune diseases, including AD, systemic lupus erythematosus, and asthma [45]. Based on the results of this study, we found that *Staphylococcus epidermidis* could significantly increase the proportion of $CD4^{\circ}+^{\circ}CD25^{\circ}+^{\circ}Foxp3^{\circ}+^{\circ}$Treg cells in the lymph nodes of AD mice. These findings suggested that *Staphylococcus epidermidis* could regulate mice's immune balance to reduce AD-induced damage.

5. Conclusion

Staphylococcus epidermidis alleviated MC903-induced skin damage and improved AD symptoms in mice with AD. It may exert its function by reducing immune proteins, alleviating inflammation, inducing the proliferation of $CD4^{\circ}+^{\circ}CD25^{\circ}+^{\circ}Foxp3^{\circ}+^{\circ}$Treg cells, and restoring the immune function of AD mice. However, the target of *Staphylococcus epidermidis* in exerting its biological function remains unknown. Therefore, further studies are needed to comprehensively elucidate the specific mechanism of *Staphylococcus epidermidis* in regulating immune balance, thereby providing more accurate theory evidence for clinical application.

Data Availability

The data used to support the findings of this study are available from the corresponding author upon request.

Ethical Approval

This study was approved by the Ethics Committee of the 920th Hospital of Joint Logistics Support Force of Chinese People's Liberation Army (no. 2022-01-01), and the experiment was performed according to relevant guidelines and regulations.

Conflicts of Interest

The authors declare that they have no conflicts of interest.

Supplementary Materials

Supplementary Table 1: primer sequences used in qRT-PCR. (*Supplementary Materials*)

References

[1] T. Zheng, J. Yu, M. H. Oh, and Z. Zhu, "The atopic march: progression from atopic dermatitis to allergic rhinitis and asthma," *Allergy, Asthma & Immunology Research*, vol. 3, no. 2, pp. 67–73, 2011.

[2] M. Boguniewicz and D. Y. Leung, "Recent insights into atopic dermatitis and implications for management of infectious complications," *The Journal of Allergy and Clinical Immunology*, vol. 125, no. 1, pp. 4–13, 2010.

[3] S. Nutten, "Atopic dermatitis: global epidemiology and risk factors," *Annals of Nutrition & Metabolism*, vol. 66, no. 1, pp. 8–16, 2015.

[4] A. M. Drucker, A. R. Wang, W. Q. Li, E. Sevetson, J. K. Block, and A. A. Qureshi, "The burden of atopic dermatitis: summary of a report for the national eczema association," *Journal of Investigative Dermatology*, vol. 137, no. 1, pp. 26–30, 2017.

[5] U. Nygaard, M. Hvid, C. Johansen et al., "TSLP, IL-31, IL-33 and sST2 are new biomarkers in endophenotypic profiling of adult and childhood atopic dermatitis," *Journal of the European Academy of Dermatology and Venereology*, vol. 30, no. 11, pp. 1930–1938, 2016.

[6] L. Misery, "La TSLP, clé du prurit dans la dermatite atopique," *Medical Science*, vol. 30, no. 2, pp. 142–144, 2014.

[7] L. T. Hellman, S. Akula, M. Thorpe, and Z. Fu, "Tracing the origins of IgE, mast cells, and allergies by studies of wild animals," *Frontiers in Immunology*, vol. 8, p. 1749, 2017.

[8] H. Long, G. Zhang, L. Wang, and Q. Lu, "Eosinophilic skin diseases: a comprehensive review," *Clinical Reviews in Allergy and Immunology*, vol. 50, no. 2, pp. 189–213, 2016.

[9] B. Cabanillas, A. C. Brehler, and N. Novak, "Atopic dermatitis phenotypes and the need for personalized medicine," *Current Opinion in Allergy and Clinical Immunology*, vol. 17, no. 4, pp. 309–315, 2017.

[10] J. Klonowska, J. Glen, R. J. Nowicki, and M. Trzeciak, "New cytokines in the pathogenesis of atopic dermatitis-new therapeutic targets," *International Journal of Molecular Sciences*, vol. 19, pp. 3086–10, 2018.

[11] A. Patrizi, B. Raone, and G. M. Ravaioli, "Management of atopic dermatitis: safety and efficacy of phototherapy," *Clinical, Cosmetic and Investigational Dermatology*, vol. 8, pp. 511–520, 2015.

[12] E. A. Grice and J. A. Segre, "The skin microbiome," *Nature Reviews Microbiology*, vol. 9, no. 4, pp. 244–253, 2011.

[13] N. Kaur, C. C. Chen, J. Luther, and J. Y. Kao, "Intestinal dysbiosis in inflammatory bowel disease," *Gut Microbes*, vol. 2, no. 4, pp. 211–216, 2011.

[14] D. Y. Leung, "New insights into atopic dermatitis: role of skin barrier and immune dysregulation," *Allergology International*, vol. 62, no. 2, pp. 151–161, 2013.

[15] N. T. Stevens, I. Sadovskaya, S. Jabbouri et al., "Staphylococcus epidermidis polysaccharide intercellular adhesin induces IL-8 expression in human astrocytes via a mechanism involving TLR2," *Cellular Microbiology*, vol. 11, no. 3, pp. 421–432, 2009.

[16] L. Gong, Q. Bao, C. Hu et al., "Exosomal miR-675 from metastatic osteosarcoma promotes cell migration and invasion by targeting CALN1," *Biochemical and Biophysical Research Communications*, vol. 500, no. 2, pp. 170–176, 2018.

[17] R. J. Stuyt, S. H. Kim, L. L. Reznikov et al., "Regulation of staphylococcus epidermidis-induced IFN-gamma in whole human blood: the role of endogenous IL-18, IL-12, IL-1, and TNF," *Cytokine*, vol. 21, no. 2, pp. 65–73, 2003.

[18] T. Bieber, "Atopic dermatitis," *New England Journal of Medicine*, vol. 358, no. 14, pp. 1483–1494, 2008.

[19] S. Naik, N. Bouladoux, J. L. Linehan et al., "Commensal-dendritic-cell interaction specifies a unique protective skin immune signature," *Nature*, vol. 520, no. 7545, pp. 104–108, 2015.

[20] T. Nakatsuji, T. H. Chen, S. Narala et al., "Antimicrobials from human skin commensal bacteria protect against *Staphylococcus aureus* and are deficient in atopic dermatitis," *Science Translational Medicine*, vol. 9, Article ID eaah4680, 2017.

[21] Z. F. Y. J. Chang, D. Zhang, and L. Wang, "Study on mechanism of compound glycyrrhizin in treatment of atopic dermatitis in mice based on miR-155/SOCS1 axis," *Chinese Journal of Immunology*, vol. 36, no. 13, pp. 1583–1588.

[22] M. Li, P. Hener, Z. Zhang, S. Kato, D. Metzger, and P. Chambon, "Topical vitamin D3 and low-calcemic analogs induce thymic stromal lymphopoietin in mouse keratinocytes and trigger an atopic dermatitis," *Proceedings of the National Academy of Sciences of the United States of America*, vol. 103, no. 31, pp. 11736–11741, 2006.

[23] L. Cox and M. A. Calderon, "Allergen immunotherapy for atopic dermatitis: is there room for debate?" *Journal of Allergy and Clinical Immunology: In Practice*, vol. 4, no. 3, pp. 435–444, 2016.

[24] V. Soumelis, "Molecular and cellular discoveries in inflammatory dermatoses," *Journal of the European Academy of Dermatology and Venereology*, vol. 31, no. Suppl 5, pp. 3–7, 2017.

[25] L. S. Chiu, V. C. Y. Chow, J. M. L. Ling, and K. L. Hon, "*Staphylococcus aureus* carriage in the anterior nares of close contacts of patients with atopic dermatitis," *Archives of Dermatology*, vol. 146, no. 7, pp. 748–752, 2010.

[26] I. Bekeredjian-Ding, S. Inamura, T. Giese et al., "*Staphylococcus aureus* protein A triggers T cell-independent B cell proliferation by sensitizing B cells for TLR2 ligands," *The Journal of Immunology*, vol. 178, no. 5, pp. 2803–2812, 2007.

[27] T. Glatthardt, J. C. d. M. Campos, R. C. Chamon et al., "Small molecules produced by commensal Staphylococcus epidermidis disrupt formation of biofilms by *Staphylococcus aureus*," *Applied and Environmental Microbiology*, vol. 86, no. 5, Article ID e02539-19, 2020.

[28] J. E. Totte, W. T. van der Feltz, M. Hennekam, A. van Belkum, E. J. van Zuuren, and S. G. Pasmans, "Prevalence and odds of *Staphylococcus aureus* carriage in atopic dermatitis: a systematic review and meta-analysis," *British Journal of Dermatology*, vol. 175, no. 4, pp. 687–695, 2016.

[29] L. Cau, M. R. Williams, A. M. Butcher et al., "Staphylococcus epidermidis protease EcpA can be a deleterious component of the skin microbiome in atopic dermatitis," *The Journal of Allergy and Clinical Immunology*, vol. 147, no. 3, pp. 955–966.e16, 2021.

[30] C. Y. Chu, "Targeting the cutaneous microbiota in atopic dermatitis: 'A new hope' or 'attack of the CoNS," *Clinical and Translational Medicine*, vol. 12, no. 5, p. e865, 2022.

[31] Y. Kitamura and A. Ito, "Mast cell-committed progenitors," *Proceedings of the National Academy of Sciences of the United States of America*, vol. 102, no. 32, pp. 11129-11130, 2005.

[32] S. J. Galli, M. Maurer, and C. S. Lantz, "Mast cells as sentinels of innate immunity," *Current Opinion in Immunology*, vol. 11, no. 1, pp. 53–59, 1999.

[33] S. J. Galli and M. Tsai, "IgE and mast cells in allergic disease," *Nature Medicine*, vol. 18, no. 5, pp. 693–704, 2012.

[34] B. Zhang, K. D. Alysandratos, A. Angelidou et al., "Human mast cell degranulation and preformed TNF secretion require mitochondrial translocation to exocytosis sites: relevance to atopic dermatitis," *The Journal of Allergy and Clinical Immunology*, vol. 127, no. 6, pp. 1522–1531.e8, 2011, e1528.

[35] R. Saluja, M. Khan, M. K. Church, and M. Maurer, "The role of IL-33 and mast cells in allergy and inflammation," *Clinical and Translational Allergy*, vol. 5, no. 1, p. 33, 2015.

[36] Y. Meng, Z. Liu, C. Zhai et al., "Paeonol inhibits the development of 1chloro2, 4dinitrobenzeneinduced atopic dermatitis via mast and T cells in BALB/c mice," *Molecular Medicine Reports*, vol. 19, no. 4, pp. 3217–3229, 2019.

[37] P. Korosec, B. F. Gibbs, M. Rijavec, A. Custovic, and P. J. Turner, "Important and specific role for basophils in acute allergic reactions," *Clinical and Experimental Allergy*, vol. 48, no. 5, pp. 502–512, 2018.

[38] K. Eyerich and N. Novak, "Immunology of atopic eczema: overcoming the Th1/Th2 paradigm," *Allergy*, vol. 68, no. 8, pp. 974–982, 2013.

[39] A. Otsuka, T. Nomura, P. Rerknimitr, J. A. Seidel, T. Honda, and K. Kabashima, "The interplay between genetic and environmental factors in the pathogenesis of atopic dermatitis," *Immunological Reviews*, vol. 278, no. 1, pp. 246–262, 2017.

[40] D. E. Lee, A. K. Clark, K. A. Tran, and V. Y. Shi, "New and emerging targeted systemic therapies: a new era for atopic dermatitis," *Journal of Dermatological Treatment*, vol. 29, no. 4, pp. 364–374, 2018.

[41] D. Simon, S. Hosli, G. Kostylina, N. Yawalkar, and H. U. Simon, "Anti-CD20 (rituximab) treatment improves atopic eczema," *The Journal of Allergy and Clinical Immunology*, vol. 121, no. 1, pp. 122–128, 2008.

[42] L. A. Beck, D. Thaci, J. D. Hamilton et al., "Dupilumab treatment in adults with moderate-to-severe atopic dermatitis," *New England Journal of Medicine*, vol. 371, no. 2, pp. 130–139, 2014.

[43] S. Sakaguchi, "Naturally arising CD4+ regulatory t cells for immunologic self-tolerance and negative control of immune responses," *Annual Review of Immunology*, vol. 22, pp. 531–562, 2004.

[44] S. Z. Josefowicz, L. F. Lu, and A. Y. Rudensky, "Regulatory T cells: mechanisms of differentiation and function," *Annual Review of Immunology*, vol. 30, no. 1, pp. 531–564, 2012.

[45] S. Sakaguchi, T. Yamaguchi, T. Nomura, and M. Ono, "Regulatory T cells and immune tolerance," *Cell*, vol. 133, no. 5, pp. 775–787, 2008.

Hindawi
Evidence-Based Complementary and Alternative Medicine
Volume 2022, Article ID 3512582, 17 pages
https://doi.org/10.1155/2022/3512582

Research Article

Analysis of the Distribution and Antibiotic Resistance of Pathogens Causing Infections in Hospitals from 2017 to 2019

Guoliang Liu and Mingzhao Qin

Department of Geriatrics, Beijing Tongren Hospital, Capital Medical University, Beijing 100730, China

Correspondence should be addressed to Guoliang Liu; drliuguoliang@163.com

Received 3 July 2022; Revised 31 July 2022; Accepted 4 August 2022; Published 16 September 2022

Academic Editor: Xueliang Wu

Background. Antibiotic resistance is a global public health problem, leading to high mortality and treatment costs. To achieve more efficient treatment protocols and better patient recovery, the distribution and drug resistance of pathogens in our hospital were investigated, allowing significant clinical guidance for the use of antimicrobials. *Methods*. In this retrospective study (2017–2019), 3482 positive samples were isolated from 43,981 specimens in 2017; 3750 positive specimens were isolated from 42,923 specimens in 2018; and 3839 positive pathogens were isolated from 46,341 specimens in 2019. These samples were from various parts of the patients, including the respiratory tract, urine, blood, wound secretions, bile, and puncture fluids. The distribution and antibiotic resistance of these isolated pathogens from the whole hospital were analyzed. *Results*. The results from pathogen isolation showed that *Escherichia coli* (12.8%), *Staphylococcus aureus* (11%), *Klebsiella pneumoniae* (10.8%), *Pseudomonas aeruginosa* (10.7%), and *Acinetobacter baumannii* (6.4%) represented the five main pathogenic bacteria in our hospital. *Pseudomonas aeruginosa* (16.2% and 17.5%) occupied the largest proportion in the central intensive care unit (central ICU) and respiratory intensive care unit (RICU), while *Acinetobacter baumannii* (15.4%) was the most common pathogen in the emergency intensive care unit (EICU). The resistance rate of *Escherichia coli* to trimethoprim and minocycline was 100%, and the sensitivity rate to ertapenem, furantoin, and amikacin was above 90%. The resistance rate of *Pseudomonas aeruginosa* to all antibiotics, such as piperacillin and ciprofloxacin, was under 40%. The sensitivity rate of *Acinetobacter baumannii* to tigecycline and minocycline was less than 30%, and the resistance rate to many drugs such as piperacillin, ceftazidime, and imipenem was above 60%. Extended-spectrum β-lactamases (ESBLs)-producing *Klebsiella pneumoniae* (ESBLs-KPN) and carbapenem-resistant *Klebsiella pneumoniae* (CRE-KPN), ESBLs-producing *Escherichia coli* (ESBLs-ECO) and carbapenem-resistant *Escherichia coli* (CRE-ECO), multidrug-resistant *Acinetobacter baumannii* (MDR-AB), multidrug-resistant *Pseudomonas aeruginosa* (MDR-PAE), and methicillin-resistant *Staphylococcus aureus* (MRSA) are all important multidrug-resistant bacteria found in our hospital. The resistance rate of ESBLs-producing *Enterobacteriaceae* to ceftriaxone and amcarcillin-sulbactam was above 95%. CRE *Enterobacteriaceae* bacteria showed the highest resistance to amcarcillin-sulbactam (97.1%), and the resistance rates of MDR-AB to cefotaxime, cefepime, and aztreonam were 100%. The resistance rates of MDR-PAE to ceftazidime, imipenem, and levofloxacin were 100%, and the sensitivity rate to polymyxin B was above 98%. The resistance rate of MRSA to oxacillin was 100%, and the sensitivity rate to linezolid and vancomycin was 100%. *Conclusion*. The distribution of pathogenic bacteria in different hospital departments and sample sources was markedly different. Therefore, targeted prevention and control of key pathogenic bacteria in different hospital departments is necessary, and understanding both drug resistance and multiple drug resistance of the main pathogenic bacteria may provide guidance for the rational use of antibiotics in the clinic.

1. Introduction

Due to the complexity and universality of infectious diseases, antibacterial agents have been widely used in clinical practice. Since the application of antibacterial agents in clinical practice, they have saved the lives of countless patients. However, bacterial resistance caused by overuse not only has a negative impact on individual users but also on the social group as a whole. Globally, various institutes and agencies have recognized this serious public health issue.

Antibiotics are a subset of antimicrobial agents that play a key role in the inhibition of essential bacterial functions and are used widely to treat and prevent bacterial infections in humans and other animals [1]. Treatment by antibiotics is one of the main approaches used by modern medicine to combat infectious diseases [2]. Antibiotics have not only saved countless lives but also have played a pivotal role in achieving significant advances in medicine and surgery and have successfully prevented or treated infections that occur in patients [3]. However, antibiotic resistance has emerged because of their overuse and inappropriate prescribing, as well as their extensive use in agriculture [4]. A minimum of 700,000 people die from antimicrobial-resistant infections each year around the world, and drug-resistant infections are expected to kill 10 million people a year within 30 years, greatly exceeding deaths from cancer. It has also been estimated that this resistance problem will be the biggest challenge facing healthcare systems by 2050 [1]. The rapid and sustained spread of antibiotic resistance poses a growing threat to the public, animal, and environmental health worldwide. The abuse of antibiotics in clinical practice, poor public health conditions, and insufficient public awareness are the main causes cited [5].

Multidrug resistance (MDR) relates to bacteria becoming resistant to multiple classes of antibiotics and [6, 7] is now classified as follows: multidrug resistance (MDR) that is not susceptible to at least one representative from each of the three categories of selected antimicrobial compound families [7]. Extreme drug resistance (XDR) is not susceptible to at least a single representative of all but very few categories of antimicrobial compounds. Pan-drug resistance (PDR) is not susceptible to any of the tested representatives of all known antimicrobial compound families [7]. Compared with other infections, MDR infections are associated with poorer clinical outcomes, resulting in increased morbidity and mortality rates and higher healthcare costs [8]. There is concern that the emergence of pan-resistant strains (pathogens resistant to all available antibiotics) will render some infections untreatable. How to effectively slow down the emergence of multidrug-resistant bacteria and block the spread of multidrug-resistant bacteria has attracted extensive attention from the medical community, government, and society.

In this study, the isolation, culture, and identification of pathogenic microorganisms and antimicrobial sensitivity tests were carried out, the detection results for different pathogenic microorganisms were provided, and the changes to and the mechanism of drug resistance were analyzed. This study provides a theoretical basis for exploring the clinical application of antibacterial drugs and further monitoring bacterial resistance and multidrug-resistant bacteria.

2. Samples and Methods

2.1. Source of Pathogenic Samples. Pathogen samples, including sputum, mid-section urine, blood, wound secretions, chest and gastric juices, bile, and puncture fluids, were taken from hospitalized patients from 2017 to 2019. To avoid overestimating antibiotic resistance, duplicate strains obtained from the same patient were deleted from the study. The study protocol was approved by the Ethics Committee of our hospital and given that medical records and patient information were anonymously reviewed and collected in this observational study, informed consent was not needed.

In 2017, the total number of microbial culture samples submitted for inspection was 43,981, and the top five infection sites were the lower respiratory tract (271/28.65%), urinary tract (125/13.21%), upper respiratory tract (107/11.31%), eyes, ears, and oral cavities (67/7.08%), and blood (64/6.77%). Respiratory tract infection, however, has always represented the main site of infection.

In 2018, the total number of microbial culture samples submitted for inspection was 42,923, a slight decrease from last year. The respiratory tract, urine, blood, stool, and female reproductive tract samples ranked in the top five, of which the respiratory tract samples, urine specimens, and blood specimens accounted for 43.93%, 12.35%, and 9.98% of the total, respectively. Stool specimens accounted for 6.73%, and female reproductive tract specimens accounted for 6.12%, a significant increase from last year by 4% and were related to *Streptococcus agalactiae* screening in obstetrics and gynecology.

The total number of microbial culture specimens submitted for inspection in 2019 was 46,341, also representing an increase from last year. The lower respiratory tract, urine, and blood specimens ranked in the top three, accounting for 39.6%, 11.0%, and 8.8% of the total, respectively, and the female reproductive tract specimens accounted for 6.7%, an increase of 6.12% from 2018. The main reason is related to *Streptococcus agalactiae* screening in the obstetrics and gynecology department, and stool specimens accounted for 6.5% and were related to the decline in the number of intestinal outpatients in recent years.

2.2. Strain Isolation, Strain Identification, and Antimicrobial Susceptibility Testing. We isolated and identified bacteria using standard microbiological and biochemical methods. According to the clinical operation requirements of the National Clinical Inspection Operation Regulations (3rd Edition), various specimens were cultured and bacterial identification was performed using a Vitek 2 Company instrument and supporting identification cards with microbiological tubes. Extended-spectrum β-lactamases (ESBLs)-producing *Klebsiella pneumoniae* (ESBLs-KPN), ESBLs-producing *Escherichia coli* (ESBLs-ECO), carbapenem-resistant (CRE) *Klebsiella pneumoniae* (CRE-KPN), CRE *Escherichia coli* (CRE-ECO), multidrug-resistant *Acinetobacter baumannii* (MDR-AB), multidrug-resistant *Pseudomonas aeruginosa* (MDR-PAE), and methicillin-resistant *Staphylococcus aureus* (MRSA) were defined based on their resistance to all antimicrobial agents as reported previously [6].

In addition, instrument drug sensitivity cards and Kirby–Bauer agar diffusion methods were used to define antibiotic resistance. The results were interpreted according to the minimum inhibitory concentration (MIC) interpretive breakpoints recommended by the Clinical and Laboratory

Table 1: The top 15 isolated pathogens in the three districts of the hospital in 2017, 2018, and 2019.

Year	2017			2018			2019		
Rankings	Bacteria	Number	Proportion	Bacteria	Number	Proportion	Bacteria	Number	Proportion (%)
1	*Escherichia coli*	456	0.131	*Escherichia coli*	497	0.133	*Escherichia coli*	465	0.121
2	*Staphylococcus aureus*	384	0.11	*Klebsiella pneumoniae*	462	0.123	*Staphylococcus aureus*	410	0.107
3	*Pseudomonas aeruginosa*	370	0.106	*Staphylococcus aureus*	420	0.112	*Pseudomonas aeruginosa*	409	0.107
4	*Klebsiella pneumoniae*	356	0.102	*Pseudomonas aeruginosa*	406	0.108	*Klebsiella pneumoniae*	382	0.1
5	*Acinetobacter baumannii*	212	0.061	*Acinetobacter baumannii*	219	0.058	*Acinetobacter baumannii*	282	0.073
6	*Enterococcus faecalis*	156	0.045	*Staphylococcus epidermidis*	176	0.047	*Staphylococcus epidermidis*	251	0.065
7	*Vibrio parahaemolyticus*	135	0.039	*Enterococcus faecalis*	147	0.039	*Enterococcus faecium*	149	0.039
8	*Staphylococcus epidermidis*	129	0.037	*Enterococcus faecium*	120	0.032	*Stenostomonas maltophilia*	129	0.034
9	*Stenostomonas maltophilia*	103	0.03	*Streptococcus agalactiae*	116	0.031	*Streptococcus agalactiae*	123	0.032
10	*Streptococcus agalactiae*	99	0.028	*Enterobacter cloacae*	113	0.03	*Enterococcus faecalis*	122	0.032
11	*Enterobacter cloacae*	92	0.026	*Stenostomonas maltophilia*	87	0.023	*Enterobacter cloacae*	101	0.026
12	*Enterococcus faecium*	92	0.026	*Corynebacterium striatum*	84	0.022	*Haemophilus influenzae*	69	0.018
13	*Corynebacterium striatum*	68	0.02	*Streptococcus pneumoniae*	68	0.018	*Corynebacterium striatum*	68	0.018
14	*Streptococcus pneumoniae*	59	0.017	*Vibrio parahaemolyticus*	60	0.016	*Streptococcus pneumoniae*	64	0.017
15	*Proteus mirabilis*	58	0.017	*Proteus mirabilis*	52	0.014	*Streptococcus astragali*	53	0.014
	Other bacteria	714	0.205	Other bacteria	723	0.193	Other bacteria	762	0.198
	Total	3483	1	Total	3750	1	Total	3839	1

Standards Institute (CLSI) of 2016. The quality-control strains were *Escherichia coli* ATCC 25922, *Pseudomonas aeruginosa* ATCC 27853, *Klebsiella pneumoniae* ATCC 700603, *Acinetobacter baumannii* ATCC 19606, *Staphylococcus aureus* ATCC 25923, *Staphylococcus epidermidis* ATCC 13518, and *Enterococcus faecium* ATCC 29212.

2.3. Monitoring and Analysis of Multidrug-Resistant Bacteria. Our hospital microbiology laboratory uses special statistical software MDR for drug resistance analysis to conduct multidrug resistance analysis on the main pathogenic bacteria (*Enterobacteriaceae, Acinetobacter baumannii, Pseudomonas aeruginosa*, and *Staphylococcus aureus*). An interim standard definition of MDR, XDR, and PDR terms coauthored by experts from the United States, Israel, Greece, Switzerland, and Australia [6] was used to identify the drug resistance of the samples.

2.4. Statistical Analyses. Data from our study were analyzed with SPSS (version 22.0, IBM Corp., Armonk, NY) and Microsoft Excel software 2007 (Microsoft Corporation, Redmond, WA). Proportions were used to summarize categorical data as appropriate.

3. Results

3.1. Isolation of Pathogenic Bacteria. According to the results from the pathogen bacteria isolation from the three hospital departments from 2017 to 2019 (Table 1), the top five pathogenic bacteria in three years were always *Escherichia coli* (12.8%), *Staphylococcus aureus* (11%), *Klebsiella pneumoniae* (10.8%), *Pseudomonas aeruginosa* (10.7%), and *Acinetobacter baumannii* (6.4%), which were relatively concentrated, and accounted for 51%, 53.4%, and 50.7% of the total cases each year. The average share of *Enterococcus faecalis* and *Enterococcus faecium* was 7.1% within three years.

From 2017 to 2019, the results of pathogenic bacterial isolation in the central intensive care unit (central ICU), respiratory intensive care unit (RICU), and emergency intensive care unit (EICU) were surveyed. Within the three ICU departments, *Escherichia coli*, *Staphylococcus aureus*, *Klebsiella pneumoniae*, *Pseudomonas aeruginosa,* and *Acinetobacter baumannii* were always in the top eight within the three years. In central ICU, *Pseudomonas aeruginosa* was ranked first over three years and had the highest proportion between 15.4% and 17.3%, followed by *Klebsiella pneumoniae* (36/13.7%), and both showed an upward trend from

Table 2: Isolation of pathogenic bacteria in central intensive care units (central ICUs) in 2017, 2018, and 2019 years.

2017			2018			2019		
Bacteria	Number	Proportion	Bacteria	Number	Proportion	Bacteria	Number	Proportion
Pseudomonas aeruginosa	40	0.154	*Pseudomonas aeruginosa*	48	0.160	*Pseudomonas aeruginosa*	39	0.173
Klebsiella pneumoniae	32	0.123	*Klebsiella pneumoniae*	41	0.137	*Klebsiella pneumoniae*	34	0.150
Acinetobacter baumannii	26	0.100	*Escherichia coli*	29	0.097	*Acinetobacter baumannii*	25	0.111
Burkholderia cepacia	19	0.073	*Acinetobacter baumannii*	22	0.073	*Staphylococcus aureus*	19	0.084
Staphylococcus aureus	16	0.062	*Enterococcus faecium*	17	0.057	*Burkholderia cepacia*	17	0.075
Escherichia coli	14	0.054	*Enterococcus faecalis*	16	0.053	*Stenostomonas maltophilia*	15	0.066
Enterococcus faecium	14	0.054	*Staphylococcus aureus*	15	0.050	*Enterococcus faecium*	15	0.066
Enterobacter cloacae	12	0.046	*Enterobacter cloacae*	14	0.047	*Escherichia coli*	12	0.053
Enterococcus faecalis	10	0.038	*Staphylococcus epidermidis*	14	0.047	*Enterobacter cloacae*	10	0.044
Staphylococcus epidermidis	8	0.031	*Burkholderia cepacia*	9	0.030	*Staphylococcus epidermidis*	8	0.035
Stenostomonas maltophilia	8	0.031	*Corynebacterium striatum*	9	0.030	*Streptococcus pneumoniae*	8	0.035
Corynebacterium striatum	8	0.031	*Stenostomonas maltophilia*	9	0.030	*Enterococcus faecalis*	8	0.035
Streptococcus pneumoniae	6	0.023	*Haemophilus influenzae*	7	0.023	*Corynebacterium striatum*	6	0.027
Klebsiella aerogenes	6	0.023	*Klebsiella aerogenes*	7	0.023	*Klebsiella aerogenes*	6	0.027
Other bacteria	41	0.158	Other bacteria	43	0.143	Other bacteria	4	0.018
Total	260	1.000	Total	300	1.000	Total	226	1.000

2017 to 2019. *Acinetobacter baumannii* (24 strains) and *Escherichia coli* (18 strains) came in third and fourth, with a proportion of 9.5% and 6.8%, respectively. *Staphylococcus aureus* (17/6.5%) and *Enterococcus faecium* (15/5.9%) also consistently ranked in the top eight for three years (Table 2). In RICUs, six pathogenic bacteria always ranked in the top eight. *Pseudomonas aeruginosa* (17/17.5%) had the largest average share over three years among the three ICU departments. The next was *Klebsiella pneumoniae* (14/14.8%), *Escherichia coli* (11/11%), *Acinetobacter baumannii* (7/7.7%), and *Staphylococcus aureus* (6/6.3%). In addition, *Stenotrophomonas maltophilia* (9 strains) accounted for 9.1%, and the average proportion was highest in the three ICU departments (Table 3). In EICUs, *Acinetobacter baumannii* (14/15.4%) had the highest average proportion from 2017 to 2019, followed by *Klebsiella pneumoniae* (14/14.7%), which ranked second for three consecutive years. *Pseudomonas aeruginosa* (13/13.7%), *Escherichia coli* (12/13.4%), *Enterococcus faecium* (8/8.1%), *Staphylococcus aureus* (7/7.1%), and *Corynebacterium striatum* (6/6.7%) are also consistently ranked in the top eight for three years and their average proportion was highest in the three ICU departments, respectively (Table 4).

3.2. Distribution of Isolated Strains from Blood, Urine, and Sputum Samples. The composition of isolates from different sources from 2017 to 2019 was analyzed, and the results are shown in Tables 5–7. From 2017 to 2019, the average proportion of *Escherichia coli* isolates (61/22.8%) in blood samples was the highest, showing a downward trend. At the same time, *Staphylococcus epidermidis* (48/18.1%) and *Klebsiella pneumoniae* (32/12%) occupied the second and third places in each of the three years. The mean proportion of *Staphylococcus epidermidis* in blood specimens was higher than that seen in urine within the three years, but it was not found in sputum specimens. The composition of blood samples in 2017 and 2019 ranked fourth and *Acinetobacter baumannii* accounted for about 6.7%, but *Staphylococcus hominis* ranked fourth in 2018, accounting for 7.5%, *Staphylococcus hominis* ranked fifth for the three years, accounting for 8.1%, and was unique to blood samples (Table 5).

It was found that *Escherichia coli* (39.7%), *Enterococcus faecium* (11.3%), *Enterococcus faecalis* (9.4%), and *Klebsiella pneumoniae* (9.1%) ranked in the top four pathogenic bacteria from urine sample isolates. The most predominant pathogen in the urine samples was *Escherichia coli* accounting for 42.2%, 39.3%, and 37.8% from 2017 to 2019. Within the three years, compared to the blood and sputum samples, *Escherichia coli* accounted for the highest proportion of the urine samples isolated strains. *Enterococcus faecium* and *Enterococcus faecalis* have a higher proportion in urine than in blood samples, and they were not present in samples (Table 6).

Pseudomonas aeruginosa (22.5%), *Klebsiella pneumoniae* (20.6%), and *Acinetobacter baumannii* (16.6%) were the top three in sputum sample isolated strains. *Staphylococcus*

Table 3: Isolation of pathogenic bacteria in respiratory intensive care units (RICUs) in 2017, 2018, and 2019.

2017			2018			2019		
Bacteria	Number	Proportion	Bacteria	Number	Proportion	Bacteria	Number	Proportion
Escherichia coli	18	0.176	*Pseudomonas aeruginosa*	22	0.204	*Pseudomonas aeruginosa*	14	0.184
Pseudomonas aeruginosa	14	0.137	*Klebsiella pneumoniae*	17	0.157	*Klebsiella pneumoniae*	12	0.158
Klebsiella pneumoniae	13	0.127	*Stenostomonas maltophilia*	11	0.102	*Stenostomonas maltophilia*	7	0.092
Stenostomonas maltophilia	8	0.078	*Corynebacterium striatum*	9	0.083	*Acinetobacter baumannii*	6	0.079
Acinetobacter baumannii	8	0.078	*Acinetobacter baumannii*	8	0.074	*Escherichia coli*	6	0.079
Staphylococcus aureus	7	0.069	*Burkholderia cepacia*	8	0.074	*Staphylococcus aureus*	5	0.066
Staphylococcus epidermidis	7	0.069	*Escherichia coli*	8	0.074	*Burkholderia cepacia*	4	0.053
Enterococcus faecalis	6	0.059	*Staphylococcus aureus*	6	0.056	*Morganella morganii*	3	0.039
Proteus mirabilis	4	0.039	*Proteus mirabilis*	4	0.037	*Staphylococcus epidermidis*	3	0.039
Enterobacter cloacae	3	0.029	*Enterobacter cloacae*	2	0.019	*Proteus mirabilis*	3	0.039
Streptococcus pneumoniae	2	0.020	*Enterococcus faecalis*	2	0.019	*Staphylococcus hominis*	2	0.026
Corynebacterium striatum	2	0.020	*Enterococcus faecium*	2	0.019	*Corynebacterium striatum*	2	0.026
Staphylococcus capitis	2	0.020	*Streptococcus pneumoniae*	2	0.019	*Enterobacter cloacae*	2	0.026
Enterococcus faecium	1	0.010	*Staphylococcus capitis*	1	0.009	*Enterococcus faecalis*	2	0.026
Other bacteria	7	0.069	Other bacteria	6	0.056	Other bacteria	5	0.066
Total	102	1.000	Total	108	1.000	Total	76	0.704

Table 4: Isolation of pathogenic bacteria in emergency intensive care units (EICUs) in 2017, 2018, and 2019.

2017			2018			2019		
Bacteria	Number	Proportion	Bacteria	Number	Proportion	Bacteria	Number	Proportion
Pseudomonas aeruginosa	15	0.140	*Acinetobacter baumannii*	19	0.200	*Escherichia coli*	13	0.163
Klebsiella pneumoniae	13	0.121	*Klebsiella pneumoniae*	16	0.168	*Klebsiella pneumoniae*	12	0.150
Acinetobacter baumannii	12	0.112	*Pseudomonas aeruginosa*	15	0.158	*Acinetobacter baumannii*	12	0.150
Escherichia coli	12	0.112	*Escherichia coli*	12	0.126	*Pseudomonas aeruginosa*	9	0.113
Enterococcus faecium	10	0.093	*Enterococcus faecium*	6	0.063	*Enterococcus faecium*	7	0.088
Staphylococcus aureus	8	0.075	*Staphylococcus aureus*	6	0.063	*Staphylococcus aureus*	6	0.075
Corynebacterium striatum	8	0.075	*Corynebacterium striatum*	5	0.053	*Corynebacterium striatum*	6	0.075
Stenostomonas maltophilia	8	0.075	*Stenostomonas maltophilia*	4	0.042	*Stenostomonas maltophilia*	4	0.050
Enterococcus faecalis	6	0.056	*Proteus mirabilis*	3	0.032	*Enterococcus faecalis*	4	0.050
Burkholderia cepacia	4	0.037	*Burkholderia cepacia*	2	0.021	*Staphylococcus epidermidis*	2	0.025
Proteus mirabilis	2	0.019	*Enterococcus faecalis*	2	0.021	*Proteus mirabilis*	2	0.025
Staphylococcus haemolyticus	1	0.009	*Staphylococcus haemolyticus*	1	0.011	*Staphylococcus haemolyticus*	1	0.013
Corynebacterium afermentans	1	0.009	*Corynebacterium urealyticum*	1	0.011	*Staphylococcus capitis*	1	0.013
Staphylococcus capitis	1	0.009	*Enterobacter avium*	1	0.011	*Saprophytic staphylococcus*	1	0.013
Other bacteria	6	0.056	Other bacteria	2	0.021	Other bacteria	0	0.000
Total	107	1.000	Total	95	1.000	Total	80	1.000

Table 5: Composition of blood specimen isolates in 2017, 2018, and 2019 years.

2017			2018			2019		
Bacteria	Number	Proportion	Bacteria	Number	Proportion	Bacteria	Number	Proportion
Escherichia coli	62	0.238	*Escherichia coli*	70	0.228	*Escherichia coli*	50	0.218
Staphylococcus epidermidis	45	0.173	*Staphylococcus epidermidis*	57	0.186	*Staphylococcus epidermidis*	42	0.183
Klebsiella pneumoniae	30	0.115	*Klebsiella pneumoniae*	42	0.137	*Klebsiella pneumoniae*	25	0.109
Acinetobacter baumannii	20	0.077	*Staphylococcus hominis*	23	0.075	*Acinetobacter baumannii*	13	0.057
Pseudomonas aeruginosa	12	0.046	*Staphylococcus aureus*	13	0.042	*Staphylococcus hominis*	11	0.048
Staphylococcus aureus	11	0.042	*Enterococcus faecalis*	12	0.039	*Enterococcus faecium*	10	0.044
Staphylococcus hominis	10	0.038	*Acinetobacter baumannii*	11	0.036	*Staphylococcus aureus*	9	0.039
Enterobacter cloacae	9	0.035	*Pseudomonas aeruginosa*	7	0.023	*Staphylococcus haemolyticus*	9	0.039
Enterococcus faecium	8	0.031	*Enterobacter cloacae*	6	0.020	*Pseudomonas aeruginosa*	7	0.031
Staphylococcus haemolyticus	4	0.015	*Enterococcus faecium*	4	0.013	*Burkholderia cepacia*	3	0.013
Other bacteria	49	0.188	Other bacteria	62	0.202	Other bacteria	50	0.218
Total	260	1.000	Total	307	1.000	Total	229	1.000

Table 6: Composition of urine specimen isolates in 2017, 2018, and 2019.

2017			2018			2019		
Bacteria	Number	Proportion	Bacteria	Number	Proportion	Bacteria	Number	Proportion
Escherichia coli	258	0.422	*Escherichia coli*	262	0.393	*Escherichia coli*	265	0.377
Klebsiella pneumoniae	75	0.123	*Enterococcus faecium*	69	0.103	*Enterococcus faecium*	86	0.123
Enterococcus faecium	70	0.114	*Enterococcus faecalis*	63	0.094	*Enterococcus faecalis*	59	0.084
Enterococcus faecalis	63	0.103	*Klebsiella pneumoniae*	51	0.076	*Klebsiella pneumoniae*	51	0.073
Pseudomonas aeruginosa	34	0.056	*Pseudomonas aeruginosa*	34	0.051	*Pseudomonas aeruginosa*	34	0.048
Staphylococcus epidermidis	22	0.036	*Staphylococcus epidermidis*	21	0.031	*Staphylococcus epidermidis*	28	0.040
Proteus mirabilis	17	0.028	*Proteus mirabilis*	18	0.027	*Streptococcus agalactiae*	18	0.026
Enterobacter cloacae	15	0.025	*Streptococcus agalactiae*	16	0.024	*Proteus mirabilis*	15	0.021
Streptococcus agalactiae	14	0.023	*Morganella morganii*	12	0.018	*Acinetobacter haemolyticus*	14	0.020
Acinetobacter haemolyticus	11	0.018	*Corynebacterium glutamicum*	11	0.016	*Enterobacter cloacae*	12	0.017
Other bacteria	33	0.054	Other bacteria	110	0.165	Other bacteria	120	0.171
Total	612	1.000	Total	667	1.000	Total	702	1.000

aureus (8.3%) and *Stenotrophomonas maltophilia* (6.1%) were also common in sputum specimens and ranked fourth and fifth. Moreover, *Stenotrophomonas maltophilia* is a pathogen specific to sputum samples, and its proportion was increasing from 5.2% to 7.7% during 2017 to 2019 (Table 7).

3.3. Antibiotic Resistance Analysis. Combining the isolation of the pathogenic bacteria from the three hospital departments from 2017 to 2019 and the distribution of isolated strains from blood, urine and sputum specimens, it can be seen that the bacteria that are susceptible and have a high titer in each specimen were mainly *Escherichia coli*, *Klebsiella pneumoniae*, *Pseudomonas aeruginosa*, *Staphylococcus aureus,* and *Acinetobacter baumannii* and their antibiotic resistance was found to be unchanged.

From 2017 to 2019, *Escherichia coli* was generally resistant to trimethoprim and minocycline, with a resistance rate of up to 100% and with high sensitivity to imipenem, amikacin, ertapenem, and other drugs (Table 8). The resistance rate of *Klebsiella pneumoniae* to trimethoprim, cefuroxime, piperacillin, piperacillin-sulbactam, and

Table 7: Composition of sputum specimen isolates in 2017, 2018, and 2019.

2017			2018			2019		
Bacteria	Number	Proportion	Bacteria	Number	Proportion	Bacteria	Number	Proportion
Pseudomonas aeruginosa	280	0.233	*Klebsiella pneumoniae*	286	0.224	*Pseudomonas aeruginosa*	295	0.220
Klebsiella pneumoniae	262	0.218	*Pseudomonas aeruginosa*	282	0.221	*Acinetobacter baumannii*	247	0.185
Acinetobacter baumannii	203	0.169	*Acinetobacter baumannii*	183	0.143	*Klebsiella pneumoniae*	234	0.175
Staphylococcus aureus	100	0.083	*Staphylococcus aureus*	110	0.086	*Staphylococcus aureus*	108	0.081
Escherichia coli	85	0.071	*Stenostomonas maltophilia*	71	0.056	*Stenostomonas maltophilia*	103	0.077
Stenostomonas maltophilia	62	0.052	*Escherichia coli*	60	0.047	*Escherichia coli*	59	0.044
Corynebacterium striatum	48	0.040	*Corynebacterium striatum*	50	0.039	*Enterobacter cloacae*	52	0.039
Enterobacter cloacae	41	0.034	*Enterobacter cloacae*	48	0.038	*Corynebacterium striatum*	42	0.031
Streptococcus pneumoniae	36	0.030	*Streptococcus pneumoniae*	33	0.026	*Haemophilus influenzae*	40	0.030
Burkholderia cepacia	29	0.024	*Burkholderia cepacia*	31	0.024	*Burkholderia cepacia*	30	0.022
Other bacteria	54	0.045	Other bacteria	123	0.096	Other bacteria	128	0.096
Total	1200	1.000	Total	1277	1.000	Total	1338	1.000

Table 8: Drug resistance rates of *Escherichia coli* from 2017 to 2019.

	2017		2018		2019	
Escherichia coli	Drugs	Drug resistance rate (%)	Drugs	Drug resistance rate (%)	Drugs	Drug resistance rate (%)
	Trimethoprim	100	Ampicillin-sulbactam	71.3	Ampicillin-sulbactam	76.8
	Minocycline	100	Ciprofloxacin	60.4	Cefuroxime	54.3
	Cefazolin	90.27	Levofloxacin	55.9	Ciprofloxacin	54.1
	Ampicillin	87.7	Ceftriaxone	55.2	Levofloxacin	49.9
	Ceftriaxone	78	Cotrimoxazole	49.5	Ceftriaxone	48.3
	Ciprofloxacin	78	Gentamicin	39.6	Cotrimoxazole	45.3
	Levofloxacin	73.2	Aztreonam	36.5	Gentamicin	34.9
	Ampicillin-sulbactam	65.9	Ceftazidime	26.4	Aztreonam	27.9
	Compound sulfadiazine	64	Cefepime	23.3	Ceftazidime	20.3
	Aztreonam	55.2	Tobramycin	14.3	Cefepime	17.4
	Piperacillin	50	Cefoperazone-sulbactam	7.9	Tobramycin	10.5
	Tobramycin	49.2	Fosfomycin	7	Fosfomycin	7.0
	Cefepime	36.4	Ertapenem	5.2	Cefoperazone-sulbactam	3.4
	Gentamicin	36.3	Piperacillin-tazobactam	4.6	Nitrofurantoin	2.5
	Cefotaxime	32.4	Imipenem	4	Piperacillin-tazobactam	2.4
	Ceftazidime	32	Nitrofurantoin	2.9	Amikacin	1.7
			Amikacin	1.4	Ertapenem	0.7
					Imipenem	0.6

ampicillin was higher than 90%. However, its resistance to cefoperazone-sulbactam, ertapenem, and amikacin was lower than 40% (Table 9). The resistance of *Pseudomonas aeruginosa* to most antibiotics such as piperacillin, ciprofloxacin, amikacin, and tobramycin was less than 30%, and resistance to polymyxin B was less than 5%, and even reached a sensitivity of 100% in 2018 and 2019 (Table 10). *Acinetobacter baumannii* had high sensitivity to tigecycline

Table 9: Drug resistance rates of *Klebsiella pneumoniae* from 2017 to 2019.

	2017		2018		2019	
	Drugs	Drug resistance rate (%)	Drugs	Drug resistance rate (%)	Drugs	Drug resistance rate (%)
Klebsiella pneumoniae	Trimethoprim	100	Ampicillin-sulbactam	71.7	Ampicillin-sulbactam	66.7
	Cefuroxime	100	Nitrofurantoin	34.8	Nitrofurantoin	33.9
	Piperacillin	100	Fosfomycin	34.1	Cotrimoxazole	29.6
	Piperacillin-sulbactam	100	Ceftriaxone	30	Aztreonam	26.7
	Ampicillin	96.3	Cotrimoxazole	27	Cotrimoxazole	23.8
	Cefazolin	81.7	Levofloxacin	25.6	Ciprofloxacin	22.2
	Nitrofurantoin	78.8	Aztreonam	25.2	Ceftazidime	20.9
	Fosfomycin	72.5	Ciprofloxacin	25.1	Levofloxacin	19.9
	Ampicillin-sulbactam	70.8	Ceftazidime	23.9	Gentamicin	18.9
	Ceftriaxone	65.7	Gentamicin	22.7	Cefepime	17.1
	Cefepime	53.5	Cefepime	22.2	Tobramycin	13.5
	Tobramycin	52.6	Tobramycin	19	Imipenem	11.8
	Aztreonam	51.3	Cefoperazone-sulbactam	18.9	Piperacillin-tazobactam	11.3
	Compound sulfadiazine	50.8	Imipenem	17.8	Cefoperazone-sulbactam	11.1
	Ceftazidime	50	Ertapenem	17.3	Ertapenem	8.8
	Cefotaxime	50	Piperacillin-tazobactam	17	Amikacin	6.0
	Ciprofloxacin	49.2	Amikacin	12.2	Tigecycline	0.0
	Cefoperazone	48.6				
	Levofloxacin	47.2				
	Gentamicin	46.1				
	Piperacillin-tazobactam	44.3				
	Imipenem	40.2				
	Cefoperazone-sulbactam	32.4				

Table 10: Drug resistance rates of *Pseudomonas aeruginosa* from 2017 to 2019.

	2017		2018		2019	
	Drugs	Drug resistance rate (%)	Drugs	Drug resistance rate (%)	Drugs	Drug resistance rate (%)
Pseudomonas aeruginosa	Aztreonam	37.2	Meropenem	22	Meropenem	18.4
	Cefepime	34	Aztreonam	18.8	Imipenem	15.8
	Imipenem	33.5	Levofloxacin	18.8	Levofloxacin	13.7
	Piperacillin	29.1	Cefepime	18.7	Aztreonam	13.4
	Meropenem	27.1	Imipenem	18.2	Gentamicin	12.2
	Gentamicin	25.2	Gentamicin	15.6	Cefepime	12.1
	Piperacillin-sulbactam	25.1	Ciprofloxacin	13.5	Piperacillin	11.6
	Ceftazidime	23.7	Piperacillin	12.8	Cefoperazone-sulbactam	9.2
	Levofloxacin	20	Ceftazidime	12.2	Ciprofloxacin	8.6
	Ciprofloxacin	18.4	Cefoperazone-sulbactam	11.1	Tobramycin	7.7
	Tobramycin	13.5	Tobramycin	9.9	Piperacillin-tazobactam	7.2
	Amikacin	10	Amikacin	9.2	Ceftazidime	6.8
	Polymyxin B	2.5	Piperacillin-tazobactam	8.6	Amikacin	3.5
			Polymyxin B	0	Polymyxin B	0.0

Table 11: Drug resistance rates of *Acinetobacter baumannii* from 2017 to 2019.

	2017		2018		2019	
	Drugs	Drug resistance rate (%)	Drugs	Drug resistance rate (%)	Drugs	Drug resistance rate (%)
Acinetobacter baumannii	Piperacillin	73.5	Piperacillin	63	Piperacillin	73.2
	Moxifloxacin	74.7	Moxifloxacin	63.8	Imipenem	72.2
	Cefepime	73.6	Cefepime	63.7	Piperacillin-tazobactam	71.2
	Piperacillin-tazobactam	74.6	Piperacillin-tazobactam	63.6	Cefepime	70.0
	Ceftazidime	73.9	Ceftazidime	63.6	Ceftazidime	69.8
	Imipenem	73.1	Imipenem	62.7	Gentamicin	69.6
	Levofloxacin	72.5	Levofloxacin	62.6	Ciprofloxacin	67.7
	Gentamicin	69.7	Gentamicin	60.6	Levofloxacin	61.5
	Amikacin	66.5	Amikacin	58.1	Tobramycin	55.4
	Tobramycin	65.3	Tobramycin	57.2	Amikacin	42.2
	Cefoperazone-sulbactam	37.3	Cefoperazone-sulbactam	32.9	Minocycline	27.3
	Minocycline	25.6	Minocycline	21.5	Tigecycline	0.0
	Tigecycline	0	Tigecycline	0		

Table 12: Drug resistance rates of *Staphylococcus aureus* from 2017 to 2019.

	2017		2018		2019	
	Drugs	Drug resistance rate (%)	Drugs	Drug resistance rate (%)	Drugs	Drug resistance rate (%)
Staphylococcus aureus	Penicillin	91.3	Penicillin	87.6	Penicillin	89.6
	Erythromycin	61.8	Erythromycin	59.8	Erythromycin	62.7
	Clindamycin	58.6	Clindamycin	57.1	Clindamycin	58.4
	Oxacillin	35.2	Oxacillin	32.3	Oxacillin	36.8
	Tetracycline	24.2	Tetracycline	23.2	Cotrimoxazole	24.1
	Cotrimoxazole	17.3	Cotrimoxazole	16.3	Tetracycline	18.3
	Ciprofloxacin	16.5	Ciprofloxacin	15	Ciprofloxacin	18.0
	Gentamicin	14.8	Gentamicin	14	Moxifloxacin	15.7
	Moxifloxacin	14	Moxifloxacin	13.3	Levofloxacin	14.2
	Levofloxacin	13	Levofloxacin	10	Gentamicin	14.1
	Rifampicin	3.5	Rifampicin	3.3	Rifampicin	3.7
	Nitrofurantoin	1.2	Nitrofurantoin	0.8	Nitrofurantoin	0.8
	Linezolid	0	Linezolid	0	Linezolid	0.0
	Vancomycin	0	Vancomycin	0	Vancomycin	0.0
	Teicoplanin	0	Teicoplanin	0	Teicoplanin	0.0
	Tigecycline	0	Tigecycline	0	Tigecycline	0.0

and minocycline of less than 30%, and the resistance rate to tigecycline was zero but was greater than 60% resistant to many drugs such as piperacillin, ceftazidime, gentamicin, and imipenem (Table 11). *Staphylococcus aureus* had the highest resistance rate to penicillin, at more than 80%, and the resistance rate to erythromycin was approximately 60%. However, no strains were resistant to antibiotics such as vancomycin, teicoplanin, tigecycline, and linezolid (Table 12).

3.4. Multidrug Resistance Analysis. Analysis of multiple drug resistance for the main pathogenic bacteria in our hospital in 2017 is shown in Figure 1. In 2017, a total of 1181 multidrug-resistant bacterial strains of *Enterobacteriacea*e were isolated, accounting for the largest proportion of the detected multidrug-resistant strains; of which 491 strains of multidrug-resistant organisms (MDRO) accounted for 41.6%, and no XDR and PDR strains were found (Figure 1(a)). ESBLs-KPN is highly resistant to amoxicillin and ceftriaxone, with resistance rates of 100% and 99.4%, respectively, and the sensitivity to ertapenem, imipenem, and piperacillin/tazobactam was above 95% (Table 13). The resistance rate of CRE-KPN to all drugs was above 50%, among which ampicillin, cefoperazone-sulbactam, ampicillin-sulbactam, ceftazidime, and ceftriaxone were all resistant by 100%. The resistance rates to nitrofurantoin, ciprofloxacin, levofloxacin, aztreonam, and cefepime were all greater than 95% (Table 14) and the resistance rates of ESBLs-producing *Escherichia coli* (ESBLs-ECO) to ampicillin and ceftriaxone were over 99%, and sensitivities to drugs such as amikacin,

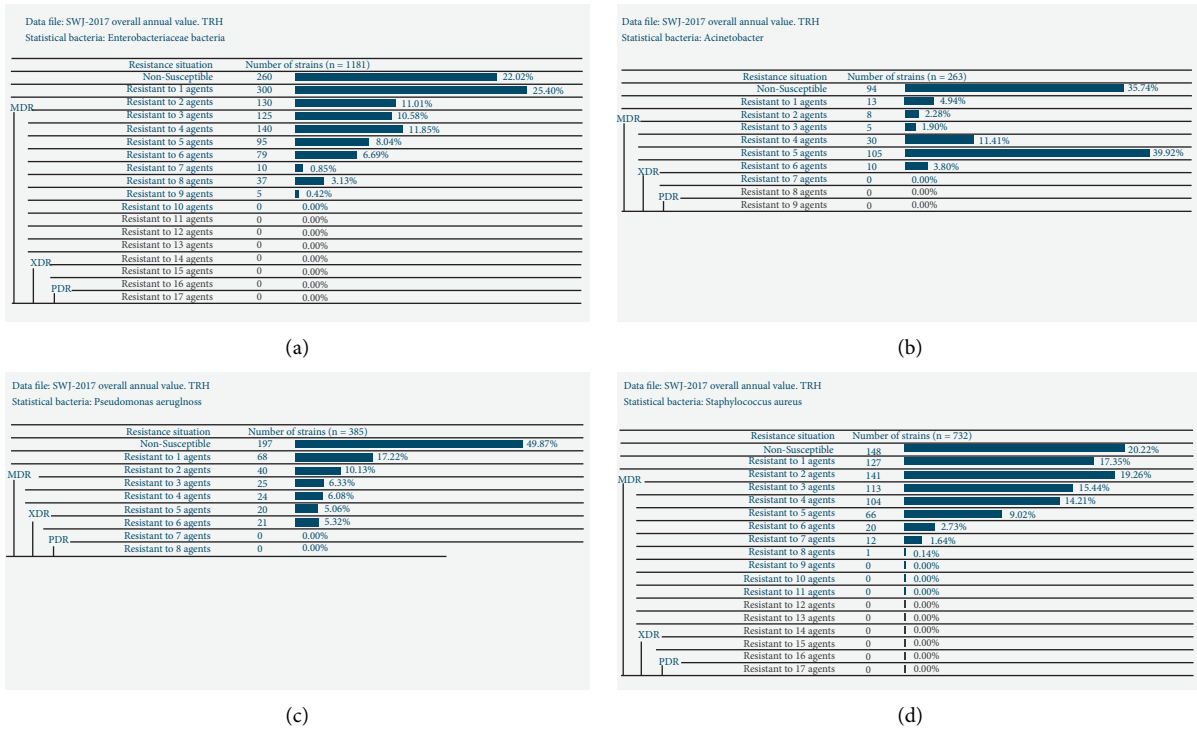

Figure 1: Analysis of multiple drug resistance for the main pathogenic bacteria in our hospital in 2017. (a) The analysis of multiple drug resistance of *Enterobacteriaceae* bacteria. (b) The analysis of multiple drug resistance of *Acinetobacter* bacteria. (c) The analysis of multiple drug resistance of *Pseudomonas aeruginosa*. (d) The analysis of multiple drug resistance of *Staphylococcus* bacteria.

Table 13: Analysis of multiple drug resistance rate of ESBLs-KPN in 2017.

	Drugs	Drug resistance rate (%)
ESBLs-KPN	Ertapenem	1.8
	Imipenem	2.8
	Piperacillin-tazobactam	8
	Amikacin	9.7
	Cefoperazone-sulbactam	21.7
	Tobramycin	27.8
	Gentamicin	40.9
	Fosfomycin	42.3
	Nitrofurantoin	48.3
	Levofloxacin	49.4
	Cefepime	50
	Ciprofloxacin	60.8
	Ceftazidime	63.1
	Aztreonam	73.9
	Cotrimoxazole	80.7
	Ampicillin-sulbactam	90.3
	Ceftriaxone	99.4
	Ampicillin	100

Table 14: Analysis of multiple drug resistance rates of CRE-KPN in 2017.

	Drugs	Drug resistance rate (%)
CRE-KPN	Cotrimoxazole	52.7
	Fosfomycin	60
	Amikacin	72.8
	Tobramycin	79
	Gentamicin	82.1
	Nitrofurantoin	96.3
	Ciprofloxacin	98.3
	Levofloxacin	98.3
	Aztreonam	98.6
	Cefepime	98.9
	Piperacillin-tazobactam	99.4
	Ampicillin	100
	Cefoperazone-sulbactam	100
	Ampicillin-sulbactam	100
	Ceftazidime	100
	Ceftriaxone	100
	Ertapenem	100
	Imipenem	100

nitrofurantoin, and cefepime were all greater than 60%, with no strains being resistant to ertapenem, piperacillin-tazobactam, or imipenem (Table 15). A total of 263 strains of *Acinetobacter* were isolated, including 150 strains of MDRO, accounting for 57%, and no XDR and PDR strains were found (Figure 1(b)). The resistance rate of MDR-*Acinetobacter baumannii* (MDR-AB) to levofloxacin, moxifloxacin, and ampicillin was up to 100%, and the drug resistance to cotrimoxazole, amikacin, and other drugs was also more than 70% (Table 16). Of the 395 strains of *Pseudomonas aeruginosa* isolated, 90 strains of MDRO accounted for 22.8%, and 21 strains of XDR accounted for 5.3%. No PDR strain was found (Figure 1(c)). MDR-*Pseudomonas aeruginosa* (MDR-PAE) showed more than 97% resistance to ciprofloxacin, piperacillin, and amtronam, among which the resistance rate for ceftazidime, imipenem, and levofloxacin

Table 15: Analysis of multiple drug resistance rate of ESBLs-ECO in 2017.

	Drugs	Drug resistance rate (%)
ESBLs-ECO	Ertapenem	0
	Piperacillin-tazobactam	0
	Imipenem	0
	ASmikacin	2.2
	Nitrofurantoin	3
	Cefoperazone-sulbactam	6.4
	Fosfomycin	12.3
	Tobramycin	17.5
	Cefepime	32.9
	Gentamicin	41.1
	Ceftazidime	43.4
	Cotrimoxazole	53.9
	Aztreonam	66.3
	Ampicillin-sulbactam	66.8
	Levofloxacin	71.6
	Ciprofloxacin	75.8
	Ampicillin	99.3
	Ceftriaxone	99.5

Table 16: Analysis of multiple drug resistance rate of MDR-AB in 2017.

	Drugs	Drug resistance rate (%)
MDR-AB	Cotrimoxazole	74.7
	Amikacin	78.1
	Tobramycin	81.1
	Gentamicin	82.2
	Minocycline	84.3
	Ampicillin	100
	Piperacillin	100
	Piperacillin-tazobactam	100
	Ceftazidime	100
	Ceftriaxone	100
	Cefotaxime	100
	Cefepime	100
	Aztreonam	100

Table 17: Analysis of multiple drug resistance rate of MDR-PAE in 2017.

	Drugs	Drug resistance rate (%)
MDR-PAE	Polymyxin B	1.3
	Tobramycin	19.4
	Amikacin	46.6
	Gentamicin	69.2
	Cefoperazone-sulbactam	81
	Piperacillin/tazobactam	93.3
	Ciprofloxacin	97.7
	Piperacillin	99.3
	Aztreonam	99.3
	Cefepime	99.7
	Ceftazidime	100
	Imipenem	100
	Levofloxacin	100

Table 18: Analysis of multiple drug resistance rate of MRSA in 2017.

	Drugs	Drugresistance rate (%)
MRSA	Linezolid	0
	Vancomycin	0
	Nitrofurantoin	4.5
	Cotrimoxazole	10
	Rifampicin	28.9
	Gentamicin	39.1
	Levofloxacin	46.9
	Moxifloxacin	48.6
	Ciprofloxacin	51.1
	Clindamycin	51.7
	Tetracycline	52.5
	Erythromycin	61.1
	Oxacillin	100

was 100%. While sensitivity to polymyxin B and tobramycin had a sensitivity of 98.7% (Table 17). A total of 732 strains of *Staphylococcus* were isolated, of which 316 were MDRO strains, accounting for 43.2%, and no XDR and PDR strains were found (Figure 1(d)). Methicillin-resistant *Staphylococcus aureus* (MRSA) was 100% resistant to benzacillin, 60% resistant to erythromycin, 50% resistant to ciprofloxacin, clindamycin, and tetracycline, but 100% sensitive to linezolid and vancomycin (Table 18).

In 2018, a total of 1293 strains of multidrug-resistant bacteria such as *Enterobacteriaceae* were isolated, of which MDRO (574 strains) accounted for 44.4%, while XDR and PDR strains were not found (Figure 2(a)). A total of 270 strains of *Acinetobacter* were isolated, including 145 strains of MDRO, accounting for 53.7%, and no XDR and PDR strains were found (Figure 2(b)). A total of 406 strains of *Pseudomonas aeruginosa* were isolated, among which 107 strains of MDRO accounted for 26.4%, while 26 strains of XDR accounted for 6.4%, and no PDR strains were found (Figure 2(c)). A total of 704 strains of *Staphylococcus* bacteria were isolated, including 300 strains (42.6%) of MDRO, with no XDR and PDR strains being found (Figure 2(d)). The resistance rates of MRSA to benzacillin and penicillin were 100% and 99.2%, respectively. No strains were found to be resistant to linezolid, vancomycin, teicoplanin, and tigecycline (Table 19).

As shown in Figure 3(a), in 2019, a total of 1166 strains of *Enterobacteriaceae* were isolated, of which 484 strains were isolated by MDR, accounting for 41.5%, and no XDR and PDR strains were found. The high resistance of ESBLs-producing *Enterobacteriaceae* to ceftriaxone and amcarcillin-sulbactam was observed, both more than 95%. Its drug resistance to cephalosporin, tobramycin, and furantoin was less than 40%, among which the drug resistance rate for tigecycline, imipenem, and amikacin was less than 5% (Table 20). Carbapenem-resistant (CRE) *Enterobacteriaceae* bacteria showed the highest resistance to amcarcillin-sulbactam (97.1%), and the resistance rate to most drugs ranged from 70% to 90%, but they were sensitive to tigecycline and amikacin (Table 21). A total of 325 strains of *Acinetobacter* were isolated, of which 213 strains were isolated from MDR, accounting for 65.5%, and no XDR and PDR strains were

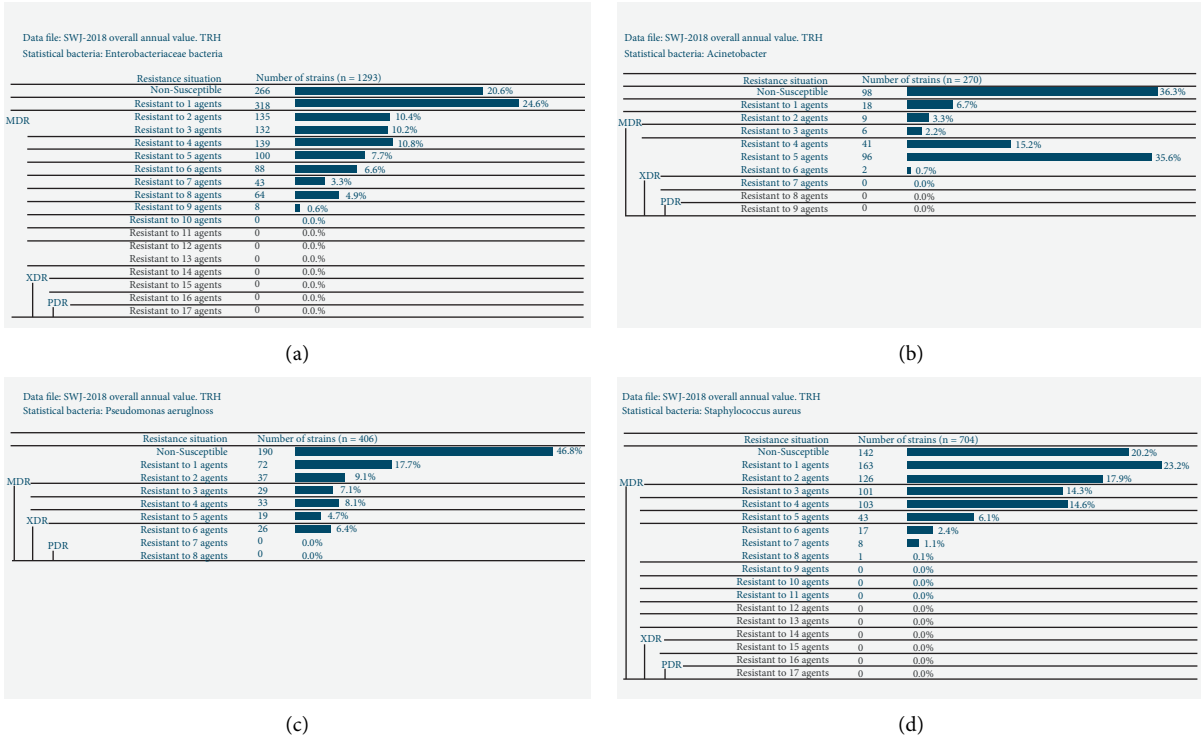

Figure 2: Analysis of multiple drug resistance for the main pathogenic bacteria in our hospital in 2018. (a) The analysis of multiple drug resistance of *Enterobacteriaceae* bacteria. (b) The analysis of multiple drug resistance of *Acinetobacter* bacteria. (c) The analysis of multiple drug resistance of *Pseudomonas aeruginosa*. (d) The analysis of multiple drug resistance of *Staphylococcus* bacteria.

Table 19: Analysis of multiple drug resistance rate of MRSA in 2018.

	Drugs	Drug resistance rate (%)
MRSA	Penicillin	100
	Oxacillin	100
	Erythromycin	74.3
	Clindamycin	69.1
	Tetracycline	38.4
	Ciprofloxacin	31.8
	Moxifloxacin	30.3
	Levofloxacin	28.3
	Cotrimoxazole	23.8
	Gentamicin	20.5
	Rifampicin	9.9
	Nitrofurantoin	1.3
	Linezolid	0
	Vancomycin	0
	Teicoplanin	0
	Tigecycline	0

found (Figure 3(b)). A total of 409 strains of *Pseudomonas aeruginosa* were isolated, of which 86 strains were isolated by MDR, accounting for 21.0%, and 23 strains were isolated by XDR, accounting for 5.6%, with no PDR strain being found (Figure 3(c)). A total of 768 strains of *Staphylococcus* were isolated, of which 356 strains were isolated by MDRO, accounting for 46.4%, and no XDR and PDR strains were found (Figure 3(d)). Similar to 2018, MRSA showed 100% resistance to penicillin and benzacillin, and the sensitivity to tetracycline, ciprofloxacin, and other drugs was more than 60%, and no strains resistant to linezolid, vancomycin, and other four drugs were found (Table 22).

3.5. The Trend of Isolate Major Multidrug-Resistant Bacteria in Our Hospital in the Past Four Years. As shown in Figure 4, the isolation rate of MDR-AB, which remained at the top for three years, declined in 2018 but increased again in 2019. ESBLs-ranked second in the three-year average separation rate, while MDR-PAB showed a continuous downward trend, whereas MRSA was the opposite, with a continuous increase being observed and CRE also exhibited a rise.

4. Discussion

The discovery of antibiotics in the last century is considered one of the most important achievements in the history of medicine, and its use has greatly reduced morbidity and mortality associated with bacterial infections [2]. However, the evolution of new bacterial strains, as well as the excessive use and reckless consumption of antibiotics, has led to the development of antibiotic resistance. Multidrug resistance is a potential threat worldwide and is escalating at an extremely high rate [9]. Poor public health conditions, lack of awareness concerning drug-resistant bacteria among the public, high incidences of disease, ease of access, and their misuse are the major factors exacerbating the problem [5]. In the context of antibiotic resistance, due to the emergence and increased prevalence of multidrug-resistant (MDR) superbugs such as *Staphylococcus aureus*, *Escherichia coli*,

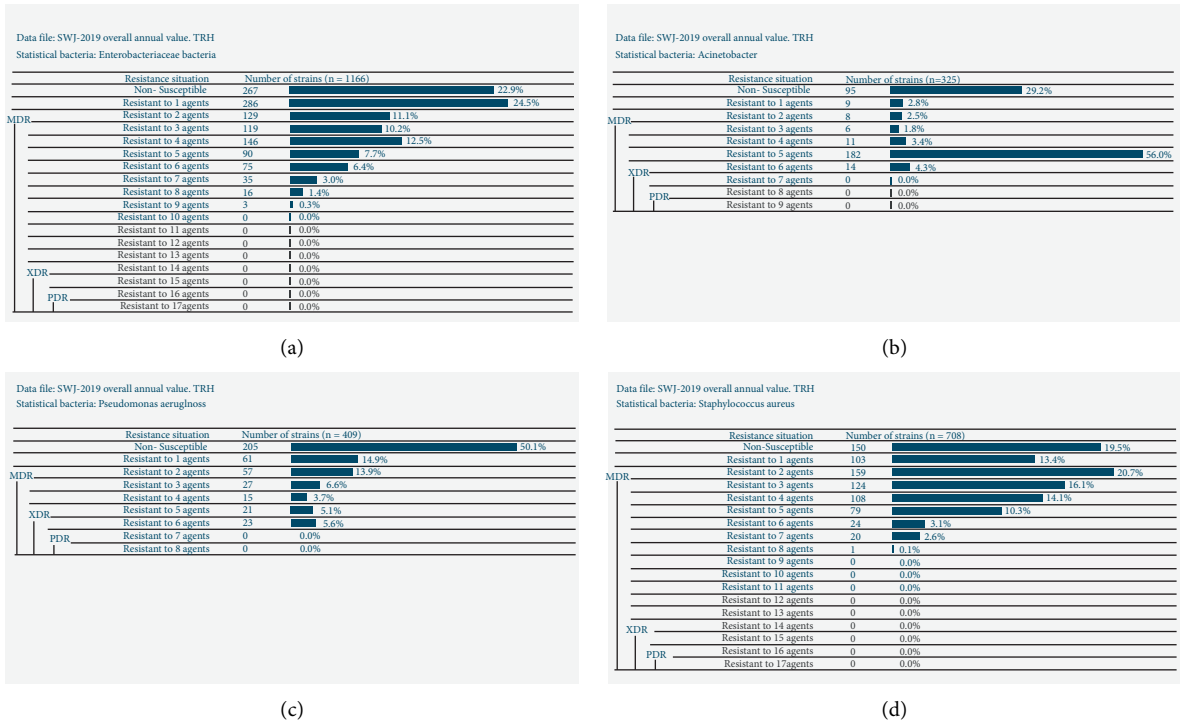

Figure 3: Analysis of multiple drug resistance for the main pathogenic bacteria in our hospital in 2019. (a) The analysis of multiple drug resistance of *Enterobacteriaceae* bacteria. (b) The analysis of multiple drug resistance of *Acinetobacter* bacteria. (c) The analysis of multiple drug resistance of *Pseudomonas aeruginosa*. (d) The analysis of multiple drug resistance of *Staphylococcus* bacteria.

Table 20: Analysis of multiple drug resistance rate of ESBLs in 2019.

	Drugs	Drug resistance rate (%)
ESBLs	Ceftriaxone	96.7
	Ampicillin-sulbactam	96.5
	Ciprofloxacin	67.2
	Aztreonam	64.7
	Levofloxacin	61.3
	Cotrimoxazole	56.2
	Ceftazidime	44.0
	Gentamicin	43.1
	Cefepime	36.2
	Tobramycin	21.5
	Nitrofurantoin	14.2
	Fosfomycin	13.6
	Cefoperazone-sulbactam	8.2
	Piperacillin-tazobactam	4.0
	Ertapenem	3.0
	Amikacin	2.7
	Imipenem	1.0

Table 21: Analysis of multiple drug resistance rate of CREs in 2019.

	Drugs	Drug resistance rate (%)
CREs	Ampicillin-sulbactam	97.1
	Imipenem	88.9
	Ceftriaxone	84.9
	Ertapenem	83.6
	Ceftazidime	82.7
	Nitrofurantoin	79.4
	Ciprofloxacin	78.9
	Aztreonam	77.3
	Levofloxacin	76.8
	Cefepime	75.8
	Piperacillin-tazobactam	74.5
	Cefoperazone-sulbactam	70.4
	Gentamicin	53.5
	Tobramycin	50.0
	Cotrimoxazole	43.3
	Amikacin	31.6
	Tigecycline	0.0

and *Klebsiella pneumoniae*, human health is being treated as a priority for the health of interdependent animals and related environments and is estimated to impose a significant health burden on the global population [10]. Therefore, we identified the clinical isolates obtained in the hospital from 2017 to 2019, carried out drug susceptibility tests and epidemiological infection analysis, obtained information about the pathogens for the whole hospital, and conducted a summary analysis, hoping to promote the rational use of antibiotics and play an active role in reducing the emergence of resistant bacteria in hospitals and controlling the spread of multidrug-resistant strains.

From 2017 to 2019, the isolation of pathogenic bacteria in the three departments of the hospital showed that the top five pathogens remained unchanged. These included *Escherichia coli*, *Staphylococcus aureus*, *Pseudomonas aeruginosa*, *Klebsiella pneumoniae,* and *Acinetobacter baumannii*, which, together with *Enterobacter faecium* as the

Table 22: Analysis of multiple drug resistance rate of MRSA in 2019.

	Drugs	Drug resistance rate (%)
MRSA	Oxacillin	100
	Penicillin	99.2
	Erythromycin	79.5
	Clindamycin	76.5
	Tetracycline	51.6
	Ciprofloxacin	31.5
	Moxifloxacin	29.5
	Levofloxacin	28.2
	Gentamicin	20.3
	Rifampicin	10.6
	Cotrimoxazole	6.1
	Nitrofurantoin	2.3
	Linezolid	0
	Vancomycin	0
	Teicoplanin	0
	Tigecycline	0

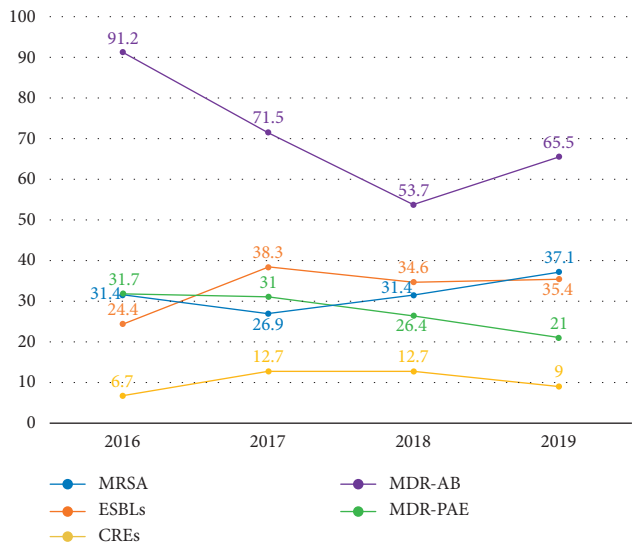

Figure 4: The trend of separation rate (%) of main multidrug-resistant strains in our hospital in recent four years.

most problematic clinical pathogens, were summarized as "ESKAPE" bugs by Louis Rice [11]. ESKAPEE pathogens have developed resistance mechanisms against most antibiotic treatments, including those that are the last line of defense, such as carbapenems and polymyxins [12]. According to the results of pathogen isolation in three ICU departments in the past three years, the five pathogens mentioned above always ranked among the top eight. The total number of isolates from central ICUs was always higher than that from specialized ICUs, namely RICUs and ICUs. The isolation rates of *Pseudomonas aeruginosa*, *Klebsiella pneumoniae,* and *Stenotrophomonas maltophilia* in the RICUs were the highest among the three ICU wards because they were all closely associated with lower respiratory tract infections [13]. In the last three years, the average proportion of *Pseudomonas aeruginosa* isolates was 17.5% in RICUs, similar to studies in the United States during the early years that found *P. aeruginosa* (17.0%) as a relatively common organism isolated in RICU with respiratory infections [14]. In EICUs, *Acinetobacter baumannii* occupies the highest isolation rate among the three ICU wards, and critically ill patients tend to be more susceptible to infection. Because *Acinetobacter baumannii* infection is associated with invasive surgery, the reason for hospitalization includes host factors, length of ICU stay, and prior use of broad-spectrum antibiotics [15].

The composition of isolates from different sources from 2017 to 2019 was analyzed, and we found that the isolation rate of *Staphylococcus epidermidis* was higher in blood samples than in urine samples, but no isolates were found in sputum samples. *Staphylococcus hominis* isolates were only present in blood samples, and as previously reported, these two bacteria both produce biofilms that allow them to adhere to internal medical devices and are commonly isolated from bloodstream infections [16, 17]. Among the three sources, blood, urine, and sputum, *Escherichia coli* isolates accounted for the highest proportion in urine specimens. *Enterococcus faecium* and *Enterococcus faecalis* were distributed at higher levels in urine samples than in blood samples and were absent in sputum samples. As previously reported, the above three bacteria are the main pathogenic bacteria of urinary tract infections [18, 19]. The top five frequent isolates from sputum samples are *Pseudomonas aeruginosa*, *Klebsiella pneumoniae*, *Acinetobacter baumannii*, *Staphylococcus aureus,* and *Stenotrophomonas maltophilia*, and this is similar to previous findings [13].

Measures for the management and clinical application of antibiotics in China are as follows: according to the notice of the Health and Family Planning Commission of the People's Republic of China on further strengthening the management of the clinical application of antibacterial drugs to effectively curb bacterial resistance, medical institutions should carry out monitoring of bacterial resistance, establish bacterial resistance early warning mechanisms, and take the following corresponding measures: (1) If the antimicrobial drug resistance rate of the main target bacteria exceeds 30%, warning information should be reported to the medical staff of the institution in a timely manner; (2) Antibiotics with a resistance rate of more than 40% for the major target bacteria should be used cautiously and empirically; (3) Antibiotics with drug resistance rates of over 50% for the major target bacteria should be selected according to drug sensitivity test results; (4) Clinical application of antibacterial drugs with drug resistance rates exceeding 75% for the main target bacteria should be suspended, and clinical application should be decided according to results based on bacterial resistance.

Regarding antibiotic resistance, *Escherichia coli* showed low resistance to most third-generation cephalosporins and aminoglycoside antibiotics, the resistance rate is between 30% and 50%, which is similar to the study conducted by Miller et al. [20]. It is highly sensitive to imipenem, nitrofurantoin, piperacillin-tazobactam, and amikacin and is recommended for clinical use. *Klebsiella pneumoniae*, also belonging to the *Enterobacteriaceae* family, exhibited low

resistance to imipenem and cefoperazone-sulbactam. Similar antibiotic resistance rates have been reported by Liu et al. [21]. In 2018-2019, its resistance rate to amikacin, piperacillin-tazobactam, ertapenem, and other antibacterial drugs was less than 20%, indicating a wide range of drug choices that can be used as a good choice for current clinical treatment. *Pseudomonas aeruginosa* showed low to moderate rates of drug resistance to commonly used anti-pseudomonal drugs and most antibiotics such as carbapenems, amikacin, cefoperazone-sulbactam, piperacillin-tazobactam, and ceftazidime, were less than 30%, similar to the results of previous studies [22]. Thus, there are many options for medication. Especially in 2018 and 2019, no strains resistant to polymyxin B were found, and therefore, it is the recommended drug for clinical treatment. The drug resistance of *Acinetobacter baumannii* is relatively serious, and the resistance rate to most antibiotics is greater than 60%. Therefore, carbapenems are not recommended for single *Acinetobacter baumannii* infections, which can easily increase the risk of multidrug resistance. *Acinetobacter baumannii* has relatively high sensitivity to cefoperazone-sulbactam, which is the first choice for empirical medication in confirmed cases of infection to improve the curative effect. *Staphylococcus aureus* is resistant to penicillin by more than 85%, so the clinical application for these target bacteria should be suspended. No resistant strains were found to linezolid, vancomycin, teicoranin, and tigecycline. Hence they represent a good choice for empirical treatment.

From 2017 to 2019, the important multidrug-resistant bacteria in our hospital included extended-spectrum β-lactamases (ESBLs)-producing *Klebsiella pneumoniae* (ESBLs-KPN) and carbapenem-resistant *Klebsiella pneumoniae* (CRE-KPN), ESBLs-producing *Escherichia coli* (ESBLs-ECO) and carbapenem-resistant *Escherichia coli* (CRE-ECO), multidrug-resistant *Acinetobacter baumannii* (MDR-AB), multidrug-resistant *Pseudomonas aeruginosa* (MDR-PAE), and methicillin-resistant *Staphylococcus aureus* (MRSA), which were mainly detected by Chinese Antimicrobial Resistance Surveillance System.

Acinetobacter baumannii, Enterobacteriaceae, and *Pseudomonas aeruginosa* are the common clinical carbapenem-resistant Gram-negative bacteria. Several drugs that are active against carbapenem-resistant *Acinetobacter baumannii* have been approved for clinical use or have entered late-stage clinical development, including eravacycline, cefiderocol, and plazomicin [23]. For MDR-AB, carbapenems are not recommended for empirical use, not only because of their high resistance rate, but more importantly, they further increase the risk of multidrug resistance caused by high intensity antimicrobial use. For pan-resistant *Acinetobacter baumannii*, some clinical departments have chosen tigecycline for treatment, but CLSI (American Institute of Clinical and Laboratory Standards) lacks the criteria for determining the susceptibility of *Acinetobacter baumannii* to tigecycline, and its efficacy remains to be validated.

The detection rate of multidrug-resistant bacteria in the *Enterobacteriaceae* family was the highest and was mainly concentrated on the detection of ESBLs-ECO, ESBLs-KPN, CRE-KPN, and CRE-ECO. The number of ESBLs-KPN and CRE-KPN isolates ranked first in 2017, followed by MDR-AB, and these results are in agreement with those obtained by Talaat et al. [24], who showed that the most predominant Gram-rods in the hospital were *Klebsiella pneumoniae* (28.7%) and Acinetobacter sp. (13.7%). ESBLs-producing isolates showed resistance to β-lactam antibiotics, including third-generation cephalosporins; in addition, they often exhibit resistance to other classes of drugs such as aminoglycosides, cotrimoxazole, and fluoroquinolones [25]. Tigecycline and imipenem can be used as empirical drugs for ESBL-producing bacteria. It should be emphasized that ESBLs-ECO and ESBLs-KPN have high drug resistance rates to ceftriaxone and amcarcillin-sulbactam, and the risk of induced drug resistance is also very high. Therefore, the drug sensitivity test results should be referred to for selection. The detection rate of CRE bacteria in 2019 was higher than the national average in 2018, and therefore, it is necessary to reduce the overuse of carbapenem antibiotics and prevent the spread of bacteria in hospitals and regions. The resistance rate of CRE bacteria to amcarcillin-sulbactam exceeded 95%, and their clinical use should be suspended. No strains sensitive to tigecycline have been found, and they can be used as clinically recommended drugs, usually in combination with other drugs. *Enterobacteriaceae* represents a key family of carbapenem-resistant bacteria. Colistin, tigecycline, ceftazidime-avibactam, plazomicin, eravacycline, and cefiderocol can all be used for their clinical treatment [23].

The average separation rate of MDR-PAE ranks third (31.7%), with no major fluctuations in recent years. It is also a common clinical carbapenem-resistant Gram-negative bacterium. Our results showed that MDR-PAE and XDR-PAE occupy 23.4% and 5.8% of the average proportion of *Pseudomonas aeruginosa* isolates, higher than the results from other studies. In 2015, the European Centers for Disease Prevention and Control stated that MDR-PAE and XDR-PAE isolates accounted for 13.7% and 5.5% [26]. The high prevalence of resistant species in developing countries could be due to noncompliance with infection control regulations and to the lack of or an imperfect antibiotic policy. Studies [26] have shown that multiple antibiotic combinations can be used as a clinical solution for MDR-PAE and XDR-PAE infections. Previous studies [27, 28] have reported that combinations of polymyxins with these anti-*pseudomonas* drugs (such as imipenem, piperacillin, aztreonam, ceftazidime, or ciprofloxacin) are more effective than polymyxins alone against MDR-PAE, providing a reference for the treatment of MDR-PAE infection. Yadav et al. [29] demonstrated substantially enhanced death *in vivo* against an MDR-PAE clinical isolate with an optimized imipenem-plus-tobramycin combination regimen, which was an alternative to colistin therapy, especially in patients with renal insufficiency. In addition, drugs such as cefiderocol and fosfomycin are potential treatment options in the near future [26]. The available clinical solution for MDR-PAE infections requires a precise diagnostic and combination antibiotic therapy based on diagnostics. Several infections which are recurrent need additional care to stop the proliferation of MDR-PAE contaminating the surrounding environment.

MRSA is a virulent and difficult-to-treat "superbug," and our results show that MRSA accounted for 30% to 50% of *Staphylococcus aureus* infections in hospital settings over the three-year period, which was slightly higher than the 25% to 50% reported in previous studies [30]. As previously reported [31], the infection rates of resistant *Staphylococcus*, *Pseudomonas*, *Acinetobacter*, and *Klebsiella* vary by country and region, with Asia being higher than North America and Western Europe. This may be due to the apparent wide variations in health care systems, ICU facilities, and policies for infectious disease control in the different geographical regions. Drug resistance, however, is consistent with previous research results, where MRSA is resistant to penicillin-like beta-lactam antibiotics [32], and the resistance to penicillin was observed to be as high as 99.2%, and clinical use of this target bacterium should be suspended. Many drugs remain active against MRSA, including glycopeptides (vancomycin and teicoranin), linezolid, and tigecycline, to which no resistant strains have been found and are, therefore, good choices for empirical treatment. Even some newer lactams, such as ceftazlorin and cefdipropanol, can be used as treatment options for MRSA [33].

With the promotion of rational applications for antibiotics, the isolation spectrum of pathogenic bacteria and the isolation rate of multidrug-resistant strains in our hospital have also changed accordingly, mainly reflected by the fact that although the isolation and drug resistance rates of MDR-AB always ranked first. After 2016, the separation rate of MDR-AB decreased significantly, which is probably due to the implementation of the Guiding Principles of Clinical Use of Antibiotics in 2015. The prevalence of CRE *Enterobacteriaceae* bacteria has increased in recent years, which is consistent with the national drug resistance monitoring information. The isolation rates of other bacteria did not fluctuate greatly, but the epidemiology of these bacteria still needs to be addressed.

The emergence of multidrug-resistant bacteria, or superbugs, poses a serious threat to public health and requires multilevel efforts to prevent them from overcoming antibiotic resistance. Governments must allocate sufficient funds to improve and develop new drug products, monitor the use of antibiotics, and establish strict policies and regulations. In addition, infection control measures must be strictly implemented in hospitals, but management practices must be considered for the use of antibiotics and microbicides and appropriate disposal or discharge of medical waste. Clinicians should avoid prescribing unnecessary and excessive antibiotics to patients with normal infections and advise patients to follow good hygiene practices such as hand washing and appropriate infection control measures. As an individual, we can take antibiotics that are prescribed only by our doctors, take them exactly as prescribed, and use them sensibly. Efforts to address the spread of antibiotic resistance include limiting the overuse of antibiotics in the food and animal sectors.

Nonantibiotic strategies for the treatment of antibiotic-resistant pathogens have been reported, such as gene editing techniques, immunotherapies, and vaccines, and antivirulence inhibitor bacteriophages [5, 10]. Antimicrobial adjuvants, fecal microbiota transplant (FMT), and competitive exclusion of pathogens through genetically modified probiotics and postbiotics are prospective alternative, unconventional strategies [5]. In addition, epidemiological and surveillance studies should be carried out and powerful tools should be used to deepen our understanding of antibiotic resistance and provide a timely and precise diagnosis of antibiotic use and consumption. Therefore, a multidisciplinary approach is needed to eliminate the serious threat of multidrug resistance.

However, this study also has some limitations. When analyzing multiple drug resistance, multiple bacteria in the same family and genus were not studied separately. In the future, a specific analysis should be carried out for important multidrug-resistant pathogens.

5. Conclusion

The distribution of pathogenic bacteria in different hospital departments and sample sources is variable. Therefore, targeted prevention and control of key pathogenic bacteria in different hospital departments must be carried out. Understanding the drug resistance and multiple drug resistance of the main pathogenic bacteria can provide guidance for the rational use of antibiotics in clinic.

Data Availability

The data used to support the findings of this study are available from the corresponding author upon request.

Ethical Approval

The study protocol was approved by the ethics committee of our hospital.

Conflicts of Interest

The authors declare that there are no conflicts of interest.

References

[1] N. A. Lerminiaux and A. D. S. Cameron, "Horizontal transfer of antibiotic resistance genes in clinical environments," *Canadian Journal of Microbiology*, vol. 65, no. 1, pp. 34–44, 2019.

[2] B. Aslam, W. Wang, M. I. Arshad et al., "Antibiotic resistance: a rundown of a global crisis," *Infection and Drug Resistance*, vol. 11, pp. 1645–1658, 2018.

[3] C. L. Ventola, "The antibiotic resistance crisis: part 1: causes and threats," *P and T: A Peer-Reviewed Journal for Formulary Management*, vol. 40, no. 4, pp. 277–283, 2015.

[4] A. Mann, K. Nehra, J. S. Rana, and T. Dahiya, "Antibiotic resistance in agriculture: perspectives on upcoming strategies to overcome upsurge in resistance," *Current research in microbial sciences*, vol. 2, Article ID 100030, 2021.

[5] M. Kumar, D. K. Sarma, S. Shubham et al., "Futuristic non-antibiotic therapies to combat antibiotic resistance: a review," *Frontiers in Microbiology*, vol. 12, Article ID 609459, 2021.

[6] A. P. Magiorakos, A. Srinivasan, R. B. Carey et al., "Multidrug-resistant, extensively drug-resistant and pandrug-resistant bacteria: an international expert proposal for interim standard

definitions for acquired resistance," *Clinical Microbiology and Infections*, vol. 18, no. 3, pp. 268–281, 2012.

[7] M. E. El Zowalaty, A. A. Al Thani, T. J. Webster et al., "*Pseudomonas aeruginosa*: arsenal of resistance mechanisms, decades of changing resistance profiles, and future antimicrobial therapies," *Future Microbiology*, vol. 10, no. 10, pp. 1683–1706, 2015.

[8] H. H. Chang, T. Cohen, Y. H. Grad, W. P. Hanage, T. F. O'Brien, and M. Lipsitch, "Origin and proliferation of multiple-drug resistance in bacterial pathogens," *Microbiology and Molecular Biology Reviews*, vol. 79, no. 1, pp. 101–116, 2015.

[9] M. Saha and A. Sarkar, "Review on multiple facets of drug resistance: a rising challenge in the 21st century," *Journal of xenobiotics*, vol. 11, no. 4, pp. 197–214, 2021.

[10] B. Aslam, M. Khurshid, M. I. Arshad et al., "Antibiotic resistance: one health one world outlook," *Frontiers in Cellular and Infection Microbiology*, vol. 11, Article ID 771510, 2021.

[11] L. B. Rice, "Federal funding for the study of antimicrobial resistance in nosocomial pathogens: no ESKAPE," *Journal of Infectious Diseases*, vol. 197, no. 8, pp. 1079–1081, 2008.

[12] Y. K. Schneider, "Bacterial natural product drug discovery for new antibiotics: strategies for tackling the problem of antibiotic resistance by efficient bioprospecting," *Antibiotics*, vol. 10, no. 7, p. 842, 2021.

[13] N. Duan, J. Du, C. Huang, and H. Li, "Microbial distribution and antibiotic susceptibility of lower respiratory tract infections patients from pediatric ward, adult respiratory ward, and respiratory intensive care unit," *Frontiers in Microbiology*, vol. 11, p. 1480, 2020.

[14] S. K. Fridkin, "Increasing prevalence of antimicrobial resistance in intensive care units," *Critical Care Medicine*, vol. 29, pp. N64–N68, 2001.

[15] M. F. Lin and C. Y. Lan, "Antimicrobial resistance in Acinetobacter baumannii: from bench to bedside," *World Journal of Clinical Cases*, vol. 2, no. 12, pp. 787–814, 2014.

[16] S. Mendoza-Olazaran, R. Morfin-Otero, L. Villarreal-Trevino et al., "Antibiotic susceptibility of biofilm cells and molecular characterisation of Staphylococcus hominis isolates from blood," *PLoS One*, vol. 10, no. 12, Article ID e0144684, 2015.

[17] L. E. Cole, J. Zhang, A. Kesselly et al., "Limitations of murine models for assessment of antibody-mediated therapies or vaccine candidates against Staphylococcus epidermidis bloodstream infection," *Infection and Immunity*, vol. 84, no. 4, pp. 1143–1149, 2016.

[18] S. S. Magill, J. R. Edwards, W. Bamberg et al., "Multistate point-prevalence survey of health care-associated infections," *New England Journal of Medicine*, vol. 370, no. 13, pp. 1198–1208, 2014.

[19] K. A. Kline and A. L. Lewis, "Gram-positive uropathogens, polymicrobial urinary tract infection, and the emerging microbiota of the urinary tract," *Microbiology Spectrum*, vol. 4, no. 2, 2016.

[20] E. A. Miller, T. J. Johnson, G. Omondi et al., "Assessing transmission of antimicrobial-resistant *Escherichia coli* in wild giraffe contact networks," *Applied and Environmental Microbiology*, vol. 85, no. 1, Article ID e02136-18, 2019.

[21] C. Liu, E. J. Yoon, D. Kim et al., "Antimicrobial resistance in South Korea: a report from the Korean global antimicrobial resistance surveillance system (Kor-GLASS) for 2017," *Journal of Infection and Chemotherapy*, vol. 25, no. 11, pp. 845–859, 2019.

[22] M. A. Khan and A. Faiz, "Antimicrobial resistance patterns of *Pseudomonas aeruginosa* in tertiary care hospitals of Makkah and Jeddah," *Annals of Saudi Medicine*, vol. 36, no. 1, pp. 23–28, 2016.

[23] Y. Doi, "Treatment options for carbapenem-resistant gram-negative bacterial infections," *Clinical Infectious Diseases*, vol. 69, pp. S565–S575, 2019.

[24] M. Talaat, M. El-Shokry, J. El-Kholy et al., "National surveillance of health care-associated infections in Egypt: developing a sustainable program in a resource-limited country," *American Journal of Infection Control*, vol. 44, no. 11, pp. 1296–1301, 2016.

[25] S. V. Gajul, S. T. Mohite, S. S. Mangalgi, S. M. Wavare, and S. V. Kakade, "Klebsiella pneumoniae in septicemic neonates with special reference to extended spectrum beta-lactamase, AmpC, metallo beta-lactamase production and multiple drug resistance in tertiary care hospital," *Journal of Laboratory Physicians*, vol. 7, pp. 032–037, 2015.

[26] J. P. Horcajada, M. Montero, A. Oliver et al., "Epidemiology and treatment of multidrug-resistant and extensively drug-resistant *Pseudomonas aeruginosa* infections," *Clinical Microbiology Reviews*, vol. 32, no. 4, Article ID e00031-19, 2019.

[27] S. I. Ahmad, "Treatment of post-burns bacterial infections by bacteriophages, specifically ubiquitous Pseudomonas spp. notoriously resistant to antibiotics," *Medical Hypotheses*, vol. 58, no. 4, pp. 327–331, 2002.

[28] P. Pachori, R. Gothalwal, and P. Gandhi, "Emergence of antibiotic resistance *Pseudomonas aeruginosa* in intensive care unit; a critical review," *Genes & Diseases*, vol. 6, no. 2, pp. 109–119, 2019.

[29] R. Yadav, J. B. Bulitta, J. Wang, R. L. Nation, and C. B. Landersdorfer, "Evaluation of pharmacokinetic/pharmacodynamic model-based optimized combination regimens against multidrug-resistant *Pseudomonas aeruginosa* in a murine thigh infection model by using humanized dosing schemes," *Antimicrobial Agents and Chemotherapy*, vol. 61, no. 12, Article ID e01268-17, 2017.

[30] D. J. Diekema, M. A. Pfaller, F. J. Schmitz et al., "Survey of infections due to Staphylococcus species: frequency of occurrence and antimicrobial susceptibility of isolates collected in the United States, Canada, Latin America, Europe, and the Western Pacific region for the SENTRY Antimicrobial Surveillance Program, 1997-1999," *Clinical Infectious Diseases*, vol. 32, 2001.

[31] J. L. Vincent, J. Rello, J. Marshall et al., "International study of the prevalence and outcomes of infection in intensive care units," *Jama*, vol. 302, no. 21, pp. 2323–2329, 2009.

[32] S. Lakhundi and K. Zhang, "Methicillin-resistant *Staphylococcus aureus*: molecular characterization, evolution, and epidemiology," *Clinical Microbiology Reviews*, vol. 31, no. 4, Article ID e00020-18, 2018.

[33] G. M. Rossolini, F. Arena, P. Pecile, and S. Pollini, "Update on the antibiotic resistance crisis," *Current Opinion in Pharmacology*, vol. 18, pp. 56–60, 2014.

Hindawi
Evidence-Based Complementary and Alternative Medicine
Volume 2023, Article ID 9793852, 1 page
https://doi.org/10.1155/2023/9793852

Retraction

Retracted: Surfactant without Endotracheal Tube Intubation (SurE) versus Intubation-Surfactant-Extubation (InSurE) in Neonatal Respiratory Distress Syndrome: A Systematic Review and Meta-Analysis

Evidence-Based Complementary and Alternative Medicine

Received 10 October 2023; Accepted 10 October 2023; Published 11 October 2023

This article has been retracted by Hindawi following an investigation undertaken by the publisher [1]. This investigation has uncovered evidence of one or more of the following indicators of systematic manipulation of the publication process:

(1) Discrepancies in scope

(2) Discrepancies in the description of the research reported

(3) Discrepancies between the availability of data and the research described

(4) Inappropriate citations

(5) Incoherent, meaningless and/or irrelevant content included in the article

(6) Peer-review manipulation

The presence of these indicators undermines our confidence in the integrity of the article's content and we cannot, therefore, vouch for its reliability. Please note that this notice is intended solely to alert readers that the content of this article is unreliable. We have not investigated whether authors were aware of or involved in the systematic manipulation of the publication process.

Wiley and Hindawi regrets that the usual quality checks did not identify these issues before publication and have since put additional measures in place to safeguard research integrity.

We wish to credit our own Research Integrity and Research Publishing teams and anonymous and named external researchers and research integrity experts for contributing to this investigation.

The corresponding author, as the representative of all authors, has been given the opportunity to register their agreement or disagreement to this retraction. We have kept a record of any response received.

References

[1] L. Wang, M. Zhang, and Q. Yi, "Surfactant without Endotracheal Tube Intubation (SurE) versus Intubation-Surfactant-Extubation (InSurE) in Neonatal Respiratory Distress Syndrome: A Systematic Review and Meta-Analysis," *Evidence-Based Complementary and Alternative Medicine*, vol. 2022, Article ID 6225282, 16 pages, 2022.

Hindawi
Evidence-Based Complementary and Alternative Medicine
Volume 2022, Article ID 6225282, 16 pages
https://doi.org/10.1155/2022/6225282

Research Article

Surfactant without Endotracheal Tube Intubation (SurE) versus Intubation-Surfactant-Extubation (InSurE) in Neonatal Respiratory Distress Syndrome: A Systematic Review and Meta-Analysis

Lirong Wang, Min Zhang, and Qingfeng Yi

Department of Neonatology, YongZhou Central Hospital, Yongzhou, Hunan 425100, China

Correspondence should be addressed to Lirong Wang; uspfd269@163.com

Received 21 July 2022; Revised 11 August 2022; Accepted 1 September 2022; Published 16 September 2022

Academic Editor: Xueliang Wu

Neonatal respiratory distress syndrome (NRDS) is generally treated with surfactant by intubation-surfactant-extubation (InSurE) technique, an invasive method of surfactant administration. Surfactant without endotracheal tube intubation (SurE) is a noninvasive technique that avoids intubation and has been found to have improved the delivery of exogenous surfactants, thereby decreasing lung damage in neonates. This systematic review aimed to provide insights into the efficacy of SurE over InSurE in neonates who received respiratory support and to evaluate the progression and onset of concurrent diseases after treatment. The CENTRAL, PubMed, and Embase databases were searched for data collection. In all, 21 research articles were eligible, comprising 19,976 study participants. The data showed a significant reduction in the composite outcome of stage 2 necrotizing enterocolitis, bronchopulmonary dysplasia, and onset of hemodynamically significant patent ductus arteriosus when treated with SurE. The trend towards lower pneumothorax rates with SurE was also evident. These findings were robust due to the sensitivity analyses performed. There were no differences in the outcome of death or rates of other neonatal morbidities. Overall, SurE was identified as a better substitute for InSurE to treat neonates with RDS.

1. Introduction

Lung development starts early after conception and is followed by consecutive branching of the bronchial tree [1]. Usually, lung development takes place in five overlapping stages, including the embryonic, pseudo-glandular, canalicular, saccular, and alveolar stages [2]. During development, factors such as insufficient levels of pulmonary surfactant, impeding normal gas exchange due to deregulation of acinar surface tension, lack of septation, and maturation of alveoli in developing fetus compromise alveolar integrity, resulting in neonatal respiratory syndrome or respiratory distress syndrome (RDS) [3–5]. RDS can cause permanent damage to preterm lungs, increase the risk of lower respiratory tract infections, and commonly progress through hypoxemia, respiratory acidosis, and hypoventilation, leading to a high risk of infant mortality every year [6–8].

Neonatal respiratory distress syndrome (NRDS) is caused by the deficiency or delayed production and secretion of pulmonary surfactants [9]. Deficiency in surfactants significantly reduces lung compliance in infants with NRDS and increases the chances of alveolar atelectasis [10, 11]. In postnatal, exposures to invasive mechanical ventilation (MV), excessive ventilator pressures, and overdistention of the neonatal lung can also impact surfactant production [12]. Results from autopsies of newborns who died from NRDS have observed airless lungs and diffused atelectasis in them 13. Among other pathophysiological features of NRDS, an increase in immature epithelial transport proteins may also aggravate NRDS due to the inability to remove excessive fetal lung fluids, leading to pulmonary edema and thereby

exacerbating respiratory distress [14]. Complications associated with RDS, such as air leaks such as pneumothorax or pneumomediastinum, intraventricular hemorrhage (IVH), and bronchopulmonary dysplasia, require continuous MV and treatment for cure.

The use of antenatal corticosteroids has significantly reduced RDS-associated mortalities as antenatal corticosteroids can trigger the activity of enzymes responsible for fetal lung maturity [15]. Recent treatments focus on replacing invasive mechanical treatments with noninvasive respiratory support through continuous positive airway pressure (CPAP). Continuous monitoring of arterial blood gases, including pH, partial pressure of carbon dioxide ($PaCO_2$), and PaO_2, is ensured in neonates with RDS to assess the blood's carbon dioxide and oxygen levels. Another widely used strategy is the exogenous administration of surfactant molecules to treat RDS, which has significantly reduced morbidity and mortality in neonates [16]. Numerous randomized trials have been performed to compare the efficacy and standard dosage of surfactants, and several research studies are focusing on the timing of prophylactic therapy and time of administration of exogenous surfactants with initial respiratory support [17]. The American Academy of Pediatrics recommends that CPAP must be immediately given to preterm infants with RDS, followed by surfactant rescue therapy [17, 18].

Although surfactant treatment is the most widely used to treat RDS, however, the current literature lacks proper information on the optimal timing and dosage of exogenous surfactant. In this study, we systematically reviewed and compared existing literature on surfactant administration through intubation-surfactant-extubation (InSurE) technique versus surfactant without endotracheal tube intubation (SurE) technique, which avoids intubation, by comparing several parameters to investigate the effectiveness of these two methods in treating RDS in neonates.

2. Materials and Methods

2.1. Search Strategy. This systematic review was conducted and is reported according to the guidelines of the Preferred Reporting Items for Systematic Reviews and Meta-Analyses (PRISMA) statement [19, 20]. Electronic searches were performed in multiple databases, including Cochrane Central Register of Controlled Trials (CENTRAL) via Cochrane Library (from inception to date), PubMed, and EMBASE, to have an in-depth look into the relevant articles published from the inception of the databases up to May 20, 2021. The database searches were conducted using the following terms: "neonatal respiratory distress syndrome" OR "respiratory distress syndrome" OR "NRDS" AND "InSurE" OR "intubation surfactant and extubation" OR "SurE".

For verification purposes, bibliographies of relevant searched items were manually confirmed to identify any additional articles of relevance. Relevant research groups were also accessed to identify any significant ongoing research projects; however, no data were obtained through this channel.

2.2. Inclusion Criteria and Study Selection. The inclusion criteria for study selection were (1) randomized control clinical trial evaluating interventions with a temporary effect; (2) neonates were properly randomized for receiving respiratory support such as nasal high-frequency oscillation ventilation (nHFOV), nasal CPAP/blood pressure (BP)-CPAP; and (3) reported more than one parameter such as type of MV, surfactant dosage, desaturation, onset of sepsis, mortality, etc. The exclusion criteria were (1) studies with experimental and basic research characterized as nonclinical studies; (2) duplicated reports and reports of post hoc analyses of the same study population; (3) studies with significant lack of information and presenting only baseline data; (4) articles written in languages other than English; (5) review articles and meeting abstracts; and (6) unpublished studies.

2.3. Data Extraction. Two reviewers independently screened eligible research studies to include in this meta-analysis. Issues and discrepancies were discussed with a third reviewer and resolved by mutual discussion. The following data were extracted: first author's name, year of publication, country, type of study, sample size, age, intervention information, and outcome measure information.

2.4. Assessment of Risk and Bias. The risk of bias in individual studies was independently assessed by two reviewers, and bias domains across studies were accessed using the Cochrane Collaboration tool [21]. Disagreements and differences were resolved through discussions with a third reviewer, and the studies were categorized as unclear, low, and high risk of bias. Methodological quality was based on concealment of allocation, blinding of participants/parents and personnel, blinding of outcome assessment, sequence generation, incomplete outcome data, and selective outcome reporting.

2.5. Statistical Analysis. The study-specific log odds ratios (ORs) were weighted by the inverse of variance for the calculation of pooled ORs with relative 95% confidence intervals (CIs). I^2 of Higgins and Thompson was used to evaluate heterogeneity among studies [22]. Data for the effect of various MV on treating NRDS were evaluated and used for statistical analysis. The random-effect model (REM) was used as the pooling method, and meta-regression analysis was used to explore potentially important covariates having significant effects on the between-study heterogeneity [23]. Treatment effect estimates for all trials were calculated and expressed as typical relative risk for dichotomous outcomes and weighted mean difference (WMD) for continuous outcomes using a 95% CI. The between-trial presence of heterogeneity among the recorded treatment effects was analyzed using the χ^2 test for heterogeneity and the I^2 statistic, which expresses the proportion of heterogeneity that cannot be explained by chance [24]. Heterogeneity was deemed significant when the corresponding *P-value* was <0.1 or when the I^2 percentage was

>50, at which point the REM was used. All statistical analyses were performed using Stata software (version 15.0; Stata Corp, College Station, Texas, USA).

3. Results

3.1. Study Selection, Description, and Assessment. The search strategy resulted in 16,834 potentially relevant citations. The PRISMA flow diagram (Figure 1) summarizes the process of the literature search and study selection. After screening the titles and abstracts of the obtained citations, 89 full-text articles were assessed for this meta-analysis eligibility. 21 articles ($n = 19976$ participants), utilizing SurE and InSurE, were selected for the final analysis [25–45]. Overall, there were nine trials that recruited 900 infants, which focused on the development of stage 2 necrotizing enterocolitis (NEC) and the use of SurE and InSurE. Eleven trials contained 1100 infants as study participants and focused on the need for MV besides exogenous surfactant administration using these methods. Mortality was observed in 700 infants from seven studies, whereas 1300 infants in thirteen trials were analyzed for the development of grade ≥2 IVH. Only four studies ($n = 400$ infants) compared transient bradycardia. Nine hundred infants from nine studies were for pneumothorax development and administration of surfactant using SurE and InSurE. Similarly, there were available data from 900 infants in whom the progression of retinopathy (ROP) was assessed in intensive neonatal care using SurE or InSurE. The evaluation and analysis of a second dose of surfactant were analyzed in 800 infants, while 600 infants from six studies were compared for the development of sepsis. Study samples of 900 patients were analyzed to evaluate the development of hemodynamically significant patent ductus arteriosus when treated with SurE or InSurE for RDS. Data sets of 1300 neonates were compared for the onset of bronchopulmonary dysplasia (BPD), and BPD-associated death was evaluated in a data set of 800 infants.

3.2. Characteristics of the Selected Studies and Risk of Bias. All the study groups were well matched. Birth weight and gestational ages, specifically assessed for only minor changes and all the aspects of respiratory support such as resuscitation devices, and use of antenatal glucocorticoids and surfactants were adequately described in the analyzed studies. All the studies were carefully assessed for the risk of bias. Most of the bias stemmed from blinding the participants and personnel and the outcome assessments. The randomization method was determined as adequate in all studies. Four studies were found to have adequate concealment of allocation (Table 1).

3.3. Meta-Analysis Results

3.3.1. Development of NEC. Among the investigated trials, when meta-analysis was performed for the use of SurE and InSurE for the treatment of NRDS, significant effectiveness of SurE over InSurE was observed. When comparing the efficacy of SurE and InSurE, a significant decrease in the

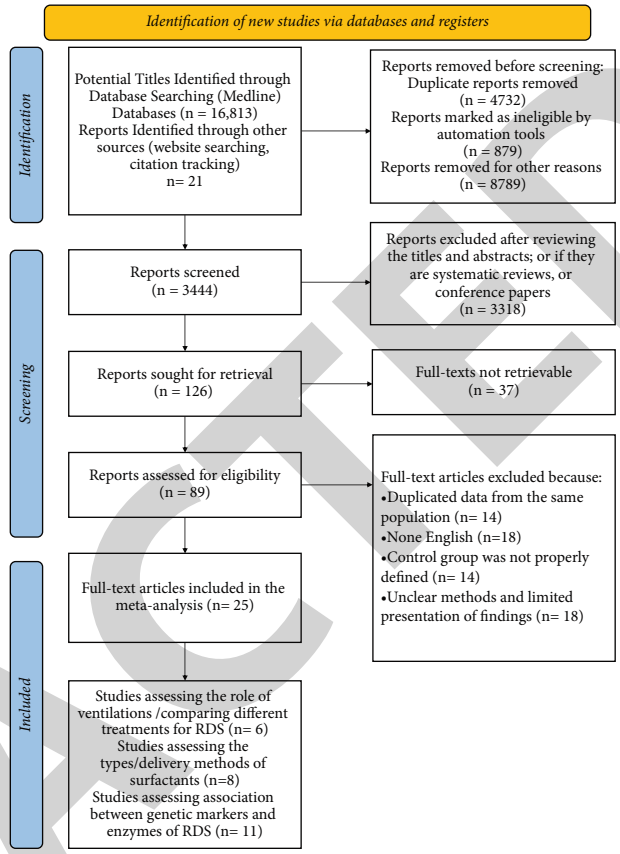

Figure 1: PRISMA flow chart of the selection of eligible studies.

progression and development of stage 2 NEC in infants suffering from RDS in the SurE group was observed (Figure 2). To investigate the association between the use of surfactant therapy and development of stage 2 NEC, a total of 9 studies were pooled for analysis. Of the 900 infants, 31 infants with RDS had NEC in the SurE group, compared with 71/900 infants in the InSurE group. The odds for the occurrence of NEC were less than one (OR, 0.451; 95% CI, 0.287–0.708; I^2, 0%; $P = 0.589$).

3.3.2. Need for MV. In total, eleven studies used MV with surfactant therapy through SurE and InSurE. We observed a significant reduction in the need for MV in the SurE group compared with the InSurE group (Figure 3). Out of the 1100 neonates with RDS, 324 required MV in comparison to 629 infants who were given surfactant through InSurE. Further assessment showed that only one study demonstrated odds for increased MV with SurE, indicating a low demand for high MV support when infants were subjected to this method of RDS treatment in neonates. The data showed characteristic significance with OR of 0.223 (95% CI, 0.111–0.447; I^2, 87.19%; $P < 0.001$).

3.3.3. Mortality Rate. Out of 700 neonates who suffered from RDS, 25 died during the treatment when subjected to SurE, whereas 54 died in the InSurE group (Figure 4). Only seven studies compared the mortality rate in infants when

Table 1: Summary of the included articles in the meta-analysis.

Author	Country	Methods	Sample size	Study type	Gestational age (weeks)	Necessity or type of MV	Intervention	Current findings	Future recommendation/ limitation/comments
Jena et al. 2019	India	Surfactant therapy	350	Original study	29–33	CPAP	SurE and InSurE	The need for MV in the first 72 hours of life was significantly lower in the SurE group. Similarly, duration of oxygen therapy, hospital stay, and BPD were significantly lower in the SurE group.	Studies with larger sample size are required along with a pain medication, which was absent in this study.
Gupta et al. 2020	India	Surfactant therapy	58	Original study	28–34	NIPPV	InSurE and MIST	No significant difference was found in need of IMV in first 72 h between MIST and InSurE (relative risk with MIST, 0.62; 95% confidence interval, 0.22 to 1.32).	Larger multicenter studies are needed.
Yang et al. 2020	China	Surfactant therapy	97	Observational study	32–36	CPAP	LISA and InSurE	LISA could be used to treat premature infants with RDS with stronger spontaneous breathing ability.	Further clinical studies are needed to determine the optimal strategy of LISA administration and the most suitable population of patients.
Aldana-Aguirre et al. 2017	Canada	Surfactant therapy	895	Review study	36	CPAP	LISA and endotracheal intubation	LISA for surfactant delivery resulted in less demand for MV in infants with RDS.	No data are provided for long-term neurodevelopmental outcomes.
Wang et al. 2019	China	Minimally invasive surfactant therapy	53	Original study	32	nCPAP	InSurE and MIST	MIST was feasible and safe, and it might reduce the composite outcome of death.	Single-center study

Table 1: Continued.

Author	Country	Methods	Sample size	Study type	Gestational age (weeks)	Necessity or type of MV	Intervention	Current findings	Future recommendation/ limitation/comments
Kamaz et al. 2013	Turkey	Noninvasive surfactant therapy	200	Original randomized controlled trial	<32	nCPAP	Noninvasive SurE and InSurE	The Take Care technique was feasible for the treatment of respiratory distress syndrome in infants with very low birth weight. It significantly reduced both the need and duration of MV, as well as the BPD rate in preterm infants.	Further studies about the effect on BPD with sufficient power and meta-analysis are needed.
Kribs et al. 2015	Germany	Nonintubated surfactant therapy	211	Multicenter, randomized, clinical, parallel-group study	36	CPAP	LISA via a thin catheter and conventional treatment	LISA did not increase survival without BPD but was associated with increased survival without major complications.	LISA is a promising new therapy for extremely preterm infants with respiratory distress syndrome, but this requires further investigation.
Langhammer et al. 2018	Germany	Surfactant therapy	407	Observational cross-sectional multicenter study	26–29	nCPAP	LISA and intubation therapy	LISA-treated infants needed less MV and shorter duration with supplemental oxygen. It also required less analgesics and sedatives. SGA infants seem to have higher risks of LISA failure.	Further studies are needed to demonstrate that LISA-treated infants require shorter duration of supplemental oxygen and lower needs for analgesics and sedatives. Also, it needs to be confirmed whether there are fewer ROP infants in the LISA group.

Table 1: Continued.

Author	Country	Methods	Sample size	Study type	Gestational age (weeks)	Necessity or type of MV	Intervention	Current findings	Future recommendation/ limitation/comments
Hartel et al. 2018	Germany	Less-invasive surfactant administration	7533	Original cohort study	22–28	NIPPV-CPAP	No surfactant, LISA, and ETT	LISA was superior to intubation for surfactant delivery for short-term outcomes. It was associated with focal intestinal perforation in the extremely preterm infants.	Whether "protective" or earlier intubation of extremely preterm infants with significant abdominal distension is beneficial, needs to be investigated further in clinical trials.
Tomar et al. 2017	India	Surfactant therapy	136	Single-center, prospective observational study	24–34	CPAP	MIST and InSurE	The modified MIST technique was an effective method for the treatment of RDS in preterm infants with better clinical efficacy than and comparable outcomes to the more invasive InSurE procedure	Further investigation with multicentric trials is needed.
Klebermass-Schrehof et al. 2013	Austria	Surfactant therapy	224	Single-center original study	23–27	CPAP	LISA	LISA resulted in significant improvement in MV, intraventricular hemorrhage, leukomalacia, PDA, and ROP.	Need for a retrospective design and a randomized control group.
Dargaville et al. 2014	Australia	Surfactant therapy	156	Open feasibility study	25–28	CPAP	MIST and InSurE	Surfactant was successfully administered via MIST in all cases, with a rapid and sustained reduction in FiO2 thereafter.	Further investigation with clinical trials is needed.

Table 1: Continued.

Author	Country	Methods	Sample size	Study type	Gestational age (weeks)	Necessity or type of MV	Intervention	Current findings	Future recommendation/ limitation/comments
Mirnia et al. 2013	Iran	Surfactant administration	136	Multicenter randomized clinical trial study	27–32	CPAP	TEC and InSurE	TEC method was effective in treating RDS, NEC, and BPD. Mortality was significantly decreased in the TEC group.	TEC procedure is a new method of surfactant administration, and there are few studies on it. Thus, there is a need for more studies to fully understand this procedure.
Li et al. 2016	China	Surfactant therapy	44	Original study	28–30	nCPAP	LISA and InSurE	Both InSurE and LISA caused a transient impairment in cerebral autoregulation of RDS infants. LISA was superior to InSurE in terms of the effect duration.	Further evaluation of neurological functions of RDS is required.
Gopel et al. 2011	Germany	Surfactant therapy	220	Parallel-group, randomized group trial	26–28	Oxygen supplementation + CPAP	SurE and InSurE	Surfactant administered via a thin catheter to spontaneously breathing preterm infants in addition to CPAP reduced the need for MV.	In the future, surfactant given to spontaneously breathing preterm infants via a thin catheter might be included for individualized and gentler care for preterm infants.
Bao et al. 2015	China	Surfactant therapy	90	Original study	28–32	nCPAP	LISA and InSurE	LISA in spontaneously breathing infants on nCPAP was an alternative therapy for PS delivery, avoiding intubation with an endotracheal tube.	Further clinical trials are required.

Table 1: Continued.

Author	Country	Methods	Sample size	Study type	Gestational age (weeks)	Necessity or type of MV	Intervention	Current findings	Future recommendation/ limitation/comments
Mohammadizadeh et al. 2015	Iran	Surfactant therapy	38	Original study	<35	nCPAP	Surfactant administration via thin intratracheal catheter vs. endotracheal tube	Both methods had similar efficacy, feasibility, and safety.	N/A
Abdel-Latif et al. 2021	Australia	Surfactant therapy	2164	Analytical study	<37	CPAP and rescue surfactant administration	Surfactant administration via thin catheter and via ETT tube	Administration of surfactant via thin catheter was compared with administration via an ETT. The former approach was associated with reduced risk of death or BPD, less intubation in the first 72 hours, incidence of major complications, and in-hospital mortality.	Further well-designed studies with adequate size and power are needed to clarify whether surfactant therapy via thin tracheal catheter provides benefits over continuation of noninvasive respiratory support without surfactant. Moreover, uncertainties related to special subgroups and the role of sedation need to be addressed.
More et al. 2014	Canada	Surfactant therapy	3081	Narrative review	<35	CPAP	MIST	Surfactant administration via a thin catheter might be an efficacious and potentially safe method.	Further investigations are recommended for better surfactant administration.
Dekker et al. 2016	Netherlands	Surfactant therapy	38	Original study	25–36	--	MIST	Preterm infants receiving MIST were more comfortable when sedation was given.	Neonates required more ventilation.

Table 1: Continued.

Author	Country	Methods	Sample size	Study type	Gestational age (weeks)	Necessity or type of MV	Intervention	Current findings	Future recommendation/ limitation/comments
Panza et al. 2020	Italy	Surfactant therapy	4926	Analytical study	20–36	CPAP and nCPAP	SurE, Take Care, LISA, MIST, and InSurE	Compared with InSurE to deliver surfactant to newborn preterm infants with RDS, using thin catheters was associated with a reduced incidence of BPD and less need for MV.	More evidence on premedication, the dose of surfactant, use of caffeine, and use of high flow are needed. In addition, information about pain level, physiological responses, and implementation protocols are required in the future studies.

MV : mechanical ventilation; N/A : not applicable; SurE : surfactant without endotracheal tube intubation; InSurE : intubation, surfactant, and extubation; MIST : minimally invasive surfactant therapy; CPAP : continuous positive airway pressure; nCPAP: nasal continuous positive airway pressure; LISA : less invasive surfactant administration; ETT: endotracheal tube; BPD : bronchopulmonary dysplasia; NEC: necrotizing enterocolitis; TEC: thin endotracheal catheter; NIPPV: noninvasive positive pressure ventilation.

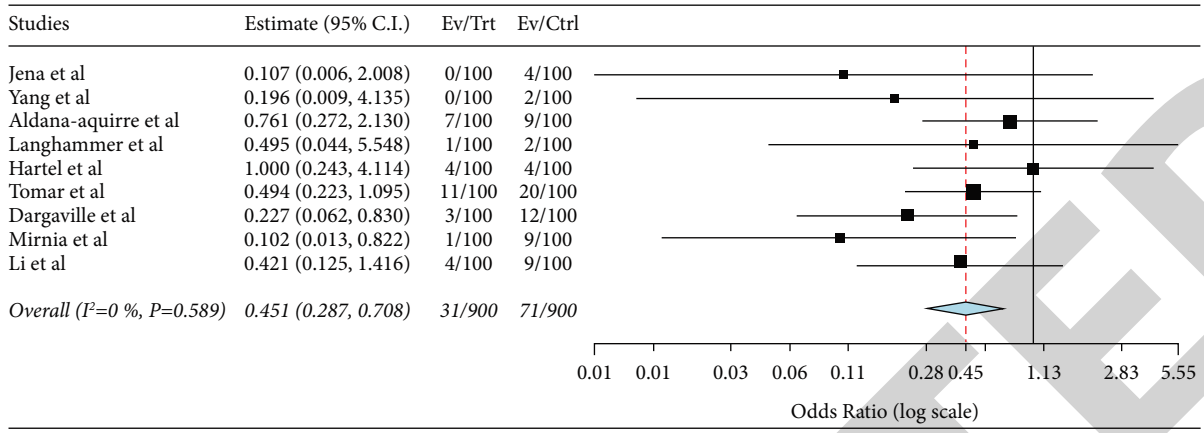

Figure 2: Meta-analysis of development of stage 2 necrotizing enterocolitis when SurE and InSurE were used.

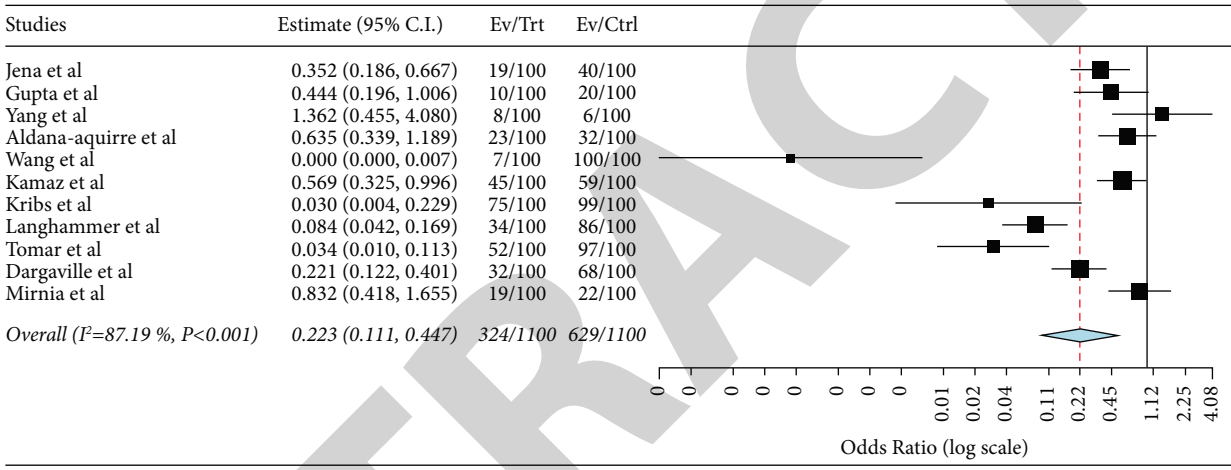

Figure 3: Meta-analysis of the need for mechanical ventilation when SurE and InSurE were used.

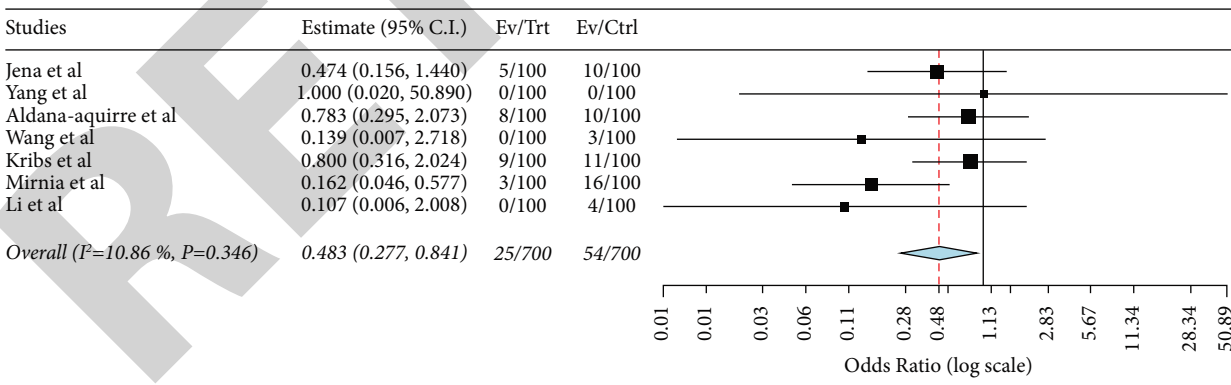

Figure 4: Meta-analysis of mortality rate when SurE and InSurE were used.

treated with SurE *vs*. InSurE. Although three studies showed a relatively higher odds ratio, four showed that treatment with InSurE was associated with a lower likelihood of death. However, due to a relatively small sample size available for analysis (OR, 0.483; 95% CI, 0.277–0.841; I^2, 10.86%; $P = 0.346$), no significant differences were observed between the two groups to fully understand the infants' mortality rate.

3.3.4. Development of IVH. In the SurE group, 76 out of 1300 neonates with RDS had IVH, whereas there were 129 neonates with IVH in the InSurE group (Figure 5). Of the 22 included studies, 13 were included for subsequent analyses. Although only one of the included studies showed an odd greater than one, the remaining were in range and tended to have lesser chances of developing IVH after SurE treatment, but the difference was not statistically significant (95% CI,

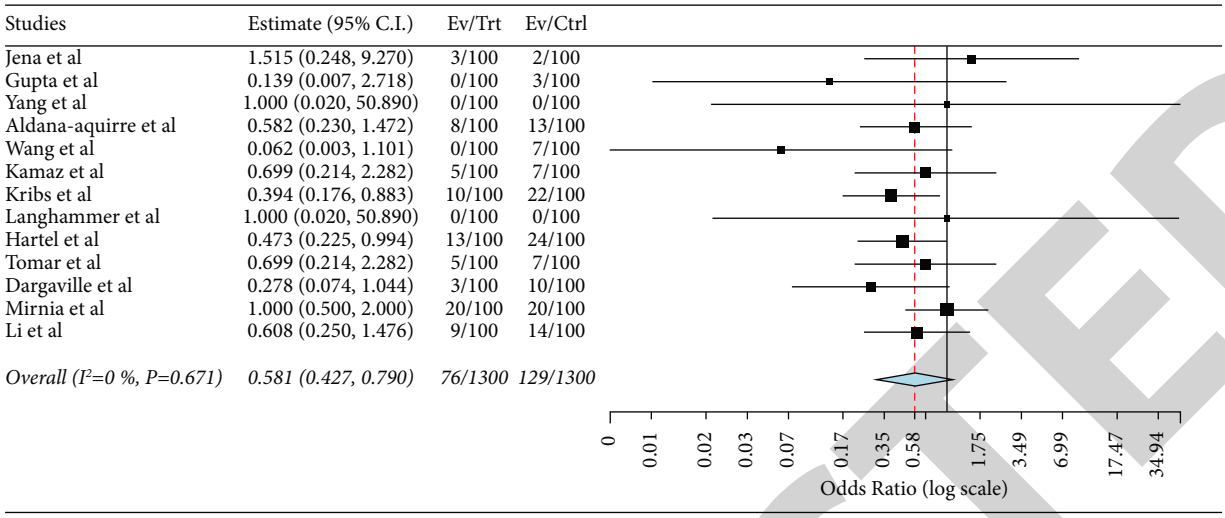

Figure 5: Meta-analysis of intraventricular hemorrhage ≥ grade 2 (IVH) when SurE and InSurE were used.

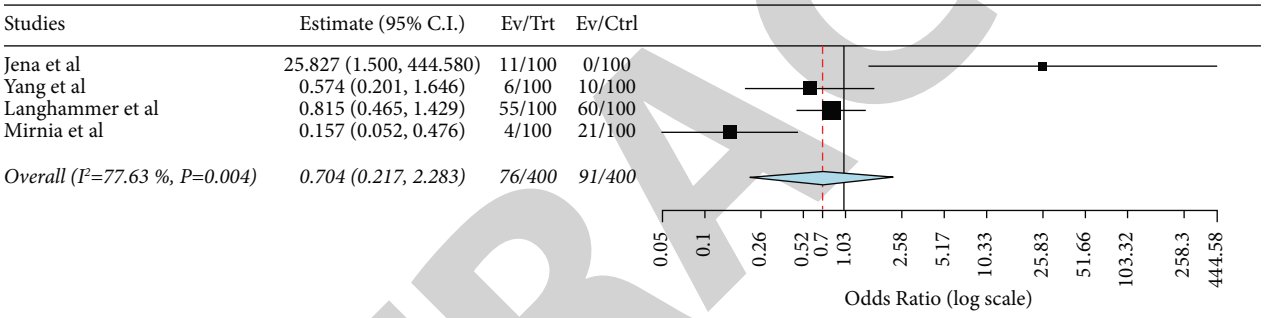

Figure 6: Meta-analysis of the development of transient bradycardia when SurE and InSurE were used.

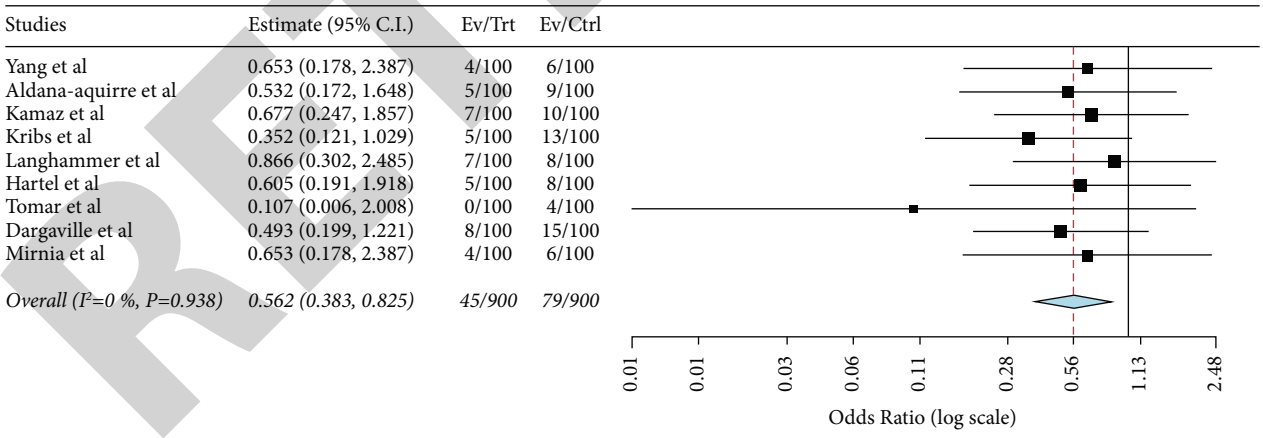

Figure 7: Meta-analysis of the development of pneumothorax when SurE and InSurE were used.

0.427–0.790; I^2, 0%; $P = 0.671$), suggesting that SurE and InSurE treatment did not affect the development of IVH.

3.3.5. Development of Transient Bradycardia or Desaturation. Four studies significantly compared the effects of SurE and InSurE on transient bradycardia or desaturation. According to the comparison, only one study indicated that the use of SurE could increase the odds of transient bradycardia or desaturation (Figure 6). However, no such observation was found in the other three studies, as the odds for the occurrence of bradycardia were less than 1 for each of them, suggesting that there was a 0.004 chance that infants would suffer from desaturation after using SurE, making SurE a more viable approach to treating RDS than InSurE.

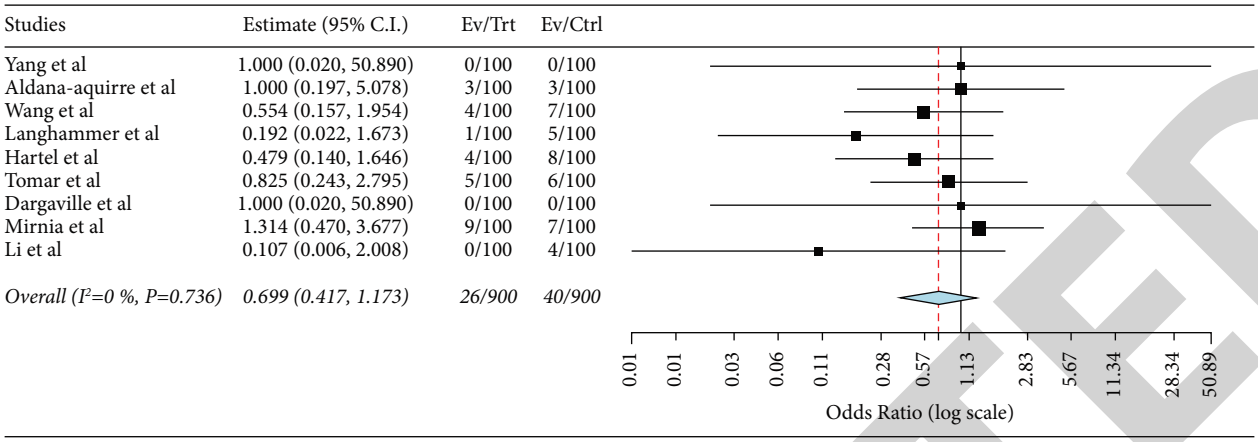

Figure 8: Meta-analysis of the progression of retinopathy (ROP) when SurE and InSurE were used.

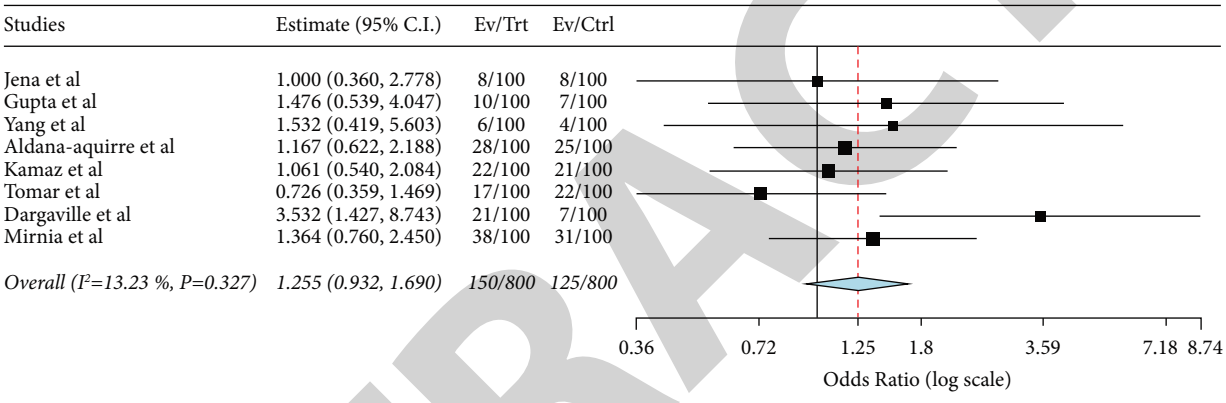

Figure 9: Meta-analysis of the need for a second-dose surfactant when SurE and InSurE were used.

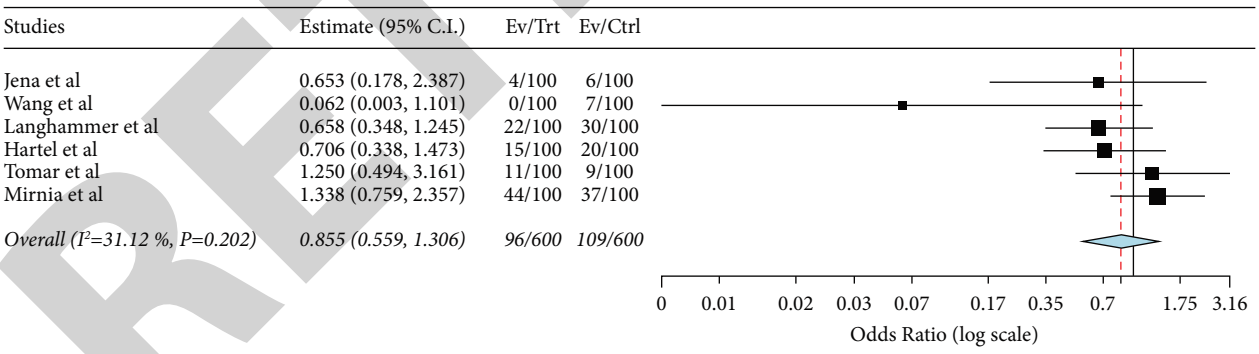

Figure 10: Meta-analysis of the occurrence of sepsis when SurE and InSurE were used.

3.3.6. Development of Pneumothorax. In total, 9 studies compared the development of pneumothorax with the use of SurE *vs*. InSurE. The average odds for the development of pneumothorax were less than one, indicating minute chances of pneumothorax after surfactant treatment. There were 45 patients who developed pneumothorax in the SurE group, compared with 79 in the InSurE group. However, the difference was not statistically significant (OR, 0.562; 95% CI, 0.383–0.825; I^2, 0%; $P = 0.938$) (Figure 7).

3.3.7. Onset of ROP. Nine studies compared the onset of ROP after the reception of SurE vs. InSurE. Overall, the odds for five studies were recorded as less than 0.57, whereas the

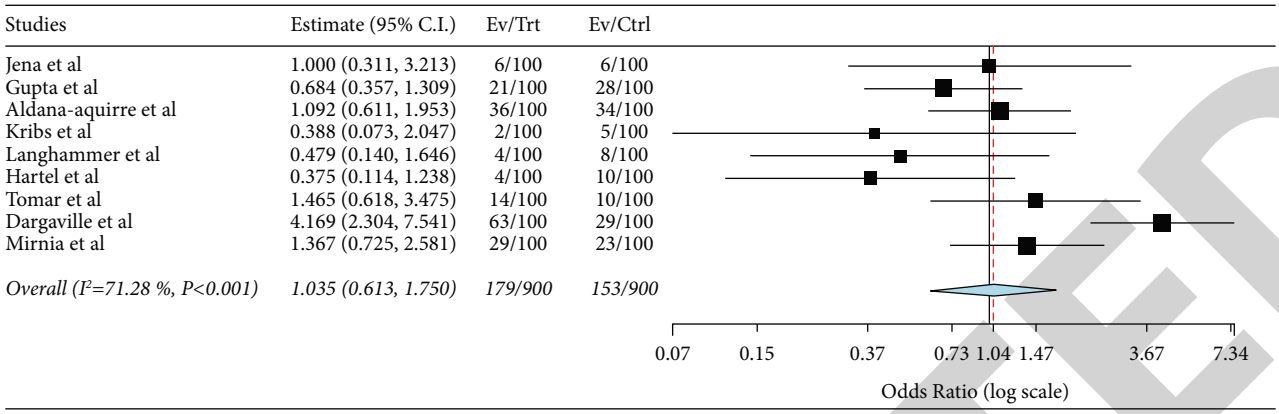

Figure 11: Meta-analysis of the occurrence of hemodynamically significant patent ductus arteriosus when SurE and InSurE were used.

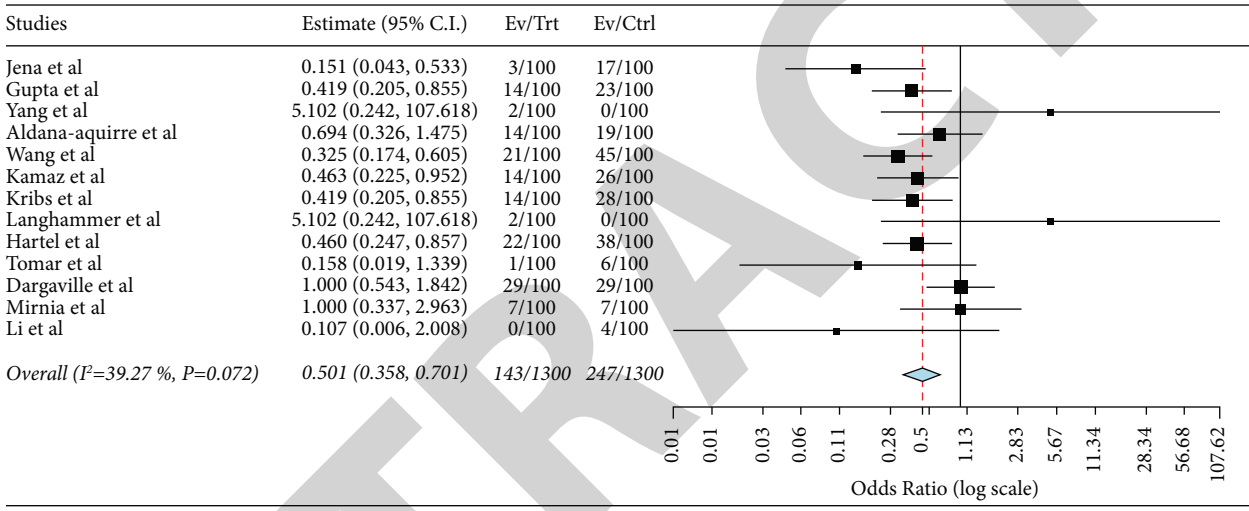

Figure 12: Meta-analysis of the occurrence of bronchopulmonary dysplasia (BPD) when SurE and InSurE were used.

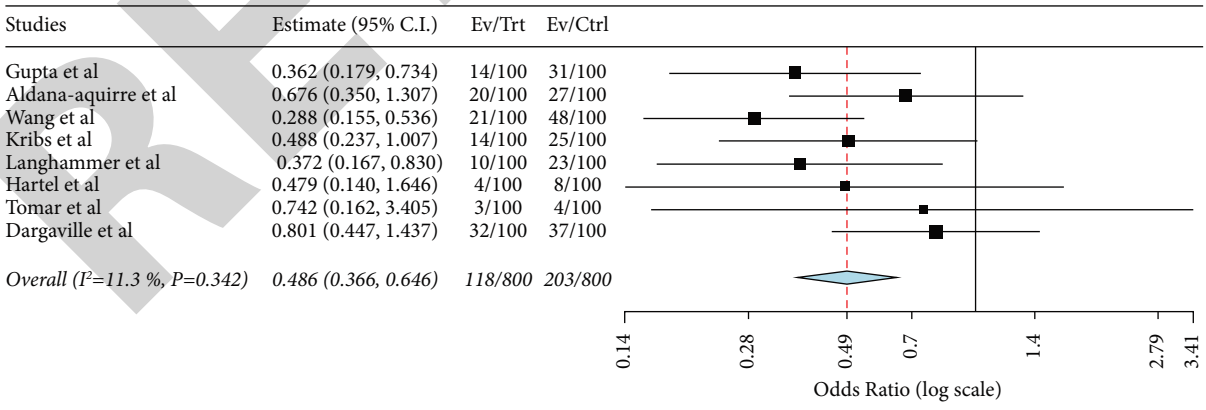

Figure 13: Meta-analysis of the occurrence of bronchopulmonary dysplasia (BPD) leading to death when SurE and InSurE were used.

odds for the remaining four studies were in the range of 0.57–1 (Figure 8). No significant difference in the onset of ROP between the SurE and InSurE groups was observed (95% CI, 0.417–1.173; I^2, 0%; $P = 0.736$).

3.3.8. Effect of Second-Dose Surfactant. Eight studies analyzed the effect of second-dose surfactant. No significant differences were observed between the two groups (OR, 1.255; 95% CI, 0.932–1.690; I^2, 13.23%; $P = 0.327$) (Figure 9).

3.3.9. Development of Sepsis. Six studies analyzed the development of sepsis after using SurE and InSurE for the treatment of RDS in 96 and 109 preterm infants, respectively. No significant difference was observed between the two treatment methods (OR, 0.855; 95% CI, 0.559–1.306; I^2, 31.12%; $P = 0.202$) (Figure 10).

3.3.10. Onset of BPD. In regard to the onset of hemodynamically significant patent ductus arteriosus and onset of BPD, a significant difference between the use of SurE and InSurE was observed (OR, 1.035; 95% CI, 0.613–1.750; I^2, 71.28%; $P < 0.001$, and OR, 0.501; 95% CI, 0.358–0.701; I^2, 39.27%; $P = 0.072$, respectively) (Figures 11 and 12). However, when BPD-related deaths were taken into account, no significant difference between the two groups was observed (Figure 13).

4. Discussion

This meta-analysis analyzed 21 research studies that agglomerated to a total of 19,976 research participants for comparing the progression and development of different diseases in preterm neonates treated with SurE *vs*. InSurE for exogenous surfactant administration. The results showed that, in noninvasively treated preterm infants, the use of SurE technique compared with that of endotracheal intubation for surfactant delivery was more beneficial [30, 36–45]. The data showed a reduction in the composite outcome of significant reduction in the composite outcome of stage 2 NEC, BPD, and onset of hemodynamically significant patent ductus arteriosus when treated with SurE. The trend towards lower pneumothorax rates with SurE was also evident.

In InSurE procedures, infants are first intubated, and then the surfactant is administered for a brief period with MV, followed by extubation and continued noninvasive respiratory support [46, 47]. However, InSurE may not always be successful because there are some infants who cannot be extubated after the procedure and some needing reintubation following hours or days after InSurE due to complications such as hypoxia or hypercapnia [46]. Such situations could lead to fluctuations in blood pressure and have been associated with an increased risk of intracranial hemorrhage [48]. However, this does not mean that InSurE should be neglected in clinical practice. The main problem could be the selection of patients who would benefit more from InSurE than other techniques. For instance, in order to improve patient selection, clinicians could assess the severity of RDS in the first hours after birth. However, an important clinical dilemma is which parameter and cutoff point to use. Further, current literature does not recommend the use of respiratory indices or clinical scores to assess RDS severity to reliably select infants in the first hours of life [49–51], mainly, because they were generally poorly investigated [10], thus making the clinical use of InSurE difficult for such cases. All these findings from the current literature support the findings of this study, which suggest the superiority of less invasive procedures such as SurE in these cases.

In this study, we carefully ensured that the exclusion of patients would not bias the main findings of this review. The analyses were restricted to SurE *vs*. InSurE treatments used for exogenous surfactant administration, and other methods were excluded due to limited available information. Further, this study can be considered as one of the largest systemic reviews of clinical trials comparing the effects of SurE and InSurE. Here, we observed no difference in the outcome of death or in the rates of other neonatal morbidities between the two treatment groups. In a study by Aldan et al. [28], which comprised 895 patients, the investigators observed no differences in the outcome of death and other neonatal morbidities. The pulmonary benefits associated with SurE are multifactorial such as the avoidance of intubation with MV, which can lead to lung injury as described in several studies [52]. Other advantages are reducing the duration of CPAP and the need for oxygen therapy [52], which could benefit maintaining functional residual capacity and preventing atelectotrauma in premature lungs [53]. Moreover, SurE has the advantage of spontaneous breathing in newborns to distribute surfactant in the lungs compared with InSurE, which can cause repeated inflations in the newborns' lungs. Recently, there have been newer minimally invasive strategies to provide surfactant therapy for managing RDS [54, 55]. These techniques incorporate the utilization of a small catheter placed into the trachea to administer the surfactant, which not only avoids intubation but also allows CPAP to continue and reduces injury to the young preterm lungs.

With regard to the strengths and limitations of this study, we performed a comprehensive search from large databases to minimize the risk of selection and publication bias. The steps of the review process were independently performed by 3 reviewers. All potential predictive factors were evaluated to maintain treatment homogeneity and thus present a complete overview for determining the clinical effects of SurE *vs*. InSurE. Some of the limitations of this systematic review include that no data were available from the retrieved studies in regard to long-term neurodevelopmental issues. Further, some studies did not provide a clear mandate for InSurE and procedure-related adverse events were not clearly demonstrated.

In conclusion, we systematically assessed the effects of SurE and InSurE in neonates who received respiratory support. Overall, the study findings suggested that noninvasive treatment with SurE was associated with better surfactant delivery than InSurE. In terms of BPD-related deaths, no significant difference between the two treatment groups was observed. Thus, noninvasive surfactant delivery strategies should be further researched to decrease the risk of injury using MV in neonates' preterm lungs.

Data Availability

The data that support the findings of this study are available from the corresponding author upon reasonable request.

Conflicts of Interest

The authors declare that they have no conflicts of interest.

References

[1] D. Mullassery and N. P. Smith, "Lung development," *Seminars in Pediatric Surgery*, vol. 24, pp. 152–155, 2015.

[2] J. W. DiFiore and J. M. Wilson, "Lung development," *Semin Pediatr Surg*, vol. 4, pp. 221–232, 1994.

[3] C. St Clair, E. R. Norwitz, K. Woensdregt et al., "The probability of neonatal respiratory distress syndrome as a function of gestational age and lecithin/sphingomyelin ratio," *American Journal of Perinatology*, vol. 25, no. 08, pp. 473–480, 2008.

[4] G. A. Agrons, S. E. Courtney, J. T. Stocker, and R. I. Markowitz, "Lung disease in premature neonates: radiologic-pathologic correlation," *RadioGraphics*, vol. 25, pp. 1047–1073, 2005.

[5] D. G. Sweet, V. Carnielli, G. Greisen et al., "European consensus guidelines on the management of respiratory distress syndrome – 2019 update," *Neonatology*, vol. 115, pp. 432–450, 2019.

[6] B. J. Stoll, N. I. Hansen, E. F. Bell et al., "Neonatal outcomes of extremely preterm infants from the NICHD neonatal research network," *Pediatrics*, vol. 126, pp. 443–456, 2010.

[7] D. De Luca, A. H. van Kaam, D. G. Tingay et al., "The Montreux definition of neonatal ARDS: biological and clinical background behind the description of a new entity," *The Lancet Respiratory Medicine*, vol. 5, pp. 657–666, 2017.

[8] C. L. Hermansen and A. Mahajan, ""Newborn respiratory distress" Am fam physician, vol," *92, no*, vol. 11, pp. 994–1002, 2015.

[9] P. Reynolds, P. Bustani, C. Darby et al., "Less-invasive surfactant administration for neonatal respiratory distress syndrome: a consensus guideline," *Neonatology*, vol. 118, pp. 586–592, 2021.

[10] B. De Bisschop, F. Derriks, and F. Cools, "Early predictors for INtubation-SURfactant-extubation failure in preterm infants with neonatal respiratory distress syndrome: a systematic review," *Neonatology*, vol. 117, pp. 33–45, 2020.

[11] M. Hallman, V. Glumoff, and M. Rämet, "Surfactant in respiratory distress syndrome and lung injury," *Comparative Biochemistry and Physiology Part A: Molecular & Integrative Physiology*, vol. 129, pp. 287–294, 2001.

[12] B. J. Stoll, N. I. Hansen, E. F. Bell et al., "Trends in care practices, morbidity, and mortality of extremely preterm neonates, 1993–2012," *314, no*, vol. 314, pp. 1039–1051, 2015.

[13] R. G. Wunderink, L. S. Woldenberg, J. Zeiss, C. M. Day, J. Ciemins, and D. A Lacher, "The radiologic diagnosis of autopsyproven ventilator-associated pneumonia," *Chest*, vol. 101, pp. 458–463, 1992.

[14] L. Jain, ""Respiratory morbidity in late-preterm infants: prevention is better than cure!." Am J Perinatol, vol," *25, no*, vol. 2, pp. 75–78, 2008.

[15] D. Roberts, J. Brown, N. Medley, and S. R. Dalziel, "Antenatal corticosteroids for accelerating fetal lung maturation for women at risk of preterm birth," *Cochrane Database Syst Rev*, vol. 3, Article ID Cd004454, 2017.

[16] J. J. Ho, P. Subramaniam, and P. G. Davis, "Continuous positive airway pressure (CPAP) for respiratory distress in preterm infants," *Cochrane Database Syst Rev*, vol. 10, no. 10, Article ID Cd002271, 2020.

[17] C. H. Backes, J. L. Notestine, J. M. Lamp et al., "Evaluating the efficacy of Seattle-PAP for the respiratory support of premature neonates: study protocol for a randomized controlled trial," *Trials*, vol. 20, p. 63, 2019.

[18] C. O. F. A. Newborn and A. A. O. Pediatrics, ""Respiratory support in preterm infants at birth."," *Pediatrics*, vol. 133, pp. 171–174, 2014.

[19] J. Li, X. Li, X. Huang, and Z. Zhang, "Noninvasive high-frequency oscillatory ventilation as respiratory support in preterm infants: a meta-analysis of randomized controlled trials," *Respiratory Research*, vol. 20, p. 58, 2019.

[20] X. W. Zhu, J. N. Zhao, S. F. Tang, J. Yan, and Y. Shi, "Noninvasive high-frequency oscillatory ventilation versus nasal continuous positive airway pressure in preterm infants with moderate-severe respiratory distress syndrome: a preliminary report," *Pediatric Pulmonology*, vol. 52, pp. 1038–1042, 2017.

[21] M. Cumpston, T. Li, and M. J. Page, "Updated guidance for trusted systematic reviews: a new edition of the Cochrane handbook for systematic reviews of interventions," *Cochrane database syst rev*, vol. 10, Article ID 000142, 2019.

[22] M. J. Page, J. E. McKenzie, and P. M. Bossuyt, "The PRISMA 2020 statement: an updated guideline for reporting systematic reviews," *Bmj*, vol. 372, 2021.

[23] J. Bowden, J. F. Tierney, A. J. Copas, and S. Burdett, "Quantifying, displaying and accounting for heterogeneity in the meta-analysis of RCTs using standard and generalised Q statistics," *BMC Medical Research Methodology*, vol. 11, no. 1, p. 41, 2011 no.

[24] J. P. T. Higgins and S. G. Thompson, "Controlling the risk of spurious findings from meta-regression," *Statistics in Medicine*, vol. 23, pp. 1663–1682, 2004.

[25] S. R. Jena, H. S. Bains, A. Pandita et al., "Surfactant therapy in premature babies: SurE or InSurE," *Pediatric Pulmonology*, vol. 54, pp. 1747–1752, 2019.

[26] B. K. Gupta, A. K. Saha, S. Mukherjee, and B. Saha, "Minimally invasive surfactant therapy versus InSurE in preterm neonates of 28 to 34 weeks with respiratory distress syndrome on non-invasive positive pressure ventilation—a randomized controlled trial," *European Journal of Pediatrics*, vol. 179, pp. 1287–1293, 2020.

[27] G. Yang, M. Hei, Z. Xue, Y. Zhao, X. Zhang, and C Wang, "Effects of less invasive surfactant administration (LISA) via a gastric tube on the treatment of respiratory distress syndrome in premature infants aged 32 to 36 weeks," *Medicine (Baltimore)*, vol. 99, no. 9, e19216, p. e19216, 2020.

[28] J. C. Aldana-Aguirre, M. Pinto, R. M. Featherstone, and M. Kumar, "Less invasive surfactant administration versus intubation for surfactant delivery in preterm infants with respiratory distress syndrome: a systematic review and meta-analysis," *Arch Dis Child Fetal Neonatal*, vol. 102, no. 1, pp. F17–f23, 2017.

[29] X. A. Wang, L. J. Chen, S. M. Chen, P. H. Su, and J. Y. Chen, "Minimally invasive surfactant therapy versus intubation for surfactant administration in very low birth weight infants with respiratory distress syndrome," *Pediatrics & Neonatology*, vol. 61, pp. 210–215, 2020.

[30] H. G. Kanmaz, O. Erdeve, F. E. Canpolat, B. Mutlu, and U. Dilmen, "Surfactant administration via thin catheter during spontaneous breathing: randomized controlled trial," *Pediatrics*, vol. 131, no. 2, pp. e502–9, 2013.

[31] A. Kribs, C. Roll, W. Göpel et al., ""Nonintubated surfactant application vs conventional therapy in extremely preterm infants: a randomized clinical trial." jama pediatr," *JAMA Pediatrics*, vol. 169, pp. 723–730, 2015.

[32] K. Langhammer, B. Roth, A. Kribs, W. Gopel, L. Kuntz, and F Miedaner, "Treatment and outcome data of very low birth weight infants treated with less invasive surfactant

Hindawi
Evidence-Based Complementary and Alternative Medicine
Volume 2023, Article ID 9797136, 1 page
https://doi.org/10.1155/2023/9797136

Retraction

Retracted: The Change of Aqueous Humor Cytokine Levels after Anti-VEGF in Diabetic Macular Edema: A Systematic Review and Meta-Analysis

Evidence-Based Complementary and Alternative Medicine

Received 8 August 2023; Accepted 8 August 2023; Published 9 August 2023

This article has been retracted by Hindawi following an investigation undertaken by the publisher [1]. This investigation has uncovered evidence of one or more of the following indicators of systematic manipulation of the publication process:

(1) Discrepancies in scope

(2) Discrepancies in the description of the research reported

(3) Discrepancies between the availability of data and the research described

(4) Inappropriate citations

(5) Incoherent, meaningless and/or irrelevant content included in the article

(6) Peer-review manipulation

The presence of these indicators undermines our confidence in the integrity of the article's content and we cannot, therefore, vouch for its reliability. Please note that this notice is intended solely to alert readers that the content of this article is unreliable. We have not investigated whether authors were aware of or involved in the systematic manipulation of the publication process.

Wiley and Hindawi regrets that the usual quality checks did not identify these issues before publication and have since put additional measures in place to safeguard research integrity.

We wish to credit our own Research Integrity and Research Publishing teams and anonymous and named external researchers and research integrity experts for contributing to this investigation.

The corresponding author, as the representative of all authors, has been given the opportunity to register their agreement or disagreement to this retraction. We have kept a record of any response received.

References

[1] A. Wang and H. Wang, "The Change of Aqueous Humor Cytokine Levels after Anti-VEGF in Diabetic Macular Edema: A Systematic Review and Meta-Analysis," *Evidence-Based Complementary and Alternative Medicine*, vol. 2022, Article ID 9779951, 10 pages, 2022.

Hindawi
Evidence-Based Complementary and Alternative Medicine
Volume 2022, Article ID 9779951, 10 pages
https://doi.org/10.1155/2022/9779951

Research Article

The Change of Aqueous Humor Cytokine Levels after Anti-VEGF in Diabetic Macular Edema: A Systematic Review and Meta-Analysis

Aoxiang Wang and Haiyan Wang

Beijing Tongren Eye Center, Beijing Tongren Hospital, Capital Medical University, Beijing Ophthalmology & Visual Sciences Key Lab, Beijing 100730, China

Correspondence should be addressed to Haiyan Wang; wangaox3@mail2.sysu.edu.cn

Received 20 June 2022; Revised 27 July 2022; Accepted 2 August 2022; Published 16 September 2022

Academic Editor: Xueliang Wu

Background. Diabetic macular edema (DME) is a vision-threatening complication that severely impairs vision, and VEGF has a certain improvement effect on it as a growth factor. *Objective*. To assess the alterations of different aqueous humor cytokine concentrations after intravitreal antivascular endothelial growth factor (VEGF) treatment for diabetic macular edema (DME). *Methods*. We searched PubMed, EMBASE, and the Cochrane Library from inception up to May 2022 for studies evaluating the alterations of different aqueous humor cytokine concentrations after intravitreal anti-VEGF treatment for diabetic macular edema. The estimates from eligible studies were meta-analyzed by the Hartung–Knapp/Sidik–Jonkman random-effects method. Egger's regression test was used to determine the publications' bias. A 95% confidence interval was calculated across studies. The analysis was performed using STATA™ Version 15 software. *Results*. Nine eligible studies involving a total of 209 eyes for our systematic review were identified through our search strategy. The mean differences in 1-month and 2-month changes of VEGF were 110.681 pg/ml ($P < 0.001$) and 283.474 pg/ml ($P = 0.003$), respectively. The mean difference in 2-month changes of interleukin 6 (IL-6) was −24.784 pg/ml ($P = 0.037$). The mean difference in 3-month changes of central macular thickness was 130.372 μm ($P < 0.001$). *Conclusions*. Intravitreal injection of anti-VEGF exerts a protective effect on macular edema secondary to diabetic retinopathy by affecting various cytokine concentrations, especially reducing aqueous VEGF concentrations and interleukin 6 in patients with DME.

1. Introduction

Diabetic retinopathy (DR) is a common retinal vascular disease in ophthalmology. It is a diabetic microvascular complication characterized by neovascularization. Hypoxic injury to endothelial cells leads to increased vascular permeability, mainly its early pathological changes. In the middle and late stages, retinal neovascularization and the gradual appearance of fundus proliferative membranes can eventually develop into retinal detachment, vitreous hemorrhage, and severe visual impairment. Diabetic macular edema (DME) is a sight-threatening complication that arises from the breakdown of the blood-retinal barrier (BRB) and a consequent increase in vascular permeability. Approximately 20% and 40% of patients with type 1 and type 2 diabetes mellitus, respectively, have the potential to develop into DME. One-third of patients with a diabetes mellitus duration of more than twenty years will develop DME. [1, 2].

Oxidative processes and inflammatory reactions have been considered significant procedures in the pathogenesis of DME, which lead to the upregulation of multiple cytokines and growth factors. [3, 4] The overexpression of these molecules, including vascular endothelial growth factor (VEGF), angiopoietins, tumor necrosis factor (TNF), monocyte chemoattractant protein (MCP), and so on, is responsible for the dysfunction of BRB and the development of DME. [4].

Tremendous progress has been made in the treatment of DME in recent years. Especially, the recognition of VEGF as the potent regulator to cause vascular leakage has led to the development of VEGF-inhibiting drugs. Anti-VEGF therapy has become the initial treatment option for patients with macular edema secondary to DR. Several anti-VEGF drugs target the VEGF molecule and have slightly different action mechanisms. Ranibizumab is a monoclonal antibody that blocks all isoforms of VEGF-A. Bevacizumab is a full-length humanized monoclonal antibody and blocks all isoforms of VEGF-A. Aflibercept is a soluble protein that contains extracellular VEGF receptor 1 and 2 sequences fused to the Fc domain of a human immunoglobulin-G1 molecule and blocks all isoforms of VEGF [4]. Besides steroids and nonsteroids, anti-inflammatory drugs are also widely used in the clinic because of the important role of inflammation in the pathogenesis of DME. Visual acuity improvement after intravitreal dexamethasone has been confirmed in the previous study [5].

A variety of studies concerning the change of aqueous humor cytokine levels in patients with macular edema caused by DR have been submitted. Despite the growing evidence of clear results, systematic and comprehensive evaluations of cytokine levels after anti-VEGF to treat DME have yet to be published. Therefore, we undertook a meta-analysis of multiple cytokines in aqueous humor to assess the change in those after anti-VEGF intravitreal injection in patients with DME.

2. Methods

2.1. Search and Identification Strategy. We conducted searches of PubMed, EMBASE, and the Cochrane Library from their inception until May 1, 2022, using the terms *diabetic macular edema or DM* and *bevacizumab, ranibizumab, aflibercept, conbercept, anti-VEGF agents,* and *aqueous humor cytokine*. Language or study-design restrictions were not used. When titles and/or abstracts fit our search terms, the abstracts were reviewed to exclude irrelevant studies (e.g., case reports, reviews, or experimental treatments). We then carefully read all the remaining articles to determine whether they contained data that was applicable to our study.

2.2. Inclusion and Exclusion Criteria. The studies were included in the meta-analysis if they fulfilled the following criteria [1]: all observational studies investigating the change of aqueous humor cytokine levels after anti-VEGF treatment in patients with DME [2]; data of aqueous humor cytokine levels pretherapy and post-treatment were reported [3]; all measured data were reported as mean/mean difference and standard deviation. The studies where the mean difference could be calculated indirectly from the data provided in the study were considered eligible for inclusion in our meta-analysis.

We excluded conference abstracts, letters to the editor, case-report studies, systematic reviews, meta-analyses, nonhuman studies, and full texts without raw data for retrieval (a detailed analysis of this study is not possible without the original data).

2.3. Data Extraction and Quality Assessment. The following information on study characteristics and clinical treatments was collected from all included studies: publication metrics (name of the first author), year of publication, location of study, subject information (age, gender, and length of follow-up period), treatment information (applied treatment, injection frequency, and number of subjects in each interventional group), and outcomes at a specific time, including VEGF, interleukin 6 (IL-6), interleukin 8 (IL-8), inducible protein 10 (IP-10), MCP-1, and central macular thickness (CMT). The two authors independently extracted the data from each of these studies using the standardized data extraction format prepared in a Microsoft™Excel worksheet. The two investigators mentioned above assessed the methodologic quality of included studies through a modified version of the Newcastle-Ottawa Scale (NOS) for cohort studies [6]. The NOS was used to assess the risk of bias of the studies by analyzing the following eight items: representativeness of the exposed cohort, selection of nonexposed cohort, ascertainment of exposure, the outcome of the interest declared at the start of the study, comparability of a cohort, assessment of outcome, follow-up duration, and adequacy of follow-up of cohorts [6]. All eligible studies were of moderate or high quality (scored ≥6).

2.4. Statistical Analysis. Means and standard deviations from each outcome group were used to calculate weighted mean differences (WMDs) of each cytokine measurement between different outcome groups, with corresponding 95% confidence intervals (95% CI). In cases where values of cytokine measurement outcomes were not directly available, for example, some studies reported the value using the median, the minimum, and maximum values, and/or the first and third quartiles. We transformed those data into the mean and standard deviation by adopting the Dehui Luo and Xiang Wan method [7, 8]. If there were two subgroups (such as responders and nonresponders) in one study, we used the following formula to combine the two groups into one intervention group [9]:

$$\text{combined } SD = \sqrt{\frac{(N_1 - 1)SD_1^2 + (N_2 - 1)SD_2^2 + (N_1N_2/N_1 + N_2)\left(\left(M_1^2 + M_2^2 - 2M_1M_2\right)\right)}{N_1 + N_2 - 1}}. \quad (1)$$

Table 1: Nine studies were included in our systematic review and were eligible for meta-analysis.

Study	Selection				Comparability	Exposure			
	Represent	Selection	Ascertain	Demon	Comparability of cohorts	Assessment of outcome	Follow-up long enough for outcomes	Adequacy of follow-up	Scores
Japan, Takuya utsumi	☆	☆	☆	—	☆	☆	—	☆	6
Japan, Tomoyasu	☆	☆	☆	—	☆	☆	—	☆	6
Austria, Dominika	☆	☆	☆	—	☆☆	☆	☆	☆	8
Italy, Mastropasqua	☆	☆	☆	—	☆☆	☆	☆	☆	8
Canada, Verena	☆	☆	☆	—	☆	☆	—	☆	6
Canada, Tina	☆	☆	☆	—	☆	☆	—	☆	6
Australia, Shueh	☆	☆	☆	—	☆	☆	—	☆	6
Canada, Roxane	☆	☆	☆	—	☆	☆	—	☆	6
Korea, Hee Jin Sohn	☆	☆	☆	—	☆☆	☆	—	☆	7

Note. represent, representativeness; ascertain, ascertainment; demon, demonstration.

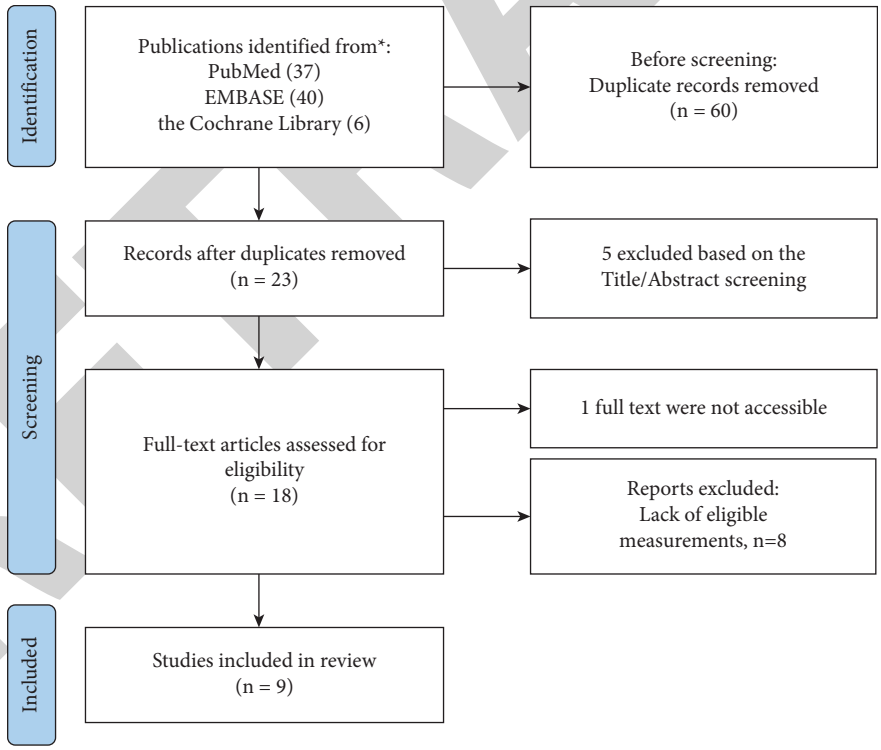

Figure 1: The flow diagram of the literature selective process and reasons for exclusion.

Where N = sample size and M = mean.

We analyzed the quantitative evidence with Stata 15.0 software for Mac. Continuous data were expressed as means and standard deviations and WMD were calculated. Cochran's Q chisquare statistics and I^2 statistical tests were conducted to assess the random variations in primary studies [10]. Herein, $P < 0.1$ and $I^2 \geq 50\%$ indicated considerable heterogeneity. Random effect models were used to pool the data since the interventions varied among the included studies. Potential publication bias was assessed by visually inspecting funnel plots and objectively using the Egger bias test with $P > 0.05$, indicating negative publication

Table 2: Study characteristics of the nine trials in the meta-analysis.

Country, author, year	Study design	Treatment	S.S	Age (y) (Mean ± SD)	Baseline CFT (μm)	Baseline BCVA, logMAR	Cytokine recorded in our meta-analysis	Follow-up month
Japan, Takuya et al., 2021	Self-control (prospective)	Ranibizumab	25	62.9 ± 9.6	560 ± 166	0.51 ± 0.30	VEGF, IL-6, IL-8, IP-10, and MCP-1	1
Austria, Dominika et al., 2020	Self-control (prospective)	Ranibizumab and dexamethasone	9	66.9 ± 8.8; 64.6 ± 9.0*	440 ± 144; 471.3 ± 122.6*	0.70; 0.35*	VEGF, IL-6, IL-8, and MCP-1	2
Canada, Verena et al., 2020	Self-control (prospective)	Aflibercept	17	57.2 ± 8.1	430.9 ± 85.5	0.39 ± 0.16	VEGF, IL-6, IL-8, IP-10, and MCP-1	1 and 2
Canada, Tina et al., 2019	Self-control (prospective)	Ranibizumab	35	62.4 ± 7.3	480.4 ± 117.4	0.60 ± 0.30	VEGF, IL-6, IL-8, and MCP-1	2
Italy, Mastropasqua et al., 2018	Self-control (prospective)	Aflibercept	20	63.4 ± 7.3	469.43 ± 181.91	0.46 ± 0.24	VEGF, IL-6, IL-8, IP-10, and MCP-1	2
Australia, Shueh et al., 2018	Self-control (prospective)	Ranibizumab	25	63.8 ± 9.6	484.5 ± 134.3	0.48 ± 0.20	IL-6, IL-8, IP-10, MCP-1	2
Canada, Roxane et al., 2018	Self-control (prospective)	Ranibizumab	48	61.9 ± 7.1	495.0 ± 134.6	0.60 ± 0.30	VEGF, IL-6, IL-8, and MCP-1	2
Japan, Tomoyasu et al., 2017	Self-control (prospective)	Ranibizumab	13	62.5 ± 11.9	570.0 ± 109.8	0.47 ± 0.25	IL-6, IL-8, IP-10, and MCP-1	1
Korea, Hee Jin Sohn et al., 2011	Self-control (prospective)	Bevacizumab	11	54.4 ± 10.2	387.7 ± 111.3	0.44 ± 0.32	VEGF, IL-6, IL-8, IP-10, and MCP-1	1

Note. S.S, sample size; *the BCVA of two groups in the original text was 74.78 ± 14.85 and 67.22 ± 10.52 presented by Early Treatment Diabetic Retinopathy Study (ETDRS) letter scores. The SD was not available due to lack of raw data.

bias. A sensitivity analysis was used to see the effect of a single study on the overall effect estimation. P values less than 0.05 were defined as significant.

2.5. Presentation and Reporting of Results. The results of this review were reported based on the Preferred Reporting Items for Systematic Review and Meta-Analyses (PRISMA) statement guidelines [11]. The entire process of study screening, selection, and inclusion was described with a flow diagram. The results were presented using forest plots and summary tables.

3. Results

3.1. Baseline Characteristics of Included Studies. We identified 83 publications by the search terms prior to August 2021. After the removal of duplicates, 23 articles were selected for the title and abstract screening, and 5 of them were excluded. The remaining 18 articles were eligible for full-text review. We excluded nine articles since one of them was not available, and eight articles did not include eligible measurements. Thus, nine prospective studies were included in our systematic review and were eligible for meta-analysis [12–19] (Table 1). The literature selection process and reasons for exclusion are summarized in (Figure 1).

Overall, sample sizes varied from 9 to 48 eyes, with a total of 209 eyes included in the analyses, and the duration of follow-up time ranged from 1 to 2 months. The study (ETDRS) letter scores or Snellen acuity fraction were transposed to the logarithm of the minimum angle of resolution (log MAR) units [20]. The mean age ranged from 54.45 to 69.25 years, and the mean baseline BCVA logMAR scores and CMT ranged from 387.7 to 570.0 μm, respectively. There were 5 studies treated with ranibizumab, 2 studies with aflibercept, and 1 with bevacizumab. All eyes received monthly anti-VEGF injection monotherapy in nine studies. To unify this meta-analysis, the selected cytokines in our study were VEGF, IL-6, IL-8, IP-10, and MCP-1 (pm/ml). See Table 2.

3.2. VEGF Level Declined in the Two-Month following after Treatment. The VEGF level of each study from baseline to different follow-up times. One-month following intravitreal treatment, VEGF levels in 53 eyes across three studies declined with a mean of 110.68 pg/ml (95% CI: −163.581 to −57.782 pg/ml, $P = 0.203$, I2=37.2%; figure 2(a)). Two-month following the treatment, VEGF of 169 eyes in five studies with a mean reduction of 283.47 pg/ml (95% CI: −470.40 to 96.54 pg/ml, $P < 0.001$, I2=97.0%; Figure 2(b)).

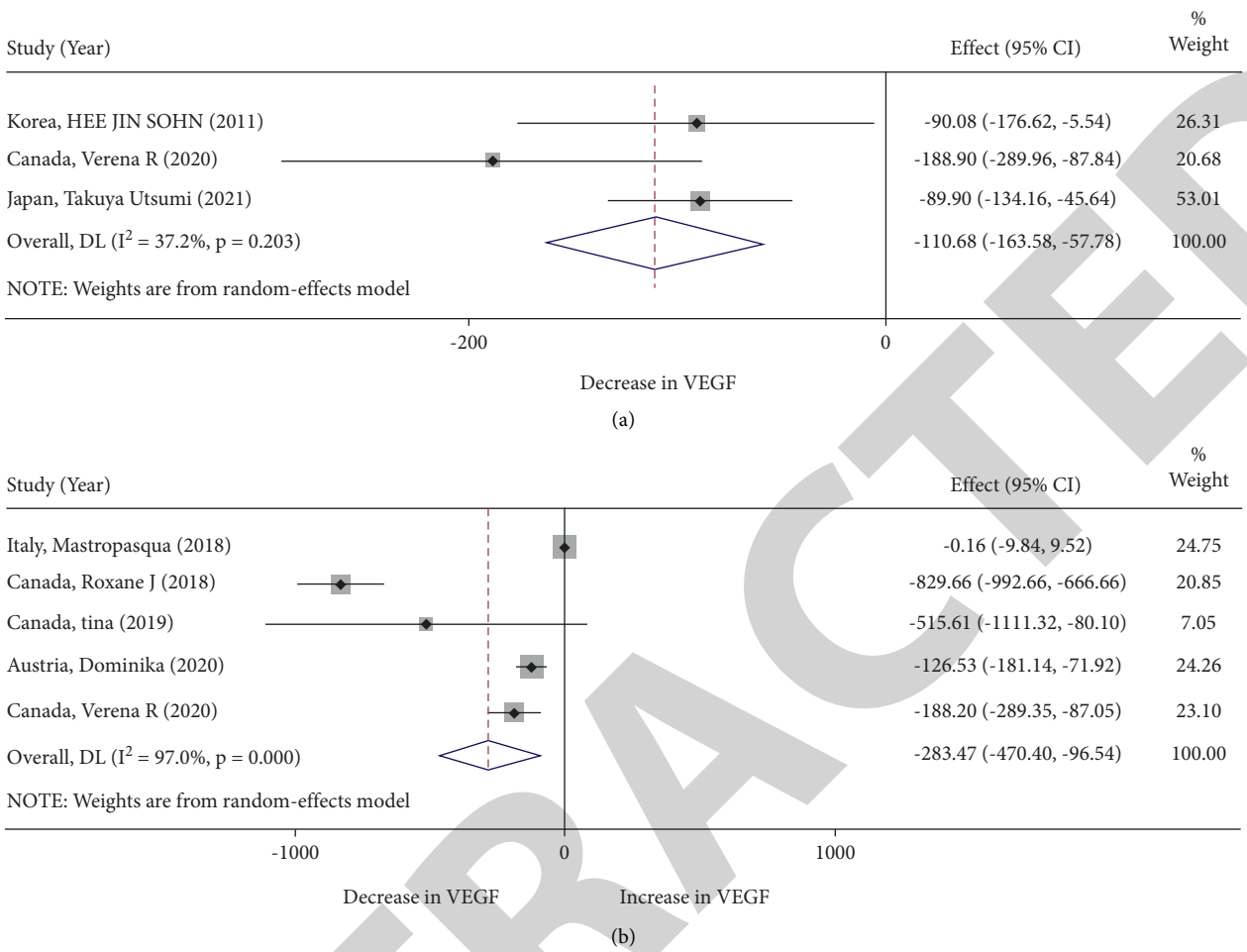

Figure 2: (a) VEGF of 53 eyes in three studies in one month following the intravitreal treatment; (b) VEGF of 169 eyes in five studies in two-month following the intravitreal treatment.

The evidence from Egger's test showed no significant proof of publication bias ($P = 0.07$).

3.3. The IL-6 Level Was Downregulated in One-Month and Two-Month following after Treatment. Four types of research showed IL-6 levels after one-month following the treatment. The IL-6 level was obviously decreased 1 month after treatment (mean level=−16.569 pg/ml, 95% CI: −40.36 to 7.22 pg/ml, $P = 0.029$, I^2=66.7%) and the evidence showed no significant proof of publication bias that was showed after Egger's test ($P = 0.99$). While a mean reduction of −24.78 pg/ml could be found at the 2-month time point (95% CI: −48.13 to −1.43 pg/ml, $P = 0.002$, I^2=73.6%). Sensitivity analysis did not show the effect of a single study on the overall effect estimation as shown in Figure 3.

3.4. The Mean Change of MCP-1, IL-8, and IP-10 in the Posttreatment. There was no significant difference between baseline and posttreatment (including month 1 and month 2) during the mean change of MCP-1(MCP-1 : WMD=−215.18 pg/ml, 95% CI: −599.72 to 169.35 pg/ml, $P = 0.985$, I^2=0.0%; WMD=−102.49 pg/ml, 95% CI: −235.57 to 30.59 pg/ml, $P = 0.192$, $I^2 = 32.5\%$) and IP-10 (WMD=22.54 pg/ml, 95%CI: −55.72 to 100.80 pg/ml, $P = 0.337$, I^2=11.1%; WMD=29.44 pg/ml, 95% CI: −73.66 to 132.54 pg/ml, $P = 0.088$, I^2=58.8%, Egger's test: $P = 0.633$). On the other hand, no alteration of the level of IL-8 was found in the one-month following treatment (WMD=1.85 pg/ml, 95% CI: −5.39 to 9.08 pg/ml, $P = 0.931$, I^2=0.0%); however, a mild drop appeared after two months of treatment (WMD=−0.31 pg/ml, 95% CI: −4.03 to 3.41 pg/ml, $P = 0.045$, I^2=55.9%, Egger's test: $P = 0.55$). The details are shown in Table 3, Figures 4 and 5.

3.5. Central Macular Thickness. Among the nine studies, three recorded the CMT change at the three-month follow-up time. We found a mean thickness of CMT (130.37 μm) of 106 eyes (95% CI: −163.72 to −97.02 μm, $P = 0.388$, I^2=0.0%). The result is displayed in Figure 6.

4. Discussion

Diabetic macular edema is the most common manifestation of DR, which can cause vision impairment in patients with diabetes [19]. In addition, many intraocular cytokines have

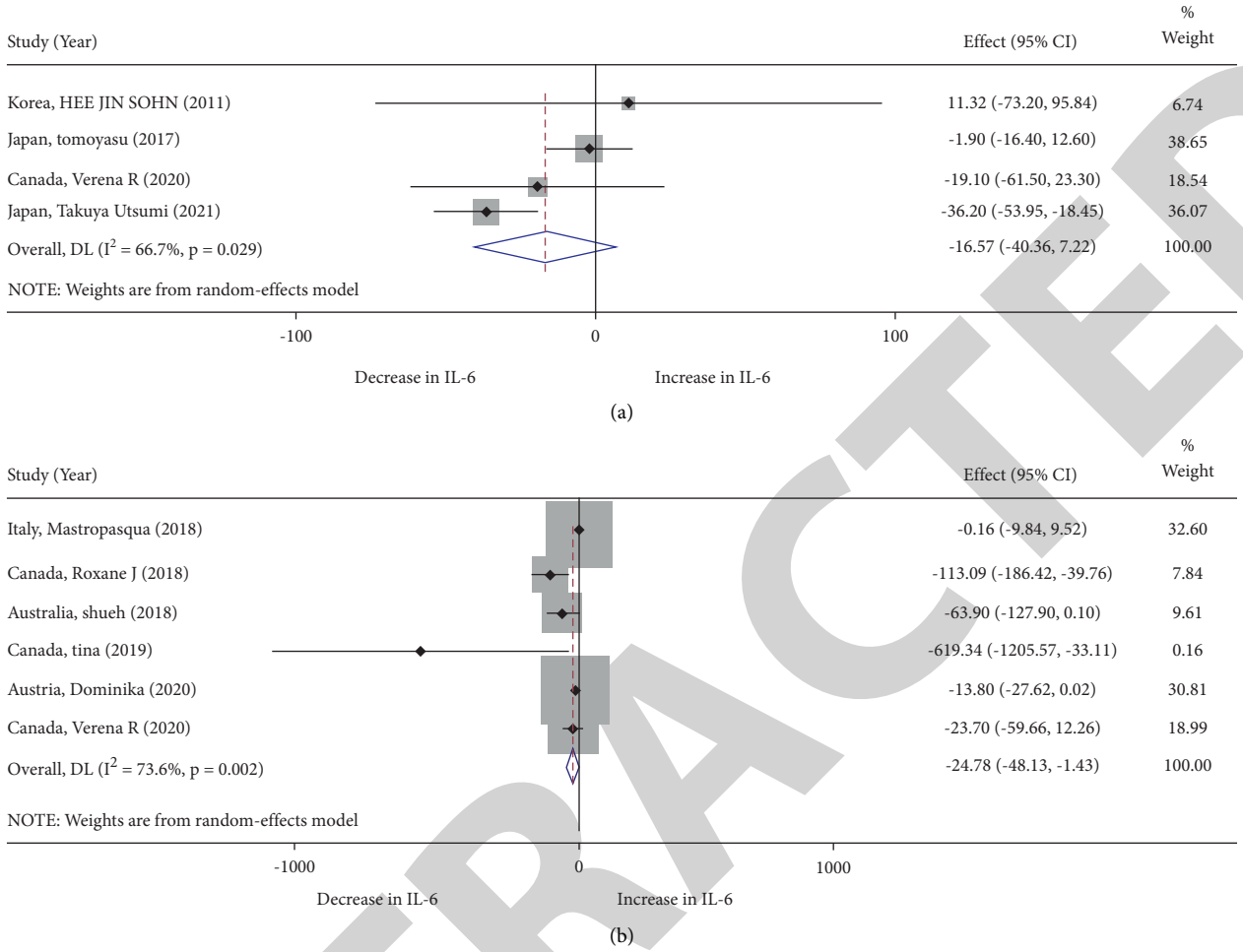

Figure 3: (a) The level of IL-6 in four studies of one-month following the treatment; (b) IL-6 level in six studies of two-month following the treatment.

Table 3: The mean changes of MCP-1, IL-8, and IP-10 after treatment.

Index	WMD (95%CI) pg/ml	I^2 (%)	*P*
After one-month treatment			
MCP	−215.18(−599.72,169.35)	0.0	0.985
IL-8	1.85(−5.39,9.08)	0.0	0.931
IP-10	22.54(−55.72,100.80)	11.1	0.337
After two-month treatment			
MCP	−102.49(−235.57,30.59)	32.5	0.192
IL-8	−0.31(−4.03,3.41)	55.9	0.045*
IP-10	29.44(−73.66,132.54)	58.8	0.088

Note. WMD, weighted mean difference; $^*P < 0.05$.

been involved in the development of DME, which have been reported to demonstrate the severity of DME and have been found to positively correlate with the CMT and cytokine levels [14]. In this meta-analysis, we examined nine studies representing 209 eyes based on a robust search method and precise data extraction following a systematic review process. Based on the studies enrolled in this meta-analysis, most articles reported obvious alterations in VEGF and IL-6, which were consistent with our overall results. Our analysis showed synthesized evidence on the change of different aqueous humor cytokine levels in patients with DME globally. Due to the limited data, it was impossible to evaluate treatment efficacy at longer time points.

Based on the pooled data analysis, VEGF significantly decreased at 1 month and 2 months after anti-VEGF treatment, and the decline of IL-6 and IL-8 can be observed at the

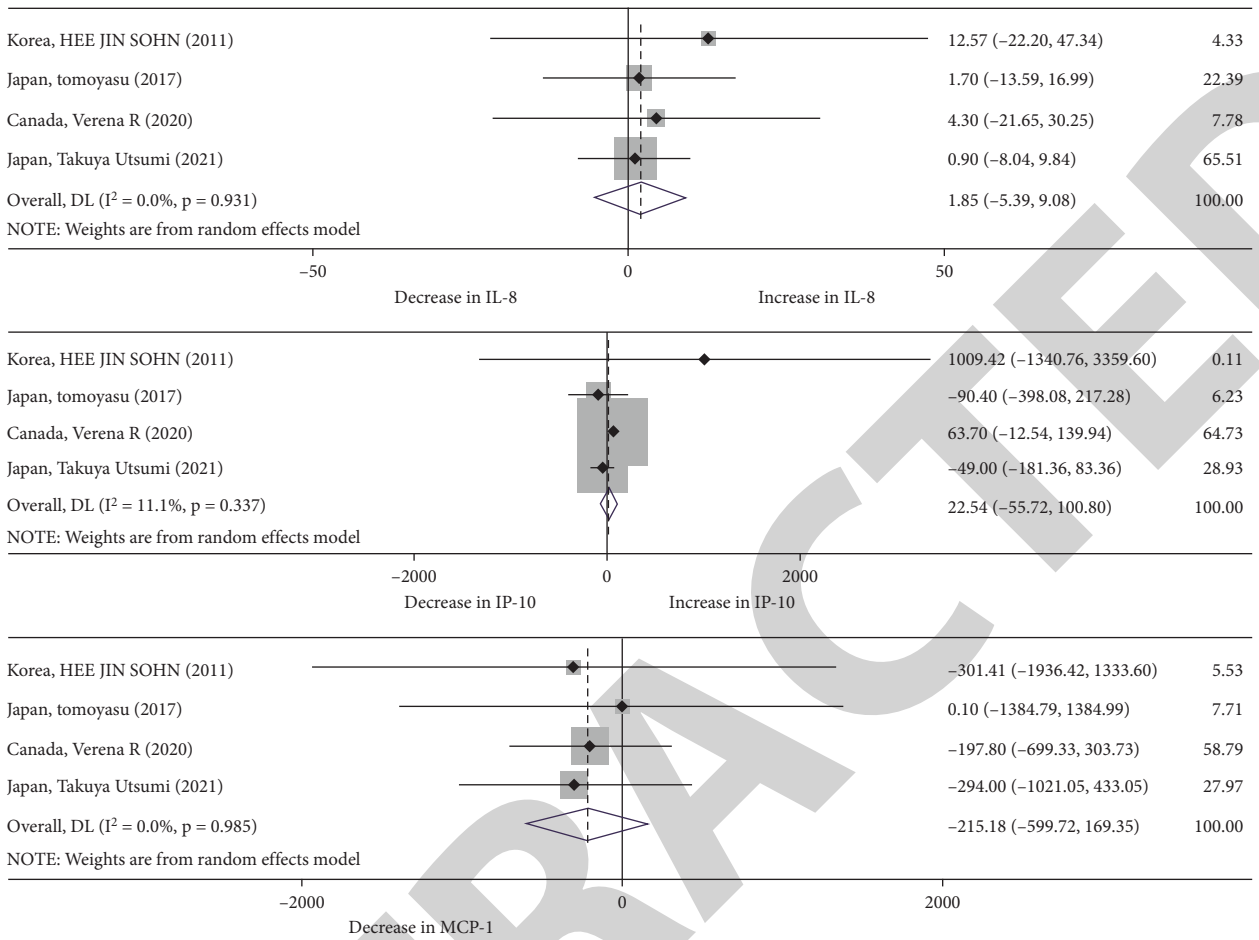

Figure 4: The mean change of IL-8, IP-10, and MCP-1 after 1-month treatment.

2-month follow-up point. The statistical differences were not demonstrated in the alterations of MCP-1 and IP-10 during the follow-up period. In addition, CMT significantly decreased after two monthly intravitreal anti-VEGF injections.

VEGF is a dominant proangiogenic factor and increases microvascular permeability. Vitreous or aqueous levels of VEGF are reportedly related to retinal vascular permeability and the severity of DME. Also, injections of anti-VEGF reagents have become the first-line treatment worldwide in DME patients [21]. Notably, our results demonstrated a decrease in VEGF and CMT. This was evident, which proved the validity of the anti-VEGF treatment during the follow-up time. Our results have demonstrated the statistically significant relationship between eyes with DME undergoing anti-VEGF therapy and lower aqueous humor VEGF concentration early in treatment. Although there was a considerably lower concentration of VEGF in all eyes following two months of anti-VEGF treatment, the 2-month follow-up VEGF concentration was remarkably downregulated compared to that of the baseline.

Some secreted cytokines and growth factors are activated and involved in the procedure of the BRB alteration [20]. IL-6 is an inflammatory cytokine involved in the enhancement of vascular permeability and the alterations of BRB in DME. The level of VEGF has been reported to be strongly correlated with IL-6 concentration in aqueous humor and vitreous, although it has not been found to have any close association between IL-6 and the severity of DME (22). Our results showed that at the 1-month follow-up, the decline was not observed. At the 2-month follow-up, there was a significant decrease in IL-6. Whereas, IL-8 is a main activator and attractant of neutrophils and T lymphocytes and is reported to be related to proliferative DR and related to the IL-8 level change in the aqueous humor which may be difficult to observe in the short term [22, 23]. At the 2-month follow-up, a mild drop in IL-8 level was discovered in our results. Moreover, a previous study has indicated that IL-8 may be a representative marker of chronicity in DR [24]. Therefore, the upregulation of IL-8 may remain for a long time in the aqueous humor.

IP-10 is a cytokine that can enhance immune reactivity but is a potent inhibitor of both IL-8- and FGF-induced angiogenic activity. MCP-1 induces monocyte and macrophage infiltration into tissues without activating neutrophils. A previous study found that IP-10 and MCP-1 were much higher in severe nonproliferative diabetic retinopathy and proliferative DR than in less severe DR (26). In addition, Hideharu and his colleagues

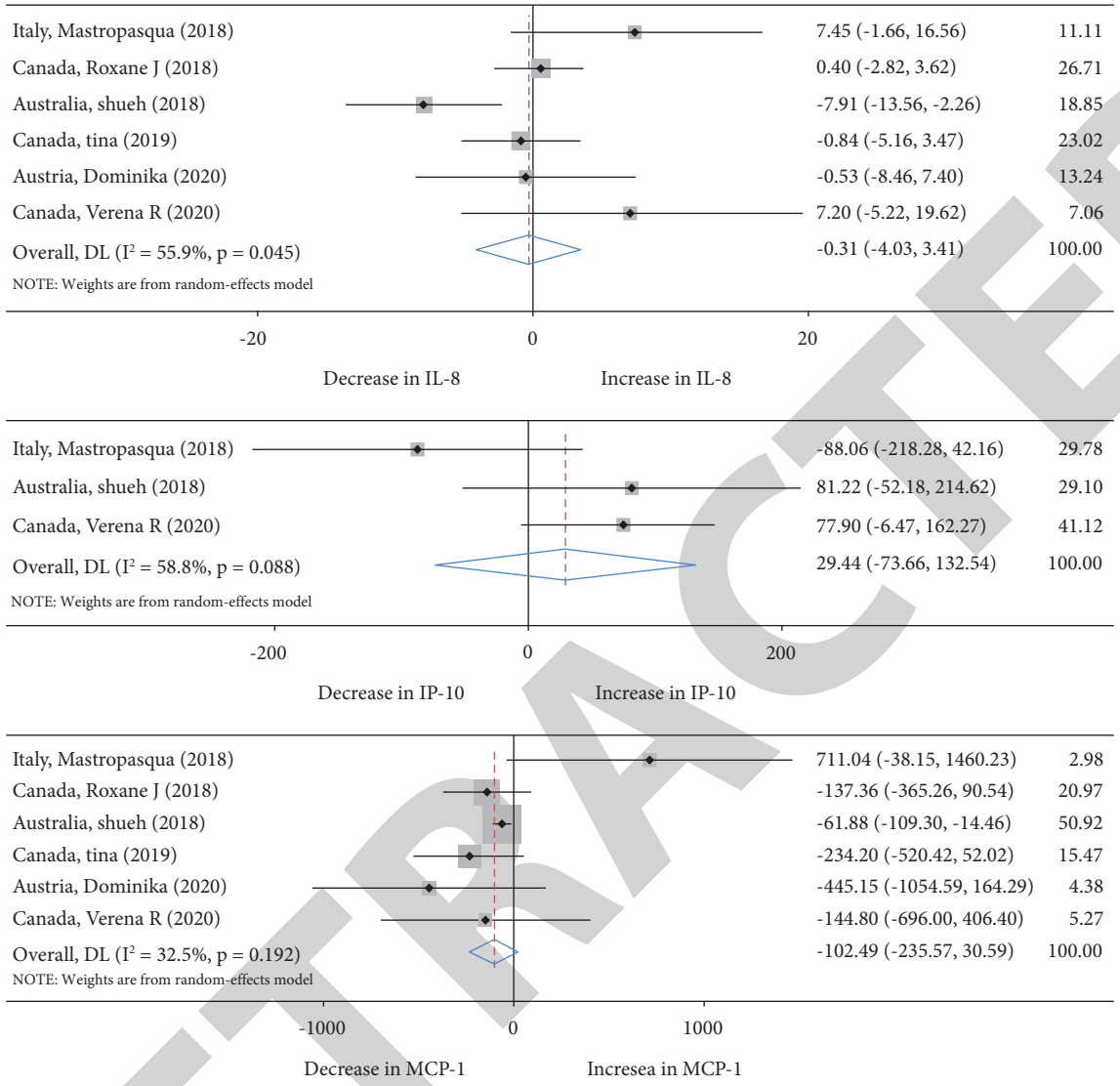

Figure 5: The mean change of IL-8, IP-10, and MCP-1 after two-month treatment.

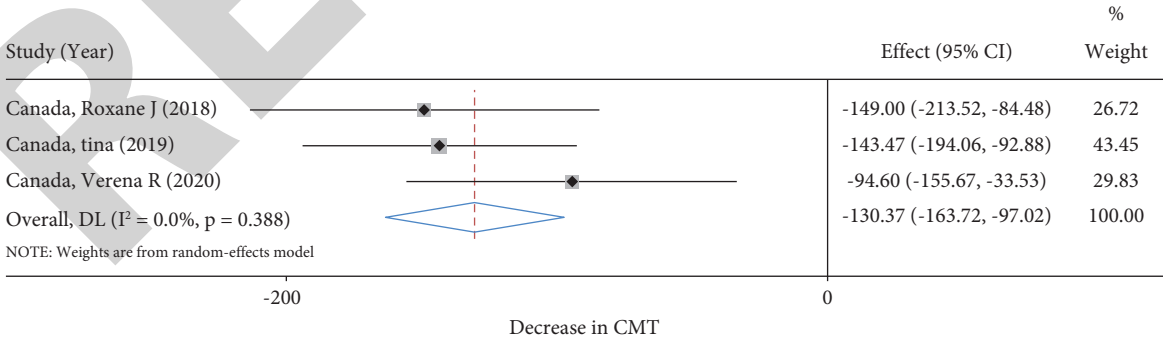

Figure 6: The change in the CMT at the three-month follow-up time.

[25] found that MCP-1 played a relatively less important role than VEGF in DR and DME. These findings may explain why the great changes in MCP-1 and IL-8 cannot be observed in chronic inflammation without a long course of DR.

This study still has a few limitations. First, some cytokines in DME eyes were reported to decrease compared to healthy eyes in previous cross-section studies, but the trends of decline were not found in our results of 2-month follow-up in comparison with the baseline [12, 18, 22, 25–27]. In

addition, more kinds of cytokines should be recruited for further analysis. At last, the efficacy of the change may be related to the category of anti-VEGF drugs. For example, study [14] found that ranibizumab could have a more potent effect on the profile of the intraocular cytokine than bevacizumab. Consequently, a larger sample size and long-term studies are required to investigate changes in different cytokines in aqueous patients suffering from DME and better understand the timing of therapy efficacy for clinics.

5. Conclusion

This study aimed to provide new insights into changes in aqueous humor cytokines following anti-VEGF intravitreal injections in DME. Our results have presented positive evidence for the change of different aqueous cytokine levels after anti-VEGF treatment in patients with DME. These findings may lead to further understanding of the disease process and aid future treatment strategies. Even so, more long-term data are needed to improve this meta-analysis accuracy and provide clinical guidance.

Data Availability

The datasets used and analyzed during the present study are available from the corresponding author upon reasonable request.

Conflicts of Interest

The authors declare that there are no conflicts of interest.

References

[1] R. Klein, M. D. Knudtson, K. E. Lee, R. Gangnon, and B. E. K. Klein, "The Wisconsin Epidemiologic Study of Diabetic Retinopathy XXIII: the twenty-five-year incidence of macular edema in persons with type 1 diabetes," *Ophthalmology*, vol. 116, no. 3, pp. 497–503, 2009.

[2] J. W. Y. Yau, S. L. Rogers, R. Kawasaki et al., "Global prevalence and major risk factors of diabetic retinopathy," *Diabetes Care*, vol. 35, no. 3, pp. 556–564, 2012.

[3] C. Haritoglou, M. Maier, A. S. Neubauer, and A. J. Augustin, "Current concepts of pharmacotherapy of diabetic macular edema," *Expert Opinion on Pharmacotherapy*, vol. 21, no. 4, pp. 467–475, 2020.

[4] A. Das, P. G. McGuire, and S. Rangasamy, "Diabetic macular edema: pathophysiology and novel therapeutic targets," *Ophthalmology*, vol. 122, no. 7, pp. 1375–1394, 2015.

[5] D. S. Boyer, Y. H. Yoon, R. Belfort et al., "Three-year, randomized, sham-controlled trial of dexamethasone intravitreal implant in patients with diabetic macular edema," *Ophthalmology*, vol. 121, no. 10, pp. 1904–1914, 2014.

[6] G. S. B. S. B. Wells and D. O'Connell, "The Newcastle–Ottawa Scale (NOS) for assessing the quality of nonrandomised studies in meta-analyses," https://www.ohri.ca/programs/clinical_epidemiology/..

[7] X. Wan, W. Wang, J. Liu, and T. Tong, "Estimating the sample mean and standard deviation from the sample size, median, range and/or interquartile range," *BMC Medical Research Methodology*, vol. 14, no. 1, p. 135, 2014.

[8] D. Luo, X. Wan, J. Liu, and T. Tong, "Optimally estimating the sample mean from the sample size, median, mid-range, and/or mid-quartile range," *Statistical Methods in Medical Research*, vol. 27, no. 6, pp. 1785–1805, 2018.

[9] S. Zhou, J. Gao, and X. Xu, "Antivascular endothelial growth factors in the treatment of macular oedema secondary to central retinal vein occlusion: a meta-analysis," *Clinical and Experimental Ophthalmology*, vol. 42, no. 7, pp. 637–649, 2014.

[10] T. B. Huedo-Medina, J. Sánchez-Meca, F. Marín-Martínez, and J. Botella, "Assessing heterogeneity in meta-analysis: Q statistic or I2 index?" *Psychological Methods*, vol. 11, no. 2, pp. 193–206, 2006.

[11] M. J. Page, J. E. McKenzie, P. M. Bossuyt et al., "The PRISMA 2020 statement: an updated guideline for reporting systematic reviews," *BMJ*, vol. 372, p. n71, 2021.

[12] H. J. Sohn, D. H. Han, I. T. Kim et al., "Changes in aqueous concentrations of various cytokines after intravitreal triamcinolone versus bevacizumab for diabetic macular edema," *American Journal of Ophthalmology*, vol. 152, no. 4, pp. 686–694, 2011.

[13] R. J. Hillier, E. Ojaimi, D. T. Wong et al., "Aqueous humor cytokine levels and anatomic response to intravitreal ranibizumab in diabetic macular edema," *JAMA ophthalmology*, vol. 136, no. 4, pp. 382–388, 2018.

[14] S. W. Lim, E. Bandala-Sanchez, M. Kolic et al., "The influence of intravitreal ranibizumab on inflammation-associated cytokine concentrations in eyes with diabetic macular edema," *Investigative Ophthalmology & Visual Science*, vol. 59, no. 13, pp. 5382–5390, 2018.

[15] R. Mastropasqua, R. D'Aloisio, M. Di Nicola et al., "Relationship between aqueous humor cytokine level changes and retinal vascular changes after intravitreal aflibercept for diabetic macular edema," *Scientific Reports*, vol. 8, no. 1, Article ID 16548, 2018.

[16] T. Felfeli, V. R. Juncal, R. J. Hillier et al., "Aqueous humor cytokines and long-term response to anti-vascular endothelial growth factor therapy in diabetic macular edema," *American Journal of Ophthalmology*, vol. 206, pp. 176–183, 2019.

[17] T. Shiraya, S. Kato, F. Araki, and T. Ueta, "Effect of intravitreal ranibizumab injection on aqueous humour cytokine levels in patients with diabetic macular oedema," *Acta Ophthalmologica*, vol. 95, no. 4, pp. e340–e341, 2017.

[18] V. R. Juncal, M. Y. K. Mak, M. Bamakrid, and R. H. Muni, "Changes in aqueous cytokine levels following intravitreal aflibercept in treatment-naive patients with diabetic macular edema," *Journal of Ocular Pharmacology and Therapeutics*, vol. 36, no. 9, pp. 697–702, 2020.

[19] T. Utsumi, H. Noma, K. Yasuda, H. Goto, and M. Shimura, "Effects of ranibizumab on growth factors and mediators of inflammation in the aqueous humor of patients with diabetic macular edema," *Graefe's archive for clinical and experimental ophthalmology*, vol. 259, 2021.

[20] N. Z. Gregori, W. Feuer, and P. J. Rosenfeld, "Novel method for analyzing snellen visual acuity measurements," *Retina*, vol. 30, no. 7, pp. 1046–1050, 2010.

[21] Y. Liu, J. Cheng, Y. Gao, L. Qin, X. Min, and M. Zhang, "Efficacy of switching therapy to aflibercept for patients with persistent diabetic macular edema: a systematic review and meta-analysis," *Annals of Translational Medicine*, vol. 8, no. 6, p. 382, 2020.

[22] N. Dong, B. Xu, L. Chu, and X. Tang, "Study of 27 aqueous humor cytokines in type 2 diabetic patients with or without

Hindawi
Evidence-Based Complementary and Alternative Medicine
Volume 2022, Article ID 6880974, 7 pages
https://doi.org/10.1155/2022/6880974

Research Article

Aberrant Expression of SIRT6 and VNN1 in Peripheral Blood Monocytes of Children with Primary Nephrotic Syndrome and Its Diagnostic and Prognostic Values

Peitong Han, Xiaohong Xi, Xiaoying Yuan, Chunzhen Li, Ling Liu, and Jieyuan Cui

Department of Nephrology and Immunology, Children's Hospital of Hebei Province, Shijiazhuang, Hebei Province 050031, China

Correspondence should be addressed to Jieyuan Cui; cjyuan_0@cqmu-edu.cn

Received 27 June 2022; Revised 30 July 2022; Accepted 2 August 2022; Published 15 September 2022

Academic Editor: Xueliang Wu

Objective. The objective is to explore the aberrant sirtuin-6 (SIRT6) and Vanin-1 (VNN1) protein expression in peripheral blood monocytes (PBM) of children with primary nephrotic syndrome (PNS) and its diagnostic and prognostic values. *Methods*. 83 child patients with nephrotic syndrome (NS) and 65 healthy volunteers were enrolled in the study. The test of SIRT6 and VNN1 was performed by the Western blot. The receiver operator characteristic (ROC) curve was used to analyze the diagnostic and prognostic value of SIRT6 and VNN1 for child patients with NS. The logistic regression was used to analyze the association of SIRT6 and VNN1 with the prognosis of NS child patients. *Results*. SIRT6 in monocytes in the study group was inferior versus the control, while VNN1 outweighed it. The AUC of the combined detection of SIRT6 and VNN1 for the diagnosis of NS was 0.854, with a sensitivity of 80.0% and a specificity of 80.7%. The AUC of combined detection of SIRT6 and VNN1 for the prognosis of NS was 0.860, with a sensitivity of 84.6% and a specificity of 79.2%. The logistic regression analysis showed that less than 21.09 in SIRT6 was the number of risk factors for the prognosis of NS child patients ($P < 0.05$). *Conclusion*. SIRT6 and VNN1 are provided with diagnostic and prognostic values for NS.

1. Introduction

Primary nephrotic syndrome (PNS) in children is a group of clinical syndromes in which elevated glomerular basement membrane permeability and loss of large amounts of protein from urine are due to multiple factors [1, 2]. Relevant studies manifest that aberrant nicotinamide adenine dinucleotide-dependent protein deacetylase sirtuin-6 (SIRT6) is available to aggravate renal insufficiency, renal tubular injury, and renal fibrosis, which is closely associated with the occurrence of renal disease [3, 4]. The maintenance of normal renal function requires a great deal of energy, and most of that required for life activities is provided via synthesized adenosine triphosphate (ATP) through the mitochondria. Furthermore, mitochondrial dysfunction is available to affect the renal function of patients, leading to the occurrence of renal disease, while SIRT6 is available to prevent renal tubulointerstitial fibrosis via ameliorating mitochondrial dysfunction, implying that its aberrant expression is supposed to lead to mitochondrial dysfunction and aggravate renal function injury. Vanin-1 (VNN1) is a kind of glycosylated phospholipid adenoinositol-anchored hydrolase in epithelial cells, which is augmented in the liver and kidney [5]. It has been reported that VNN1 is available to repress the antioxidant capacity of platelets, aggravate the oxidative stress response of the body cells, or affect renal function [6, 7]. VNN1 is able to mediate oxidative stress on the body's cells and inflammation. However, its association with the occurrence of nephrotic syndrome (NS) and diagnostic value for this disease are not yet clearly reported. Therefore, this study was to explore SIRT6 and VNN1 in peripheral blood monocytes (PBM) of NS and their values in clinical diagnosis and prognosis, offering references for the clinical diagnosis and evaluation of this disease.

Table 1: Comparison of clinical data between the two.

Classification	The study ($n = 83$)	The control ($n = 65$)	χ^2/t	P
Gender (male/female)	51/32	44/21	0.619	0.432
Age (years)	7.14 ± 1.35	7.36 ± 1.41	0.965	0.336
24 h urine protein quantification (mg/d)	261.35 ± 50.08	115.08 ± 21.35	22.020	<0.001
Serum albumin (g/L)	19.68 ± 3.85	22.31 ± 1.89	5.049	<0.001

2. Materials and Methods

2.1. Clinical Data. From January 2019 to February 2021, 83 child patients with NS were selected for the study group. This study has been approved by the ethics committee of the Children's Hospital of Hebei Province, and informed consent was signed by the guardian of every subject. All of whom met the diagnostic criteria for NS in Evidence-based Guidelines on Diagnosis and Treatment of Primary Nephrotic Syndrome in Children (Trial) [8]. The course of disease of the child patients ranged from 4 months to 2 years, with an average of (0.93 ± 0.13) years. Pathological types: 49 cases of simple NS and 34 cases of nephritis. Clinical symptoms: 79 cases of proteinuria and 69 cases of edema, and the selection of 65 healthy volunteers served as the control. Inclusion criteria: ① under the age of 14; ② complete clinical data. Exclusion criteria: ① child patients with severe cardiovascular and cerebrovascular diseases; ② child patients with autoimmune diseases involving systemic lupus erythematosus and allergic purpura; ③ child patients with congenital NS; ④ child patients with other types of nephropathies; ⑤ child patients with combined tumor diseases. No distinct differences were found in gender and age between the two ($P < 0.05$), as proved in Table 1.

2.2. Methods. Protein determinations of SIRT6 and VNN1 in monocytes are as follows: the collection of 20 mL fasting venous blood was from child patients within 24 h after admission and children in the control, and the division of samples was into two parts. SIRT6 protein in the samples was determined, and dilution was with an equal volume of Hank solution, and the addition of 20 mL of Ficoll solution was with a density of 1.007 (all the Institute of Bioengineering, Chinese Academy of Medical Sciences). The adoption of a SORVALL cryogenic centrifuge (Kojun Instrument Co., Ltd., USA) was for centrifugation. The mononuclear cell was sucked from the milky layer and centrifuged again after washing with Hank's solution. After trypan blue staining, a cell culture was performed in Roswell Park Memorial Institute 1640 medium, and the addition of 80 μL sodium dodecyl sulfate (SDS) and a phenylmethylsulfonyl fluoride mixture of (100 : 1) was made into each culture well. Placement of the culture plate was on the ice for lysis, and the shift of the cell lysis solution to an Eppendorf (EP) tube. After centrifugation, the shift of the protein solution was to a clean EP tube and the determination of the sample protein concentration was via the Bio-Rad QuantaPhase II radioassay enzyme-linked immunosorbent assay. The remaining proteins were added to a quarter volume of 5 × SDS loading buffer, boiled for 10 min, and stored in a refrigerator after cooling as a standby. The addition of 1 × SDS loading buffer was made into a 20 μL protein sample, and centrifugation was carried out at the same rate. After collecting the supernatant, the equivalent protein was added to 12% sodium dodecyl sulfate polyacrylamide gel electrophoresis gel well, then electroblotted onto a Polyvinylidene fluoride membrane, and sealed with a phosphate buffer solution involving 5% skim milk powder. The addition of diluted rabbit anti-SIRT6 (Abcam, UK, 1 : 5000) after equilibrium was reached at temperature, and then the accretion of 5 mL of diluted goat anti-rabbit secondary antibody (1 : 5000) was for the reaction. Meanwhile, the adoption of the Leica Quantimet 550 DMRXA chemiluminescence and image analysis system was for analysis, and calculation was with the ratio of the target and the internal reference gray values. The determination of VNN1 was done via the same method as the control. Monoclonal rabbit antihuman VNN1 primary antibody and sheep antimouse VNN1 secondary antibody (all Abcam, Britain) were adopted.

2.3. Observation Indexes. (1) The test of SIRT6 and VNN1 in monocytes of patients in the study group and healthy subjects in the control was performed via Western blot, comparison, and then analysis their diagnostic value for NS. (2) The division of child patients was into the severe and the mild groups in line with the occurrence of complications (acute renal failure, thrombosis, electrolyte disturbance, infection, renal tubular dysfunction, etc.), analysis of the assessed values of SIRT6 and VNN1, and the severity of NS child patients. (3) The treatment of child patients was via referring to evidence-based Guidelines for Diagnosis and Treatment of Primary Nephrotic Syndrome in Children (Trial) [8], and the division into good prognosis (positive urinary protein <+++) and unpleasing prognosis (positive urinary protein ≥+++) was in line with the disease outcome after 4 weeks of treatment. An analysis of the predictive values of SIRT6 and VNN1 on the prognosis of child patients with NS and its association with an unpleasing prognosis was adopted.

2.4. Statistical Treatment. Application of SPSS24.0 software was to process the data, representation of enumeration data was as percent, and the comparison of the differences of groups was via χ^2 test. Expression of the measurement data was as $(\overline{x} \pm s)$ after the normal test. The comparison of the differences between groups was via the t-test. The exertion of the receiver operator characteristic (ROC) curve was to analyze the diagnostic value of SIRT6 and VNN1 for NS and the assessed value for the disease of child patients. The

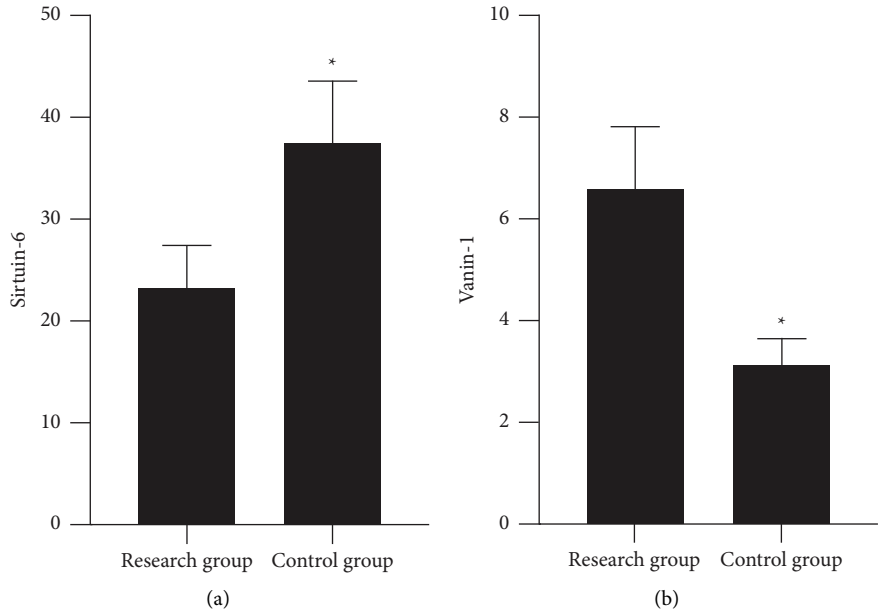

Figure 1: The comparison of SIRT6 and VNN1 is between the study and the control versus the study; $^*P < 0.05$. (a) The SIRT6 in two groups. (b) The VNN1 in two groups.

Table 2: Analysis of diagnostic value of SIRT6 and VNN1 for NS.

Indexes	Cut-off values	AUC	SE	95% CI	Specificity	Sensitivity
SIRT6	25.07	0.751	0.040	0.673~0.830	0.663	0.785
VNN1	5.26	0.794	0.037	0.721~0.866	0.675	0.862
Combined detection		0.854	0.031	0.794~0.914	0.807	0.800

employment of logistic regression was to analyze the association of SIRT6 with VNN1 and the unpleasing prognosis of NS child patients. $P < 0.05$ was accepted as indicative of distinct differences.

3. Results

3.1. Comparison of SIRT6 and VNN1 is between the Study and the Control Groups. SIRT6 in monocytes in the study declined versus the control, while VNN1 ascended ($P < 0.05$), as proved in Figures 1(a) and 1(b).

3.2. The Diagnostic Value of SIRT6 and VNN1 in NS Is Analyzed. The AUC of SIRT6 and VNN1, jointly detecting NS, outweighed the two alone ($P < 0.05$), as proved in Table 2 and Figure 2.

3.3. Comparison of SIRT6 and VNN1 is between the Mild and the Severe. SIRT6 in monocytes in the severe declined versus the mild, while VNN1 was elevated ($P < 0.05$), as proved in Figure 3.

3.4. Assessed Value of SIRT6 and VNN1 is on the Degree of Renal Function Impairment. The AUC of SIRT6 and VNN1, jointly examining and assessing the degree of renal function

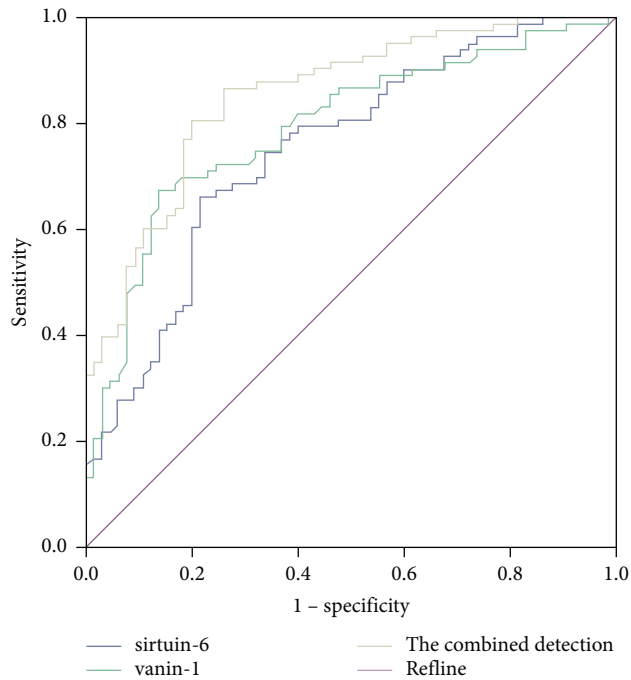

Figure 2: The ROC curve analysis of SIR6 and VNN1 is for the diagnosis of NS.

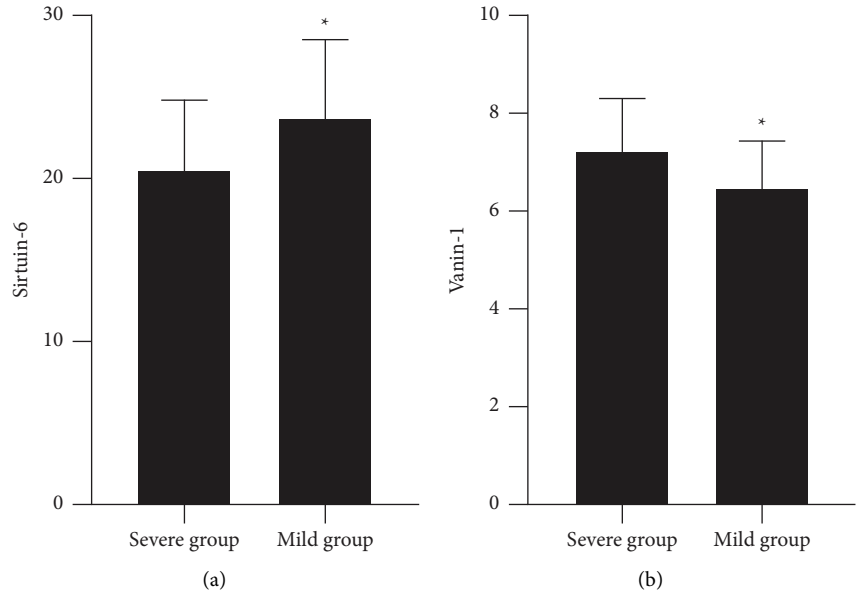

Figure 3: The comparison of SIRT6 and VNN1 is between the mild and the severe versus the severe, $^{*}P < 0.05$.

Table 3: Analysis of assessed value of SIRT6 and VNN1 on the degree of renal function impairment.

Indexes	Cut-off values	AUC	SE	95% CI	Specificity	Sensitivity
SIRT6	21.68	0.630*	0.084	0.465~0.795	0.602	0.778
VNN1	5.37	0.672	0.085	0.506~0.839	0.566	0.831
Combined detection		0.705	0.090	0.528~0.881	0.653	0.815

Versus combined detection, $^{*}P < 0.05$.

impairment in NS child patients, outweighed SIRT6 alone ($P < 0.05$), as proved in Table 3 and Figure 4.

3.5. Comparison of SIRT6 and VNN1 is between the Good and the Unpleasing Prognosis. SIRT6 in monocytes with an unpleasing prognosis was inferior than in those with a good prognosis, while VNN1 ascended ($P < 0.05$), as shown in Figure 5.

3.6. Assessed Value of SIRT6 and VNN1 in Prognosis Is Analyzed. The AUC of SIRT6 and VNN1, jointly detecting and assessing prognosis in NS child patients, outweighed SIRT6 alone ($P < 0.05$), as proved in Table 4 and Figure 6.

3.7. Correlation of SIRT6 with VNN1 is with Prognosis of NS Child Patients. Less than 21.09 in SIRT6 was the number of risk factors for the prognosis of NS child patients ($P < 0.05$), as shown in Tables 5 and 6.

4. Discussion

VNN1 is the critical molecule that modulates the dependent reaction of glutathione to oxidative damage in epithelial cells. Relevant studies have testified that urinary VNN1 distinctly ascends in patients with nephropathy, implying that urinary VNN1 is able to be employed as a biomarker of renal tubular injury [9, 10]. Presently, the role of SIRT6 in a

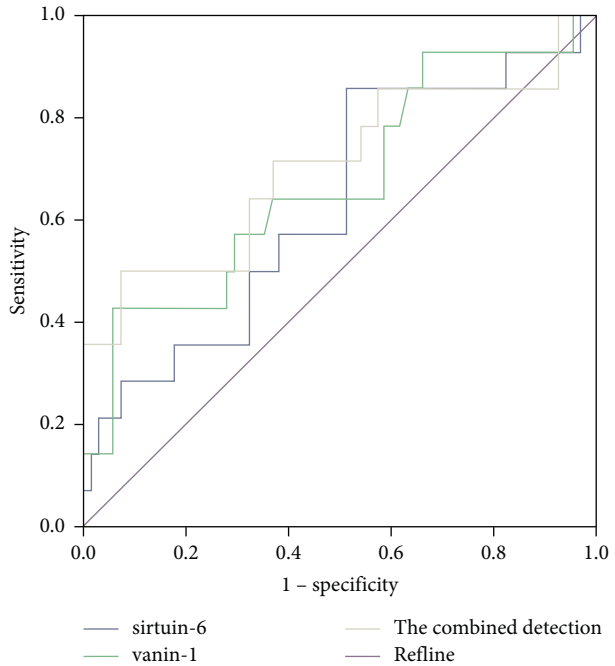

Figure 4: The ROC curve analysis of SIRT6 and VNN1 is to assess the degree of renal function impairment.

variety of diseases is yet disputable, and some scholars maintain that it is a tumor suppressor modulating the

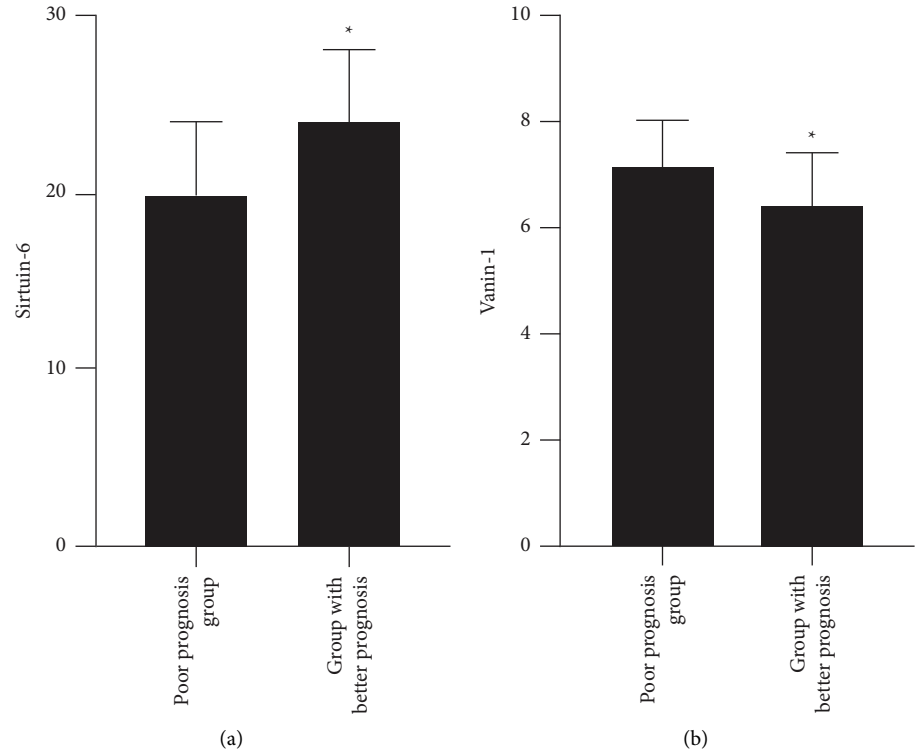

Figure 5: The comparison of SIRT6 and VNN1 is between the good and unpleasing prognosis versus the unpleasing prognosis; $^{*}P < 0.05$.

Table 4: Analysis of assessed value of SIRT6 and VNN1 in prognosis.

Indexes	Cut-off values	AUC	SE	95% CI	Specificity	Sensitivity
SIRT6	21.09	0.699*	0.072	0.557~0.841	0.554	0.762
VNN1	5.54	0.829	0.049	0.733~0.924	0.751	0.815
Combined detection		0.860	0.041	0.779~0.942	0.792	0.846

Versus combined detection, $^{*}P < 0.05$.

occurrence and advancement of multiple tumor diseases [11, 12]. However, SIRT6 is elevated in cancers involving prostate cancer or breast cancer and is available to exert a role as an oncogene [13, 14]. Additionally, it is the same in small-cell lung cancer. SIRT6 is available to modulate glucose metabolic homeostasis via repressing glycolysis-related genes. When SIRT6 is inactivated, acetylation of glycolysis gene promoters and multiple metabolic genes are elevated, ultimately affecting the glycolysis process [15]. Relevant studies manifest the correlation of SIRT6 with diversified cell functions, involving DNA repair, antioxidant activity, cell proliferation, and mitochondrial energy homeostasis [16]. Nevertheless, cellular mitochondrial function was associated with renal function. SIRT6 is supposed to be correlated with renal dysfunction. In this study, aberrant SIRT6 and VNN1 in monocytes were verified in child patients with NS. Additionally, the study documented that the combined detection of SIRT6 and VNN1 is provided with diagnostic values for NS, so SIRT6 and VNN1 in monocytes are supposed to be applied to the initial diagnosis of NS.

The kidney is one of the most energy-demanding organs in the human body, which requires a great deal of ATP production via mitochondria to meet its physiological requirements [17]. Relevant studies testify that SIRT6 is nearly

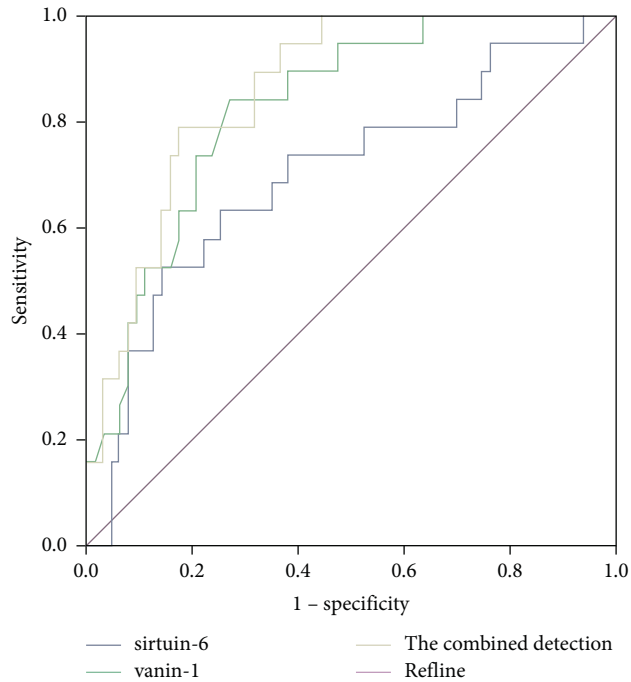

Figure 6: The ROC curve analysis of SIRT6 and VNN1 is conducted to predict prognosis.

Table 5: Univariate analysis of SIRT6 and VNN1 and prognosis of NS child patients.

Indexes		The unpleasing prognosis ($n = 19$)	The good prognosis ($n = 64$)	χ^2	P
SIRT6	≥21.09	5	52	20.552	<0.001
	<21.09	14	12		
VNN1	≥5.54	12	11	15.456	<0.001
	<5.54	7	53		

Table 6: Logistic regression analysis of SIRT6 and VNN1 and prognosis of NS child patients.

Indexes	β	SE	Wald χ^2	OR	95% CI	P
SIRT6	−0.155	0.078	3.949	0.856	0.735~0.998	0.048
VNN1	1.822	0.527	2.433	2.275	0.810~6.391	0.120
Constant	−7.141	4.260	2.810	0.001	0.000~3.349	0.094

Value assignment: SIRT6 (21.09 or more is 1, less than 21.09 is 0); VNN1 (5.54 or more is 1, less than 5.54 is 0).

correlated to the mitochondrial function of body cells [18, 19]. SIRT6 exerts a critical role in antioxidant stress, mitochondrial substrate metabolism, and cell survival, and is able to mitigate the severity of renal tubular injury via protecting mitochondrial integrity [20, 21]. The study manifested that the AUC of SIRT6 and VNN1 jointly examining and evaluating the degree of renal function impairment in NS child patients outweighed SIRT6 alone, illustrating that the combined detection of SIRT6 and VNN1 provides an assessed value in the severity of the disease in NS child patients.

Renal injury mainly affects renal tubules, and tubular cells involve more mitochondria. It has been reported that SIRT deficiency aggravates early fibrosis in acute renal injury induced via ischemia-reperfusion in mice [22, 23]. The authors maintain that aberrant SIRT6 is supposed to exacerbate renal tissue fibrosis or critically affect the prognosis of child patients. This study documented that less than 21.09 of SIRT6 exerts a deteriorative influence on the prognosis of NS child patients, and its specific mechanism is yet unknown. Furthermore, the author maintains that this is supposed to be correlated to the fact that declined SIRT6 is available to augment the apoptosis and mitochondrial damage of renal tubular epithelial cells. Additionally, declining SIRT6 is able to aggravate the oxidative stress response and augment inflammatory damage, which is also one of the reasons for the unpleasing prognosis [24, 25]. The study stated that the AUC of the combined examination of SIRT6 and VNN1 to assess the prognosis of NS child patients outweighed SIRT6 alone, manifesting that the combined assay provided predictive value for the prognosis of NS child patients.

In short, aberrant SIRT6 and VNN1 in monocytes are proven in NS child patients, which provides diagnostic value for NS and assesses value for disease severity and prognosis.

Data Availability

The data used to support the findings of this study are available from the corresponding author upon request.

Conflicts of Interest

The author(s) declare that there are conflicts of interest.

Acknowledgments

The authors would like to thank a series of studies on the correlation between CD20 expression and the pathogenesis and recurrence mechanism of childhood nephrotic syndrome and anti-CD20 monoclonal antibody treatment.

References

[1] A. M. Schijvens, L. van der Weerd, J. A. E. van Wijk et al., "Practice variations in the management of childhood nephrotic syndrome in The Netherlands," *European Journal of Pediatrics*, vol. 180, no. 6, pp. 1885–1894, 2021.

[2] M. Kallash and J. D. Mahan, "Mechanisms and management of edema in pediatric nephrotic syndrome," *Pediatric Nephrology*, vol. 36, no. 7, pp. 1719–1730, 2021.

[3] A. P. Waller, J. P. Troost, S. V. Parikh et al., "Nephrotic syndrome disease activity is proportional to its associated hypercoagulopathy," *Thrombosis Research*, vol. 201, no. 5, pp. 50–59, 2021.

[4] Y. Sun, X. Hu, G. Hu, C. Xu, and H. Jiang, "Curcumin attenuates hydrogen peroxide-induced premature senescence via the activation of SIRT1 in human umbilical vein endothelial cells," *Biological and Pharmaceutical Bulletin*, vol. 38, no. 8, pp. 1134–1141, 2015.

[5] N. D'Onofrio, L. Servillo, and M. L. Balestrieri, "SIRT1 and SIRT6 signaling pathways in cardiovascular disease protection," *Antioxidants and Redox Signaling*, vol. 28, no. 8, pp. 711–732, 2018.

[6] C. Zhaohui and W. Shuihua, "Protective effects of SIRT6 against inflammation, oxidative stress, and cell apoptosis in spinal cord injury," *Journal of Inflammation*, vol. 43, no. 5, pp. 1751–1758, 2020.

[7] D. W. Ferreira, P. Naquet, and J. E. Manautou, "Influence of VNN1 and catalytic products in liver during normal and oxidative stress conditions," *Current Medicinal Chemistry*, vol. 22, no. 20, pp. 2407–2416, 2015.

[8] A. Liu, "Interpretation of evidence-based Guidelines for diagnosis and treatment of primary nephrotic syndrome in children (trial)," *Zhejiang Medical*, vol. 32, no. 8, pp. 1139-1140, 2010.

[9] M. Karami, F. Mehrabi, A. Allameh, M. Pahlevan Kakhki, M. Amiri, and M. S. Emami Aleagha, "Klotho gene expression decreases in peripheral blood monocytes cells (PBMCs) of patients with relapsing-remitting multiple sclerosis," *Journal of Neurological Sciences*, vol. 381, no. 10, pp. 305–307, 2017.

[10] N. Kavian, S. Mehlal, W. Marut et al., "Imbalance of the VNN1 pathway in systemic sclerosis," *The Journal of Immunology*, vol. 197, no. 8, pp. 3326–3335, 2016.

[11] C. Fang, Y. Liu, L. Chen et al., "α-Hederin inhibits the growth of lung cancer A549 cells in vitro and in vivo by decreasing SIRT6 dependent glycolysis," *Pharmacien Biologiste*, vol. 59, no. 1, pp. 11–20, 2021.

[12] C. Zhang, Y. Yu, Q. Huang, and K. Tang, "SIRT6 regulates the proliferation and apoptosis of hepatocellular carcinoma via the ERK1/2 signaling pathway," *Molecular Medicine Reports*, vol. 20, no. 2, pp. 1575–1582, 2019.

[13] B. Sosnowska, M. Mazidi, P. Penson, A. Gluba-Brzózka, J. Rysz, and M. Banach, "The sirtuin family members SIRT1, SIRT3 and SIRT6: their role in vascular biology and atherogenesis," *Atherosclerosis*, vol. 265, no. 10, pp. 275–282, 2017.

[14] A. Dijk, F. W. Hoff, E. Bont et al., "Signatures of histone modification marks and proteins in pediatric acute myeloid leukemia: a comparison to adults," *Blood*, vol. 132, no. 1, p. 2761, 2018.

[15] S. L. M. Blokland, M. R. Hillen, A. A. Kruize et al., "Increased CCL25 and T helper cells expressing CCR9 in the salivary glands of patients with primary sjögren's syndrome: potential new Axis in lymphoid neogenesis," *Arthritis & Rheumatology*, vol. 69, no. 10, pp. 2038–2051, 2017.

[16] J. Guo, J. Zhao, R. Liu et al., "Metabolomics analysis of serum in pediatric nephrotic syndrome based on targeted and non-targeted platforms," *Metabolomics*, vol. 17, no. 4, p. 38, 2021.

[17] M. Simon, M. Van Meter, J. Ablaeva et al., "LINE1 derepression in aged wild-type and SIRT6-deficient mice drives inflammation," *Cell Metabolism*, vol. 29, no. 4, pp. 871–885, 2019.

[18] N. Tripathi, A. Singh, and P. Agarwal, "Worsening anasarca on a child with severe steroid-dependent nephrotic syndrome without proteinuria: answers," *Pediatric Nephrology*, vol. 25, no. 5, pp. 1–6, 2021.

[19] A. Watanabe, M. S. Guaragna, V. M. S. Belangero et al., "APOL1 in an ethnically diverse pediatric population with nephrotic syndrome: implications in focal segmental glomerulosclerosis and other diagnoses," *Pediatric Nephrology*, vol. 36, no. 8, pp. 2327–2336, 2021.

[20] X. Fan, K. Yan, and Q. Meng, "Aberrant expression of SIRTs in psoriasis: decreased expression of SIRT 1-5 and increased expression of SIRT 6 and 7," *International Journal of Molecular Medicine*, vol. 44, no. 2, pp. 157–171, 2019.

[21] S. Raj, L. A. Dsouza, S. P. Singh, and A. Kanwal, "Sirt6 deacetylase: a potential key regulator in the prevention of obesity, diabetes and neurodegenerative disease," *Frontiers in Pharmacology*, vol. 11, no. 7, Article ID 598326, 2020.

[22] S. Washino, K. Hosohata, and M. Oshima, "MP77-08 VNN1, a novel acute kidney injury marker, is a useful biomarker for adult upper urinery tract obstruction induced kidey injury," *Journal d'Urologie*, vol. 201, no. 4, pp. 1–7, 2019.

[23] K. Hosohata, D. Jin, S. Takai, and K. Iwanaga, "Involvement of VNN1 in ameliorating effect of oxidative renal tubular injury in dahl-salt sensitive rats," *International Journal of Molecular Sciences*, vol. 20, no. 18, p. 4481, 2019.

[24] O. Govaere, J. Palmer, M. Zhuang, and M. Y. W. Zaki, "The vanin 1-cysteamine pathway regulates immune tolerance upon lipid-induced oxidative stress in non-alcoholic fatty liver disease," *Journal of Hepatology*, vol. 68, no. 3, p. S339, 2018.

[25] K. Hosohata, D. Jin, S. Takai, and K. Iwanaga, "VNN1 in renal pelvic urine reflects kidney injury in a rat model of hydronephrosis," *International Journal of Molecular Sciences*, vol. 19, no. 10, p. 3186, 2018.

Hindawi
Evidence-Based Complementary and Alternative Medicine
Volume 2022, Article ID 7332337, 11 pages
https://doi.org/10.1155/2022/7332337

Research Article

HBV Promotes the Proliferation of Liver Cancer Cells through the hsa_circ_0000847/miR-135a Pathway

Jianjun Lin,[1] **Xiang Lian**,[2] **Shihang Xue**,[3] **Lian Ouyang**,[4] **Lihui Zhou**,[4] **Yuyang Lu**,[5] **and Longteng Xie**[2]

[1]*Department of Clinical Laboratory, Xiangshan First People's Hospital, Ningbo Fourth Hospital, Ningbo 315700, China*
[2]*Hepatology Department, Xiangshan First People's Hospital, Ningbo Fourth Hospital, Ningbo 315700, China*
[3]*Department of General Surgery, Xiangshan First People's Hospital, Ningbo Fourth Hospital, Ningbo 315700, China*
[4]*Department of Orthopaedic Surgery, Xiangshan First People's Hospital, Ningbo Fourth Hospital, Ningbo 315700, China*
[5]*Xiangshan County Center for Disease Control and Prevention, Ningbo 315700, China*

Correspondence should be addressed to Yuyang Lu; 390487428@qq.com and Longteng Xie; xfxlt@126.com

Received 23 July 2022; Revised 18 August 2022; Accepted 23 August 2022; Published 15 September 2022

Academic Editor: Xueliang Wu

Hepatocellular carcinoma (HCC) is currently one of the most common tumors, with a high morbidity and mortality rate. HCC induced by persistent hepatitis *B* virus (HBV) infection is the most common liver cancer subtype at present, and HBV-related HCC is highly malignant and its development mechanism still needs to be explored in depth. This study aimed to explore the molecular mechanism of hsa_circ_0000847 targeting miR-135a-5p (miR-135a) to regulate the proliferation, invasion, and apoptosis of liver cancer cells. The study found that the expression level of hsa_circ_0000847 in liver cancer tissues and cells was significantly increased, while the expression level of miR-135a was significantly decreased. Hsa_circ_0000847 promoted the proliferation of liver cancer cells and elevated the expression of the proliferation-related protein. In addition, hsa_circ_0000847 could promote the invasion of HBV-infected liver cancer cells and inhibit the cell apoptosis of liver cancer cells. At the same time, it significantly promoted the expression of antiapoptotic proteins and inhibited the expression of proapoptotic protein. Interestingly, the dual luciferase experiment proved that hsa_circ_0000847 directly targeted miR-135a. On the other hand, the combined effect of hsa_circ_0000847 and miR-135a further illustrated the effect of hsa_circ_0000847 on the proliferation, invasion, and apoptosis of liver cancer cells. In addition, further experiments have also found that HBV could promote the expression of p-p38, p-ERK, and p-JNK through the hsa_circ_0000847/miR-135a axis, thereby further activating the MAPK pathway. In short, HBV promotes the proliferation and invasion of liver cancer cells and inhibits apoptosis by regulating the hsa_circ_0000847/miR-135a pathway, which provided a theoretical basis for effective treatment of HBV-infected liver cancers.

1. Introduction

Hepatocellular carcinoma (HCC) is currently one of the most common malignant tumors, with a high incidence and fatality rate worldwide [1]. Although liver transplantation and surgical treatment have obtained good results as the first-line treatment of liver cancers, the clinical data show that the 5-year survival rate of patients with liver cancers is still not high [2]. The main reason is that liver cancers exert a markedly high survival rate, high degree of malignancy, rapid growth and proliferation ability, and high metastasis rate [3]. Therefore, a better understanding of the molecular mechanism of the growth and metastasis of liver cancer cells is essential for the treatment of HCC. Studies have pointed out that the loss of control of tumor cell growth and the malignant proliferation of tumor cells is an important reason for the malignant development of tumors [4]. On the one hand, the malignant proliferation of tumor cells may lead to the activation of oncogenes, which accelerates the cell cycle process [5]. On the other hand, the cell apoptosis might be inhibited and the cell gains "immortality," so that it loses control and proliferates malignantly [6]. In addition to the malignant proliferation, tumor metastasis is also an important cause of cancer death [7]. The main cause of

metastasis is the acquisition of tumor cell migration and invasion capability. The occurrence and development of liver cancer is an extremely complex process, which is triggered by many factors. Among them, hepatitis *B* virus (HBV) is an important cause of hepatocellular carcinoma. About 80% of liver cancers are caused by HBV infection [8]. Recent studies have shown that the viral protein of HBV itself can promote the malignant development of liver cancer by promoting the malignant proliferation and distant metastasis of tumor cells. For example, in HBV-related HCC, HBV's genomic product preS2 protein can enhance the proliferation of liver cancer cells [9]. HBV *X* protein, that is, HBV promotes the migration and invasion of liver cancer cells by upregulating the expression of FoxM1, causing liver cancer metastasis, ultimately leading to a poor prognosis [10].

Circular RNAs (circRNAs) are a type of endogenous noncoding RNAs with a closed circular structure, which are mainly produced by the variable shearing process of precursor RNAs (pre-mRNAs) [11]. CircRNAs are widely present in all eukaryotes and are very stable. Studies have found that circRNA occupies a considerable proportion of transcripts, and some expression abundance is even significantly higher than other transcripts. At the same time, circRNAs exert an important regulatory effect on gene expression and play an important biological function in the development of organisms, such as acting as a miRNA sponges, endogenous RNAs, and biomarkers [12]. circRNAs also play an important role in the diagnosis and treatment of diseases. Studies have found that circRNAs play an important role in the occurrence of some diseases, including arteriosclerosis, nervous system disorders, diabetes, and cancer. miRNA sponge is the most frequently reported roles of circRNA in many tumors [13–16]. Many RNA transcripts share binding sites with miRNAs, and they compete with each other to act as competitive endogenous RNAs (ceRNAs) to further regulate tumor development [17, 18]. For example, circHIPK3 sponge miR-558 can inhibit the expression of heparanase in bladder cancer cells [19]. In addition, the circular RNA profile of circPVT1 identified it as a proliferation factor and prognostic marker of gastric cancer, and circular RNAMTO1 was used as a sponge of miR-9 to inhibit the progression of hepatocellular carcinoma [20].

In the previous experiment, the differentially expressed circRNAs in HBV-infected liver cancer cells were screened by high-throughput sequencing, and the present study found that hsa_circ_0000847 was significantly highly expressed in liver cancer tissues and cells. Therefore, the study aims to explore the specific mechanism of hsa_circ_0000847 in HBV infection of liver cancer cells.

2. Methods

2.1. Clinical Samples. HBV-positive liver cancer specimens ($n = 10$) and HBV-negative liver cancer specimens ($n = 10$) were collected from HCC patients who underwent hepatectomy at Xiangshan First People's Hospital. The pathological diagnosis has been confirmed, and the patients have not received chemotherapy or radiotherapy. All the patients have written the consent for approval of the application of clinical samples for basic research, and this study was approved by the research medical ethics committee at the hospital.

2.2. Cell Culture. Human normal hepatocytes (LO2), liver cancer cells (Bel-7402, Huh7, and HepG2), and HepG2.2.15 (HBV-infected liver cancer cells) were cultured in Dulbecco's Modified Eagle Medium (DMEM) containing 10% fetal bovine serum (FBS) and 1% penicillin, and streptomycin at 37°C in a 5% CO_2 incubator. When the degree of cell association reached 80%–90%, the cells were passed into next passage at a ratio of 1 : 2 to 1 : 3.

2.3. CCK-8 Assay. The cells were seeded at a density of 1×10^5 cells/mL in a 96-well plate, and the five replicate groups were set up for each group. The experiments were performed according to the experimental requirements as previously described [21]. After the treatment, the DMEM medium containing 10% CCK-8 was added. 1–4 h later, a microplate reader was used to detect the absorbance (OD value) at a wavelength of 450 nm. The proliferation capacity of the cell was directly proportional to the absorbance of the cells.

2.4. Real-Time Quantitative PCR (RT-qPCR). The TRIzol reagent was used to extract total RNAs from the tissues and cells as previously described [22]. According to the instructions, 1000 ng of total RNA was reversed and recorded into cDNAs. Then, the cDNAs were used as a template to perform the fluorescence quantitative PCR reaction of the target genes according to the SYBR Green *I* method. The design and synthesis of primers were obtained from Shanghai Sanitary Industry Co., Ltd., using β-actin or U6 as the internal reference. The $2^{-\Delta\Delta CT}$ method was used to analyze the relative expression level of the target gene.

2.5. Western Blotting. The protein lysate was used to extract the total proteins in the cells, and the extracted proteins were quantified by the BCA method [23, 24]. In each group, samples of the same concentration of protein were subjected to SDS-PAGE electrophoresis; then, the protein was electrotransferred to the PVDF membrane. The 5% skimmed milk powder was used to block for 1 h at room temperature and the primary antibody was incubated overnight at 4°C and washed 3 times with PBST. Then, the HRP-labeled secondary antibody was incubated for 1 hour at room temperature. After washing with PBST 3 times, the expression of proteins was analyzed by the ECL chemiluminescence method.

2.6. Transwell Assay. The experiments were carried out according to the previous study [25]. Briefly, the cells were cultured in a serum-free medium for 24 h, and the concentration was adjusted to 5×10^5/mL. Then, 100 μL cells were seeded into the polycarbonate membrane in the upper chamber of the small chamber and 600 μL of the serum-

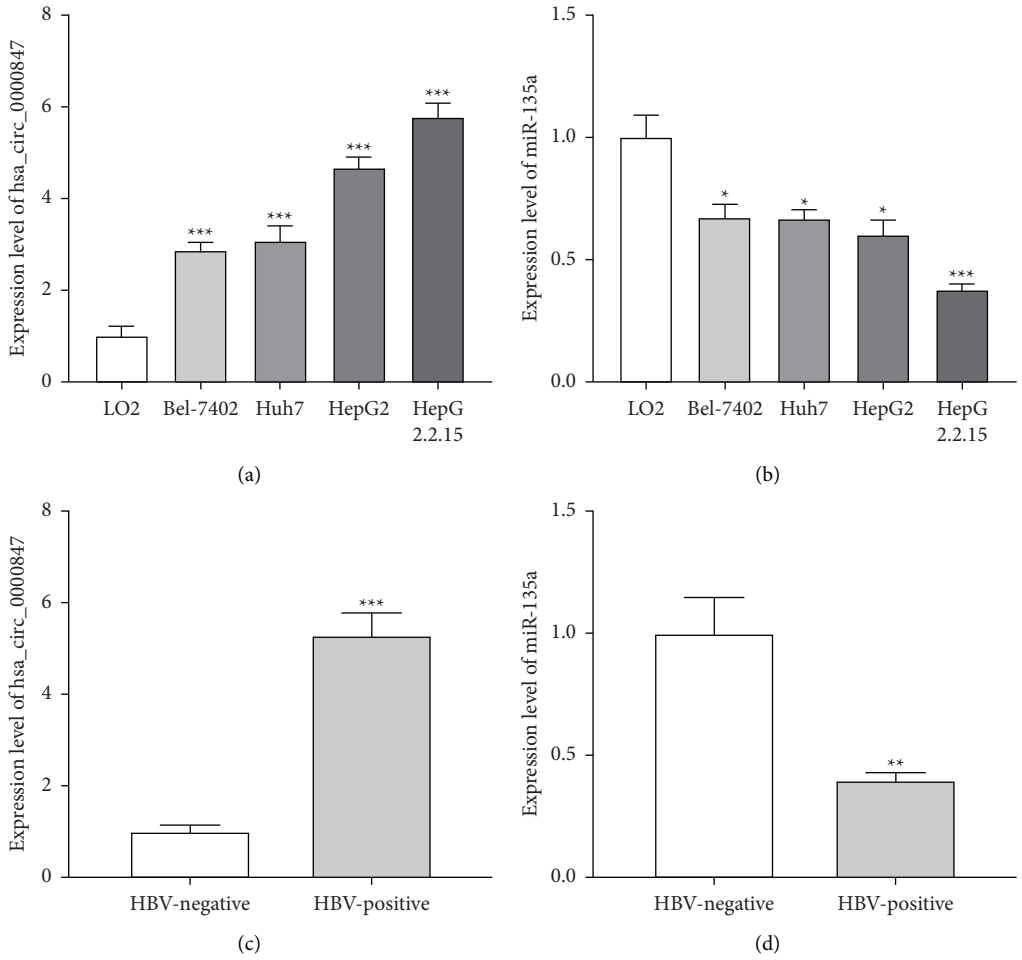

Figure 1: The expression level of hsa_circ_0000847/miR-135a in liver cancer cells. (a and b) Elevated expression of hsa_circ_0000847 and decreased expression of miR-135a in liver cancer cell lines ($n = 3$, mean ± SD, $^{*}p < 0.05$, $^{**}p < 0.01$, $^{***}p < 0.001$ vs LO2 cells). (c and d) Elevated expression of hsa_circ_0000847 and decreased level of miR-135a in HBV-positive liver cancer specimens ($n = 10$, mean ± SD, $^{*}p < 0.05$, $^{**}p < 0.01$, $^{***}p < 0.001$ vs HBV-negative liver cancer specimens).

containing culture medium were added to the lower chamber. The cells were placed in a 37°C, 5% CO_2 cell culture incubator for 24 h and then removed. The cells were carefully wiped off the lower surface of the polycarbonate membrane of the upper chamber with a cotton swab, fixed with methanol, stained with crystal violet, and the number of invaded cells were observed under a microscope.

2.7. Double Fluorescein Enzyme Report Assay. The miR-135a mimics or its negative control (miR-135a mimics NC) was co-transfected with the luciferase reporter vector WT-hsa_circ_0000847 or MUT-hsa_circ_0000847 into HEK293T cells, respectively; miR-135a mimics NC and WT-hsa_circ_0000847 co-transfection, miR-135a mimics and WT-hsa_circ_0000847 co-transfection, miR-135a mimics NC and mut-hsa_circ_0000847 co-transfection, and miR-135a mimics and MUT-hsa_circ_0000847 co-transfection. After 24 h of transfection, the cells were collected and the relative luciferase activity was detected by the dual luciferase reporter gene detection system.

2.8. Flow Cytometry Assay. Cell transfection was carried out according to the experimental requirements. After 24 h of transfection, the culture medium was discarded. The cells were washed twice with 1×PBS and discarded. The cells were digested with 0.3% trypsin without EDTA and collected. The cells were centrifuged at 2000 rpm at room temperature for 5 min, and then the supernatant was discarded and 1 ml 1 × PBS was added to resuspend the cells. The cells were centrifuged at 2000 rpm for 5 min at room temperature, and then the supernatant was discarded. The cells were resuspended in 300 μL 1×binding buffer and 5 μL AnnexinV-FITC was added in a dark room for 10 min. Then, 5 μL PI solution was added in a dark room for 5 min. Then, 200 μL 1 × binding buffer was added, and flow detection was performed within 1 h.

2.9. Statistical Analysis. The data were analyzed using the SPSS 20.0 statistical package (IBM, USA). The results of this study were expressed as means ± standard deviation. The comparisons among multiple groups were performed using

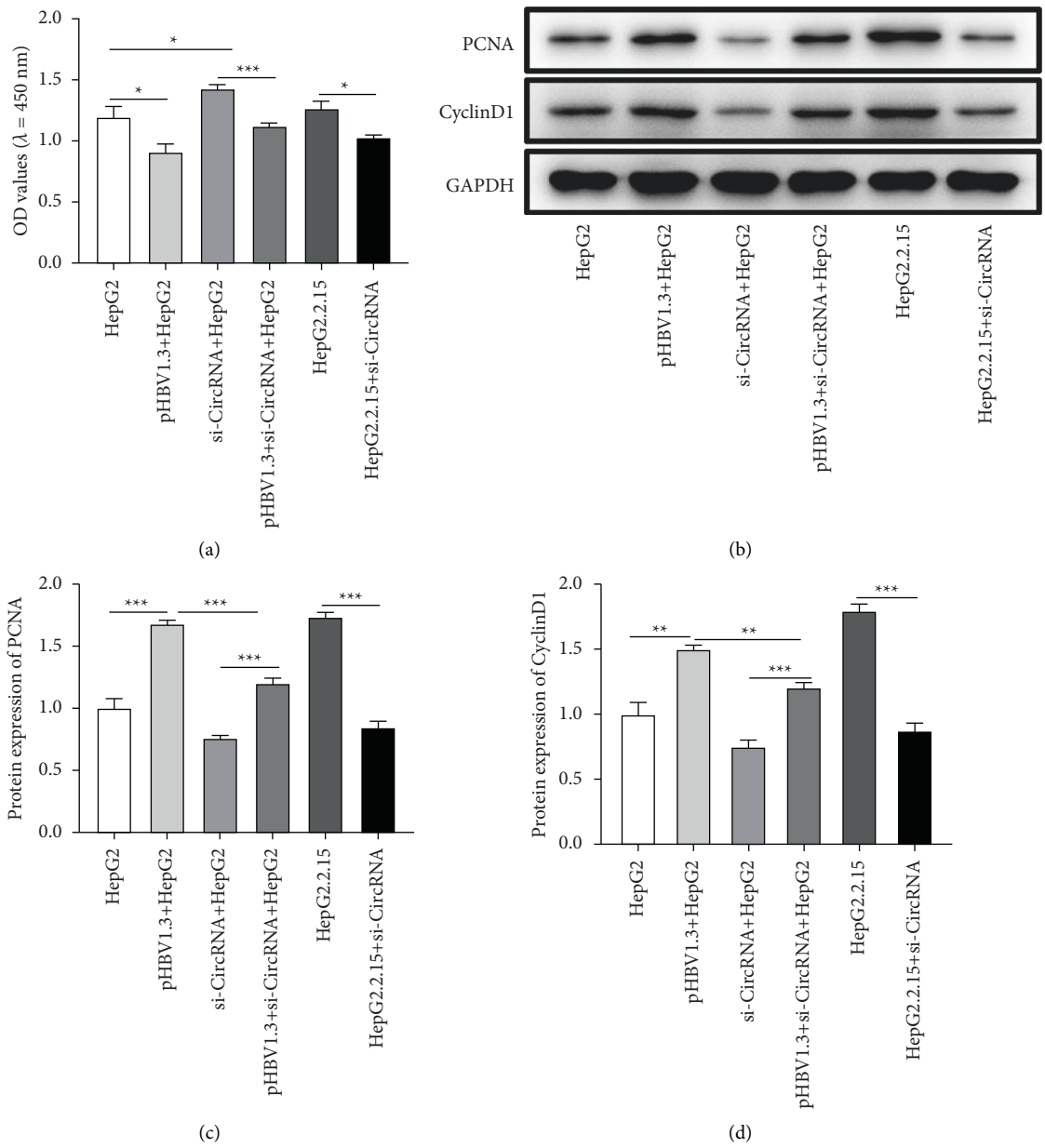

Figure 2: The effects of si-hsa_circ_0000847 on cell proliferation and the protein expression of PCNA and CyclinD1. (a) si-circRNA reduced the proliferation of HepG2, pHBV1.3 + HepG2, and HepG2.2.15 cells. (b-d) si-circRNA reduces the protein expression of PCNA and CyclinD1 ($n = 3$, Mean ± SD, $^{*}p < 0.05$, $^{**}p < 0.01$, $^{***}p < 0.001$.

one-way analysis of variance (ANOVA) followed by post-hoc test for multiple comparisons. $P < 0.05$ indicated a significant difference.

3. Results

3.1. The Expression of hsa_circ_0000847 and miR-135a in Liver Cancer Cells and Tissues. In order to explore the expression of hsa_circ_0000847 in liver cancers, we detected the expression levels of hsa_circ_0000847 and miR-135a in liver cancer cells and HBV-infected liver cancer cells. The results showed that the expression level of hsa_circ_0000847 in liver cancer cells was significantly higher than that of normal liver cells, especially in HBV-infected liver cancer cells (Figure 1(a)). While the expression level of miR-135a was significantly lower in liver cancer cells than that of normal liver cells, especially in HBV-infected liver cancer cells (Figure 1(b)). In addition, compared with HBV-negative liver cancer specimens, the expression level of hsa_circ_0000847 was significantly increased in HBV-positive liver cancer specimens, while the expression level of miR-135a was significantly decreased (Figures 1(c) and 1(d)). The results suggested that hsa_circ_0000847 and miR-135a might be related to the development and occurrence of liver cancer.

3.2. The Effects of hsa_circ_0000847 on the Cell Proliferation of Liver Cancer Cells. This study explored the effects of hsa_circ_0000847 on the cell proliferation through CCK-8

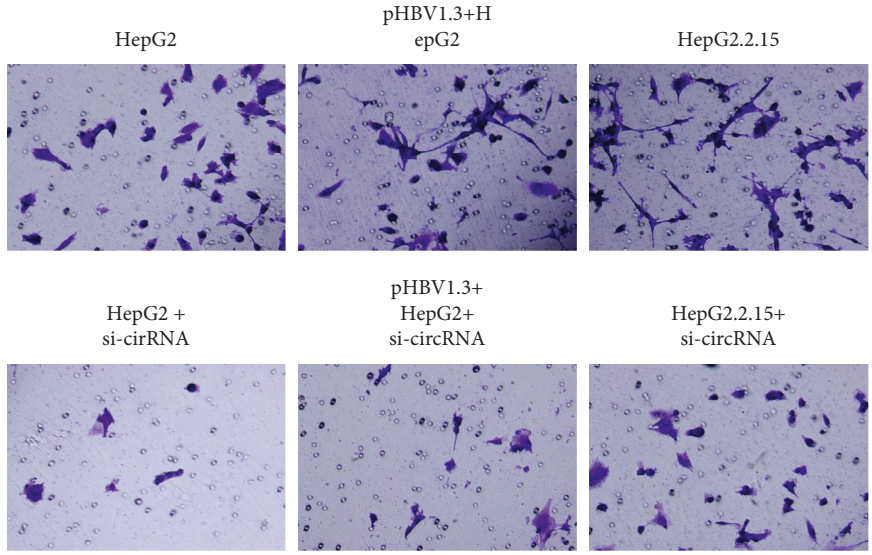

FIGURE 3: The effects of si-hsa_circ_0000847 on cell invasion. Transwell assay was applied to detect the invasion ability of liver cancer cells ($n = 3$).

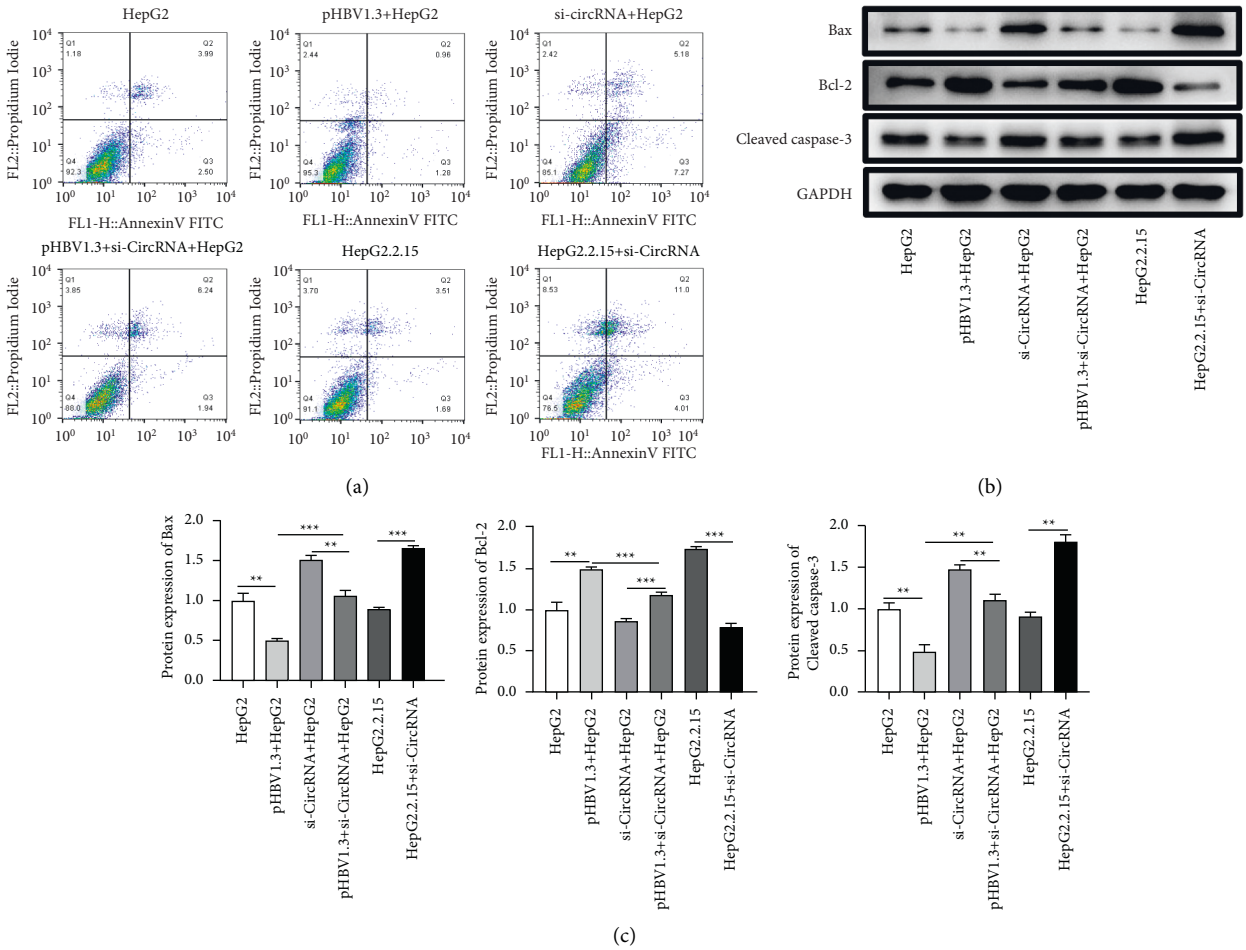

FIGURE 4: The effect of si-hsa_circ_0000847 on cell apoptosis in liver cancer cells. (a). Flow cytometry was used to detect the effect on cell apoptosis. (b and c) The expression levels of apoptosis-related proteins Bcl-2, Bad, and cleaved caspase-3 ($n = 3$, Mean ± SD, $^{**}p < 0.01$, $^{***}p < 0.001$.

assay and detecting the expression of proliferation-related proteins. Compared with the HepG2 group, the OD values of the cells in pHBV1.3 + HepG2 group were markedly increased, which were reduced by pHBV1.3 + si-hsa_circ_0000847 + HepG2 (Figure 2(a)). Compared with the HepG2 group, the OD values of the cells were obviously decreased in si-hsa_circ_0000847 + HepG2 group (Figure 2(a)). Besides, the OD values of HepG2.2.15 group were inhibited by si-hsa_circ_0000847 + HepG2.2.15 (Figure 2(a)).

Furthermore, the results of western blot showed that the expression of proliferation-related proteins (PCNA and CyclinD1) was much higher in pHBV1.3 + HepG2 group than that in HepG2 group, which was reduced by si-hsa_circ_0000847+HepG2 (Figures 2(b)–2(d)). Furthermore, the expression of proliferation-related proteins (PCNA and CyclinD1) in si-hsa_circ_0000847 + HepG2.2.15 group was much lower than that in HepG2.2.15 group (Figures 2(b)–2(d)). The results indicated that HBV promoted the proliferation of liver cancer cells through hsa_circ_0000847.

3.3. The Effects of hsa_circ_0000847 on the Invasion of Liver Cancer Cells. To further analyze the effects of hsa_circ_0000847 on the invasion of liver cancer cells, the transwell experiments were carried out. The results showed that compared with the HepG2 group, the number of invasive cells in pHBV1.3 + HepG2 group was markedly increased, which were inhibited by pHBV1.3 + si-hsa_circ_0000847 + HepG2 (Figure 3). Compared with the HepG2 group, the number of invasive cells in HepG2.2.15 group was significantly increased, which was blocked by si-hsa_circ_0000847 + HepG2.2.15 (Figure 3). The results suggested that the number of cells in the si-circRNA group was significantly lower than that in the untransfected si-circRNA group (Figure 3). Therefore, hsa_circ_0000847 and HBV significantly enhanced the invasion ability of liver cancer cells.

3.4. The Effects of hsa_circ_0000847 on the Cell Apoptosis of Liver Cancer Cells. In addition, the experiments were applied to detect the effects of hsa_circ_0000847 in the apoptosis of liver cancer cells by flow cytometry and western blotting. The results showed that compared with the HepG2 group, the apoptosis rate of liver cancer cells in pHBV1.3 + HepG2 group was much lower, which was elevated by si-hsa_circ_0000847 (Figure 4(a)). Moreover, compared with HepG2.2.15 group, the apoptosis rate of liver cancer cells in si-hsa_circ_0000847 + HepG2.2.15 group was significantly increased (Figure 2(a)).

In addition, western blotting experiments also proved the results. The results of western blotting showed that compared with the HepG2 group, the apoptosis-related proteins (Bax and cleaved caspase-2) of liver cancer cells in pHBV1.3 + HepG2 group was much lower, which was upregulated by si-hsa_circ_0000847 (Figures 4(b)–4(c)). While the antiapoptosis-related protein Bcl-2 of liver cancer cells in pHBV1.3 + HepG2 group was much higher, which was decreased by si-hsa_circ_0000847 (Figures 4(b)–4(c)). Moreover, compared with the HepG2.2.15 group, the expression of Bax and cleaved caspase-2 of liver cancer cells in si-hsa_circ_0000847 + HepG2.2.15 group was significantly increased, while the expression of Bcl-2 was decreased (Figures 4(b)––4(c)). The results suggested that knockdown of hsa_circ_0000847 could significantly promote the apoptosis of liver cancer cells. In short, hsa_circ_0000847 exerted a significant antiapoptotic effect on liver cancer cells.

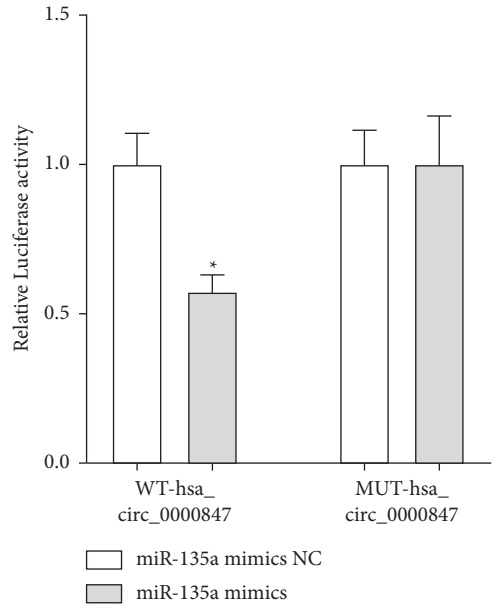

Figure 5: The relationship between hsa_circ_0000847 and miR-135a. Double luciferase reporter gene assay was performed in 293T cells, and the ratio of firefly/Renilla activity represents luciferase activity ($n = 3$, mean ± SD, $^{*}p < 0.5$.

3.5. Targeting Relationship between hsa_circ_0000847 and miR-135a. Through the dual luciferase experiment, we found that the luciferase activity of the miR-135a mimics + MUT-hsa_circ_0000847 group was significantly lower than that of the MUT-hsa_circ_0000847 and miR-135a mimics NC co-transfection group (Figure 5). However, compared with the MUT-hsa_circ_0000847 and mimics NC co-transfection group, the luciferase activity of the MUT-hsa_circ_0000847 + miR-135a mimics group did not change significantly (Figure 5). The results suggested that hsa_circ_0000847 might directly target miR-135a.

3.6. The Effect of hsa_circ_0000847 and miR-135a on Cell Proliferation of Liver Cancer Cells. The cell proliferation experiments found that si-hsa_circ_0000847 + miR-135a-5p mimics can significantly inhibit the proliferation of liver cancer cells in the HepG2 + pHBV1.3 cell group (Figure 6(a)). Similarly, the HepG2.2.15 cell group has similar results, and the ability to inhibit the proliferation of liver cancer cells is stronger (Figure 6(b)). In addition, in HepG2.2.15 cells or HepG2 transfected with pHBV1.3, the

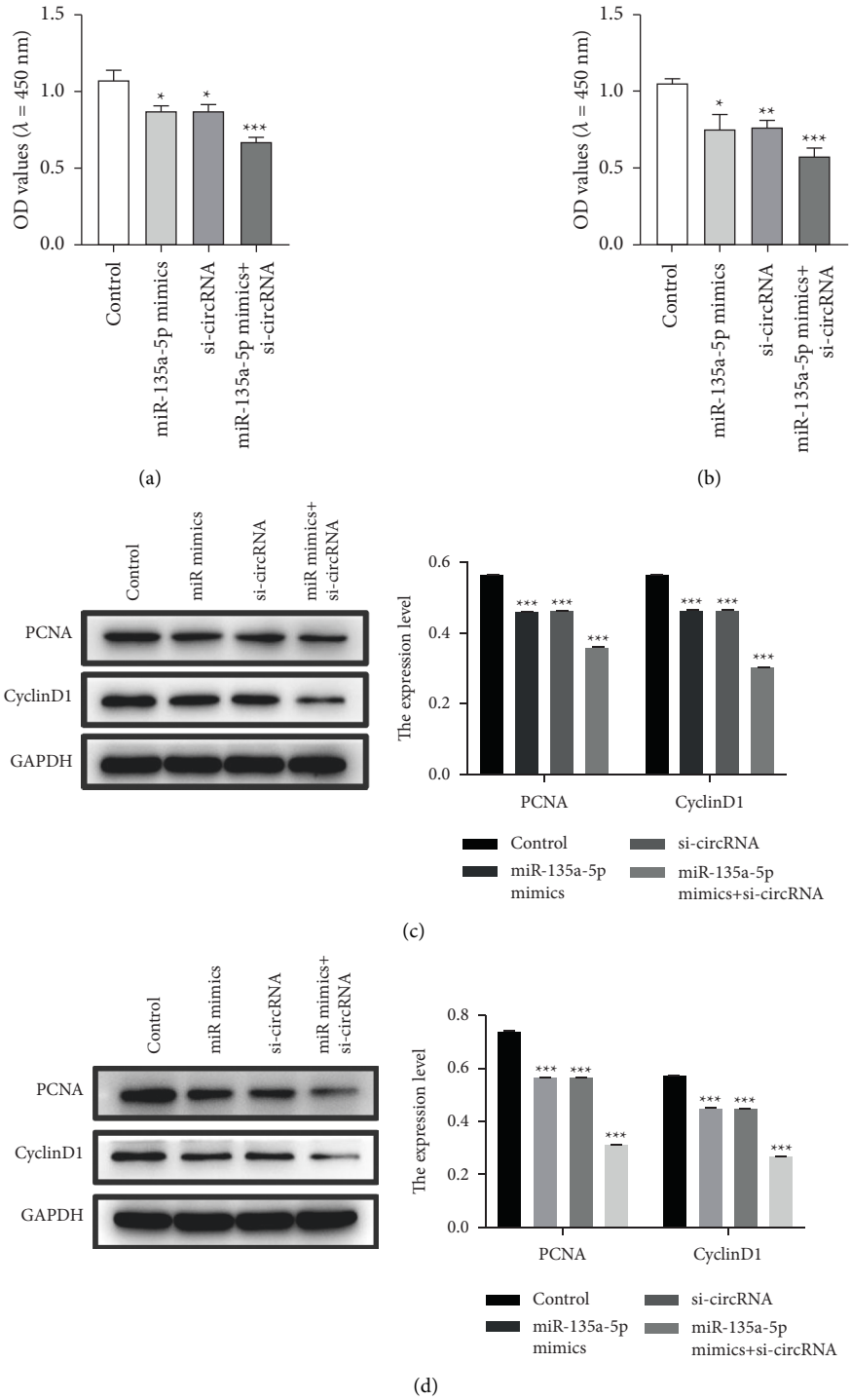

Figure 6: The effects of si-circRNA on cell proliferation and the protein expression of PCNA and CyclinD1. (a and b) The proliferation of HepG2 + pHBV1.3 cells (a) and HepG2.2.15 cell group (b) tested by CCK-8. (c and d) The expression levels of apoptosis-related proteins PCNA and CyclinD1 in HepG2 + pHBV1.3 cell group (c) and HepG2.2.15 cell group (d). $n = 3$, Mean ± SD, $^{*}p < 0.05$, $^{**}p < 0.01$, $^{***}p < 0.001$ vs control.

miR-135a mimics + si-hsa_circ_0000847 group significantly reduced the expression levels of proliferation-related proteins PCNA and CyclinD1 (Figures 6(c) and 6(d)). All these results indicated that HBV promoted the proliferation of liver cancer cells through the hsa_circ_0000847/miR-135a axis.

3.7. The Effects of hsa_circ_0000847 + miR-135a on Cell Invasion of Liver Cancer Cells. Experiments have proved that hsa_circ_0000847 can promote the invasion ability of liver cancer cells. Therefore, the next step is to test the effects of si-circRNA + miR-135a on cell invasion of liver cancer cells. After experiment silencing hsa_circ_0000847, it was found that in the

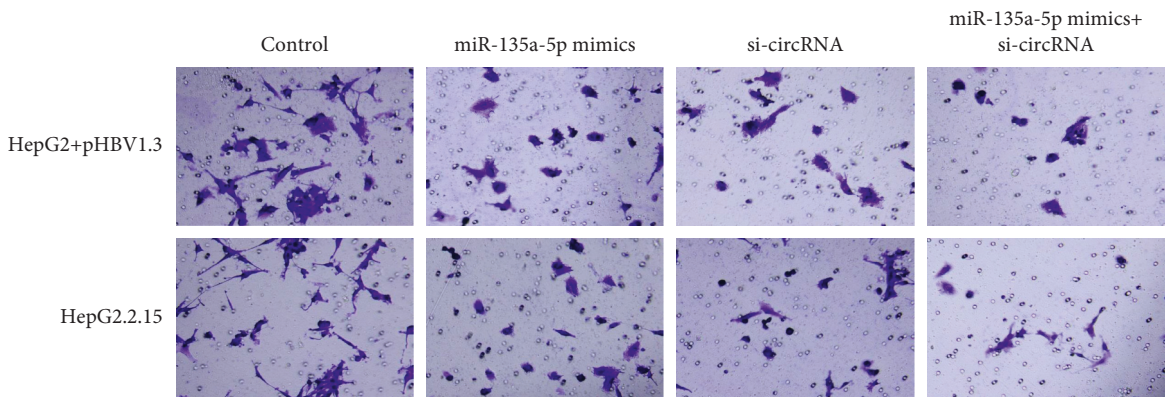

FIGURE 7: The effects of si-hsa_circ_0000847 and miR-135a on cell invasion. The effects of miR-135a-5p, mimics si-hsa_circ_0000847, and miR-135a-5p mimics + si-hsa_circ_0000847 on cell invasion in HepG2 + pHBV1.3 and HepG2.2.15 groups, respectively ($n = 3$).

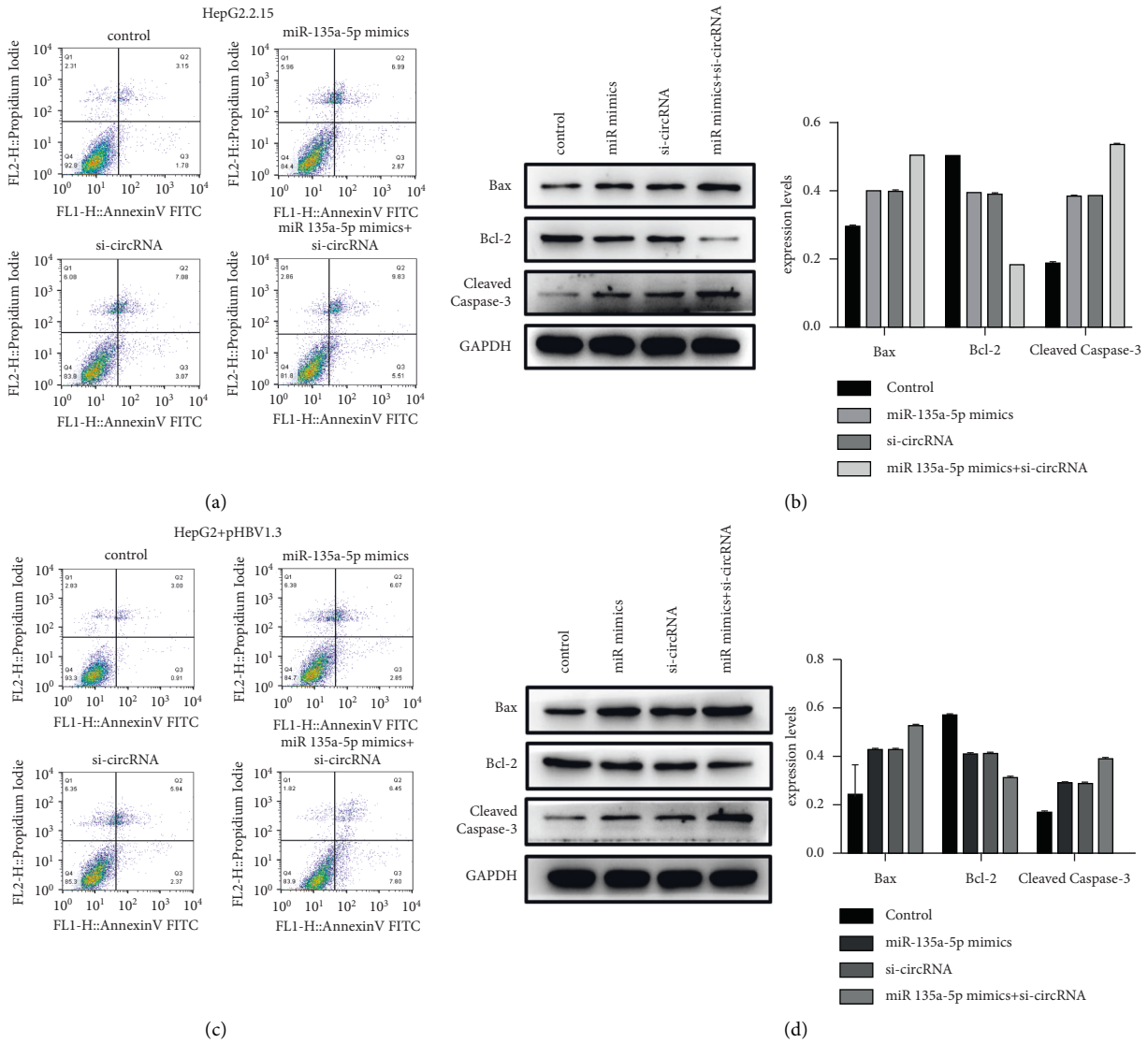

FIGURE 8: The roles of si-hsa_circ_0000847 and miR-135a on cell apoptosis. (a) Flow cytometry was used to detect cell apoptosis in HepG2.2.15 cells. (b) The expression levels of apoptosis-related proteins Bcl-2, Bad, and cleaved caspase-3 in HepG2.2.15 cells. (c) Flow cytometry was used to detect cell apoptosis in HepG2+pHBV1.3 cells. (d) The expression levels of apoptosis-related proteins Bcl-2, Bad, and cleaved caspase-3 in HepG2 + pHBV1.3 cells. $n = 3$, mean ± SD, $^{*}p < 0.05$, $^{**}p < 0.01$, $^{***}p < 0.001$ vs control.

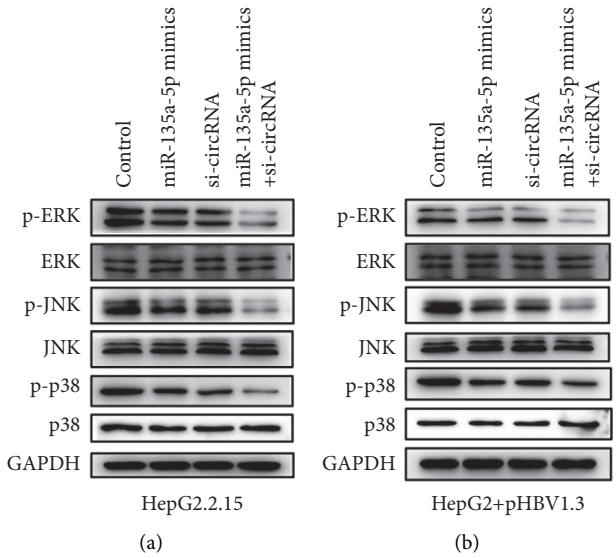

Figure 9: The roles of si-hsa_circ_0000847 and miR-135a on the activation of MAPK pathway. (a and b) The expression levels of p-ERK, ERK, p-JNK, JNK, p-p38, and p38 in the HepG2.2.15 group (a) and the HepG2 + pHBV1.3 group (b).

HepG2+pHBV1.3 cell group, miR-135a-5p mimics can significantly inhibit the invasion ability of liver cancer cells (Figure 7). Similarly, in the HepG2.2.15 cell group, miR-135a mimics also significantly inhibited the invasion of liver cancer cells (Figure 7). Therefore, whether in liver cancer cells or HBV-infected liver cancer cells, si-hsa_circ_0000847 can inhibit the invasion of liver cancer cells through miR-135a. Therefore, si-hsa_circ_0000847 + miR-135a can significantly inhibit the invasion of liver cancer cells.

3.8. The Effect of hsa_circ_0000847 + miR-135a on Cell Apoptosis of Liver Cancer Cells. In the HepG2.2.15 group, the co-transfection of miR-135a mimics and si-hsa_circ_0000847 significantly promoted the apoptosis of liver cancer cells (Figure 8(a)). At the same time, it elevated the expression level of the proapoptotic protein Bcl-2 and cleaved caspase-3 but inhibited the expression level of the protein Bax (Figure 8(b)). Importantly, the HepG2+pHBV1.3 group also got the same result (Figures 8(c) and 8(d)). The above-mentioned results indicated that co-transfection of miR-135a mimics and si-hsa_circ_0000847 promoted the apoptosis of liver cancer cells.

3.9. The Effect of hsa_circ_0000847 + miR-135a on the Activation of the MAPK Pathway. The MAPK pathway plays an important role in the occurrence and development of cancers. In this study, compared with the control group, the si-hsa_circ_0000847 + miR-135a mimics group significantly reduces the expression levels of phosphorylated proteins p-p38, p-ERK, and p-JNK in HepG2.2.15 cells (Figure 9(a)). In HepG2 cells transfected with pHBV1.3, the expression levels of p-p38, p-ERK, and p-JNK were also significantly inhibited by miR-135a/ hsa_circ_0000847 (Figure 9(b)). Therefore, the findings showed that miR-135a/hsa_circ_0000847 will significantly inhibit the activation of the MAPK pathway.

4. Discussion

The development of liver cancer is a multistep process involving multiple genetic and epigenetic changes. Several studies have confirmed that dysregulated circRNAs are related to the progression of liver cancer. It is reported that the downregulation of hsa_circ_0001445 expression is significantly related to the aggressiveness of liver cancer, and it can be used as an independent risk factor for overall survival and recurrence-free survival of patients after hepatectomy [26]. Overexpression of hsa_circ_0001445 exerts an inhibitory effect on the proliferation and migration of liver cancer cells [26]. It has found that knockdown of circRNAs significantly inhibited the proliferation, cycle progression, and migration of liver cancer cells [27]. Therefore, restoring the expression of liver cancer-related circRNAs might exert an inhibitory effect on the progression of liver cancer. In our study, the expression of hsa_circ_0000847 in liver cancer tissues was significantly increased, suggesting that the dysregulated expression in hsa_circ_0000847 might be related to the progression of liver cancer. Besides, the knockdown of hsa_circ_0000847 significantly reduces the viability of liver cancer cells HepG2 and HepG2.2.15, suggesting that hsa_circ_0000847 exerted a pro-proliferation effect in liver cancer cells.

As we all know, Bax, Bcl-2, and cleaved caspase-3 proteins play an important role in the apoptosis of tumor cells, and their abnormal expression is critical to the occurrence and development of cancer [24, 28, 29]. This study showed that knockdown of hsa_circ_0000847 significantly increased the expression of Bax and cleaved caspase-3 proteins, and decreased the expression of Bcl-2 protein. In addition, the MAPK pathway is a classic inflammation and tumor-related pathway, which plays an important role in the regulation of liver cancer. The previous studies have shown that circ-MAPK4 inhibits glioma cell apoptosis through the MAPK signaling pathway by secreting miR-125a-3p [30].

circ_0001721 promotes the progression of osteosarcoma through the miR-372-3p/MAPK7 axis [31]. Therefore, to explore the effects of hsa_circ_0000847 on liver cancers, it is necessary to focus on the roles of MAPK pathway. In this study, si-hsa_circ_0000847 significantly inhibited the expression levels of p-p38, p-ERK1/2, and p-JNK1/2/3 in HepG2.2.15 cells. Therefore, hsa_circ_0000847 participates in the regulation of liver cancer cells by activating the MAPK pathway.

miRNA is an endogenous noncoding small RNA consisting of about 22 nucleotides and is an essential epigenetic regulatory factor in cancer [32–34]. A number of studies have shown that circRNAs can directly interact with miRNAs to regulate the expression of target genes and participate in the progression of liver cancers [35–37]. For example, circMAT2B promotes glycolysis of liver cancer cells by regulating the miR-338-3p/PKM2 axis under hypoxic conditions, thereby promoting liver cancer progression [38]. miR-21 is involved in cellular processes, such as cell proliferation, angiogenesis, invasion, and metastasis, and resistance to chemotherapy and radiotherapy. It is a carcinogenic factor for breast cancer and non-small cell lung cancers [39, 40]. The high expression of miR-21 in liver cancer is associated with shortened 5-year overall survival and 5-year disease-free survival of liver cancer patients, which suggests miE-21 is a potential prognostic marker of liver cancer [41]. This study confirmed that miR-135a binds directly and specifically to circRNAs, and the expression of miR-135a is negatively regulated by circRNAs. Analysis of the function of miR-135a showed that inhibiting the expression of miR-135a significantly downregulated the expression of Bcl-2 protein, upregulated expression of Bax, and cleaved caspase-3 proteins, and inhibited the proliferation and invasion of HepG2.2.15 cells.

In summary, the expression of hsa_circ_0000847 in liver cancer tissues is upregulated. The knockdown of hsa_circ_0000847 can reduce the proliferation and invasion of liver cancer cells and its mechanism is related to the negative regulation of miR-135a expression. This provides new clues for understanding the role of circRNAs/miRNAs regulatory network in liver cancer and provides a valuable target for liver cancer treatment.

Data Availability

All data included in this study are available upon request by contacting the corresponding author.

Conflicts of Interest

The authors declare that they have no conflicts of interest.

Authors' Contributions

Longteng Xie and Yuyang Lu designed the study. Jianjun Lin, Xiang Lian, and Shihang Xue provided experimental support to this research. Lian Ouyang and Jianjun Lin analyzed the data. Lihui Zhou and Yuyang Lu provided statistical support to this research. Jianjun Lin and Longteng Xie wrote this study. Yuyang Lu and Longteng Xie revised this manuscript.

Acknowledgments

This work was supported by Basic Public Welfare Research Program of Zhejiang Natural Science Foundation (LY20H160002).

References

[1] H. J. Alter, "To have B or not to have B: vaccine and the potential eradication of hepatitis B," *Journal of Hepatology*, vol. 57, pp. 715–717, 2012.

[2] M. Maluccio and A. Covey, "Recent progress in understanding, diagnosing, and treating hepatocellular carcinoma," *CA: A Cancer Journal for Clinicians*, vol. 62, pp. 394–399, 2012.

[3] A. Forner, J. M. Llovet, and J. Bruix, "Hepatocellular carcinoma," *The Lancet*, vol. 379, no. 9822, pp. 1245–1255, 2012.

[4] Y. Chen, Q. Liu, M. Wu et al., "GAB2 promotes cell proliferation by activating the ERK signaling pathway in hepatocellular carcinoma," *Tumor Biology*, vol. 37, no. 9, pp. 11763–11773, 2016.

[5] Y. Chen, S. Yang, J. Hu, C. Yu, M. He, and Z. Cai, "Increased expression of SETD7 promotes cell proliferation by regulating cell cycle and indicates poor prognosis in hepatocellular carcinoma," *PLoS One*, vol. 11, no. 5, Article ID e0154939, 2016.

[6] S. Ahmadi, M. Sharifi, and R. Salehi, "Locked nucleic acid inhibits miR-92a-3p in human colorectal cancer, induces apoptosis and inhibits cell proliferation," *Cancer Gene Therapy*, vol. 23, no. 7, pp. 199–205, 2016.

[7] L. Wan, K. Pantel, and Y. Kang, "Tumor metastasis: moving new biological insights into the clinic," *Nature Medicine*, vol. 19, no. 11, pp. 1450–1464, 2013.

[8] D. S. Chen, "From hepatitis to hepatoma: lessons from type B viral hepatitis," *Science*, vol. 262, no. 5132, pp. 369-370, 1993.

[9] P. Liu, H. Zhang, X. Liang et al., "HBV preS2 promotes the expression of TAZ via miRNA-338-3p to enhance the tumorigenesis of hepatocellular carcinoma," *Oncotarget*, vol. 6, no. 30, pp. 29048–29059, 2015.

[10] L. Xia, W. Huang, D. Tian et al., "Upregulated FoxM1 expression induced by hepatitis B virus X protein promotes tumor metastasis and indicates poor prognosis in hepatitis B virus-related hepatocellular carcinoma," *Journal of Hepatology*, vol. 57, no. 3, pp. 600–612, 2012.

[11] R. Ashwal-Fluss, M. Meyer, N. R. Pamudurti et al., "circRNA biogenesis competes with pre-mRNA splicing," *Molecular Cell*, vol. 56, pp. 55–66, 2014.

[12] Y. Shi, X. Jia, and J Xu, "The new function of circRNA: translation," *Clinical and Translational Oncology*, vol. 22, no. 12, pp. 2162–2169, 2020.

[13] M. Zhang, X. Bai, X. Zeng, J. Liu, F. Liu, and Z. Zhang, "circRNA-miRNA-mRNA in breast cancer," *Clinica chimica acta; international journal of clinical chemistry*, vol. 523, pp. 120–130, 2021.

[14] Z. Y. Zhang, X. H. Gao, M. Y. Ma, C. L. Zhao, Y. L. Zhang, and S. S. Guo, "CircRNA_101237 promotes NSCLC progression via the miRNA-490-3p/MAPK1 axis," *Scientific Reports*, vol. 10, no. 1, p. 9024, 2020.

[15] Y. Li, C. Feng, M. Gao et al., "MicroRNA-92b-5p modulates melatonin-mediated osteogenic differentiation of bone marrow mesenchymal stem cells by targeting ICAM-1," *Journal of*

Cellular and Molecular Medicine, vol. 23, no. 9, pp. 6140–6153, 2019.

[16] Y. Li, F. Yang, M. Gao et al., "miR-149-3p Regulates the Switch between Adipogenic and Osteogenic Differentiation of BMSCs by Targeting FTO," *Molecular Therapy–Nucleic Acids*, vol. 17, pp. 590–600, 2019.

[17] X. Qi, D. H. Zhang, N. Wu, J. H. Xiao, X. Wang, and W. Ma, "ceRNA in cancer: possible functions and clinical implications," *Journal of Medical Genetics*, vol. 52, no. 10, pp. 710–718, 2015.

[18] L. Yang, Y. Li, R. Gong et al., "The long non-coding RNA-ORLNC1 regulates bone mass by directing mesenchymal stem cell fate," *Molecular Therapy*, vol. 27, no. 2, pp. 394–410, 2019.

[19] Y. Li, F. Zheng, X. Xiao et al., "Circ HIPK 3 sponges miR-558 to suppress heparanase expression in bladder cancer cells," *EMBO Reports*, vol. 18, no. 9, pp. 1646–1659, 2017.

[20] Y. Liu, Y. Dong, L. Zhao, L. Su, and J. Luo, "Circular RNA-MTO1 suppresses breast cancer cell viability and reverses monastrol resistance through regulating the TRAF4/Eg5 axis," *International Journal of Oncology*, vol. 53, no. 4, pp. 1752–1762, 2018.

[21] R. Hua, J. Zou, Y. Ma et al., "Psoralidin prevents caffeine-induced damage and abnormal differentiation of bone marrow mesenchymal stem cells via the classical estrogen receptor pathway," *Annals of Translational Medicine*, vol. 9, no. 15, p. 1245, 2021.

[22] Z. Zhang, Y. Song, S. I. Wang et al., "Osteoblasts/osteocytes sirtuin6 is vital to preventing ischemic osteonecrosis through targeting VDR-RANKL signaling," *Journal of Bone and Mineral Research*, vol. 36, no. 3, pp. 579–590, 2021.

[23] F. Yang, L. Yang, Y. Li et al., "Melatonin protects bone marrow mesenchymal stem cells against iron overload-induced aberrant differentiation and senescence," *Journal of Pineal Research*, vol. 63, no. 3, Article ID e12422, 2017.

[24] H. J. Park, J. S. Bae, K. M. Kim et al., "The PARP inhibitor olaparib potentiates the effect of the DNA damaging agent doxorubicin in osteosarcoma," *Journal of Experimental & Clinical Cancer Research*, vol. 37, no. 1, p. 107, 2018.

[25] K. M. Kim, U. K. Hussein, S. H. Park et al., "FAM83H is involved in stabilization of beta-catenin and progression of osteosarcomas," *Journal of Experimental & Clinical Cancer Research*, vol. 38, no. 1, p. 267, 2019.

[26] J. Yu, Q. G. Xu, Z. G. Wang et al., "Circular RNA cSMARCA5 inhibits growth and metastasis in hepatocellular carcinoma," *Journal of Hepatology*, vol. 68, no. 6, pp. 1214–1227, 2018.

[27] W. Zhan, X. Liao, Z. Chen et al., "Circular RNA hsa_circRNA_103809 promoted hepatocellular carcinoma development by regulating miR-377-3p/FGFR1/ERK axis," *Journal of Cellular Physiology*, vol. 235, no. 2, pp. 1733–1745, 2020.

[28] Y. J. Moon, Z. Zhang, I. H. Bang et al., "Sirtuin 6 in pre-osteoclasts suppresses age- and estrogen deficiency-related bone loss by stabilizing estrogen receptor α," *Cell Death & Differentiation*, vol. 26, no. 11, pp. 2358–2370, 2019.

[29] Z. Zhang, S. H. Ha, Y. J. Moon et al., "Inhibition of SIRT6 potentiates the anti-tumor effect of doxorubicin through suppression of the DNA damage repair pathway in osteosarcoma," *Journal of Experimental & Clinical Cancer Research*, vol. 39, no. 1, p. 247, 2020.

[30] J. He, Z. Huang, M. He et al., "Circular RNA MAPK4 (circ-MAPK4) inhibits cell apoptosis via MAPK signaling pathway by sponging miR-125a-3p in gliomas," *Molecular Cancer*, vol. 19, no. 1, p. 17, 2020.

[31] Y. Gao, H. Ma, Y. Gao et al., "CircRNA Circ_0001721 promotes the progression of osteosarcoma through miR-372-3p/MAPK7 Axis," *Cancer Management and Research*, vol. 12, pp. 8287–8302, 2020.

[32] J. Zou, J. Sun, H. Chen et al., "The regulatory roles of miR-26a in the development of fracture and osteoblasts," *Annals of Translational Medicine*, vol. 10, no. 2, p. 37, 2022.

[33] Q. Lu, R. Wu, M. Zhao, A. Garcia-Gomez, and E. Ballestar, "miRNAs as therapeutic targets in inflammatory disease," *Trends in Pharmacological Sciences*, vol. 40, no. 11, pp. 853–865, 2019.

[34] Z. Liu, Y. Zhou, G. Liang et al., "Circular RNA hsa_circ_001783 regulates breast cancer progression via sponging miR-200c-3p," *Cell Death & Disease*, vol. 10, no. 2, p. 55, 2019.

[35] G. Huang, M. Liang, H. Liu et al., "CircRNA hsa_circRNA_104348 promotes hepatocellular carcinoma progression through modulating miR-187-3p/RTKN2 axis and activating Wnt/β-catenin pathway," *Cell Death & Disease*, vol. 11, no. 12, p. 1065, 2020.

[36] L. L. Chen, "The expanding regulatory mechanisms and cellular functions of circular RNAs," *Nature Reviews Molecular Cell Biology*, vol. 21, no. 8, pp. 475–490, 2020.

[37] L. S. Kristensen, M. S. Andersen, L. V. W. Stagsted, K. K. Ebbesen, T. B. Hansen, and J. Kjems, "The biogenesis, biology and characterization of circular RNAs," *Nature Reviews Genetics*, vol. 20, no. 11, pp. 675–691, 2019.

[38] A. W. M. Lee, W. T. Ng, J. Y. W. Chan et al., "Management of locally recurrent nasopharyngeal carcinoma," *Cancer Treatment Reviews*, vol. 79, p. 101890, 2019.

[39] A. McGuire, J. A. L. Brown, and M. J. Kerin, "Metastatic breast cancer: the potential of miRNA for diagnosis and treatment monitoring," *Cancer and Metastasis Reviews*, vol. 34, no. 1, pp. 145–155, 2015.

[40] H. Nie, X. Xie, D. Zhang et al., "Use of lung-specific exosomes for miRNA-126 delivery in non-small cell lung cancer," *Nanoscale*, vol. 12, no. 2, pp. 877–887, 2020.

[41] Y. S. Feng, J. M. Zhou, C. H. Sun, J. Zhu, J. Yang, and L. Guo, "The diagnostic value of miR-21 combined with CT in patients with liver cancer," *Clinical and Translational Oncology*, vol. 23, no. 6, pp. 1238–1244, 2021.

Hindawi
Evidence-Based Complementary and Alternative Medicine
Volume 2022, Article ID 2075638, 15 pages
https://doi.org/10.1155/2022/2075638

Research Article

A Noval Established Cuproptosis-Associated LncRNA Signature for Prognosis Prediction in Primary Hepatic Carcinoma

Lan Luo, Xiaoyan Hu, Aoshuang Huang, Xiaofang Liu, Lingyun Wang, Tao Du, Lei Liu, and Ming Li

Department of Hematology and Oncology, The First People's Hospital of Guiyang, No. 97, Boai Road, Nanming, Guiyang, Guizhou 550002, China

Correspondence should be addressed to Lan Luo; 1621020380@stu.cpu.edu.cn

Received 8 August 2022; Revised 20 August 2022; Accepted 25 August 2022; Published 15 September 2022

Academic Editor: Xueliang Wu

The copper ion content in the body maintains homeostasis, and when dysregulated, it can produce cytotoxicity and induce cell death through a variety of pathways. Cuproptosis refers to copper ions combining directly with acylated molecules, leading to the accumulation of oligomerization of lipoylated protein and subsequent downregulation of iron-sulfur cluster proteins; this induces proteotoxic stress and cell death. This study on the relationship between cuproptosis-related lncRNAs (CRLns) and the prognosis of primary hepatic carcinoma (PHC) has important clinical guiding significance for the diagnosis and treatment of PHC. Prognosis-related CRLRs were identified via rank-sum tests, correlational analyses, and univariate Cox regression, and a CRLR risk-scoring model (CRLRSM) was constructed using LASSO Cox regression. Patients were divided into high-risk and low-risk groups based on the median CRLRSM scores. Variance analysis for cuproptosis-related genes, gene set enrichment analysis, and correlational analysis for risk and immunity were performed using boxplots. Quantitative polymerase chain reactions were used to verify the CRLR levels in PHC cell lines. The study results showed that patients in the CRLRSM high-risk group had worse survival rates than those in the low-risk group. The PHC stage and risk score were independent prognostic factors for hepatocellular carcinoma. There were 7 CRLRs (MIR210HG, AC099850.3, AL031985.3, AC012073.1, MKLN1-AS, KDM4A-AS1, and PLBD1-AS1) associated with PHC prognosis, primarily through cellular metabolism, growth, proliferation, apoptosis, and immunity. In conclusion, the overexpression of 7 CRLRs in patients with PHC indicates a poor prognosis.

1. Introduction

Copper ion is an essential metal element for bacteria, animals, and humans, and an indispensable cofactor in the process of life activities [1]. Under normal physiological conditions, copper ions maintain a low concentration in organisms and maintain dynamic balance, and excessive accumulation of copper ions induces cell death [2]. The mechanism is unknown, but in recent years, it has been found that copper ions combine with anticancer drugs to produce reactive oxygen species, form oxidative stress, inhibit antiapoptotic factors, activate apoptosis-related pathways, and thus induce apoptosis of cancer cells [3, 4]. Cu^{2+} complexes can be potent proteasome inhibitors, inhibiting proteasome activity in some tumors and subsequently inhibiting cell proliferation [5, 6]. Recently, Tsvetkov et al. found that copper ions directly bind to the lipoacylated component of the tricarboxylic acid cycle (TCA) in mitochondrial respiration, leading to the aggregation of lipoacylated proteins and subsequent downregulation of iron-sulfur cluster proteins, leading to proteotoxic stress and ultimately cell death. Copper carriers were also found to kill specific drug-resistant cancer cells. The research team identified this as a new type of cell death, termed cuproptosis [7].

Primary hepatic carcinoma (PHC) is one of the most common digestive system malignancies and comprises mainly hepatocellular carcinoma (HCC) and intrahepatic cholangiocarcinoma (ICC). The pathogenesis of PHC is a complex and multistage process, involving epigenetics and

genetics, finally leading to the cancerization of hepatic cells. Although ever-improving surgical approaches and emerging drugs have lengthened patient survival, their overall outcomes remain unsatisfactory. The five-year survival rate in patients with PHC is merely 20% [8].

In order to prolong the survival of patients with Primary hepatic carcinoma, we identified FDX1, LIAS, LIPT1, DLD, DLAT, PDHA1, PDHB, MTF1, GLS, and CDKN2A as cuproptosis-related genes [7] through previous studies. Long noncoding RNAs (lncRNAs) are nonbiased RNAs with a length of more than 200 nucleotides [9]. Accumulating evidence shows that lncRNA plays a complex and precise regulatory role in the process of tumorigenesis and development by acting as oncogenes or tumor performing factors [10–13]. They can not only regulate the proliferation, differentiation, invasion, and metastasis of cancer cells but also regulate the metabolic reprogramming of cancer cells [14–16]. There are currently few studies regarding the correlation between cuproptosis-related lncRNAs and PHC. Therefore, we built a new model of cuproptosis-related lncRNAs to predict the prognoses of PHC patients, assess the predictive performance of these lncRNAs, interpret individual differences, identify targets, and improve survival, which would be of great value in clinical practice.

2. Materials and Methods

2.1. Collection of Gene Expression and Clinical Data. There were 421 sets of public RNA-sequencing transcriptome data and clinical data extracted from UCSC Xena (http://xena.ucsc.edu/); one set of clear cell adenocarcinomas and six sets with unavailable clinical information were excluded. Thus, 414 sets were included: 364 sets of cancer tissue samples and 50 sets of normal tissue samples. HCC and HCC concomitant with ICC were the primary pathological types. The collected clinical characteristics included age, sex, pathological stage, overall cancer stage, survival state, and overall survival (OS) of the patients. Ten cuproptosis-related genes were identified through screening of genome-wide CRISPR–Cas9 deletions [7].

2.2. Cuproptosis-Related lncRNAs. There were 19266 mRNAs and 13431 lncRNAs that were recognized from the cancer tissues and normal tissues using the "Perl" software, and 10 cuproptosis-related genes were identified through screening of genome-wide CRISPR–Cas9 deletions. To assess lncRNAs associated with cuproptosis, Spearman's rank correlation coefficient was analyzed using the "limma" R package. The lncRNAs with $p < 0.001$ and a correlation coefficient of 0.4 were selected as cuproptosis-related lncRNAs. Univariate Cox regression was used to identify 106 prognosis-related lncRNAs ($p < 0.05$).

2.3. Construction of the Prediction Model. The Least Absolute Shrinkage and Selection Operator (LASSO) was processed using the "glmnet" R package to sort out cuproptosis-related lncRNAs (CRLRs), which were then plugged into a multivariate Cox model to construct a CRLR risk-scoring model (CRLRSM). The following formula was used for the risk scoring:

$$\text{Risk score} = \sum \text{Coef}_{\text{lncRNAs}} \times \text{Exp}_{\text{lncRNAs}}. \quad (1)$$

Patients were divided into high-risk and low-risk groups based on the median CRLRSM scores.

2.4. Survival Analysis and Model Validation. A total of 364 PHC patients were assigned in a 5 : 5 ratio to a training ($n = 184$) or test group ($n = 180$) for validation of the risk score. Kaplan–Meier analysis was performed, and the area under the receiver operator characteristic (ROC) curve (AUC) was calculated using R (version 4.1.3) for the three groups of low-risk and high-risk patients to estimate the accuracy and sensitivity of the OS prediction. Principal components analysis was used to evaluate differences in the expression of CRLRs in patients with PHC. To evaluate whether the risk score would be an independent prognostic factor and to identify clinical characteristics that could be regarded as independent prognostic factors, ROC univariate analysis, and Cox multivariate analysis were performed for clinical characteristics (age, sex, pathological stage, and overall stage) and the risk score. The ROC was used to compare the predictive performance between the clinical characteristics and risk score.

2.5. Nomogram Predicted Survival. A predictive nomogram for cancer risk can estimate the survival of specific cancer patients based on individual data, and they are of great value in clinical practice [17]. Using the "rms" and "Hmisc" R packages, we plotted a nomogram that included stages and risk scores. The AUC and calibration charts were used to evaluate the predictive accuracy and value of the 1-year, 3-year, and 5-year survival rates. A consistency index (C-index) was used to validate the performance of the nomogram predictions.

2.6. Variance Analysis for Cuproptosis-Related Genes. A boxplot is used to visualize the dispersion of data, which can be used to compare the distribution characteristics of multiple sets of data. Therefore, we constructed a boxplot, using the "limma" and "ggpubr" packages in R to evaluate whether there was a difference in the expression of cuproptosis-related genes between high-risk and low-risk groups.

2.7. Correlational Analysis for Risk and Immunity. The types and distributions of immune cells from the 414 patients were analyzed using the CIBERSORT algorithm, and the relationship between the risk score and the amount of immune cell invasion was assessed using Spearman's correlation analysis. Statistical significance was indicated by a p value < 0.05.

2.8. Gene Set Enrichment Analysis. The patients were assigned to the low-risk or high-risk group based on the prediction model. Gene set enrichment analysis was

Table 1: PCR primer sequences.

Primer	Sequence (5′–3′)
Human-MIR210HG-F	CAGCGTTTGGAGCCTCCTGC
Human-MIR210HG-R	AGGCAACTCGGCTTGGTTATTTC
Human-KDM4A-AS1-F	CAGGTCGTGAGCGCACCCAT
Human-KDM4A-AS1-R	TCAGCCATCCAGGCAAGAGCA
Human-PLBD1-AS1-F	GTGGATTCCATCCTAGAGGCTGTG
Human-PLBD1-AS1-R	TTCCTGCTTTCTGTCCTTCATTTCAG
Human-AC099850.3-F	TCACTGCAACCTCTGCCTCCC
Human-AC099850.3-R	TTCCCTGTTGTCACTGACCTATGTAATC
Human-AL031985.3-F	CCACAAGATGCCAGCATTCA
Human-AL031985.3-R	GCCCTTGAGCCAAACGAAAC
Human-AC012073.1-F	TATGTGGAGCTGTGGTTAGTTTCC
Human-AC012073.1-R	CAAAGTGGCACTGTTCGTAATAGAC
Human-GAPDH F	AATCCCATCACCATCTTCCA
Human-GAPDH R	AAATGAGCCCCAGCCTTCT

performed to identify significantly associated biological functions and signaling pathways, which might be potential pathways related to CRLR regulation. Statistical significance was indicated by a false discovery rate (FDR) < 0.05.

2.9. Cell Culturing. Human cell lines of normal hepatocytes (LO-2) and hepatomas (Huh7, Hep3B, and SK-Hep-1) were purchased from the Cell Collection Center of the Chinese Academy of Sciences. All cell lines were incubated in 5% CO2 at 37°C on a medium supplemented with 10% fetal bovine serum and 1% penicillin–streptomycin. The LO-2 cells were cultured using RPMI1630 medium, Huh7 cells were cultured using DMEM high-glucose medium, and Hep3B and SK-Hep-1 cells were cultured using MEM high-glucose medium.

2.10. Real-Time Polymerase Chain Reaction (PCR). RNA was extracted from 1×10^6 LO-2, Huh7, Hep3B, and SK-Hep-1 cells using TRIzol reagent, followed by reverse-transcription to synthesize cDNA using a cDNA synthesis kit according to the manufacturer's instructions. Based on the SYBR-Green method (TaKaRa), the 7500 Real-Time PCR System (Applied Biosystems) was used to measure the levels of the resulting cDNA. The reaction program was 30 s at 94°C, followed by 40 cycles of 5 s at 94°C and 35 s at 61°C. The primer sequences are shown in Table 1. Differences in the levels of targeted genes between the test and control groups were analyzed via the $2^{-\Delta\Delta CT}$ method, using the following calculation: $\triangle Ct = Ct_{\text{target gene}} - Ct_{\text{internal reference}}$. The average $\triangle Ct$ of the control group was recorded as the $\triangle Ct_{\text{control average}}$. Subtracting the $\triangle Ct_{\text{control average}}$ from the $\triangle Ct$ of each group yields the $\triangle\triangle Ct$ value, that is, $\triangle\triangle Ct = \triangle Ct_{\text{sample}} - \triangle Ct_{\text{control average}}$. The $2^{-\Delta\Delta CT}$ value of each group, indicating the relative expression of the genes in the group, was then calculated.

2.11. Data Analysis. PERL (version 5.32.1.1, https://strawberryperl.com/) was used for gene name translation, lncRNA identification, data-file expression, and phenotyping. All statistical analyses were performed using R software (version 4.1.3) or GraphPad Prism5 (GraphPad Software Inc., La Jolla, CA, USA). A p value < 0.05 indicated statistical significance. All experiments were performed twice.

3. Results

3.1. Data Processing. There were 414 cases of HCC or HCC with ICC downloaded from UCSC Xena; of these, 50 were pericarcinomatous tissues. A total of 13431 lncRNA were obtained, and 10 cuproptosis-related genes were identified through screening of genome-wide CRISPR–Cas9 deletions (Figure 1(a)). A total of 106 prognosis-related lncRNAs were identified using univariate Cox regression analysis. Seven CRLRs were identified using LASSO Cox regression: MIR210HG, AC099850.3, AL031985.3, C012073.1, MKLN1-AS, KDM4A-AS1, and PLBD1-AS1 (Figures 2(a) and 2(b)).

3.2. Construction and Validation of CRLR Risk Model for PHC. Seven CRLRs were identified via LASSO Cox regression using the following risk-scoring formula:

$$\begin{aligned}\text{Risk score} = {} & (\text{MIR210HG} \times 0.068) + (\text{AC099850.3} \times 0.017) \\ & + (\text{AL031985.3} \times 0.327) \\ & + (\text{AC012073.1} \times 0.102) \\ & + (\text{MKLN1} - \text{AS} \times 0.426) \\ & + (\text{KDM4A} - \text{AS1} \times 0.152) \\ & + (\text{KDM4A} - \text{AS1} \times 0.049).\end{aligned} \tag{2}$$

The patients were divided in a 5 : 5 ratio into training and test groups, based on the median scores of the CRLRSM (Figures 3(a), 3(f), and 3(k)). The whole group is the sum of patients in the training and test groups. The number of deaths increased as the risk score increased (Figures 3(b), 3(g), and 3(l)). A heat map showed that the 7 CRLR genes were related to a poor prognosis (Figures 3(c), 3(h), and 3(m)). There was a significant difference in survival between the high- and low-risk groups in the training group; patients in the low-risk group had longer survival times compared with those in the high-risk group. In the test group as well, patients in the low-risk group had longer survival times than

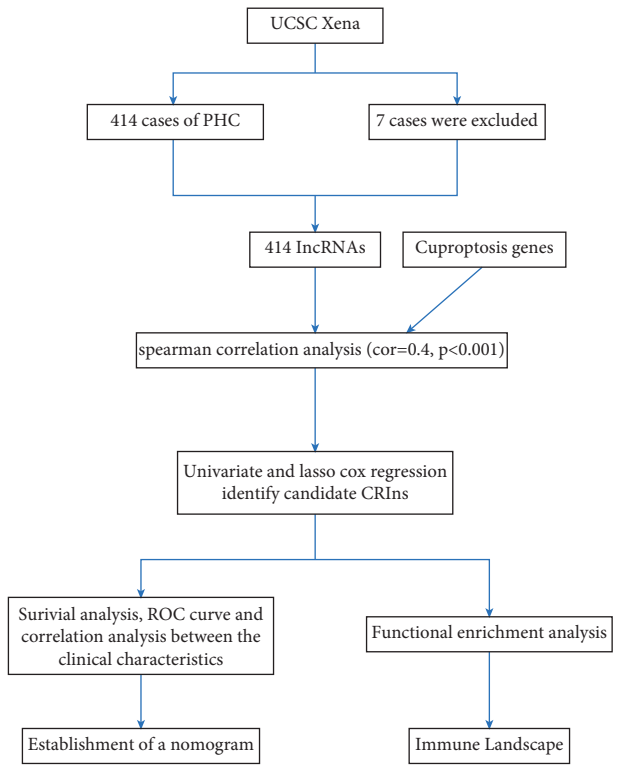

(a)

ID	HR	HR.95L	HR.95H	pvalue
SNHG1	1.372	1.103	1.707	0.004
MIR210HG	1.507	1.250	1.818	0.000
AL592435.1	3.720	1.646	8.403	0.002
GHET1	2.852	1.050	7.744	0.040
AC099850.3	1.548	1.300	1.844	0.000
AP003392.4	1.691	1.097	2.606	0.017
AC025048.4	1.751	1.162	2.639	0.007
AC025171.2	1.561	1.001	2.433	0.050
AL139393.2	2.003	1.080	3.714	0.027
US2111.1	3.326	1.044	10.592	0.042
AC012467.2	2.014	1.281	3.168	0.002
AC091057.1	2.507	1.315	4.780	0.005
AL050341.2	1.540	1.173	2.020	0.002
AC107959.3	1.753	1.326	2.318	0.000
TRAF3IP2-AS1	5.134	1.617	16.302	0.006
AC107214.1	3.181	1.538	6.580	0.002
LINC01232	2.448	1.559	3.844	0.000
KTN1-AS1	2.177	1.151	4.115	0.017
LINC01094	2.704	1.615	4.528	0.000
LINC02259	0.368	0.150	0.906	0.030
LINC01018	0.891	0.815	0.976	0.013
AL031985.3	3.250	2.229	4.738	0.000
AL139289.1	2.660	1.528	4.631	0.001
AC002116.2	1.875	1.207	2.912	0.005
AL049840.2	2.098	1.282	3.434	0.003
AC012073.1	2.555	1.837	3.552	0.000
AC090192.2	1.539	1.269	1.866	0.000
NCK1-DT	2.032	1.300	3.177	0.002
TGFB2-AS1	1.577	1.194	2.081	0.001
C2orf27A	2.127	1.514	2.988	0.000
AL031670.1	2.924	1.329	6.435	0.008
AC010336.2	0.711	0.509	0.994	0.046
AL035461.2	1.298	1.052	1.600	0.015
AC145207.8	1.604	1.220	2.109	0.001
AC023090.1	1.289	1.067	1.557	0.009
ZEB1-AS1	2.168	1.463	3.211	0.000
LINC00665	1.309	1.080	1.586	0.006
AL137186.2	1.850	1.343	2.550	0.000
LINC00294	1.462	1.017	2.102	0.040
AC115837.1	1.374	1.033	1.828	0.029
AC092614.1	2.852	1.194	6.813	0.018
DDX11-AS1	4.980	2.352	10.547	0.000
WAC-AS1	1.813	1.364	2.411	0.000
AP001372.2	1.731	1.107	2.708	0.016
CASC15	2.038	1.044	3.978	0.037
MKLN1-AS	4.312	2.623	7.087	0.000
AL137127.1	4.625	1.491	14.354	0.008
AL049840.3	1.600	1.018	2.516	0.042
AC010761.2	1.777	1.222	2.584	0.003
FAM111A-DT	1.688	1.057	2.696	0.028
AC006252.1	4.531	2.062	9.958	0.000
BACE1-AS	1.755	1.279	2.409	0.001
AC040970.1	1.431	1.137	1.801	0.002
AL117335.1	1.704	1.198	2.424	0.003
MAFG-DT	1.384	1.162	1.648	0.000
PTOV1-AS1	1.736	1.183	2.546	0.005
HMGN3-AS1	2.912	1.691	5.014	0.000
AC073254.1	4.257	1.423	12.735	0.010
AC006305.1	1.747	1.056	2.891	0.030
GIHCG	1.437	1.141	1.810	0.002
TMCO1-AS1	3.370	1.450	7.831	0.005
SNHG4	2.340	1.691	3.239	0.000
AC116351.1	1.367	1.057	1.768	0.017
LINC01011	2.357	1.426	3.896	0.001
AC007541.1	1.585	1.099	2.286	0.014
AC004816.1	1.622	1.247	2.110	0.000
AC005562.1	6.456	1.833	22.745	0.004
WARS2-AS1	1.779	1.132	2.794	0.012
KDM4A-AS1	3.376	1.977	5.764	0.000
AC073842.2	2.119	1.257	3.572	0.005
AL603839.2	2.948	1.555	5.590	0.001
CDKN2B-AS1	1.927	1.014	3.663	0.045
SCAT2	1.629	1.124	2.363	0.010
ARRDC1-AS1	1.426	1.028	1.978	0.033
AC115619.1	0.806	0.715	0.908	0.000
AC087289.1	1.178	1.002	1.385	0.047
PLRD1-AS1	1.731	1.292	2.317	0.000
ABALON	1.917	1.011	3.635	0.046
AC004943.2	2.122	1.188	3.791	0.011
AC108676.1	2.047	1.294	3.239	0.002
LENG8-AS1	1.564	1.067	2.294	0.022
AC107068.1	2.329	1.341	4.045	0.003
AC002310.1	1.937	1.082	3.467	0.026
AC026401.3	1.485	1.208	1.827	0.000
AC009299.2	2.449	1.282	4.678	0.007
AC098484.1	2.632	1.485	4.663	0.001
MCM3AP-AS1	7.122	2.425	20.919	0.000
AL356481.1	4.395	1.636	11.809	0.003
FOXD2-AS1	1.511	1.210	1.887	0.000
AC008771.1	1.460	1.095	1.946	0.010
AP003469.2	1.631	1.270	2.095	0.000
SLC16A1-AS1	2.596	1.420	6.318	0.004
PSMD6-AS2	4.581	1.056	19.868	0.042
ZNF32-AS2	1.827	1.033	3.233	0.038
AC026356.1	4.205	2.242	7.884	0.000
AC025580.1	1.802	1.260	2.577	0.001
AC068580.1	1.365	1.022	1.822	0.035
AL161668.4	0.823	0.690	0.981	0.030
AC026412.3	9.340	3.349	26.047	0.000
AC145343.1	1.720	1.269	2.330	0.000
AC010186.3	1.812	1.005	3.267	0.048
AC019080.1	11.854	2.746	51.181	0.001
AL135488.1	1.437	1.081	1.910	0.013
LINC00205	1.559	1.195	2.034	0.001
AC018904.1	1.324	1.016	1.725	0.038
LINC00654	2.305	1.332	3.988	0.003

(b)

Figure 1: (a) Flow chart of the study. (b) Univariate Cox results for prognosis-associated lncRNA.

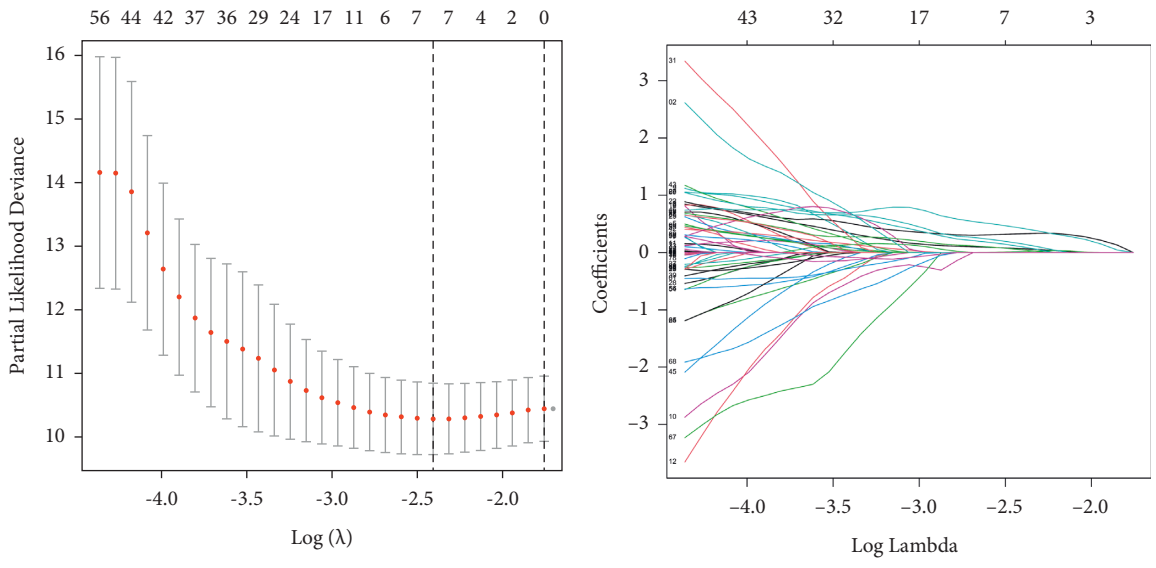

(a) (b)

Figure 2: (a) LASSO cross-validation plot based on seven CRLRs. (b) LASSO coefficient of the seven CRLRs in PHC.

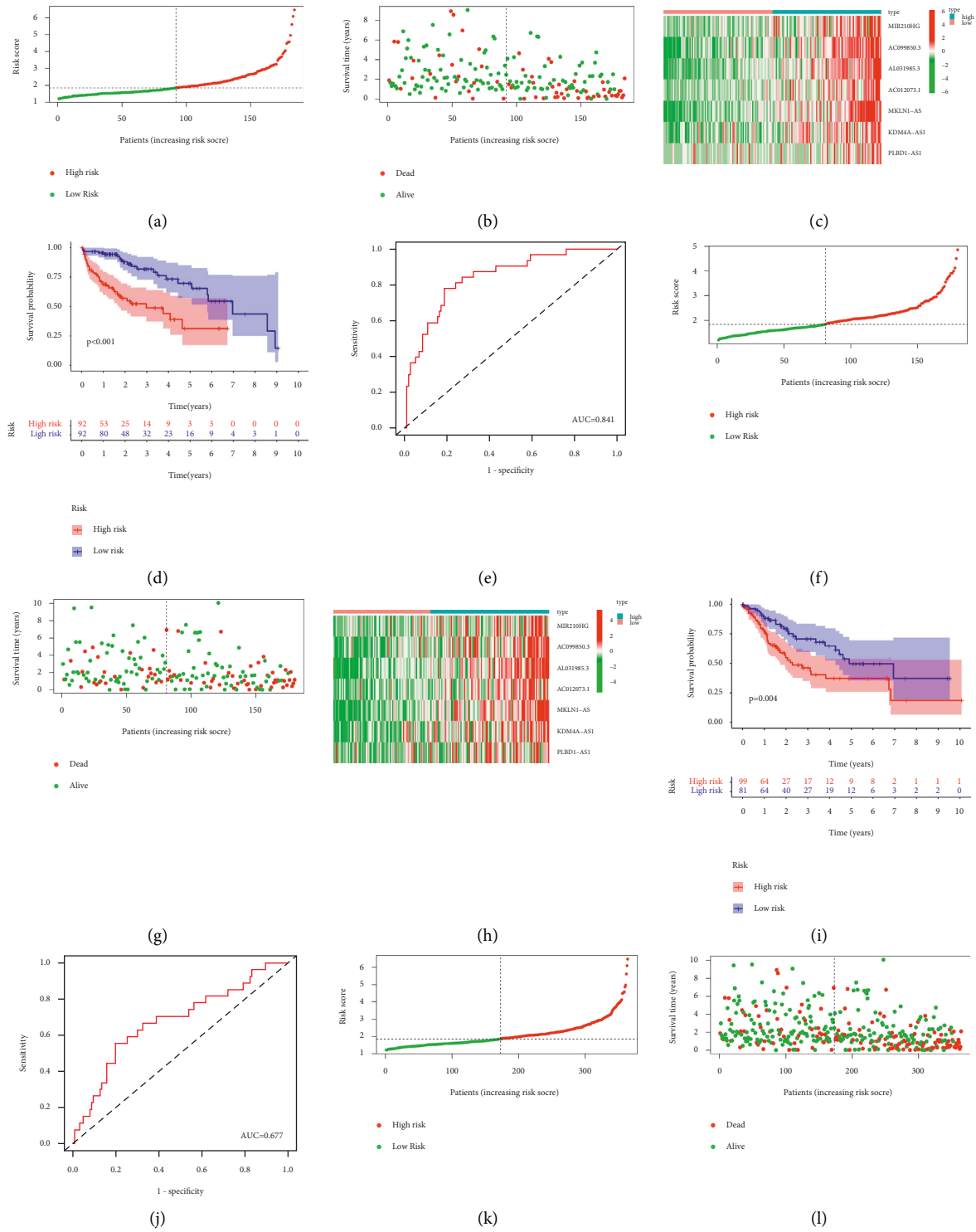

Figure 3: Continued.

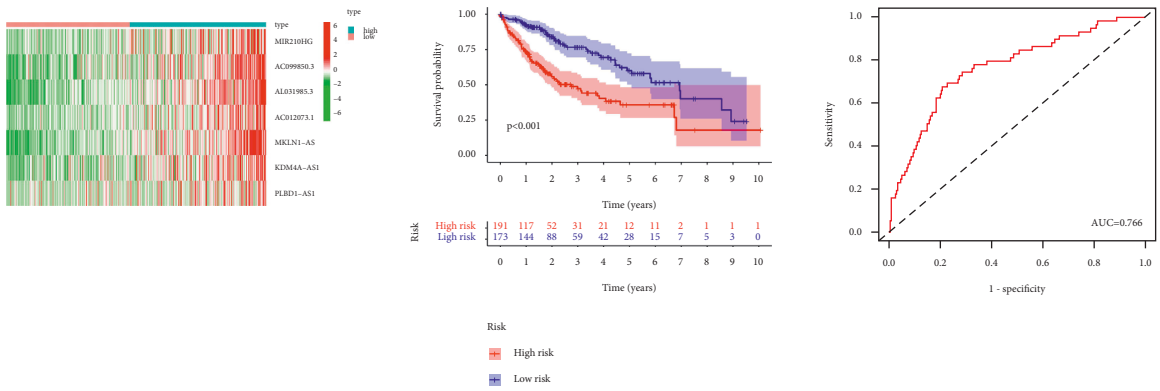

(m) (n) (o)

Figure 3: (a) Distribution of risk scores in the training cohort of patients with PHC, based on CRLRs. (b) Scatter plots show the association between the OS and the risk score in the training cohort of PHC patients, according to prognostic features of CRLRs. (c) A heat map shows seven CRLRs (MIR210HG, AC099850.3, AL031985.3, AC012073.1, MKLN1-AS, KDM4A-AS1, and PLBD1-AS1) with high expression in high-risk patients in the training cohort. (d) KM survival curve analysis of the training cohort. (e) Area under the ROC curve for the training cohort, based on CRLR-based prognostic features at 12 months. (f) Distribution of risk scores in the testing cohort of patients with PHC, based on CRLRs. (g) Scatter plots show the association between the OS and the risk score in the testing cohort of PHC patients, according to prognostic features of CRLRs. (h) A heat map shows the same seven CRLRs with high expression in high-risk patients in the testing cohort. (i) KM survival curve analysis of the testing cohort. (j) Area under the ROC curve for the testing cohort, based on CRLRs-based prognostic features at 12 months. (k) Distribution of risk scores for the entire cohort of patients with PHC, based on CRLRs. (l) Scatter plots show the association between the OS and the risk score for the entire cohort of PHC patients, according to prognostic features of CRLRs. (m) Heat map shows the same seven CRLRs with high expression in high-risk patients among the entire cohort. (n) KM survival curve analysis of the entire cohort. (o) Area under the ROC curve for the entire cohort, based on CRLRs-based prognostic features at 12 months.

those in the high-risk group (Figure 3(i), $p = 0.004$). Likewise, among the whole group, patients in the high-risk group had worse survival times than those in the low-risk group (Figure 3(n), $p < 0.001$).

A ROC curve was plotted to predict the 1-year survival and assess the accuracy and sensitivity of the prediction model. The AUC was 0.814 in the training group, 0.677 in the test group, and 0.766 in the whole group, indicating excellent accuracy for the model (Figures 3(e), 3(j), and 3(o)). Principal components analysis confirmed the differential expression of CRLRs in PHC patients (Figures 4(a)–4(d)). To compare the effects of the clinical characteristics and risk score on prognosis, univariate Cox proportional regression was performed. This showed that the overall PHC stage and risk score were correlated with the prognosis of PHC in both the training group (Figure 5(a), $p < 0.001$) and the test group (Figure 5(d), ($p < 0.01$). Multivariate Cox regression analysis showed that the overall stage and risk score in both the training and test groups were independent factors for the prognosis of PHC (Figures 5(b) and 5(e), $p < 0.05$); the risk score was the most significant. A ROC curve was drawn according to the clinical characteristics and risk score, and it showed that the AUC of the risk score was maximized in the training, test, and whole groups; this indicates that the CRLRSM had high accuracy and sensitivity for predicting the prognoses of PHC patients (Figures 5(c), 5(f), and 5(g)).

3.3. Predictive Nomogram. A predictive nomogram for cancer risk can estimate the survival of specific cancer patients based on individual data Based on multivariate Cox regression, the overall stage and risk score were included to construct the nomogram (Figure 6(a)). The whole group was internally validated using the C-index (Figure 6(b)). The 1-year, 3-year, and 5-year AUCs of the nomogram were 0.766, 0.716, and 0.693, respectively, suggesting that the nomogram had excellent specificity and sensitivity for predicting the OS time (Figure 6(c)). The calibrated nomogram was consistent with the diagonal, indicating the predictive value of the nomogram for 1-year, 3-year, and 5-year OS (Figure 6(d)). These results demonstrated that the CRLRSM-based nomogram had good prediction performance for the prognoses of patients with PHC.

3.4. Enrichment Analysis of Function Pathway Sets. Boxplots were used to analyze the FDX1, CDKN2A, MTF1, and GLS genes of the patients in the two groups. FDX1 expression levels in the low-risk group of patients were significantly increased (Figure 7(a), $p < 0.001$); CDKN2A, GLS, and MTF1 expression levels were significantly increased in the high-risk group of patients (Figures 7(b)–7(d), $p < 0.001$). This shows that PHC patients with high expression of FDX1 had better prognoses, whereas those with high expression of CDKN2A, MTF1, and GLS had worse prognoses. We conducted gene set enrichment analysis to explore the potential biological functions and signaling pathways between the two groups. There were 52 active pathways in the high-risk group (Figure 8(a), FDR < 0.05). The enrichment pathways were associated with cellular metabolism, repair, growth, proliferation, apoptosis, and immunity. There were 2 active pathways were related to

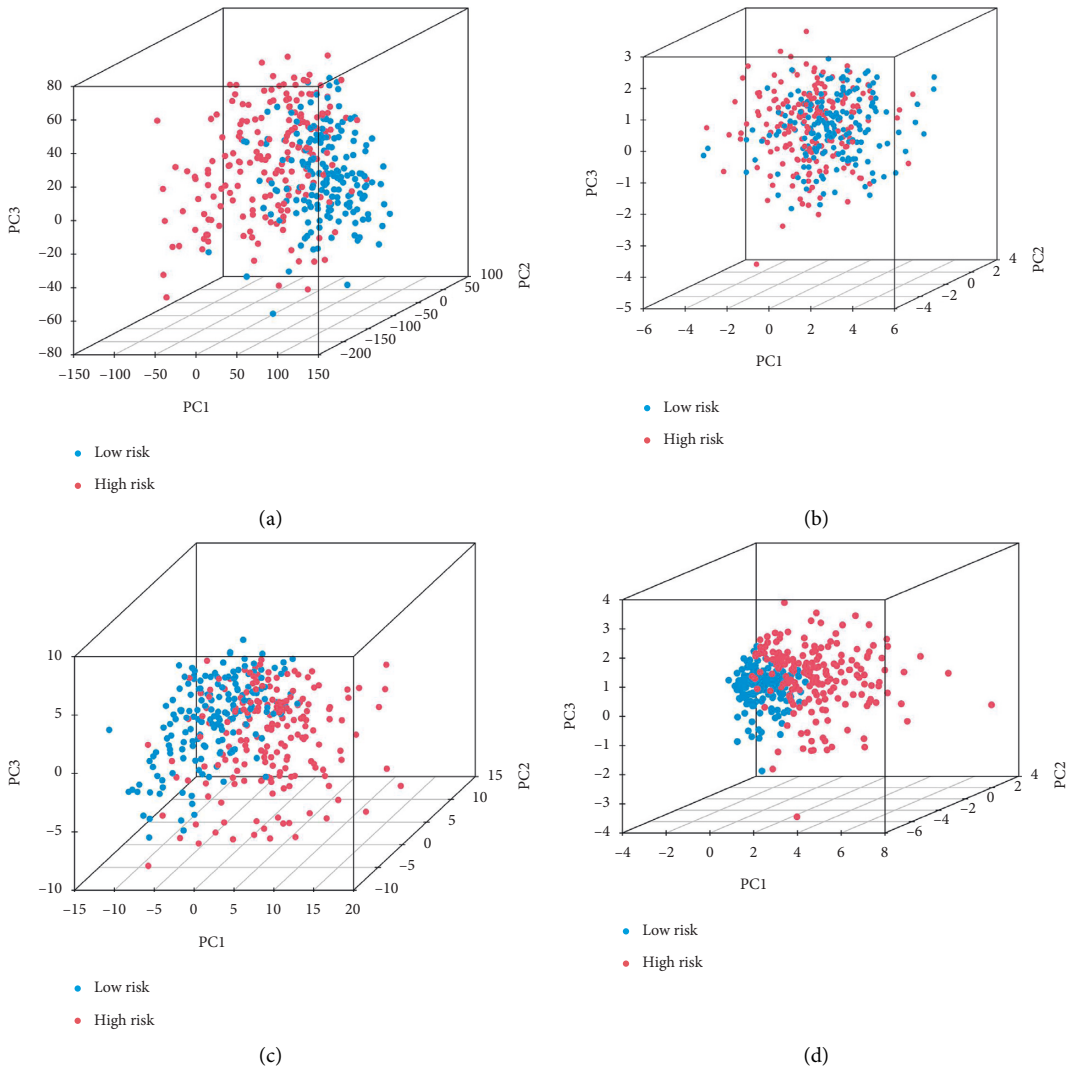

Figure 4: The high-risk and low-risk groups are analyzed using (a) the whole gene set, (b) the cuproptosis gene set, (c) the cuproptosis lncRNA set, and (d) the cuproptosis risk lncRNA set.

tricarboxylic acid metabolism in the low-risk group (Figure 8(a), FDR < 0.05).

3.5. Correlation between Prognostic Risk Scores and Immune Cells. The CIBERSORT algorithm was used to analyze 22 different immune cells for the two groups of patients. There were positive correlations between the risk score and M0 macrophages ($R = 0.36$, $p = 8.1 \times 10^{-10}$), neutrophils ($R = 0.15$, $p = 0.015$), and follicular helper T cells ($R = 0.23$, $p = 9.3 \times 10^{-05}$) (Figures 9(a)–9(c)). Negatively correlations were found between the risk score and resting mast cells ($R = -0.23$, $p = 9.9 \times 10^{-05}$), monocytes ($R = -0.14$, $p = 0.018$), activated natural killer (NK) cells ($R = -0.13$, $p = 0.027$), $CD8^+$ T cells ($R = -0.12$, $p = 0.046$), gamma delta T cells ($R = -0.19$, $p = 0.0013$), and naive B cells ($R = -0.12$, $p = 0.038$) (Figures 9(d)–9(i)). This indicates that PHC prognosis is associated with immune cell infiltration.

3.6. Overexpression of MIR210HG, MKLN1-AS, and PLBD1-A in PHC Patients. The expression levels of the seven CRLRs in liver cancer cells and normal hepatocytes were measured using PCR. The results showed that MIR210HG, MKLN1-AS, and PLBD1-AS were overexpressed in liver cancer cells (Figures 10(a) fig10–10(c)); the expression of the other four CRLRs was decreased. This might be attributed to the variances among the different cell lines and false-positive results of the prediction (Figure 10(d)).

4. Discussion

Cell death is a physiological process. The mechanism of cell death varies. Apoptosis [18], pyroptosis [19], necrosis [20], and ferroptosis [21–23] are the most commonly observed. Recently, Tsvetkov et al. found a copper-based mechanism that was completely different from the known mechanisms of cell death, and they named it "cuproptosis" [7]. LncRNAs

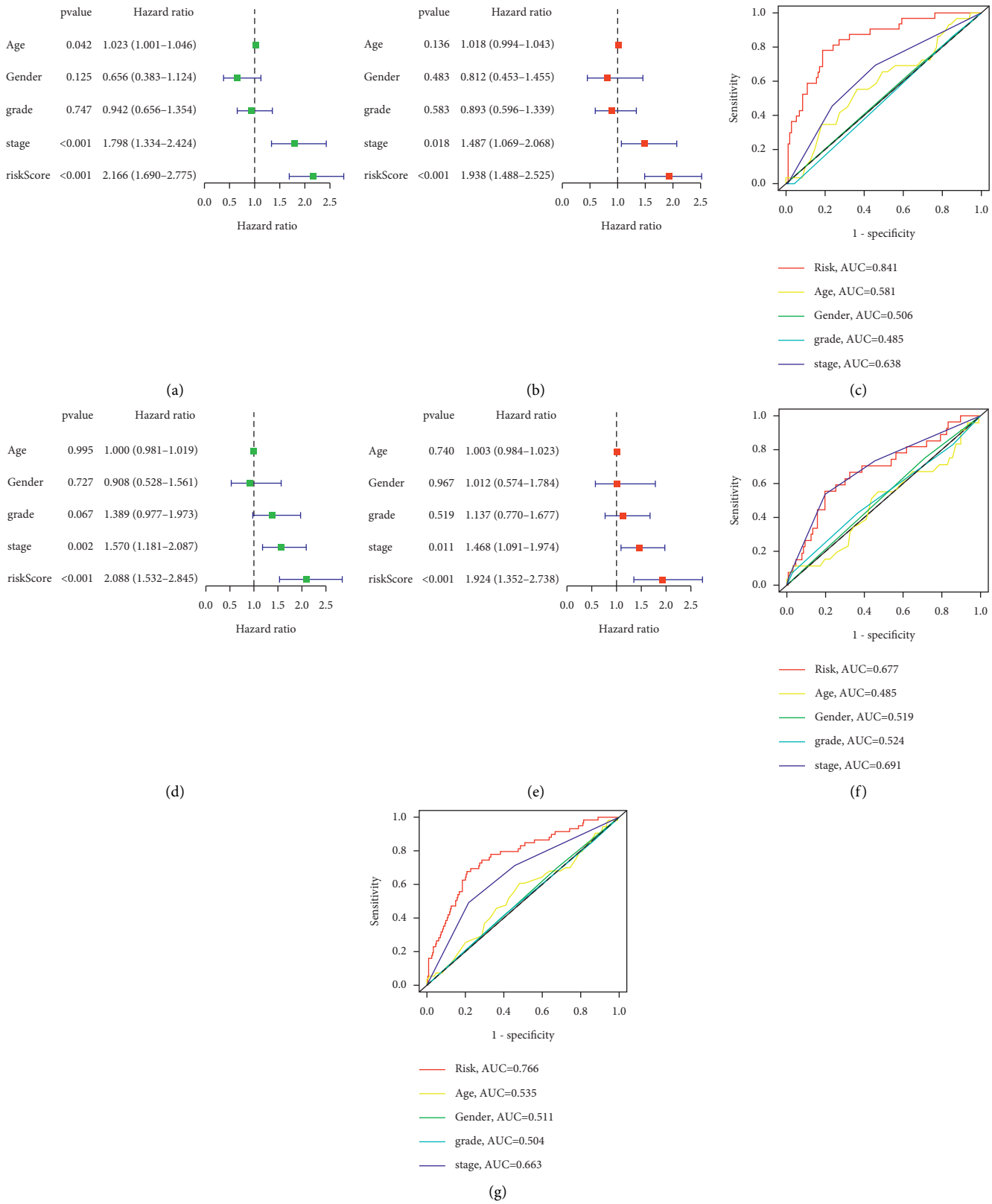

Figure 5: (a) Univariate Cox regression showing that the age, stage, and risk score are associated with OS in the training cohort ($p < 0.05$). (b) Multivariate Cox regression shows that the stage and risk score ($p < 0.05$) are independent prognostic indicators of OS in patients with PHC in the training cohort. (c) ROC curve shows that the stage and risk score have the highest prognostic accuracy in the training cohort. (d) Univariate Cox regression shows that the stage and risk score are associated with OS in the testing cohort ($p < 0.01$). (e) Multivariate Cox regression shows that the stage and risk score ($p < 0.05$) are independent prognostic indicators of OS in patients with PHC in the testing cohort. (f) ROC curve shows that the stage and risk score have the highest prognostic accuracy in the testing cohort. (g) ROC curve shows that the stage and risk score have the highest prognostic accuracy for the entire cohort.

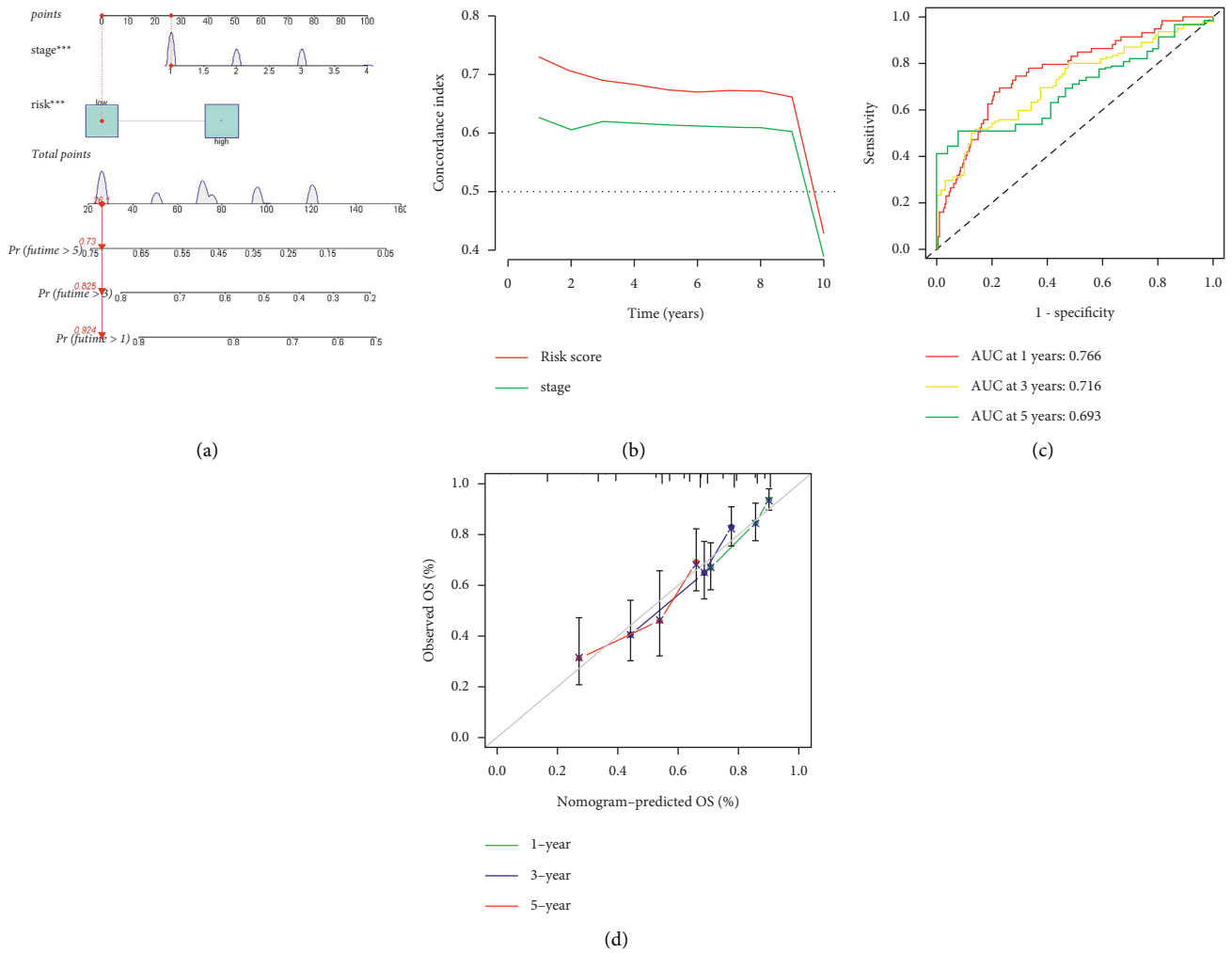

Figure 6: (a) Survival nomogram on risk score and stage. (b) Concordance index on risk score and stage. (c) ROC curve comparing the prognostic power of the nomogram at 1, 3, and 5 years for the entire cohort. (d) Calibration curves were corrected for predicting liver cancer patients at 1, 3, and 5 years for the entire cohort.

have been shown to be associated with hepatic carcinoma [24, 25]. Therefore, we built a cuproptosis-related lncRNA prognostic risk model to predict the prognoses of patients with PHC, explore its potential pathogenesis, and facilitate individualized treatment.

Hepatoma tissue samples were divided into CRLRSM high-risk and low-risk groups. The OS of patients in the high-risk group was worse than that of patients in the low-risk group. The CRLRSM was an independent prognostic factor for PHC and had a good predictive performance for the prognoses of patients with PHC. Correlation analyses between the CRLRSM and cuproptosis-related genes showed that patients with high FDX1 expression had better prognoses, indicating that high expression of FDX1 might promote cancer cell death. patients with high expression of CDKN2A, MTF1, and GLS had worse prognoses, suggesting that CDKN2A, MTF1, and GLS might promote the proliferation of cancer cells. This is consistent with the findings of Tsvetkov et al. [7], who identified FDX1 as a key regulator of cuproptosis and an upstream regulator of protein lipoacylation, and the abundance of FDX1 and lipoacylated proteins is highly correlated with a variety of human tumors. The results also suggest that CDKN2A, MTF1, and GLS are negative feedback genes that inhibit apoptosis and promote cell survival. At the same time, the enrichment pathway of the CRLRSM high-risk group was related to tumor cell genesis and proliferation. The enrichment pathway of the CRLRSM low-risk group was mainly related to the tricarboxylic acid cycle, and was mainly in the upstream pathway entering the tricarboxylic acid cycle, indicating that the progress of the tricarboxylic acid cycle was blocked. Therefore, these seven CRLns may be potential targets for the treatment of PHC.

We validated the expression of the seven CRLRs in hepatic cancer cells and normal hepatocytes and found that MIR210HG, MKLN1-AS, and PLBD1-AS were highly overexpressed in hepatic cancer cells. Recent studies have shown that overexpression of MKLN1-AS is associated with a lower OS rate and shorter disease-free survival. The downregulation of MKLN1-AS reduces the proliferation, migration, and invasion of cancer cells and induces apoptosis. *In vivo* inhibition can also suppress the proliferation

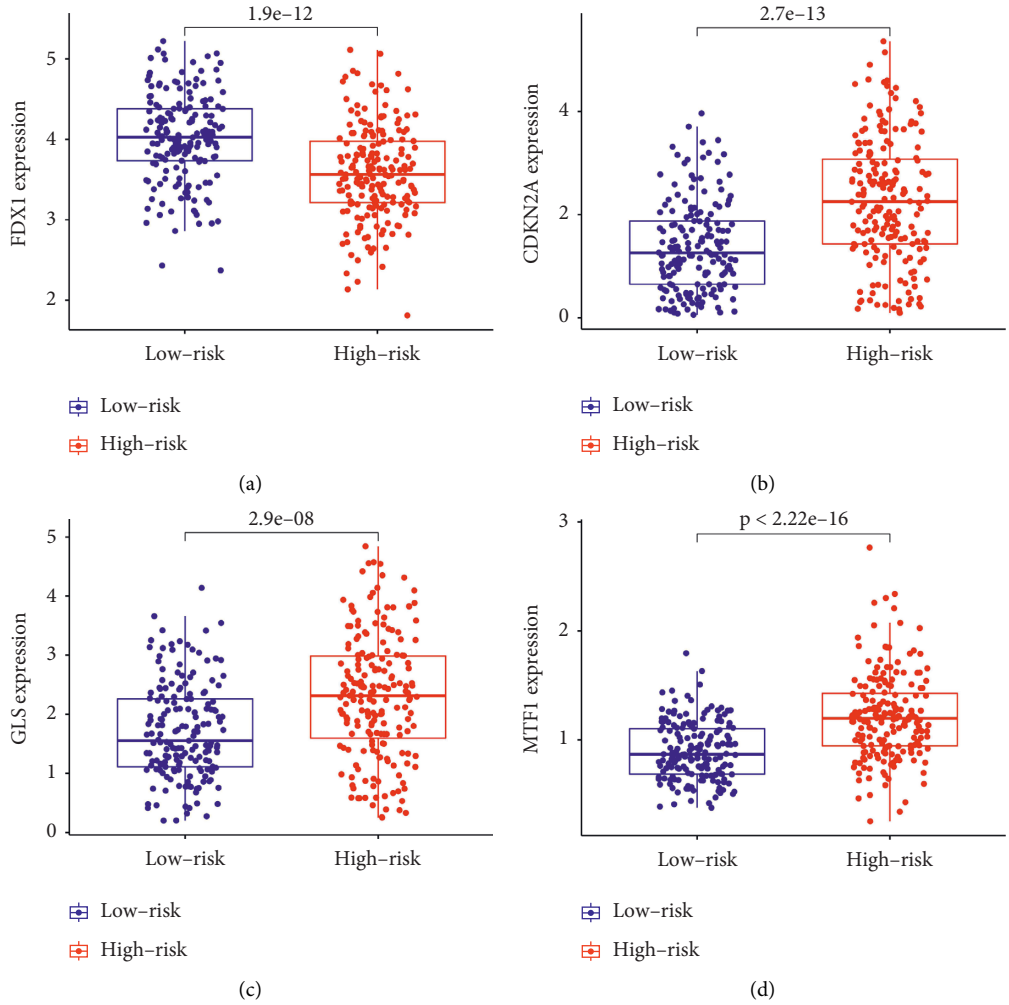

Figure 7: Different expression of (a) FDX1, (b) CDKN2A, (c) GLS, and (d) MTF1 in the high- and low-risk groups.

of hepatic cancer cells. MKLN1-AS has been shown to serve as a molecular sponge for miR-654-3p, upregulate the expression of HCC-derived growth factor (HDGF), and promote cancer growth [26]. The upregulation of MKLN1-AS also leads to poor prognoses in patients with PHC. MKLN1-AS positively regulates the expression of YAP1 via targeting and stabilizing YAP1 mRNA, and it enhances the proliferation, migration, and invasion of hepatic cancer cells through YAP1. It can also induce the expression of YAP1 *in vivo* to cause hepatic carcinogenesis [27].

MIR210H was first found to be overexpressed in osteosarcoma and glioma. Wang et al. discovered that hepatic cancer cells overexpressing MIR210H contributed to poor prognoses in patients, whereas silencing MIR210H inhibited proliferation, migration, and invasion of cancer cells [28]. AC099850.3 and KDM4A-AS1 are newly identified lncRNAs, and their overexpression indicates an adverse prognosis in PHC patients. Knockout of AC099850.3 might significantly inhibit the proliferative and migratory potential of hepatic cancer cells and promoted their death. A previous study proposed that AC099850.3 served as an oncogene through the PRR11/PI3K/AKT pathway [29]. KDM4A-AS1 promotes the proliferation, migration, and invasion of hepatic cancer cells *in vitro* and promotes the growth of hepatic cancer cells and lung metastasis *in vivo*. It is suggested that KDM4A-AS1 is regulated retrograde by miR-411-5p at the post-transcriptional level and promotes the expression of KPNA2 by competitively binding to miR-411-5p to activate the AKT pathway. KPN2 silencing, miR-411-5p overexpression, and AKT inhibitors (e.g., MK2206) can reverse KDM4A-AS1-enhanced hepatoma cell proliferation, migration, and epithelial-mesenchymal transformation. KDM4A-AS1 is considered to be a new hypoxia response gene that promotes the growth and metastasis of hepatic cancer [30] through KDM4A-AS1/KPNA2/HIF-1α signaling.

Gene set enrichment analysis showed that the mTOR, p53, ErbB, and insulin signaling pathways, ubiquitin-mediated proteolysis, inositol phosphate metabolism, and the phosphatidylinositol signaling system were associated with the metabolism, growth, proliferation, and apoptosis of cancer cells. The ubiquitin-proteasome system (UPS) had the strongest correlation. The UPS is a multicomponent system for protein degradation in cells and is involved in multiple cellular biological activities such as cell growth and differentiation, DNA replication and repair, cellular

IncRNA set name	NES	NOM p-val	FDR q-val
KEGG_UBIQUITIN_MEDIATED_PROTEOLYSIS	1.947	0.000	0.014
KEGG_NUCLEOTIDE_EXCISION_REPAIR	1.951	0.000	0.015
KEGG_PURINE_METABOLISM	1.953	0.000	0.017
KEGG_BASE_EXCISION_REPAIR	1.849	0.002	0.018
KEGG_SPHINGOLIPID_METABOLISM	1.852	0.000	0.018
KEGG_NON_SMALL_CELL_LUNG_CANCER	1.898	0.000	0.018
KEGG_DNA_REPLICATION	1.840	0.000	0.018
KEGG_PYRIMIDINC_METABQLISM	1.967	0.000	0.019
KEGG_VASOPRESSIN_REGULATED_WATER_REABSORPTION	1.853	0.004	0.019
KEGG_ENDOMETRIAL_CANCER	1.905	0.002	0.019
KEGG_INOSITOl_PHOSPHATC_METABOLISM	1.864	0.000	0.019
KEGG_RNA_POLYMERASE	1.857	0.000	0.019
KEGG_HOMOLOGOUS_RECOMBINATION	1.916	0.000	0.019
KEGG_ERBB_SIGNALING_PATHWAY	1.865	0.000	0.019
KEGG_BASAL_TRANSCRIPTION_FACTORS	1.832	0.002	0.020
KEGG_GLIOMA	1.866	0.000	0.020
KEGG_PROGESTERONC_MEDIATED_OOCYTE_MATURATION	1.872	0.000	0.020
KEGG_MISMATCH_REPAIR	1.882	0.000	0.021
KEGG_CHRONIC_MYELOID_LEUKEMIA	1.874	0.002	0.021
KEGG_INSULIN_SIGNALING_PATHWAY	1.824	0.002	0.021
KEGG_ENDOCYTOSIS	1.918	0.000	0.021
KEGG_OOCYTC_MEIOSIS	1.978	0.000	0.022
KEGG_SPLICEOSOME	1.817	0.006	0.022
KEGG_ADHERENS_JUNCTION	1.794	0.006	0.025
KEGG_BLADDER_CANCER	1.797	0.004	0.025
KEGG_SNARE_INTERACTIONS_IN_VESICULAR_TRANSPORT	1.800	0.004	0.025
KEGG_PANCREATIC_CANCER	1.803	0.002	0.025
KEGG_PATHWAYS_IN_CANCER	1.803	0.006	0.026
KEGG_PHOSPHATIDYLINOSITOl_SIGNALlNG_SYSTEM	1.776	0.002	0.028
KEGG_P53_SIGNALING_PATHWAY	1.779	0.000	0.029
KEGG_RNA-DEGRADATION	1.988	0.000	0.029
KEGG_PROSTATE_CANCER	1.767	0.008	0.030
KEGG_LYSOSOME	1.752	0.018	0.032
KEGG_MTOR_SIGNALING_PATHWAY	1.753	0.002	0.033
KEGG_N_GLYCAN_BIOSYNTHESIS	1.755	0.014	0.033
KEGG_COLORECTAL_CANCER	1.746	0.004	0.034
KEGG_RIG_I_LIKE_RECEPTOR_SIGNALING_PATHWAY	1.743	0.008	0.034
KEGG_THYROID_CANCER	1.739	0.004	0.035
KEGG_NEUROTROPHIN_SIGNALING_PATHWAY	1.734	0.006	0.036
KEGG_ACUTE_MYELOID_LEUKEMIA	1.732	0.008	0.037
KEGG_REGULATION_OF_AUTOPHAGY	1.727	0.009	0.037
KEGG_SMALL_CELL_LUNG_CANCER	1.728	0.014	0.037
KEGG_SELENOAMINO_ACID_METABOLISM	1.719	0.008	0.038
KEGG_REGULATION_OF_ACTIN_CYTOSKELETON	1.720	0.010	0.039
KEGG_CYTOSOLIC_DNA-SENSING_PATHWAY	1.715	0.016	0.039
KEGG_LYSINE_DEGRAOATION	1.701	0.014	0.042
KEGG_FC_GAMMA_R_MEDIATED_PHAGOCYTOSIS	1.703	0.008	0.042
KEGG_MELANOGENESIS	1.696	0.002	0.043
KEGG_CELL_CYCLE	2.021	0.000	0.044
KEGG_RENAL_CElL_CARCINOMA	1.690	0.010	0.045
KEGG_HUNTINGTONS_DISEASE	1.685	0.029	0.046
KEGG_VIBRIO_CHOLERAE_INFECTION	1.679	0.018	0.047

NES, normalized enrichment score; NOM, nominal; FDR, false discovery rate.

(a)

IncRNA set name	NES	NOM p-val	FDR q-val
KEGG_PRIMARY_BILE_ACID_BIOSYNTH	-1.88642	0	0.025761865
KEGG_FATTY_ACID_METABOLISM	-1.89435	0.00203252	0.035317067

NES, normalized enrichment score; NOM, nominal; FDR, false discovery rate.

(b)

Figure 8: CRLRs set enrichment analysis for the (a) high-risk group and (b) low-risk group.

metabolism, and the immune response, affecting the degradation of most proteins in eukaryotic cells [31].UPS dysfunction has been found to be closely related to multiple diseases, including neurodegenerative diseases, cancer, cardiovascular diseases, and respiratory diseases [32].

UPS dysfunctions can be divided into two categories based on specific mechanisms. The first involves genetic mutation of the enzymes or substrates of the UPS system, in which normal UPS targets are no longer subject to being ubiquitinated and degraded; subsequently, they constantly accumulate in the cells. The second category is abnormal activation of the UPS, which accelerates the degradation of intracellular proteins. There are also UPS inhibitors, such as bortezomib, which inhibit the catalytic activity of the proteasome subunits, resulting in mitochondrial membrane depolarization and cell apoptosis. Apoptosis is induced mainly by an increase in intracellular p27 and p53 levels [33]. Second-generation proteasome inhibitors, including kafizomib and oral isazomib, are used for the treatment of multiple myeloma. TP53 encodes a transcription factor, and the tumor suppressor p53 is activated and stabilized simultaneously in response to cellular stress and DNA

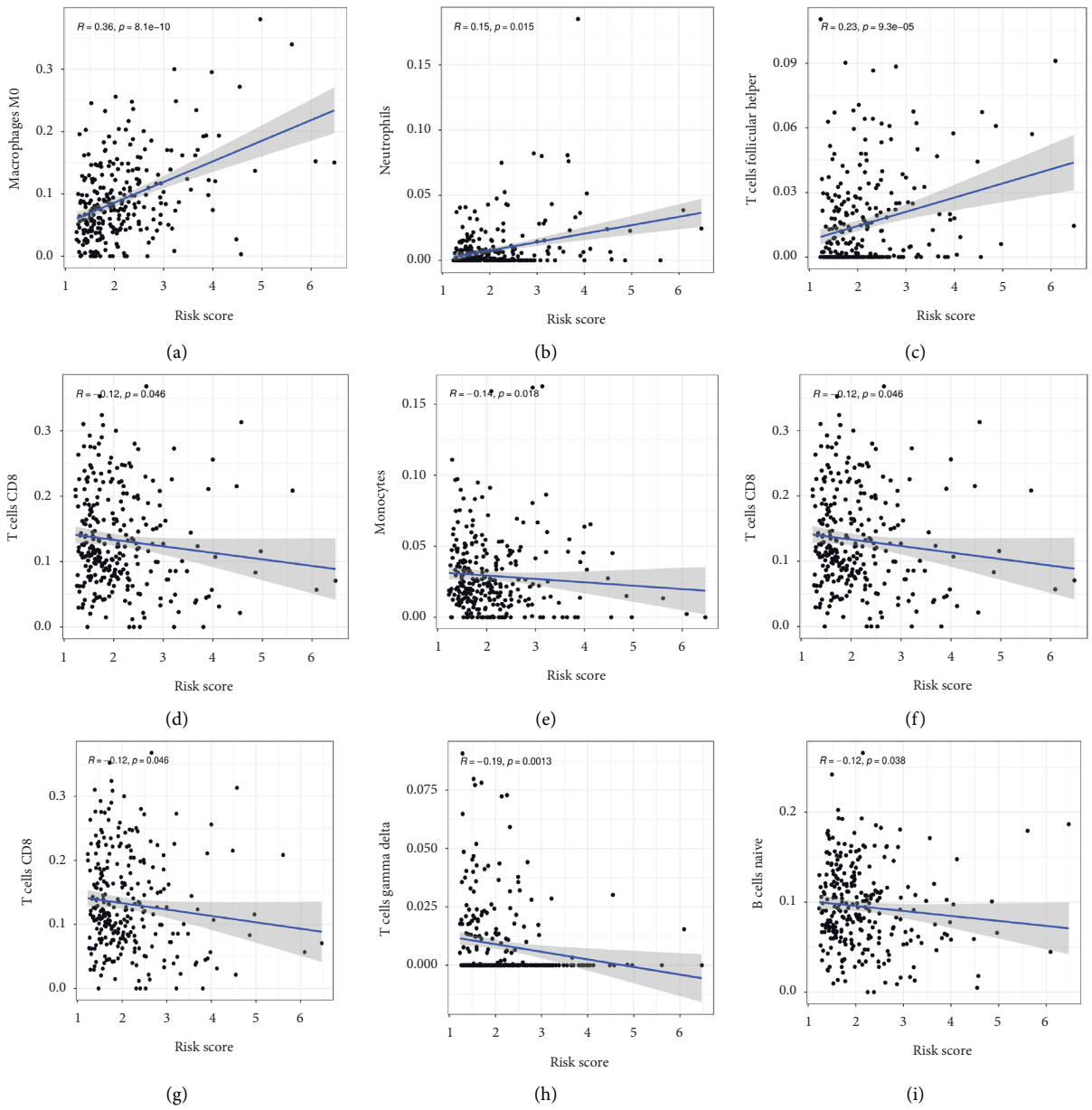

Figure 9: Relationships between the CRLRs and infiltration abundances of nine types of immune cells, as analyzed using Spearmen's correlation analysis. (a) M0 macrophages; (b) neutrophils; (c) follicular helper T cells; (d) resting mast cells; (e) monocytes; (f) activated NK cells; (g) $CD8^+$ T cells; (h) gamma delta T cells; (i) naive B cells.

damage; this is the basis for its central role as a tumor suppressor [34, 35].

It has been found that the MDM2 gene is expressed in the UPS and p53 signal pathways. MDM2 inhibits p53-induced apoptosis and is the most connected functional target of p53. Its N-terminal domain binds to the transcriptional activation domain of p53, hinders the binding of p53 to its cotranscriptional activators, and subsequently inhibits the activation of p53 target genes [36]. The RING domain in the C-terminus of MDM2 has E3 ubiquitin ligase activity and can ubiquitinate and degrade p53 [37]. In some human tumors, MDM2 has been demonstrated to be upregulated abnormally due to gene magnification, increased transcription, and enhanced translation; these would induce increased degradation and decreased activity of p53 [38]. Based on the strategy of blocking the protein interaction between p53 and MDM2, some small molecules have been developed, including BI-907828 [39], miladematan [40], and APG-115 [41]. Among these agents, APG-115 and miladematan have been approved for clinical trials and have yielded preliminary clinical data [42, 43]. Upregulation of the phosphocreatine kinase signal pathway, insulin signal pathway, and ErbB signal pathway can activate the PI3K/AKT pathway and mTOR, which plays a critical role in the

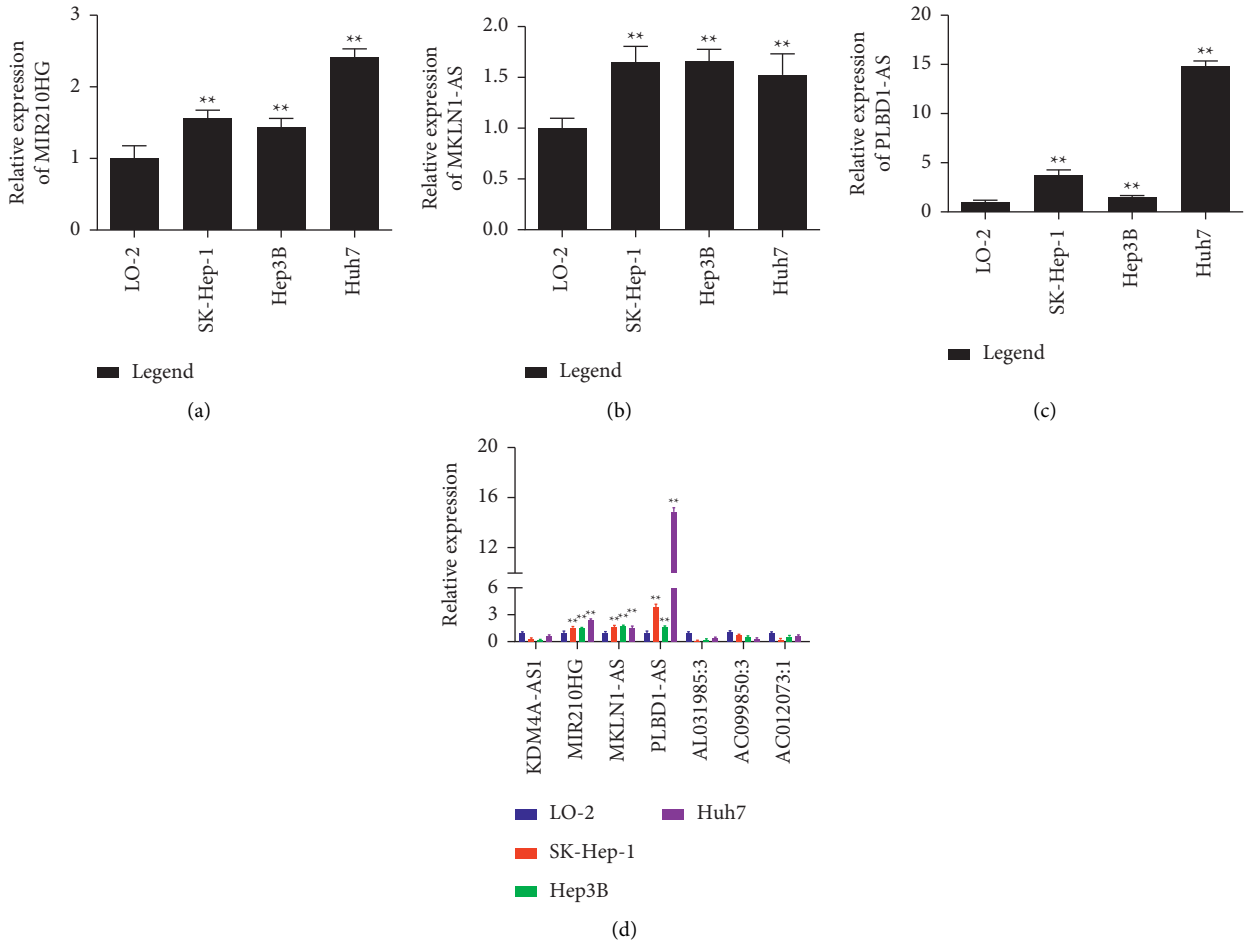

FIGURE 10: The results of RT-qPCR for (a) MIR210HG, (b) MKLN1-AS, and (c) PLBD1-AS in the hepatoma cell lines. (d) The results of RT-qPCR for the seven CRLRs in the hepatoma cell lines. ** $p < 0.01$.

regulation of autophagy [44]. The mTOR signal is highly activated in most cancers, especially in the process of cell transformation, growth, and survival [45].

The correlations between risk scores and immune cells showed that immune cell infiltration is associated with the prognosis of PHC. Several enriched pathways were associated with the immune response. For example, the ErbB pathway downregulates the chemokine ligand CXCL10 through PI3K–AKT signaling and interferon regulatory factor IRF1, which results in the reduction of effector $CD8^+$ T cells and recruitment of T_{reg} cells into the tumor microenvironment; this leads to immune escape and cancer growth [46]. PI3K–AKT–mTOR regulates many characteristics of the immunosuppressive microenvironment. The latest data from clinical trials and preclinical mouse models suggest that the therapeutic inhibition of the PI3K–AKT–mTOR signaling network might have dual benefits: preventing tumor progression by suppressing proliferation, migration, and survival of cancer cells, and enhancing the tumor immune surveillance pathway and intrinsic antitumor immune characteristics by inhibiting the activation of immunosuppressants [47]. Shishir et al. believed that the tumor microenvironment of HCC still remains a major challenge to therapeutic success. To explore a new strategy of combined immunotherapy will hopefully lead to major improvements in survival for patients [48].

In conclusion, hepatic carcinogenesis is a complicated process that involves multiple biological functions and pathways. This often results in unsatisfactory therapeutic outcomes and poor survival rates in patients with PHC. The seven CRLns in the high-risk group were found to be involved in multiple pathways to promote the growth, proliferation, invasion, and migration of PHC. The low-risk group was involved in multiple pathways related to the tricarboxylic acid cycle, therefore, silencing the seven CRLns may promote tumor cell death, which is a potential target for the treatment of PHC, and further research is needed to verify its mechanism and efficacy in the future. This study has several limitations. First, the data were obtained from the UCSC Xena public database, which has a limited sample size. Second, we did not explore further functional genomics and pathways, although we assessed the expression of CRLR in hepatoma cells and normal hepatocytes. Lastly, our study lacks further validation from cohort, prospective, multicenter, and real data.

Data Availability

The raw data could be obtained from the corresponding author.

Conflicts of Interest

The authors declare that they have no conflicts of interest

References

[1] B. E. Kim, T. Nevitt, and D. J. Thiele, "Mechanisms for copper acquisition, distribution and regulation," *Nature Chemical Biology*, vol. 4, no. 3, pp. 176–185, 2008.

[2] T. D. Rae, P. J. Schmidt, R. A. Pufahl, V. C. Culotta, and T. O'Halloran, "Undetectable intracellular free copper: the requirement of a copper chaperone for superoxide dismutase," *Science*, vol. 284, no. 5415, pp. 805–808, 1999.

[3] K. Shimada, E. Reznik, M. E. Stokes et al., "Copper-binding small molecule induces oxidative stress and cell-cycle arrest in glioblastoma-patient-derived cells," *Cell Chemical Biology*, vol. 25, no. 5, pp. 585–594, 2018.

[4] N. C. Yip, I. S. Fombon, P. Liu et al., "Disulfiram modulated ROS-MAPK and NFκB pathways and targeted breast cancer cells with cancer stem cell-like properties," *British Journal of Cancer*, vol. 104, no. 10, pp. 1564–1574, 2011.

[5] D. Chen, Q. C. Cui, H. Yang, and Q. P. Dou, "Disulfiram, a clinically used anti-alcoholism drug and copper-binding agent, induces apoptotic cell death in breast cancer cultures and xenografts via inhibition of the proteasome activity," *Cancer Research*, vol. 66, no. 21, pp. 10425–10433, 2006.

[6] Z. Skrott, M. Mistrik, K. K. Andersen et al., "Alcohol-abuse drug disulfiram targets cancer via p97 segregase adaptor NPL4," *Nature*, vol. 552, no. 7684, pp. 194–199, 2017.

[7] P. Tsvetkov, S. Coy, B. Petrova et al., "Copper induces cell death by targeting lipoylated TCA cycle proteins," *Science*, vol. 375, no. 6586, pp. 1254–1261, 2022.

[8] R. L. Siegel, K. D. Miller, H. E. Fuchs, and A. Jemal, "Cancer statistics, 2022," *CA: A Cancer Journal for Clinicians*, vol. 72, no. 1, pp. 7–33, 2022.

[9] A. Bhan, M. Soleimani, and S. S. Mandal, "Long noncoding RNA and cancer: a new paradigm," *Cancer Research*, vol. 77, no. 15, pp. 3965–3981, 2017.

[10] Y. Li, J. Zou, B. Li, and J. Du, "Anticancer effects of melatonin via regulating lncRNA JPX-Wnt/β-catenin signalling pathway in human osteosarcoma cells," *Journal of Cellular and Molecular Medicine*, vol. 25, no. 20, pp. 9543–9556, 2021.

[11] L. Yang, Y. Li, R. Gong et al., "The long non-coding RNA-ORLNC1 regulates bone mass by directing mesenchymal stem cell fate," *Molecular Therapy*, vol. 27, no. 2, pp. 394–410, 2019.

[12] R. Esposito, N. Bosch, A. Lanzós, T. Polidori, C. Pulido-Quetglas, and R. Johnson, "Hacking the cancer genome: profiling therapeutically actionable long non-coding RNAs using CRISPR-cas9 screening," *Cancer Cell*, vol. 35, no. 4, pp. 545–557, 2019.

[13] J. Kim, H. L. Piao, B. J. Kim et al., "Long noncoding RNA MALAT1 suppresses breast cancer metastasis," *Nature Genetics*, vol. 50, no. 12, pp. 1705–1715, 2018.

[14] J. D. Ransohoff, Y. Wei, and P. A. Khavari, "The functions and unique features of long intergenic non-coding RNA," *Nature Reviews Molecular Cell Biology*, vol. 19, no. 3, pp. 143–157, 2018.

[15] M. Huarte, "The emerging role of lncRNAs in cancer," *Nature Medicine*, vol. 21, no. 11, pp. 1253–1261, 2015.

[16] J. Luo, L. F. Langer, and J. Liu, "A novel role of LncRNA in regulating tumor metabolism and angiogenesis under hypoxia," *Cancer Communications*, vol. 39, no. 1, p. 2, 2019.

[17] S. Y. Park, "Nomogram: an analogue tool to deliver digital knowledge," *The Journal of Thoracic and Cardiovascular Surgery*, vol. 155, no. 4, p. 1793, 2018.

[18] X. Yao, C. Sun, B. Fan et al., "Neurotropin exerts neuroprotective effects after spinal cord injury by inhibiting apoptosis and modulating cytokines," *Journal of Orthopaedic Translation*, vol. 26, pp. 74–83, 2021.

[19] Z. Rao, Y. Zhu, P. Yang et al., "Pyroptosis in inflammatory diseases and cancer," *Theranostics*, vol. 12, no. 9, pp. 4310–4329, 2022.

[20] F. Yang, Y. Li, G. Yan et al., "Inhibition of iron overload-induced apoptosis and necrosis of bone marrow mesenchymal stem cells by melatonin," *Oncotarget*, vol. 8, no. 19, pp. 31626–31637, 2017.

[21] S. Q. Feng, X. Yao, Y. Zhang et al., "Deferoxamine promotes recovery of traumatic spinal cord injury by inhibiting ferroptosis," *Neural Regeneration Research*, vol. 14, no. 3, pp. 532–541, 2019.

[22] Y. Zhang, C. Sun, C. Zhao et al., "Ferroptosis inhibitor SRS 16-86 attenuates ferroptosis and promotes functional recovery in contusion spinal cord injury," *Brain Research*, vol. 1706, pp. 48–57, 2019.

[23] J. Li, J. Zhang, S. Tao, J. Hong, Y. Zhang, and W. Chen, "Prognostication of pancreatic cancer using the cancer genome atlas based ferroptosis-related long non-coding RNAs," *Frontiers in Genetics*, vol. 13, Article ID 838021, 2022.

[24] T. Guo, C. Gong, P. Wu et al., "LINC00662 promotes hepatocellular carcinoma progression via altering genomic methylation profiles," *Cell Death & Differentiation*, vol. 27, no. 7, pp. 2191–2205, 2020.

[25] A. Xia, W. Yuan, Q. Wang et al., "The cancer-testis lncRNA lnc-CTHCC promotes hepatocellular carcinogenesis by binding hnRNP K and activating YAP1 transcription," *Naturaliste Canadian*, vol. 3, no. 2, pp. 203–218, 2022.

[26] W. Gao, X. Chen, W. Chi, and M. Xue, "Long non-coding RNA MKLN1-AS aggravates hepatocellular carcinoma progression by functioning as a molecular sponge for miR-654-3p, thereby promoting hepatoma-derived growth factor expression," *International Journal of Molecular Medicine*, vol. 46, no. 5, pp. 1743–1754, 2020.

[27] C. Guo, S. Zhou, W. Yi et al., "Long non-coding RNA muskelin 1 antisense RNA (MKLN1-AS) is a potential diagnostic and prognostic biomarker and therapeutic target for hepatocellular carcinoma," *Experimental and Molecular Pathology*, vol. 120, Article ID 104638, 2021.

[28] Y. Wang, W. Li, X. Chen, Y. Li, P. Wen, and F. Xu, "MIR210HG predicts poor prognosis and functions as an oncogenic lncRNA in hepatocellular carcinoma," *Biomedicine & Pharmacotherapy*, vol. 111, pp. 1297–1301, 2019.

[29] F. Zhong, S. Liu, D. Hu, and L. Chen, "LncRNA AC099850.3 promotes hepatocellular carcinoma proliferation and invasion through PRR11/PI3K/AKT axis and is associated with patients prognosis," *Journal of Cancer*, vol. 13, no. 3, pp. 1048–1060, 2022.

[30] T. Chen, R. Liu, Y. Niu et al., "HIF-1α-activated long non-coding RNA KDM4A-AS1 promotes hepatocellular carcinoma progression via the miR-411-5p/KPNA2/AKT pathway," *Cell Death & Disease*, vol. 12, p. 1152, 2021.

[31] A. Hershko and A. Ciechanover, "The ubiquitin system," *Annual Review of Biochemistry*, vol. 67, no. 1, pp. 425–479, 1998.

[32] A. H. P. Jansen, E. A. J. Reits, and E. M. Hol, "The ubiquitin proteasome system in glia and its role in neurodegenerative diseases," *Frontiers in Molecular Neuroscience*, vol. 7, p. 73, 2014.
[33] P. Robak and T. Robak, "Bortezomib for the treatment of hematologic malignancies: 15 years later," *Drugs in R & D*, vol. 19, no. 2, pp. 73–92, 2019.
[34] B. Vogelstein, D. Lane, and A. J. Levine, "Surfing the p53 network," *Nature*, vol. 408, no. 6810, pp. 307–310, 2000.
[35] A. C. Joerger and A. R. Fersht, "The p53 pathway: origins, inactivation in cancer, and emerging therapeutic approaches," *Annual Review of Biochemistry*, vol. 85, no. 1, pp. 375–404, 2016.
[36] C. A. Brady, D. Jiang, S. S. Mello et al., "Distinct p53 transcriptional programs dictate acute DNA-damage responses and tumor suppression," *Cell*, vol. 145, no. 4, pp. 571–583, 2011.
[37] O. Laptenko, I. Shiff, W. Freed-Pastor et al., "The p53 C terminus controls site-specific DNA binding and promotes structural changes within the central DNA binding domain," *Molecular Cell*, vol. 57, no. 6, pp. 1034–1046, 2015.
[38] J. Momand, D. Jung, S. Wilczynski, and J. Niland, "The MDM2 gene amplification database," *Nucleic Acids Research*, vol. 26, no. 15, pp. 3453–3459, 1998.
[39] L. Skalniak, E. Surmiak, and T. A. Holak, "A therapeutic patent overview of MDM2/X-targeted therapies (2014-2018)," *Expert Opinion on Therapeutic Patents*, vol. 29, no. 3, pp. 151–170, 2019.
[40] V. Arnhold, K. Schmelz, J. Proba et al., "Reactivating TP53 signaling by the novel MDM2 inhibitor DS-3032b as a therapeutic option for high-risk neuroblastoma," *Oncotarget*, vol. 9, no. 2, pp. 2304–2319, 2018.
[41] A. Aguilar, J. Lu, L. Liu et al., "Discovery 4-((3′R,4′S,5′R)-6″-Chloro-4′-(3-chloro-2-fluorophenyl)-1′-ethyl-2″-oxodispiro [cyclohexane-1,2′-pyrrolidine-3′,3″-indoline]-5′-carboxamido)bicyclo[2.2.2]octane-1-carboxylic acid (AA-115/APG-115): a potent and orally active murine double minute 2 (MDM2) inhibitor in clinical development," *Journal of Medicinal Chemistry*, vol. 60, pp. 2819–2839, 2017.
[42] D. W. Rasco, N. J. Lakhani, Y. Li et al., "A phase I study of a novel MDM2 antagonist APG-115 in patients with advanced solid tumors," *Journal of Clinical Oncology*, vol. 37, no. 15, p. 3126, 2019.
[43] T. M. Bauer, M. M. Gounder, A. M. Weise et al., "A phase 1 study of MDM2 inhibitor DS-3032b in patients with well/dedifferentiated liposarcoma (WD/DD LPS), solid tumors (ST) and lymphomas (L)," *Journal of Clinical Oncology*, vol. 36, no. 15, Article ID 11514, 2018.
[44] R. A. Saxton and D. M. Sabatini, "mTOR signaling in growth, metabolism, and disease," *Cell*, vol. 169, no. 2, pp. 361–371, 2017.
[45] D. Mossmann, S. Park, and M. N. Hall, "mTOR signalling and cellular metabolism are mutual determinants in cancer," *Nature Reviews Cancer*, vol. 18, no. 12, pp. 744–757, 2018.
[46] S. Kumagai, S. Koyama, and H. Nishikawa, "Antitumour immunity regulated by aberrant ERBB family signalling," *Nature Reviews Cancer*, vol. 21, no. 3, pp. 181–197, 2021.
[47] G. Xue, A. Zippelius, A. Wicki et al., "Integrated Akt/PKB signaling in immunomodulation and its potential role in cancer immunotherapy," *JNCI Journal of the National Cancer Institute*, vol. 107, no. 7, p. djv171, 2015.
[48] S. Shetty, A. Lujambio, and F. Tacke, "Editorial: overcoming the immune microenvironment of hepatocellular cancer," *Frontiers in Immunology*, vol. 12, Article ID 707329, 2021.

Hindawi
Evidence-Based Complementary and Alternative Medicine
Volume 2022, Article ID 6913315, 8 pages
https://doi.org/10.1155/2022/6913315

Research Article

The Predictive Values of MMP-9, PLTs, ESR, and CRP Levels in Kawasaki Disease with Cardiovascular Injury

Yinan Yang[1] **and Xiaobin Hu**[2]

[1]*Department of Pediatrics, Lanzhou University Second Hospital, Lanzhou University, Lanzhou, Gansu, China*
[2]*Epidemiology and Health Statistics, School of Public Health, Lanzhou University, Lanzhou, Gansu, China*

Correspondence should be addressed to Xiaobin Hu; huyang_0001@163.com

Received 5 July 2022; Revised 1 August 2022; Accepted 6 August 2022; Published 14 September 2022

Academic Editor: Xueliang Wu

Objective. To explore the levels of matrix metalloproteinase-9 (MMP-9), platelets (PLTs), C reactive protein (CRP), and erythrocyte sedimentation rate (ESR) and their predictive values in Kawasaki disease (KD) with cardiovascular injury. *Methods*. 128 children were diagnosed with KD in the Lanzhou University Second Hospital. 75 patients had coronary artery lesion (CAL), while 53 patients did not. The levels of MMP-9, PLTs, and CRP and ESR in the two groups were determined. The area under the curve (AUC) of the receiver-operating characteristic (ROC) curve and the Youden index (YI) were used to evaluate the efficacy of MMP-9, PLTs, ESR, and CRP for predicting CALs in KD. *Results*. The mean age of the patients was 2.7 ± 2.03 years (range, 2 months to 11 years). There were 87 boys (67.97%) and 41 girls (32.03%). In contrast to the NCAL group, the CAL group had obviously higher levels of MMP-9, PLTs, and CRP and an obviously higher ESR ($P < 0.05$). MMP-9 showed a linear positive correlation with ESR ($P < 0.05$) and CRP ($P < 0.05$). The AUC of the combined detection of the four indicators was 0.877, the sensitivity was 85.07% and the specificity was 78.95%. *Conclusion*. MMP-9, PLTs, ESR, and CRP are important indicators for a CAL in KD. The efficacy of the combined detection of MMP-9, PLTs, ESR and CRP is better than that of any single indicator for predicting a CAL in KD.

1. Introduction

Kawasaki disease (KD), also known as mucocutaneous lymph node syndrome, is a self-limiting disease whose major symptom is systemic arteritis. Doctor Tomisaku Kawasaki described KD for the first time in Japan in 1967 [1]. The highest incidences are seen in Japan, Korea, and Taiwan [2]. KD was also reported in China in the 1970s [3–5]. Currently, the disease has been reported worldwide [6–10]. Since the first report on KD was made 50 years ago, the etiology and pathogenic mechanism of KD remain unclear. The clinical manifestations of this disease include fever, a polymorphous rash, lymph node swelling in the neck, bilateral bulbar conjunctival congestion, alterations in the oral mucous membrane, and peripheral limb changes.

KD is pathologically characterized by the systemic inflammation of the walls of both small and medium-sized blood vessels, particularly the coronary arteries, and of multiple organs and tissues [11]. KD most frequently affects children under the age of five years [12]. Coronary artery lesions (CALs) are the most serious complication of KD and may last for many months or many years. Coronary artery dilatation and coronary artery aneurysm (CAA) are common in the acute phase, and the proportion of coronary artery stenosis gradually increases after convalescence [13, 14]. A large number of follow-up studies showed that approximately 50% of CAAs subsided within 1–2 years after onset, 80% of mild to moderate CAAs subsided within 5 years after onset [15–19], CAA diameter >5 mm may progress to stenosis, and that larger coronary artery abnormalities are associated with a greater possibility of stenosis [20]. Coronary artery abnormalities lead to potential hazards that are associated with ischemic heart disease (IHD), myocardial infarction (MI), and even sudden cardiac death (SCD) [21, 22].

Currently, CALs caused by KD have become one of the major causes of acquired heart diseases in children in Western countries and in China [23]. Studies have shown that children with KD have a higher risk of cardiovascular disease in adulthood, which is closely related to SCD in young adults and to coronary atherosclerosis in adults [17, 24]. Early exposure to high doses of intravenous immunoglobulin can reduce the incidence of CALs from 20% to 25%, and then to <5% [4].

It has been 50 years since the first report on KD was published in 1967 [12, 25]. KD has become a greater concern to an increasing number of pediatricians and cardiologists in recent years [24, 26] because KD patients show functional and structural alterations as adults due to coronary artery sequelae [28–30]. These patients may have coronary artery events in adulthood, long after the acute illness [5, 18, 31]. Therefore, the early diagnosis and treatment of KD is especially important. The purpose of this study was to find laboratory indicators with high sensitivity and specificity and to improve the early diagnosis and treatment of KD [32].

Matrix metalloproteinase-9 (MMP-9), an important member of the MMP family, may be involved in multiple inflammatory reactions. MMP-9 is considered to be very closely associated with vascular lesions in multiple diseases [33]. Studies have shown that MMP-9 plays an important role in the occurrence and development of vascular inflammation and can be used as a biochemical marker for the prediction and early diagnosis of CALs [34]. Platelets (PLTs), erythrocyte sedimentation rate (ESR), and CRP are classic inflammatory indicators in the peripheral blood for the early diagnosis of inflammatory diseases in clinical practice. Since KD is essentially a kind of vasculitis, these indicators have become increasingly meaningful in the clinical diagnosis of KD [35]. Thus, the present study aimed to examine the values of MMP-9, PLTs, ESR, and CRP for predicting CALs in KD via the combined detection of their levels.

2. Materials and Methods

2.1. Research Subjects. This study included 128 children who were diagnosed with KD based on clinical symptoms and color doppler echocardiography who were hospitalized from November 2015 to December 2018 at Lanzhou University Second Hospital. The age of the onset ranged from 2 months to 11 years old. There were 87 boys and 41 girls, with a male/female ratio of 2.12 : 1. The present research was approved by the Medical Ethics Committee of this hospital. The children's parents had signed the informed consents before the implementation of the study.

2.2. Diagnostic Criteria. The diagnostic criteria for the complete Kawasaki disease (CKD) were based on the 5th revised edition of the Kawasaki Disease Research Committee of Japan [36]. The diagnostic criteria for the incomplete Kawasaki disease (IKD) were based on the criteria developed by the American Heart Association (AHA) in 2004 [21]. The diagnostic criteria for CALs in KD were based on the 2015 diagnostic criteria for KD, as described in *Zhu Futang Pediatrics* (8th Edition) [37].

3. Methods

After all the patients were admitted and their diagnosis was confirmed, 3~5 ml of peripheral venous blood was collected and stored in an anticoagulation tube (EDTA) before 8 AM. After settling, the blood was centrifuged at 3000 r/min for 15 min to collect the upper layer of the serum. The serum MMP-9 level was detected by a double-antibody sandwich enzyme-linked immunosorbent assay (ELISA). An MMP-9 kit was purchased (Elabscience Biotechnology Co. Ltd., Wuhan, China), and the assay was executed in strict accordance with the instructions of the kit. Then, MMP-9 levels were detected by using an Infinite F200 Multifunctional Microplate Reader (Tecan, Sweden). The ESR was determined by the Westergren method, and the levels of PLTs and CRP were detected by using an ADVIA70 Automatic Hematology Analyzer (Bayer, Germany). The levels of albumin (ALB) were detected by using an ADVIA Chemistry XPT Fully Automatic Biochemical Analyzer (Siemens, Germany).

3.1. Statistical Methods. The data obtained were analyzed by SPSS 22.0 software and GraphPad Prism 8.0 software. Measurement data with a normal distribution are expressed as the mean ± the standard deviation (SD). Group comparisons were made by two independent-sample*t* tests. The categorical data was expressed as n (%), and the comparison of categorical data were performed by the chi-square test. Correlations between two variables were analyzed by the Spearman correlation analysis. The area under the curve (AUC) of the receiver-operating characteristic (ROC) curve and the Youden index (YI) were used to evaluate the efficacy of MMP-9, PLTs, ESR, and CRP for predicting CALs in KD. As the AUC gets closer to 1, the diagnostic efficacy increases. ($P < 0.05$) was considered statistically significant.

4. Results

The mean age of the patients was 2.7 ± 2.03 years (range, 2 months to 11 years). There were 87 boys (67.97%) and 41 girls (32.03%), with a male/female ratio of 2.12 : 1. Among the patients, the incidence of KD in infancy was obviously higher than that in other age groups, and 55 (43.0%) patients were under the age of one year. The details of the demographic data of the study participants are shown in Table 1 and Figure 1. All patients were treated with the regular medications, and 75 (58.59%) had a CAL. According to the clinical manifestations and coronary artery injury status, the patients were divided into the CKD group and the IKD group. A total of 56 patients had CKD (43.8%), and 72 (56.2%) patients had IDK. A comparison of the sex and age characteristics between the CKD and IKD groups is shown in Table 2. There was no significant difference in the age and gender between the two groups ($P > 0.05$).

Of the 56 patients with CKD, 27 patients (48.21%) had a CAL and 29 patients (51.69%) had NCALs (no coronary artery lesions). Among the 72 patients with IKD, 48 patients (66.67%) had a CAL and 24 patients (33.33%) had NCALs.

Table 1: Age and sex composition at onset in KD (*n*%).

Age (y)	Male (*n*%)	Female (*n*%)	Total (*n*%)
≤1 y	39 (44.8%)	16 (39.0%)	55 (43.0%)
1~3 y	31 (35.6%)	13 (31.7%)	44 (34.4%)
>3 y	17 (19.5%)	12 (29.3%)	29 (22.7%)
Total	87 (100.0%)	41 (100%)	128 (100.0%)

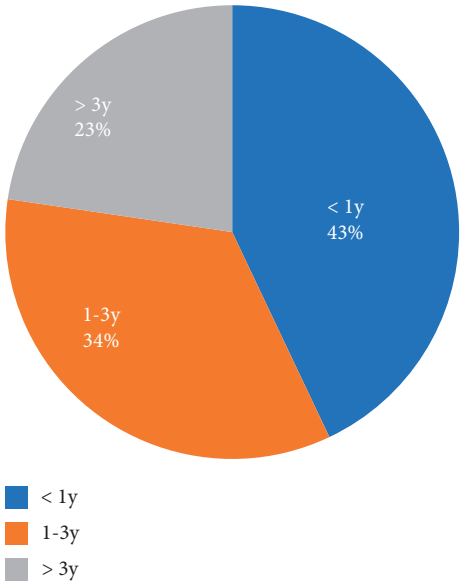

Figure 1: Age composition ratio of children with KD.

Table 2: Comparison of general characteristics between CKD and IKD.

Items	CKD	IKD	X^2	*P* value
Sex				
Male	37 (66.1%)	50 (69.4%)	0.165	0.685
Female	19 (33.9%)	22 (30.6%)		
Age (y)				
≤1 y	24 (42.9%)	31 (43.1%)	0.001	0.982
1~3 y	23 (41.1%)	21 (29.2%)	3.440	0.064
>3 y	9 (16.1%)	20 (27.8%)	2.463	0.117
Total	56 (100%)	72 (100.0%)	3.204	0.201

Note. $P < 0.05$ was considered statistically significant.

The difference between the two groups was statistically significant ($X^2 = 4.421$, $P = 0.036$, $P < 0.05$), indicating that the incidence of CALs was significantly higher in the IDK group than in the CKD group (Figure 2).

4.1. Comparisons of the Levels of MMP-9, PLTs, CRP, and ALB and ESR between the CAL Group and the NCAL Group. The statistical analysis of laboratory indicators in the CAL group and the NCAL group showed that the levels of MMP-9, PLTs, and CRP and the ESR were much higher in the CAL group, and ALB was lower in the NCAL group; these differences were statistically significant ($P < 0.01$). Compared with IKD, CKD had a significantly higher concentration of MMP-9, and this difference was statistically significant ($P < 0.05$) (Figure 3).

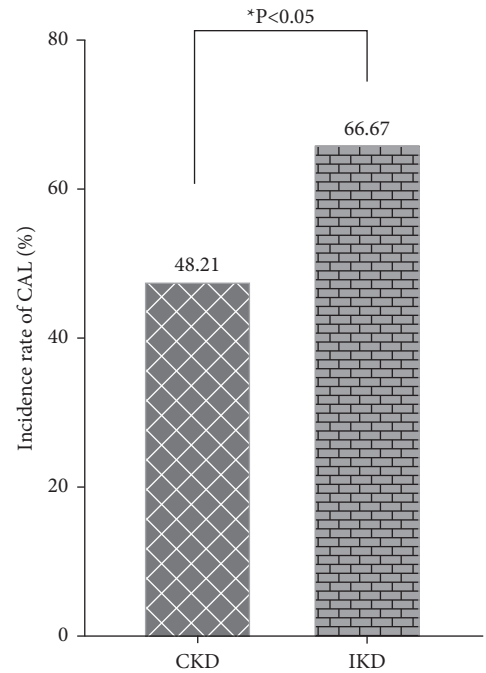

Figure 2: Comparison of the incidence rate of CAL between CKD and IKD.

4.2. Correlations of MMP-9 with PLTs, ESR, and CRP. Spearman correlation analysis suggested that MMP-9 showed a linear positive correlation with the ESR ($r = 0.224$, $P < 0.05$) and CRP ($r = 0.352$, $P < 0.05$) (Figure 4); the PLT levels were not obviously correlated with MMP-9.

4.3. The Results of the ROC Curve Analysis for MMP-9, PLTs, ESR, and CRP. The AUCs of the ROC curves for MMP-9, PLTs, ESR, and CRP were 0.636 (95% CI 0.532~0.741), 0.681 (95% CI 0.589~0.772), 0.762 (95% CI 0.671~0.853), and 0.657 (95% CI 0.564~0.750), respectively, (ESR˃PLT˃CRP˃MMP-9). The YIs of MMP-9, PLTs, te ESR, and CRP were 0.372, 0.408, 0.530, and 0.330, respectively, (ESR˃PLT˃MMP-9˃CRP). From the perspective of the best diagnostic cut-off value, when MMP-9 was set to 1120.74 ng/mL, the sensitivity and specificity for CALs and NCALs in KD were 58.21% and 78.95%, respectively. When the PLT cut-off was set to 424.5×10^9/L, the sensitivity and specificity for CALs and NCALs in KD were 42.67% and 98.11%, respectively. When the ESR cut-off was set to 74.5 mm/h, the sensitivity and specificity for CALs and NCALs in KD were 81.3% and 71.7%, respectively. When the CRP cut-off was set to was 82.5 mg/L, the sensitivity and specificity for CALs and NCALs in KD patients were 38.67% and 94.34%, respectively (Table 3).

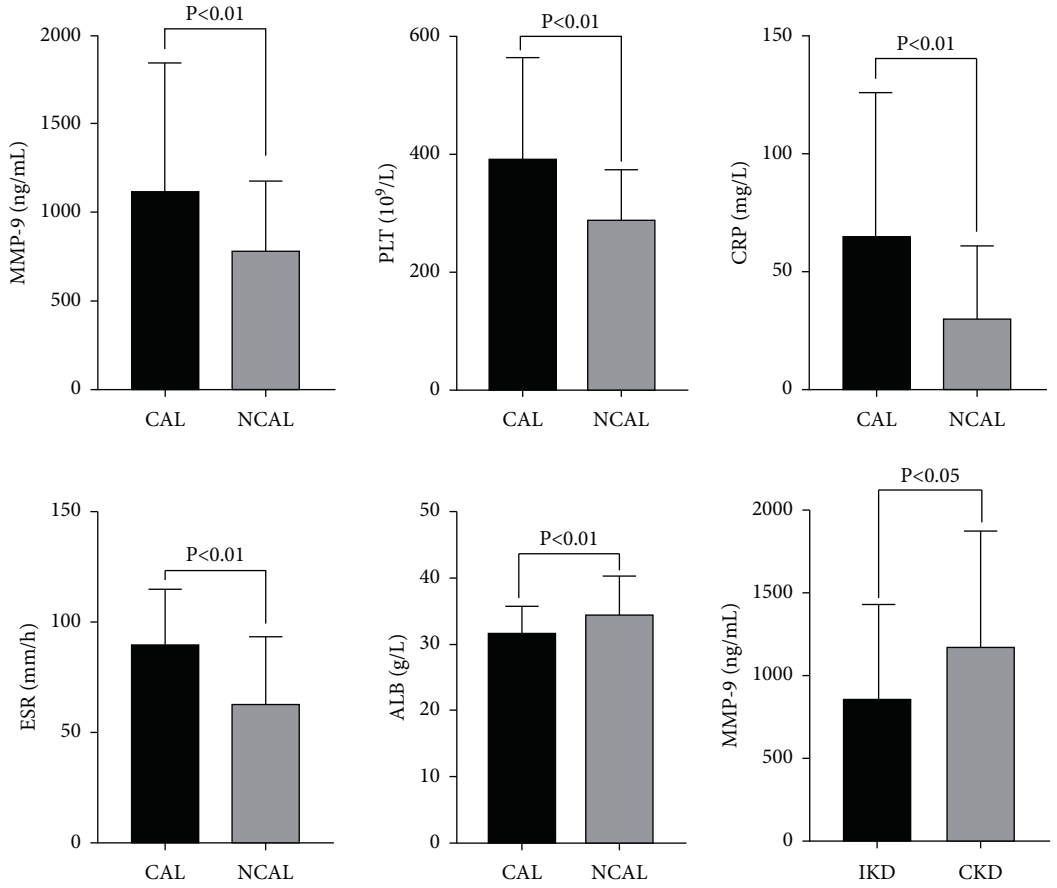

Figure 3: The CAL and NCAL groups regarding the serum levels of MMP-9, PLTs, CRP, ESR, and ALB and the concentration of MMP-9 in CKD and IKD. The level of statistical significance was set at $P < 0.05$.

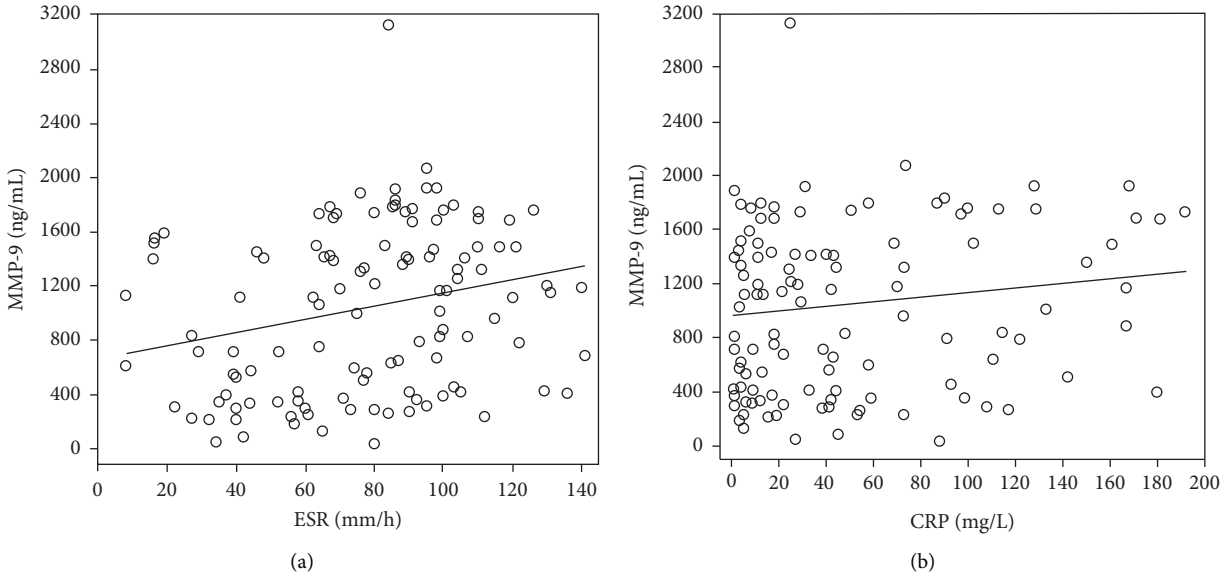

Figure 4: MMP-9 showed a linear positive correction with the (a) ESP ($r = 0.224$, $P < 0.05$) and the (b) CRP ($r = 0.352$, $P < 0.05$).

To make up for the limitation of a single diagnostic index, we determined the optimal cut-off values of MMP-9, PLTs, ESR, and CRP by using the ROC curves. The four values were converted into different combined indicators by the multiple factor logistic regression, and the regression equation of the combined indicators for diagnosis was

Table 3: Evaluation of the detection indicators (PLTs, ESR, CRP, and MMP-9) for predicting CALs.

	AUC	SE	AUC (95% CI)	Cut-off value	Youde n index	Sensitivity (%)	Specificity (%)	P
PLT	0.681	0.047	0.589~0.772	424.5	0.408	42.67	98.11	0.001
ESR	0.762	0.047	0.671~0.853	74.5	0.530	81.30	71.70	0.000
CRP	0.657	0.048	0.564~0.750	82.5	0.330	38.67	94.34	0.003
MMP-9	0.636	0.053	0.532~0.741	1120.74	0.372	58.21	78.95	0.021

Note. $P < 0.05$ was considered statistically significant.

expressed as $\log(P) = 0.0001^{*}\text{MMP-9} - 0.005^{*}\text{PLT} - 0.036^{*}\text{ESR} - 0.019^{*}\text{CRP} - 4.791$. The predicative factor $P = 1/(1 + e - (0.001 * \text{MMP-9} - 0.005 * \text{PLT} - 0.036^{*}\text{ESR} - 0.019^{*}\text{CRP} - 4.791))$ was obtained after performing a conversion. A ROC curve was drawn with the predicative factor P as the indicator for the analysis of the combined factors for diagnosis. The AUC of the combined detection of the four indicators was 0.877, the SD was 0.034, the sensitivity was 85.07%, and the specificity was 78.95%. The AUC for the combined factor diagnosis yielded the following results: compared with the AUC of MMP-9 for diagnosis, $Z = 3.84$ and $P < 0.05$; compared with the AUC of PLTs for diagnosis, $Z = 3.40$ and P<0.05; compared with the AUC of the ESR for diagnosis, $Z = 2.00$ and $P < 0.05$; and compared with the AUC of CRP for diagnosis, $Z = 3.76$ and $P < 0.05$; these differences were statistically significant ($P < 0.05$). These results show that the AUC, sensitivity, and specificity of the combined diagnosis with four indicators were superior to those of the single indicators. Thus, the combination of the four indicators was considered the most effective way to distinguish CALs and NCALs, as the efficacy was superior to that of the single indicators, and the rate of missed diagnoses and misdiagnoses was lower (Figure 5).

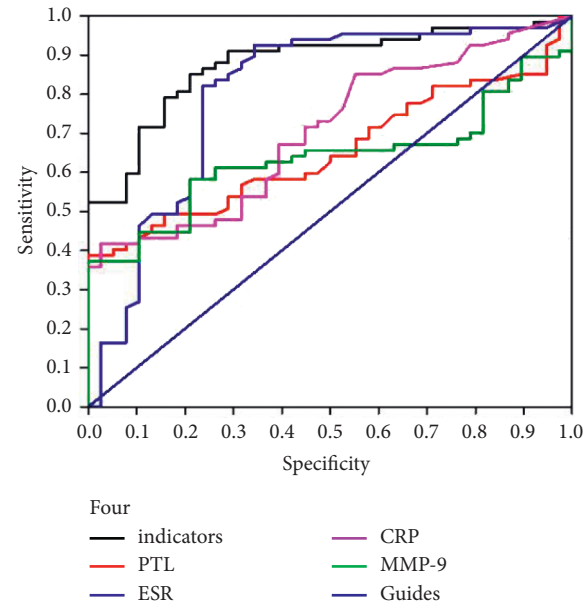

Figure 5: The ROC curve analysis for MMP-9, PLTs, EST, and CEP.

5. Discussion

KD, a kind of disease whose major symptom is vascular inflammation, mostly occurs in children. It is difficult to distinguish these conditions from infectious febrile diseases in the absence of specific laboratory diagnostic indictors [38, 39]. Thus, the early diagnosis and prediction of CALs in KD is of great significance for understanding the development, progression, and severity of this illness [40].

MMPs are zinc-dependent proteases that were first discovered in 1962 that play an important role in the cardiovascular disease [41–45]. In the MMP family, MMP-9 is the member that is most closely associated with vascular lesions [46–50], including acute MI, atherosclerosis, heart failure, and aortic aneurysm [51, 52]. MMP-9 activity contributes to the decomposition of elastin, and blocking this activity can decrease coronary artery inflammation in KD animals [53, 54]. In our study, we found that MMP-9 was not only upregulated in KD but was also significantly correlated with CALs, which is consistent with a report by Kuo et al. [55].

Elevations in MMP-9, PLTs, ESR, and CRP in children should be given adequate attention in clinical practice, thus avoiding the occurrence or further development of CALs. Lai [56] found that serum MMP-9 was positively correlated with serum CRP and the ESR in CALs based on partial correlation analysis, which may be explained by the fact that the ESR is mainly affected by changes in immunoglobulins and fibrinogens in the blood. MMP-9 may be activated by neutrophil elastase, plasminogen activators, and fibrin plasmin in the inflammatory response, further accelerating ECM degradation and leading to the destruction of the vascular wall [57]. Thus, there is a mechanism through which the ESR and MMP-9 can simultaneously increase, leading to the positive correlation of these factors. CRP is involved in the entire process of the inflammatory response, as it activates complement proteins and increases the ability of monocytes to release [58], while monocytes are stimulated by IL-1β to produce prostaglandin E2 and, therefore, to generate MMP-9 [59]; in addition, CRP is synthesized and secreted by hepatocytes that are stimulated by cytokines, such as IL-6 and IL-1β, revealing the interaction between CRP and MMP-9. CRP is able to induce an increase in the MMP-9 expression. Hence, there is a certain correlation between CRP and MMP-9.

The combined detection of MMP-9, PLTs, ESR, and CRP is superior to the detection of any single indicator for predicting CALs in KD. The etiology and pathogenesis of KD are not fully understood, and clinicians lack specific laboratory criteria for diagnosis, making it difficult to make an early diagnosis of KD. Moreover, many KD patients come to

the hospital for medical treatment because of a fever of an unknown cause and have no typical clinical characteristics. The progressive aggravation of inflammation leads to the persistence of a vascular inflammatory response that increases in severity, thus causing CALs [60]. Therefore, KD should be considered in patients with a fever of an unknown origin in the acute stage if the index of the appeal is abnormally increased.

Because CAL in KD usually appears two weeks after the onset of the disease, it is more difficult to make an early diagnosis of IKD [61]. PLTs, ESR, CRP, and other inflammatory indicators have been increasingly useful for the clinical diagnosis of KD and have been widely recognized by the majority of clinicians. However, reports comparing the efficacy of these indicators in the early diagnosis and prediction of CALs are rare. The detection results of MMP-9, PLTs, ESR, and CRP in this study showed that the ESR has good sensitivity and specificity, while PLTs, CRP, and MMP-9 have lower sensitivity and higher specificity, and thus have limited diagnostic values. After combining the four indicators into a singer diagnostic indicator by logistic stepwise regression, the ROC analysis suggested that the sensitivity and specificity has improved. Therefore, combined detection was considered to have a higher efficacy for predicting CALs in KD and to perform better than single-indicator detection, suggesting that both missed diagnoses and the misdiagnosis rate would be reduced.

There are some limitations in this study. This study was a single center clinical study, with limited sample size and less variables. In the future, large sample and long follow-up studies are needed to verify the role of MMP-9, PLTs, ESR, and CRP levels in Kawasaki disease with cardiovascular injury.

6. Conclusions

In conclusion, the combined detection of MMP-9, PLTs, ESR, and CRP is of great significance for predicting CALs in children with KD and provides a theoretical basis for clinicians to achieve the early diagnosis of KD.

Data Availability

The data used to support the findings of this study are available from the corresponding author upon request.

Ethical Approval

A corresponding approval from the Lanzhou University Second Hospital ethics committee was obtained.

Conflicts of Interest

The authors declare that they have no conflicts of interest.

Acknowledgments

This work was supported by the Natural Science Foundation of Gansu Province (20JR10RA599) and Cuiying Scientific and Technological Innovation Plan of Lanzhou University Second Hospital (2020QN-22). This study received funding from the government (item number: 18JR3RA323) from the Natural Science Foundation of Gansu Province.

References

[1] Y. W. Park, I. S. Park, C. H. Kim et al., "Epidemiologic study of kawasaki disease in Korea, 1997-1999: comparison with previous studies during 1991-1996," *Journal of Korean Medical Science*, vol. 17, no. 4, pp. 453–456, 2002.

[2] M. T. Lin and M. H. Wu, "The global epidemiology of kawasaki disease: review and future perspectives," *Global Cardiology Science & Practice*, vol. 2017, no. 3, Article ID e201720, 2017.

[3] K. Matsushita, T. Tamura, M. Nishiga, K. Kaitani, C. Izumi, and Y. Nakagawa, "Acute myocardial infarction and 30-year coronary aneurysm follow-up by serial angiography in a young adult with kawasaki disease," *Cardiovascular Intervention and Therapeutics*, vol. 30, no. 2, pp. 142–146, 2015.

[4] J. W. Newburger, M. Takahashi, M. A. Gerber et al., "Diagnosis, treatment, and long-term management of kawasaki disease: a statement for health professionals from the committee on rheumatic fever, endocarditis and kawasaki disease, council on cardiovascular disease in the young, american heart association," *Circulation*, vol. 110, no. 17, pp. 2747–2771, 2004.

[5] J. B. Gordon, A. M. Kahn, and J. C. Burns, "When children with kawasaki disease grow up: myocardial and vascular complications in adulthood," *Journal of the American College of Cardiology*, vol. 54, no. 21, pp. 1911–1920, 2009.

[6] S. Singh, A. Bansal, A. Gupta, R. M. Kumar, and B. R. Mittal, "Kawasaki disease: a decade of experience from north India," *International Heart Journal*, vol. 46, no. 4, pp. 679–689, 2005.

[7] R. P. Khubchandani and C. Khemani, "Kawasaki disease registries reap results experience in Mumbai," *Indian Journal of Pediatrics*, vol. 73, pp. 545-546, 2006.

[8] D. K. Paul, A. Gupta, and M. Lahiri, "Kawasaki disease in Calcutta," *Indian Pediatrics*, vol. 37, no. 11, pp. 1264-1265, 2000.

[9] S. N. Narayanan and K. Sabarinathan, "Kawasaki disease," *Indian Pediatrics*, vol. 34, no. 2, pp. 139–143, 1997.

[10] N. Suresh, V. V. Varadarajan, and M. S. Ranjith, "Kawasaki disease in south India: a prospective, case-control study," *Annals of Tropical Paediatrics*, vol. 27, no. 4, pp. 277–283, 2007.

[11] S. Amano, F. Hazama, H. Kubagawa, K. Tasaka, H. Haebara, and Y. Hamashima, "General pathology of kawasaki disease: on the morphological alterations corresponding to the clinical manifestations," *Pathology International*, vol. 30, no. 5, pp. 681–694, 1980.

[12] T. Kawasaki, F. Kosaki, S. Okawa, I. Shigematsu, and H. Yanagawa, "A new infantile acute febrile mucocutaneous lymph node syndrome (MLNS) prevailing in Japan," *Pediatrics*, vol. 54, no. 3, pp. 271–276, 1974.

[13] Y. Lu, L. Wu, F. Liu, X. Hu, X. Liang, and X. Ma, "Long-termfollow-up assessment of coronary artery complications in children with kawasaki disease: a comparision between echocardiography and coronary angiography," *Chinese Journal of Evidence Based Pediatrics*, vol. 05, no. 6, pp. 430–435, 2010.

[14] E. Tsuda, T. Kamiya, Y. Ono, K. Kimura, and S. Echigo, "Dilated coronary arterial lesions in the late period after kawasaki disease," *Heart*, vol. 91, no. 2, pp. 177–182, 2005.

[15] T. Akagi, V. Rose, L. N. Benson, A. Newman, and R. M. Freedom, "Outcome of coronary artery aneurysms after

kawasaki disease," *The Journal of Pediatrics*, vol. 121, no. 5, pp. 689–694, 1992.

[16] H. Kato, T. Sugimura, T. Akagi et al., "Long-term consequences of kawasaki disease. a 10- to 21-yearfollow-up study of 594 patients," *Circulation*, vol. 94, no. 6, pp. 1379–1385, 1996 Sep 15.

[17] R. M. R. Tulloh, R. Mayon-White, A. Harnden et al., "Kawasaki disease: a prospective population survey in the UK and ireland from 2013 to 2015," *Archives of Disease in Childhood*, vol. 104, no. 7, 2020.

[18] J. C. Burns, H. Shike, J. B. Gordon, A. Malhotra, M. Schoenwetter, and T. Kawasaki, "Sequelae of kawasaki disease in adolescents and young adults," *Journal of the American College of Cardiology*, vol. 28, no. 1, pp. 253–257, 1996.

[19] J. Fukushige, N. Takahashi, K. Ueda, T. Hijii, H. Igarashi, and A. Ohshima, "Long-term outcome of coronary abnormalities in patients after kawasaki disease," *Pediatric Cardiology*, vol. 17, no. 2, pp. 71–76, 1996.

[20] A. Suzuki, T. Kamiya, Y. Arakaki, Y. Kinoshita, and K. Kimura, "Fate of coronary arterial aneurysms in kawasaki disease," *The American Journal of Cardiology*, vol. 74, no. 8, pp. 822–824, 1994.

[21] J. W. Newburger, M. Takahashi, M. A. Gerber et al., "Diagnosis, treatment and long-term management of kawasaki disease: a statement for health professionals from the committee on rheumatic fever, endocarditis, and kawasaki disease, council on cardiovascular disease in the young, American heart association," *Pediatrics*, vol. 114, no. 6, pp. 1708–1733, 2004.

[22] L. Huiling, L. Yaping, and H. Xiufen, "Prediction of the risk of coronary arterial lesions in kawasaki disease by N-terminalpro-brain natriuretic peptide," *Chinese Journal of Pediatrics*, vol. 53, no. 4, pp. 300–303, 2015.

[23] J. Fuyong, *Kawasaki Disease*, People's Publishing House, Beijing, China, 2014.

[24] R. Fukazawa and S. Ogawa, "Long-term prognosis of patients with kawasaki disease: at risk for future atherosclerosis," *Journal of Nippon Medical School*, vol. 76, no. 3, pp. 124–133, 2009.

[25] T. Kawasaki, "Acute febrile mucocutaneous syndrome with lymphoid involvement with specific desquamation of the fingers and toes in children," *Arerugi*, vol. 16, no. 3, pp. 178–222, 1967.

[26] Y. Mitani, Y. Okuda, H. Shimpo et al., "Impaired endothelial function in epicardial coronary arteries after kawasaki disease," *Circulation*, vol. 96, no. 2, pp. 454–461, 1997.

[27] R. Yamakawa, M. Ishii, T. Sugimura et al., "Coronary endothelial dysfunction after kawasaki disease: evaluation by intracoronary injection of acetylcholine," *Journal of the American College of Cardiology*, vol. 31, no. 5, pp. 1074–1080, 1998.

[28] Y. Mitani, H. Sawada, H. Hayakawa et al., "Elevated levels of high-sensitivityC-reactive protein and serum amyloid-A late after kawasaki disease: association between inflammation and late coronary sequelae in kawasaki disease," *Circulation*, vol. 111, no. 1, pp. 38–43, 2005.

[29] Y. Mitani, H. Ohashi, H. Sawada et al., "*In vivo* plaque composition and morphology in coronary artery lesions in adolescents and young adults long after kawasaki disease: a virtual histology-intravascular ultrasound study," *Circulation*, vol. 119, no. 21, pp. 2829–2836, 2009.

[30] K. Suda, N. Tahara, Y. Kudo et al., "Persistent coronary arterial inflammation in a patient long after the onset of kawasaki disease," *International Journal of Cardiology*, vol. 154, no. 2, pp. 193-194, 2012.

[31] E. Tsuda, T. Abe, and W. Tamaki, "Acute coronary syndrome in adult patients with coronary artery lesions caused by kawasaki disease: review of case reports," *Cardiology in the Young*, vol. 21, no. 1, pp. 74–82, 2011.

[32] L. B. Daniels, M. S. Tjajadi, H. H. Walford et al., "Prevalence of kawasaki disease in young adults with suspected myocardial ischemia," *Circulation*, vol. 125, no. 20, pp. 2447–2453, 2012.

[33] D. M. Hovsepian, S. J. Ziporin, M. K. Sakurai, J. K. Lee, J. A. Curci, and R. W. Thompson, "Elevated plasma levels of matrix metalloproteinase-9 in patients with abdominal aortic aneurysms: a circulating marker of degenerative aneurysm disease," *Journal of Vascular and Interventional Radiology*, vol. 11, no. 10, pp. 1345–1352, 2000.

[34] Q. Peng, T. F. Zhou, C. Chen et al., "Clinical value of serum matrix metalloproteinase-9 and tissue inhibitor of metalloproteinase-1 for the prediction and early diagnosis of coronary artery lesion in patients with kawasaki disease," *Chinese Journal of Pediatrics*, vol. 43, no. 9, pp. 676–680, 2005.

[35] B. Li and X. Zhang, "Diagnosis and differential diagnosis of kawasaki disease," *Chinese Pediatrics Of Integrated Traditional and Western Medicin*, vol. 8, no. 2, pp. 125–128, 2016.

[36] M. Ayusawa, T. Sonobe, S. Uemura et al., "Revision of diagnostic guidelines for kawasaki disease (the 5th revised edition)," *Pediatrics International*, vol. 47, no. 2, pp. 232–234, 2005.

[37] H. Yamei and J. Zaifang, *Zhufutang Practical Pediatrics*, People's Health Publishing House, Beijing, China, 2015.

[38] S. Singh, A. K. Jindal, and R. K. Pilania, "Diagnosis of kawasaki disease," *International Journal of Rheumatic Diseases*, vol. 21, no. 1, pp. 36–44, 2018.

[39] S. Singh, P. Vignesh, and D. Burgner, "The epidemiology of kawasaki disease: a global update," *Archives of Disease in Childhood*, vol. 100, no. 11, pp. 1084–1088, 2015.

[40] J. M. Zhao and X. H. Wang, "Clinical significance of anti-neutrophil cytoplasmic antibodies and anti-endothelial cell antibodies in children with kawasaki disease," *Chinese Journal of Contemporary Pediatrics*, vol. 16, no. 7, pp. 740–744, 2014.

[41] G. M. Longo, W. Xiong, T. C. Greiner, Y. Zhao, N. Fiotti, and B. T. Baxter, "Matrix metalloproteinases 2 and 9 work in concert to produce aortic aneurysms," *Journal of Clinical Investigation*, vol. 110, no. 5, pp. 625–632, 2002.

[42] S. L. Parsons, S. A. Watson, P. D. Brown, H. M. Collins, and R. J. C. Steele, "Matrix metalloproteinases," *British Journal of Surgery*, vol. 84, no. 2, pp. 160–166, 1997.

[43] E. Hopps and G. Caimi, "Matrix metalloproteinases in metabolic syndrome," *European Journal of Internal Medicine*, vol. 23, no. 2, pp. 99–104, 2012.

[44] G. Berg, V. Miksztowicz, and L. Schreier, "Metalloproteinases in metabolic syndrome," *Clinica Chimica Acta*, vol. 412, no. 19-20, pp. 1731–1739, 2011.

[45] E. Hopps and G. Caimi, "Matrix metalloproteases as a pharmacological target in cardiovascular diseases," *European Review for Medical and Pharmacological Sciences*, vol. 19, no. 14, pp. 2583–2589, 2015.

[46] S. R. Mirhafez, A. Avan, M. Tajfard et al., "Relationship between serum cytokines receptors and matrix metalloproteinase 9 levels and coronary artery disease," *Journal of Clinical Laboratory Analysis*, vol. 31, no. 5, Article ID e22100, 2017.

[47] T. A. A. El-Aziz and R. H. Mohamed, "Matrix metalloproteinase-9 polymorphism and outcome after acute

myocardial infarction," *International Journal of Cardiology*, vol. 227, pp. 524–528, 2017.

[48] McE. C. M. Yasmin, S. Wallace, C. M. McEniery et al., "Matrix metalloproteinase-9 (MMP-9), MMP-2, and serum elastase activity are associated with systolic hypertension and arterial stiffness," *Arteriosclerosis, Thrombosis, and Vascular Biology*, vol. 25, no. 2, pp. 372–378, 2005.

[49] E. Furenes, M. Trøseid, E. Hjerkinn et al., "Prediction of cardiovascular events by matrix metalloproteinase (MMP)-9 in elderly men," *Thrombosis & Haemostasis*, vol. 103, no. 03, pp. 679–681, 2010.

[50] M. Li, G. Yang, B. Xie, K. Babu, and C. Huang, "Changes in matrix metalloproteinase-9 levels during progression of atrial fibrillation," *Journal of International Medical Research*, vol. 42, no. 1, pp. 224–230, 2014.

[51] A. Briasoulis, D. Tousoulis, N. Papageorgiou et al., "Novel therapeutic approaches targeting matrix metalloproteinases in cardiovascular disease," *Current Topics in Medicinal Chemistry*, vol. 12, no. 10, pp. 1214–1221, 2012.

[52] H. Cai, Y. Ma, L. Jiang et al., "Hypoxia response element-regulated MMP-9 promotes neurological recovery via glial scar degradation and angiogenesis in delayed stroke," *Molecular Therapy*, vol. 25, no. 6, pp. 1448–1459, 2017.

[53] A. C. Lau, T. T. Duong, S. Ito, and R. S. M. Yeung, "Matrix metalloproteinase 9 activity leads to elastin breakdown in an animal model of kawasaki disease," *Arthritis & Rheumatism*, vol. 58, no. 3, pp. 854–863, 2008.

[54] A. C. Lau, T. T. Duong, S. Ito, G. J. Wilson, and R. S. M. Yeung, "Inhibition of matrix metalloproteinase-9 activity improves coronary outcome in an animal model of kawasaki disease," *Clinical and Experimental Immunology*, vol. 157, no. 2, pp. 300–309, 2009.

[55] H. C. Kuo, S. C. Li, L. H. Huang, and Y. H. Huang, "Epigenetic hypomethylation and upregulation of matrix metalloproteinase 9 in kawasaki disease," *Oncotarget*, vol. 8, no. 37, pp. 60875–60891, 2017.

[56] Y. Lai, "Changes of matrix metalloproteinase-9 and tissue inhibitors of metalloproteinase-1 in the patients with acute coronary syndrome," *Journal of Chinese Practical Diagnosis and Therapy*, vol. 23, no. 1, pp. 17–19, 2009.

[57] S. Ye, C. R. Gale, and C. N. Martyn, "Variation in the matrix metalloproteinase-1 gene and risk of coronary heart disease," *European Heart Journal*, vol. 24, no. 18, pp. 1668–1671, 2003.

[58] T. Chen and J. Gao, "Expression and correlation of IL-6, hs-CRP and TNF-α in patients with acute myocardial infarction," *Hebei Medical Journal*, vol. 40, no. 24, pp. 3725–3728, 2018.

[59] F. Cipollone, M. L. Fazia, A. Iezzi et al., "Association between prostaglandin E receptor subtype EP4 overexpression and unstable phenotype in atherosclerotic plaques in human," *Arteriosclerosis, Thrombosis, and Vascular Biology*, vol. 25, no. 9, pp. 1925–1931, 2005.

[60] T. Kim, W. Choi, C. W. Woo et al., "Predictive risk factors for coronary artery abnormalities in Kawasaki disease," *European Journal of Pediatrics*, vol. 166, no. 5, pp. 421–425, 2007.

[61] X. Wang, X. Wang, W. Wang, and W. Dong, "Changes in heart type fatty acid binding protein and brain natriuretic peptide of children with kawasaki disease and their relationship with heart function," *Chinese Journal of Applied Clinical Pediatrics*, vol. 32, no. 9, pp. 705–707, 2017.

[62] J. Zhang, C. C. Li, W. Zhao et al., "Association between sleep quality and cardiovascular damage in predialysis patients with chronic kidney disease," *BMC Nephrology*, vol. 15, no. 1, p. 131, 2014.

[63] A. S. Hussain, M. H. Shah, M. Lakhdir et al., "Effectiveness of transcutaneous bilirubin measurement in managing neonatal jaundice in postnatal ward of a tertiary care hospital in Pakistan," *BMJ paediatrics open*, vol. 1, no. 1, Article ID e000065, 2017.

[64] S. Xiu-Yu, H. Jia-Yu, H. Qiang, and D. Shu-Hui, "Platelet count and Erythrocyte Sedimentation Rate are good predictors of kawasaki disease: ROC analysis," *Journal of Clinical Laboratory Analysis*, vol. 24, no. 6, pp. 385–388, 2010.

Hindawi
Evidence-Based Complementary and Alternative Medicine
Volume 2022, Article ID 2501846, 11 pages
https://doi.org/10.1155/2022/2501846

Research Article

CMaf-Inducing Protein Promotes LUAD Proliferation and Metastasis by Activating the MAPK/ERK Pathway

Xiao-Yan Yu,[1] Ming Wang,[2] and Juan-Juan Qian[1]

[1]*Respiratory Medicine, The Second Affiliated Hospital of Jiaxing University, Jiaxing, Zhejiang 314099, China*
[2]*Cardiothoracic Surgery, Shulan (Hangzhou) Hospital, Hangzhou, Zhejiang 310015, China*

Correspondence should be addressed to Juan-Juan Qian; yymcabc@126.com

Received 27 July 2022; Revised 19 August 2022; Accepted 25 August 2022; Published 14 September 2022

Academic Editor: Xueliang Wu

Objective. Previous studies have shown that cMaf-inducing protein (CMIP) promotes tumorigenesis and progression, however, the role of CMIP in lung adenocarcinoma (LUAD) and its molecular mechanism remain unclear. *Methods*. In this study, the Human Protein Atlas and Kaplan–Meier Plotter database were used to analyze the expression and prognostic value of CMIP in LUAD. Then, the expression levels of CMIP in LUAD tissues and cells were detected by qRT-PCR and western blot. The lentiviral vector was used to establish a stable transfected cell line, and the transfection efficiency was detected by qRT-PCR. MTT assay, colony formation assay, transwell assay, and wound healing assay were used to evaluate the function of CMIP in LUAD. In addition, the effect of CMIP on the MAPK/ERK pathway in LUAD cells was analyzed by western blot. *Results*. The expression level of CMIP was significantly increased in LUAD cell and tissue samples, and the high expression of CMIP was associated with overall survival (OS) and progression-free survival (PFS) in LUAD patients. In vitro experiments showed that CMIP overexpression significantly promoted the proliferation, migration, and invasion of A549 cells. CMIP knockout significantly inhibited the proliferation, migration, and invasion of H1299 cells. In addition, it was observed that the expression levels of the MAPK/ERK pathway-related proteins were significantly increased in CMIP-overexpressed A549 cells, and promoted cell proliferation, migration, and invasion, while U0126 could significantly reverse the activation of the MAPK/ERK pathway by CMIP overexpression, and inhibit the proliferation, migration, and invasion of A549 cells. *Conclusion*. Our study shows that CMIP, as an oncogene, is associated with poor patient prognosis, and may promote the proliferation and metastasis of LUAD by activating the MAPK/ERK pathway. Therefore, CMIP may be a new potential therapeutic target for LUAD.

1. Introduction

According to the latest data from GLOBOCAN in 2020, lung cancer is still the malignant tumor with the highest number of cancer-related deaths in the world, and its mortality rate accounts for about 18.0% of cancer-related deaths [1]. Nonsmall cell lung cancer (NSCLC) accounts for approximately 90% of all lung cancer types, of which adenocarcinoma (LUAD) and squamous cell carcinoma (LUSC) are the most common subtypes [2–4]. At present, radical resection, radiotherapy, and chemotherapy are the traditional methods for clinical treatment of LUAD [5, 6], but the treatment and prognosis of LUAD are poor due to the lack of precise targeting and large side effects and other adverse factors [7]. In addition, due to the high probability of postoperative recurrence and early development of metastatic propensity in LUAD patients [8], the 5-year survival rate of lung cancer patients is only 17% [9], and the 5-year relative survival rate among metastatic patients is only 5% lower[10]. Although many genes involved in LUAD tumorigenesis have been identified at this stage, only a few of them have been developed for clinical treatment. Therefore, finding potential cancer-related genes and elucidating their biological mechanisms related to tumor malignant behavior has important therapeutic significance.

Cmaf-inducing protein (CMIP) was originally discovered in the podocytes of patients with acquired idiopathic nephrotic syndrome [11]. The protein structure of CMIP

consists of an N-terminal region of the pleckstrin homology domain (PH), an intermediate region containing multiple interacting docking sites (a 14-3-3 module, a PKC domain, and an SH3 domain similar to the p85, the regulatory subunit of phosphatidylinositol 3-kinase (PI3K)) and a C-terminal region containing a leucine-rich repeat (LRR) domain [12]. At present, he function of CMIP is still unclear. Previous studies have shown that intravenous injection of small interfering RNA-targeting CMIP can prevent lipopolysaccharide-induced proteinuria in rats by inhibiting the interaction between Src kinase Fyn and cytoskeletal regulator N-WASP (neural Wiskott Aldrich syndrome protein) and between adaptor proteins Nck and nephrin [11]. CMIP interacts with RelA to inhibit the degradation of I-kappaBα and prevent the dissociation of the NF-kappad/I-kappα complex, resulting in down-regulation of NF-kB activity [13]. In addition, Kamal et al. found that CMIP has a dual effect in undifferentiated T cells, when CMIP inactivates Lck by interacting with the p85 subunit of PI3 kinase, leading to activation of the extracellular signal-regulated kinase (ERK) 1/2 and P38 MAPK pathways, but when CMIP interacts with death-associated protein kinase (DAPK)-interacting protein-1 (DIP-1) and upregulates DAPK, it blocks the nuclear translocation of ERK1/2 and thus plays a key role in preventing the development of immune responses [14]. Studies have found that two isoforms of adaptor proteins of CMIP are expressed in the human brain [15, 16] and play an important role in human reading [16] and language [17]-related behavioral traits by participating in the cMaf signaling pathway. To date, little is known about CMIP in cancer. Zhang et al. showed that high expression of CMIP in gastric cancer tissue is associated with poorer clinical parameters, RFS, and OS, and CMIP works by upregulating mitogen-activated protein kinase (MAPK) Its expression plays an oncogenic role in human gastric cancer cells [18]. However, the relationship and mechanism of action of CMIP in LUAD have not been reported.

In the present study, CMIP protein expression was significantly elevated in LUAD tissue compared with normal lung tissue and correlated with poorer overall survival (OS) and progression-free survival (PFS). In addition, CMIP overexpression promoted the proliferation, migration, and invasion of lung cancer cells. Notably, CMIP overexpression activated the MAPK/ERK signaling pathways to promote LUAD development, while U0126 reversed the oncogenic effects of CMIP. It indicated that CMIP may promote the proliferation and metastasis of LUAD by activating the MAPK/ERK pathway. CMIP can be further studied as a prognostic biomarker and clinical therapeutic target for LUAD.

2. Materials and Methods

2.1. Clinical Samples. We collected a total of 20 tumor tissue samples (LUAD) and paired adjacent normal tissue (Normal) from patients diagnosed with LUAD between June 2018 and December 2020. All patients were admitted to Shulan (Hangzhou) Hospital, and all participants signed informed consent voluntarily. In this study, two pathologists diagnosed LUAD based on the pathological results, and analyzed the histological type and tumor stage of the patients according to the eighth edition of the Lung Cancer Tumor, Lymph Node, Metastasis (TNM) Staging System [19]. This study was approved by the Research Ethics Committee of Shulan (Hangzhou) Hospital (KY2022042). The study was conducted in accordance with the Declaration of Helsinki (revised 2013).

The inclusion criteria are as follows [20]: (1) Have not received chemotherapy and radiotherapy; (2) No history of any other malignant tumor within 5 years; (3) No pregnancy or breastfeeding; (4) No cardiopulmonary insufficiency and severe cardiovascular disease; (5) No severe infection and severe malnutrition.

2.2. Data Collection. The human protein atlas (HPA; https://www.proteinatlas.org), immunohistochemical (IHC) staining data of CMIP in normal lung tissues, and LUAD tissues were obtained. In the HPA database, protein expression was scored on four levels of undetected, low, medium, and high based on the proportion of stained cells and the intensity of staining [21].

The Kaplan–Meier Plotter database (http://www.kmplot.com) was used for survival analysis of CMIP mRNA expression in LUAD patients, including OS and PFS, to evaluate LUAD patients prognosis. The LUAD patients were divided into high-expression group and low-expression group according to the median expression value, and the "Automatically select the best cutoff" model was selected during the analysis and the threshold with the best performance was used as the cutoff value. Results are shown graphically with hazard ratios (HR) and log-rank test P values with 95% confidence intervals, and log-rank test P values of $p < 0.05$ were considered statistically significant [22].

2.3. Cell Culture and Transfection. Cell culture human normal lung epithelial cells (BEAS-2B) and human nonsmall cell lung cancer cell lines (A549, H460 and H1299) were purchased from American type culture collection (ATCC). The cells were cultured in DMEM or RPMI-1640 medium (GIBCO, USA) supplemented with 10% fetal bovine serum (FBS; GIBCO, USA) and 100 U/ml of penicillin streptomycin mixed antibiotics, and the cells were cultured in a humidified incubator at 37°C and 5% CO_2.

Cell transfection CMIP siRNA plasmid (si-CMIP) and negative siRNA plasmid (siNC), empty plasmid pcDNA3.1 (Vector), and CMIP overexpression plasmid pcDNA3.1-CMIP (OE-CMIP) were designed and synthesized by Thermo Fisher Scientific. H460 and H1299 cells (1×10^6 cells/mL) were seeded in 6-well plates, grouped, and transfected when the cells grew to 80%–90%. Transfected H460 cells grouped: vector group and OE-CMIP group. Transfected H1299 cells grouped: siNC group and si-CMIP group. The plasmids were transfected into H460 and H1299 cells, respectively, using Lipofectamine™ 2000 transfection reagent (11668500, Invitrogen, Thermo Fisher Scientific, Inc.) according to the manufacturer's instructions. After 6 h

Table 1: Primers.

Gene	Sequences (5′ to 3′)
CMIP	F: AAATTCCTGAGGCGCTG R: CTTCAATTGCGCTGTAGGA
β-actin	F: TTCCTGGGCATGGAGTC R: CAGGTCTTTGCGGATGTC

of transfection, the medium was changed and the cells were cultured for another 48 h. Cells are collected. Transfection efficiency was detected using qRT-PCR.

2.4. Quantitative Real-Time PCR Analysis (qRT-PCR). Total RNA from cells and tissues was extracted using the TRIzol™Plus RNA Purification Kit (Invitrogen, Thermo Fisher Scientific, Inc.) according to the manufacturer's instructions, and RNA was reverse transcribed into cDNA according to the instructions of PrimeScript RTMaster Mix (Takala, Japan). Also, the concentration and purity of cDNA were checked. qRT-PCR was performed using the SYBR PremixEx Taq II kit (Takala, Japan) to detect the relative expression levels of CMIP. PCR amplification steps: 95°C for 30 s; 95°C for 5 s, 60°C for 30 s, 72°C for 45 s, 40 cycles; 72°C for 10 min. β-actin was used as an internal reference gene and the data were analyzed by the $2^{-\Delta\Delta Ct}$ method [23]. The primer sequences are shown in Table 1.

2.5. Cell Viability Assays. Transfected H1299 and H460 cells were seeded in 96-well plates at 5×10^3 cells/well. H460 cells were treated with or without the addition of 10 μM U0126 [24–26] (#9903S, Cell Signal Technology, Danvers, MA, USA). After 24 h of cell culture, 10 μL of MTT (5 mg/ml) (Biyuntian, China) was added to each well, and then incubated at 37°C for 4 h. The supernatant was aspirated and 150 μL of DMSO was added to each well. The absorbance of each well was measured at 570 nm using a microplate reader (Bio-Rad Laboratory, Inc.) [27]. All experiments were repeated three times.

2.6. Cell Colony Formation Assay. Transfected H1299 cells and H460 cells were seeded into 6-well plates at 500 cells/well, and H460 cells were treated with or without the addition of 10 μM U0126. The new medium was replaced every 3 days, and after 2 weeks of culture, cells were fixed with 4% paraformaldehyde for 30 min at room temperature and stained with 0.1% crystal violet for 30 min. Photographs were taken using a light microscope (Olympus Corporation, Japan) and the number of visible colonies were manually counted. Groups of cells containing >50 cells were identified as colonies, and the number of clones in each group was counted [28]. All experiments were repeated three times.

2.7. Wound Healing Assay. Transfected H1299 cells and H460 cells were seeded into 6-well plates at 5×10^4 cells/well, and H460 cells were treated with or without the addition of 10 μM U0126. When the cells reached 90% confluency, a 20 μl pipette tip was used to scratch directly on the cell monolayer and wash the cells with PBS. They were then incubated in serum-free RPMI-1640 for 24 h. Images were taken at 0 h and 24 h using a light microscope (Leica, Germany), and ImageJ software was used to quantitatively assess the wound area and calculate cell migration rates for each group [28]. All experiments were repeated three times.

2.8. Transwell Assay. Matrigel (364262, BD Biosciences) was coated on a 24-well transwell chamber (Costar; Corning, Inc.) at 37°C and placed in a cell incubator overnight. After suspending transfected H1299 cells and H460 cells with FBS-free medium, 100 μL of cells were seeded into the upper chamber at 5×10^5 cells/ml, and 500 μL of RPMI-1640 containing 10% FBS was added to the lower chamber. H460 cells were treated with or without the addition of 10 μM U0126. After culturing at 37°C for 24 h, cells on the underside of the membrane were fixed with 5% glutaraldehyde for 30 min at 4°C, and then stained with 0.5% crystal violet for 30 min at room temperature. Images were taken using an inverted light microscope (Leica, Germany) and invading cells in different areas were counted and analyzed using ImageJ software [29]. All experiments were repeated three times.

2.9. Western Blot Analysis. Transfected H1299 cells and H460 cells were seeded into 6-well plates at 1×10^6 cells/well, and the cells were collected when the cells reached a certain number. Total cell and tissue proteins were extracted using RIPA lysis buffer (Beyotime, Shanghai, China) containing protease and phosphatase inhibitors. Protein concentrations were determined using the BCA protein assay kit (Beyotime). Equal amounts of protein samples (30 μg/lane) were separated on 8–12% SDS–polyacrylamide gel electrophoresis (PAGE), and proteins were transferred to polyvinylidene fluoride membranes (PVDF, Immobilon-P, Millipore). Afterward, membranes were blocked with 5% skim milk or bovine serum albumin (BSA) (for phosphorylated proteins) for 1 h at room temperature. Then at 4°C with primary antibodies CMIP (PA5-65870, Invitrogen); P38 (#9212, Cell Signaling Technology); ERK (#4695, Cell Signaling Technology); p-P38 (#9215, Cell Signaling Technology); p-ERK (#4370, Cell Signaling Technology) and β-actin (#3700, Cell Signaling Technology) were incubated overnight. After TBST washes, the membranes were incubated with the appropriate horseradish peroxidase-conjugated secondary antibodies goat anti-rabbit IgG H&L (HRP) (ab205718, Abcam) and goat anti-mouse IgG H&L (HRP) (ab97023, Abcam) was incubated for 2 h. Images of protein bands were obtained using ECL chemiluminescent liquid (PE0010, Solebao). The target protein expression levels were calculated and normalized using Image J software.

2.10. Statistical Analysis. All experiments were repeated at least three times and all statistical analyses were analyzed using SPSS 26.0 software or GraphPad Prism 8.0. All data are presented as mean ± SD. Differences between multiple groups were analyzed using one-way ANOVA and

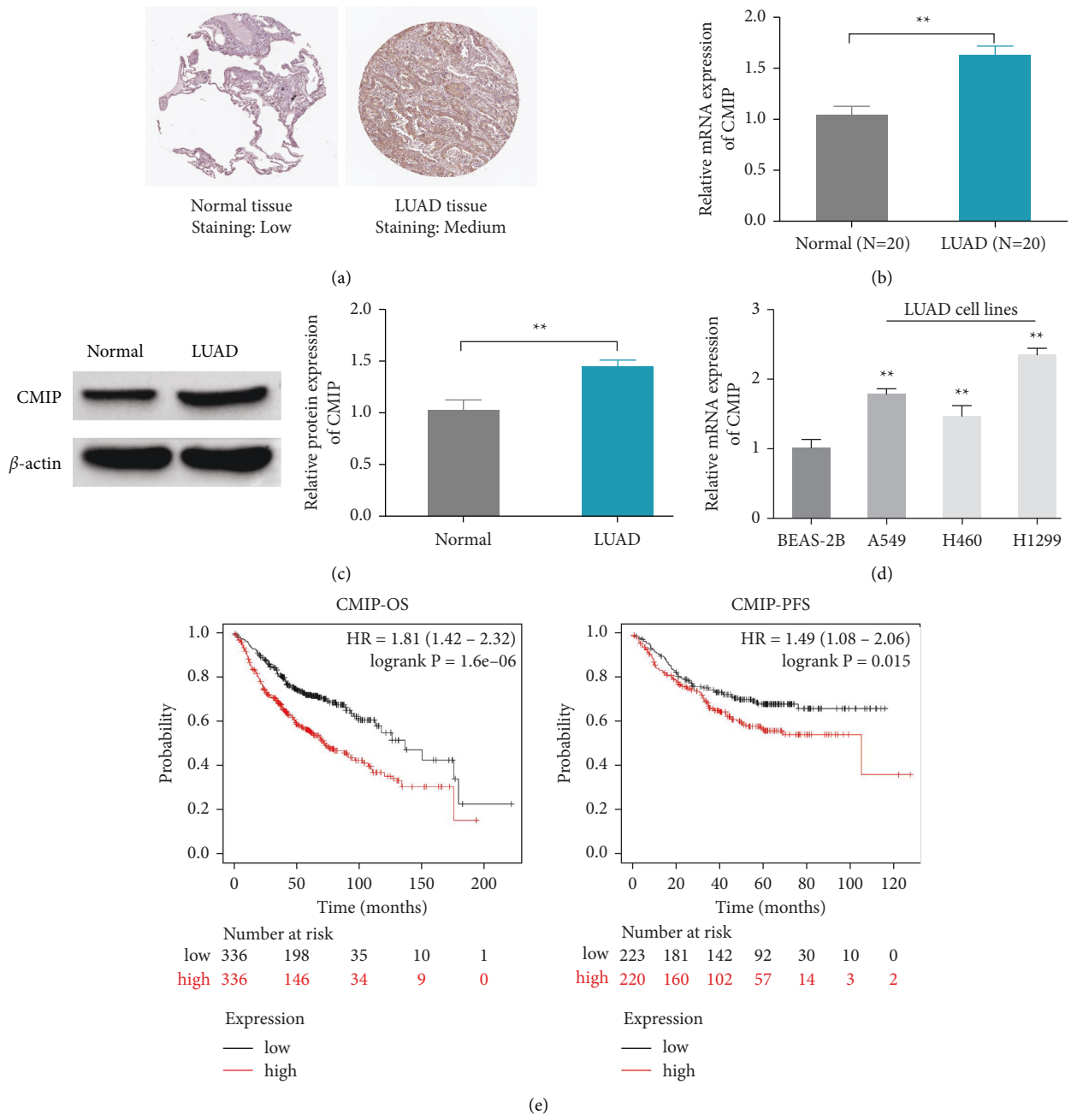

Figure 1: CMIP is upregulated in LUAD and associated with poor prognosis. (a) Immunohistochemical tissue microarray image (HPA) of CMIP protein. (b) qRT-PCR detection of CMIP mRNA levels in normal lung tissue and LUAD tissue ($n = 20$); (c) Western blot detection of CMIP protein expression in normal lung tissue and LUAD tissue ($n = 3$); (d) mRNA levels of CMIP detected by qRT-PCR in BEAS-2B, A549, H460, and H1299 cells ($n = 3$); (e) OS and PFS in LUAD patients obtained from the Kaplan–Meier plotter online database; $^{**}P < 0.01$ vs. (Normal group or BEAS-2B group).

Bonferroni's multiple comparison post hoc test. $P < 0.05$ was considered to be statistically significant.

3. Results

3.1. CMIP Is Upregulated in LUAD and Associated with Poor Prognosis. To determine the relationship between CMIP expression and LUAD, tissue microarray IHC according to the HPA database showed that the expression of CMIP was significantly higher in LUAD tissue than in normal lung tissue (Figure 1(a)). Similarly, CMIP protein levels were significantly elevated in LUAD tissues and cells were confirmed by qRT-PCR and Western blot analysis. It is worth noting that among the three lung cancer cell lines, CMIP expression was highest in H1299 cells and lowest in H460 cells (Figures 1(b)b–e1(e)), therefore, knockdown of CMIP in H1299 cells and overexpression of CMIP in H460 cells were selected for subsequent experimental studies.

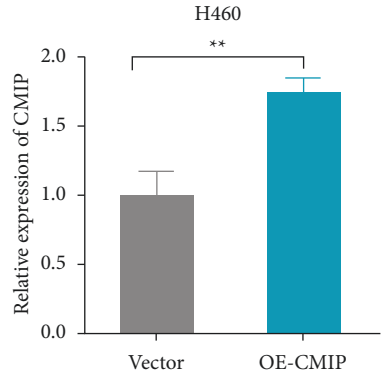

(a)

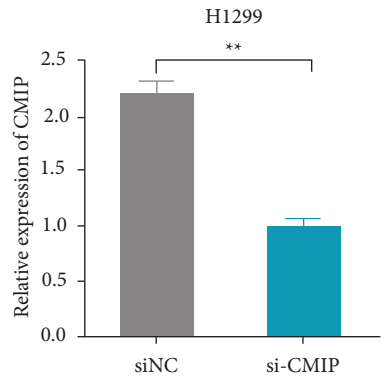

(b)

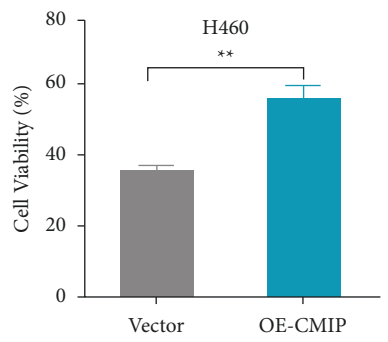

(c)

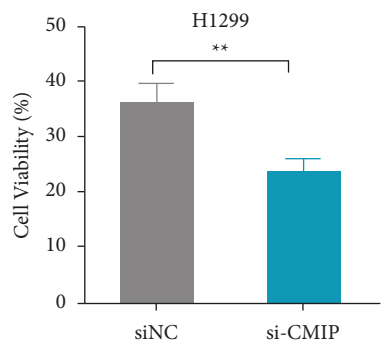

(d)

Figure 2: Continued.

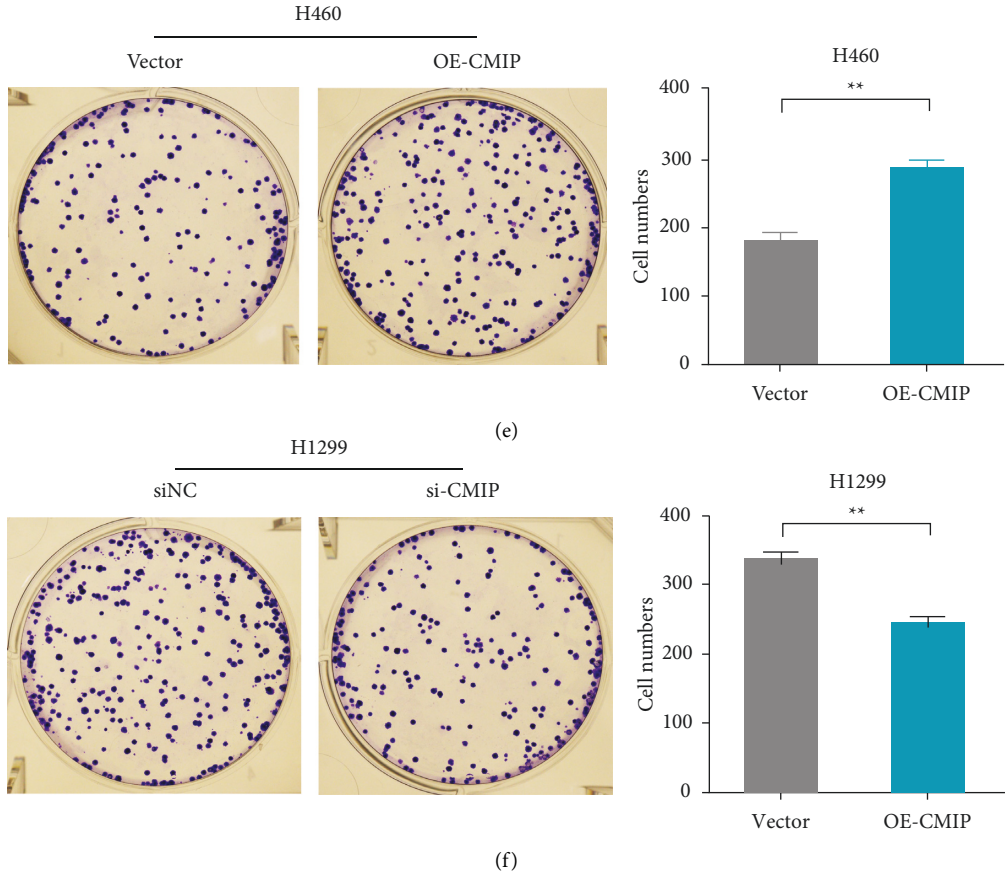

Figure 2: CMIP overexpression promotes the proliferation of H460 cells. (a/b) The mRNA levels of CMIP in H460 (a) and H1299 (b) cells after transfection were detected by qRT-PCR; (c/d) MTT assay was used to detect the difference of CMIP expression after transfection on H460 (c) and H1299 (d) Effect of cell viability. (e/f) Cell colony formation assay to assess the effect of CMIP expression on the proliferation of H460 (e) and H1299 (f) cells after transfection. $^{**}P < 0.01$ vs. (siNC group or vector group).

Furthermore, using Kaplan–Meier survival curves, it was found that patients with high CMIP expression in LUAD had worse OS ($P = 0.0068$) and PFS ($P = 0.015$) (Figure 1(f)). Therefore, these results suggest that CMIP is involved in the occurrence and development of LUAD, which is worthy of further study.

3.2. CMIP Overexpression Promotes H460 Cell Proliferation. In order to explore the effect of CMIP on the occurrence and development of LUAD, this study firstly transfected CMIP overexpression or knockdown plasmids into H460 and H1299 cells, respectively. qRT-PCR detection showed that in H460 cells, compared with the vector group, CMIP mRNA level in the OE-CMIP group was significantly increased (Figure 2(a)). In H1299 cells, CMIP mRNA levels were significantly decreased in the si-CMIP group compared with the siNC group (Figure 2(b)). Subsequently, the effect of CMIP expression on the viability of H460 and H1299 cells was examined by MTT. The results showed that CMIP overexpression significantly enhanced H460 cell viability compared with the vector group (Figure 2(c)), while in H1299 cells, knockdown of CMIP significantly inhibited cell viability compared with the siNC group (Figure 2(d)). In addition, the cell colony formation assay showed that CMIP overexpression significantly increased the number of H460 cell colonies compared with the vector group (Figure 2(e)). Compared with the siNC group, knockdown of CMIP significantly reduced the number of H1299 cell colonies (Figure 2(f)).

3.3. CMIP Overexpression Promotes H460 Cell Migration and Invasion. Subsequently, we further assessed the effect of CMIP expression on the migration and invasion of H460 and H1299 cells. The results showed that CMIP overexpression significantly promoted H460 cell migration and invasion compared with the vector group (Figures 3(a) and 3(c)), and knockdown of CMIP significantly inhibited H1299 cell migration and invasion compared with the siNC group (Figures 3(b) and 3(d)). These results indicate that high expression of CMIP promotes the occurrence and development of LUAD.

3.4. CMIP Overexpression Promotes Activation of MAPK/ERK Signaling Pathway. In order to explore the molecular mechanism of abnormal expression of CMIP in the

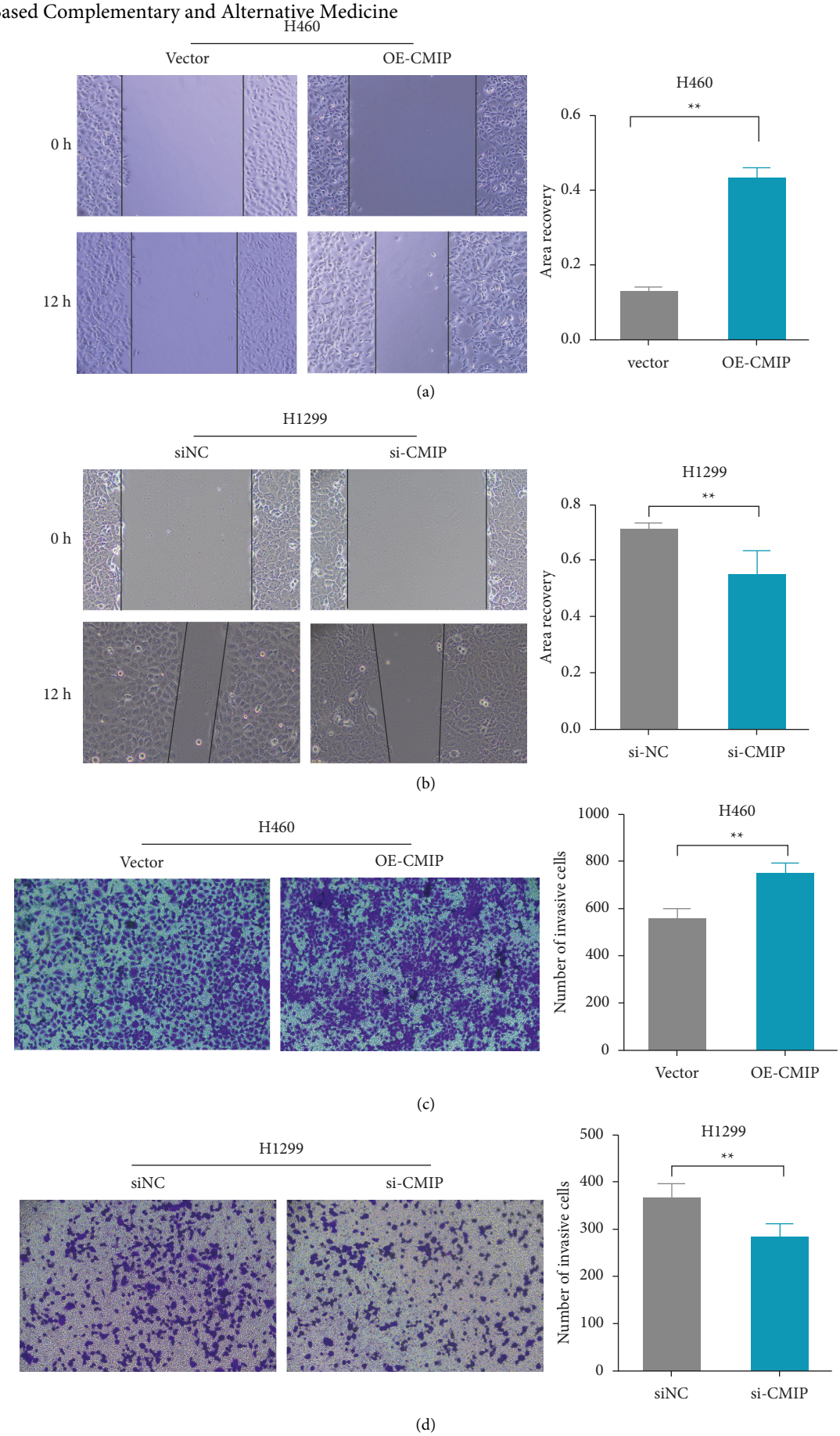

Figure 3: CMIP overexpression promotes H460 cell migration and invasion. (a/b) The wound healing assay was used to analyze the effect of CMIP expression on the migration of H460 (a) and H1299 (b) cells after transfection. (c/d) The effect of CMIP expression on H460 (c) and H1299 (d) cell invasion after transfection was assessed using Transwell analysis. $^{**}P < 0.01$ vs. (siNC group or vector group).

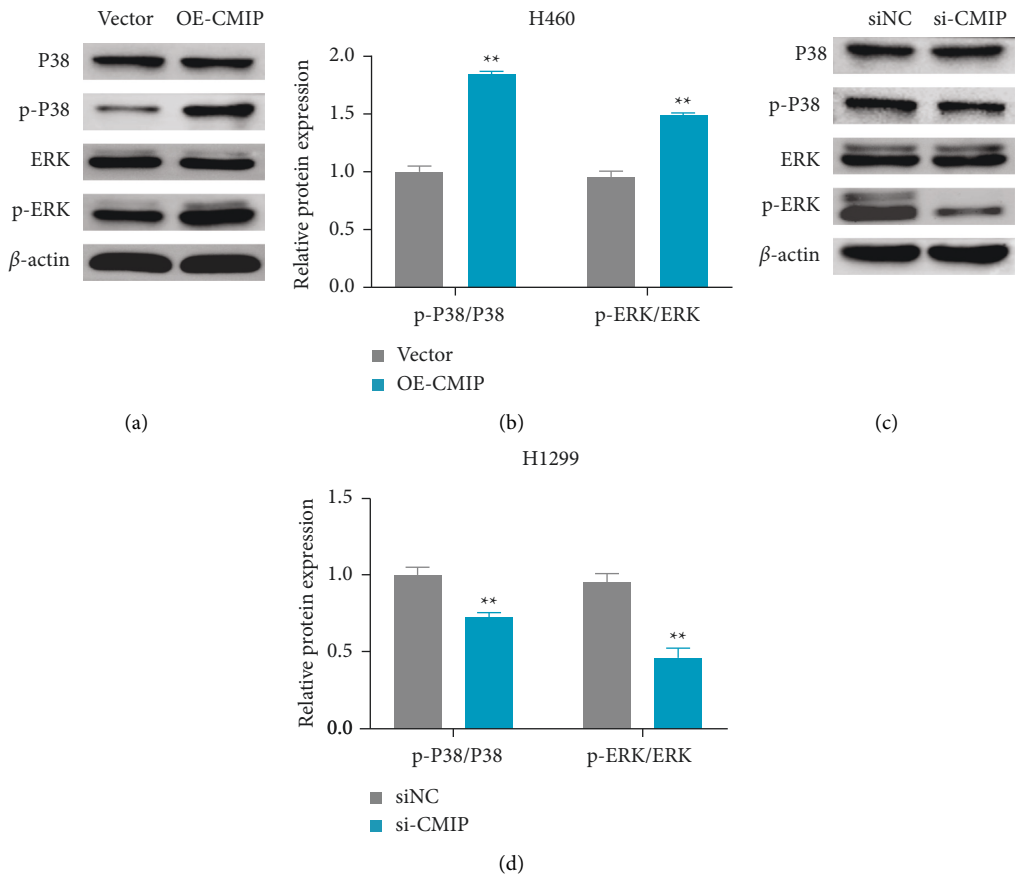

Figure 4: CMIP overexpression promotes activation of the MAPK/ERK pathway. (a, b) Western blot detection of P38, ERK, p-P38 and p-ERK protein expression, and the relative expression of p-P38/P38 and p-ERK/ERK in H1299 cells. (c, d) Western blot detection of P38, ERK, p-P38 and p-ERK protein expression, and the relative expression of p-P38/P38 and p-ERK/ERK in H460 cells. $^{**}P < 0.01$ vs. (siNC group or vector group).

occurrence and development of LUAD, this study detected the expression of the MAPK/ERK pathway-related proteins. Western blot analysis showed that knockdown of CMIP significantly reduced p-P38 and p-ERK protein expressions, and p-P38/P38 and p-ERK/ERK ratios in H1299 cells compared with the siNC group (Figures 4(a) and 4(b)). In H460 cells, CMIP overexpression significantly increased p-P38 and p-ERK protein expression, and p-P38/P38 and p-ERK/ERK ratios compared with the vector group (Figures 4(c) and 4(d)). These results suggest that the MAPK/ERK pathways may be involved in the pathogenesis of LUAD by CMIP.

3.5. CMIP Overexpression Promotes H460 Cell Proliferation, Migration, and Invasion by Activating the MAPK/ERK Pathway. In addition, in order to further verify whether CMIP overexpression promotes the occurrence and development of LUAD through MAPK/ERK, H460 cells were treated with 10 μM U0126, and the results of MTT assay showed that compared with the OE-CMIP group, OE-CMIP + U0126 group significantly reduced the number of cells viability (Figure 5(a)). Colony formation assays also showed similar results, with U0126 intervention significantly reducing the number of H460 cell colonies compared to the OE-CMIP group (Figure 5(b)). In addition, wound healing assay and transwell analysis showed that the migration and invasion of H460 cells were significantly inhibited after U0126 intervention compared with the OE-CMIP group (Figures 5(c) and 5(d)). These results suggest that CMIP overexpression promotes the progression of LUAD by activating the MAPK/ERK pathway.

4. Discussion

At present, lung cancer is still one of the malignant tumors that seriously endanger human health and life [1]. With the rapid development of various omics technologies and bioinformatics, more and more genes have been identified as biomarkers for certain cancers for disease screening, diagnosis, prognosis, or further development as therapeutic targets corresponding biological reagents. Wei et al. found that EHD2 can inhibit the invasive ability of LUAD, improve patient prognosis, and can be used as a prognostic biomarker for LUAD [30]. Huang et al. showed through bioinformatics analysis and cellular experiments that high expression of GRSF1 promotes the occurrence and development of LUAD tumors and can be used as an effective prognostic biomarker for LUAD patients [31]. Previous studies have shown that CMIP, as an oncogene, promotes the progression of human

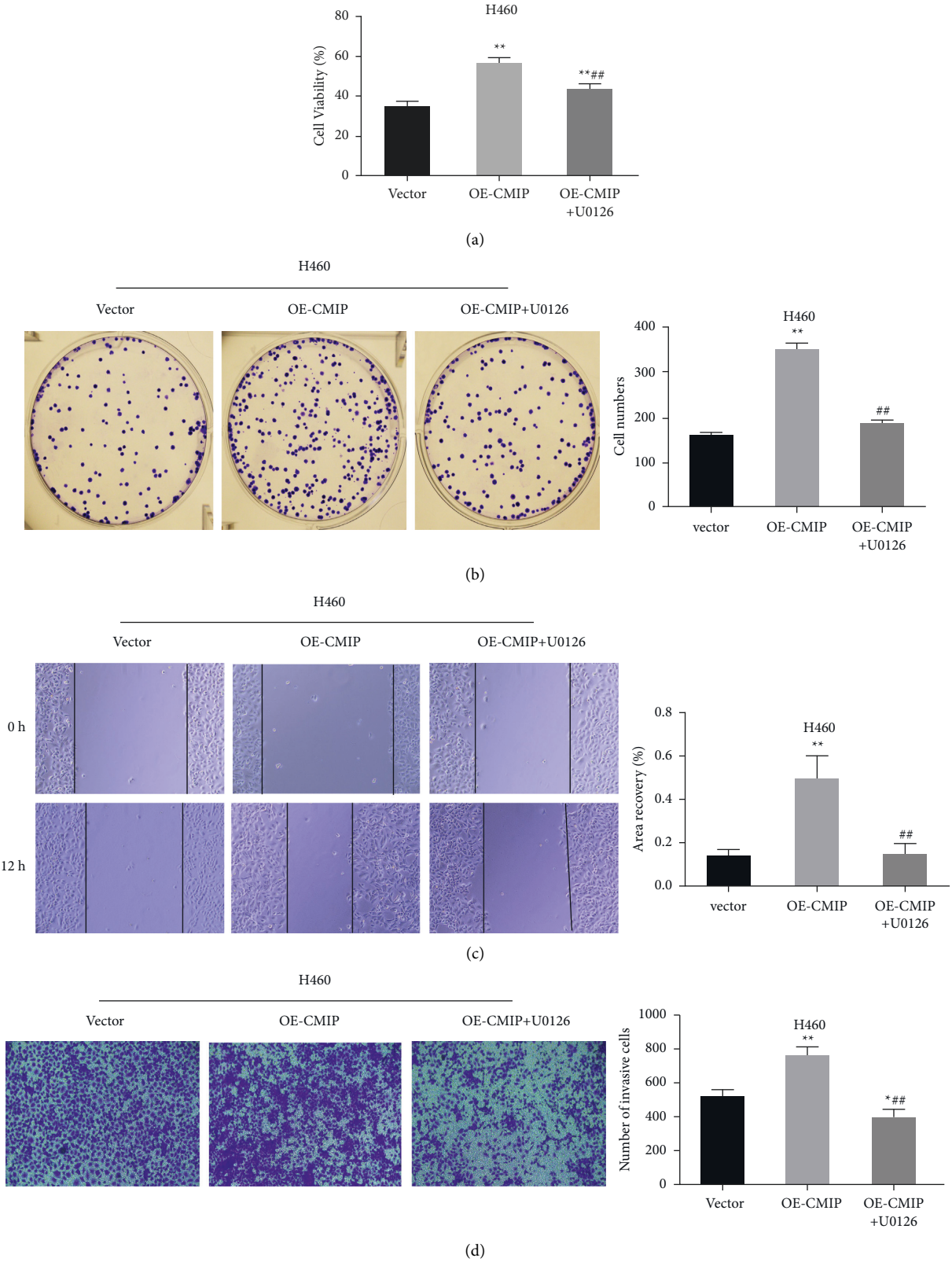

Figure 5: CMIP promotes H460 cell proliferation, migration, and invasion by activating the MAPK/ERK pathway. (a) MTT assay to detect cell viability in each group; (b) cell clone formation assay to detect the number of cell clones in each group; (c) wound healing assay to detect cell migration in each group; (d) Transwell analysis to detect cell invasion ability of each group. $^{*}P < 0.05$ and $^{**}P < 0.01$ vs. vector group, $^{\#\#}P < 0.01$ vs. OE-CMIP group.

gastric cancer and human glioma, and may be a potential target for the diagnosis and treatment of human glioma [18, 32]. However, so far, no studies have addressed the relationship between CMIP and LUAD. In the present study, bioinformatics analysis found that CMIP was highly expressed in LUAD tissues and correlated with poor patient prognosis. Subsequently, by detecting the expression of CMIP at the mRNA and protein levels, the results showed that the expression of CMIP in LUAD tissues and cells was significantly higher than that in the control group. These findings suggest that CMIP can serve as a prognostic biomarker for LUAD and is a new potential target worth investigating.

In order to explore the role of CMIP in LUAD and its molecular mechanism, this study found that CMIP overexpression promoted the proliferation, migration, and invasion of H460 cells through *in vitro* cell experiments, however, CMIP knockout significantly inhibited the proliferation, migration of H1299 cells, and invasive capacity, these results are consistent with Wang et al. [32]. In contrast, Zhang et al., in addition to demonstrating that CMIP knockout significantly reduced the proliferation, migration, and invasion abilities of MKN-28 gastric cancer cells, also showed that apoptosis was significantly increased after CMIP knockout by flow cytometry [18]. Based on this, the apoptotic role of CMIP in LUAD needs to be addressed in future studies.

Previous studies have shown that CMIP can directly inhibit Src kinase and cause urinary protein in mice [11]. In addition, Src homologous collagen (Shc) protein stimulates Raf through GTPase-Ras to activate the MAPK pathway, especially the ERK pathway to promote cell proliferation [33]. It has been reported that overactivation of the MAPK pathway promotes the occurrence and development of LUAD [34–36]. A previous study reported that EphA10 drives tumor progression and immune evasion by regulating the MAPK/ERK cascade in LUAD, and the MEK inhibitor U0126 significantly reversed the promoting effect of EphA10 overexpression on LUAD cells [37]. In this study, western blot experiments showed that CMIP overexpression significantly increased the expression of MAPK/ERK pathway-related proteins in H460 cells, while U0126 could significantly reversed the function of CMIP overexpression on the activation of the MAPK/ERK pathway. Therefore, CMIP may play pro-proliferation, migration and invasion effects in LUAD by activating the MAPK/ERK pathway.

To our knowledge, this study is the first to report the oncogenic role of CMIP in LUAD. Through bioinformatics analysis, clinical tissue samples and *in vitro* cell experiments, it was proved that high expression of CMIP is associated with poor prognosis of patients, and may promote the development of LUAD by activating the MAPK/ERK pathway. However, this study has some limitations. For the first time, the effect of CMIP on the malignant characteristics of LUAD by activating the MAPK/ERK pathway was not further explored in animal models by breeding CMIP knockout mice or injecting CMIP-targeting small interfering RNAs in LUAD mice. Second, epithelial-mesenchymal transition (EMT) promotes the spread of early epithelial cancer cells and is an important parameter for assessing the ability of epithelial cancer to metastasize and invade [38, 39] the degree of tumor resistance to anticancer drugs [40–42], but, which we did not explore in this study. Therefore, these issues will be addressed in future studies.

5. Conclusion

In conclusion, CMIP expression was significantly elevated in both LUAD cell lines and tissues, and was significantly associated with poor patient prognosis. Furthermore, CMIP promoted the proliferation and metastasis of LUAD cells by activating the MAPK/ERK pathway. Therefore, CMIP can serve as a prognostic biomarker and potential therapeutic target for LUAD.

Data Availability

The data used to support the findings of this study are available from the corresponding author upon request.

Conflicts of Interest

The authors declare that they have no conflicts of interest.

References

[1] H. Sung, J. Ferlay, R. L. Siegel et al., "Global cancer statistics 2020: GLOBOCAN estimates of incidence and mortality worldwide for 36 cancers in 185 countries," *CA: A Cancer Journal for Clinicians*, vol. 71, no. 3, pp. 209–249, 2021.

[2] J. R. Molina, P. Yang, S. D. Cassivi, S. E. Schild, and A. A. Adjei, "Non-small cell lung cancer: epidemiology, risk factors, treatment, and survivorship," *Mayo Clinic Proceedings*, vol. 83, no. 5, pp. 584–594, 2008.

[3] W. D. Travis, E. Brambilla, M. Noguchi et al., "International association for the study of lung cancer/American thoracic society/European respiratory society: international multidisciplinary classification of lung adenocarcinoma: executive summary," *Proceedings of the American Thoracic Society*, vol. 8, no. 5, pp. 381–385, 2011.

[4] Z. Chen, C. M. Fillmore, P. S. Hammerman, C. F. Kim, and K. K. Wong, "Non-small-cell lung cancers: a heterogeneous set of diseases," *Nature Reviews Cancer*, vol. 14, no. 8, pp. 535–546, 2014.

[5] U. Testa, G. Castelli, and E. Pelosi, "Lung cancers: molecular characterization, clonal heterogeneity and evolution, and cancer stem cells," *Cancers*, vol. 10, no. 8, p. 248, 2018.

[6] J. Hanaoka, M. Yoden, K. Hayashi et al., "Dynamic perfusion digital radiography for predicting pulmonary function after lung cancer resection," *World Journal of Surgical Oncology*, vol. 19, no. 1, p. 43, 2021.

[7] L. N. R. Buddharaju and A. K. Ganti, "Immunotherapy in lung cancer: the chemotherapy conundrum," *Chinese Clinical Oncology*, vol. 9, no. 4, p. 59, 2020.

[8] J. Zhang, J. Fujimoto, J. Zhang et al., "Intratumor heterogeneity in localized lung adenocarcinomas delineated by multiregion sequencing," *Science (New York, N.Y.)*, vol. 346, no. 6206, pp. 256–259, 2014.

[9] Y. Zhao, F. Varn, G. Cai, F. Xiao, C. Amos, and C. Cheng, "A P53-deficiency gene signature predicts recurrence risk of patients with early-stage lung adenocarcinoma," *Cancer Epidemiology, Biomarkers & Prevention*, vol. 27, no. 1, pp. 86–95, 2018.

[10] R. L. Siegel, K. D. Miller, and A. Jemal, "Cancer statistics, 2020," *CA: A Cancer Journal for Clinicians*, vol. 70, no. 1, pp. 7–30, 2020.

[11] S. y. Zhang, M. Kamal, K. Dahan et al., "c-mip impairs podocyte proximal signaling and induces heavy proteinuria," *Science Signaling*, vol. 3, no. 122, p. ra39, 2010.

[12] D. Sahali, K. Sendeyo, M. Mangier et al., "Immunopathogenesis of idiopathic nephrotic syndrome with relapse," *Seminars in Immunopathology*, vol. 36, no. 4, pp. 421–429, 2014.

[13] M. Kamal, A. Valanciute, K. Dahan et al., "C-mip interacts physically with RelA and inhibits nuclear factor kappa B activity," *Molecular Immunology*, vol. 46, no. 5, pp. 991–998, 2009.

[14] M. Kamal, A. Pawlak, F. BenMohamed et al., "C-mip interacts with the p85 subunit of PI3 kinase and exerts a dual effect on ERK signaling via the recruitment of Dip1 and DAP kinase," *FEBS Letters*, vol. 584, no. 3, pp. 500–506, 2010.

[15] K. Szymańska, K. Szczałuba, A. Lugowska et al., "The analysis of genetic aberrations in children with inherited neurometabolic and neurodevelopmental disorders," *BioMed Research International*, vol. 2014, pp. 1–8, 2014.

[16] D. F. Newbury, L. Winchester, L. Addis et al., "CMIP and ATP2C2 modulate phonological short-term memory in language impairment," *The American Journal of Human Genetics*, vol. 85, no. 2, pp. 264–272, 2009.

[17] T. S. Scerri, A. P. Morris, L. L. Buckingham et al., "DCDC2, KIAA0319 and CMIP are associated with reading-related traits," *Biological Psychiatry*, vol. 70, no. 3, pp. 237–245, 2011.

[18] J. Zhang, J. Huang, X. Wang et al., "CMIP is oncogenic in human gastric cancer cells," *Molecular Medicine Reports*, vol. 16, no. 5, pp. 7277–7286, 2017.

[19] R. Rami-Porta, V. Bolejack, J. Crowley et al., "The IASLC lung cancer staging project: proposals for the revisions of the T descriptors in the forthcoming eighth edition of the TNM classification for lung cancer," *Journal of Thoracic Oncology*, vol. 10, no. 7, pp. 990–1003, 2015.

[20] L. Wang, L. Meng, X. w. Wang, G. y. Ma, and J. h. Chen, "Expression of RRM1 and RRM2 as a novel prognostic marker in advanced non-small cell lung cancer receiving chemotherapy," *Tumor Biology*, vol. 35, no. 3, pp. 1899–1906, 2014.

[21] A. Digre and C. Lindskog, "The Human Protein Atlas-Spatial localization of the human proteome in health and disease," *Protein Science*, vol. 30, no. 1, pp. 218–233, 2021.

[22] A. Lánczky and B. Győrffy, "Web-based survival analysis tool tailored for medical Research (KMplot): development and implementation," *Journal of Medical Internet Research*, vol. 23, no. 7, Article ID e27633, 2021.

[23] K. J. Livak and T. D. Schmittgen, "Analysis of relative gene expression data using real-time quantitative PCR and the 2−ΔΔCT method," *Methods*, vol. 25, no. 4, pp. 402–408, 2001.

[24] M. Y. Li, Y. Liu, L. Z. Liu et al., "Estrogen receptor alpha promotes smoking-carcinogen-induced lung carcinogenesis via cytochrome P450 1B1," *Journal of Molecular Medicine (Berlin)*, vol. 93, no. 11, pp. 1221–1233, 2015.

[25] J. H. Joo, G. Liao, J. B. Collins, S. F. Grissom, and A. M. Jetten, "Farnesol-induced apoptosis in human lung carcinoma cells is coupled to the endoplasmic reticulum stress response," *Cancer Research*, vol. 67, no. 16, pp. 7929–7936, 2007.

[26] M. L. Janmaat, J. A. Rodriguez, M. Gallegos-Ruiz, F. A. Kruyt, and G. Giaccone, "Enhanced cytotoxicity induced by gefitinib and specific inhibitors of the Ras or phosphatidyl inositol-3 kinase pathways in non-small cell lung cancer cells," *International Journal of Cancer*, vol. 118, no. 1, pp. 209–214, 2006.

[27] P. Twentyman and M. Luscombe, "A study of some variables in a tetrazolium dye (MTT) based assay for cell growth and chemosensitivity," *British Journal of Cancer*, vol. 56, no. 3, pp. 279–285, 1987.

[28] L. Dai, S. Li, X. Li, and B. Jiang, "Propofol inhibits the malignant development of osteosarcoma U2OS cells via AMPK/FOXO1-mediated autophagy," *Oncology Letters*, vol. 24, no. 3, p. 310, 2022.

[29] S. J. Wang, W. W. Li, C. J. Wen, Y. L. Diao, and T. L. Zhao, "MicroRNA-214 promotes the EMT process in melanoma by downregulating CADM1 expression," *Molecular Medicine Reports*, vol. 22, no. 5, pp. 3795–3803, 2020.

[30] S. Wei, J. Shao, J. Wang et al., "EHD2 inhibits the invasive ability of lung adenocarcinoma and improves the prognosis of patients," *Journal of Thoracic Disease*, vol. 14, no. 7, pp. 2652–2664, 2022.

[31] R. Huang, L. Xu, Q. Chen et al., "GRSF1 predicts an unfavorable prognosis and promotes tumorigenesis in lung adenocarcinoma based on bioinformatics analysis and *in vitro* validation," *Annals of Translational Medicine*, vol. 10, no. 13, p. 747, 2022.

[32] B. Wang, Z. s. Wu, and Q. Wu, "CMIP promotes proliferation and metastasis in human glioma," *BioMed Research International*, vol. 2017, pp. 1–8, 2017.

[33] A. Józefiak, M. Larska, M. Pomorska-Mól, and J. J. Ruszkowski, "The IGF-1 signaling pathway in viral infections," *Viruses*, vol. 13, no. 8, p. 1488, 2021.

[34] L. Zhou, W. Chen, H. Yang, J. Liu, and H. Meng, "*β*Circ_001042 inhibits TGF-1/P38 MAPK signaling axis-mediated epithelial-mesenchymal transition and metastasis in lung adenocarcinoma," *Evidence-based Complementary and Alternative Medicine*, vol. 2022, pp. 1–11, 2022.

[35] Y. Li, R. Dong, M. Lu et al., "Let-7b-3p inhibits tumor growth and metastasis by targeting the BRF2-mediated MAPK/ERK pathway in human lung adenocarcinoma," *Translational Lung Cancer Research*, vol. 10, no. 4, pp. 1841–1856, 2021.

[36] J. Cheng, L. Xia, X. Hao et al., "Targeting STT3A produces an anti-tumor effect in lung adenocarcinoma by blocking the MAPK and PI3K/AKT signaling pathway," *Translational Lung Cancer Research*, vol. 11, no. 6, pp. 1089–1107, 2022.

[37] W. Zhao, L. Liu, X. Li, and S. Xu, "EphA10 drives tumor progression and immune evasion by regulating the MAPK/ERK cascade in lung adenocarcinoma," *International Immunopharmacology*, vol. 110, Article ID 109031, 2022.

[38] S. Yang, Y. Liu, M. Y. Li et al., "FOXP3 promotes tumor growth and metastasis by activating Wnt/*β*-catenin signaling pathway and EMT in non-small cell lung cancer," *Molecular Cancer*, vol. 16, no. 1, p. 124, 2017.

[39] Y. r. Zhao, J. l. Wang, C. Xu, Y. m. Li, B. Sun, and L. y. Yang, "HEG1 indicates poor prognosis and promotes hepatocellular carcinoma invasion, metastasis, and EMT by activating Wnt/*β*-catenin signaling," *Clinical Science*, vol. 133, no. 14, pp. 1645–1662, 2019.

[40] K. R. Fischer, A. Durrans, S. Lee et al., "Epithelial-to-mesenchymal transition is not required for lung metastasis but contributes to chemoresistance," *Nature*, vol. 527, no. 7579, pp. 472–476, 2015.

[41] X. Zheng, J. L. Carstens, J. Kim et al., "Epithelial-to-mesenchymal transition is dispensable for metastasis but induces chemoresistance in pancreatic cancer," *Nature*, vol. 527, no. 7579, pp. 525–530, 2015.

[42] E. Galle, B. Thienpont, S. Cappuyns et al., "DNA methylation-driven EMT is a common mechanism of resistance to various therapeutic agents in cancer," *Clinical Epigenetics*, vol. 12, no. 1, p. 27, 2020.

Hindawi
Evidence-Based Complementary and Alternative Medicine
Volume 2023, Article ID 9782478, 1 page
https://doi.org/10.1155/2023/9782478

Retraction

Retracted: Evaluation of lncRNA FOXD3-AS1 as a Biomarker for Early-Stage Lung Cancer Diagnosis and Subtype Identification

Evidence-Based Complementary and Alternative Medicine

Received 3 October 2023; Accepted 3 October 2023; Published 4 October 2023

This article has been retracted by Hindawi following an investigation undertaken by the publisher [1]. This investigation has uncovered evidence of one or more of the following indicators of systematic manipulation of the publication process:

(1) Discrepancies in scope
(2) Discrepancies in the description of the research reported
(3) Discrepancies between the availability of data and the research described
(4) Inappropriate citations
(5) Incoherent, meaningless and/or irrelevant content included in the article
(6) Peer-review manipulation

The presence of these indicators undermines our confidence in the integrity of the article's content and we cannot, therefore, vouch for its reliability. Please note that this notice is intended solely to alert readers that the content of this article is unreliable. We have not investigated whether authors were aware of or involved in the systematic manipulation of the publication process.

Wiley and Hindawi regrets that the usual quality checks did not identify these issues before publication and have since put additional measures in place to safeguard research integrity.

We wish to credit our own Research Integrity and Research Publishing teams and anonymous and named external researchers and research integrity experts for contributing to this investigation.

The corresponding author, as the representative of all authors, has been given the opportunity to register their agreement or disagreement to this retraction. We have kept a record of any response received.

References

[1] X. Liu, W. Chen, Y. Qi, and Y. Zhu, "Evaluation of lncRNA FOXD3-AS1 as a Biomarker for Early-Stage Lung Cancer Diagnosis and Subtype Identification," *Evidence-Based Complementary and Alternative Medicine*, vol. 2022, Article ID 5702014, 11 pages, 2022.

Hindawi
Evidence-Based Complementary and Alternative Medicine
Volume 2022, Article ID 5702014, 11 pages
https://doi.org/10.1155/2022/5702014

Research Article

Evaluation of lncRNA FOXD3-AS1 as a Biomarker for Early-Stage Lung Cancer Diagnosis and Subtype Identification

Xiaofeng Liu, Wenyan Chen, Yu Qi, and Yongqian Zhu

Department of Pathology, Traditional Chinese Medicine Hospital of LuAn, Lu'an 237006, Anhui, China

Correspondence should be addressed to Xiaofeng Liu; liuxifnla@163.com

Received 2 July 2022; Revised 22 July 2022; Accepted 20 August 2022; Published 14 September 2022

Academic Editor: Xueliang Wu

Purpose. Lung cancer (LC) is the most commonly diagnosed cancer and the leading cause of cancer-related deaths. More and more long noncoding RNA (lncRNA) are associated with cancer. This study aimed to assess whether plasma lncRNA could be used to diagnose early-stage LC and identify subtypes of LC. *Methods*. For bioinformatic analysis, we used genetic data from the Cancer Genome Atlas, lung adenocarcinoma (LUAD), and lung squamous cell carcinoma (LUSC) datasets and a small cell lung cancer (SCLC) dataset from the Gene Expression Omnibus. Real-time quantitative polymerase chain reaction (RT-qPCR) was used to examine the relative expression of lncRNA in LC tissues and plasma samples. The patients' clinical information was obtained at the time of sample collection. *Results*. According to public datasets, the lncRNA forkhead box D3 antisense 1 (FOXD3-AS1) was significantly upregulated in LUAD, LUSC, and SCLC tissues over controls. RT-qPCR assays confirmed this finding in LUAD, LUSC, and SCLC tissues and plasma samples. Even early-stage receiver operating characteristic analysis showed that plasma FOXD3-AS1 could be used to discriminate LUAD, LUSC, and SCLC from normal controls and identify LC subtypes SCLC. *Conclusion*. FOXD3-AS1 is significantly upregulated in LC tissues and plasma. FOXD3-AS1 could be a potential biomarker for LC subtype identification and early diagnosis.

1. Introduction

Lung cancer (LC) is the leading cause of cancer-related morbidity and mortality in China, accounting for 36.98% of cases and 39.21% of deaths worldwide, posing a significant challenge to the medical system and research [1, 2]. Non-small cell lung cancer (NSCLC) is the most common histological subtype of LC, accounting for 85% of diagnosed LCs [3]. It has always progressed to unresectable stage III or IV at the time of diagnosis. The most common types of NSCLC are lung adenocarcinoma (LUAD) and lung squamous cell carcinoma (LUSC), which arise from alveolar cells in the smaller airway epithelium and cells in the airway epithelium, respectively, and have divergent oncogenic driver mutations and pathways [4, 5]. Small cell lung cancer (SCLC) is an aggressive neuroendocrine tumor that arises as a perihilar mass from the airway submucosa. It is usually diagnosed at metastasis extensive-stage or unresectable limited-stage [6, 7]. Early LC screening with low-dose computed tomography is most effective in reducing mortality, but it has a high false-positive rate. Many types of imaging, particularly high-resolution computed tomography and preoperative pathology, aid in the clinical diagnosis and treatment planning of LC [8–10]. However, repeated ionizing radiation is expensive and may increase cancer risk. As a result, finding novel biomarkers for early and accurate LC detection is critical. Furthermore, a noninvasive and sensitive method to identify LC histological subtypes would greatly improve LC therapy.

Long noncoding RNAs (lncRNAs) are transcripts with a length of more than 200 nucleotides and no open reading frame or protein-coding function. They encompass a large and diverse group of transcripts with varying biogenesis and biological functions [11]. LncRNAs could induce chromatin remodeling and histone modification by invading chromatin structure or regulating chromatin/histone accessibility of the regulator/modifier; regulate transcription by gene-dosage compensation, acting as enhancers, or lncRNAs regulatory

networks; regulate splicing, degradation, or sponging absorbing of transcription products; and act in cellular organelles function, structural functions, and genome integrity primarily through protein interactions [12, 13].

LncRNA forkhead box D3 antisense 1 (FOXD3-AS1) is a 963 bp antisense transcript of the gene FOXD3, whose abnormal expression has been linked to pathophysiological characteristics of several diseases [14]. FOXD3-AS1, for example, affects the development of breast cancer, nasopharyngeal carcinoma, colon adenocarcinoma, and hepatocellular carcinoma via competing for the endogenous RNAs (ceRNAs) mechanism [15–17]. FOXD3-AS1 binds to poly (ADP-ribose) polymerase 1 in neuroblastoma, preventing the CCCTC-binding factor from being PARylated and thus derepressing the production of downstream tumor-suppressive genes [18]. According to Yang's research, FOXD3-AS1 binds to Y-box binding protein 1 to mediate the H3K27ac enrichment in the promoter region in nasopharyngeal carcinoma [19]. Through the PI3K/Akt pathway, FOXD3-AS1 interacts with and activates RNA-binding protein ELAV-like RNA-binding protein 1, causing LC cell proliferation, invasion, and 5-fluorouracil resistance [20]. FOXD3-AS1 has also been shown to keep mediator subunit 28, murine double minute 2, and cyclin-dependent kinase 6 expressions in NSCLC by sequestering miRNAs [21–23]. We confirmed that FOXD3-AS1 is overexpressed in both blood and tissues of LUAD, LUSC, and SCLC samples when compared to control in the current study, based on hints from the Cancer Genome Atlas (TCGA) lung adenocarcinoma projects, lung squamous carcinoma projects, and Gene Expression Omnibus (GEO) datasets (GSE60052) as well as our RT-qPCR assays. Furthermore, FOXD3-AS1 has the potential to aid in the early detection of LC and identifying SCLC subtypes.

2. Materials and Methods

2.1. RNA Sequencing (RNA-Seq) Data Collection from TCGA and GEO Databases. The gene expression matrix and clinical data for LUAC projects were downloaded from TCGA's official website (527 tumor vs. 58 normal, https://xenabrowser.net/datapages/?cohort=GDC%20TCGA%20Lung%20Adenocarcinoma%20(LUAD)&removeHub=https%3A%2F%2Fxena.treehouse.gi.ucsc.edu%3A443), LUSC (501 tumor vs. 49 normal, https://xenabrowser.net/datapages/?cohort=GDC%20TCGA%20Lung%20Squamous%20Cell%20Carcinoma%20(LUSC)&removeHub=https%3A%2F%2Fxena.treehouse.gi.ucsc.edu%3A443), and GEO official website for SCLC (79 tumor vs. 7 normal, https://www.ncbi.nlm.nih.gov/geo/query/acc.cgi?acc=GSE60052).

2.2. Bioinformatic Analysis. Gene categories lncRNA was screened based on human genome annotation files (gif files) downloaded from the Gencode database. On the lncRNA expression matrices, differential expression analysis of tumor versus normal was performed for each of the three datasets using the *R* package DESeq2. |log2 fold change (FC)| >1 and adjusted *P* value <0.05 were used to screen differentially expressed lncRNAs (DELs). To visualize the findings, volcano plots were created. The *R* package heatmap was used to plot heat maps of differential expressed lncRNAs. The results of the up and downregulated genes of the three subtypes of tumors were analyzed separately and presented in a Venn diagram. The *R* package ggplot2 was used to plot the expression Boxplot.

2.3. Patients and Clinical Samples. This study included 150 patients with LC (50 with LUAD, 50 with LUSC, and 50 with SCLC) and 50 health subjects (HS) of similar sex and age. All surgical specimens were obtained between January 2020 and December 2021, and the clinical data were collected at the same time (Table 1). Three months prior to surgery, no patients received chemotherapy or radiotherapy. The Ethics Committee of Traditional Chinese Medicine Hospital of LuAn approved the study protocol on scientific research, and all participants provided written informed consent. The tissues were immediately frozen in liquid nitrogen and then stored at −80°C for RNA extraction. Before the operation, blood samples were collected in a vacutainer with an anticoagulant. The whole blood samples were centrifuged at 3000 rpm at 4°C for 10 min, and the supernatant plasma was frozen at −80°C.

2.4. RNA Isolation and Real-Time Quantitative Polymerase Chain Reaction (RT-qPCR). TRIzol reagent (Invitrogen) and QIAGEN RNeasy Serum/Plasma Maxi Kit (QIAGEN) were used to extract total RNA from tissues and plasma, respectively, according to the manufacturer's instructions. The Prime ScriptTM RT reagent kit (Takara) was used for reverse transcription, which was carried out according to the manufacturer's protocol. For RT-qPCR, the SYBR Premix Ex Taq kit (Takara) was used. The endogenous reference glyceraldehyde-3-phosphate dehydrogenase (GAPDH) was used to calibrate the initial mRNA concentrations. The $2^{-\Delta\Delta CT}$ method [24] was used to determine relative gene expression. The primer sequences were as follows: FOXD3-AS1, forward 5′-GAATAGTTGCCGAGAGAAA-3′ and reverse 5′-GACAGACAGGGATTGGGTT-3′; GAPDH, forward 5′-GGGGCTCTCCAGAACATC-3′ and reverse 5′-TGACACGTTGGCAGTGG-3′.

2.5. Statistical Analysis. R (v.4.1.0) and SPSS (IBM Corp., Armonk, USA) were used to conduct all statistical analyses. The *t*-test was used to compare the two groups of continuous data. The difference between the two groups was analyzed using the chi-square test, which was used to express the enumeration data in a fourfold table. The receiver operating characteristic curve (ROC) and the area under the curve (AUC) were performed to evaluate the diagnostic value of FOXD3-AS1. $P < 0.05$ was considered statistically significant.

Table 1: The clinicopathological parameters of patients with lung cancer.

Characteristics	HS ($n = 50$)	LC			P value (HS vs. LC)
		SCLC ($n = 50$)	LUAD ($n = 50$)	LUSC ($n = 50$)	
Age in years median (range)	69.98 ± 11.25	70.26 ± 12.05	74.14 ± 8.76	71.96 ± 11.72	0.237
Gender					0.280
Male	33	35	28	23	
Female	17	15	22	27	
Smoking status					0.612
Yes	30	36	32	28	
No	20	14	18	22	
Stage					—
I-II	—	19	16	18	
III-IV	—	31	34	32	
Lymph metastasis					
No	—	16	14	15	—
Yes	—	34	36	35	
Distal metastasis					—
Yes	—	16	18	14	
No	—	34	32	36	

HS, healthy subjects; LC, lung cancer; SCLC, small cell lung cancer; LUAD, lung adenocarcinoma; LUSC, lung squamous cell carcinoma.

3. Results

3.1. Identification of Key lncRNAs from TCGA and the GEO RNA-Seq Data. Mining of TCGA, LUAD, and LUSC RNA sequencing (RNA-seq) datasets, as well as GEO, SCLC, and RNA-seq datasets (GSE60052) was performed to find lncRNAs as diagnostic biomarkers in patients with LC. The LUAD cohort, LUSC cohort, and SCLC cohort each had 527 LUAD samples vs. 58 paracancer tissue samples, 501 LUSC samples vs. 49 paracancer tissue samples, and 79 SCLC tumors vs. 7 normal lung tissue samples. We found 1368, 1436, and 524 significantly upregulated lncRNAs and 755, 1386, and 153 downregulated lncRNAs (|log2 FC|>1 and adjusted $P < 0.001$ value <0.05), associated with the histological subtypes of LUAD, LUSC, and SCLC, respectively (Tables S1–S3). Heatmaps were created using differentially expressed lncRNAs (DELs) (Figures 1(a)–1(c)). Volcano maps were used to show the two-dimensional distribution of −log10 (adjusted P value) and log2 (FC) of three sets of DELs (Figures 1(d)–1(f)). Among these DELs, 66 upregulated lncRNAs coexisted in all three LC subtypes (Figure 1(g) and Table S4), while 10 lncRNAs were downregulated (Figure 1(h) and Table S5).

We ranked the DELs of each comparison by FC or adjusted P value. We performed a Venn diagram analysis using the top 10 lncRNAs of each comparison to find the most significant DELs. Finally, FOXD3-AS1 was identified using FC and adjusted P value screening. In contrast, HOXC-AS2 was identified using adjusted P value screening (Figure 2(a) and 2(b)). When compared to normal controls ($P < 0.0001$), the expression of FOXD3-AS1 was significantly higher in lung tumors, regardless of whether they were LUAD, LUSC, or SCLC (Figures 2(c)–2(e)). FOXD3-AS1 was selected for further research.

3.2. Participants and Clinical Characteristics of the Validation Phase. A total of 50 healthy candidates and 150 patients with LC (50 SCLC, 50 LUAD, and 50 LUSC) were enrolled in the study to verify the diagnostic potential of FOXD3-AS1. Table 1 summarizes the demographic and clinical parameters. In the healthy and LC groups, sex ratios (males: females) and smoking rates were similar. According to disease characteristics, there were 53 patients with stages I-II and 97 with stages III-IV.

3.3. FOXD3-AS1 Expression in Tissues and Plasma Was Correlated with the LC Progression. In all LUAD, LUSC, and SCLC patients, FOXD3-AS1 expression in tumor tissues (CA) was much higher than in paracancer tissues (PC) ($P < 0.001$, Figure 3(a)). We investigated whether FOXD3-AS1 could be secreted into circulating plasma by tumor cells because it has been shown to stimulate invasion in NSCLC [23]. As we can see, lncRNA FOXD3-AS1 was found in plasma and expressed significantly higher in LUAD, LUSC, and SCLC blood samples than in HS ($P < 0.001$, Figure 3(b)). We also looked at how the expression of FOXD3-AS1 changed as LC progressed. In all three subtypes, FOXD3-AS1 production in blood was significantly higher in stages III-IV than in stages I-II ($P < 0.001$, Figure 3(c)).

Based on the median FOXD3-AS1 expression threshold (5.045 for SCLC, 3.52 for LUAD, and 4.04 for LUSC), we divided the cancer plasma samples into low and high-FOXD3-AS1 subgroups (L-lncRNA and H-lncRNA for short). We analyzed their relationship with the clinical characteristics of the patients. As shown in Table 2, there were no significant differences in gender or smoking history between the H-lncRNA and L-lncRNA groups, but the patients who expressed high levels of FOXD3-AS1 were more likely older than 65 in LUAD ($P = 0.047$) and LUSC ($P = 0.022$). Furthermore, a high level of FOXD3-AS1 indicated a more advanced stage of LUAD ($P = 0.012$) and LUSC ($P = 0.010$), a greater probability of lymph metastasis in LUAD ($P = 0.025$) and LUSC ($P < 0.001$), and a greater probability of distal metastasis in SCLC ($P = 0.032$). These findings showed that the level of FOXD3-AS1 increased as LC progressed and that the fluctuating levels of FOXD3-AS1

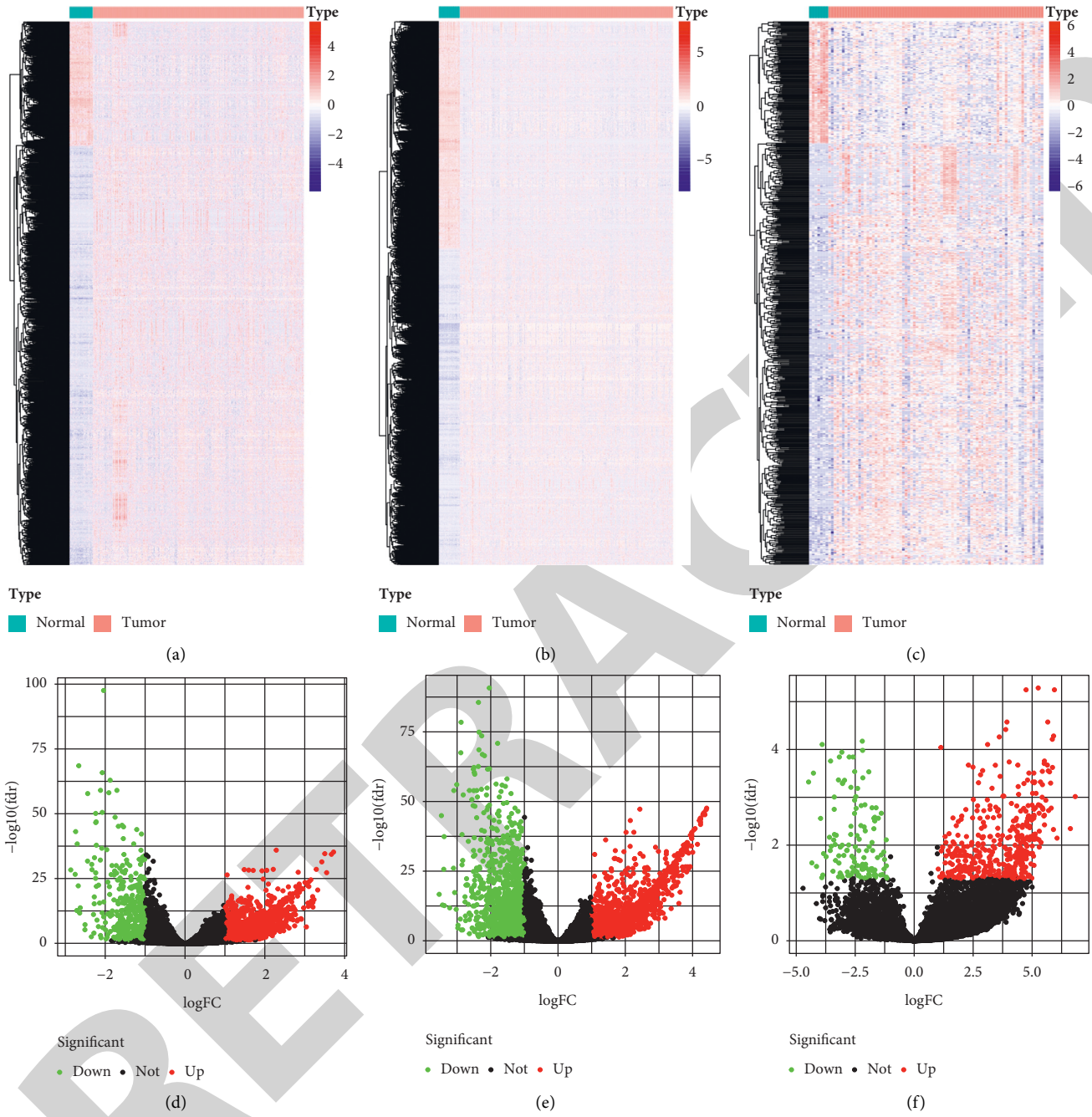

Figure 1: Continued.

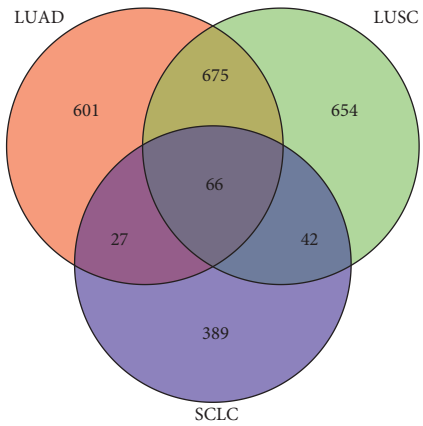

(g)

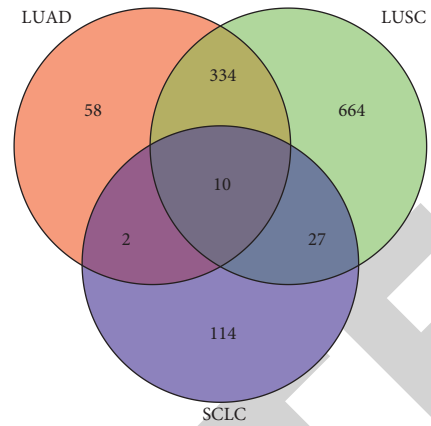

(h)

Figure 1: Bioinformatic analysis of dysregulated lncRNAs in different subtypes of LC. (a)–(c) Heatmap and (d)–(f) volcano plot of differentially expressed lncRNAs (DELs) between paracancer tissues and cancer tissues in TCGA LUAD project (a and d), TCGA LUSC project (b and e), and GEO SCLC dataset (c and f). (g)-(h) A Venn diagram of the upregulated (g) and downregulated (h) DELs overlapping between LUAD, LUSC, and SCLC.

in tissues were primarily related to the presence of disease lesions rather than factors such as gender or smoking.

3.4. Role of Plasma FOXD3-AS1 in LC Diagnosis and Identifying LC Subtypes. The diagnostic efficacy of plasma FOXD3-AS1 in three subtypes of LC was assessed using ROC analysis. FOXD3-AS1 had an AUC of 0.959 (95% confidence interval (CI): 0.926–0.992) in identifying patients with SCLC out of HS (Figure 4(a) and Table 3), an AUC of 0.763 (95% CI: 0.670–0.855) in identifying patients with LUAD out of HS (Figure 4(b) and Table 3), an AUC of 0.854 (95% CI: 0.782–0.927) in identifying patients with LUSC out of HS (Figure 4(c) and Table 3), and an AUC of 0.859 (95% CI: 0.802–0.915) in identifying patients with LC out of HS (Figure 4(d) and Table 3).

We further looked at the discrimination efficiency of FOXD3-AS1 between them. With a sensitivity of 78% and a specificity of 92%, it created an AUC value of 0.888 (95% CI: 0.822–0.953) in distinguishing patients with SCLC from patients with LUAD (Figure 4(e) and Table 3). With a sensitivity of 78% and a specificity of 80%, it created an AUC value of 0.821 (95% CI: 0.737–0.905) in distinguishing patients with SCLC from patients with LUSC (Figure 4(f) and Table 3). In contrast, with a sensitivity of 80% and a specificity of 52%, it created an AUC value of 0.658 (95% CI: 0.552–0.765) in determining patients with LUAD from patients with LUSC (Figure 4(g) and Table 3).

3.5. Diagnostic Accuracy of FOXD3-AS1 as Diagnostic Biomarkers to Detect Early-Stage LC. Because the expression of FOXD3-AS1 in LC was higher than in healthy people and increased as the disease progressed, we hypothesized that FOXD3-AS1 was activated early in the disease. We specifically analyzed stages I-II LC samples to estimate the efficiency of FOXD3-AS1 in the early detection of LC. FOXD3-AS1 yielded an AUC of 0.906 (95% CI: 0.831–0.982), a sensitivity of 73%, a specificity of 92%, and a Yoden index of 3.94 in distinguishing between SCLC and HS subjects (Figure 5(a) and Table 4). In terms of LUAD early detection, the AUC value, sensitivity, specificity, and Yoden index was 0.591 (95% CI: 0.453–0.729), 100%, 30%, and 2.46, respectively (Figure 5(b) and Table 4). In LUSC early detection, the AUC value, sensitivity, specificity, and Yoden index was 0.686 (95% CI: 0.562–0.809), 100%, 42%, and 2.750, respectively (Figure 5(c) and Table 4). In total, FOXD3-AS1 produced an AUC value of 0.751 (95% CI: 0.658–0.845), a sensitivity of 73.6%, a specificity of 66%, and a Yoden index of 3.195 in discriminating early LC samples from HS (Figure 5(d) and Table 4).

FOXD3-AS1 was also found to be effective in identifying LC subtypes SCLC. The AUC values for SCLC versus LUAD, SCLC versus LUSC, and LUAD versus LUSC were found to be 0.901 (95% CI: 0.802–1) (Figure 5(e) and Table 4), 0.857 (95% CI: 0.730–0.983) (Figure 5(f) and Table 4), and 0.674 (95% CI: 0.489 0.858) (Figure 5(g) and Table 4), respectively.

4. Discussion

Despite the numerous diagnostic and treatment options available for LC [25, 26], it remains one of the most dangerous malignancies worldwide because it is often asymptomatic and detected late [1]. Early diagnosis is the most important factor in influencing the prognosis of patients with LC. We aimed to find an abnormally expressed lncRNA in patients with LC and investigate how effective this lncRNA is at diagnosing LC. Through bioinformatics analysis of public datasets, we discovered that FOXD3-AS1, a lncRNA, was significantly upregulated in three primary subtypes of LC, SCLC, LUAD, and LUSC. An RT-qPCR assay confirmed the finding in SCLC, LUAD, and LUSC tissues and plasma. Furthermore, ROC analysis revealed that plasma FOXD3-AS1 could be used to discriminate SCLC, LUAD, and LUSC from healthy subjects. On the other side, SCLC samples produced much more FOXD3-AS1 than LUAD or LUSC, and FOXD3-AS1 was more sensitive in

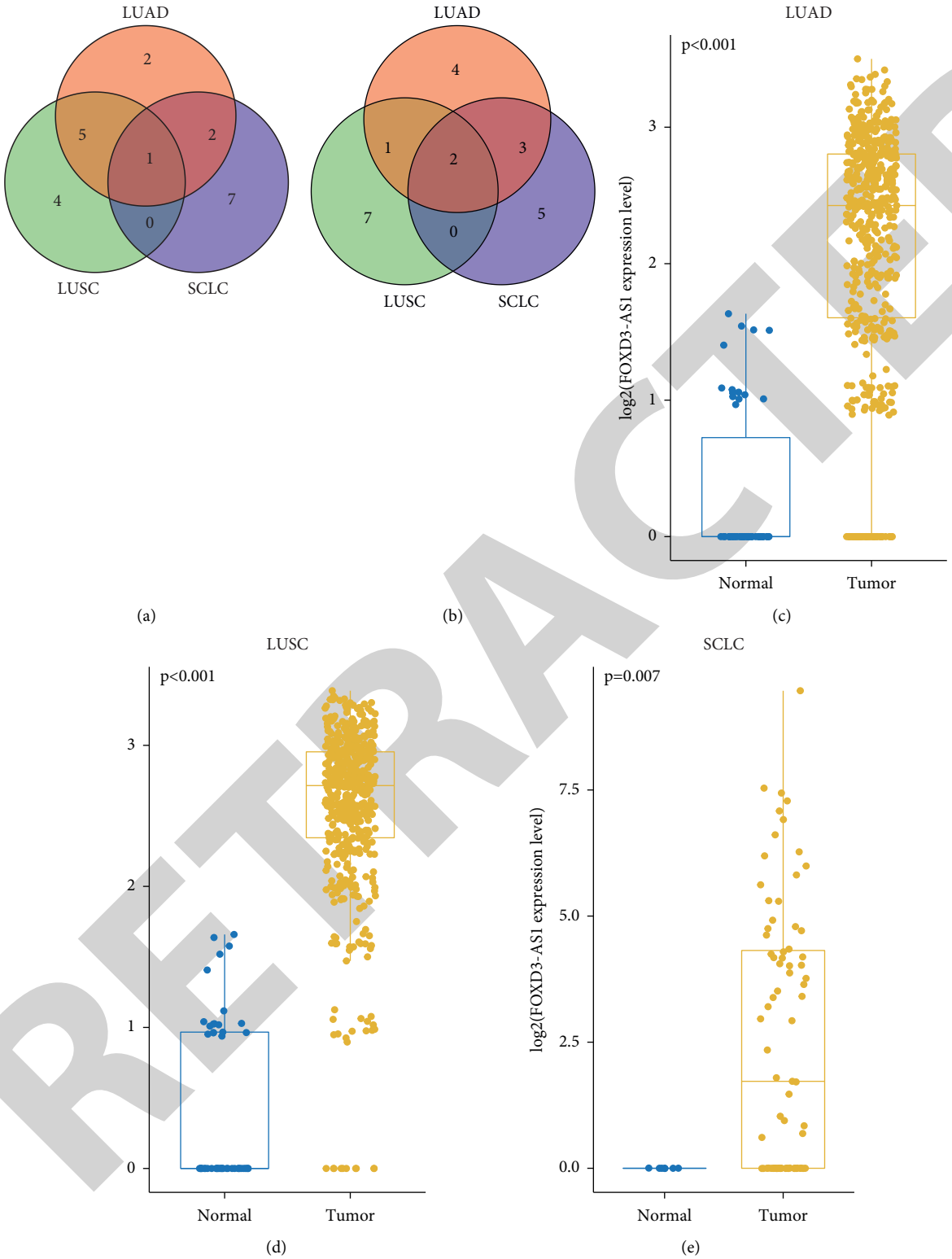

Figure 2: FOXD3-AS1 was the most significantly upregulated lncRNA in LUAD, LUSC, and SCLC according to public datasets. Venn diagram of the intersection of top 10 DELs ranked by FC (a) and adjusted *P* value (b). FOXD3-AS1 expression determined in cancer specimens (tumor) and paracancer specimens (normal) using TCGA LUAD dataset (c), TCGA LUSC dataset (d), and GEO SCLC dataset (e). The *t*-test was used to calculated *P* value.

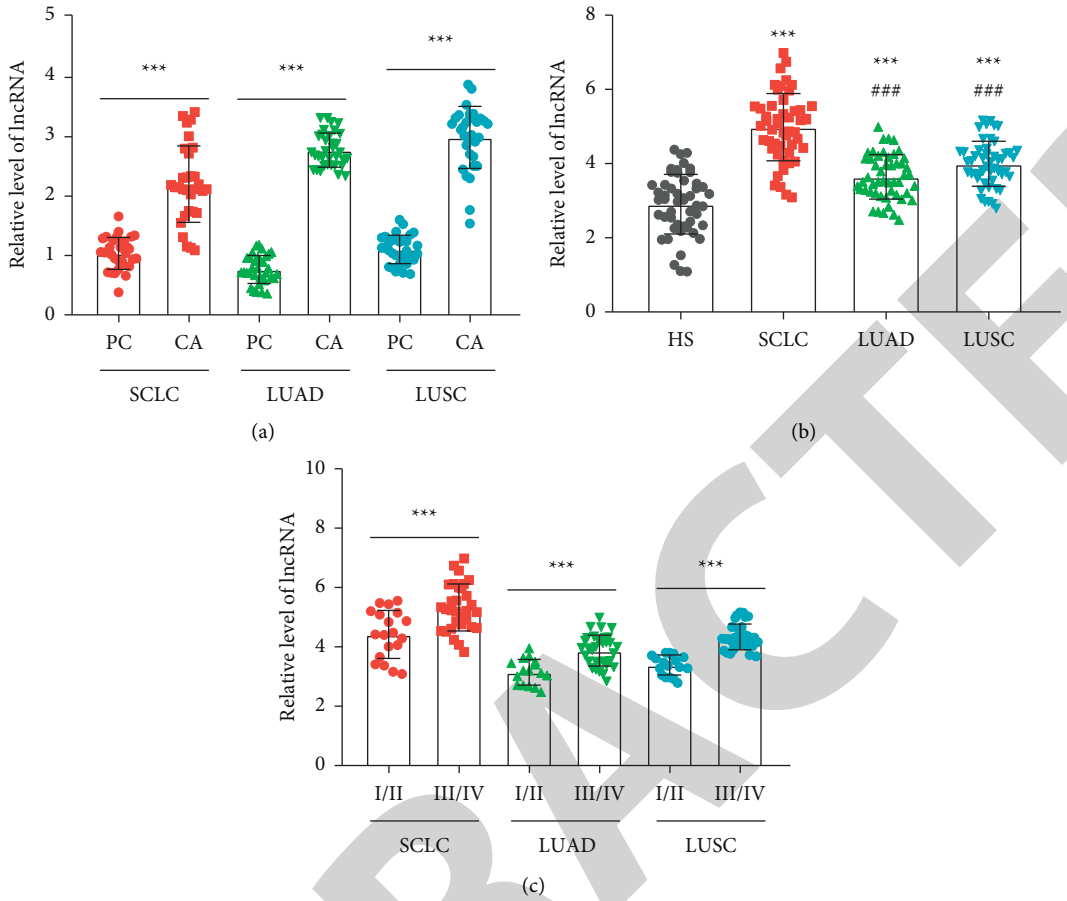

Figure 3: FOXD3-AS1 was verified to be overexpressed in SCLC, LUAD, and LUSC tissues and plasma comparing with healthy subjects. (a) RT-qPCR assay performed to detect the expression of FOXD3-AS1 in cancer tissues and paracancer tissues from patients with SCLC, LUAD, and LUSC. P value was obtained by the t-test. $^{***}P < 0.001$. (b) RT-qPCR analysis of FOXD3-AS1 in the plasma of healthy candidates (HS) and patients with SCLC, LUAD, and LUSC. The asterisk sign indicated the comparison with the HS group, while the hash sign represented the SCLC group as the control. P value was obtained by the t-test. $^{***}P < 0.001$. $^{###}P < 0.001$. (c) RT-qPCR analysis of FOXD3-AS1 in the plasma samples of patients with SCLC, LUAD, and LUSC at stages I-II (I/II) and stages III-IV (III/IV). P value was obtained by the t-test. $^{***}P < 0.001$.

Table 2: Relationship between lncRNA FOXD3-AS1 expression in serum and clinicopathological parameters of patients with lung cancer.

Characteristics	SCLC			LUAD			LUSC		
	H-lncRNA ($n = 25$)	L-lncRNA ($n = 25$)	P value	H-lncRNA ($n = 25$)	L-lncRNA ($n = 25$)	P value	H-lncRNA ($n = 25$)	L-lncRNA ($n = 25$)	P value
Gender (male/female)	17/8	18/7	1	13/12	15/10	0.776	14/11	18/7	0.377
Age (<65 y/≥65 y)	7/18	14/11/	0.085	4/21	15/20	0.047	7/18	16/9	0.022
Smoking story (yes/no)	19/6	17/8	0.754	17/8	15/10	0.769	13/12	15/10	0.776
Stage (I-II/III-IV)	19/6	13/12	0.140	22/3	13/12	0.012	25/0	18/7	0.010
Lymph metastasis (yes/no)	20/5	14/11	0.128	22/3	14/11	0.025	25/0	10/15	<0.001
Distal metastasis (yes/no)	12/13	4/21	0.032	10/15	8/17	0.769	10/15	4/21	0.114

discriminating SCLC from LUAD or LUSC by ROC analysis. Thus, FOXD3-AS1 would be an accurate molecular marker for the diagnosis of LC and SCLC subtype identification.

Previous research found that the transcription factor specificity protein 1 promoted lymphatic invasion and distant metastasis in cervical cancer by inducing FOXD3-AS1 expression [27]. However, the factors that activate FOXD3-AS1 in LC are unknown, and more research studies are needed. FOXD3-AS1 has been shown to have predictive value and functional roles in various diseases, including

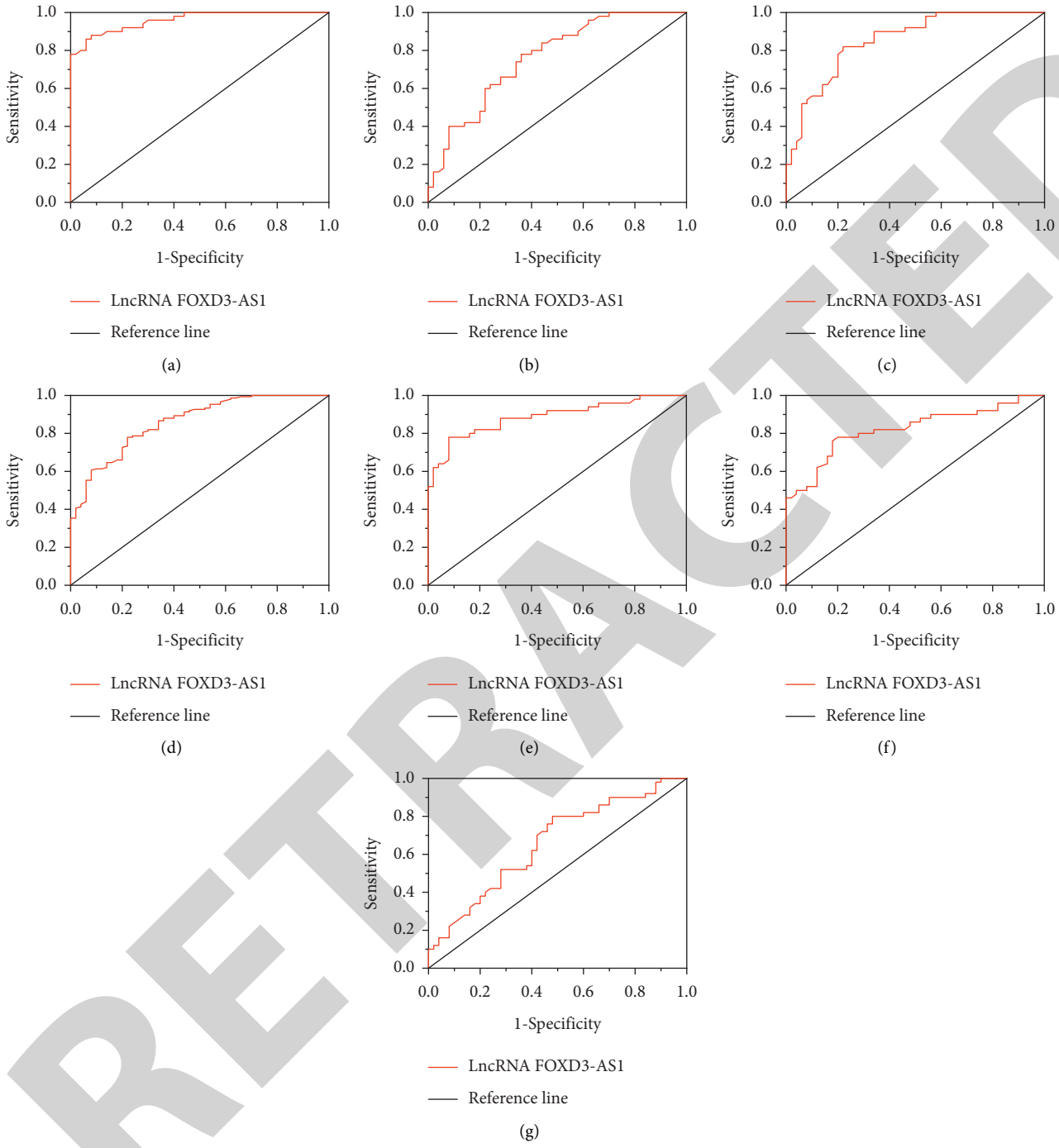

Figure 4: The efficiency of plasma FOXD3-AS1 in cancer diagnosis and SCLC identification. (a)–(g) ROC curves used to validate the discrimination efficiency of plasma FOXD3-AS1 for SCLC vs. HS (a), LUAD vs. HS (b), LUSC vs. HS (c), LC vs. HS (d), SCLC vs. LUAD (e), SCLC vs. LUSC (f), and LUAD vs. LUSC (g).

Table 3: The diagnostic values of lncRNA FOXD3-AS1 in discriminating lung cancer subtypes.

Index	AUC	95% CI		*P* value	Sensitivity	Specificity	Critical value	Yoden index
		Down	Up					
SCLC vs. HS	0.959	0.926	0.992	<0.001	88.000	92.000	0.800	3.940
LUAD vs. HS	0.763	0.670	0.855	<0.001	78.000	64.000	0.420	3.195
LUSC vs. HS	0.854	0.782	0.927	<0.001	82.000	78.000	0.600	3.465
LC vs. HS	0.859	0.802	0.915	<0.001	78.000	78.000	0.560	3.465
SCLC vs. LUAD	0.888	0.822	0.953	<0.001	78.000	92.000	0.700	4.375
SCLC vs. LUSC	0.821	0.737	0.905	<0.001	78.000	80.000	0.580	4.380
LUAD vs. LUSC	0.658	0.552	0.765	0.006	80.000	52.000	0.320	3.535

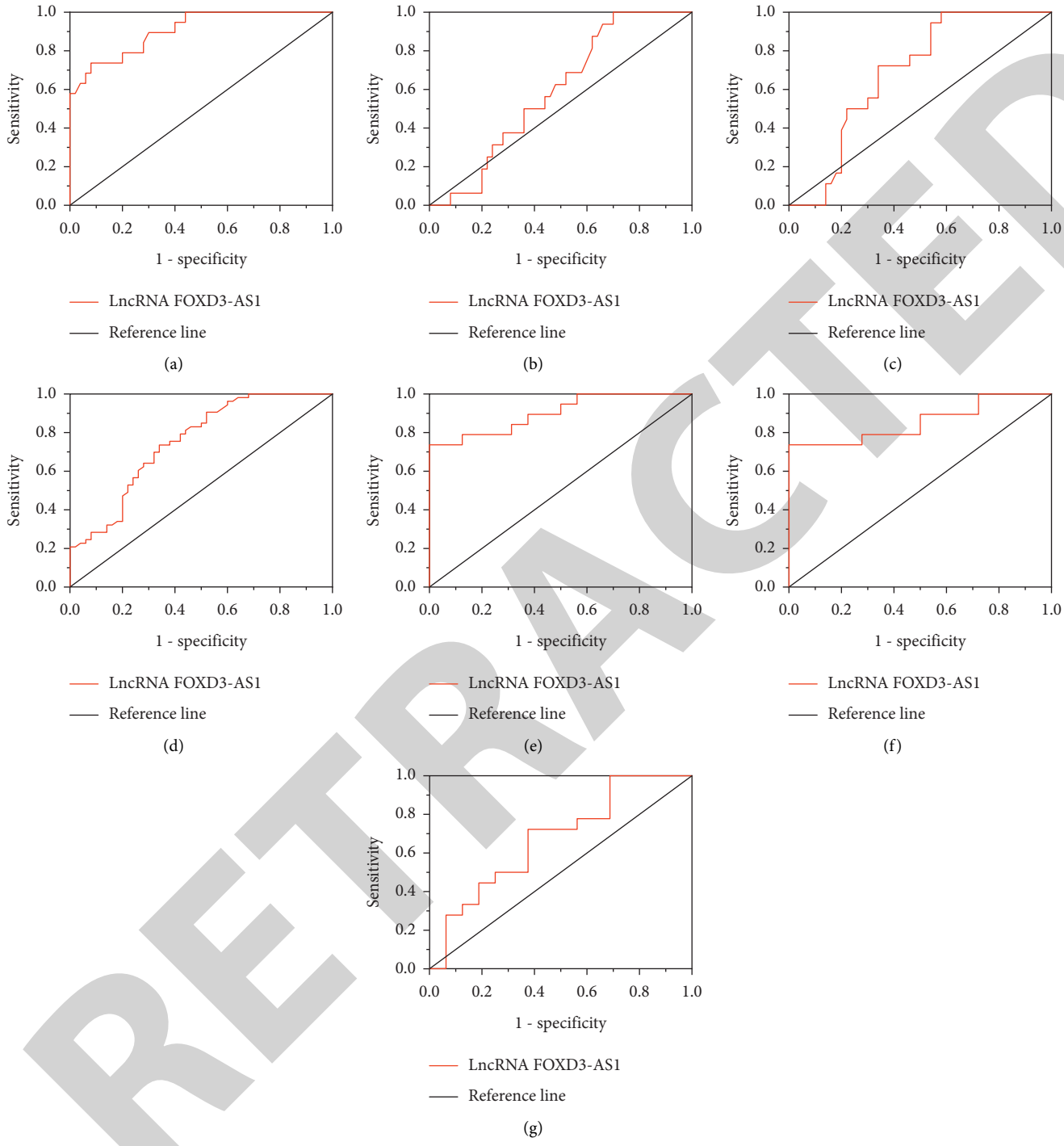

Figure 5: The efficiency of plasma FOXD3-AS1 in LC diagnosis and SCLC identification at early stage. (a)–(g) ROC curves used to validate the discrimination efficiency of plasma FOXD3-AS1 for early-stage SCLC vs. HS (a), early-stage LUAD vs. HS (b), early-stage LUSC vs. HS (c), early-stage LC vs. HS (d), early-stage SCLC vs. early-stage LUAD (e), early-stage SCLC vs. early-stage LUSC (f), and early-stage LUAD vs. early-stage LUSC (g).

breast cancer, cervical cancer, nasopharyngeal carcinoma, cerebral ischemia/reperfusion injury, cardiomyocyte injury, allergic rhinitis, and so on [15–17, 27, 28]. Furthermore, FOXD3-AS1 has been found in nuclear or cytoplasm fractions, and its molecular mechanisms include acting as competing endogenous RNA [15, 29], acting as mediators for gene promotor loci and histone modification factor interaction [19], stimulating proteins expression [20], interacting and sequestering proteins, and so on [14, 18]. In this study, we found that FOXD3-AS1 was upregulated in all primary subtypes of LC at an early stage and increased as the disease progressed. Furthermore, consistent trends in FOXD3-AS1 expression in tissues with disease progression suggest that plasma is partly derived from tumor tissues.

Table 4: The diagnostic values of lncRNA FOXD3-AS1 in discriminating early-stage lung cancer.

Index	AUC	95% CI		*P* value	Sensitivity	Specificity	Critical value	Yoden index
		Down	Up					
SCLC vs. HS	0.906	0.831	0.982	<0.001	73.700	92.000	0.657	3.940
LUAD vs. HS	0.591	0.453	0.729	0.275	100.000	30.000	0.300	2.460
LUSC vs. HS	0.686	0.562	0.809	0.020	100.000	42.000	0.420	2.750
LC vs. HS	0.751	0.658	0.845	<0.001	73.600	66.000	0.396	3.195
SCLC vs. LUAD	0.901	0.802	1.000	<0.001	73.700	100.000	0.737	3.980
SCLC vs. LUSC	0.857	0.730	0.983	<0.001	73.700	100.000	0.737	3.905
LUAD vs. LUSC	0.674	0.489	0.858	0.084	72.200	62.500	0.347	3.240

Therefore, we have reason to believe that FOXD3-AS1 is a potential marker for the diagnosis of LC. On the contrary, Ji et al. discovered that FOXD3-AS1 expression was downregulated in NSCLC tissues and cell lines, linked to lymph node metastasis and a high tumor grade [29]. FOXD3-AS1 may thus play a variety of roles and be involved in multiple stages of LC development. Furthermore, the more aggressive expression of FOXD3-AS1 in SCLC over that in NSCLC (LUAD and LUSC) at early or all stages may be due to the fact that SCLC has a different pathological mechanism from NSCLC, such as a strong predilection for early metastasis [30].

In our study, analysis displayed that FOXD3-AS1was significantly associated with tumor stage, lymph node metastasis, and distant metastasis. It is further suggested that FOXD3-AS1 may be helpful to distinguish LC subtypes. Interestingly, our results that not only did FOXD3-AS1 accurately distinguish LC patients from healthy subjects with the highest AUC but also distinguished LC subtypes very well, providing an objective basis for distinguishing among LC subtypes. Previous studies have shown that increased lncRNA levels can be used as a potential biomarker for LC detection, particularly at the early stage. For example, Li et al. reported that lncRNA GAS5 in exosomes may function as an ideal noninvasive marker for identifying patients with early NSCLC [31]. In this study, the results of ROC analysis demonstrated that FOXD3-AS1 had an advantage in the diagnostic efficiency of detecting early-stage SCLC patients. FOXD3-AS1 as a predictive biomarker in the clinical application might significantly enhance the efficacy of SCLC screening.

Although the current study has improved our understanding of the relationship between FOXD3-AS1 and LC, it has some limitations. First, longitudinal cohort studies with large populations are required to determine the true value of FOXD3-AS1 in LC early diagnosis and subtype identification. Second, a logistic model based on multiple genes may be more efficient because LC is heterogeneous. Furthermore, evaluating a combination of biomarkers may offer more predictive value than assessing FOXD3-AS1 alone.

5. Conclusions

The overexpression of FOXD3-AS1 in LC tissues and plasmas was discovered in our study. Plasma FOXD3-AS1 has the potential to be a molecular biomarker for early diagnosis and identification SCLC subtype. Our study points to a new direction for early diagnosis of patients with LC, which may play an important role in diagnosing and treating patients with LC and prolonging their survival.

Data Availability

The gene expression matrix and clinical data for LUAC projects and LUSC projects were downloaded from TCGA (https://www.cancer.gov/about-nci/organization/ccg/research/structural-genomics/tcga) and SCLC data were downloaded from GEO under accession GSE60052 (https://www.ncbi.nlm.nih.gov/geo/).

Conflicts of Interest

The authors declare that they have no conflicts of interest.

Authors' Contributions

XFL conceptualized and designed the study and critically revised the manuscript. Data collection and analysis were performed by XFL and WYC. The first draft of the manuscript was written by XFL and YQ. WYC, YQ, and YQZ were responsible for data visualization and literature search. All authors read and approved the final manuscript.

Supplementary Materials

Table S1: Basic characteristics of the DELs in LUAD. Table S2: Basic characteristics of the DELs in LUSC. Table S3: Basic characteristics of the DELs in SCLC. Table S4: The significantly upregulated lncRNAs. Table S5: The significantly downregulated lncRNAs. (*Supplementary Materials*)

References

[1] S. Gao, N. Li, S. Wang et al., "Lung cancer in people's Republic of China," *Journal of Thoracic Oncology*, vol. 15, no. 10, pp. 1567–1576, 2020.

[2] S. He, H. Li, M. Cao et al., "Trends and risk factors of lung cancer in China," *Chinese Journal of Cancer Research*, vol. 32, no. 6, pp. 683–694, 2020.

[3] N. Duma, R. Santana-Davila, and J. R. Molina, "Non-small cell lung cancer: epidemiology, screening, diagnosis, and treatment," *Mayo Clinic Proceedings*, vol. 94, no. 8, pp. 1623–1640, 2019.

[4] Y. Guo, R. Cao, X. Zhang et al., "Recent progress in rare oncogenic drivers and targeted therapy for non-small cell lung

Hindawi
Evidence-Based Complementary and Alternative Medicine
Volume 2022, Article ID 5765233, 14 pages
https://doi.org/10.1155/2022/5765233

Research Article

Investigation of Anti-Liver Cancer Activity of the Herbal Drug FDY003 Using Network Pharmacology

Ho-Sung Lee,[1,2] **In-Hee Lee**,[1,2] **Sang-In Park**,[3] **Minho Jung**,[4] **Seung Gu Yang**,[5] **Tae-Wook Kwon**,[2] **and Dae-Yeon Lee**[1,2]

[1]*The Fore Research Institute, 33 Saemunan-ro 5ga-gil, Jongno-gu, Seoul 03170, Republic of Korea*
[2]*Forest Hospital, 33 Saemunan-ro 5ga-gil, Jongno-gu, Seoul 03170, Republic of Korea*
[3]*Forestheal Hospital, 173 Ogeum-ro, Songpa-gu, Seoul 05641, Republic of Korea*
[4]*Forest Hospital, 129 Ogeum-ro, Songpa-gu, Seoul 05549, Republic of Korea*
[5]*Forest Hospital, 67 Dolma-ro, Bundang-gu, Seongnam 13586, Republic of Korea*

Correspondence should be addressed to Ho-Sung Lee; forehslee@gmail.com and Dae-Yeon Lee; foresthrnd@gmail.com

Received 11 April 2022; Accepted 10 August 2022; Published 9 September 2022

Academic Editor: Bashar Saad

Globally, liver cancer (LC) is the sixth-most frequently occurring and the second-most fatal malignancy, responsible for 0.83 million deaths annually. Although the application of herbal drugs in cancer therapies has increased, their anti-LC activity and relevant mechanisms have not been fully studied from a systems perspective. To address these issues, we conducted a system-perspective network pharmacological investigation into the activity and mechanisms underlying the action of the herbal drug. FDY003 reduced the viability of human LC treatment. FDY003 reduced the viability of human LC cells and elevated their chemosensitivity. There were a total of 16 potential bioactive chemical components in FDY003 and they had 91 corresponding targets responsible for the pathological processes in LC. These FDY003 targets were functionally involved in regulating the survival, proliferation, apoptosis, and cell cycle of LC cells. Additionally, we found that FDY003 may target key signaling cascades connected to diverse LC pathological mechanisms, namely, PI3K-Akt, focal adhesion, IL-17, FoxO, MAPK, and TNF pathways. Overall, this study contributed to integrative mechanistic insights into the anti-LC potential of FDY003.

1. Introduction

Liver cancer (LC) is the sixth-most frequently occurring and the second-most fatal malignancy, responsible for 0.83 million deaths annually [1]. Molecular-targeted and immune checkpoint therapies serve as the main treatment strategies for LC in clinical settings [2]. However, such treatment options and their efficacy are largely restricted to a few patients, which emphasizes the need to design and develop effective therapeutics for LC treatment [2]. There is growing recognition of herbal drugs as potent therapeutics for LC treatment to augment treatment efficacy while minimizing the adverse effects of anticancer strategies [3–7]. Herbal drugs possess beneficial properties, increasing survival and tumor response rates, enhancing the treatment efficacies and immune functions, increasing the quality of life, and inhibiting the development of side effects caused by anti-cancer treatments in patients with LC [3–7].

FDY003 is an herbal drug composed of *Cordyceps militaris* (Cm), *Artemisia capillaris* Thunberg (AcT), and *Lonicera japonica* Thunberg (LjT). It has antiproliferative and proapoptotic activities in cancer cells [8–11]. These anticancer activities arise primarily from the functional regulation of many oncogenes, tumor suppressors, and their cancer-associated signaling cascades [8–11]. However, the anticancer activity of FDY003 against LC and its mechanistic characteristics from an integrated systems view remain unclear.

Network pharmacology is a field that is efficient for dissecting synergistic mechanistic characteristics of herbal drugs based on their related pharmacological and biomedical data [12–19]. This strategy merges the herbal drug-

associated comprehensive information into networks that represent the interaction between herbal medicines, bioactive components, and therapeutically targeted genes and proteins [12–19]. Network pharmacology seeks the synergistic mechanisms of herbal drugs by assessing the functional, structural, and topological nature of their associated networks [12–19]. Based on the network pharmacology, we assessed the therapeutic role of FDY003 in LC and evaluated the underlying systematic mechanisms.

2. Materials and Methods

2.1. Cell Culture. The HepG2 human LC cell line was obtained from the Korean Cell Line Bank (Seoul, Korea) and cultured in Dulbecco's modified Eagle medium (WELGENE Inc., Gyeongsang, Korea) supplemented with antibiotics (penicillin-streptomycin) (Thermo Fisher Scientific, Inc., Waltham, MA, USA) and 10% fetal bovine serum (FBS) (WELGENE Inc.). The cells were grown in a humidified incubator at 37°C with 5% CO_2.

2.2. Herbal Drug Preparation. For the preparation of FDY003, dried raw AcT (150.0 g), LjT (150.0 g), and Cm (100.0 g) were obtained from Hanpure Pharmaceuticals (Pocheon, Korea), mixed, and ground. The herbal mixture was dispersed in 70% ethanol (500 mL) and subjected to a 3 h reflux extraction process at −80°C. After purifying the herbal extracts with 80% and 90% ethanol solutions successively, they were lyophilized at −80°C and the resulting 50.4 g of freeze-dried extracts were stored at −20°C. We used distilled water to dissolve the prepared FDY003 samples before further experiments.

2.3. Analysis of Cell Viability upon Drug Treatment. The viability of the drug-treated cells was analyzed by water-soluble tetrazolium salt (WST-1) experiments. Cells (1.0×10^4) were seeded and cultured in 96-well plates and treated with FDY003, sorafenib (Sigma-Aldrich, St. Louis, MO, USA), or both for 72 h. Next, cells were incubated for 2 h with WST-1 solution (Daeil Lab Service Co. Ltd., Seoul, Korea) at 37°C and 5% CO_2. The cell viability was assessed by measuring the absorbance (450 nm) of the samples on an xMark microplate absorbance spectrophotometer (Bio-Rad, Hercules, CA, USA).

2.4. Screening for Bioactive Chemical Components. First, we investigated comprehensive herbal medicine-related databases (e.g., a bioinformatics analysis tool for the molecular mechanism of traditional Chinese medicine [20], an anticancer herbs database of systems pharmacology [21], and the traditional Chinese medicine systems pharmacology [22]) and acquired large-scale data for the chemical composition of FDY003. For these components, we used pharmacokinetic parameters, namely drug-likeness, Caco-2 permeability, and oral bioavailability, for the screening of the bioactive chemical components, as previously described [14, 22, 23]. Drug-likeness determines whether a given chemical component can adequately serve as a drug based on its molecular structure and physicochemical properties [22, 24]. A chemical component with a drug-likeness equal to or greater than 0.18 (the mean drug-likeness based on the currently available drugs) is considered to have adequate drug-like functions [22, 24]. The Caco-2 permeability determines whether a given chemical component has adequate intestinal absorption and permeability [22, 25–27]; a chemical component with Caco-2 permeability equal to or greater than −0.4 is considered to have adequate intestinal permeability and absorption activity [28, 29]. Oral bioavailability determines whether an orally administered chemical component has an adequate delivery rate to reach the target sites of drug action [22, 30]. A chemical component with an oral bioavailability equal to or more than 30% is considered to have adequate absorption in the human body [22, 30]. Thus, chemical components with drug-likeness ≥ 0.18, Caco-2 permeability ≥ -0.4, and oral bioavailability $\geq 30\%$ [14, 22, 23] were considered bioactive.

2.5. Target Screening. To screen the targets of the identified bioactive chemical components of FDY003, we investigated their simplified molecular input line entry system notation using PubChem [28] and imported the information into the diverse tools and databases used to evaluate the molecular interactions between the chemical components and genes and proteins as follows: PharmMapper [29], Similarity Ensemble Approach [31], SwissTargetPrediction [32], and Search Tool for Interactions of Chemicals 5 [33]. Among the FDY003 targets, the genes and proteins significantly associated with the LC pathological mechanisms were examined using "liver cancer" and "hepatocellular carcinoma" as query keywords in the following tools and databases: Pharmacogenomics Knowledgebase [34], Online Mendelian Inheritance in Man [35], Human Genome Epidemiology Navigator [36], DisGeNET [37], Comparative Toxicogenomics Database [38], Therapeutic Target Database [39], GeneCards [40], and DrugBank [41].

2.6. Generation and Analysis of Herbal Drug-Associated Networks. Herbal drug-associated networks consist of nodes (which refer to the herbal components, chemical components, targeted genes and proteins, and pathways) and edges (which refer to the interactions among the network nodes) [42]. The node degree represents the number of edges for a given node [42]. The herbal component–chemical component–target (H-C-T) network uses herbal components, chemical components, and targeted genes and proteins of FDY003 as nodes and their molecular interactions and associations as the edges. The H-C-T-Pathway (H-C-T-P) network was created by linking the targets of the H-C-T network to their correspondingly enriched LC-related signaling cascades. The protein-protein interaction (PPI) network used FDY003 targets as nodes and their interaction information (interactions with high confidence obtained from STRING [43]) as edges. Network generation and analysis were performed using the Cytoscape tool [44].

2.7. Analysis of Correlation between the Survival of Patients with LC and the Expression Profiles of FDY003 Targets. The correlations between the survival of patients with LC and the expression profiles of LC-associated targets of FDY003 were analyzed using the Kaplan–Meier Plotter [45], a commonly used database for the survival analysis with large-scale gene expression profiles and survival information of patients with various cancer types obtained from The Cancer Genome Atlas (TCGA) [46], the Gene Expression Omnibus (GEO) [47], and the European Genome-phenome Archive (EGA) [48]. The survival analysis was performed using an auto-selected best cut-off and the results with $p < 0.05$ (log-rank test) were regarded to be statistically significant. The clinical information of the included patients for the survival analysis is provided in Supplementary Table S1.

2.8. Exploration of Functional Enrichment of FDY003 Targets. The Gene Ontology (GO) and pathway enrichment of FDY003 targets were analyzed using the Database for Annotation, Visualization, and Integrated Discovery (DAVID) [49] and the Kyoto Encyclopedia of Genes and Genomes (KEGG) [50], respectively, and the results having $p < 0.05$ were regarded to be statistically significant.

2.9. Investigation of Binding Affinities between the Chemical Components and Targets of FDY003. To assess the binding affinities between the chemical components and corresponding targets of FDY003, we calculated the binding energies. First, we imported the molecular structures of the bioactive components of FDY003 (obtained from the RCSB Protein Data Bank [51]) and their targets (obtained from PubChem [28]) into AutoDock Vina [52] and calculated the resulting binding energies. As suggested earlier [53, 54], the binding affinities between the chemical components and targets were considered to be highly significant if their corresponding binding energies were ≤ -5.0.

3. Results

3.1. Inhibitory Role of FDY003 in LC. To assess the action of FDY003 against LC, HepG2 human LC cells were treated with FDY003 and/or sorafenib (a first-line therapeutic agent for LC treatment [2]), and the effects of the treatment on the cells were monitored. FDY003 significantly reduced the viability of HepG2 cells; the viability of the cells was further inhibited upon treatment with a combination of the herbal drug and sorafenib (Supplementary Figures S1A and S1B). These observations suggest that FDY003 exhibits inhibitory and chemosensitizing effects on the LC cells.

3.2. Identification of Bioactive Components and Targets of FDY003. As previously described, we selected FDY003 constituents with Caco-2 permeability ≥ -0.4, drug-likeness ≥ 0.18, and oral bioavailability $\geq 30\%$, and considered them as bioactive components (Supplementary Tables S2 and S3) [8, 14, 22, 23]. Several components having potent anticancer functions against LC were also included in the list of bioactive components, despite their failure to meet the inclusion criteria (Supplementary Tables S2 and S3). Using the databases for examining the molecular binding interactions between the chemical components and genes and proteins, a total of 379 targets were investigated. Among them, 91 were determined to be associated significantly with the LC pathological mechanisms based on previous cancer biology and oncological studies (Figure 1, and Supplementary Tables S4 and S5).

3.3. Network Analysis of Poly-Pharmacological Mechanisms Underlying FDY003 Effects in LC Treatment. For the network pharmacology analysis, first, we united the FDY003-associated data and knowledge into an H-C-T network (Figure 2, and Supplementary Table S4 and S5). Among the targets in this network, 20.1% (19 of 91 targets), 23.1% (21 of 91 targets), and 74.7% (68 of 91 targets) were linked to the chemical components kaempferol, luteolin, and quercetin, respectively (Figure 2 and Supplementary Table S4), which demonstrated their key roles in exerting anti-LC effects of FDY003. Moreover, 70.3% (64 of 91 targets) were linked to two or more chemical components (Figure 2), which indicated the synergistic poly-pharmacological nature of the herbal drug.

Analytical investigation of complex interactions among the therapeutic targets of a given drug is pivotal for understanding the underlying treatment mechanisms [55–59]. Thus, we constructed a PPI network consisting of large-scale interactions among the FDY003 targets to further dissect their pharmacological features (Figure 3). For analyzing the network topology of the PPI network, we identified the network hubs having a relatively large number of interacting partners as compared to the nonhubs; they had a high probability of being effective drug targets [60, 61]. As described previously, nodes with number of edges $\geq 2 \times$ the average node degree were considered hubs [62, 63]. As a result, the identified hubs were AKT1, AR, EGFR, ESR1, JUN, PIK3R1, SRC, TP53, and VEGFA (Figure 3), which suggests that they were the primary nodes mediating the therapeutic roles of FDY003 in LC. Additionally, the expression status of these hubs could estimate the survival rate of patients with LC (Figure 4), which suggests their prognostic roles.

To understand the mechanisms of action of FDY003 in LC treatment, we evaluated the GO terms and pathways that were functionally enriched for the targets. The results showed that the FDY003 targets were functionally involved in the control of survival and proliferative behaviors, apoptosis, and cell cycle of LC cells (Supplementary Figure S2), which suggests the potential FDY003 mechanisms in the LC treatment. Additionally, FDY003 could target key signaling cascades connected to diverse LC pathological mechanisms (Figure 5 and Supplementary Figure S2) as analyzed by the KEGG pathway enrichment investigation, which demonstrated that these pathways were important mediators of the FDY003 drug activity against LC.

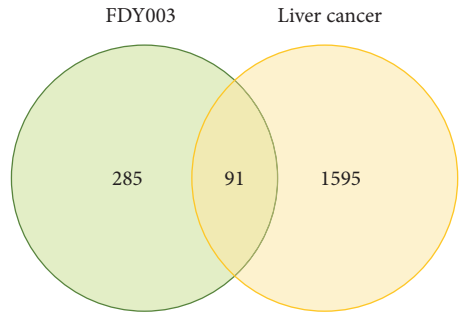

Figure 1: A Venn diagram of targets of FDY003 (green circle) and LC-associated genes (yellow circle).

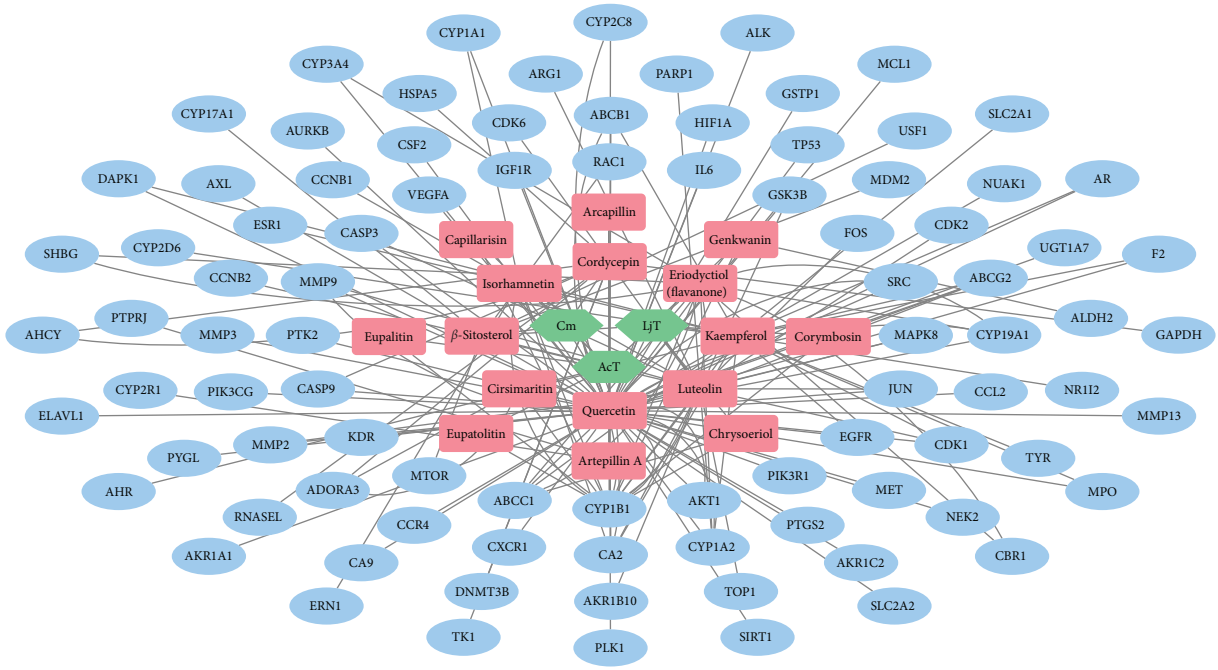

Figure 2: The herbal component–bioactive chemical component-target network for FDY003. Green nodes, herbal components; red nodes, bioactive chemical components; blue nodes, liver cancer-associated targets.

3.4. Assessing the Binding Affinities of Chemical Components of FDY003 and Their Targets. We performed a molecular docking study to assess the binding affinities and active binding sites between the chemical components of FDY003 and their targets. The resulting binding energies of the chemical component-target pairs were less than −5.0 kcal/mol (Figure 6 and Supplementary Figure S3 and Supplementary Table S6), which indicated their high pharmacological binding potentials.

4. Discussion

Globally, LC is the sixth-most frequently occurring and the second-most fatal malignancy, responsible for 0.83 million deaths annually [1]. Although the application of herbal drugs in cancer therapies has increased, their anti-LC activity and relevant mechanisms have not been fully studied from a systems view [3–7]. To address these issues, we conducted a system-perspective network pharmacological investigation into the activity and mechanisms of action of the herbal drug, FDY003, for LC treatment. Treatment with FDY003 significantly reduced the viability of human LC cells and elevated their chemosensitivity. A total of 16 potential bioactive chemical components of FDY003 and corresponding 91 targets were identified for the pathological process of LC. The FDY003 targets were functionally involved in the regulating survival, proliferation, apoptosis, and cell cycle of LC cells. Additionally, we found that FDY003 may target key signaling cascades connected to the diverse LC pathological mechanisms, namely, phosphoinositide 3-kinase (PI3K)-Akt, focal adhesion, interleukin (IL)-17, forkhead box O (FoxO), mitogen-activated protein kinase (MAPK), and tumor necrosis factor (TNF) pathways. Overall, this study added to the integrative mechanistic insights into the anti-LC potential of FDY003.

The hub targets identified from the analysis of the FDY003-associated PPI network modulate crucial LC pathological mechanisms, and this targeting may result in effective therapeutic effects against LC. *AKT1* is an important regulator of the tumorigenic processes, migration,

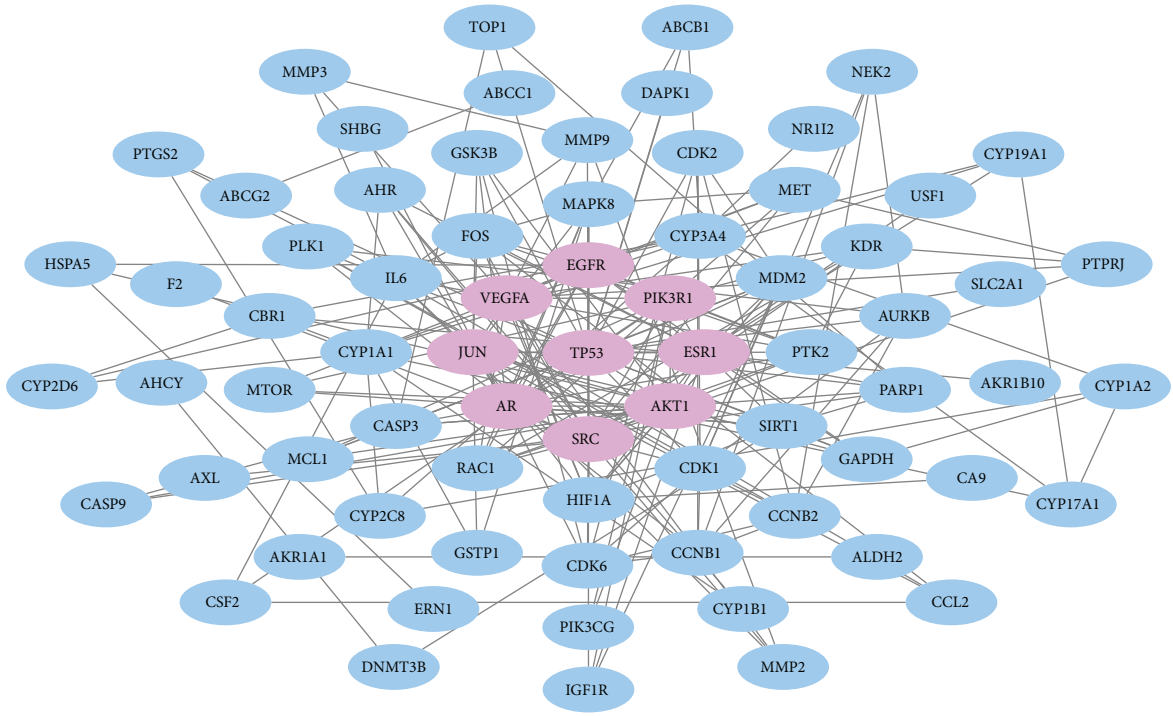

Figure 3: The protein-protein interaction network for liver cancer-associated targets of FDY003. Purple nodes, hubs.

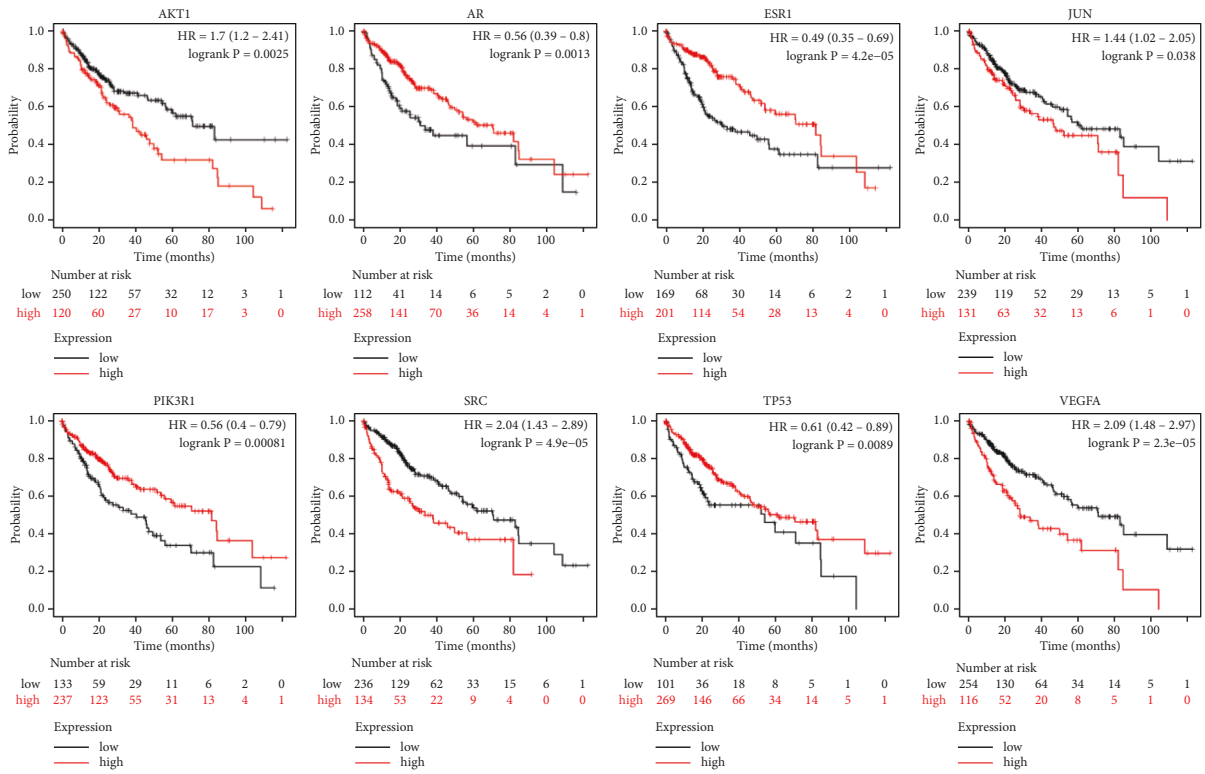

Figure 4: Analysis of the survival probability of patients for corresponding liver cancer-associated targets of FDY003. The Kaplan–Meier curves for the survival of liver cancer patients are associated with the expression levels of the indicated targets.

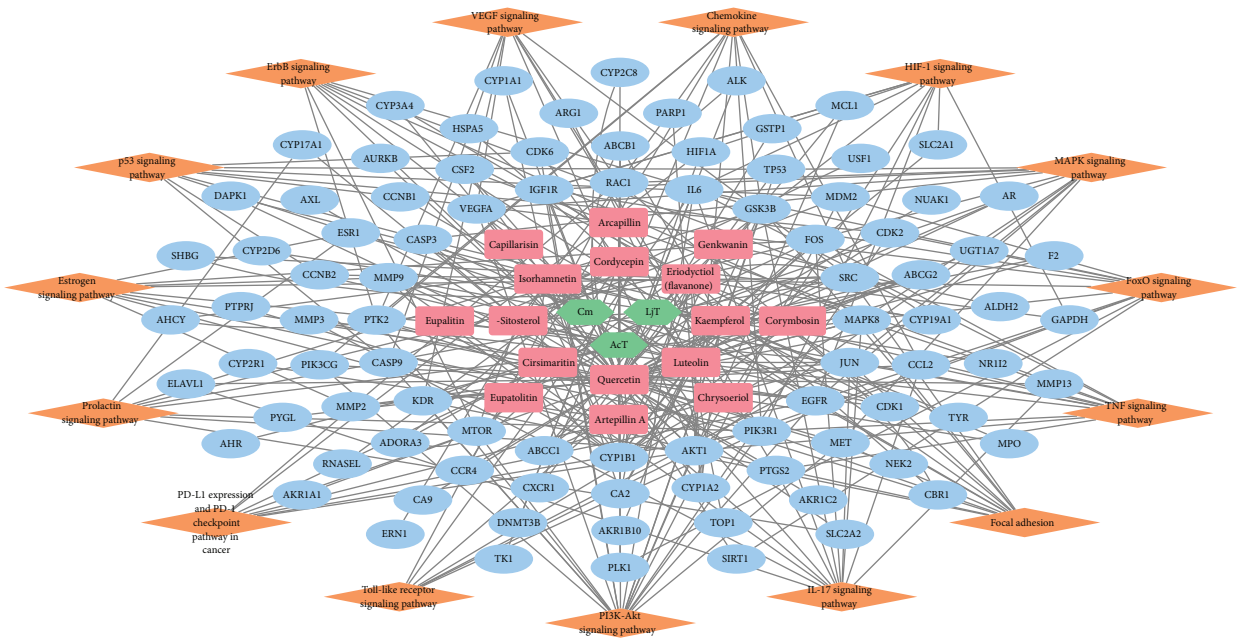

FIGURE 5: The herbal component–bioactive chemical component-target-pathway network for FDY003. Green nodes, herbal components; red nodes, bioactive chemical components; blue nodes, liver cancer-associated targets; orange nodes, liver cancer-associated pathways.

spreading, therapeutic sensitivity, resistance, survival, and proliferation of LC cells, and is a promising theragnostic target [64–67]. *AR* expression and activity influence angiogenesis, stemness, invasion, angiogenesis, epithelial-mesenchymal transition (EMT), migration, and oncogenesis of LC cells, and it is a prognostic determinant and responsive marker for anticancer therapies [68–73]. *EGFR* is responsible for the modulation of proliferation, metastasis, migration, self-renewal potential, EMT, angiogenesis, anchorage-independent growth, invasion, and drug sensitivity of LC cells and tumors, and its expression and activity are implicated in the initiation, recurrence, progression, metastasis, and aggressiveness of LC in patients [74–83]. *ESR1* is involved in the coordination of migration, angiogenesis, cancer stem-like properties, mobility, proliferation, and invasion of LC cells, and its genetic and expression status correlate with cancer susceptibility, tumor growth, metastasis, and prognosis of LC [84–89]. *JUN* is an oncogenic transcription factor that promotes tumor formation, chemoresistance, invasion, proliferation, migration, and metastasis, and serves as a marker for evaluating chemotherapeutic responses [90–92]. *PIK3R1* is highly expressed and activated in LC cells and tumors, and it stimulates their migration, proliferation, invasion, and survival [93, 94]. Its elevated expression level is associated with poor prognostic outcomes [93, 94]. *Src* is highly expressed in LC cells and tumors, and its targeting can repress anoikis resistance, metastasis, treatment resistance, growth, stemness, invasion, tumorigenesis, migration, and mobility [95–101]. The expression and mutations of *TP53* serve as biomarkers of prognosis, therapeutic response, aggressiveness, progression, and survival in LC [102–107]. *VEGFA* contributes to the malignant processes in LC by inducing angiogenesis, growth, invasion, prosurvival, metastasis, lymphangiogenesis, and migration of LC cells and tumors, and its expression and polymorphisms are related to the therapeutic responsiveness, prognosis, and cancer susceptibility of patients with LC [108–113].

FDY003 may pharmacologically intervene in various signaling cascades that are key factors in the LC pathophysiology as well as potent treatment targets. The chemokine pathway impacts the pathological processes of LC in various aspects, including inflammation, immune response, angiogenesis, metastasis, invasion, carcinogenesis, migration, EMT, tumorigenic potential, tumor microenvironment remodeling, and proliferation of LC cells and tumors [114–117]. Its activity is further associated with decreased survival and poor prognosis in patients with LC [114–117]. The abnormally controlled function of the erythroblastic leukemia viral oncogene homolog (ErbB), focal adhesion, hypoxia-inducible factor (HIF)-1, MAPK, p53, PI3K-Akt, and vascular endothelial growth factor (VEGF) pathways may contribute to the malignant tumorigenic and progressive processes in LC by inducing uncontrolled survival and proliferation, angiogenesis, EMT, invasion, migration, and metastasis of LC cells and tumors [118–121]. Thus, they can function as key therapeutic targets [118–121]. The estrogen pathway exerts a protective role against LC by inhibiting cancerous inflammation [122, 123]. The FoxO pathway is a tumor-suppressing cascade whose activation induces antiproliferation and apoptosis of LC cells and confers the pharmacological effects of anticancer therapeutics [124–127]. The inflammatory IL-17, TNF, and toll-like receptor pathways are responsible for the modulation of not only the protumorigenic inflammation but also the proliferation, invasion, metastasis, migration, immune microenvironment, and treatment sensitivity of LC cells and tumors [128–134]. Their activities correlate with poor prognostic outcomes in patients with LC [128–134]. The programmed death-ligand 1 (PD-1)/

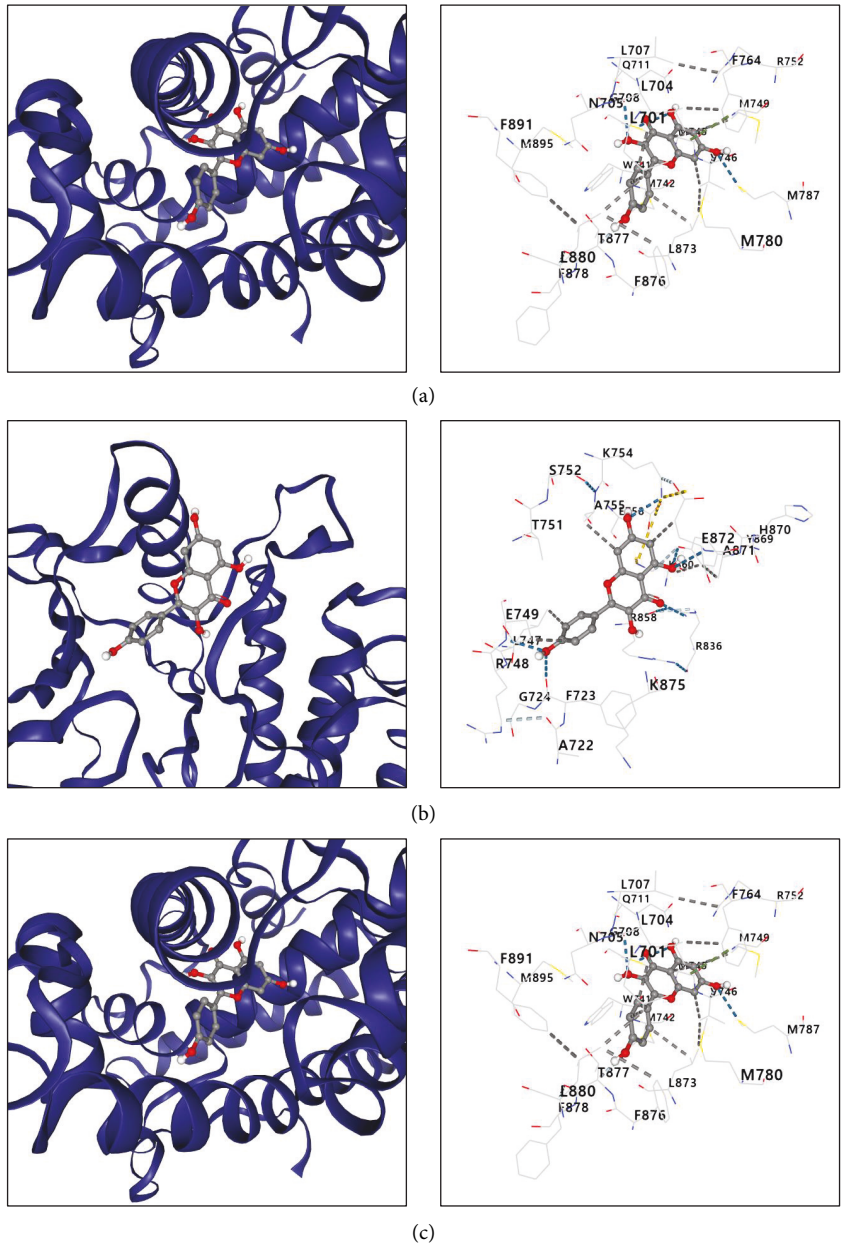

Figure 6: Analysis of binding affinities between the bioactive chemical components of FDY003 and their targets. (a) Kaempferol–AR (binding energy = −8.0 kcal/mol). (b) Kaempferol–EGFR (binding energy = −8.1 kcal/mol). (c) Kaempferol–ESR1 (binding energy = −8.6 kcal/mol).

programmed cell death-ligand 1 (PD-L1) pathway drives the immune escape of LC cells and tumors and is the major target of immune checkpoint therapies [135, 136]. The activity of the prolactin pathway is enhanced in LC tissues and is a marker for disease stage, survival, and progression of LC [137–140].

The herbal and bioactive components of FDY003 are known to function as anti-LC pharmacological agents. AcT represses survival, invasion, growth, angiogenesis, and migration of LC cells by blocking the PI3K/Akt and IL-6/signal transducer and activator of transcription (STAT) 3 pathways [141–144]. Cm exerts antisurvival, antigrowth, and anti-angiogenic effects in LC cells [145, 146]. Cordycepin targets integrin, focal adhesion kinase (FAK), c-Jun N-terminal kinases (JNK), PI3K/Akt/mammalian target of rapamycin (mTOR), nuclear factor erythroid-2-related factor 2 (Nrf2)/heme oxygenase 1 (HO-1)/nuclear factor kappa-light-chain-enhancer of activated B cells (NF-κB), IL-6, IL-1β, TNF-α, extracellular-signal-regulated kinase (ERK), Fas, B-cell lymphoma-2 (Bcl-2), caspase, and C-X-C motif chemokine receptor (CXCR) 4 cascades, thereby leading to the repression of angiogenesis, metastasis, EMT, proliferation, viability, and invasion of LC cells [147–153]. Eriodyctiol induces cell cycle arrest and apoptosis of LC cells by targeting the poly ADP-ribose polymerase (PARP), Bcl-2, and BCL2-associated X (Bax) signaling [154]. Isorhamnetin and β-sitosterol suppress the survival, viability, and proliferation

of LC cells [155, 156]. Kaempferol enhances the efficacy of anticancer agents whilst reducing the proliferative, migratory, and invasive behaviors of LC cells by modulating PI3K/mTOR/matrix metalloproteinase (MMP), endoplasmic reticulum (ER) stress/CCAAT/enhancer binding protein (CHOP)/autophagy, 5′ adenosine monophosphate-activated protein kinase (AMPK), reactive oxygen species (ROS), and caspase pathways [157–161]. Luteolin induces autophagy, cell cycle arrest, growth suppression, chemosensitization, proapoptosis, anti-invasion, antimigration, antiadhesion, and antiangiogenesis effects on LC cells [162–170]. These pharmacological effects are conferred through cyclin, p53, JNK, death receptor, Akt/osteopontin, PARP, caspase, myeloid cell leukemia 1 (Mcl-1), X-linked inhibitor of apoptosis protein (XIAP), Beclin-1, Bcl-2, Bax, BH3 interacting domain death agonist (Bid), and the ER stress signaling pathways [162–170]. Quercetin represses chemoresistance, survival, growth, migration, and proliferation of LC cells by perturbing the activities of p53, B-cell lymphoma-extra-large (Bcl-xL), Janus kinase (JAK)/STAT, β-catenin, casein kinase (CK) 2α, Notch1, hedgehog, cyclin, PI3K/Akt, protein kinase C (PKC), cyclooxygenase-2 (COX-2), Bax, specificity protein 1 (SP1), and mitogen-activated protein kinase (MEK)/ERK pathways [171–180].

5. Conclusions

In conclusion, we performed a system-perspective network pharmacological investigation into the activity and mechanisms underlying the effects of the herbal drug, FDY003, for LC treatment. FDY003 could reduce the viability of human LC cells and elevate their chemosensitivity. A total of 16 potential bioactive chemical components of FDY003 that pharmacologically regulate diverse LC-related drug targets and signaling cascades were identified. Further studies should focus on enhancing the therapeutic potential of herbal drugs as efficacious clinical agents for anticancer treatment, including investigations into their mechanisms of action in the modulation of a variety of cancerous and protumorigenic phenotypes and therapeutic sensitivities.

Data Availability

All data generated or analyzed during this study are included in this published article and its supplementary materials file.

Conflicts of Interest

The authors declare that there are no conflicts of interest.

Acknowledgments

This work was supported by the National Research Foundation of Korea (NRF) grant funded by the Korea government (MSIT) (No. 2021R1F1A1049472).

Supplementary Materials

Supplementary Figure S1. Pharmacological role of FDY003 on the viability of human liver cancer cells. Supplementary Figure S2. Gene ontology and pathway enrichment analysis for the liver cancer-related targets of FDY003. Supplementary Figure S3. Analysis of binding affinities between the bioactive chemical components of FDY003 and their targets. Supplementary Table S1. Clinical information of the included patients for the survival analysis. Supplementary Table S2. List of chemical components of FDY003. Supplementary Table S3. List of bioactive chemical components of FDY003. Supplementary Table S4. List of targets for active phytochemical ingredients of FDY003. Supplementary Table S5. List of the genes and proteins associated with the pathological mechanisms of liver cancer. Supplementary Table S6. Binding energies between the bioactive chemical components of FDY003 and their targets. (*Supplementary Materials*)

References

[1] H. Sung, J. Ferlay, R. L. Siegel et al., "Global cancer statistics 2020: GLOBOCAN estimates of incidence and mortality worldwide for 36 cancers in 185 countries," *CA: A Cancer Journal for Clinicians*, vol. 71, no. 3, pp. 209–249, 2021.

[2] Z. Liu, Y. Lin, J. Zhang et al., "Molecular targeted and immune checkpoint therapy for advanced hepatocellular carcinoma," *Journal of Experimental & Clinical Cancer Research*, vol. 38, no. 1, p. 447, 2019.

[3] F. Chen, Z. Zhong, H. Y. Tan et al., "Uncovering the anticancer mechanisms of Chinese herbal medicine formulas: therapeutic alternatives for liver cancer," *Frontiers in Pharmacology*, vol. 11, p. 293, 2020.

[4] W. C. Cho and H. Y. Chen, "Transcatheter arterial chemoembolization combined with or without Chinese herbal therapy for hepatocellular carcinoma: meta-analysis," *Expert Opinion on Investigational Drugs*, vol. 18, no. 5, pp. 617–635, 2009.

[5] M. B. Meng, Q. L. Wen, Y. L. Cui, B. She, and R. M. Zhang, "Meta-analysis: traditional Chinese medicine for improving immune response in patients with unresectable hepatocellular carcinoma after transcatheter arterial chemoembolization," *Explore*, vol. 7, no. 1, pp. 37–43, 2011.

[6] X. Shu, M. McCulloch, H. Xiao, M. Broffman, and J. Gao, "Chinese herbal medicine and chemotherapy in the treatment of hepatocellular carcinoma: a meta-analysis of randomized controlled trials," *Integrative Cancer Therapies*, vol. 4, no. 3, pp. 219–229, 2005.

[7] Z. Yang, X. Liao, and Y. Lu, "Add-on therapy with traditional Chinese medicine improves outcomes and reduces adverse events in hepatocellular carcinoma: a meta-analysis of randomized controlled trials," *Evidence-Based Complementary and Alternative Medicine*, vol. 2017, Article ID 3428253, 11 pages, 2017.

[8] H. S. Lee, I. H. Lee, K. Kang et al., "A network pharmacology study on the molecular mechanisms of FDY003 for breast cancer treatment," *Evidence-Based Complementary and Alternative Medicine*, vol. 2021, Article ID 3919143, 18 pages, 2021.

[9] D. Y. Lee and I. H. Lee, "FDY003 inhibits colon cancer in a Colo205 xenograft mouse model by decreasing oxidative stress," *Pharmacognosy Magazine*, vol. 15, no. 65, pp. 675–681, 2019.

[10] H.-S. Lee, I.-H. Lee, K. Kang et al., "Systems pharmacology study of the anticervical cancer mechanisms of FDY003," *Natural Product Communications*, vol. 15, no. 12, 2020.

[11] H.-S. Lee, I.-H. Lee, K. Kang et al., "Network pharmacology-based dissection of the comprehensive molecular mechanisms of the herbal prescription FDY003 against estrogen receptor-positive breast cancer," *Natural Product Communications*, vol. 16, no. 9, Article ID 1934578X2110443, 2021.

[12] P. Poornima, J. D. Kumar, Q. Zhao, M. Blunder, and T. Efferth, "Network pharmacology of cancer: from understanding of complex interactomes to the design of multi-target specific therapeutics from nature," *Pharmacological Research*, vol. 111, pp. 290–302, 2016.

[13] W. Y. Lee, C. Y. Lee, Y. S. Kim, and C. E. Kim, "The methodological trends of traditional herbal medicine employing network pharmacology," *Biomolecules*, vol. 9, no. 362, p. 8, 2019.

[14] H. S. Lee, I. H. Lee, S. I. Park, and D. Y. Lee, "Network pharmacology-based investigation of the system-level molecular mechanisms of the hematopoietic activity of samultang, a traditional Korean herbal formula," *Evidence-Based Complementary and Alternative Medicine*, vol. 2020, Article ID 9048089, 17 pages, 2020.

[15] R. He, S. Ou, S. Chen, and S. Ding, "Network pharmacology-based study on the molecular biological mechanism of action for compound kushen injection in anti-cancer effect," *Medical Science Monitor*, vol. 26, Article ID e918520, 2020.

[16] J. L. Mi, C. Liu, M. Xu, and R. S. Wang, "Network pharmacology to uncover the molecular mechanisms of action of LeiGongTeng for the treatment of nasopharyngeal carcinoma," *Medical Science Monitor Basic Research*, vol. 26, Article ID e923431, 2020.

[17] Y. Wang, B. Dong, W. Xue et al., "Anticancer effect of radix astragali on cholangiocarcinoma in vitro and its mechanism via network pharmacology," *Medical Science Monitor*, vol. 26, Article ID e921162, 2020.

[18] T. Xu, Q. Wang, and M. Liu, "A network pharmacology approach to explore the potential mechanisms of huangqin-baishao herb pair in treatment of cancer," *Medical Science Monitor*, vol. 26, Article ID e923199, 2020.

[19] S. Q. Zhang, H. B. Xu, S. J. Zhang, and X. Y. Li, "Identification of the active compounds and significant pathways of Artemisia annua in the treatment of non-small cell lung carcinoma based on network pharmacology," *Medical Science Monitor*, vol. 26, Article ID e923624, 2020.

[20] Z. Liu, F. Guo, Y. Wang et al., "BATMAN-TCM: a bioinformatics analysis tool for molecular mechanism of traditional Chinese medicine," *Scientific Reports*, vol. 6, no. 1, p. 21146, 2016.

[21] W. Tao, B. Li, S. Gao et al., "CancerHSP: anticancer herbs database of systems pharmacology," *Scientific Reports*, vol. 5, no. 1, p. 11481, 2015.

[22] J. Ru, P. Li, J. Wang et al., "TCMSP: a database of systems pharmacology for drug discovery from herbal medicines," *Journal of Cheminformatics*, vol. 6, no. 1, p. 13, 2014.

[23] S. J. Yue, L. T. Xin, Y. C. Fan et al., "Herb pair Danggui-Honghua: mechanisms underlying blood stasis syndrome by system pharmacology approach," *Scientific Reports*, vol. 7, no. 1, p. 40318, 2017.

[24] A. Y. Lee, W. Park, T. W. Kang, M. H. Cha, and J. M. Chun, "Network pharmacology-based prediction of active compounds and molecular targets in Yijin-Tang acting on hyperlipidaemia and atherosclerosis," *Journal of Ethnopharmacology*, vol. 221, pp. 151–159, 2018.

[25] Y. Kono, A. Iwasaki, K. Matsuoka, and T. Fujita, "Effect of mechanical agitation on cationic liposome transport across an unstirred water layer in caco-2 cells," *Biological & Pharmaceutical Bulletin*, vol. 39, no. 8, pp. 1293–1299, 2016.

[26] D. A. Volpe, "Variability in Caco-2 and MDCK cell-based intestinal permeability assays," *Journal of Pharmaceutical Sciences*, vol. 97, no. 2, pp. 712–725, 2008.

[27] M. N. Garcia, C. Flowers, and J. D. Cook, "The Caco-2 cell culture system can be used as a model to study food iron availability," *Journal of Nutrition*, vol. 126, no. 1, pp. 251–258, 1996.

[28] S. Kim, J. Chen, T. Cheng et al., "PubChem 2019 update: improved access to chemical data," *Nucleic Acids Research*, vol. 47, no. D1, pp. D1102–D1109, 2019.

[29] X. Wang, Y. Shen, S. Wang et al., "PharmMapper 2017 update: a web server for potential drug target identification with a comprehensive target pharmacophore database," *Nucleic Acids Research*, vol. 45, pp. W356–W360, 2017.

[30] C. K. Wang and D. J. Craik, "Cyclic peptide oral bioavailability: lessons from the past," *Biopolymers*, vol. 106, no. 6, pp. 901–909, 2016.

[31] M. J. Keiser, B. L. Roth, B. N. Armbruster, P. Ernsberger, J. J. Irwin, and B. K. Shoichet, "Relating protein pharmacology by ligand chemistry," *Nature Biotechnology*, vol. 25, no. 2, pp. 197–206, 2007.

[32] A. Daina, O. Michielin, and V. Zoete, "SwissTargetPrediction: updated data and new features for efficient prediction of protein targets of small molecules," *Nucleic Acids Research*, vol. 47, no. W1, pp. W357–W364, 2019.

[33] D. Szklarczyk, A. Santos, C. von Mering, L. J. Jensen, P. Bork, and M. Kuhn, "STITCH 5: augmenting protein-chemical interaction networks with tissue and affinity data," *Nucleic Acids Research*, vol. 44, no. D1, pp. D380–D384, 2016.

[34] M. Whirl-Carrillo, E. M. McDonagh, J. M. Hebert et al., "Pharmacogenomics knowledge for personalized medicine," *Clinical Pharmacology & Therapeutics*, vol. 92, no. 4, pp. 414–417, 2012.

[35] J. S. Amberger, C. A. Bocchini, F. Schiettecatte, A. F. Scott, and A. Hamosh, "OMIM.org: online mendelian inheritance in man (OMIM(R)), an online catalog of human genes and genetic disorders," *Nucleic Acids Research*, vol. 43, pp. D789–D798, 2015.

[36] W. Yu, M. Gwinn, M. Clyne, A. Yesupriya, and M. J. Khoury, "A navigator for human genome epidemiology," *Nature Genetics*, vol. 40, no. 2, pp. 124-125, 2008.

[37] J. Pinero, A. Bravo, N. Queralt-Rosinach et al., "DisGeNET: a comprehensive platform integrating information on human disease-associated genes and variants," *Nucleic Acids Research*, vol. 45, no. D1, pp. D833–D839, 2017.

[38] A. P. Davis, C. J. Grondin, R. J. Johnson et al., "The comparative toxicogenomics database: update 2019," *Nucleic Acids Research*, vol. 47, no. D1, pp. D948–D954, 2019.

[39] F. Zhu, B. Han, P. Kumar et al., "Update of TTD: therapeutic target database," *Nucleic Acids Research*, vol. 38, no. suppl_1, pp. D787–D791, 2010.

[40] M. Safran, I. Dalah, J. Alexander et al., "GeneCards version 3: the human gene integrator," *Database*, vol. 2010, p. baq020, 2010.

[41] D. S. Wishart, Y. D. Feunang, A. C. Guo et al., "DrugBank 5.0: a major update to the DrugBank database for 2018," *Nucleic Acids Research*, vol. 46, no. D1, pp. D1074–D1082, 2018.

[42] A. L. Barabasi and Z. N. Oltvai, "Network biology: understanding the cell's functional organization," *Nature Reviews Genetics*, vol. 5, no. 2, pp. 101–113, 2004.

[43] D. Szklarczyk, A. L. Gable, D. Lyon et al., "STRING v11: protein-protein association networks with increased coverage, supporting functional discovery in genome-wide experimental datasets," *Nucleic Acids Research*, vol. 47, no. D1, pp. D607–D613, 2019.

[44] P. Shannon, A. Markiel, O. Ozier et al., "Cytoscape: a software environment for integrated models of biomolecular interaction networks," *Genome Research*, vol. 13, no. 11, pp. 2498–2504, 2003.

[45] A. Nagy, A. Lanczky, O. Menyhart, and B. Gyorffy, "Validation of miRNA prognostic power in hepatocellular carcinoma using expression data of independent datasets," *Scientific Reports*, vol. 8, no. 1, p. 9227, 2018.

[46] J. N. Weinstein, E. A. Collisson, G. B. Mills et al., "The cancer genome Atlas pan-cancer analysis project," *Nature Genetics*, vol. 45, no. 10, pp. 1113–1120, 2013.

[47] T. Barrett, S. E. Wilhite, P. Ledoux et al., "NCBI GEO: archive for functional genomics data sets–update," *Nucleic Acids Research*, vol. 41, no. D1, pp. D991–D995, 2013.

[48] I. Lappalainen, J. Almeida-King, V. Kumanduri et al., "The European genome-phenome archive of human data consented for biomedical research," *Nature Genetics*, vol. 47, no. 7, pp. 692–695, 2015.

[49] D. W. Huang, B. T. Sherman, and R. A. Lempicki, "Systematic and integrative analysis of large gene lists using DAVID bioinformatics resources," *Nature Protocols*, vol. 4, no. 1, pp. 44–57, 2009.

[50] M. Kanehisa, M. Furumichi, M. Tanabe, Y. Sato, and K. Morishima, "KEGG: new perspectives on genomes, pathways, diseases and drugs," *Nucleic Acids Research*, vol. 45, no. D1, pp. D353–D361, 2017.

[51] S. K. Burley, H. M. Berman, C. Bhikadiya et al., "RCSB protein data bank: biological macromolecular structures enabling research and education in fundamental biology, biomedicine, biotechnology and energy," *Nucleic Acids Research*, vol. 47, no. D1, pp. D464–D474, 2019.

[52] O. Trott and A. J. Olson, "AutoDock vina: improving the speed and accuracy of docking with a new scoring function, efficient optimization, and multithreading," *Journal of Computational Chemistry*, vol. 31, no. 2, pp. 455–461, 2010.

[53] Z. Zhuang, J. Wen, L. Zhang et al., "Can network pharmacology identify the anti-virus and anti- inflammatory activities of Shuanghuanglian oral liquid used in Chinese medicine for respiratory tract infection?" *European Journal of Integrative Medicine*, vol. 37, Article ID 101139, 2020.

[54] M. Zhang, Y. Yuan, W. Zhou et al., "Network pharmacology analysis of Chaihu Lizhong Tang treating non-alcoholic fatty liver disease," *Computational Biology and Chemistry*, vol. 86, Article ID 107248, 2020.

[55] A. Athanasios, V. Charalampos, T. Vasileios, and G. M. Ashraf, "Protein-protein interaction (PPI) network: recent advances in drug discovery," *Current Drug Metabolism*, vol. 18, no. 1, pp. 5–10, 2017.

[56] L. H. Chu and B. S. Chen, "Construction of a cancer-perturbed protein-protein interaction network for discovery of apoptosis drug targets," *BMC Systems Biology*, vol. 2, no. 1, p. 56, 2008.

[57] J. Huang, C. Niu, C. D. Green, L. Yang, H. Mei, and J. D. J. Han, "Systematic prediction of pharmacodynamic drug-drug interactions through protein-protein-interaction network," *PLoS Computational Biology*, vol. 9, no. 3, Article ID e1002998, 2013.

[58] M. A. Yildirim, K. I. Goh, M. E. Cusick, A. L. Barabasi, and M. Vidal, "Drug-target network," *Nature Biotechnology*, vol. 25, no. 10, pp. 1119–1126, 2007.

[59] M. Zhu, L. Gao, X. Li et al., "The analysis of the drug-targets based on the topological properties in the human protein-protein interaction network," *Journal of Drug Targeting*, vol. 17, no. 7, pp. 524–532, 2009.

[60] D. Y. Cho, Y. A. Kim, and T. M. Przytycka, "Chapter 5: network biology approach to complex diseases," *PLoS Computational Biology*, vol. 8, no. 12, Article ID e1002820, 2012.

[61] H. Jeong, S. P. Mason, A. L. Barabasi, and Z. N. Oltvai, "Lethality and centrality in protein networks," *Nature*, vol. 411, no. 6833, pp. 41-42, 2001.

[62] J. Zhu, X. Yi, Y. Zhang, Z. Pan, L. Zhong, and P. Huang, "Systems pharmacology-based approach to comparatively study the independent and synergistic mechanisms of danhong injection and naoxintong capsule in ischemic stroke treatment," *Evidence-Based Complementary and Alternative Medicine*, vol. 2019, Article ID 1056708, 16 pages, 2019.

[63] J. Zhong, Z. Liu, X. Zhou, and J. Xu, "Synergic anti-pruritus mechanisms of action for the radix sophorae flavescentis and fructus cnidii herbal pair," *Molecules*, vol. 22, no. 1465, p. 9, 2017.

[64] X. Wu, Y. Niu, G. Tang, and C. Wu, "LncRNA NEAT1 modulates sorafenib resistance in hepatocellular carcinoma through regulating the miR-149-5p/AKT1 axis," *Saudi Journal of Gastroenterology*, vol. 26, no. 4, p. 194, 2020.

[65] H. Tian, C. Ge, H. Li et al., "Ribonucleotide reductase M2B inhibits cell migration and spreading by early growth response protein 1-mediated phosphatase and tension homolog/Akt1 pathway in hepatocellular carcinoma," *Hepatology*, vol. 59, no. 4, pp. 1459–1470, 2014.

[66] Y. W. Wang, K. T. Lin, S. C. Chen et al., "Overexpressed-eIF3I interacted and activated oncogenic Akt1 is a theranostic target in human hepatocellular carcinoma," *Hepatology*, vol. 58, no. 1, pp. 239–250, 2013.

[67] X. Yang, L. Liu, H. Zou, Y. W. Zheng, and K. P. Wang, "circZFR promotes cell proliferation and migration by regulating miR-511/AKT1 axis in hepatocellular carcinoma," *Digestive and Liver Disease*, vol. 51, no. 10, pp. 1446–1455, 2019.

[68] S. Acosta-Lopez, D. Diaz-Bethencourt, T. Concepcion-Massip et al., "The androgen receptor expression and its activity have different relationships with prognosis in hepatocellular carcinoma," *Scientific Reports*, vol. 10, no. 1, p. 22046, 2020.

[69] T. Kanda, X. Jiang, and O. Yokosuka, "Androgen receptor signaling in hepatocellular carcinoma and pancreatic cancers," *World Journal of Gastroenterology*, vol. 20, no. 28, pp. 9229–9236, 2014.

[70] H. Khan, W. Jia, Z. Yu et al., "Emodin succinyl ester inhibits malignant proliferation and migration of hepatocellular carcinoma by suppressing the interaction of AR and EZH2," *Biomedicine & Pharmacotherapy*, vol. 128, Article ID 110244, 2020.

[71] H. C. Lai, W. M. Chung, C. M. Chang et al., "Androgen receptor enhances the efficacy of sorafenib against hepatocellular carcinoma through enriched EpCAM stemness," *Anticancer Research*, vol. 40, no. 3, pp. 1285–1295, 2020.

[72] G. Liu, X. Ouyang, Y. Sun et al., "The miR-92a-2-5p in exosomes from macrophages increases liver cancer cells invasion via altering the AR/PHLPP/p-AKT/β-catenin

signaling," *Cell Death & Differentiation*, vol. 27, no. 12, pp. 3258–3272, 2020.

[73] Y. Xiao, Y. Sun, G. Liu et al., "Androgen receptor (AR)/miR-520f-3p/SOX9 signaling is involved in altering hepatocellular carcinoma (HCC) cell sensitivity to the sorafenib therapy under hypoxia via increasing cancer stem cells phenotype," *Cancer Letters*, vol. 444, pp. 175–187, 2019.

[74] Z. Ezzoukhry, C. Louandre, E. Trecherel et al., "EGFR activation is a potential determinant of primary resistance of hepatocellular carcinoma cells to sorafenib," *International Journal of Cancer*, vol. 131, no. 12, pp. 2961–2969, 2012.

[75] F. T. Fan, C. S. Shen, L. Tao et al., "PKM2 regulates hepatocellular carcinoma cell epithelial-mesenchymal transition and migration upon EGFR activation," *Asian Pacific Journal of Cancer Prevention*, vol. 15, no. 5, pp. 1961–1970, 2014.

[76] L. Huang, C. Zhao, K. Sun et al., "Downregulation of CLDN6 inhibits cell proliferation, migration, and invasion via regulating EGFR/AKT/mTOR signalling pathway in hepatocellular carcinoma," *Cell Biochemistry and Function*, vol. 38, no. 5, pp. 541–548, 2020.

[77] J. W. Jang, Y. Song, S. H. Kim et al., "CD133 confers cancer stem-like cell properties by stabilizing EGFR-AKT signaling in hepatocellular carcinoma," *Cancer Letters*, vol. 389, pp. 1–10, 2017.

[78] L. Kang, Z. H. Zhang, and Y. Zhao, "SCAMP3 is regulated by miR-128-3p and promotes the metastasis of hepatocellular carcinoma cells through EGFR-MAPK p38 signaling pathway," *American Journal of Translational Research*, vol. 12, no. 12, pp. 7870–7884, 2020.

[79] C. Leng, Z. G. Zhang, W. X. Chen et al., "An integrin beta4-EGFR unit promotes hepatocellular carcinoma lung metastases by enhancing anchorage independence through activation of FAK-AKT pathway," *Cancer Letters*, vol. 376, no. 1, pp. 188–196, 2016.

[80] R. Y. Wang, L. Chen, H. Y. Chen et al., "MUC15 inhibits dimerization of EGFR and PI3K-AKT signaling and is associated with aggressive hepatocellular carcinomas in patients," *Gastroenterology*, vol. 145, no. 6, pp. 1436–1412, 2013.

[81] H. Xiao, R. Tong, C. Ding et al., "γ-H2AX promotes hepatocellular carcinoma angiogenesis via EGFR/HIF-1α/VEGF pathways under hypoxic condition," *Oncotarget*, vol. 6, no. 4, pp. 2180–2192, 2015.

[82] D. Zhao, B. Zhai, and C. He, "Upregulation of HIF-2alpha induced by sorafenib contributes to the resistance by activating the TGF-alpha/EGFR pathway in hepatocellular carcinoma cells," *Cellular Signalling*, vol. 26, no. 5, pp. 1030–1039, 2014.

[83] Y. N. Zhao, J. Cao, and F. X. Wu, "Expression and significance of EGF mRNA and EGFR mRNA in hepatocellular carcinoma," *Ai Zheng*, vol. 23, no. 7, pp. 762–766, 2004.

[84] M. Hishida, S. Nomoto, Y. Inokawa et al., "Estrogen receptor 1 gene as a tumor suppressor gene in hepatocellular carcinoma detected by triple-combination array analysis," *International Journal of Oncology*, vol. 43, no. 1, pp. 88–94, 2013.

[85] J. Meng, L. Wang, J. Hou et al., "CCL23 suppresses liver cancer progression through the CCR1/AKT/ESR1 feedback loop," *Cancer Science*, vol. 112, no. 8, pp. 3099–3110, 2021.

[86] M. L. Sheng, G. L. Xu, C. H. Zhang et al., "Aberrant estrogen receptor alpha expression correlates with hepatocellular carcinoma metastasis and its mechanisms," *Hepato-Gastroenterology*, vol. 61, no. 129, pp. 146–150, 2014.

[87] L. Wang, M. Cui, D. Cheng et al., "miR-9-5p facilitates hepatocellular carcinoma cell proliferation, migration and invasion by targeting ESR1," *Molecular and Cellular Biochemistry*, vol. 476, no. 2, pp. 575–583, 2021.

[88] Y. Wu, M. Zhang, X. Bi, L. Hao, R. Liu, and H. Zhang, "ESR1 mediated circ_0004018 suppresses angiogenesis in hepatocellular carcinoma via recruiting FUS and stabilizing TIMP2 expression," *Experimental Cell Research*, vol. 408, no. 2, 2021.

[89] Y. Zhai, G. Zhou, G. Deng et al., "Estrogen receptor alpha polymorphisms associated with susceptibility to hepatocellular carcinoma in hepatitis B virus carriers," *Gastroenterology*, vol. 130, no. 7, pp. 2001–2009, 2006.

[90] W. Chen, W. Xiao, K. Zhang et al., "Activation of c-Jun predicts a poor response to sorafenib in hepatocellular carcinoma: preliminary clinical evidence," *Scientific Reports*, vol. 6, no. 1, p. 22976, 2016.

[91] R. K. K. Chow, S. Tsz-Kwan Sin, M. Liu et al., "AKR7A3 suppresses tumorigenicity and chemoresistance in hepatocellular carcinoma through attenuation of ERK, c-Jun and NF-κB signaling pathways," *Oncotarget*, vol. 8, no. 48, pp. 83469–83479, 2017.

[92] C. Liu, X. Peng, Y. Li et al., "Positive feedback loop of FAM83A/PI3K/AKT/c-Jun induces migration, invasion and metastasis in hepatocellular carcinoma," *Biomedicine & Pharmacotherapy*, vol. 123, Article ID 109780, 2020.

[93] X. Ai, L. Xiang, Z. Huang et al., "Overexpression of PIK3R1 promotes hepatocellular carcinoma progression," *Biological Research*, vol. 51, no. 1, p. 52, 2018.

[94] S. He, J. Zhang, W. Zhang, F. Chen, and R. Luo, "FOXA1 inhibits hepatocellular carcinoma progression by suppressing PIK3R1 expression in male patients," *Journal of Experimental & Clinical Cancer Research*, vol. 36, no. 1, p. 175, 2017.

[95] J. Bao, X. Chen, Y. Hou, G. Kang, Q. Li, and Y. Xu, "LncRNA DBH-AS1 facilitates the tumorigenesis of hepatocellular carcinoma by targeting miR-138 via FAK/Src/ERK pathway," *Biomedicine & Pharmacotherapy*, vol. 107, pp. 824–833, 2018.

[96] Z. Dai, S. L. Zhou, Z. J. Zhou et al., "Capn4 contributes to tumour growth and metastasis of hepatocellular carcinoma by activation of the FAK-Src signalling pathways," *The Journal of Pathology*, vol. 234, no. 3, pp. 316–328, 2014.

[97] W. C. Huang, S. L. Tung, Y. L. Chen, P. M. Chen, and P. Y. Chu, "IFI44L is a novel tumor suppressor in human hepatocellular carcinoma affecting cancer stemness, metastasis, and drug resistance via regulating met/Src signaling pathway," *BMC Cancer*, vol. 18, no. 1, p. 609, 2018.

[98] G. M. Lau, G. M. Lau, G. L. Yu et al., "Expression of Src and FAK in hepatocellular carcinoma and the effect of Src inhibitors on hepatocellular carcinoma in vitro," *Digestive Diseases and Sciences*, vol. 54, no. 7, pp. 1465–1474, 2009.

[99] C. F. Mo, J. Li, S. X. Yang et al., "IQGAP1 promotes anoikis resistance and metastasis through Rac1-dependent ROS accumulation and activation of Src/FAK signalling in hepatocellular carcinoma," *British Journal of Cancer*, vol. 123, no. 7, pp. 1154–1163, 2020.

[100] R. Zhao, L. Tin, Y. Zhang et al., "EF24 suppresses invasion and migration of hepatocellular carcinoma cells in vitro via inhibiting the phosphorylation of src," *BioMed Research International*, vol. 2016, Article ID 8569684, 8 pages, 2016.

[101] R. Zhao, Y. Wu, T. Wang et al., "Elevated Src expression associated with hepatocellular carcinoma metastasis in northern Chinese patients," *Oncology Letters*, vol. 10, no. 5, pp. 3026–3034, 2015.

[102] S. P. Hussain, J. Schwank, F. Staib, X. W. Wang, and C. C. Harris, "TP53 mutations and hepatocellular carcinoma:

insights into the etiology and pathogenesis of liver cancer," *Oncogene*, vol. 26, no. 15, pp. 2166–2176, 2007.

[103] J. Long, A. Wang, Y. Bai et al., "Development and validation of a TP53-associated immune prognostic model for hepatocellular carcinoma," *EBioMedicine*, vol. 42, pp. 363–374, 2019.

[104] H. G. Woo, X. W. Wang, A. Budhu et al., "Association of TP53 mutations with stem cell-like gene expression and survival of patients with hepatocellular carcinoma," *Gastroenterology*, vol. 140, no. 3, pp. 1063–1070, 2011.

[105] S. Ye, X. Y. Zhao, X. G. Hu et al., "TP53 and RET may serve as biomarkers of prognostic evaluation and targeted therapy in hepatocellular carcinoma," *Oncology Reports*, vol. 37, no. 4, pp. 2215–2226, 2017.

[106] P. Zhan and Y. N. Ji, "Prognostic significance of TP53 expression for patients with hepatocellular carcinoma: a meta-analysis," *Hepatobiliary Surgery and Nutrition*, vol. 3, no. 1, pp. 11–17, 2014.

[107] P. Zhan, Y. N. Ji, and L. K. Yu, "TP53 mutation is associated with a poor outcome for patients with hepatocellular carcinoma: evidence from a meta-analysis," *Hepatobiliary Surgery and Nutrition*, vol. 2, no. 5, pp. 260–265, 2013.

[108] A. Ghosh, D. Dasgupta, A. Ghosh et al., "MiRNA199a-3p suppresses tumor growth, migration, invasion and angiogenesis in hepatocellular carcinoma by targeting VEGFA, VEGFR1, VEGFR2, HGF and MMP2," *Cell Death & Disease*, vol. 8, no. 3, p. e2706, 2017.

[109] E. Horwitz, I. Stein, M. Andreozzi et al., "Human and mouse VEGFA-amplified hepatocellular carcinomas are highly sensitive to sorafenib treatment," *Cancer Discovery*, vol. 4, no. 6, pp. 730–743, 2014.

[110] C. R. Oh, S. Y. Kong, H. S. Im et al., "Genome-wide copy number alteration and VEGFA amplification of circulating cell-free DNA as a biomarker in advanced hepatocellular carcinoma patients treated with sorafenib," *BMC Cancer*, vol. 19, no. 1, p. 292, 2019.

[111] Y. Shi, X. Yang, X. Xue et al., "HANR promotes lymphangiogenesis of hepatocellular carcinoma via secreting miR-296 exosome and regulating EAG1/VEGFA signaling in HDLEC cells," *Journal of Cellular Biochemistry*, vol. 120, no. 10, pp. 17699–17708, 2019.

[112] X. Wu, Z. Xin, W. Zhang et al., "Polymorphisms in the VEGFA promoter are associated with susceptibility to hepatocellular carcinoma by altering promoter activity," *International Journal of Cancer*, vol. 133, no. 5, pp. 1085–1093, 2013.

[113] J. J. Yan, Y. N. Zhang, J. Z. Liao et al., "MiR-497 suppresses angiogenesis and metastasis of hepatocellular carcinoma by inhibiting VEGFA and AEG-1," *Oncotarget*, vol. 6, no. 30, pp. 29527–29542, 2015.

[114] F. Huang and X. P. Geng, "Chemokines and hepatocellular carcinoma," *World Journal of Gastroenterology*, vol. 16, no. 15, pp. 1832–1836, 2010.

[115] C. M. Liang, L. Chen, and H. Hu, "Chemokines and their receptors play important roles in the development of hepatocellular carcinoma," *World Journal of Hepatology*, vol. 7, no. 10, pp. 1390–1402, 2015.

[116] X. Pan, A. C. Kaminga, S. W. Wen, and A. Liu, "Chemokines in hepatocellular carcinoma: a meta-analysis," *Carcinogenesis*, vol. 41, no. 12, pp. 1682–1694, 2020.

[117] D. Xue, Y. Zheng, J. Wen et al., "Role of chemokines in hepatocellular carcinoma (review)," *Oncology Reports*, vol. 45, no. 3, pp. 809–823, 2021.

[118] S. M. Akula, S. L. Abrams, L. S. Steelman et al., "RAS/RAF/MEK/ERK, PI3K/PTEN/AKT/mTORC1 and TP53 pathways and regulatory miRs as therapeutic targets in hepatocellular carcinoma," *Expert Opinion on Therapeutic Targets*, vol. 23, no. 11, pp. 915–929, 2019.

[119] C. Chen and T. Lou, "Hypoxia inducible factors in hepatocellular carcinoma," *Oncotarget*, vol. 8, no. 28, pp. 46691–46703, 2017.

[120] Y. Guo, Z. Xiao, L. Yang et al., "Hypoxiainducible factors in hepatocellular carcinoma (review)," *Oncology Reports*, vol. 43, no. 1, pp. 3–15, 2020.

[121] X. Meng, D. A. Franklin, J. Dong, and Y. Zhang, "MDM2-p53 pathway in hepatocellular carcinoma," *Cancer Research*, vol. 74, no. 24, pp. 7161–7167, 2014.

[122] L. Shi, Y. Feng, H. Lin, R. Ma, and X. Cai, "Role of estrogen in hepatocellular carcinoma: is inflammation the key?" *Journal of Translational Medicine*, vol. 12, no. 1, p. 93, 2014.

[123] O. A. Sukocheva, "Estrogen, estrogen receptors, and hepatocellular carcinoma: are we there yet?" *World Journal of Gastroenterology*, vol. 24, no. 1, pp. 1–4, 2018.

[124] M. Abd-Elbaset, A. M. Mansour, O. M. Ahmed, and A. M. Abo-Youssef, "The potential chemotherapeutic effect of beta-ionone and/or sorafenib against hepatocellular carcinoma via its antioxidant effect, PPAR-gamma, FOXO-1, Ki-67, Bax, and Bcl-2 signaling pathways," *Naunyn-Schmiedeberg's Archives of Pharmacology*, vol. 393, no. 9, pp. 1611–1624, 2020.

[125] Y. Li, P. Li, and N. Wang, "Effect of let-7c on the PI3K/Akt/FoxO signaling pathway in hepatocellular carcinoma," *Oncology Letters*, vol. 21, no. 2, p. 96, 2021.

[126] K. Lou, N. Chen, Z. Li et al., "MicroRNA-142-5p overexpression inhibits cell growth and induces apoptosis by regulating FOXO in hepatocellular carcinoma cells," *Oncology Research Featuring Preclinical and Clinical Cancer Therapeutics*, vol. 25, no. 1, pp. 65–73, 2017.

[127] F. Yamaguchi, Y. Hirata, H. Akram et al., "FOXO/TXNIP pathway is involved in the suppression of hepatocellular carcinoma growth by glutamate antagonist MK-801," *BMC Cancer*, vol. 13, no. 1, p. 468, 2013.

[128] V. Kairaluoma, N. Kemi, H. Huhta, V. M. Pohjanen, and O. Helminen, "Toll-like receptor 5 and 8 in hepatocellular carcinoma," *Acta Pathologica, Microbiologica et Immunologica Scandinavica*, vol. 129, no. 8, pp. 470–479, 2021.

[129] Z. Sepehri, Z. Kiani, F. Kohan, S. M. Alavian, and S. Ghavami, "Toll like receptor 4 and hepatocellular carcinoma; A systematic review," *Life Sciences*, vol. 179, pp. 80–87, 2017.

[130] S. N. Wang, S. T. Wang, and K. T. Lee, "The potential interplay of adipokines with toll-like receptors in the development of hepatocellular carcinoma," *Gastroenterol Res Pract*, vol. 2011, Article ID 215986, 2011.

[131] R. Bansal, "Battling IL-17, the troublemaker in alcohol-induced hepatocellular carcinoma," *Journal of Hepatology*, vol. 72, no. 5, pp. 809–812, 2020.

[132] R. Liao, J. Sun, H. Wu et al., "High expression of IL-17 and IL-17RE associate with poor prognosis of hepatocellular carcinoma," *Journal of Experimental & Clinical Cancer Research*, vol. 32, no. 1, p. 3, 2013.

[133] O. Hammam, O. Mahmoud, M. Zahran et al., "A possible role for TNF-alpha in coordinating inflammation and angiogenesis in chronic liver disease and hepatocellular carcinoma," *Gastrointestinal Cancer Research*, vol. 6, no. 4, pp. 107–114, 2013.

[134] W. Tan, X. Luo, W. Li et al., "TNF-alpha is a potential therapeutic target to overcome sorafenib resistance in hepatocellular carcinoma," *EBioMedicine*, vol. 40, pp. 446–456, 2019.

[135] A. D'Alessio, L. Rimassa, A. Cortellini, and D. J. Pinato, "PD-1 blockade for hepatocellular carcinoma: current research and future prospects," *Journal of Hepatocellular Carcinoma*, vol. 8, pp. 887–897, 2021.

[136] D. J. Pinato, N. Guerra, P. Fessas et al., "Immune-based therapies for hepatocellular carcinoma," *Oncogene*, vol. 39, no. 18, pp. 3620–3637, 2020.

[137] T. Garcia-Caballero, H. M. Mertani, A. Lambert et al., "Increased expression of growth hormone and prolactin receptors in hepatocellular carcinomas," *Endocrine*, vol. 12, no. 3, pp. 265–272, 2000.

[138] X. Kong, W. Wu, Y. Yuan et al., "Human growth hormone and human prolactin function as autocrine/paracrine promoters of progression of hepatocellular carcinoma," *Oncotarget*, vol. 7, no. 20, pp. 29465–29479, 2016.

[139] W. W. Wang, S. F. Ang, R. Kumar et al., "Identification of serum monocyte chemoattractant protein-1 and prolactin as potential tumor markers in hepatocellular carcinoma," *PLoS One*, vol. 8, no. 7, Article ID e68904, 2013.

[140] Y. T. Yeh, K. T. Lee, C. J. Tsai, Y. J. Chen, and S. N. Wang, "Prolactin promotes hepatocellular carcinoma through Janus kinase 2," *World Journal of Surgery*, vol. 36, no. 5, pp. 1128–1135, 2012.

[141] E. Jang, S. Y. Kim, N. R. Lee et al., "Evaluation of antitumor activity of Artemisia capillaris extract against hepatocellular carcinoma through the inhibition of IL-6/STAT3 signaling axis," *Oncology Reports*, vol. 37, no. 1, pp. 526–532, 2017.

[142] K. H. Jung, M. Rumman, H. Yan et al., "An ethyl acetate fraction of Artemisia capillaris (ACE-63) induced apoptosis and anti-angiogenesis via inhibition of PI3K/AKT signaling in hepatocellular carcinoma," *Phytotherapy Research*, vol. 32, no. 10, pp. 2034–2046, 2018.

[143] J. Kim, K. H. Jung, H. H. Yan et al., "Artemisia capillaris leaves inhibit cell proliferation and induce apoptosis in hepatocellular carcinoma," *BMC Complementary and Alternative Medicine*, vol. 18, no. 1, p. 147, 2018.

[144] H. Yan, K. H. Jung, J. Kim, M. Rumman, M. S. Oh, and S. S. Hong, "Artemisia capillaris extract AC68 induces apoptosis of hepatocellular carcinoma by blocking the PI3K/AKT pathway," *Biomedicine & Pharmacotherapy*, vol. 98, pp. 134–141, 2018.

[145] K.-M. Kim, C. Park, Y.-H. Choi, and W.-H. Lee, "Induction of apaopotis by water extract of Cordyceps militaris (WECM) in human hepatocellular carcinoma HepG2 cells," *Journal of Life Sciences*, vol. 18, no. 6, pp. 804–813, 2008.

[146] Z. Li, Z. Guo, and J. Zhu, "Cordyceps militaris fraction inhibits angiogenesis of hepatocellular carcinoma in vitro and in vivo," *Pharmacognosy Magazine*, vol. 16, no. 67, p. 169, 2020.

[147] Z. Guo, W. Chen, G. Dai, and Y. Huang, "Cordycepin suppresses the migration and invasion of human liver cancer cells by downregulating the expression of CXCR4," *International Journal of Molecular Medicine*, vol. 45, no. 1, pp. 141–150, 2020.

[148] H. H. Lee, J. W. Jeong, J. H. Lee et al., "Cordycepin increases sensitivity of Hep3B human hepatocellular carcinoma cells to TRAIL-mediated apoptosis by inactivating the JNK signaling pathway," *Oncology Reports*, vol. 30, no. 3, pp. 1257–1264, 2013.

[149] H. Lu, X. Li, J. Zhang, H. Shi, X. Zhu, and X. He, "Effects of cordycepin on HepG2 and EA.hy926 cells: potential anti-proliferative, antimetastatic and anti-angiogenic effects on hepatocellular carcinoma," *Oncology Letters*, vol. 7, no. 5, pp. 1556–1562, 2014.

[150] L. W. Shao, L. H. Huang, S. Yan, J. D. Jin, and S. Y. Ren, "Cordycepin induces apoptosis in human liver cancer HepG2 cells through extrinsic and intrinsic signaling pathways," *Oncology Letters*, vol. 12, no. 2, pp. 995–1000, 2016.

[151] W. L. Yao, B. S. Ko, T. A. Liu et al., "Cordycepin suppresses integrin/FAK signaling and epithelial-mesenchymal transition in hepatocellular carcinoma," *Anti-Cancer Agents in Medicinal Chemistry*, vol. 14, no. 1, pp. 29–34, 2014.

[152] Y. Zeng, S. Lian, and D. Li, "Anti-hepatocarcinoma effect of cordycepin against NDEA-induced hepatocellular carcinomas via the PI3K/Akt/mTOR and Nrf2/HO-1/NF-kappaB pathway in mice," *Biomedicine & Pharmacotherapy*, vol. 95, pp. 1868–1875, 2017.

[153] Y. Zhou, Z. Guo, Q. Meng et al., "Cordycepin affects multiple apoptotic pathways to mediate hepatocellular carcinoma cell death," *Anti-Cancer Agents in Medicinal Chemistry*, vol. 17, no. 1, pp. 143–149, 2017.

[154] F. Wang, Y.-H. Wang, J.-J. Wang, H.-L. Xu, and C.-M. Wang, "Eriodictyol-induced anti-cancer and apoptotic effects in human hepatocellular carcinoma cells are associated with cell cycle arrest and modulation of apoptosis-related proteins," *Bangladesh Journal of Pharmacology*, vol. 11, no. 2, pp. 285–291, 2016.

[155] R. Fei and H. Wei, "Quantitative proteomic analysis of Isorhamnetin treatment in human liver cancer cells," *Journal of Medicinal Plants Research*, vol. 12, no. 7, pp. 77–88, 2018.

[156] T. K. Vo, Q. T. H. Ta, Q. T. Chu, T. T. Nguyen, and V. G. Vo, "Anti-hepatocellular-cancer activity exerted by beta-sitosterol and beta-sitosterol-glucoside from Indigofera zollingeriana miq," *Molecules*, vol. 25, no. 3021, p. 13, 2020.

[157] H. Guo, W. Lin, X. Zhang et al., "Kaempferol induces hepatocellular carcinoma cell death via endoplasmic reticulum stress-CHOP-autophagy signaling pathway," *Oncotarget*, vol. 8, no. 47, pp. 82207–82216, 2017.

[158] B. Han, Y. Q. Yu, Q. L. Yang, C. Y. Shen, and X. J. Wang, "Kaempferol induces autophagic cell death of hepatocellular carcinoma cells via activating AMPK signaling," *Oncotarget*, vol. 8, no. 49, pp. 86227–86239, 2017.

[159] B. Nair, R. J. Anto, and L. R. Nath, "Kaempferol-Mediated sensitization enhances chemotherapeutic efficacy of sorafenib against hepatocellular carcinoma: an in silico and in vitro approach," *Advanced Pharmaceutical Bulletin*, vol. 10, no. 3, pp. 472–476, 2020.

[160] E. Seydi, A. Salimi, H. R. Rasekh, Z. Mohsenifar, and J. Pourahmad, "Selective cytotoxicity of luteolin and kaempferol on cancerous hepatocytes obtained from rat model of hepatocellular carcinoma: involvement of ROS-mediated mitochondrial targeting," *Nutrition and Cancer*, vol. 70, no. 4, pp. 594–604, 2018.

[161] G. Yang, J. Xing, B. Aikemu, J. Sun, and M. Zheng, "Kaempferol exhibits a synergistic effect with doxorubicin to inhibit proliferation, migration, and invasion of liver cancer," *Oncology Reports*, vol. 45, no. 32, p. 4, 2021.

[162] Z. Cao, H. Zhang, X. Cai et al., "Luteolin promotes cell apoptosis by inducing autophagy in hepatocellular carcinoma," *Cellular Physiology and Biochemistry*, vol. 43, no. 5, pp. 1803–1812, 2017.

[163] X. Q. Feng, L. W. Rong, R. X. Wang et al., "Luteolin and sorafenib combination kills human hepatocellular carcinoma cells through apoptosis potentiation and JNK activation," *Oncology Letters*, vol. 16, no. 1, pp. 648–653, 2018.

[164] E. Im, C. Yeo, and E. O. Lee, "Luteolin induces caspase-dependent apoptosis via inhibiting the AKT/osteopontin pathway in human hepatocellular carcinoma SK-Hep-1 cells," *Life Sciences*, vol. 209, pp. 259–266, 2018.

[165] Y. Lee and Y. H. Kwon, "Regulation of apoptosis and autophagy by luteolin in human hepatocellular cancer Hep3B cells," *Biochemical and Biophysical Research Communications*, vol. 517, no. 4, pp. 617–622, 2019.

[166] U. M. Nazim and S. Y. Park, "Luteolin sensitizes human liver cancer cells to TRAILinduced apoptosis via autophagy and JNKmediated death receptor 5 upregulation," *International Journal of Oncology*, vol. 54, no. 2, pp. 665–672, 2019.

[167] H. Xu, T. Yang, X. Liu et al., "Luteolin synergizes the antitumor effects of 5-fluorouracil against human hepatocellular carcinoma cells through apoptosis induction and metabolism," *Life Sciences*, vol. 144, pp. 138–147, 2016.

[168] Y. Su Bog, L. Jung Hwa, C. Hae Young et al., "Inhibitory effects of luteolin isolated from Ixeris sonchifolia hance on the proliferation of HepG2 human hepatocellular carcinoma cells," *Archives of Pharmacal Research*, vol. 26, no. 2, pp. 151–156, 2003.

[169] X. Meng, W.-Q. Zhong, and X.-R. Zhang, "Effect of luteolin on HepG2 liver cancer cell proliferation in vitro and angiogenesis activity," *Journal of Hainan Medical University*, vol. 23, no. 23, pp. 9–12, 2017.

[170] Q. Wang, S. Shen, and X. G. Li, "Effects of luteolin on invasion, migration and adhesion of human hepatocellular carcinoma HepG2 cells," *Chinese Journal of Pathophysiology*, vol. 33, no. 9, pp. 1606–1610, 2017.

[171] Z. Chen, C. Huang, T. Ma et al., "Reversal effect of quercetin on multidrug resistance via FZD7/β-catenin pathway in hepatocellular carcinoma cells," *Phytomedicine*, vol. 43, pp. 37–45, 2018.

[172] Y. Ding, X. Chen, B. Wang, B. Yu, J. Ge, and X. Shi, "Quercetin suppresses the chymotrypsin-like activity of proteasome via inhibition of MEK1/ERK1/2 signaling pathway in hepatocellular carcinoma HepG2 cells," *Canadian Journal of Physiology and Pharmacology*, vol. 96, no. 5, pp. 521–526, 2018.

[173] I. Igbe, X. F. Shen, W. Jiao et al., "Dietary quercetin potentiates the antiproliferative effect of interferon-alpha in hepatocellular carcinoma cells through activation of JAK/STAT pathway signaling by inhibition of SHP2 phosphatase," *Oncotarget*, vol. 8, no. 69, pp. 113734–113748, 2017.

[174] Y. Ji, L. Li, Y. X. Ma et al., "Quercetin inhibits growth of hepatocellular carcinoma by apoptosis induction in part via autophagy stimulation in mice," *The Journal of Nutritional Biochemistry*, vol. 69, pp. 108–119, 2019.

[175] R. H. Lee, J. H. Cho, Y. J. Jeon et al., "Quercetin induces antiproliferative activity against human hepatocellular carcinoma (HepG2) cells by suppressing specificity protein 1 (Sp1)," *Drug Development Research*, vol. 76, no. 1, pp. 9–16, 2015.

[176] A. K. Maurya and M. Vinayak, "Anticarcinogenic action of quercetin by downregulation of phosphatidylinositol 3-kinase (PI3K) and protein kinase C (PKC) via induction of p53 in hepatocellular carcinoma (HepG2) cell line," *Molecular Biology Reports*, vol. 42, no. 9, pp. 1419–1429, 2015.

[177] Y. A. Salama, A. El-Karef, A. M. El Gayyar, and N. Abdel-Rahman, "Beyond its antioxidant properties: quercetin targets multiple signalling pathways in hepatocellular carcinoma in rats," *Life Sciences*, vol. 236, Article ID 116933, 2019.

[178] G. Wang, J. Zhang, L. Liu, S. Sharma, and Q. Dong, "Quercetin potentiates doxorubicin mediated antitumor effects against liver cancer through p53/Bcl-xl," *PLoS One*, vol. 7, no. 12, Article ID e51764, 2012.

[179] L. Wu, J. Li, T. Liu et al., "Quercetin shows anti-tumor effect in hepatocellular carcinoma LM3 cells by abrogating JAK2/STAT3 signaling pathway," *Cancer Medicine*, vol. 8, no. 10, pp. 4806–4820, 2019.

[180] N. Yamada, R. Matsushima-Nishiwaki, and O. Kozawa, "Quercetin suppresses the migration of hepatocellular carcinoma cells stimulated by hepatocyte growth factor or transforming growth factor-α: attenuation of AKT signaling pathway," *Archives of Biochemistry and Biophysics*, vol. 682, Article ID 108296, 2020.

Hindawi
Evidence-Based Complementary and Alternative Medicine
Volume 2022, Article ID 9092311, 10 pages
https://doi.org/10.1155/2022/9092311

Research Article

Febuxostat Alleviates Allergic Rhinitis by Inhibiting Inflammation and Monocyte Adhesion in Human Nasal Epithelial Cells via Regulating KLF6

Yuting Yao, Ran Wei, and Hui Jiang

Otorhinolaryngology, Dongfang Hospital Beijing University of Chinese Medicine, No. 6 Fangxingyuan, Fengtai District, Beijing 100078, China

Correspondence should be addressed to Ran Wei; b01229@bucm.edu.cn

Received 13 July 2022; Accepted 16 August 2022; Published 8 September 2022

Academic Editor: Xueliang Wu

Introduction. Febuxostat is a novel inhibitor of xanthine oxidase that suppresses cell adhesion molecules-mediated (CAMs) inflammation by activating KLF6. In this study, we explored the therapeutic function and potential mechanisms of febuxostat against allergic rhinitis (AR). *Methods*. We investigated the role of febuxostat through *in vitro* cell and *in vivo* animal experiments. Human nasal epithelial cells (hNECs) were cultured with histamine as an *in vitro* model. To establish the AR animal model, rats were exposed to ovalbumin. Rats were randomly grouped into control, model, 7.5 mg/kg febuxostat, and 15 mg/kg febuxostat groups. *Results*. In the *in vitro* study, we found significantly increased release of lactate dehydrogenase, elevated production of inflammatory factors and chemokines, and upregulated CAMs in histamine-treated hNECs. However, these results were significantly reversed for the 10 and 20 μM febuxostat treatments. The enhanced adhesion between hNECs and monocytes induced by histamine was dramatically repressed by febuxostat. In the *vivo* experiments, we observed that febuxostat ameliorated the increased sneezing times, the number of nose scratching episodes, and elevated HE pathological scores as well as alleviated the inflammation in nasal mucous tissues of AR mice. We found that KLF6, which was downregulated in histamine-treated hNECs, was significantly upregulated by febuxostat. The inhibitory effects of febuxostat on the expression levels of CAMs and adhesion between histamine-treated hNECs and monocytes were significantly abolished by the knockdown of *KLF6*. *Conclusion*. Febuxostat alleviates AR by inhibiting inflammation and monocyte adhesion in human nasal epithelial cells through the regulation of KLF6.

1. Introduction

Allergic rhinitis (AR) is a common rhinitis with clinical symptoms such as itchy nose, sneezing, and runny nose, which cause significant inconvenience in the normal lives of AR patients [1]. At present, approximately 30% of the global population is affected by AR and the morbidity rate in America is 5%-22%. The annual cost for AR treatment in America is approximately 7 billion dollars [2]. In addition, with economic development, acceleration of industrialization, and lifestyle changes in China, the morbidity rate of AR has increased. It has been reported that approximately 30 million patients are diagnosed with AR in China every year [3, 4]. Therefore, AR has triggered significant public health problems worldwide.

After AR patients are stimulated with allergens, immunoglobulin E (Ig E) is excessively produced in the nasal mucosa and binds with the receptor located on mast cells, which further induces degranulation in mast cells and the release of multiple inflammatory mediators such as histamine and leukotrienes. Consequently, the development of AR is induced under the regulation of multiple inflammatory cells and inflammatory factors [5]. The pathological mechanism of AR is complicated. Currently, the theory of imbalance between type 1 helper T (Th1) and type 2 helper T (Th2) cells is widely accepted [6]. The relationship between the pathogenesis of AR and cytokines has been extensively investigated such as interleukin 4 (IL-4) and interleukin 9 (IL-9) released by Th2 cells [7, 8], interleukin 5 (IL-5)

produced by $CD4^+$ T cells and mast cells [9], interleukin 12 (IL-12) released by antigen-presenting cells (APCs) [10], and tumor necrosis factor-alpha (TNF-α) secreted by macrophages [11]. Additionally, the disorder of the cytokine network is the molecular basis for developing AR [12]. For investigating the pathological mechanism of AR, the function of cell adhesion molecules (CAMs) released by Th cells in the development of AR has received considerable attention [13]. The infiltration and adhesion of inflammatory cells in local or systemic inflammatory tissues are keys to the progression of inflammation. In clinical investigations, a significantly higher number of neutrophils, eosinophils (EOS), and lymphocytes are observed in AR patients [14]. The involvement of inflammatory cells in immunologic processes depends on the regulation of CAMs [15]. Recently, KLF6, which is a transcriptional factor, was reported to suppress the expression of CAMs to mediate the inflammatory reaction [16]. Therefore, KLF6 might be an important target for the treatment of clinical AR due to its function in regulating CAMs-mediated inflammation.

Febuxostat is a novel inhibitor of xanthine oxidase and was developed for treating hyperuricemia by reducing the production of uric acid [17]. Animal experiments revealed that febuxostat showed a promising protective property in renal ischemia-reperfusion injury [18], diabetic nephropathy (DN) [19], and myocardial ischemia-reperfusion injury [20] by inhibiting oxidative stress. Recently, febuxostat was reported to suppress adhesion between monocytes and endothelial cells by regulating the expression level of CAMs, which is associated with the activation of KLF6 [21]. In this study, we explored the inhibitory function of febuxostat on inflammation to determine the therapeutic function of febuxostat on AR.

2. Materials and Methods

2.1. Cells and Treatments. Human nasal epithelial cells (hNECs) and U937 cells were obtained from ATCC (ATCC, California, USA) and cultured in a DMEM medium containing 10% FBS under the condition of 37°C and 5% CO_2.

2.2. The MTT Assay. After different treatment strategies, cells were added with 0.25 mg/ml MTT (Sigma, Missouri, USA) at 37°C for 3 h, followed by removing the medium and adding the dimethyl sulfoxide for the production of blue formazan. Then, the microplate reader (Mindray, Shenzhen, China) was used to measure the absorbance at 630 nm.

2.3. The Lactate Dehydrogenase (LDH) Release Assay. In brief, treated hNECs were seeded in the 96-well plate to be incubated for 24 hours. Subsequently, the collected supernatants were added to the CytoTox 96 Reagent (Promega, Wisconsin, USA), followed by incubating it with the stop solution. Lastly, the percentage of LDH released was calculated by the following equation: LDH releases (%) = (experimental LDH release spontaneous LDH release)/maximum LDH release.

2.4. Real-Time qPCR. The trizol reagents were utilized to extract the cellular total RNA from treated hNECs and the concentration of RNA was measured by detecting the optical density at 260 nm, followed by being transcribed into cDNA by utilizing the PrimeScript RT Master Mix Kit (Takara, Tokyo, Japan). The Sybr Premix Ex Taq Kit (Takara, Tokyo, Japan) was used to perform the RT-qPCR in the present study. The $2^{-\Delta\Delta Ct}$ method was utilized to calculate the expression of genes after normalization to Gapdh. The primers used in the qRT-PCR analysis are as follows:

Gapdh primer F: 5′- GCACCGTCAAGGCTGAGAAC -3′

Gapdh primer R: 5′- TGGTGAAGACGCCAGTGGA -3′

IL-6 primer F: 5′-TCCAGAACAGATTTGA-GAGTAGTG-3′

IL-6 primer R: 5′-GCATTTGTGGTTGGGTCAGG-3′

TNF-αprimer F: 5′-CCTGTGAGGAGGACGAAC-3′

TNF-α primer R: 5′-CCTGTGAGGAGGACGAAC-3′

IL-12 primer F: 5′-TTCTTATCGATATGGGTCAC CAGCAGTTGGTCAT-3′

IL-12 primer R: 5′-TTTTTATCGATGGAAGCATT-CAGATAGCTCATCA-3′

2.5. ELISA Assay. The secretion of cytokines was determined by the ELISA assay (Elabscience, Wuhan, China). In brief, 5 gradient concentrations of the standard were obtained and added to the 96-well plates, along with the supernatant collected from the culture medium of each group. The samples and the standards were incubated in the wells for half an hour at 37°C, followed by removing the medium and washing it 3 times. Then, conjugate reagents were added into each well to be incubated for half an hour at 37°C. After adding 3,3′,5,5′-Tetramethyl benzidine (TMB) solution it was incubated again for 15 min, and the stop reagent was introduced to end the reaction. Lastly, the microplate reader (Bio Tek, Vermont, USA) was used for the detection of absorbance at 450 nm.

2.6. Western Blotting Assay. Following the extraction of total proteins from the treated hNECs using the lysis buffer, a BCA kit was used to quantify the isolated proteins and approximately 40 μg proteins were loaded and separated by 12% SDS-PAGE and transferred to the PVDF membrane (Millipore, Massachusetts, USA). The membrane was then incubated with 5% BSA followed by incubation with the primary antibody against VCAM-1 (1 : 1000, Affinity Biosciences, Melbourne, Australian), E-Selectin (1 : 1000, Affinity Biosciences, Melbourne, Australian), KLF6 (1 : 1000, Affinity Biosciences, Melbourne, Australian), and Gapdh (1 : 1000, Affinity Biosciences, Melbourne, Australian). Subsequently, the membrane was incubated with the secondary antibody (1 : 2000, Affinity Biosciences, Melbourne, Australia). Lastly, the bands were visualized by ECL solution,

and the relative expression level of target proteins was quantified by the Image J software.

2.7. Calcein Acetoxymethyl Ester (Calcein Am) Staining. The attachment of U937 monocytes to hNECs was measured by the calcein-AM staining assay. After being stained with 1 μM calcein-AM in the dark for 30 min, 5×10^5 U937 monocytes were added to approximately 1×10^5 hNECs for 2 hours, followed by removing the unbounded cells and visualizing the attached cells under a fluorescent microscope (Olympus, Tokyo, Japan).

2.8. AR Modeling and Grouping. 24 male C57BL/6 mice were obtained from Shanghai SLAC Laboratory Animal Co.,Ltd (Shanghai, China) and 18 mice were used to establish the AR model, with the remaining 6 mice as the control group. For the establishment of the AR model, mice were injected with ovalbumin (OVA) and aluminium hydroxide intraperitoneally, followed by stimulation on days 21, 28, 35, and 39 postinjection using OVA nasal drops. Animals in the control group were administered with normal saline and nasal drops with ultrapure water on days 21, 28, 35, and 39 postinjection.They were then divided into following four groups: control, model, 7.5 mg/kg febuxostat, and 15 mg/kg febuxostat. Animals in the control (normal mice) and model group (AR mice) were dosed with normal saline for 21 days. AR mice in the 7.5 mg/kg febuxostat group and in the15 mg/kg febuxostat group were administered orally with 7.5 mg/kg/day febuxostat and 15 mg/kg/day febuxostat for 21 days, respectively [22].

2.9. Behavioral Experiments. The symptom of AR was evaluated by sneezing times and the number of nose scratchesin 15 mins, which were recorded for the statistical analysis.

2.10. Hematoxylin and Eosin (HE) Staining. After collecting the nasal mucous tissues from each mouse, tissues were dehydrated with different concentrations of ethanol solution and ethanol and xylene until the tissues looked transparent, followed by embedding, sectioning and staining them with H&E. Lastly, the images were taken using the inverted microscope (Leica, Wetzlar, Germany). The degree of pathology was rated as follows: 0–5 points: 0: no lesion; 1: very mild lesion; 2: mild lesion; 3: moderate lesions; 4: severe lesions; and 5: extremely severe lesions.

2.11. Transfection. The specially designed siRNA against KLF6 was synthesized by Nanjing Genscript (Nanjing, China), the sequences of which were 5′ CACACAGGAGAAAAGCCUUACAGAU-3′. In brief, cells were seeded in 6-well plates, followed by the addition of 40 nM siRNAs and lipofectamine 2000 (Sigma-Aldrich, Missouri, USA), following which the transfecting efficacy was evaluated using the Western blotting assay.

2.12. Statistical Analysis. Data were analyzed using the Graphpad software and were presented as the mean ± SD. Students't test was used to compare two independent data and the data among groups were compared using the one-way ANOVA method, while $p < 0.05$ was taken as the significant difference.

3. Results

3.1. Screening the Optimized Concentration of Febuxostat. To obtain an optimized concentration of febuxostat, hNECs were incubated at different concentrations (0.1, 0.2, 1, 2, 10, 20, 100, and 200 μM) for 24 hours, followed by an evaluation of cell viability using the CCK-8 assay. Cell viability (Figure 1(a)) was slightly changed under concentrations ranging from 0.1 to 20 μM. When the concentration was higher than 100 μM, cell viability dramatically declined. In subsequent experiments, 10 and 20 μM were used for incubation.

3.2. Febuxostat Alleviated the Inflammatory State in Histamine-Treated hNECs. hNECs were treated with 0.1 μM histamine [23] in the absence or presence of 10 and 20 μM febuxostat, respectively. hNECs cells without treatment were utilized as the negative control. Compared to the control, we found that the LDH release (Figure 1(b)) was significantly elevated from 5% to 40.1% by the stimulation of histamine, which was dramatically suppressed by 23.9% and 15.0% in the 10 and 20 μM febuxostat groups, respectively. The upregulated IL-6, TNF-α, and IL-12 (Figure 1(c)) in histamine-stimulated hNECs were dramatically downregulated by the treatment with 10 and 20 μM febuxostat. Compared to the control, the release of TNF-α (Figure 1(d)) was greatly promoted from 72.9 pg/mL to 254.6 pg/mL in the histamine group and significantly declined to 186.8 pg/mL and 145.1 pg/mL in the 10 and 20 μM febuxostat group, respectively. Concentrations of IL-6 in the control, histamine, 10, and 20 μM febuxostat groups were 105.2, 445.1, 368.3, and 296.8 pg/mL, respectively. Finally, the production of IL-12 was greatly elevated from 99.4 pg/mL to 402.2 pg/mL in the histamine group, and significantly decreased to 245.7 pg/mL and 176.6 pg/mL in the 10 and 20 μM febuxostat groups ($p < 0.01$), respectively. These results imply that cell injury and the inflammatory state in hNECs induced by histamine were significantly alleviated by febuxostat.

3.3. Febuxostat Suppressed the Expression Level of Chemokines and Adhesion Molecules in Histamine-Treated hNECs. We explored the impact of febuxostat on the expression level of chemokines and adhesion molecules to explore potential mechanisms. CXCL-1, PDPN, and CXCL8 (Figure 2(a)) were dramatically upregulated by histamine, which was significantly reversed by 10 and 20 μM febuxostat. Compared with the control, the secretion of CXCL-1 (Figure 2(b)) significantly increased from 125.3 pg/mL to 488.5 pg/mL in the histamine group, which was significantly decreased to 389.8 pg/mL and 323.6 pg/mL in the 10 and 20 μM febuxostat group, respectively. Concentrations of

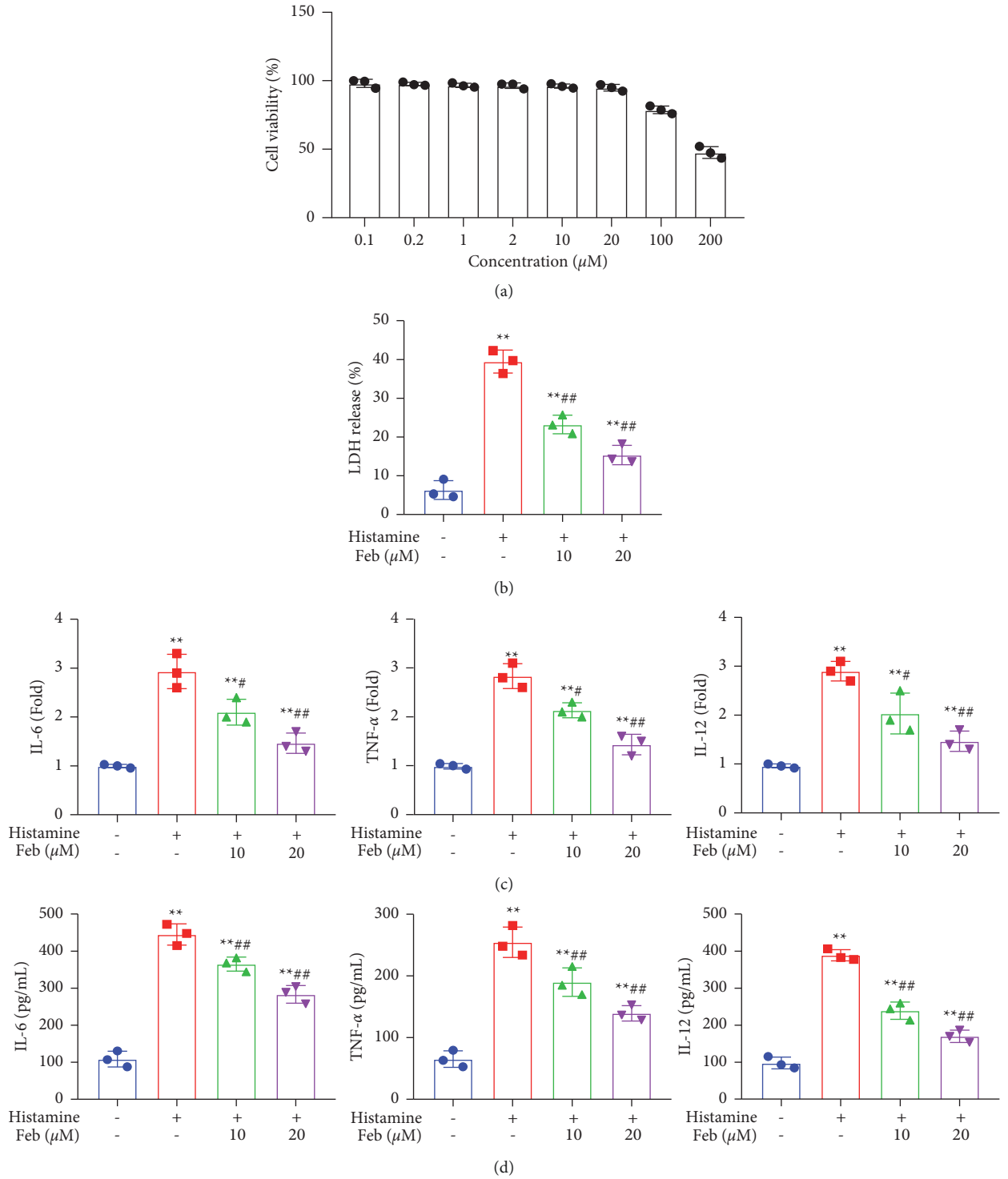

FIGURE 1: The cell injury and inflammatory state in histamine-treated hNECs were alleviated by Febuxostat. (a) The cell viability was detected by utilizing the MTT assay, (b) LDH release was measured, (c) the expression level of IL-6, TNF-α, and IL-12 was determined by RT-qPCR assay, and (d) the release of IL-6, TNF-α, and IL-12 was measured by the ELISA assay ($p < 0.01$).

PDPN in the control, histamine, 10, and 20 μM febuxostat groups were 49.6, 152.4, 129.3, and 97.0 pg/mL, respectively. Finally, the release of CXCL8 was dramatically promoted from 63.2 pg/mL to 183.7 pg/mL in the histamine group and was dramatically suppressed to 157.5 pg/mL and 126.1 pg/mL in the 10 and 20 μM febuxostat groups, respectively. VCAM-1 and E-Selectin (Figures 2(c) and 2(d)) were greatly upregulated in the histamine group, which was significantly downregulated by 10 and 20 μM of febuxostat ($p < 0.05$ and $p < 0.01$), respectively.

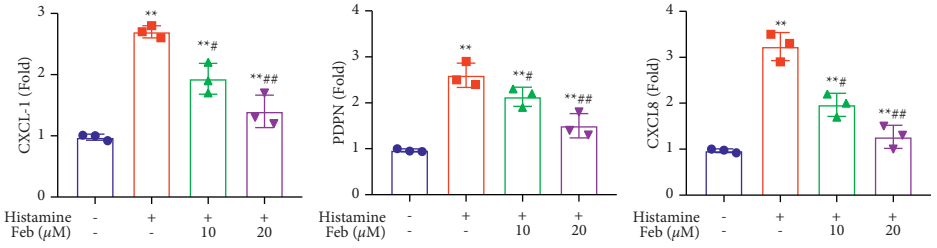

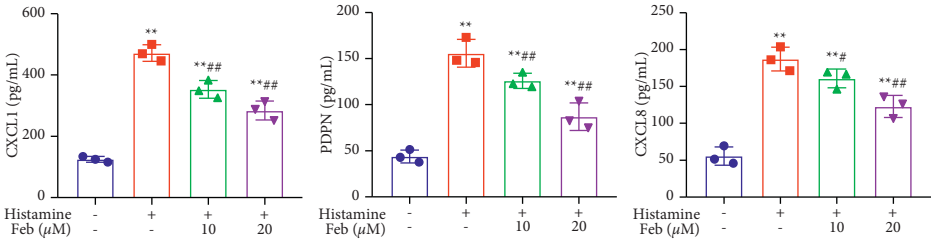

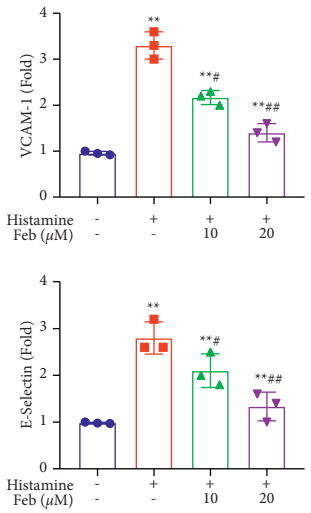

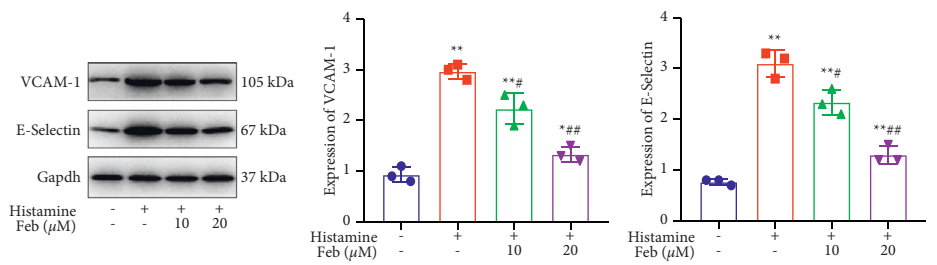

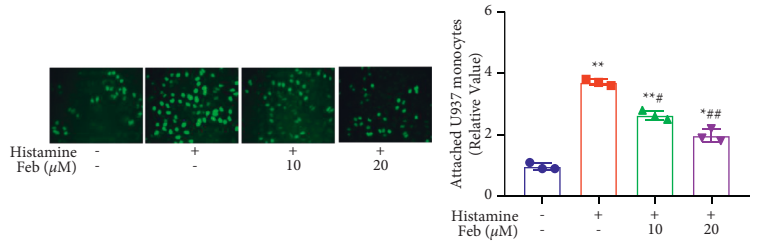

Figure 2: Continued.

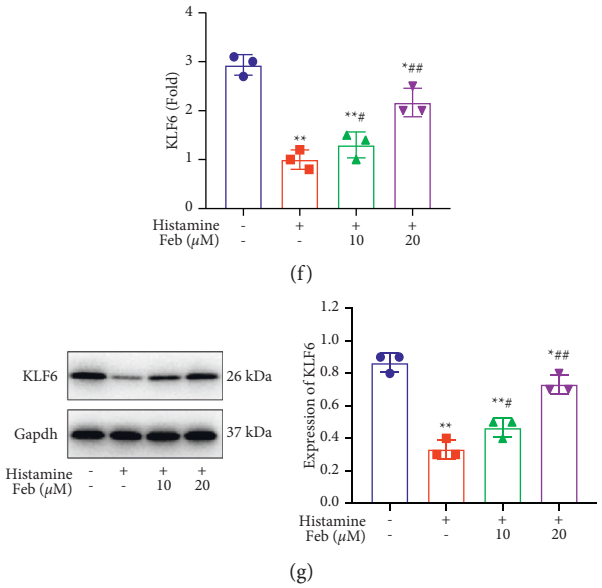

Figure 2: The expression level of chemokines, adhesion molecules, and KLF6 expression in histamine-treated hNECs were repressed by febuxostat. (a). The expression level of chemokines was measured by the RT-qPCR assay, (b) the production of chemokines was evaluated by the ELISA assay, (c) the expression level of CAMs was checked by the RT-qPCR assay, (d) the expression level of CAMs was measured by the Western blotting assay ($p < 0.05$ and $p < 0.01$), (e) the adhesion between hNECs and U937 monocytes was inhibited by febuxostat. The attached U937 monocytes were detected using the calcein-AM staining assay ($p < 0.05$ and $p < 0.01$), (f) the expression level of KLF6 was evaluated by the RT-qPCR assay, and (g) the expression level of KLF6 was determined by the Western blotting assay ($p < 0.05$ and $p < 0.01$). Immunofluorescence magnification was 10×.

3.4. Febuxostat Inhibited Adhesion between hNECs and U937 Monocytes. To confirm the effect of febuxostat on adhesion between hNECs and inflammatory cells, a calcein-AM staining assay was performed. The attached U937 monocytes (Figure 2(e)) were dramatically promoted in the histamine group but 10 and 20 μM febuxostat significantly and dose-dependently suppressed these ($p < 0.05$ and $p < 0.01$, respectively). This indicated a promising inhibitory effect of febuxostat on the attachment between hNECs and U937 monocytes.

3.5. Febuxostat Elevated the Expression Level of KLF6 in Histamine-Treated hNECs. We explored the effects of febuxostat on KLF6 and found that compared to the control, KLF6 (Figures 2(f) and 2(g)) was greatly downregulated in histamine-treated hNECs. Additionally, this was significantly reversed by 10 and 20 μM febuxostat ($p < 0.05$ and $p < 0.01$, respectively), which indicated that KLF6 might be involved in the therapeutic function of febuxostat.

3.6. Febuxostat Ameliorated the Pathological Symptoms of AR Mice. To verify the therapeutic effect of febuxostat on AR, AR mice were treated with 7.5 mg/kg/day and 15 mg/kg/day for 21 consecutive days and evaluated for pathological changes. We found that compared to the control group, sneezing times and the number of nose scratches (Figure 3(a)) were significantly elevated in the model group but were dramatically decreased in the 7.5 mg/kg and 15 mg/kg febuxostat groups. The results of HE staining on nasal mucous tissues (Figure 3(b)) indicated that compared to the control group, significant infiltration of inflammatory cells and increased HE scores were observed in the model group but these results were dramatically abolished by 7.5 mg/kg and 15 mg/kg of febuxostat. Additionally, elevated production of TNF-α, IL-6, and IL-12 in nasal mucous tissues (Figure 3(c)) in AR mice was greatly suppressed by 7.5 mg/kg and 15 mg/kg of febuxostat ($p < 0.05$ and $p < 0.01$, respectively). Results of the expression of CAMs (VCAM-1 and E-selectin) and KLF6 (Figure 3(d)) were consistent with detection results of inflammatory factors (TNF-α, IL-6, and IL-12). These results collectively revealed that pathological changes in AR mice were significantly ameliorated by febuxostat.

3.7. Febuxostat Inhibited Adhesion between hNECs and U937 Monocytes by Activating KLF6. To verify the febuxostat mechanism, hNECs were transfected with siRNA targeting KLF6 to establish KLF6-knockdown hNECs. The knockdown efficacy (Figure 4(a)) was identified using a Western blotting assay ($p < 0.01$). Subsequently, hNECs were introduced with febuxostat in the presence or absence of siRNA-KLF6. The elevated expression level of VCAM-1 and E-selectin (Figure 4(b)) in histamine-treated hNECs was significantly repressed by febuxostat, which was significantly abolished by the knockdown of KLF6. The increased attachment of U937 monocytes in histamine-treated hNECs was dramatically inhibited by febuxostat (Figure 4(c)) but this was greatly reversed by the knockdown of KLF6

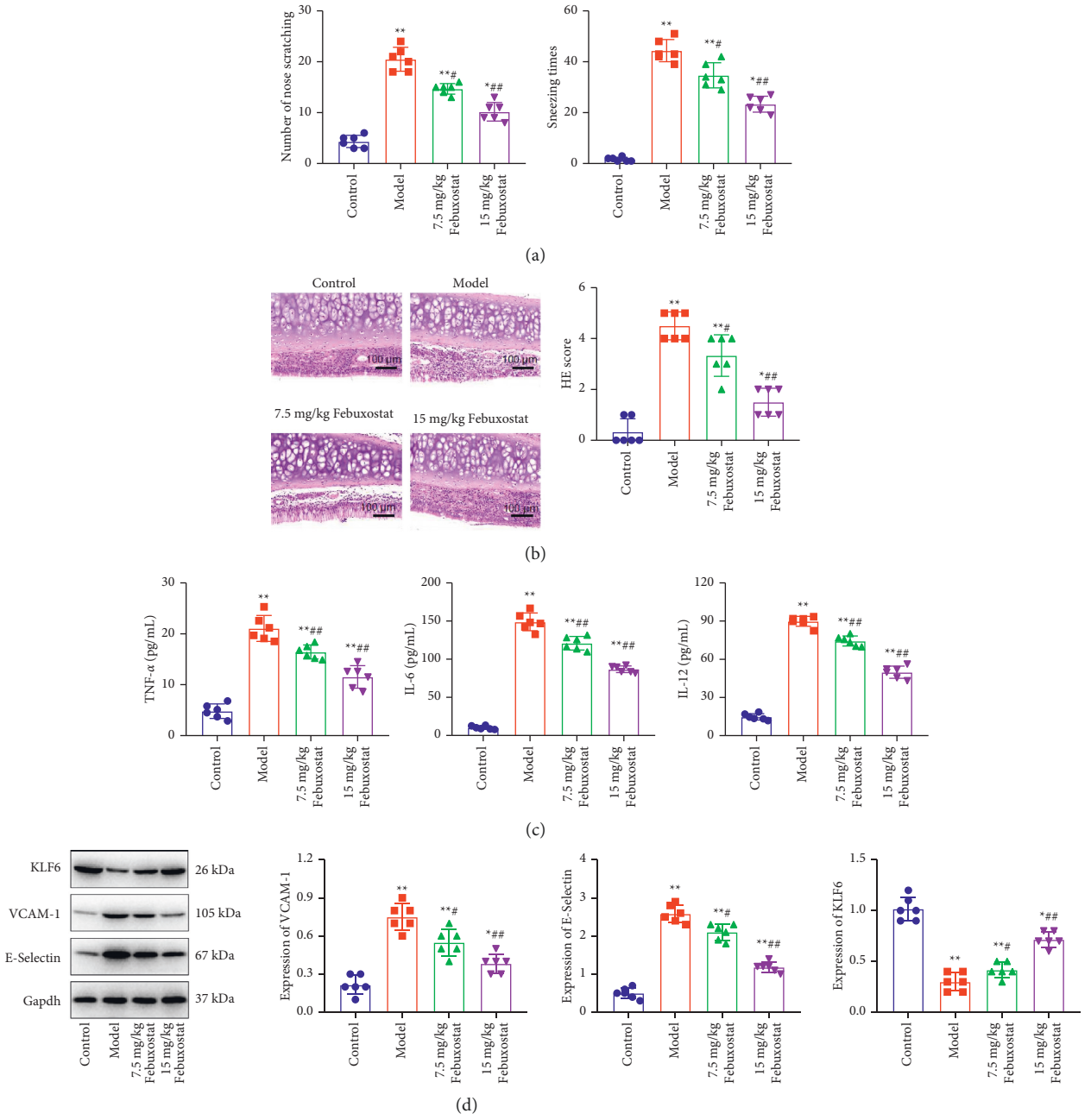

Figure 3: The AR pathological symptom was alleviated by febuxostat. (a) The sneezing times and the number of nose scratching were recorded, (b) the pathological state in nasal mucosa tissues was determined by HE staining, (c) the secretion of TNF-α, IL-6, and IL-12 in nasal mucosa tissues was measured by the ELISA assay ($p < 0.05$ and $p < 0.01$), and (d) the expression level of CAMs and KLF6 were measured by the Western blotting assay ($p < 0.05$ and $p < 0.01$).

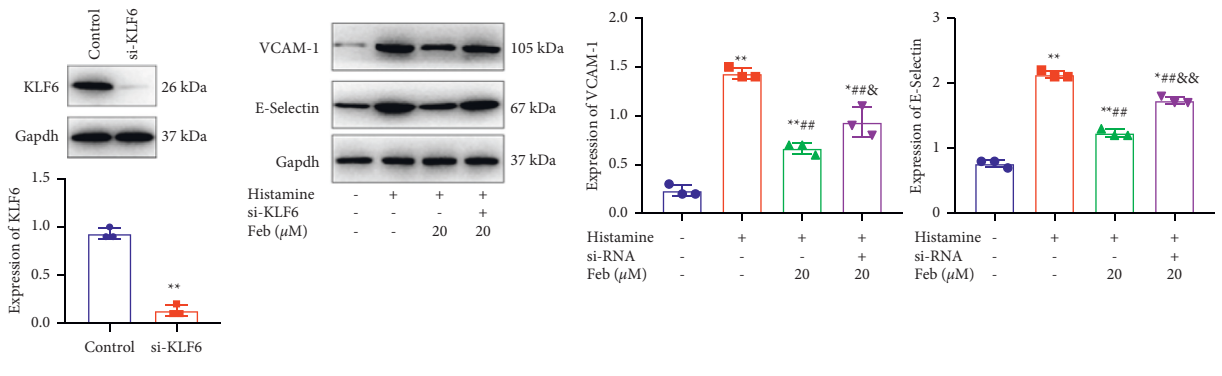

Figure 4: Continued.

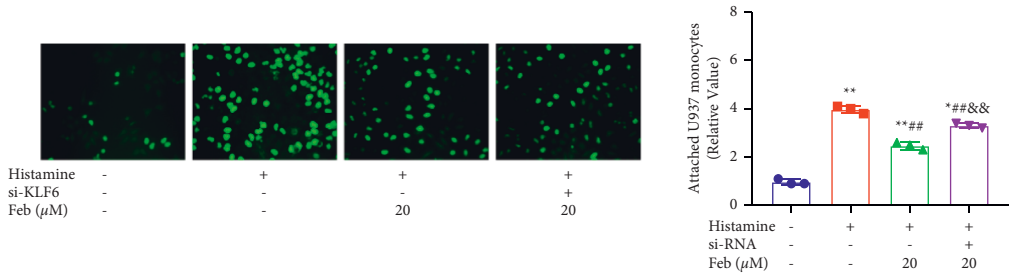

(c)

Figure 4: The inhibitory effect of febuxostat on the adhesion between hNECs and U937 monocytes. (a) The knockdown efficacy on KLF6 was evaluated by the Western blotting assay, (b) the expression level of CAMs was determined by theWestern blotting assay, and (c) the adhesion between hNECs and U937 monocytes was inhibited by febuxostat. The attached U937 monocytes were detected using the calcein-AM staining assay ($p < 0.05$ and $p < 0.01$). Immunofluorescence magnification was 10×.

($p < 0.05$ and $p < 0.01$, respectively). These results indicate that the inhibitory function of febuxostat on adhesion between hNECs and U937 monocytes may be mediated by the activation of KLF6.

4. Discussion and Conclusion

CAMs are a group of molecules that mediate the interaction among cells or between cells and a matrix, which are mainly distributed in the extracellular matrix (ECM) and exert regulatory functions by binding to specific receptors [24]. CAMs are involved in multiple types of pathological and physiological processes including the recognition of cell types, activation of cellular signal pathways, maintenance of the cellular structure, wound healing, coagulation, and tumor metastasis [25, 26]. CAMs are mainly divided into four categories as follows: the selectin family, integrin family, immunoglobulin superfamily, and cadherin family [27]. During the pathological progression of AR, CAMs bind with lymphocyte function-associated antigens to induce adhesion between T-cells and target cells such as antigen-presenting cells (APCs), epithelial cells, and endothelial cells, which further mediate the selective accumulation and adhesion of inflammatory cells including eosinophils (EOS). The accumulation and adhesion of inflammatory cells are closely related to the development of AR [28, 29]. In this study, *in vitro* results indicated that excessive production of inflammatory factors and elevated expression levels of CAMs were observed in histamine-treated hNECs, which was similar to a previous report [30]. After the treatment with febuxostat, the secretion of inflammatory factors and expression of CAMs in histamine-treated hNECs were dramatically reversed, which indicated a promising anti-inflammatory effect of febuxostat against histamine-induced inflammation.

Compared to healthy subjects, in AR patients, the expression of adhesion molecules was significantly and highly expressed in vascular endothelial cells, gland cells, submucosal lymphocytes, and EOS cells [31]. Under the stimulation of inflammation, CAMs were further upregulated by the induction of elevated and released TNF-α and IL-1 in EOS and mast cells [32, 33]. Dissociative CAMs, such as VCAMs, were significantly upregulated in the serum when the intranasal allergen was activated [34]. The important role of CAMs in the pathogenesis of AR is currently receiving considerable attention [35]. Functional experiments in this study revealed that the adhesion between histamine-treated hNECs and monocytes was significantly repressed by febuxostat, and this verified the inhibitory effect of febuxostat on CAMs. *In vivo* experiments indicated that AR pathological symptoms were significantly ameliorated by febuxostat. This was also accompanied by the alleviation of the inflammatory state in nasal mucous tissues in AR mice, which indicated that the therapeutic effect of febuxostat on AR was mediated by its anti-inflammatory properties.

Krüppel-like factor (KLF)6 is a nuclear transcription factor commonly located in mammals and is also called zinc finger factor 9(Zf9) or core promoter element binding protein. The carboxyl-terminal of KLF6 is composed of 3 sequential C_2H_2 type zinc finger structures, which regulate the expression level of downstream genes by specifically targeting and binding the CACCC and GC cassette located in the promoter [36, 37]. KLF6 is involved in multiple types of cellular progression, such as cell development, growth, signaling transition, proliferation, differentiation, and apoptosis, and the deficiency of KLF is closely associated with the development of malignant tumors [38, 39]. Recently, KLF6 was reported to regulate the expression of CAMs and mediate adhesion between endothelial cells and monocytes [21, 40]. In this study, we found that KLF6 was dramatically downregulated in histamine-treated hNECs but elevated by febuxostat, which is consistent with previous reports [21]. Further, we found that the inhibitory effects of febuxostat on the expression of CAMs and adhesion between histamine-treated hNECs and monocytes were significantly abolished by the knockdown of KLF6, which indicated that febuxostat exerted an anti-inflammatory effect by activating KLF6. In future studies, the direct interaction between febuxostat and KLF6 will be investigated to determine molecular regulatory mechanisms underlying the effects of febuxostat on monocyte adhesion and inflammation. Collectively, our data indicate that febuxostat alleviates AR by inhibiting inflammation and monocyte adhesion in human nasal epithelial cells through the regulation of KLF6.

Data Availability

The data used to support the findings of this study are included within the article.

Ethical Approval

The experiments were performed with the approval for ethical clearance from the experimental animal ethics committee of Dongfang Hospital Beijing University of Chinese Medicine (Reference number: JDF-IRB-2021031302).

Conflicts of Interest

The authors declare that there are no conflicts of interest.

Acknowledgments

This project was funded by the 2018 National Key R&D Program: Innovative research on the inheritance of famous and old Chinese medicine experiences based on the idea of "combination of Taoism" and multiple integration methods, and research on the methodological system and paradigm of the excavation and inheritance of famous and old Chinese medicine experience. NO. 2018YFC1704100; NO. 2018YFC1704101.

References

[1] S. M. Nur Husna, H. T. T. Tan, N. Md Shukri, N. S. Mohd Ashari, and K. K. Wong, "Allergic rhinitis: a clinical and pathophysiological overview," *Frontiers of Medicine*, vol. 9, Article ID 874114, 2022.

[2] J. R. May and W. K. Dolen, "Management of allergic rhinitis: a review for the community pharmacist," *Clinical Therapeutics*, vol. 39, no. 12, pp. 2410–2419, 2017.

[3] M. Feng, X. Zeng, and J. Li, "House dust mite subcutaneous immunotherapy in Chinese patients with allergic asthma and rhinitis," *Journal of Thoracic Disease*, vol. 11, no. 8, pp. 3616–3625, 2019.

[4] B. A. Stuck and T. Hummel, "Olfaction in allergic rhinitis: a systematic review," *The Journal of Allergy and Clinical Immunology*, vol. 136, no. 6, pp. 1460–1470, 2015.

[5] J. B. Morjaria, M. Caruso, R. Emma, C. Russo, and R. Polosa, "Treatment of allergic rhinitis as a strategy for preventing asthma," *Current Allergy and Asthma Reports*, vol. 18, no. 4, p. 23, 2018.

[6] F. Chen, D. He, and B. Yan, "Apigenin attenuates allergic responses of ovalbumin-induced allergic rhinitis through modulation of Th1/Th2 responses in experimental mice," *Dose Response*, vol. 18, no. 1, Article ID 155932582090479, 2020.

[7] Z. W. Gu, Y. X. Wang, and Z. W. Cao, "Neutralization of interleukin-9 ameliorates symptoms of allergic rhinitis by reducing Th2, Th9, and Th17 responses and increasing the Treg response in a murine model," *Oncotarget*, vol. 8, no. 9, pp. 14314–14324, 2017.

[8] Z. Song, C. Tu, and Y. Wang, "Effect of nose sensitive pill (NSP) on serum IFN-γ and il-4 levels in allergic rhinitis using rats model," *Pakistan Journal of Pharmaceutical Sciences*, vol. 33, no. 2, pp. 611–614, 2020.

[9] L. Lin, Z. Chen, F. Dai, J. J. Wei, X. Y. Tang, and G. B. Sun, "CD4(+) T cells induce productions of IL-5 and IL-13 through MHCII on ILC2s in a murine model of allergic rhinitis," *Auris Nasus Larynx*, vol. 46, no. 4, pp. 533–541, 2019.

[10] J. D. Marshall, H. Secrist, R. H. DeKruyff, S. F. Wolf, and D. T. Umetsu, "IL-12 inhibits the production of IL-4 and IL-10 in allergen-specific human CD4+ T lymphocytes," *The Journal of Immunology*, vol. 155, no. 1, pp. 111–117, 1995.

[11] M. Nonaka, R. Nonaka, M. Jordana, and J. G. M.-C. S. F. Dolovich, "GM-CSF, IL-8, IL-1R, TNF-alpha R, and HLA-DR in nasal epithelial cells in allergic rhinitis," *American Journal of Respiratory and Critical Care Medicine*, vol. 153, no. 5, pp. 1675–1681, 1996.

[12] L. X. Zhang and T. Liu, "[Treg influences the pathogenesis of allergic rhinitis through TICAM-1 pathway]," *Lin Chung Er Bi Yan Hou Tou Jing Wai Ke Za Zhi*, vol. 32, no. 22, pp. 1763–1766, 2018.

[13] J. Bi, Y. Hu, Z. Peng, H. Liu, and Y. Fu, "Changes and correlations of serum interleukins, adhesion molecules and soluble E-selectin in children with allergic rhinitis and asthma," *Pakistan Journal of Medical Sciences*, vol. 34, no. 5, pp. 1288–1292, 2018.

[14] J. Arebro, S. Ekstedt, E. Hjalmarsson, O. Winqvist, S. Kumlien Georén, and L. O. Cardell, "A possible role for neutrophils in allergic rhinitis revealed after cellular subclassification," *Scientific Reports*, vol. 7, no. 1, Article ID 43568, 2017.

[15] S. Xie, H. Zhang, F. Wang et al., "Activated leukocyte cell adhesion molecule as a biomarker for disease severity and efficacy of sublingual immunotherapy in allergic rhinitis," *International Immunopharmacology*, vol. 88, Article ID 106975, 2020.

[16] G. Wei, D. Zhu, Y. Sun et al., "The protective effects of azilsartan against oscillatory shear stress-induced endothelial dysfunction and inflammation are mediated by KLF6," *Journal of Biochemical and Molecular Toxicology*, vol. 35, no. 6, pp. 1–8, 2021.

[17] K. Kimura, T. Hosoya, S. Uchida et al., "Febuxostat therapy for patients with stage 3 ckd and asymptomatic hyperuricemia: a randomized trial," *American Journal of Kidney Diseases*, vol. 72, no. 6, pp. 798–810, 2018.

[18] H. Tsuda, N. Kawada, J. Y. Kaimori et al., "Febuxostat suppressed renal ischemia-reperfusion injury via reduced oxidative stress," *Biochemical and Biophysical Research Communications*, vol. 427, no. 2, pp. 266–272, 2012.

[19] S. J. Hwang, K. H. Lee, H. H. Jang et al., "Febuxostat contributes to improvement of endothelial dysfunction in an experimental model of streptozocin-induced diabetic rats," *International Journal of Cardiology*, vol. 171, no. 3, pp. e110–2, 2014.

[20] A. N. Shafik, "Febuxostat improves the local and remote organ changes induced by intestinal ischemia/reperfusion in rats," *Digestive Diseases and Sciences*, vol. 58, no. 3, pp. 650–659, 2013.

[21] J. Hao, W. Zhang, R. Tong, and Z. Huang, "Febuxostat prevents the cytotoxicity of propofol in brain endothelial cells," *ACS Omega*, vol. 6, no. 8, pp. 5471–5478, 2021.

[22] S. Jagtiani, K. Chitnis, and A. Karve, "Evaluation of effect of allopurinol and febuxostat in behavioral model of depression in mice," *Indian Journal of Pharmacology*, vol. 45, no. 3, pp. 244–247, 2013.

[23] B. Sun, B. Wang, and M. Xu, "Esculetin inhibits histamine-induced expression of inflammatory cytokines and mucin in nasal epithelial cells," *Clinical and Experimental Pharmacology and Physiology*, vol. 46, no. 9, pp. 821–827, 2019.

[24] N. Milošević, M. Rütter, and A. David, "Endothelial cell adhesion molecules- (un)Attainable targets for nanomedicines," *Front Med Technol*, vol. 4, Article ID 846065, 2022.

[25] M. N. Opiłka, Z. Lorenc, M. Starzewska, J. Lorenc, and A. Rajs, "Cell adhesion molecules in terms of carcinogenesis," *Polski Przeglad Chirurgiczny*, vol. 86, no. 3, pp. 151–157, 2014.

[26] J. Rico-Jimenez, J. H. Lee, A. Alex et al., "Non-invasive monitoring of pharmacodynamics during the skin wound healing process using multimodal optical microscopy," *BMJ Open Diabetes Research & Care*, vol. 8, no. 1, p. e000974, 2020.

[27] N. J. Gibson, "Cell adhesion molecules in context: CAM function depends on the neighborhood," *Cell Adhesion & Migration*, vol. 5, no. 1, pp. 48–51, 2011.

[28] E. M. Minshall, L. Cameron, F. Lavigne et al., "Eotaxin mRNA and protein expression in chronic sinusitis and allergen-induced nasal responses in seasonal allergic rhinitis," *American Journal of Respiratory Cell and Molecular Biology*, vol. 17, no. 6, pp. 683–690, 1997.

[29] M. A. Calderón, J. L. Devalia, A. J. Prior, R. J. Sapsford, and R. J. Davies, "A comparison of cytokine release from epithelial cells cultured from nasal biopsy specimens of atopic patients with and without rhinitis and nonatopic subjects without rhinitis," *The Journal of Allergy and Clinical Immunology*, vol. 99, no. 1, pp. 65–76, 1997.

[30] N. Terada, N. Hamano, K. I. Maesako et al., "Diesel exhaust particulates upregulate histamine receptor mRNA and increase histamine-induced IL-8 and GM-CSF production in nasal epithelial cells and endothelial cells," *Clinical and Experimental Allergy*, vol. 29, no. 1, pp. 52–59, 1999.

[31] C. Bachert, M. Wagenmann, and G. Holtappels, "Cytokines and adhesion molecules in allergic rhinitis," *American Journal of Rhinology*, vol. 12, no. 1, pp. 3–8, 1998.

[32] F. M. Baroody, B. J. Lee, M. C. Lim, and B. S. Bochner, "Implicating adhesion molecules in nasal allergic inflammation," *European Archives of Oto-Rhino-Laryngology*, vol. 252, no. S1, pp. S50–S58, 1995.

[33] R. P. Schleimer, S. A. Sterbinsky, J. Kaiser et al., "IL-4 induces adherence of human eosinophils and basophils but not neutrophils to endothelium. Association with expression of VCAM-1," *The Journal of Immunology*, vol. 148, no. 4, pp. 1086–1092, 1992.

[34] M. F. Kramer, T. R. Jordan, C. Klemens et al., "Factors contributing to nasal allergic late phase eosinophilia," *American Journal of Otolaryngology*, vol. 27, no. 3, pp. 190–199, 2006.

[35] J. Mullol, F. de Borja Callejas, M. A. Martínez-Antón et al., "Mometasone and desloratadine additive effect on eosinophil survival and cytokine secretion from epithelial cells," *Respiratory Research*, vol. 12, no. 1, p. 23, 2011.

[36] S. E. Syafruddin, M. A. Mohtar, W. Wan Mohamad Nazarie, T. Low, and T. Y. Low, "Two sides of the same coin: the roles of KLF6 in physiology and pathophysiology," *Biomolecules*, vol. 10, no. 10, p. 1378, 2020.

[37] C. Dumayne, D. Tarussio, A. R. Sanchez-Archidona et al., "Klf6 protects β-cells against insulin resistance-induced dedifferentiation," *Molecular Metabolism*, vol. 35, Article ID 100958, 2020.

[38] A. DiFeo, J. A. Martignetti, and G. Narla, "The role of KLF6 and its splice variants in cancer therapy," *Drug Resistance Updates*, vol. 12, no. 1-2, pp. 1–7, 2009.

[39] V. Andreoli, R. C. Gehrau, and J. L. Bocco, "Biology of Krüppel-like factor 6 transcriptional regulator in cell life and death," *IUBMB Life*, vol. 62, no. 12, pp. 896–905, 2010.

[40] H. Wang, G. Yang, Q. Zhang et al., "Apremilast ameliorates ox-LDL-induced endothelial dysfunction mediated by KLF6," *Aging (Albany NY)*, vol. 12, no. 19, pp. 19012–19021, 2020.

Hindawi
Evidence-Based Complementary and Alternative Medicine
Volume 2022, Article ID 1408948, 6 pages
https://doi.org/10.1155/2022/1408948

Research Article

Influence of Sevoflurane Inhalation Anesthesia on Clinical Outcomes of Morbidly Obese Patients Undergoing Laparoscopic Bariatric Surgery

Wei Li, Ying Zhang, Jianrui Lv, Yong Zhang, and Jie Bai

Department of Anesthesia, The Second Affiliated Hospital of Xi'an Jiaotong University, Xi'an 710004, Shaanxi, China

Correspondence should be addressed to Wei Li; 13891960816@163.com

Received 8 July 2022; Revised 8 August 2022; Accepted 25 August 2022; Published 6 September 2022

Academic Editor: Xueliang Wu

Background. Morbid obesity is one of the fastest-growing subgroups of obesity and is associated with high mortality, with an estimated 2.8 million people dying from obesity each year. *Objective*. This research sets out to elucidate the impact of sevoflurane (Sevo) inhalation anesthesia on the clinical outcome of morbidly obese (MO) patients undergoing laparoscopic bariatric surgery (LBS). *Methods*. A retrospective study was conducted on 150 MO patients undergoing LBS in the Second Affiliated Hospital of Xi'an Jiaotong University from November 2019 to November 2021. According to the difference of anesthesia methods, 100 patients with Sevo anesthesia were set as group A, and 50 patients with propofol (P) anesthesia were set as group B. Intergroup comparisons were performed in terms of eye-opening time, tracheal intubation removal time, directional force recovery, heart rate (HR), mean arterial pressure (MAP), peak airway pressure (P_{peak}), plateau pressure (P_{plat}), standard time out of PACU, postoperative food intake (FI), length of stay (LOS), and complication rate. *Results*. Group A had a shorter time to open eyes, remove tracheal intubation, and restore directional force than Group B, with better recovery of HR, MAP, P_{peak}, and P_{plat}. Group A was also superior to Group B in the standard time out of PACU, postoperative FI, and LOS, with a lower complication rate. *Conclusions*. Sevo inhalation anesthesia is more effective and safer for MO patients undergoing LBS.

1. Introduction

Obesity is a chronic condition defined as body mass index (BMI) > 30 kg/m^2, of which morbid obesity, defined as body mass index (BMI) > 40 kg/m^2, is one of the fastest-growing subgroups [1, 2]. In recent years, there has been a gradual increase in the rate of obesity, accompanied by a dramatic increase in obesity-related metabolic diseases, including type 2 diabetes [3, 4], and ileal Crohn's disease [5]. Morbid-obesity-related conditions such as stroke, acute myocardial infarction, hypertension, type 2 diabetes, hyperlipidemia, and obstructive sleep apnea are associated with high mortality rates, with approximately 2.8 million deaths per year among obesity-affected adults [6, 7]. In recent years, treatments for morbid obesity, such as weight-reducing drugs and insulin resistance therapy, have been constantly improved. But bariatric surgery is still very important for morbidly obese (OB) patients. Therefore, this study aims to improve the surgical protocol for MO patients in order to provide a better choice for the clinical treatment of such a patient population.

Bariatric surgery has long been considered the most effective method to treat severe obesity and its complications, with mortality rates falling below 0.1 per cent in the past decade [8]. Currently, the number of patients undergoing bariatric surgery is steadily increasing globally due to increased demand, accessibility, and advances in laparoscopic surgery. However, laparoscopic surgery is associated with a high incidence of complications that can predispose patients to readmission or even death in the absence of strict protection measures [9]. It is shown that appropriate anesthesia can speed up patient recovery and reduce the risk of infection [10]. Therefore, anesthesia for patients is very important. Among them, the application of sevoflurane

(Sevo) inhalation anesthesia is becoming more and more extensive [11]. However, a randomized controlled study suggested that Sevo may produce stress responses of varying degrees during laparoscopic surgery [12]. And among previous studies on Sevo's application in laparoscopic surgery, there are relatively few studies investigating its role in MO patients. Accordingly, in this study, we combined a series of indicators to study the impact of this anesthesia approach on the clinical outcomes of laparoscopic bariatric surgery (LBS) for MO patients.

2. Methods

2.1. General Data. From November, 2019 to November, 2021, 150 MO patients undergoing LBS were selected and assigned to Sevo anesthesia Group A ($n = 100$) and Propofol (P) anesthesia Group B ($n = 50$) according to the difference in inhaled anesthetics during surgery. Inclusion criteria: the participants were all MO patients undergoing LBS in our hospital, with BMI >40 kg/m^2, normal psychology, and communication ability, as well as the consent and signed relevant agreements from patients and their families. Exclusion criteria: surgical contraindications; drug allergies or endocrine system diseases; history of cerebral hemorrhage and cerebral infarction within 1 year; and severe heart and brain organ lesions. This research was conducted after obtaining approval from the Ethics Committee of the Second Affiliated Hospital of Xi'an Jiaotong University.

2.2. Methods. All patients were fasted for 10h and abstained from drinking for 6h preoperatively. The airway was established by tracheal intubation before anesthesia, and preoperative airway pressure monitoring and results recording were performed. All patients underwent LBS in the supine position. Pneumoperitoneum was established during the operation, and pulmonary recruitment maneuver (PRM) were performed every 30 min. The steps of PRM are as follows: (1) The respiration rate and pressure limit were set as 8 beats/min and 40 cm H_2O, respectively; (2) The positive end-expiratory pressure (PEEP) was set as 5 cm H_2O when initiating the ventilation, which was increased by 10 cm H_2O and 15 cm H_2O after 5 times of ventilation to gradually increase the tidal volume (TV) until the peak airway pressure (P_{peak}) reached 40 cm H_2O; (3) TV was restored to the level before PRM by gradually reducing the PEEP to 10 cm H_2O, 5 cm H_2O and 0 cm H_2O. Scopolamine was injected intramuscularly 30 min before anesthesia. After opening the patient's venous access, 10 ml/(kg·h) Sodium Lactate Ringer's Injection was administered intravenously, and the mask oxygen inhalation was maintained at 2–4 L/min. The patient's heart rate (HR) and mean arterial pressure (MAP) were detected by puncture and catheterization around the left artery under local anesthesia. Besides, the patient was given an iv bolus of 0.2 mg/kg atracurium and 0.4 g/kg sufentanil. Furthermore, Group B was given 3 mg/kg P, while Group A was given Sevo with an initial and a maximum inhalation concentration of 7.0% and 8.0%, respectively. The patient underwent mechanical ventilation after spontaneous breathing disappeared, with a respiratory ratio of 1 : 1.5, a frequency of 12 times/min and a TV of 8–9 ml/kg. The anesthesia concentration was adjusted according to the bispectral index scale (BIS), HR, and blood pressure (BP) of patients, and BIS was maintained at 40–50 to keep the HR stable. Urapidil was given if BIS <40 and BP was 120% above normal. Phenylephrine was administered if the patient's BP was below 70% of normal; in cases with HR > 90 beats/min, esmolol was given, while atropine was given to those with HR < 50 beats/min. The anesthetic concentration was increased once BIS >50 was observed; 5 μg of sufentanil was administered when the patient's HR was more than 90 beats/min or the BP was 120% higher than normal. Phenylephrine was given if BP was below 70% of normal. And in those with a HR < 50 beats/min, atropine was given. The inhalation of P and Sevo was gradually reduced 15 min before surgery, and withdrawn after the completion of the operation. When patients resumed spontaneous breathing, 0.5 mg atropine, and 1 mg neostigmine were injected. Airway pressures were remonitored in all patients postoperatively and the results were recorded.

2.3. Endpoints

2.3.1. Anesthesia Recovery Time. The times of eye-opening time (from stopping anesthetics to being awakened to open eyes), the time of tracheal intubation removal (from withdrawal of anesthetics to removal of bronchial intubation) and the time of restoring orientation (from withdrawal of anesthetics to blinking and coughing as instructed) were observed and recorded.

2.3.2. Hemodynamics. The preoperative and postoperative hemodynamics (HR, MAP) were compared.

2.3.3. Pulmonary Function (PF). The pre- and posttreatment PF (P_{peak}, plateau pressure (P_{plat})) of the two groups was compared.

2.3.4. Postoperative Recovery. The two cohorts were also compared in terms of postoperative recovery as assessed by the following indices: the standard time out of post-anesthesia care unit (PACU), postoperative food intake, and length of stay (LOS).

2.3.5. Complication Rate. The postoperative complications were compared. The related indicators included nausea, vomiting, labored breathing, and chills.

2.4. Statistical Processing. SPSS19.0 (Asia Analytics Formerly SPSS China) and GraphPad Prism 6 (GraphPad Software, San Diego, USA) were employed for comprehensive statistical analysis and visualization of data, respectively. Enumeration data (sex, family status, etc.), denoted by number of cases/percentage (n/%), were compared by the $\chi 2$ test; the t-test was used to identify the

Table 1: General data of two groups of patients.

Classification	Group A ($n = 100$)	Group B ($n = 50$)	t/χ^2	P
Sex			0.487	0.485
Male	54 (54.00)	30 (60.00)		
Female	46 (46.00)	20 (40.00)		
Age (years)	47.10 ± 6.04	48.72 ± 6.43	1.080	0.284
BMI (kg/m^2)	42.01 ± 3.08	42.70 ± 2.76	0.969	0.336
Family type			0.642	0.423
Nuclear family	83 (83.00)	44 (88.00)		
Others	17 (17.00)	6 (12.00)		
Place of residence			0.269	0.604
Urban	74 (74.00)	35 (70.00)		
Rural	26 (26.00)	15 (30.00)		
Drinking			0.085	0.770
Yes	80 (80.00)	41 (82.00)		
No	20 (20.00)	9 (18.00)		
Eating habits				
Heavy	75 (75.00)	36 (72.00)	0.156	0.693
Light	25 (25.00)	14 (28.00)		

difference of quantitative data (age, BMI, etc.) denoted by $(\overline{x} \pm s)$. A significance level of $P < 0.05$ was used in this study.

3. Results

3.1. General Information. Groups A and B differed insignificantly in a series of general data like sex, age, BMI, family status, and drinking (yes/no) ($P > 0.05$) (Table 1).

3.2. Recovery Time from Anesthesia. After comparing patients' anesthesia recovery, it was found that the eye-opening time, tracheal intubation removal time and directional force recovery time were significantly shorter in Group A compared with Group B, with statistical significance ($P < 0.05$) (Figure 1).

3.3. Hemodynamics. The comparison of patients' hemodynamics revealed statistically higher posttreatment HR and MAP in Group A versus Group B, showing statistical significance ($P < 0.05$) (Figure 2).

3.4. PF. The intergroup comparison of patients' PF also determined statistically lower posttreatment P_{peak} and P_{plat} in Group A compared with Group B ($P < 0.05$) (Figure 3).

3.5. Comparison of Postoperative Recovery. The comparison of postoperative recovery between groups showed statistically shorter standard time out of PACU, postoperative eating time and LOS in Group A compared with Group B ($P < 0.05$) (Figure 4).

3.6. Complication Rate. Comparing the complication rate between Groups A and B, we found a statistically lower postoperative complication rate in Group A ($P < 0.05$) (Table 2).

4. Discussion

Morbid obesity is an extremely challenging disease that affects every aspect of patients' lives [13]. Minimally invasive bariatric surgery is becoming increasingly popular because of the disappointing long-term outcomes of medical and behavioral interventions [14]. Of these, LBS is by far the most popular, accounting for more than 50 to 60 percent of global bariatric surgery [15]. Although various clinical studies have shown that LBS has a favorable effect on weight reduction, it will still bring a series of complications if not performed with good anesthesia [16, 17]. In this section, we will discuss the anesthetic effect of Sevo based on the findings of this clinical study.

From the perspective of anesthesia recovery time, Group A using Sevo had shorter eye-opening time, earlier tracheal intubation removal, and faster directional force recovery than Group B using *P*. Although anesthesia benefits various surgical procedures and patients, improper anesthesia puts patients at greater risk of neurocognitive impairment and even reduces their processing speed and impairs their fine motor abilities [18]. In an animal model, neuroinflammation and other damage in addition to cognitive impairment, have been found if anesthetics are poorly chosen [19, 20]. So, the choice of anesthetics is very important in surgery. Sevo, a recognized inhalation anesthetic extensively used in various surgical procedures [21], has antioxidant stress and anti-inflammatory properties, which are important in protecting organs from stress-induced damage [22]. *P*, another drug most commonly used in international anesthesia and intensive care, also has good pharmacokinetics and rapid and reversible sedation [23]. However, it comes with obvious disadvantages, as it will not only cause complications such as severe metabolic acidosis and bradycardia-induced cardiac arrest, but even lead to rhabdomyolysis and acute kidney injury (AKI), all of which compromise the anesthetic effect [24]. Therefore, the recovery from anesthesia was faster in Group A. And combining the results of PF and hemodynamics, it is clear

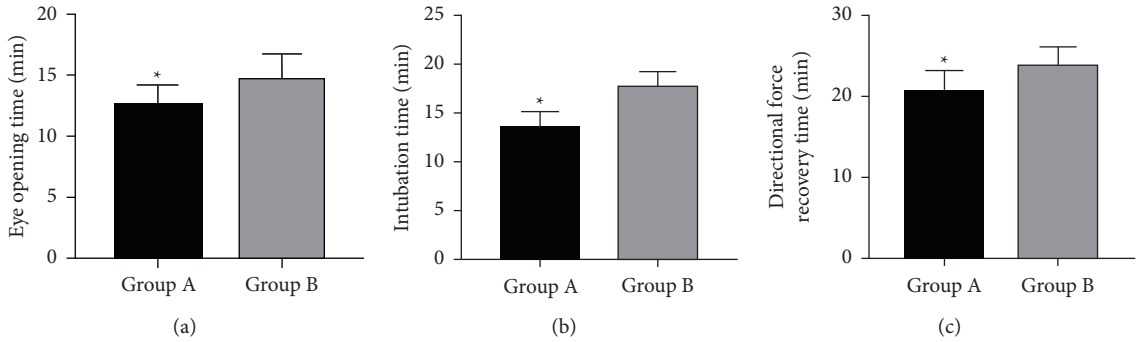

Figure 1: Time of recovery from anesthesia. (a) Eye-opening time: Group A presented shorter eye opening time than Group B ($P < 0.05$). (b) Intubation time: Group A had shorter intubation time than Group B ($P < 0.05$). (c) Directional force recovery time: the directional force recovery time was significantly shorter in Group A than in Group B ($P < 0.05$). Note: $^{*}P < 0.05$ vs. Group B.

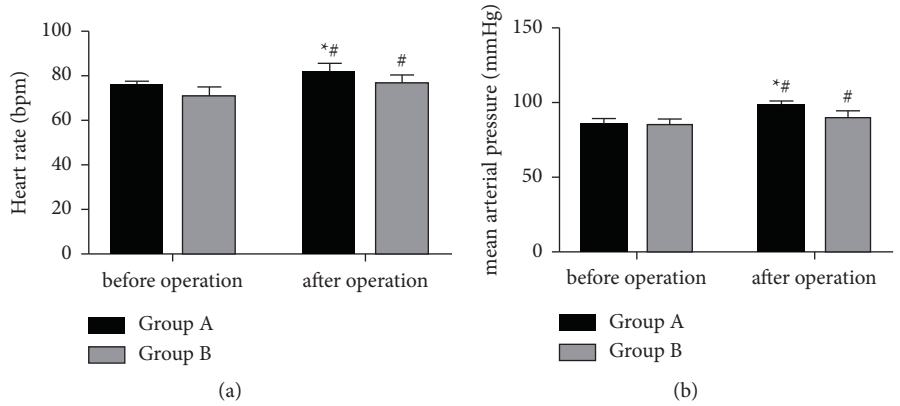

Figure 2: Hemodynamics. (a) Heart rate: After surgery, the heart rate of both groups showed significant changes, with a high level in Group A compared with Group B ($P < 0.05$). (b) Mean arterial pressure: There were significant changes in the mean arterial pressure in both groups after operation, and the level was significantly higher in Group A versus Group B ($P < 0.05$). Note: $^{*}P < 0.05$ vs. Group B; $^{\#}P < 0.05$ vs. after treatment.

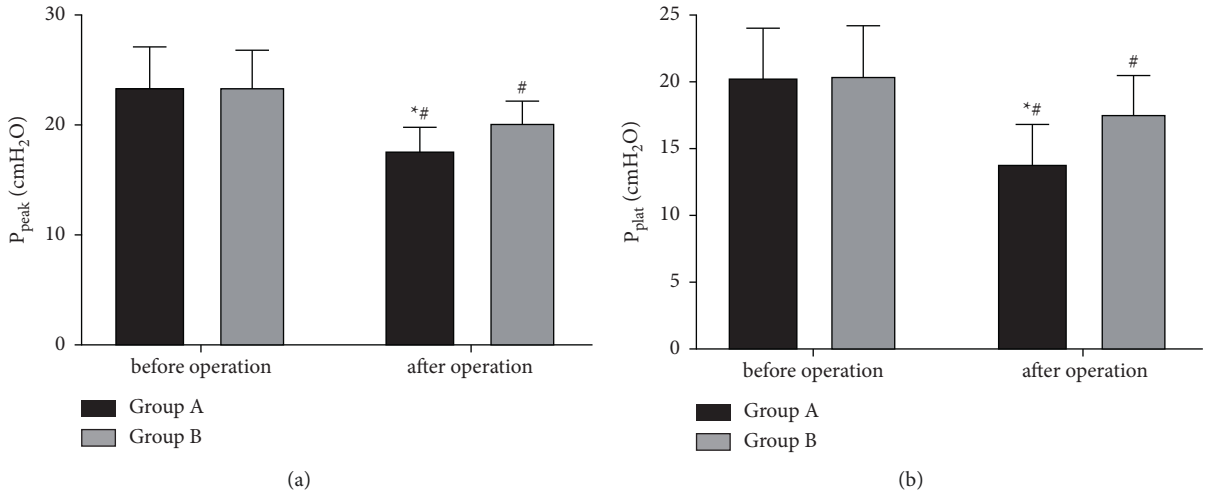

Figure 3: Pulmonary function. (a) P_{peak}: There were significant changes in P_{peak} in both groups postoperatively, with a lower $_{P}$peak in Group A versus Group B ($P < 0.05$). (b) Pplat: Postoperatively, the P_{plat} changed statistically in both groups and was lower in Group A ($P < 0.05$). Note: $^{*}P < 0.05$ vs. Group B; $^{\#}P < 0.05$ vs. after treatment.

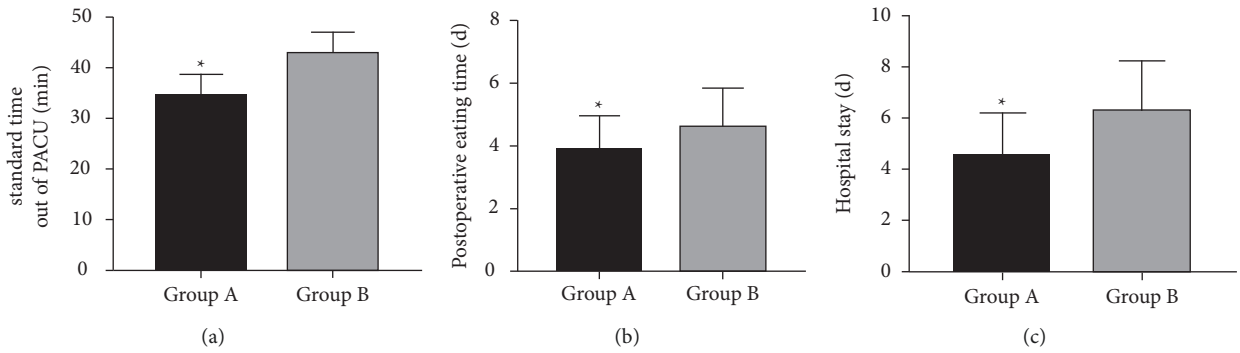

Figure 4: Postoperative recovery. (a) Standard time out of PACU : The standard time out of PACU was significantly shorter in Group A than in Group B ($P < 0.05$). (b) Postoperative feeding time: Group A showed shorter postoperative feeding time than Group B ($P < 0.05$). (c) Hospital stay: The hospital stay was significantly shorter in Group A than in Group B ($P < 0.05$). Note: $^*P < 0.05$ vs. B group.

Table 2: Incidence of complications after treatment in two groups.

	Group A ($n = 100$)	Group B ($n = 50$)	χ^2	P
Nausea	2 (2.00)	3 (6.00)	—	—
Vomiting	0 (0.00)	2 (4.00)	—	—
Labored breathing	0 (0.00)	1 (2.00)	—	—
Chills	1 (1.00)	4 (8.00)		
Complication rate	3 (3.00)	10 (20.00)	12.170	<0.001

that Sevo used in Group A protected the lungs and heart from pressure, resulting in better PF and hemodynamics than Group B. It suggests that not only may the effects of anesthesia be impaired if improper anesthetics are used, but also the recovery of PF and hemodynamics. In the present work, Sevo allowed patients in Group A to wake up more quickly than *P*, with better and effective recovery of PF and hemodynamics. In the study on the application of Sevo in elderly patients with lung cancer, Qin et al. [25] also suggested that compared with *P*, Sevo inhalation general anesthesia can more effectively improve PF with less effect on patients' cognitive function, which is consistent with our results.

In terms of postoperative complication rate and patient recovery, a lower complication rate and better recovery of various indicators were determined in Group A. It has been indicated that volatile anesthetics are safe and effective. The use of Sevo promotes early extubation and facilitates rapid transfer of patients from the operating room to the recovery room, which has a positive effect on patient recovery and restores the degree of respiratory protective reflexes and arousal as quickly as possible [26, 27]. *P* anesthesia is not only less effective than volatile anesthetics such as Sevo but also less safe, with greater side effects [28]. Therefore, the postoperative complication rate in Group A is lower, indicating better safety. In combination with these findings, Sevo has more favorable anesthetic effects, better recovery effects on PF and hemodynamics of patients, and higher safety than *P*, which explains better postoperative recovery in patients who used Sevo.

There are still many deficiencies in this study. Due to the limitations of research conditions, we were unable to detect the relevant molecular indicators of patients. Nor have we investigated patients' status during surgery and their satisfaction with the two surgical anesthesia methods. In future studies, we will supplement these tests while continuously improving the surgical procedures to facilitate patients' recovery.

5. Conclusion

Collectively, Sevo inhalation anesthesia has a better anesthetic effect for MO patients undergoing LBS, with a higher safety profile, which is worthy of clinical promotion [29].

Data Availability

The labeled dataset used to support the findings of this study are available from the corresponding author upon request.

Conflicts of Interest

The author declare that there are no conflicts of interest.

References

[1] S. Milic, D. Lulic, and D. Stimac, "Non-alcoholic fatty liver disease and obesity: biochemical, metabolic and clinical presentations," *World Journal of Gastroenterology*, vol. 20, no. 28, pp. 9330–9337, 2014.

[2] K. Kido, J. C. Lee, T. Hellwig, and M. P. Gulseth, "Use of direct oral anticoagulants in morbidly obese patients," *Pharmacotherapy: The Journal of Human Pharmacology and Drug Therapy*, vol. 40, no. 1, pp. 72–83, 2020.

[3] P. Saeedi, I. Petersohn, P. Salpea et al., "Global and regional diabetes prevalence estimates for 2019 and projections for 2030 and 2045: results from the international diabetes federation diabetes atlas, 9th edition," *Diabetes Research and Clinical Practice*, vol. 157, Article ID 107843, 2019.

[4] D. Trico, D. Moriconi, R. Berta et al., "Effects of low-carbohydrate versus mediterranean diets on weight loss, glucose metabolism, insulin kinetics and beta-cell function in morbidly obese individuals," *Nutrients*, vol. 13, no. 4, p. 1345, 2021.

[5] D. Blumberg, "Morbidly obese patients with ileocolic Crohn's disease may benefit from robotic surgery," *Journal of the Society of Laparoendoscopic Surgeons*, vol. 25, 2021.

[6] K. M. Flegal, B. K. Kit, H. Orpana, and B. I. Graubard, "Association of all-cause mortality with overweight and obesity using standard body mass index categories: a systematic review and meta-analysis," *JAMA*, vol. 309, no. 1, pp. 71–82, 2013.

[7] G. M. Sangiorgi, A. Cereda, N. Porchetta et al., "Endovascular bariatric surgery as novel minimally invasive technique for weight management in the morbidly obese: review of the literature," *Nutrients*, vol. 13, no. 8, p. 2541, 2021.

[8] P. Mousapour, E. Tasdighi, A. Khalaj et al., "Sex disparity in laparoscopic bariatric surgery outcomes: a matched-pair cohort analysis," *Scientific Reports*, vol. 11, no. 1, Article ID 12809, 2021.

[9] N. T. Nguyen, H. Masoomi, C. P. Magno, X. M. T. Nguyen, K. Laugenour, and J. Lane, "Trends in use of bariatric surgery, 2003-2008," *Journal of the American College of Surgeons*, vol. 213, no. 2, pp. 261–266, 2011.

[10] L. Gannam-Somri, I. Matter, C. Hadjittofi et al., "Combined epidural-general anaesthesia vs general anaesthesia in neonatal gastrointestinal surgery: a randomized controlled trial," *Acta Anaesthesiologica Scandinavica*, vol. 64, no. 1, pp. 34–40, 2020.

[11] C. Han, Z. Zhang, N. Guo et al., "Effects of sevoflurane inhalation anesthesia on the intestinal microbiome in mice," *Frontiers in Cellular and Infection Microbiology*, vol. 11, Article ID 633527, 2021.

[12] L. Miao, X. Lv, C. Huang, P. Li, Y. Sun, and H. Jiang, "Long-term oncological outcomes after oral cancer surgery using propofol-based total intravenous anesthesia versus sevoflurane-based inhalation anesthesia: a retrospective cohort study," *PLoS One*, vol. 17, no. 5, Article ID e0268473, 2022.

[13] S. F. Gullaam Rasul, N. Draman, R. Muhamad et al., "Lived experience after bariatric surgery among patients with morbid obesity in east coast peninsular Malaysia: a qualitative study," *International Journal of Environmental Research and Public Health*, vol. 19, 2022.

[14] W. J. English, E. J. DeMaria, S. A. Brethauer, S. G. Mattar, R. J. Rosenthal, and J. M. Morton, "American Society for Metabolic and Bariatric Surgery estimation of metabolic and bariatric procedures performed in the United States in 2016," *Surgery for Obesity and Related Diseases*, vol. 14, no. 3, pp. 259–263, 2018.

[15] L. Angrisani, A. Santonicola, P. Iovino et al., "Bariatric surgery and endoluminal procedures: IFSO worldwide survey 2014," *Obesity Surgery*, vol. 27, no. 9, pp. 2279–2289, 2017.

[16] R. Peterli, B. K. Wolnerhanssen, T. Peters et al., "Effect of laparoscopic sleeve gastrectomy vs laparoscopic roux-en-Y gastric bypass on weight loss in patients with morbid obesity: the SM-BOSS randomized clinical trial," *JAMA*, vol. 319, no. 3, pp. 255–265, 2018.

[17] P. Salminen, M. Helmio, J. Ovaska et al., "Effect of laparoscopic sleeve gastrectomy vs laparoscopic roux-en-Y gastric bypass on weight loss at 5 Years among patients with morbid obesity: the SLEEVEPASS randomized clinical trial," *JAMA*, vol. 319, no. 3, pp. 241–254, 2018.

[18] D. O. Warner, M. J. Zaccariello, S. K. Katusic et al., "Neuropsychological and behavioral outcomes after exposure of young children to procedures requiring general anesthesia: the mayo anesthesia safety in kids (MASK) study," *Anesthesiology*, vol. 129, no. 1, pp. 89–105, 2018.

[19] L. Vutskits and Z. Xie, "Lasting impact of general anaesthesia on the brain: mechanisms and relevance," *Nature Reviews Neuroscience*, vol. 17, no. 11, pp. 705–717, 2016.

[20] Y. Yu, Y. Yang, H. Tan et al., "Tau contributes to sevoflurane-induced neurocognitive impairment in neonatal mice," *Anesthesiology*, vol. 133, no. 3, pp. 595–610, 2020.

[21] Y. Wang, X. Zhang, J. Tian, G. Liu, X. Li, and D. Shen, "Sevoflurane alleviates LPS-induced acute lung injury via the microRNA-27a-3p/TLR4/MyD88/NF-κB signaling pathway," *International Journal of Molecular Medicine*, vol. 44, no. 2, pp. 479–490, 2019.

[22] T. Y. Liang, H. Y. Li, M. Ma, S. Y. Peng, Z. Wang, and G. Chen, "Protective effects of sevoflurane in cerebral ischemia reperfusion injury: a narrative review," *Medical Gas Research*, vol. 11, no. 4, pp. 152–154, 2021.

[23] K. M. Ho and J. Y. Ng, "The use of propofol for medium and long-term sedation in critically ill adult patients: a meta-analysis," *Intensive Care Medicine*, vol. 34, no. 11, pp. 1969–1979, 2008.

[24] S. Hemphill, L. McMenamin, M. C. Bellamy, and P. M. Hopkins, "Propofol infusion syndrome: a structured literature review and analysis of published case reports," *British Journal of Anaesthesia*, vol. 122, no. 4, pp. 448–459, 2019.

[25] Y. Qin, J. Ni, L. Kang, Z. Zhong, L. Wang, and S. Yin, "Sevoflurane effect on cognitive function and the expression of oxidative stress response proteins in elderly patients undergoing radical surgery for lung cancer," *Journal of College of Physicians and Surgeons*, vol. 29, no. 1, pp. 12–15, 2019.

[26] J. Jakobsson, "Desflurane: a clinical update of a third-generation inhaled anaesthetic," *Acta Anaesthesiologica Scandinavica*, vol. 56, no. 4, pp. 420–432, 2012.

[27] Y. Xu, Y. Dong, C. Wang, Q. Jiang, H. Chu, and Y. Tian, "Lovastatin attenuates sevoflurane-induced cognitive disorder in aged rats via reducing Aβ accumulation," *Neurochemistry International*, vol. 148, Article ID 105078, 2021.

[28] K. Varnas, S. J. Finnema, P. Johnstrom et al., "Effects of sevoflurane anaesthesia on radioligand binding to monoamine oxidase-B in vivo," *British Journal of Anaesthesia*, vol. 126, no. 1, pp. 238–244, 2021.

[29] H. C. Tan, J. W. Hsu, E. S. Tai et al., "De novo Glycine synthesis is reduced in adults with morbid obesity and increases following bariatric surgery," *Frontiers in Endocrinology*, vol. 13, Article ID 900343, 2022.

Hindawi
Evidence-Based Complementary and Alternative Medicine
Volume 2023, Article ID 9795602, 1 page
https://doi.org/10.1155/2023/9795602

Retraction

Retracted: *Vitis vinifera* L. Flavones Regulate Hippocampal Neurons via Autophagy in APP/PS1 Alzheimer Model Mice

Evidence-Based Complementary and Alternative Medicine

Received 8 August 2023; Accepted 8 August 2023; Published 9 August 2023

This article has been retracted by Hindawi following an investigation undertaken by the publisher [1]. This investigation has uncovered evidence of one or more of the following indicators of systematic manipulation of the publication process:

(1) Discrepancies in scope
(2) Discrepancies in the description of the research reported
(3) Discrepancies between the availability of data and the research described
(4) Inappropriate citations
(5) Incoherent, meaningless and/or irrelevant content included in the article
(6) Peer-review manipulation

The presence of these indicators undermines our confidence in the integrity of the article's content and we cannot, therefore, vouch for its reliability. Please note that this notice is intended solely to alert readers that the content of this article is unreliable. We have not investigated whether authors were aware of or involved in the systematic manipulation of the publication process.

Wiley and Hindawi regrets that the usual quality checks did not identify these issues before publication and have since put additional measures in place to safeguard research integrity.

We wish to credit our own Research Integrity and Research Publishing teams and anonymous and named external researchers and research integrity experts for contributing to this investigation.

The corresponding author, as the representative of all authors, has been given the opportunity to register their agreement or disagreement to this retraction. We have kept a record of any response received.

References

[1] P. Zhang, Z. Maimaiti, G. Aili, F. Yuan, and H. Xiao, "*Vitis vinifera* L. Flavones Regulate Hippocampal Neurons via Autophagy in APP/PS1 Alzheimer Model Mice," *Evidence-Based Complementary and Alternative Medicine*, vol. 2022, Article ID 8554184, 7 pages, 2022.

Hindawi
Evidence-Based Complementary and Alternative Medicine
Volume 2022, Article ID 8554184, 7 pages
https://doi.org/10.1155/2022/8554184

Research Article

Vitis vinifera L. Flavones Regulate Hippocampal Neurons via Autophagy in APP/PS1 Alzheimer Model Mice

Peng Zhang,[1] **Znafuguli Maimaiti**,[2] **Gulixiati Aili**,[1] **Fang Yuan**,[2] **and Hui Xiao**[1]

[1]*College of Public Health, Xinjiang Medical University, Urumqi, Xinjiang, China*
[2]*College of Basic Medical, Xinjiang Medical University, Urumqi, Xinjiang, China*

Correspondence should be addressed to Fang Yuan; yuanfang398@163.com and Hui Xiao; xh20108262@sina.com

Received 6 July 2022; Revised 1 August 2022; Accepted 5 August 2022; Published 1 September 2022

Academic Editor: Xueliang Wu

Background. Alzheimer's disease (AD) is a neurodegenerative disease and our current treatment approach can only delay its course rather than cure it completely. Flavones from *Vitis vinifera* L. have been reported to promote synaptic plasticity and indirectly affect the expression of cholinergic neurotransmitters in a rat model of Alzheimer's disease. *Objective*. The aim of the study is to explore the effect of *Vitis vinifera* L. in APP/PS1 Alzheimer model mice. *Methods*. APP/PS1 AD mice were used as the research subjects, and the mice were divided into a model group, donepezil group, VTF low-dose group, VTF medium-dose group, and VTF high-dose group. C57BL/6 mice served as a control group. The autophagosomes were observed by a transmission electron microscope, and the expressions of LC3I, LC3IIand Beclin-1 were determined by Western blotting. The results of qRT-PCR are consistent with Western blotting. *Results*. VTF can exert a positive regulatory effect on AD mice by inhibiting autophagy. *Conclusion*. Our study supports that intragastrically administration of VTF is effective and operable in Alzheimer's disease mice, and that inhibition of excessive autophagy may be one of the potential reasons why VTF exerts a therapeutic effect on AD.

1. Introduction

Alzheimer's disease is a neurodegenerative disease that affects the elderly and is the most common cause of dementia in the elderly population [1]. The pathological hallmarks and typical symptoms of AD are the accumulation of senile plaques, neurofibrillary tangles, and progressive loss of memory [2–6]. However, the specific pathogenesis and causes of AD are still unclear. Currently, the scholars generally believe that it may be related to the environment, genetics, and aging. Conventional drugs in clinical practice at present, such as cholinesterase inhibitors and glutamate receptor antagonists, can only alleviate the disease process but cannot completely cure the disease [1, 7]. Therefore, exploring effective treatment strategies for AD is still an urgent problem to be solved in the scientific community.

Autophagy plays a crucial role in the development of many neurodegenerative diseases, and autophagy is considered to be a double-edged sword [8, 9]. Interestingly, most of our current scientific research on AD agrees that autophagy is beneficial in AD, and it might initiate self-protection through removing excessive intracellular peptide deposits and damaged organelles [10–15]. Beclin-1 is regarded as a marker protein of autophagosome formation and inhibiting the expression of beclin1 increases the deposition of Aβ in AD animal/cell models [16–18]. However, in some cases, hyperactivated autophagy has a negative effect on neuron survival. Therefore, inhibition of excessive autophagy may be an effective target for the treatment of AD.

Eating flavonoid-rich plants and fruits can repair damaged neurons [19]. *Vitis vinifera* L. flavones (VTF) is a flavonoid extracted from grapes. Recent studies have reported that VTF can promote synaptic plasticity, affect the expression of cholinergic neurotransmitters, and improve the learning and memory abilities in AD model rats [20]. However, it is unclear whether VTF can prevent hippocampal neurons damage through inhibiting autophagy. In this study, the changes of autophagy-related protein expression in the brain tissues were analyzed by qRT-PCR and

western blotting. Our work revealed that the mechanism by which VTF exerts neuroprotective effects in AD models may be related to the suppression of excessive autophagy.

2. Materials and Methods

2.1. Animals. We purchased 6-month-old APP/PS-1 double-transgenic male mice (body weight (30 ± 10) g) from Promoter Biotechnology Co., Ltd. (Beijing, China) and used C57BL/6 mice as controls. A total of 90 mouse were selected, 15 in each group. Mice were housed under specific pathogen-free conditions, the environmental parameters were temperature 23 ± 2°C, humidity 60 ± 5%. The animal room where the mice were housed performed a 12 h light/12 h dark cycle, and the mice were given sufficient food, water and living space. All of the experiments followed the ethical guidelines of Xinjiang Medical University (Ethical approval number: IACUC-20210507-07.).

2.2. Preparation of Flavones from Vitis vinifera L. We added 95% ethanol to *V. vinifera* L. for extraction, then concentrated the extract into paste and mixed with water to form a suspension. AB-8 macroporous resin were used to elute and purify. Finally, the freeze-dried brown-yellow powder is VTF.

2.3. Animal Grouping and Drug Administration. We placed the experimental mice in the SPF laboratory and then administered the gavage after 1 week of adaptive feeding. 6-Month-old APP/PS1 AD mice were randomly divided into a model group and treatment group. The treatment group including a donepezil group (positive control), VTF low-dose group (70 mg/kg), a VTF medium-dose group (210 mg/kg), and a VTF high-dose group (420 mg/kg). The wild-type C57BL/6 male mice were taken as the control group, there are 6 groups in total. The model group were given the same concentration of CMC-Na solution (1.0 ml/100 g). All of the mice were intragastrically administered once a day (1.0 ml/100 g) for 8 weeks. Double blind method is adopted to avoid subjective influence. Mouse in normal control group were given distilled water by gavage; The positive control group was given donepezil solution (donepezil powder dissolve in distilled water and shake well with 0.5 mg/kg) by gavage.

2.4. Western Blot. We collected mice hippocampus tissues and extracted the protein solution. We then tested the protein concentration in each sample with BCA kit. We separated the protein through SDS-PAGE and transferred it onto PVDF membranes. After blocking the excess binding sites on the membrane with nonfat dry milk, the PVDF membranes were incubated at 4°C with the following antibodies for one night (primary antibodies): LC3-I (1: 500, Abcam, LC3-II (1: 500, Abcam), Beclin-1 (1: 500, Abcam) and GAPDH (1: 500, Abcam). The PVDF membranes were washed with PBS supplemented with 0.1% Tween 20 and then incubated with the corresponding secondary antibody for 1 h at room temperature. The membranes were visualized using an LAS-4000 chemiluminescence detection system. We used Image J software to quantify the band densities.

2.5. Quantitative Reverse Transcription-Polymerase Chain Reaction (qRT-PCR). According to the kit instructions (ThermoFisher Scientific., Carlsbad, United States), total RNA from hippocampus tissues was extracted and reverse-transcribed into cDNA. After adding the fluorescent dye, the quantitative real-time PCR was performed using quantitative PCR (Applied Biosystems, CA, United States) with corresponding primers (Table 1). The levels of mRNA were normalized in relevance to GAPDH.

2.6. Transmission Electron Microscopy. Brain tissues were fixed with 6% glutaraldehyde and cut into slices, and then we stained these slices with lead. We observed and photographed autophagosomes in the mice hippocampus using transmission electron microscopy.

2.7. Statistical Analysis. We used SPSS software (version 20.0) and GraphPad Prism 6 software (version 4.0) to performed statistical analyses and data are presented as mean ± SEM. The data of western blot and qRT-PCR were analyzed by one-way ANOVA followed by the *post hoc* Bonferroni multiple comparison test. $P < 0.05$ was considered statistically significant.

3. Results

3.1. Vitis vinifera L. Flavones Can Inhibit Excessive Autophagy in Hippocampus. The autophagy-related proteins LC3-I, LC3-II, and Beclin-1 were identified. Western blot results showed that the protein expression of Beclin-1 in the model group was significantly higher than that in the treatment group (Figure 1. $P < 0.05$), and in the treatment group, the expression level of Beclin-1 was negatively correlated with the dose of VTF. We speculate that the significantly decreased expression of beclin1 after treatment was related to the repression of autophagy. In addition, we tested the change trend of LC3-II/LC3-I, our result indicated that the excessive autophagy in hippocampus was inhibited, which further confirmed our previous conjecture.

To further verify the role of VTF in regulating autophagy from the gene level, we extracted total RNA from mice hippocampus and performed RT-qPCR. The mRNA levels of LC3 and Beclin-1 in the hippocampus of the model group were much higher than those of the treatment group, and the decrease of LC3 and Beclin-1 in the treatment group were VTF concentration-dependent, and the difference among the groups was statistically significant ($P < 0.01$, Figure 2). The gene expression trend of p62 is consistent with Beclin-1 and LC3; we speculate that this may be because the mechanism by which VTF exert the positive effects through inhibiting excessive accumulation of autophagy. Our results demonstrate that VTF can repress the expression of pro-

Table 1: Primer sequence of q RT-PCR.

Gene	Primer	Sequence (5′-3′)	PCR products
Mus GAPDH	Forward Reverse	ATGGGTGTGAACCACGAGA CAGGGATGATGTTCTGGGCA	229bp
Mus Beclin-1	Forward Reverse	GATTGGACCAGGAGGAAG AAGGTGGCATTGAAGACA	160bp
Mus LC3	Forward Reverse	AATGCTAACCAAGCCTTCTTCCTCC AGCCGTCTTCATCTCTCTCACTCTC	103bp
Mus p62	Forward Reverse	CCTGAAGAATGTGGGGGAGAGTGTG TGGAACTTTCTGGGGTAGTGGGTGT	122bp

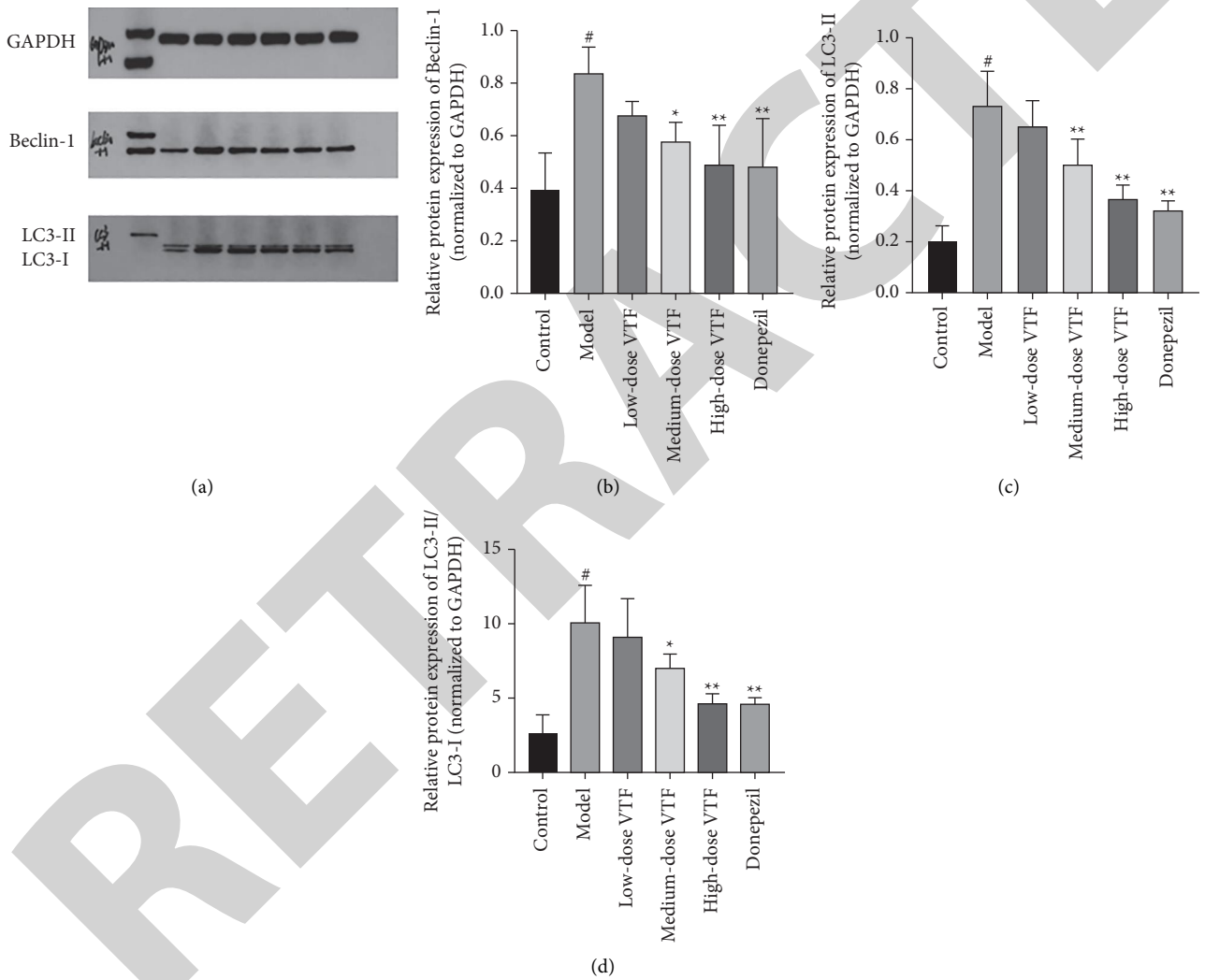

Figure 1: VTF administration inhibits excessive autophagy In AD models. Representative western blots and quantitation data of apoptosis-related proteins. (a) The levels of the apoptosis-related proteins are reported as the value normalized to GAPDH for each sample. (b–d) Compared to the model group, the mean percentage of beclin1, LC3-II, LC3-II/LC3-I was significantly decreased in the treatment group. Relative expression expressed as the mean ± SEM. #The p-value was less than 0.01 compared with the control group. *The p value was less than 0.05 compared with the model group. **The p value was less than 0.01 compared with the model group.

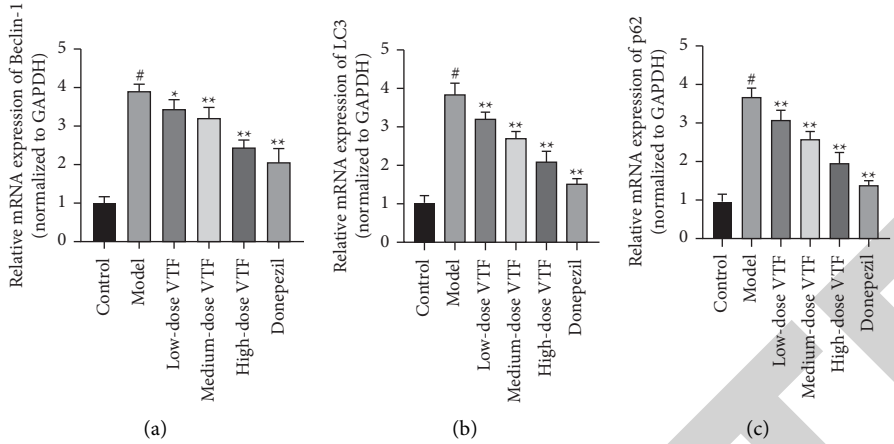

Figure 2: Comparison of relative mRNA expression of autophagy-relate proteins in different groups. (a–c) Compared to the model group, the mean percentage of beclin1, LC3, P62 was significantly decreased in the treatment group. Relative expression expressed as the mean ± SEM. #The p-value was less than 0.01 compared with the control group. *The p value was less than 0.05 compared with the model group. **The p value was less than 0.01 compared with the model group.

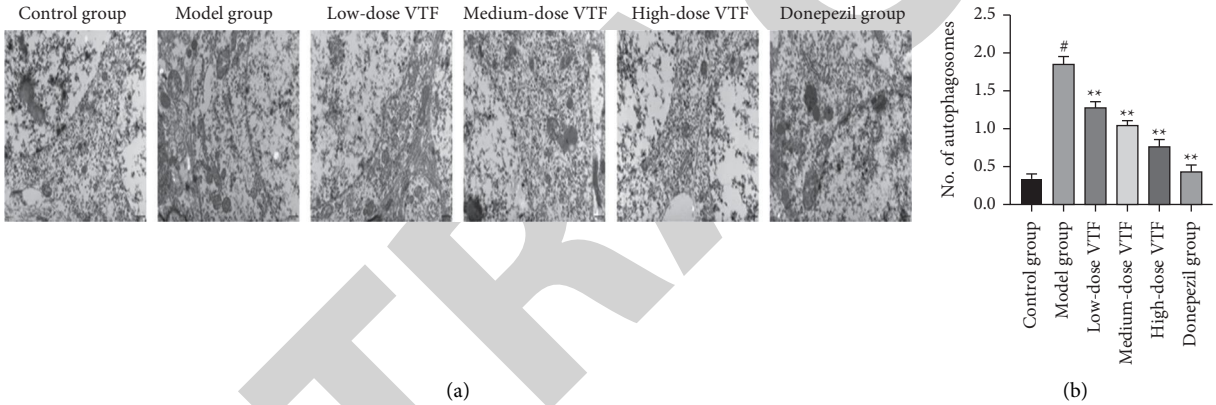

Figure 3: Electron microscopy-based detection of autophagosome in hippocampal neurons. Representative images of autophagosome in the six groups, the autophagosome was observed under an electron microscope at ×4.0 k magnification (bar = 500 nm). Compared with the model group, the number of autophagosomes in the treatment group grow in number with the decreasing dose of VTF. *The p value was less than 0.05 compared with the model group. **The p value was less than 0.01 compared with the model group.

autophagy-related proteins in the hippocampus. These results confirm those of the Western blot.

The autophagosomes were detected in the hippocampus using TEM in a ×4.0 k field of view (Figure 3). Compared with the model group, the number of autophagosomes in the treatment group grow in number with the decreasing dose of VTF. In fact, the model group has the highest number of autophagosomes. Therefore, the researchers speculated that VTF could exert its positive effects by suppression autophagy in the hippocampus.

Based on the above experimental results, we believe that *Vitis vinifera* L. Flavones. can inhibit excessive autophagy in hippocampus.

4. Discussion

Flavonoids are polyphenolic compounds that are widely present in plants and can be successfully extracted from tea, cocoa, and wine [21–23]. Emerging evidence suggests that flavonoids can act as oxygen free radical scavengers and antioxidants [24, 25]. Flavonoids can smoothly cross the blood-brain barrier (BBB) in neurological diseases [26], it can exert neuroprotective and anti-inflammatory effects in the central nervous system and improve learning and memory in memory-impaired mice [27–30]. Studies have shown that a variety of flavonoids may have positive therapeutic effects on AD. Vepsäläinen et al. and colleagues fed APP/PS1 mice with anthocyanin-enriched bilberry and blackcurrant extracts, they found that it alleviated spatial working memory deficits and altered amyloid precursor protein (APP) processing [31]. In addition, Nobiletin, a citrus flavonoid, was found to improve memory impairment and Abeta pathology in a transgenic mice model of Alzheimer's disease [32]. Flavonoids can also reduce amyloid beta production in AD by mediating presenilin-1 phosphorylation [33]. In general, flavonoids are currently very promising drugs for the treatment of AD.

Previous studies have shown that VTF can promote synaptic plasticity and indirectly affect the expression of cholinergic neurotransmitters [20]. Our work attempts to explore the underlying mechanisms more deeply from the perspective of autophagy. We believe that this positive effect of VTF may be related to inhibiting excessive autophagy in Alzheimer's disease model mice.

The metabolism of Aβ and Tau is strongly associated with autophagy, regulating autophagy is regard as one of the most promising therapeutic strategies [34–37]. Under normal circumstances, activation or a certain degree of enhancement of autophagy can significantly eliminate Aβ deposition, promote Tau clearance, and alleviate neurodegeneration [34, 38, 39]. Some researchers added $A\beta_{1-42}$ to SH-SY5Y cells and found that it can cause a certain cytotoxic effect on the cells. After administering rapamycin (an autophagy inducer), it can not only reduce the level of $A\beta_{1-42}$ but also exert a protective effect in SH-SY5Y cells [40]. In the APP/PS1 AD mouse model, it was also found that activating autophagy could reduce senile plaques formed by Aβ deposition and alleviate memory and cognitive impairment in mice [14, 41–44]. In addition, the formation of autophagosomes is also often accompanied by a decrease in the content of phosphorylated Tau [45, 46]. However, there are also some research results supporting that autophagy does not always play a positive role in AD models. ATG7 is an essential protein for cellular degradation and recycling associated with autophagy. Some scholars have tried to cross the amyloid precursor protein (APP) transgenic mice with ATG7-selective knockout mice. It was found that Aβ secretion was inhibited due to the lack of autophagy, and it was surprising to find that the burden of extracellular Aβ protein was greatly reduced. [47, 48]. Both of these opposite results have been scientifically verified in a certain degree. Our team believes that the reason for this phenomenon may be because the two-sided nature of autophagy itself makes it play different effects in different situations. Maybe it is a good choice to bring the level of autophagy back to a balanced level.

A previous interesting study observed that VTF can enhance synaptic plasticity and improve cognitive impairment in AD model mice, which indicates that VTF has a great therapeutic potential in neurodegenerative diseases [20]. Our work attempts to build on the previous work to further investigate the reasons why VTF plays a positive role and its possible relationship with autophagy.

4.1. Limitation. "Autophagy" itself is a complex concept. We did not evaluate the change of autophagy flow nor did we conduct a control experiment to observe whether the positive effect of VTF can be reversed after using autophagy inhibitors. Relevant research will be further carried out in the future.

5. Conclusion

Based on the above research work, we believe that VTF can affect the pathological changes of Alzheimer's disease by inhibiting excessive autophagy. This discovery provides a new theoretical basis for the therapeutic prospects of VTF in the treatment of Alzheimer's disease.

Data Availability

The data used to support the findings of this study are available from the corresponding author upon request.

Conflicts of Interest

The authors declare that they have no conflicts of interest.

Acknowledgments

The study was supported by the National Natural Science Foundation of China, China (No. 8196140312).

References

[1] H. Mai, W. Fan, Y. Wang et al., "Intranasal administration of miR-146a agomir rescued the pathological process and cognitive impairment in an AD mouse model," *Molecular Therapy-Nucleic Acids*, vol. 18, pp. 681–695, 2019.

[2] M. K. Shin, M. S. Choi, H. J. Chae, J. W. Kim, H. G. Kim, and K. L. Kim, "Ganglioside GQ1b ameliorates cognitive impairments in an Alzheimer's disease mouse model, and causes reduction of amyloid precursor protein," *Scientific Reports*, vol. 9, no. 1, p. 8512, 2019.

[3] D. J. Selkoe, "Normal and abnormal biology of the beta-amyloid precursor protein," *Annual Review of Neuroscience*, vol. 17, no. 1, pp. 489–517, 1994.

[4] T. E. Golde, D. R. Borchelt, B. I. Giasson, and J. Lewis, "Thinking laterally about neurodegenerative proteinopathies," *Journal of Clinical Investigation*, vol. 123, no. 5, pp. 1847–1855, 2013.

[5] G. S. Bloom, "Amyloid-β and tau: the trigger and bullet in Alzheimer disease pathogenesis," *JAMA Neurology*, vol. 71, no. 4, pp. 505–508, 2014.

[6] M. G. Spillantini and M. Goedert, "Tau pathology and neurodegeneration," *The Lancet Neurology*, vol. 12, no. 6, pp. 609–622, 2013.

[7] J.-Y. Han, L. M. Besser, C. Xiong, W. A. Kukull, and J. C. Morris, "Cholinesterase inhibitors may not benefit mild cognitive impairment and mild Alzheimer disease dementia," *Alzheimer Disease and Associated Disorders*, vol. 33, no. 2, pp. 87–94, 2019.

[8] S. Krishnan, Y. Shrestha, D. P. W. Jayatunga, S. Rea, R. Martins, and P. Bharadwaj, "Activate or inhibit? implications of autophagy modulation as a therapeutic strategy for Alzheimer's disease," *International Journal of Molecular Sciences*, vol. 21, no. 18, p. 6739, 2020.

[9] D. J. Klionsky, G. Petroni, R. K. Amaravadi et al., "Autophagy in major human diseases," *The EMBO Journal*, vol. 40, no. 19, Article ID e108863, 2021.

[10] M. Eshraghi, A. Adlimoghaddam, A. Mahmoodzadeh et al., "Alzheimer's disease pathogenesis: role of autophagy and mitophagy focusing in microglia," *International Journal of Molecular Sciences*, vol. 22, no. 7, p. 3330, 2021.

[11] R. Luo, L.-Y. Su, G. Li et al., "Activation of PPARA-mediated autophagy reduces Alzheimer disease-like pathology and cognitive decline in a murine model," *Autophagy*, vol. 16, no. 1, pp. 52–69, 2020.

[12] Q. Feng, Y. Luo, X.-N. Zhang et al., "MAPT/Tau accumulation represses autophagy flux by disrupting IST1-regulated ESCRT-III complex formation: a vicious cycle in Alzheimer neurodegeneration," *Autophagy*, vol. 16, no. 4, pp. 641–658, 2020.

[13] A. Wani, M. Gupta, M. Ahmad et al., "Alborixin clears amyloid-β by inducing autophagy through PTEN-mediated inhibition of the AKT pathway," *Autophagy*, vol. 15, no. 10, pp. 1810–1828, 2019.

[14] A. Wani, S. B. Al Rihani, A. Sharma et al., "Crocetin promotes clearance of amyloid-β by inducing autophagy via the STK11/LKB1-mediated AMPK pathway," *Autophagy*, vol. 17, no. 11, pp. 3813–3832, 2021.

[15] Y. Zhao, Y. Zhang, J. Zhang, X. Zhang, and G. Yang, "Molecular mechanism of autophagy: its role in the therapy of Alzheimer's disease," *Current Neuropharmacology*, vol. 18, no. 8, pp. 720–739, 2020.

[16] M. Deng, L. Huang, and X. Zhong, "β-asarone modulates Beclin-1, LC3 and p62 expression to attenuate Aβ40 and Aβ42 levels in APP/PS1 transgenic mice with Alzheimer's disease," *Molecular Medicine Reports*, vol. 21, no. 5, pp. 2095–2102, 2020.

[17] Y. Yang, S. Chen, J. Zhang et al., "Stimulation of autophagy prevents amyloid-β peptide-induced neuritic degeneration in PC12 cells," *Journal of Alzheimer's Disease*, vol. 40, no. 4, pp. 929–939, 2014.

[18] M. B. Fonseca, S. Solá, J. M. Xavier, P. A. Dionísio, and C. M. P. Rodrigues, "Amyloid β peptides promote autophagy-dependent differentiation of mouse neural stem cells: aβ-mediated neural differentiation," *Molecular Neurobiology*, vol. 48, no. 3, pp. 829–840, 2013.

[19] A. Rodriguez-Mateos, D. Vauzour, C. G. Krueger et al., "Bioavailability, bioactivity and impact on health of dietary flavonoids and related compounds: an update," *Archives of Toxicology*, vol. 88, no. 10, pp. 1803–1853, 2014.

[20] L. Ma, H. Xiao, J. Wen, Z. Liu, Y. He, and F. Yuan, "Possible mechanism of *Vitis vinifera* L. flavones on neurotransmitters, synaptic transmission and related learning and memory in Alzheimer model rats," *Lipids in Health and Disease*, vol. 17, no. 1, p. 152, 2018.

[21] C. M. Liu, J. Q. Ma, S. S. Liu, G. H. Zheng, Z. J. Feng, and J. M. Sun, "Proanthocyanidins improves lead-induced cognitive impairments by blocking endoplasmic reticulum stress and nuclear factor-κB-mediated inflammatory pathways in rats," *Food and Chemical Toxicology*, vol. 72, pp. 295–302, 2014.

[22] G. R. Beecher, "Overview of dietary flavonoids: nomenclature, occurrence and intake," *Journal of Nutrition*, vol. 133, no. 10, pp. 3248s–3254s, 2003.

[23] M. Samsuzzaman, M. S. Uddin, M. A. Shah, and B. Mathew, "Natural inhibitors on airway mucin: molecular insight into the therapeutic potential targeting MUC5AC expression and production," *Life Sciences*, vol. 231, Article ID 116485, 2019.

[24] M. S. Uddin, M. T. Kabir, D. Tewari, B. Mathew, and L. Aleya, "Emerging signal regulating potential of small molecule biflavonoids to combat neuropathological insults of Alzheimer's disease," *The Science of the Total Environment*, vol. 700, Article ID 134836, 2020.

[25] M. S. Uddin, M. T. Kabir, K. Niaz et al., "Molecular insight into the therapeutic promise of flavonoids against Alzheimer's disease," *Molecules*, vol. 25, no. 6, p. 1267, 2020.

[26] A. Elbaz, L. Carcaillon, S. Kab, and F. Moisan, "Epidemiology of Parkinson's disease," *Revue Neurologique*, vol. 172, no. 1, pp. 14–26, 2016.

[27] J. P. Spencer, K. Vafeiadou, R. J. Williams, and D. Vauzour, "Neuroinflammation: modulation by flavonoids and mechanisms of action," *Molecular Aspects of Medicine*, vol. 33, no. 1, pp. 83–97, 2012.

[28] D. H. Kim, S. Kim, S. J. Jeon et al., "Tanshinone I enhances learning and memory, and ameliorates memory impairment in mice via the extracellular signal-regulated kinase signalling pathway," *British Journal of Pharmacology*, vol. 158, no. 4, pp. 1131–1142, 2009.

[29] D. Prakash and G. Sudhandiran, "Dietary flavonoid fisetin regulates aluminium chloride-induced neuronal apoptosis in cortex and hippocampus of mice brain," *The Journal of Nutritional Biochemistry*, vol. 26, no. 12, pp. 1527–1539, 2015.

[30] A. Gomes, R. C. Pimpão, S. Fortalezas et al., "Chemical characterization and bioactivity of phytochemicals from Iberian endemic Santolina semidentata and strategies for ex situ propagation," *Industrial Crops and Products*, vol. 74, pp. 505–513, 2015.

[31] S. Vepsäläinen, H. Koivisto, E. Pekkarinen et al., "Anthocyanin-enriched bilberry and blackcurrant extracts modulate amyloid precursor protein processing and alleviate behavioral abnormalities in the APP/PS1 mouse model of Alzheimer's disease," *The Journal of Nutritional Biochemistry*, vol. 24, no. 1, pp. 360–370, 2013.

[32] H. Onozuka, A. Nakajima, K. Matsuzaki et al., "Nobiletin, a citrus flavonoid, improves memory impairment and Aβ pathology in a transgenic mouse model of Alzheimer's disease," *Journal of Pharmacology and Experimental Therapeutics*, vol. 326, no. 3, pp. 739–744, 2008.

[33] K. Rezai-Zadeh, R. Douglas Shytle, Y. Bai et al., "Flavonoid-mediated presenilin-1 phosphorylation reduces Alzheimer's disease beta-amyloid production," *Journal of Cellular and Molecular Medicine*, vol. 13, no. 3, pp. 574–588, 2009.

[34] H. Kuang, C.-Y. Tan, H.-Z. Tian et al., "Exploring the bi-directional relationship between autophagy and Alzheimer's disease," *CNS Neuroscience and Therapeutics*, vol. 26, no. 2, pp. 155–166, 2020.

[35] W. Zhang, C. Xu, J. Sun, H.-M. Shen, J. Wang, and C. Yang, "Impairment of the autophagy-lysosomal pathway in Alzheimer's diseases: pathogenic mechanisms and therapeutic potential," *Acta Pharmaceutica Sinica B*, vol. 12, no. 3, pp. 1019–1040, 2022.

[36] M. A. Rahman, M. S. Rahman, M. H. Rahman et al., "Modulatory effects of autophagy on APP processing as a potential treatment target for Alzheimer's disease," *Biomedicines*, vol. 9, no. 1, p. 5, 2020.

[37] M. Manczak, R. Kandimalla, X. Yin, and P. H. Reddy, "Hippocampal mutant APP and amyloid beta-induced cognitive decline, dendritic spine loss, defective autophagy, mitophagy and mitochondrial abnormalities in a mouse model of Alzheimer's disease," *Human Molecular Genetics*, vol. 27, no. 8, pp. 1332–1342, 2018.

[38] J. L. Chen, C. Luo, D. Pu et al., "Metformin attenuates diabetes-induced tau hyperphosphorylation in vitro and in vivo by enhancing autophagic clearance," *Experimental Neurology*, vol. 311, pp. 44–56, 2019.

[39] E. Schmukler and R. Pinkas-Kramarski, "Autophagy induction in the treatment of Alzheimer's disease," *Drug Development Research*, vol. 81, no. 2, pp. 184–193, 2020.

[40] A. K. Singh, A. Bissoyi, M. P. Kashyap, P. K. Patra, and S. I. Rizvi, "Autophagy activation alleviates amyloid-β-induced oxidative stress, apoptosis and neurotoxicity in human neuroblastoma SH-SY5Y cells," *Neurotoxicity Research*, vol. 32, no. 3, pp. 351–361, 2017.

Hindawi
Evidence-Based Complementary and Alternative Medicine
Volume 2022, Article ID 3306771, 4 pages
https://doi.org/10.1155/2022/3306771

Research Article

Clinical Value Analysis of Hepatectomy Based on Minimally Invasive Surgical Imaging for Hepatolithiasis

Shubin Zhang, Zhongqiang Xing, Xinbo Zhou, Zixuan Hu, and Jianhua Liu

Department of General Surgery, The Second Hospital of Hebei Medical University, Shijiangzhuang 050000, Hebei, China

Correspondence should be addressed to Jianhua Liu; liujianhua2981@163.com

Received 28 June 2022; Revised 22 July 2022; Accepted 29 July 2022; Published 31 August 2022

Academic Editor: Xueliang Wu

Objective. To investigate the clinical value of hepatectomy based on minimally invasive surgical images in the treatment of hepatolithiasis. *Methods.* The clinical data of 87 patients with hepatolithiasis who received treatment in the Department of General Surgery of our hospital from February 2020 to September 2021 were retrospectively analyzed. According to different surgical methods, the patients were divided into minimally invasive group ($n = 43$) and laparotomy group ($n = 44$). Perioperative conditions and stone clearance rate were compared. *Results.* The preoperative conditions of patients in the two groups were comparable, and the average operation time in the minimally invasive group was significantly longer than that in the laparotomy group ($t = 18.783, P < 0.001$). There was no significant difference in intraoperative bleeding, postoperative fasting time, postoperative complications, and stone clearance between the two groups ($P > 0.05$). Postoperative hospital stay was significantly lower in the minimally invasive group than that in the laparotomy group ($t = -0.486, P < 0.001$). *Conclusion.* Hepatectomy based on minimally invasive surgical imaging for hepatolithiasis is safe and feasible, has high clinical value, and can achieve similar short-term clinical efficacy to laparotomy and reduce the postoperative hospital stay of patients, reflecting its minimally invasive advantages, and it is worthy of clinical application.

1. Introduction

Hepatolithiasis is a common biliary tract disease in China, and the incidence of hepatolithiasis accounts for 16% to 18% of cholelithiasis [1]. The treatment is relatively complex, and the residual rate of stones and the incidence of complications after surgery are relatively high. Hepatectomy is still the preferred treatment [2]. At present, there are laparotomy and minimally invasive surgery (endoscopy). The choice of surgery needs to be based on the preoperative auxiliary examination and diagnosis. Traditional laparotomy is invasive and risky. In recent years, with the rapid development of endoscopic surgical techniques in biliary surgery, the advantages of minimally invasive surgical imaging in the treatment of hepatolithiasis have been gradually highlighted and gradually applied in clinical practice [3]. However, due to the complexity and extensiveness of the distribution of hepatolithiasis, minimally invasive surgery still lacks detailed criteria in terms of preoperative planning, ultrasound navigation, hemobilia and biliary stricture treatment, and postoperative management, and the safety and effectiveness need to be studied in depth. Therefore, this study investigated the clinical value of hepatectomy based on minimally invasive surgical images in the treatment of hepatolithiasis in order to provide a reference for the surgical treatment of intrahepatic and extrahepatic bile duct stones.

1.1. Study Subjects and Methods

1.1.1. Study Subjects. The clinical data of 87 patients with hepatolithiasis who received diagnosis and treatment in the Department of General Surgery of our hospital from February 2020 to September 2021 were retrospectively analyzed. They were divided into minimally invasive surgery group and laparotomy group according to surgical methods. There were 43 patients in the minimally invasive group and 44 patients in the laparotomy group.

Inclusion criteria were as follows: (1) hepatolithiasis diagnosed by imaging examination; (2) hepatectomy; (3) complete clinical data; and (4) agreed to sign informed consent.

Exclusion criteria were as follows: (1) combined with other serious systemic diseases; (2) combined with suppurative cholecystitis, gangrenous cholecystitis, and acute pancreatitis; and (3) coagulation disorders.

The study was approved by the ethics committee of The Second Hospital of Hebei Medical University (No.hbmu021), and the patients signed the informed consent.

2. Methods

2.1. Preoperative Preparation. All patients underwent preoperative examinations such as enhanced CT, MRCP, chest radiograph, electrocardiogram, and blood routine before operation. Preoperation education and adaptive exercise shall be carried out for patients to prepare their gastrointestinal tract. All patients took Shugan Jianpi Rongshi decoction. The compound includes Bupleurum chinense, Paeonia lactiflora, tangerine peel, Pinellia ternata, Codonopsis pilosula, Poria cocos, Atractylodes macrocephala, Glycyrrhiza, Magnolia officinalis, qianqiancao, haijinsha, Chuanpo stone, chenneijin, Burmese wormwood, and neem.

2.2. Surgical Methods. Open hepatectomy: the patient was under general anesthesia, and a vertical incision with a length of about 15cm was made on the right side of rectus abdominis. The scope of resection was determined according to the patient's condition. The blood flow of hepatic portal was blocked by the same method as that of laparoscopy. The diseased liver was severed by clamp method. The wound was covered with hemostatic sponge and greater omentum, and a drainage tube was placed.

Minimally invasive hepatectomy operation steps refer to Guidelines for Minimally Invasive Surgical Treatment of Hepatolithiasis (Edition 2019). Preoperative ultrasonography, choledochoscopy, CT scan, and arteriography were performed to determine the extent of liver resection margin. General anesthesia was performed with endotracheal intubation. During the resection, the liver segment and lobe could be used as units. The lesion could be removed by minimally invasive surgery. The diseased liver was divided by the clamping method. Adequate hemostasis was performed. The wound surface was washed. The diseased liver lobe and the pipeline in the Glisson fiber sheath of the liver were dissected. The harmonic scalpel could be used to achieve hemostatic effect and relieve pneumoperitoneum for the small pipeline in the liver.

2.3. Outcome Measures. Patients' clinical data were collected as follows: gender, age, BMI, Child–Pugh classification, smoking status, history of diabetes, and history of hypertension. The operation time, intraoperative blood loss, intraoperative abdominal drainage volume, postoperative hospital stay, drainage tube placement time, postoperative incision infection, bile leakage, pulmonary infection and other complications, and postoperative stone clearance rate were observed in the two groups. The calculation formula of stone clearance rate is as follows: the number of cases without residual stones in postoperative imaging and choledochoscopy in the minimally invasive surgery group or open surgery group/the total number of cases in the laparoscopic surgery group or open surgery group.

2.4. Data Analysis. SPSS 24.0 software was used to statistically describe and analyze the data. When quantitative data conformed to normal distribution, they were described as mean ± standard deviation, and enumeration data were expressed as rate. Measurement data of patients in the two groups were compared by the t-test, and enumeration data were analyzed by χ^2 or Fisher exact probability test. P values represent 2-sided probabilities, with $P < 0.05$ considered statistically different.

3. Results

3.1. Baseline Data. The comparison of preoperative general data showed that there was no significant difference in age, gender, body mass index, Child–Pugh classification, and past medical history between the two groups ($P > 0.05$), as shown in Table 1.

3.2. Comparison of Intraoperative Conditions. The differences in the operation time, intraoperative blood loss, and intraoperative laparoscopic drainage volume between the laparoscope group and laparotomy group had statistical significance ($P < 0.05$). There was no significant statistical difference in the proportion of T-tube drainage placement ($P > 0.05$), as shown in Table 2.

3.3. Comparison of Postoperative Conditions. Patients in the minimally invasive group had shorter postoperative hospital stays and drainage tube placement days than the laparotomy group. Postoperative complications occurred in 4 cases in the minimally invasive group and 8 cases in the laparotomy group, and the difference had no different significance between the two groups. The difference in stone clearance rate between the two groups was not significant ($P > 0.05$), as shown in Table 3.

4. Discussion

The most effective treatment for patients with hepatobiliary calculi is partial hepatectomy, which can remove the stones, remove the narrow area of the bile duct and the atrophic liver parenchyma, thereby reducing the risk of stone recurrence [4]. Open hepatectomy is effective but invasive to patients. Minimally invasive surgical image-based hepatectomy for hepatolithiasis is minimally invasive, and there were many reports [5]. There is still a lack of sufficient evidence to support its advantages in terms of safety and efficacy compared with open hepatectomy. The results of this study showed that minimally invasive hepatectomy was

Table 1: Baseline characteristics.

Characteristics	Minimally invasive group ($n = 43$)	Laparotomy group ($n = 44$)	t/χ^2	P
Age	53.19 ± 2.37	53.89 ± 2.33	−1.387*	0.169
Gender			0.335	0.563
Male	15 (34.9%)	18 (65.1%)		
Female	28 (40.9%)	26 (59.1%)		
Body mass index	21.50 ± 0.71	22.00 ± 0.82	−0.730*	0.506
Child–Pugh classification			0.859	0.354
Grade A	39 (90.07%)	37 (84.1%)		
Grade B	4 (9.3%)	7 (15.9%)		
Smoking history			0.186	0.666
Yes	10 (23.3%)	12 (27.3%)		
No	33 (76.7%)	32 (72.7%)		
Diabetes			0.132	0.716
Yes	6 (14%)	5 (11.4%)		
No	37 (86%)	38 (88.6%)		
Hypertension			0.055	0.814
Yes	7 (16.3%)	8 (18.2%)		
No	36 (83.7%)	36 (81.8%)		

Note. *refers to the use of *t*-test.

Table 2: Comparison of intraoperative conditions.

	Minimally invasive group ($n = 43$)	Laparotomy group ($n = 44$)	t/χ^2	P
T-tube drainage	36 (83.7%)	32 (72.7%)	1.540	0.215
Procedure time	214.60 ± 13.78	139.82 ± 0.75	18.783*	<0.001
Intraoperative bleeding	201.44 ± 8.37	200.09 ± 1.04	0.536*	0.599
Intraoperative abdominal drainage	146.63 ± 0.74	187.11 ± 4.29	−26.281	<0.001

Note. *refers to the use of *t*-test.

Table 3: Comparison of postoperative conditions.

	Minimally invasive group ($n = 43$)	Laparotomy group ($n = 44$)	t/χ^2	P
Postoperative hospital stay	6.71 ± 0.95	9.09 ± 1.04	−4.864*	<0.001
Postoperative fasting time	1.43 ± 0.79	1.89 ± 0.79	−1.165*	0.263
Drainage tube placement days	3.56 ± 0.73	5.56 ± 0.73	−5.840*	<0.001
Postoperative complications	4 (9.3%)	8 (18.2%)	1.442	0.230
Incision infection	1	2		
Biliary fistula	2	3		
Lung infection	1	3		
Stone clearance			0.001	0.969
Yes	38 (88.4%)	39 (88.6%)		
No	5 (11.6%)	5 (11.4%)		

Note. *refers to the use of *t*-test.

comparable to open hepatectomy in removing stones and had significant advantages in reducing operation time, intraoperative blood loss, intraoperative abdominal drainage volume, and postoperative complications and shortening hospital stay.

Intraoperative bleeding control is a difficult point in minimally invasive hepatectomy. Perfect imaging data, reasonable hepatic blood flow occlusion, liver transection and hemostatic devices, control of central venous pressure, and skilled microscopic operation are considered the key to control intraoperative blood loss. Patients with hepatolithiasis tend to have varying degrees of inflammatory adhesions in the diseased liver segment, which can become difficult to perform laparoscopically [6], and hemostatic techniques used for open hepatectomy such as vascular ligation and compression hemostasis are equal to laparoscopic inability to flexibly use. In this study, intraoperative blood loss in the minimally invasive group was not significantly higher than that in the laparotomy group, which was consistent with the results of Ye et al. [7]. This result may be due to the high-resolution magnification of the surgical field provided by laparoscopy and the more meticulous dissection of the liver parenchyma using a laparoscopic multifunctional surgical dissector. Hepatobiliary surgeons can combine preoperative imaging data and mark the hepatic resection line under the guidance of ultrasound to monitor the separation of blood vessels and bile ducts in real time. It may also be related to the maturity of

hepatobiliary surgeons' concept awareness, proficiency in operation techniques, and continuous improvement of laparoscopic surgical instruments. It is inconsistent with the research results of Li et al. [8] and Wang et al. [9]. The results show that the amount of intraoperative bleeding in the minimally invasive surgery group is less than that in the open surgery group, and the difference between the two groups is statistically significant.

In this study, the operation time of the minimally invasive group was longer than that of the laparotomy group. It was considered that the main reason was not only that laparoscopic surgery required hepatectomy but also that laparoscopic bile duct exploration, stone extraction, liver section bile duct suture, and other operations were completed, and the operation steps were complicated compared with open left hepatectomy; in addition, bile duct inflammation caused by long-term bile duct stones led to adhesion of the first porta hepatis to the surrounding tissues, increasing the difficulty of laparoscopic anatomical separation of the first porta hepatis, resulting in prolonged operation time.

n this study, the postoperative hospital stay of the minimally invasive group was shorter than that of the laparotomy group. Considering that the laparoscopic technique has less irritation to organs and tissues around the liver, the abdominal wall surgical incision is reduced, the incision infection rate is reduced, and with the surgeon 's laparoscopic technique becoming more skilled, the postoperative hospital stay of the patients is shortened. The total incidence rate of complications in the minimally invasive group was lower than that in the laparotomy group, but the difference between the two groups had no significant difference. Considering that the sample size was small, it had a certain impact on the statistical results.

Stone clearance rate is an important indicator to evaluate the effect of hepatectomy in the treatment of hepatolithiasis. In this study, the stone clearance rate was 88.4% in the minimally invasive group and 88.6% in the laparotomy group, and there was no significant difference between the two groups. In accordance with relevant domestic and foreign studies [3, 10], it was reported that there was no significant difference in stone clearance rate between the minimally invasive group and the laparotomy group. It may be related to the routine application of ultrasonography and choledochoscopy in minimally invasive surgery to detect stones deep in the liver parenchyma and identify the location, size, and extent of stones and the location of biliary strictures.

In summary, laparoscopic hepatectomy for left hepatolithiasis is safe and feasible and has high clinical value. It can achieve similar short-term clinical efficacy to laparotomy, reflecting the advantages of minimally invasive surgery. It is superior to laparotomy in controlling intraoperative bleeding and shortening postoperative hospital stay. However, because this study is a single center retrospective study, in order to provide a higher level of evidence-based medical evidence support for the safety and effectiveness of laparoscopic hepatectomy in the treatment of hepatolithiasis, a prospective randomized controlled trial with a sufficient number of cases is also needed.

Data Availability

The data used to support the findings of this study are available from the corresponding author upon request.

Conflicts of Interest

The authors declare that they have no conflicts of interest.

References

[1] S. Chen, L. Huang, F. N. Qiu et al., "Total laparoscopic partial hepatectomy versus open partial hepatectomy for primary left-sided hepatolithiasis: a propensity, long-term follow-up analysis at a single center," *Surgery*, vol. 163, no. 4, pp. 714–720, 2018.

[2] E. Lorio, P. Patel, L. Rosenkranz, S. Patel, and H. Sayana, "Management of hepatolithiasis: review of the literature," *Current Gastroenterology Reports*, vol. 22, no. 6, p. 30, 2020.

[3] D. Yao and S. Wu, "Application of laparoscopic technique in the treatment of hepatolithiasis," *Surgical Laparoscopy Endoscopy & Percutaneous Techniques*, vol. 31, no. 2, pp. 247–253, 2021.

[4] H. Xia, X. Meng, X. Xin et al., "Resection of extrahepatic bile ducts with partial hepatectomy for treating intra- and extrahepatic hepatolithiasis," *BMC Surgery*, vol. 21, no. 1, p. 420, 2021.

[5] L. Peng, J. Xiao, Z. Liu, Y. Li, and W. Xiao, "Laparoscopic versus open left-sided hepatectomy for hepatolithiasis: a systematic review and meta-analysis," *Journal of Laparoendoscopic & Advanced Surgical Techniques*, vol. 27, no. 9, pp. 951–958, 2017.

[6] L. Peng, J. Xiao, Z. Liu et al., "Laparoscopic left-sided hepatectomy for the treatment of hepatolithiasis: a comparative study with open approach," *International Journal of Surgery*, vol. 40, pp. 117–123, 2017.

[7] X. Ye, K. Ni, X. Zhou, K. Xie, and X. Hong, "Laparoscopic versus open left hemihepatectomy for hepatolithiasis," *Journal of Surgical Research*, vol. 199, no. 2, pp. 402–406, 2015.

[8] H. Li, J. Zheng, J. Y. Cai et al., "Laparoscopic VS open hepatectomy for hepatolithiasis: an updated systematic review and meta-analysis," *World Journal of Gastroenterology*, vol. 23, no. 43, 2017.

[9] X. Wang, A. Chen, Q. Fu, and C. Cai, "Comparison of the safety and efficacy of laparoscopic left lateral hepatectomy and open left lateral hepatectomy for hepatolithiasis: a meta-analysis," *Front Surg*, vol. 8, Article ID 749285, 2021.

[10] X. Cai, Y. Wang, H. Yu, X. Liang, and S. Peng, "Laparoscopic hepatectomy for hepatolithiasis: a feasibility and safety study in 29 patients," *Surgical Endoscopy*, vol. 21, no. 7, 2007.

Hindawi
Evidence-Based Complementary and Alternative Medicine
Volume 2022, Article ID 4304361, 11 pages
https://doi.org/10.1155/2022/4304361

Research Article

Six Genes Associated with Lymphatic Metastasis in Colon Adenocarcinoma Linked to Prognostic Value and Tumor Immune Cell Infiltration

Baoquan Wang,[1,2] **Changjun Yin**,[3] **Xu Yang**,[3] **Huibo Shi**,[4] **Zheng Zhang**,[1,2] **Jun Zhou**,[3,5] **and Peitong Zhang**[1]

[1]*Department of Oncology, China Aacdemy of Chinese Medical Sciences Guang'anmen Hospital, Beijing 100053, China*
[2]*Graduate School, Beijing University of Chinese Medicine, Beijing 100029, China*
[3]*Department of Gastrointestinal Surgery, Sun Yat-Sen Memorial Hospital of Sun Yat-Sen University, Guangzhou 510120, China*
[4]*Graduate School, Liaoning Technical University, Fuxin 123000, China*
[5]*Department of Gastrointestinal Surgery, The Third Affiliated Hospital of Guangzhou Medical University, Guangzhou 510150, China*

Correspondence should be addressed to Jun Zhou; zhoujun2@mail.sysu.edu.cn and Peitong Zhang; gamzpt@163.com

Received 12 July 2022; Revised 26 July 2022; Accepted 2 August 2022; Published 29 August 2022

Academic Editor: Xueliang Wu

Objective. The aim of the study is to explore the relationship between lymphatic metastasis genes, prognosis, and immune cell infiltration in patients with colon cancer. *Methods*. Based on the Cancer Genome Atlas Program (TCGA) database, differentially expressed genes and prognostic genes related to colon adenocarcinoma (COAD) lymphatic metastasis were screened and intersected. We used lasso and univariate Cox regression analysis to screen core genes and establish a preliminary prediction model. GO and KEGG enrichment analysis was used for lymphatic metastasis-related genes, and single GSEA was used for the final screening results. Finally, we evaluated the relationship between identified genes and immune cell infiltration. *Results*. A total of 1727 genes were differentially expressed between COAD patients with TNM stages of N0 and N1. After further screening, six core genes (RNU4-2, ZNF556, RNVU1-15, NSA2P6, RN7SL767P, and RN7SL473P) were obtained, and a preliminary prediction model was established, in which ZNF556 was a risk factor, and the rest were protective factors. Single GSEA showed that pathways such as systemic lupus erythematosus might play an important role in the initial lymphatic metastasis of COAD. GO and KEGG enrichment analysis of 1727 genes supported this result. Immune infiltration analysis showed that six genes were significantly correlated with T cell and NK cell families. *Conclusion*. Six core genes may affect COAD initial lymphatic metastasis through the systemic lupus erythematosus pathway and immune cell infiltration.

1. Introduction

Colorectal cancer (CRC) represents approximately 10% of all cancers and is the second most common cause of cancer deaths [1, 2]. Colon adenocarcinoma (COAD), one of the most common pathological types of CRC, has a high fatality rate worldwide [3]. Currently, the standard treatment for COAD is surgery combined with adjuvant chemotherapy or radiotherapy as per the clinical stages [4]. Patients with advanced COAD frequently cannot receive radical treatment because of distant metastasis, and their prognosis is very poor.

Lymphatic metastasis is a precursor of distant metastasis and a key determinant in the prognosis of patients [5]. Most solid tumors release growth factors such as vascular endothelial growth factor C (VEGF-C) to induce lymphatic vessel expansion (lymphangiogenesis) in primary tumors and in draining sentinel lymph nodes (LNs), thereby promoting LN metastasis [6]. It is worth noting that the occurrence of lymphatic metastasis is not accidental but a well-designed

event, and the immune microenvironment may play an important role in this process [7].

For COAD, the potential molecular mechanism of lymphatic metastasis is still unknown; it is essential to explore its potential biomarkers. Immune cells in the tumor microenvironment participate in tumor cell lymph node metastasis through their complex interaction and biochemical function depth. Studies have shown that tumor-infiltrating lymphocytes (TILs) and CD57 play an important role in lymphatic metastasis of COAD by mediating local immune response and can also be used as independent prognostic factors [8]. Jianwei Lin's research was based on transcription factors (TFs) and established a prognostic risk model to predict the prognosis of patients with COAD and finally obtained a 7-gene prognostic model [9]. Appropriate biomarkers should effectively monitor disease progression and, to some extent, predict the patient's prognosis [10]. This study investigated the genes that affect initial lymphatic metastasis of COAD, speculated their mechanism, and discussed the relationship between them and immune infiltration to provide a new idea for clinical treatment of COAD lymphatic metastasis.

2. Materials and Methods

2.1. Data Access. This study used level 3 HT Seq-Counts format and HT Seq-FPKM format RNASeq data from the TCGA (https://portal.gdc.cancer.gov/) COAD project [11, 12], and we converted the data in fragments per kilobase per million (FPKM) format to transcripts per million (TPM) format. It comprised 521 COAD samples, with 41 from paracancerous tissues and 480 from tumor tissues. To verify the relationship between the gene expression and the immunophenoscore (IPS), we download the relevant information of COAD patients from The Cancer Immunome Atlas (TCIA) (https://tcia.at/home) [13, 14].

2.2. Differences in Gene Expression with Initial Lymphatic Metastasis. The clinical specimens with TNM stages of N0 and N1 were extracted and divided into two groups based on whether they had initial lymphatic metastasis or not.The purpose of this grouping is to explore the possible molecular mechanism of COAD initial lymphatic metastasis. The data format used in this part of the study is Counts. The differences in gene expression were analyzed by the DESeq2 package [15] of R software. The screening threshold was "adjusted $p$value <0.05 and log2 (fold change) > 1 or log2 (fold change) <−1."

2.3. Genes Related to Prognosis. The survival package of R software was used for molecular screening of COAD prognosis [16]. In this part, we used data in the TPM format. The clinical information was retained after the paracancerous tissue group was removed from the data. Additional prognostic data were obtained from a Cell article [17]. "p cox <0.05" was taken as the screening threshold.

2.4. Enrichment Analysis. Gene Ontology (GO) enrichment analysis (BP: biological process; CC: cellular component; MF: molecular function) and Kyoto Encyclopedia of Genes and Genomes (KEGG) pathway analysis were performed on the selected differential lymphoid metastasis molecules [18–20]. "q value <0.2 and p. adj <0.1" were used as the threshold to enrich functional categories and pathways. The *R* software was used to examine the single GSEA of the six core genes [21, 22]. In terms of reference gene sets, we chose "c2 cp v7.2 symbols gmt." "FDR (q value) < 0.25 and p adjust <0.05" were used as the threshold to filter pathways.

2.5. Screening of Genes and Establishment of the Prognostic Model. The selected prognosis and lymphatic metastasis-related genes were intersected. The intersection results were then screened using the "lasso regression methods" through the R package "glmnet" [23]. To assess the screening results of "lasso regression methods," the Kaplan–Meier (K–M) survival curves were used to compare survival between low and high-risk groups using the survival package. Additionally, the time-dependent receiver operating characteristic (ROC) curve analysis (including 1-year, 3-year, and 5-year survival) was established to reflect the sensitivity and specificity of the results by the time ROC package [24]. We used univariate Cox regression analysis to further screen core genes [25]. For the corresponding variables of "$p < 0.1$," multivariate Cox regression analysis was used to establish the model. The prognosis nomogram of the model results was drawn, and calibration analysis was performed to evaluate the actual prediction effect of the model [26].

2.6. Differential mRNA Expression of Genes and Its Relationship with Prognosis. The R software was used to validate the differential expression of six genes in different groups of COAD patients. The Kaplan–Meier survival curve of six genes was plotted by using a survival package [16]. Additional prognostic data were derived from an article of Liu's research [17]. The RNASeq data format of COAD patients used above is TPM.

2.7. Immune Infiltration Assessment. The immune cell infiltration of the obtained gene in COAD patients was evaluated by the ssGSEA algorithm [27]. We used the GSVA package in R software to complete this part of the research. The selected correlation analysis method is Spearman. The classification and description of specific immune cells can be found in Bindea's research [28]. The horizontal coordinate represents the gene, the vertical coordinate represents the immune cell, and the correlation coefficient is between −1 and 1. The difference was statistically significant when $p < 0.05$.

3. Results

3.1. Genes Screening and Results Evaluation. A total of 1727 lymphatic metastasis-related genes (Figure 1(a)) and 2118 prognosis-related genes (Figure 1(b)) were screened. Among the genes related to initial lymphatic metastasis, 1682 genes were downregulated and 45 genes were upregulated. Among

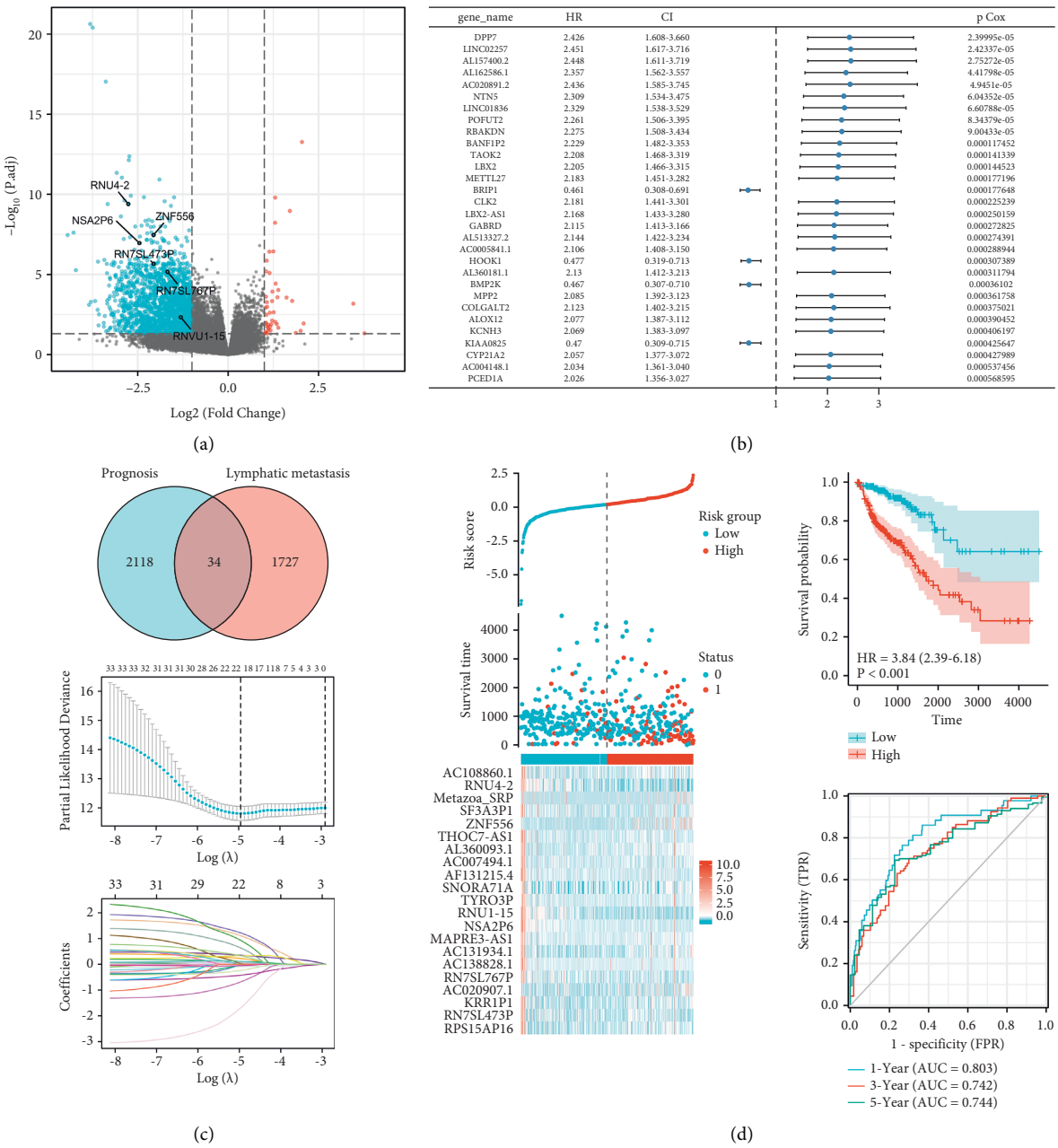

Figure 1: Screening of genes and evaluation of related results. (a) Volcano plot of lymphoid metastasis-related genes; (b) forest plot of prognosis-related genes only shows top 30; (c) Venn diagram and lasso regression method results; (d) lasso regression risk factor diagram, K–M survival curves, and ROC curve analysis.

the prognosis-related genes, 1572 genes were caused by risk factors, while 546 genes were induced by protective factors. As shown in the Venn diagram, the intersection of the two types of genes yielded 34 genes. The variables were screened by lasso regression analysis, and the lambda.min was 21 (Figure 1(c)). Based on the results of the lasso regression analysis, the risk factor map was drawn, and the risk score, risk grouping, survival outcome, and 21 gene expression heat maps (Figure 1(d)) of COAD patients under lasso regression were obtained. The K–M curve and ROC curve (Figure 1(d)) were drawn based on the risk grouping of lasso regression results. There is a significant difference in prognosis between the high-risk and low-risk groups ($p < 0.001$, HR = 3.84). The ROC curve shows that the area under the curve (AUC) of the model obtained by lasso analysis for one year, three years, and five years is 0.803, 0.742, and 0.744, respectively, which has good prediction efficiency. It shows the reliability of lasso results.

3.2. GO and KEGG Enrichment Analysis of Initial Lymphatic Metastasis-Related Genes. A total of 1727 genes related to initial lymphatic metastasis were analyzed using GO and KEGG enrichment analysis to examine the possible

molecular mechanism in the early stage of lymphatic metastasis in COAD patients. Under the condition of q value <0.2 and *p*.adj <0.1, there were 65 BP, 17 CC, 10 MF, and 7 KEGG (Figure 2). The main enrichment by BP analysis (Figure 3(a)) is nucleosome assembly, nucleosome organization, chromatin assembly or disassembly, DNA packaging, and protein-DNA complex assembly. This demonstrated that the biological process plays an important role in the initial lymphatic metastasis of COAD, and the results of CC and MF enrichment analysis supported this conclusion (Figures 3(b) and 3(c)). The main pathways enriched by KEGG analysis (Figure 3(d)) were systemic lupus erythematosus, alcoholism, and viral carcinogenesis. Furthermore, KEGG analysis revealed that transcriptional misregulation in cancer and necroptosis might be important in COAD lymph node metastasis.

3.3. Establishment of the Prognostic Model. Genes obtained by lasso regression were analyzed by Cox regression analysis (used coxph function) to further screen core genes (Table 1). Univariate analysis showed that RNU4-2, ZNF556, RNVU1-15, NSA2P6, RN7SL767P, and RN7SL473P were significant and could be included in the multivariate regression model. Among them, HR < 1 of RNU4-2 and HR > 1 of ZNF556 were protective factors, and HR > 1 of RN7SL473P was a risk factor. Based on the results of multiple regression analysis of genes, the predictive map was formed by adding common clinicopathological factors (Figure 4(a)), and calibration analysis (Figure 4(b)) shows the results of the line chart. The advanced analysis parameters were as follows: several samples were recalculated in each group: 100, method: boot, data filtering: remove the normal group and retain clinical information. This part of the study aimed to develop a quantitative analysis tool that can predict the survival risk of individual patients. The nomogram calibration curve demonstrated that in the entire TCGA queue, when the index is one year, three years, and five years, the actual probability agrees with the model prediction probability.

3.4. Differential mRNA Expression of Genes and Its Relationship with Prognosis. We used the TCGA database to confirm the differential expression of six genes in different grouping samples. It was discovered that there was a difference in the expression of mRNA between RNU4-2 and COAD tissues (Figure 5(a)). When the overall survival (OS) was used as an indicator, there were significant differences in the expression of six genes between survival patients and dead patients. When disease-specific survival (DSS) was used as an index, there were significant differences in gene expression except for ZNF556 (Supplement Figure 1). *Moreover, the expression of six genes in different groups had significant differences in prognosis (Figure 5(b)). Amongthem, ZNF556 was found to be a risk factor, and the high expression group had a shorter survival time.Whereas the other genes were protective factors, and the high expression group had a longer survival time.*

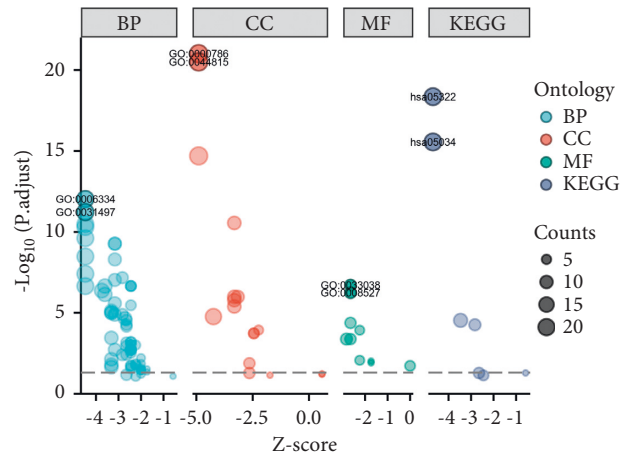

Figure 2: Bubble plot of lymphoid metastasis-related genes enrichment analysis.

3.5. GSEA of Six Genes. Single GSEA was performed on the six selected genes to investigate their possible functional pathways and mechanisms of action in COAD. ZNF556 was not enriched into the pathway that met the conditions, and the enrichment results of other genes were as follows (Figure 6). The findings revealed that "KEGG systemic lupus erythematosus" was significantly enriched in all five genes. This pathway plays an important role in the initial lymph node metastasis of COAD, and the previous GO and KEGG enrichment analysis results support this conclusion. Furthermore, we found "Reactome cellular senescence" "Reactome-activated pkn1 stimulates transcription of androgen receptor-regulated genes klk2 and klk3," and "Reactome activation of anterior Hox genes in hindbrain development during early embryogenesis" played an important role in GSEA enrichment.

3.6. Immune Infiltration Assessment. We investigated the relationship between six genes expression and the infiltration of 24 different types of immune cells (Figure 7(a)). It can be observed that there is a significant correlation between T cell and NK cell families and the expression of six genes. Previously, we discovered that the initial lymphatic metastasis of COAD may be highly related to the "KEGG systemic lupus erythematosus" pathway. Systemic lupus erythematosus is characterized by overactivation of the immune system, abnormal function of many immune cells, and the production of antibodies that attack their components [29–31]. These can significantly affect the tumor microenvironment. This conclusion was supported by immune cell infiltration analysis in COAD. Subsequently, we explored the relationship between the overall risk score of the six genes and IPS (Figure 7(b)). IPS is a good predictor of immunosuppressant response [32]. The immune checkpoints explored in this study include CTLA-4 and PD-1. Figure 7(b) shows the four types of IPS in TCIA: CTLA4 negative PD-1 negative, CTLA4 positive PD-1 negative, CTLA4 negative PD-1 positive, and CTLA4 positive PD-1 positive. The findings revealed a significant difference

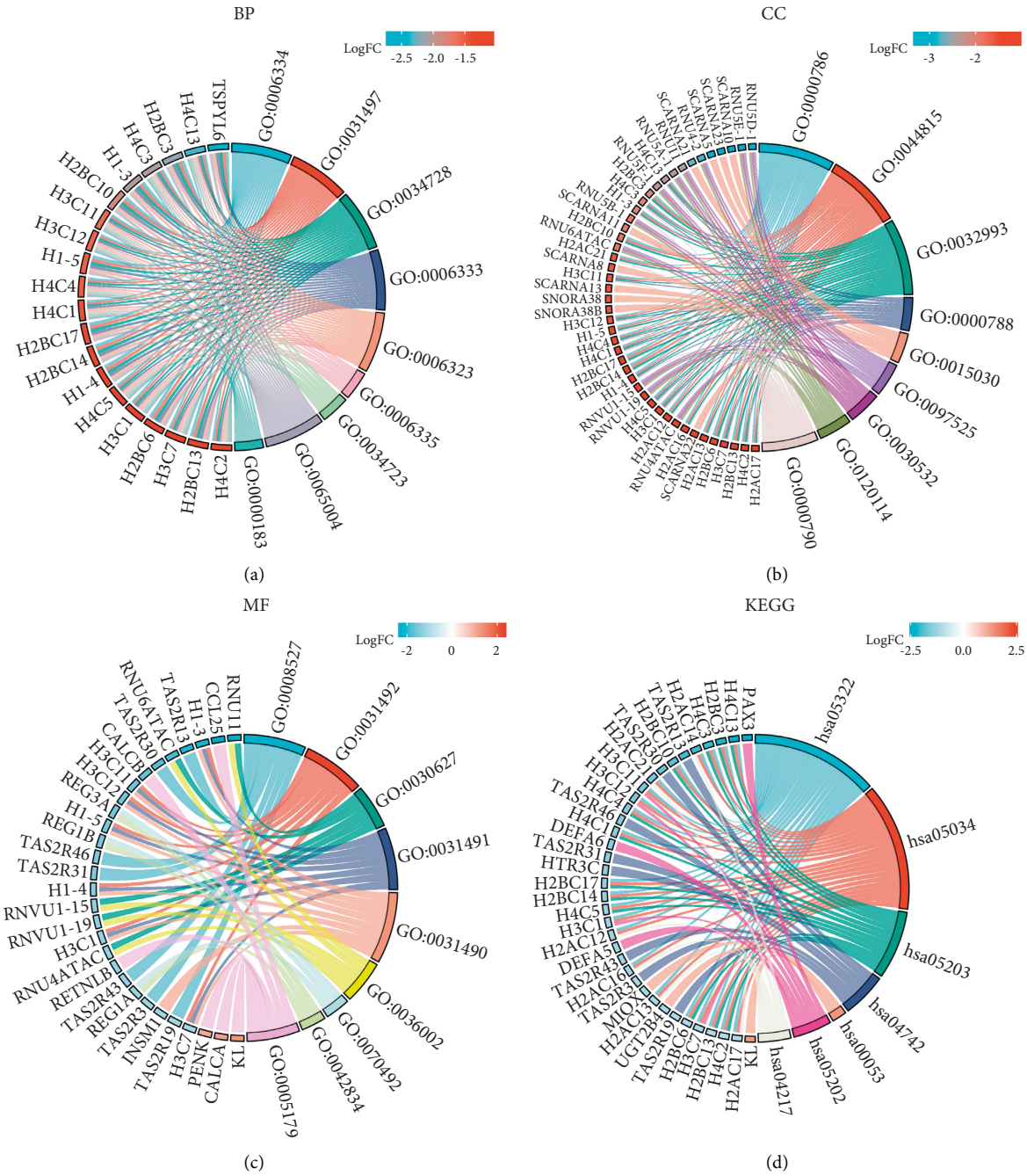

FIGURE 3: Circle plot of lymphoid metastasis-related genes GO and KEGG enrichment analysis. (a) BP: biological process; (b) CC: cellular component; (c) MF: molecular function; (d) KEGG: Kyoto Encyclopedia of Genes and Genomes.

between high and low-risk scores in the "ctla4_positive_pd1_negative" group. This indicated that the overall risk score of the six genes may predict the response of anti-CTLA4 immunotherapy.

4. Discussion

Lymphatic metastasis plays a crucial role in tumor progression, enabling cancer cells to spread from primary tumors to distant organs [33]. Lymphatic metastasis is directly related to distant recurrence and prognosis in most tumors [34]. Moreover, the survival prognosis for N0 and N1 tumor patients has changed significantly, and even after surgical treatment, N1 patients also have a poor overall survival [35]. The molecular mechanism of lymphatic metastasis in COAD has not been thoroughly investigated. However, it is critical to investigate the molecular mechanism affecting the initial lymphatic metastasis of COAD and to explore biomarkers. Some scholars have examined the predictive value of miRNA in lymphatic metastasis and preliminarily determined miRNA that can predict lymphatic metastasis of colon cancer; however, the molecular mechanism has not been

Table 1: Univariate and multivariate Cox regression analysis results.

Characteristics	Total (*N*)	Univariate analysis		Multivariate analysis	
		Hazard ratio (95% CI)	*p* value	Hazard ratio (95% CI)	*p* value
AC108860.1	462	0.975 (0.768–1.238)	0.836		
RNU4-2	462	0.879 (0.792–0.977)	0.017	0.920 (0.806–1.051)	0.220
Metazoa_SRP	462	2.088 (0.669–6.522)	0.205		
SF3A3P1	462	0.885 (0.565–1.386)	0.593		
ZNF556	462	1.384 (1.079–1.775)	0.010	1.440 (1.119–1.853)	0.005
THOC7-AS1	462	0.686 (0.404–1.163)	0.161		
AL360093.1	462	1.015 (0.689–1.494)	0.941		
AC007494.1	462	0.907 (0.607–1.356)	0.635		
AF131215.4	462	0.614 (0.327–1.154)	0.130		
SNORA71 A	462	0.998 (0.895–1.113)	0.970		
TYRO3P	462	0.864 (0.428–1.743)	0.683		
RNVU1-15	462	0.732 (0.559–0.957)	0.023	0.788 (0.563–1.102)	0.163
NSA2P6	462	0.505 (0.225–1.134)	0.098	0.672 (0.233–1.940)	0.462
MAPRE3-AS1	462	0.937 (0.528–1.660)	0.823		
AC131934.1	462	1.139 (0.856–1.515)	0.373		
AL138828.1	462	0.577 (0.217–1.537)	0.271		
RN7SL767P	462	0.770 (0.571–1.039)	0.088	1.063 (0.713–1.586)	0.765
AC020907.1	462	1.166 (0.920–1.478)	0.203		
KRR1P1	462	1.011 (0.828–1.235)	0.913		
RN7SL473P	462	0.778 (0.577–1.048)	0.098	1.030 (0.675–1.572)	0.890
RPS15AP16	462	0.978 (0.765–1.251)	0.858		

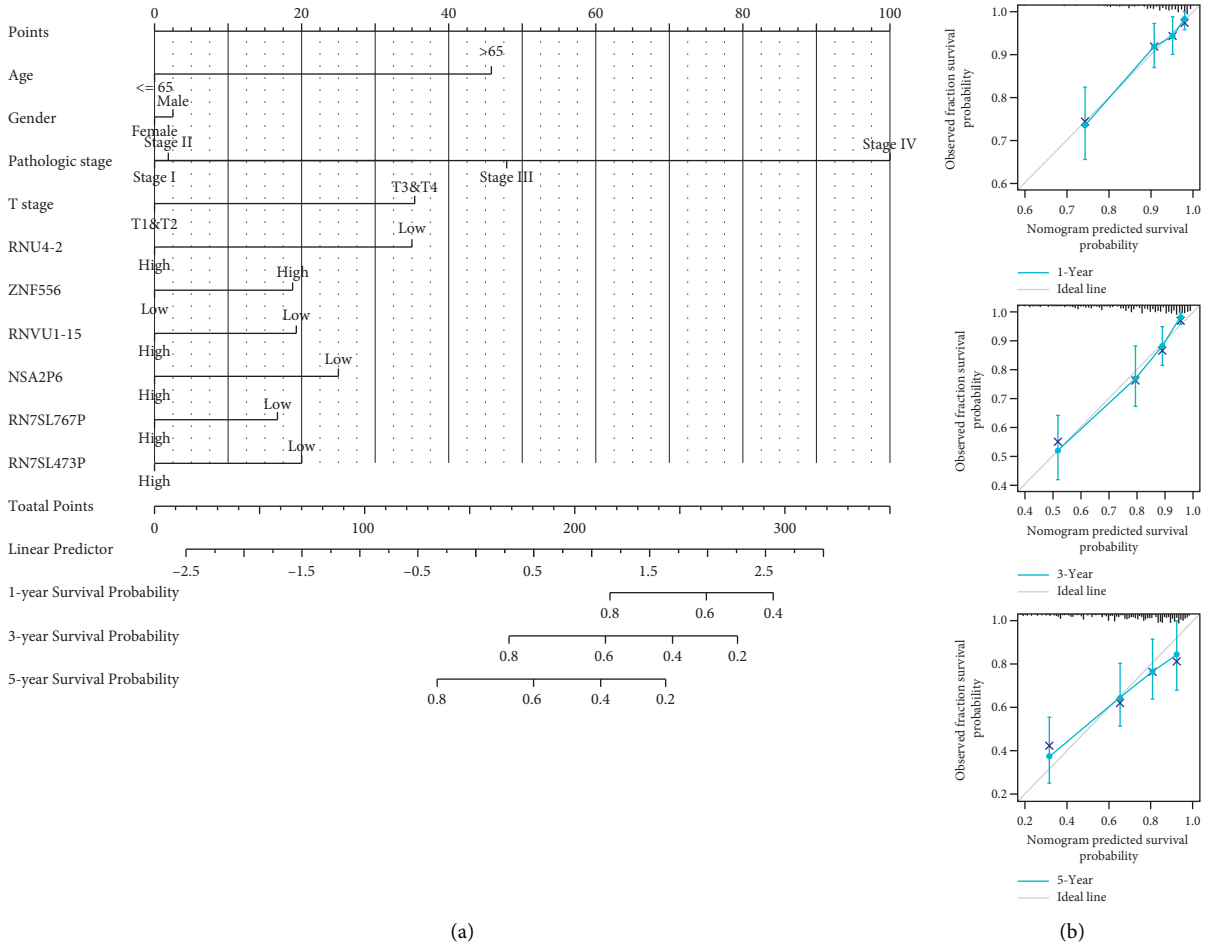

(a) (b)

Figure 4: Nomogram for predicting and its evaluation. (a) Nomogram for predicting 1-year, 3-year, and 5-year OS in the entire TCGA cohort; (b) calibration curves of the nomogram on consistency between predicted and observed 1-year, 3-year, and 5-year survival in the entire TCGA cohort.

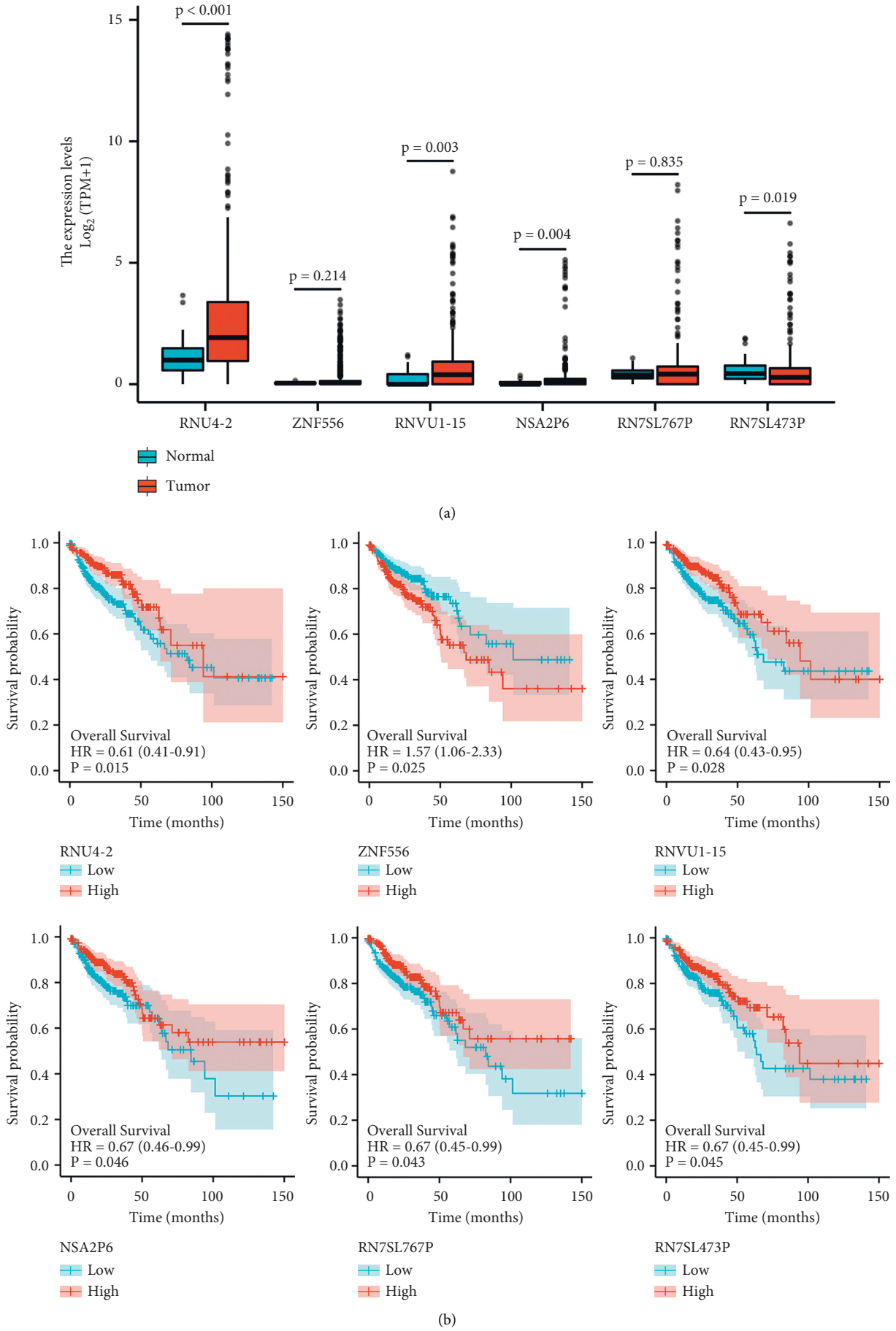

Figure 5: Differential mRNA expression of genes and its relationship with prognosis. (a) Box plot of differential expression of six genes in tumor tissues and normal tissues; (b) K–M survival curves between low and high expressions of each gene.

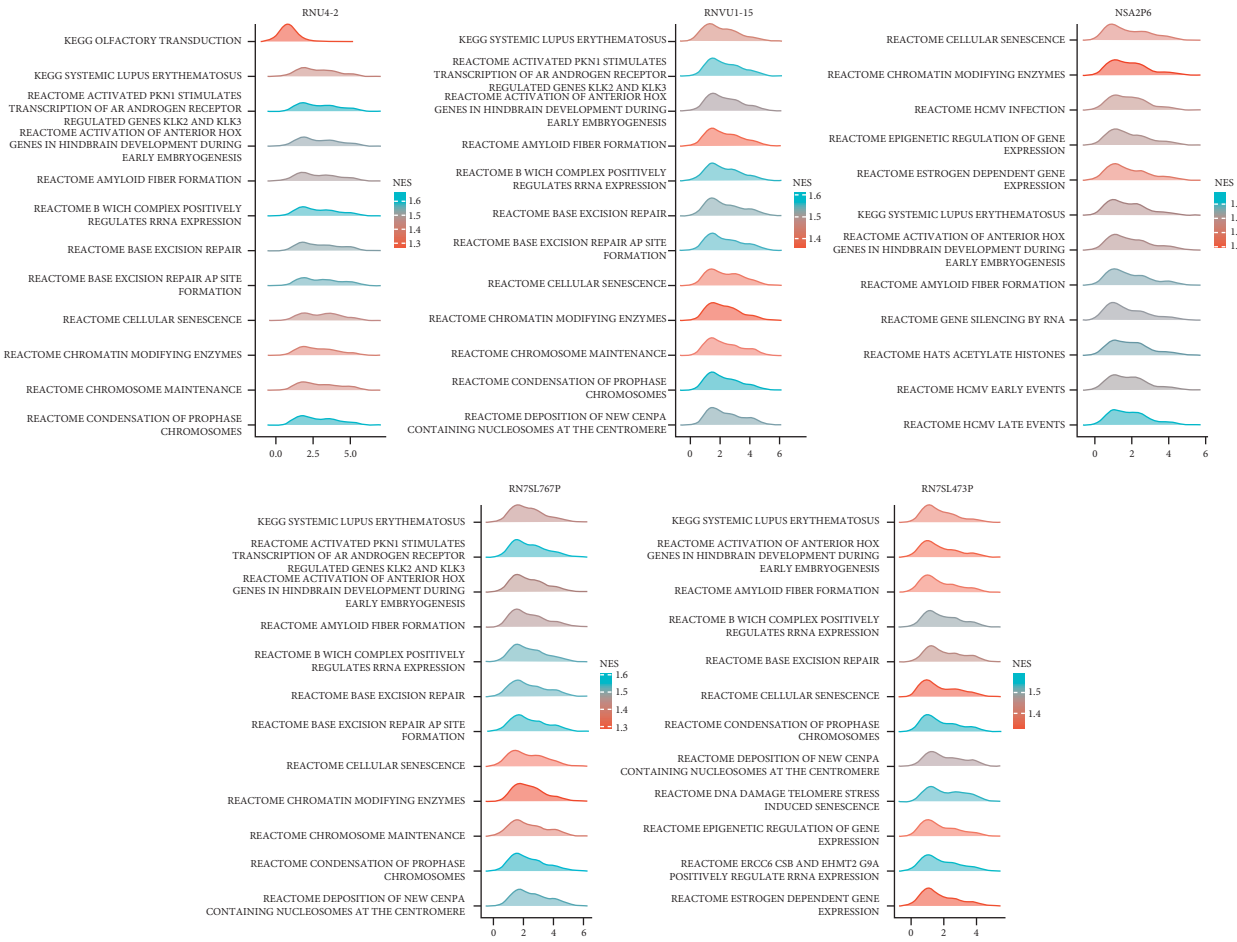

Figure 6: Mountain plot of GSEA enrichment analysis of six genes only shows top 12.

examined [36]. Based on the TCGA database, this study investigated the molecular mechanism affecting the initial lymphatic metastasis of COAD patients and preliminarily identified six core genes (RNU4-2, ZNF556, RNVU1-15, NSA2P6, RN7SL767P, and RN7SL473P).

ZNF556, as a colon cancer biomarker, has been demonstrated to possess a robust predictive ability, which validates the results of this study [37]. Unfortunately, ZNF556 was not enriched to the pathway in further the single GSEA in this study. RNU4-2 and RNVU1-15 are involved in RNA processing related to suicide and autism [38, 39]. This study revealed the potential of RNU4-2, RNVU1-15, NSA2P6, RN7SL767P, and RN7SL473P as biomarkers of COAD for the first time.

In GO enrichment analysis, cell division-related biological processes such as nucleosome assembly, nucleosome organization, chromatin assembly, or disassembly were found to be deeply involved in the initial lymphatic metastasis of COAD. This might be due to increased cancer cell division and the proliferation of new lymphatic vessels [40, 41]. KEGG enrichment analysis revealed that systemic lupus erythematosus was the most significantly enriched pathway, and furthermore, the single GSEA validated this result, suggesting that the systemic lupus erythematosus pathway may be crucial for initial lymphatic metastasis in COAD. According to relevant clinical studies, systemic lupus erythematosus enhances the risk for occurrence of various cancers and can lead to increased cancer-related mortality [42, 43]. However, its mechanism of action has not been elucidated. Systemic lupus erythematosus is an autoimmune disease that causes chronic multiorgan inflammatory damage and is characterized by the presence of nuclear autoantibodies, leading to the formation of autoimmune complexes, which are further deposited throughout the tissue, causing chronic inflammatory lesions. Its chronic inflammation might have a role in apoptosis, immunosuppression, or activation by influencing the tumor microenvironment, consequently affecting the occurrence and progression of tumors. The elucidation of the exact mechanism can be used as the direction of further research.

According to the findings of the above single GSEA enrichment analysis, immune infiltration in the tumor microenvironment may play a role in the initial lymphatic metastasis of COAD. As a result, this study examined the relationship between 24 different types of immune cells and the expression of six genes. The results revealed that the expression of these six genes was significantly associated with T cell and NK cell families. Further investigation revealed that IPS scores of patients also differed between different groups of

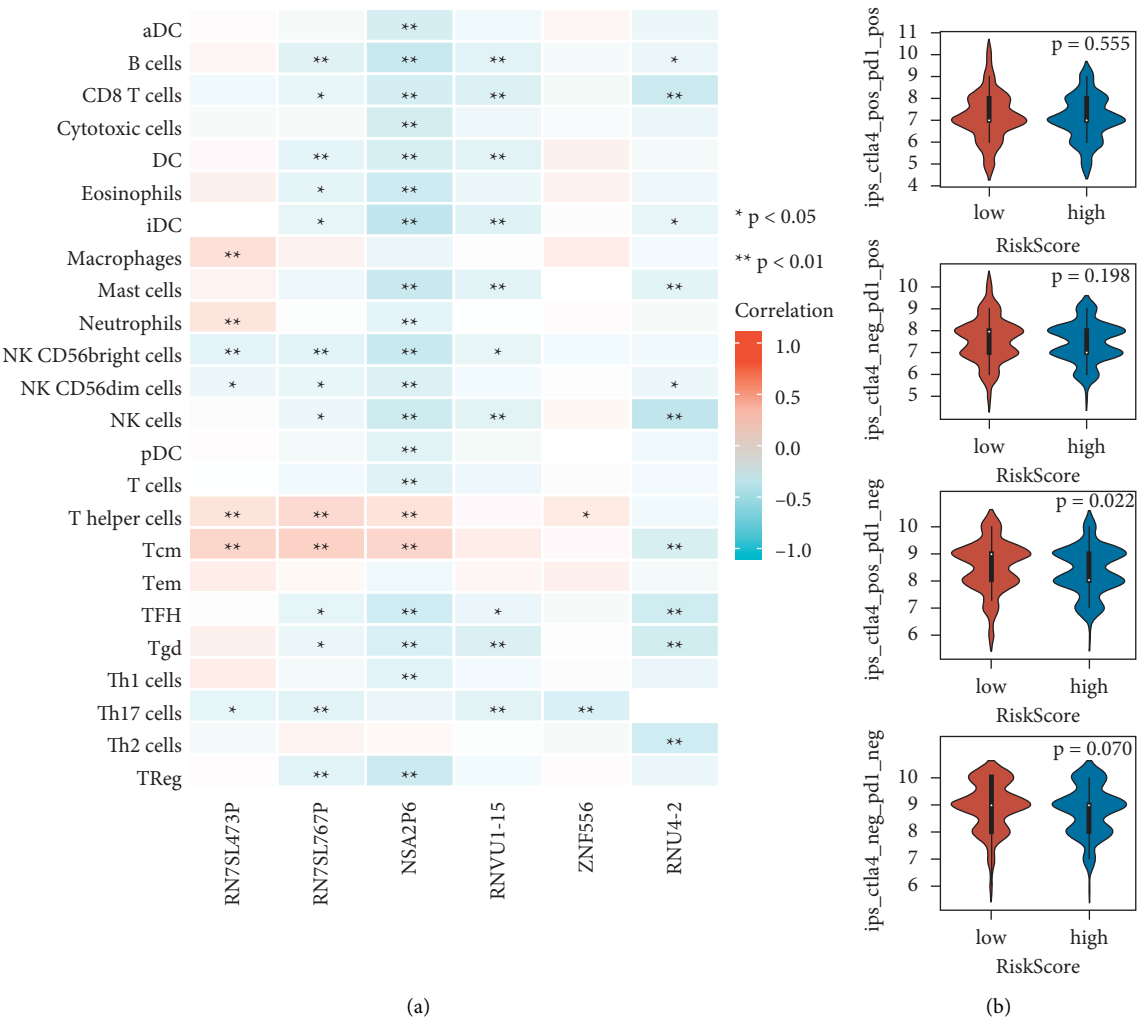

FIGURE 7: Six genes, respectively, associated with immune cell infiltration. (a) Correlation heat plot of immune infiltration; (b) correlations of six gene risk scores with IPS.

six-gene risk scores. Similar studies have selected IRF1 as a biomarker to explore its relationship with immune cell infiltration and COAD metastasis [44]. IRF1 is associated with metastasis and the degree of immune infiltration of $CD8^+$ T cells (general), dendritic cells, T-helper 1 cells, and T cell exhaustion in COAD, further demonstrating that immune cell infiltration can affect COAD lymphatic metastasis. Combined with this study, it can be seen that the above process is closely related to the expression of these six genes, although the specific mechanism remains to be explored.

In summary, based on the TCGA database, this study investigated the genes associated with the initial lymphatic metastasis of COAD and their mechanisms and initially established a predictive model. Finally, six core genes were obtained, and systemic lupus erythematosus was considered to play a significant role as its action pathway. Moreover, immune infiltration assessment showed that these six genes may promote COAD lymphatic metastasis by influencing immune cell infiltration. These provide potential targets for immunotherapy to prevent COAD development.

However, there are some unavoidable limitations in our research. As the study is based on bioinformatics analysis, there are no in vivo or in vitro experiments verifying the conclusions of this study. The research on the mechanism has not been thoroughly explained and verified. These should be further investigated for improvement.

Data Availability

The data supporting the findings of this study are available from the corresponding author upon request.

Conflicts of Interest

The authors declare that they have no conflicts of interest.

Authors' Contributions

Wang B, Zhang P, and Zhou J designed the work. Wang B, Yin C, Yang X, and Shi H acquired and analyzed data. Yin C,

Yang *X,* and Zhang *Z* were responsible for interpretation of data. Wang B drafted the work and substantively revised it. All authors reviewed the manuscript. Baoquan Wang, Changjun Yin, and Xu Yang contributed equally to this work and share first authorship.

Acknowledgments

This work was supported by the https://doi.org/10.13039/501100005089Beijing Municipal Natural Science Foundation (7182142).

Supplementary Materials

Supplement Figure 1: expression of six genes in different groups. (*Supplementary Materials*)

References

[1] F. Ciardiello, D. Ciardiello, G. Martini, S. Napolitano, J. Tabernero, and A. Cervantes, "Clinical management of metastatic colorectal cancer in the era of precision medicine," *CA: A Cancer Journal for Clinicians*, vol. 72, no. 4, pp. 372–401, 2022.

[2] K. D. Miller, L. Nogueira, T. Devasia et al., "Cancer treatment and survivorship statistics, 2022," *CA Cancer Journal for Clinicians*, 2022.

[3] R. L. Siegel, K. D. Miller, and A. Jemal, "Cancer statistics, 2019," *CA: A Cancer Journal for Clinicians*, vol. 69, no. 1, pp. 7–34, 2019.

[4] A. W. Rosen, T. H. Degett, and I. Gögenur, "Individualized treatment of colon cancer," *Weekly Laeger*, vol. 178, no. 31, Article ID V11150916, 2016.

[5] Y. Hashiguchi, K. Muro, Y. Saito et al., "Japanese Society for Cancer of the Colon and Rectum (JSCCR) guidelines 2019 for the treatment of colorectal cancer," *International Journal of Clinical Oncology*, vol. 25, no. 1, pp. 1–42, 2020.

[6] S. Karaman and M. Detmar, "Mechanisms of lymphatic metastasis," *Journal of Clinical Investigation*, vol. 124, no. 3, pp. 922–928, 2014.

[7] Z. Xiao, G. Luo, C. Liu et al., "Molecular mechanism underlying lymphatic metastasis in pancreatic cancer," *BioMed Research International*, vol. 2014, Article ID 925845, 15 pages, 2014.

[8] O. Vycital, M. Dubova, R. Palek et al., "The impact of immune interaction on the metastatic infiltration of colorectal carcinoma to lymph nodes," *Anticancer Research*, vol. 38, no. 7, pp. 4159–4167, 2018.

[9] J. Lin, Z. Cao, D. Yu, and W. Cai, "Identification of transcription factor-related gene signature and risk score model for colon adenocarcinoma," *Frontiers in Genetics*, vol. 12, Article ID 709133, 2021.

[10] M. A. S. Broggi, L. Maillat, C. C. Clement et al., "Tumor-associated factors are enriched in lymphatic exudate compared to plasma in metastatic melanoma patients," *Journal of Experimental Medicine*, vol. 216, no. 5, pp. 1091–1107, 2019.

[11] K. Tomczak, P. Czerwińska, and M. Wiznerowicz, "Review the cancer genome Atlas (TCGA): an immeasurable source of knowledge," *Contemporary Oncology*, vol. 1A, pp. A68–A77, 2015.

[12] Z. Wang, M. A. Jensen, and J. C. Zenklusen, "A practical guide to the cancer genome Atlas (TCGA)," *Methods in Molecular Biology*, vol. 1418, pp. 111–141, 2016.

[13] P. Charoentong, F. Finotello, M. Angelova et al., "Pan-cancer immunogenomic analyses reveal genotype-immunophenotype relationships and predictors of response to checkpoint blockade," *Cell Reports*, vol. 18, no. 1, pp. 248–262, 2017.

[14] M. Zanfardino, K. Pane, P. Mirabelli, M. Salvatore, and M. Franzese, "TCGA-TCIA impact on radiogenomics cancer research: a systematic review," *International Journal of Molecular Sciences*, vol. 20, no. 23, 2019.

[15] M. I. Love, W. Huber, and S. Anders, "Moderated estimation of fold change and dispersion for RNA-seq data with DESeq2," *Genome Biology*, vol. 15, no. 12, p. 550, 2014.

[16] S. Liu, Y. Cai, E. Changyong, J. Sheng, and X. Zhang, "Screening and validation of independent predictors of poor survival in pancreatic cancer," *Pathology and Oncology Research*, vol. 27, Article ID 1609868, 2021.

[17] J. Liu, T. Lichtenberg, K. A. Hoadley et al., "An integrated TCGA pan-cancer clinical data resource to drive high-quality survival outcome analytics," *Cell*, vol. 173, 2018.

[18] W. Walter, F. Sánchez-Cabo, and M. Ricote, "GOplot: an R package for visually combining expression data with functional analysis," *Bioinformatics*, vol. 31, no. 17, pp. 2912–2914, 2015.

[19] G. Y. Chen, J. Luo, Y. Liu, X. B. Yu, X. Y. Liu, and Q. W. Tao, "Network pharmacology analysis and experimental validation to investigate the mechanism of total flavonoids of rhizoma drynariae in treating rheumatoid arthritis," *Drug Design, Development and Therapy*, vol. 16, pp. 1743–1766, 2022.

[20] G. Y. Chen, X. Y. Liu, J. Luo, X. B. Yu, Y. Liu, and Q. W. Tao, "Integrating network pharmacology and experimental validation to explore the key mechanism of gubitong recipe in the treatment of osteoarthritis," *Computational and Mathematical Methods in Medicine*, vol. 2022, Article ID 7858925, 25 pages, 2022.

[21] G. Yu, L. G. Wang, Y. Han, and Q. Y. He, "lusterProfiler: an R Package for comparing biological themes among gene clusters," *OMICS: A Journal of Integrative Biology*, vol. 16, no. 5, pp. 284–287, 2012.

[22] A. Subramanian, P. Tamayo, V. K. Mootha et al., "Gene set enrichment analysis: a knowledge-based approach for interpreting genome-wide expression profiles," *Proceedings of the National Academy of Sciences*, vol. 102, no. 43, pp. 15545–15550, 2005.

[23] J. Friedman, T. Hastie, and R. Tibshirani, "Regularization paths for generalized linear models via coordinate descent," *Journal of Statistical Software*, vol. 33, no. 1, pp. 1–22, 2010.

[24] Y. Fang, S. Huang, L. Han, S. Wang, and B. Xiong, "Comprehensive analysis of peritoneal metastasis sequencing data to identify LINC00924 as a prognostic biomarker in gastric cancer," *Cancer Management and Research*, vol. 13, pp. 5599–5611, 2021.

[25] S. Sun, W. Guo, Z. Wang et al., "Development and validation of an immune related prognostic signature in lung adenocarcinoma," *Cancer Medicine*, vol. 9, no. 16, pp. 5960–5975, 2020.

[26] J. Su, L. F. Miao, X. H. Ye, M. S. Cui, and X. F. He, "Development of prognostic signature and nomogram for patients with breast cancer," *Medicine*, vol. 98, no. 11, Article ID e14617, 2019.

[27] S. Hänzelmann, R. Castelo, and J. Guinney, "GSVA: gene set variation analysis for microarray and RNA-Seq data," *BMC Bioinformatics*, vol. 14, no. 1, p. 7, 2013.

[28] G. Bindea, B. Mlecnik, M. Tosolini et al., "Spatiotemporal dynamics of intratumoral immune cells reveal the immune

landscape in human cancer," *Immunity*, vol. 39, no. 4, pp. 782–795, 2013.

[29] L. Zhang, P. Qing, H. Yang, Y. Wu, Y. Liu, and Y. Luo, "Gut microbiome and metabolites in systemic lupus erythematosus: link, mechanisms and intervention," *Frontiers in Immunology*, vol. 12, Article ID 686501, 2021.

[30] M. Kiriakidou and C. L. Ching, "Systemic lupus erythematosus," *Annals of Internal Medicine*, vol. 172, no. 11, pp. ITC81–ITC96, 2020.

[31] H. Yu, Y. Nagafuchi, and K. Fujio, "Clinical and immunological biomarkers for systemic lupus erythematosus," *Biomolecules*, vol. 11, no. 7, p. 928, 2021.

[32] S. Yang, Y. Wu, Y. Deng et al., "Identification of a prognostic immune signature for cervical cancer to predict survival and response to immune checkpoint inhibitors," *OncoImmunology*, vol. 8, no. 12, Article ID e1659094, 2019.

[33] N. Fujimoto and L. C. Dieterich, "Mechanisms and clinical significance of tumor lymphatic invasion," *Cells*, vol. 10, no. 10, p. 2585, 2021.

[34] J. Yao, Q. Chen, Y. Deng et al., "Nomograms predicting primary lymph node metastases and prognosis for synchronous colorectal liver metastasis with simultaneous resection of colorectal cancer and liver metastases," *Annals of Palliative Medicine*, vol. 10, no. 4, pp. 4220–4231, 2021.

[35] A. R. Dezube and M. T. Jaklitsch, "Minimizing residual occult nodal metastasis in NSCLC: recent advances, current status and controversies," *Expert Review of Anticancer Therapy*, vol. 20, no. 2, pp. 117–130, 2020.

[36] I. H. Lee, G. Kim, S. G. Kwak et al., "Predictive value of circulating miRNAs in lymph node metastasis for colon cancer," *Genes*, vol. 12, no. 2, p. 176, 2021.

[37] J. Liu, C. Dong, G. Jiang, X. Lu, Y. Liu, and H. Wu, "Transcription factor expression as a predictor of colon cancer prognosis: a machine learning practice," *BMC Medical Genomics*, vol. 13, 2020.

[38] D. Glavan, V. Gheorman, A. Gresita, D. M. Hermann, I. Udristoiu, and A. Popa-Wagner, "Identification of transcriptome alterations in the prefrontal cortex, hippocampus, amygdala and hippocampus of suicide victims," *Scientific Reports*, vol. 11, no. 1, Article ID 18853, 2021.

[39] J. Zhou, Q. Hu, X. Wang, W. Cheng, C. Pan, and X. Xing, "Development and validation of a novel and robust blood small nuclear RNA signature in diagnosing autism spectrum disorder," *Medicine*, vol. 98, no. 45, Article ID e17858, 2019.

[40] F. A. C. da Luz, E. da Costa Marinho, C. P. Nascimento et al., "Prognosis value of lymphovascular invasion in patients with invasive ductal breast carcinoma according to lymph node metastasis status," *Ecancermedicalscience*, vol. 16, 2022.

[41] X. J. Chen, W. F. Wei, Z. C. Wang et al., "A novel lymphatic pattern promotes metastasis of cervical cancer in a hypoxic tumour-associated macrophage-dependent manner," *Angiogenesis*, vol. 24, no. 3, pp. 549–565, 2021.

[42] M. Zhang, Y. Wang, Y. Wang, Y. Bai, and D. Gu, "Association between systemic lupus erythematosus and cancer morbidity and mortality: findings from cohort studies," *Frontiers in Oncology*, vol. 12, Article ID 860794, 2022.

[43] S. Mao, H. Shen, and J. Zhang, "Systemic lupus erythematosus and malignancies risk," *Journal of Cancer Research and Clinical Oncology*, vol. 142, no. 1, pp. 253–262, 2016.

[44] Y. J. Shao, J. J. Ni, S. Y. Wei et al., "IRF1-mediated immune cell infiltration is associated with metastasis in colon adenocarcinoma," *Medicine*, vol. 99, no. 37, Article ID e22170, 2020.

Hindawi
Evidence-Based Complementary and Alternative Medicine
Volume 2022, Article ID 5045869, 8 pages
https://doi.org/10.1155/2022/5045869

Research Article

Ultrasound-Guided Percutaneous Transhepatic Gallbladder Drainage Improves the Prognosis of Patients with Severe Acute Cholecystitis

Xin Jin, Yunshan Jiang, and Jiongjiong Tang

Department of Ultrasound Medicine, The Central Hospital of Yongzhou, Yongzhou, Hunan 425006, China

Correspondence should be addressed to Yunshan Jiang; 3434123465@qq.com and Jiongjiong Tang; yonglingtjj@outlook.com

Received 12 July 2022; Revised 29 July 2022; Accepted 3 August 2022; Published 29 August 2022

Academic Editor: Xueliang Wu

The aim of this study was to investigate the clinical efficacy of ultrasound-guided percutaneous transhepatic gallbladder drainage (PTGD) for the treatment of severe acute cholecystitis (AC). The data of 40 patients diagnosed with severe AC at our hospital between August 2020 and June 2021 were retrieved and classified into a PTGD group, open cholecystostomy (OC) group, laparoscopic cholecystectomy (LC) group, and conventional conservative treatment (CT) group. Before treatment and on days 1, 3, 5, and 7 after treatment, their serum levels of alanine aminotransferase (ALT), alkaline phosphatase (ALP), aspartate aminotransferase (AST), total bilirubin (TBIL), triglyceride (TG), high-density lipoprotein (HDL), low-density lipoprotein (LDL), white blood cell count (WBC), IL-2, IL-4, IL-6, IL-8, and cancer antigen 19–9 (CA19-9) were measured. Additionally, clinical manifestations such as body temperature and pain score were monitored before treatment and at 24, 48, and 72 hours after treatment. The recovery time and complications/adverse reactions were statistically analyzed, and the Kaplan–Meier survival curve was plotted. After treatment, compared with the other three groups, the PTGD group had a significant reduction in serum indicators, including WBC and inflammatory factors, recovery time, pain score, and complications, and benefitted from better treatment efficacy and higher survival rate. Thus, ultrasound-guided PTGD was found to be more effective in treating severe AC patients and was associated with improved patient prognoses.

1. Introduction

Humans have long suffered from gallstones. According to research statistics, about 10%–15% of Americans have gallstones [1]. However, most patients with gallstones are asymptomatic. Population-based studies showed that 10–18% of patients with asymptomatic gallstones may experience biliary pain, of whom 7% might require surgical intervention and 1–4% could lead to complications such as acute cholecystitis (AC), gallstone pancreatitis, and choledocholithiasis [2]. It has been reported that the incidence of gallbladder disease increases with age, threatening the health of the aging population [3]. Gallstones sometimes migrate out of the gallbladder, block the normal flow of bile, and cause inflammation and infection of the gallbladder. This resulting condition is called cholecystitis and can lead to persistent and intense abdominal pain, fever, nausea, and vomiting [4].

AC accounts for 14–30% of cholecystectomies [5] and is defined as an inflammation of the gallbladder, usually caused by cystic duct obstruction [6]. The most common causes of cystic duct obstruction are gallstones and cholestasis. Other less common causes include masses (primary tumors or gallbladder polyps), parasites, or foreign bodies. Acute calculous cholecystitis is a common disease that requires surgical treatment. It was reported that approximately 120,000 cholecystectomies are performed in the United States annually [7]. If left treated, AC could lead to persistent obstruction of the cystic duct, causing mucus accumulation due to its continued production, and no outlet for drainage. As a result, the gallbladder pressure increases and venous stasis occurs, followed by arterial

stasis and ischemic gallbladder necrosis. Necrotic tissue then causes complications such as gallbladder perforation and empyema.

Laparoscopic cholecystectomy (LC) is currently the gold standard for treating AC [8]. However, cholecystectomy is not suitable for many elderly patients with multiple comorbidities. For patients who are not candidates for surgery, less invasive interventions, such as percutaneous transhepatic gallbladder drainage (PTGD), are performed to reduce surgery-related morbidity and mortality [9]. PTGD is a minimally invasive surgery to decompress the gallbladder and is usually used in critically ill patients [10]. In clinical practice, the indications for PTGD include calculous and acalculous cholecystitis, gallbladder perforation, malignant obstruction, percutaneous gallstone removal, and biliary drainage [11]. In addition, PTGD is often used as one of the auxiliary examination methods for cholangiography, gallstone dissolution, and lithotripsy [12]. In the diagnosis of cholecystitis, imaging examinations such as ultrasound, CT, and hepatobiliary scan are essential for surgery to determine the specific circumstances of the gallbladder, as well as to select the appropriate access for gallbladder decompression [13]. Previous clinical studies showed that the overall success rate of PTGD was higher than 95% [14], achieving a clinical improvement in 56%–93% of patients, with only 3%–13% developing complications such as biliary peritonitis, massive hemorrhage, and hemothorax/pneumothorax [14].

However, the effects of PTGD in treating severe AC patients remain controversial. Thus, in this study, we compared PTGD with other surgical methods to determine its clinical efficacy and impact on the survival of severe AC patients to provide evidence for its clinical significance in severe AC.

2. Materials and Methods

2.1. Study Subjects. In this study, severe AC was defined as a gallbladder inflammation complicated with acute pain and serum markers abnormalities, such as an increase in WBC levels $>15 \times 10^9$/L, and diagnosed via imaging. The data of patients diagnosed with severe AC in our hospital between August 2016 and June 2019 were retrospectively retrieved, analyzed, and divided into four groups based on their treatment methods, namely, the ultrasound-guided PTGD group (PTGD, $n = 14$), open cholecystostomy group (OC, $n = 12$), LC group (LC, $n = 8$), and conventional conservative treatment group (CT, $n = 6$). The study inclusion criteria were as follows: (1) all patients underwent color Doppler ultrasound, CT, or MRI to confirm the diagnosis; (2) did not receive any treatments, such as antibiotics, prior to diagnosis; and (3) had typical clinical manifestations of AC such as the presence of fever/shivering, right upper abdominal pain/tenderness, diffuse pain/tenderness, nausea/vomiting, and/or positive Murphy's sign; and (4) had almost similar postoperative management, unless they had postoperative complications, which were treated on an individualized basis. The exclusion criteria were as follows: (1) the presence of malignant tumors and dysfunction of vital organs; (2) severe systemic infection; (3) gastrointestinal diseases, such as gastrointestinal perforation and bleeding; (4) a history of abdominal surgery; and (5) poor coagulation, mental illness, severe cognitive impairment, or language problems. The baseline data of the patients, including age, gender, body mass index (BMI), onset symptoms, gallbladder diameter, stage of septic shock, site of infection, duration of abdominal pain, and disease history, were recorded. Since this was a retrospective study, the patients' treatments were based on the treating physician's discretion and after consultation with the patients and/or relatives. The study protocol was approved by the Ethics Committee of The Central Hospital of Yongzhou. All the methods were performed in accordance with the Declaration of Helsinki.

2.2. Surgical Methods. In the PTGD group, patients were placed in the supine position. Then, the size and location of the gallbladder and surrounding organs were scanned using an ultrasound machine, based on which an appropriate puncture site and puncture route were selected. After anesthetic infiltration into the peritoneum at the puncture site, the gallbladder was punctured using a disposable pigtail drainage catheter under ultrasound guidance. The puncture needle was made to enter the gallbladder cavity, and the outflow of bile was observed. Then, the guidewire was inserted into the gallbladder, and the chest wall was expanded to insert the drainage tube. The extracted bile or pus was connected to a drainage bag, and the fixed line of the drainage tube was tightened. Last, after the drainage tube was fixed, the body surface was sutured. After treatment, routine anti-infection, semiliquid, low-fat food, and other symptomatic and supportive treatment were given.

In the OC group, patients were placed in the supine position. Then, a paramidline incision of about 10 cm in length was made. The drainage tube was inserted in the gallbladder, and the incision was sutured. After treatment, the patients received symptomatic and supportive treatment such as conventional anti-infection and intravenous nutrition.

In the LC group, patients were treated with four-port LC. During the procedure, the conditions of Calot's triangle and abdominal cavity were observed. After clarifying the relationship between the three ducts, the neck and duct of the gallbladder were disconnected. Lastly, the gallbladder was removed using a combined antegrade and retrograde approach, and an abdominal drainage tube was inserted routinely.

In the CT group, surgical treatment was recommended after admission, but the patients and their families refused. Therefore, during hospitalization, the patients only received conventional anti-infective conservative treatment, and symptomatic treatment was performed according to the condition.

2.3. Detection of Biochemical Indicators. Fasting serum was collected from all patients on days 1, 3, 5, and 7 after treatment. After 2-h standing, the supernatant was collected after centrifugation at 3500 rpm for 10 min. Then, an automatic biochemical analyzer (Mindray, China) was

employed to measure the expression of alanine aminotransferase (ALT), alkaline phosphatase (ALP), aspartate aminotransferase (AST), total bilirubin (TBIL), triglyceride (TG), high-density lipoprotein (HDL), low-density lipoprotein (LDL), and white blood cell count (WBC) in the serum.

2.4. ELISA. Fasting serum was collected from all patients on days 1, 3, 5, and 7 after treatment. After 2-h standing, the supernatant was collected after centrifugation at 3500 rpm for 10 min. Then, the corresponding ELISA kits (MULTI-SCIENCES (LIANKE), China) were utilized to detect the expression of interleukin (IL)-2, IL-4, IL-6, IL-8, and cancer antigen 19–9 (CA19-9) in serum.

2.5. Detection of Clinical Indicators. Before treatment and at 24, 48, and 72 hours after treatment, the following clinical indicators were recorded, including pain score, body temperature, systolic blood pressure, and diastolic blood pressure. Additionally, the duration of abdominal pain, recovery time of WBC, operation duration, extubation time, and length of hospital stay were observed after treatment. The occurrence of complications/adverse reactions was also recorded.

2.6. Follow-Up. All patients were followed up for 2 years, and the data on patients' survival status were obtained to calculate the survival rate of each treatment group.

2.7. Statistical Analysis. All data were statistically analyzed using the SPSS 26.0 software (SPSS Inc., Chicago, IL, USA). Measurement data were expressed as mean ± standard deviation (SD), and one-way analysis of variance (ANOVA) was used for comparison between groups. Enumeration data were expressed as frequency (n) and rate (%), and the chi-squared test or Fisher's exact test was used for statistical analysis. Survival curve was plotted using the Kaplan–Meier and compared with the log-rank test. $P < 0.05$ was set as a cutoff for statistical significance.

3. Results

3.1. Baseline Data of Patients. A total of 40 patients were found eligible for this study. The patients in all groups were over 60 years of age. There were no significant differences in age, gender, BMI, clinical symptoms, time from onset to admission, trigger, history of diseases disease, ASA grade, and APACHE II score among the groups (Table 1). Therefore, the comparability of the patients was ensured.

3.2. Comparison of Preoperative Clinical Indicators among the Four Groups. The preoperative clinical parameters were compared, including WBC, neutrophil count, ALT, ALP, AST, TBIL, TG, HDL, LDL, and systolic and diastolic blood pressure. The results showed no significant difference in these indicators among the four groups (Table 2).

3.3. Comparison of Postoperative Clinical Indicators among the Four Groups. Their postoperative clinical symptoms were compared, and the results including that the duration of abdominal pain (18.03 ± 3.02), recovery time of WBC (3.21 ± 0.40), operation duration (58.31 ± 10.09), extubation time (2.10 ± 0.40), and length of hospital stay (2.99 ± 1.31) were the shortest in the PTGD group, while the CT group had the worst effect (Table 3).

3.4. Comparison of Postoperative Serum Indicators at Different Time Points among the Four Groups. Clinical biochemical parameters and inflammatory factors were measured on days 1, 3, 5, and 7 after treatment in the four groups. The results showed that the ALT, AST, ALP, TBIL, WBC, and CA19-9 on days 3, 5, and 7 after treatment in the four groups gradually decreased compared with Day 1 and returned to the normal range, with the PTGD group demonstrating the most significant decrease (Figure 1(a)). Further examination of the serum levels of inflammatory factors in the four groups showed that the IL-2, IL-6, and IL-8 and IL-4 levels in the four groups also gradually returned to the normal range on 3, 5, and 7 days after treatment compared with Day 1. Compared with the other groups, the PTGD group had the lowest expression of inflammatory factors and the highest expression of anti-inflammatory factors from day 1 to day 7 after treatment (Figure 1(b)).

3.5. Comparison of Postoperative Complications among the Four Groups. The results showed that all four groups had some complications or adverse reactions after treatment. The patients in the PTGD group mainly had four complications, including wound infection ($n = 1$), stress ulcer ($n = 1$), urinary tract infection ($n = 2$), and incomplete intestinal obstruction ($n = 1$). Seven kinds of complications or adverse reactions occurred in the other three groups, with the CT group having the highest number of complications than the other groups. For instance, the results showed that the probability of upper gastrointestinal bleeding in the CT group was as high as 50%. Overall, the PTGD group had the lowest probability of complications (Table 4).

3.6. Comparison of Survival among the Four Groups. Forty patients were followed up for two years, and their survival status and duration were analyzed. The results showed that during follow-up, there were 2 deaths (14.3%) in the PTGD group, 4 deaths (33.3%) in the LC group, 4 deaths (50%) in the OC group, and 4 deaths (66.7%) in the CT group (Figure 2). Thus, the survival rate of the PTGD group was the highest (85.7%), while the CT group showed the lowest survival rate (33.3%).

Table 1: Baseline data of the severe acute cholecystitis patients included in this study.

Variables	PTGD ($n = 14$)	LC ($n = 12$)	OC ($n = 8$)	CT ($n = 6$)	P value
Age (year)	62.5 ± 12.0	63.3 ± 13.9	66.5 ± 9.9	60.8 ± 15.7	NS
Gender (male/female)	6/8	7/5	3/5	3/3	NS
BMI (kg/m^2)	28.23 ± 5.02	26.78 ± 6.03	28.23 ± 6.93	26.03 ± 4.02	NS
Clinical symptoms/signs (n (%))					
Fever/shivering	10 (71.4)	8 (66.7)	5 (62.5)	4 (66.7)	NS
Right upper abdominal pain/tenderness	13 (92.9)	12 (100.0)	7 (87.5)	6 (100.0)	NS
Diffuse pain/tenderness	7 (50.0)	5 (41.7)	5 (62.5)	2 (33.3)	NS
Nausea/vomiting	5 (35.7)	4 (33.3)	3 (37.5)	3 (50.0)	NS
Positive Murphy's sign	8 (57.1)	5 (41.7)	3 (37.5)	3 (50.0)	NS
Time from onset to admission (d)	4.0 ± 1.5	3.5 ± 1.3	4.5 ± 1.7	4.3 ± 2.5	NS
Trigger (n (%))					
Calculous	10 (71.4)	8 (66.7)	7 (87.5)	4 (66.7)	NS
Noncalculous	4 (28.6)	4 (33.3)	1 (12.5)	2 (33.3)	NS
Thickness of gallbladder wall (cm)	0.68 ± 0.23	0.73 ± 0.26	0.66 ± 0.30	0.70 ± 0.34	NS
History of diseases (n (%))					
Cardiovascular diseases	9 (64.3)	6 (50.0)	5 (62.5)	4 (66.7)	NS
Lung diseases	3 (21.4)	2 (16.7)	2 (25.0)	1 (16.7)	NS
Diabetes	4 (28.6)	2 (16.7)	3 (37.5)	2 (33.3)	NS
Chronic kidney disease	2 (14.3)	1 (8.3)	1 (12.5)	1 (16.7)	NS
ASA grade (n (%))					
≤II	5 (35.7)	4 (33.3)	4 (50.0)	2 (33.3)	NS
III-IV	9 (64.3)	8 (66.7)	4 (50.0)	4 (66.7)	NS
APACHE II score (point)	15.6 ± 3.6	14.2 ± 4.5	13.6 ± 2.8	14.7 ± 3.5	NS

Note: PTGD, percutaneous transhepatic gallbladder drainage; LC, laparoscopic cholecystectomy; OC: open cholecystostomy; CT, conventional conservative treatment; BMI, body mass index.

Table 2: Comparison of preoperative clinical indicators among the four treatment groups.

Variables	PTGD ($n = 14$)	LC ($n = 12$)	OC ($n = 8$)	CT ($n = 6$)	P value
WBC (×10^9/L)	16.71 ± 3.60	15.89 ± 2.49	16.30 ± 3.98	17.10 ± 4.56	0.898
Neutrophil count (%)	88.68 ± 6.64	88.05 ± 7.15	89.76 ± 5.32	88.82 ± 6.50	0.954
ALT (U/L)	73.35 ± 30.04	70.10 ± 29.03	76.35 ± 24.99	72.49 ± 32.05	0.973
ALP (U/L)	142.96 ± 32.76	140.66 ± 36.12	139.64 ± 30.09	138.17 ± 31.30	0.991
AST (U/L)	81.22 ± 24.92	77.81 ± 22.06	79.35 ± 26.20	83.52 ± 31.11	0.970
TBIL (μmol/L)	41.67 ± 11.7	38.35 ± 12.89	38.91 ± 14.2	44.57 ± 16.14	0.767
TG (mmol/mL)	3.21 ± 0.40	3.29 ± 0.45	3.27 ± 0.36	2.9 ± 0.25	0.184
HDL (mmol/mL)	0.9 ± 0.25	0.91 ± 0.30	0.89 ± 0.28	0.93 ± 0.23	0.996
LDL (mmol/mL)	3.1 ± 0.7	3.0 ± 0.6	3.2 ± 0.5	2.9 ± 0.6	0.847
Systolic blood pressure (mmHg)	146.64 ± 26.05	145.75 ± 31.97	144.50 ± 28.65	145.93 ± 27.85	0.999
Diastolic blood pressure (mmHg)	93.36 ± 13.11	90.92 ± 11.07	92.38 ± 14.02	94.0 ± 15.10	0.956

Note: PTGD, percutaneous transhepatic gallbladder drainage; LC, laparoscopic cholecystectomy; OC: open cholecystostomy; CT, conventional conservative treatment; WBC, white blood cell count; ALT, alanine aminotransferase; ALP, alkaline phosphatase; AST, aspartate aminotransferase; TBIL, total bilirubin; TG, triglyceride; HDL, high-density lipoprotein; LDL, low-density lipoprotein.

Table 3: Comparison of postoperative clinical indicators among the four groups.

Variables	PTGD ($n = 14$)	LC ($n = 12$)	OC ($n = 8$)	CT ($n = 6$)	P value
Duration of abdominal pain (h)	18.03 ± 3.02	22.48 ± 3.32	28.46 ± 3.96	31.70 ± 5.94	<0.001***
Recovery time of WBC (d)	3.21 ± 0.40	4.00 ± 1.00	5.54 ± 2.01	7.00 ± 2.20	<0.001***
Operation duration (h)	58.31 ± 10.09	66.07 ± 12.12	71.65 ± 14	83.58 ± 23.12	0.005**
Extubation time (h)	2.10 ± 0.40	2.59 ± 0.59	2.98 ± 1.01	4.18 ± 1.49	<0.001***
Length of hospital stay (d)	2.99 ± 1.31	3.99 ± 1.1.51	5.99 ± 2	8.07 ± 2.98	<0.001***

Note: *** $P < 0.001$ vs. CT group; PTGD, percutaneous transhepatic gallbladder drainage; LC, laparoscopic cholecystectomy; OC: open cholecystostomy; CT, conventional conservative treatment; WBC, white blood cell count.

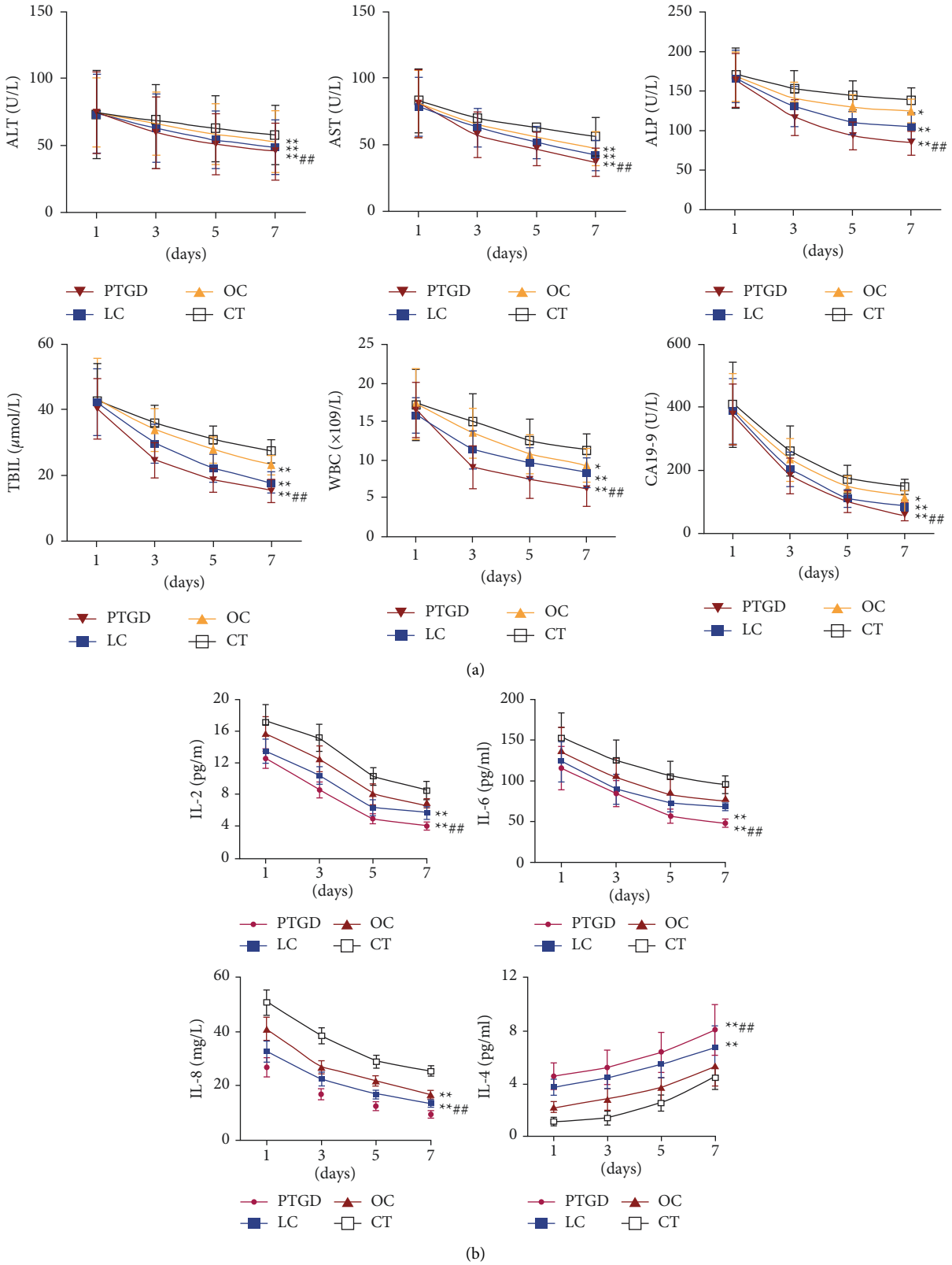

Figure 1: Comparison of serum indicators at different time points after treatment among the four treatment groups. (a) Serum ALT, AST, ALP, TBIL, WBC, and CA19-9 levels on days 1, 3, 5, and 7 after treatment. (b) Serum IL-2, IL-4, IL-6, and IL-8 levels on days 1, 3, 5, and 7 after treatment. $^{*}P < 0.05$, $^{**}P < 0.01$ *vs.* the CT group, $^{\#\#}P < 0.01$ *vs.* the LC group. PTGD, percutaneous transhepatic gallbladder drainage; LC, laparoscopic cholecystectomy; OC, open cholecystostomy; CT, conventional conservative treatment.

Table 4: Comparison of postoperative complications among the four treatment groups.

Complication (n (%))	PTGD ($n = 14$)	LC ($n = 12$)	OC ($n = 8$)	CT ($n = 6$)	P value
Wound infection	1 (7.14)	2 (16.7)	3 (37.5)	0 (0.0)	0.198
Upper gastrointestinal bleeding	0 (0.0)	1 (8.3)	2 (25.0)	3 (50.0)	0.026
Stress ulcer	1 (7.14)	4 (33.3)	3 (37.5)	4 (66.7)	0.045
Urinary tract infection	2 (14.3)	0 (0.0)	0 (0.0)	1 (16.7)	0.350
Incomplete intestinal obstruction	1 (7.14)	1 (8.3)	2 (25.0)	2 (33.3)	0.346
Infectious pneumonia	0 (0.0)	2 (16.7)	1 (12.5)	2 (33.3)	0.206
Acute renal failure	0 (0.0)	1 (8.3)	2 (25.0)	1 (16.7)	0.317
Death during hospitalization	0 (0.0)	1 (8.3)	2 (25.0)	1 (16.7)	0.317

Note: PTGD, percutaneous transhepatic gallbladder drainage; LC, laparoscopic cholecystectomy; OC: open cholecystostomy; CT, conventional conservative treatment.

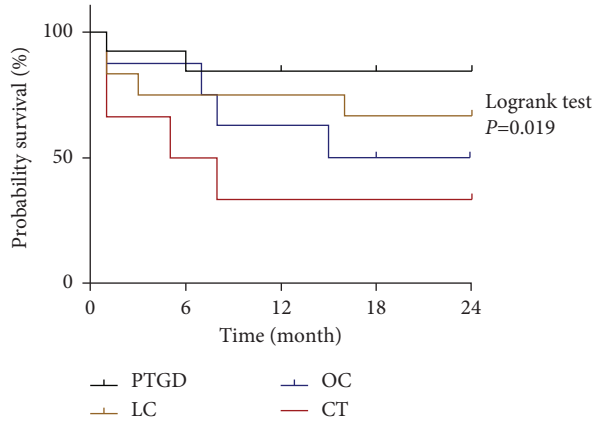

Figure 2: Comparison of survival among the four treatment groups.

3.7. Typical Case Report of Severe AC from Hospitalization to Discharge. A 38-year-old woman was hospitalized in our hospital for 3 days with persistent distending pain in the upper abdomen, no pain radiating to other parts of the body, no correlation between pain and position change, no self-remission after rest, and absence of nausea, vomiting, diarrhea, chills, fever, and acid reflux. Physical examination showed that the pressure pain was located in the epigastrium and subxiphoid process, with percussion pain in the liver area. No rebound tenderness or obvious mass was observed, and the liver and spleen were not enlarged. An abdominal ultrasound showed that the diameter of the gallbladder was 200×48 mm (Figure 3). Based on these observations, acute severe cholecystitis was considered, and the patient underwent ultrasound-guided percutaneous transcatheter gallbladder puncture placement. She was placed in a supine position. After routine disinfection, real-time color ultrasound was used to guide and monitor the needle entry to avoid large vessels. It passed through a portion of liver tissue, and after its tip reached the gallbladder, the needle core was withdrawn, and brown viscous bile was aspirated. Then, the support was removed, and the traction line was pulled. After successfully placing the catheter, it was externally fixed (Figure 4). Following this procedure, the patient's abdominal distention and discomfort were significantly relieved, and she was discharged on the third day of hospitalization.

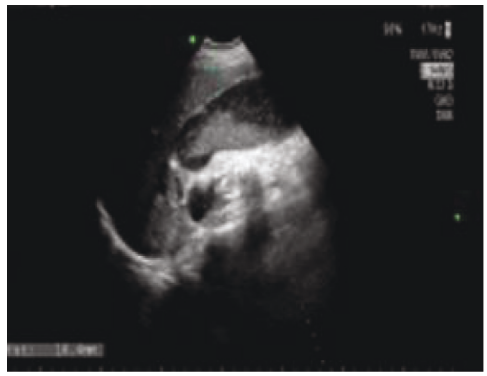

Figure 3: Illustration of an enlarged gallbladder, of size approximately 200×48 mm.

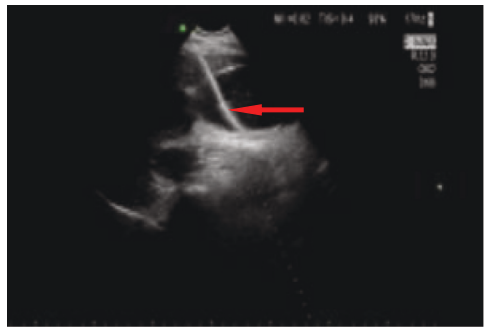

Figure 4: Illustration of a successfully cannulated gallbladder. The catheter was successfully punctured into the gallbladder, as indicated by the red arrow.

4. Discussion

Our results showed the levels of ALT, AST, ALP, TBIL, WBC, and CA19-9 in all four treatment groups gradually decreased from Day 1 to Day 7, with the PTGD group demonstrating the most significant decrease, and the levels

of IL-2, IL-6, IL-8, and IL-4 gradually returned within normal ranges, with the PTGD group demonstrating the lowest expression of inflammatory factors and highest expression of anti-inflammatory factors. These findings indicate that ultrasound-guided PTGD was the most effective treatment for AC patients, at least in this present study. AC is an acute inflammation triggered by cystic duct obstruction caused by various factors [15]. Studies have shown that ultrasound-guided PTGD has a high success rate in elderly AC patients and was associated with a low level of inflammation after surgery [16], which was concordant with the results of our study.

Like most inflammatory diseases, AC is usually associated with leukocytosis, but the manifestations may vary in different patients [17]. According to statistics, 32–53% of patients have fever when they come to the hospital, and 51–53% have leukocytosis [6]. In this study, we found that after treatment, the level of WBC was decreased in all four groups compared with before treatment, and the decrease was most prominent in the PTGD group, while it was least favorable in the CT group. Kim et al. also reported that PTGD could rapidly reverse local inflammation and reduce its systemic effects in patients who could not undergo surgery due to severe comorbidities [18].

Recently, ultrasound-guided PTGD has received significant attention as a potential method of internal gallbladder drainage and is indicated for high-risk patients who cannot undergo cholecystectomy [19]. This study confirmed that ultrasound-guided PTGD was associated with the shortest operation duration, extubation time, and length of hospital stay compared with the other three treatments. This could be because ultrasound-guided PTGD can be effectively performed with ultrasound assistance to directly observe the whole procedure, thereby reducing the risk of complications. Therefore, compared with traditional conventional surgery, ultrasound-guided PTGD is associated with more accurate localization, a clearer field of vision, less trauma, and lower risk of complications [20]. In our typical case, a middle-aged woman was hospitalized due to persistent epigastric pain and discomfort. After completing relevant examinations, she was diagnosed with acute severe cholecystitis and was immediately treated with ultrasound-guided percutaneous transcatheter cholecystocentesis, during which the patient's vital signs were stable. In a randomized study of 61 patients, it was observed that patients treated with PTGD had a shorter hospital stay than those who received LC after conservative treatment [21]. Regarding the treatment response rate, this study also found that patients in the PTGD group had the best prognosis among the four groups. Another randomized controlled trial, including 58 severe AC patients, demonstrated that PTGD was clinically effective in 90% of patients, while OC was effective in 61% of patients [22]. In addition, a systematic review of PTGD for AC patients reported that PTGD was clinically successful, with 85.6% of the patients showing clinical improvement within 48–72 hours, and only 6.24% experienced adverse events. Although the mortality related to the surgery was only 0.36%, the overall mortality was 15% [23]. In contrast to our study, patients in the PTGD group had the lowest incidence of complications and adverse reactions.

The efficacy and safety of PTGD are still somewhat controversial. A study reported that in a case series of high-risk elderly AC patients, the mortality rate of cholecystectomy was 0%, while that of PTGD was 17.2% [24]. The main reason for such controversy could be that the guiding modalities for PTGD were different. PTGD, according to multiple meta-analyses, is reliable under ultrasound guidance, and even ultrasound-guided PTGD has higher success rates and lower readmission and reintervention rates, with a 1-year adverse event rate relative to other modalities [25–28].

Despite the clinically important results in this study, some limitations have to be mentioned. First, this study was limited due to its retrospective nature and small cohort size. Second, the follow-up time was relatively short, and long-term follow-ups are required to further confirm the efficacy of PTGD. Third, this was a single-center study based on Chinese patients, and whether these observations would be similar in a multicenter and multiethnicity cohort remained to be determined.

5. Conclusion

In summary, compared with open cholecystostomy, LC, and conventional conservative treatment, ultrasound-guided PTGD was associated with the greatest normalization of serum indicators, fastest recovery time, lowest risk of complications, and highest survival rate; supporting the clinical application of PTGD in severe AC patients. However, due to the limited number of cases and additional limitations, further investigations in multicenter prospective settings are required to confirm the efficacy of PTGD.

Data Availability

The datasets generated and/or analyzed in the experiment are available from the corresponding author upon request.

Ethical Approval

The study protocol was approved by the Ethics Committee of the Central Hospital of Yongzhou. All the methods were carried out in accordance with the Declaration of Helsinki.

Conflicts of Interest

The authors declare that they have no conflicts of interest.

Authors' Contributions

Xin Jin and Yunshan Jiang designed the study. Yunshan Jiang collected the data. Jiongjiong Tang accomplished the statistical analyses. Xin Jin and Jiongjiong Tang drafted and revised the manuscript. All authors read and approved the final manuscript.

References

[1] L. M. Stinton, R. P. Myers, and E. A. Shaffer, "Epidemiology of gallstones," *Gastroenterology Clinics of North America*, vol. 39, no. 2, pp. 157–169, 2010.

[2] E. A. Shaffer, "Gallstone disease: epidemiology of gallbladder stone disease," *Best Practice & Research Clinical Gastroenterology*, vol. 20, no. 6, pp. 981–996, 2006.

[3] I. Halldestam, E. L. Enell, E. Kullman, and K. Borch, "Development of symptoms and complications in individuals with asymptomatic gallstones," *British Journal of Surgery*, vol. 91, no. 6, pp. 734–738, 2004.

[4] C. K. McSherry, H. Ferstenberg, W. F. Calhoun, E. Lahman, and M. Virshup, "The natural history of diagnosed gallstone disease in symptomatic and asymptomatic patients," *Annals of Surgery*, vol. 202, no. 1, pp. 59–63, 1985.

[5] D. F. Ransohoff, W. A. Gracie, L. B. Wolfenson, and D. Neuhauser, "Prophylactic cholecystectomy or expectant management for silent gallstones. A decision analysis to assess survival," *Annals of Internal Medicine*, vol. 99, no. 2, pp. 199–204, 1983.

[6] A. Hafif, M. Gutman, O. Kaplan, E. Winkler, R. R. Rozin, and Y. Skornick, "The management of acute cholecystitis in elderly patients," *The American Surgeon*, vol. 57, no. 10, pp. 648–652, 1991.

[7] S. M. Strasberg, "Acute calculous cholecystitis," *New England Journal of Medicine*, vol. 358, no. 26, pp. 2804–2811, 2008.

[8] M. H. Heim, "Epidemiology of diseases of the bile ducts and gallbladder," *Diseases of the Gallbladder and Bile Ducts: Diagnosis and Treatment*, Blackwell Publishing Ltd, Hoboken, NJ, USA, 2007.

[9] R. E. Glasgow, M. Cho, M. M. Hutter, and S. J. Mulvihill, "The spectrum and cost of complicated gallstone disease in California," *Archives of Surgery*, vol. 135, no. 9, pp. 1021–1025, 2000.

[10] A. De Santis, A. F. Attili, S. G. Corradini et al., "Gallstones and diabetes: a case-control study in a free-living population sample," *Hepatology*, vol. 25, no. 4, pp. 787–790, 1997.

[11] P. A. Myer, A. Mannalithara, G. Singh, G. Singh, P. J. Pasricha, and U. Ladabaum, "Clinical and economic burden of emergency department visits due to gastrointestinal diseases in the United States," *American Journal of Gastroenterology*, vol. 108, no. 9, pp. 1496–1507, 2013.

[12] C. de la Serna-Higuera, M. Perez-Miranda, P. Gil-Simon et al., "EUS-guided transenteric gallbladder drainage with a new fistula-forming, lumen-apposing metal stent," *Gastrointestinal Endoscopy*, vol. 77, no. 2, pp. 303–308, 2013.

[13] K. Kamata, M. Takenaka, M. Kitano et al., "Endoscopic ultrasound-guided gallbladder drainage for acute cholecystitis: long-term outcomes after removal of a self-expandable metal stent," *World Journal of Gastroenterology*, vol. 23, no. 4, pp. 661–667, 2017.

[14] P. A. Clavien, J. Barkun, M. L. de Oliveira et al., "The Clavien-Dindo classification of surgical complications: five-year experience," *Annals of Surgery*, vol. 250, no. 2, pp. 187–196, 2009.

[15] R. W. Xing, H. Q. Nie, and Y. Zhang, "Efficacy of laparoscopic cholecystectomy at different times after gallbladder puncture and drainage in elderly patients with acute cholecystitis," *Zhejiang Medical Journal*, vol. 43, no. 1, pp. 70–73, 2014.

[16] K. L. Li, F. Wang, and W. J. Gu, "Clinical observation of percutaneous transhepatic gallbladder drainage in the treatment of calculouscholecystitis," *China Continuing Medical Education*, vol. 9, no. 31, pp. 79-80, 2017.

[17] P. J. Gruber, R. A. Silverman, S. Gottesfeld, and E. Flaster, "Presence of fever and leukocytosis in acute cholecystitis," *Annals of Emergency Medicine*, vol. 28, no. 3, pp. 273–277, 1996.

[18] I. G. Kim, J. S. Kim, J. Y. Jeon et al., "Percutaneous transhepatic gallbladder drainage changes emergency laparoscopic cholecystectomy to an elective operation in patients with acute cholecystitis," *Journal of Laparoendoscopic & Advanced Surgical Techniques*, vol. 21, no. 10, pp. 941–946, 2011.

[19] S. M. Chan, A. Y. B. Teoh, H. C. Yip, V. W. Y. Wong, P. W. Y. Chiu, and E. K. W. Ng, "Feasibility of per-oral cholecystoscopy and advanced gallbladder interventions after EUS-guided gallbladder stenting (with video)," *Gastrointestinal Endoscopy*, vol. 85, no. 6, pp. 1225–1232, 2017.

[20] P. H. Yuan, "Clinical effect of ultrasound-guided percutaneous puncture and drainage of gallbladder for elderly patients with acute cholecystitis," *Chinese Remedies and Clinics*, vol. 21, no. 21, pp. 3556–3558, 2021.

[21] N. Akyurek, B. Salman, O. Yuksel et al., "Management of acute calculous cholecystitis in high-risk patients: percutaneous cholecystotomy followed by early laparoscopic cholecystectomy," *Surgical Laparoscopy Endoscopy & Percutaneous Techniques*, vol. 15, no. 6, pp. 315–320, 2005.

[22] K. Ito, N. Fujita, Y. Noda et al., "Percutaneous cholecystostomy versus gallbladder aspiration for acute cholecystitis: a prospective randomized controlled trial," *American Journal of Roentgenology*, vol. 183, no. 1, pp. 193–196, 2004.

[23] A. Winbladh, P. Gullstrand, J. Svanvik, and P. Sandstrom, "Systematic review of cholecystostomy as a treatment option in acute cholecystitis," *International Hepato-Pancreato-Biliary Association*, vol. 11, no. 3, pp. 183–193, 2009.

[24] J. C. Rodriguez-Sanjuan, A. Arruabarrena, L. Sanchez-Moreno, F. Gonzalez-Sanchez, L. A. Herrera, and M. Gomez-Fleitas, "Acute cholecystitis in high surgical risk patients: percutaneous cholecystostomy or emergency cholecystectomy?" *The American Journal of Surgery*, vol. 204, no. 1, pp. 54–59, 2012.

[25] S. Irani, S. Ngamruengphong, A. Teoh et al., "Similar efficacies of endoscopic ultrasound gallbladder drainage with a lumen-apposing metal stent versus percutaneous transhepatic gallbladder drainage for acute cholecystitis," *Clinical Gastroenterology and Hepatology*, vol. 15, no. 5, pp. 738–745, 2017.

[26] J. H. Choi, H. W. Kim, J. C. Lee et al., "Percutaneous transhepatic versus EUS-guided gallbladder drainage for malignant cystic duct obstruction," *Gastrointestinal Endoscopy*, vol. 85, no. 2, pp. 357–364, 2017.

[27] A. Y. B. Teoh, C. Serna, I. Penas et al., "Endoscopic ultrasound-guided gallbladder drainage reduces adverse events compared with percutaneous cholecystostomy in patients who are unfit for cholecystectomy," *Endoscopy*, vol. 49, no. 02, pp. 130–138, 2016.

[28] A. Tyberg, M. Saumoy, E. V. Sequeiros et al., "EUS-Guided versus percutaneous gallbladder drainage: isn't it time to convert?" *Journal of Clinical Gastroenterology*, vol. 52, no. 1, pp. 79–84, 2018.

Hindawi
Evidence-Based Complementary and Alternative Medicine
Volume 2023, Article ID 9787616, 1 page
https://doi.org/10.1155/2023/9787616

Retraction

Retracted: The Analysis of the Effect of Blood Transfusion on Changes of Blood Platelet Parameters in Patients with Leukemia Treated with Chemotherapy

Evidence-Based Complementary and Alternative Medicine

Received 15 August 2023; Accepted 15 August 2023; Published 16 August 2023

This article has been retracted by Hindawi following an investigation undertaken by the publisher [1]. This investigation has uncovered evidence of one or more of the following indicators of systematic manipulation of the publication process:

(1) Discrepancies in scope
(2) Discrepancies in the description of the research reported
(3) Discrepancies between the availability of data and the research described
(4) Inappropriate citations
(5) Incoherent, meaningless and/or irrelevant content included in the article
(6) Peer-review manipulation

The presence of these indicators undermines our confidence in the integrity of the article's content and we cannot, therefore, vouch for its reliability. Please note that this notice is intended solely to alert readers that the content of this article is unreliable. We have not investigated whether authors were aware of or involved in the systematic manipulation of the publication process.

Wiley and Hindawi regrets that the usual quality checks did not identify these issues before publication and have since put additional measures in place to safeguard research integrity.

We wish to credit our own Research Integrity and Research Publishing teams and anonymous and named external researchers and research integrity experts for contributing to this investigation.

The corresponding author, as the representative of all authors, has been given the opportunity to register their agreement or disagreement to this retraction. We have kept a record of any response received.

References

[1] Y. He, S. Liang, Y. Xu, C. Wan, F. Ma, and B. Wang, "The Analysis of the Effect of Blood Transfusion on Changes of Blood Platelet Parameters in Patients with Leukemia Treated with Chemotherapy," *Evidence-Based Complementary and Alternative Medicine*, vol. 2022, Article ID 2901993, 4 pages, 2022.

Hindawi
Evidence-Based Complementary and Alternative Medicine
Volume 2022, Article ID 2901993, 4 pages
https://doi.org/10.1155/2022/2901993

Research Article

The Analysis of the Effect of Blood Transfusion on Changes of Blood Platelet Parameters in Patients with Leukemia Treated with Chemotherapy

Yangxin He, Shanshan Liang, Yali Xu, Chunjing Wan, Feng Ma, and Baoyan Wang

Department of Blood Transfusion, The First Affiliated Hospital of Xi'an Jiaotong University, Xi'an 710061, Shannxi, China

Correspondence should be addressed to Baoyan Wang; he.yangxin@stu.xjtu.edu.cn

Received 29 June 2022; Revised 22 July 2022; Accepted 25 July 2022; Published 29 August 2022

Academic Editor: Xueliang Wu

Objective. To study and analyze the effect of blood transfusion on the change of blood platelet parameters in patients with leukemia treated with chemotherapy. *Methods*. Ninety-eight patients with leukemia treated with chemotherapy in the First Affiliated Hospital of Xi'an Jiaotong University from January 2021 to January 2022 were selected to observe the changes of platelet parameters before and after blood transfusion. *Results*. There was significant difference between pre-transfusion and post-transfusion indexes (platelet count, mean platelet volume, and hematocrit) ($P < 0.05$). After binary logistic regression analysis, the use of antibiotics (OR = 2.235), blood transfusion history (OR = 3.086), abnormal white blood cell count (OR = 1.134), and frozen plasma transfusion (OR = 3.121) were the main factors of blood platelet parameters after transfusion in leukemia patients ($P < 0.05$). *Conclusion*. Blood transfusion is beneficial to improve blood platelet parameters and prevent bleeding in patients with leukemia treated with chemotherapy. Attention should be paid to patients with risk factors for poor response to blood platelet transfusion and early intervention.

1. Introduction

Acute leukemia is a malignant clonal disease of hematopoietic stem cells. Abnormal proliferation of primitive and immature cells inhibits normal hematopoiesis of bone marrow and can also infiltrate extramedullary organs such as the liver, spleen, and lymph nodes. It is mainly divided into two types: acute lymphoblastic leukemia and acute myeloid leukemia [1], and the mortality is high in malignancies [2]. To prevent thrombocytopenia or bleeding, blood transfusion therapy is one of the supportive care measures for leukemia patients following cytotoxic chemotherapy [3, 4]. However, during blood transfusion therapy, the body is stimulated to produce anti-platelet-associated antibodies due to the immune effect of leukocytes in blood products, affecting the effect of platelet transfusion, resulting in no significant increase in platelet count, bleeding symptoms are not significantly controlled, fever, allergy, and other adverse reactions may also occur, and intracranial hemorrhage may also be caused in severe cases [5, 6]. At present, there is no unified theory about the changes of platelet coefficient and related influencing factors after blood transfusion treatment, and there are few related studies. Therefore, it is of great significance to identify the effect of blood transfusion on blood platelet parameters in leukemia patients treated with chemotherapy as early as possible and take effective intervention in a timely manner.

2. Study Subjects and Methods

A total of 98 leukemia patients who were treated with chemotherapy in the department of hematology from January 2021 to January 2022 in the First Affiliated Hospital of Xi'an Jiaotong University were selected by convenience sampling. All patients were diagnosed by bone marrow examination and met the Criteria for the Diagnosis and Efficacy of Hematological Diseases. Chemotherapy regimen is in line with the National Comprehensive Cancer Network

(NCCN) guidelines for adult leukemia treatment. All patients received adjuvant treatment with traditional Chinese medicine. Compound ingredients: Angelica sinensis, Astragalus membranaceus, Ligustrum lucidum, Atractylodes macrocephala, Radix Pseudostellariae, Radix Scutellariae, Radix Polygoni Multiflori, wolfberry, dodder seed, Fructus Psoraleae, Morinda officinalis. The patient took the prescription orally once in the morning and once in the evening. This study was approved by the medical ethics committee of the First Affiliated Hospital of Xi'an Jiaotong University (no. xjt122), which is in line with the Declaration of Helsinki. All patients signed informed consent.

2.1. Inclusion Criteria. Inclusion criteria were as follows: (1) patients who signed the informed consent form of blood transfusion products and (2) patients having clear consciousness.

2.2. Exclusion Criteria. Exclusion criteria were as follows: (1) combined with other diseases that can lead to thrombocytopenia such as malignant tumors, rheumatism, and immune system diseases; (2) combined with important organ dysfunction; (3) patients with mental disorders who cannot cooperate with this study; and (4) breastfeeding or pregnant women.

2.3. Methods of Blood Transfusion. Whole blood and blood components were all included. According to the specific implementation of conventional chemotherapy regimen, when the patient developed clinical abnormalities after chemotherapy, multiple transfusions of whole blood were required, each transfusion volume was 300 ml, blood was transfused every other day for 3 consecutive transfusions, and another 10 U therapeutic dose of blood platelets was transfused.

2.4. Outcome Measures. Baseline data such as gender, age, disease type, antibiotic use, history of blood transfusion, and platelet type (frozen platelets and fresh platelets) were collected. Within 24 hours after the end of chemotherapy, 2 ml of fasting peripheral venous blood was extracted with EDTA anticoagulation tube. Platelet count (PLT), mean platelet volume (MPV), platelet volume distribution width (PDW), and platelet volume (PCT) were measured by automatic blood cell analyzer within 24 hours. The corrected count of increment (CCI) was calculated. CCI = (post-transfusion platelet count transfusion-pre-platelet count) (10^9/L) × body surface area (m^2))/(total number of platelets transfused (10^{11}/L)). If the CCI value at 24 hours after transfusion was less than 4.5×10^9/L, it indicated that the platelet transfusion was ineffective.

2.5. Data Analysis. Data analysis was performed using the software SPSS 24.0, expressed as mean ± standard deviation, qualitative data were described as percentages, and quantitative data were tested by normality. The platelet correlation coefficient of patients before and after blood transfusion was compared by paired sample *t*-test. Binary logistic regression analysis was used to analyze the influencing factors of platelet transfusion efficacy. $P < 0.05$ indicated a statistically significant difference.

3. Results

3.1. Baseline Characteristics. This study included 52 cases of acute lymphoblastic leukemia (ALL), 22 cases of acute myeloid leukemia (AML), and 24 cases of acute promyelocytic leukemia (APL). The mean age of patients was 42.13 ± 1.02 years old (range 34 to 69 years old), males accounted for 44.9% (44/98), antibiotics were used in 38.8% (38/98), frozen plasma was transfused in 20.4% (20/98), and white blood cell count was abnormal in 24.5% (24/98). Patients who had a blood transfusion history before this transfusion accounted for 42.9%, 32 patients developed clinically abnormal changes during the chemotherapy period, and 66 patients developed clinically abnormal changes during the interval between chemotherapies (within 2 weeks after the end of the chemotherapy course), and 15 patients did not respond to platelet transfusion.

3.2. Changes in Blood Platelet Parameters before and after Transfusion. Comparative analysis of blood platelet parameters before and after transfusion showed that MPV, PCT, and PLT were significantly improved in patients after transfusion, as shown in Table 1.

3.3. Influencing Factors of Blood Platelet Parameter Changes after Transfusion. The CCI value at 24 hours after transfusion was bounded by 4.5×10^9/L to determine whether this blood platelet transfusion was effective or ineffective, and the CCI value at 24 hours was used as the outcome measure. Among all the patients, 15 patients who failed to respond to transfusion were selected, and 15 patients were randomly selected in a ratio of 1 : 1 among 83 patients who responded to transfusion for secondary analysis. Binary logistic regression analysis showed that the use of antibiotics, history of blood transfusion, abnormal white blood cell count, and frozen plasma transfusion were the main factors affecting the changes of blood platelet parameters after transfusion in leukemia patients ($P < 0.05$), as shown in Table 2.

4. Discussion

Leukemia is a clonal malignant disease with abnormal hematopoietic stem cells, which has a great impact on the life safety of patients. Clinical manifestations of patients were anemia, infection, severe bleeding symptoms, and death in severe cases. At present, chemotherapy is mainly used to improve the clinical symptoms of patients in clinical practice, mainly to change blood platelet parameters, and specific treatment is carried out [7]. Different degrees of bleeding caused by thrombocytopenia in patients with

Table 1: Changes in blood platelet parameters before and after transfusion.

	MPV (fL)	PDW (%)	PCT (%)	PLT ($\times 10^9$/L)
Pre-infusion	10.39 ± 0.68	16.17 ± 0.03	0.024 ± 0.005	55.90 ± 0.16
24 hours after infusion	10.23 ± 0.79	16.23 ± 0.05	0.053 ± 0.004	60.08 ± 0.92
T	−5.397	−2.359	−15.158	−9.469
P	0.006	0.078	<0.001	0.001

Table 2: Influencing factors of blood platelet parameter changes after transfusion.

	B value	Standard error	Wald value	OR	95% CI	P value
Gender	0.731	0.671	2.537	4.105	2.147–8.092	0.347
Age	0.257	0.833	17.246	7.136	4.099–10.765	0.134
Antibiotic use	0.804	0.645	1.552	2.235	0.631–7.918	0.213
History of transfusion	2.674	0.746	11.412	3.086	2.766–5.908	0.007
Abnormal white blood cell count	3.705	0.842	19.673	1.134	0.91–2.419	0.001
Platelet species	1.788	0.564	10.335	3.121	2.034–8.132	0.03

leukemia after chemotherapy are the main factors leading to death. Blood transfusion is currently one of the common methods to treat and prevent bleeding in patients with acute leukemia. However, in repeated blood transfusion, bone marrow megakaryocytes divide and proliferate, significantly reducing the effect of blood transfusion [8]. Adverse reactions of blood transfusion may occur, which can seriously interfere the therapeutic effect and lead to various serious consequences such as blood transfusion lung injury and pulmonary microvascular embolism, increasing the risk of death [9]. Exploring the changes of blood platelet parameters and influencing factors in patients with leukemia treated with after blood transfusion and giving targeted suggestions are the key to guide the planning of treatment options and improve the therapeutic effect.

In this study, patients with leukemia treated with chemotherapy received blood transfusion treatment, including whole blood transfusion and blood components. The main purpose was to prevent bleeding and regulate platelet-related parameters. MPV, PCT, and PLT were significantly different before and after transfusion, which indicated that blood transfusion could improve blood platelet parameters and prevent bleeding in patients with leukemia received chemotherapy. This finding is partially in contrast to the findings of Comont et al.'s study [10], which showed that in multiple transfusions, patients developed platelet antibodies, PCT and PLT gradually decreased, and MPV gradually increased. Although transfusion of whole blood and component blood can bring obvious therapeutic effect, it affects the therapeutic effect due to the complex components of blood products [11].

At present, the effect of blood transfusion on blood platelet parameters in patients with leukemia who received chemotherapy is influenced by multiple factors, but the results of various studies are not uniform [12, 13]. In this study, the results of binary logistic regression analysis showed that the use of antibiotics, history of blood transfusion, abnormal white blood cell count, and frozen plasma transfusion were the main influencing factors of ineffective platelet transfusion after blood transfusion in leukemia patients. However, there was no significant difference regardless of age or gender. Leukemia patients can be affected by a variety of factors, causing fever, infection, and other complications, requiring the use of antibiotics, resulting in a large number of platelet consumption. Inflammatory reactions can produce a variety of antibodies, resulting in rapid reduction of platelet counts and affecting platelet transfusion [14]. Frozen blood platelets increase the risk of exposure to phosphatidylserine moieties during freezing, prompting platelet activation, which in turn accelerates the rate at which blood platelets damage the mononuclear phagocytic system after entering the body, resulting in insignificant improvement in blood platelet counts and poor response to transfusions after treatment with blood platelet transfusions [15]. The study by Tantanate et al. [16] indicated that multiple blood platelet transfusions resulted in decreased platelet counts and increased risk of bleeding, similar to the finding that a blood transfusions history was a risk factor for platelet transfusion efficacy in this study. Research [17] showed that when patients receive platelet infusion, leukocytes in the body can secrete a large number of histamines, leukotrienes, and other components, which promote the body to have allergic reactions, increase the risk of hemolysis and allergy, and then affect the effect of infusion treatment, which is similar to the result that abnormal leukocytes increase the risk of ineffective infusion in this study. The sample size of this study is less, which may affect the authenticity of the results. The research is still limited, and large-sample research is needed to explore and analyze.

5. Conclusion

Blood transfusion is beneficial to improve blood platelet parameters and prevent bleeding in patients with leukemia treated with chemotherapy.

Data Availability

The data used to support the findings of this study are available from the corresponding author upon request.

Hindawi
Evidence-Based Complementary and Alternative Medicine
Volume 2023, Article ID 9786270, 1 page
https://doi.org/10.1155/2023/9786270

Retraction

Retracted: Analysis of Influencing Factors for Exercise Ventilation Efficiency of COPD Patients

Evidence-Based Complementary and Alternative Medicine

Received 3 October 2023; Accepted 3 October 2023; Published 4 October 2023

This article has been retracted by Hindawi following an investigation undertaken by the publisher [1]. This investigation has uncovered evidence of one or more of the following indicators of systematic manipulation of the publication process:

(1) Discrepancies in scope

(2) Discrepancies in the description of the research reported

(3) Discrepancies between the availability of data and the research described

(4) Inappropriate citations

(5) Incoherent, meaningless and/or irrelevant content included in the article

(6) Peer-review manipulation

The presence of these indicators undermines our confidence in the integrity of the article's content and we cannot, therefore, vouch for its reliability. Please note that this notice is intended solely to alert readers that the content of this article is unreliable. We have not investigated whether authors were aware of or involved in the systematic manipulation of the publication process.

Wiley and Hindawi regrets that the usual quality checks did not identify these issues before publication and have since put additional measures in place to safeguard research integrity.

We wish to credit our own Research Integrity and Research Publishing teams and anonymous and named external researchers and research integrity experts for contributing to this investigation.

The corresponding author, as the representative of all authors, has been given the opportunity to register their agreement or disagreement to this retraction. We have kept a record of any response received.

References

[1] Y.-m. Ge, S. Nie, N. Jia, Q.-F. Xu, B. Xu, and H.-Y. Wang, "Analysis of Influencing Factors for Exercise Ventilation Efficiency of COPD Patients," *Evidence-Based Complementary and Alternative Medicine*, vol. 2022, Article ID 8376085, 7 pages, 2022.

Hindawi
Evidence-Based Complementary and Alternative Medicine
Volume 2022, Article ID 8376085, 7 pages
https://doi.org/10.1155/2022/8376085

Research Article

Analysis of Influencing Factors for Exercise Ventilation Efficiency of COPD Patients

Yu-mei Ge, Shan Nie, Nan Jia, Qiu-Fen Xu, Bo Xu, and Hao-Yan Wang

Department of Respiratory Medicine, Beijing Friendship Hospital, Capital Medical University, Beijing, China

Correspondence should be addressed to Shan Nie; nieshan0211@126.com and Hao-Yan Wang; haoyanw@ccmu.edu.cn

Received 1 July 2022; Revised 25 July 2022; Accepted 5 August 2022; Published 29 August 2022

Academic Editor: Xueliang Wu

Dynamic pulmonary hyperinflation and abnormal air exchange are the primary causes of the exercise limitation of chronic obstructive pulmonary disease (COPD) patients. During exercise, COPD sufferers' lungs are dynamically hyperinflated. Increased inefficient ventilation reduces ventilation efficiency and causes a mismatch between ventilation volume and blood flow. The ventilatory equivalent for CO_2 ($VeqCO_2$) is a physiological parameter that can be measured using cardiopulmonary exercise testing. Therefore, the aim of this exploratory study was to perform cardiopulmonary exercise testing on people with COPD, investigate the impact of static pulmonary function on ventilation efficiency under the exercise state, and screen the predictive indicators of ventilation efficiency. *Subject*. The aim of this study was to look at the factors that influence the exercise ventilation efficiency of people with COPD. *Method*. A total of 76 people with COPD were recruited during the stable period. Age, gender, body height, body mass, and other basic information were recorded. The body mass index (BMI) was determined, and forced vital capacity (FVC), forced expiratory volume in one second (FEV1), residual volume/total lung capacity (RV/TLC), diffusing capacity of the lung for carbon monoxide (DLCO), and DLCO divided by the alveolar volume (DLCO/VA) were measured. The ventilatory equivalent for carbon dioxide (VE/VCO2) under the rest state ($EqCO_2$rest), anaerobic threshold ($EqCO_2$at), and maximum exercise state ($EqCO_2$ max) were calculated to investigate the influencing factors for ventilation efficiency of people with COPD. *Results*. FEV1% was negatively correlated with $EqCO_2$rest ($r = -0.277$, P value <0.05); FEV1/FVC % was negatively correlated with EqCO2rest and EqCO2at ($r = -0.311$, -0.287, P value <0.05); DLCO% was negatively correlated with $EqCO_2$rest, $EqCO_2$at, and $EqCO_2$max ($r = -0.408$, -0.462, and -0.285, P value <0.05); DLCO/VA% was negatively correlated with $EqCO_2$rest, $EqCO_2$at, and $EqCO_2$max ($r = -0.390$, -0.392, and -0.245, P value <0.05); RV/TLC was positively correlated with EqCO2rest and EqCO2at ($r = 0.289$, 0.258, P-value <0.05). The prediction equation from the multivariable regression analysis equation was $Y = 40.04–0.075X$ ($Y = EqCO_2$, $X =$ DLCO/VA%). *Conclusions*. As the degree of ventilatory obstruction increased, the ventilation efficiency of the stable people with COPD under the exercise state showed a progressive decrease; the ventilation efficiency of the people with COPD decreased significantly under the maximum exercise state, and the ventilation capacity and diffusion capacity were the significant factors that affected the exercise ventilation efficiency. The diffusion function may predict the maximum ventilation efficiency and enable primary hospitals without exercise test equipment in developing countries to predict and screen patients at risk for current exercise based on limited information.

1. Introduction

Due to chronic airway limitation and poor pulmonary function, the cardiopulmonary exercise functions of people with COPD are aberrant. [1] However, studies have demonstrated that during exercise, the rate of decline in cardiopulmonary function is higher than the rate of progression of poor pulmonary function. [2] It is possible that it is linked to a decrease in inspiratory vital capacity and effective ventilation volume and abnormality of pulmonary air exchange caused by pulmonary hyperinflation. [3].

The ventilatory equivalent for CO_2 ($VeqCO_2$) is a physiological parameter that can be measured using cardiopulmonary exercise testing. According to previous research findings, people with COPD have significantly higher $EqCO_2$ than people with normal lung function under the peak exercise state. It may be linked to the increase in physiological dead space volume/tidal volume (VD/VT)

during exercise. [4] Studies have proved that it has low ventilation efficiency; that is, the rise in VE/VCO_2 response during exercise is an independent predictor of the mortality rate in patients with chronic heart failure (CHF), pulmonary hypertension (PH), and chronic obstructive pulmonary disease (COPD). At present, there are few studies on the $EqCO_2$ influencing factors, both at home and abroad. The goal of this study was to examine the factors that influence the ventilation efficiency of people with COPD in order to help primary care hospitals predict and screen patients at risk for exercise based on limited information.

2. Participants and Methods

2.1. Research Participants. From January 2016 to December 2019, 76 people with COPD who were receiving regular treatment during the stable period were recruited from the outpatients of Beijing Friendship Hospital's Respiratory Department. The study was carried out with the approval of the Beijing Friendship Hospital's Ethics Committee, and each participant provided written informed consent.

2.1.1. Inclusion Criteria. (1) Diagnosed people with COPD: according to the GOLD Guidelines for COPD, [1] patients with dyspnea, chronic cough, or sputum expectoration and a history of exposure to COPD risk factors, having FEV1/FVC <70% after inhalation of bronchodilators and showing continuous airway limitation. (2) People with COPD during the stable period: the duration of the clinical stability was ≥6 weeks after the standardized treatment, that is, the drug treatment plan and drug dosage had not been changed due to changes in the patients' condition over the past 6 weeks. (3) The patients ranged in age from 40 to 85 years old. (4) The percutaneous oxygen saturation (SPO_2) was >88% under the condition of inhalation of air under the rest state.

2.1.2. Exclusion Criteria. (1) With a medical history of other pulmonary diseases, such as bronchiectasis (except for COPD complicated with bronchiectasis), interstitial lung disease, bronchial asthma, cystic fibrosis, infectious lung disease, thoracic deformity, and pneumonectomy, and without a history of respiratory tract infection over the past 6 weeks; (2) with severe cardiovascular diseases, such as acute left heart failure, malignant arrhythmia, uncontrolled hypertension, or with a medical history of the acute coronary syndrome within nearly one month; (3) with a medical history of major diseases of other systems, such as a malignant tumor, severe liver and kidney dysfunction, active autoimmune disease, lower limb bone and joint diseases that affect body activity, and limb activity disorder, cognitive disorder, and mental disorder caused by cerebrovascular diseases.

2.2. Research Methods

2.2.1. General Data. Subjects were recruited, their genders and ages were recorded, body heights and body masses were measured, and the BMI [BMI = body mass (kg)/body height square (m^2)] was calculated. Blood pressure, pulses, and SPO_2 when inhaling air under the rest state were also measured. It was confirmed that the subjects had not been orally, intramuscularly, or intravenously treated with H1 receptor antagonists and adrenocortical hormone agents within 72 hours prior to the pulmonary function testing procedure, had not been treated with inhaled long-acting muscarinic antagonists (LAMA) and long-acting β_2 receptor agonists/inhaled corticosteroids (LABA/ICS) within 24 hours prior to the pulmonary function testing procedure, and had not been treated with inhaled short-acting muscarinic antagonists (SAMA) and short-acting β_2 receptor agonists/inhaled corticosteroids (SABA/ICS) within 4 hours prior to the pulmonary function testing procedure.

2.2.2. Methods. All patients' static pulmonary functions (Master Screen Body, Care Fusion, Hochberg, Germany) were evaluated to determine the degree of airway restriction based on the GOLD stage and GOLD group.

The cardiopulmonary exercise testing (CPET) procedure was then carried out. The patients sat on an electronically braked cycle ergometer (ER 900L, Jaeger, Germany), which was equipped with an expiratory air collecting tube, an electrocardiograph, a blood pressure cuff, and an infrared blood oxygen saturation monitor. Their noses were clamped with a nose clip. The patients clenched their lips around the mouth bite. After 3 min of rest, the patients underwent 3 min of unloaded pedaling, followed by an incremental phase of exercise at a 10 W/min work rate. All participants were encouraged to cycle as long as they could until they were exhausted, then the load was reduced to a 20 W/min work rate, and the exercise was stopped after 4 to 6 minutes of slow exercise. Throughout the exercise test, the cardiopulmonary exercise tester (Oxycon Delta, JAEGER, Germany) was used to measure the parameters, such as oxygen uptake (VO_2), carbon dioxide production (VCO_2), and ventilation (VE), breath by breath. The anaerobic threshold (AT) was established via the V-slope method. According to the formula, $EqCO_2 = VE/VCO_2$, $EqCO_2$rest, $EqCO_2$at, and $EqCO_2$max were calculated at rest, AT, and peak exercise. The direct measurement data were calculated based on the average value of 30 s measurement data.

2.2.3. Statistical Processing. Data were analyzed using SPSS Statistics for Windows, Version 23.0. The normal distribution of data was confirmed using the Kolmogorov–Smirnov test. The results of the continuous variables were presented by mean and standard deviation, while the categorical variables were presented by percentage. The correlation analysis was assessed by the Pearson correlation coefficient. The screen influencing factors were analyzed using multiple linear regression (MLR). The results were considered statistically significant when the P value was <0.05.

3. Results

3.1. General Data. All 76 patients finished pulmonary function testing and CPET.

Table 1: Anthropometric, functional characteristics in COPD.

Items	Value(Mean ± SD)
Male/female	61/15
Age	64.35 ± 8.14
Body height (cm)	167.99 ± 7.68
Body weight (kg)	69.14 ± 13.82
BMI (kg/m^2)	24.44 ± 4.29
Static pulmonary function	
FEV1%pred	59.41 ± 18.99
FEV1/FVC%	55.54 ± 11.77
RV/TLC	55.54 ± 12.13
DLCO%	59.88 ± 19.91
DLCO/VA%	76.60 ± 223.39

Table 2: CPET variables in COPD.

Items	Value
VO_2max	1268.55 ± 289.12
VO_2max/pred%	69.75 ± 13.89
Watts-at	60.21 ± 20.60
Watts-max	83.70 ± 25.72
Watts-max (W)	95.31 ± 26.3
HR-base	88.58 ± 11.85
HR-max	130.41 ± 18.77
HR-%	83.59 ± 10.96
VE-base	20.01 ± 5.37
VEmax	47.56 ± 12.08
VE%	58.30 ± 18.33
AT/($mL \cdot min^{-1} \cdot kg^{-1}$) ($n = 66$)	13.05 ± 2.67
$EqCO_{2rest}$	36.63 ± 6.17
$EqCO_{2at}$	33.91 ± 5.21
$EqCO_{2max}$	33.04 ± 5.38

The anthropometric, functional characteristics of the objects were as shown in Table 1.

The characteristics of the cardiopulmonary exercise indicators of the test objects were as shown in Table 2.

3.2. $EqCO_2$ Parameter Influencing Factors of People with COPD during the Stable Period

3.2.1. General Influencing Factors. A correlation analysis was performed between the parameters $EqCO_2$rest, $EqCO_2$at, and $EqCO_2$ max and age, body height, body mass, and BMI. Table 3 shows the results: $EqCO_2$at and $EqCO_2$-base were negatively correlated with BMI ($r = -0.437$, -0.308, P value <0.05), and $EqCO_2$rest was positively correlated with body height ($r = 0.274$, P value <0.05).

3.2.2. Pulmonary Function Influencing Factors. A correlation analysis was performed between the parameters $EqCO_2$rest, $EqCO_2$at, and $EqCO_2$ max and the pulmonary function indicators FEV1, FEV1/FVC, RV/TLC, DLCO, DLCO/VA, RV, and VC-FVC. As shown in Table 4, FEV1% was negatively correlated with $EqCO_2$rest ($r = -0.277$, P value <0.05); FEV1/FVC% was negatively correlated with $EqCO_2$rest and $EqCO_2$at ($r = -0.311$, -0.287, P value <0.05); DLCO% was negatively correlated with $EqCO_2$rest, $EqCO_2$at, and $EqCO_2$max ($r = -0.408$, -0.462, -0.285, P value <0.05); DLCO/VA% was negatively correlated with $EqCO_2$-rest, $EqCO_2$at, and $EqCO_2$max ($r = -0.390$, -0.392, -0.245, P value <0.05); RV/TLC was positively correlated with $EqCO_2$rest and $EqCO_2$at ($r = 0.289$, 0.258, P value <0.05).

In the group as a whole, there was a significant correlation of all pulmonary functions and $EqCO_2$at, such as FEV1/FVC %, DLCO%, DLCO/VA%, and RV/TLC, except for FEV1%. Multivariable regression analysis revealed that the pulmonary function parameter DLCO/VA% was the only variable that significantly entered the regression as EqCO2at (Table 5). The prediction equation from the multivariable regression analysis equation was $Y = 40.04 - 0.075X$ ($Y = EqCO_2$, $X =$ DLCO/VA%).

3.2.3. Differences between Ventilation Efficiencies at Different Pulmonary Function Levels. Table 6 shows the differences between ventilation efficiencies at different pulmonary function levels. The numbers of cases at GOLD Level 1 and GOLD Level 4 were less than 10; therefore, the t-testing was only performed for GOLD Level 2 and GOLD Level 3.

4. Discussions

According to previous research findings, the subjective exertional dyspnea symptoms of people with COPD did not completely match the static pulmonary function indicators; clinical symptoms were not obvious, especially for mild and moderate patients; the decrease in pulmonary function was also not obvious under the rest state, but the patients' cardiopulmonary reserve functions significantly decreased. [5, 6].

CPET can play an important role in judging the severity of the disease, predicting survival time, identifying the cause of dyspnea, diagnosing complicated pulmonary vascular lesions, evaluating the treatment effect, and guiding pulmonary rehabilitation training. [7] Although CPET is not as valuable as conventional pulmonary function testing in the diagnosis of COPD, CPET is a sensitive method that can accurately quantify exercise tolerance. $EqCO_2$ (ventilatory equivalent for carbon dioxide) is a critical parameter in the CPET, which is calculated using the equation: $VeqCO_2 = [V'_E - (d_{syst} \times RR)]/V'_{CO2}$. $EqCO_2$ was the focus of this study because previous research demonstrated that this parameter is most useful in the diagnosis of dysfunctional breathing [8]. The increase in $EqCO_2$ indicates a decrease in ventilation efficiency [9, 10]. According to recent research, under the peak exercise state, the $EqCO_2$ of people with COPD was significantly higher than that of people with normal lung function [10]. The reason can be correlated to an increase in the physiological dead space volume or tidal volume, which indicates a significant decrease in the ventilation efficiency of people with COPD [4]. Previous findings suggest that exercise ventilatory inefficiency is a physiological marker associated with clinically relevant endpoints in patients with mild to end-stage COPD [11].

The previous research findings revealed that $EqCO_2$rest, $EqCO_2$at, and $EqCO_2$max of people with COPD showed a

Table 3: Correlation of $EqCO_2$ and anthropometric characteristics.

		BMI	Body height	Body weight	Age
$EqCO_2$ at	Pearson correlation	−0.308*	0.162	−0.214	0.246*
	P value	0.012	0.194	0.085	0.046
	n	66	66	66	66
$EqCO_2$ max*	Pearson correlation	−0.185	0.113	−0.124	0.250*
	P value	0.117	0.343	0.297	0.033
	n	73	73	73	73
$EqCO_2$ rest	Pearson correlation	−0.437**	0.271*	−0.219	0.178
	P value	0.000	0.028	0.078	0.154
	n	66	66	66	66

*significant difference, $P < 0.05$.

Table 4: Correlation of $EqCO_2$ and key variables of pulmonary function.

		FEV1%	FEV1/FVC %	DLCO%	DLCO/VA%	RV/TLC
$EqCO_2$rest	Pearson correlation	−0.277*	−0.311*	−0.408**	−0.390**	0.289*
	P-value	0.024	0.011	0.001	0.002	0.023
	n	66	66	63	63	62
$EqCO_2$at	Pearson correlation	−0.224	−0.287*	−0.462**	−0.392**	0.258*
	P-value	0.070	0.020	0.000	0.002	0.043
	n	66	66	63	63	62
$EqCO_2$max *	Pearson correlation	−0.024	−0.086	−0.285*	−0.245*	0.095
	P-value	0.837	0.468	0.017	0.041	0.436
	n	73	73	70	70	69

*significant difference, $P < 0.05$.

Table 5: Multiple linear regression with $EqCO_2$ at as the dependent variable.

Model		Coefficients			*t*	*P*
		Unstandardized coefficients		Standardized coefficients		
		B	Std. error	Beta		
1	(Constant)	40.040	2.387		16.771	0.000
	DLCO/VA%	−0.075	0.030	−0.321	−2.534	0.014

Table 6: $EqCO_2$, RR, and VE at different exercise intensities by the GOLD stage.

	GOLD level 1	GOLD level 2	GOLD level 3	GOLD level 4	*t* value	*P* value
Number of cases	9	44	21	2		
$EqCO_2$rest	32.33 ± 1.75	35.83 ± 1.02	39.64 ± 1.67	36.3 ± 2.26	−9.63	0.00
$EqCO_2$at	29.46 ± 1.49	33.62 ± 0.87	35.58 ± 1.46	/	−5.68	0.00
$EqCO_2$max	29.72 ± 1.32	32.99 ± 0.94	33.21 ± 1.39	29.05 ± 0.21	−0.657	0.51
RRrest	18.85 ± 5.31	21.95 ± 4.41	22.25 ± 5.94	23.5 ± 0.71	−0.38	0.71
RRat	24.86 ± 5.40	23.58 ± 3.66	26.70 ± 5.27	/	−2.26	0.03
RRmax	34.22 ± 7.43	31.05 ± 4.46	31.65 ± 6.02	30.0 ± 1.41	−0.52	0.61
%	79.7% ± 18,26	76.77 ± 16.56	76.38 ± 15.00	72.5 ± 3.54	0.02	0.98
VErest	15.71 ± 5.50	20.38 ± 5.51	20.31 ± 4.42	23.0 ± 5.66	0,10	0,92
VEat	28.30 ± 9.57	28.05 ± 8.07	31.31 ± 6.20	/	−1.32	0.19
VEmax	55.22 ± 9.24	48.61 ± 12.29	42.95 ± 10.09	32.5 ± 7.78	1.75	0.09
%	72.7 ± 14.97	60.15 ± 12.52	49.63 ± 10.76	36.5 ± 6.36	2.85	0.01

*significant difference, $P < 0.05$.

progressive decline, while the $EqCO_2$ of people with normal lung function hyperbolically decreased with increasing power during exercise. [12].

The research by Sun et al. [13] showed that for people with normal lung function, during the initial period of exercise, due to the hysteresis of nerve conduction, the increase in VE was relatively lower than that of VCO_2, and $EqCO_2$ was lower than that in the static state; when the exercise load increased to the point where the body began anaerobic glycolysis, intracellular bicarbonate neutralized

lactic acid to produce a large amount of CO_2, and chemoreceptors were excited, causing VE and $EqCO_2$ to increase. Small airway obstruction and decreased compliance in people with COPD resulted in an increased residual air volume and thoracic expansion in the inspiratory state, limiting diaphragm function, shortening of inspiratory muscle fibers, and weakening of muscle strength; therefore, respiratory muscle fatigue was prone to occur during exercise. They have shown that reduced ventilatory efficiency during exercise is common in mild COPD, and this is primarily due to high physiological dead space (rather than alveolar hyperventilation or a relatively reduced tidal volume), resulting in a preponderance of lung units with high ventilation-perfusion ratios. [12] Because of the loss of gas exchange areas, increased dead space can reduce DLCO and KCO. We believe that the increase in $EqCO_2$ is due to dead space rather than DLCO. We did not measure the dead space because artery blood was required.

Relevant studies revealed that the $EqCO_2$ level of people with COPD was significantly higher than that of people with normal lung function under the high exercise state, which was correlated to an increase in the ratio between the physiological dead space volume and the tidal volume, indicating that the ventilation efficiency of people with COPD significantly decreased. [14] The research by Yuan and Wang [15] found that VE/VCO_2 levels of people with COPD during the stable period progressively decreased at rest, AT, and peak exercise states, which was consistent with our findings.

Our study conducted a correlation analysis between multiple parameters of pulmonary function ventilation, diffusion, and VE/VCO_2, demonstrating that for mild and moderate airway obstruction patients, ventilation efficiency at the AT state was clearly correlated with the degree of pulmonary function airway obstruction, diffusion function, and the ratio of the total residual. According to the GOLD classification, the greater the airway obstruction, the lower the ventilation efficiency, that is, the higher the VE/VCO2, indicating that the air exchange between people with COPD of varying severity had changed. [16] When the patient reached the maximum exercise state, ventilation efficiency was only correlated with the diffusion function and not with ventilation capacity. The most likely explanation is that after the anaerobic threshold, as exercise power increased, the body switched from aerobic metabolism to anaerobic metabolism, and the output of CO_2 obviously increased, stimulating more VE and VCO_2; furthermore, during exercise, the development of dynamic hyperinflation with a progressive increase in the end-expiratory lung volume (EELV) imposed additional elastic load on the ventilator system and was closely related to exertional dyspnea, and it, therefore, contributed to exercise limitation [17]. The ventilation efficiency calculated using VE/VCO_2 was only correlated with the effective respiratory area, that is, the diffusion function but not with basic ventilation capacity under the rest state. Previous research proved that in patients who underwent lung volume reduction surgery, due to the improvement of alveolar ventilation, peak VE, VCO_2, peak VE/VCO_2, and other indicators were improved. [18, 19] The research on people with COPD based on exercise rehabilitation revealed that pulmonary rehabilitation has no significant effect on the improvement of ventilation efficiency in people with COPD. [20] This phenomenon also indirectly supported our research finding, that is, diffusion function is the only indicator of maximum ventilation efficiency, rather than ventilation and other indicators.

Alveolar ventilation and arterial blood gases PCO_2 were used to adjust CO_2 removal during exercise [21]. When the power was gradually increased, VE increased linearly with the increase in CO_2 emissions within a considerable range of power. After the carbonic acid buffer period, the increase in VE was faster than that of VCO_2 (an increase in the VE/VCO_2 ratio). In our study, people with COPD did not exhibit the same ventilation characteristics at maximum exercise intensity as people with normal lung function under the maximum exercise state; that is, $EqCO_2$ increased from the carbonic acid buffer period to the maximum exercise state. The probable reasons were that the people with COPD due to the increase in physiological dead cavities [14] had a ratio imbalance of ventilation volume and blood flow, and their VE/VCO_2 was higher than that of people with normal lung function; furthermore, because of respiratory limitations caused by respiratory drive, respiratory muscle dysfunction, and other conditions, the VT of people with COPD could not be correspondingly increased according to the metabolic acidosis that occurred after the AT. $EqCO_2$max was lower than $EqCO_2$ during the period from W_{at} to W_{max}. In addition to the aforementioned causes, it may also be due to the fact that the CPET examination is a test of self-control, COPD patients have poor exercise ability and reach MAX shortly after reaching AT, as indicated by the data, and W_{max} is similar to W_{at}. At the same time, they may be afraid of unusual symptoms such as coughing and chest tightness and decide to skip the test.

The precise matching of alveolar ventilation with the metabolic rate during exercise is achieved by increasing minute ventilation. This increase is accomplished by increases in both the tidal volume and breathing frequency. During low-to-moderate intensity exercise, both tidal volume and breathing frequency increase roughly in proportion to exercise intensity [8], whereas at higher intensities, as our results showed that for COPD patients with a heavier GOLD grade, the expected ventilate ratio of maximum intensity exercise was lower. Therefore, due to the limitation of ventilatory function, it is necessary to rely more on the increased respiratory rate to meet metabolic requirements during certain intensity exercises.

Compared with the main ventilatory indicator of static lung function, diffusion function predicted decreased ventilatory efficiency during exercise (although it was not a particularly strong predictor). Although there are certain limitations to our study: the slope of VE/VCO_2 indicates the efficiency of lung ventilation very well, $EqCO_2$ is more convenient to obtain. Therefore, $EqCO_2$ was selected for our research because it is more consistent with clinical practice. Due to the limited number of included GOLD1 and GOLD4 patients, the analysis of factors related to $EqCO_2$ may not be clear, but based on existing data, the correlation between

dispersion function indicators and $EqCO_2$ has been shown. It may be possible for people who are difficult to implement CPET and institutions with limited medical conditions to screen people with hypoxia during exercise at an early stage and provide corresponding medical advice for the related risks.

5. Conclusion

In conclusion, the current study revealed the following trends: the ventilation efficiency of people with COPD during the stable period under the exercise state demonstrated a progressive decrease, and ventilation capacity and diffusion capacity were significant factors influencing ventilation efficiency. Among all lung function indicators, though not particularly strong predictors, the diffusion function may be able to predict the maximum ventilation efficiency.

Our study showed that DLCO/VA% was associated with $EqCO_2$, which may be used as a means to screen hypoxia subjects during exercise, especially in primary hospitals without exercise test equipment, and implement relevant exercise prescriptions as early as possible.

Data Availability

The data used to support the findings of this study are included within the article.

Conflicts of Interest

The authors declare no conflicts of interest.

Authors' Contributions

Shan Nie and Hao-Yan Wang contributed equally to this work. The manuscript has been read and approved by all the authors.

Acknowledgments

This study was supported by Capital's Funds for Health Improvement and Research (grant no. 2018-2-2-24) and the Key Clinical Specialty Construction Program of Beijing (2020-2022).

References

[1] D. E. O'Donnell, M. Lam, and K. A. Webb, "Spirometric correlates of improvement in exercise performance after anticholinergic therapy in chronic obstructive pulmonary disease," *American Journal of Respiratory and Critical Care Medicine*, vol. 160, no. 2, pp. 542–549, 1999.

[2] T. Oga, K. Nishimura, M. Tsukino, S. Sato, T. Hajiro, and M. Mishima, "Exercise capacity deterioration in patients with COPD: longitudinal evaluation over 5 years," *Chest*, vol. 128, no. 1, pp. 62–69, 2005.

[3] W. Stringer and D. Marciniuk, "The role of cardiopulmonary exercise testing (CPET) in pulmonary rehabilitation (PR) of chronic obstructive pulmonary disease (COPD) patients," *COPD: Journal of Chronic Obstructive Pulmonary Disease*, vol. 15, no. 6, pp. 621–631, 2018.

[4] D. B. Phillips, S. E. Collins, and M. K. Stickland, "Measurement and interpretation of exercise ventilatory efficiency," *Frontiers in Physiology*, vol. 11, p. 659, 2020.

[5] D. Murciano, A. Ferretti, J. Boczkowski, C. Sleiman, M. Fournier, and J. Milic-Emili, "Flow limitation and dynamic hyperinflation during exercise in COPD patients after single lung transplantation," *Chest*, vol. 118, no. 5, pp. 1248–1254, 2000.

[6] K. Krol, M. A. Morgan, and S. Khurana, "Pulmonary function testing and cardiopulmonary exercise testing: an overview," *Medical Clinics of North America*, vol. 103, no. 3, pp. 565–576, 2019.

[7] A. K. Boutou, A. Zafeiridis, G. Pitsiou, K. Dipla, I. Kioumis, and I. Stanopoulos, "Cardiopulmonary exercise testing in chronic obstructive pulmonary disease: an update on its clinical value and applications," *Clinical Physiology and Functional Imaging*, vol. 40, no. 4, pp. 197–206, 2020.

[8] M. Watson, M. F. Ionescu, K. Sylvester, and J. Fuld, "Minute ventilation/carbon dioxide production in patients with dysfunctional breathing," *European Respiratory Review*, vol. 30, no. 160, Article ID 200182, 2021.

[9] R. Maekura, T. Hiraga, K. Miki et al., "Differences in physiological response to exercise in patients with different COPD severity," *Respiratory Care*, vol. 59, no. 2, pp. 252–262, 2014.

[10] I. R. Caviedes, I. Delgado, and R. Soto, "Ventilatory inefficiency as a limiting factor for exercise in patients with COPD," *Respiratory Care*, vol. 57, no. 4, pp. 583–589, 2012.

[11] J. A. Neder, F. F. Arbex, M. C. N. Alencar et al., "Exercise ventilatory inefficiency in mild to end-stage COPD," *European Respiratory Journal*, vol. 45, no. 2, pp. 377–387, 2015.

[12] A. F. Elbehairy, C. E. Ciavaglia, K. A. Webb et al., "Pulmonary gas exchange abnormalities in mild chronic obstructive pulmonary disease. Implications for dyspnea and exercise intolerance," *American Journal of Respiratory and Critical Care Medicine*, vol. 191, no. 12, pp. 1384–1394, 2015.

[13] X. G. Sun, J. E. Hansen, N. Garatachea, T. W. Storer, and K. Wasserman, "Ventilatory efficiency during exercise in healthy subjects," *American Journal of Respiratory and Critical Care Medicine*, vol. 166, no. 11, pp. 1443–1448, 2002.

[14] E. Teopompi, P. Tzani, M. Aiello et al., "Ventilatory response to carbon dioxide output in subjects with congestive heart failure and in patients with COPD with comparable exercise capacity," *Respiratory Care*, vol. 59, no. 7, pp. 1034–1041, 2014.

[15] W. Yuan and H. Wang, "Correlation analysis of ventilation efficiency and exercise capacity of COPD patients," *Journal of Cardiovascular and Pulmonary Diseases*, vol. 32, no. 1, pp. 57–60, 2013.

[16] W. Thirapatarapong, H. F. Armstrong, B. M. Thomashow, and M. N. Bartels, "Differences in gas exchange between severities of chronic obstructive pulmonary disease," *Respiratory Physiology and Neurobiology*, vol. 186, no. 1, pp. 81–86, 2013.

[17] D. E. O'Donnell and K. A. Webb, "Exertional breathlessness in patients with chronic airflow limitation: the role of lung hyperinflation," *American Review of Respiratory Disease*, vol. 148, no. 5, pp. 1351–1357, 1993.

[18] G. J. Criner, P. Belt, A. L. Sternberg et al., "Effects of lung volume reduction surgery on gas exchange and breathing pattern during maximum exercise," *Chest*, vol. 135, no. 5, pp. 1268–1279, 2009.

Hindawi
Evidence-Based Complementary and Alternative Medicine
Volume 2023, Article ID 9865432, 1 page
https://doi.org/10.1155/2023/9865432

Retraction

Retracted: Valproic Acid Inhibits Peripheral T Cell Lymphoma Cells Behaviors via Restraining PI3K/AKT Pathway

Evidence-Based Complementary and Alternative Medicine

Received 8 August 2023; Accepted 8 August 2023; Published 9 August 2023

This article has been retracted by Hindawi following an investigation undertaken by the publisher [1]. This investigation has uncovered evidence of one or more of the following indicators of systematic manipulation of the publication process:

(1) Discrepancies in scope

(2) Discrepancies in the description of the research reported

(3) Discrepancies between the availability of data and the research described

(4) Inappropriate citations

(5) Incoherent, meaningless and/or irrelevant content included in the article

(6) Peer-review manipulation

The presence of these indicators undermines our confidence in the integrity of the article's content and we cannot, therefore, vouch for its reliability. Please note that this notice is intended solely to alert readers that the content of this article is unreliable. We have not investigated whether authors were aware of or involved in the systematic manipulation of the publication process.

Wiley and Hindawi regrets that the usual quality checks did not identify these issues before publication and have since put additional measures in place to safeguard research integrity.

We wish to credit our own Research Integrity and Research Publishing teams and anonymous and named external researchers and research integrity experts for contributing to this investigation.

The corresponding author, as the representative of all authors, has been given the opportunity to register their agreement or disagreement to this retraction. We have kept a record of any response received.

References

[1] Z. Peng, J. Xiong, and H. Dong, "Valproic Acid Inhibits Peripheral T Cell Lymphoma Cells Behaviors via Restraining PI3K/AKT Pathway," *Evidence-Based Complementary and Alternative Medicine*, vol. 2022, Article ID 7350489, 9 pages, 2022.

Hindawi
Evidence-Based Complementary and Alternative Medicine
Volume 2022, Article ID 7350489, 9 pages
https://doi.org/10.1155/2022/7350489

Research Article

Valproic Acid Inhibits Peripheral T Cell Lymphoma Cells Behaviors via Restraining PI3K/AKT Pathway

Zhiqiang Peng,[1,2] **Jianping Xiong**,[1] **and Hanzhi Dong**[3]

[1]*Department of Oncology, The First Affiliated Hospital of Nanchang University, Nanchang 330006, Jiangxi, China*
[2]*Department of Lymphatic Hematology and Oncology, Jiangxi Cancer Hospital, Nanchang 330029, Jiangxi, China*
[3]*General Department of Oncology, Jiangxi Cancer Hospital, Nanchang 330029, Jiangxi, China*

Correspondence should be addressed to Jianping Xiong; xjppzq@163.com

Received 27 April 2022; Revised 30 June 2022; Accepted 5 July 2022; Published 5 August 2022

Academic Editor: Xueliang Wu

Objective. Alproic acid (VPA) is a clinic antiepileptic drug. Antitumor role of VPA has been studied. The aim of this study was to clarify the treatment effect and potential mechanism of VPA on peripheral T cell lymphomas (PTCLs). *Materials and Methods*. Hut 78 cells were obtained from the Shanghai Cell Bank, Chinese Academy of Sciences, and randomly divided into six groups: control, VPA (8 mM), empty vector (NC), miR-3196 mimics, miR-3196 inhibitor, and VPA + miR-3196 mimics groups. CCK-8 assay was performed to clarify the regulative role of VPA on cell proliferation. Flow cytometry was applied to determine the apoptotic rate and ROS levels. miR-3196 was tested by RT-qPCR. Western blot was used to test the level of p-PI3K and p-AKT. Biochemical experiments were used to detect changes in the content of ATP, lactate level, and glucose content. Electron microscopy was used to show the structure of mitochondria in Hut 78 cells. *Results*. VPA greatly promoted the expression of miR-3196 and inhibited cell proliferation in a dose-dependent manner. Compared with the NC group, the cell apoptosis rate, Bax and cleaved-caspase-3 expression, lactate level, ROS expression, and glucose content in the VPA group were significantly increased ($P < 0.05$), and cell proliferation, ATP production, and the expression of Bcl-2, p-PI3K and p-AKT was decreased significantly ($P < 0.05$). The role of mir-3196 mimics is similar to VPA. While, the miR-3196 inhibitor had the opposite effect to VPA and mimics. The combination of VPA and miR-3196 mimics has the most obvious effect. *Conclusion*. VPA can inhibit the proliferation of Hut 78 cells and promote cell apoptosis and the structure and dysfunction of mitochondria by regulating the activity of the PI3K/AKT pathway.

1. Introduction

Peripheral T cell lymphomas (PTCLs) are a group of heterogeneous lymphoproliferative diseases caused by mature T cells or natural killer cells, accounting for about 10%–15% of the total malignant lymphoma [1–3]. The incidence of PTCL has distinct geographical and ethnic characteristics, accounting for 25%–30% of non-Hodgkin lymphoma (NHL) incidence in the oriental population [4–6], which is significantly higher than 10%–15% reported in European and American countries [7, 8]. As PTCL has diverse clinical symptoms, PTCL could affect upper digestive tract to induce esophageal stricture and dysphagia [9]. Tongue could also be the target tissue of lymphoma [10]. The symptoms of digestive lymphoma are similar to that of Crohn's disease [11]. It is prone to missed diagnosis and misdiagnosis. The main frontline therapies include brentuximab vedotin [12], histone deacetylase inhibitors [13], pralatrexate [14], mogamulizumab [15], alemtuzumab [16], lenalidomide [17], azacitidine [18], PI3Ki [19], and consolidative stem cell transplantation [20]. However, its overall treatment efficacy is still poor, with a 5-year survival of only 10%–30% [21]. Further studies are needed to investigate the pathogenesis of PTCLs, which are of great significance for the prevention and treatment of PTCLs.

Alproic acid (VPA) is a commonly used antiepileptic drug in clinics. Due to its histone deacetyltransferase inhibitor function, its potential antitumor effect has been

widely valued. Many studies have shown that VPA has a certain antitumor effect [22–24]. In the combined treatment research of VPA and other chemotherapeutics, it is found that VPA itself has the effect of inhibiting tumor cells, and it can also increase the sensitivity of tumor cells to certain chemotherapeutic drugs and reduce the drug resistance of tumor cells [25, 26]. VPA can also regulate the expression of miRNAs in tumor cells to play an antitumor role [27]. However, the effects of VPA on miRNAs in peripheral T lymphocytic lymphoma and their specific regulatory mechanisms are currently poorly studied and still need further study.

miRNAs have been widely studied in various disease. They are a group of short noncoding RNA that inhibits the function of target gene via binding to its mRNA [28]. The role of miRNAs in PTCLs has been confirmed by some studies. miRNA-126-3p and miR-145-5p are increased in PTCL and perform T cell migrative regulation [29]. Hsa-miR-372-5p regulates NLRP3 inflammasome activation via targeting in NK/T cell lymphoma [30]. miR-548 could inhibit the progression of NK/T cell lymphoma via targeting FOXO1 [31]. These evidences reveal the potential regulation role of miRNAs in PTCL. However, the role of miRNAs in PTCL is still not fully clarified. The involved miRNAs and their target genes need to be uncovered. miR-3196 has been confirmed to regulate lung adenocarcinoma cell migration and invasion via Sox12 [32]. miR-3196 could regulate cell proliferation, migration, and EMT (epithelial-mesenchymal transition) via STRN4 in drug-resistant cells of liver cancer [33]. However, the role of miR-3196 in PTCL has not been explored. Whether miR-3196 was the downstream gene in VPA treating needs to be verified.

In this study, we used VPA to process Hut 78 cells and then observed the effects of VPA on the proliferation, apoptosis, mitochondrial structure, and function of Hut 78 cells and further explore whether its effect is achieved by regulating the PI3K/AKT pathway.

2. Materials and Methods

2.1. Cell Culture. To detect the role of VPA PTCL cells, Hut 78 cells (TCHu206, Shanghai Cell Bank, Chinese Academy of Sciences), a commonly used T cell lymphoma cell in tumor research studies [34], were cultured and in vitro analysis was conducted. These cells were purchased from IMDM (SH30228.01B; Hyclone), adding 20% fetal bovine serum (FBS, 10270-106; Gibco) was applied to culture the cell in vitro. The cells were cultured in a 37°C constant temperature incubator (5% CO_2). The culture medium was changed every day.

2.2. Cell Transfection. The sequence of miR-3196 (GI: 301171776) was checked at the NCBI database. miR-3196 mimics (5′-CGGGGCGGCAGGGCCUC-3′) or inhibitor (5′-CGGGGCGGCAGGGCCUC-3′) was transported into the cell with Lipofectamine 2000. The transfection was conducted according to the manufacturer's instructions. 24 hours before transfection, inoculate 1×10^5 cells in 500 μL medium and adjust the cell number to 6×10^5/well during transfection. siRNA (1 μl, 10 μM) was diluted with Opti-MEM (50 μL). Then, 5 μl Lipofectamine® RNAiMAX was added into 50 μL Opti-MEM. These reagents were mixed and maintained in the fridge (4°C, 5 minutes). Finally, the cells were kept in an incubator at 37°C and 5% CO_2 for 24 hours.

Cells were intervened with miR-3196 mimics or miR-3196 inhibitor for 48 h and, respectively, divided into six groups: control, VPA, empty vector (NC), miR-3196 mimics, miR-3196 inhibitor, and VPA + miR-3196 mimics groups.

2.3. Cell Counting Kit-8 (CCK-8). To detect the cell viability, CCK-8 assay was used. The suspending cells were cultured in 96-well plates at a density of 1×10^4 cells/ml with IMDM adding 20% FBS for 48 h. Then, 10 μl CCK-8 reagent was added to each well of the plates. The cells with CCK-8 were incubated at 37°C for 4 h. The optical density (450 nm) was determined with a microplate reader (Multiskan FC, Thermo, USA).

2.4. Flow Cytometry. After culturing for 48 h, the cell samples from different groups were harvested, added in 1 ml precooled PBS, and centrifuged at 1000g for 5 min. The supernatant was discarded. The cells were resuspended with cold PBS, and Annexin V-FITC and PI were added. The cell apoptotic rate and ROS level of cells were analyzed using flow cytometry according to the manufacturer's instructions, and the data were analyzed by flow cytometry (Beckman Coulter, USA).

2.5. The Detection of Glucose, A095-1, and A019-2. To detect the level of lactic acid (A019-2), ATP (A095-1), and glucose (F006), the assay kits were brought from Nanjing Jiancheng Bioengineering Institute. The experiments were conducted according to the manufacturer's instruction.

2.6. Transmission Electron Microscopy (TEM). After rinsing the cells with cold PBS for three times, 2.5% glutaraldehyde was applied to prefix the cells (4°C, 30 min). Then, 1% osmic acid was used to fix the cells for 1 h. Then, after dehydrating, the samples were incubated in acetone and epoxy mixture (1 : 1) at 40°C for 6 h. After further fixing with pure epoxy resin (40°C, 4 h), the samples were embedded and sliced. The slices were double stained and stained with lead citrate for 15 min. The slices were rinsed with double-distilled water. Finally, the mitochondria ultrastructure was recorded with TEM (HT7700, Hitachi).

2.7. Western Blot Analysis. The total proteins from cells were extracted, and the concentration was measured by the BCA protein assay kit (Beyotime, China). Total protein was separated in SDS-PAGE (12%). The proteins were then transferred to the PVDF membrane. The membranes were blocked with a blocking buffer (5% nonfat milk, 0.05% Tween-20) which was used to block the membranes. Then, the membranes were labeled with primary antibody

Table 1: Primer sequences.

Primers	Sequence (5′-3′)
miR-3196-F	GGGCGGGGCGGCAGGG
miR-3196-R	AACTGGTGTCGTGGAGTCGGC
U6-F	CTCGCTTCGGCAGCACA
U6-R	AACGCTTCACGAATTTGCGT

including anti-Bad antibody (1 : 1000, MAB37156, Bioswamp), anti-Bcl-2 antibody (1 : 1000, PAB33482, Bioswamp), anti-cleaved-caspase-3 antibody (1 : 1000, MAB37300, Bioswamp), anti-PI3K antibody (1 : 1000, PAB30009, Bioswamp), anti-AKT antibody (1 : 1000, PAB34089, Bioswamp), and anti-GAPDH antibody (1 : 1000, PAB36264, Bioswamp). The membranes were rinsed with PBS/Tween-20 three times. Then, the membranes were further labeled with horseradish peroxidase-conjugated secondary goat anti-rabbit IgG (1 : 10000, SAB43711, Bioswamp) for 2 h at room temperature. The blots were visualized by enhanced chemiluminescence color detection (Tanon-5200, TANON, China).

2.8. Quantitative Real-Time Polymerase Chain Reaction (qRT-PCR). The total RNAs of the cultured cell were extracted with TRIzol (Beyotime, China) kit. The cDNAs were synthesized with the reverse transcriptase kit (TAKARA, USA). RT-qPCR was conducted with the SYBR Green PCR Kit (KM4101, KAPA Biosystems) on the real-time system (Bio-Rad. The $2^{-\triangle\triangle Ct}$ method was used to analyze the expression of the RNAs. The primers sequences are given in Table 1 (Nanjing Kingsy Biotechnology Co., Ltd.) (Table 1).

2.9. Statistical Analysis. The data were recorded as the mean ± standard deviation. *t* tests were used to analyze the differences between two groups. One-way ANOVA was used to analyze differences between groups. SPSS 22 statistical software was used to conduct statistical analysis. $P < 0.05$ was considered statistically significant.

3. Results

3.1. VPA Promotes miR-3196 Expression and VPA and miR-3196 Promote Cell Proliferation in a Synergistic way. We first detected miR-3196 expression in Hut 78 cells after different concentrations of VPA intervention. Compared with the control group, different doses of VPA could significantly increase the expression of miR-3196 ($P < 0.05$) (Figure 1(a)). CCK-8 analysis was conducted to clarify the effect of VPA on the Hut 78 cell proliferation. The results showed that compared with the control group, the cell proliferation rate in the VPA group (0 mM, 0.5 mM, 1 mM, 2 mM, 4 mM, 8 mM, 16 mM, and 32 mM) [35] was significantly reduced ($P < 0.05$), and the 32 mM VPA group had the lowest cell proliferation rate (Figure 1(b)). The CCK-8 experiment showed that IC50 of VPA on Hut 78 cells was 16 mM. Therefore, we use 0.5 IC50 (8 mM) as the VPA intervention concentration for subsequent experiments. The transfection efficiency of miR-3196 mimics/inhibitor was further detected by RT-qPCR (Figure 1(c)). The expression of miR-3196 in the miR-3196 mimics group was evidently increased compared with the control group ($P < 0.05$). The expression level of miR-3196 was significantly decreased in the miR-3196 inhibitor group compared with the control group ($P < 0.05$). These data suggested that miR-3196 mimics and miR-3196 inhibitor were successfully transfected. As shown in Figure 1(d), the cell proliferation rate of the VPA group was greatly reduced compared with that in the control group ($P < 0.05$). Compared with the NC group, the cell proliferation rate was decreased in the miR-3196 mimics group and VPA + miR-3196 mimics group ($P < 0.05$). While, it was increased in the miR-3196 inhibitor group ($P < 0.05$).

3.2. VPA and miR-3196 Promote Cell Apoptosis in a Synergistic way. Flow cytometry was performed to determine the apoptotic rate of cultured Hut 78 cells. As shown in Figure 2(a), the apoptotic rate of the VPA, miR-3196 mimics, and VPA + miR-3196 mimics group was greatly promoted compared with that in the control group ($P < 0.05$). The apoptotic rate of the miR-3196 inhibitor group was evidently inhibited compared with that in the control group ($P < 0.05$). The apoptotic rates of the miR-3196 mimics group and VPA + miR-3196 mimics group were greatly promoted compared with that in the NC group ($P < 0.05$), while the apoptotic rate of the miR-3196 inhibitor group was evidently reduced ($P < 0.05$). We further detected the expression of related apoptotic proteins, and the results showed that compared with the control, Bax and cleaved-caspase-3 expressions were significantly increased in the VPA, miR-3196 mimics, and VPA + miR-3196 mimics group ($P < 0.05$), and the level of Bcl-2 was greatly reduced in the VPA, miR-3196 mimics, and VPA + miR-3196 mimics group ($P < 0.05$) (Figure 2(b)). Compared to the NC group, the expression of Bax and cleaved-caspase-3 in the miR-3196 mimics group and VPA + miR-3196 mimics group increased significantly ($P < 0.05$), while Bcl-2 expression in these groups was evidently inhibited ($P < 0.05$).

3.3. VPA and miR-3196 Affect Mitochondrial Morphology, ROS Production, and Cell Metabolism. In Figure 3(a), TEM was conducted to show the impact of VPA and miR-3196 on mitochondrial structure of Hut 78 cells. The shape of mitochondria in the control group was oval or rod with neat mitochondria cristae. The cristae lumen was not dilated. In the VPA group and miR-3196 mimics group, the swelling and deformation of mitochondria showed spherical structure, the internal cristae decreased, and some vacuolization. Compared with the control group, the production of ROS was greatly promoted in the VPA group ($P < 0.05$). Compared with the NC group, ROS levels in miR-3196 mimics and VPA + miR-3196 mimics groups were significantly increased ($P < 0.05$), while ROS level was significantly decreased ($P < 0.05$) in the miR-3196 inhibitor group ($P < 0.05$) (Figure 3(b)). We further tested the effects of VPA on the cell metabolism. As the result shown in Figure 3(c), compared with the control group, the ATP production in the VPA group decreased ($P < 0.05$), and the lactate level and glucose

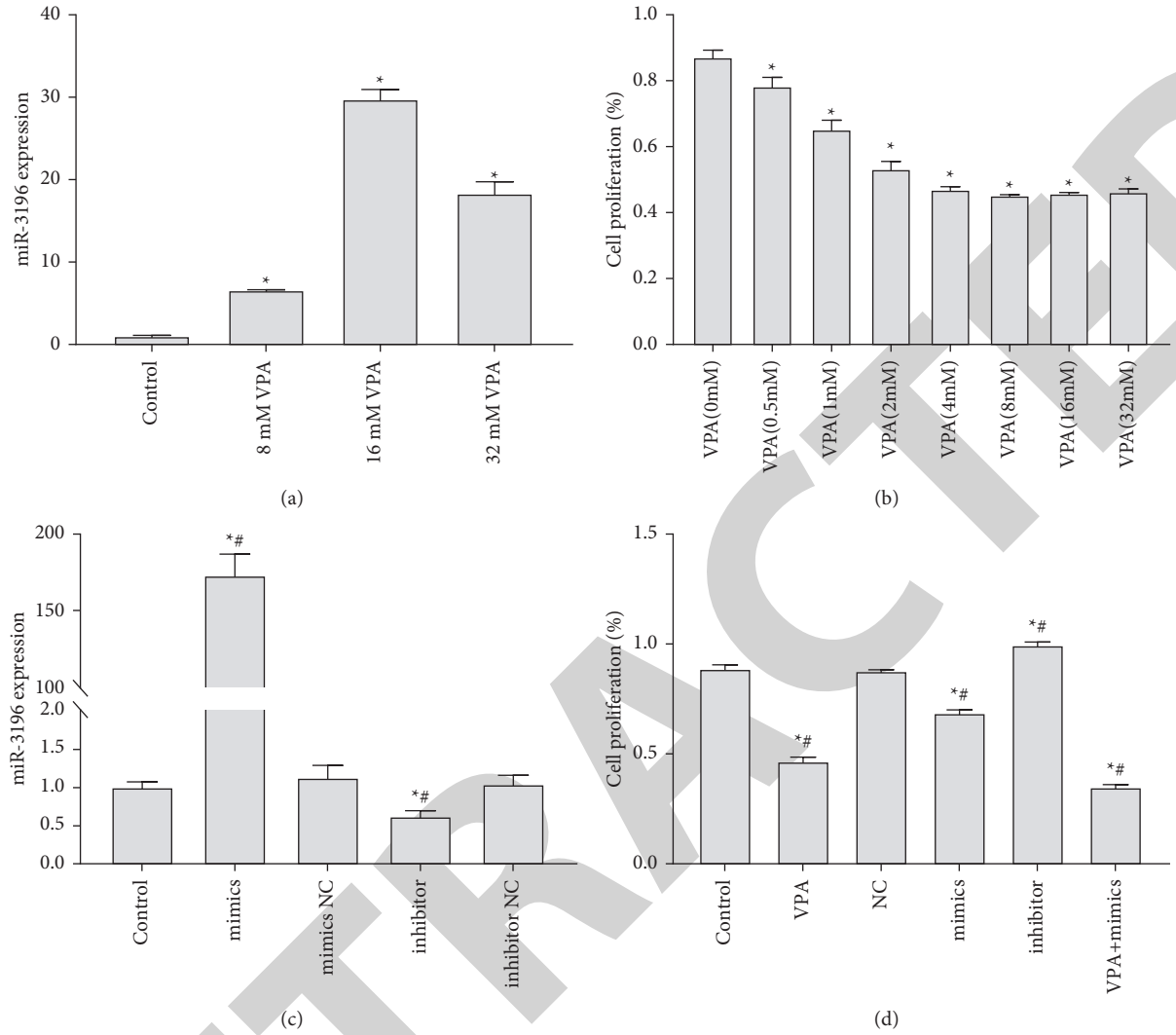

Figure 1: VPA promotes miR-3196 expression, and VPA and miR-3196 promote cell proliferation in a synergistic way. (a) RT-qPCR used to detect miR-3196 expression. ((b) and (d)) CCK-8 used to detect Hut 78 cell proliferation after 48 hours of valproic acid intervention. (c) miR-3196 expression detected by RT-qPCR. $^{*}P < 0.05$ vs. control; $^{\#}P < 0.05$ vs. NC. $N = 3$.

content increased ($P < 0.05$). Compared with the NC group, the ATP production in the miR-3196 mimics group and VPA + miR-3196 mimics increased ($P < 0.5$) and the lactic acid content and glucose content decreased ($P < 0.5$).

3.4. VPA and miR-3196 Regulate PI3K/AKT Pathway. To study whether VPA and miR-1396 play its role through the PI3K/AKT pathway, we used Western blot to detect key proteins in the PI3K/AKT pathway. The level of p-PI3K and p-AKT were decreased in the VPA group compared with that in the control group ($P < 0.05$). Compared with the NC group, the expression of p-PI3K and p-AKT was decreased in the miR-3196 mimics group and VPA + miR-3196 mimics group ($P < 0.05$) and increased significantly in the miR-3196 inhibitor group ($P < 0.05$). These results suggested VPA and miR-3196 can play a protective role by inhibiting the PI3K/AKT pathway (Figure 4).

4. Discussion

Peripheral T cell lymphoma (PTCL) is a type of heterogeneous lymphoproliferative diseases that affect multiorgan including the digestive system. When PTCLs occur in the digestive system, dysphagia, digestive tract stenosis, and other type of symptoms like Crohn's disease could occur [9–11]. Clarifying the pathogenic mechanism of PTCLs is important to the development of effective therapeutic methods.

Aberrant epigenetic dysregulation, including DNA methylation, histone modification, chromatin remodeling, gene imprinting, and random chromosome (x) inactivation, plays a key role in tumorigenesis. Histone deacetylases (HDACs) and histone acetyltransferases (HATS) are involved in epigenetic regulation of genes by controlling the acetylation status of lysine residues in the histone tail [36]. HATS acetylate histone tails to form an "open" chromatin

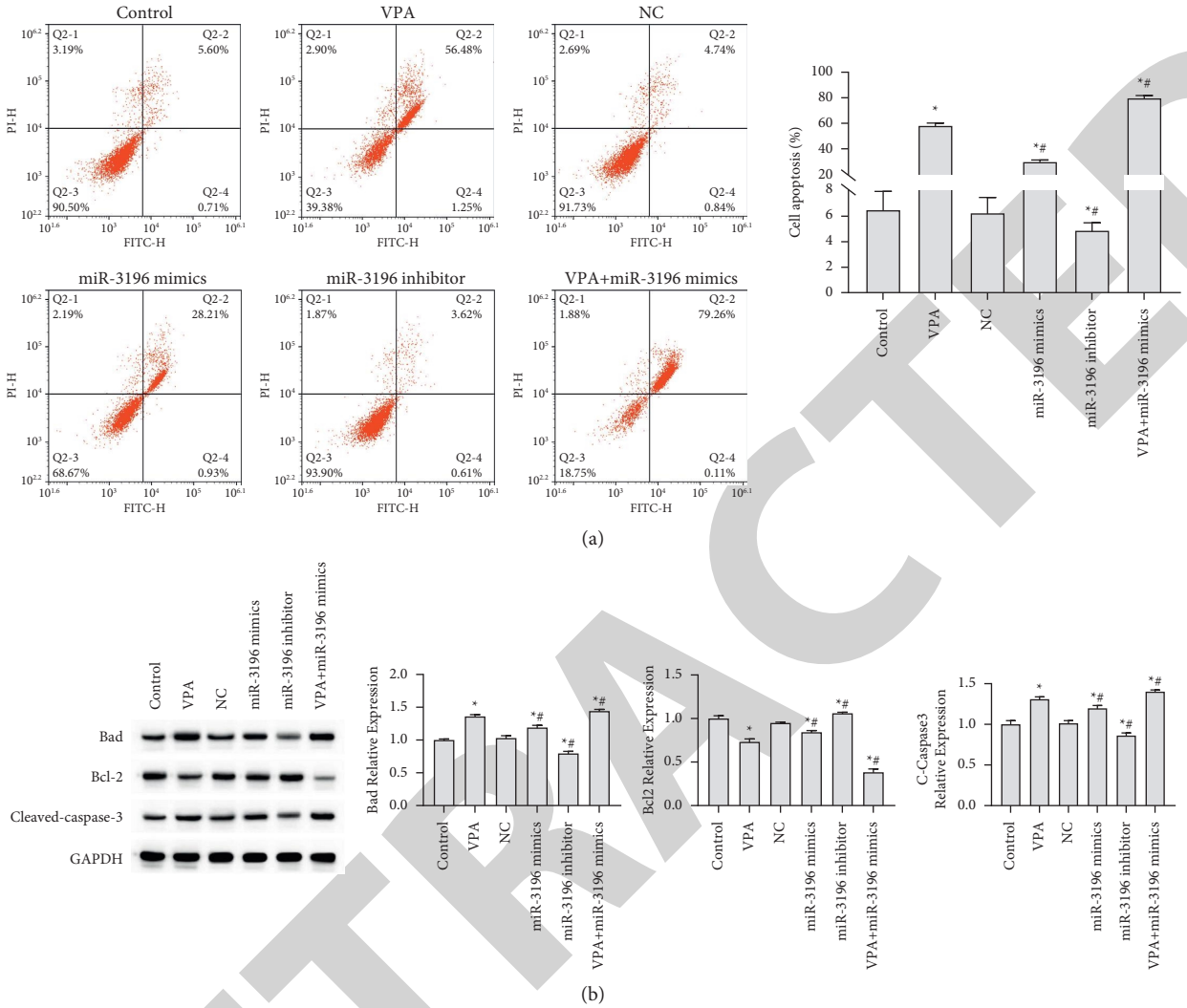

Figure 2: VPA and miR-3196 promote cell apoptosis in a synergistic way. (a) Cell apoptosis detected by flow cytometry. (b) Expression of Bcl-2, Bax, and cleaved-caspase-3 tested by Western blot. $^{*}P < 0.05$ vs. control; $^{\#}P < 0.05$ vs. NC. $N = 3$.

structure that facilitates the execution of gene transcription. In contrast, HDACs control the deacetylation of histone tails, which holds chromatin in a "closed" state and causes the expression silencing of relevant genes [37]. Normally, HDACs and hats are in a dynamic equilibrium between each other, and the disruption of their balance is closely related to tumor initiation and progression. HDACs, which regulate the deacetylation of histones and certain nonhistone proteins, including the activation of tumor initiation related transcription factors as well as posttranslational modifications of key proteins including tumor suppressor genes [38–40], have emerged as a potential anticancer target because of their close association with cancer cell proliferation, apoptosis, differentiation, migration, and metastasis [40]. Studies have found that VPA is able to exert its anticancer effects by altering the histone acetylation levels of tumor cells, while also downregulating the expression levels of the antiapoptotic protein survivin, counteracting its antiapoptotic effect, and playing a role in inducing tumor cell apoptosis. Thus, in this experiment, we first detected the effect of VPA on the proliferation and apoptosis of PTCLs. The results showed that compared with the control group, the treatment of VPA can significantly inhibit the proliferation of Hut 78 cells and promote its apoptosis, suggesting that VPA can significantly inhibit the proliferation of PTCLs and promote cell apoptosis.

Mitochondria are an important source of energy in cells, and their morphology is a dynamic change process in the cell process. Mitochondria are extremely vulnerable to the attack of reactive oxygen species, which leads to the breakdown of the dynamic balance of mitochondrial fission and polymerization, and ultimately leads to cell apoptosis [41–44]. Studies have found [45] that histone deacetylase inhibitors can inhibit the formation of reactive oxygen species in tumor cells, promote the activation of caspase-8, caspase-9, caspase-3 and PARP, and ultimately lead to cell apoptosis.

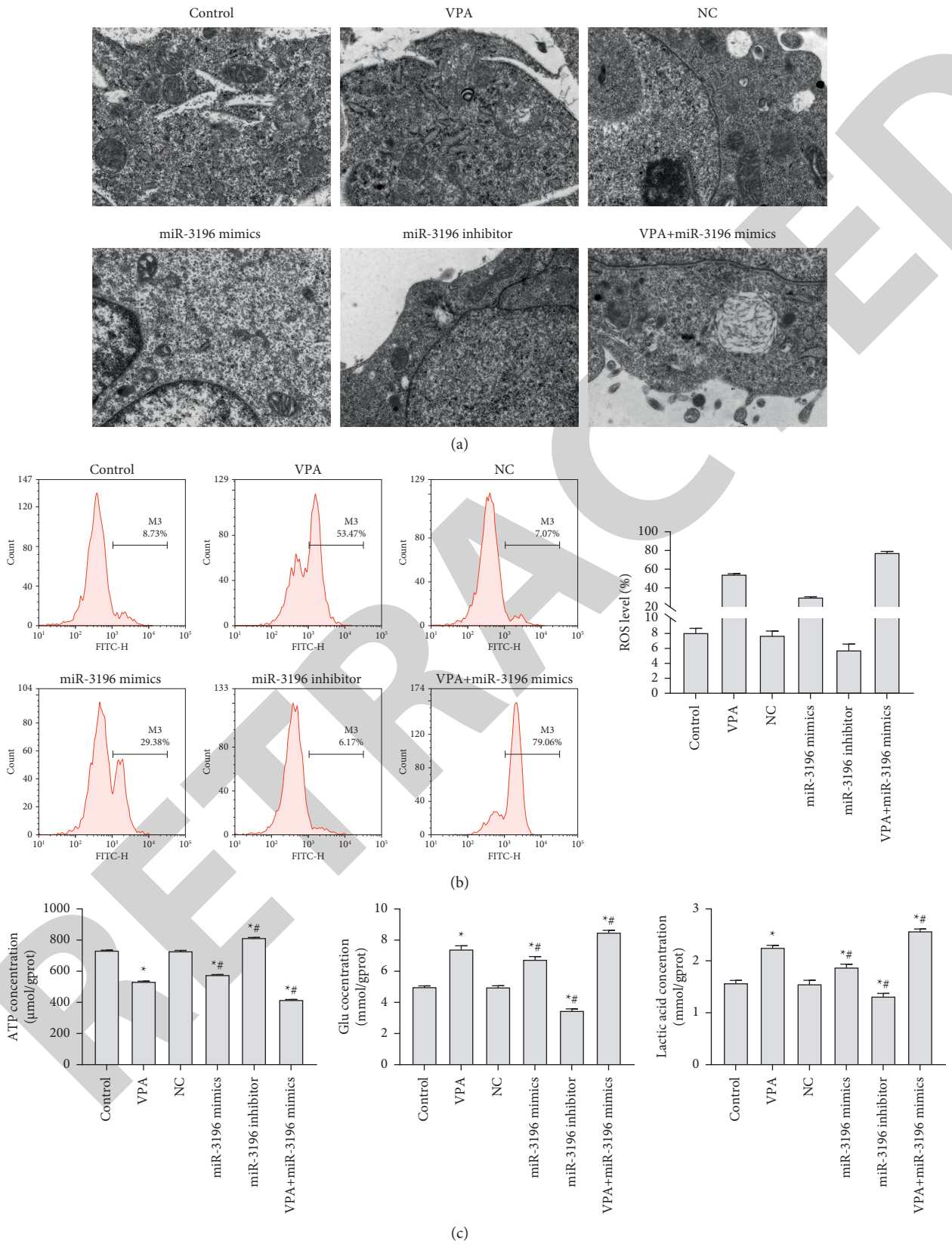

Figure 3: VPA and miR-3196 affect mitochondrial morphology, ROS production, and cell metabolism. (a) Mitochondrial morphology examined by electron microscopy (scale bar = 1 mM). (b) ROS level detected by flow cytometry. (c) ATP production, lactate level, and glucose content observed by biochemical analysis. $^{*}P < 0.05$ vs. control; $^{\#}P < 0.05$ vs. NC. $N = 3$.

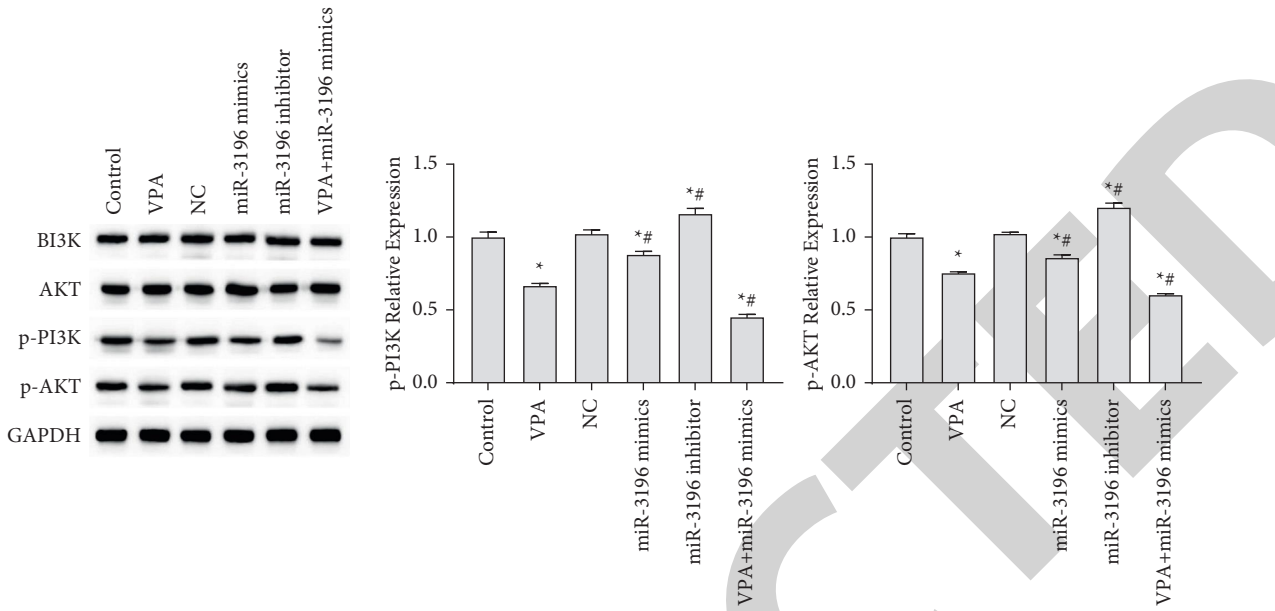

Figure 4: VPA and miR-3196 regulate the PI3K/AKT pathway. Expression of p-PI3K and p-AKT protein observed by Western blot. $^{*}P < 0.05$ vs. control; $^{\#}P < 0.05$ vs. NC. $N = 3$.

However, it is rarely reported whether VPA regulates the mitochondrial function of T lymphocyte tumors and promotes cell apoptosis. Thus, in this experiment, we first detected the expression of ROS in each group; the results showed that the expression of ROS in the VPA group was significantly increased compared to the control, suggesting that VPA can effectively promote the expression of ROS. We further observed the effect of VPA on mitochondrial structure of Hut 78 cells and found that the mitochondria in the control group were oval or rod-shaped, and the cristae in the mitochondria was neat, and the lumen of the cristae was not dilated. In the VPA group and miR-3196 mimics group, the swelling and deformation of mitochondria showed spherical structure, the internal cristae decrease, and some vacuolization.

The PI3K/AKT/mTOR signaling pathway is a classical pathway that regulates cell growth and proliferation and is closely related to a variety of diseases. In the previous experiments of this study, we found that VPA could inhibit the proliferation of Hut 78 cells, promote cell apoptosis, and the structure and dysfunction of mitochondria. Therefore, we speculate that VPA may be achieved by regulating the PI3K/AKT pathway. The results showed that the expression of p-PI3K and p-AKT decreased in the VPA group compared to the control, prompting that VPA can inhibit the activity of the PI3K/AKT pathway. There are some limitations of this study. The target gene of miR-3196 could be confirmed. The animal verification is also suggested. We will complete these in further study.

In conclusion, VPA can inhibit the proliferation of Hut 78 cells and promote cell apoptosis and the structure and dysfunction of mitochondria, and its effect may be achieved by regulating the activity of the PI3K/AKT pathway. VPA could be a potential treatment drug on PTCLs.

Data Availability

The data used to support this study are available from the corresponding author upon request.

Conflicts of Interest

The authors declare that they have no conflicts of interest.

References

[1] J. O. Armitage, "The aggressive peripheral T-cell lymphomas: 2015," *American Journal of Hematology*, vol. 90, no. 7, pp. 665–673, 2015.

[2] K. J. Savage, "Peripheral T-cell lymphomas," *Blood Reviews*, vol. 21, no. 4, pp. 201–216, 2007.

[3] F. M. Foss, P. L. Zinzani, J. M. Vose, R. D. Gascoyne, S. T. Rosen, and K. Tobinai, "Peripheral T-cell lymphoma," *Blood*, vol. 117, no. 25, pp. 6756–6767, 2011.

[4] Q. P. Yang, W. Y. Zhang, J. B. Yu et al., "Subtype distribution of lymphomas in Southwest China: analysis of 6, 382 cases using WHO classification in a single institution," *Diagnostic Pathology*, vol. 6, no. 1, 2011.

[5] J. Sun, Q. Yang, Z. Lu et al., "Distribution of lymphoid neoplasms in China: analysis of 4, 638 cases according to the world health organization classification," *American Journal of Clinical Pathology*, vol. 138, no. 3, pp. 429–434, 2012.

[6] L. I. Xiao-Qiu, L. I. Gan-Di, Z. F. Gao, X. G. Zhou, and X. Z. Zhu, "Distribution pattern of lymphoma subtypes in China: a nationwide multicenter study of 10002 cases," *Journal of Diagnostics Concepts & Practice*, vol. 11, 2012.

[7] B. T. Hennessy, E. O. Hanrahan, and P. A. Daly, "Non-Hodgkin lymphoma: an update," *The Lancet Oncology*, vol. 5, no. 6, pp. 341–353, 2004.

[8] International T-Cell Lymphoma Project, J. Armitage, and D. Weisenburger, "International peripheral T-cell and natural killer/T-cell lymphoma study: pathology findings and clinical

outcomes," *Journal of Clinical Oncology*, vol. 26, no. 25, pp. 4124–4130, 2008.

[9] Q. Zhang, C. Liu, Z. Liu et al., "Esophageal peripheral T-cell lymphoma treated with radiotherapy: a case report," *Medicine (Baltimore)*, vol. 100, no. 4, Article ID e24455, 2021.

[10] Y. Kim, J. Song, D. Sun, Y. Hong, and G. Park, "MALT lymphoma at the base of tongue of a 29-year-old woman treated with radiation therapy alone," *Journal of Cancer Research and Therapeutics*, vol. 10, no. 2, pp. 407–409, 2014.

[11] P. Coppo, B. Fabiani, C. Marzac, and H. Sokol, "Mature CD8 (+) T-cell clonal expansion in the oral cavity and digestive tract: a severe lymphoid malignancy that mimics Crohn's disease," *Clinical Case Reports*, vol. 4, no. 12, pp. 1088–1090, 2016.

[12] M. A. Fanale, S. M. Horwitz, A. Forero-Torres et al., "Five-year outcomes for frontline brentuximab vedotin with CHP for CD30-expressing peripheral T-cell lymphomas," *Blood*, vol. 131, no. 19, pp. 2120–2124, 2018.

[13] I. C. Chen, B. Sethy, and J. P. Liou, "Recent update of HDAC inhibitors in lymphoma," *Frontiers in Cell and Developmental Biology*, vol. 8, Article ID 576391, 2020.

[14] O. A. O'Connor, B. Pro, L. Pinter-Brown et al., "Pralatrexate in patients with relapsed or refractory peripheral T-cell lymphoma: results from the pivotal PROPEL study," *Journal of Clinical Oncology*, vol. 29, pp. 1182–1189, 2011.

[15] Y. H. Kim, M. Bagot, L. Pinter-Brown et al., "Mogamulizumab versus vorinostat in previously treated cutaneous T-cell lymphoma (MAVORIC): an international, open-label, randomised, controlled phase 3 trial," *The Lancet Oncology*, vol. 19, no. 9, pp. 1192–1204, 2018.

[16] A. Gallamini, F. Zaja, C. Patti et al., "Alemtuzumab (campath-1H) and CHOP chemotherapy as first-line treatment of peripheral T-cell lymphoma: results of a GITIL (gruppo italiano terapie innovative nei linfomi) prospective multicenter trial," *Blood*, vol. 110, no. 7, pp. 2316–2323, 2007.

[17] E. Toumishey, A. Prasad, G. Dueck et al., "Final report of a phase 2 clinical trial of lenalidomide monotherapy for patients with T-cell lymphoma," *Cancer*, vol. 121, no. 5, pp. 716–723, 2015.

[18] J. Ruan, A. J. Moskowitz, N. Mehta-Shah et al., "Multi-center phase II study of oral azacitidine (CC-486) plus CHOP as initial treatment for peripheral T-cell lymphoma (PTCL)," *Blood*, vol. 136, pp. 33-34, 2020.

[19] S. M. Horwitz, R. Koch, P. Porcu et al., "Activity of the PI3K-δ, γ inhibitor duvelisib in a phase 1 trial and preclinical models of T-cell lymphoma," *Blood*, vol. 131, no. 8, pp. 888–898, 2018.

[20] Z. Al-Mansour, H. Li, J. R. Cook et al., "Autologous transplantation as consolidation for high risk aggressive T-cell non-Hodgkin lymphoma: a SWOG 9704 intergroup trial subgroup analysis," *Leukemia and Lymphoma*, vol. 60, no. 8, pp. 1934–1941, 2019.

[21] Y. Zhang, W. Xu, H. Liu, and J. Li, "Therapeutic options in peripheral T cell lymphoma," *Journal of Hematology & Oncology*, vol. 9, no. 1, 2016.

[22] P. J. Tofilon and K. Camphausen, "HDAC inhibitors in cancer care," *Oncology*, vol. 24, no. 2, pp. 180–185, 2010.

[23] S. H. Kim, J. G. Kang, C. S. Kim et al., "Synergistic cytotoxicity of BIIB021 with triptolide through suppression of PI3K/Akt/mTOR and NF-κB signal pathways in thyroid carcinoma cells," *Biomedicine & Pharmacotherapy*, vol. 83, pp. 22–32, 2016.

[24] Y. K. Shi, Z. H. Li, X. Q. Han et al., "The histone deacetylase inhibitor suberoylanilide hydroxamic acid induces growth inhibition and enhances taxol-induced cell death in breast cancer," *Cancer Chemotherapy and Pharmacology*, vol. 66, no. 6, pp. 1131–1140, 2010.

[25] T. Ueda, N. Takai, M. Nishida, K. Nasu, and H. Narahara, "Apicidin, a novel histone deacetylase inhibitor, has profound anti-growth activity in human endometrial and ovarian cancer cells," *International Journal of Molecular Medicine*, vol. 19, no. 2, pp. 301–308, 2007.

[26] M. Bazzaro, Z. Lin, A. Santillan et al., "Ubiquitin proteasome system stress underlies synergistic killing of ovarian cancer cells by bortezomib and a novel HDAC6 inhibitor," *Clinical Cancer Research*, vol. 14, no. 22, pp. 7340–7347, 2008.

[27] W. Xia, X. Lan, J. Lv, and J. Ma, "Valproic acid (VPA) suppresses the expression of SMAD4 in prostate carcinoma by up-regulating miR-34a," *International Journal of Clinical and Experimental Medicine*, vol. 9, pp. 20466–20473, 2016.

[28] B. Li, Z. Wang, M. Yu et al., "miR223p enhances the intrinsic regenerative abilities of primary sensory neurons via the CBL/pEGFR/pSTAT3/GAP43/pGAP43 axis," *Journal of Cellular Physiology*, vol. 235, no. 5, pp. 4605–4617, 2020.

[29] W. Lone, A. Bouska, S. Sharma et al., "Genome-wide miRNA expression profiling of molecular subgroups of peripheral T-cell lymphoma," *Clinical Cancer Research*, vol. 27, no. 21, pp. 6039–6053, 2021.

[30] Q. Chen, S. Liu, K. Zhang et al., "Hsa-miR-372-5p regulates the NIMA related kinase 7 and IL-1β release in NK/T-cell lymphoma," *Leukemia and Lymphoma*, vol. 62, no. 11, pp. 2648–2656, 2021.

[31] C. C. Wang, L. Han, Y. H. Hou, and X. Y. Ying, "MiRNA-584 suppresses the progression of NK/T-cell lymphoma by targeting FOXO1," *European Review for Medical and Pharmacological Sciences*, vol. 24, no. 8, pp. 4404–4411, 2020.

[32] Q. Wu and J. Jiang, "LncRNA MAFG-AS1 promotes lung adenocarcinoma cell migration and invasion by targeting miR-3196 and regulating SOX12 expression," *Molecular Biotechnology*, 2022.

[33] T. Chen, B. Huang, and Y. Pan, "Long non-coding RNA MAFG-AS1 promotes cell proliferation, migration, and EMT by miR-3196/STRN4 in drug-resistant cells of liver cancer," *Frontiers in Cell and Developmental Biology*, vol. 9, Article ID 688603, 2021.

[34] A. Verma, P. Gupta, N. Rai et al., "Assessment of biological activities of fungal endophytes derived bioactive compounds isolated from amoora rohituka," *Journal of Fungi*, vol. 8, no. 3, 2022.

[35] Z. Zheng, S. Cheng, W. Wu et al., "c-FLIP is involved in tumor progression of peripheral T-cell lymphoma and targeted by histone deacetylase inhibitors," *Journal of Hematology & Oncology*, vol. 7, no. 1, 2014.

[36] A. J. D. Ruijter, A. H. V. Gennip, H. N. Caron, S. Kemp, and A. B. V. Kuilenburg, "Histone deacetylases (HDACs): characterization of the classical HDAC family," *Biochemical Journal*, vol. 370, no. 3, pp. 737–749, 2003.

[37] A. Mengel, A. Ageeva, E. Georgii et al., "Nitric oxide modulates histone acetylation at stress genes by inhibition of histone deacetylases," *Plant Physiology*, vol. 173, no. 2, pp. 1434–1452, 2017.

[38] K. Lu, N. Chen, X. X. Zhou et al., "The STAT3 inhibitor WP1066 synergizes with vorinostat to induce apoptosis of mantle cell lymphoma cells," *Biochemical and Biophysical Research Communications*, vol. 464, no. 1, pp. 292–298, 2015.

[39] J. Tan, S. Cang, Y. Ma, R. L. Petrillo, and D. Liu, "Novel histone deacetylase inhibitors in clinical trials as anti-cancer agents," *Journal of Hematology & Oncology*, vol. 3, no. 1, 2010.

Hindawi
Evidence-Based Complementary and Alternative Medicine
Volume 2022, Article ID 8701779, 5 pages
https://doi.org/10.1155/2022/8701779

Research Article

Treatment Alternative and High Safety Profile of Acupuncture Plus Chemotherapy for Advanced Gastric Cancer

Xiaomei Miao,[1] **Hongying Wu**,[1] **Yan Liu**,[2] **Shu Zhang**,[1] **Chaohui Li**,[1] **and Jie Hao**[3]

[1]*National Physician Hall, Cangzhou Central Hospital, Cangzhou, China*
[2]*Department of Hepatopancreatobiliary Surgery, Cangzhou Central Hospital, Cangzhou, China*
[3]*Department of Oncology, Cangzhou Central Hospital, Cangzhou, China*

Correspondence should be addressed to Xiaomei Miao; miaozhiguxiong1928@163.com

Received 10 April 2022; Revised 11 June 2022; Accepted 4 July 2022; Published 30 July 2022

Academic Editor: Xueliang Wu

Objective. The aim of this study is to evaluate the safety and tumor marker level changes of acupuncture plus chemotherapy (FOLFOX4) for advanced gastric cancer. *Methods*. One hundred and twenty patients with advanced gastric cancer who were treated at our hospital between May 2019 and April 2021 were recruited for prospective analysis, and all patients were allocated to the control and experimental groups in a 1 : 1 ratio using the random number table method, with 60 patients in each group. They received either chemotherapy using the FOLFOX4 regimen (control group) or the FOLFOX4 chemotherapy plus acupuncture (experimental group). Outcome measures included tumor marker levels, quality of life, and adverse events. *Results*. Before treatment, the two groups showed similar tumor markers levels and the MOS 36-item short-form health survey (SF-36) scores ($P > 0.05$). FOLFOX4 chemotherapy plus acupuncture was associated with significantly lower levels of carcinoembryonic antigen (CEA), carbohydrate antigen (CA) 19-9, and CA72-4 versus FOLFOX4 chemotherapy alone ($P < 0.05$). The patients who were given FOLFOX4 chemotherapy plus acupuncture showed significantly increased SF-36 scores versus monotherapy of the FOLFOX4 regimen ($P < 0.05$). The joint therapy resulted in a significantly lower incidence of adverse events versus the monotherapy ($P < 0.05$). *Conclusion*. Acupuncture plus chemotherapy using the FOLFOX4 regimen can effectively regulate the serum tumor marker levels of patients with advanced gastric cancer, with a high safety profile, which provides a viable treatment alternative.

1. Introduction

Gastric cancer is a malignant tumour disease with a very high incidence, ranking second in terms of incidence and mortality of malignant tumours in China and posing a serious threat to the health of the population [1–4]. Due to the atypical early symptoms of gastric cancer, the disease mostly progresses to advanced stages by the time of diagnosis [5, 6]. Chemotherapy is the main treatment modality for patients with inoperable advanced gastric cancer [7]. The FOLFOX4 regimen (oxaliplatin + 5-fluorouracil) is a common chemotherapy regimen used to treat patients with advanced gastric cancer and may also involve the use of calcium folinic acid injection (a sensitising agent for fluorouracil injection) [8]. Studies have shown that FOLFOX4 chemotherapy is safe and effective in reducing the pathological stage of gastric cancer, reducing postoperative recurrence and metastasis, and prolonging patient survival [9, 10]. Given the low selectivity in targeting tumour cells and the tendency to harm normal cells, chemotherapy may lead to adverse effects, reduced compliance, poor tolerance, and impaired therapeutic efficacy [11, 12].

Acupuncture provides disease management and health care by treating with acupuncture, whose stimulation of body acupoints regulates the function of breath power, blood, and internal organs [13, 14]. Acupuncture has been reported to reduce adverse events after chemotherapy in patients with gastric cancer, but few studies have combined it with the FOLFOX4 regimen. Therefore, the aim of this study was to evaluate the safety and changes in tumour marker levels of acupuncture combined with chemotherapy (FOLFOX4) in the treatment of advanced gastric cancer.

2. Materials and Methods

2.1. Baseline Data. One hundred and twenty patients with advanced gastric cancer who underwent consultation at our hospital between May 2019 and April 2021 were recruited for prospective analysis, and all patients were allocated to the control and experimental groups in a 1 : 1 ratio using the random number table method, with 60 patients in each group. All patients and their families were informed and asked to sign a consent form, and the study was approved for implementation by the ethics committee of Cangzhou Central Hospital, No. 297901-117.

2.2. Inclusion and Exclusion Criteria

2.2.1. Inclusion Criteria. The inclusion criteria were as follows:

(1) those who met the diagnostic criteria of gastric cancer in the Clinical Diagnostic and Treatment Guidelines Oncology Branch [15]

(2) those who met the soft tissue tumor staging criteria for gastric cancer stage IIIB and stage IV by the American Joint Committee on Cancer (AJCC)

(3) those with an expected survival of ≥3 months

2.2.2. Exclusion Criteria. The exclusion criteria were as follows:

(1) those with serious cardiovascular, cerebrovascular, hepatic, renal, and hematological diseases

(2) those with cardiopulmonary dysfunction

(3) those with brain metastases

2.3. Treatment Methods. The patients in the control group were given chemotherapy (FOLFOX4 regimen) [16]. Oxaliplatin injection (Qilu Pharmaceutical Co., Ltd.) 85 mg/m^2 was given intravenously for 2 h on the first day, calcium folinate injection (Jiangsu Hengrui Pharmaceutical Co., Ltd.) 200 mg/m^2 was given intravenously for 2 h on the first and second days, and 5-fluorouracil (Shanghai Xudong Haipu Pharmaceutical Co., Ltd.) 400 mg/m^2 was pushed intravenously, followed by 2 h continuous intravenous of 5-fluorouracil 600 mg/m^2. A course of treatment was given every 2 weeks for a total of 4 courses of treatment [17].

The patients in the experimental group were given acupuncture plus chemotherapy (FOLFOX4 regimen). A millineedle of 40 mm or more was used to perform acupuncture at the following acupoints, including Guanyuan, Qihai, Zusanli, Daheng, Neiguan, Xuehai, Diji, Shuidao, and Guilai, followed by the needling techniques of the lifting-thrusting method and the reinforcing-reducing method. A moxa stick about 2 cm long is placed above the needle handle, about 2-3 cm from the skin, lit from the lower end and the skin of the acupuncture point is covered with kraft paper, and the patient feels proper warmth at the point. The acupuncture takes about 20 minutes and the moxa strips are burnt out and the needles are withdrawn. During acupuncture, if the patient feels unbearable heat, a piece of cardboard can be placed over the acupuncture point to reduce the heat. Acupuncture was performed at Zusanli and Hangjian acupoints for patients with liver and stomach disharmony, at Zusanli, Piyu, Geyu, and Sanyinjiao for spleen and kidney yang deficiency. The needles remained at the points for 6 h. Acupuncture once every other day, 20 times as a course of treatment, a total of 28 courses of treatment.

2.4. Outcome Measures

(1) Tumor markers: At the end of the procedure, 2–5 ml of fasting venous blood was collected from the patient, clotted, and centrifuged at 2500 r/min. The serum was separated to determine carcinoembryonic antigen (CEA), carbohydrate antigen (CA) 19-9, and CA72-4 using electrochemiluminescence immunoassay (ECLIA) with original matching reagents.

(2) Quality of survival [18]: The MOS 36-item Short Form Health Survey (SF-36) was used to assess quality of life 3 months after the end of treatment in 8 domains: physical functioning, physical role, physical pain, general health, vitality, social functioning, role emotion, and mental health. The total score for each dimension is 100, with higher scores representing a better quality of life for the patient.

(3) Adverse events: Adverse events, including anaemia, nausea and vomiting, malaise, leucopenia, and peripheral neuropathy, occurred during treatment in both groups were recorded and the incidence of adverse events was calculated.

2.5. Statistical Analysis. SPSS 22.0 was used for data analyses, and GraphPad Prism 8 was used for image rendering. The measurement data were expressed as ($\overline{x} \pm s$) and processed using the *t*-test. The count data were expressed as the number of cases (rate) and analyzed using the chi-square test. Differences were considered statistically significant at $P < 0.05$.

3. Results

3.1. Baseline Data. The baseline characteristics of the control group (33 males, 27 females, aged 38–63 (50.45 ± 5.68) years, 42 cases of stage IIIB, and 18 cases of stage IV) were comparable with those of the experimental group (31 males, 29 females, aged 39–66 (50.18 ± 5.94) years, 37 cases of clinical-stage IIIB, and 23 cases of stage IV) ($P > 0.05$) (Table 1).

3.2. Tumor Markers Levels. Before treatment, the two groups showed similar tumor markers levels ($P > 0.05$). FOLFOX4 chemotherapy plus acupuncture was associated with significantly lower levels of CEA, CA19-9, and CA72-4 (13.21 ± 1.31 μg/ml, 158.14 ± 5.14 U/ml, 56.74 ± 5.27 U/ml)

Table 1: Comparison of baseline data ($\overline{x} \pm s$).

Groups	n	Gender		Age		Clinical stage	
		Male	Female	Range	Mean age	IIIB	IV
Control group	60	33	27	42–71	50.45 ± 5.68	42	18
Experimental group	60	31	29	40–72	50.18 ± 5.94	37	23
t value	—			0.251			
P value	—			0.802			

Table 2: Comparison of tumor markers levels ($\overline{x} \pm s$).

Groups	n	Before treatment			After treatment		
		CEA (μg/ml)	CA19-9 (U/ml)	CA72-4 (U/ml)	CEA (μg/ml)	CA19-9 (U/ml)	CA72-4 (U/ml)
Control group	60	24.23 ± 2.27	255.54 ± 8.17	78.25 ± 3.47	16.25 ± 2.12	228.52 ± 9.14	70.08 ± 4.13
Experimental group	60	24.51 ± 2.11	256.08 ± 7.94	77.94 ± 3.86	13.21 ± 1.31	158.14 ± 5.14	56.74 ± 5.27
t value	—	0.718	0.367	0.462	9.471	51.967	15.433
P value	—	0.474	0.714	0.645	<0.001	<0.001	<0.001

* indicates a statistically significant difference ($P < 0.05$) in the same group between before and after treatment.

versus FOLFOX4 chemotherapy alone (16.25 ± 2.12 μg/ml, 228.52 ± 9.14 U/ml, 70.08 ± 4.13 U/ml) ($P < 0.001$) (Table 2).

3.3. Quality of Life. The patients who were given FOLFOX4 chemotherapy plus acupuncture showed significantly increased SF-36 scores (75.23 ± 6.17) versus monotherapy of the chemotherapy (68.17 ± 6.88) ($P < 0.001$) (Figure 1).

3.4. Incidence of Adverse Events. The joint therapy resulted in a significantly lower incidence of adverse events (3.34%, including 1 (1.67%) case of nausea and vomiting and 1 (1.67%) case of fatigue) versus the monotherapy (41.67%, including 8 (13.34%) cases of anaemia, 11 (18.34%) cases of nausea and vomiting, 4 (6.67%) cases of fatigue, 1 (1.67%) case of leukopenia, and 1 (1.67%) case of peripheral neuropathy) ($P < 0.05$) (Table 3).

4. Discussion

Advanced gastric cancer refers to the invasion of tumour tissue into the stroma or stromal layer of the stomach or the occurrence of extrastromal metastasis. The main clinical manifestations are emaciation, epigastric pain, anaemia, loss of appetite, and corresponding clinical manifestations in distant sites. Currently, the FOLFOX4 regimen is a common chemotherapy regimen in clinical practice [19, 20]. Acupuncture features extensive indications and significant efficacy [21]. The results of this study showed a significant reduction in CEA, CA19-9 and CA72-4 levels after acupuncture combined with FOLFOX4 regimen chemotherapy, indicating the effectiveness of FOLFOX4 regimen chemotherapy in reducing tumour marker levels. It has been shown that CEA is highly sensitive to gastric cancer and its changes correlate with the sensitivity of gastric cancer to chemotherapy, showing great benefit in prognostic assessment and efficacy observation. CA19-9 is a highly specific gastrointestinal tumour-associated antigen whose expression correlates positively with the degree of tumour progression and has a sensitivity of approximately 40% for gastric cancer. CA72-4 is a tumour marker for gastrointestinal tract tumours and ovarian cancer and plays a role in detecting residual tumours and early gastric cancer recurrence. It has been confirmed in numerous studies that serum CEA, CA19-9, and CA72-4 are all common clinical serum tumor markers for gastric cancer, with considerable clinical significance in the diagnosis and treatment of gastric cancer. In traditional Chinese medicine, the process of disease development and regression is essentially the process of the struggle between the positive and evil breath power. Acupuncture plus chemotherapy has a wide range of indications and significant efficacy to better exploit its anticancer effects. Here, the patients given FOLFOX4 chemotherapy plus acupuncture showed significantly increased SF-36 scores and a lower incidence of adverse events versus monotherapy of the chemotherapy, indicating the benefits of quality of life after the intervention of acupuncture, as it stimulates the acupoints to unblock breath power and blood of the stomach, harmonize the Yin and Yang, and the dispel evil breath power, which resulted in enhanced quality of life and fewer adverse events.

The study of Xu demonstrated that acupuncture can reduce adverse events in gastric cancer patients after chemotherapy, for example, a large number of studies have shown that acupuncture at certain specific acupoints, such as the Neiguan point, not only has an effect on the release of wuqiang acid in the vomiting centre but also has a regulatory effect on the release of wuqiang acid in the local tissues of the gastrointestinal tract, providing a good antiemetic effect from effectively reducing damage to the gastric mucosa from chemotherapy drugs and restoring gastrointestinal motility [21]. It has also been shown that acupuncture can have a prestimulatory effect, i.e., some acupuncture can reduce the degree of damage when the body is injured only before the body is injured [22]. A related study by Zhou et al. also showed that acupuncture used early in chemotherapy was

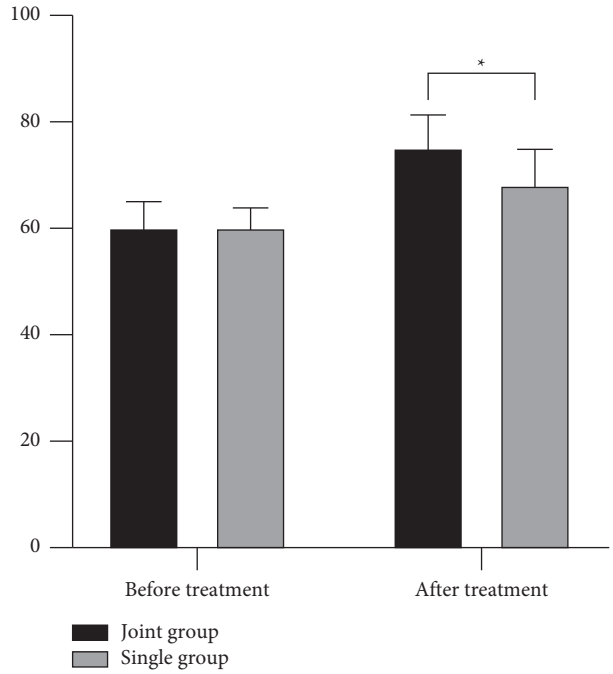

Figure 1: Comparison of SF-36 scores. * indicates a statistically significant difference ($P < 0.05$) between the two groups.

Table 3: Comparison of incidence of adverse events (%).

Groups	n	Anemia	Nausea and vomiting	Fatigue	Leukopenia	Peripheral neuropathy	Total incidence
Control group	60	8 (13.34)	11 (18.34)	4 (6.67)	1 (1.67)	1 (1.67)	25 (41.67)
Experimental group	60	0 (0.00)	1 (1.67)	1 (1.67)	0 (0.00)	0 (0.00)	2 (3.34)
χx^2	—				25.281		
P value	—				<0.001		

more effective in improving gastric motility than later in the course of chemotherapy, suggesting that if acupuncture is used early and at the right time in chemotherapy, it may prevent the onset of vomiting and nausea, or reduce its symptoms when it occurs [23].

However, there are obvious limitations to our study. First, our experimental sample was small, which may lead to some error in the results. Second, we need to improve the monitoring indicators in subsequent trials by adding indicators such as survival after treatment and the clinical remission rate of the efficacy evaluation criteria for solid tumours (RECIST) [24].

5. Conclusion

To sum up, acupuncture plus chemotherapy using the FOLFOX4 regimen can effectively regulate the serum tumor marker levels of patients with advanced gastric cancer, with a high safety profile, which provides a viable treatment alternative.

Data Availability

The datasets used during the present study are available from the corresponding author upon reasonable request.

Conflicts of Interest

The authors declare that they have no conflicts of interest.

Acknowledgments

This study was supported by Cangzhou Science and Technology Support Program Project, No. 213106044.

References

[1] Z. Song, Y. Wu, J. Yang, D. Yang, and X. Fang, "Progress in the treatment of advanced gastric cancer," *Tumor Biology*, vol. 39, no. 7, Article ID 101042831771462, 2017.

[2] A. Digklia and A. D. Wagner, "Advanced gastric cancer: current treatment landscape and future perspectives," *World Journal of Gastroenterology*, vol. 22, no. 8, pp. 2403–2414, 2016.

[3] V. Pasechnikov, S. Chukov, E. Fedorov, I. Kikuste, and M. Leja, "Gastric cancer: prevention, screening and early diagnosis," *World Journal of Gastroenterology*, vol. 20, no. 38, pp. 13842–13862, 2014.

[4] M. Venerito, A. Link, T. Rokkas, and P. Malfertheiner, "Gastric cancer—clinical and epidemiological aspects," *Helicobacter*, vol. 21, pp. 39–44, 2016.

[5] Q. Li, X. Xu, D. Su, T. Zhou, G. Wang, and Z. Li, "Long-term survival of an elderly patient with advanced gastric cancer after combination therapy: a case report and literature review," *BMC Cancer*, vol. 19, no. 1, p. 459, 2019.

[6] A. R. Siebenhüner, S. De Dosso, D. Helbling et al., "Advanced gastric cancer: current treatment landscape and a future outlook for sequential and personalized guide: swiss expert statement article," *Oncology Research and Treatment*, vol. 44, no. 9, pp. 485–494, 2021.

[7] H. Liu, J. Song, Z. Yang, and X. Zhang, "Effects of cytokine-induced killer cell treatment combined with FOLFOX4 on the recurrence and survival rates for gastric cancer following surgery," *Experimental and Therapeutic Medicine*, vol. 6, no. 4, pp. 953–956, 2013.

[8] S. Haghighi, H. Kasbkar, K. Esmaeilpour, and M. Yasaei, "Oxaliplatin, 5fluorouracil and leucovorin (FOLFOX4) as first line chemotherapy in elderly patients with advanced gastric cancer," *Asian Pacific Journal of Cancer Prevention*, vol. 17, no. 7, pp. 3277–3280, 2016.

[9] H. Xie, Q. Lu, H. Wang, X. Zhu, and Z. Guan, "Two post-operative chemotherapies for gastric cancer: FOLFOX4 vs. TPF," *Oncology Letters*, vol. 17, no. 1, pp. 933–936, 2019.

[10] M. Shi, J. Ji, J. Wu et al., "Cetuximab combined with FOLFOX4 as the first-line treatment for advanced gastric cancer: report of 25 cases from a single institution," *Hepato-Gastroenterology*, vol. 59, no. 116, pp. 1054–1058, 2012.

[11] H. Li, S. Qin, Y. Liu et al., "Camrelizumab combined with FOLFOX4 regimen as first-line therapy for advanced hepatocellular carcinomas: a sub-cohort of a multicenter phase ib/II study," *Drug Design, Development and Therapy*, vol. 15, pp. 1873–1882, 2021.

[12] A. Passardi, I. G. Rapposelli, E. Scarpi et al., "Neoadjuvant treatment (FOLFOX4 plus hypofractionated tomotherapy) for patients with locally advanced rectal cancer: a multicenter phase II trial," *Therapeutic Advances in Medical Oncology*, vol. 12, Article ID 175883592097713, 2020.

[13] K. Zhang, "Acupuncture for quality of life in gastric cancer patients: methodological issues," *Journal of Pain and Symptom Management*, vol. 63, no. 4, pp. e447–e448, 2022.

[14] Y. J. Zhang, Q. Min, Y. Huang et al., "Efficacy of acupuncture and moxibustion as a subsequent treatment after second-line chemotherapy in advanced gastric cancer," *Evidence-Based Complementary and Alternative Medicine*, vol. 2020, Article ID 8274021, 9 pages, 2020.

[15] T. Aoyama and T. Yoshikawa, "Adjuvant therapy for locally advanced gastric cancer," *Surgery Today*, vol. 47, no. 11, pp. 1295–1302, 2017.

[16] T. André, T. Iveson, R. Labianca et al., "The IDEA (international duration evaluation of adjuvant chemotherapy) collaboration: prospective combined analysis of phase III trials investigating duration of adjuvant therapy with the FOLFOX (FOLFOX4 or modified FOLFOX6) or XELOX (3 versus 6 months) regimen for patients with stage III colon cancer: trial design and current status," *Current Colorectal Cancer Reports*, vol. 9, no. 3, pp. 261–269, 2013.

[17] Z. Sun, R. J. Zhu, G. F. Yang, and Y. Li, "Neoadjuvant chemotherapy with FOLFOX4 regimen to treat advanced gastric cancer improves survival without increasing adverse events: a retrospective cohort study from a Chinese center," *Scientific World Journal*, vol. 2014, Article ID 418694, 10 pages, 2014.

[18] E. de Beurs, I. Carlier, and A. van Hemert, "Psychopathology and health-related quality of life as patient-reported treatment outcomes: evaluation of concordance between the brief symptom inventory (BSI) and the short form-36 (SF-36) in psychiatric outpatients," *Quality of Life Research*, vol. 31, no. 5, pp. 1461–1471, 2021.

[19] Y. Zhang, L. Jiang, J. Ouyang, X. Du, and L. Jiang, "Efficacy and safety of traditional Chinese medicine injections joint with FOLFOX4 regimen for gastric cancer: a protocol for systematic review and network meta-analysis," *Medicine (Baltimore)*, vol. 100, no. 41, Article ID e27525, 2021.

[20] Y. Chi, J. Yang, S. Yang, Y. Sun, B. Jia, and Y. Shi, "Phase I dose-finding study of sorafenib with FOLFOX4 as first-line treatment in patients with unresectable locally advanced or metastatic gastric cancer," *Chinese Journal of Cancer Research*, vol. 27, no. 3, pp. 239–246, 2015.

[21] X. Xu, "The effect of warm acupuncture on the recovery of gastrointestinal function after gastric cancer surgery," *China Medical Device Information*, vol. 22, p. 2, 2016.

[22] H. Choi, "Surface-modified acupuncture needles offering enhanced therapeutic properties," Ph D. dissertation, DGIST, Daegu, Republic of Korea, 2018.

[23] J. Zhou, L. Fang, W. Y. Wu et al., "The effect of acupuncture on chemotherapy-associated gastrointestinal symptoms in gastric cancer," *Current Oncology*, vol. 24, no. 1, pp. e1–e5, 2017.

[24] Y. J. Zhu, Xy Wu, W. Wang et al., "Acupuncture for quality of life in gastric cancer patients undergoing adjuvant chemotherapy," *Journal of Pain and Symptom Management*, vol. 63, no. 2, pp. 210–220, 2022.

Hindawi
Evidence-Based Complementary and Alternative Medicine
Volume 2022, Article ID 8266321, 5 pages
https://doi.org/10.1155/2022/8266321

Research Article

Impact of *Helicobacter pylori* Infection and Outcome of Anti-*Helicobacter pylori* Therapy in Patients with Reflux Laryngopharyngitis

Huili Shen,[1,2] Yijie Chen,[3] Xiaohui Li,[3] Jing Yan,[1] Junjie Zhao,[1] Demin Kong,[1] Yanxia Shi,[1] Zhihui Li,[1] Jihong Wang,[1] Na Shao,[1] and Zhenghui Wang[1]

[1]*Department of Otolaryngology-Head and Neck Surgery, The Second Affiliated Hospital of Xi'an Jiaotong University, Xi'an, China*
[2]*Department of Otolaryngology-Head and Neck Surgery, The Fourth People's Hospital of Shaanxi Province, Xi'an, China*
[3]*College of Medicine, Xi'an Jiaotong University, Xi'an, China*

Correspondence should be addressed to Zhenghui Wang; hezhuozhezhui7983@163.com

Received 14 April 2022; Accepted 8 June 2022; Published 5 July 2022

Academic Editor: Xueliang Wu

Objectives. This study was designed to explore the relationship between *Helicobacter pylori* (Hp) infection and reflux laryngopharyngitis (RLP) and to evaluate the outcome of anti-Hp therapy in improving RLP symptoms. *Methods*. A total of 410 patients with RLP were enrolled and tested for Hp infection. The association of Hp infection with reflux symptom index (RSI) and reflux finding score (RFS) was determined. Hp-positive patients received either a proton pump inhibitor (PPI) omeprazole alone (control group) or a combination regimen (experimental group) consisting of omeprazole, mosapride citrate, amoxicillin, and clarithromycin. Therapeutic outcomes were compared 4 weeks later. *Results*. Of the 410 participants, 290 were Hp-positive and 120 Hp-negative. Both RSI and RFS were significantly higher in Hp-positive patients than in Hp-negative patients. Hp infection status was positively correlated with RSI ($P < 0.05$) and RFS ($P < 0.05$). The overall response rate was higher in the experimental group than in the control group. Both the groups had a significant reduction in RSI and RFS after therapy, with a greater improvement in the experimental group ($P < 0.05$). *Conclusion*. Our findings establish a link between Hp infection and RLP. Anti-Hp therapy improves RSI and RFS in RLP patients. Therefore, Hp eradication drugs may be added to the PPI-based regimen in the treatment of RLP.

1. Introduction

Reflux pharyngitis (RLP), also known as laryngopharyngeal reflux disease, is characterised by inflammatory damage to the tissues of the upper aerodigestive tract caused by reflux of gastric contents [1]. Common symptoms include throat clearing, voice quality alteration, and globus pharyngeus. Although RLP has an adverse impact on the life quality of patients, its pathogenesis is still unclear. Moreover, there were no standard diagnostic and therapeutic methods available for RLP [2, 3]. For a long time in the past, reflux pharyngitis was often considered an extra-oesophageal manifestation of reflux gastro-oesophagitis, but now more and more scholars agree that these are two relatively independent diseases [4]. Reflux pharyngitis is characterised by acid reflux and heartburn in the stomach, with a higher incidence when lying down. Patients are associated with abnormal oesophageal peristalsis and prolonged exposure to gastric acid, with a daily repetition rate of up to 50 times and more [5]. Gastric manifestations such as acid reflux and heartburn are generally not present in reflux pharyngitis. Patients have only pharyngeal symptoms, which tend to occur in the upright position and are considered abnormal if they exceed four times per day [6].

Helicobacter pylori (Hp) is a pathogenic bacterium that inhabits the gastric mucosa of humans. Hp infection has

been suggested as an important etiological factor for gastroesophageal reflux diseases [7]. Clinically, the main drugs taken to treat HP are antibiotics (e.g., clarithromycin and amoxicillin), drugs to inhibit gastric acid secretion (e.g., omeprazole), and drugs to protect the gastric mucosa (e.g., bismuth potassium citrate), and triple therapy or quadruple therapy to kill *H. pylori* [6, 8, 9]. *H. pylori* is contagious and can be transmitted through food and utensils. Patients must develop good hygiene habits in daily life, wash their hands regularly before and after meals, and eat clean food, and disinfect utensils regularly can effectively kill *H. pylori* in their lives [10].

However, the relationship between Hp infection and RLP is still unclear. In the present study, we retrospectively analysed clinical data of RLP patients admitted in our hospital and assessed the association of Hp infection status and RLP. We also explored the outcomes of Hp therapy in patients with RLP.

2. Materials and Methods

2.1. General Information. A total of 410 patients diagnosed with RLP between August 2015 and August 2019 were recruited for retrospective analysis. Patients with Hp-positive RLP were sequentially assigned equally to the control and experimental groups according to the different treatment modalities. The study was approved by the Ethics Committee of Xi'an Jiaotong University (Xi'an, China) (approval no.#19879). Written informed consent for the study was obtained from each patient.

2.2. Inclusion and Exclusion Criteria. Inclusion criteria: (1) duration of disease >1 month; (2) patient age ≥18 years; (3) Hp-positive RLP patients.

Exclusion criteria: (1) presence of laryngopharyngeal trauma or systemic disease; (2) treatment with Hp within 3 months prior to RLP diagnosis; (3) receipt of a proton pump inhibitor (PPI) within 1 month; (4) laryngopharyngeal tumour.

2.3. Hp Detection. Hp infection was examined using the ^{14}C urea breath test [11]. Briefly, all the participants took an urea ^{14}C capsule on an empty stomach 15 min before tests. The ^{14}C content in the gas blew out from the patients was recorded by a YH04E Hp detector. The ^{14}C results (expressed in dmp) were defined as: ≤99 dmp, negative; 99< dpm ≤149, uncertain; dpm >149, positive; 149< dpm ≤499, "+"; 499< dpm ≤1499, "++"; 1499< dpm ≤2499, "+++"; dpm >249, "++++."

2.4. Treatment Protocol. The patients in the control group received a daily oral dose of 40 mg of omeprazole (Changzhou Siyao Pharmaceutical co., Ltd., Changzhou, China). For those with severe reflux symptoms, domperidone was added to the treatment regimen.

The patients in the experimental group were treated with a combination of omeprazole (40 mg/day), mosapride citrate (15 mg/day), amoxicillin (1 g BID), and clarithromycin (500 mg BID). The treatment was continued for 4 weeks in both the groups [12]. All the patients were advised to follow recommended dietary guidelines: i.e., intake of a restricted amount of food and no consumption of alcohol, coffee, tea, soda beverage, chocolate, or peppermint. Eating food should be avoided 3 h before sleep.

2.5. Reflux Measurements. Reflux symptom index (RSI) [13, 14] is a 9-item patient questionnaire scoring system used to assess severity of reflux symptoms. The parameters tested included hoarseness or dysphonia, chronic cough, difficulty swallowing, excess laryngeal secretions, heartburn or regurgitation, difficulty breathing, constant throat clearing, throat pain, and foreign-body sensation in the throat. Each item of RSI was scored from 0 (no symptom) to 5 (the most serious symptom). The total score of RSI was 45. Reflux finding score (RFS) [14, 15] is a 8-item clinical severity scale based on laryngoscopic findings. The parameters included subglottic edema, ventricular obliteration, mucosal hyperemia, vocal cord edema, laryngeal edema, posterior commissure hypertrophy, and thick endolaryngeal mucus. RFS scale ranges from 0 (no abnormal findings) to a maximum 26 (worst findings).

2.6. Therapeutic Outcome Assessment. Therapeutic outcome was graded as complete response (resolution of all symptoms in the throat and RSI ≤13), partial response (partial remission of symptoms, relief of mucosal hyperemia, edema, and hypertrophy, and RSI reduction but more than 13), and no response (no improvement in clinical symptoms, laryngoscopic findings, or RSI). The overall response rate (OR) was calculated using the formula of OR = (number of CR + number of PR)/145 × 100%, in which CR and PR means complete response and partial response, respectively.

2.7. Statistical Analysis. Statistical analysis was performed using SPSS version 17.0. Differences in proportions were calculated using the chi-square test. The results expressed as mean ± standard deviation were compared using Student's *t*-test. Correlation analysis was determined using Pearson's correlation test. A level of $P < 0.05$ was significant.

3. Results

3.1. General Information. The control group had 80 males and 65 females, with a mean age of 55.6 ± 10.0 years (19–78 years). The experimental group also had 80 men and 65 women, with a mean age of 56.2 ± 11.9 years (22–80 years). There was no significant difference in clinicodemographic data of the 2 groups ($P > 0.05$).

3.2. Hp Detection Results. Of the 410 patients enrolled, 290 were Hp-positive and 120 Hp-negative (Table 1). No significant difference was noted between the Hp-positive and Hp-negative patients regarding gender ($P = 0.734$) and age ($P = 0.366$).

Table 1: *Helicobacter pylori* (Hp) detection results in 410 patients with reflux laryngopharyngitis.

Parameter	Hp infection status		P value
	Positive	Negative	
Gender			0.734
Male	160	64	
Female	130	56	
Age, years			0.366
≤35	28	16	
36–55	50	22	
56–75	124	55	
≥76	88	27	
Total	290	120	

3.3. RSI and RFS Measurement Results. Table 2 shows comparisons of RSI and RFS between Hp-positive and Hp-negative patients. Of note, compared to Hp-negative patients, Hp-positive patients had a significantly higher RSI (32.66 ± 3.21 *vs*. 17.52 ± 2.53; $P < 0.05$) and RFS (21.68 ± 1.23 *vs*. 16.25 ± 1.04; $P < 0.05$).

3.4. Association of Hp Status with RSI and RFS. The Hp infection rate was positively associated with RSI ($r = 0.770$, $P < 0.05$) and RFS ($r = 0.615$, $P < 0.05$) in patients with RLP (Table 3), suggesting that Hp infection may be a risk factor of RLP.

3.5. Treatment Outcome Comparison. Hp treatment resulted in a significantly higher OR rate compared to the control group (90.34% vs. 74.48%, $P < 0.05$; Table 4). There was no significant difference in baseline RSI and RFS between the two groups before treatment ($P > 0.05$; Table 5). After treatment, RSI and RFS improved significantly in both groups. In addition, RSI and RFS were significantly lower in the Hp-treated group than in the control group ($P < 0.05$), indicating that patients derived better benefit from Hp treatment.

4. Discussion

RLP is a common laryngopharyngeal disorder that presents as an inflammatory injury to the upper aerodigestive tract. The incidence of RLP has increased in recent years, and this may be related to changes in dietary habits. It is estimated that over 50% of patients with voice abnormalities have reflux symptoms [16]. Multiple factors including oesophageal sphincter function, retention time of reflux contents, and pharyngeal mucosa susceptibility have an impact on the progression of RLP. Direct injury of pharyngeal mucosa by gastric reflux contents is regarded as an important cause of RLP [17]. RLP also involves vasovagal reflex-related injuries [18]. However, little is known about the exact pathogenesis of its RLP.

Hp is a common pathogenic bacterium that lives in gastric mucosa. Accumulating evidence has linked Hp infection to gastric reflux diseases [19, 20]. Hp infection can cause excessive secretion of gastric acid, which can lead to abdominal distention, nausea, chronic gastritis, and gastric ulcers. In addition, Hp infection can cause oesophageal sphincter dysfunction and overproduction of acidic contents, which may exacerbate damage to the pharyngeal mucosa from acid reflux [21]. It has been reported that over 3 months of acid stimulation reduces the expression of E-cadherin and impairs the junction among laryngopharyngea mucosal cells, leading to submucosal muscle hypertrophy [22]. Another report suggests that Hp infection may contribute to the pathogenesis of RLP by altering the endocrine secretion of the gastric glands [23–25]. As a result of insufficient gastric acid, large amounts of undigested food are retained in the stomach, releasing spoiled gas and thus aggravating pharyngeal reflux [26–28].

Table 2: RSI and RFS in patients with or without *Helicobacter pylori* (Hp) infection.

Group	n	RSI	RFS
Hp-positive	290	32.66 ± 3.21	21.68 ± 1.23
Hp-negative	120	17.52 ± 2.53	16.25 ± 1.04
P value		<0.001	<0.001

RSI = reflux symptom index; RFS = reflux finding score.

Table 3: Association of *Helicobacter pylori* infection with RSI and RFS.

Parameter	n	r	P value
RSI	290	0.770	<0.001
RFS	120	0.615	<0.001

RSI = reflux symptom index; RFS = reflux finding score.

It has also been confirmed that *H. pylori* prevents gastric acid production, which in turn can prevent reflux; that is, *H. pylori* infection is negatively associated with the development of a wide range of gastroesophageal reflux disease, contrary to the results of our study here [29, 30]. This occurs when the inflammatory infection of the stomach caused by *H. pylori* affects the entire gastric body, especially when it involves areas of gastric acid secretion [31]. The secretion of gastric acid is reduced because of the inhibitory effect of inflammatory cells on the mural cells [32]. Thus, in cases where *H. pylori* infection inhibits gastric acid secretion, *H. pylori* infection inhibits GERD episodes [33]. In some cases, however, the areas of the gastric body involved in gastric acid secretion are largely unaffected by *H. pylori* infection, so that gastric acid secretion is not reduced, but instead also leads to an increase in serum gastrin levels [34]. In this case, the risk of GERD associated with *H. pylori* infection is actually thought to be increased, which is consistent with the findings derived from our study.

In the present study, we show that Hp-positive RLP patients have a significantly higher RSI and RFS than Hp-negative RLP patients. There are positive correlations between Hp infection and RSI and RFS. The prevalence of Hp infection secondary to modification of dietary habits is emerging as a crucial factor of RLP progression. Therefore, we speculated that Hp eradication therapy may provide benefits in improving RLP symptoms. In our Hp-positive RLP patients, we compared the outcome of PPI and Hp

Table 4: Therapeutic outcome in the Hp therapy and control groups.

Group	*n*	CR (*n*, %)	PR (*n*, %)	NR (*n*, %)	OR (*n*, %)	*P* value[a]
Control	**145**	35 (24.14)	73 (50.34)	37 (25.52)	108 (74.48)	<0.001
Hp therapy	**145**	69 (47.59)	62 (42.76)	14 (9.66)	131 (90.34)	

CR = complete responses; Hp = *Helicobacter pylori*; NR = no response; OR = overall response; PR = partial response. [a]*P* value was determined for the difference in OR between the control and experimental groups.

Table 5: RSI and RFS before and after treatment.

Group	*n*	RSI		*P*	RFS		*P*
Control	**145**	32.67 ± 0.41	18.07 ± 1.05	≤0.001	21.66 ± 1.22	15.44 ± 0.54	<0.001
Hp therapy	**145**	32.65 ± 0.70	11.50 ± 1.73	≤0.001	21.72 ± 0.82	12.97 ± 1.50	<0.001
P		0.722	≤0.001		0.279	<0.001	

Hp = *Helicobacter pylori*.

therapies. It was found that anti-Hp therapy yields a significantly higher OR than PPI treatment (90.34% vs. 74.48%). Moreover, both RSI and RFS are improved to a greater extent in the experimental group than in the control group. Our results suggest the benefits of anti-Hp therapy in RLP patients.

However, the limitations of the trial are clear, not least of which, Hp infection has not been assessed quantitatively, and we need a standard method of assessing treatment outcomes. We did not know the facts about the oesophageal status of these patients, so it was not clear if they had GERD, which was associated with RLP. Secondly, because this study was a retrospective analysis, the eradication rate was a missing number for us. Therefore, in a follow-up trial the investigators will be looking more closely at the response to eradication in HP-positive patients divided into eradicated and noneradicated patients. Finally, we consider that although ^{14}C-UBT is proven to be safe, appropriate safety precautions must be taken for the storage, handling, and disposal of the radioactive test components. Our next step may be to choose the ^{13}C isotope, as it is nonradioactive.

In summary, we indicate that Hp infection has a positive impact on RLP severity and progression. Compared to PPI treatment alone, Hp eradication therapy yields additional benefits in improving RSI and RFS in patients with RLP. These results warrant further studies in larger cohorts of patients with RLP.

Data Availability

All data generated or analysed during this study are included in this published article.

Conflicts of Interest

The authors declare that there are no conflicts of interest related to this study.

Acknowledgments

The work was funded by Shaanxi Province Government, grant/award number: 2022SF-387.

References

[1] A. Aldhahrani, J. Powell, S. Ladak et al., "The potential role of bile acids in acquired laryngotracheal stenosis," *Laryngoscope*, vol. 128, no. 9, pp. 2029–2033, 2018.

[2] J. R. Li, S. Xiao, X. Li, Q. Lyu, Y. Yan, and L. Zhang, "Explanation of the experts consensus on diagnosis and treatment of laryngopharyngeal reflux disease," *Chinese Journal of Otorhinolaryngology Head and Neck Surgery*, vol. 51, no. 5, pp. 327–332, 2016.

[3] R. Yadlapati, J. E. Pandolfino, A. K. Lidder et al., "Oropharyngeal pH testing does not predict response to proton pump inhibitor therapy in patients with laryngeal symptoms," *American Journal of Gastroenterology*, vol. 111, no. 11, pp. 1517–1524, 2016.

[4] M. Durazzo, G. Lupi, F. Cicerchia et al., "Extra-esophageal presentation of gastroesophageal reflux disease: 2020 update," *Journal of Clinical Medicine*, vol. 9, no. 8, p. 2559, 2020.

[5] D. M. Clarrett and C. Hachem, "Gastroesophageal reflux disease (GERD)," *Missouri Medicine*, vol. 115, no. 3, p. 214, 2018.

[6] S. Tauber, M. Gross, and W. J. Issing, "Association of laryngopharyngeal symptoms with gastroesophageal reflux disease," *Laryngoscope*, vol. 112, no. 5, pp. 879–886, 2002.

[7] J. H. Rubenstein, J. M. Inadomi, J. Scheiman et al., "Association between *Helicobacter pylori* and barrett's esophagus, erosive esophagitis, and gastroesophageal reflux symptoms," *Clinical Gastroenterology and Hepatology*, vol. 12, no. 2, pp. 239–245, 2014.

[8] S. Y. Kim, D. J. Choi, and J. W. Chung, "Antibiotic treatment for *Helicobacter pylori*: is the end coming?" *World Journal of Gastrointestinal Pharmacology and Therapeutics*, vol. 6, no. 4, p. 183, 2015.

[9] J. C. Yang, C. W. Lu, and C. J. Lin, "Treatment of *Helicobacter pylori* infection: current status and future concepts," *World Journal of Gastroenterology*, vol. 20, no. 18, p. 5283, 2014.

[10] S Kayali, M. Manfredi, F. Gaiani et al., "*Helicobacter pylori*, transmission routes and recurrence of infection: state of the art," *Acta BioMedica: Atenei Parmensis*.vol. 89, no. 8-S, pp. 72–76, 2018.

[11] F. Imanzadeh, A. Imanzadeh, A. A. Sayyari, M. Yeganeh, H. Javaherizadeh, and B. Hatamian, "*Helicobacter pylori* infection," *The Professional Medical Journal*, vol. 17, no. 04, pp. 543–545, 201017.

[12] B. Tepes, A. O'Connor, J. P. Gisbert, and C. O'Morain, "Treatment of *Helicobacter pylori* infection 2012," *Helicobacter*, vol. 17, pp. 36–42, 2012.

[13] P. C. Belafsky, G. N. Postma, and J. A. Koufman, "Validity and reliability of the reflux symptom index (RSI) flux symptom index (RSI)," *Journal of Voice*, vol. 16, no. 2, pp. 274–277, 2002.

[14] R. Hutnik, A. Zlatopolsky, S. Mehraban-Far et al., "Laryngopharyngeal reflux: comparing improvements in reflux symptom index with reflux finding score," *American Journal of Otolaryngology*, vol. 41, no. 6, Article ID 102730, 2020.

[15] P. C. Belafsky, G. N. Postma, and J. A. Koufman, "The validity and reliability of the reflux finding score (RFS)," *Laryngoscope*, vol. 111, no. 8, pp. 1313–1317, 2001.

[16] J. R. Li, "Standardized diagnosis and treatment of throat reflux disease," *Chinese Journal of Otorhinolaryngology Head and Neck Surgery*, vol. 50, no. 9, pp. 435–437, 2015.

[17] E. Eren, S. Arslanoğlu, A. Aktaş et al., "Factors confusing the diagnosis of laryngopharyngeal reflux: the role of allergic rhinitis and inter-rater variability of laryngeal findings," *European Archives of Oto-Rhino-Laryngology*, vol. 271, no. 4, pp. 743–747, 2014.

[18] T. A. Mesallam, K. H. Malki, M. Farahat, M. Bukhari, and S. Alharethy, "Voice problems among laryngopharyngeal reflux patients diagnosed with oropharyngeal pH monitoring," *Folia Phoniatrica et Logopaedica*, vol. 65, no. 6, pp. 280–287, 2013.

[19] F. Paolo, M. Brezzi, S. Barbieri et al., "Blood loss, predictors of bleeding, transfusion practice and strategies of blood cell salvaging during liver transplantation," *World Journal of Hepatology*, vol. 5, no. 1, p. 1, 2013.

[20] L. Cristina, P. Alberto, N. Giordano et al., "H pylori infection and systemic antibodies to CagA and heat shock protein 60 in patients with coronary heart disease," *World Journal of Gastroenterology*, vol. 12, no. 48, pp. 7815–7820, 2006.

[21] J. H. Rubenstein, H. Morgenstern, D. McConell et al., "Associations of diabetes mellitus, insulin, leptin, and ghrelin with gastroesophageal reflux and Barrett's esophagus," *Gastroenterology*, vol. 145, no. 6, pp. 1237–1244, 2013.

[22] H. B. El-Serag, A. Sonnenberg, M. M. Jamal et al., "Corpus gastritis is protective against reflux oesophagitis," *Gut*, vol. 45, no. 2, pp. 181–185, 1999.

[23] J. Luther, M. Zhang, M. Liu et al., "*Helicobacter pylori* DNA decreases pro-inflammatory cytokine production by dendritic cells and attenuates dextran sodium sulphate-induced colitis," *Gut*, vol. 60, no. 11, pp. 1479–1486, 2011.

[24] O. Emre, G. . Kubat, and Y. İrfan, "Immunoserologic pepsin detection in the saliva as a non-invasive rapid diagnostic test for laryngopharyngeal reflux," *Balkan Medical Journal*, vol. 32, no. 1, pp. 46–50, 2015.

[25] A. R. Assun, J. Priston, R. Heidrich Thoen, T. Medeiros, and A. Regina Assunção, "Laryngopharyngeal reflux: diagnosis, treatment, and latest Research," *International Archives of Otorhinolaryngology*, vol. 18, no. 2, pp. 184–191, 2014.

[26] S. Y. Han and G. H. Kim, "Clinical manifestations of laryngopharyngeal reflux," *Journal of neurogastroenterology and motility*, vol. 22, no. 3, pp. 351-352, 2016.

[27] V. Becker, R. Drabner, S. Graf et al., "New aspects in the pathomechanism and diagnosis of the laryngopharyngeal reflux-clinical impact of laryngeal proton pumps and pharyngeal pH metry in extraesophageal gastroesophageal reflux disease," *World journal of gastroenterology*, vol. 21, no. 3, pp. 982–987, 2015.

[28] J. R. Lechien, V. Delvaux, K. Huet et al., "Phonetic approaches of laryngopharyngeal reflux disease: a prospective study," *Journal of Voice*, vol. 31, no. 1, 2017.

[29] A. M. Saad, A. Choudhary, and M. L. Bechtold, "Effect of *Helicobacter pylori* treatment on gastroesophageal reflux disease (GERD): meta-analysis of randomized controlled trials," *Scandinavian Journal of Gastroenterology*, vol. 47, no. 2, pp. 129–135, 2012.

[30] S. Take, M. Mizuno, K. Ishiki et al., "*Helicobacter pylori* eradication may induce de novo, but transient and mild, reflux esophagitis: prospective endoscopic evaluation," *Journal of Gastroenterology and Hepatology*, vol. 24, no. 1, pp. 107–113, 2009.

[31] F. J. Xie, Y. P. Zhang, Q. Q. Zheng et al., "*Helicobacter pylori* infection and esophageal cancer risk: an updated meta-analysis," *World Journal of Gastroenterology*, vol. 19, no. 36, p. 6098, 2013 Sep 28.

[32] T. Xie, X. Cui, H. Zheng, D. Chen, L. He, and B. Jiang, "Meta-analysis: eradication of: *Helicobacter pylori*: infection is associated with the development of endoscopic gastroesophageal reflux disease," *European Journal of Gastroenterology and Hepatology*, vol. 25, no. 10, pp. 1195–205, 2013 Oct 1.

[33] M Yaghoobi, F Farrokhyar, Y. Yuan, and R. H. Hunt, "Is there an increased risk of GERD afterhelicobacter pyloriEradication?: a meta-analysis," *American Journal of Gastroenterology*, vol. 105, no. 5, pp. 1007–1013, 2010.

[34] K. Iijima, T. Koike, and T. Shimosegawa, "Reflux esophagitis triggered after *Helicobacter pylori* eradication: a noteworthy demerit of eradication therapy among the Japanese?" *Frontiers in Microbiology*, vol. 6, p. 566, 2015.

Hindawi
Evidence-Based Complementary and Alternative Medicine
Volume 2022, Article ID 8769889, 6 pages
https://doi.org/10.1155/2022/8769889

Research Article

Effectiveness of Quantitative Shear Wave Elastography for the Prediction of Axillary Lymph Node Metastasis

Yingying Cheng,[1] Guofu Li,[2] Hui Jing,[1] Shasha Yuan,[1] Lei Zhang,[1] and Wen Cheng[1]

[1]*Department of Ultrasound, Harbin Medical University Cancer Hospital, Harbin, China*
[2]*Department of Neurosurgery, Harbin Medical University Cancer Hospital, Harbin, China*

Correspondence should be addressed to Guofu Li; liguofu1012@hrbmu.edu.cn and Wen Cheng; hrbchengwen@163.com

Received 28 April 2022; Revised 22 May 2022; Accepted 28 May 2022; Published 28 June 2022

Academic Editor: Xueliang Wu

Objective. Invasive breast cancer can be metastasized through axillary lymph nodes (LNs). This study was to evaluate the effectiveness of quantitative shear wave elastography (SWE) to predict axillary LN metastasis, which also provides prognostic implication of SWE as a histopathologic element of invasive breast cancer. *Methods*. 72 prospectively enrolled patients received B-mode ultrasound (BUS) and SWE, and the elasticity index (EI) of SWE at the stiffest part of lymph nodes (LNs) was measured. EI of SWE was closely associated with pathologic results and the histopathologic elements. The receiver operating characteristics (ROC) curve was drawn to evaluate the optimal cut-off value for the assessment of disease severity. *Results*. A significantly longer short-axis diameter and a larger maximal cortex were observed in malignant LNs than that in healthy LNs. The absence of the hilum was associated with metastatic LNs. The EI of SWE varied markedly between the benign and malignant LNs. The combination of $E_{\max \text{ and}}$ BUS showed higher area under the curve (AUC) than BUS alone to predict metastatic LNs (0.7762 vs. 0.7230). EI of SWE in malignant lymph nodes those with extranodal extension are higher than those without extranodal extension. *Conclusions*. Quantitative SWE provides a viable alternative for the assessment of axillary LN and shows great potential to predict pathological prognostic elements of metastatic axillary LNs in invasive breast cancer. Joint use of SWE and BUS allows examination of the predictive outcome of BUS for axillary lymph node metastasis in invasive breast cancer.

1. Introduction

The correlation between axillary lymph node metastasis and prognostic of invasive breast cancer remains elusive. Lymph node (LNs) metastasis affects prognosis and treatment decisions [1, 2], so assessment of lymph node metastasis in breast cancer is of great importance. Clinical results revealed that axillary lymph node metastasis showed low sensitivity of 45.4% to 68% [3–5]. Axillary ultrasonography is an important tool for lymph node metastases inspection. However, the sensitivity of axillary ultrasonography only ranges from 35% to 82%, with specificity being 73% to 97.9% [6–9]. The average sensitivity of ultrasound-guided core needle biopsy (CNB) is 89.8% for suspicious axillary lymph nodes, 60.3% for large metastases, and 26.7% for micrometastases [10]. It is obvious that the current detection of lymph node metastasis may still result in missed diagnosis. Compared with axillary lymph node dissection (ALND), sentinel lymph node biopsy (SLNB) features higher precision and less invasiveness as a treatment. However, SLNB may give rise to complications such as lymphedema and seroma formation [11]. Therefore, there exists a need to explore a noninvasive imagological examination to predict metastatic axillary lymph nodes of invasive breast cancer.

The stiffness of LNs can be objectively assessed by ultrasound elastography given the different stiffness between benign and malignant LNs [12, 13]. Nonetheless, the results of strain elastography are impacted by the proficiency of the radiologists and the variations of measured organizational elasticity [14–17]. With the advancement in medical technology, shear wave elastography (SWE) was developed to overcome the relevant limitations by providing quantitative

statistics about tissue elasticity. SWE is a quantitative elastography technique that generates sheer wave using professional sensors and ultrafast ultrasonic tracking technology to obtain the velocity of induced shear wave and the real-time output displayed on tissue stiffness based on elastic diagram [18–21]. Recent studies reported the application of SWE for inspection of many organs such as the breast, thyroid, prostate, cervix, and liver [19,22–24]. SWE is scarcely used to predict axillary lymph node metastasis in invasive breast cancer. This study was undertaken to assess the effectiveness of quantitative SWE to predict axillary LNs metastasis in invasive breast cancer and to predict the correlation of elasticity index (EI) of SWE with histopathologic elements of axillary lymph node metastasis.

2. Materials and Methods

This retrospective study was approved by the ethics committee of the Cancer Hospital of Harbin Medical University, Harbin, China. Undersigned informed consent was obtained from all patients.

2.1. Patients. Women with ultrasound-detected abnormalities and those with symptoms were included in the study [25]. Axillary lymph nodes were determined as abnormal (round, absence of fat hilus, calcification, cystic changes, cortical heterogeneity, and confusion of vascular pattern) [26], whereas they were deemed benign without the abovementioned. From January 2014 to February 2015, 72 patients (115 lymph nodes) with invasive breast cancer underwent routine B-mode ultrasonography (BUS) and SWE examination before operation.

The enrolled patient underwent conventional BUS and SWE of the enlarged or suspicious axillary lymph nodes, and the imaging was performed with the patients in the supine or slightly (30°) left lateral decubitus position with the right arm elevated above the head. BUS and SWE were performed using the ultrasound imaging equipment produced by AIKE in Provence, France, with a 15-4 MHz linear array transducer SWE and gray-scale ultrasound images were obtained, using the default elasticity settings for penetration, persistence, smoothing, and kilopascal (kPa) display scale (0–180 kPa). On SWE, a square frame was used to include axillary lymph nodes and surrounding tissue cells. LNs with a depth over 3 cm were excluded given the signal loss in SWE at such depth. Red and blue areas on SWE correspond to stiff and soft regions, respectively. Three or more SWE/US cineloop fragments were obtained by using different parts of each node. The duration of the obtained fragments was displayed for 10 seconds, and the sensor remained still during capture. For each cineloop, the first few seconds were omitted as the elastogram during which is not stable, and single still images, with the least artifacts, such as vertical linear color bands passing through different tissues or other high hardness color parts in the surrounding fascia, were selected. For each selected still image, the hardest part of lymph node cortex and portal was selected by visual inspection, on which a circular electronic region of interest or Q-box was placed [27]. The software determines the relevant index for each Q-box, in which the maximum (E_{max}) and average (emean) and minimum (E_{min}) elastic values (kPa) were analyzed (Figure 1). The elastic index (EI) of surrounding muscles was calculated to clarify the Emean comparison value (Emean-m) of LNs and surrounding muscles. By moving a delineated region of interest (ROI) over the color map, the values of elasticity were obtained. ROI were placed of stiffest areas on color maps to obtain max ROI, mean ROI, min ROI, and mean-m ROI for analysis [28]. The selection of the highest value to measure the entire lymph node determines the absence of complete infiltration of the lymph node by tumor cells or spatial heterogeneity due to tumor necrosis.

2.2. Histopathologic Diagnosis. Of 61 suspicious axillary lymph nodes, 43 were treated with surgery and 18 with neoadjuvant chemotherapy after CNB. Of the remaining 54 LNs, 38 were treated with surgery or SLNB due to discordant ultrasound results or clinician request, and 12 LNs had ultrasound follow-up for 6 to 9 months. To facilitate accurate comparison between imaging results and histopathological results, the tissues were fixed by 10% formalin, paraffin embedded and sectioned, followed by eosin and hematoxylin staining. The histopathological diagnosis of LNs was reviewed, which was closely related to SWE results. The histopathological manifestations of metastatic LN were determined by the ratio of surgical specimens and the number of metastatic LN divided by the number of anatomical LN (metastatic ln/anatomical LN).

2.3. Statistical Analysis. Data analyses were performed based on the histopathologic results from LN dissections. SWE elasticity indices (E_{max}, E_{mean}, E_{min}, and $E_{mean\text{-}m}$) were closely associated with the pathological and histopathological results of metastatic lymph nodes, which was obtained with Student's *t*-test age's differences and short-axis diameter between benign and metastatic LNs. Wilcoxon rank sum test was used to determine the long/short-axis ratio, maximal cortex, E_{max}, Emean and Emin between benign and metastatic LNs. The *t*-test was used to determine the differences in Emean-m between benign and metastatic LNs. Chi-square experiment was applied to clarify the different selection methods for the absence and presence of hilum between benign and metastatic LNs. Spearman correlation coefficient and Student's *t*-test were used to analyze the correlation between EI of SWE and histopathological results of metastatic LNs [29]. The ability of EI of SWE and BUS category values to differentiate between benign and malignant LNs was evaluated using the ROC curve. After obtaining the best cut-off data, x2 test was used to measure the sensitivity, specificity, accuracy, positive predictive value (PPV), and negative predictive value (NPV). The generalized estimation equation was adopted to effectively analyze the optimal cut-off data based on the logistic regression model, and assessments were performed on the basis of the comparative analysis of the area under the curve (AUC) value

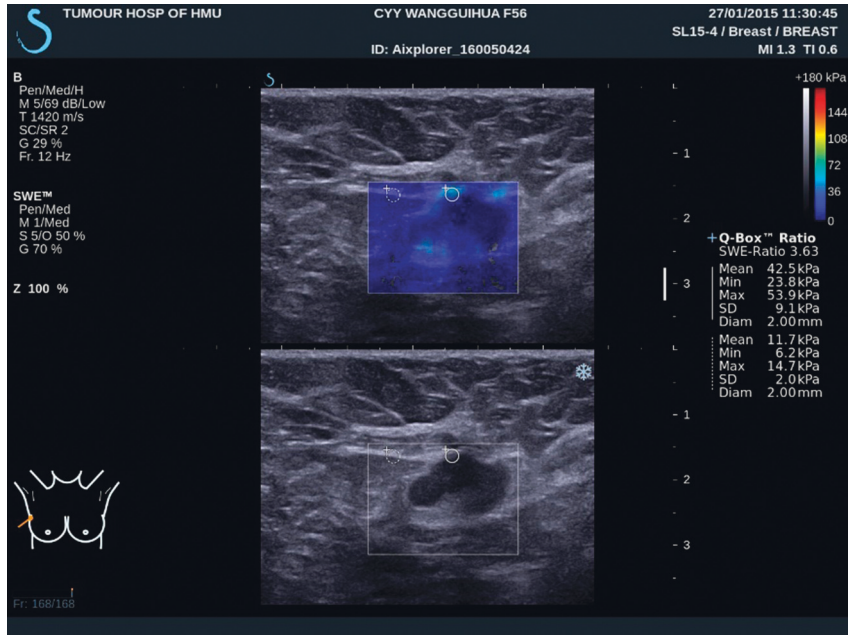

Figure 1: Shear wave elastography (SWE) and B-mode ultrasonography (BUS) images of a metastatic axillary lymph node from an invasive breast cancer in a 56-year-old women. Findings consistent with malignancy on BUS included loss of hilar fat and cortical heterogeneous echogenicity (lower image). SWE was performed for the lymph node and a Q-box is placed over the stiffest region, as assessed by visual inspection. A 2-mm-size circular region of interest was selected at the stiffest portion and elasticity scores of 42.5 kPa (E_{max}), 53.9 kPa (E_{mean}), 23.8 kPa (E_{min}), and 3.63 ($E_{mean\text{-}m}$)were obtained. $E_{max,}$ maximal elasticity score of the lesion; $E_{mean,}$ mean elasticity score of the lesion; $E_{min,}$ minimal elasticity score of the lesion; $E_{mean\text{-}m,}$ ratio of E_{mean} mean of the lesions divided by E_{mean} of surrounding muscles.

and 95% confidence interval (CI) diagnostic performance of ultrasonic classification. The statistical analysis was implemented in SAS version 9.2 (Cary SAS Institute, North Carolina, USA). $P < 0.05$ was set as the cut-off for statistical significance.

3. Results

3.1. Correlation of SWE and Pathologic Results of LNs. 115 LNs in 72 patients were examined by BUS and SWE from January 2014 to February 2015.115 LNs were dissected by ultrasound-guided labeling. 70 cases (60.9%) were metastatic lymph nodes, and 45 cases (39.1%) were benign lymph nodes. Malignant LNs were associated with a longer short-axis diameter and a larger maximal cortex versus healthy LNs (Table 1; $P < 0.0001$). The absence of the hilum was associated with metastatic LNs (Table 1; $P < 0.0001$). E_{max}, E_{mean}, $E_{min,}$ and Emean-m were significantly larger in malignant LNs than in healthy LNs (Table 1; $P < 0.0001$).

The diagnostic performances of E_{max}, E_{mean}, $E_{min,}$ and $E_{mean\text{-}m}$ using sensitivity, specificity, accuracy, PPV, NPV, and estimated critical value were used to predict the actual situation of metastasis and distinguish benign lymph nodes from metastatic lymph nodes 21.10 kPa (E_{max}), 13.10 kPa (E_{mean}), 9.00 kPa (E_{min}), and 1.58 ($E_{mean\text{-}m}$), as presented in Table 2. The comparison of AUC values between SWE and BUS is shown in Table 3. AUC values of E_{max}, E_{mean}, $E_{min,}$ and $E_{mean\text{-}m}$ were not different from those of BUS ($P > 0.05$). However, AUC of E_{max} plus BUS is higher than that of BUS alone ($P = 0.0208$; Table 3).

3.2. Correlation between EI of SWE and Histopathology of Metastatic LNs. Table 4 presents the relationship between EI of SWE and histopathological results of metastatic LN, in which there is a relationship between EI of SWE of E_{max}, E_{mean}, $E_{min,}$ and $E_{mean\text{-}m}$ and the number of metastatic LNs, and the ratio of malignant LNs/dissected LNs and the L/S (Long-/short-axis ratio) were not significantly different ($P < 0.05$). EI of SWE in malignant lymph nodes those with extranodal extension are higher than those without extranodal extension ($P < 0.0001$ for E_{max}, $E_{mean,}$ and E_{min}; Table 4).

4. Discussion

Lymph node metastasis compromises the outcome of surgical treatment, radiotherapy, and neoadjuvant therapy, so the prediction of axillary lymph node status is of great significance in the prognosis of patients with invasive breast cancer. The 5-year survival of patients with positive lymph nodes is 40%, which is lower than that of patients without lymph node metastasis [30]. Previous studies have reported that BUS features including low long-to-short-axis diameter ratio, heterogeneous cortical thickening, and absence of fat gates and peripheral blood flow are associated with lymph node metastasis. Several studies have investigated the significance of quantitative SWE in patients with breast cancer [31, 32]. However, SWE has not been evaluated for metastatic LN in invasive breast cancer.

Here, metastatic LNs were associated with a longer short-axis diameter and a larger maximal cortex versus

Table 1: Statistic analysis between benign and malignant lymph nodes ($n = 115$).

Variable	Benign ($n = 45$)	Malignant ($n = 70$)	Statistic value	P value
Age (year)	53.31 ± 9.84	51.8 ± 9.04	0.84	0.4000[a]
Short-axis diameter (mm)	5.30 ± 1.50	11.5 ± 6.20	7.95	<0.0001[a]
Long/short-axis ratio	1.76(1.55,2.21)	1.585(1.34,2.08)	3.71	0.0541[b]
Maximal cortex (mm)	2.20(1.40,3.20)	5.20(2.30,7.20)	20.19	<0.0001[b]
Hilum			19.35	<0.0001[d]
Absent, n (%)	2.00 (4.4%)	31.00 (44.3%)		
Present, n (%)	43.00 (95.6%)	39.00 (55.7%)		
E_{max} (kPa)	16.80 (14.50,19.40)	25.45 (19.0,41.50)	46.12	<0.0001[b]
E_{mean} (kPa)	11.70 (9.90,12.60)	15.45 (13.20,24.70)	34.61	<0.0001[b]
E_{min} (kPa)	7.90 (6.50,9.80)	11.15 (9.00,13.80)	24.32	<0.0001[b]
$E_{mean\text{-}m}$ (kPa)	1.36 ± 0.28	2.03 ± 0.61	−8.05	<0.0001[c]

$E_{max,}$ maximal elasticity score of the lesion; $E_{mean,}$ mean elasticity score of the lesion; $E_{min,}$ minimal elasticity score of the lesion; $E_{mean\text{-}m,}$ ratio of E_{mean} mean of the lesions divided by E_{mean} of surrounding muscles.[a]Student's t test.[b]Wilcoxon rank sum test.[c]Student's t' test.[d]Chi-square test.

Table 2: Diagnostic performance of BUS and SWE for predicting axillary lymph node metastasis.

Variables	Cutoff values	Sensitivity (%)	Specificity (%)	PPV (%)	NPV (%)	Accuracy (%)
BUS		75.71	68.89	79.10	64.58	73.04
E_{max}	21.10	70.00	93.33	94.23	66.67	79.13
E_{mean}	13.10	78.57	80.00	85.94	70.59	79.13
E_{min}	9.00	75.71	68.89	79.10	64.58	73.04
$E_{mean\text{-}m}$	1.58	81.43	82.22	87.69	74.00	81.74
BUS + E_{max}	21.10	88.57	66.67	80.52	78.95	80.00
BUS + E_{mean}	13.10	91.43	57.78	77.11	81.25	78.26
BUS + E_{min}	9.00	91.43	51.11	74.42	79.31	75.65
BUS + $E_{mean\text{-}m}$	1.58	95.71	60.00	78.82	90.00	81.74

BUS, B-mode ultrasound category; SWE, shear wave elastography; PPV, positive predictive value; NPV, negative predictive value; $E_{max,}$ maximal elasticity score of the lesion;, $E_{mean,}$ mean elasticity score of the lesion; $E_{min,}$ minimal elasticity score of the lesion; $E_{mean\text{-}m,}$ ratio of E_{mean} mean of the lesions divided by E_{mean} of surrounding muscles; BUS + $E_{max,}$ combined use of E_{max} and BUS; BUS + E_{mean}, combined use of E_{mean} and BUS; BUS + $E_{min,}$ combined use of E_{min} and BUS; BUS + $E_{mean\text{-}m,}$ combined use of $E_{mean\text{-}m}$ and BUS.

Table 3: Comparison of diagnostic performances of BUS and SWE.

Parameters	AUC (95% CI)	P value (compared with BUS)
BUS	0.7230 (0.6379,0.8081)	
E_{max}	0.8167 (0.7512,0.8821)	0.0574
E_{mean}	0.7929 (0.7165,0.8692)	0.1913
E_{min}	0.7230 (0.6379,0.8081)	1.0000
$E_{mean\text{-}m}$	0.8183 (0.7455,0.8910)	0.0768
BUS + E_{max}	0.7762 (0.6971,0.8553)	0.0208
BUS + E_{mean}	0.7460 (0.6659,0.8261)	0.4756
BUS + E_{min}	0.7127 (0.6318,0.7936)	0.7756
BUS + $E_{mean\text{-}m}$	0.7786 (0.7024,0.8548)	0.0849

BUS, B-mode ultrasound category; SWE, shear wave elastography; AUC, area under the curve; CI, confidence interval; P value is for parameter compared with the ultrasound category; $E_{max,}$ maximal elasticity score of the lesion; $E_{mean,}$ mean elasticity score of the lesion; $E_{min,}$ minimal elasticity score of the lesion; $E_{mean\text{-}m,}$ ratio of E_{mean} mean of the lesions divided by E_{mean} of surrounding muscles; BUS + $E_{max,}$ combined use of E_{max} and BUS; BUS + $E_{mean,}$ combined use of E_{mean} and BUS; BUS + $E_{min,}$ combined use of E_{min} and BUS; BUS + $E_{mean\text{-}m,}$ combined use of $E_{mean\text{-}m}$ and BUS.

benign LNs, and the absence of hilum was associated with metastatic LNs. These results were similar to those from previous studies [33]. The present study found that EI of SWE of E_{max}, E_{mean}, $E_{min,}$ and $E_{mean\text{-}m}$ were significantly higher in malignant LNs when compared with benign LNs. In addition, the results showed the highest sensitivity (81.43%), accuracy (81.74%), and NPV (74%) with $E_{mean\text{-}m}$ (cutoff lever of 1.58), highest specificity (93.33%), and PPV (94.23%) with E_{max} (cutoff lever of 21.10 kPa). These results are similar to the results of previous research [34]. The difference of diagnostic performance between BUS and SWE did not come up to the statistical standard. However, our study found E_{max} plus BUS outperformed BUS only (AUC 0.7762 vs. 0.7230; $P = 0.0208$). These findings suggest that SWE may serve as an important auxiliary diagnostic tool for invasive breast cancer.

In this study, quantitative SWE may be closely related to histopathological prognostic factors of metastatic lymph nodes, and the ratio (L/S), number of malignant LNs, and the ratio of metastatic LN/dissected LN were not significantly correlated with the quantitative EI of SWE. However, the mean values of Emax, Emean, Emin, and Emean-m with

Table 4: Correlation of Emean-m and histopathologic factors in metastatic LN of invasive breast cancer.

Variables	No. of metastatic LN[#]		Ratio of metastatic LN/dissected LN[#]		L/S[#]		Extranodal extension[*]		
	Coefficient	P value	Coefficient	P value	Coefficient	P value	Without extension	With extension	P value
E_{max}	0.0657	0.6573	0.0662	0.6550	−0.1238	0.1876	24.01 ± 8.46	44.35 ± 6.06	<0.0001
E_{mean}	0.2037	0.1650	0.1350	0.3602	−0.0392	0.6772	15.71 ± 6.21	28.42 ± 8.81	<0.0001
E_{min}	0.0970	0.5120	0.2136	0.1449	0.0237	0.8018	10.01 ± 3.61	16.59 ± 5.41	<0.0001
$E_{mean\text{-}m}$	0.1574	0.2852	0.1159	0.4328	−0.0082	0.9309	1.70 ± 0.41	2.71 ± 0.67	<0.0001

SWE, shear wave elastography; EI, elasticity indices; LN, lymph node; $E_{max,}$ maximal elasticity score of the lesion; $E_{mean,}$ mean elasticity score of the lesion; $E_{mi,}$ minimal elasticity score of the lesion; $E_{mean\text{-}m,}$ ratio of E_{mean} mean of the lesions divided by E_{mean} of surrounding muscles. [#]Spearman correlation coefficient. [*]Student's t test.

extranodal infiltration and metastasis were significantly different from those without lymph nodes (44.35 ± 6.06 vs. 24.01 ± 8.46 kPa, 28.42 ± 8.81 vs. 25.71 ± 6.21 kPa, 16.59 ± 5.41 vs. 10.01 ± 3.61 kPa, and 2.71 ± 0.67 vs. 1.70 ± 0.41 kPa, respectively; $P < 0.0001$). These results were similar to those of previous studies and suggested that EI of SWE is available to help determine the degree of the benignity of LN to decide the use of surgery or neoadjuvant therapy for invasive breast cancer patients.

Real-time shear wave elastography, as a new concept for tissue hardness evaluation, overcomes the objective impacts such as the size and frequency of probe pressure in static/quasistatic elastography and features the advantages of good repeatability, rapidity, and no dependence.

There were several limitations in the current study. First, the number of our samples is small, and the follow-up duration was short. Furthermore, evaluation of factors affecting the elasticity measurements including degree, depth, size, and location of calcification in a single lymph node was absent. Second, SWE was performed in preoperative staging ultrasound in patients with invasive breast cancer, which may result in a selection bias. Third, the accuracy of the examinations used in this study was correlated with LNs removed in the surgery. However, the removed LNs herein were fixed in formalin which may lead to alterations in the sizes of the LNs. Finally, this study did not obtain a detailed correlation between the EI of SWE and histopathological elements of metastatic breast cancer in metastatic LNs. Future multicenter studies will be carried out with a larger sample size, a longer follow-up duration, and improvement of the above limitations to provide more convincing data.

5. Conclusions

Quantitative SWE provides a viable alternative for the assessment of axillary LN and shows great potential to predict pathological prognostic elements of metastatic axillary LNs in invasive breast cancer. Joint use of SWE and BUS allows examination of the predictive outcome of BUS for axillary lymph node metastasis in invasive breast cancer.

Data Availability

The data sets used and analyzed in this study can be obtained from the corresponding authors in combination with specific requirements.

Conflicts of Interest

The authors declare that they have no conflicts of interest.

Authors' Contributions

Yingying Cheng and Guofu Li contributed equally to this work

Acknowledgments

This research was supported by the Fundamental Research Funds for the Provincial Universities (31041180116) and the Health and Family Planning Commission of Heilongjiang Province (2018-371).

References

[1] B. Fisher, M. Bauer, D. L. Wickerham, C. K. Redmond, E. R. Fisher, and A. B. Cruz, "Relation of number of positive axillary nodes to the prognosis of patients with primary breast cancer. An NSABP update," *Cancer*, vol. 52, no. 9, pp. 1551–1557, 1983.

[2] P. L. Fitzgibbons, D. L. Page, D. Weaver, A. D. Thor, D. C. Allred, and G. M. Clark, "Prognostic factors in breast cancer," *Archives of pathology & laboratory medicine*, vol. 124, no. 7, pp. 966–978, 2000.

[3] J. N. Bruneton, E. Caramella, M. Héry, D. Aubanel, J. J. Manzino, and J. L. Picard, "Axillary lymph node metastases in breast cancer: preoperative detection with US," *Radiology*, vol. 158, no. 2, pp. 325-326, 1986.

[4] M. C. van Rijk, H. J. Teertstra, J. L. Peterse, O. E. Nieweg, R. A. Olmos, and C. A. Hoefnagel, "Ultrasonography and fine-needle aspiration cytology in the preoperative evaluation of melanoma patients eligible for sentinel node biopsy," *Annals of Surgical Oncology*, vol. 13, no. 11, pp. 1511–1516, 2006.

[5] R. de Freitas Jr., M. V. Costa, S. V. Schneider, M. A. Nicolau, and E. Marussi, "Accuracy of ultrasound and clinical examination in the diagnosis of axillary lymph node metastases in breast cancer," *European Journal of Surgical Oncology: The Journal of the European Society of Surgical Oncology and the British Association of Surgical Oncology*, vol. 17, pp. 240–244, 1991.

[6] M. D. Alkuwari and M. A. Auger, "Accuracy of fine-needle aspiration cytology of axillary lymph nodes in breast cancer patients," *Cancer*, vol. 114, no. 2, pp. 89–93, 2008.

[7] S. Sidibé, A. Coulibaly, S. Traoré, M. Touré, and I. Traoré, "[Role of ultrasonography in the diagnosis of axillary lymph

node metastases in breast cancer: a systematic review],” *Le Mali Médical*, vol. 22, pp. 9–13, 2007.

[8] C. Balu-Maestro, C. Chapellier, P. Carrier, J. Darcourt, F. Ettore, and I. Raoust, “Imagerie dans le bilan d’extension ganglionnaire et métastatique du cancer du sein,” *Journal de Radiologie*, vol. 86, no. 11, pp. 1649–1657, 2005.

[9] M. Sianesi, G. Ceci, A. Ghirarduzzi, P. Del Rio, A. Guazzi, and B. Pisanelli, “Use of axillary ultrasonography in breast cancer: a useful tool to reduce sentinel node procedures,” *Annali Italiani di Chirurgia*, vol. 80, pp. 315–318, 2009.

[10] P. D. Britton, A. Goud, S. Godward, S. Barter, A. Freeman, and M. Gaskarth, “Use of ultrasound-guided axillary node core biopsy in staging of early breast cancer,” *European Radiology*, vol. 19, no. 3, pp. 561–569, 2009.

[11] K. M. McMasters, T. M. Tuttle, D. J. Carlson, C. M. Brown, R. D. Noyes, and R. L. Glaser, “Sentinel lymph node biopsy for breast cancer: a suitable alternative to routine axillary dissection in multi-institutional practice when optimal technique is used,” *Journal of Clinical Oncology*, vol. 18, no. 13, pp. 2560–2566, 2000.

[12] L. ., . Gao, K. J. Parker, R. M. Lerner, and S. F. Levinson, “Imaging of the elastic properties of tissue-A review,” *Ultrasound in Medicine and Biology*, vol. 22, no. 8, pp. 959–977, 1996.

[13] B. S. Garra, E. I. Cespedes, J. Ophir, S. R. Spratt, R. A. Zuurbier, and C. M. Magnant, “Elastography of breast lesions: initial clinical results,” *Radiology*, vol. 202, no. 1, pp. 79–86, 1997.

[14] E. S. Burnside, T. J. Hall, A. M. Sommer, G. K. Hesley, G. A. Sisney, and W. E. Svensson, “Differentiating benign from malignant solid breast masses with US strain imaging,” *Radiology*, vol. 245, no. 2, pp. 401–410, 2007.

[15] E. D. C. Fleury, J. C. V. Fleury, S. Piato, and D. Roveda, “New elastographic classification of breast lesions during and after compression,” *Diagnostic and interventional radiology*, vol. 15, no. 2, pp. 96–103, 2009.

[16] D. M. Regner, G. K. Hesley, N. J. Hangiandreou, M. J. Morton, M. R. Nordland, and D. D. Meixner, “Breast lesions: evaluation with US strain imaging-clinical experience of multiple observers,” *Radiology*, vol. 238, no. 2, pp. 425–437, 2006.

[17] M. Tanter, J. Bercoff, A. Athanasiou, T. Deffieux, J. L. Gennisson, and G. Montaldo, “Quantitative assessment of breast lesion viscoelasticity: initial clinical results using supersonic shear imaging,” *Ultrasound in Medicine and Biology*, vol. 34, no. 9, pp. 1373–1386, 2008.

[18] J. Bercoff, M. Tanter, and M. Fink, “Supersonic shear imaging: a new technique for soft tissue elasticity mapping,” *IEEE Transactions on Ultrasonics, Ferroelectrics, and Frequency Control*, vol. 51, no. 4, pp. 396–409, 2004.

[19] A. Athanasiou, A. Tardivon, M. Tanter, B. Sigal-Zafrani, J. Bercoff, and T. D. Deffieux, “Breast lesions: quantitative elastography with supersonic shear imaging-preliminary results,” *Radiology*, vol. 256, no. 1, pp. 297–303, 2010.

[20] K. Bhatia, C. S. Tong, C. C. Cho, E. H. Yuen, J. Lee, and A. T. Ahuja, “Reliability of shear wave ultrasound elastography for neck lesions identified in routine clinical practice,” *Ultraschall in der Medizin - European Journal of Ultrasound*, vol. 33, no. 5, pp. 463–468, 2012.

[21] K. S. Bhatia, C. S. Tong, C. C. Cho, E. H. Yuen, Y. Y. Lee, and A. T. Ahuja, “Shear wave elastography of thyroid nodules in routine clinical practice: preliminary observations and utility for detecting malignancy,” *European Radiology*, vol. 22, no. 11, pp. 2397–2406, 2012.

[22] L. S. Taylor, D. J. Rubens, B. C. Porter, Z. Wu, R. B. Baggs, and S. A. P. di Sant’Agnese, “Prostate cancer: three-dimensional sonoelastography for in vitro detection,” *Radiology*, vol. 237, no. 3, pp. 981–985, 2005.

[23] E. Bavu, J. L. Gennisson, M. Couade, J. Bercoff, V. Mallet, and M. Fink, “Noninvasive in vivo liver fibrosis evaluation using supersonic shear imaging: a clinical study on 113 hepatitis C virus patients,” *Ultrasound in Medicine and Biology*, vol. 37, no. 9, pp. 1361–1373, 2011.

[24] A. Thomas, S. Kümmel, O. Gemeinhardt, and T. Fischer, “Real-time sonoelastography of the cervix: tissue elasticity of the normal and abnormal cervix,” *Academic Radiology*, vol. 14, no. 2, pp. 193–200, 2007.

[25] A. Evans, P. Rauchhaus, P. Whelehan, K. Thomson, C. A. Purdie, and L. B. Jordan, “Does shear wave ultrasound independently predict axillary lymph node metastasis in women with invasive breast cancer?” *Breast Cancer Research and Treatment*, vol. 143, no. 1, pp. 153–157, 2014.

[26] J. H. Yoon, Y. K. Kim, H. J. Moon, H. Y. Youk, E. J. Son, and E. K. Kim, “Contribution of computed tomography to ultrasound in predicting lateral lymph node metastasis in patients with papillary thyroid carcinoma,” *Annals of Surgical Oncology*, vol. 18, no. 6, pp. 1734–1741, 2011.

[27] W. S. Jung, J. A. Kim, E. J. Son, J. H. Youk, and C. S. Park, “Shear wave elastography in evaluation of cervical lymph node metastasis of papillary thyroid carcinoma: elasticity index as a prognostic implication,” *Annals of Surgical Oncology*, vol. 22, no. 1, pp. 111–116, 2015.

[28] J. P. Yun, J. A. Kim, E. J. Son, H. Y. Ji, and C. S. Park, “Quantitative shear wave elastography as a prognostic implication of papillary thyroid carcinoma (PTC): elasticity index can predict extrathyroidal extension (ETE),” *Annals of Surgical Oncology*, vol. 20, pp. 2765–2771, 2013.

[29] Y. J. Choi, J. H. Lee, H. K. Lim, S. Y. Kim, M. W. Han, and K. J. Cho, “Quantitative shear wave elastography in the evaluation of metastatic cervical lymph nodes,” *Ultrasound in Medicine and Biology*, vol. 39, no. 6, pp. 935–940, 2013.

[30] C. L. Carter, C. Allen, and D. E. Henson, “Relation of tumor size, lymph node status, and survival in 24,740 breast cancer cases,” *Cancer*, vol. 63, no. 1, pp. 181–187, 1989.

[31] C. Tourasse, J. F. Dénier, A. Awada, A.-C. Gratadour, K. Nessah-Bousquet, and J. Gay, “Elastography in the assessment of sentinel lymph nodes prior to dissection,” *European Journal of Radiology*, vol. 81, no. 11, pp. 3154–3159, 2012.

[32] J. J. Choi, B. J. Kang, S. H. Kim, J. H. Lee, S. H. Jeong, and H. W. Yim, “Role of sonographic elastography in the differential diagnosis of axillary lymph nodes in breast cancer,” *Journal of Ultrasound in Medicine*, vol. 30, no. 4, pp. 429–436, 2011.

[33] Y. J. Choi, E. Y. Ko, B. K. Han, J. H. Shin, S. S. Kang, and S. Y. Hahn, “High-resolution ultrasonographic features of axillary lymph node metastasis in patients with breast cancer,” *The Breast*, vol. 18, no. 2, pp. 119–122, 2009.

[34] K. S. Bhatia, C. C. Cho, C. S. Tong, E. H. Yuen, and A. T. Ahuja, “Shear wave elasticity imaging of cervical lymph nodes,” *Ultrasound in Medicine and Biology*, vol. 38, no. 2, pp. 195–201, 2012.

Hindawi
Evidence-Based Complementary and Alternative Medicine
Volume 2022, Article ID 9647325, 6 pages
https://doi.org/10.1155/2022/9647325

Research Article

Effectiveness of Comfort Nursing Combined with Continuous Nursing on Patients with Colorectal Cancer Chemotherapy

Jing Miao,[1] Mengting Liu,[2] Jie Ma,[3] and Han Wang[1]

[1]*Oncology Chemotherapy Day Ward, Peking Union Medical College Hospital, Beijing 100010, China*
[2]*Pneumology and Critical Care Medicine, Peking Union Medical College Hospital, Beijing 100010, China*
[3]*Cardiac Intensive Care Unit, Peking Union Medical College Hospital, Beijing 100010, China*

Correspondence should be addressed to Han Wang; hangmodi106@163.com

Received 11 April 2022; Revised 9 May 2022; Accepted 16 May 2022; Published 8 June 2022

Academic Editor: Xueliang Wu

Purpose. To analyze the application effect of continuous nursing combined with comfort nursing on patients with colorectal cancer chemotherapy and its influence on sleep quality and immune function. *Methods*. The data of 96 patients with colorectal cancer in the Oncology Department of Peking Union Medical College Hospital from July 2018 to July 2020 were collected and randomized into the control group and study group according to the odd and even numbers, with 48 cases in each group. The control group received routine care during chemotherapy, and the study group implemented continuous care combined with comfort care. *Results*. After intervention, the results were in favor of the study group than the control group with higher compliance, higher level of various immune indicators, higher quality of life scores, and higher nursing satisfaction rate. In addition, the Generalized Anxiety Disorder (GAD-7) scores and the average Pittsburgh Sleep Quality Index (PSQI) score of the study group after intervention was drastically lower than the control group ($P < 0.001$). *Conclusion*. The implementation of continuous care combined with comfort care for patients with colorectal cancer undergoing chemotherapy can effectively improve sleep quality and quality of life, relieve anxiety, and yield high patient compliance, which is worthy of clinical promotion.

1. Introduction

Colorectal cancer is a common gastrointestinal tumor disease, which can be divided into colon cancer and rectal cancer according to different diseased sites [1, 2]. Surgery is currently the primary option for the treatment of colorectal cancer. Unfortunately, due to its hidden characters, most patients have entered the middle and advanced stages when they are diagnosed. In this regard, surgery cannot benefit patients; thus, chemotherapy is frequently used. As a damaging treatment, chemotherapy can produce strong side effects, making it prone to hair loss, abdominal pain, liver and kidney function damage [3], and further damaging the body's immune cells to undermine immune function. In addition, up to 65% of patients develop psychological stress reaction during chemotherapy, in the most direct manner of poor psychological state and sleep quality. Hence, it is essential to implement nursing intervention for patients with colorectal cancer during chemotherapy [4]. The nursing focuses on psychiatric state, nutrition support, bowel preparation for surgery, pain care, and complication care.

Continuous nursing, also known as extended nursing, is a high-quality clinical nursing service concept first proposed by the United States [5]. Its purpose is to improve patient compliance with treatment and provide patients with out-of-hospital health guidance and professional nursing. As an important part of high-quality nursing care, comfort care can organically integrate the physiology, psychology, and society of patients by providing creative and personalized nursing services for chemotherapy patients, so as to promote physical recovery and improve the quality of life in the most comfortable form [6, 7]. Traditional Chinese medicine (TCM) nursing based on "holistic concept, syndrome differentiation and treatment, meridian theory," through skin absorption, acupoint stimulation, and meridian conduction, effectively alleviate various uncomfortable symptoms of patients with advanced cancer and has become an important content of cancer care [8, 9]. In light of these, this study

explores the application effect of continuous care combined with comfort care on patients with colorectal cancer chemotherapy and its impact on sleep quality and immune function and provides more evidence for follow-up clinical care.

2. Materials and Methods

2.1. Baseline Data. The data of 96 patients with colorectal cancer in the Oncology Department of Peking Union Medical College Hospital from July 2018 to July 2020 were selected for retrospective analysis. According to the odd and even numbers of hospitalization numbers, they were divided into the study group and control group, with 48 cases in each group. The study was authorized and reviewed by hospital ethics committee (approved no. 2017-DW651).

2.2. Inclusion and Exclusion Criteria. Inclusion criteria were as follows: age 18–80 years old, diagnosed as colorectal cancer by pathology and treated by surgery, with normal cognitive function and audiovisual function, and the expected survival time ≥6 months.

Exclusion criteria were as follows: associated with other primary cancers, history of chemotherapy contraindications, hearing or language communication impairment, previous craniocerebral nervous system diseases such as senile dementia, craniocerebral trauma, and Parkinson's disease, and serious damage to the brain, heart, liver, kidney, and other organs.

2.3. Methods

2.3.1. Routine Care. The control group received clinical routine care during chemotherapy, such as instructed patients to take medication on time, created a tidy and clean ward environment, strengthened daily inspection work, monitored the physical condition of patients during chemotherapy, and took preventive measures for complications.

2.3.2. Continuous Care Combined with Comfort Care. The study group received clinical routine care during chemotherapy, and the specific methods were as follows.

Continuous care: (1) Established a nursing intervention team, with members including the attending physician, head nurse, and 4 nurses, with the head nurse as the team leader to carry out clinical nursing work. (2) Before enrollment, based on the clinical condition of the patients, provided psychological care and health education about bowel cancer, explained the pathogenesis and treatment process of bowel cancer, and emphasized the importance of chemotherapy to help patients understand their own diseases more comprehensively and reduced inner fears to improve his confidence in treatment and compliance with treatment [10]. (3) Strictly controlled use of analgesics of patients with severe pain while carrying out nursing care and informed patients of medication precautions. (4) Once the patient presented an abnormal condition during chemotherapy, promptly notified the doctor for corresponding treatment. Paid particular attention to the patient's physical changes during and within 1 hour after the use of chemotherapy drugs and formulated predictive nursing measures for possible complications [11]. (5) For those with sleep disorders, implemented appropriate interventions with drugs to ensure that the patients maintain adequate sleep, created a good treatment environment for the patients, and kept the ward clean and tidy.

Comfort care: (1) Recorded the patient's condition, examination results, and treatment plan in detail. Before chemotherapy, called the patients in advance to make relevant preparations and explained precautions. (2) Informed patients of the chemotherapy regimen at revisit, the progress of the disease and the duration of treatment in a timely manner based on the results of the examination. (3) After the patient is discharged from the hospital, followed up by telephone at least once a week to understand the patient's disease and guided and supervised the patient to develop a scientific diet, exercise appropriately, maintain a happy mood, and answered questions raised by the patient [12]. (4) Informed patients that they should receive chemotherapy on a regular basis, follow the doctor's advice to develop good living habits, and improved their treatment compliance and self-care ability. (5) Carry out TCM health guidance for cancer pain: according to patients' syndrome type, guide self-adjustment methods such as deep breathing, music therapy, wet hot compress, and metastatic acupoint massage.

2.4. Evaluation Indicators

2.4.1. Treatment Compliance. The self-made chemotherapy patient compliance questionnaire by our department was used to evaluate the treatment compliance of patients after intervention. The scale includes adherence to radiotherapy, regular physical examination, scientific diet, self-protection, and disease recognition, and the results were divided into yes and no. The compliance rate was conculcated.

2.4.2. Anxiety Scores. With reference to the Generalized Anxiety Disorder Scale [13] (GAD-7), the anxiety was evaluated after intervention. The scale includes 7 scoring items, each with a full score of 3 points and a total score of 21 points. The higher the score, the greater the degree of anxiety.

2.4.3. Sleep Quality. With reference to the Pittsburgh Sleep Quality Index [14] (PSQI), the sleep quality of patients was evaluated after intervention. The scale includes 7 scoring items, each on a scale of 0–3, with a total score of 21 points. The higher the value, the worse the quality of sleep.

2.4.4. T Cell Subsets. 5 ml fasting venous blood before and after the intervention of the two groups of patients was collected and centrifuged to obtain upper serum; flow cytometry (model: Attune NxT; manufacturer: Shanghai Mojin Medical Equipment Co., Ltd.) was used to detect T cell differentiation group CD4+, CD8+, and CD4+/CD8+ ratio.

2.4.5. Nursing Satisfaction. A self-made questionnaire on clinical nursing satisfaction for patients with bowel cancer chemotherapy by our department was used to evaluate the clinical satisfaction of the two groups. According to the degree of satisfaction, it was divided into very satisfied, satisfied, basically satisfied, and dissatisfied; total satisfaction = (very satisfied + satisfied + basically satisfied) number of cases/total number of cases.

2.4.6. Quality of Life. The quality of life (QOL) rating scale [15] was used to evaluate the quality of life of the two groups of patients after intervention. It was evaluated from six dimensions including psychology, physiology, spirit, environment, social relations, and independence, each with a full score of 100 points; the higher the score, the higher the quality of life;

2.5. Statistical Methods. The data were statistically analyzed and processed by the SPSS 21.0 software, and GraphPad Prism 7 (GraphPad Software, San Diego, USA) was used to map graphics. The enumeration data were represented by (n %) and analyzed by the χ^2 test, and the measurement data were expressed as ($\overline{x} \pm s$) and examined by the t-test. Statistical significance was accepted at $P < 0.05$.

3. Results

3.1. Comparison of Baseline Data. There was no significant difference between the two groups in gender ratio, average age, BMI value, marital status, disease type, pathological type, residence, and education level ($P < 0.05$, Table 1).

3.2. Comparison of Treatment Compliance. The compliance of the study group after intervention was significantly higher than that of the control group ($P < 0.05$), as given in Table 2.

3.3. Comparison of GAD-7 and PSQI Scores. A drastically lower GAD-7 scores and PSQI scores of the study group after intervention than the control group were observed ($P < 0.001$), as shown in Figure 1.

3.4. Comparison of Various Immune Indicators. The levels of various immune indicators in the study group after intervention were observed to be considerably superior to those in the control group ($P < 0.05$), as given in Table 3.

3.5. Comparison of Patient Care Satisfaction. The total nursing satisfaction comparison results proved to be in favor of the study group with higher satisfaction as compared to the control group ($P < 0.05$), as given in Table 4.

3.6. Comparison of Quality of Life Scores. A markedly higher quality of life scores of patients in the study group after intervention was yielded in contrast to the control group ($P < 0.001$), as given in Table 5.

4. Discussion

With the changes in modern dietary habits, the prevalence of bowel cancer is rising, with a trend in younger population. Surgery is currently the mainstay for the treatment of the disease, yet patients in progressed stages are prone to metastasis and recurrence after surgery [16, 17]. As a result, combined adjuvant chemotherapy is urgent to improve the treatment effect and prolong the survival time of patients. Studies have found that surgery and chemotherapy can damage the immune function of patients, and the immune function is closely related to tumor recurrence and growth rate. Effective implementation is of great necessity and significance to improve the immune function, quality of life, and prognosis [18]. At present, most of the nursing work for these patients is conducted in hospitals, with the main purpose to relieve the patient's physical and mental burden, improve treatment compliance, and prevent adverse reactions that may occur during treatment. However, out-of-hospital care services are unavailable, leading to somber compliance and impeding the prognosis [19, 20].

Continuous care can realize the continuation of care from the hospital to the home, so that nursing work is no longer simply limited to the hospital, meeting the health needs of patients after discharge. Therefore, continuous care can promote the recovery of patients and plays a significant role in improving the prognosis [21, 22]. Comfortable care integrates the concept of human-centered care into the nursing process in the practice, takes the individual needs of patients as the starting point, and carries out nursing services based on the clinical conditions of the patients, effectively regulating the physical and mental conditions of the patients, keeping them in favorable condition, and consolidating the treatment effect [23]. Due to the influence by the side effects of chemotherapy and the negative emotions during cancer, the symptoms of insomnia may occur. This study showed that the average PSQI score of the study group after treatment was significantly lower than that of the control group, indicating that continuous care combined with comfort care can significantly improve the sleep quality of patients undergoing chemotherapy for colon cancer, which has been confirmed in a prior trial [24].

As is known that the lesions in patients with bowel cancer can consume nutrients in the patient's body, plus the adverse reactions caused by chemotherapy drugs, it can result in loss of appetite, weakened immunity, and high catabolism and negative nitrogen balance, compromising the chemotherapy effect [25]. This study provides continuous care for patients undergoing chemotherapy for colon cancer, develops them with scientific dietary plans, helps them establish healthy living habits, improves the body's nutritional status, and enhances immune function. And the results showed that the immune indicators of the study group after intervention are superior to the control group, suggesting that combined nursing intervention can improve

Table 1: Comparison of baseline data between the two groups.

	Study group ($n = 48$)	Control group ($n = 48$)	χ^2/t	P
Gender (male/female)	26/22	25/23	0.042	0.838
Age ($\overline{x} \pm s$, years)	52.16 ± 4.51	52.21 ± 4.48	0.054	0.957
BMI ($\overline{x} \pm s$, kg/m^2)	21.62 ± 1.05	21.58 ± 1.15	0.178	0.859
Disease type				
Rectal	39 (81.25%)	41 (85.42%)	0.300	0.584
Colon	9 (18.75%)	7 (14.58%)		
Pathological type				
Adenocarcinoma	42 (87.50%)	40 (83.33%)	0.335	0.563
Squamous carcinoma	6 (12.50%)	8 (16.67%)		
Residence				
City	23 (47.92%)	19 (39.58%)	0.677	0.411
Rural	25 (52.08%)	29 (60.42%)		

Table 2: Treatment compliance (n, %).

	Radiotherapy adherence	Physical examination	Scientific diet	Self-protection	Disease recognition
Study group ($n = 48$)	44 (91.67)	47 (97.92)	43 (89.58)	42 (87.50)	47 (97.92)
Control group ($n = 48$)	36 (75.00)	39 (81.25)	35 (72.92)	33 (68.75)	40 (83.33)
χ^2	4.800	7.144	4.376	4.937	6.008
P	0.028	0.008	0.036	0.026	0.014

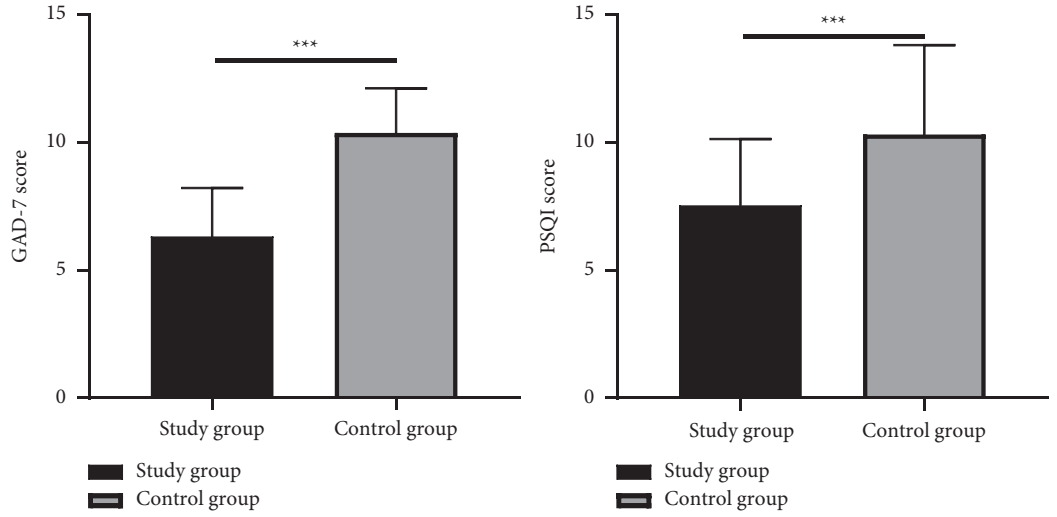

Figure 1: Comparison of GAD-7 scores and PSQI scores, $^{***}P < 0.001$.

Table 3: T cell subsets ($\overline{x} \pm s$).

Group	$CD4^+$ (%)		$CD8^+$ (%)		$CD4^+/CD8^+$	
	Before	After	Before	After	Before	After
Study group ($n = 48$)	32.46 ± 4.27	43.27 ± 3.28	22.81 ± 4.26	32.18 ± 3.17	1.26 ± 0.24	1.51 ± 0.35
Control group ($n = 48$)	32.52 ± 4.21	36.78 ± 3.57	22.85 ± 4.31	27.47 ± 3.26	1.31 ± 0.27	1.36 ± 0.33
t	0.069	9.2275	0.046	7.176	0.959	2.160
P	0.945	<0.001	0.964	<0.001	0.340	0.033

Table 4: Nursing satisfaction (n, %).

Group	Very satisfied	Satisfied	Generally satisfied	Unsatisfied	Total satisfaction rate
Study group ($n = 48$)	21 (43.75)	19 (39.58)	6 (12.50)	2 (4.17)	46 (95.83)
Control group ($n = 48$)	16 (33.33)	15 (31.25)	8 (16.67)	9 (18.75)	39 (81.25)
χ^2					5.031
P					0.025

Table 5: Quality of life scores ($\overline{x} \pm s$, points).

Group	Psychology	Physiology	Spirit	Environment	Social relation	Independence
Study group ($n = 48$)	64.38 ± 3.19	70.27 ± 3.65	68.92 ± 4.27	66.38 ± 3.28	66.26 ± 4.27	60.28 ± 4.28
Control group ($n = 48$)	58.37 ± 3.27	62.18 ± 3.28	60.27 ± 4.19	57.82 ± 3.56	59.28 ± 4.28	52.36 ± 3.76
t	9.115	11.422	10.018	12.252	7.999	9.632
P	<0.001	<0.001	<0.001	<0.001	<0.001	<0.001

the immune function of patients with colorectal cancer chemotherapy and ensure the quality of chemotherapy.

5. Conclusion

The implementation of continuous care combined with comfort care for patients undergoing chemotherapy for colorectal cancer can effectively improve the patient's sleep quality, enhance immune function, and produce higher satisfaction with clinical care, which is worthy of clinical promotion.

Data Availability

The datasets used during the present study are available from the corresponding author upon request.

Conflicts of Interest

The authors declare that they have no conflicts of interest.

References

[1] L. Gavens, L. Whiteley, A. Belencsak et al., "Market segmentation tools provide insights into demographic variations in bowel cancer screening uptake," *Journal of Epidemiology and Community Health*, vol. 73, no. 8, pp. 778–785, 2019.

[2] S. Pompili, R. Sferra, E. Gaudio et al., "Can Nrf2 modulate the development of intestinal fibrosis and cancer in inflammatory bowel disease?" *International Journal of Molecular Sciences*, vol. 20, no. 16, 2019.

[3] K. Cerna, J. Ivarsson, A. Weilenmann, and G. Steineck, "Supporting self-management of radiation-induced bowel and bladder dysfunction in pelvic-cancer rehabilitation: an ethnographic study," *Journal of Clinical Nursing*, vol. 28, no. 13-14, pp. 2624–2634, 2019.

[4] J. A. Burns, A. B. Weiner, W. J. Catalona et al., "Inflammatory bowel disease and the risk of prostate cancer," *European Urology*, vol. 75, no. 5, pp. 846–852, 2019.

[5] T. J. Borody, G. D. Eslick, and R. L. Clancy, "Fecal microbiota transplantation as a new therapy: from Clostridioides difficile infection to inflammatory bowel disease, irritable bowel syndrome, and colon cancer," *Current Opinion in Pharmacology*, vol. 49, pp. 43–51, 2019.

[6] I. Mert, A. Kumar, D. Torres et al., "Should mucosal bowel invasion in ovarian cancer be assigned to FIGO stage IV disease?" *Gynecologic Oncology*, vol. 153, no. 2, pp. 238–241, 2019.

[7] C. Hoppenot, P. Peters, M. Cowan et al., "Malignant bowel obstruction due to uterine or ovarian cancer: are there differences in outcome?" *Gynecologic Oncology*, vol. 154, no. 1, pp. 177–182, 2019.

[8] W.-W. Tao, H. Jiang, X.-M. Tao, P. Jiang, L.-Y. Sha, and X.-C. Sun, "Effects of acupuncture, tuina, tai chi, qigong, and traditional Chinese medicine five-element music therapy on symptom management and quality of life for cancer patients: a meta-analysis," *Journal of Pain and Symptom Management*, vol. 51, no. 4, pp. 728–747, 2016.

[9] W. Tao, X. Luo, B. Cui et al., "Practice of traditional Chinese medicine for psycho-behavioral intervention improves quality of life in cancer patients: a systematic review and meta-analysis," *Oncotarget*, vol. 6, no. 37, pp. 39725–39739, 2015.

[10] C. Stevens, C. Vrinten, S. Smith, and J. Waller, "Acceptability of receiving lifestyle advice at cervical, breast and bowel cancer screening," *Preventive Medicine: An International Journal Devoted to Practice and Theory*, vol. 120, pp. 19–25, 2019.

[11] A. Kable, A. Baker, D. Pond, E. Southgate, A. Turner, and C. Levi, "Health professionals' perspectives on the discharge process and continuity of care for stroke survivors discharged home in regional Australia: a qualitative, descriptive study," *Nursing and Health Sciences*, vol. 21, no. 2, pp. 253–261, 2019.

[12] Y. H. Kao, W. T. Lin, W. H. Chen, S. C. Wu, and T. S. Tseng, "Continuity of outpatient care and avoidable hospitalization: a systematic review," *American Journal of Managed Care*, vol. 25, no. 4, pp. E126–E134, 2019.

[13] A. Macdonald, D. Adamis, T. Craig, and R. Murray, "Continuity of care and clinical outcomes in the community for people with severe mental illness," *The British Journal of Psychiatry*, vol. 214, no. 5, pp. 273–278, 2019.

[14] M. Hustoft, E. Biringer, S. Gjesdal, V. P. Moen, J. Abmus, and Ø. Hetlevik, "The effect of team collaboration and continuity of care on health and disability among rehabilitation patients: a longitudinal survey-based study from western Norway," *Quality of Life Research*, vol. 28, no. 10, pp. 2773–2785, 2019.

[15] H. G. Varnell and M. E. O'Connor, "Continuity of infant well care in a community health center resident clinic," *Journal of Community Health*, vol. 44, no. 1, pp. 143–148, 2019.

[16] C. Loranger and M.-J. Fleury, "Factors associated with perceived continuity of care among patients suffering from mental disorders," *Community Mental Health Journal*, vol. 56, no. 4, pp. 670–679, 2020.

[17] A. Cummins, R. Coddington, D. Fox, and A. Symon, "Exploring the qualities of midwifery-led continuity of care in Australia (MiLCCA) using the quality maternal and newborn care framework," *Women and Birth*, vol. 33, no. 2, pp. 125–134, 2020.

[18] G. Facchinetti, D. D'Angelo, M. Piredda et al., "Continuity of care interventions for preventing hospital readmission of older people with chronic diseases: a meta-analysis," *International Journal of Nursing Studies*, vol. 101, 2020.

[19] A. Lele, C. Cheever, L. Healey, K. Hurley, L. J. Kim, and C. J. Creutzfeldt, "Operationalization of the transition to comfort measures only in the neurocritical care unit: a quality improvement project," *American Journal of Hospice and Palliative Medicine*, vol. 36, no. 1, pp. 38–44, 2019.

[20] A. Stacy, K. Magdic, M. Rosenzweig, B. Freeman, and D. Verosky, "Improving Knowledge, comfort, and confidence of nurses providing end-of-life care in the hospital setting

through use of the CARES tools," *Journal of Hospice and Palliative Nursing*, vol. 21, no. 3, pp. 200–206, 2019.

[21] M. A. Bender, C. H. A. Andrilla, A. Holly et al., "Moral distress and attitudes about timing related to comfort care for hospitalized patients: a survey of inpatient providers and nurses," *American Journal of Hospice and Palliative Medicine*, vol. 36, no. 11, pp. 967–973, 2019.

[22] J. R. Linzey, J. F. Burke, J. L. Nadel et al., "Incidence of the initiation of comfort care immediately following emergent neurosurgical and endovascular procedures," *Journal of Neurosurgery*, vol. 131, no. 6, pp. 1725–1733, 2019.

[23] W. Santivasi, K. Wu, M. Litzow, T. LeBlanc, and J. Strand, "Palliative care physician comfort (and discomfort) with discussing prognosis in hematologic diseases: results of a nationwide survey (SA528B)," *Journal of Pain and Symptom Management*, vol. 57, no. 2, p. 454, 2019.

[24] J. M. Morrison, S. Wu, and H. H. Keller, "Beyond tube-feeding: relationship-centered, comfort care for individuals with eating challenges in dementia," *Journal of the American Geriatrics Society*, vol. 67, no. 1, pp. 185-186, 2019.

[25] T. Lane, D. Ramadurai, and J. Simonetti, "Public awareness and perceptions of palliative and comfort care," *The American Journal of Medicine*, vol. 132, no. 2, pp. 129–131, 2019.

Hindawi
Evidence-Based Complementary and Alternative Medicine
Volume 2022, Article ID 6581127, 5 pages
https://doi.org/10.1155/2022/6581127

Research Article

Diagnostic Value of Multislice Spiral Computed Tomography Combined with Serum AFP, TSGF, and GP73 Assay in the Diagnosis of Primary Liver Cancer

Chuanwen Yu and Chuang Sun

Department of Radiology, The Second Hospital of Dalian Medical University, Dalian 116004, Liaoning, China

Correspondence should be addressed to Chuang Sun; chuishisunsrv@163.com

Received 14 April 2022; Revised 6 May 2022; Accepted 16 May 2022; Published 7 June 2022

Academic Editor: Shangxiang Chen

Objective. To explore the diagnostic value of multislice spiral computed tomography (MSCT) scan combined with serum alpha-fetoprotein (AFP), tumor-specific growth factor (TSGF), and Golgi protein73 (GP73) assays in the diagnosis of primary liver cancer (PLC). *Methods*. Totally, 60 patients with PLC admitted to The Second Hospital of Dalian Medical University from January 2019 to January 2020 were included in group A, 60 patients with liver cirrhosis were included in group B, and 60 healthy subjects were included in group C. The serum AFP, TSGF, and GP73 levels were determined, and all participants received MSCT scanning. The diagnostic efficacy of MSCT, assays of serum AFP, TSGF, and GP73, and their combined detection was analyzed. *Results*. Group A had the highest levels of AFP, TSGF, and GP73, followed by group B, and then group C. The sensitivity, specificity, positive predictive value, and negative predictive value of MSCT for PLC were 80.0%,91.7%, 82.8%, and 90.2%, respectively, while those of combined detection of MSCT plus serum AFP, TSGF, and GP73 for PLC were 100.0%, 93.3%, 88.2%, and 100.0%. The combined detection was associated with significantly a higher detection rate of PLC versus stand-alone detection. *Conclusion*. MSCT plus serum AFP, TSGF, and GP73 has a higher detection rate versus stand-alone detection, which shows great potential in the diagnosis of PLC.

1. Introduction

The incidence of primary liver cancer (PLC) accounts for more than 50% of the total prevalence of liver cancer. The early stage of PLC is mostly asymptomatic, and the disease may have progressed to an advanced stage by the time of diagnosis where surgical outcomes are unfavorable [1, 2]. Thus, early diagnosis is crucial for the improvement of the prognosis of patients [3]. At present, diagnosis of PLC is mostly achieved by imaging examination, and multislice spiral computed tomography (MSCT) can clearly display the liver conditions, which is of high clinical application value [4, 5]. It was found that the detection rate of contrast-enhanced CT scans was about 80.0%, but its diagnostic efficiency might be compromised in the detection of small tumors, which requires additional diagnostic means to enhance the diagnostic accuracy [6, 7]. Tumor markers such as alpha-fetoprotein (AFP), tumor-specific growth factor (TSGF), and Golgi protein 73 (GP73) are commonly used for tumor diagnosis. AFP is commonly used for PLC diagnosis but is associated with poor sensitivity and specificity. Recent research has shown that the combined assay of AFP with other tumor markers might potentiate the diagnostic efficiency [8]. TSGF is a polypeptide secreted during the production and proliferation of malignant tumors, and its secretion mechanism is irrelevant to liver injuries caused by benign liver diseases such as liver cysts and cirrhosis [9]. Therefore, the determination of serum TSGF may facilitate the differentiation between PLC and liver cirrhosis. GP73 is a transmembrane protein of the Golgi apparatus and is rarely detected in the liver cells of healthy people. The elevation of its expression indicates cancerous changes of liver cells [10]. The serum levels of GP73 increase with the severity of liver inflammatory responses, but not significantly. The

Table 1: Comparison of baseline characteristics.

Group	Group A ($n = 60$)	Group B ($n = 60$)	Group C ($n = 60$)	P value
Gender (male/female)	35/25	34/26	33/27	>0.05
Age (year)	53.26 ± 5.11	53.24 ± 5.26	53.20 ± 5.21	
Income (¥)				>0.05
<3000	25	26	27	
≥3000	35	34	33	
Education level				>0.05
High school or below	20	21	19	
College or above	40	39	41	
Drinking	28	27	29	>0.05
BIM over standard	4	5	2	>0.05

combination of AFP, TSGF, and GP73 contributes to a higher diagnostic efficiency for PLC [11]. Accordingly, this study was conducted to explore the diagnostic value of MSCT plus serum AFP, TSGF, and GP73 levels in PLC.

2. Materials and Methods

2.1. General Materials. Totally 60 patients with PLC admitted to The Second Hospital of Dalian Medical University from January 2019 to January 2020 were included in group A, 60 patients with liver cirrhosis were included in group B, and 60 healthy subjects were included in group C. There were no significant differences between the three groups in terms of baseline characteristics ($P > 0.05$), as shown in Table 1.

2.2. Inclusion Criteria. The inclusion criteria were as follows: (1) participants and their family members fully understood the research procedures and signed the informed consent. (2) patients of group A were diagnosed with PLC by surgery or biopsy; (3) patients of group B were confirmed with cirrhosis after the examination.

2.3. Exclusion Criteria. Exclusion criteria were as follows: (1) patients with mental illness that prevented normal communication; (2) with other organic diseases; (3) who were in pregnancy or lactation.

2.4. Methods. This study was approved by the ethics committee of The Second Hospital of Dalian Medical University. All the methods were carried out per the Declaration of Helsinki [12].

(1) Detection of serum AFP, TSGF, and GP73 levels: 3 ml of morning fasting venous blood was collected from the patients and centrifuged to obtain the serum. The serum AFP was determined using the electrochemiluminescence method (Cobase 411 electrochemical luminescence device with original auxiliary reagent, Approval No. 3402843 2011), with the range of markers given on the kit as the normal range. The serum TSGF was determined using the colorimetric method (Tai'an City Kangyu Medical Equipment Co. Ltd., Approval No. 2400498). The serum GP73 was determined using the enzyme-linked immunoassay (Beijing Kewei Clinical Diagnostic Reagents Co., Ltd., S20060028). Positive determination of content: serum AFP ≥ 20 ng/mL, TSGF ≥ 70 U/mL, GP73 ≥ 80 ng/mL [13].

(2) MSCT scan: patients were required to lie supine, a 64-row helical CT scanner (Philips, drug safety food machinery into the word no. 3303600 2008) was used for scanning. The scanning parameters were pitch of 1.5, scanning thickness of 0.5 cm, transverse reconstruction thickness of 0.2 cm, current of 160 mA, and voltage of 120 kV. A plain CT scan was performed from the diaphragm to the lower margin of the phalangeal joint. After scanning, 100 mL of iohexol contrast agent was injected at a rate of 2.5–3.0 ml/s, followed by scanning 25 s after injection for the arterial phase and 30 s after injection for the venous phase. The examination results were interpreted independently by two radiologists, and consensus was made after discussion with a third radiologist in the event of discrepancies.

2.5. Observation Criteria. (1) The levels of AFP, TSGF, and GP73 of the participants were analyzed. (2) The diagnostic efficiency of MSCT was analyzed. (3) The diagnostic efficiency of AFP, TSGF, and GP73 was analyzed. (4) The diagnostic efficiency of combined detection was analyzed.

Diagnostic efficacy includes (1) sensitivity: the ratio of positive cases in group A to the total in that group. (2) Specificity: the ratio of (number of negative cases in group B + number of negative cases in group C) to (total number of cases in group B + total number of cases in group C). (3) Positive predictive value: the ratio of the number of positive cases in group A to (number of positive cases in groups A, B, and C). (4) Negative predictive value: the ratio of (number of negative cases in group B + number of negative cases in group C) to (number of negative cases in groups A, B, and C).

2.6. Statistical Analysis. SPSS20.0 was used for data analyses, and GraphPad Prism 7 (GraphPad Software, San Diego, USA) was to plot the graphics. The counting data are analyzed using the chi-square test, and the measurement data are analyzed using the t-test. Statistically significant results were defined as $P < 0.05$.

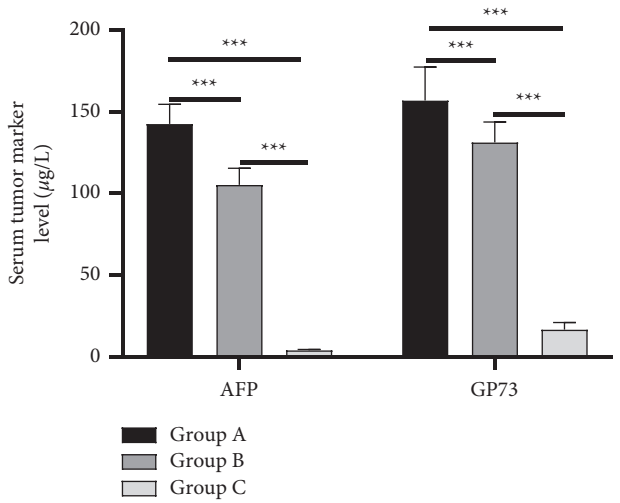

Figure 1: Analysis of AFP and GP73 levels ($\overline{x} \pm s$, μg/L). The horizontal axis from left to right was AFP and GP73, and the vertical axis referred to the level of serum tumor markers (μg/L); the black area in the figure was group A the dark gray indicated group B and the light gray area was for group C. The level of AFP was (142.56 ± 12.10) μg/L in group A, (105.26 ± 10.23) μg/L in group B, and (3.89 ± 0.56) μg/L in group C; the level of GP73 was (156.89 ± 20.56) μg/L in group A, (131.20 ± 12.48) μg/L in group B, and (16.58 ± 4.26) μg/L in group C; $^{***}P < 0.001$.

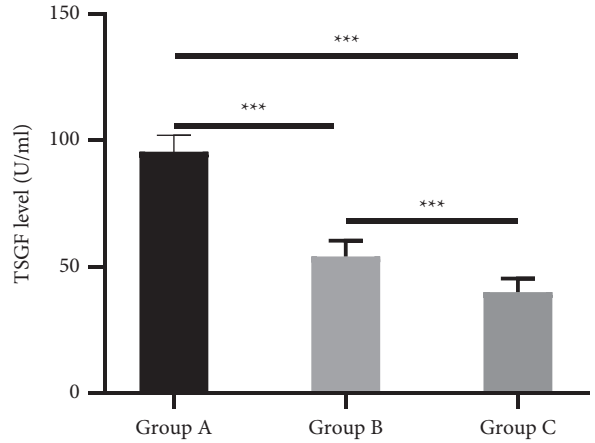

Figure 2: Analysis of TSGF level ($\overline{x} \pm s$,U/ml). The horizontal axis from left to right was group A group B and group C, respectively, and the vertical axis indicated TSGF level (U/ml). The level of TSGF was (95.56 ± 6.56) U/ml in group A, (54.11 ± 6.26) U/ml in group B, and (39.89 ± 5.48) U/ml in group C; $^{***}P < 0.001$.

3. Results

3.1. Analysis of AFP, TSGF, and GP73 Levels. Group A had the highest levels of AFP, TSGF, and GP73, followed by group B, and then group C ($P < 0.001$), as shown in Figures 1 and 2.

3.2. Analysis of Diagnostic Efficiency of Multislice Spiral CT Scanning. The sensitivity, specificity, positive predictive value, and negative predictive value of MSCT were 80.0% (48/60), 91.7% (110/120), 82.8% (48/58), and 90.2% (110/122), respectively, as shown in Table 2.

Table 2: Analysis of diagnostic efficiency of multislice spiral CT scanning.

Multislice CT	Pathologic examination		Total
	Positive	Negative	
Positive	48	10	58
Negative	12	110	122
Total	60	120	180

3.3. Diagnostic Efficacy of Serum AFP, TSGF, and GP73. The diagnostic efficiency of serum AFP, TSGF, and GP73 is shown in Table 3.

3.4. Diagnostic Efficacy of Combined Detection. The sensitivity, specificity, positive predictive value, and negative predictive value of multislice spiral CT combined with serum AFP, TSGF, and GP73 were 100.0%, 93.3%, 88.2%, and 100.0%, respectively. The combined detection was associated with significantly a higher detection rate of PLC versus stand-alone detection ($P < 0.05$), as shown in Table 4.

4. Discussion

Imaging examination and tumor marker detection are the main methods for PLC diagnosis, but their detection efficiency for small tumors was unsatisfactory [14].

AFP is a serum glycogen protein and its level reaches a peak in the fetal period and declines after delivery. However, injuries and cancerous changes in liver cells can upregulate the expression of AFP [15]. Therefore, the detection of serum AFP levels may contribute to better PLC diagnostic efficiency [16]. However, recent studies found that AFP lacked sensitivity in the diagnosis of early PLC with a high false-positive rate, which compromised its clinical value [17, 18]. In the present study, the sensitivity and specificity of AFP detection for PLC were 66.7% and 70.0%, respectively, which were consistent with the previous research results [19].

TSGF is a polypeptide and exists in the peripheral blood at the early stage of tumor generation [20]. Accordingly, its expression levels in the serum are associated with tumor development. GP73 is a transmembrane glycoprotein that belongs to bile duct epithelial cells in normal tissues [21]. It participates in the inflammatory responses in the body and exerts a great impact on the protein stability of patients [22]. The results of the present study showed that the level of GP73 in patients with PLC was significantly higher than that in healthy people, and the sensitivity of GP73 for PLC was 83.3%, indicating a positive role of GP73 in PLC diagnosis.

TSGF is present in the serum of patients with early-stage PLC and can discriminate tumor properties. Both GP73 and AFP are sensitive to PLC, so the combined detection efficiency is superior to that of stand-alone detection. The sensitivity, specificity, positive predictive value, and negative

Table 3: Diagnostic efficacy of serum AFP, TSGF, and GP73.

	Sensitivity (%)	Specificity (%)	Positive predictive value (%)	Negative predictive value (%)
AFP	66.7 (40/60)	70.0 (84/120)	52.6 (40/76)	80.8 (84/104)
TSGF	63.3 (38/60)	75.0 (90/120)	55.9 (38/68)	80.4 (90/112)
GP73	83.3 (50/60)	81.7 (98/120)	69.4 (50/72)	90.7 (98/108)

The sensitivity, specificity, positive predictive value and negative predictive value of MSCT combined with serum AFP, TSGF and GP73 were 100.0% (60/60), 93.3% (112/120), 88.2% (60/68) and 100.0% (112/112), respectively.

Table 4: Diagnostic efficiency of combined detection of tumor markers.

	Sensitivity (%)	Specificity (%)	Positive predictive value (%)	Negative predictive value (%)
AFP + TSGF	70.0 (42/60)	75.0 (90/120)	58.3 (42/72)	83.3 (90/108)
AFP + GP73	85.0 (51/60)	75.0 (90/120)	63.0 (51/81)	90.9 (90/99)
GP73 + TSGF	83.3 (50/60)	78.3 (94/120)	65.8 (50/76)	90.4 (94/104)
AFP + TSGF + GP73	90.0 (54/60)	80.0 (96/120)	69.2 (54/78)	94.1 (96/102)
AFP + TSGF + GP73 + MSCT	100.0 (60/60)	93.3 (112/120)	88.2 (60/68)	100.0 (112/112)

predictive value of TSGF, GP73, and AFP were 90.0 (54/60), 80.0 (96/120), 69.2 (54/78), and 94.1 (96/102), respectively, indicating that the combined detection of tumor markers produced a favorable diagnostic yield.

The main blood supply source of healthy liver tissue is the portal vein, while that of PLC patients is the hepatic artery [23]. With blood circulation, the liver cancer lesions of patients gradually disperse, and the diffusion rate of cancer cells rapidly increases through blood metastasis. Multilayer spiral CT scans can clearly visualize the liver lesions of PLC patients [24]. In the present study, contrast-enhanced scanning was performed to compensate for the insufficiency of the original plain scanning, and the sensitivity and specificity of MSCT were 80.0% and 91.7%, respectively, which confirmed the high diagnostic efficiency of MSCT. The sensitivity, specificity, positive predictive value, and negative predictive value of multislice spiral CT combined with serum AFP, TSGF, and GP73 were 100.0%, 93.3%, 88.2%, and 100.0%, respectively. The combined detection was associated with significantly a higher detection rate of PLC versus stand-alone detection ($P < 0.05$), which was in line with the research results of Poynard T [25]. The sensitivity of multislice spiral CT scan combined with serum AFP, TSGF, and GP73 detection was 98.3% (118/120), proving that the combined detection could increase the early detection rate of PLC. However, this study still has the following deficiencies. First, this study is a single-center study without a blind method, which is prone to researcher bias. Secondly, this study is a cross-sectional diagnostic study, and the relationship between the dynamic changes in the above indicators and the severity and prognosis of primary liver cancer remains unclear. Future studies are to include more cases with long-term follow-up of relevant markers to systematically reflect changes in these markers during disease onset and progression and to provide a more accurate basis for prognosis prediction.

5. Conclusion

MSCT plus serum AFP, TSGF, and GP73 has a higher detection rate versus stand-alone detection, which shows great potential in the diagnosis of PLC.

Data Availability

All the data generated or analyzed during this study are included in this published article.

Ethical Approval

This study was approved by the Ethics Committee of The Second Hospital of Dalian Medical University. All the methods were carried out in accordance with the Declaration of Helsinki.

Consent

The research subjects or their family members have fully recognized research procedures and signed the informed consents.

Conflicts of Interest

The authors declare that they have no conflicts of interest.

References

[1] A. K. Ram, B. Pottakat, and B. Vairappan, "Increased systemic zonula occludens 1 associated with inflammation and independent biomarker in patients with hepatocellular carcinoma," *BMC Cancer*, vol. 18, no. 1, p. 572, 2018.

[2] N. Tsuchiya, Y. Sawada, I. Endo, K. Saito, Y. Uemura, and T. Nakatsura, "Biomarkers for the early diagnosis of hepatocellular carcinoma," *World Journal of Gastroenterology*, vol. 21, no. 37, pp. 10573–10583, 2015.

[3] W. K. Jeong, N. Jamshidi, E. R. Felker, S. S. Raman, and D. S. Lu, "Radiomics and radiogenomics of primary liver cancers," *Clinical and Molecular Hepatology*, vol. 25, no. 1, pp. 21–29, 2019.

[4] L. A. Daamen, V. P. Groot, H. D. Heerkens, M. P. W. Intven, H. C. van Santvoort, and I. Q. Molenaar, "Systematic review on the role of serum tumor markers in the detection of recurrent pancreatic cancer," *International Hepato-Pancreato-Biliary Association*, vol. 20, no. 4, pp. 297–304, 2018.

[5] M. Sojoodi, L. Wei, D. J. Erstad et al., "Epigallocatechin gallate induces hepatic stellate cell senescence and attenuates development of hepatocellular carcinoma," *Cancer Prevention Research*, vol. 13, no. 6, pp. 497–508, 2020.

[6] W. Guo, Y. Pang, L. Yao et al., "Imaging fibroblast activation protein in liver cancer: a single-center post hoc retrospective analysis to compare [68Ga] Ga-FAPI-04 PET/CT versus MRI and [18F]-FDG PET/CT," *European Journal of Nuclear Medicine and Molecular Imaging*, vol. 48, no. 5, pp. 1604–1617, 2021.

[7] T. Millard, A. Gupta, C. Brenin, P. Marshall, and P. Dillon, "Radiographically occult carcinomatous spread of breast cancer to the liver: a challenging case," *Case Reports in Oncological Medicine*, vol. 2019, Article ID 4935615, 5 pages, 2019.

[8] S. Hirose, K. Ishige, M. Yamaura et al., "A case report: long-term complete response of metastatic hepatocellular carcinoma obtained after discontinuation of 2-month sorafenib monotherapy," *Clin J Gastroenterol*, vol. 13, no. 5, pp. 902–906, 2020.

[9] T. Aboushousha, S. Mamdouh, H. Hamdy et al., "Immunohistochemical and biochemical expression patterns of TTF-1, RAGE, GLUT-1 and SOX2 in HCV-associated hepatocellular carcinomas," *Asian Pacific Journal of Cancer Prevention*, vol. 19, no. 1, pp. 219–227, 2018.

[10] T. Wakabayashi, F. Ouhmich, C. Gonzalez-Cabrera et al., "Radiomics in hepatocellular carcinoma: a quantitative review," *Hepatol Int*, vol. 13, no. 5, pp. 546–559, 2019.

[11] Y. Zhang, Z. Liu, K. Ji et al., "Clinical application value of circulating cell-free DNA in hepatocellular carcinoma," *Frontiers in Molecular Biosciences*, vol. 8, Article ID 736330, 2021.

[12] World Medical Association, "World Medical Association Declaration of Helsinki: ethical principles for medical research involving human subjects," *JAMA*, vol. 310, no. 20, pp. 2191–2194, 2013.

[13] X. Zhang and Z. Chen, "Tumor-specificity growth factor combined with tumor markers in nuclear medicine imaging to identify prostate cancer osteonosus," *Journal of Healthcare Engineering*, vol. 2021, Article ID 7380120, 9 pages, 2021.

[14] A. E. El-Sisi, S. S. Sokar, H. A. Ibrahim, and S. E. Abu-Risha, "Enhanced anticancer activity of combined treatment of imatinib and dipyridamole in solid Ehrlich carcinoma-bearing mice," *Naunyn-Schmiedeberg's Archives of Pharmacology*, vol. 393, no. 6, pp. 1113–1129, 2020.

[15] M. Taniai, E. Hashimoto, M. Tobari et al., "Clinicopathological investigation of steatohepatitic hepatocellular carcinoma: a multicenter study using immunohistochemical analysis of adenoma-related markers," *Hepatology Research*, vol. 48, no. 12, pp. 947–955, 2018.

[16] F. Kanwal, J. R. Kramer, S. Mapakshi et al., "Risk of hepatocellular cancer in patients with non-alcoholic fatty liver disease," *Gastroenterology*, vol. 155, no. 6, pp. 1828–1837.e2, 2018.

[17] P. S. Harris, R. M. Hansen, M. E. Gray, O. I. Massoud, B. M. McGuire, and M. G. Shoreibah, "Hepatocellular carcinoma surveillance: an evidence-based approach," *World Journal of Gastroenterology*, vol. 25, no. 13, pp. 1550–1559, 2019.

[18] A. J. Weaver, R. Stafford, J. Hale, D. Denning, J. R. Sanabria, and GBD Collaborators, "Geographical and temporal variation in the incidence and mortality of hepato-pancreato-biliary primary malignancies:1990-2017," *Journal of Surgical Research*, vol. 245, pp. 89–98, 2020.

[19] M. Spadaccini, A. Lleo, R. Ceriani et al., "Alpha-fetoprotein screening in patients with hepatitis C-induced cirrhosis who achieved a sustained virologic response in the direct-acting antiviral agents era," *Hepatobiliary and Pancreatic Diseases International*, vol. 17, no. 6, pp. 570–574, 2018.

[20] E. Ha, F. Kim, J. Blanchard, and H. S. Juon, "Prevalence of chronic hepatitis B and C infection in Mongolian immigrants in the Washington, District of Columbia, metropolitan area, 2016–2017," *Preventing Chronic Disease*, vol. 16, Article ID 180104, 2019.

[21] O. Golubnitschaja, J. Polivka Jr, K. Yeghiazaryan, and L. Berliner, "Liquid biopsy and multiparametric analysis in management of liver malignancies: new concepts of the patient stratification and prognostic approach," *The EPMA Journal*, vol. 9, no. 3, pp. 271–285, 2018.

[22] G. Duininck, A. G. Lopez-Aguiar, R. M. Lee et al., "Optimizing cancer care for hepatocellular carcinoma at a safety-net hospital: the value of a multidisciplinary disease management team," *Journal of Surgical Oncology*, vol. 20, no. 8, pp. S81–S82, 2018.

[23] A. Turcanu, E. Pitel, V. T. Dumbrava et al., "Profile of hepatocellular carcinoma in the Republic of Moldova: first-hand information on the presentation, distribution and etiologies," *Romanian Journal of Internal Medicine*, vol. 57, no. 1, pp. 37–46, 2019.

[24] T. M. Drake and T. G. Bird, "Editorial: simplifying screening for primary liver cancer - do the LCR1 and LCR2 tests hold the key?" *Alimentary Pharmacology & Therapeutics*, vol. 49, no. 5, pp. 612-613, 2019.

[25] F. Yang, L. Shi, T. Liang et al., "Anti-tumor effect of evodiamine by inducing Akt-mediated apoptosis in hepatocellular carcinoma," *Biochemical and Biophysical Research Communications*, vol. 485, no. 1, pp. 54–61, 2017.

Hindawi
Evidence-Based Complementary and Alternative Medicine
Volume 2022, Article ID 9483762, 5 pages
https://doi.org/10.1155/2022/9483762

Research Article

The Effect of Comfort Care on Postoperative Quality of Life, Psychological Status, and Satisfaction of Pancreatic Cancer Patients

Yingliang Miao

Department of Gastroenterology, Hai'an People's Hospital, Nantong, China

Correspondence should be addressed to Yingliang Miao; miaobashahe244@163.com

Received 18 April 2022; Revised 6 May 2022; Accepted 20 May 2022; Published 30 May 2022

Academic Editor: Shangxiang Chen

Objective. To evaluate the effect of comfort care on postoperative quality of life, psychological status, and satisfaction of pancreatic cancer patients. *Methods*. From June 2019 to March 2021, 136 pancreatic cancer patients undergoing pancreatectomy in Hai'an People's Hospital were recruited and randomly assigned via the random number table method at a ratio of 1 : 1 to receive either conventional care (control group) or comfort care (study group), with 68 cases in each group. *Results*. Before the intervention, the two groups had similar visual analog scale (VAS) scores, the Medical Outcomes Study 36-Item Short-Form Health Survey (SF-36) scores, and psychological status scores. The study group resulted in a significantly lower VAS score than the control group. The study group required a lower dose of analgesics than the control group. After the intervention, the study group showed significantly higher scores in social functioning, role emotional, mental health, role physical, and bodily pain than the control group. The study group had significantly lower Self-Rating Anxiety Scale (SAS) and Self-Rating Depression Scale (SDS) scores than the control group. The study group showed a significantly lower incidence of complications and a higher satisfaction rate than the control group. *Conclusion*. Comfort care effectively alleviates the pain of patients after pancreatectomy, reduces the incidence of complications, and improves their quality of life, psychological status, and satisfaction, so it is worthy of clinical application.

1. Introduction

Pancreatic cancer is a common tumor of the gastrointestinal tract with a high degree of malignancy [1, 2]. Its clinical manifestations vary depending on the lesion site, disease course, metastasis, and adjacent organ involvement, and common symptoms include upper abdominal discomfort or abdominal pain, abdominal mass and ascites, jaundice, and weakness [3]. With insidious early symptoms, rapid progression, high surgical mortality, low cure rate, and poor survival, pancreatic cancer is considered one of the malignant tumors with the worst prognosis. According to the Lancet, the five-year survival of pancreatic cancer after diagnosis is only about 10% [4]. Moreover, a report from the World Health Organization (WHO) in 2012 showed that the global prevalence and mortality rate of pancreatic cancer ranked 13th and 7th in malignant tumors, respectively [5], and data from the National Cancer Center of China showed that the incidence and mortality rate of pancreatic cancer ranked 10th and 6th in malignant tumors in 2019, respectively, with a male-to-female ratio of 1.5–2 : 1 [6]. Currently, surgical resection is the clinical radical treatment for pancreatic cancer. However, a large body of evidence shows a poor surgical outcome and unfavorable five-year postoperative survival.

It has been confirmed that surgical outcomes could be ameliorated by efficient postoperative care interventions. Comfort care [7] is a new and effective nursing modality providing physiological and psychological care to enhance patient comfort and satisfaction [8, 9]. It includes care in the postural comfort to prevent compression of nerves and blood vessels, environmental comfort to help the patient maintain a positive treatment attitude, temperature and humidity management to ensure physical comfort [10], and active communication and psychological guidance to eliminate negative emotions [11]. Different from the traditional nursing

concept, comfort care focuses on the mitigation of patients' unpleasantness and psychological disorders management of patients in treatment. However, the nursing efficiency of comfort care for postpancreatectomy patients is marginally explored. Accordingly, this study was undertaken to evaluate the effect of comfort care on postoperative quality of life, psychological status, and satisfaction of pancreatic cancer patients to provide a reference for the clinical postoperative care of pancreatic cancer patients.

2. Materials and Methods

2.1. Participants. Between June 2019 and March 2021, 136 patients with pancreatic cancer (77 males and 59 females, aged 26–71 years, mean age of 42.89 ± 5.08 years) undergoing pancreatectomy in our hospital were recruited and assigned via the random number table method at a ratio of 1 : 1 to receive either conventional care (control group) or comfort care (study group), with 68 patients in each group The research was approved by the Ethics Committee of Hai'an People's Hospital (97770/1)

2.2. Inclusion and Exclusion Criteria. Patients who met the diagnostic criteria for pancreatic cancer after examinations; who underwent pancreatectomy in our hospital; and who provided written informed consent were included in the present study.

Patients with serious dysfunction of the heart, liver, and kidney; with psychiatric diseases or unconsciousness; and who revoked their consent were excluded.

2.3. Treatment. Patients in the control group received conventional care, including monitoring of vital signs, instructions on antibiotics use, hemostatic and analgesic drugs administration, observation of the properties and color of drains, and timely management of other medical conditions such as hemorrhage. One day postoperatively, nursing staff helped patients perform out-of-bed activities and provided discharge instructions and postdischarge follow-up.

Patients in the study group received comfort care. (1) Environmental care: the ward was maintained quiet, and the temperature, humidity, and light in the ward were regulated to provide the patients with a good recovery environment. (2) Psychological care: patients may experience psychological pressure and anxiety after surgery due to postoperative pain and fear of disease recurrence, so the psychological changes in patients were closely monitored. Targeted psychological care protocols were developed according to each patient's situation for the management of psychological disorders of patients. (3) Social comfort care: the nursing staff actively communicated with the patient's family members and timely informed them of the patient's physical and psychological condition, which contributed to potentiating the psychological care efficiency and helped the patients strengthen their treatment confidence. (4) Postoperative comfort care: patients with severe pain were given intramuscular injections of analgesics intermittently, and analgesic pumps were used when necessary. The patients were also given dietary guidance and were advised to follow a high-calorie, high-protein diet, low-fat, and low-salt diet after surgery to ensure a balanced intake of nutrients. The nursing staff closely monitored the changes in patients' vital signs and drainage fluid and timely informed the doctors of any abnormalities, so as to maximize the physical and mental comfort of patients after surgery.

2.4. Outcome Measures

(1) Patients' pain level was rated using the visual analog scale (VAS) with a score of 0–10 points [12]. A score of ≤3 points indicated mild pain with no effect on daily life, 4–6 points indicated moderate pain that was tolerable, and ≥7 points indicated severe pain that was unbearable. The scores were proportional to the degree of pain, and the use of analgesics in the two groups was recorded in detail and compared.

(2) The patients' quality of life was assessed using the MOS 36-Item Short-Form Health Survey (SF-36) [13], which was divided into physical health (physical functioning, role physical, bodily pain, general health) and psychological health (vitality, social functioning, role emotional, mental health). Each domain had a total score of 100 points, and higher scores indicated better quality of life of patients.

(3) The patients' negative emotions were assessed using the Self-Rating Anxiety Scale (SAS) and the Self-Rating Depression Scale (SDS) [14], both with a total score of 100 points. For SAS, a score of 50–70 points indicated mild anxiety, 71–90 points indicated moderate anxiety, and >90 points indicated severe anxiety. For SDS, a score of 53–62 points indicated mild depression, 63–72 points indicated moderate depression, and 72 points or more indicated severe depression. The higher the score, the more severe the patient's anxiety and depression.

(4) The complications of the two groups were recorded in detail, including infection, pressure sores, oral ulcers, and venous thrombosis. The total incidence of complications in the two groups was calculated and compared.

(5) The "Nursing Satisfaction Questionnaire" was adopted for nursing satisfaction evaluation including three items, namely, the attitude of medical staff, nursing efficiency, and disease education. The questionnaire was designed by our hospital, and the result was divided into four levels (highly satisfied, satisfied, less satisfied, and dissatisfied) to obtain the satisfaction of patients in both groups with Cronbach's α of 0.921.

2.5. Statistical Analysis. GraphPad Prism 8 software was used to plot the graphics, and SPSS22.0 software was used for data analyses. Count data are expressed as n (%) and analyzed using the chi-square test, and measurement data are

Table 1: Comparison of baseline patient profile.

	Control group ($n = 68$)	Study group ($n = 68$)	t/χ^2	P
Gender (male/female)	30/38	39/29	2.383	0.123
Age ($\overline{x} \pm s$, years)	43.03 ± 4.87	42.65 ± 5.61	0.422	0.674
Disease duration	2.23 ± 0.71	2.37 ± 0.58	1.259	0.210
Pathological type			0.127	0.938
HDA	24	26		
MDA	25	24		
DCC	19	18		

Note. HDA = highly differentiated adenocarcinoma, MDA = moderately differentiated adenocarcinoma, DCC = ductal cell carcinoma.

expressed as mean ± standard deviation and analyzed using Student's t-test. Differences were considered statistically significant at $P < 0.05$.

3. Results

3.1. Baseline Patient Profile. The baseline characteristics of the control group (38 males and 30 females, aged 26–71 years, mean age of 43.03 ± 4.87 years, disease duration of 1–4 years, mean disease duration of 2.23 ± 0.71 years, 24 cases of highly differentiated adenocarcinoma, 25 cases of moderately differentiated adenocarcinoma, and 19 cases of ductal cell carcinoma) were comparable with those of the study group (39 males and 29 females, aged 28–70 years, mean age of 42.65 ± 5.61 years, disease duration of 1–4 years, mean disease duration of 2.37 ± 0.58 years, 26 cases of highly differentiated adenocarcinoma, 24 cases of moderately differentiated adenocarcinoma, and 18 cases of ductal cell carcinoma) ($P > 0.05$) (Table 1).

3.2. VAS Scores and Analgesic Use. Before the intervention, the two groups had similar VAS scores ($P > 0.05$). After intervention, the study group had a significantly lower VAS score (2.17 ± 0.31) than the control group (6.51 ± 0.98) ($P < 0.05$) (Table 2). The medication rate was 70.59% (48/68) in the control group and 35.29% (24/68) in the study group. The study group required a lower dose of analgesics than the control group ($P < 0.05$) (Table 3).

3.3. Quality of Life. Before intervention, the two groups had similar SF-36 scores ($P > 0.05$). After intervention, the study group showed significantly higher scores of social functioning, role emotional, mental health, role physical, and bodily pain (84.02 ± 9.88, 83.29 ± 10.03, 81.94 ± 10.46, 83.82 ± 11.61, and 82.48 ± 10.14) than the control group (73.41 ± 13.54, 70.46 ± 11.52, 72.17 ± 10.45, 73.99 ± 14.51, and 71.98 ± 12.12) ($P < 0.05$) (Table 4).

3.4. Psychological Status. Before intervention, the two groups showed comparable psychological status scores ($P > 0.05$). After treatment, the study group had significantly lower SAS and SDS scores (46.08 ± 4.45 and 49.95 ± 4.02) than the control group (55.21 ± 5.89 and 58.48 ± 6.17) ($P < 0.05$) (Table 5).

Table 2: Comparison of VAS scores ($\overline{x} \pm s$).

	Before intervention	After intervention
Control group ($n = 68$)	8.03 ± 1.11	6.51 ± 0.98
Study group ($n = 68$)	7.98 ± 1.32	2.17 ± 0.31
t	0.239	34.818
P	0.811	<0.001

3.5. Complications. In the study group, there were 3 cases of infections, 1 case of pressure sores, and 1 case of oral ulcers, with an incidence of 7.35% (5/68). In the control group, there were 8 cases of infections, 6 case of pressure sores, 4 cases of oral ulcers, and 3 cases of venous thrombosis with an incidence of 30.88% (21/68). The study group was associated with a significantly lower incidence of complications than the control group (Table 6).

3.6. Satisfaction Rate. In the study group, there were 32 cases of highly satisfied, 33 cases of satisfied, 2 cases of less satisfied, and 1 case of dissatisfied, with a satisfaction rate of 98.53% (67/68). In the control group, there were 18 cases of highly satisfied, 24 cases of satisfied, 19 cases of less satisfied, and 7 cases of dissatisfied, with a satisfaction rate of 89.71% (61/68). The study group showed a higher satisfaction rate than the control group ($P < 0.05$) (Table 7).

4. Discussion

Pancreatic cancer is a common malignant tumor of the gastrointestinal tract, with the clinical characteristics of short disease duration and rapid progression. Currently, pancreatectomy is a well-recognized radical treatment, but it is associated with a high perioperative mortality rate of patients [15]. It has been demonstrated that the amelioration of poor surgical outcomes could be achieved by incorporating effective care after pancreatic cancer surgery, but specific care methods are still inconclusive. Comfort care is an effective nursing modality that maintains the continuity and coordination of care and assists patients to master self-care skills, which boosts recovery and improves the quality of life of patients [16]. Taemin et al. stated that comfort care contributes to improving clinical outcomes and reducing the incidence of postoperative complications in pancreatic cancer patients. Accordingly, this study aims to analyze the effects of comfort care on the quality of life, psychological status, and nursing satisfaction of postoperative pancreatic

Table 3: Comparison of analgesic use (n, (%)).

	Dezocine	Flurbiprofen axetil	No medicine	Medication rate
Control group ($n = 68$)	23	25	20	48 (70.59)
Study group ($n = 68$)	11	13	44	24 (35.29)
χ^2				17.00
P				<0.001

Table 4: Comparison of SF-36 scores ($\overline{x} \pm s$).

		Control group ($n = 68$)	Study group ($n = 68$)	t	P
Social functioning	Before	62.87 ± 10.85	63.01 ± 10.64	0.076	0.940
	After	73.41 ± 13.54*	84.02 ± 9.88*	5.220	<0.001
Role emotional	Before	65.65 ± 12.37	65.54 ± 11.17	0.054	0.957
	After	70.46 ± 11.52*	83.29 ± 10.03*	6.926	<0.001
Mental health	Before	63.45 ± 12.03	63.78 ± 11.72	0.162	0.872
	After	72.17 ± 10.45*	81.94 ± 10.46*	5.449	<0.001
Role physical	Before	62.41 ± 10.95	62.74 ± 10.21	0.182	0.856
	After	73.99 ± 14.51*	83.82 ± 11.61*	4.362	<0.001
Bodily pain	Before	62.87 ± 10.33	62.62 ± 10.34	0.141	0.888
	After	71.98 ± 12.12*	82.48 ± 10.14*	5.479	<0.001

Note. *indicates $P < 0.05$ between before and after intervention in the same group.

Table 5: Comparison of SAS and SDS scores ($\overline{x} \pm s$).

	SAS scores		SDS scores	
	Before	After	Before	After
Control group ($n = 68$)	65.84 ± 8.23	55.21 ± 5.89	64.98 ± 6.78	58.48 ± 6.17
Study group ($n = 68$)	66.07 ± 7.88	46.08 ± 4.45	64.73 ± 6.98	49.95 ± 4.02
t	0.166	10.199	0.212	9.552
P	0.868	<0.001	0.832	<0.001

Table 6: Comparison of complications (n, (%)).

	Infections	Pressure sores	Oral ulcers	Venous thrombosis	Incidence
Control group ($n = 68$)	8	6	4	3	21 (30.88)
Study group ($n = 68$)	3	1	1	0	5 (7.35)
χ^2			12.173		
P			<0.001		

Table 7: Comparison of satisfaction (n, (%)).

	Highly satisfied	Satisfied	Not very satisfied	Dissatisfied	Satisfaction rate
Control group ($n = 68$)	18	24	19	7	61 (89.71)
Study group ($n = 68$)	32	33	2	1	67 (98.53)
χ^2					4.781
P					0.029

cancer patients to provide a reference for clinical practice [17].

The causes of postoperative pain in pancreatic cancer include psychological factors, misplaced drains, environmental influences, postoperative infection, and mechanical irritation. In the present study, patients receiving comfort care showed a significantly lower VAS score and required a lower dose of analgesics than those receiving conventional care, indicating milder pain in patients given comfort care than those receiving conventional care. The reason may be that comfort care effectively relieves the pain of patients through disease education, psychological guidance, and medication instruction and helps patients have a correct understanding of their condition, thereby reducing the use of analgesics [18]. Moreover, comfort care herein resulted in a better quality of life for patients and lower SAS and SDS scores than conventional care, indicating better quality of life benefits and psychological status management of patients. Conventional care focuses more on disease care yet overlooks the physiological and psychological needs of patients. By contrast, comfort care is a new patient-centered nursing model that satisfies patients' physical and psychological

needs in addition to the treatment of disease. Therefore, the quality of life and psychological status of patients were better after comfort care than after conventional care, which is similar to the findings of Nikio et al. [19]. Besides, comfort care was associated with a significantly lower incidence of complications and a higher nursing satisfaction than conventional care. The reason may be that comfort care requires a three-step approach to drug relief for patients with postoperative pain and enhanced skin and oral care, thereby effectively preventing complications such as oral ulcers and pressure sores [20]. Furthermore, comfort care provides environmental care, meticulous psychological care, social comfort care, and physical comfort care to efficiently alleviate patients' pain and improve their quality of life and psychological status, resulting in fewer complications and high patient satisfaction.

5. Conclusion

Comfort care effectively alleviates the pain of patients after pancreatectomy, reduces the incidence of complications, and improves their quality of life, psychological status, and satisfaction, so it shows good potential for clinical application.

Data Availability

All data generated or analyzed during this study are included in this published article.

Disclosure

This research did not receive any specific grant from funding agencies in the public, commercial, or not-for-profit sectors.

Conflicts of Interest

The authors declare that they have no conflicts of interest.

References

[1] R. J. Torphy, Y. Fujiwara, and R. D. Schulick, "Pancreatic cancer treatment: better, but a long way to go," *Surgery Today*, vol. 50, no. 10, pp. 1117–1125, 2020.

[2] J. P. Neoptolemos, J. Kleeff, P. Michl, E. Costello, W. Greenhalf, and D. H. Palmer, "Therapeutic developments in pancreatic cancer: current and future perspectives," *Nature Reviews Gastroenterology & Hepatology*, vol. 15, no. 6, pp. 333–348, 2018.

[3] M. A. Tempero, "NCCN guidelines updates: pancreatic cancer," *Journal of the National Comprehensive Cancer Network*, vol. 17, no. 5, pp. 603–605, 2019.

[4] D. Ansari, B. Tingstedt, B. Andersson et al., "Pancreatic cancer: yesterday, today and tomorrow," *Future Oncology*, vol. 12, no. 16, pp. 1929–1946, 2016.

[5] M. Ilic and I. Ilic, "Epidemiology of pancreatic cancer," *World Journal of Gastroenterology*, vol. 22, no. 44, pp. 9694–9705, 2016.

[6] V. Goral, "Pancreatic cancer: pathogenesis and diagnosis," *Asian Pacific Journal of Cancer Prevention*, vol. 16, no. 14, pp. 5619–5624, 2015.

[7] C. Chabanolle, "Preventive approach of oral care for comfort and hydration," *Revue de l'Infirmiere*, vol. 67, no. 245, pp. 34–36, 2018.

[8] E. H. Stephens, J. A. Dearani, M. Y. Qureshi et al., "Toward eliminating perinatal comfort care for prenatally diagnosed severe congenital heart defects: a vision," *Mayo Clinic Proceedings*, vol. 96, no. 5, pp. 1276–1287, 2021.

[9] P. Yates, "Symptom management and palliative care for patients with cancer," *Nursing Clinics of North America*, vol. 52, no. 1, pp. 179–191, 2017.

[10] M. Yabrodi and C. W. Mastropietro, "Hypoplastic left heart syndrome: from comfort care to long-term survival," *Pediatric Research*, vol. 81, no. 1-2, pp. 142–149, 2017.

[11] J. L. Vincent, Y. Shehabi, T. S. Walsh et al., "Comfort and patient-centred care without excessive sedation: the eCASH concept," *Intensive Care Medicine*, vol. 42, no. 6, pp. 962–971, 2016.

[12] Y. T. Sung and J. S. Wu, "The visual analogue scale for rating, ranking and paired-comparison (VAS-RRP): a new technique for psychological measurement," *Behavior Research Methods*, vol. 50, no. 4, pp. 1694–1715, 2018.

[13] E. Takeuchi, Y. Kim, K. M. Shaffer, R. S. Cannady, and C. S. Carver, "Fear of cancer recurrence promotes cancer screening behaviors among family caregivers of cancer survivors," *Cancer*, vol. 126, no. 8, pp. 1784–1792, 2020.

[14] D. A. Dunstan, N. Scott, and A. K. Todd, "Screening for anxiety and depression: reassessing the utility of the Zung scales," *BMC Psychiatry*, vol. 17, no. 1, p. 329, 2017.

[15] E. Wittenberg, A. Reb, and E. Kanter, "Communicating with patients and families around difficult topics in cancer care using the COMFORT communication curriculum," *Seminars in Oncology Nursing*, vol. 34, no. 3, pp. 264–273, 2018.

[16] P. Kasvis and R. D. Kilgour, "Diet and exercise interventions in patients with pancreatic cancer: a scoping review," *Pancreas*, vol. 50, no. 5, pp. 657–666, 2021.

[17] E. J. Lee, S. Y. Seo, I. H. Kim et al., "Effect of cancer awareness on treatment decision for pancreatic cancer patients," *Korean Journal of Gastroenterology*, vol. 75, no. 4, pp. 198–206, 2020.

[18] S. Partelli, F. Sclafani, S. T. Barbu et al., "European cancer organisation essential requirements for quality cancer care (ERQCC): pancreatic cancer," *Cancer Treatment Reviews*, vol. 99, Article ID 102208, 2021.

[19] Y. Lei, B. Liu, L. Su et al., "Perioperative nursing of patients with pancreatic cancer treated with a nanoknife," *Journal of Nanoscience and Nanotechnology*, vol. 20, no. 10, pp. 6584–6590, 2020.

[20] L. H. Eaton, J. Brant, K. McLeod, and C. Hsing Yeh, "Nonpharmacologic pain interventions: a review of evidence-based practices for reducing chronic cancer pain," *Clinical Journal of Oncology Nursing*, vol. 21, no. 3, pp. 54–79, 2017.